

AD-A149 163

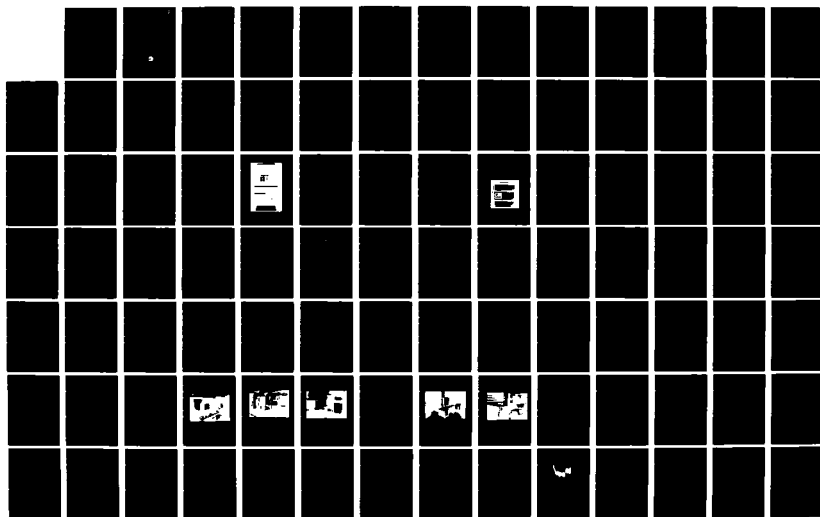
PROCEEDINGS OF THE ANNUAL PRECISE TIME AND TIME
INTERVAL (PTTI) APPLICATI. (U) NAVAL RESEARCH LAB
WASHINGTON DC J A MURRAY 02 APR 84

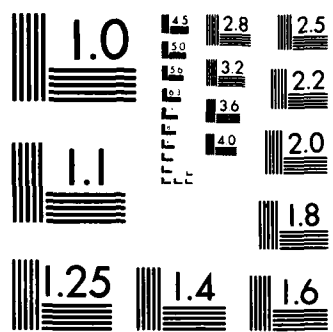
1/8

UNCLASSIFIED

F/G 5/9

NL





MICROCOPY RESOLUTION TEST CHART
NATIONAL BUREAU OF STANDARDS-1963-A

AD-A149 163

2

Proceedings of the Fifteenth Annual Precise Time and Time Interval (PTTI) Applications and Planning Meeting

A meeting held at the
Naval Research Laboratory
Washington, D.C.
December 6-8, 1983

FILE COPY



DTIC
ELECT
NOV 5 1984
S

D

Approved for public release; distribution unlimited.

34 1 10 131

Proceedings of the Fifteenth Annual Precise Time and Time Interval (PTTI) Applications and Planning Meeting

A meeting held at the
Naval Research Laboratory
Washington, D.C.
December 6-8, 1983

Accession For	
NTIS GRA&I	<input checked="" type="checkbox"/>
DTIC TAB	<input type="checkbox"/>
Unannounced	<input type="checkbox"/>
Justification	

A/11



Sponsored by

Naval Observatory
NASA Goddard Space Flight Center
Naval Electronic Systems Command
Naval Research Laboratory
Defense Communications Agency
Chief of Naval Operations
National Bureau of Standards
Army Electronics Technology
and Devices Laboratory
Rome Air Development Center

DISTRIBUTION STATEMENT A

Approved for public release;
Distribution Unlimited

SECURITY CLASSIFICATION OF THIS PAGE

REPORT DOCUMENTATION PAGE				
1a REPORT SECURITY CLASSIFICATION UNCLASSIFIED		1b RESTRICTIVE MARKINGS None		
2a SECURITY CLASSIFICATION AUTHORITY		3 DISTRIBUTION / AVAILABILITY OF REPORT		
2b DECLASSIFICATION / DOWNGRADING SCHEDULE		Approved for public release; distribution unlimited.		
4 PERFORMING ORGANIZATION REPORT NUMBER(S) None		5 MONITORING ORGANIZATION REPORT NUMBER(S)		
6a NAME OF PERFORMING ORGANIZATION Naval Research Laboratory	6b OFFICE SYMBOL (if applicable) 7962	7a NAME OF MONITORING ORGANIZATION		
6c ADDRESS (City, State, and ZIP Code) Washington, DC 20375		7b ADDRESS (City, State, and ZIP Code)		
8a NAME OF FUNDING / SPONSORING ORGANIZATION Naval Research Laboratory*	8b OFFICE SYMBOL (if applicable) 7962	9. PROCUREMENT INSTRUMENT IDENTIFICATION NUMBER		
8c ADDRESS (City, State, and ZIP Code) Washington, DC 20375		10 SOURCE OF FUNDING NUMBERS		
		PROGRAM ELEMENT NO	PROJECT NO	TASK NO
		WORK UNIT ACCESSION NO 1356-0-4		
11 TITLE (Include Security Classification) Proceedings of the Fifteenth Annual Precise Time and Time Interval (PTTI) Applications and Planning Meeting				
12. PERSONAL AUTHOR(S) James A. Murray, Editor				
13a. TYPE OF REPORT Proceedings	13b. TIME COVERED FROM 12/6/83 TO 12/8/83	14 DATE OF REPORT (Year, Month, Day) 84 April 2	15 PAGE COUNT 770	
16 SUPPLEMENTARY NOTATION (See page ii)				
17 COSATI CODES			18 SUBJECT TERMS (Continue on reverse if necessary and identify by block number)	
FIELD	GROUP	SUB-GROUP	Time, Time transfer, Time dissemination, Time measurement, Hydrogen masers, Frequency standards	
19 ABSTRACT (Continue on reverse if necessary and identify by block number)				
<p>These proceedings contain the papers presented at the Fifteenth Annual Precise Time and Time Interval (PTTI) Applications and Planning Meeting, including questions and answers following presentations. The purpose of the meeting was to give PTTI managers, systems engineers, and program planners a transparent view of the state of the art, and opportunity to express needs, a view of important future trends, and a review of relevant past accomplishments; to provide PTTI users with new and useful applications, procedures, and techniques; to allow the PTTI researcher to better assess fruitful directions for research efforts.</p>				
20 DISTRIBUTION / AVAILABILITY OF ABSTRACT <input type="checkbox"/> UNCLASSIFIED/UNLIMITED <input checked="" type="checkbox"/> SAME AS RPT <input type="checkbox"/> DTIC USERS			21 ABSTRACT SECURITY CLASSIFICATION UNCLASSIFIED	
22a NAME OF RESPONSIBLE INDIVIDUAL J. A. Murray			22b TELEPHONE (Include Area Code) 202-767-2595	22c OFFICE SYMBOL 7962

DD FORM 1473, 84 MAR

83 APR edition may be used until exhausted
All other editions are obsolete

SECURITY CLASSIFICATION OF THIS PAGE

16. SUPPLEMENTARY NOTATION (Continued)

***Sponsors:** U.S. Naval Observatory; NASA Goddard Space Flight Center; Naval Electronic Systems Command; Naval Research Laboratory; Defense Communications Agency; Chief of Naval Operations; National Bureau of Standards; Rome Air Development Center; and Army Electronics Technology and Devices Laboratory

EXECUTIVE COMMITTEE

Schuyler C. Wardrip, Chairman
NASA Goddard Space Flight Center

James A. Buisson
Naval Research Laboratory

Jimmie B. Collie
Naval Electronic Systems Command

Hugh S. Fosque
NASA Headquarters

Dr. William J. Klepczynski
Naval Observatory

Dr. Arthur O. McCoubrey
National Bureau of Standards

James A. Murray, Jr.
Naval Research Laboratory

Dr. Samuel R. Stein
National Bureau of Standards

Dr. Harris A. Stover
Defense Communications Agency

Dr. John R. Vig
Army Electronics Technology and Devices Laboratory

Dr. Gernot M. R. Winkler
Naval Observatory

Dr. Nicholas F. Yannoni
Rome Air Development Center

Sheila C. Faulkner
Naval Observatory
Administrative Assistant

GENERAL CHAIRMAN
Dr. Nicholas F. Yannoni
Rome Air Development Center

TECHNICAL PROGRAM COMMITTEE
CHAIRMAN
Dr. William J. Klepczynski
Naval Observatory

EDITORIAL COMMITTEE CHAIRMAN
L. J. Rueger
Johns Hopkins University/Applied Physics Laboratory

PUBLICITY CHAIRMAN
James A. Buisson
Naval Research Laboratory

SESSION CHAIRMEN

SESSION I

Advances in Time and Frequency Services

Dr. Derek Morris

National Research Council

Canada

SESSION II

GPS Time Transfer

Dr. Victor Reinhardt

Bendix Field Engineering Corporation

SESSION III

Time Transfer/Synchronization

Hugh S. Fosque

NASA Headquarters

SESSION IV

Mathematical and Statistical Techniques and

Their Applications to PTI

Dr. James A. Barnes

Austron Inc.

SESSION V

PTI Components

Dr. Arthur O. McCoubrey

National Bureau of Standards

SESSION VI

Classified Session

Dr. Gernot M. R. Winkler

Naval Observatory

ARRANGEMENTS

James A. Murray, Jr. NRL
Stella Scates, NRL
Susan Ramey, NRL

FINANCE COMMITTEE

James A. Buisson, NRL
S. Clark Wardrip, GSFC

PUBLICATIONS

Elaine Bowers, BFEC
L. J. Rueger, APL
S. Clark Wardrip, GSFC

NRL TECHNICAL ASSISTANCE

James Eng
Stanley Falvey
Alick Frank
Robert Hersh
Chester Kleczek
Mark Lister
Wayne Lloyd
Wade Root
Leighton Williams

PRINTING

Charles V. Hardesty, GSFC
Donald E. Ellis, GSFC

RECEPTIONISTS

Elaine Bowers, BFEC
Sheila Faulkner, USNO
Stella Scates, NRL
Betty Wardrip, GSFC

BANQUET SPEAKER

Robert E. Fischell, APL/JHU

SUBJECT: Time Controlled Release of
Medication By Implantable Devices

FOREWORD

These proceedings contain the papers presented at the Fifteenth Annual Precise Time and Time Interval Applications and Planning Meeting which was held December 6-8, 1983 at the Naval Research Laboratory. The discussions following the presentations are also included. There were 261 registered attendees, of which 31 were from 13 foreign countries.

The objective of the meeting was to provide an opportunity for program planners to meet those who are engaged in research and development and to keep abreast of the state-of-the-art and latest technological developments. At the same time, it provided an opportunity for the engineers and scientists to meet program planners. This objective is clearly reflected by the title of the meeting.

This year, the program emphasized advances in Time and Frequency Services of the various national laboratories, the use of the NAVSTAR Global Positioning Service for time transfer, and the mathematics and statistical techniques used in PTTI. Specialized PTTI applications and systems for Time Transfer/Synchronization and PTTI System Components were also included in the program. For the second time in the history of the PTTI meetings, a well-attended classified session was held.

The Executive Committee wishes to express its appreciation of the excellent work of the Session Chairman and the Technical Program Committee. The quality of the program remains excellent as is evidenced by the increasing registration and continuing support of our sponsors. The key to the success of a meeting such as this depends on the unstinting support of many volunteers. We are fortunate to have such support from the sponsors. In particular, the efforts of Mesers. S. Clark Wardrip and James Murray must be recognized, as well as the hospitality of the Naval Research Laboratory.

CONTENTS

	<u>Page</u>
CALL TO SESSION Dr. William J. Klepczynski	1
WELCOMING ADDRESS Jim Murray	3
OPENING COMMENTS Dr. William J. Klepczynski	5

SESSION I ADVANCES IN TIME AND FREQUENCY SERVICES

Timing Accuracy of LF and TV Synchronization Techniques Miao Yun-rui and Pan Xiao-pei	9
New Time and Frequency Services at the National Bureau of Standards S. R. Stein, G. Kamas and D. W. Allan	17
Recent Improvements in the Atomic Time Scales of the National Bureau of Standards D. W. Allan, D. J. Glaze, J. E. Gray, R. H. Jones, J. Levine, and S. R. Stein	29
Automation of Precise Time Reference Stations (PTRS) Paul J. Wheeler	41
U.S. Naval Observatory Collection and Utilization of Time Comparison Data F. Neville Withington	53
International Time Comparison by a GPS Timing Receiver M.-K. Fujimoto, K. Fujiwara, and S. Aoki	71

SESSION II GPS TIME TRANSFER

First Results of GPS Time Transfer to Australia John McK. Luck, John R. Woodger, James E. Wells, Peter N. Churchill and Philip A. Clements	87
Separating the Variances of Noise Components in the Global Positioning System David W. Allan and Marc Weiss	115
Enhancements to the TTS-502 Time Transfer System Dr. A. J. Van Dierendonck and Dr. Q. D. Hua	133

CONTENTS (continued)

	<u>Page</u>
A New Precision Time and Frequency Source for Stationary PTTI Applications	155
Javad M. Ashjaee, Roger J. Helkey and Ron C. Hyatt	
On-Orbit Frequency Stability Analysis of the GPS NAVSTAR's 3 and 4 Rubidium Clocks and NAVSTAR's 5 and 6 Cesium Clocks	171
Thomas B. McCaskill, James A. Buisson and Sarah B. Stebbins	
GPS Navigation Experiment Using High Precision GPS Timing Receivers . . .	211
J. Buisson, O. J. Oaks, M. Lister, S. C. Wardrip, S. Leschiutta, P. G. Galliano, F. Cordara, V. Pettiti, E. Detoma, P. Dachel, H. Warren, T. Stalder, F. Fedele and R. Azzarone	
Improved Master Clock Reference System at USNO	237
Gernot M. R. Winkler	
The Steering of GPS Time	249
H. F. Fliegel	
Test Results for Prototype GPS Rubidium Clocks	269
T. J. Lynch and W. J. Riley	

SESSION III TIME TRANSFER/SYNCHRONIZATION

International Time Transfer and Portable Clock Evaluation Using GPS Timing Receivers: Preliminary Results	283
S. C. Wardrip, J. Buisson, O. J. Oaks, M. Lister, E. Detoma, P. Dachel, T. Stalder, H. Warren, G. Winkler, G. Luther, S. Leschiutta, P. G. Galliano, F. Cordara, V. Pettiti, R. Azzarone and F. Fedele	
Spread Spectrum Time Transfer Experiment Via INTELSAT	331
Dr. P. Hartl, L. Veenstra, N. Gieschen, K.-M. Mussener, W. Schafer, C.-M. Wende, Dr. W. Klepczynski, H.-H. Nau and R. Stoiber	
Unattended TV Time Transfer Results	357
John A. Waak and John H. Spencer	
The Role of a Low Earth Orbiter in Intercontinental Time Synchronization Via GPS Satellites	371
Sien-Chong Wu and V. John Ondrasik	
Timing of Spacecraft Data	389
H. P. Dworak	

CONTENTS (continued)

	<u>Page</u>
UHF IRIG G Distribution System	413
M. Tope	
Timing System Design Considerations for a Mobile Astrolabe	423
Carl F. Lukac, Paul J. Wheeler, Richard E. Keating, and Randolph T. Clarke	
Precise Time Transfer Using MKIII VLBI Technology	443
K. J. Johnston, J. A. Buisson, M. J. Lister, O. J. Oaks, J. H. Spencer, W. B. Waltman, G. Elgered, G. Lundqvist, A. E. E. Rogers, T. A. Clark, C. Ma, A. C. Johnson, K. Kingham, W. J. Klepczynski, G. Luther, A. J. Kubic, and D. D. McCarthy	

SESSION IV

MATHEMATICAL AND STATISTICAL TECHNIQUES AND THEIR APPLICATION TO PTTI

Clock Characterization Tutorial	459
David W. Allan	
Methods for Optimal Recursive Estimation of Non-Stationary Time Series, Applications to Atomic Time and Frequency Metrology	477
Z. Y. Weng, J. Rutman and J. Uebersfeld	
Applied Kalman Filtering: An Overview	503
R. Grover Brown	
Kalman Filtering with a Two-State Clock Model	519
Fran B. Varnum	
Kalman Filter Estimates of the NAVSTAR Satellite Clock Parameters	531
Paul S. Jorgensen	
The Measurement of Linear Frequency Drift in Oscillators	551
James A. Barnes	
A Plan for the Development of Inertial Reconstruction of Initial State Clock (IRIS)	583
Ernest G. Kimme, Ph.D.	

SESSION V

PTTI COMPONENTS

High Performances from a New Design of Crystal Oscillator	621
G. Beauvy, G. Marotel and P. Renoult	
Design of SC Cut 10 MHz H.Q. Crystals with G. Sensitivity Better than $2.10^{-10}/G$	635
A. Debaisieux, J. P. Aubry and J. Gros Lambert	

CONTENTS (continued)

	<u>Page</u>
Recent Results on the Performance of EFOS, NP and NX Hydrogen Masers V. Reinhardt, J. Ingold, T. Stalder, M. Saifi, P. Dachel and S. C. Wardrip	653
Physics Element Design Aspects for a Tactical Rubidium Frequency Standard. . Bruce Grover and Tae M. Kwon	677
Crystal Resonator/Oscillator Test Facility and Test Results. V. J. Rosati and R. L. Filler	693
Time Synchronization Experiments with Apple. C. L. Jain, K. Kumar, M. R. Sivaraman, B. S. Mathur, P. Banerjee, A. Sengupta, Mithlesh Saxana, A. K. Hanjura and A. K. Suri	707
The Superconducting Cavity Stabilized Ruby Maser Oscillator. G. J. Dick and D. M. Strayer	723
CLOSING REMARKS.	741

CALL TO SESSION

Dr. William J. Klepczynski
Program Chairman
United States Naval Observatory

DR. KLEPCZYNSKI: My name is Bill Klepczynski, and I am the program chairman for this meeting. Unfortunately, the general chairman of the meeting, Dr. Nicholas Yannoni, is ill and could not, therefore, make it for today. So, on his behalf, I would like to extend to you a hearty welcome for your attendance here at the Fifteenth Annual P.T.T.I. Meeting.

Authors of papers, Lauren Rueger, who is here, I'll ask him to stand up, he is to receive your paper sometime, during the three days of the meeting, for publication in the Proceedings of the Fifteenth Annual Precision Time and Time Interval Planning Conference.

For our welcoming address I would like to introduce Jim Murray of the Naval Research Laboratory.

WELCOMING ADDRESS

Jim Murray
Naval Research Laboratory

MR. MURRAY: I am sorry that our Commanding Officer, Captain McMorris, will not be able to be here for the welcoming address; but, on his behalf, I would like to extend to you a wish for a very successful meeting.

The laboratory is not new to this meeting. We have been associated with it for the past fifteen years, back to when it first started. During that time we have seen the number of sponsors increase by an order of magnitude; from one to ten, and we have seen the nanosecond replace the microsecond as the most talked about unit of time; and now we can even use picoseconds without a footnote. These are all signs of progress, and these are things that the timing community has done; but there's another sign of progress, and that's the growing number of users that describe their systems in terms of these units. For this, our meetings can take proper credit.

We are responsible for letting the potential users know what has been done, what is being done, and what is planned in timing. In this way, we have helped them to take advantage of the kinds of precise timing that can improve their systems.

P.T.T.I. meetings have been very successful in accomplishing their purposes, and I am sure this meeting will enjoy the same productivity as those in the past.

We have many foreign visitors here and we are very happy to have them. We are sorry for the inconvenience that our entry procedures have caused, but this is just part of our system that we cannot do without.

I welcome you here and I wish you success in your meeting.

OPENING COMMENTS

Dr. William J. Klepczynski
Technical Program Committee
United States Naval Observatory

DR. KLEPCZYNSKI: I would like to talk about the program very briefly. As Jim mentioned, today microsecond timing is available throughout most of the world; and in some instances, we have nanosecond timing. This has really taken place in the last fifteen or sixteen years. I think the first Hewlett-Packard cesium box came out about 1967 or '68, and ever since that time the timing community and users of precise time have made quantum leaps in their systems; and the programs reflect some of these advances.

The first session we have is devoted to advances in the services provided by the various national laboratories.

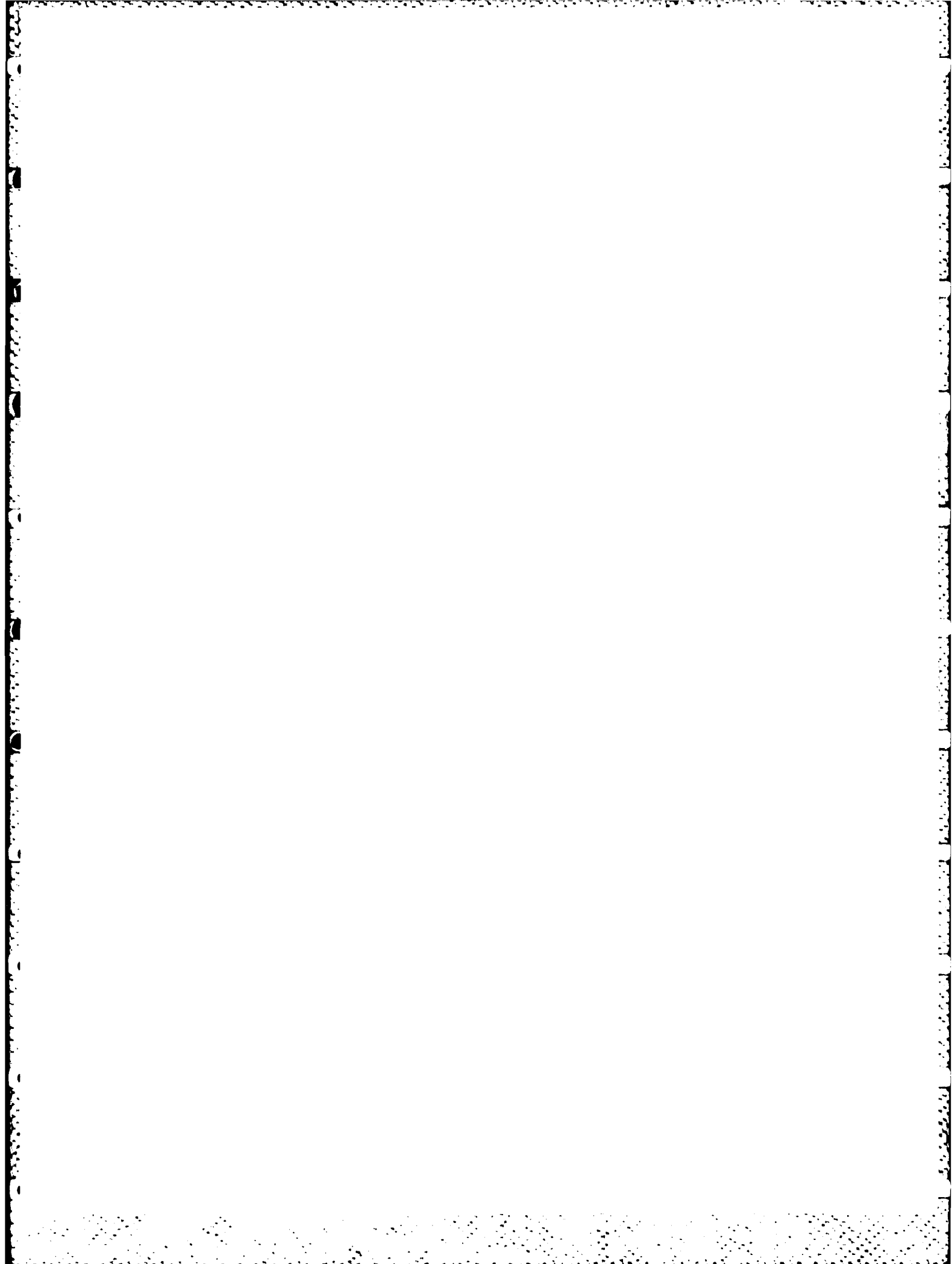
We have another session on G.P.S. time transfer; one of the most up-to-date systems, which will assure nanosecond timing throughout the world.

One session is devoted to the mathematics of precision time and frequency. Since we have not dealt with that for a long time, we thought some interesting tutorials would be worthwhile for the people who attend the meetings.

There is one classified session which will not be held in this auditorium; it will be held in a separate building and is restricted to cleared U.S. citizens. So please take this into consideration.

If you have a question would you identify yourself, because the sessions are being recorded for the proceedings of the conference, and we can then get your name and affiliation as well as your words.

With that, I would like to introduce the chairman of the first session, Dr. Derek Morris, National Research Council of Canada.



SESSION I

ADVANCES IN TIME AND FREQUENCY SERVICES

Dr. Derek Morris, Chairman
National Research Council
Canada

CALL TO SESSION I

DR. DEREK MORRIS: Good morning. This session is called Advances in Time and Frequency Services, and I understand at the moment that five of the six papers will be given. If the authors of the last paper are here, I would appreciate it if they would identify themselves to me; if not, we will start right away, and I would ask the speakers, please, to keep to twenty minutes for their presentations. If it's slightly less than that, we will have time for one or two questions; but we have a deadline to reach lunch by 11:50, so we will have to keep the session moving.

TIMING ACCURACY OF LF AND TV SYNCHRONIZATION TECHNIQUES

Miao Yun-rui and Pan Xiao-pei¹
Shaanxi Astronomical Observatory
P. O. Box 18
Lintong (near Xian)
Shaanxi
People's Republic of China

ABSTRACT

LF and TV synchronization techniques have been widely used in China for several years. Shaanxi, Shanghai and Beijing Astronomical Observatories have cooperated with the U. S. Naval Observatory in making two portable clock calibration experiments in 1981 and 1982. The results indicate that the LF synchronization method can reach a timing accuracy of $\pm 1 \mu\text{s}$ and a precision of $\pm 0.05 \mu\text{s}$ to $\pm 0.20 \mu\text{s}$ over a range of 2000km with complex mixed paths. In addition, it has been found that there is a systematic difference of about 4 μs between USNO and other laboratories via the North-West Pacific Loran-C chain. The experiment also shows that the timing accuracy for the passive TV synchronization method is about $\pm 1 \mu\text{s}$ and the precision of daily frequency calibrations is better than 2 parts in 10 to the 12th.

1. INTRODUCTION

Precise time and frequency comparison among Shaanxi, Shanghai and Beijing Astronomical Observatories has been accomplished via different techniques. Since 1974, Loran-C has been used in China for the determination of the accuracy and the long-term stability of many types of atomic frequency standards. In 1978, an experimental LF pulse-coded transmitter station (BPL), which is controlled by Shaanxi Astronomical Observatory, was put into service for precise time and frequency in China. The equivalent values of conductivity over land in China for the LF signal were measured, and the signal strength and the time delay of the ground wave at 100kHz were predicted for most of the timing centers. Now, the LF pulse-coded sync technique has been widely used for time and frequency in China.

Time and frequency comparisons via television signals have been used on a daily basis for more than seven years between these observatories. This is a very simple and valuable method. Time delays between Beijing and other cities, such as Xian, Shanghai, etc., through microwave relay routing of the Chinese Television Network have been measured. Passive TV Line-6 comparison is used not only for frequency calibration but also for time distribution.

¹ This cooperative program also includes the following people:
Luo Ding-chang (Beijing Astronomical Observatory)
Zhuang Qi-xiang (Shanghai Astronomical Observatory)
Song Jin-an (Shaanxi Astronomical Observatory)
Bian Yu-jing (Shaanxi Astronomical Observatory)

The portable clock is still the best technique available for the remote synchronization of clocks because it is independent of propagation errors. Shaanxi, Beijing and Shanghai Observatories cooperated with the U. S. Naval Observatory in making two portable clock experiments in 1981 and 1982 in order to evaluate the timing accuracy and precision of the LF and TV techniques.

II. RESULTS AND ANALYSIS FOR LF SYNCHRONIZATION TECHNIQUE

The results of the comparison between the portable clock, received Loran-C signals, and local master clocks in different labs are given in Tables 1 and 2, separately. It is obvious that precisions for Loran-C reception (sample time = 1 hour) at SO, CSAO and BAO are 0.046, 0.178 and 0.089 μ s, respectively.

Table 1. Time difference (in μ s) between portable clock and local Loran-C received (PC-LCr) in August 1982

	PC-LCr(SO)		PC-LCr(CSAO)		PC-LCr(BAO)	
Period	Aug	19 ^d 15 ^h -20 ^d 15 ^h	Aug	21 ^d 10 ^h -22 ^d 10 ^h	Aug	25 ^d 14 ^h -26 ^d 14 ^h
Mean		62286.023		66224.050		65706.870
rms		<u>+0.046</u>		<u>+0.178</u>		<u>+0.089</u>

* Abbreviations used here are:

CSAO Shaanxi Observatory
SO Shanghai Observatory
BAO Beijing Observatory

PC Portable Clock
LCr Loran-C Received

Table 2. Results (in μ s) of comparison between portable clock and local master clock in August 1982

	MC(SO)-PC		MC(CSAO)-PC		MC(BAO)-PC	
Period	Aug	19 ^d 15 ^h -21 ^d 01 ^h	Aug	21 ^d 10 ^h -25 ^d 05 ^h	Aug	25 ^d 14 ^h -26 ^d 21 ^h
Frequency offset		-7.0x10 ⁻¹³		-4.7x10 ⁻¹³		-3.1x10 ⁻¹³
stability (τ = 3 hour)		<u>+6.0x10⁻¹³</u>		<u>+5.5x10⁻¹³</u>		<u>+6.1x10⁻¹³</u>

The accuracy of Loran-C timing mainly depends upon a knowledge of the distance, the earth conductivity and the refractive index of the air between transmitting and receiving sites. It also depends upon the measurement of the delay of the receiving system. The time difference between the portable clock and the received Loran-C signal from Table 1 is

$$\begin{aligned} (PC-LCr)_t = & (UTC(USNO,MC)-LCe)t \\ & -(UTC(USNO,MC)-PC)_{t_0} \\ & +\Delta PC(t-t_0) \\ & + (LCe-LCr), \end{aligned}$$

where $(UTC(USNO,MC)-LC)$ is the time signal correction at some moment, t , that comes from USNO publication, Series 4,
 $(UTC(USNO,MC)-PC)$ is the time difference of the portable clock with respect to the Master Clock (USNO),
 $\Delta PC(t-t_0)$ is the rate correction of the portable clock during the period $(t - t_0)$
 $LCe-LCr$ is the total delay between the transmitting and receiving sites, which includes emission delay, propagation delay, receiving delay and the cycle correction. The results of the calculations are summarized in Table 3 (Ref. 1).

The results of calculations and the calibration experiment with portable clocks are compared in Table 4. Sync errors for each pair of observatories are summarized in Table 5. Although these observatories have different distances from the transmitter stations, different paths and receiving conditions, the average sync error for two labs, as derived from the data from Table 4, is $0.57 \pm 0.27 \mu s$.

Table 3. Measured time delays (in μs) of the Y slave station of the Northwest Pacific Loran-C Chain (GRP=99700 μs) as determined at three observatories.

	SO	CSAO	BAO
Distance	828.840 km	2006.232 km	1853.607 km
Emission delay	59463.18	59463.18	59463.18
Cycle correction	30.00	30.00	30.00
Receiving delay	25.9	28.9	25.3
Propagation delay	2767.39	6702.67	6189.74
Total Delay	62286.47	66224.75	65708.22

Table 4. Results of experiment and calculation for the Loran-C sync (unit = μs)

	Shanghai		Shaanxi		Beijing	
	1981	1982	1981	1982	1981	1982
UTC(MC)-LCe	2.6	3.6	2.6	3.6	2.6	3.6
-(UTC(MC)-PC)	-0.95	-0.4	-0.95	0.4	-0.95	-0.4
LCe-LCr	62286.47	62286.47	66222.20	66224.75	65708.22	65708.22
(PC-LCr)cal	62288.12	62289.67	66223.85	66227.95	65709.97	65711.42
(PC-LCr)meas	62283.81	62286.02	66219.00	66224.05	65704.85	65706.87
Meas. - Cal. (PC-LCr)	-4.31	-3.65	-4.85	-3.90	-5.12	-4.55

Table 5. Sync error between two observatories via LC/9970

	CSAO-SO	BAO-CSAO	SO-BAO
1981	-0.54	-0.27	-0.81
1982	-0.25	-0.65	-0.90

Note also from Table 5 that the annual change in the sync error between SO and BAO is very small, less than $0.1 \mu\text{s}$. This means that the Loran-C time signal in different years and different months is rather stable. A conservative estimation is that it is stable to better than $0.5 \mu\text{s}$. Even for the CSAO, which changed receivers and their location, the variation of the sync error is only $0.95 \mu\text{s}$. It is clear that a timing accuracy at the level of $1 \mu\text{s}$ within the range of 2000 km over complex mixed paths via LF can be reached.

It is worthwhile to notice that the average difference between measurement and calculation in Table 4 is

$$-4.39 \pm 0.56 \mu\text{s},$$

which, in fact, implies that there is a common systematic error between the USNO and each of the three observatories. In Japan there is a similar result. For example, Tokyo Astronomical Observatory (TAO), in October 18, 1982, measured $\text{UTC}(\text{TAO})-\text{PC} = 6.5 \mu\text{s}$. From TAO publications, one can deduce that the time difference of the Loran-C time signal relative to $\text{UTC}(\text{TAO})$ is $\text{UTC}(\text{TAO})-\text{LCe} = 5.4 \mu\text{s}$. Thus from measurement, we have $\text{PC}-\text{LCe} = -0.9 \mu\text{s}$. On the other hand, the time difference between the portable clock and the Loran-C signal at the emission station, calculated from USNO publication Series 4, is

$$\text{PC}-\text{LCe} = (\text{UTC}(\text{USNO}, \text{MC})-\text{LCe}) - (\text{UTC}(\text{USNO}, \text{MC})-\text{PC}) = 3.25 \mu\text{s}.$$

It is evident that the difference between measurement and calculation for the USNO relative to TAO is $-4.15 \mu\text{s}$. This systematic error is consistent not only with the results from Shaanxi, Shanghai and Beijing Observatories, but also with the historical results from TAO (Ref. 2). The reason for this error should be investigated further.

In addition, one can see from the results in Table 4 that the average difference between measurement and calculation in 1981 is $-4.39 \mu\text{s}$, but in 1982 is $-3.43 \mu\text{s}$. The difference of about $1 \mu\text{s}$ reflects the precision of the correction values in Series 4 published by the USNO.

III. RESULTS AND ANALYSIS FOR TV SYNC TECHNIQUE

Beijing, Shaanxi and Shanghai observatories have developed a TV Line-6 system (line 6 pulse of the odd field in the 625 line system) as a method of comparing remotely located clocks in China. The results of TV comparison during the period of portable clock calibration experiment in October, 1982 are listed in Table 6. According to the measurement of time delay for the microwave relay network and calculation of the propagation delay between the local TV transmitter and the receiver (Ref. 3), we can get the time delays between the Beijing Microwave Master Station (BMMS) and each lab as follows:

Time delay of (BMMS-CSAO) = $3611.0 \mu\text{s}$,
 Time delay of (BMMS-SO) = $6835.1 \mu\text{s}$,
 Time delay of (BMMS-BAO) = $75.3 \mu\text{s}$.

Using the above data during the period of portable clock trip, the measurement error of single time difference from day to day for TV method is as follows:

$+0.027 \mu\text{s}$ for (CSAO-BAO),
 $+0.061 \mu\text{s}$ for (SO-BAO),
 $+0.025 \mu\text{s}$ for (SO-CSAO).

The relative frequency offsets measured by the portable clock and the TV Line-6 technique are summarized in Table 7.

Table 6. Time differences between the CCTV signal and the local master clocks during the October 1982 clock trip in μs

	MC(BAO)-TV	MC(CSAO)-TV	MC(SO)-TV
October 19	17216.35	20748.86	3947.94
20	38794.79	2326.94	5558.07
21	12518.86	16051.27	39250.49
22	4023.83	7556.28	30755.62
23	920.34	4452.63	---
24	28677.47	32209.80	---
25	32663.43	36195.74	---

Table 7. Relative frequency offset between local master clocks measured by different techniques

	CSAO-BAO	SO-BAO	SO-CSAO
TV	-3.6×10^{-13}	7.5×10^{-13}	10.1×10^{-13}
PC	-1.6×10^{-13}	-3.9×10^{-13}	-2.3×10^{-13}
Δ PC-TV	-2.0×10^{-13}	11.4×10^{-13}	12.4×10^{-13}

It is obvious that the precision of frequency comparisons via TV is:

and 2×10^{-13} /day for CSAO - BAO,
 2×10^{-12} /day for SO - CSAO and SO - BAO.

The results of time comparisons by use of portable clocks and passive TV techniques are given in Tables 8 and 9. It shows that the sync error between CSAO and BAO is $-0.78 \mu\text{s}$; the error for CSAO and SO is $-1.82 \mu\text{s}$; and the average timing accuracy is $1.3 \pm 0.74 \mu\text{s}$.

Table 8. Comparison between time differences (SO-CSAO) measured by the portable clock and the TV sync on October 20, 1982 (μs)

	SO	CSAO	SO-CSAO
MC-TVr	5558.07	2326.94	
TVe-TVr	6835.1	3611.0	
MC-TVe	-1277.03	-1284.06	7.03
MC-PC	8.694	-0.153	8.85

Note: The time difference value of (MC(CSAO)-PC) on October 20, 1982 is obtained by extrapolating the values of October 21 and 22.

Table 9. Comparison between time difference (CSAO-BAO) measured by the portable clock and the TV sync on October 25, 1982 (μs)

	CSAO	BAO	CSAO-BAO
MC-TVr	36195.74	32663.43	
TVe-TVr	3611.0	75.3	
MC-TVe	32584.74	32588.13	-3.39
MC-PC	-0.392	2.22	-2.61

Note: The time difference value of (MC(CSAO)-PC) on October 25, 1982 is obtained by extrapolating the values of October 23 and 24.

IV. CONCLUSION

LF and TV sync techniques provide an excellent medium for the dissemination of precise time and frequency on a continuous basis. The portable clock is an absolute technique with a

precision of about $0.1 \mu\text{s}$. The results of the portable clock experiment indicate that LF sync technique can reach a timing accuracy of $\pm 1 \mu\text{s}$ and precision of $\pm 0.05 - \pm 0.2 \mu\text{s}$ within a range of 2000 km of the groundwave coverage. In addition, it has been found that there is a systematic error of about $4 \mu\text{s}$ between the USNO and other labs via the Northwest Pacific Loran-C Chain. For passive TV sync, the timing accuracy is about $1 \mu\text{s}$, and precision of the daily frequency calibration is better than 2×10^{-12} .

REFERENCE

1. Chen Hong-qing etc., "Problems on the computation of time delay of LF groundwave propagation," Symposium on the Jointed Atomic Time Scale, December, 1982.
2. Shigetaka Iijima, "Time and frequency in Japan," J. Inst. Electronics & Telecom. Engrs., Vol. 27, No. 10, 1981
3. Cheng Cong-ling, "Analysis of the results of the passive TV synchronization," Symposium on the Jointed Atomic Time Scale, December, 1982
4. Allan, D. W., Blair, B. E., etc., "Precision and accuracy of remote synchronization via network television broadcasts, Loran-C and portable clocks", Metrologia, 8, No. 2, pp 64-72, (April 1972)
5. Lukac, Carl "Loran-C prediction problems," Proc. 13th PTTI Meeting, pp. 217-227, December 1981

QUESTIONS AND ANSWERS

A VOICE:

Why was the four microseconds there? Do you know?

MR PAN:

We think the problem is that it is an adopted value, because we checked the receiving delay and we checked the propagation delay; and we think that for the propagation delay, we get better than one microsecond because - you see in Table 5 we listed the time difference between the different observatories in China, and we can see the difference is less than one microsecond. But, as you know, since the observatories are far away from the North-west Pacific Ocean Loran-'chain', because the distance is from 800 kilometers to 2000 kilometers, and today you have a different path, completely different. So we thought we could predict the propagation delay to better than one microsecond.

DR. WINKLER:

I would like to make a comment. About the origin of the four microseconds is clearly an adopted value for the propagation delays in some original monitor stations; but there is one thing to consider, at that time, loop antennas were used. Today, many people use whip antennas. If you use a loop antenna, there are many loops in existence which have the arrow pointing in the wrong direction. If you use one of these you have an error of five microseconds. This is a fact of life.

So, therefore, my suspicion is that somewhere in our original calibrations there must have been a loop confusion. We actually deal with a discrepancy between the computed delay and the measured delay of slightly larger than one microsecond.

Of course, we have no choice but to stick to the value which we have adopted. You cannot jump around between adopted values.

NEW TIME AND FREQUENCY SERVICES AT THE
NATIONAL BUREAU OF STANDARDS

S. R. Stein, G. Kamas, and D. W. Allan
Time and Frequency Division
National Bureau of Standards
Boulder, Colorado

INTRODUCTION

The National Bureau of Standards (NBS) established two new time and frequency services in 1983. They permit the user to obtain time and frequency traceable to the NBS with greater precision and less effort than previously possible. The new services are for users who require time transfer accuracies in the three nanosecond to one microsecond range or frequency calibration capability in the 1 part in 10^{11} to one part in 10^{14} range. However, many applications not requiring this level of precision may benefit from these services because of the high degree of automation, simplicity of use, and support from the NBS.

Frequency calibration requirements at the part in 10^{11} to part in 10^{12} level and timing requirements at the 1 microsecond level can be satisfied using low frequency radio signals broadcast from stations such as WWVB or Loran-C. The NBS Frequency Measurement Service helps the user set-up a low frequency receiver and data logging system most appropriate for his needs and location. A typical system includes a receiver, microcomputer, floppy disc units and printer-plotter. The user supplies a dial-up phone line and modem so that his data can be compared with data recorded at NBS when necessary, thus providing increased assurance that the measurements are valid. The user also receives a bulletin by mail containing NBS measurements of many signal sources. To assist the user in getting the most from his system, NBS provides specific training using the actual equipment in one of its seminars on frequency measurements.

The NBS Global Time Service provides higher precision time and frequency data and a greater degree of automation. A Global Positioning System (GPS) receiver, located at the user's facility communicates automatically with an NBS computer that stores raw data, determines which data elements are suitable for time transfer calculations and provides an optimally filtered value for the time of the user's clock with respect to the NBS atomic time scales. The user is assigned an "account" on one of the NBS computers through which he may access the results of the NBS analysis. Tests, based

upon receivers in Colorado, Germany, France, Washington, DC, Wyoming, and California, demonstrate that the system can perform time comparisons with a precision of three nanoseconds and frequency comparisons with a precision of one part in 10^{-14} after four days of operation.

THE MEASUREMENT ASSURANCE APPROACH

The most common way to relate industrial calibration measurements to the national standards is to have the local reference standards calibrated in a way that provides traceability to the national standards. Depending upon the required level of accuracy, these calibrations may be performed by private or governmental laboratories at the local, regional or national level. NBS provides approximately 12,000 calibrations per year for this purpose. NBS Calibration services are described in Special Publication 250 (available from the Office of Physical Measurement Services, National Bureau of Standards, Washington, DC 20234). The cost of each calibration is published in an Appendix to this publication.

The ordinary calibration process has serious deficiencies. First, the standard or instrument to be calibrated must travel to the calibration laboratory, so it is out of service for a period of time. For example, the complete characterization of a cesium beam frequency standard requires that it be at NBS for a period of not less than five weeks. Even more serious is that the confidence in the calibration deteriorates with the passage of time. The fact that the instrument must be shipped to and from the calibration laboratory contributes substantially to this problem. Finally, only selected individual standards or instruments are calibrated and thus little information is available concerning whether or not the total measurement process is under control.

A general goal of the NBS program is to increase the reliability and effectiveness of the national measurement system. The two new time and frequency services are examples of what is frequently called "measurement assurance". In a measurement assurance program, most of the measurements are performed at the user's site rather than at the NBS and feedback and analysis of measured information is an important part of the process. In addition, the NBS establishes a long term interaction with the user and assists in training user personnel. The complete measurement process undergoes repeated scrutiny and is therefore likely to remain under control at all times. Of the six base units of measurement -the kilogram, the second, the Kelvin, the candella, the ampere, and the mole -the second is unique by the relative ease with which it may be compared by radio at remote locations without the transport of physical

artifacts[†]. Because of the unique property of the second, the new services provide the user the accuracy he requires through a simple program of coordinated measurements made at his site and at the NBS. No artifacts need be shipped to NBS, and the user exchanges calibration data with the NBS via telephone. Thus, the user obtains NBS traceable frequency measurements and time synchronization in real time. Traceability is provided at whatever level is required up to the ultimate stability of the NBS atomic time scales and the full accuracy of the NBS primary frequency standard. Since the link to NBS is established on a regular basis, the user's confidence in the performance of his in-house standards is greatly increased. Because of the high degree of automation, inherent in both of the new services, the improvements in precision and accuracy are obtained with negligible operational burden on the user.

NBS FREQUENCY MEASUREMENT SERVICE

This new Frequency Measurement Service, using straight forward measurement techniques [1], utilizes precision navigation and timing broadcasts from Loran-C and WWVB to provide frequency traceability to the NBS at approximately a one part in 10^{-11} level. Prior to the introduction of this service, there did not exist a total measurement system with the following features: LF receiver and antenna; time interval counter; dual floppy disc data storage system; printer/plotter; instrument controller; and telephone modem data line to the NBS.

Figure 1 shows the Loran-C version of the frequency measurement system. Using the NBS software, this system is capable of monitoring Loran-C transmissions, storing, listing and plotting the frequency calibration data. Figure 2 is a sample plot of phase vs time. The slope calculated by the system program is the frequency offset of the user's clock. The numerical value of the calibration is printed on each plot. The plots are made automatically once each day. Four separate frequency sources can be calibrated simultaneously.

The new NBS Frequency Measurement Service is more than an automated data acquisition system. It begins with consultation between NBS staff and the user to determine the best method of satisfying the user's requirements. If the Frequency Measurement Service is selected, consultation continues to determine the most appropriate radio transmission including an analysis of possible propagation and reception problems. The second step is training of the user's technical staff. A general foundation in time and frequency measurement techniques is provided by the two yearly NBS Seminars: "Frequency Measurements" and "Frequency Stability and Its Measurement". Direct experience with the equipment used in the

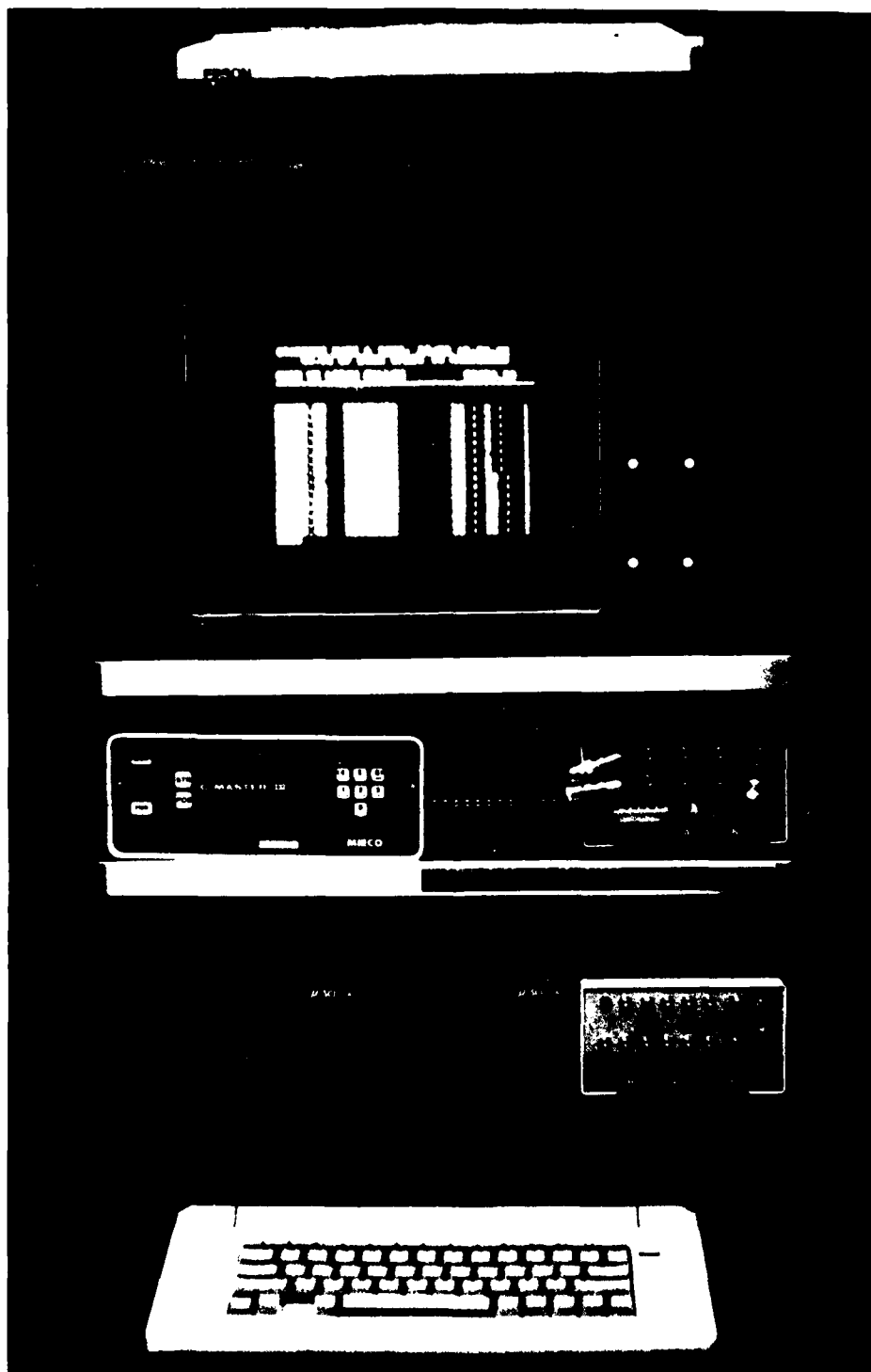
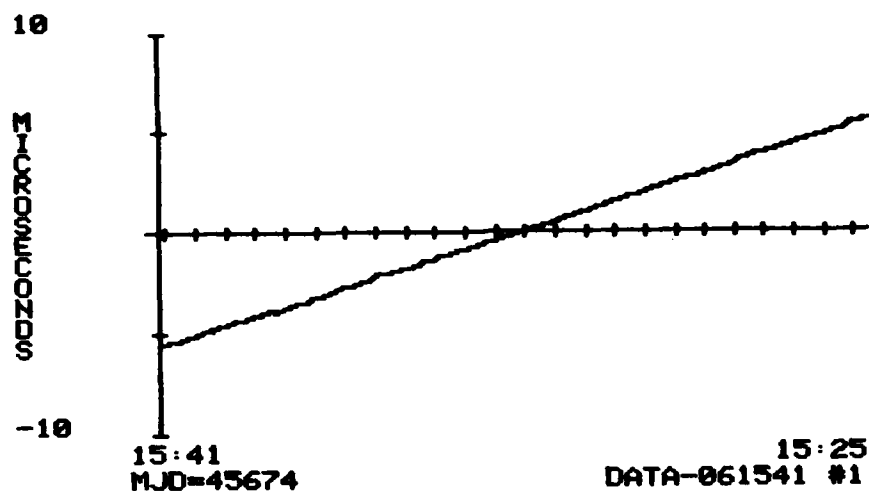


Figure 1. Photograph of frequency measurement system^{††}.

USER'S FREQUENCY REFERENCE VS LORAN-C



RELATIVE FREQUENCY $\approx 1.31E-10$ 500 / 185

Figure 2. Sample plot of calibration data from the frequency measurement system.

frequency dissemination service will be provided using equipment now operating at the NBS facility in Boulder, Colorado. Step three is the acquisition of the necessary measurement equipment. If desired, NBS can provide the complete integrated measurement system, insuring that all the parts are compatible and operate with the NBS software. Finally, the NBS will consult with the user during the installation of the antenna, the initial set-up of the equipment and verification of proper operation. Interaction between the NBS and the user will continue throughout the program and the user will receive NBS data via the monthly "Time and Frequency Bulletin." Also, through direct computer-to-computer data exchanges, the NBS will monitor the user's data without interfering with the operation of the user's measurement system. Thus the NBS will be able to help diagnose any anomalies. Finally, the NBS will provide additional training for newer staff members and will upgrade the calibration service with future releases of improved software and calibration equipment.

NBS GLOBAL TIME SERVICE

With this new service the user can synchronize his reference clock with respect to UTC(NBS) with state-of-the-art precision and accuracy. The service utilizes the clear access signal broadcast from the Global Positioning System (GPS) satellites. The time transfer measurements are made using a common-view technique, thereby eliminating the noise contribution from the clock errors of the GPS system and greatly reducing the effect of ephemeris errors [2]. When the NBS calculated corrections are applied to the user's clock, that clock becomes a high performance reference with the following characteristics. Between one and four days,

$\text{mod } \sigma_y(\tau) \approx 10^{-13} \tau^{-3/2}$ [3]. For longer times, up to approximately one-month, $\sigma_y(\tau) \approx 10^{-14}$. Figure 3 shows the results of an analysis of data taken between Boulder and Paris confirming this performance level. As a result of these very high precision time transfers, the user not only has access to a very stable frequency reference but also gains direct access to the U. S. primary frequency standard, NBS-6. Access to NBS-6 makes it possible to set an absolute limit of one part in 10^{13} on the frequency excursions of the user's clock. Another way to express the quality of this service is to say that, for time periods longer than approximately four days, the user can take advantage of the full capability of the NBS atomic time scale. The performance is almost the same as if the user were located in the next room and connected by a coaxial cable.

The NBS Global Time Service is more than just a GPS time transfer receiver. A receiver alone provides only short term measurements of the time of the user's clock relative to the time of a space vehicle clock or GPS time. The NBS service provides, in addition: determination of the user's position (necessary for time transfer measurements); scheduling of common view measurements between the user and the NBS; automatic collection by the NBS of the data from the user's receiver; computation by the NBS of the UTC(NBS)-user clock time differences; and optimum filtering of the data to provide a daily best estimate of the time of the user's clock with respect to UTC(NBS). The NBS provides each user with a monthly report giving the computed daily time differences, the computed daily frequency differences and the Allan variance of the user's clock. Figure 4 is a plot of time difference data taken from one of the Global Time Service reports. The user is assigned an "account" on one of the NBS computers through which he may directly access the results of the NBS analysis.

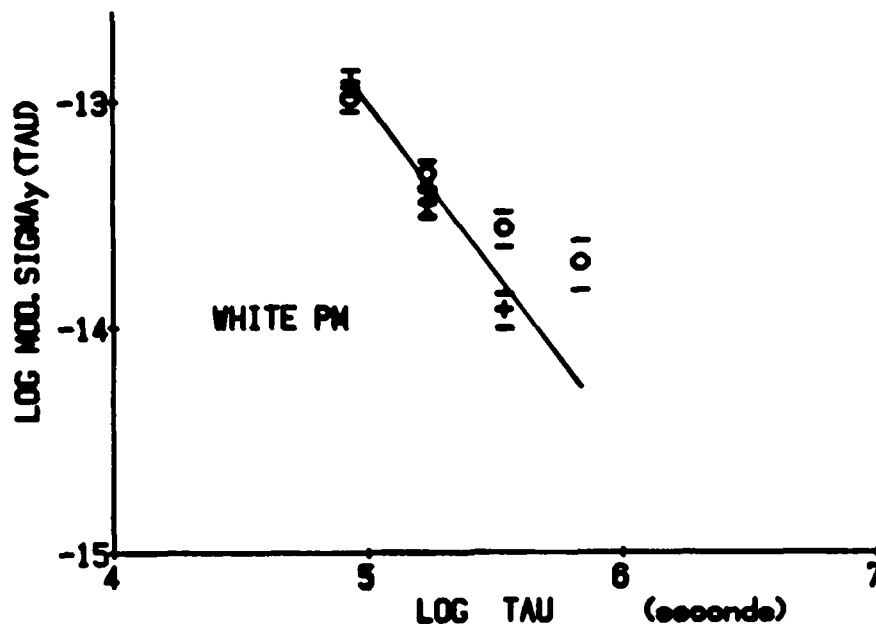


Figure 3. Modified Allan variance analysis of the NBS Global Time Service. The plus signs refer to measurement system noise and the circles refer to the noise of the reference clocks.

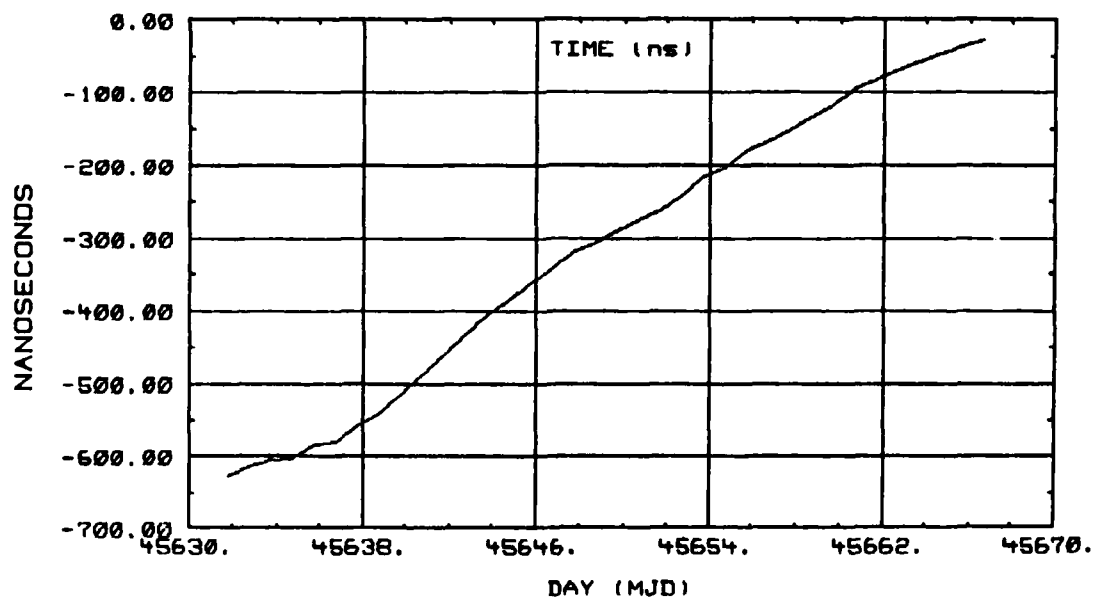


Figure 4. Sample plot of time transfer data provided monthly to users of the Global Time Service.

The service utilizes a GPS receiver developed at the NBS and now in commercial production [4]. Figure 5 is a photo of the NBS prototype. The receiver has 0.1 ns precision and nonvolatile memory for data storage. A simple, small omni-directional antenna makes it possible to lock on to any satellite whose elevation angle is greater than 5 degrees. The receiver, interfaced to a printer, allows local display of the raw GPS measurements and a telephone modem provides communications with NBS. The user is responsible for providing a dial-up telephone line so that the NBS may directly access the data from the receiver. This telephone link is an essential element of the data communications that gives the user access to UTC(NBS).

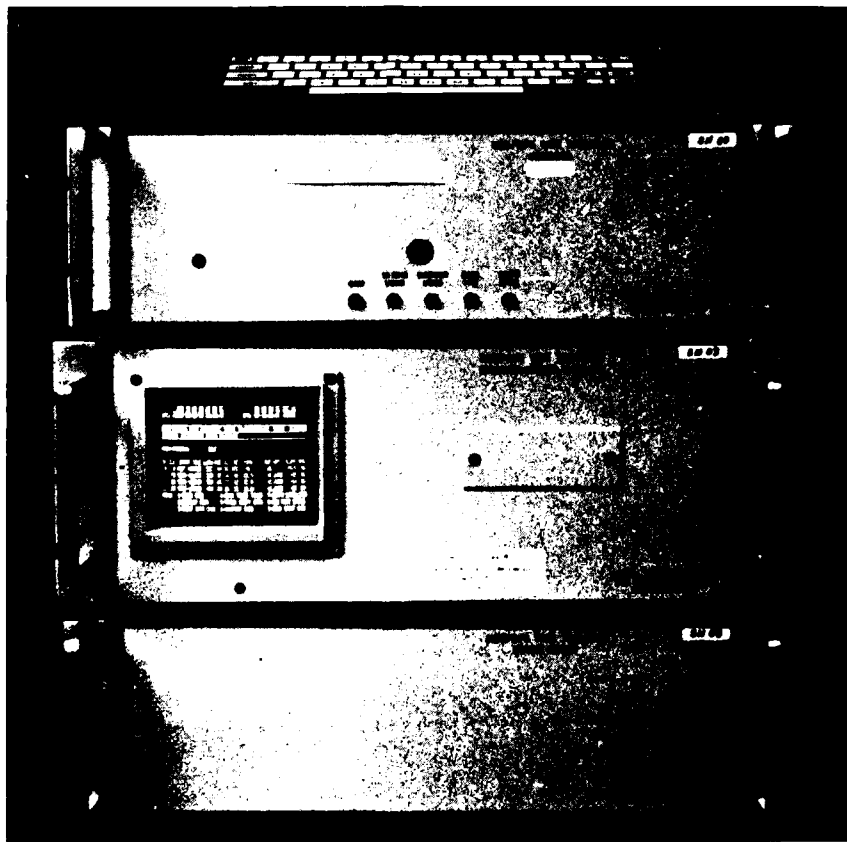


Figure 5. Photograph of prototype receiver for the NBS Global Time Service.

SUMMARY

The two new measurement services offered in 1983 extend the range and capability of the other frequency and time services offered by NBS: telephone time of day; high frequency broadcasts (WWV and WWVH); low frequency broadcast (WWVB), the GOES satellite time code; and laboratory calibrations. These services previously provided routine time synchronization capability in the one second to 25 microsecond range. The new services offer enhanced automation and a greater confidence in the results of the measurements. In addition, NBS provides consultation to assist the user in selecting the best solution to his problems, initial training and follow-up consultation whenever measurement problems are detected. The new time and frequency services provide traceability to NBS and a direct link to one of the world's best time scales. They greatly reduce the need for the user to become an expert on the intricacies of navigation systems such as Loran-C and GPS. The systems reliability will be high because all the components are "off-the-shelf" commercial equipment and because NBS maintains the systems to minimize hardware failures.

[†] The seventh base unit, the mole, is now defined in terms of the second.

^{††} Certain commercial equipment, instruments, or materials are identified in this paper in order to adequately specify the experimental procedure. Such identification does not imply recommendation or endorsement by the National Bureau of Standards, nor does it imply that the materials or equipment identified are necessarily the best available for that purpose.

[1] *Time and Frequency Users Manual*, George Kamas and Sandra L. Howe Eds., National Bureau of Standards Special Publication 559. Available from the Superintendent of Documents, U. S. Govt. Printing Office, Washington, DC 20402. Stock #003-003-02137-1. Price \$6.00.

[2] Dick D. Davis, Marc Weiss, Alvin Clements and David W. Allan, "Construction and Performance Characteristics of a Prototype NBS/GPS Receiver", Proc. 35th Annual Frequency Control Symposium, May 1981.

[3] David W. Allan and James A. Barnes, "A Modified Allan Variance with Increased Oscillator Characterization Ability", Proc. 35th Annual Frequency Control Symposium, May 1981.

[4] David W. Allan, "National and International Time and Frequency Comparisons," Proc. 37th Annual Frequency Control Symposium, June 1983.

QUESTIONS AND ANSWERS

MR. WARD:

Samuel Ward, Jet Propulsion Laboratory. It's not a question, it's a statement. On the data that you presented against the GPS for the GSC-12. We discovered there was an error that was not on the GSC-12 clock. It was on a cesium standard 1636 that was a part of our master clock ensemble and it was in a rather poorly controlled temperature environment. So that would explain some of the noise that you saw.

DR. STEIN:

It certainly would.

MR. CARLSON:

J. R. Carlson, SCS, Canada. I would be interested in the performance of a system like yours with a distributed ensemble of clock, perhaps tied to a central control, and then feeding data to your lab. It's just a proposal, but have you done any work with a distributed system or user system? I am thinking of considering a baseline interferometer type application.

DR. STEIN:

Of course there already is a major distributed ensemble in the international atomic time; and one of the things that I think that I would like to avoid is an overlap in that kind of operation; but we have considered the question of an ensemble time, say, for an individual user who has his own distributed set of clocks. For example, we have some separated clocks at our radio stations which we like to use at least for redundancy purposes.

The answer to your question is, the one-day performance of the G.P.S. System over thousands of kilometer baselines; using this common mode technique, with a high quality receiver could be as good as approximately eight nanoseconds RMS.

It's not quite as good as, say, a very high quality cesium standard, but it's better than a standard performance device in general, or at least comparable. So that for time periods somewhat longer than a day, one can begin to construct a very high quality time reference this way and, of course, that's what is done internationally.

I think G.P.S. is already beginning to replace Loran-C to some extent in international time scales.

MR. WARD:

Again, a comment to the last gentleman. I have with me a comparative analysis of GPS versus VLBI for intercoupling an ensemble of standards that includes cesiums and hydrogen masers. So if you come to see me I can give you a sample.

RECENT IMPROVEMENTS IN THE ATOMIC TIME SCALES OF THE NATIONAL BUREAU OF STANDARDS

D. W. Allan, D. J. Glaze, J. E. Gray, R. H. Jones, J. Levine, and S. R. Stein
Time and Frequency Division
Boulder, Colorado 80303

ABSTRACT

Coincident with the installation of a new measurement system, the National Bureau of Standards has also developed a new philosophy for the generation of both UTC(NBS) and atomic time, TA(NBS). Several benefits have resulted from this new direction. First, a more uniform UTC(NBS) scale was achieved in order to meet the increased requirements of our users. Second, improved synchronization of UTC(NBS) with UTC (Universal Time Coordinated) has been achieved. The frequency stability of UTC(NBS) is typically about 1×10^{-14} for averaging times of one day and longer and synchronism is now maintained to within about 1 microsecond of UTC indefinitely. Previously five microseconds was a realistic goal. Third, a new Kalman type algorithm with more robust performance is used to generate TA(NBS) totally independent of the generation of UTC(NBS). TA(NBS) is still steered in rate toward the frequency given by the NBS primary frequency standards. Fourth, a significantly improved working time and frequency reference is readily available. This reference supports the research and development of new frequency standards, and also supports our calibration services. This improved time and frequency reference is constructed by computing UTC(NBS) in final form every two hours. A real-time output signal is then steered in frequency to keep its time within a few nanoseconds of the officially computed value. And fifth, a very stable frequency reference is obtained by using all of the clocks available in the NBS clock ensemble. This time scale -- denoted AT1 -- is used for all of the NBS frequency stability calibrations, and is also used to generate UTC(NBS). This new approach has been tested for more than a year and the resulting improvements have now been documented.

INTRODUCTION

As of MJD 45195.5 (14 Aug. '82) NBS has been generating three time scales: UTC(NBS), TA(NBS), and AT1. Frequency steps introduced in the past to synchronize UTC(NBS) with UTC were objectionable to some of the NBS's more sophisticated users. These steps have been reduced by an order of magnitude and the frequency stability and the time accuracy of the new UTC(NBS) have been improved by about an order of magnitude. With the introduction of a new measurement system (1) with a measurement precision of about 1 picosecond, UTC(NBS) is computed every two hours, and a real-time clock is kept within a few nanoseconds of this computed time. The coordination of UTC(NBS) is accomplished with a one year time constant so that the monthly frequency steps introduced to maintain synchronization are of the order of one part in 10^{-14} comparable to the order of the noise and hence are imperceptible. Coordination with UTC has been enhanced by more than an order of magnitude by

placing into operation, in July of 1983, the measurement of UTC - UTC(NBS) via global positioning system satellites in common-view between Boulder, Colorado and Paris, France (2,3). The measurement precision of this technique is about 10 ns.

The "second" used in generating the independent and proper time scale, TA(NBS) continues to be steered toward the NBS "best estimate" of the SI second as determined by periodic calibrations with the NBS primary frequency standard (4). Hence, this time scale is syntonized with the definition of the second as realized at Boulder, Colorado--limited only by the inaccuracies of the NBS primary frequency standards and the algorithms involved, currently 8×10^{-14} . At the last calibration (July 1983) -- after applying the 1.8×10^{-13} gravitational potential correction of Boulder, Colorado with respect to the geoid -- the second used in UTC and TAI was found to be too long by 3×10^{-14} with respect to the NBS "best estimate". The algorithm employed in generating TA(NBS) is based on Kalman filter and prediction techniques (5). Though it uses measurements from the same set of clocks, its operating algorithm is independent of that used to generate UTC(NBS) and AT1. A new clock noise parameter estimation procedure has also been introduced (6,7), which has provided better clock noise model development and noise parameter estimation for each of the clocks in the NBS ensemble. This improvement in parameter estimation has enhanced the frequency stability of all three time scales.

The AT1 time scale is a proper time scale designed to run in real time with state-of-the-art frequency stability. UTC(NBS) differs from AT1 by a preset (steering) time and frequency offset. AT1 is a totally independent scale generated by a choice of optimum weighting factors for each of the clocks in the NBS ensemble so that, in principle, the scale's stability is better than that of the best clock in the ensemble. This scale provides a local frequency reference for NBS research and development efforts, and also for clocks being calibrated by NBS. These clocks may be either on site or at remote locations. When the clocks are at remote locations, they are compared with the NBS time scales via the GPS in common-

view technique or via Loran-C. The frequency stability of AT1 is estimated to be about 1×10^{-14} for sample times of one day to about one month.

The body of the paper will give the details of the formulation and the performance of the above three scales. Figure 1 is a block diagram illustrating how the time scales are generated.

The Time Scale UTC(NBS)

An International Radio Consultative Committee (CCIR) regulation states that all UTC(i) scales should be synchronized to within 1 millisecond of the international scale, UTC, maintained by the BIH (8). Well within that regulation and in accordance with the intent to minimize the disparity between scales, NBS has designed UTC(NBS) to be synchronous with UTC within practical limits. In the past that limit has been 5 μ s. With the new UTC(NBS), the goal is 1 μ s. UTC(NBS) is also kept nearly as stable as AT1, a scale designed specifically for optimum frequency stability. Because UTC(NBS) is synchronous with UTC in long term, the syntonization accuracy of UTC(NBS) is approximately the same as that of the international primary frequency standards utilized in the determination of the SI second for TAI (currently CS1 at the PTB, CS5 at the NRC, and NBS-6 at the NBS all with accuracies equal to or less than 1×10^{-13}). UTC is derived from TAI by subtracting

"leap seconds" as needed in order to keep UTC within 0.9 seconds of the earth time scale UT1.

Synchronizing to UTC presents two challenging logistic problems: 1) In the past the measurement noise using the Loran-C navigation chain as the time transfer mechanism required averaging times of the order of several months before the instabilities of state-of-the-art clocks began to appear. With GPS satellites used in common-view, that measurement noise becomes negligible for sample times of a few days and longer. However, this technique is currently only available to a small set of timing laboratories. 2) There have been indications that either the propagation noise and/or temperature coefficients in the clocks involved in the generation of TAI may be causing an annual variation to appear. The BIH is paying strict attention to the temperature environment of the clocks involved in order to reduce any potential effect from that source. While this problem is being worked out, NBS has adopted a steering servo technique with a one year time constant in order to average out any annual term which may be present. This servo technique has been applied since November 1982, and the improved performance is illustrated in Figure 2. The GPS satellite data used in common-view between Boulder, CO and Paris, France has only been available since July 1983. As more of this data becomes available the smoothness and synchronization accuracy of UTC(NBS) should continue to improve. ¹⁴Theoretical estimates indicate that frequency stabilities in the range of 1×10^{-14} may be maintained for sample times from one day to a month and longer for UTC(NBS). Synchronization accuracies should drop well below a microsecond as annual term problems in the clocks and in the propagation are solved.

The most stringent users of UTC(NBS) desire it to be as smooth and accurate as possible. Time steps to synchronize it to UTC would be objectionable. Excellent frequency stability and time accuracy can be obtained simultaneously by inserting imperceptible frequency steps (of the same size as the noise) on a monthly basis in order to steer it toward UTC. Prior to this new procedure for steering UTC(NBS), only annual frequency steps were inserted. They were sufficiently large so that they became objectionable to NBS's most stringent users such as the NASA Deep Space Network. Table 1 lists the steering corrections published in the NBS Time and Frequency Bulletin, yielding the results shown in Figure 2.

The Time Scale TA(NBS)

The NBS goal is to smoothly syntonize TA(NBS) with the frequency given by the NBS primary frequency standard -- currently NBS-6. TA(NBS) is a proper time scale in the sense of general relativity -- its time being determined only by the clocks and standards in the NBS laboratories. Since frequency steps are objectionable for this time scale, frequency syntonization is achieved for TA(NBS) by inserting frequency drift of the order of the noise (≤ 1 part in 10^{13} per year). The frequency drift inserted is computed using an algorithm (4) which uses the periodic calibrations of the primary frequency standards. The relationship between the frequencies of TA(NBS) and UTC(NBS) are listed in the right column of Table 1.

The algorithm used in generating TA(NBS) employs the same clock data used in generating the other two time scales. However, the algorithm has been developed using Kalman filter and prediction techniques (5). The noise model for the clocks in the ensemble used to generate the NBS time scales is composed of two coefficients:

a coefficient which gives the level of white noise frequency modulation (FM) and a coefficient which gives the random walk FM. A maximum likelihood parameter estimation procedure is used to estimate these coefficients for each of the clocks. Their values are listed in Table 2. A test for whiteness of the residuals has been conducted to assess the goodness of the model. The test was affirmative indicating the model is statistically adequate to describe the behavior of the clocks in the NBS ensemble.

Equation 1 gives the relationship of these coefficients to the "Allan Variance".

$$\sigma_y^2(n\tau_o) = \frac{\sigma_\epsilon^2}{n\tau_o^2} + \frac{\sigma_\eta^2 (2n^2 + 1)}{6n\tau_o^2}, \quad (1)$$

where the sample time $\tau = n\tau_o$, τ_o is the measurement and prediction interval and σ_ϵ and σ_η are measures of the magnitude of the rms prediction error in the clock over an interval τ_o for the white noise FM and the random walk noise FM respectively.

The Time Scale AT1

AT1 is a basic time and frequency metrology tool for the Time and Frequency Division of NBS. It is also used as a stable frequency reference for remotely measuring and calibrating clocks as well as for measuring and calibrating clocks sent to the NBS.

AT1 is automatically computed every two hours. The computation algorithm uses an "optimum" weighted set of the data from each of the clocks in the NBS ensemble. The time differences are measured with a precision of the order of a picosecond. A two-parameter representation of the noise characteristics is also used in this algorithm. There is a one-to-one correspondence between these two parameters and the two parameters referenced above. (See Table 2) The values of these parameters, their relationships, and how the algorithm works is described elsewhere (9).

To evaluate a clock such as AT1 which is designed to be better than the best clock available is a very difficult task. However, there are ways to estimate the frequency stability of AT1: First, by simulation, using the clock models estimated from the maximum likelihood approach; second, by measuring against an independent clock, either remote or local; third, by using the three corner-hat (10) technique with three nominally comparable and independent clocks or time scales. One further twist on the last option is to permute three separate algorithms around three independent clock ensembles, allowing one to independently estimate the performance of each of the algorithms and each of the ensembles. The data available were only sufficient to perform the first two options.

Figure 3 shows the frequency stability model for each of the clocks in the NBS ensemble. Once the model elements had been estimated using the maximum likelihood technique, each clock was simulated and then processed through the AT1 algorithm as if the data were real. The computed time could then be compared against perfect (true) time since the data were simulated. Two different sets were simulated and

processed and the resulting frequency stability is indicated by the squares in this figure. One estimates that for sample times ranging from about one day to about a month the stability of AT1 so computed should be of the order of or below about 1×10^{-14} .

Using the second option and the GPS common-view technique we have measured the frequency stability of AT1 versus UTC(USNO MC) an operational time scale provided by the U.S. Naval Observatory. The time difference so deduced is shown in Figure 4 for the period July through October 1983. The $\sigma_y(\tau)$ analysis of these data is shown in Figure 5 with and without an apparent frequency drift being removed. The frequency drift is tiny -- amounting to only -8×10^{-16} per day. For sample times of one, two, and four days, the stability values are probably significantly contaminated by measurement noise. A probable proper conclusion from this data set is that both time scales are better than about 2×10^{-14} for $4 \text{ days} \leq \tau \leq 1 \text{ month}$.

Because of the previously determined white phase measurement noise present when using the GPS in common-view technique (11), it is appropriate to use the modified $\sigma_y(\tau)$ analysis technique (12). Using this technique, Figure 6 shows AT1 versus both UTC(USNO MC) and UTC(OP), the time scale provided by the Paris Observatory. Because of a frequency step introduced in UTC(OP) during the above analysis period, a stable period prior to this step during July 1983 was analyzed. In figure 6, the measurement noise is limiting for sample times of one and two days but for sample times of from 4 to 32 days it appears that none of the above three scales has instabilities worse than about 1×10^{-14} for mod. $\sigma_y(\tau)$ and for the analysis period covered. Assuming flicker noise FM as the stability model and translating to $\sigma_y(\tau)$ increases the instability value by only a factor of about 1.2.

Recently some repair work was performed on the NBS prototype passive hydrogen maser (PHM4). Because of this repair work the maser was not included in the NBS computation of AT1. This provided an opportunity to use the maser as an independent local reference to measure the stability of AT1. Because of the maser's excellent white noise FM characteristics, its absence from the time scale computation increased the over-all white noise FM level of AT1 as compared to Figure 3. Even so, as shown in Figure 7, the long term stability of AT1 versus the passive maser is still very good -- of the order of 1×10^{-14} for sample times of one to four days. The stability of AT1 versus UTC(USNO MC) from Figure 5 is plotted for comparison -- it should be noted that this data is contaminated by measurement noise. A conservative conclusion from the data shown in Figure 7 is that the stability of AT1 is better than 2×10^{-14} for sample times in the range of one day to a month.

To test if the steering of UTC(NBS) was affecting the long term stability, UTC(NBS) was measured against UTC(USNO MC) via GPS in common-view and no significant change in the $\sigma_y(\tau)$ diagram resulted compared to that obtained in Figure 5. One can apparently also say that the time scales UTC(NBS) and/or UTC(USNO MC) have stabilities better than 2×10^{-14} for sample times from a few days to a month.

Conclusion

The new NBS time scale measurement system (1) coupled with the time scale algorithm research (13) has provided NBS with a solid foundation for developing the

time scales UTC(NBS), TA(NBS), and AT1 as explained above. All three scales have frequency stabilities of the order of 1×10^{-14} for sample times from one day to a month. UTC(NBS) is synchronized to UTC, and TA(NBS) is syntonized to the NBS "best estimate" of the frequency given by the NBS primary frequency standards (currently NBS-6). AT1 provides state-of-the-art frequency stability for sample times of the order of one day and longer with the ability to include and to calibrate clocks of diverse as well as of state-of-the-art quality. As new and better clocks are added, AT1, UTC(NBS), and TA(NBS) will continue to improve in their frequency stabilities.

With the advent of GPS used in the common-view measurement mode, the full frequency stability and accuracy of the above time scales is available at a remote user's location for sample times of about 4 days and longer (14). This measurement is about a factor of 20 times better than using Loran-C. With this measurement technique, not only will the time difference UTC(USNO MC) - UTC(NBS) be known in near real time to an accuracy of about 10 ns (3), but also it is anticipated that UTC(NBS) will be able to maintain synchronization with UTC, which is calculated two months after the fact, with an accuracy of about 100 ns.

Acknowledgments

The authors are deeply appreciative for the helpful comments given in review by Dr. Karl Kessler and by Dr. Lindon Lewis.

References

1. Stein, S. Glaze, D., Levine, J., Gray, J., Hilliard, D., Howe, D., and Erb, L. A., Automated High Accuracy Phase Measurement System, IEEE Transactions on Instrumentation and Measurement, Vol. IM-32, No. 1, 1983.
2. Allan, D. and Weiss, M., Accurate Time and Frequency Transfer During Common View of a GPS Satellite, Proc. 34th Annual Symp. on Frequency Control 334 1980.
3. Davis, D., Weiss, M., and Clements, A., Remote Syntonization Within a Few Nanoseconds by Simultaneous Viewing of the 1.575 GHz GPS Satellite Signals, Conference on Precision and Electromagnetic Measurements, 1982.
4. Allan, D., Hellwig, H., and Glaze, D., An Accuracy Algorithm for An Atomic Time Scale, Metrologia 11, 133 1975.
5. Jones, R. and Tryon, P., Estimating Time From Atomic Clocks, Journal of Research, Vol. 88 No. 1 1983.
6. Tryon, P. and Jones, R., Estimation of Parameters in Models for Cesium Beam Atomic Clocks, Journal of Research, Vol. 88 No. 1, 1983.
7. Barnes, J., Jones, R., Tryon, P. and Allan, D., Noise Models for Atomic Clocks, 14th Annual Precise Time and Time Interval Meeting 1982.
8. C.C.I.R. Recommendation 460-3. ITU, Geneva, Switzerland. Available from Places des Nations, CH-1311, Geneva 20, Switzerland.
9. Allan, D., Gray, J., and Machlan, H., The National Bureau of Standards Atomic Time Scale: Generation, Stability, Accuracy, and Accessibility, NBS Monograph 140, 207.
10. Gray, J. and Allan, D., A Method for Estimating the Frequency Stability of an Individual Oscillator, 28th Annual Symposium on Frequency Control 1974.
11. Davis, D., Weiss, M., Clements, A., and Allan, D., Construction and Performance Characteristics of a Prototype NBS/GPS Receiver, Proc. 35th Annual

- Frequency Control Symposium, 1981.
12. Allan, D. and Barnes, J., A Modified "Allan Variance" with Increased Oscillator Characterization Ability, Proc. 35th Annual Frequency Control Symposium, 1981.
 13. 2nd Symposium on Atomic Time Scale Algorithm, held in Boulder, Colorado, June 23-25, 1982.
 14. Stein, S., Kamas, G., and Allan, D. W., "New Time and Frequency Services at the National Bureau of Standards," Proceedings of the Fifteenth Annual Precise Time and Time Interval (PTTI) Applications and Planning Meeting, Dec. 6-8, 1983, Washington, DC.

Table 1 is a list of changes in time scale frequencies of both TA(NBS) and UTC(NBS) as well as a list of the time and frequency differences between TA(NBS) and UTC(NBS) at the dates of leap seconds, and/or frequency or frequency drift changes.

TABLE 1

DATE	(MJD)	FREQUENCY CHANGES		TA(NBS) - UTC(NBS)	$y_{UTC(NBS)} - y_{TA(NBS)}$
		TA(NBS)	UTC(NBS)		
1 Jan 80	44239			19.045 071 350 s	-0.36×10^{-13}
1 Apr 80	44330	$+1.0 \times 10^{-13}$ /year	+50 ns/day	19.045 071 432 s	$+5.43 \times 10^{-13}$
1 July 80	44421	(Drift continued)	-35 ns/day	19.045 067 262 s	$+0.88 \times 10^{-13}$
1 July 81	44786		+ 4 ns/day	20.045 065 283 s	$+0.59 \times 10^{-13}$
1 July 82	45151	$+1.0 \times 10^{-13}$ /year	- 3 ns/day	21.045 063 425 s	$+0.24 \times 10^{-13}$
1 Sept 82	45213	(Drift stopped)	-3.7 ns/day	21.045 063 341 s	-0.36×10^{-13}
1 Oct 82	45243			21.045 063 464 s	-0.45×10^{-13}
1 Nov 82	45274	$+1.0 \times 10^{-13}$ /year	+1.4 ns/day	21.045 063 583 s	-0.34×10^{-13}
1 Dec 82	45304	(Drift continued)	+0.77 ns/day	21.045 063 671 s	-0.25×10^{-13}
1 Jan 83	45335	(Drift continued)	+1.49 ns/day	21.045 063 715 s	-0.08×10^{-13}
1 Feb 83	45366	(Drift continued)	+2.51 ns/day	21.045 063 716 s	$+0.11 \times 10^{-13}$
1 Mar 83	45394	(Drift continued)	+1.28 ns/day	21.045 063 656 s	$+0.30 \times 10^{-13}$
1 Apr 83	45424	(Drift continued)	+0.93 ns/day	21.045 063 565 s	$+0.21 \times 10^{-13}$
1 May 83	45455	(Drift continued)	-0.17 ns/day	21.045 063 547 s	$+0.08 \times 10^{-13}$
1 Jun 83	45486	(Drift continued)	-0.44 ns/day	21.045 063 522 s	-0.11×10^{-13}
1 July 83	45516	(Drift continued)	-0.94 ns/day	22.045 063 605 s	-0.37×10^{-13}
1 Aug 83	45547	(Drift continued)	-1.04 ns/day	22.045 063 721 s	-0.47×10^{-13}
1 Sept 83	45578	(Drift continued)	-1.20 ns/day	22.045 063 856 s	-0.62×10^{-13}
1 Oct 83	45608	(Drift continued)	0.00 ns/day	22.045 064 070 s	-0.72×10^{-13}

TABLE 2 Estimated values of σ_e and σ_n and 95% confidence intervals.

Clock	Length of data (days)	σ_e (ns)			σ_n (ns)		
		Lower Limit	Est.	Upper Limit	Lower Limit	Est.	Upper Limit
1316	364	3.81	4.14	4.53	0.53	0.80	1.23
167	361	12.58	13.52	14.67	0.57	1.11	2.07
137	358	10.41	11.31	12.27	1.76	2.49	3.56
61	67	5.48	6.77	8.43	1.53	2.80	4.83
352	354	8.12	8.85	9.74	2.42	3.32	4.41
323	255	2.06	2.37	2.74	0.63	0.94	1.34
1375	357	9.93	10.71	11.64	0.96	1.48	2.25
NBS4	66	0	0.88	1.86	0.72	1.34	2.16
113	354	8.73	9.48	10.38	2.49	3.18	4.11
8	360	7.98	8.65	9.49	2.11	2.76	3.66
601	298	1.89	2.13	2.41	0	0.06	0.52
PHM4	203	0	0.65	1.19	0.55	0.77	1.09

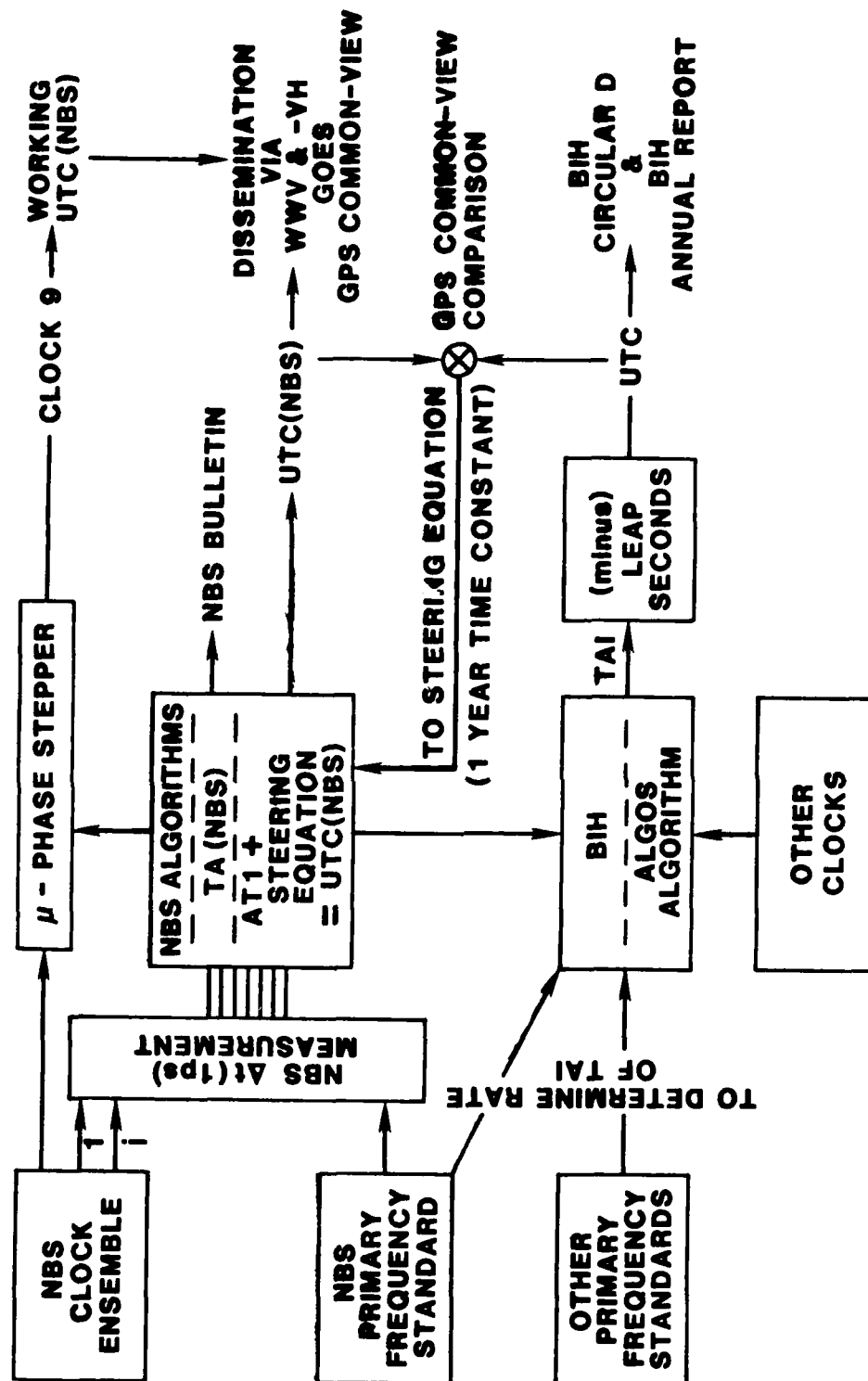


Figure 1. Conceptual block diagram illustrating how the International Time scales and the NBS Time scales are generated.

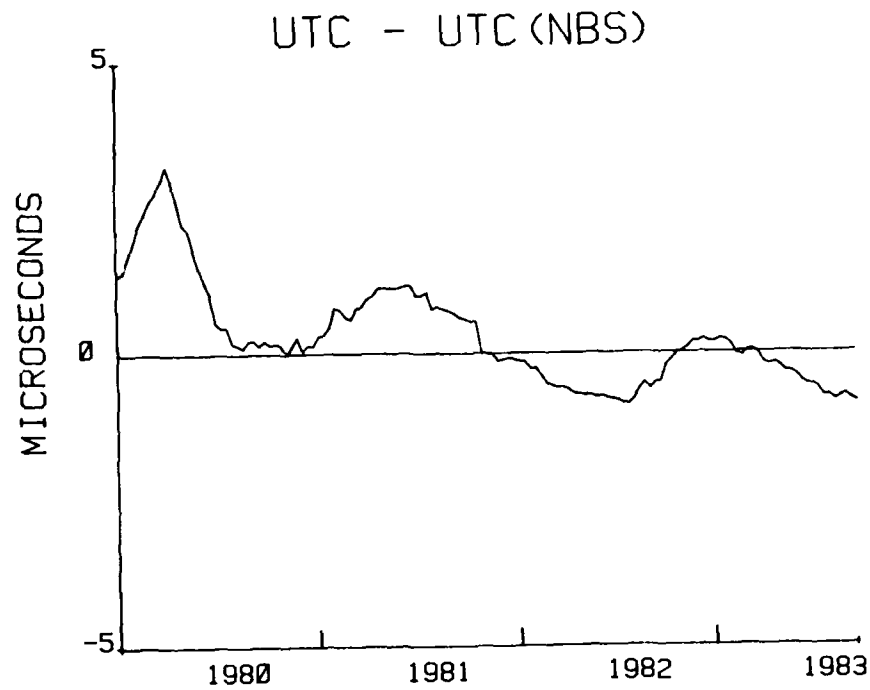


Figure 2. Universal Time Coordinated (UTC) minus UTC(NBS) via Loran-C.

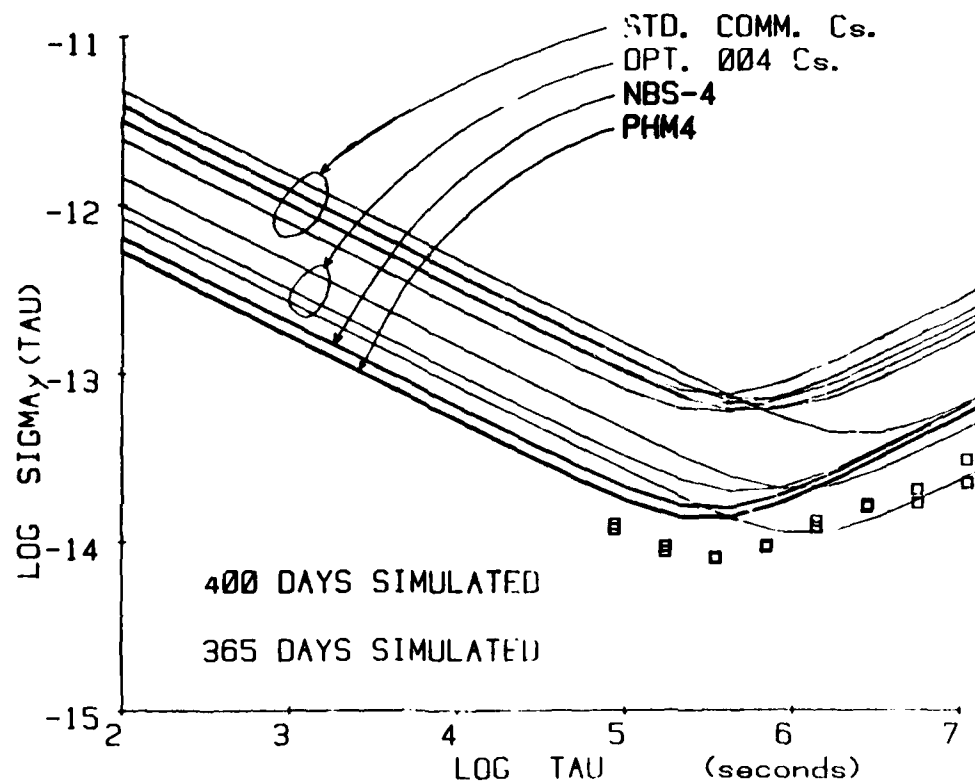


Figure 3. Frequency stability models of clocks in NBS ensemble. The squares are estimates of the stability of NBS.AT1 and UTC(NBS) via the NBS algorithm.

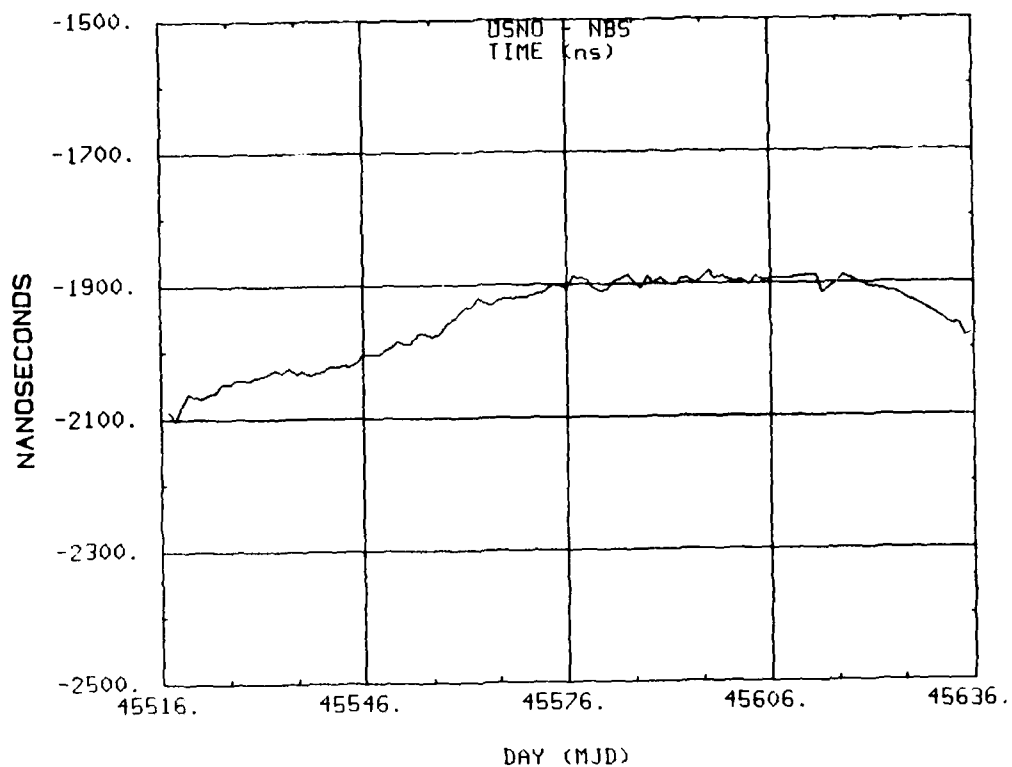


Figure 4. USNO master clock, UTC(USNO MC), minus UTC(NBS) via GPS in common-view (July through October 1983).

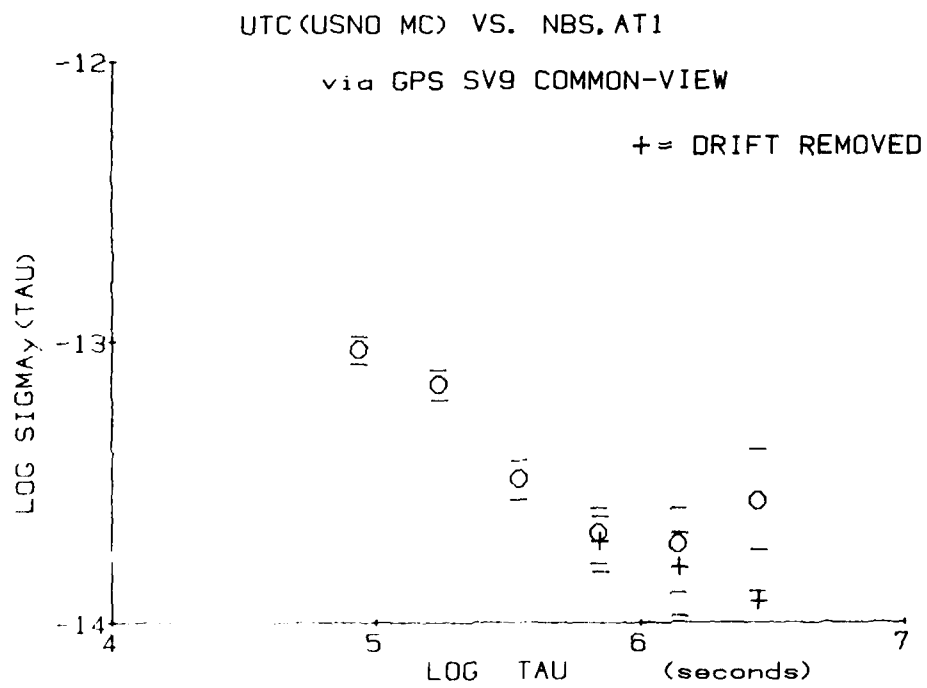


Figure 5. Frequency stability of UTC(USNO-MC) vs AT1 with and without an apparent frequency drift removed.

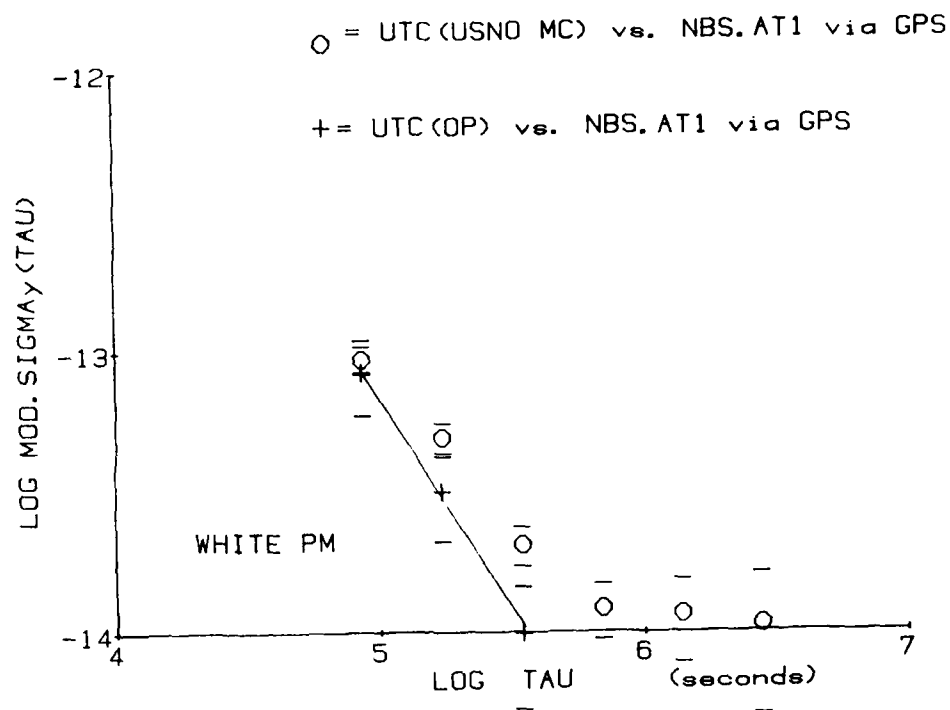


Figure 6. Frequency stability of NBS.AT1 vs. UTC(USNO-MC) and UTC(OP) via GPS in common-view using the modified $\sigma_y(\tau)$ analysis technique.

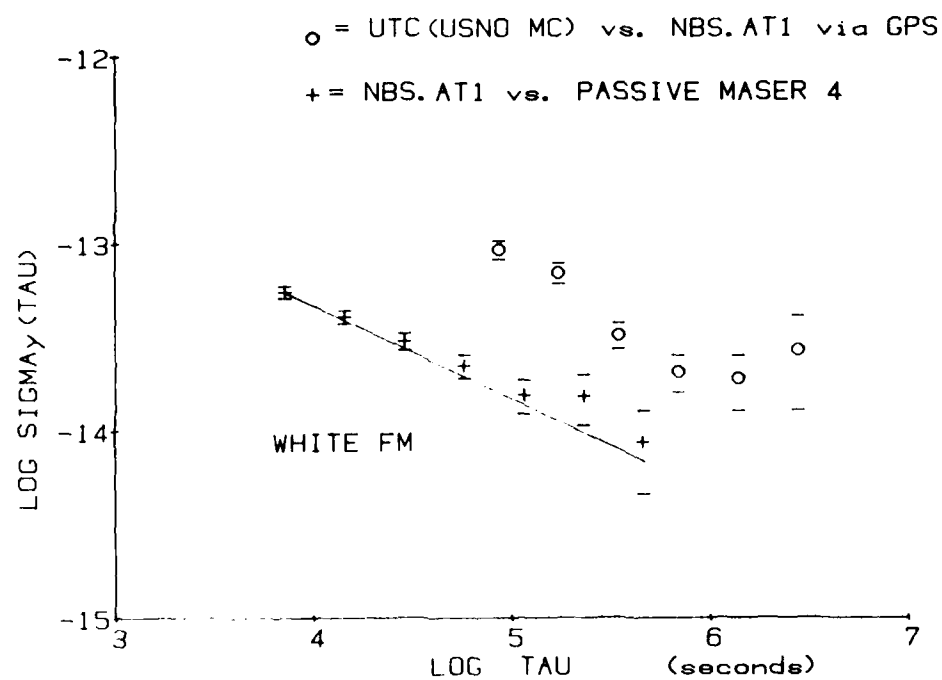


Figure 7. The frequency stability of NBS.AT1 vs. a passive hydrogen maser and vs. UTC(USNO-MC) via the GPS in common-view technique.

QUESTIONS AND ANSWERS

MR. WARD:

Sam Ward, Jet Propulsion Laboratory. When did you start using this smoother rate?

MR. ALLAN:

Basically, October of last year, all of this year. Roughly, about a year ago.

MR. WARD:

Well, as a matter of added information, we had been having a problem with hydrogen masers, and one of them in particular had been left open for an excessive period and it cooled down, and when it came back up it had a very high drift rate. Now, normally, this drift rate is around a few parts in 10^{15} per day; so we have been trying to use the G.P.S. to measure that drift rate. So you can see why we didn't like it being diddled.

MR. ALLAN:

That's right.

MR. WARD:

But we, indeed, found the rate, after about three months, had settled down to a rate that was approaching a part in 10^{14} ; and before it was taken off the line last month, it had settled down to 3.5×10^{-15} per day.

MR. ALLAN:

In fact, J.P.L. was one of the driving forces why N.B.S. improved their performance.

AUTOMATION OF PRECISE TIME REFERENCE STATIONS (PTRS)

Paul J. Wheeler
U. S. Naval Observatory
Washington, D. C.

ABSTRACT

The U. S. Naval Observatory is presently engaged in a program of automating precise time stations (PTS) and precise time reference stations (PTRS) by using a versatile mini-computer controlled data acquisition system (DAS). The data acquisition system is configured to monitor locally available PTTI signals such as LORAN-C, OMEGA, and/or the Global Positioning System. In addition, the DAS performs local standard intercomparison. Computer telephone communications provide automatic data transfer to the Naval Observatory. Subsequently, after analysis of the data, results and information can be sent back to the precise time reference station to provide automatic control of remote station timing. The DAS configuration is designed around state of the art standard industrial high reliability modules. The system integration and software are standardized but allow considerable flexibility to satisfy special local requirements such as stability measurements, performance evaluation and printing of messages and certificates. The DAS operates completely independently and may be queried or controlled at any time with a computer or terminal device (control is protected for use by authorized personnel only). Such DAS equipped PTS are operational in Hawaii, California, Texas and Florida.

INTRODUCTION

One of the functions of the U. S. Naval Observatory is to provide a data base of precise time measurements which reference navigation systems timing to UTC (USNO). This is accomplished with measurements made at the Naval Observatory and at precise time stations (PTS) around the world. The quality of the measurements made at a PTS is often affected by personnel changes at the stations. In addition, the quantity of data is limited by the number of available man-hours. To improve both quality and quantity of this data the Naval Observatory has developed an automated data acquisition system (DAS) that is being installed in different configurations at the PTS's. There are operational systems presently installed in Hawaii, Texas, Florida and three in California. In the near future systems will be installed in Ohio, West Virginia and a second system in Hawaii.

The following will describe the different configurations and capabilities of these systems.

System Description (Figure 1)

The DAS is a mini-computer controlled system capable of monitoring locally available precise time signals such as LORAN-C, OMEGA and/or the Global Positioning System. In addition, the DAS can perform local standard intercomparisons. Computer telephone communications provide automatic data transfer to the Naval Observatory. After the data has been analyzed,

results and information can be sent back to the PTS to provide automatic control of remote station timing. Data analysis can also be performed by PTS personnel by utilizing the plotting and data printout capabilities of the DAS. The DAS also provides automated portable clock measurements, and printing of messages and certificates.

System Design (Figure 2)

The heart of the DAS is a Hewlett Packard (H/P) 9915 computer. The computer controls two interfaces, one an RS232 interface that is primarily used for data communications and an IEEE-488 (HPIB) interface for equipment control. In a basic system the HPIB connects to the computer one or two H/P 59307 VHF switches, an H/P 5328 or 5335 universal counter, and an Austron 2100 LORAN-C timing receiver. Once per hour under computer control the VHF switches connect up to 14 different timing signals (1PPS) into the universal counter. The universal counter is configured to make time interval measurements and transfer them to the computer for storage and subsequent transfer to the Naval Observatory. Each hour, under computer control, the LORAN receiver is locked onto a selected station, a time of arrival measurement is made, the data is transferred to the computer, and the LORAN receiver is initialized to acquire a different station. This computer control of the LORAN receiver allows different stations and/or chains to be monitored with a single receiver. A time tag for the data is obtained from the LORAN receiver or from an internal clock in the computer if the LORAN receiver malfunctions. The data is also labeled with the Modified Julian Date that is maintained by the computer, and the LORAN data is labeled with the chain repetition rate and station ID. A DAS in this configuration can store two days of data in computer memory and up to 30 days on the built in tape drive. To reduce the problems caused by magnetic tape and tape transport wear, the system programs are stored on EPROMs (erasable programmable read only memory) in the computer. These programs are loaded and run on power-up without human intervention, eliminating the need for computer back-up power.

The RS232 interface connects the computer to a standard dial up telephone line via a 1200 baud modem. This allows data transfer, system control, and/or *system diagnostics to be performed* with a remote computer or communications terminal. To communicate with a remote DAS, dial the telephone number, respond to the request for your ID, then respond to the request for your operation codes. The ID "USNO" is provided for PTTI users; this code allows access to the DAS data without the capability of interfering with the DAS operation. The operation code in most cases is a one or two digit number that tells the DAS what data you would like transferred (refer to Table 1 for example). Upon request the DAS stored data is transferred to the USNO or PTTI user in the form of Modified Julian Date, Universal Time, clock time interval measurements, LORAN-C chain, and LORAN-C time interval measurements. Remote system control provides, for example, the ability to update the DAS date, time of day, and the number of leap seconds, as well as to monitor clock time interval measurements and LORAN-C data in real time. Time of day, station GRI (Group Repetition Interval), receiver gain, signal to noise ratio, receiver status, and cycle number from the LORAN receiver can also be monitored. Remote system diagnostics can be performed on the VHF switches, LORAN-C receiver, and time interval counter. In addition to the precoded diagnostics any allowable interface bus commands can be sent to each piece of equipment allowing complete equipment control from a remote terminal. Other diagnostics include a table of amplitude and frequency measurements of each clock signal connected to the VHF switches. Comparing these measurements to the measurements in the table made during system initialization helps to determine the integrity of the signals and cables in the system. The number of power failures at the PTS are counted and stored to help analyze equipment failures. The programs are designed so that when a software or firmware error occurs, the program will recover and continue; however, the error code and the program line number where the error occurred are stored and may be read during data communications. This aids in software debugging while the DAS is operating at the PTS.

Soon after installation of DAS's in the field new requirements evolved and subsequently the DAS's capabilities were expanded (refer to Figure 3).

One of the new requirements was to provide a printout of the USNO's GPS timing data in the computer facility at the GPS master control site located at Vandenberg AFB, California. The printer was to be located 1000 feet from the DAS and the data printed out had to be free of any transmission errors. To connect the printer to the DAS, short-haul modems and a Black Box "Fall Back Switch" (FBS) were used. The modems extend the RS-232 communications from the DAS to the printer. The FBS allows both the data communications modem and the printer via short-haul modems to be connected to a single RS-232 computer interface. To insure error free data, two error check numbers are calculated by the USNO computer and transmitted with the data. When the data is received at the DAS, the error check numbers are calculated by the DAS computer and compared to those sent with the data. An affirmative acknowledgement is returned by the DAS if the calculations agree; otherwise, retransmission of the data is requested. Data and messages can also be sent from a data terminal. However, calculation of the error check codes by hand is not practical. To solve this problem, a special error check code is sent with the message. This code tells the DAS to transmit the entire message back to the sender. The sender can then check the message for errors and transmit an affirmative acknowledgment or retransmit the message.

Another requirement was to monitor the OMEGA navigation system. The Black Box FBS was used to connect a Magnavox 1104 OMEGA monitor to the DAS, and an H/P Winchester disc was added to accommodate the storage of the large amount of data provided by the OMEGA receiver. The OMEGA data is stored in a 100 day circular file on the disc. With the use of the DAS data communications this data is available to the U.S. Coast Guard for analysis. The communications modem used in this DAS was a dual speed modem, 300 and 1200 baud. This modem and the computer identify the speed of the call-in modem and set their own communications speed accordingly. This feature allows a larger variety of data terminals and even the most inexpensive computers to communicate with the DAS.

In January 1983, the Vandenberg AFB contracted with the USNO to design and build an automated timing system for their Precise Measurement Electronics Laboratory (PMEL). This PMEL is a Precise Time Reference Station (PTRS). This was the beginning of a second generation DAS with several new capabilities (refer to Figure 4). This new system consisted of the computer, two VHF switches, the LORAN receiver, time interval counter, Winchester disc, a second H/P 9915 computer with keyboard and monitor, a Timing Systems Technology (TST) precision digital multi-timescale clock, TST microphase stepper, Stanford Telecommunications Inc. (STI) 502 GPS receiver, an H/P graphics plotter, and an H/P printer.

The keyboard, monitor and second computer are used as a local terminal. This terminal provides for local control of the system, data analysis, plots and printouts of the collected data, and the printing of reports and messages. The programs for the local terminal are soft-key controlled. Programs are loaded and run by pressing a single key and require no programming knowledge. The terminal computer is connected to the DAS computer and the other equipment in the system by the HPIB. Both computers, in turn, can act as the system controller. This allows both computers to access the same disc in order to store and retrieve data or to control the other equipment in the DAS in order to collect the data. The plotter and printer are connected to the terminal computer with the H/P interface loop (HPIL). The use of the HPIL allows the printer and plotter to be located with the keyboard and monitor in an office, while the computers and other equipment are kept in a laboratory environment. Plotting, printing and programming can also be performed with the terminal computer without tying up the HPIB interface which is required by the DAS for data collection.

The DAS computer, as in other DAS's, is for control of the system, timing equipment and communications. The DAS computer maintains priority control over the HPIB and, therefore, priority control over the equipment in the system. In order for the terminal computer to access the disc or control the equipment the terminal computer must obtain HPIB control from the DAS computer. The DAS computer may pass control, deny or take control away from the terminal computer.

The microphase stepper and digital clock were added to provide a computer slewable 1pps and are connected to the system via the HPIB. With the microphase stepper, the 1pps from the digital clock can be stepped in time in one picosecond steps or the 1pps can be slewed in parts as small as ten to the minus seventeenth. This control of station timing can be done with the local terminal, remote terminal or remote computer. The microphase stepper and digital clock are completely programmable by remote computer or terminal. This provides for automated insertion of leap seconds into the station timing and allows for remote diagnostics in the event of equipment failure.

The GPS receiver provides primary data for control of the station timing. A tracking schedule is loaded into the DAS computer from the USNO. This schedule is initialized so that the GPS receiver at the remote station and the GPS receiver at the USNO collect data from the same GPS satellite at the same time. The data is reduced and stored on disc with the start time, stop time, space vehicle number, slope and rms of the data, and the number of samples. Each day the USNO computer calls and collects the GPS, clock and LORAN data from the DAS. The DAS GPS data is compared with the USNO GPS data. The difference between the remote station timing and UTC USNO is then calculated and when needed control information is sent back to the DAS to automatically correct station timing. To prevent transmission errors in the timing control message, the entire message is retransmitted to the sender. The sender must then acknowledge whether the message was received correctly or if retransmission is required. After an affirmative acknowledgment is received by the DAS, the DAS sends the control message to the microphase stepper. If no errors are indicated by the microphase stepper the DAS computer queries the microphase stepper for the last control message received. The control messages are compared by the computer and the results are sent back to the sender informing him that the control was accepted or that retransmission is required. If an error occurs in the microphase stepper, an error code, the date and time are stored on disc. This information can then be retrieved by USNO for analysis.

The graphics plotter and associated software provide plots of any of the collected time interval data. This includes the data from the GPS receiver, the LORAN receiver, and all equipment connected to the VHF switches. The data is collected once each hour and stored on disc in a ten day circular file and may be used to produce plots one to ten days long. This data can also be printed on the printer for numerical analysis or to edit bad data points. Plots with reduced resolution can be produced on the monitor for quick analysis.

A connection through the VHF switches is provided for automated portable clock measurements. The computer asks the operator pertinent information for printing a portable clock measurement certificate; i.e., clock serial and model number, owner's name and address, and the personnel making the measurement. The computer then instructs the operator through a procedure that calibrates the cables being used to connect the clock to the measurement system, measures the time interval between the system time and portable clock, and prints out a certificate of the measurements made. The data that is printed on the certificate is also stored on the disc for transfer to the USNO.

One of the functions of the Vandenberg PMEL is to calibrate other PTS's. A computer program was added to this DAS which significantly reduces the amount of labor previously required to calculate and report these measurements. After portable clock measurements are made at the

PMEL and the remote PTS, the data is entered into the computer. The computer then locates data on the disc from previous clock measurements made at the PTS, calculates the long term drift rate of the PTS timing, calculates the present time offset between the PTS and UTC (USNO), prints out an extensive form with all pertinent data, and stores the data on the disc for future reference.

SUMMARY

The DAS's described are systems that are already operational at several PTS's. Some of the DAS's have been operating for two years providing data for the USNO. The equipment used in these systems was selected for its reliability, accuracy, and availability. The DAS can be easily configured in many different ways to tailor the system to the needs of the particular PTS. The software for the computers is written as modules and can be connected together to conform with the equipment in the system. Other equipment and software can be easily added to the DAS as requirements evolve.

The USNO will continue to install these DAS's at selected PTS's and PTRS's in order to improve the monitoring and dissemination of precise time. The USNO is also willing to design, build and control DAS's for other precise time users.

USNO AUTOMATED REMOTE DATA ACQUISITION SYSTEM (DAS)

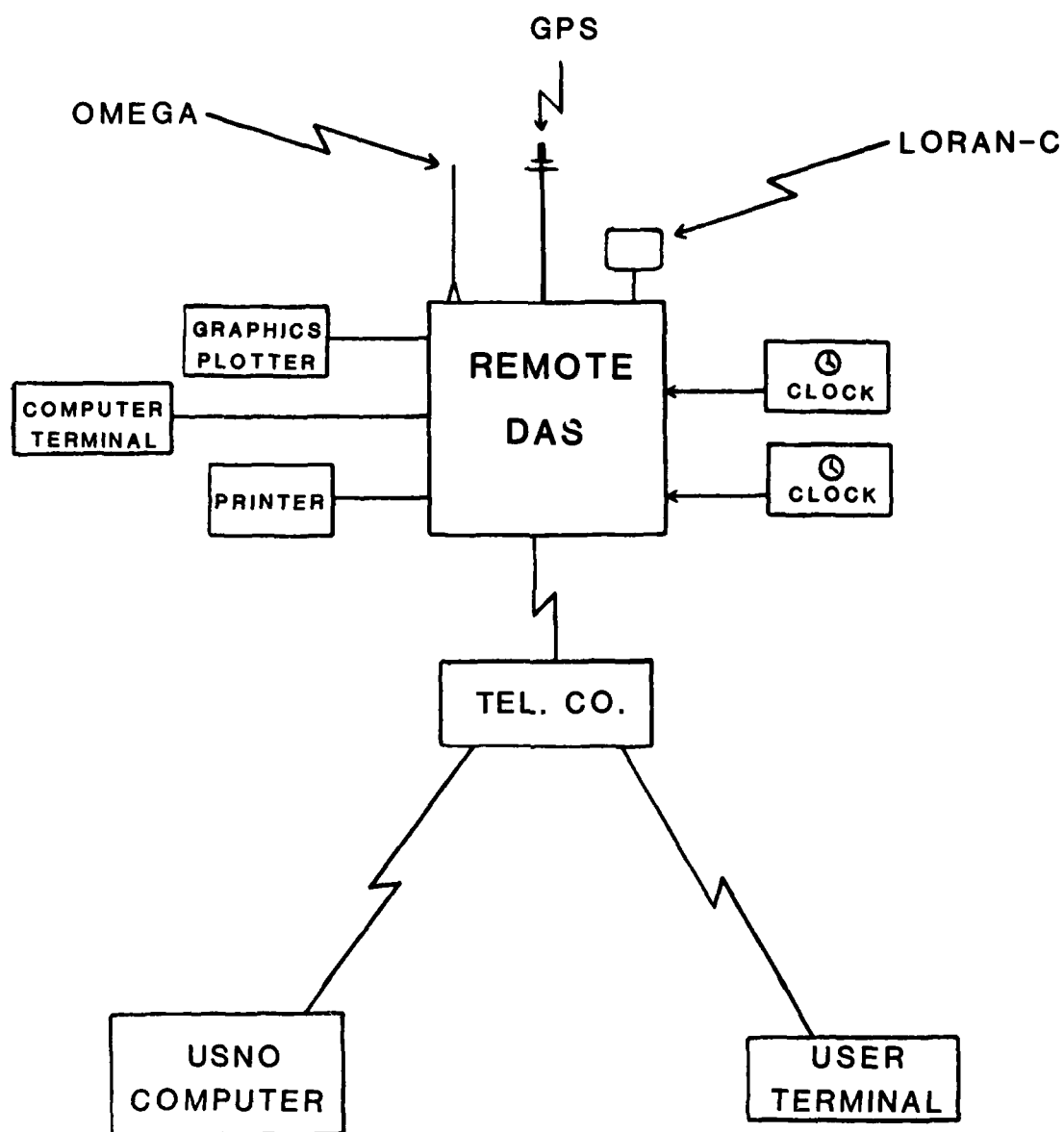


FIGURE 1

PTS DAS

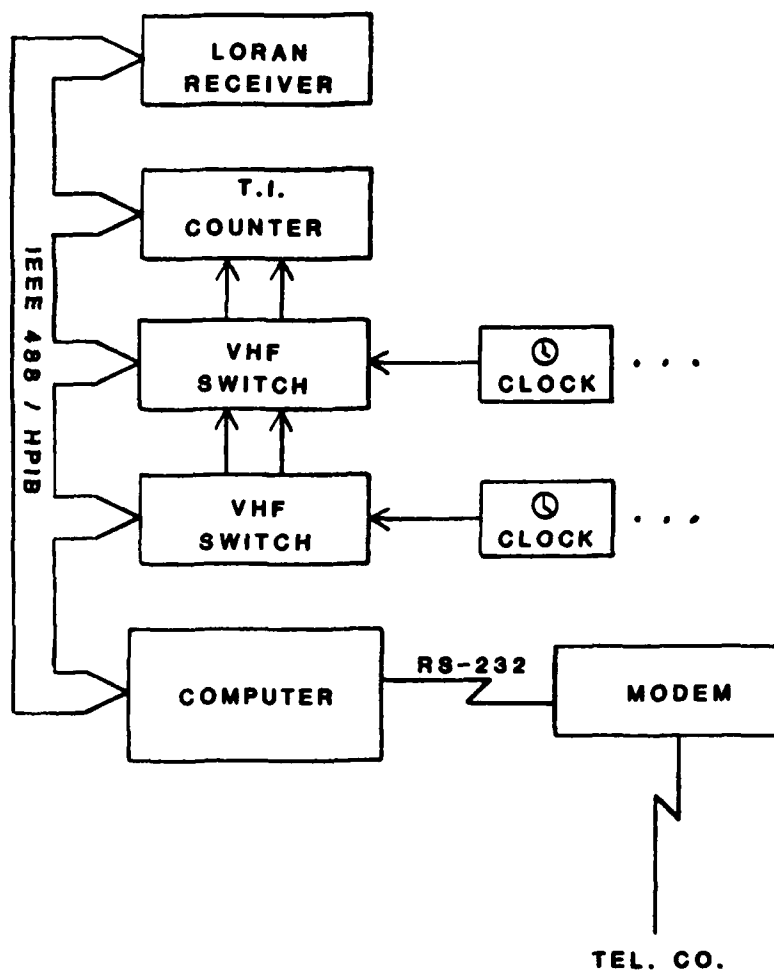


FIGURE 2

DAS OPTIONS

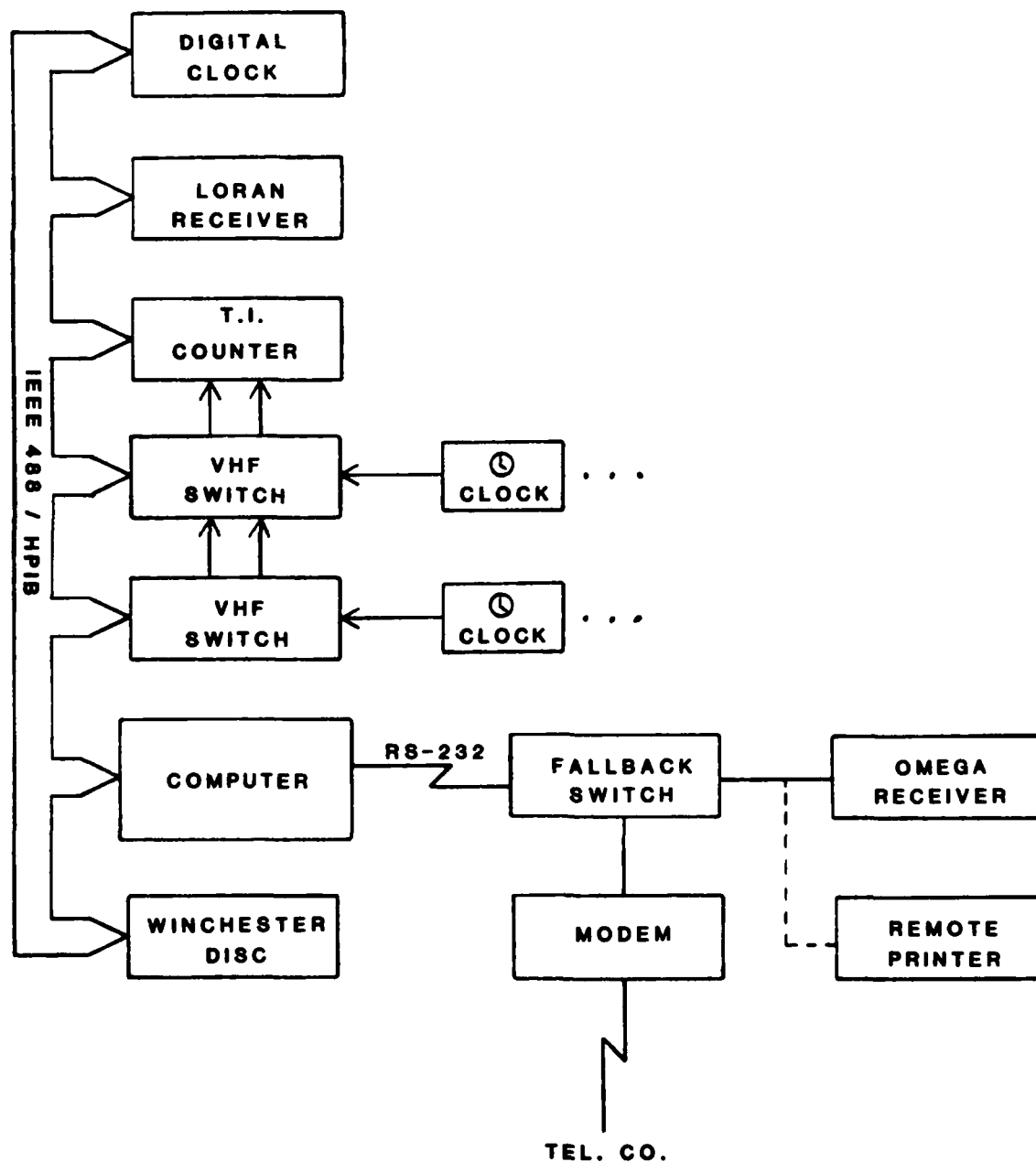


FIGURE 3 48

PTRS DAS

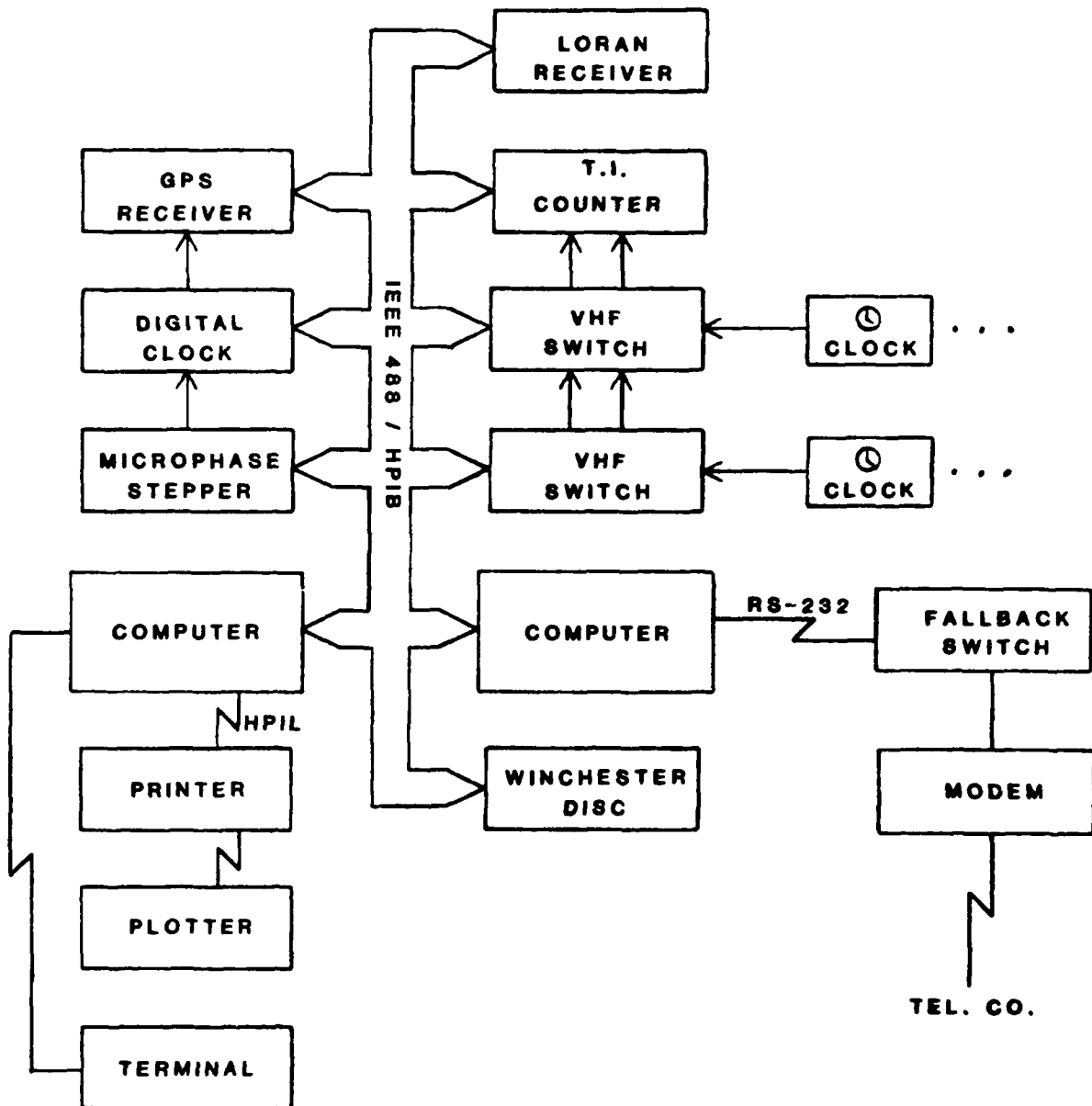


FIGURE 4 49

COMMUNICATION CODES

	1	=	TERMINATE COMMUNICATIONS
	2XXZ	=	DATA TRANSFER (XX = # OF CHANNELS, Z = # OF DAYS, DEFAULT = 2162)
	3X...	=	TIME INTERVAL COUNTER CONTROL (X... = ANY VALID HPIB COMMAND)
	31	=	PERFORM A TIME INTERVAL MEASUREMENT
	32	=	T.I. COUNTER SELF CHECK
	4X...	=	VHF SWITCH CONTROL
P	5X...	=	LORAN RECEIVER CONTROL
P	6XX	=	LEAP SECONDS CONTROL (XX = LEAP SECOND COUNT) IF XX IS INCREMENTED BY 1 THEN THE TST DIGITAL CLOCK IS CORRECTED AT 2400 UT.
	7	=	NUMBER OF STATION POWER FAILURES
A	71	=	PRINT OUT VHF SWITCH SIGNAL TABLE
B	71	=	PRINT OUT THE LAST 10 PORTABLE CLOCK MEASUREMENTS
	72	=	PERFORM ALL T.I. MEASUREMENTS WITHOUT STORING DATA
P A	73	=	RESET POWER FAILURE COUNT
B	73	=	PRINT OUT THE LAST 10 DAYS OF GPS DATA
P	74	=	PRINT OUT PROGRAM AND MICROSTEPPER ERROR LIST AND OPTION TO ERASE DATA FILES ON TAPE
A	75	=	PERFORM VHF SWITCH SIGNAL ANALYSIS
B	75	=	GPS RECEIVER INTERNAL TRACKING SCHEDULE
P A	76	=	CORRECT VHF SWITCH SIGNAL TABLE
P B	76	=	RESET POWER FAILURE COUNT
P	77	=	RESET AND INITIALIZE LORAN RECEIVER
P	78	=	READ COMPUTER INTERNAL CLOCK (TIME OF DAY)
P	79	=	SET COMPUTER INTERNAL CLOCK
	8	=	PRINT OUT LORAN RECEIVER STATUS TABLE
P A	81	=	REMOTE PRINTER INPUT (1,1 = DEFAULT CHECK SUM AFTER cntl D)
B	81	=	PRINT OUT VHF SWITCH CLOCK LABELS
P	82	=	HPIB OR HPIL PRINTER INPUT (1,1 = DEFAULT CHECK SUM AFTER cntl D)
P	83	=	MICROSTEPPER CONTROL INPUT
P A	84	=	READ DATA ON MAGNETIC TAPE
B	84X...	=	CONTROL TST CLOCK (DEFAULT = T read clock), (1C = UTC)
	85	=	PRINT OUT THE LAST 24 HOURS OF OMEGA DATA
P	86	=	GPS RECEIVER DATA REDUCTION SCHEDULE
	OMEGA	=	PRINT OUT 1 TO 100 DAYS OF OMEGA DATA

NOTE: (P) INDICATES THAT THE CODE ACCESS IS PROTECTED AND DEPENDENT ON ID ENTRY
 (A) INDICATES CODES THAT ARE USED FOR PRECISE TIME STATIONS
 (B) INDICATES CODES THAT ARE USED FOR PRECISE TIME REFERENCE STATIONS

TABLE 1

QUESTIONS AND ANSWERS

MR. WARD:

Samuel Ward, Jet Propulsion Laboratory. Why weren't multiple-time interval counters used?

MR. WHEELER:

We haven't had a problem with a single-time interval counter. We didn't deem it necessary to have more than one time interval counter.

MR. WARD:

But with a single-time interval counter, the epoch of the measurement is different for each. You can't make two measurements at the same time, nor can you use the integrating features that are built into the counter.

MR. WHEELER:

Yes, measurements are made sequentially.

MR. WARD:

But in cross correlating data from the different measurements, if the epochs are not the same, then you really have to make adjustments because it's not truly simultaneous measurement.

MR. WHEELER:

Yes. The simultaneous data from the G.P.S. receiver is not measured to the time interval counter.

MR. WARD:

Well, G.P.S. has its own counter built in.

MR. WHEELER:

Yes.

MR. WARD:

We think that for the measurements made on the Loran and Omega and some of the other measurements, the time interval counter was used.

MR. WHEELER:

We aren't depending on the true common view measurements of the clocks, of the locally available clocks in the Loran.

DR. WINKLER:

I would like to comment on that, on the question: "Why are these measurements not being made simultaneously and what is the maximum error which you get by not doing so?"

Well, if you make your measurements sequentially between high performance clocks, the maximum time error which you make in a measurement which is done in ten seconds or fifteen seconds is less than one nanosecond; and considering all your other errors in the system, that is not important, of course. That's the main reason why in the interest of being economical, the multiple counter system has not been selected.

U.S. NAVAL OBSERVATORY COLLECTION AND UTILIZATION OF TIME COMPARISON DATA

F. Neville Withington
U. S. Naval Observatory
Washington, D. C.

ABSTRACT

Through the years, the amount of PTTI data collected by, disseminated through and utilized at the U. S. Naval Observatory has steadily grown. Approximately 10 years ago, the USNO began computerizing collection and reduction of these data. At that time this process was automated as much as possible, given the technical constraints involved. In the last few years, the advent of more sophisticated equipment and techniques has improved and further automated data handling. Not only has data collection been modernized, but new systems for disseminating data, bulletins, and other information have been introduced and are being developed. This paper is an overview of the development of automated PTTI data handling at the Naval Observatory, generally describes the current data handling practices, and briefly discusses near future trends in the management of data.

INTRODUCTION

The mission of the United States Naval Observatory (USNO), requires the determination and dissemination of uniform clock and astronomical time to "United States Naval vessels and aircraft as well as to all availing themselves thereof" (SecNav Notice 5450). This mission statement, coupled with DoD Directive 5160.51 of 31 August 1971, which requires the Naval Observatory to supply traceability to the Master Clock for all DoD time, defines the primary function of the USNO Time Service Division. The Time Service must not only determine accurate time, but disseminate the information quickly and efficiently, and provide the Master clock time to those with timing requirements.

To carry out its mission, Time Service receives, disseminates, and utilizes PTTI and Earth Rotation data from sources located throughout the world. These sources include national and international laboratories, DoD field installations, and observatories which maintain time standards, make measurements of systems capable of being used for time synchronization, and/or make observations for Astronomical time and latitude data. The types of data handled are as varied as the sources. These data include OMEGA and LORAN-C measurements, earth rotation observations, navigation and communication satellite timing information, portable clock trip results, and much more. Over the last decade, the amount and frequency of data collected and disseminated has grown steadily, and, at times, even dramatically. To process the constant influx and growth of timing information, the Time Service has automated to a great extent, and continues to update, the data collection, dissemination, and analysis techniques. This process is aided by advancements in computer technology, by the addition of new modes of collecting information and by the use of statistical software to assist in the analysis of data.

Types of Data

As mentioned above, the types of data collected and analyzed by the Time Service Division in fulfillment of its mission are quite varied. Not only do the data from local sources, such as USNO clocks and telescopes have to be retrieved, but data of all kinds from remote sources must be collected and processed as well. Figure 1 lists the various types of data which are collected and maintained in databases whose integrity must be ensured.

The astronomical databases contain astronomical time and polar motion information from the optical Photographic Zenith Tubes (PZT) and the Connected Element Radio Interferometer which are run by the Naval Observatory. However, these data only comprise a part of the Earth Orientation data utilized by the Naval Observatory. Polar Motion data from the Doppler Navigation Satellites and from satellite laser ranging programs run by the University of Texas are collected regularly. Very Long Baseline Interferometry earth orientation data from both the Polaris project of the National Geodetic Survey and the TEMPO project of the Jet Propulsion Laboratory contribute to the earth orientation database. All of these are analyzed and utilized for earth orientation production and research. Both the preliminary (Rapid Service) and the final (Circular D) international earth orientation parameters, as determined by the Bureau International de l'Heure (BIH), are included in the data collected into the databases.

Data which are used for determining remote time scales, timing LORAN-C chains, and/or satellite time transfer information are all maintained in machine readable form. LORAN-C, OMEGA, TRANSIT and GPS data are monitored by the USNO, and by international laboratories and DoD field sites. Figure 2 is a list of some of the LORAN-C chains and where they are monitored. Time transfers from Defense Satellite Communications System (DSCS) are available, and used to calibrate other systems as well as maintain DSCS synchronization with the USNO master clock. It is with these systems that traceability back to the Master Clock can be realized.

Local timescale data are kept on a separate database. The hourly readings of the clocks are used to maintain the local timescales, and to steer the master clock. Portable clock data are also collected and stored with local timescale data. Since the portable clocks are very important for ensuring that remote time scales are remaining on time, this aspect of the database is also very important. An historical file of measurements obtained during portable clock trips is maintained. The local clock measurements are not only used to formulate USNO time scales, but are also transmitted to the BIH for use in the formation of International Atomic Time (TAI). Presently USNO is a major contributor to TAI.

Collection of Data

Prior to the 1970s, the data collected by the Observatory were all logged manually. These included PZT measures, OMEGA and VLF readings, and local clock comparisons. Initially, only locally monitored time pulses from LORAN-C, and OMEGA, were available to the USNO. However, it was soon evident that remote LORAN-C chains should also be monitored in order that time at wherever there were chains available could be traced back to the Master Clock. This was accomplished by establishing Precise Time Reference Stations (PTRS), laboratories and Observatories which maintain one or more clocks coordinated with the USNO master clock. Many of these could monitor LORAN chains locally and send the information to Time Service via TWX, mail or telephone messages. To further assist in the timing of remote LORAN chains, time transfers received from DSCS terminals also began to be utilized for this purpose.¹

The arrival of an IBM 1800 Data Acquisition and Control System (DACS) (pictured in figure 3) in the early seventies enabled local clock data to be collected more accurately and more frequently. The IBM 1800 began collecting clock comparisons hourly and regularly monitored the local time scales. The frequency of collection had a beneficial effect on the accuracy of the time scales. The DACS was soon also being utilized to control the PZT and collect the timing ticks for each observation. The IBM 1800 would trigger the shutter of the PZT at a given computed time with far more precision than a human observer. It could also "observe" on cloudy nights, which meant that, if the clouds broke in the early morning, it was possible to retrieve data from the nights observation. As with the clocks, the increased amounts of data added weight to USNO time and polar motion determinations.

The amounts of external data being collected by the Observatory grew as remote chains and PTRSs were added. The data were entered into the computer on punched cards which, at the start, were punched manually from the TWX messages, telephone messages, and data received via US mail. It very quickly became impractical to process and manipulate these data by hand.

Approximately ten years ago, the decision was made to automate, as much as possible, the data handling for the timing of LORAN chains, and any other applicable PTTI function.² Utilizing equipment and technology available in Time Service at that time, (a TWX that punched paper tape, and the IBM 1800 DACS), a system was set up whereby data sent from the field via TWX would no longer have to be manually entered. A standard format for TWX PTTI input was devised which allowed the 1800 to sort through the messages on the tape and to locate the necessary data. These data were then punched onto cards in the correct format for the database on the mainframe computer. This system was originally used for DSCS data, but was soon expanded to include other types of data, such as LORAN-C readings, TRANSIT satellite timing data, and photographic zenith tube (PZT) results from the Time Service substation near Miami, Florida.

By the late seventies, it was evident that the Data Acquisition needs of the Time Service were beginning to outrun the currently available DACS. The daily paper tape from the TWX was getting longer as more data were sent, and the IBM 1800 was taking longer to read it. Cards were starting to jam in the 1800 with increasing regularity, and the number of service calls was growing. The types of data being sent were becoming more diversified. New technology was, of course, available, and by 1981, the IBM 1800 had been replaced by newer, faster, more complex, machines.

The functions of the IBM 1800 were taken over by an IBM SERIES/1 (figure 4) and an HP1000 (figure 5). The far more sophisticated capabilities of these two machines opened new methods of data collection and data handling.

The SERIES/1 is the primary DACS for local clock comparison collection and time scale monitoring. It is backed up in this function by the HP1000. The SERIES/1 also collects the raw timing data from the Global Positioning System (GPS) navigation satellites which the Observatory receives directly, and continues the role of the IBM 1800 in the control of the PZT.

The HP1000 is used to back up the SERIES/1 for local clock collection. However, it also has a data collection role of its own. It collects the data from the automatic receivers for the locally monitored LORAN-C chains. It also receives daily the clock comparison and LORAN-C data from the new automatic data collection systems that the USNO is installing in remote field sites. More information on these systems may be found in reference 3.

The basic philosophy of data collection via TWX has not changed with the replacements in data acquisition systems. The data are still processed through the DACS. However, the mode of collection has changed dramatically from the paper tape/ punched card method.

Since the SERIES/1 has no paper tape reader and no card punch, the basic automatic data handling process had to change somewhat. A line was run from the Telex machine so that all incoming messages could be read directly on to a circular file on the SERIES/1. The PTTI data output from the TWX input was initially carried to the mainframe computer via magnetic tape, but it now can be sent directly from the SERIES/1 through a fiber optic line using remote job entry (RJE) software. The TWX file is also transferred daily to the HP1000.

In themselves, these improvements are significant. However, as stated before, the new machines have opened up other avenues of data manipulation. The TWX is no longer the sole source of remote machine readable data input.

As it is important that Time Service receive field measurements as quickly as possible in order to best utilize them, outside contributors are encouraged to send their data by the swiftest means at their disposal. For a significant number of these, the TWX is the best method (and, indeed, it is very efficient). Many contributors have only the mails or the telephone at their disposal. These are not as efficient as the mails take time, and all the data must be handled manually. This, in turn, can also lead to errors. The Observatory now uses another method of obtaining machine readable timing measurements - the General Electric MARK III international computer network

Use of the G.E. MARK III began for the Observatory with The MERIT (Measuring of Earth Rotation and Intercomparing Techniques) campaign. A subsection or 'catalog' of the General Electric MARK III international computer network was created to enable laboratories and observatories all over the world to transmit and utilize earth rotation data during the mini-campaign in 1980. This catalog was so successful that it was kept active after the campaign. In 1982, Time Service became administrator of this catalog, and began to expand the catalog to include different kinds of timing information. This catalog allows dissemination and utilization of data with laboratories that are willing to pay G.E. to be part of the service. Figure 6 is a list of the current users of the MARK III RC28 catalog. In terms of data collection, the Naval Observatory receives LORAN-C data from members of the catalog who previously sent the data via TWX or mail. GPS timing information from other laboratories is also received in this manner. By utilizing an automatic dialler and a modem, these data are transmitted directly into the IBM SERIES/1.

Most of the databases are stored and manipulated on the USNO's mainframe computer. At the start of automatic data handling of Time data, this computer was an IBM 360/40 (figure 7). It ran in a batch mode, using punched cards or magnetic tape for input. About the same period that the IBM 1800 DACS was becoming obsolete, the computing needs of the Observatory as a whole began to outrun the capabilities of the computer. In 1980, the IBM 360 was replaced by an IBM 4341, shown in figure 8, which not only offers batch capabilities with OS/MVT, but also offers an interactive operating system.

Dissemination of Data

Up until very recently, almost the sole method of general data dissemination was via the U.S. mail. A few military users were authorized to get PTTI data via TWX daily, and, because of requirements for determining earth orientation on a quick turn around basis, the BIH received USNO data via TWX weekly. With the advent of the HP1000 and the MARK III, the mails are no longer the sole source of data dissemination. The weekly bulletins are available electronically, and transmission to the BIH no longer requires a TWX.

The HP1000 has also been set up as an Automatic Data Service (ADS). This service, described more fully in reference 4, is a telephone service which allows the outside user to connect to the HP1000 and extract data and information. A 'mailbox' service also allows the input of messages, data, or anything else a user would care to share with the Naval Observatory. The addition of this service has allowed a new method of disseminating information. Anyone with a modem and terminal is now able to retrieve SERIES 4, SERIES 7, SERIES 17, GPS data, OMEGA data, LORAN information, status reports of various systems, and much more. Figure 9 shows the Table of Codes which guide the user to files which are of interest. The explanations contain other codes for files which may be accessed.

The G.E. MARK III is also an efficient method of data dissemination. When it was created in 1980, the RC28 catalog's main purpose was to allow data dissemination to the BIH. After the mini-MERIT campaign, Time Service continued to send earth rotation data to the BIH in this manner. The expansion of the catalog, both in terms of users and of data types, has meant that international laboratories and observatories are now able to receive Bulletins 4,7, and 17 from Time Service much more quickly. Now, not only do the earth rotation data go via this method to the BIH, but local clock data, essential for determining TAI are also sent via the MARK III. GPS data and USNO observing schedules are available as well.

Internal Transmissions

The HP1000, IBM SERIES/1, IBM 4341 and the G. E. Mark III do not operate in a vacuum. As may be deduced from above, there must be interaction between the machines in order that the various types of data collected and disseminated can be most efficiently utilized. There is, of course, a "traditional method" of moving data between machines: via magnetic tape. However, in the case of the four machines utilized for time service purposes, magnetic tape is only a backup method of transferring data. There are direct communications links between the three on site machines and the MARK III is accessed directly through the SERIES/1 via automatic dialer. This configuration is illustrated in figure 10.

The SERIES/1 is linked to both the HP1000 and the IBM 4341. This means that data from the SERIES/1, or the 4341, such as GPS, local clock intercomparisons, or Earth rotation data, may be sent to the HP1000, or data from the HP1000 may be sent to the SERIES/1 and/or the 4341. In this way, calculations made, or bulletins created on any of the machines may be made available on the HP1000 for the public.

The G. E. MARK III is accessed through a modem and automatic dialer on the SERIES/1. This configuration allows transmission to and reception from the MARK III of data files, which can then be sent wherever appropriate in the Time Service network.

Much of the data transmission is completely automated throughout the network. For example, the SERIES/1 telephones the MARK III once a day and checks to see whether there are any LORAN-C data. If there are, these data are appended to the TWX file and are processed with the other data. The raw GPS data from the receivers is collected by the SERIES/1 and sent twice a day to the HP1000, where it is processed and put into final form. Final GPS data is then automatically sent back up to the SERIES/1 where it is stored until it is placed on the MARK III. Data from the automatic systems are transmitted to the SERIES/1 once a day, after being automatically collected by the HP1000. These totally automated transmissions mean that fewer person hours have to be spent in transmitting data from place to place, freeing the staff for the analysis of the data collected.

Although much of the transmission has been automated, it has not all been done by any means. There is automatic transmission from the MARK III, for example, but none to it. There are no

automatic transmissions to and from the 4341, nor are all transmissions between the SERIES/1 and the HP1000 automated. However, even the 'manual' processes between the machines are expedited because of the efficiency and speed of various links.

Analysis and Utilization

The local and remote data collected by the Time Service are processed and analyzed for both production and research purposes. It is not the function of this paper to describe in great detail the reduction techniques or statistical analyses that form the work of Time Service. However, a brief mention of some of the purposes of the data handling techniques is pertinent.

The earth orientation data are used to determine as accurately as possible, UT1-UTC and polar motion, and to predict the position of the Earth in space with as small a standard deviation as possible. To do this, observations from many different techniques must be used. Analysis of these data is performed to determine the accuracy and precision of the observations, and how they may best be used for prediction purposes.

For timing remote LORAN-C chains, data from many different sources are essential. With only occasional calibrations via portable clock measurements or DSCS transfers available for these chains, intercomparison between systems is necessary to determine individual clock rates to keep the chains steered as closely as possible with U.S. Naval Observatory master clock. Data not only from the chains themselves, but from laboratories, field sites, or observatories which can monitor these chains are analyzed for this purpose.

These, and other projects of the Time Service Division call for large amounts of data. Statistical analyses done with either software packets such as BMDP, or by programs written at the Observatory, require as large a sample as can be utilized in order to get an accurate picture of the data as possible. Much of the production work, as well, such as earth orientation predictions, or LORAN chain timing and prediction, also require a large baseline of data. The numerous databases are required by Time Service for both the production and analysis.

The Near Future

The network that has been developed between the IBM SERIES/1, HP1000, IBM 4341, and the G. E. MARK III has added much to the efficiency of processing and of dissemination of PTTI and earth rotation data. However, improvements are continuing to be made. The amounts of data are still increasing as automatic systems are installed, new LORAN chains are established, additional DSCS modems are fielded, and more GPS satellites are launched. This increasing data load means that still greater automation is required to ensure that the available manpower can fully utilize the vast amounts of data available.

As intimated above, there are plans and ideas to continue to develop the automatic processing of data which pass through Time Service. Although some of these plans are just extremely tentative, others are very real concepts. Projects which are being implemented include improvements and enhancements in all aspects of data management in Time Service.

Redesigning the database on the mainframe computer is one of the realistic near future goals of the Time Service. Currently the database exists on a batch mode operating system. Although this system is good, the 4341 has acquired an operating system which is interactive in nature. By changing the database so that it runs on this new system, the door is open to better utilize the capabilities of the 4341.

New remote automatic collection systems are being added at many PTRS sites. This fact, coupled with increased usage of the automatic data service, means that the HP1000's responsibilities will eventually move beyond its capabilities. It has been definitely decided that the current HP1000 will be replaced by a more powerful machine that will be able to handle more efficiently the increased data load. The plans for this have already begun, and the present configuration will be replaced within two years.

Further enhancements are also planned for the SERIES/1. The SERIES/1 already consists of two processors, which doubles its efficiency, but more disk space is needed. Upgrading the operating system is also on the agenda.

Increased use and further automation of the data flow of the MARK III are both being planned. The number of laboratories and Observatories on the system is steadily growing, and it is hoped that this growth will continue. It is also anticipated that the types of data available on the MARK III shall also grow as the needs and desires of the timing community for easily accessible, machine readable data grow. Further automating the current data flow is also planned. Many of the transmissions are routine, and automating them would free additional personnel for other projects.

The newer types of data will be more fully utilized in the near future. There is a great deal of potential still to be tapped in the GPS data, the DSCS data, and the automatic systems. Currently studies are being made on how best to utilize these data, as fully and as effectively as possible. The necessary computer programming is being done for these studies.

As more technology and new types of data are made available, ideas of improvements in the existing data handling structure will naturally occur. Perhaps many of the concepts that exist today will also be eventually incorporated into the structure of data handling at the Naval Observatory.

CONCLUSION

In carrying out its mission requirements, the Time Service Division of the U. S. Naval Observatory quickly and efficiently collects, utilizes and disseminates time data of all sorts. Not only the methods of utilizing the collected data, but also the means of data collection and utilization are essential for the successful Time Service operation. Automating the flow of data through the Naval Observatory to the greatest extent possible has been one means of improving the service provided for the Timing user community. By automating, or at least streamlining, the routine data flow, skilled personnel are released to work on the data analysis which is necessary to ensure precise, accurate and timely information. Using machines, rather than people, for data entry also minimizes the risk of error in data exchange. Thus far, the Observatory has been highly successful in utilizing available technology for rapid dissemination to the many users of PTTI and Earth rotation data.

REFERENCES

1. Charron, L.G. and Lukac, C.F., "Evolution of LORAN-C Timing Techniques" in The Proceedings of the Wild Goose Association Meeting, October, 1983. (in press)
2. Fisher, L.C., "Precise Time and Time Interval Data Handling and Reduction" in Proceedings of the Fifth Precise Time and Time Interval Meeting: (Greenbelt, MD., 1973), pp. 215-231.

3. Wheeler, P.J., "Automation of Precise Time Reference Stations (PTRS)" in Proceedings of the Fifteenth Annual Precise Time and Time Interval Meeting: (in press).
4. Miranian, M., "The U.S. Naval Observatory Automated Data Service" (unpublished) copies available through Time Service Division. U.S. Naval Observatory.

DATA TYPES

INTERCOMPARISON OF CESIUM CLOCKS
 OMEGA MEASUREMENTS
 LORAN-C MEASUREMENTS
 REMOTE TIME SCALES FOR MONITORING SITES
 PORTABLE CLOCK REDUCTIONS
 NAVOBSY TIME SCALES
 SATELLITE TIMING INFORMATION
 (DSCS, TRANSIT)
 UTC(BIH) - UTC(II)
 EARTH ORIENTATION PARAMETERS
 (UT1, POLAR COORDINATES)
 GPS TIME TRANSFER MEASUREMENTS
 ASTRONOMICAL OBSERVATIONS

FIGURE 1

REPRESENTATIVE SAMPLE of MONITORING STATIONS

7970 <u>NORWEGIAN SEA</u>		7980 <u>SOUTHEAST USA</u>		7990 <u>MEDITERRANEAN SEA</u>	
OP	FRANCE	NAVOBSY		OP	FRANCE
HP	SWITZERLAND	NOTSS	RICHMOND, FL	HP	SWITZERLAND
ON	SWITZERLAND	AGMC	NEWARK AFS, OH	ON	SWITZERLAND
NPL	ENGLAND	WHITE SANDS MISSILE		LEN	ITALY
RGO	ENGLAND	RANGE, NM		RGO	ENGLAND
NAVSECGRU	SCOTLAND			NAVSECGRU	ITALY
8970 <u>GREAT LAKES</u>		9960 <u>NORTHEAST USA</u>		9990 <u>NORTH PACIFIC</u>	
NAVOBSY		NAVOBSY		PHEL	ELMENDORF
		NOTSS	RICHMOND, FL	NASA	FAIRBANKS
		AGMC	NEWARK AFS, OH	SHENYA	AFB, AK
		MBS	BOULDER, CO	*DSCS	ELMENDORF

*INDIRECT MEASURE

FIGURE 2



FIGURE 3



FIGURE 4



FIGURE 5

USER #	ACTIVITY/USER	QUIK-COMM	ACRONYM
RC28000	CATALOG ADMINISTRATOR (USNO)	USNO	-
RC28210	ASTRONOMY DEPT. UNIV. OF TEXAS, USA	AUTA	UTEXA
RC28210	CENTER FOR SPACE RESEARCH, U OF TEXAS	AUTA	CSR
RC28235	JET PROPULSION LABORATORY, PASADENA	JPLP	JPL
RC28240	NATIONAL GEODETIC SURVEY, ROCKVILLE	NGSV	NGS
RC28260	TIME SERVICE, US NAVAL OBSERVATORY	TIME	USNO
RC28265	INSTITUT FUER ANGEWANDTE GEODAESIE	IFAG	IFAG
RC28270	SMITHSONIAN ASTROPHYSICAL OBSERVATORY	SAOB	SAO
RC28280	EARTH PHYSICS BRANCH, OTTAWA	EPBR	EPBR
RC28300	CERGA, GRASSE, FRANCE	CERG	CERGA
RC28310	BIH, PARIS, FRANCE	BIHF	BIH
RC28311	ISTITUTO ELETTRONICO NAZIONALE	IENT	IEN
RC28314	ISTITUTO Y OBSERVATORIO DE MARINA	--	OMSF
RC28316	PHYSIKALISCH - TECHNISCHE BUNDESANSTALDT	--	PTB
RC28317	NATIONAL PHYSICS LAB., TEDDINGTON, U.K.	NPLT	NPL
RC28321	TOKYO ASTRONOMICAL OBSERVATORY	TAOB	TAO
RC28324	VAN SWINDEN LABORATORIUM, NEDERLAND	VSLA	VSL
RC28339	TECHNISCHE UNIVERSITAT, GRAZ, AUSTRIA	TECH	TUG
RC28350	SUB ADMINISTRATOR, 310 - 399 (BIH)	--	-
RC28355	OBSERVATOIRE ROYAL DE BELGIQUE	ORBB	ORB
RC28360	INSTITUT GEOGRAPHIQUE NATIONAL	IGNF	IGNF
RC28365	GROUPE DE RECHERCHES DE GEODASIE SPATIALE	--	GRGS
RC28390	EUROPEAN SPACE AGENCY OPERATING CENTER	--	ESA
RC28400	INTERNATIONAL LATITUDE OBSERVATORY	ILOM	IPMS
RC28405	RADIO RESEARCH LABORATORIES, JAPAN	---	RRL
RC28410	KANONAN GEODETIC OBSERVATORY, JAPAN	--	KGO
RC28420	NAVAL RESEARCH LABORATORIES, WASHINGTON	---	NRL
RC28430	DIVISION OF NATIONAL MAPPING, AUSTRALIA	---	NATMAP
RC28440	OHIO STATE UNIVERSITY, DEPT. OF GEODETIC SCIENCE AND SURVEYING	DGSS	DGSS

FIGURE 6

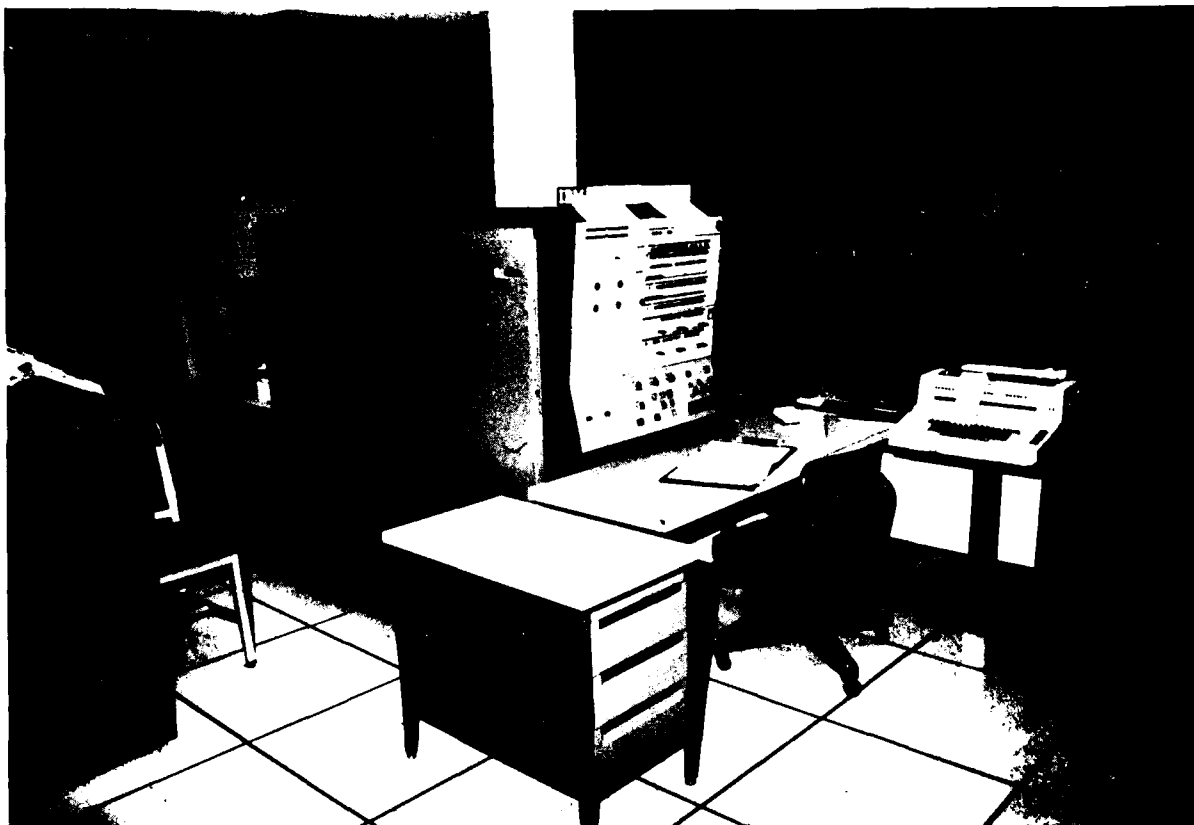


FIGURE 7



FIGURE 8

USNO AUTOMATED DATA SERVICE

TABLE OF MOST FREQUENTLY USED CODES (@TCO)
(FOR MORE CODES SEE EXPLANATIONS IN EACH CATEGORY)

SERIES EXPLANATIONS (SER4,5,7,8,9)	@SERXP		
SERIES 4: Notes of the last SER4 Bulletin	@SER49		
SERIES 5: LAST MESSAGE (AIG 100)	@SER50		
Older messages may be obtained by appending the digit 1-9 for data age for example: 5 day old message			
	@SER55		
SERIES 7: Explanations for Extrapolation	@SER70		
PREDICTION OF UT, X-Y	@SER71		
PRELIMINARY MC-UTC(USNO)	@SER73		
EXPLANATIONS, GENERAL ..	@EXP	PTTI CONFERENCE NEWS ..	@TTI
SPECIAL DAILY MESSAGE ..	@DME	TIME SERVICE DIRECTORY ..	@DIR
GENERAL PTTI MESSAGE ...	@MES	MAILBOX INFORMATION	@MBXXP
VLF STATUS	@VLF	VLF MAINTENANCE SCHED ..	@VLFD2
VLF EXPLANATIONS	@VLFXP		
OMEGA STATUS	@ONS	OMEGA MONITOR DATA	@ONSD1
OMEGA EXPLANATIONS	@ONSXP	OMEGA OFF-TIMES SCHED ..	@ONSD2
GPS STATUS	@GPS	GPS TRACKING SCHEDULE ..	@GPSD2
GPS EXPLANATION FOR DATA	@GPSXP	GPS EXTRAPOLATION	@GPSD4
GPS LATEST TIME DATA ...	@GPSD1	GPS FILE DATA	@GPSSL
TRANSIT STATUS	@TRA	TRANSIT SER17	@TRAD7
TRANSIT EXPLANATIONS ...	@TRAXP	TRANSIT FILE DATA	@TRASL
TRANSIT TIME DATA	@TRAD1	TRANSIT SAT. VISIBILITY	@TRAVS
TRANSIT NOVA DATA	@TRAD2		
LORAN STATUS	@LOR	LORAN REAL TIME MEAS ...	@MLO
LORAN EXPLANATIONS	@LORXP	LORAN PROPAGATION TIME, DIRECTION & DISTANCE ...	@LDX
TOC FOR LORAN OR TV	@TOC	TV EXPLANATIONS	@TVKXP
(TIME OF COINCIDENCE)		WTTG-TV CH-5, MEAS	@TVL
		NETWORK TV MEASUREMENTS	@TVK
PORTABLE CLOCK DATA:		SCHED. OF NEXT TRIP	@MPX
MEASUREMENTS	@MPC	TENT. PC TRIP PLANS	@MPT
SCHED. OF CURRENT TRIP .	@MPN		
NBS DATA:		OPERATIONS CONTROL:	
NBS EXPLANATIONS	@NBSXP	FOR DETAILS AND CODES ..	@OPSXP
NBS STATUS OF GOES	@NBSGO	USNO PUBLIC INFORMATION:	@STAXP
REAL TIME MEASUREMENTS:		PREDICTIONS & COMPUTATIONS:	
EXPLANATIONS	@RTMXP	SIDERIAL TIME	@STI
LORAN (4 CHAINS)	@MLO	MJD/WEEKDAY	@DAT
UTC TO +/- 50MS	@TIM	SUNRISE, SUNSET, TWILIGHT FOR ANY POINT .	@SRI
TIME SIGNAL EXPL	@TSF	SUNRISE PROG. EXPLAN ...	@SRIXP
TV READINGS (AVERAGES):		LORAN PROPAGATION TIME, DIRECTION & DISTANCE ...	@LDX
WTTG WASHINGTON, DC	@TVM	STANDARD TIME ANYWHERE .	@STTXP
NBC "	@TVN		

FIGURE 9

CURRENT CONFIGURATION

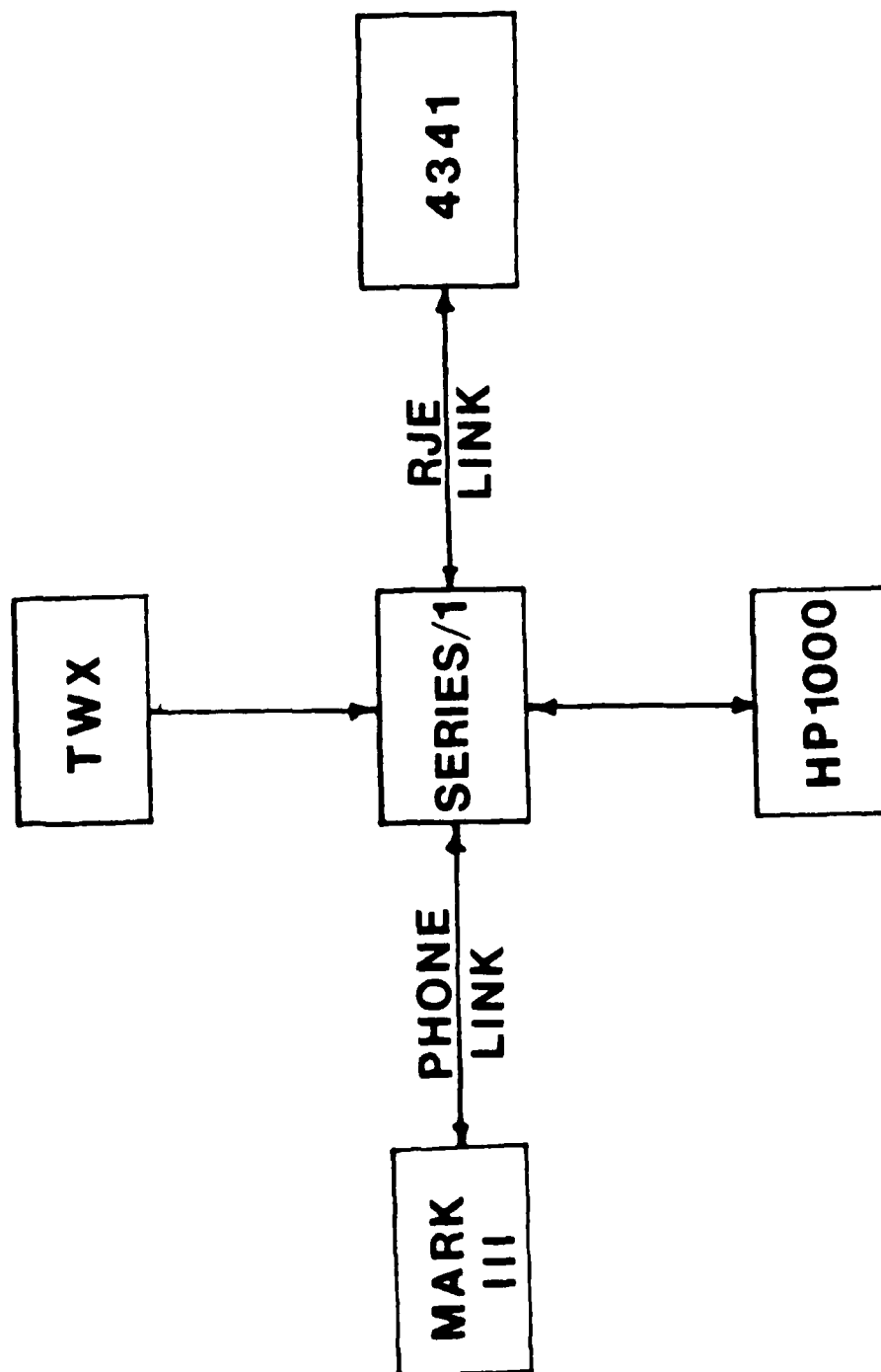


FIGURE 10

QUESTIONS AND ANSWERS

MR. WARD:

Sam Ward, J.P.L., again. For the users who get poor quality telephone lines, such as I do, before I get any useful data the thing times out, this happens to me frequently.

MRS. WITHINGTON:

You are referring to the Automated Data System?

MR. WARD:

That's right. I don't know how we solve that one, either. I worked on the telephone company but the length of time that is programmed in should be longer.

DR. WINKLER:

I appreciate hearing such comments. You are the first one who has made that request. That can easily be done. The waiting time of the computer has been set for forty-five seconds, in the interest of making the telephone line available as quickly as possible; but if there are such problems, it's a matter of one minute to increase that to one-and-a-half minutes. So we appreciate hearing from the users about such difficulties. The local telephone lines can be somewhat improved if you request from your telephone company a data line. It can be especially equalized. We had a considerable amount of trouble before our system was working reliably. Also, there is a difference between a hard connected modem, a wire connected modem compared to the acoustic couplers. Acoustic couplers are generally poorer because it depends on the microphone that you have. There are special microphones available that you can put in. So there are lots of little tricks you can put in; we will be very happy to assist a user.

MR. CAMP:

Bob Camp from Synox. I have a question. Who should one get in touch with for further information about the mechanism of accessing all this data?

MRS. WITHINGTON:

Well, for the Automated Data Service, Myron Moranian of the Naval Observatory is the one to call. For the G.E. Mark III, I'm the one to call on that. My name is Neville Withington.

INTERNATIONAL TIME COMPARISON BY A GPS TIMING RECEIVER

M.-K. Fujimoto, K. Fujiwara, and S. Aoki
Tokyo Astronomical Observatory, Mitaka, Tokyo 181

ABSTRACT

Tokyo Astronomical Observatory (TAO) has started a regular reception of the Global Positioning System (GPS) timing signals for the purpose of a precise international time comparison. A test operation of the GPS receiver was performed from September 1982 to January 1983 and achieved good accuracy in time comparisons. During the test run, a clock comparison was made by a USNO portable clock team and it was compared with the GPS reception. The difference between the comparisons was less than the error in the portable clock comparison. Since April 1983, regular reception of GPS signals has continued and the results in the GPS time error, UTC(TAO)-GPS, are transmitted every week on the General Electric (GE) Mark III system. By this means, the cesium clocks in the asian region will be related to TAI with better accuracies.

INTRODUCTION

The asian cesium clocks have been excluded from the contribution to the International Atomic Timescale (TAI) because of their poor links to the clocks in the other areas such as Europe, United States, and Canada. Loran C stations in the Northwest Pacific chain are so distant that the time-keeping organizations in the asian region cannot receive ground waves of the Loran C signals with sufficient accuracy.¹ The Global Positioning System (GPS) is considered to be one of the most promising methods for time transfers on a worldwide basis at the ten-nanosecond level.² Regular time transfers by the GPS will make it possible for the asian clocks to contribute information into the TAI.

Tokyo Astronomical Observatory (TAO) performed a test operation of a GPS timing signal receiver and achieved good accuracy in time comparisons with the U.S. Naval Observatory (USNO). During the test operation, a clock comparison was made by a USNO portable clock team and the result was compared with the one by the GPS time comparison. After the test run, some trouble-shooting and revisions were made on our receiver to increase the reliability of continuous operation. From April 1983, regular receptions of the GPS signals were started and the results are transmitted every week on the General Electric (GE) Mark III system.

This paper will deal mainly with the results of time comparisons with USNO by GPS.

GPS TIME TRANSFER SYSTEM

The GPS receiver used at TAO is a Stanford Telecommunications Inc. (STI) Time Transfer System Model 502 (TTS 502), for which a detailed description was given at the thirteenth annual PTI meeting.³ The system automatically acquires and tracks the L1 carrier and C/A code of GPS satellites according to a schedule which is initially set up by us. The system then processes the received data to calculate satellite position, satellite clock correction and propagation time between the satellite and the receiving station which includes corrections for ionospheric, tropospheric, and relativistic delays, and gives "time error" of the local clock referred to the GPS time.

Through an RS-232C port, all necessary information for calculation of the time error, obtained from the received data, are output to external peripherals; a printer and a recording system in our case. The real time recording system for GPS data is realized on a general-purpose minicomputer. All the data output from the receiver are recorded in a file of the minicomputer and are then transmitted to a large computer, by which they are processed and analyzed.

GPS DATA TRANSMISSION

We regularly transmit the results of GPS time transfers by two modes: Weekly data exchanges are made through a GE Mark III file in a format agreed upon, and monthly data are published in a printed form. Examples are shown in Figure 1 and 2. The former contains almost all of the measurements made at TAO and the latter does one measurement of good quality for each space vehicle (SV) each day, generally, a measurement at larger elevation is chosen.

We receive the GPS data of the other organizations on the GE Mark III. The data are stored in certain files on the large computer and are used in mutual time comparisons.

CLOCK COMPARISONS WITH USNO

Figure 3 shows the time differences, UTC(TAO)-GPS and UTC(USNO)-GPS, which were obtained by the GPS receptions. It covers the data in the period of half a year. Zigzag runnings appear in both the curves and are considered mainly due to the operational changes in the rate of the GPS time.

In order to see the time differences between USNO and TAO, the behavior of the GPS time against the UTC(USNO) is approximated tentatively by a broken line, denoted as REF(t), and both of the values UTC(TAO)-GPS and UTC(USNO)-GPS are corrected (subtracted) by the quantity REF(t). The results are shown in Figure 4. The upper curve, UTC(TAO)-GPS-REF(t), approximates UTC(TAO)-UTC(USNO) and the lower curve, UTC(USNO)-GPS-REF(t), shows the errors of the approximation, as well as transmission/receiving errors in the GPS clock link.

The former curve is comparable with that in Figure 5, which shows UTC(TAO)-UTC(USNO) obtained from the GPS receptions in a common view mode,⁴ where the data of the same SV were measured by both observatories within 4 minutes. The values of UTC(TAO)-UTC(USNO) in the first half of the data period are relatively scattered mostly because of small sampling numbers (less than 10) of the measurements at both or either site. Small but clear frequency drift was found in the TAO clock before the 1st of October 1983, when the master clock at TAO was replaced.

These three figures show that the time comparison between TAO and USNO by GPS is achieved, roughly speaking, to an accuracy of less than 50 ns.

TEST OPERATION

A test operation of the GPS receiver was performed from September 1982 to January 1983 as mentioned before.

Figure 6 shows the residuals of a linear-fit through approximately three months' data, UTC(TAO)-GPS, which were obtained from the reception of SV#5 during the test run. For a comparison, the corresponding data of the USNO, UTC(USNO)-GPS, are shown in the same manner. USNO data approximately once a day are taken from the USNO publication, Series 4. TAO data are plotted twice a day, when the signals from the SV of the subsequent passes are received. It is clearly seen in the figure that the values of UTC(TAO)-GPS at the different sidereal times are different from each other.

The conditions in the alternate measurements are quite different. In our case, for example, the maximum elevation changed alternately by a large amount. Differences of the elevation and of the local solar time may cause errors in the estimation of propagation delays, especially of the ionospheric delay. Figure 7 shows raw (every 6 seconds) data of UTC(TAO)-GPS during continuous tracking (about 6 hours) of the same SV. Elevation of the SV and the applied ionospheric corrections are also shown in the figure, for which a timescale is indicated by UT and Japan Standard Time (JST). From the figure, correlation is not as obvious between the variation of the time difference data and the above mentioned conditions.

Errors in the estimation of satellite position from the transmitted ephemeris may be another possible cause of the variations as was pointed out by Klepczynski.⁵

Further study on the cause of such semi-systematic variations in the GPS data may be useful to improve the GPS time links to the accuracy of 10 ns.

COMPARISON WITH A PC TIME TRANSFER

During the test operation, a USNO Portable Clock (PC) team made a clock comparison between the USNO and the TAO. Table 1 shows the results of comparison of the PC trip and the GPS time transfers.⁶ Difference of 113 ns (average) between the GPS and PC determinations for UTC(USNO)-UTC(TAO) is

not significant, because the PC time determination has an uncertainty of 170 ns as was reported by USNO. From this comparison, we know that the values of time comparisons by GPS seem to be better than or at least comparable with the PC results. As a matter of course we must check the existence of systematic differences between the two time determinations for every subsequent PC trip.

SUMMARY

GPS capability for international time transfers is established with an accuracy better than fifty nanoseconds. By regular operation of the GPS receiver at Tokyo Astronomical Observatory, the asian cesium clocks, which are connected to TAO through a Loran C chain, will contribute information to the International Atomic Timescale (TAI) very soon. This will be an epoch-making event in the history of TAI.

Further improvement in the accuracy of the time transfer may be expected by studies of the cause of data variations.

ACKNOWLEDGEMENT

The authors wish to thank Dr. Gernot Winkler and Dr. William Klepczynski for their valuable advice on purchasing and operating the GPS receiver. They acknowledge Mr. J. R. McLean and Mr. Q. D. Hua, STI, for their kind efforts in improving the reliability of the receiver. They also thank Mr. T. Yamazaki of the time division and the staff of the computing facility at TAO for their cooperative operation and management to connect the GPS receiver to the computer, FACOM M-380R, through the mini-computer, PANAFACOM U-1200. This work was supported in part by the Scientific Research Fund of the Ministry of Education, Science, and Culture under Grant No. 56420002 in the fiscal years 1981 and 1982.

REFERENCES

- 1) S. Iijima, "Time and Frequency in Japan," Journal of the Institute of Electronics and Telecommunication Engineers, Vol. 27, No. 10, pp. 372-378, 1981.
- 2) K. Putkovich, "Initial Test Results of USNO GPS Time Transfer Unit," presented at 34th Annual Symposium on Frequency Control, May 1980.
- 3) A. J. Van Dierendonck, Q. D. Hua, J. R. McLean, and A. R. Denz, "Time Transfer using Navstar GPS," presented at 13th Annual Precise Time and Time Interval (PTTI) Applications and Planning Meeting, December 1981.
- 4) D. W. Allan and M. A. Weiss, "Accurate Time and Frequency Transfer during Common-View of GPS Satellite," Proceedings, 34th Annual Frequency Control Symposium, May 1980.

- 5) W. J. Klepczynski, "Systematic Effects in GPS Time Transfer," presented at 14th Annual Precise Time and Time Interval (PTTI) Applications and Planning Meeting, December 1982, and private communication with William J. Klepczynski, USNO, August 1983.
- 6) Private communication with W. J. Klepczynski, November 1982.

TABLE 1
COMPARISON OF PC TRIP AND GPS TIME TRANSFER

	U.T.	USNO - TAO via PC	USNO - TAO via GPS	PC - GPS
1982				
15 October	1344	-6196 ns	-6329 ns	133 ns
18 October	0128	-6139	-6263	124
18 October	0131	-6147	-6263	116
18 October	0542	-6142	-6260	118
18 October	2106	-6154	-6230	76
				average 113 ns

SV	CL	MJD'	HH	MM	SS	TRCK	AG	EL	AZM	ION	MC-SATCL	SLOPE	MC-GPS	SLOPE	RMS
						SEC	HR	DG	DEG	NS	NS	PS/S	NS	PS/S	NS
6	FB	5639	03	42	00	300	11	13	331	38	829379	109	2159	38	13
8	10	5639	04	26	00	780	12	48	315	20	-355159	-54	2158	7	15
6	10	5639	04	42	00	780	12	30	310	27	829649	82	2174	11	10
9	FB	5639	05	10	00	480	12	8	333	42	9287	21	2134	18	14
6	FB	5639	05	22	00	480	13	32	287	27	829831	91	2185	20	11
11	10	5639	05	46	00	780	12	30	309	27	648356	10	2167	-1	11
8	28	5639	06	26	00	780	14	54	53	18	-355584	-56	2175	6	14
11	FB	5639	07	26	00	600	14	62	1	17	648444	5	2177	-10	14
5	10	5639	07	50	00	780	10	28	323	28	190484	16	2167	16	11
5	FB	5639	09	25	00	600	11	72	334	16	190500	8	2181	6	10
6	28	5639	15	02	00	780	23	40	39	20	832229	74	2145	4	12
6	20	5639	15	24	00	780	23	31	34	24	832319	73	2147	-40	13
9	28	5639	16	46	00	780	0	39	32	21	9283	-10	2134	-13	13
9	20	5639	17	06	00	780	0	30	33	25	9278	2	2125	-1	13
5	FB	5639	19	36	00	540	1	10	35	38	190503	5	2125	5	15
5	FB	5639	20	14	00	600	2	3	21	43	190513	-18	2135	-18	15
6	FB	5640	03	38	00	300	12	13	331	38	835463	104	2159	33	12
8	10	5640	04	22	00	780	12	48	315	20	-360392	-52	2164	9	14
6	10	5640	04	38	00	780	12	30	310	27	835739	73	2179	1	10
9	FB	5640	05	06	00	480	12	8	333	42	9314	5	2152	2	13
6	FB	5640	05	18	00	480	13	32	287	27	835920	80	2189	9	9
11	10	5640	05	42	00	780	13	30	309	27	649577	17	2170	5	11
8	28	5640	06	22	00	780	14	54	53	18	-360815	-60	2182	1	13
11	FB	5640	07	22	00	600	15	62	1	17	649659	14	2173	-1	15
5	10	5640	07	46	00	780	13	28	323	28	190593	16	2173	16	13
5	FB	5640	09	21	00	600	15	72	334	16	190619	9	2198	7	11
6	28	5640	14	58	00	780	23	40	39	20	838302	67	2125	-4	13
6	20	5640	15	20	00	780	23	31	34	24	838390	74	2122	-7	13

FIGURE 1 GPS DATA TRANSMISSION FORMAT (GE MARK III FILE)

International Precise Time Comparison

at Tokyo Astronomical Observatory

(UTC(TAO MC) - Signal)

NO. 83- 4

** Global Positioning System(GPS) **

		SV#5		SV#6		SV#8	
Date							
1983	MJD	MC-GPS	UT*	MC-GPS	UT*	MC-GPS	UT*
10	1	45608	2.359(112900)	2.334(173000)	2.354(071700)		
	2	45609	2.325(112500)	2.313(172600)	2.362(071300)		
	3	45610	2.339(112100)	2.307(172200)	2.351(070900)		
	4	45611	2.364(111700)	2.285(171800)	2.327(070500)		
	5	45612	2.322(111300)	2.288(171400)	2.307(070100)		
	6	45613	2.276(110900)	2.291(171400)	2.321(065700)		
	7	45614	2.311(110500)	2.284(171000)	2.322(065300)		
	8	45615	2.295(110100)	2.241(170600)	2.302(064900)		
	9	45616	2.323(105700)	2.262(170200)	2.324(064500)		
	10	45617	2.301(105300)	2.264(165800)	2.297(064100)		
	11	45618	2.303(104900)	2.252(165400)	2.298(063700)		
	12	45619	2.271(104500)	2.297(061400)	2.292(055800)		
	13	45620	2.291(104100)	2.293(061000)	2.301(055400)		
	14	45621	2.263(103700)	2.289(060600)	2.286(055000)		
	15	45622	2.261(103300)	2.285(060200)	2.278(054600)		
	16	45623	2.269(102900)	2.277(055800)	2.262(054200)		
	17	45624	2.274(102500)	2.283(055400)	2.267(053800)		
	18	45625	2.271(102100)	2.251(055000)	2.247(053400)		
	19	45626	2.212(101700)	2.242(054600)	2.235(053000)		
	20	45627	2.246(101300)	2.252(054200)	2.243(052600)		
	21	45628	2.267(100900)	2.233(053800)	2.226(052200)		
	22	45629	2.151(100500)	2.226(053400)	2.211(051800)		
	23	45630	1.670(201200)	-----	-----		
	24	45631	2.215(095700)	2.209(052600)	2.201(051000)		
	25	45632	2.195(095300)	2.203(052200)	2.190(050600)		
	26	45633	2.129(094900)	2.196(051800)	2.186(050200)		
	27	45634	2.178(094500)	2.187(051400)	2.179(045800)		
	28	45635	2.160(094100)	2.197(051000)	2.178(045400)		
	29	45636	2.182(093700)	2.187(050600)	2.164(045000)		
	30	45637	3.183(093300)	0.102(050200)	2.153(044600)		
10	31	45638	2.146(092900)	2.178(045800)	2.155(044200)		

FIGURE 2 A MONTHLY PUBLICATION ON TAO GPS DATA

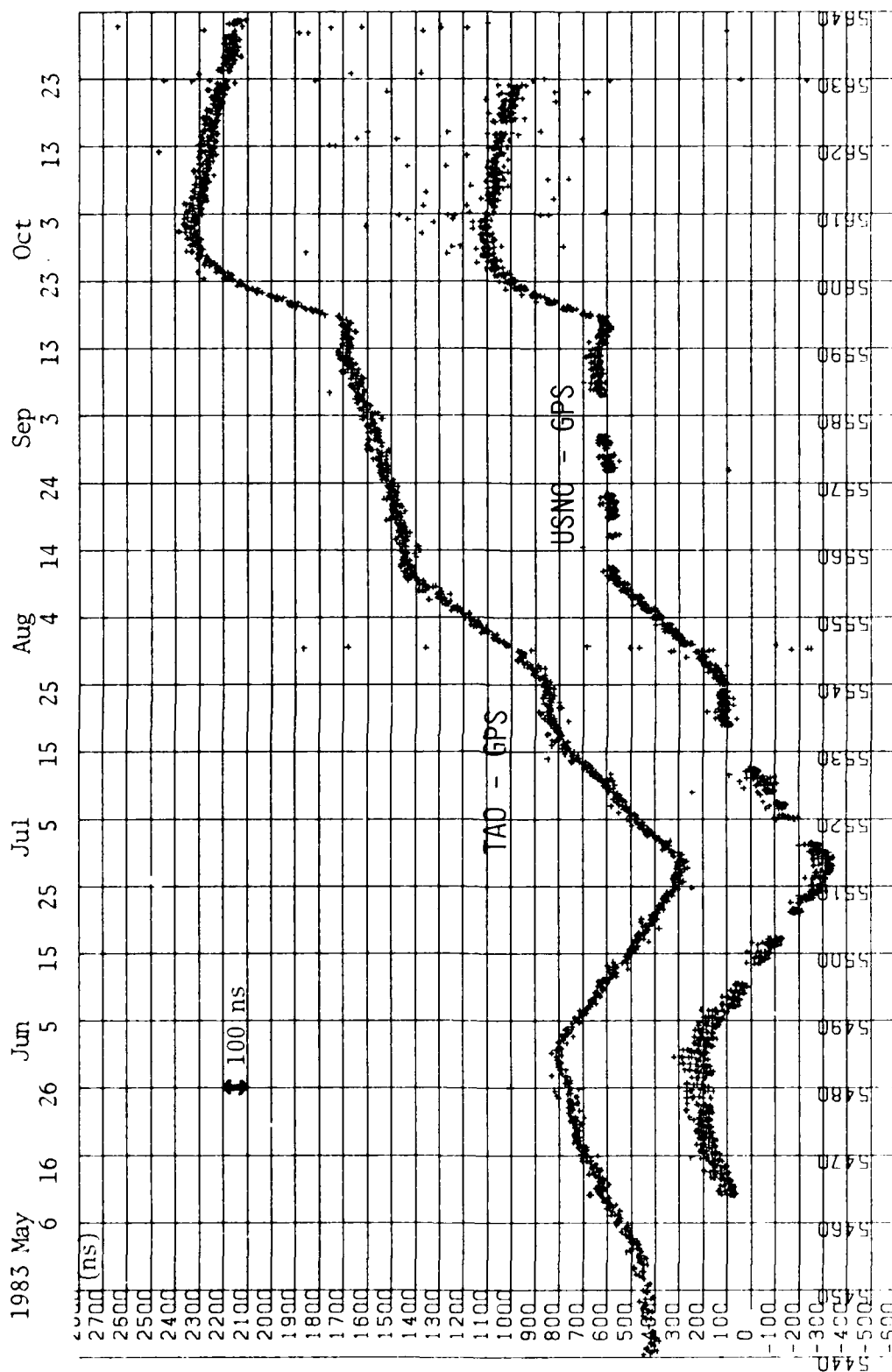


FIGURE 3 UTC(TAO)-GPS AND UTC(USNO)-GPS BY GPS TIME TRANSFER

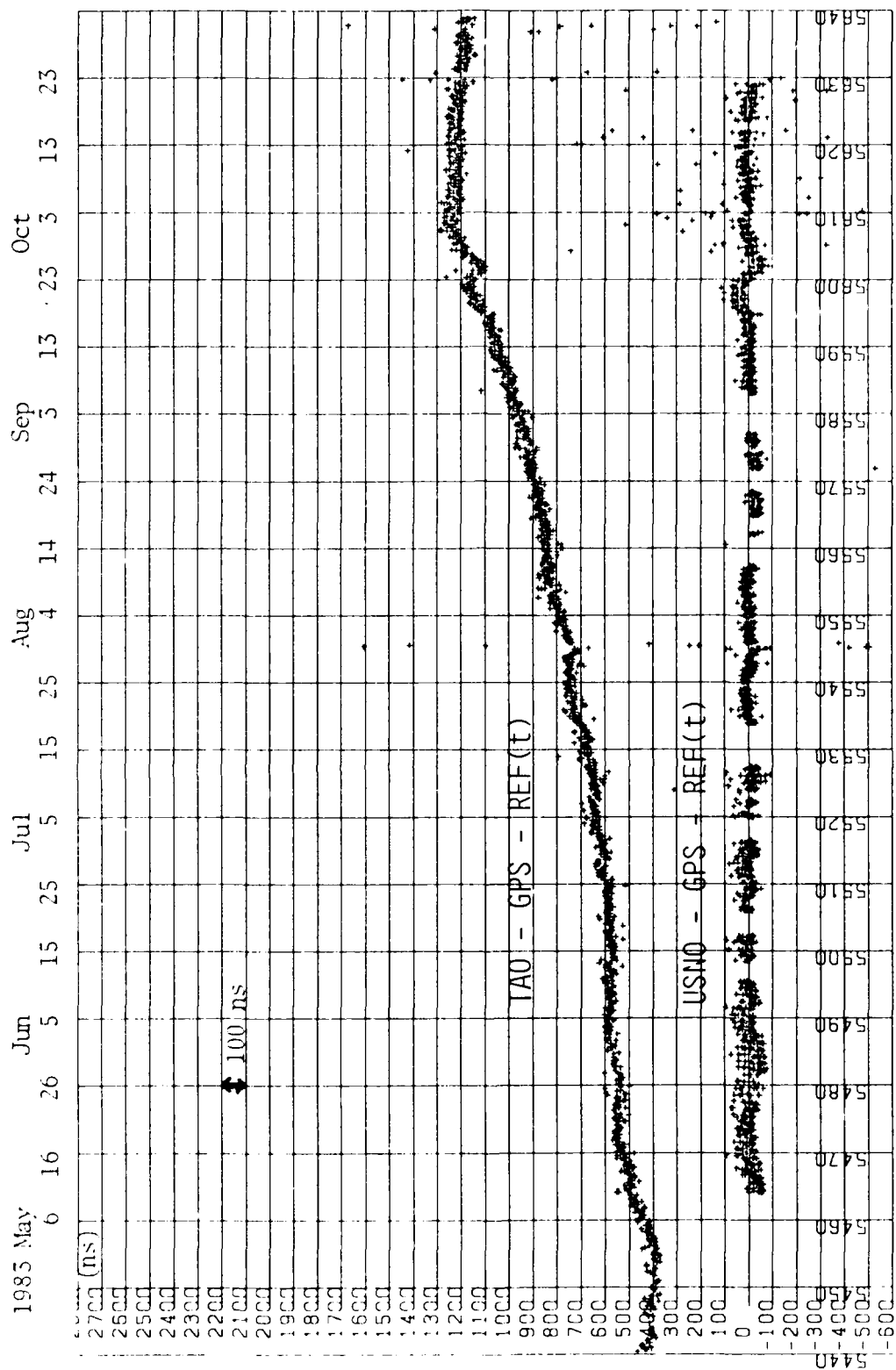


FIGURE 4 APPROXIMATION OF UTC(TAO) - UTC(USNO)

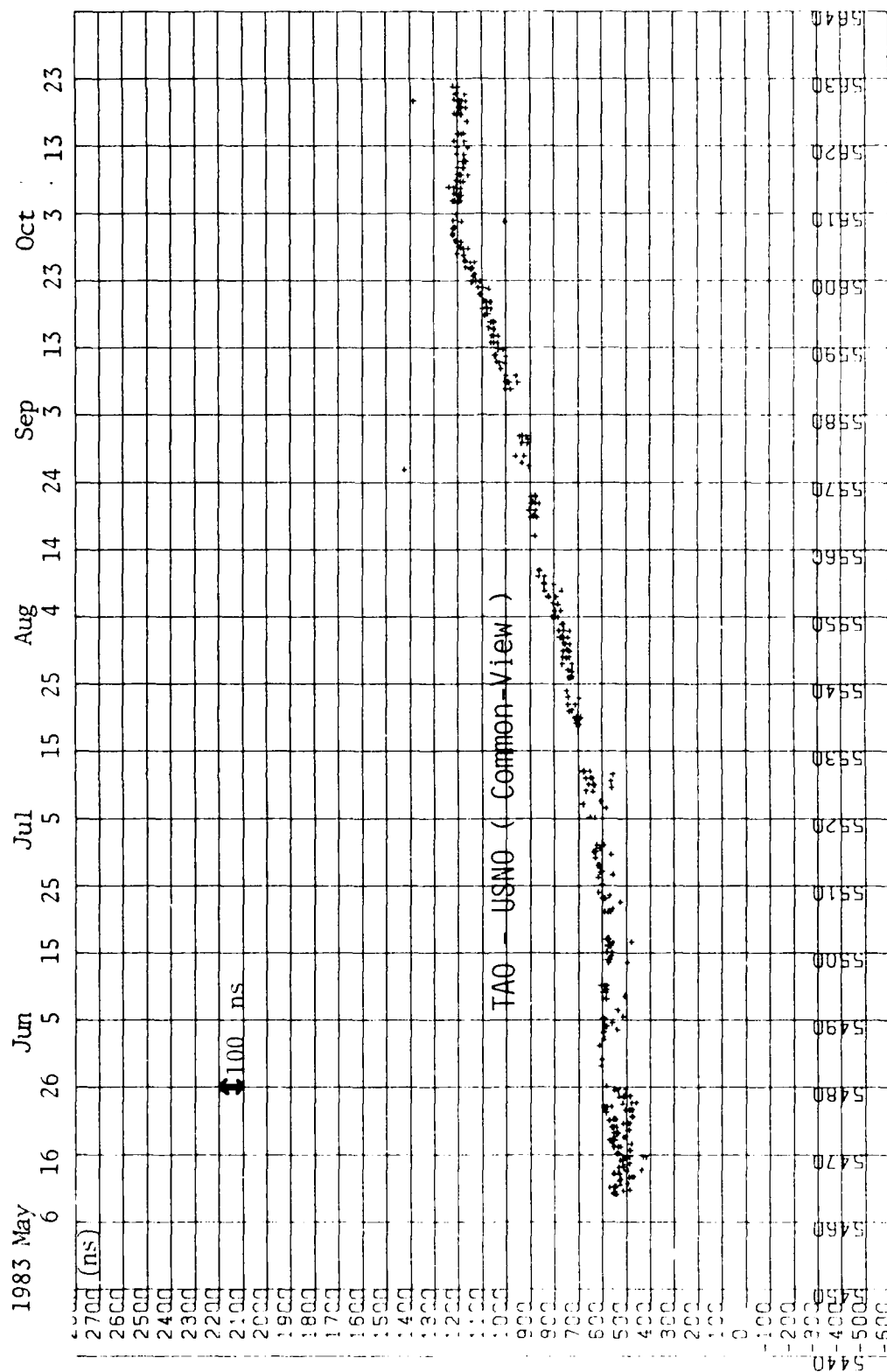


FIGURE 5 UTC(TAO) - UTC(USNO) FROM COMMON-VIEW RECEPTIONS

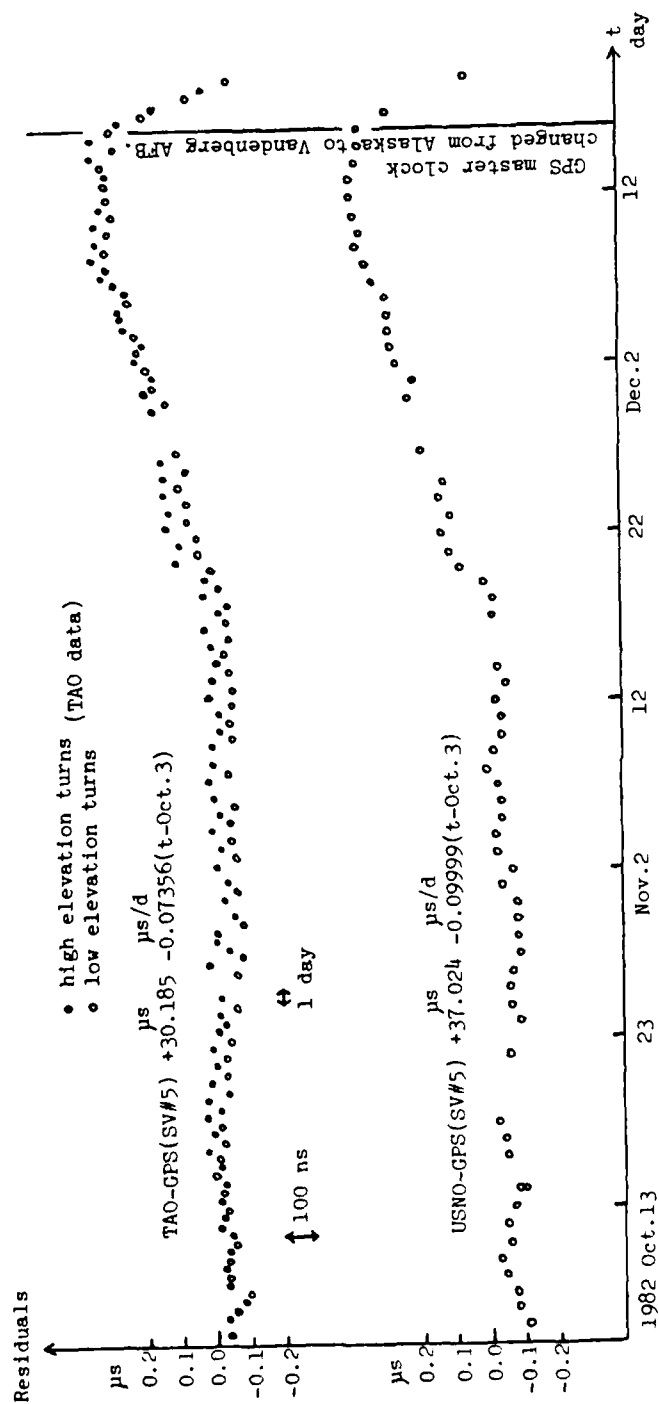


FIGURE 6 RESIDUALS OF A LINEAR FIT FOR GPS DATA DURING A TEST RUN

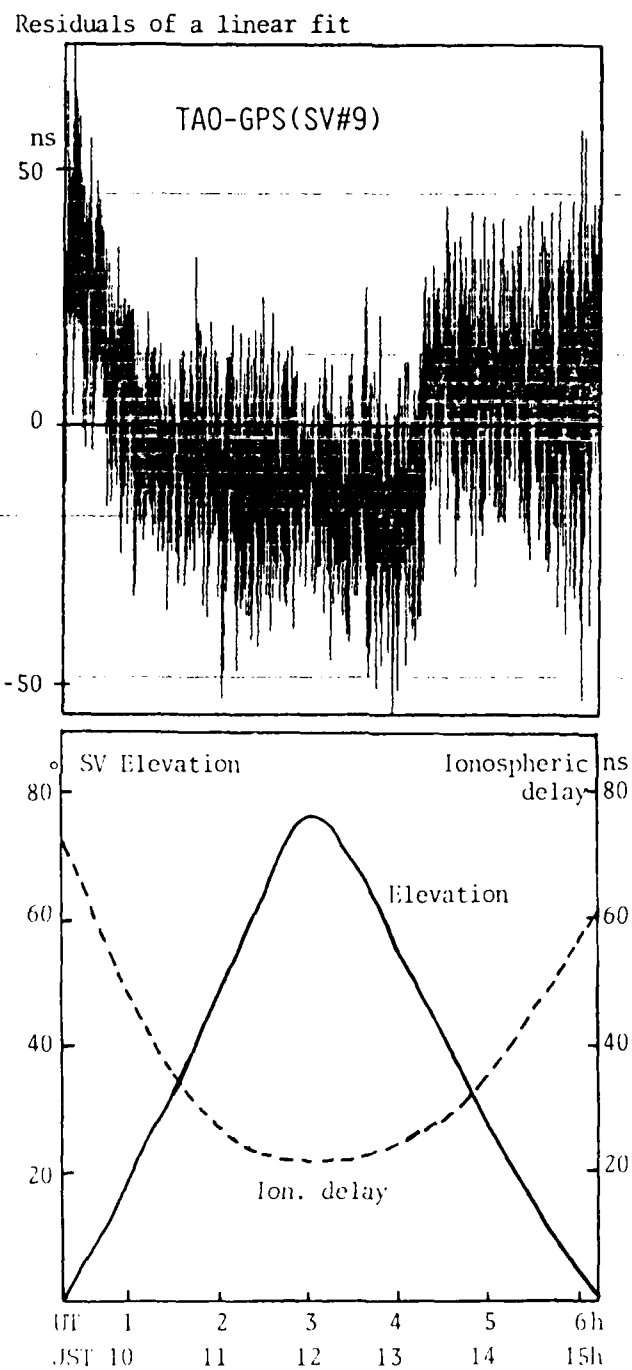


FIGURE 7 RAW DATA OF UTC(TAO)-GPS (6 HOURS TRACKING)

Paper #6 was not given.

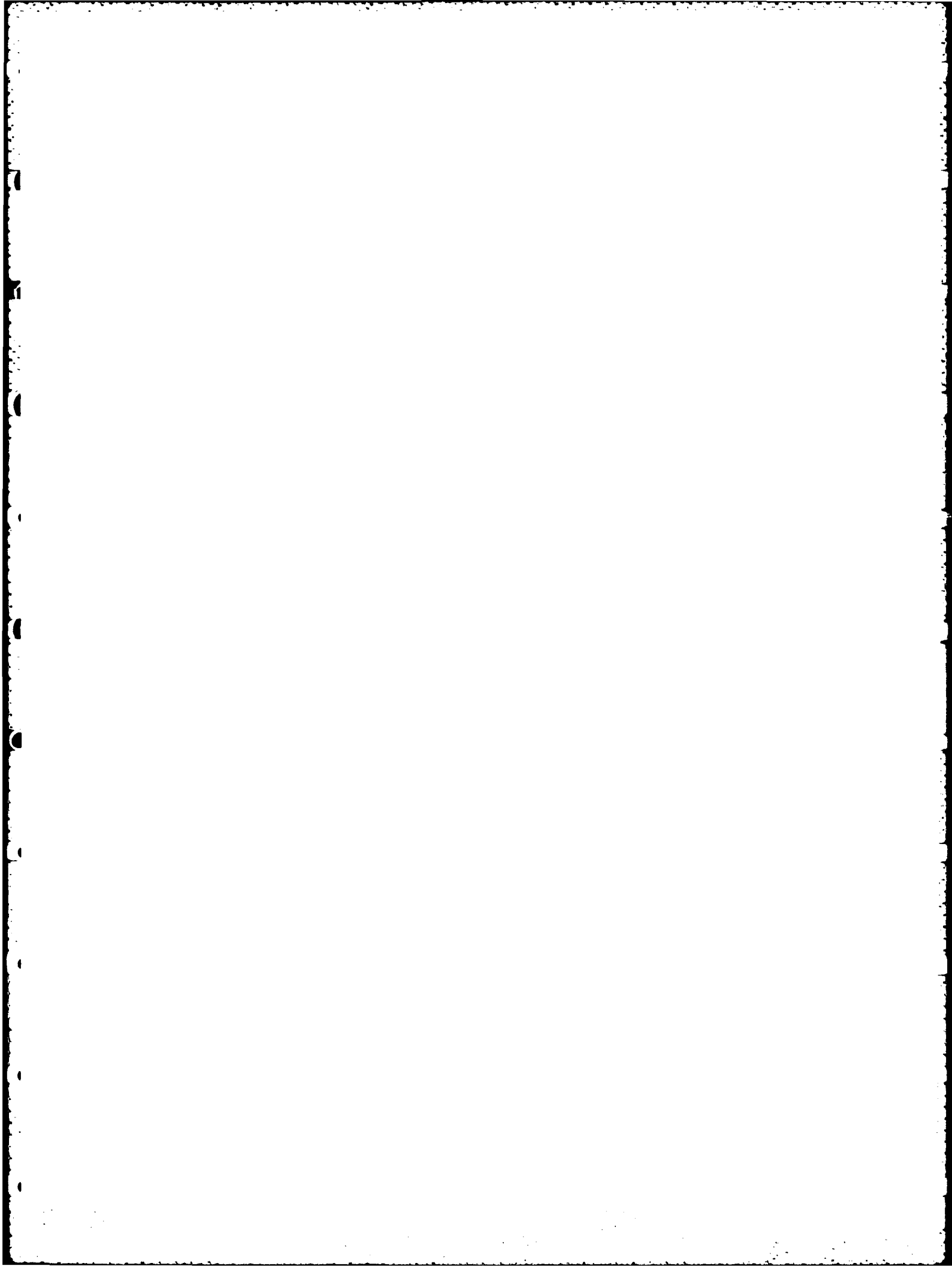
SESSION II

GPS TIME TRANSFER

Capt. Demosthenes Galanos, Chairman
United States Air Force
Airforce Space Division

CALL TO SESSION II

DR. REINHARDT: As you can see, Captain Galanos is not here, so they have asked me to take his place. We have a very tight session this afternoon. There are lots of papers and it looks very interesting. We may have to cut short the questioning period because of time constraints.



FIRST RESULTS OF GPS TIME TRANSFER TO AUSTRALIA

John McK. Luck and John R. Woodger, Division of National Mapping, Canberra, ACT, Australia, James E. Wells and Peter N. Churchill, DSS42/43, Tidbinbilla, ACT, Australia and Philip A. Clements, Jet Propulsion Laboratory, Pasadena, California.

ABSTRACT

A GPS time transfer unit built by NBS under contract to JPL was installed at Tidbinbilla Deep Space Communications Complex of the NASA Deep Space Network in June 1983. It has been used to estimate the relationship to UTC(USNO MC) of the Tidbinbilla frequency and time system TID(FTS) based on a hydrogen maser, and thence to estimate the performance of the Australian free-running time scale UTC(AUS). Data from the first three months has been analysed three ways: by two-hop "common view" using JPL as intermediary; by "long-arc" interpolation of measurements against space vehicle clocks; and by "long-arc" interpolation of GPS-Time results. Residuals from a single quadratic fit through three months of UTC(USNO MC) - TID(FTS) results were white noise with standard error 15 ns, and a flying clock measurement gave 70 ns agreement. A straight line fit through results UTC(USNO MC) - UTC (AUS) gave 90 ns standard error and 120 ns agreement. It is proposed to use the GPS measurements to steer UTC(AUS) to UTC(BIH), and to rename the existing time scale TA(AUS).

INTRODUCTION

A Global Positioning System (GPS) Time Transfer Unit (TTU) built by US National Bureau of Standards (NBS) for the NASA Deep Space Network (DSN) was installed at NASA's Deep Space Communications Complex 42/43 at Tidbinbilla (TID) in late June 1983. It was turned on in July and has operated correctly from that moment. Its principal function of interest here is to monitor the performance of the Tidbinbilla Frequency and Time System (TID(FTS)) which was derived from a SAO Model VLG11 hydrogen maser P14 during the period to November 1983. The basic results recorded are the time intervals between TID(FTS) 1 pps and the timing marks broadcast from the clocks on board each GPS space vehicle (SV), corrected in real time for propagation delay calculated from the on-board ephemeris transmitted by each SV and an assumed position for the antenna:

AD-A149 163

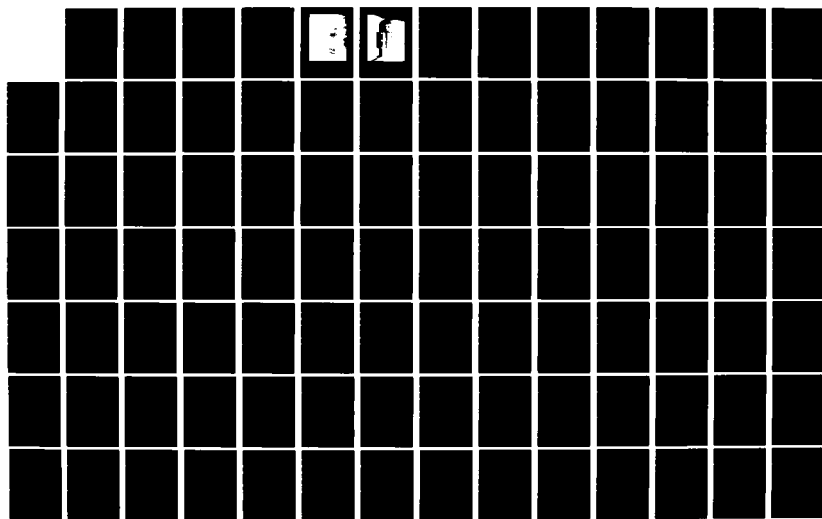
PROCEEDINGS OF THE ANNUAL PRECISE TIME AND TIME
INTERVAL (PTTI) APPLICATI. (U) NAVAL RESEARCH LAB
WASHINGTON DC J A MURRAY 02 APR 84

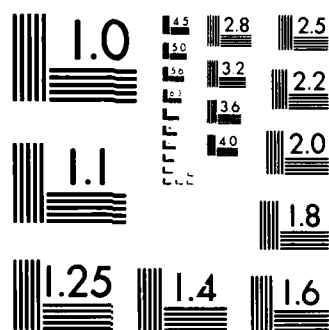
2/8

UNCLASSIFIED

F/G 5/9

NL





MICROCOPY RESOLUTION TEST CHART
NATIONAL BUREAU OF STANDARDS-1963-A

λ = 148°58'48"2018 E

ϕ = 35°24' 8"0444 S

h = 665.54 m

Also available is the time comparison between TID(FTS) and the GPS master clock (GPS TIME) in the GPS Control Segment [Kovach, 1981]. Generally two passes from each of space vehicles 5, 6, 8 and 9 are observed each day, of which only the higher altitude passes are used in this analysis.

Similar results are obtained on each SV at the US Naval Observatory (USNO) referred to their Master Clock (UTC(USNO MC)), although at different times in the day, and made available through the bulletin Series 4: Daily Phase Values, and otherwise. Time transfer between UTC (USNO MC) and TID(FTS) is obtained by linear interpolation to the time of a Tidbinbilla observation between two adjacent reported USNO observations, usually but not always one sidereal day apart. In this paper, data gaps up to two days are tolerated, and only linear interpolations are employed, hence it is tacitly assumed that on-board clock behaviour is linear over a day or two and that receiving antennae locations and broadcast orbital parameters are accurate. Because of the appreciable interpolating factors, this method is here designated "long arc" and is applied to results obtained both from SV observations and GPS TIME results.

The "common view" method in which both stations take measurements simultaneously [Davis et al, 1981; Clements, 1982] is impossible between Tidbinbilla and USNO and difficult between Tidbinbilla and Jet Propulsion Laboratory (JPL). Nevertheless a two-hop quasi-"common-view" experiment has been attempted, with a GPS TTU at JPL taking nearly simultaneous observations with Tidbinbilla on the one hand, and nearly simultaneous observations with USNO on the other. The effectiveness of the time transfer then depends on the behaviour of the JPL Frequency and Time System between the two sets of observations which may be several hours apart.

Since four satellites were available, and more can be expected, the opportunity exists for averaging. This has been done by interpolating linearly to 0^h UTC between adjacent time transfer results from each satellite prior to taking the mean. This process yields a "consolidated" result.

THE TIDBINBILLA GPS SYSTEM

Equipment

The GPS equipment installation at the Canberra Deep Space Communication Complex (CDSCC), Tidbinbilla is depicted in Figure 1. All of the equipment with the exception of the antenna unit is mounted in a short rack adjacent to the CDSCC frequency and timing system (FTS) monitor panel in the operations building (Figure 2). The antenna unit, which also includes a low noise amplifier and mixer, is a sealed enclosure located on the roof of the operations building (Figure 3).

The antenna position was obtained by carrying out a traverse from the surveyed ground monument position beneath the DSS 42 34 metre antenna. A receiver offset of 272 nanoseconds was inserted in the GPS software to correct for the delay due to cable length between antenna unit and receiver.

A 5 MHz signal is provided from the FTS as a reference frequency from which is derived the receiver 100 MHz to supply the first I.F. mixer in the antenna unit. D.C. power is also run through the 100 MHz coax cable, avoiding the requirement to provide a separate power cable. A 1 PPS signal is also connected from the FTS to provide the CDSCC clock reference to the system.

A modem phone is connected to an RS 232 port of the microprocessor to allow data acquired and stored by the system to be transmitted periodically by telephone to JPL, usually once a week. Data from a remote receiver may also be printed out locally using this modem link.

Operation of GPS Receiver

The GPS receiving system is capable of running in an automatic mode, once all relevant parameters have been entered. In this mode, the system will acquire chosen space vehicles, lock onto the downlink and accumulate relevant data. The system is normally operated in the automatic mode at DSS 43.

The software/operator interface consists of a "user friendly", menu-driven parameter selection matrix, arranged in the form of one main menu and a number of sub-menus.

In order to bring the system up to a functioning condition, it is necessary to perform a "cold start" operation. This consists of instructing the system to acquire an almanac from a satellite when such a vehicle is within reception range (usually above horizon). It is also necessary to set the system's internal UTC clock by responding to the system prompts. Under normal operating conditions, a battery back-up supply maintains the system's RAM such that a cold start is not necessary even in the event of a power failure.

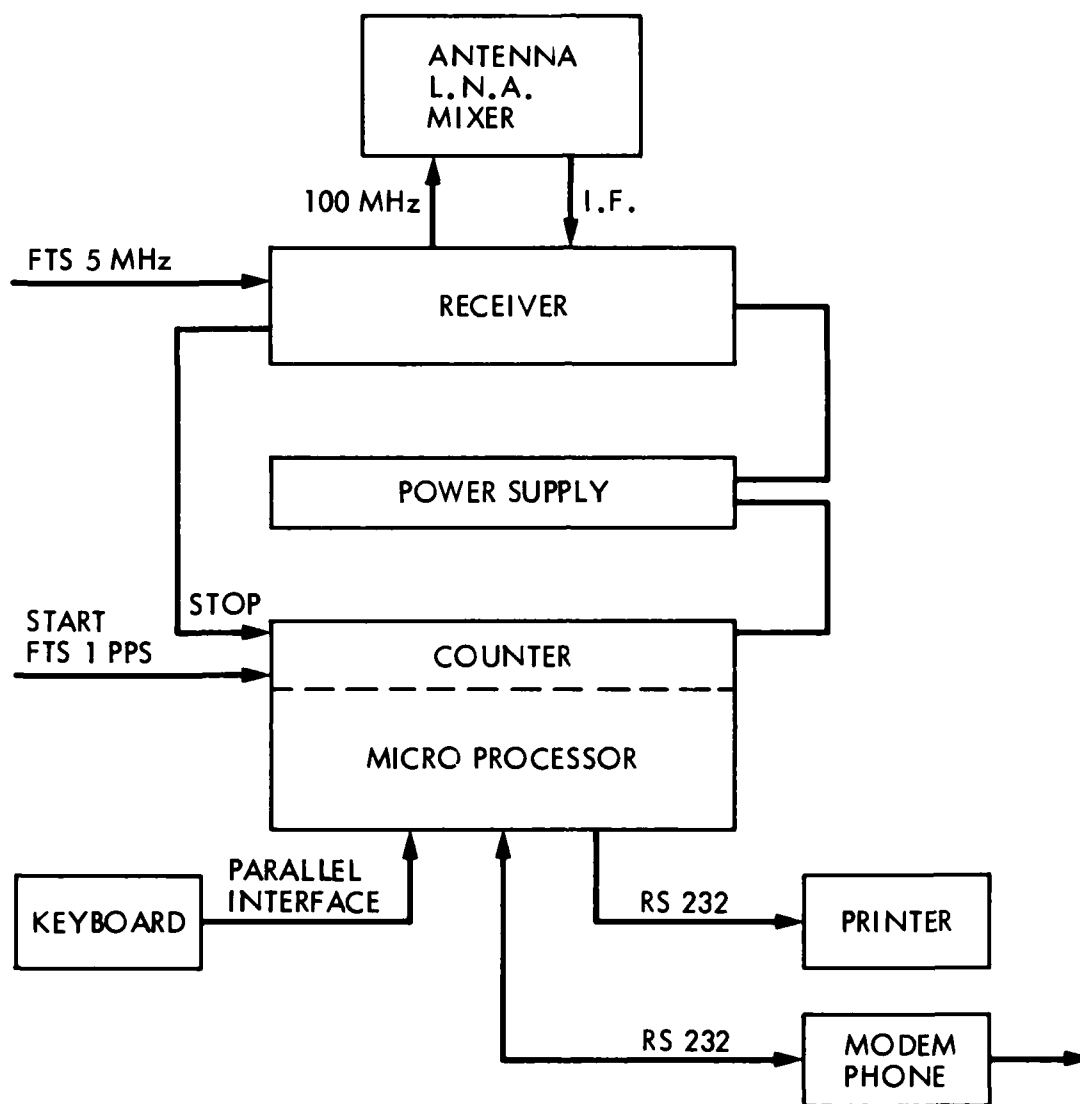


Figure 1. GPS equipment configuration at Canberra Deep Space Communications Complex, Tidbinbilla.



Figure 2. GPS receiver installation at Tidbinbilla.

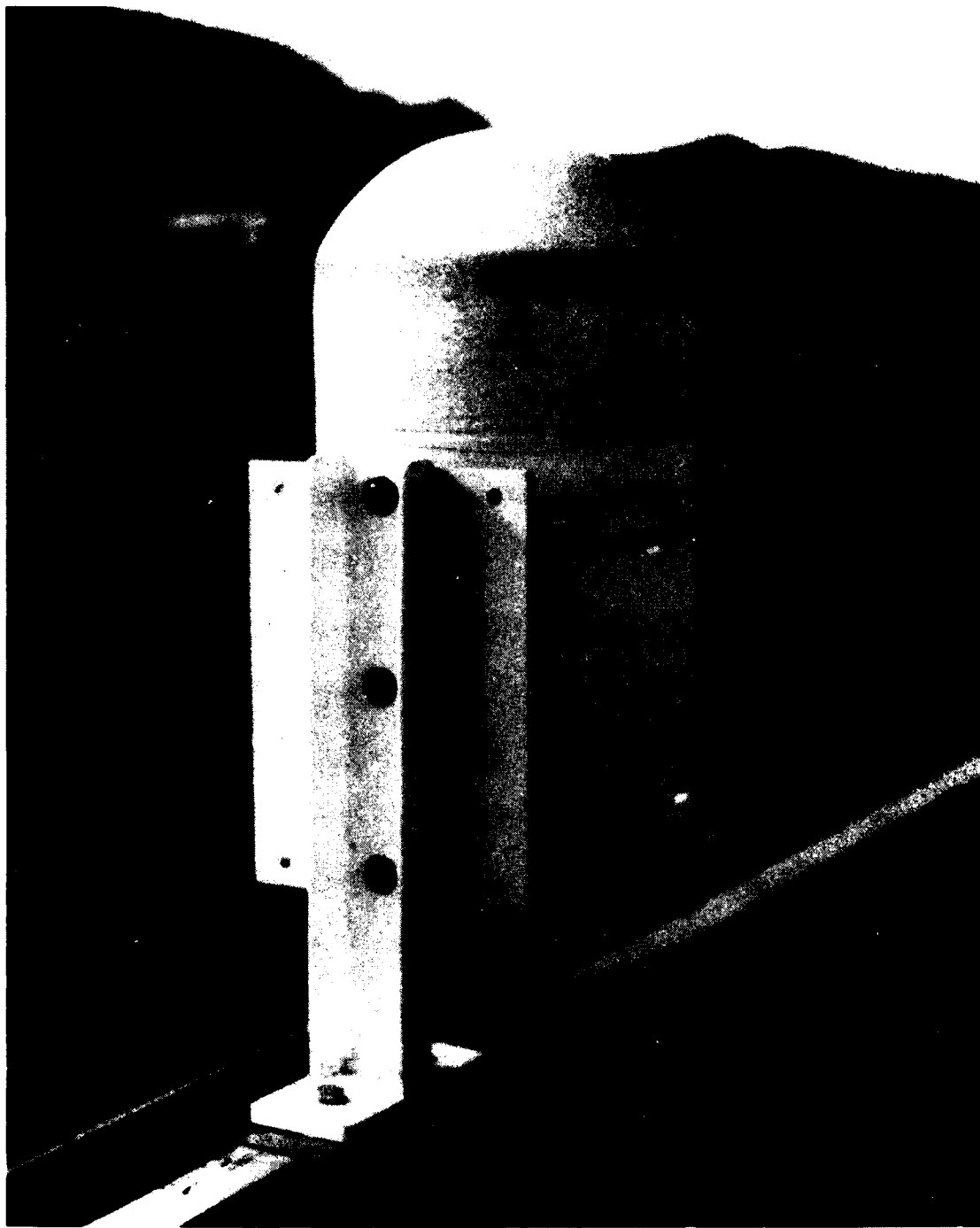


Figure 3. GPS antenna housing on roof of CDSCC.

The system software provides an aid to the selection of suitable satellites for tracking purposes. If selected, the system will print a graph of elevation and azimuth versus time for up to five vehicles, dependent, of course, on the system's knowledge of its present location. This parameter may be entered by calling up the NEW RECEIVER COORDINATES feature on the displayed menu.

Having selected suitable satellites to track, appropriate track times may be entered, derived from the aforementioned graph. The facility exists to cause the system to decrement the track start times by 4 minutes per day to account for the fact that the satellites are in sidereal orbits. The satellite may then be tracked in the same position in the sky each day.

The system may be commanded to perform position location calculations by one of two methods. The first method requires that four satellites be in view so that data of sufficient precision may be obtained for the navigation solution. The second method requires that the system lock sequentially onto four satellites every two minutes. This second method produces a solution in a shorter time than the former and has the advantage of eliminating much of the short term noise in the local clock system.

The GPS measurement computation is performed by calculating a pseudo-range value from system counter measurements and then computing the slant range, relativistic and ionospheric corrections based on data obtained from the satellite ephemeris. These corrections, along with the local receiver delay, are subtracted from the pseudo-range estimate to obtain the local clock minus satellite clock value. The satellite clock correction, transmitted from the vehicle is then added to this value to produce a figure for local clock minus GPS clock.

TABLE 1
Quadratic Fits to Observations on Satellite Clocks

Observation	Offset(a) μs	Rate(b) $\mu\text{s/d}$	Drift/2(c) $\mu\text{s/d/d}$	Av Time(\bar{t}) MJD	Std Error(σ) μs
TID(FTS)-SV(5)	188.236	0.213022	0.00009463	5571.18	0.01
TID(FTS)-SV(9)	15.809	0.075300	0.00022562	5572.31	0.01
UTC(USNOMC)-SV(5)	180.642	0.144689	-0.00009541	5575.53	0.05
UTC(USNOMC)-SV(9)	7.562	0.007514	0.00004740	5575.20	0.03

SPACE VEHICLE AND GPS TIMES

The results produced by Tidbinbilla's GPS TTU are, for each SV(i), numbers in the form TID(FTS) - SV(i) and TID(FTS) - GPS TIME via SV(i). The corresponding numbers disseminated by USNO are UTC(USNO MC) - SV(i) and UTC (USNO MC) - GPS TIME via SV(i). It has been found that the "raw" results TID-SV and USNO-SV are adequately modelled by quadratic curves over the interval MJD 5528-5618 for SV(5) and SV(9), while cubic or higher-order fits would be required for SV(6) and SV(8). The parameters of the quadratics are given in Table 1 in the form:

$$\text{TID(FTS)} - \text{SV}(i) = a(i) + b(i) * (t - \bar{t}) + c(i) * (t - \bar{t})^2 \quad (1)$$

and similarly for UTC(USNO MC) - SV(i), where $a(i)$ is the offset at the mean time \bar{t} , $b(i)$ is the rate at \bar{t} and $c(i)$ is half the drift rate. The standard errors of residuals $\sigma(i)$ are also tabled, and the residuals are displayed in Figures 4 and 5. Both graphs have many features in common, demonstrating that vagaries in on-board clock behaviour are readily detectable.

Several rate changes were observed to occur in GPS time in the interval considered, so the results were broken in to four segments and straight lines fitted through each as shown in Tables 2 and 3. The residuals are displayed all together in Figures 6 and 7, where it can be seen that results are rather better at USNO than at Tidbinbilla which is possibly a consequence of efforts made at the GPS master station to follow USNO time.

LONG-ARC TIME TRANSFER TO USNO

Time transfer from USNO to Tidbinbilla was achieved by linearly interpolating between successive daily results UTC(USNO MC) - SV(i), and subtracting the observed value of TID(FTS) - SV(i) from it. It was felt that it was better to use the USNO results to interpolate on since its time scale is the reference being accessed and is therefore to be considered definitive for these purposes. Linear interpolation was adequate and in fact desirable since the effects of drift rate over one or two days are swamped in the random noise. The "consolidated" result is shown in Figure 8, on which is also shown the value

$$\text{UTC(USNO MC)} - \text{TID(FTS)} = - 11.030 \mu\text{s}$$

by USNO/Bendix flying clock on 1 October 1983.

TABLE 2
Straight Line Fits to TID(FTS)-GPS TIME

SV#	Offset(a) μs	Rate (b) $\mu\text{s/d}$	Av.Time(\bar{t}) MJD	Std.Error(σ) μs	Smoothed Between	
5	5.861	0.08233	5530.75	.02	5528	5532
6	5.874	0.05275	5530.78	.03	5528	5532
8	5.887	0.07441	5531.21	.03	5528	5532
9	5.812	0.07190	5530.86	.02	5528	5532
5	6.282	0.05981	5537.74	.04	5532	5542
6	6.296	0.06118	5537.77	.02	5532	5542
8	6.293	0.06123	5537.69	.02	5532	5542
9	6.287	0.06314	5538.17	.02	5532	5542
5	7.269	0.08851	5549.99	.01	5542	5556
6	7.280	0.09221	5550.01	.02	5542	5556
8	7.265	0.09207	5549.66	.02	5542	5556
9	7.221	0.08997	5549.80	.03	5542	5556
5	8.979	0.06995	5573.14	.04	5556	5589
6	9.010	0.07002	5573.16	.02	5556	5589
8	9.017	0.09669	5572.96	.02	5556	5589
9	8.962	0.07134	5573.24	.03	5556	5589
5	10.339	0.06487	5592.08	.03	5589	5594
6	10.368	0.07126	5592.11	.01	5589	5594
8	10.377	0.06552	5592.04	.02	5589	5594
9	10.327	0.06830	5592.19	.02	5589	5594
5	11.060	0.14007	5598.07	.03	5594	5601
6	11.094	0.13991	5598.09	.03	5594	5601
8	11.102	0.14669	5598.02	.03	5594	5601
9	11.047	0.14017	5598.17	.03	5594	5601
5	11.763	0.08500	5604.35	.02	5601	5607
6	11.806	0.08724	5604.37	.02	5601	5607
8	11.846	0.08914	5604.44	.02	5601	5607
9	11.754	0.09100	5604.45	.02	5601	5607
5	12.401	0.07943	5612.08	.02	5607	5618
6	12.431	0.07593	5612.25	.02	5607	5618
8	12.455	0.07508	5612.18	.02	5607	5618
9	12.384	0.07606	5612.33	.01	5607	5618

TABLE 3
Straight Line Fits to UTC(USNOMC)-GPS TIME

SV#	Offset(a) μs	Rate (b) $\mu\text{s/d}$	Av.Time(\bar{t}) MJD	Std.Error(σ) μs	Smoothed Between	
5	0.054	0.02183	5529.91	.02	5528	5532
6	0.075	0.01957	5530.83	.01	5528	5532
8	0.078	0.02276	5531.24	.02	5528	5532
9	0.054	0.02202	5529.99	.01	5528	5532
5	0.115	0.00188	5537.00	.01	5532	5542
6	0.127	0.00565	5537.76	.01	5532	5542
8	0.108	0.00003	5537.70	.03	5532	5542
9	0.114	0.00349	5536.98	.01	5532	5542
5	0.360	0.03048	5549.50	.01	5542	5556
6	0.388	0.02952	5550.24	.01	5542	5556
8	0.392	0.03226	5549.92	.02	5542	5556
9	0.394	0.03135	5549.98	.02	5542	5556
5	0.630	0.00270	5582.29	.01	5556	5589
6	0.610	0.00207	5582.30	.02	5556	5589
8	0.619	0.00197	5582.36	.02	5556	5589
9	0.619	0.00197	5582.35	.02	5556	5589
5	0.637	0.00948	5592.45	.03	5589	5594
6	0.613	0.00622	5592.39	.03	5589	5594
8	0.639	-0.01150	5592.44	.01	5589	5594
9	0.620	0.00693	5592.44	.03	5589	5594
5	0.911	0.05304	5598.45	.02	5594	5601
6	0.886	0.05647	5598.37	.02	5594	5601
8	0.920	0.05879	5598.43	.06	5594	5601
9	0.897	0.05507	5598.42	.02	5594	5601
5	1.101	0.00862	5604.94	.02	5601	5607
6	1.087	0.00853	5604.85	.01	5601	5607
8	1.109	0.00625	5604.86	.01	5601	5607
9	1.090	0.00695	5604.91	.01	5601	5607
5	1.084	-0.00690	5613.41	.01	5607	5618
6	1.074	-0.00405	5613.61	.02	5607	5618
8	1.091	-0.00438	5613.64	.01	5607	5618
9	1.081	-0.00383	5613.35	.02	5607	5618

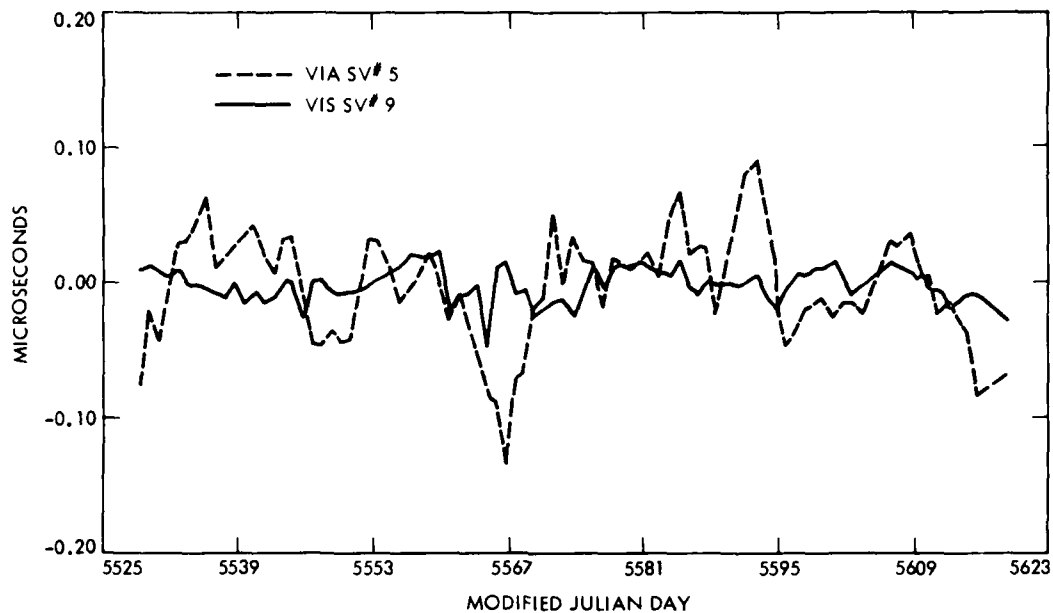


Figure 4. Residuals from quadratic fits through raw data
TID(FTS)-SV TIME, space vehicles 5 and 9 (see Table 1).

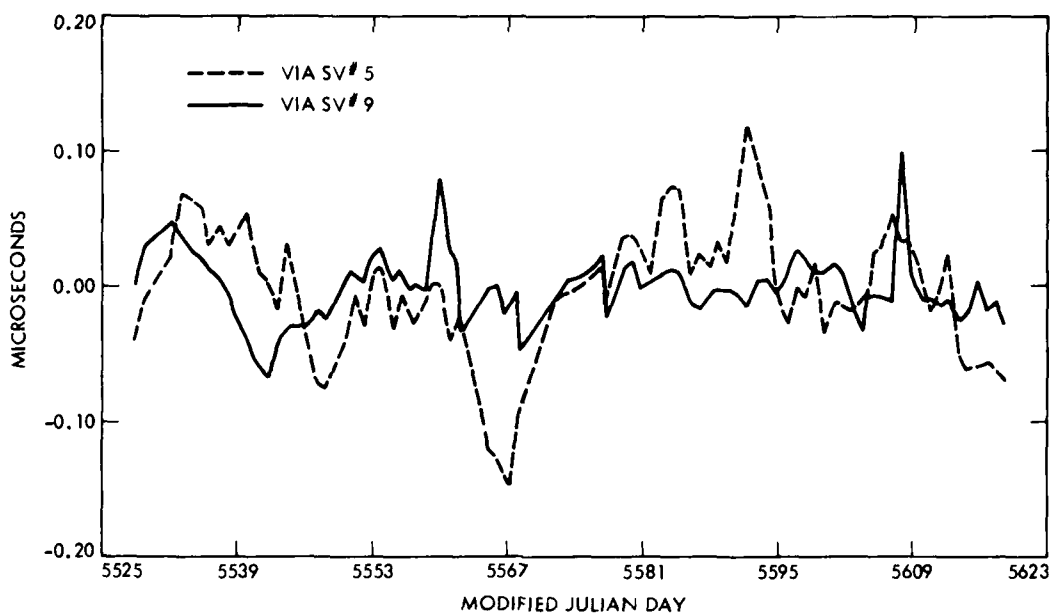


Figure 5. Residuals from quadratic fits through raw data UTC(UNSNO,MC)
-SV TIME, space vehicles 5 and 9 (see Table 1).

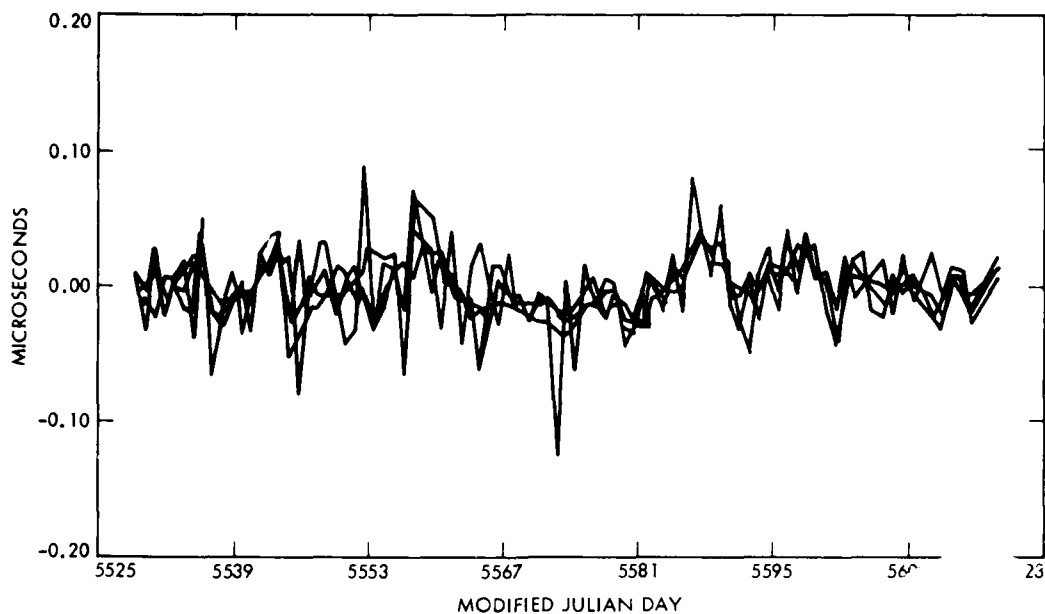


Figure 6. Residuals from straight line fits through raw TID(FTS)-GPS TIME, space vehicles 5, 6, 8, 9 segmented at MJDs 5532, 5542, 5556, 5589, 5594, 5601, 5607 and 5618 (see Table 2).

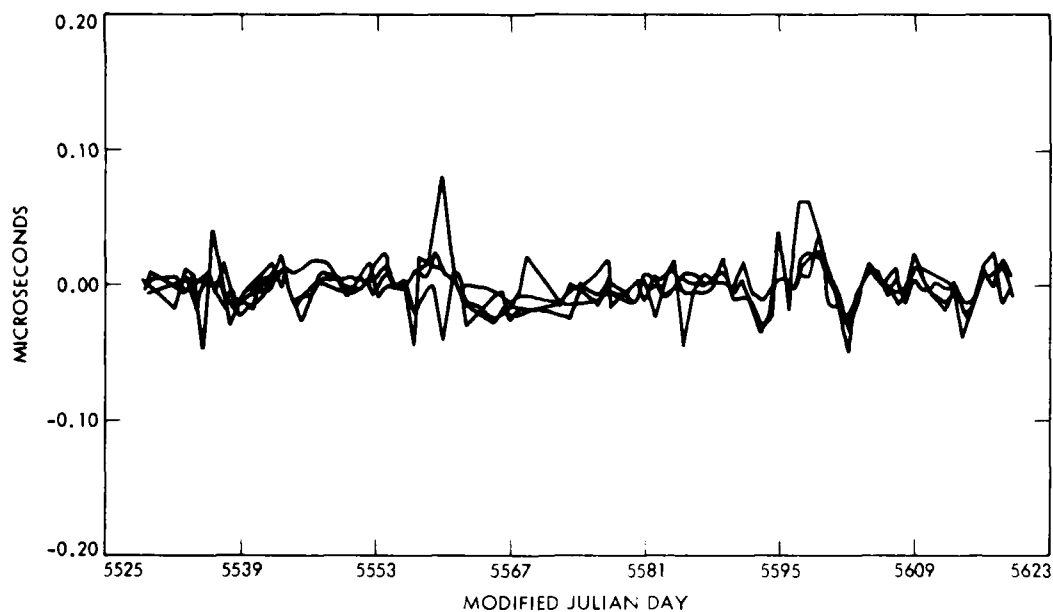


Figure 7. Residuals from straight line fits through raw data UTC(USNO,MC)-GPS TIME via space vehicles 5, 6, 8, 9, as in Figure 6 (see Table 3).

Quadratic curves in the same form as equation (2) were fitted to the outcomes using each space vehicle separately. Their parameters are given in Table 4, and the residuals therefrom are shown in Figure 9. Residuals from the "consolidated" time transfer are shown in Figure 10, and the Allan variances of these residuals are displayed in Figure 11 in which the slope is close to -1, indicating that the residuals after removal of the quadratic are very nearly random uncorrelated "white" phase noise.

Almost identical results are obtained when transfer is effected via GPS TIME instead of SV TIME. Table 4 contains their quadratic parameters. Figure 12 shows their consolidated Allan variances, Figure 13 the individual residuals and Figure 14 the consolidated residuals.

From this analysis, the drift rate of the Tidbinbilla hydrogen maser with respect to UTC(USNO MC) is -4 parts in 10^{15} per day, and is undoubtedly now well measured: the drift rate itself has not changed during three months.

COMMON VIEW MEASUREMENTS

The results given above show quite clearly that the GPS receivers can detect anomalies in the on-board clocks and in GPS TIME as small as 10 ns or less, so simultaneous observations should remove their effects. The geographical locations of Tidbinbilla and USNO make "common view" observations impossible, so a two-hop scheme is necessary. In this, the GPS TTU at JPL's Goldstone Radar Net (GRN) has been taking measurements at the same time as USNO (to within ten minutes) and also at the same time as Tidbinbilla (to within one minute) each day. The hydrogen maser based timing system at GRN has a rate of about 20 ns/day but is assumed here to be error-free in relating the two sets of measurements. Then:

$$\text{UTC(USNO MC)} - \text{TID(FTS)} = [\text{UTC(USNO MC)} - \text{JPL}] - [\text{TID(FTS)} - \text{JPL}] \quad (2)$$

Results from GPS TIME averaged over all space vehicles are shown in Figure 15, and residuals from the quadratic fit whose parameters are given in Table 4 are in Figure 16. Figure 17 shows the results in the vicinity of the 1 October flying clock measurement, while Figure 18 gives Allan variances after the quadratic curve has been removed.

Figure 19 copies Figures 10, 14 and 16 to show the residuals by each of the three methods on one graph. It can be seen that the "common view" results have some spikes not visible in the other results, but that otherwise the results are quite similar. It is noteworthy that the statistics given in Table 4 for "long-arc" using SV TIME and using GPS TIME are very similar, and differ by about 170 ns in offset and 2 ns/day in rate from the "common view" results whose standard error is also somewhat larger. It is therefore evident that the greater atmospheric effects caused by the "common view" method in this case outweigh the clock modelling errors of the "long arc" method.

TABLE 4
Quadratic Fits to UTC(USNO,MC)-TID(FTS)

Medium	Offset (a) μs	Rate (b) $\mu\text{s/d}$	Drift/2 (c) $\mu\text{s/d/d}$	Av. Time (T) MJD	Std. Error (σ) μs
SV(5)	-8.485	-0.06867	-0.0001853	5574.96	0.019
SV(6)	-8.334	-0.06841	-0.0001663	5572.08	0.010
SV(8)	-8.478	-0.06904	-0.0001788	5574.46	0.019
SV(9)	-8.510	-0.06924	-0.0001817	5575.86	0.022
All SV	-8.387	-0.06849	-0.0001764	5573.39	0.017
GPS TIME, SV(5)	-8.483	-0.06893	-0.0001872	5574.96	0.023
GPS TIME, SV(6)	-8.326	-0.06851	-0.0001752	5572.08	0.016
GPS TIME, SV(8)	-8.472	-0.06925	-0.0001896	5574.46	0.022
GPS TIME, SV(9)	-8.523	-0.06969	-0.0001830	5575.86	0.017
GPS TIME, All SV	-8.385	-0.06872	-0.0001869	5573.39	0.015
Common View	-8.559	-0.07054	-0.0001614	5573.50	0.023
UTC(USNO,MC)- UTC(AUS) Via					
GPS TIME, All SV	-12.19	-0.01680	0.0	5576.92	0.088

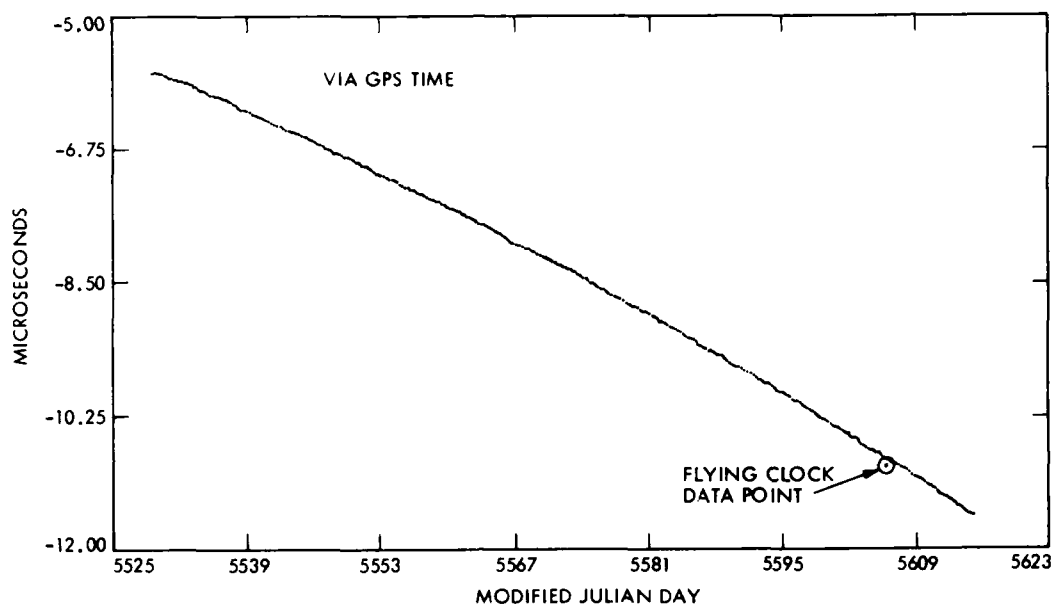


Figure 8. Interpolated UTC(USNO,MC)-TID(FTS) using GPS TIME from space vehicles 5, 6, 8, 9 together.

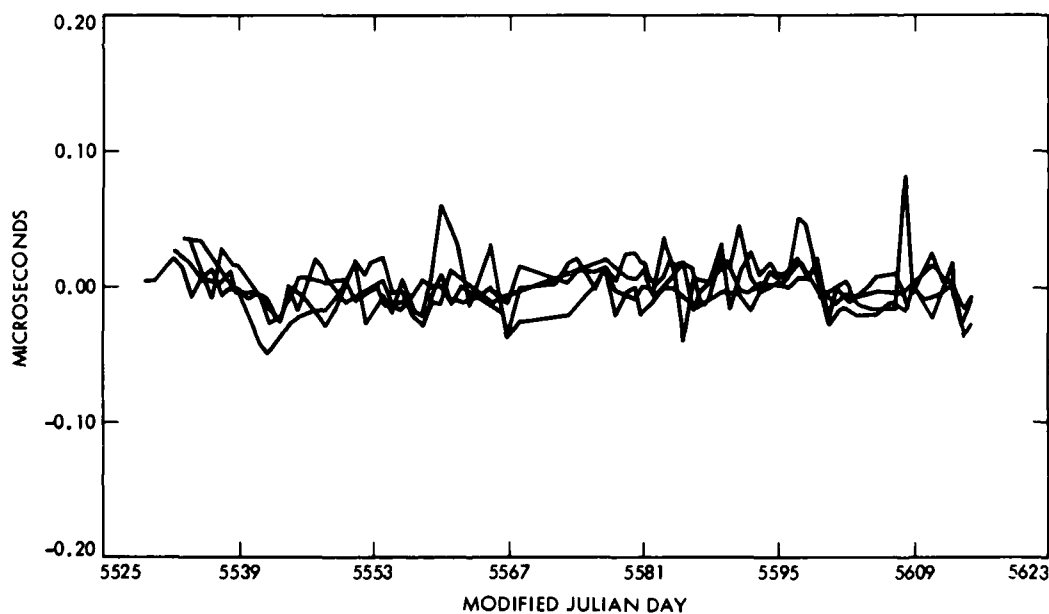


Figure 9. Residuals from quadratic fits through interpolated data UTC(USNO,MC)-TID(FTS), using SV TIME from space vehicles 5, 6, 8, 9 (see Table 4).

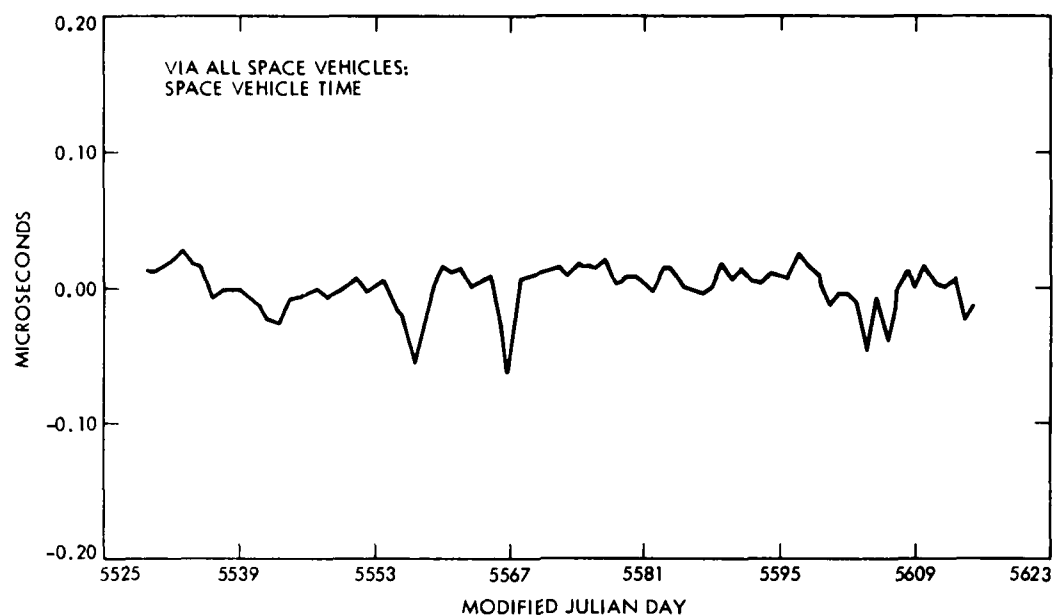


Figure 10. Residuals from quadratic fit through interpolated data UTC(USNO,MC)-TID(FTS) reduced to 0h UTC and averaged over SV TIME from space vehicles 5, 6, 8 and 9 (see Table 4).

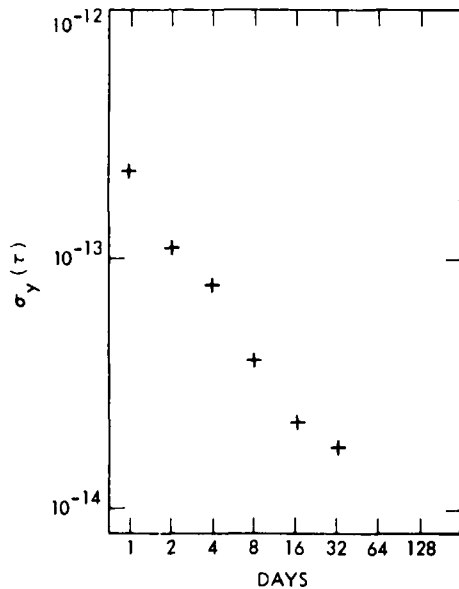


Figure 11. Allan variances of residuals in Figure 10.

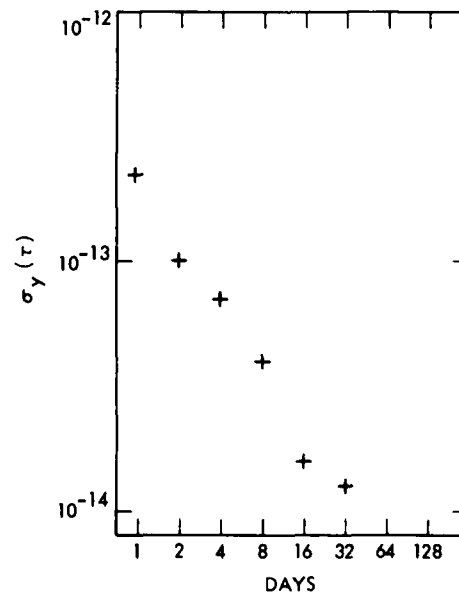


Figure 12. Allan variances of residuals in Figure 14.

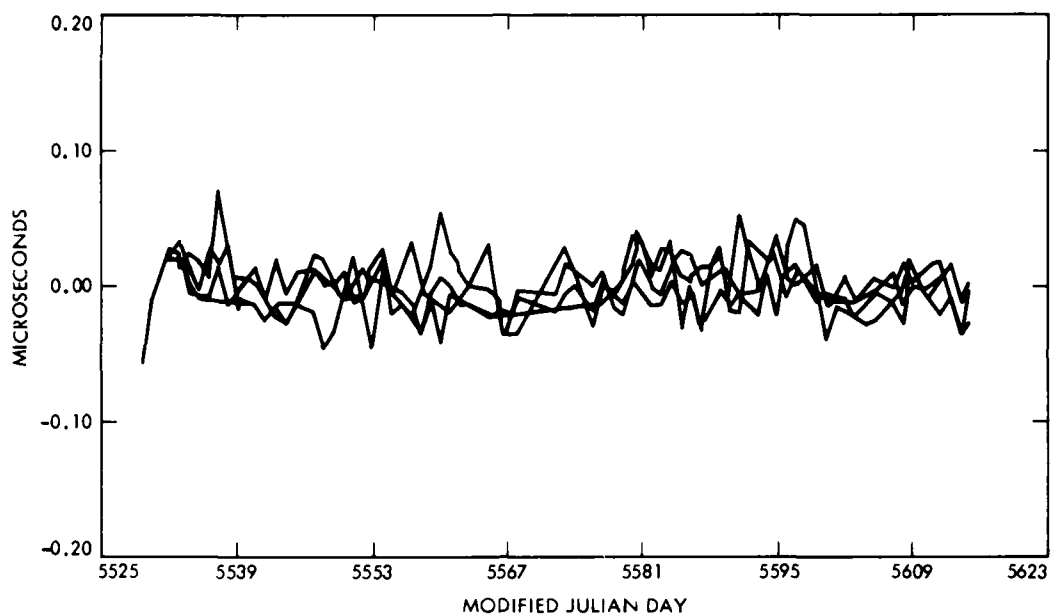


Figure 13. Residuals from quadratic fits through interpolated data UTC(USNO,MC)-TID(FTS) using GPS TIME from space vehicles 5, 6, 8 and 9 (see Table 4).

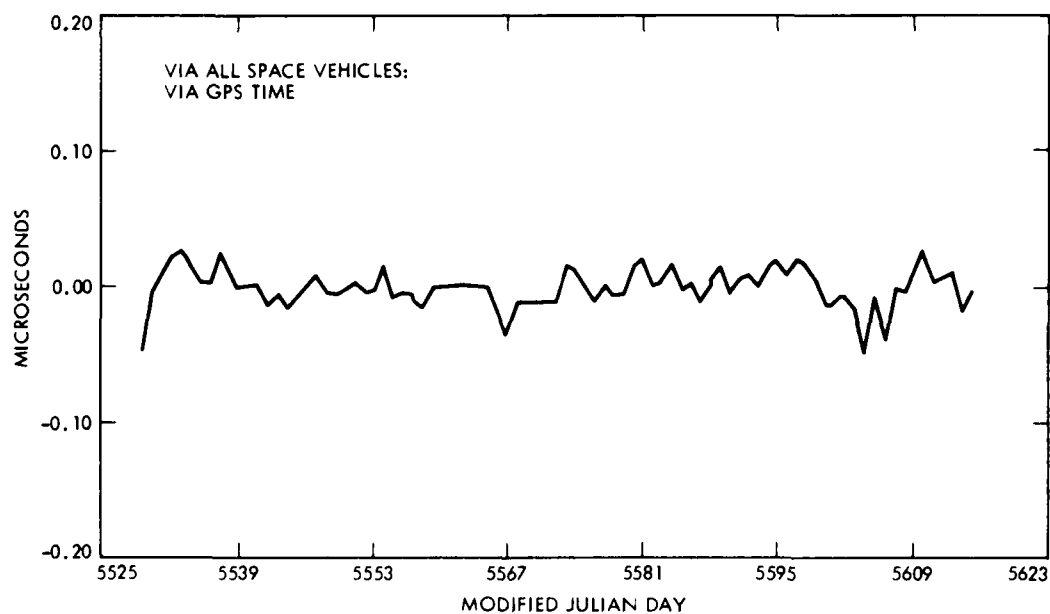


Figure 14. Residuals from quadratic fit through interpolated data UTC(USNO,MC)-TID(FTS) reduced to 0h UTC and averaged over GPS TIME from space vehicles 5, 6, 8 and 9 (see Table 4).

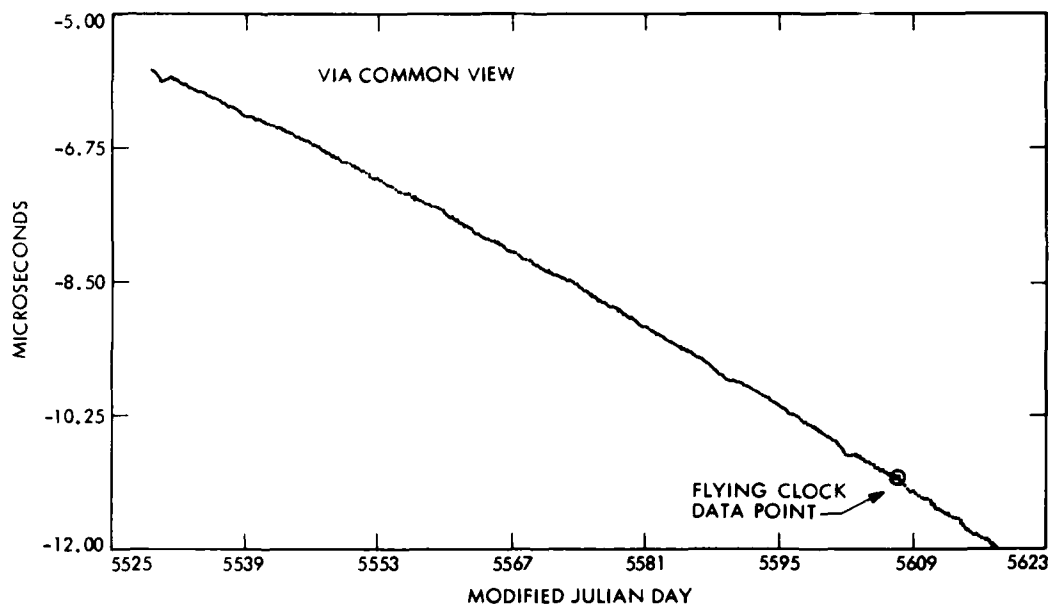


Figure 15. Common view results UTC(USNO,MC)-TID(FTS) showing flying clock result on 1 October 1983.

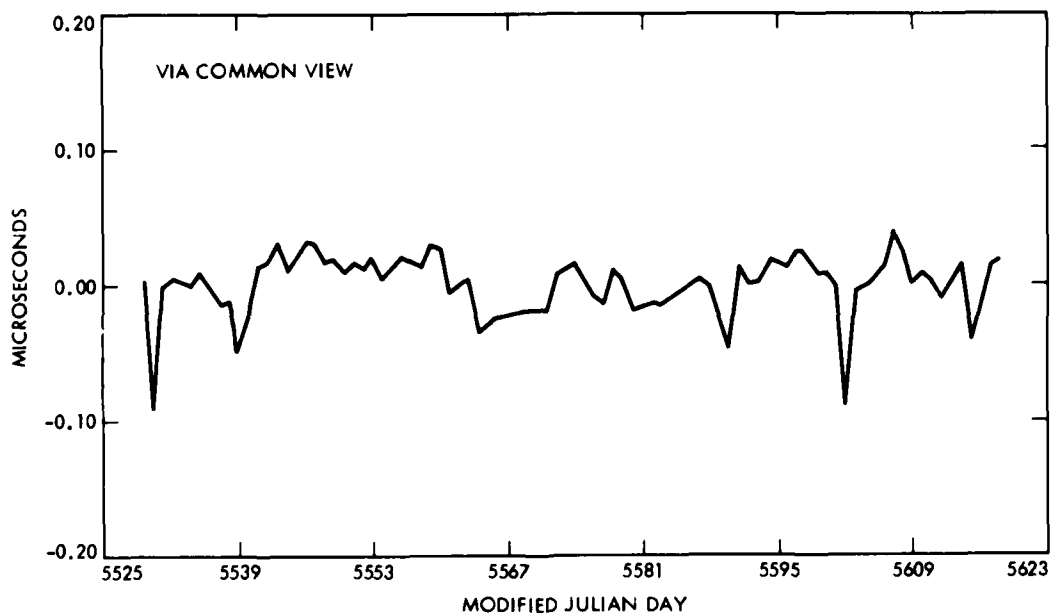


Figure 16. Residuals from quadratic fit through common view results UTC(USNO,MC)-TID(FTS), averaged over GPS TIME from space vehicles 5, 6, 8 and 9 (see Table 4).

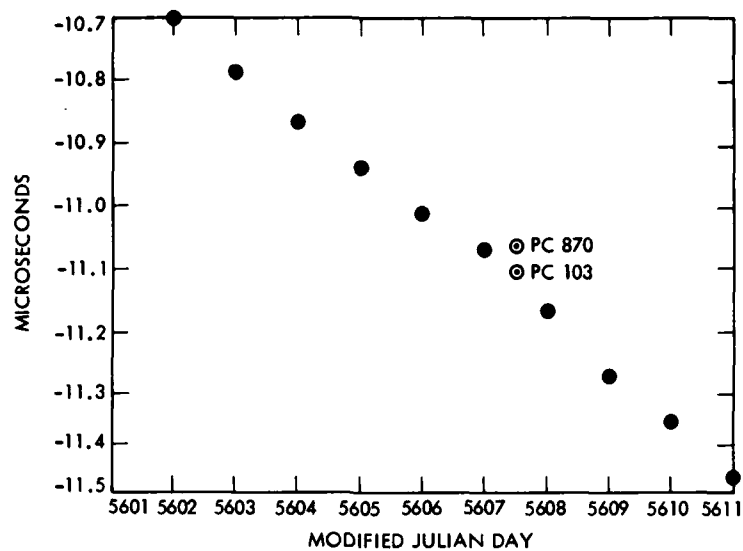


Figure 17. Common view UTC(USNO,MC)-TID(FTS) in vicinity of travelling clock data points on 1 October 1983 - "consolidated" from GPS TIME results on 0h UTC.

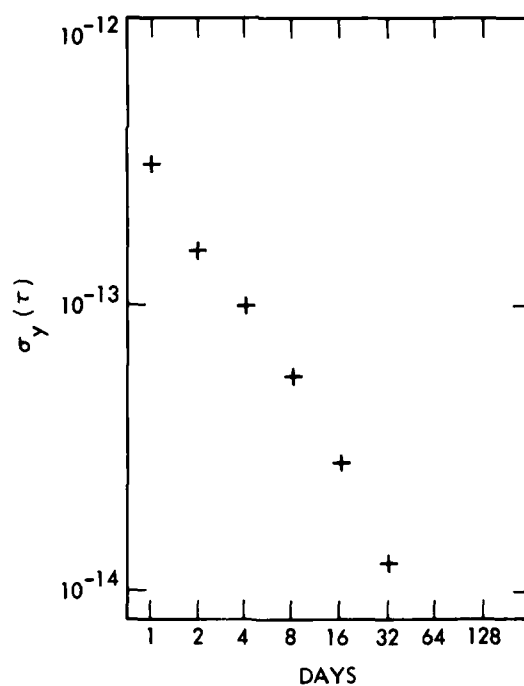


Figure 18. Allan variances from quadratic fit through data of Figure 17 (see Table 4).

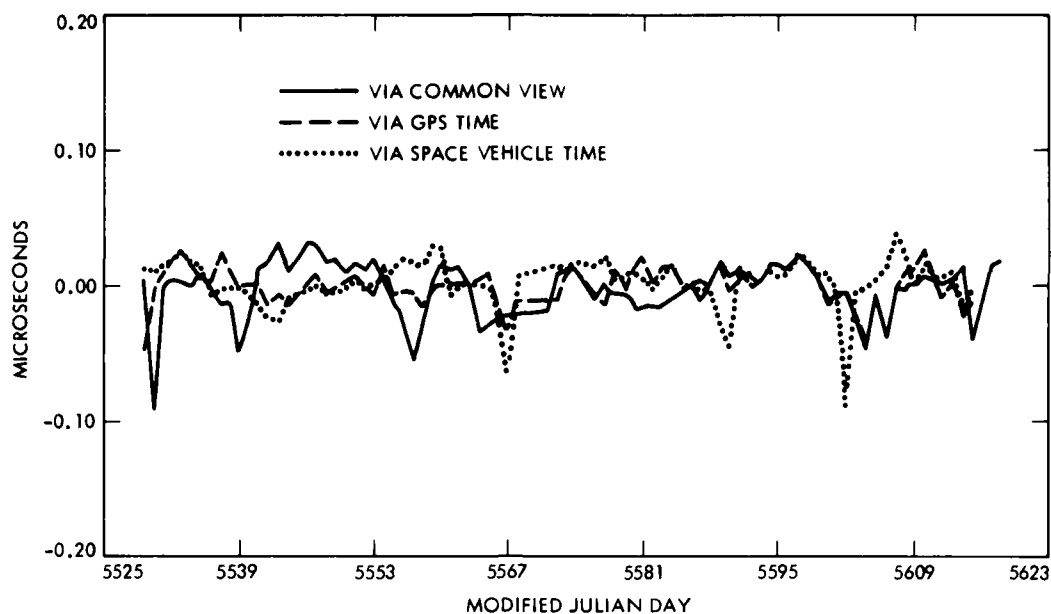


Figure 19. Composite of residuals from quadratic fits through UTC(USNO,MC)-TID(FTS) via common view (Figure 16), long-arc GPS TIME (Figure 14) and long-arc SV TIME (Figure 10).

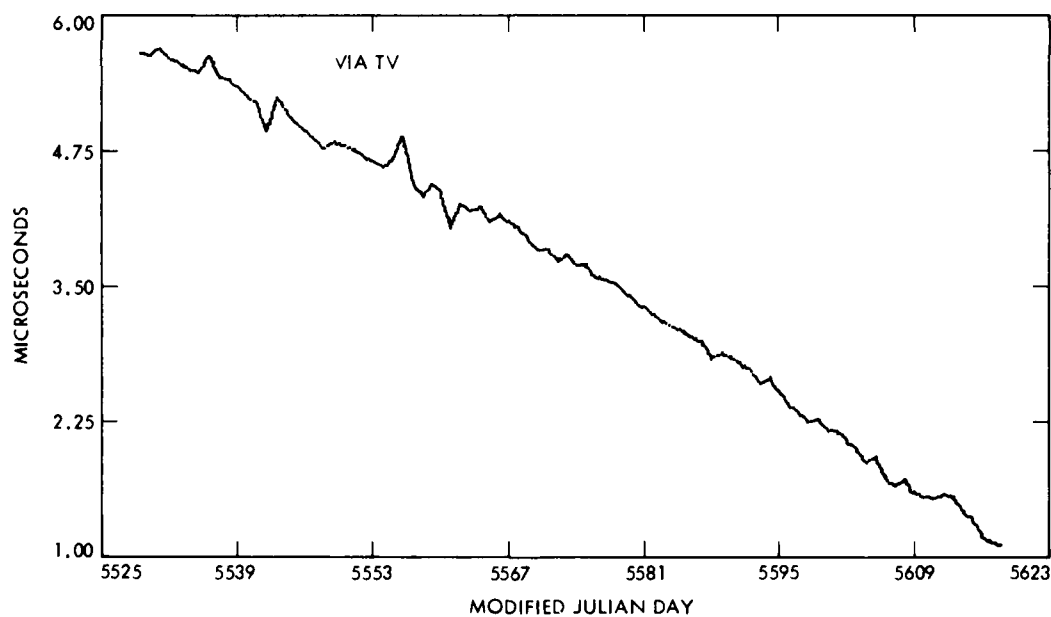


Figure 20. UTC(AUS)-TID(FTS) via TV as published in NATMAP Bulletin E.

TRANSFER TO UTC(AUS)

The free-running time scale UTC(AUS) is calculated from TV comparisons between caesium standards and hydrogen masers located mainly in Canberra, Sydney and Melbourne [Luck, 1979; Woodger 1980]. The clocks contributing to UTC(AUS) in the three month period under consideration are summarised in Table 5. Until the GPS receiver was put in to use at Tidbinbilla the only regular means of comparing UTC(AUS) with adequate precision to the outside world was by flying clock trips every three or four months organised by USNO and Bendix Corporation. It is now possible, however, to measure the relationship on a daily basis, using TID(FTS) as the intermediary.

The results UTC(AUS) - TID(FTS) as published in NATMAP's Bulletin E during July-October are shown in Figure 20. Combining these with UTC(USNO MC) - TID(FTS) as in Figure 8 gives UTC(USNO MC) - UTC(AUS) shown in Figure 21. Residuals from a straight line fit (see Table 4) are shown in Figure 22 and their Allan variances in Figure 23. It is immediately seen that the standard errors are almost an order of magnitude greater, which is directly attributable to TV noise. The flying clock trip error is 120 ns of which a substantial proportion can be attributed to the flying clocks themselves.

There is no doubt that, for as long as the GPS TTU remains at Tidbinbilla, a regular, reliable and accurate avenue is available for comparing clocks in Eastern Australia to clocks and time scales overseas. Conversely, it is now possible for 16 or more Southern Hemisphere clocks to be used in the computation of International Atomic Time (TAI) if so desired.

USE OF RESULTS TO STEER UTC(AUS)

Time scales such as UTC(AUS), UTC(BIH) and UTC(USNO) are calculated in batch mode after-the-event; for example, UTC(AUS) is calculated monthly about a fortnight in arrears. It is thus feasible to accommodate the delays in gathering GPS data and reducing them to a common time such as 0^h UTC in order to include it in the time scale algorithm. This can be done in such a way that the time scale generally follows the external clock or scale to which the GPS measurements are referred, yet continues virtually uninterrupted if the GPS results are unavailable.

Let the time shown by clock i be denoted x_i at a given time, and let the measurement against the local TV (corrected for propagation delay) be l_i :

$$l_i = x_i - TV \quad , \quad i = 1, 2, \dots, n. \quad (3)$$

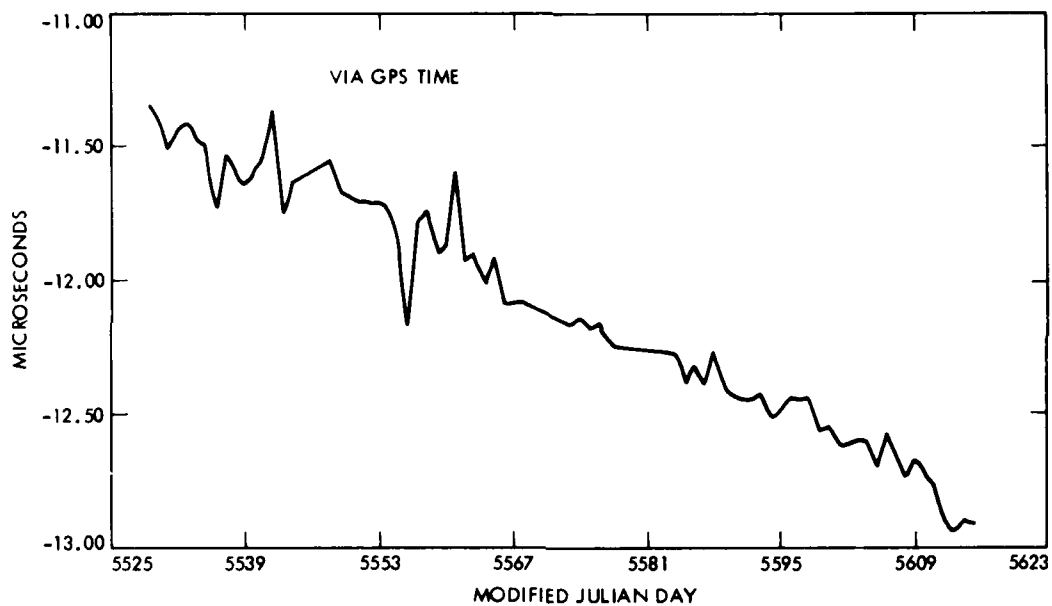


Figure 21. UTC(USNO,MC)-UTS(AUS) derived from long-arc GPS TIME results to Tidbinbilla (Figure 8) and Bulletin E (Figure 20).

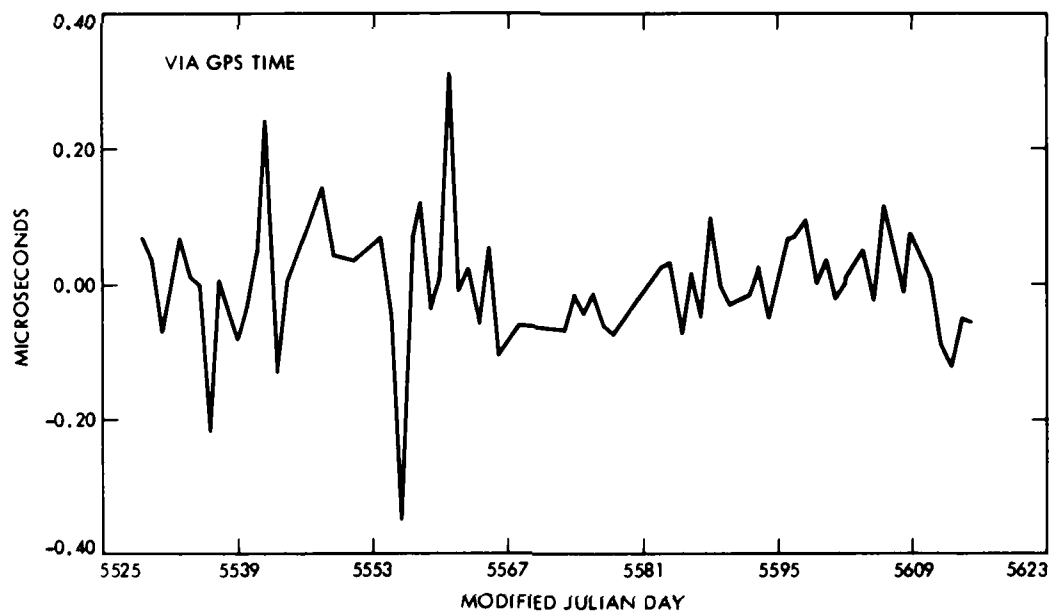


Figure 22. Residuals from straight line fit through UTC(USNO,MC)-UTC(AUS) shown in Figure 21 (see Table 4).

TABLE 5

Contributors to UTC(AUS), July-October 1983

Organisation	Location	Time Standards
Tidbinbilla DSCC	Canberra	1 hydrogen maser 2 HP caesium standards
Division of National Mapping	Canberra	2 HP caesium standards
Orroral Valley STDN	Canberra	1 HP caesium standard
CSIRO National Measurements Lab	Sydney	2 hydrogen masers 3 HP caesium standards
Royal Australian Navy	Sydney	1 HP caesium standard
TELECOM Aust Research Lab	Melbourne	5 HP caesium standards

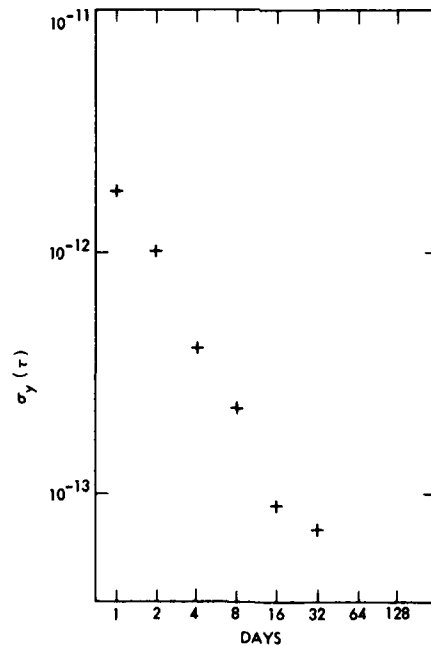


Figure 23. Allan variances of the residuals UTC(USNO,MC)-UTC(AUS) shown in Figure 22.

It is desired to calculate a time scale X , e.g. $X = \text{UTC}(\text{AUS})$, which appears in the form of a set of results z_i :

$$\begin{aligned} z_i &= X - x_i, \quad i = 1, 2, \dots, n. \\ z_0 &= X - T_V \end{aligned} \quad (4)$$

taking into account weights p_i for each clock according to some pre-arranged criteria. This is achieved by invoking the fundamental time scale equation [Percival, 1978]:

$$\sum_{i=1}^n p_i (z_i - \hat{z}_i) = 0 \quad (5)$$

where \hat{z}_i is an unbiased prediction of $\text{UTC}(\text{AUS}) - x_i$ at the time of observation [Luck, 1983]. There are n observations and one condition available to solve for the $n + 1$ unknowns $z_0, z_1, z_2, \dots, z_n$.

Now suppose that an external observation l_T is available on one of the clocks x_T ($T \in i$) against the reference time scale R , e.g. $R = \text{UTC}(\text{USNO MC})$:

$$l_T = R - x_T \quad (6)$$

and impose the steering condition:

$$X = R \quad (7)$$

i.e. $\text{UTC}(\text{AUS}) = \text{UTC}(\text{USNO MC})$ at the time of measurement. The full set of equations to be solved can then be put into the form of observation equations with a condition, from equations (6), (3) and (5) respectively:

$$\begin{aligned} l_T &= z_T, \quad T \in i \\ \sum_{i=1}^n p_i (z_i - \hat{z}_i) &= 0 \end{aligned} \quad (8)$$

which can be treated by standard least squares methods; a weight p_T should be assigned judiciously to the external direct observation l_T . This formulation can be readily extended to cater for the hypothetical situation in which several GPS units, or indeed any other international time transfer systems, were operating in Australia.

When this suggestion has been investigated and implemented, $\text{UTC}(\text{AUS})$ will be truly a coordinated scale of Universal Time. Removal of the direct external observation(s) l_T would restore it to its current position as a true free-running time scale, more appropriately designated perhaps as $\text{T}(\text{AUS})$ yet regularly monitored against TAI. It is proposed to run both solutions once certain prediction and weighting biases in the $\text{UTC}(\text{AUS})$ algorithm have been removed.

CONCLUSION

It has been demonstrated that the GPS TTU at Tidbinbilla DSCC can achieve time transfer half way around the world with 20 nanosecond precision over extended periods and with accuracy inside the measurement capability of flying clocks. Little degradation occurs by employing the "long-arc" method rather than the "common view" method because "common view" requires low observing altitudes over these distances, and use of USNO GPS TIME values is almost as good as USNO SV values, besides being easier to obtain.

The first practical application of the method has been the determination of the drift rate of Tidbinbilla's hydrogen maser as 4 parts in 10^{15} per day.

Because the user data processing has proved to be very straightforward, it is highly feasible to include the results in the computation of UTC(AUS) and indeed to steer this time scale to UTC(USNO MC) or to UTC(BIH). It is also now possible for a wider community to use Australian clocks for scientific purposes. We hope that other South-East Asian and Pacific countries will be encouraged by our results to examine the method very closely.

ACKNOWLEDGEMENTS

The authors thank Mr D. Abreu (National Mapping) and Mr J. Hoyland (Tidbinbilla) for assistance in data processing and communications; Mr M. Miranian (US Naval Observatory) for sending much USNO space vehicle data; and Mr H. Sadler (Bendix Corporation) and his associates for their frequent visits with flying clocks.

REFERENCES

- Clements, P.A. (1982): "Intercontinental Time and Frequency Transfer Using a Global Positioning System Timing Receiver", Proc. Fourteenth Annual PTTI, Goddard SFC, NASA Conference Publ. 2265, pp 517-527.
- Davis, D.D., M. Weiss, A. Clements and D.W. Allan (1981): "Unprecedented Syntonization and Synchronization Accuracy via Simultaneous Viewing with GPS Receivers and Construction Characteristics of an NBS/GPS Receiver", Proc. Thirteenth Annual PTTI, Naval Research Lab, NASA Conference Publ. 2220, pp 527-543.
- Kovach, K.L. (1981): "Using the NAVSTAR Global Positioning System as a Global Timing System", Proc. Thirteenth Annual PPTI, Naval Research Lab., NASA Conference Publ. 2220, pp 133-163.

- Luck, J. McK. (1979): "Comparison and Coordination of Time Scales", Proc. Astronomical Soc. Australia, Vol 3, No. 5, pp 357-363.
- Luck, J. McK. (1983): Construction and Comparison of Atomic Time Scale Algorithms, Division of National Mapping Tech. Report 32, Canberra.
- Percival, D.B. (1978): "The U.S. Naval Observatory Clock Time Scales", IEEE Trans. Instrumentation and Measurement, Vol IM-27, No. 4, pp 376-385.
- Woodger, J.R. (1980): "Australian Time and Frequency Standards", IREE Aust. Precise Time and Frequency Conference Record, The Institution of Radio and Electronics Engineers Australia, Sydney.

QUESTIONS AND ANSWERS

None for Paper #7.

SEPARATING THE VARIANCES OF NOISE COMPONENTS IN THE GLOBAL POSITIONING SYSTEM

David W. Allan and Marc Weiss
Time and Frequency Division
National Bureau of Standards, Boulder, Colorado

ABSTRACT

Central to the success of the GPS program is the ability to model the frequency stability characteristics of the its various components. A persistent challenge in evaluating the Global Positioning System is the separation of the errors of the satellite clocks from those due to the satellite ephemeris errors and/or the signal propagation delay errors. This information is important when one tries to improve the performance of the Global Positioning System. It is necessary to know if a particular component of the system meets specification and which component(s) limits performance.

Although one cannot separate the errors themselves, a method has been developed whereby the "Allan variances" of critical components to the GPS can be separated. Using a reference clock such as UTC(NBS) or UTC(USNO), for example, the fractional frequency stability of each of the following can be separated from each of the others: the reference clock, the space vehicle clock, the GPS clock, the clock upload correction, the ephemeris and the propagation delay. This technique has the potential to significantly assist in properly setting the parameters to obtain optimum performance from the Global Positioning System e.g. setting the Kalman filter parameters. Results will be given showing some interesting surprises in the characteristics of the system.

INTRODUCTION

During the testing of the GPS it has become evident that an independent method for the characterization of the observables of the system would be an important supplement to the Kalman estimates. Such a method would allow one to diagnose problems, make improvements, and predict system performance for variation in the system's environment. This is not an easy task in some cases. For example, an independent method for the separation of the time errors of the clocks from those due to the ephemeris variations and propagation delays has been desired for some time. Because of the natural correlation between these error sources, differences of opinion have often arisen as to the source of some errors that have been observed.

Under a reasonable set of assumptions, NBS has developed a method whereby the Allan variances of important GPS observables can be separated. Using a reference clock such as UTC(NBS) or UTC(USNO), for example, the fractional stability of each of the following can be separated from each of the other:

- the reference clock
- the space vehicle clock
- the GPS clock
- the clock upload correction
- the ephemeris and the propagation delay

This technique has the potential to significantly assist in properly setting the GPS Kalman filter parameters. Also, this technique should be useful to users who want to study the stability of their clocks, since the user's reference is one of the components separated.

GENERAL CONSIDERATIONS

This separation of variances is performed using the following general approach. When considering any time series it is convenient to divide the elements into two parts, i.e., the deterministic part and the random part which is described by stochastic measures such as spectral densities or Allan variances. First the random elements are separated from the deterministic ones. If the driving forces that cause the random perturbations are independent, then the variances of these individual components can also be separated. An example is the separation of the sum of the ephemeris errors and propagation delay variations from the clock upload correction errors. In short term these appear to be correlated but in long term they decorrelate and hence the variances of these can be separated.[1] If different space vehicles are observed within a reasonable period of time, mainly within a few hours of each other, then the clock in each of the satellites provides an independent reference having random uncorrelated errors with the clocks in other satellites and with the ground clock. Using three independent satellites allows one to calculate variances for each individual component among the three. Finally, the clock correction error is independent of the time of the space vehicle clock, thus providing a tool for the separation of the variance of the errors in that component of the system. This approach and these assumptions will be explained further as the method is developed in detail.

Suppose that we have three independent time series -- denoted by subscripts i, j, and k. Since all measurements are made in pairs one can use those pairs of measurements to estimate the individual variances (σ_i^2 , σ_j^2 , and σ_k^2) of the time series from the variances of the pairs of measurements (σ_{ij}^2 , σ_{ik}^2 , and σ_{jk}^2). The variance of each time series is estimated as follows

$$\sigma_i^2 = (\sigma_{ij}^2 + \sigma_{ik}^2 - \sigma_{jk}^2)/2, \quad (1)$$

and one permutes the i, j, and k to obtain σ_j^2 and σ_k^2 . A problem which sometimes arises with this technique is that the estimated variances are negative. This may occur when there are too little data or there are apparent correlations. The longer the data length the better the statistical confidence on the estimates. For the GPS case one can use 3 independent satellites to estimate observables for each of the satellites in question.

DERIVATION FOR GPS

Next we will describe the individual independent error sources arising in a given GPS time transfer measurement. We will define some terms as follows: Let x be the time deviation for a particular noise source in the GPS. We will subscript the x depending upon the particular source being studied.

REF... as the reference clock such as the NBS clock.

GPS'...the received estimate of the time from the GPS receiver.

GPS ...time as generated by the GPS master clock.

PE ...the combination of the propagation time error and the satellite ephemeris error.

CL' ...the error in the space vehicle clock correction.

SV' ...the time of the space vehicle clock as received by the GPS receiver

SV ...the true SV time as generated within the space vehicle.

Our goal, of course, is to have an estimate of the true variance of each one of the components in question.

We may make the following measurements for each of 3 satellites i , j , and k ; specifically we will list these for satellite i .

$$x_{\text{REF-GPS}_i} = x_{\text{REF}} - x_{\text{PE}_i} - x_{\text{CL}_i} - x_{\text{GPS}} \quad (2)$$

$$x_{\text{REF-SV}_i} = x_{\text{REF}} - x_{\text{PE}_i} - x_{\text{SV}_i} \quad (3)$$

If equation (2) is subtracted from equation (3) one obtains cancellation of the propagation plus ephemeris error.

$$x_{\text{GPS}_i - \text{SV}_i} = x_{\text{GPS}} + x_{\text{CL}_i} - x_{\text{SV}_i} \quad (4)$$

Assuming that the reference clock time deviation error is small from one satellite measurement to the next, which is a good assumption for high quality references with errors of the order of one nanosecond, one can subtract the measurements of satellite i from those of satellite j resulting in the following 2 equations:

$$x_{\text{REF-GPS}_{ij}} = x_{\text{PE}_{ij}} + x_{\text{CL}_{ij}} \quad (5)$$

$$x_{\text{REF-SV}_{ij}} = x_{\text{PE}_{ij}} + x_{\text{SV}_{ij}}, \quad (6)$$

where the ij subscripts on the right of equation (5) and (6) denote the differences $(j-i)$ in the measurement of those two components. Equations (5) and (6) can, of course, be written for satellites i and k and for j and k as well. Equations 2 through 6 comprise our measurement basis. Since (in long term) each of the components in these equations are uncorrelated we may take variances of each of these equations and the cross terms will average to zero

giving the following 5 equations:

$$\sigma_{1_i}^2 \equiv \sigma_{\text{REF-GPS}_i'}^2 = \sigma_{\text{REF}}^2 + \sigma_{\text{PE}_i}^2 + \sigma_{\text{CL}_i'}^2 + \sigma_{\text{GPS}}^2 \quad (7)$$

$$\sigma_{2_i}^2 \equiv \sigma_{\text{REF-SV}_i'}^2 = \sigma_{\text{REF}}^2 + \sigma_{\text{PE}_i}^2 + \sigma_{\text{SV}_i}^2 \quad (8)$$

$$\sigma_{3_i}^2 \equiv \sigma_{\text{GPS}_i'-\text{SV}_i'}^2 = \sigma_{\text{GPS}}^2 + \sigma_{\text{CL}_i'}^2 + \sigma_{\text{SV}_i}^2 \quad (9)$$

$$\sigma_{\text{REF-GPS}_{ij}'}^2 = \sigma_{\text{PE}_{ij}}^2 + \sigma_{\text{CL}_{ij}'}^2 \quad (10)$$

$$\sigma_{\text{REF-SV}_{ij}'}^2 = \sigma_{\text{PE}_{ij}}^2 + \sigma_{\text{SV}_{ij}}^2 \quad (11)$$

And again we can write equations (7), (8), and (9) for satellites j and k as well, and equation (10), (11), for satellite pairs ik, and jk as well. In addition we can use equation (1) to estimate the variances for i, j, and k separately from (10), and (11) respectively:

$$\sigma_{4_i}^2 \equiv \sigma_{\text{PE}_i}^2 + \sigma_{\text{CL}_i'}^2 \quad (12)$$

$$\sigma_{5_i}^2 \equiv \sigma_{\text{PE}_i}^2 + \sigma_{\text{SV}_i}^2 \quad (13)$$

and similarly for j and k. In matrix formulation we have the following representative set of equations resulting from the estimates or measures for each of the three satellites i, j and k:

$$\begin{pmatrix} \sigma_{1_i}^2 \\ \sigma_{2_i}^2 \\ \sigma_{3_i}^2 \\ \sigma_{4_i}^2 \\ \sigma_{5_i}^2 \end{pmatrix}_{i,j,k} = \begin{pmatrix} 1 & 1 & 0 & 1 & 1 \\ 1 & 0 & 1 & 0 & 1 \\ 0 & 1 & 1 & 1 & 0 \\ 0 & 0 & 0 & 1 & 1 \\ 0 & 0 & 1 & 0 & 1 \end{pmatrix} \cdot \begin{pmatrix} \sigma_{\text{REF}}^2 \\ \sigma_{\text{GPS}}^2 \\ \sigma_{\text{SV}}^2 \\ \sigma_{\text{CL}_i'}^2 \\ \sigma_{\text{PE}_i}^2 \end{pmatrix}_{i,j,k} \quad (14)$$

If the matrix is inverted we may then write the final equation for the variances of the individual components of the GPS system. Global variances are obtained through each of three space vehicles. Variances pertaining to an individual space vehicle are obtained through that space vehicle.

$$\begin{pmatrix} \sigma_{\text{REF}}^2 \\ \sigma_{\text{GPS}}^2 \\ \sigma_{\text{SV}}^2 \\ \sigma_{\text{CL}'}^2 \\ \sigma_{\text{PE}}^2 \end{pmatrix}_{i,j,k} = \begin{pmatrix} 0 & 1 & 0 & 0 & -1 \\ 1 & -1 & 0 & -1 & 1 \\ -\frac{1}{2} & \frac{1}{2} & \frac{1}{2} & 0 & 0 \\ -\frac{1}{2} & \frac{1}{2} & \frac{1}{2} & 1 & -1 \\ \frac{1}{2} & -\frac{1}{2} & -\frac{1}{2} & 0 & 1 \end{pmatrix} \cdot \begin{pmatrix} \sigma_1^2 \\ \sigma_2^2 \\ \sigma_3^2 \\ \sigma_4^2 \\ \sigma_5^2 \end{pmatrix}_{i,j,k} \quad (15)$$

Alternatively, one can write out the separation of variances in equation form for each of the i, j, and k satellites -- here written specifically for i:

$$\sigma_{\text{REF}_i}^2 = \sigma_{2_i}^2 - \sigma_{5_i}^2 \quad (16)$$

$$\sigma_{\text{GPS}_i}^2 = \sigma_{1_i}^2 - \sigma_{2_i}^2 - \sigma_{4_i}^2 + \sigma_{5_i}^2 \quad (17)$$

$$\sigma_{\text{SV}_i}^2 = \frac{1}{2} (-\sigma_{1_i}^2 + \sigma_{2_i}^2 + \sigma_{3_i}^2) \quad (18)$$

$$\sigma_{\text{CL}'_i}^2 = \frac{1}{2} (-\sigma_{1_i}^2 + \sigma_{2_i}^2 + \sigma_{3_i}^2) + \sigma_{4_i}^2 - \sigma_{5_i}^2 \quad (19)$$

$$\sigma_{\text{PE}_i}^2 = \frac{1}{2} (\sigma_{1_i}^2 - \sigma_{2_i}^2 - \sigma_{3_i}^2) + \sigma_{5_i}^2 \quad (20)$$

The subscript i on REF and on GPS, clocks which are totally independent of the satellites i, j, and k, denotes an estimate of that clock's stability calculated via that particular satellite. As a final answer one could take a simple average or a more sophisticated statistical (e.g., weighted) average of the $\sigma_{\text{REF}_i}^2$, $\sigma_{\text{REF}_j}^2$, and $\sigma_{\text{REF}_k}^2$, and of the $\sigma_{\text{GPS}_i}^2$, $\sigma_{\text{GPS}_j}^2$, and $\sigma_{\text{GPS}_k}^2$.

The Allan variance fulfills the criterion that the variance used be a well behaved stable measure of the time series in question. In fact one can do the Allan variance analysis for different sample times as well, which allows one to characterize a process. The only criterion on the sample time is that it be sufficiently long so that the processes under consideration are uncorrelated, indications are that this is of the order of one day and longer.

AN EXAMPLE

This theoretical approach was applied to data taken at NBS from June 25th, 1983 to October 1, 1983. The result was an analysis of the stability of the GPS and space vehicle clocks, as well as of the clock corrections and propagation noise plus ephemeris estimates.

The stability analysis was performed on data on file in the NBS time scale computer. Each file entry is characterized by the MJD on which the data was taken, the hour, minute and second on which the satellite pass was started, the receiver number used to receive the data, the space vehicle involved, the class byte employed, the length of the data, the age of the data, the elevation and azimuth of the satellite, the ionospheric delay, the reference minus space vehicle (SV) time to a tenth of a nanosecond resolution and its accompanying slope from a linear least squares fit to the particular data pass, the reference minus GPS time to a tenth of a nanosecond resolution and its similar accompanying slope from a linear least squares fit, and the rms fit of the linear least squares to that data set. In addition, for the NBS data, the time of the reference minus UTC(NBS) is recorded. Finally there is a column for any offsets which may be due to discontinuities from a known effect in a receiver or idiosyncrasy in the system. The NBS reference clock is typically within a few nanoseconds of UTC(NBS).

The most recent data were analyzed to give a current estimate of the stability of the clocks in the GPS. The period covered was from MJD 45510 to 45608, which is the 25th of June 1983 throughout the 1st of October 1983. The data are taken on a sidereal day basis; i.e., the receivers automatically subtract 4 minutes a day to nominally maintain the same viewing angle to the SV. On the 30th of September 1983 the starts of each track time were 1802 UT, 1855 UT, 2050 UT, 2228 UT for SV-8, -6, and -9 and -5 respectively. The track lengths were each 780 seconds. The average age of data over the analysis period was nominally 2 to 4 hours and the elevation angle in all cases was above 52 degrees.

All of the time difference plots have nanoseconds as their ordinate units and the abscissas are in MJDs. Figure 1 is a plot of UTC(USNO-MC) minus the time of the GPS steered clock sometimes called the GPS software clock. In short term this clock behaves like the cesium at Vandenberg or Alaska and in long term it should reflect the stability of UTC(USNO-MC) as the software clock is steered to UTC(USNO-MC). Only SV-8 data were used because of some problems in the other space vehicle data sets in the USNO file stored in the NBS time scale computer. One sees a fairly significant frequency step around MJD 45591 and the time at the end of September has departed more than one microsecond from UTC(USNO).

Figure 2 is the average obtained by SV-5, -6, -8 and -9 of the NBS reference (Clock 9) minus GPS steered clock. Clock 9 is kept within a few nanoseconds of UTC(NBS). One sees very similar performance between figures 1 and 2 indicating that the main effect is that of the GPS clock. The data in Figure 2 are smoother simply because of the average across additional satellites and because of somewhat quieter receiver data. The agreement between the 4 space vehicles of the time difference, Clock 9 minus GPS, was typically in the range

of 6 to 8 nanoseconds.

Figure 3 is the plot of NBS Clock 9 minus Space Vehicle Cesium 5 with a frequency removed of $1.66 \text{ parts in } 10^{12}$.

Figure 4 is NBS Clock 9 minus the SV-6 Rubidium with a mean frequency removed of $7.009 \text{ parts in } 10^{11}$. The frequency drift of the rubidium has clearly changed from negative to positive from the first and middle of the data to the last part.

Figure 5 shows the NBS Clock 9 minus SV-8 with the time reset occurring at MJD 45573. The stability analysis below was reported after the reset to take advantage of the most recent stability information.

Figure 6 is NBS Clock 9 minus SV-9 and shows some measurable frequency drift in the NAVSTAR 6 Cesium. This could be problematic as frequency drift in cesium standards is sometimes indicative of end of life.

Figure 7 is NBS Clock 9 or SV-9 after removing a mean frequency drift by using a linear least squares fit and a mean time from the data. The mean frequency removed was $.3858 \times 10^{-11}$. The drift was $-.197 \times 10^{-14}/\text{day}$ and the mean time removed was 9498 nanoseconds. If a stability analysis is performed on the residuals shown in Figure 7, one obtains the sigma tau plot shown in Figure 8 which indicates that the frequency drift is well modelled and the residual random instabilities are very small--of the order of 3 to 5 parts in 10^{14} for sample times of 4 to 32 days.

The last set of figures are $\sigma_y(\tau)$ plots as estimated from the separation of variance analysis technique. As shown earlier this technique allows one to estimate the contribution of the individual noise components to the stability. Figure 9 is the frequency stability of the GPS steered clock which appears to be of the order of 1 part in 10^{13} . An interesting phenomenon is observed in the long term, namely that the $\sigma_y(\tau)$ values tend to decrease which is indicative of the long term steering of the GPS time; the time constant appears to be of the order of a few weeks.

Figure 10 is a stability plot of the Space Vehicle 5 cesium and of the clock correction errors and of the ephemeris plus propagation errors. Because the measurements were made only a few hours after upload, the clock correction errors should be approximately one-tenth of those of the space vehicle clock errors. It is evident from this data that the clock correction errors are of the same order as the space vehicle instabilities. One possible explanation of this is that the Q value in the Kalman processor at Vandenburg is set so as to assign too much error to the SV clock and not enough to the ephemeris and propagation. One also sees from the same figure that the ephemeris and propagation errors are clearly well below those of the space vehicle clock.

Because of the three corner hat analysis technique used in the separation of variances routine and because of finite data sets, it is possible to have negative variances. A negative variance indicates that the noise level is well below the other components in the calculation. Given the data length involved in this data set one can at best resolve sigmas that are about one-

tenth that of the other sigmas being considered in the analysis. In those cases where small or negative variances occurred they were simply not plotted. Thus the interpretation for those cases where no data points are plotted is that the stability of that component is well below that of the other components for those sample times. Figure 11 is a plot for NAVSTAR 3 (Space Vehicle 6). In this case, the propagation and ephemeris errors were significantly below either the space vehicle stability or the clock correction errors. Here again it seems that too much error is being assigned to the SV clock.

Figure 12 is a stability plot of Space Vehicle 8. Here again it appears that at $\tau = 1$ day too much error is being assigned to the clock and not enough to the ephemeris and propagation. In long term however, that appears not to be the case and the clock correction error falls below that of the ephemeris plus propagation errors as well as the clock instabilities as it should.

Figure 13 is a stability plot of Space Vehicle 9. In this case we have the reverse situation where the clock correction errors were very small and were not plotted. One explanation for this behavior is that too much error is being assigned to the ephemeris and propagation and not enough to the space vehicle clock. In long term, the space vehicle clock instability was sufficiently below the other instabilities in the system that it was unmeasurable and one gets some indication of its performance by the direct measurement against NBS shown earlier (Figure 8).

More recently, the separation of variance analysis technique was used to evaluate SV#11, the newest addition to the GPS constellation. This space vehicle is now operating with a rubidium standard. A linear least squares fit to the frequency of SV#11 of -2.65×10^{-13} /day frequency drift at about a 2% confidence of the estimate was removed from the data. After subtracting the frequency drift, the variances were separated. The frequency stability of the SV#11 rubidium at tau equal one day and longer was found to be excellent. In Figure 14, we show a comparison of the frequency stability of SV#11 with the SV#9 and 5 cesiums. One sees the very exciting result that at tau equal one and two days the SV#11 rubidium is comparable to the SV#9 cesium.

The software for separation of variance at NBS continues to undergo some refinements. However, the results to date are very enlightening concerning the performance of the GPS system and provide some insight into where one might improve the performance of the system.

[1] Jack Henrich, IBM Federal Systems Division, private communication.

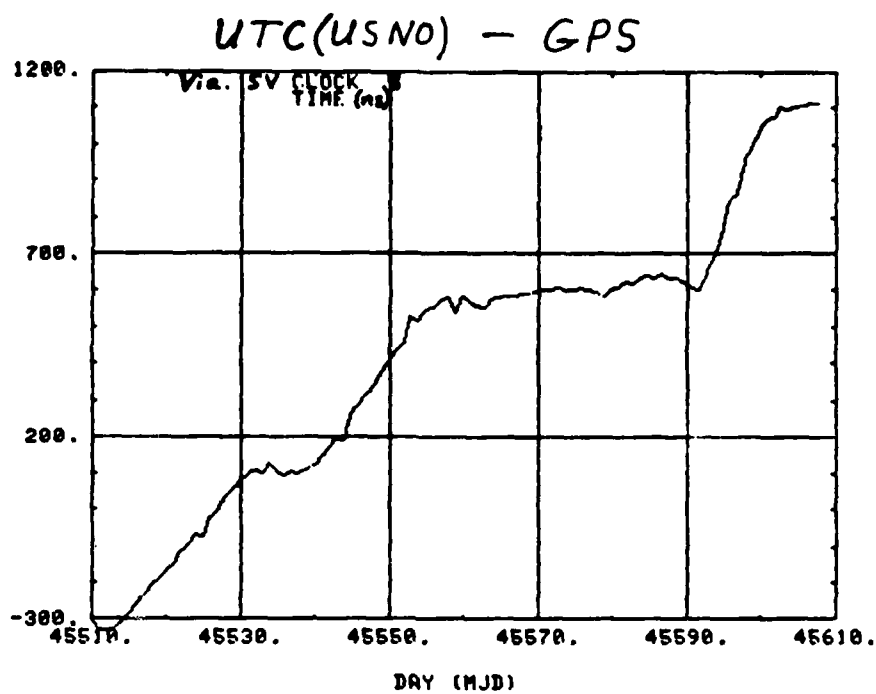


Fig. 1

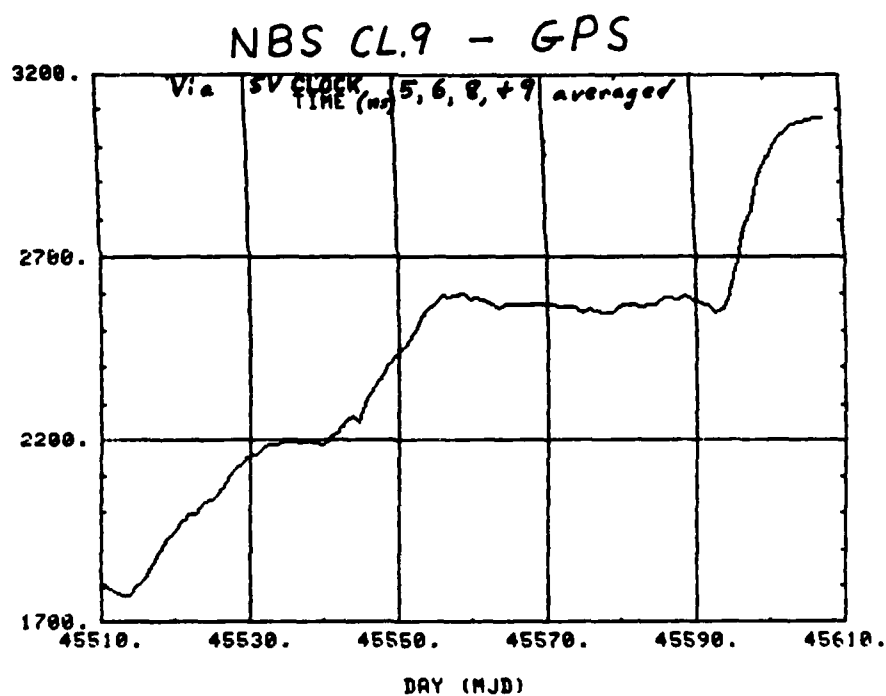


Fig. 2

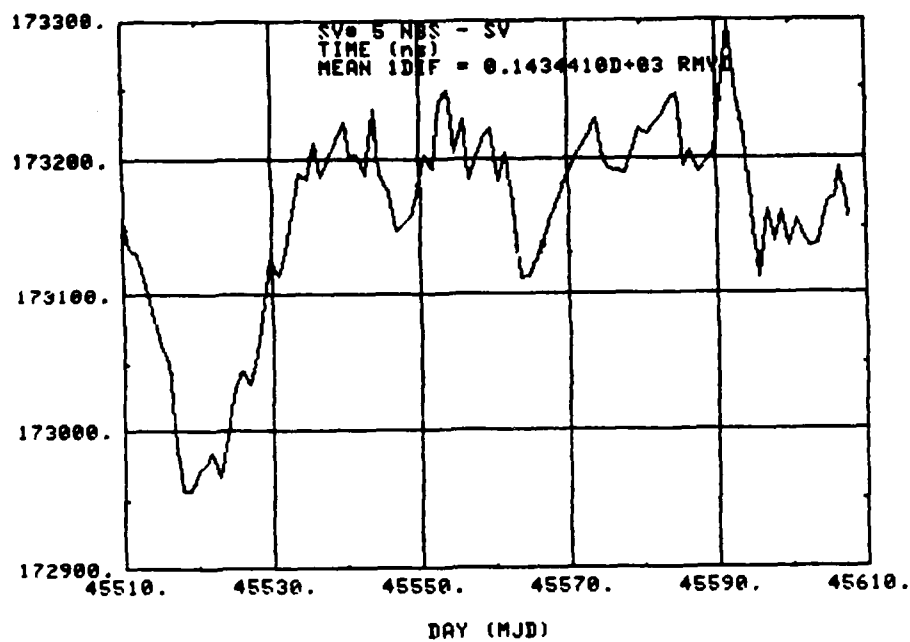


Fig. 3

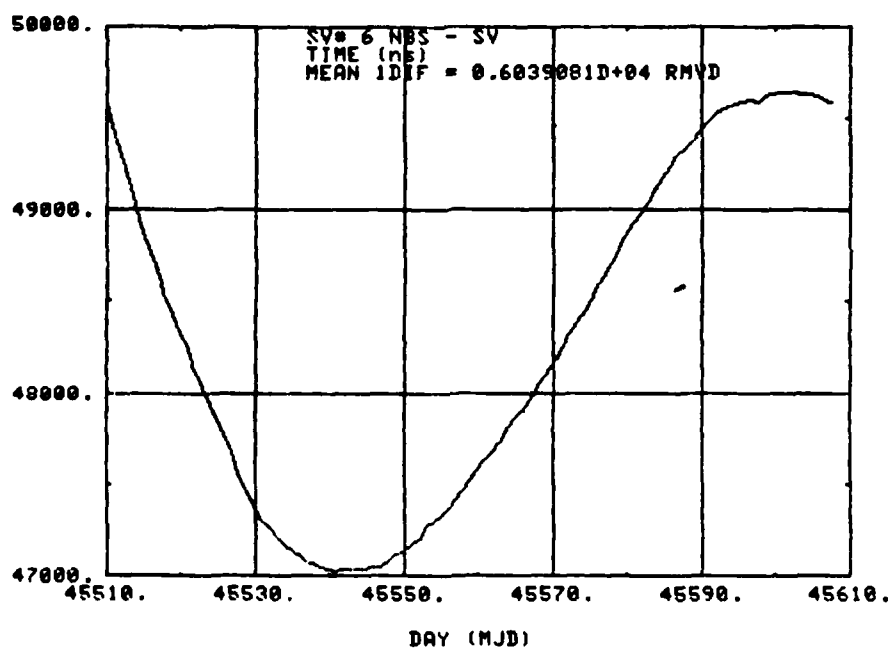


Fig. 4

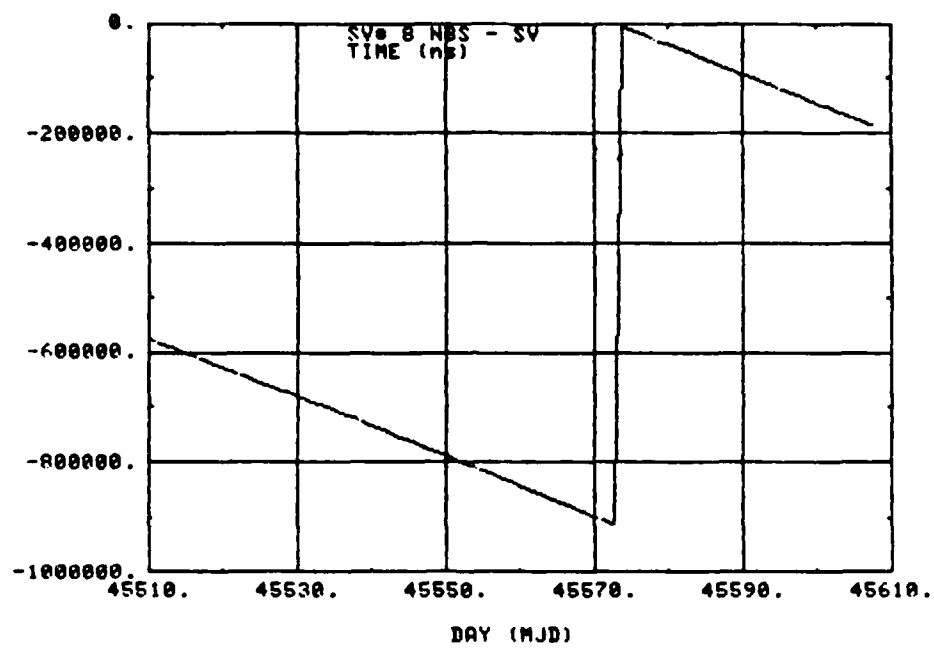


Fig. 5

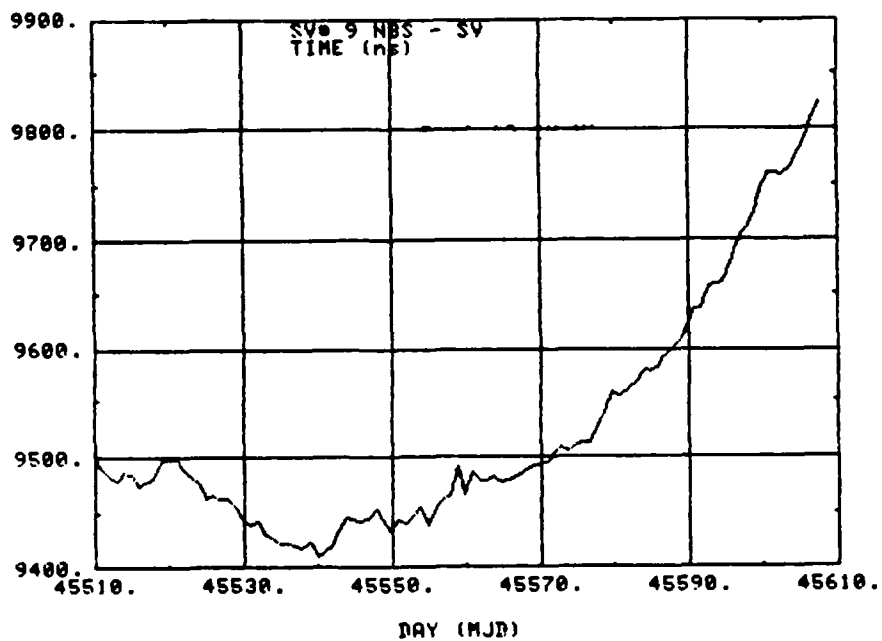


Fig. 6

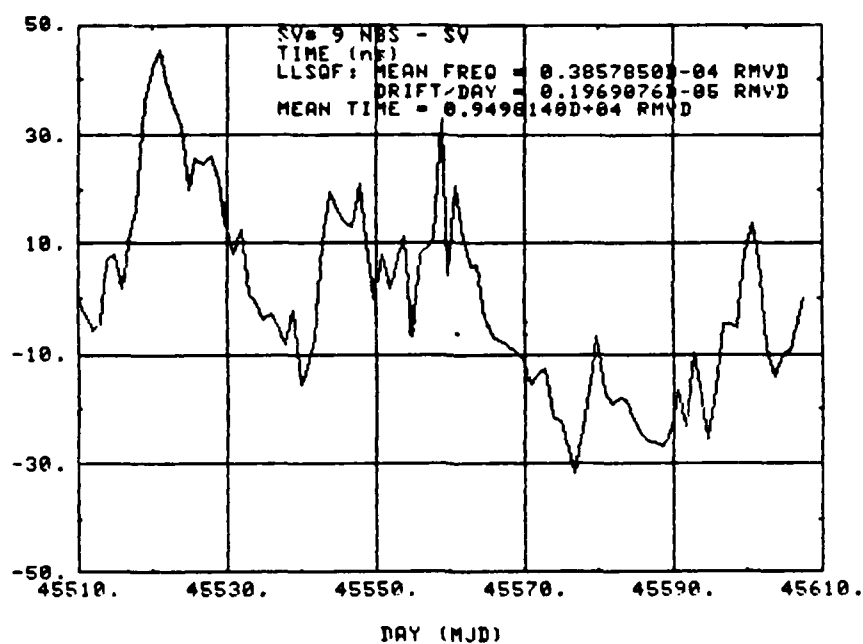


Fig. 7

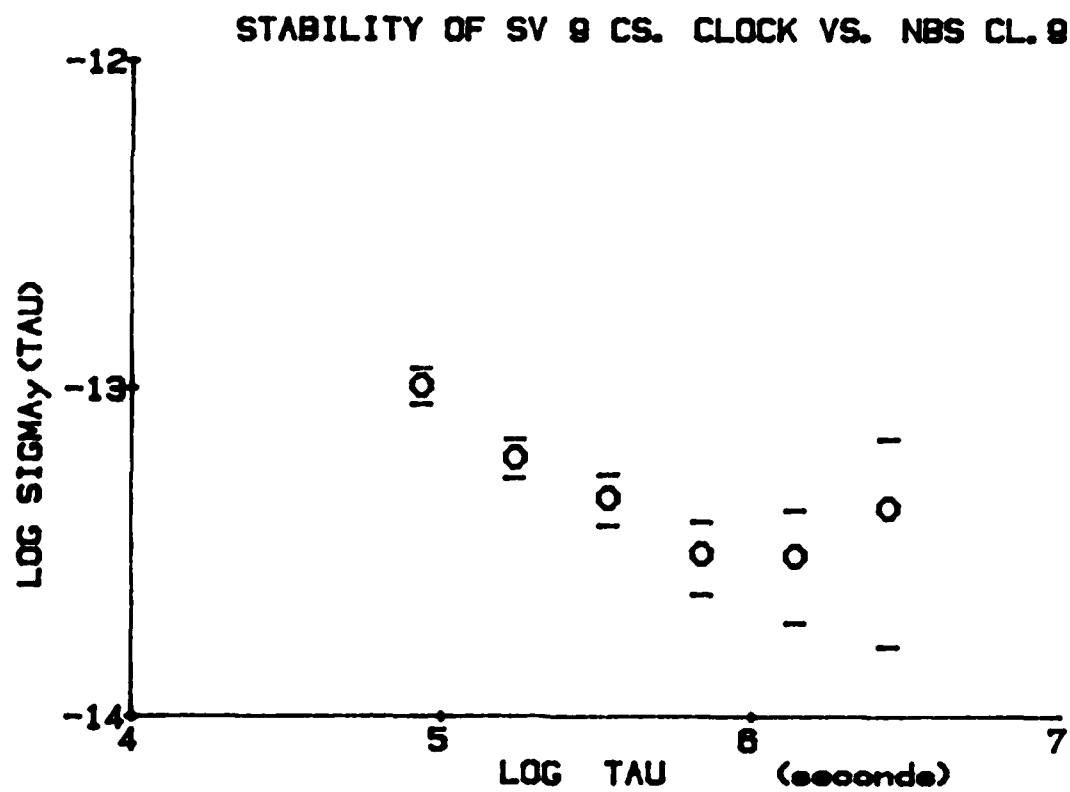


Fig. 8

STABILITY OF GPS STEERED CLOCK

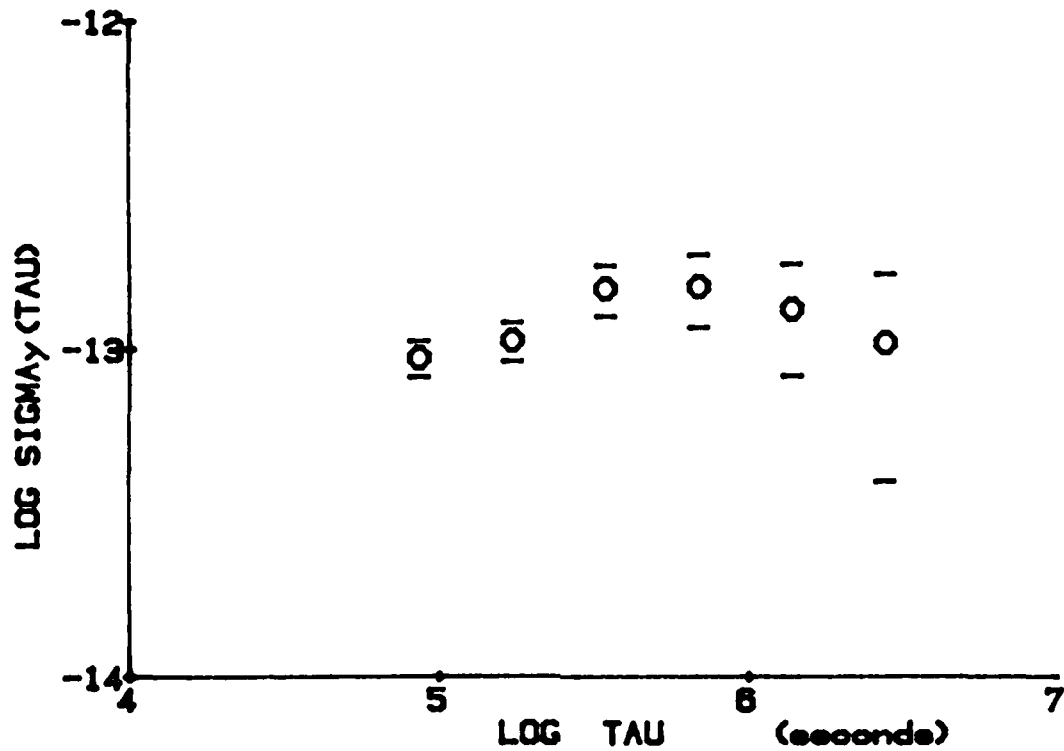


Fig. 9

SPACE VEHICLE 5 (NAVSTAR 5)

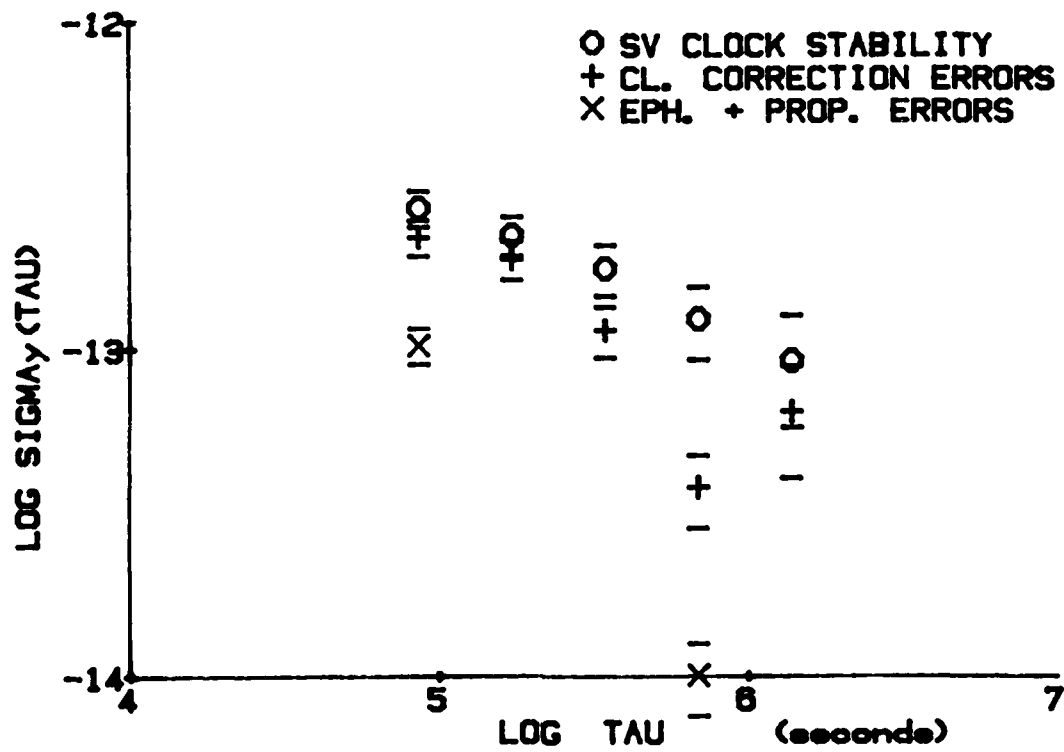


Fig. 10

SPACE VEHICLE 8 (NAVSTAR 3)

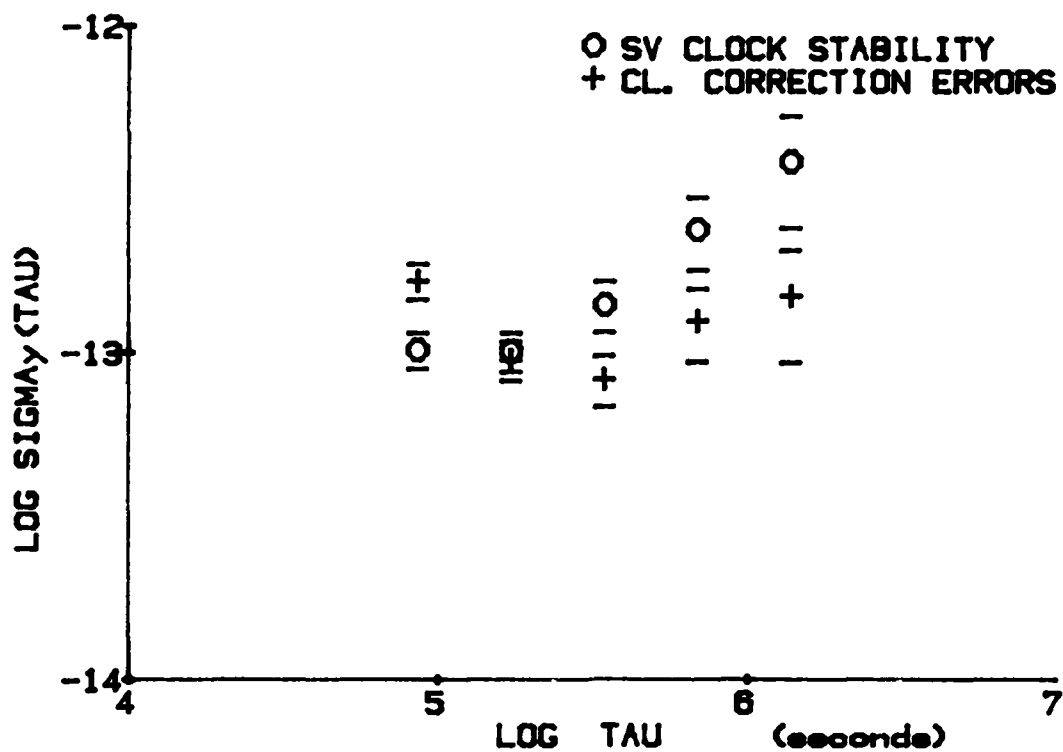


Fig. 11

SPACE VEHICLE 8 (NAVSTAR 4)

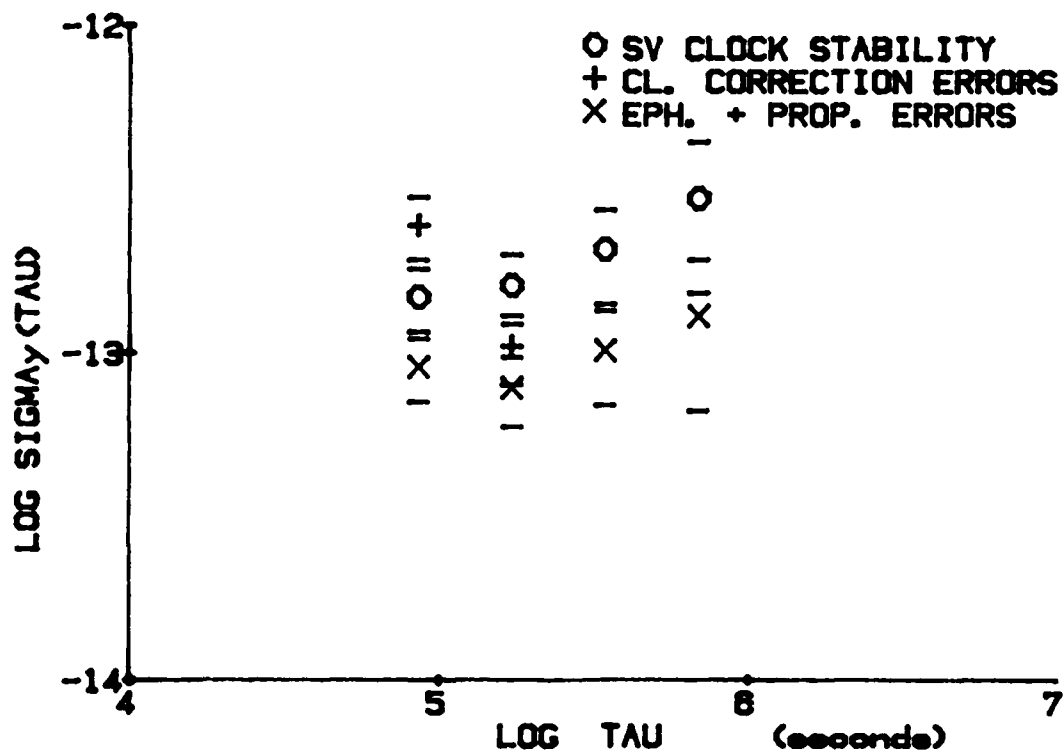


Fig. 12

SPACE VEHICLE 8 (NAVSTAR 8)

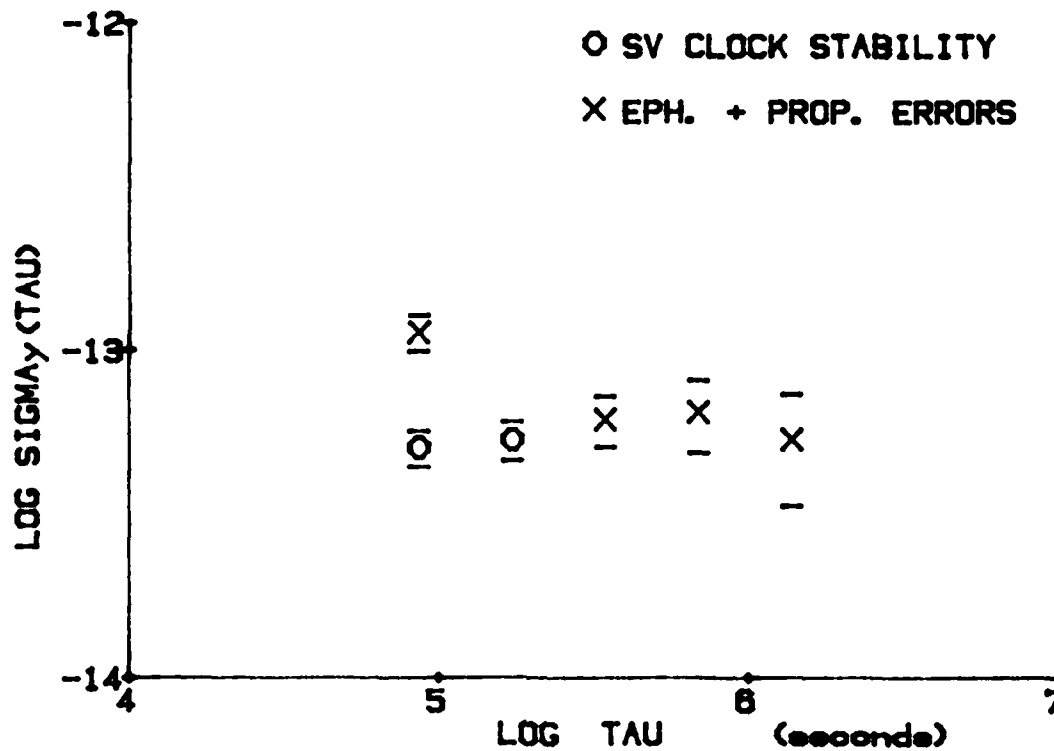


Fig. 13

STABILITY VIA NBS SEPARATION OF VARIANCE TECHNIQUE

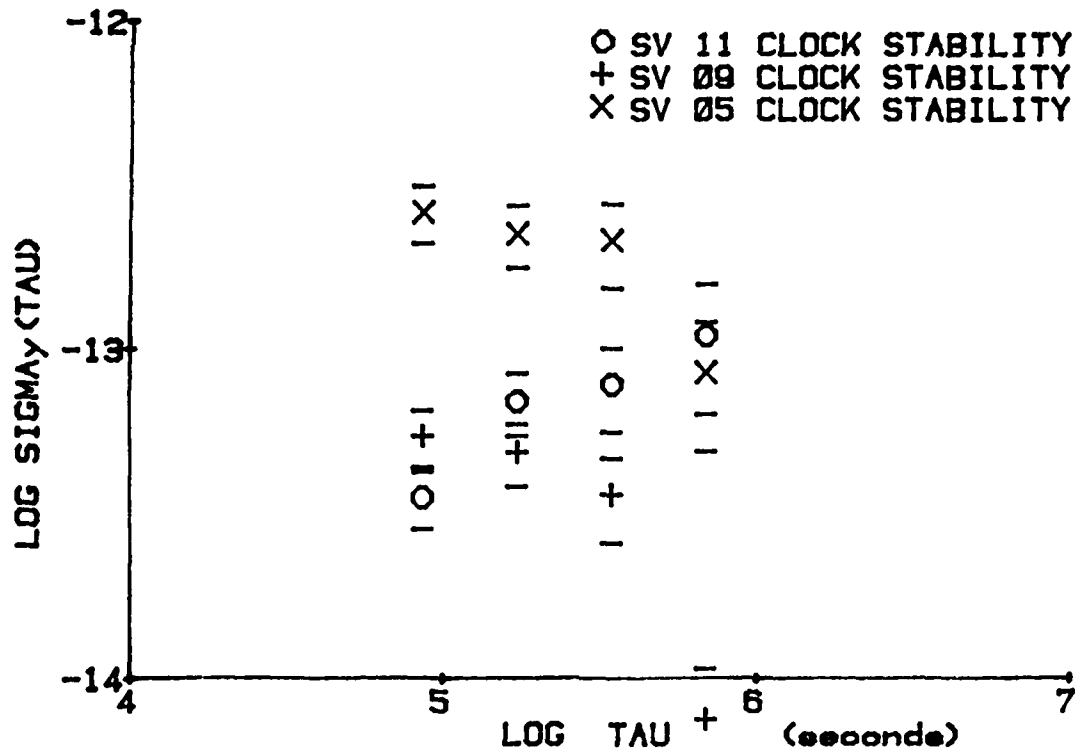


Fig. 14

QUESTIONS AND ANSWERS

MR. PAN:

I was wondering, in your three corner hat method, when you find in a case like that where σ^2 equals a negative number, how often does this occur, and what do you do about it?

MR. WEISS:

In that case we suspect that the clock that gets the negative variance is too accurate to be measured by the other two clocks in the hat, in the three corners, that it's much more stable than the other two, and so it becomes negative.

DR. REINHARDT:

What do you do when it becomes negative?

MR. WEISS:

Well, you can't plot it. You say, "Well, that's what the clock is doing." It simply is a negative variance.

DR. REINHARDT:

But you don't exclude it from the negative side?

MR. WEISS:

Well, you don't throw the clock out, if that's what you mean.

DR. REINHARDT:

No. Some people were arbitrarily setting negative errors to zero, zero variances.

MR. WEISS:

No. We don't make it positive, either.

A VOICE:

You just sum it up, the negative number? When you figure out the other ones, you just sum it up, with the rest of them?

MR. WEISS:

We assume that that number is invalid and you can't use the three-corner hat to get an accurate number.

DR. REINHARDT:

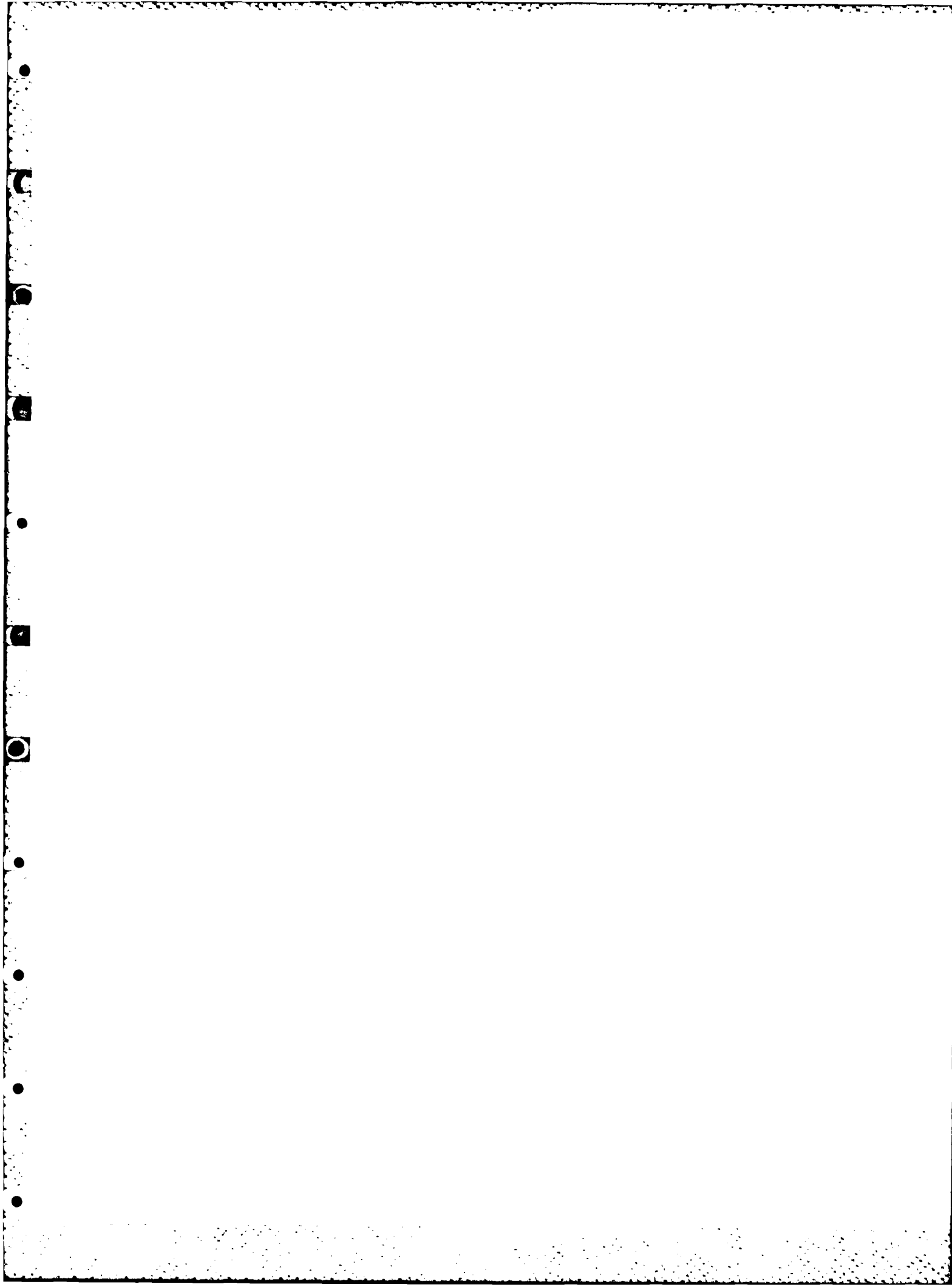
Oh, for that clock, but you can use it for the rest of the data?

MR. WEISS:

Yes.

PROFESSOR ALLEY:

This analysis was very interesting and it reveals what some of us suspected or emphasized for some time, that they were assigning errors incorrectly. May I emphasize once more that the G.P.S. planning people give serious consideration to a short laser pulse calibration technique that would unambiguously separate the ephemeris errors from the clock errors. Thank you very much.



ENHANCEMENTS TO THE TTS-502 TIME TRANSFER SYSTEM

Dr. A. J. Van Dierendonck
Dr. Q. D. Hua
Stanford Telecommunications, Inc.
2421 Mission College Blvd.
Santa Clara, CA 95050
(408) 748-1010

ABSTRACT

Two years ago STI introduced an affordable, relatively compact time transfer system on the market -- the TTS-502, and described that system at the 1981 PTTI conference. Over the past few months, that system has been improved, and new features have been added. In addition, new options have been made available to further enhance the capabilities of the system.

These enhancements include the addition of a positioning algorithm and new options providing a corrected 5 MHz output that is phase coherent with the 1 pps output, and providing an internal Rubidium Oscillator.

The Positioning Algorithm was developed because not all time transfer users had the luxury of the Defense Mapping Agency's (DMA) services for determining their position in WGS-72 coordinates. The enhanced TTS-502 determines the GPS position anywhere in the world, independent of how many GPS satellites are concurrently visible. However, convergence time to a solution is inversely proportional to the number of satellites concurrently visible and the quality of frequency standard used in conjunction with the TTS-502. Real world solution results will be presented for a variety of cases and satellite scheduling scenarios. Typically, positioning accuracies were achieved better than 5 to 10 meters r.s.s. using the C/A code only at Sunnyvale, California.

A Time and Frequency Solution allows for the output of a time corrected 1 pps (to GPS time or UTC) and a frequency corrected 5 MHz (and 1 MHz) signal that is coherent to the 1 pps. This is offered as an inexpensive option.

To make the TTS-502 a stand alone system somewhat independent of GPS satellite visibility, an option is also offered where an internal

Rubidium Standard is included in the TTS-502, eliminating the need for expensive Cesium frequency standards.

This paper presents various details and results of the Positioning Algorithm and details of the new options available. In addition, details of other enhancements are described.

INTRODUCTION AND SUMMARY

The TTS-502 and its applications are described in detail in References 1, 2 and 3. It has been recently upgraded to the TTS-502B. A new computer board has made it possible to make various functional improvements in this Time Transfer System. These improvements are the addition of a Positioning Algorithm, a new Time and Frequency Solution and a series of new commands meant to aid the user in performing his time transfer.

The upgrade to the TTS-502B from the existing TTS-502's can be accomplished by simply purchasing the new computer board along with the new PROM's containing the new software.

In addition to the computer board and software upgrades, four new options are available. These options include two different internal Rubidium Oscillators, a coherent 5 MHz and corrected 1 pps output, and a custom length antenna cable.

The Positioning Algorithm, which is a square root information filter, has been tested at Sunnyvale, California and has consistently demonstrated accuracies of 5-10 meters. It also has the capability of positioning at locations where 4 satellites are never in view simultaneously.

The new Time and Frequency Solution uses the same type of filter as does the Positioning Algorithm. It provides a extremely stable time and frequency transfer capability.

THE POSITIONING ALGORITHM

The TTS-502B Positioning Algorithm was designed with the goal of solving for a stationary position anywhere on earth without much concern of how long it would take. Its primary purpose is to solve for that position for time transfer users who don't have or don't wish to have on outside service (such as DMA) to survey their position.

To solve for a position with GPS globally can't always be done in a short period of time. The system does not currently provide the required simultaneous visibility everywhere in this world. Not only is the Geometric Dilution of Precision (GDOP) bad, it doesn't even exist. However, for a stationary user, instantaneous good geometry is not required, as long as it exists over a reasonable period of time and provided that he has a reasonably stable clock. This is somewhat the concept of the TRANSIT system, except that that system uses Doppler measurements.

The TTS 502B algorithm relies on this concept. In that way it can position itself (actually, its antenna) anywhere on earth. It does so with a square root information filter version of a sequential Kalman Filter that is a natural algorithm for this sort of problem. the square root algorithm is known as the U-D (Upper Triangular Diagonal) Covariance Factorization method of Bierman.⁽⁴⁾ However, for the purposes of this paper, the Kalman Filter implementation will be described because square root implementations are somewhat difficult to illustrate. The reader should refer to Reference 4 for those details.

The previous version of the TTS-502 software already processed measurements in a manner consistent with a Kalman Filter implementation. Corrected pseudorange measurements were computed every six seconds and compared with the equivalent computed range to derive a raw clock offset used in a polynomial smoothing algorithm. The Kalman Filter uses the same computation except that the corrected measurements are compared with a predicted pseudorange in order to define the measurement residuals for the Filter. So the structure was already there. The filtering procedures are as follows:

Filter Initialization

- 1) The initial position estimate X_0', Y_0', Z_0' at t_0 in ECEF (Earth-Centered-Earth-Fixed) Coordinates (meters) is taken to be the position stored in the TTS-502B non-volatile memory, which could have been entered by the operator or saved from a previous solution.
- 2) The initial clock time offset and drift $(\Delta t_{u_0}', \Delta \dot{t}_{u_0}')$ are taken to be zero, even if they had previously been estimated. Given the position described in 1), the filter will solve for these offsets very quickly.

- 3) The filter is a five state filter. Its initial state estimate is

$$\underline{\hat{x}}_0 = \begin{bmatrix} \hat{x}_0 \\ \hat{y}_0 \\ \hat{z}_0 \\ \hat{\Delta t}_{u_0} \\ \hat{\Delta \dot{t}}_{u_0} \end{bmatrix}$$

- 4) The initial covariance matrix P'_0 is defined based on position uncertainties entered by the operator and constants stored in the TTS-502B for the time and frequency offsets. Since the TTS-502B initially sets its time from the HOW word, the initial time uncertainty is based on the uncertainty in that setting. The frequency uncertainty is based upon worst case offsets that might prevail with the frequency standard to which the TTS-502B is being slaved. The type of frequency standard is entered by the operator (crystal, Rubidium or Cesium). the initial error covariance matrix is defined as a diagonal matrix

$$P'_0 = \begin{bmatrix} \sigma_{x_0}^2 & & & & \\ & \sigma_{y_0}^2 & & & \\ & & \sigma_{z_0}^2 & & \\ & & & \sigma_{\Delta t_{u_0}}^2 & \\ & & & & \sigma_{\Delta \dot{t}_{u_0}}^2 \end{bmatrix}$$

Filter Measurement Application

- 1) The measurement matrix $H_k(\hat{\underline{X}}_k)$ is computed at time t_k as a 5×1 column vector (T = transposed)

$$H_k(\hat{\underline{X}}_k) = [\bar{I}_{LOS}, c, 0]^T$$

where the 1×3 line-of-sight vector is

$$\bar{I}_{LOS_k} = \left[\frac{\hat{X}_k - X_{s_k}}{R'_k}, \frac{\hat{Y}_k - Y_{s_k}}{R'_k}, \frac{\hat{Z}_k - Z_{s_k}}{R'_k} \right]$$

where X_{s_k} , Y_{s_k} and Z_{s_k} are the ECEF coordinates of the satellites at time t_k less signal transmission time;

\hat{X}_k , \hat{Y}_k and \hat{Z}_k are the position estimate predicted from the time of the last measurements t_{k-1} , where

$$\begin{aligned}\hat{X}_k &= X_{k-1} \\ \hat{Y}_k &= Y_{k-1} \\ \hat{Z}_k &= Z_{k-1}\end{aligned}$$

and the range estimate R'_k is

$$R'_k = \sqrt{(X_{s_k} - \hat{X}_k)^2 + (Y_{s_k} - \hat{Y}_k)^2 + (Z_{s_k} - \hat{Z}_k)^2}$$

and c is the speed of light in meters per second.

- 2) Compute the pseudorange measurement residual variance α_k as

$$\alpha_k = H_k(\hat{\underline{X}}_k) P'_k H_k^T(\hat{\underline{X}}_k) + \Sigma$$

where \hat{P}_k is the predicted error covariance matrix at time t_k and σ is the pseudorange measurement noise variance taken to be a constant at $(15 \text{ meters})^2$.

- 3) Compute the Kalman Filter gains vector K_k (5x1) where

$$K_k = \hat{P}_k H_k (\bar{X}_k) / \alpha_k$$

- 4) Update the error covariance matrix incorporating the measurements at time t_k

$$P_k = [I - K_k H_k (\bar{X}_k)] \hat{P}_k$$

where I is a 5x5 identity matrix.

- 5) Compute the measurement residual δm_k at time t_k as

$$\delta m_k = PR_k - \hat{PR}_k$$

where PR_k is the pseudorange measurement at time t_k and \hat{PR}_k is the predicted pseudorange measurement, where

$$\hat{PR}_k = R'_k + (\Delta t_{u_k} + \tau_k - \Delta t_{sv_k}) \cdot c$$

where τ_k is the sum of pseudorange corrections (ionospheric and tropospheric delay and earth's rotation correction, all in seconds) and Δt_{sv_k} is the satellites time offset at time t_k .

- 6) Update the estimate of the state vector \bar{X}_k at time t_k , where

$$\bar{X}_k = \bar{X}_k + K_k \delta m_k$$

At this time the TTS-502 computes the change in state since the first iteration (t_0) as

$$\Delta \bar{X}_k = \bar{X}_k - \bar{X}_0$$

and the filter one sigma position uncertainty σ_{p_k} , where

$$\sigma_{p_k} = \sqrt{P_{11_k} + P_{22_k} + P_{33_k}}$$

where P_{ii_k} is the i th entry of the error covariance matrix. The TTS-502B then outputs these values on the screen, to a printer (if option is chosen) and to the auxiliary output port (if option is chosen).

Filter Time Update

- 1) At the time of the next measurement (t_{k+1}), the TTS-502 computes

$$\Delta t_k = t_{k+1} - t_k$$

and sets

$$t_k = t_{k+1}$$

It then updates the estimates (predicts), where

$$\bar{X}_k = \Phi_k \bar{X}_{k-1}$$

where Φ_k is the state transition matrix at the time t_k given as

$$\Phi_k = \begin{bmatrix} 1 & & & & \\ & 1 & & & \\ & & 1 & & \\ & & & 1 & \Delta t_k \\ & & & 0 & 1 \end{bmatrix}$$

2) The error covariance matrix P_k is then updated as

$$P_k' = \Phi_k P_{k-1} \Phi_k^T + Q_k$$

where Q_k is the process noise matrix modeling the characteristics of the frequency standard to which the TTS-502B is slaved. That is,

$$Q_k = \begin{bmatrix} 0 & 0 & 0 & 0 \\ 0 & 0 & 0 & 0 \\ 0 & 0 & q_{44} & q_{45} \\ 0 & 0 & q_{45} & q_{55} \end{bmatrix}$$

where, in general,

$$q_{44} = \frac{h_0}{2} \Delta t_k + 2h_{-1} \Delta t_k^2 + \frac{2\pi^2}{3} h_{-2} \Delta t_k^3 + \sigma_D^2 \frac{\Delta t_k^4}{4}$$

$$q_{45} = 2h_{-1} \Delta t_k + \pi^2 h_{-2} \Delta t_k^2 + \sigma_D^2 \frac{\Delta t_k^3}{2}$$

$$q_{55} = h_{-1} \ln \Delta t_k + 2\pi^2 h_{-2} \Delta t_k + \sigma_D^2 \Delta t_k^2$$

where h_0 , h_{-1} and h_{-2} are Allan variance spectral density coefficients (5) and σ_D is the one sigma frequency standard

drift rate in seconds/second². These variables are stored in the TTS-502B as typical constants for each type of frequency source (good crystal, Rubidium and Cesium).

Filter Operation

Starting with the initial estimates and error covariance defined above, at the time of the first measurement (t_0), the TTS-502B

processes a measurement in the filter every six seconds sequentially by first applying the time update from the time of the previous measurement to the time of the current measurement, and then performing the measurement update. Whenever a satellite changeover occurs, the time between the last measurement from the previous satellite to the first measurement of the current satellite could be as long as 90 seconds.

SOME EXPERIMENTAL RESULTS

The algorithms presented above were verified experimentally prior to modifying the software in the TTS-502. This was relatively easy to do because of the auxiliary port data category output options available. The data required for the filtering operations were available without modifying the unit.

The algorithms were tested using data from Category 2 - Auxiliary Time Transfer Data (6). This data was read via GPIB into an HP-85 desk top computer. Matrix manipulation PROMs augmented the HP-85 to enhance its accuracy. Even then, the square root formulation of the Kalman Filter was required to provide the numerical stability of the Positioning Algorithm. However, this provided a good test in that if the HP-85 could solve for the position of the TTS-502, then surely the MC68000 could with its double precision (64 bits) mathematics package.

The purpose of the algorithm tests using the HP-85 was not only to check out the algorithms themselves and the numerical technique of implementing them, but to test concepts for scheduling measurements from satellites, even in cases when good instantaneous GDOP is not achievable.

All tests were run using a crystal oscillator as the frequency source.

Algorithm Stability

Whenever four satellites are available with good GDOP for the Positioning Algorithm, the rate of convergence to a solution is directly proportional to the rate of switching between satellites. This is evident from the plots of R.S.S. position error in Figure 1, where

$$P_{RSS} = \sqrt{(X_k - X_T)^2 + (Y_k - Y_T)^2 + (Z_k - Z_T)^2}$$

where X_T , Y_T , Z_T is the DMA surveyed position at Sunnyvale, CA. In this plot, a filter iteration normally took 12 seconds, as the HP-85 could not keep up with the TTS-502 six second measurements when the square root algorithm was used. Additionally, there was approximately 60-90 seconds between measurements any time a satellite change was made.

When satellites were changed every 4 minutes, ultimate convergence to better than 10 meters accuracy was achieved in about 45 minutes. In contrast, if satellites were changed every 1/2 hour, convergence took up to 3 hours or so while it obviously takes at least 3 hours for one hour changes. But then, this slower change rate more closely represents the case when four satellites with good GDOP are never available simultaneously.

This is the reason why the square root filter was mechanized. Sometimes when the TTS-502 was scheduled to dwell on a particular satellite for an extended period of time before the filter converged when the conventional Kalman Filter was used, the filter became unstable. This is because the error ellipsoid, which was initialized as a spheroid, became very flat along the line-of-sight to the satellite, and very high correlations (near 1 or -1) between errors occurred. This tended to cause numerical problems. Correlations crept over 1 or below -1, causing the covariance matrix to become eventually non-positive definite. The square root algorithm improved the situation significantly. However, it could also have numerical problems in extreme cases. Thus, it is important to not schedule a single satellite for too long a period. This restriction is not serious, however, since in general a time of day can be selected when at least 2 or 3 satellites are visible for filter initialization.

The Case Where Fewer Than Four Satellites are Ever Visible

Unfortunately, in California at least four satellites are visible for an extended period of time for some time each day. Therefore, one could always take advantage of fast convergence. In order to simulate the case when four satellites (with good GDOP) are never visible at a given location, a schedule was derived where all but three satellites was purposely deleted from the schedule. When this is done, the tracking schedule must be stretched in order to effectively achieve a good geometry over a period of time, taking advantage of the movement of the satellites. Figure 2 illustrates such an example when only three satellites were tracked. The R.S.S. position is compared to that of a four satellite solution. In each case the satellites were changed once an hour. The convergence time for this

particular case of three satellites is about 4.5 hours and about 80 minutes longer than that for the four satellite case. The R.S.S. error is 10 meters as opposed to the 5 meter R.S.S. error for the four satellite case. However, that error comparison is somewhat non-conclusive, since the solutions occurred on different days.

As it turns out, the four satellite solution presented in Figure 2 also simulates a solution at a location where four satellites are not visible simultaneously because the fourth satellite was acquired three hours after the first satellite. Full accuracy was achieved with one sequence through the satellites, so the first one or two satellites need not be visible any longer. In the three satellite case, it is probably necessary to come back to previously tracked satellites.

Convergence Criteria

Fortunately, for testing purposes, the location of the TTS-502 antenna was known for the results described above. However, that would never be the case in the field for those using TTS-502B for determining their position. Therefore, a criteria was established for determining convergence, which is described below under the heading "How to Use the Positioning Feature of the TTS-502B." That procedure states to let the Positioning Algorithm run until the uncertainty level in the SIGMA column drops down to 2-3 meters, where SIGMA is the filter sigma σ_{p_k} defined in the equations presented

earlier. Figures 3 and 4 illustrate two examples of how that sigma compares to the RSS position error. In those figures σ_{p_k} never gets

to the 2-3 meter level because the positioning estimates were turned off when a σ_{p_k} of 5 meters was reached, solving for the time only

after that. That does not occur in the actual implementation, however. The "time only" solution in the actual implementation is described below.

A NEW TIME-FREQUENCY SOLUTION

The TTS-502 has always had a Time-Frequency Solution although only the time solution was displayed. The frequency solution was available via the auxiliary output port. These solutions were a function of a sliding polynomial fit (zero, first or second order) over a specified period. That fit period had a maximum value of 4 minutes (40 six second samples).

Actually, that Time-Frequency Solution is relatively noisy, especially the frequency solution. Because of that, a new Time-Frequency Solution has been implemented in the TTS-502B. That new solution is a fall out of the Positioning Algorithm defined above. In fact, a Time-Frequency Solution is part of the state vector of the positioning filter $(\Delta t_u, \Delta f_u)$. It is not desirable, however, to solve for a position during time and frequency transfers, primary because, as stated earlier, positioning is not always possible. Besides, the time solution is diluted by TDOP (Time Dilution of Precision) when solving for a position.

Therefore, a "time-only" filter solution has been implemented in the TTS-502B. This solution uses the same algorithms (5 state filter) and software used in the Positioning Algorithm with the following modifications. First of all, a position is assumed, taken to be those coordinates stored in non-volatile memory, which may have been entered by the operator or with a replace command following a positioning solution. Then, the 5-state filter is re-initialized and a "time-only" solution is selected. From that time on, the measurement matrix is defined as

$$H(\bar{X}_k) = [0 \ 0 \ 0 \ 1 \ 0]^T$$

indicating that the measurements from that time on only measure time offsets. Since the initial covariance matrix P_0 has no state cross-correlation entries, there will be no cross coupling of the measurements into the positioning states, except for the definition of the range estimate R_k used to define the measurement residuals.

Using the definition of the process noise matrix Q_k , the time constant of this time-frequency filter adapts to the type of frequency standard being used. In fact, the solution will be near optimum given that the Q_k realistically models the characteristics of the frequency standard. The fact is, however, that the parameters were selected to be somewhat pessimistic so that the filter does not become unstable. In any event, no matter which frequency standard is used, the filter has a short time constant to start with, and a relatively long time constant as the filter converges on the time frequency solution. This time constant adapts to the type of frequency standard being used and is much longer than the maximum 4 minute fit span of the previous, but still available, polynomial fit. In fact, previously noticeable measurement quantization effects are no longer noticeable using the new Time-Frequency Solution.

HOW TO USE THE POSITIONING FEATURE OF THE TTS-502B

There are two modes of operation: semi automatic and full automatic, activated by the SP and FP command, respectively. These two modes are identical except that the semi-automatic operation uses the user-setup satellite tracking schedule, while the full-automatic operation computes its own schedule.

The full automatic schedule algorithm implemented in the TTS-502B software is still experimental and does not always provide the best schedule. It is recommended that the semi-automatic mode of operation be used for positioning. Steps 2 and 3 of the following procedure will show how to set up a good tracking schedule.

Procedures

1. Use the DB command to enter the best estimate of antenna location. The location may be entered in either the Earth-Centered Earth Fixed (XYZ) coordinates or the geodetic (latitude, longitude, and height) coordinates. Also set the elevation angle mask to less than 10 degree to get more visibility and better geometry.
2. Use the HV command with P (print) option to get a copy of satellite visibility histogram to help set up a tracking schedule.
3. The best schedule would have the maximum number of satellites over the shortest time interval.

If possible, do positioning over an interval where there are four or more satellites since the position solution converges faster in this case. Over this interval, a tracking schedule may be set up that "rotates" among these satellites, with about 4 minutes per satellite. Even when four or more satellites are simultaneously visible over some time interval, one may not want to wait until such time to do positioning. In such case, a schedule may be set up that will eventually cover four or more satellites, using 4- to 30-minute time slots. At some locations this could be the only choice since there may never be more than 3 satellites simultaneously visible with the current GPS constellation of only 5 working satellites.

After setting up a schedule, use the IS command to enter the tracking schedule. The allotted time of some time slots may have to be stretched if the schedule requires more than 79 time slots.

4. Use the SP command, with P (print) option if desired, to activate the semi-automatic positioning operation. Specify three parameters as follows:
 - a. The kind of frequency standard (crystal, Rubidium, or Cesium) that is being used in positioning. This input is used to select the appropriate clock model. The kind of standard that is being used has to be specified since the system may have been configured with more than one standard, e.g., an internal crystal standard and an external Cesium standard.
 - b. A uncertainty level in the best estimate of the location. It could be as small as 10 meters if it is a very good estimate, or as big as 20,000 meters if the estimate is picked from a map. This parameter should be specified in meters even if the location is entered in geodetic coordinates.
 - c. Enter the selection of XYZ or geodetic coordinates for display. To conserve space on the screen display, only the difference between the computed position and the initial position is displayed.
5. Wait until the uncertainty level on the SIGMA column of the display drops down to 2-3 meters, and then stop the operation by entering CONTROL X. This level of uncertainty indicates that the position solution has converged.
6. Use the LP command with the R option to have the initial position estimate in non-volatile memory replaced by the last position solution.

NEW OPTIONS

There are four new options available that can be added to the TTS-502B. These options are:

- 1) Option 001-RL - an Internal Rubidium Oscillator

- 2) Option 001-RH - an Internal High Precision Rubidium Oscillator
- 3) Option 008 - - Coherent 5 MHz and Corrected 1 pps Output
- 4) Option 009 - - Antenna Cable with Customized Length up to 200 ft.

Internal Rubidium Oscillators

The first two options are identical except for the stability of the oscillator. These options are in addition to the internal crystal oscillator option previously available. Their function is the same. However, they provide a capability with the TTS-502B where it is truly a stand-alone unit as a precise time-frequency standard. This is because the Rubidium Oscillators are stable enough to provide continuous precise time even during periods of time when no GPS satellites are visible.

Currently, Option 001-RL includes the Efratom FRK-L Rubidium Oscillator with the LN₁ (Low Noise) option, whose stability (σ_τ) at $\tau=100$ seconds is 3×10^{-12} . Option 001-RH includes the Efratom FRK-H, where $\sigma_\tau = 1 \times 10^{-12}$ at $\tau = 100$ seconds. For a nominal five hour period of satellite nonvisibility, those numbers translate into time drifts of about 65 and 22 nanoseconds (one sigma) for the RL and RH options, respectively, essentially making the TTS-502B a continuous stand-alone 100 nanosecond timekeeping device.

Coherent 5 MHz and Corrected 1 pps Output

This option provides the capability of having a time-frequency source that is slaved to UTC or GPS Time. With this option the TTS-502B computed time and frequency offsets are used to correct the phase and frequency of the 5 MHz source (internal or external) and the time of the 1 pps output. In addition, the 1 pps output is coherently derived from the corrected 5 MHz. A block diagram of this option is presented in Figure 5.

When this option is being used, any external 1 pps is ignored. The TTS-502B generates its own 1 pps and corrects it so that there is no time offset in its solution. In addition, the frequency of the 5 MHz output is corrected so that there is no frequency offset in the TTS-502B's solution. Since that corrected 5 MHz is used to derive the

corrected 1 pps output, they are coherent and the frequency of the 1 pps is also correct. In effect, the TTS-502B provides a very low bandwidth second order 1 pps Phase Lock Loop.

In addition to the corrected 5 MHz and 1 pps outputs, a corrected 1 MHz output is provided. Both the 5 MHz and 1 MHz outputs are passed through crystal oscillator phase lock loops to reduce the harmonics and spurious components of the signals.

Antenna Cable

The standard length of the TTS-502B antenna cable is 82 feet (25 meters). Option 009 provides customized antenna cable lengths of up to 200 feet for a nominal charge. However, the receiver time calibration is performed with whatever cable, customized or not, is provided with the unit. If the cable or its length is changed, recalibration is required.

USER COMMAND UPGRADE

Hardware-wise, the only difference between the TTS-502 and the TTS-502B, except for options, is a new computer board. The new board is the Omnibyte OB68K1A with 96K of PROM. This board with more memory made it possible to implement the Positioning Algorithm described above. In addition, the number of user commands was increased from 17 to 32. These 32 commands are listed in Figure 6. Some of those new commands are associated with the new Positioning Algorithm and new Time-Frequency Solution. Others were added to further assist the user in operating the TTS-502B. Also, some of the original commands were improved. A summary of these user command upgrades follows.

General Upgrade

In general, three options were added to some of the commands. These are the "Replace" option [R], the "Print" option [P] and the "Output" option [O]. The Replace option is used to replace data in non-volatile memory with the corresponding data shown on the screen display. The Print option is used to output the image of the displayed data to the auxiliary RS-232-C bus. A user-provided RS-232-C printer can be used to obtain a hard copy of the screen display. The Output option is used to output a formatted data category associated with the given command to the auxiliary RS-232-C and/or the GPIB busses.

In addition, for the user's convenience most commands that require a time input will now default to system time if the time input is omitted.

New Commands

The following is a summary of new commands:

- 1) DD - Displays all operational data base parameters -- see example in Figure 7.
- 2) UT - Displays UTC/GPS parameters.
- 3) UG - Computes UTC-GPS time difference at a particular time.
- 4) HV - Displays visibility histogram, i.e., the number of visible satellites and their ID's. See example in Figure 8.
- 5) DV - Displays elevation angle, azimuth angle and Doppler of a particular satellite as a function of time on a particular date.
- 6) CD - Displays a snapshot of elevation angle, azimuth angle and Doppler of all satellites at a particular time and date.
- 7) SS - Displays, for review only, the semi-automatic tracking schedule adjusted to any particular date.
- 8) CP - Computes a fully automatic tracking schedule for positioning such that each satellite (except priority 0) is to be scheduled at least once a day.
- 9) SK,FK - Perform time transfer operation using square root filter to produce time and frequency estimates. SK uses semi-automatic schedule; FK uses fully-automatic schedule.
- 10) SP,FP - Perform positioning function using semi-automatic or fully-automatic schedule, respectively. Displays difference between updated and initial

position in XYZ or geodetic coordinates. See example in Figure 9. A new data category #12 is output every 6 seconds, if selected.

- 11) LP - Displays the last position computed by the previous SP or FP command. With Replace option, that position will be stored in non-volatile memory to be used as reference position.
- 12) CB - Stops the "beeping" alarm.
- 13) ?? - Displays format of a particular command.

REFERENCES

- [1] A.J. VanDierendonck, Q.D. Hua, J.R. McLean and A.R. Denz, "Time Transfer Using NAVSTAR GPS," Proceedings of the Thirteenth Annual Precise Time and Time Interval (PTTI) Applications and Planning Meeting, Washington, D.C., December 1981.
- [2] A.J. VanDierendonck and W.C. Melton, "Applications of Time Transfer Using NAVSTAR GPS," Proceedings of the Institute of Navigation National Aerospace Meeting, Arlington, Virginia, March 1983.
- [3] J.R. McLean and Q.D. Hua, "An Advanced Microprocessor-Controlled GPS Time Transfer System," Proceedings of the Institute of Navigation National Aerospace Meeting, Arlington, Virginia, March 1983.
- [4] Bierman, G.J., Factorization Methods for Discrete Sequential Estimation, Academic Press, 1977.
- [5] Time and Frequency: Theory and Fundamentals, Byron E. Blair, Editor, NBS Monograph 140, May 1974.
- [6] Specification for Time Transfer System TTS-502, Revision 5, STI-TM-9831, 10 November 1982.

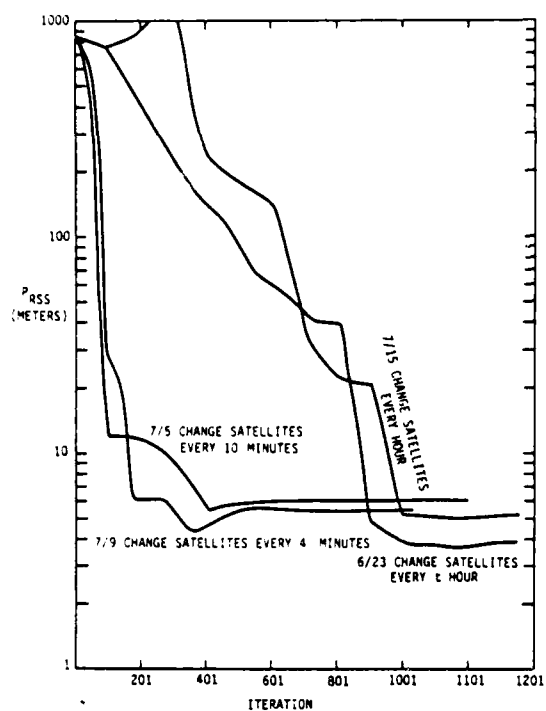


FIGURE 1 P_{RSS} VS ITERATION FOR VARYING LENGTH FOUR SATELLITE SCHEDULES

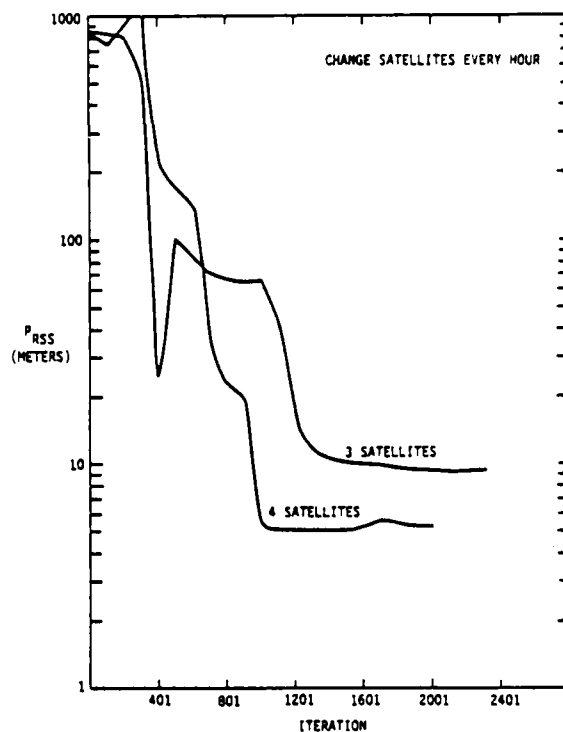


FIGURE 2 A THREE SATELLITE SCHEDULE AND FOUR SATELLITE SCHEDULE COMPARED

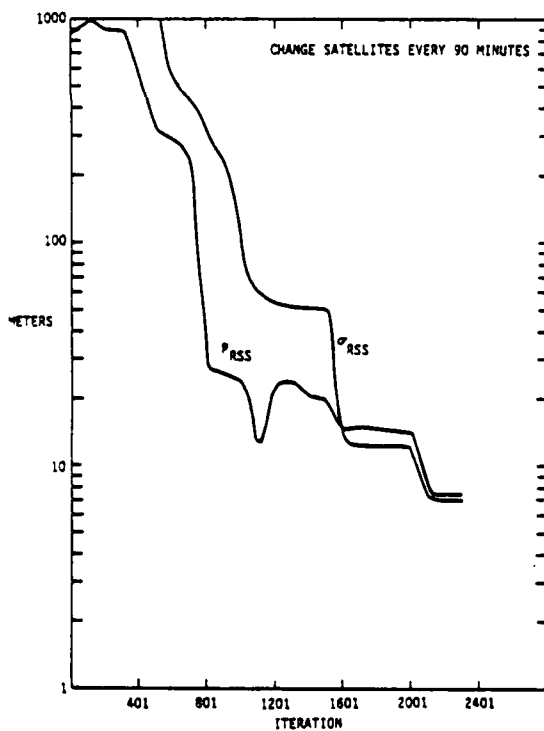


FIGURE 3 P_{RSS} AND σ_{RSS} VS ITERATION FOR A FOUR SATELLITE SCHEDULE

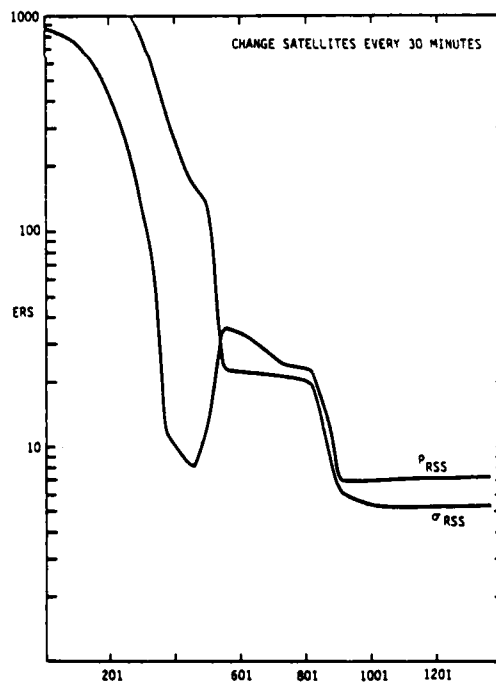


FIGURE 4 P_{RSS} AND σ_{RSS} VS ITERATION FOR THE FOUR SATELLITE SCHEDULE

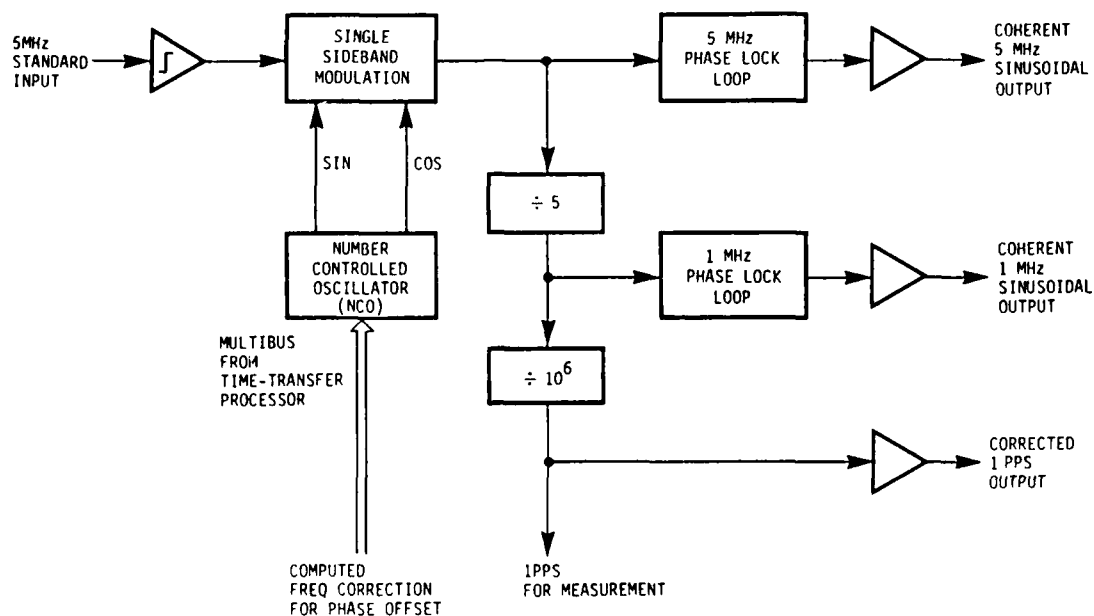


FIGURE 5. TTS 502B OPTION 8, COHERENT CORRECTED 1 PPS

ST	Set Time	IS	Input Schedule [P]
RT	Request Time [P]	SS	Shift Schedule [P]
DB	Data Base Input [D]	CS,CF ..	Compute Schedule [PR]
UD	Data Base Display [FO]	SA,FA ..	Time Transfer (Polv) [P]
AC	Almanac Collection	SP,FP ..	Time Transfer (Alman) [P]
HS	Health & Status [P]	SP,FP ..	Positioning [FO]
HC	Health & Configuration [P]	LP	Last-Computed Position [P]
SM	SV Special Message [P]	OM	Operator Message
UT	UTC/GPS Data [P]	RM	Receiver Monitor
UG	Compute UTC-GPS [P]	BC	Bias Calibration
RV	SV Visibility [FO]	DT	Diagnostic Table
HV	SV Visibility Histogram [P]	CB	Cancel Bell
DV	Daily Elv/Azm/Doppler [P]	HE	Print Command List
CD	SV Elv/Azm/Doppler [P]	CC	Command Format

FIGURE 6. TTS-502B's 32 COMMANDS

[illegible]

FIGURE 8. VISIBILITY HISTOGRAM
(HV COMMAND)

TIME	Dx	Dy	Dz	SIGMA	DF/F	ELEV	ADJUST	DATE
hh:mm:ss	meter	meter	meter	meter	10 ⁻¹⁴	deg	deg	dd/mm/yy
18:58:12	0.00	-0.00	0.00	1730	0.000	53.52	122.58	01/02/01
18:58:18	0.12	0.70	3.95	1731	0.000	53.43	122.58	01/02/01
18:58:24	-0.16	-0.92	-3.90	1729	-0.004	53.44	122.51	01/02/01
18:58:30	0.79	4.14	13.67	1726	0.019	53.40	122.73	01/02/01
18:58:36	0.53	4.11	17.30	1720	0.018	53.35	122.85	01/02/01
18:58:42	0.32	1.91	7.99	1713	0.008	53.32	121.91	01/02/01
18:58:48	1.21	5.76	28.53	1701	0.030	53.28	122.98	01/02/01
18:58:54	0.30	1.38	7.37	1688	0.007	53.24	123.05	01/02/01
18:59:00	-1.58	-8.46	-16.40	1677	-0.038	53.21	123.11	01/02/01
18:59:06	-2.36	-12.67	-54.43	1656	-0.057	53.17	123.13	01/02/01
18:59:12	-1.43	-7.59	-32.95	1639	-0.035	53.17	123.24	01/02/01
18:59:18	-1.41	-7.62	-32.71	1620	-0.034	53.09	123.31	01/02/01
18:59:24	0.65	3.28	14.65	1602	0.015	53.05	123.37	01/02/01
18:59:30	-1.14	-5.07	-26.17	1585	-0.027	53.01	123.44	01/02/01
18:59:36	0.54	2.59	11.87	1568	0.013	52.97	123.51	01/02/01
18:59:42	4.91	24.78	109.87	1557	0.118	52.93	123.57	01/02/01
18:59:48	5.66	28.53	126.57	1539	0.136	52.89	123.64	01/02/01
18:59:54	6.03	30.36	134.80	1526	0.145	52.85	123.71	01/02/01
18:59:00	8.16	40.66	181.43	1515	0.196	52.81	123.77	01/02/01
18:59:06	10.40	51.31	230.18	1504	0.249	52.77	123.83	01/02/01
18:59:12	10.24	50.55	226.64	1495	0.245	52.73	123.90	01/02/01
18:59:18	11.61	56.78	255.88	1487	0.277	52.69	123.96	01/02/01
18:59:24	13.77	64.56	292.97	1480	0.319	52.65	124.03	01/02/01
18:59:30	12.60	61.22	276.79	1473	0.301	52.61	124.09	01/02/01
18:59:36	13.45	60.61	273.77	1468	0.297	52.58	124.16	01/02/01
18:59:42	10.34	52.20	231.27	1462	0.249	52.54	124.22	01/02/01
18:59:48	9.57	49.25	216.00	1458	0.231	52.50	124.28	01/02/01
18:59:54	10.60	53.01	236.05	1454	0.254	52.46	124.35	01/02/01
18:59:00	9.17	43.04	208.72	1450	0.222	52.42	124.41	01/02/01
18:59:06	7.94	43.97	185.60	1447	0.195	52.38	124.48	01/02/01
18:59:12	6.28	38.86	155.32	1444	0.158	52.34	124.54	01/02/01
18:59:18	4.05	32.43	115.46	1442	0.109	52.30	124.60	01/02/01
18:59:24	3.74	31.60	110.04	1440	0.102	52.26	124.67	01/02/01
18:59:30	2.83	29.35	94.47	1437	0.083	52.22	124.73	01/02/01
18:59:36	2.46	28.54	88.40	1436	0.075	52.18	124.79	01/02/01
18:59:42	1.72	27.06	76.45	1434	0.059	52.14	124.86	01/02/01

FIGURE 9. POSITIONING DATA DISPLAY (SP OR FP COMMAND)

QUESTIONS AND ANSWERS

None for Paper #9.

A NEW PRECISION TIME AND FREQUENCY SOURCE FOR STATIONARY PTTI APPLICATIONS

Javad M. Ashjaee, Roger J. Helkey and Ron C. Hyatt
Trimble Navigation, Mountain View, California

ABSTRACT

The highly stable, accurate navigation signals provided by the GPS satellite navigation system are utilized in a new time and frequency source presently in the final stages of development. Integration of the latest technology in component quartz oscillators and digital electronics with a low cost, C/A receiver provides frequency and timing signals with exceptional stability and accuracy at a very cost effective level. A description of the product and results of key performance measurements will be presented in this paper.

INTRODUCTION

The Trimble 5000A GPS Time and Frequency Source is designed to satisfy a broad set of requirements for system time and frequency applications as well as calibration lab and scientific research applications. It is a fully automatic unit with self-test features to ensure proper operation on a continuous basis.

Automatic acquisition and tracking of the optimum satellite provides continuous updates to the frequency and timing outputs without the need for operator interaction. When no satellites are above the horizon, the internal oscillator or externally provided reference will determine the frequency and time based on the last update from the satellite.

The present constellation of satellites provide 14 to 18 hours per day of single satellite coverage. Figures 1-3 show the hours of coverage available at locations around the world. As additional satellites are added, the coverage will approach 24 hours.

In addition to providing a wide variety of frequency and timing signals, frequency and time interval comparisons of other sources are provided to automate calibration.

Accurate position determination capability in WGS-72 coordinates is provided to eliminate any need for precise site survey.

PRODUCT DESCRIPTION

The Trimble 5000A Time and Frequency Source consists of an omni-directional antenna/preamp assembly, coaxial cable up to 75 meters in length, and a 7" high rack mountable main unit.

The product provides isolated front and rear panel standard frequency outputs at 10 MHz, 5 MHz, 1 MHz and 100 KHz. Timing signals at 1000 PPS, 100 PPS, 10 PPS, 1 PPS and 1 PPM are available to meet most system requirements. Table 1 lists the specifications for these signals.

The main unit can be powered by 110/220 volt AC or external DC from 20-35 volts. An internal standby battery provides one hour of operation. The antenna/preamp power is provided from the main unit via the coaxial cable.

The unit contains a built-in display and keyboard with GPIB (IEEE 488) and RS 422 digital interfaces for system integration.

For those applications that require higher performance during non-tracking intervals, an optional internal rubidium oscillator is available. Also, external sources of frequency and time may be utilized as the reference. Frequency control of the external oscillator is also provided.

Calibration of other frequency and time sources can be accomplished with the time interval counter and frequency comparator built into this unit.

SYSTEM DESCRIPTION

Figure 4 shows the block diagram for the integration of a frequency and time source with a simple C/A satellite receiver. A single channel is dedicated to tracking one satellite for time and frequency transfer. Frequency corrections and time corrections are applied to the component quartz oscillator and digital clock based on range and range rate measurements of the satellite. Frequency control resolution is 1.5 parts in ten to the twelfth and time control resolution is 4 nanoseconds.

Calibration of an external source of time and frequency can be automated with the time interval counter and frequency comparator built into this product. Single shot, 1 nanosecond time difference measurements can be made against the internally generated timing signals. The frequency comparator can resolve two parts in ten to the eleventh in one second of measurement time.

Sequential measurements of four satellites will allow precision position determination necessary for accurate time and frequency transfer when tracking one satellite. Position can be determined within 50 meters after a few hours of averaging when four satellites are available.

Position determination need only be done upon initial installation in order to achieve high accuracy time and frequency transfer.

PERFORMANCE DATA

Stability, accuracy and reliability are the key measures of performance for a time and frequency source. Stability and accuracy measurements have been made on the present prototype. Reliability can be assured with simplified design that minimizes the number of components and interconnections. Component derating is essential to high reliability.

FREQUENCY STABILITY AND ACCURACY

The frequency stability of the 5 MHz and 10 MHz outputs is determined by the component quartz oscillator and output amplifiers for averaging times less than the time constant of the frequency control loop. The stability of the satellite signal plus receiver noise exceeds the oscillator stability for averaging times greater than ten seconds. The control loop has been designed with a time constant of 10-15 seconds in order to not degrade the performance for shorter averaging times, yet still remove any thermal and long term drift of the oscillator. Figure 5 shows the frequency stability for ten second averaging. The "Allan Variance" for 10 second to 300 second averaging times is shown in Table 2.

Frequency accuracy maintained by the GPS system is better than 1 part in ten to the twelfth. The quartz oscillator in the Trimble 5000A is locked to the carrier frequency and corrected to a few parts in ten to the twelfth. During non-tracking intervals, thermal and long term drift in the component oscillator may reduce accuracy to one part in ten to the tenth in reasonably controlled environments. For those applications where higher accuracy is required, the optional component rubidium will maintain better than one part in ten to the eleventh during non-tracking intervals.

TIMING STABILITY AND ACCURACY

The stability of the timing signals is determined by the amount of averaging done on the psuedo-random phase modulation. Table 3 shows the stability of the timing signals for averaging times of 10 to 300 seconds. Averaging for 100 seconds will improve the stability to near 1 nano second (one sigma). Figure 6 shows the timing stability for 10 second averaging during part of a satellite pass of satellite tracking.

Time accuracy of the GPS system is specified to be within 100 nano-seconds (one sigma) with respect to USNO (UTC). Receiver delay and position must be accurately determined to achieve this level of accuracy. The Trimble 5000A automatically calibrates the receiver delay and can determine accurate position with respect to WGS-72 coordinate system.

Table 4 shows the results of time comparisons with Hewlett-Packard HP (UTC) via time transfer and portable clock trips. The uncertainty in TV time transfer and portable clock trips amounts to as much as 100 nanoseconds presently. HP (UTC) uncertainty is 200 nanoseconds. A visit to the GPS Master Clock is planned in the near future to eliminate these uncertainties. The day to day variation of these time transfers is less than 50 nanoseconds including the TV time transfer jitter. During non-tracking intervals, the error may increase to one microsecond for eight hours of non-tracking. With the optional rubidium oscillator, this can be held to less than 200 nanoseconds. Utilizing an external cesium beam standard, less than 100 nanoseconds can be assured on a continuous basis.

CONCLUSION

The GPS satellite navigation system provides a very high performance source of time and frequency for 14-18 hours per day and will become continuous within the next few years. It will likely become the most widely used system for time and frequency distribution and comparison during the next decade.

The Trimble 5000A provides a complete time and frequency source referenced to UTC. The stability and accuracy provided by this product without any need for calibration meets most system and calibration lab requirements. Within the next few months, the Trimble 5000A Time and Frequency Source will become available at a price well below the cost of Cesium beam frequency sources. The elimination of recalibration and synchronization costs will make this source an attractive instrument for all precision time and frequency applications.

ACKNOWLEDGEMENTS

The authors wish to express their appreciation to Charles Trimble and Ralph Eschenbach of Trimble Navigation for their support and to Jim Marshall of Hewlett-Packard for his assistance with the TV time transfers and portable clock measurements.

REFERENCES

1. "NAVSTAR GPS Space Segment/Navigation User Interface", ICD-GPS-200.
2. Milliken, R.J. and Zoller, C.J., "Principle of Operation of NAVSTAR and System Characteristics", Navigation, Summer of 1978.
3. Time and Frequency: Theory and Fundamentals, NBS Monograph 140.
4. Characterization of Frequency Stability, NBS Technical Note 394.

[illegible]

159

SATELLITE VISIBILITY - WASHINGTON D.C. - 11/30/83

5 sat visibility 3, 3 hours
 4 sat visibility 4, 0 hours
 3 sat visibility 5, 0 hours
 2 sat visibility 12, 3 hours
 1 sat visibility 18, 0 hours

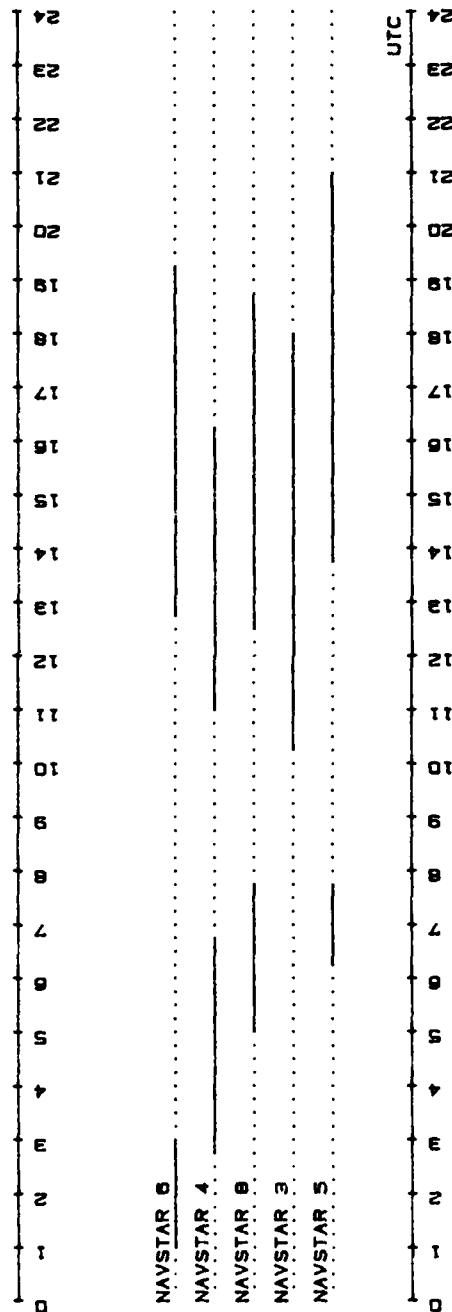
0 1 2 3 4 5 6 7 8 9 10 11 12 13 14 15 16 17 18 19 20 21 22 23 24

NAVSTAR 6
 NAVSTAR 4
 NAVSTAR 8
 NAVSTAR 3
 NAVSTAR 5

0 1 2 3 4 5 6 7 8 9 10 11 12 13 14 15 16 17 18 19 20 21 22 23 24 UTC

FIGURE 2

5 eat visibility	_____	2, 5 hours
4 eat visibility	_____	5, 3 hours
3 eat visibility	_____	8, 8 hours
2 eat visibility	_____	11, 3 hours
1 eat visibility	_____	17, 5 hours



161

TRIMBLE TIME AND FREQUENCY SOURCE SYSTEM BLOCK DIAGRAM

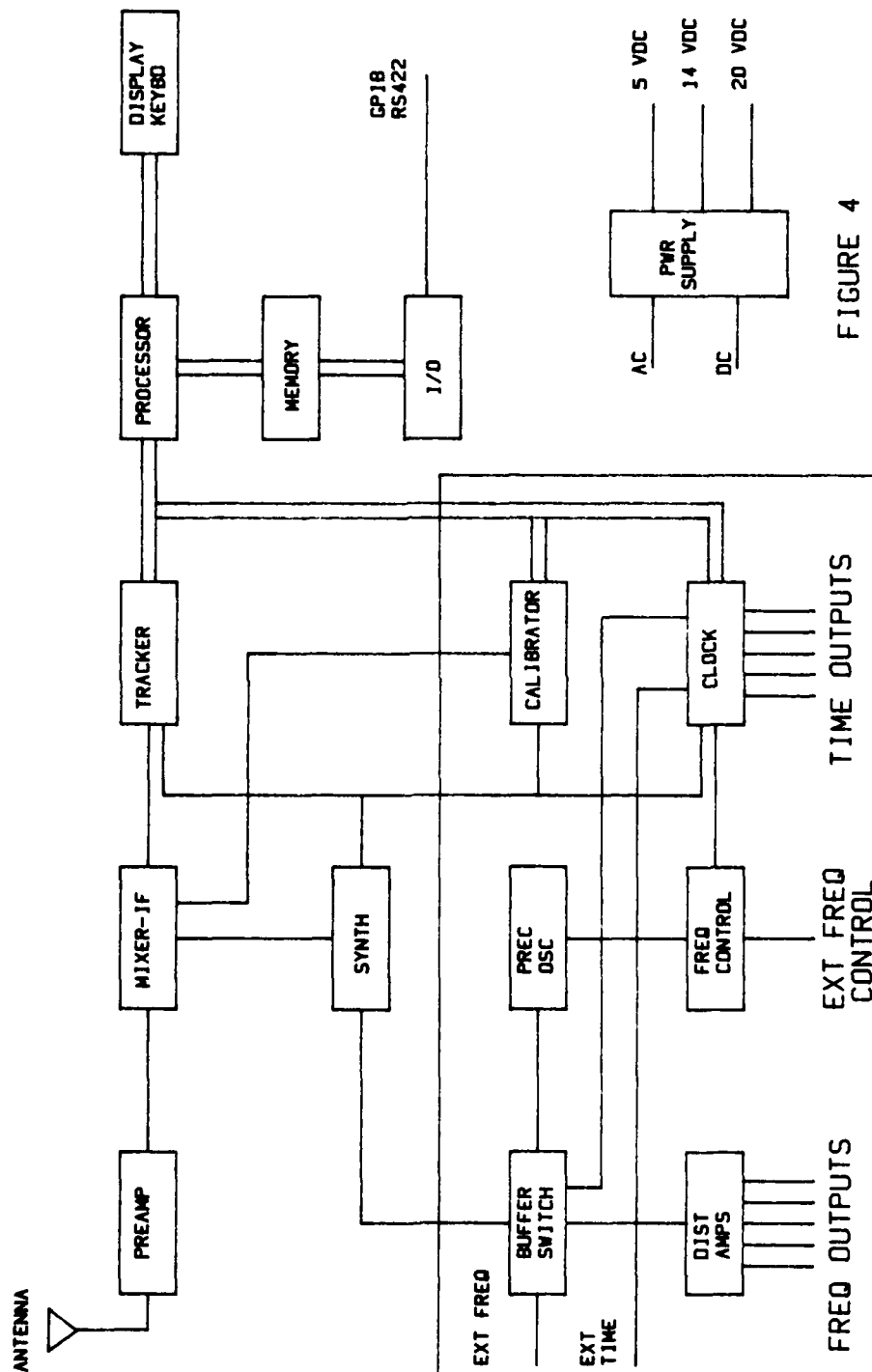


FIGURE 4

FREQUENCY STABILITY

NAVSTAR 5
NOV 19, 1983
1830 UTC

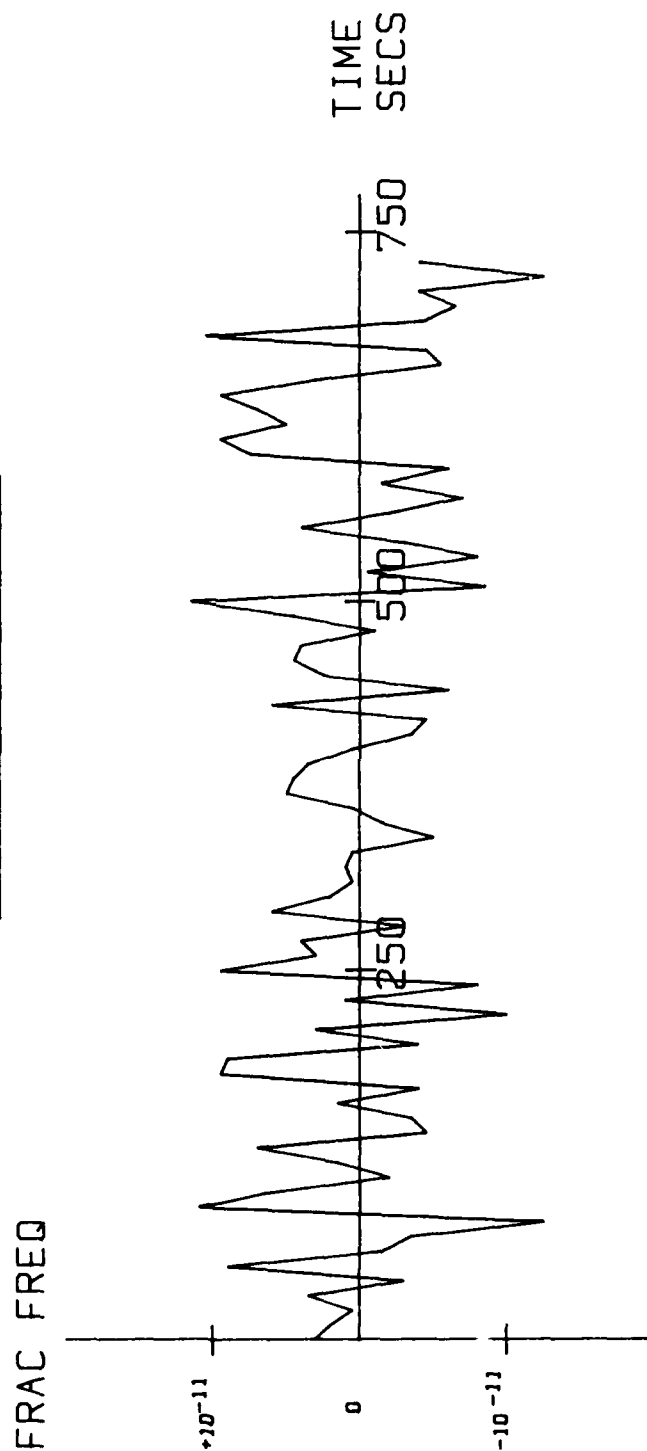


FIGURE 5

TIMING STABILITY

NAVSTAR 5
NOV 19, 1983
1830 UTC

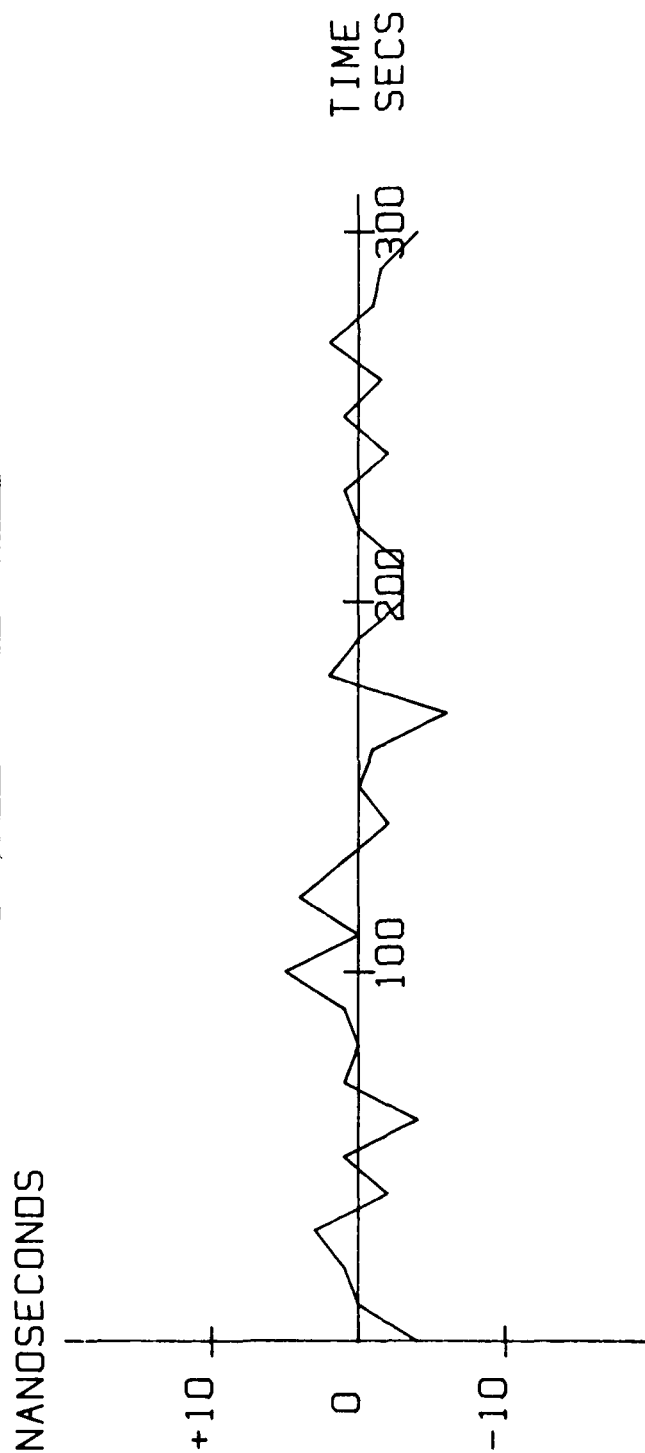


FIGURE 6

TABLE 1
TRIMBLE 5000A SPECIFICATIONS

TIMING ACCURACY:	100 nanoseconds (one sigma) with respect to USNO (UTC) during satellite tracking.
	* 1 microsecond with respect to UTC (USNO) during non-tracking intervals up to eight hours with controlled environment.
TIMING STABILITY:	Better than 20 nanoseconds (one sigma) during satellite tracking.
FREQUENCY ACCURACY:	1 part in ten to the eleventh during satellite tracking.
	* 1 part in ten to the tenth during non-tracking intervals with controlled environment.
FREQUENCY STABILITY:	Better than 1 part in ten to the eleventh for 1 second and greater averaging times.
	* Optional rubidium oscillator provides better than 1 part in ten to the eleventh and less than 200 nanoseconds during non-tracking intervals up to eight hours.
SIGNAL OUTPUTS:	5 and 10 MHz sine wave outputs. Two channels at each frequency. 0-3 volts rms into 50 ohms. Harmonic distortion -30 dB. Nonharmonic distortion -60 dB. Phase noise -140 dBc @ 1 KHz.
	1 MHz and 100 kHz sine wave outputs. Two channels at each frequency. 1 volt rms into 50 ohms. Harmonic distortion -25 dB.
	1, 10, 100 millisec, 1 PPS, 1 PPM pulses. 3 volts into 50 ohms. Positive pulse, dc coupled.

10 microsecond pulse width minimum.
 10 nanosecond rise time minimum.
 Programmable phase, 4 nanosecond steps.

SIGNAL INPUTS: 10 MHz, 5 MHz, 1 MHz sine waves.
 .3-3 volts rms into 50 ohms.

1 PPS, 1 PPM pulses.
 3 volts into 50 ohms.
 Positive pulse, dc coupled.
 10 microseconds pulse width minimum.
 10 nanosecond rise time minimum.

COMPARISONS: Frequency comparator - Two parts in ten to the
 eleventh in one second.

Time interval - 1 nanosecond, single shot.

I/O: RS 422
 GPIB (IEEE 488)

POWER SOURCES: 90/130, 180/280 v ac, 45-440 Hz, 150 va
 20-35 v dc, 60 watts
 Internal battery, 1 hour standby

DIMENSIONS: Coaxial Cable - 20 to 200 feet
 Receiver/Source - 7" x 17" x 17"

FREQUENCY STABILITY

TIMING STABILITY

$\tau(\text{secs})$	$\sigma_y (\tau)$	$\tau(\text{secs})$	$\sigma_t (\tau)$
10	6.7×10^{-12}	10	2.9×10^{-9}
30	3.6×10^{-12}	30	2.1×10^{-9}
100	1.6×10^{-12}	100	1.4×10^{-9}
300	7.1×10^{-13}	300	1.1×10^{-9}

NAVSTAR 5
NOV 19, 1983
1600-1900 UTC

TABLE 2

TABLE 3

TIME COMPARISON

WITH HP

DATE	TIME	SAT #	TV TIME DIFF	TV DELAY ¹	HP-USNO ²	TRIMBLE-USNO ³
11-23-83	16:51	5	51.10	49.72	1.45	70
11-28-83	16:51	3	51.09	49.72	1.45	80
11-29-83	16:51	3	51.10	49.72	1.45	70
11-30-83	16:51	3	51.12	49.72	1.45	50
12-01-83	16:51	6	51.09	49.72	1.45	80
			μsec	μsec	μsec	nsec

1 - UNCERTAINTY OF 100 NANoseconds

2 - UNCERTAINTY OF 200 NANoseconds

3 - UNCERTAINTY OF 225 NANoseconds RSS

TABLE 4

QUESTIONS AND ANSWERS

DR. REINHARDT:

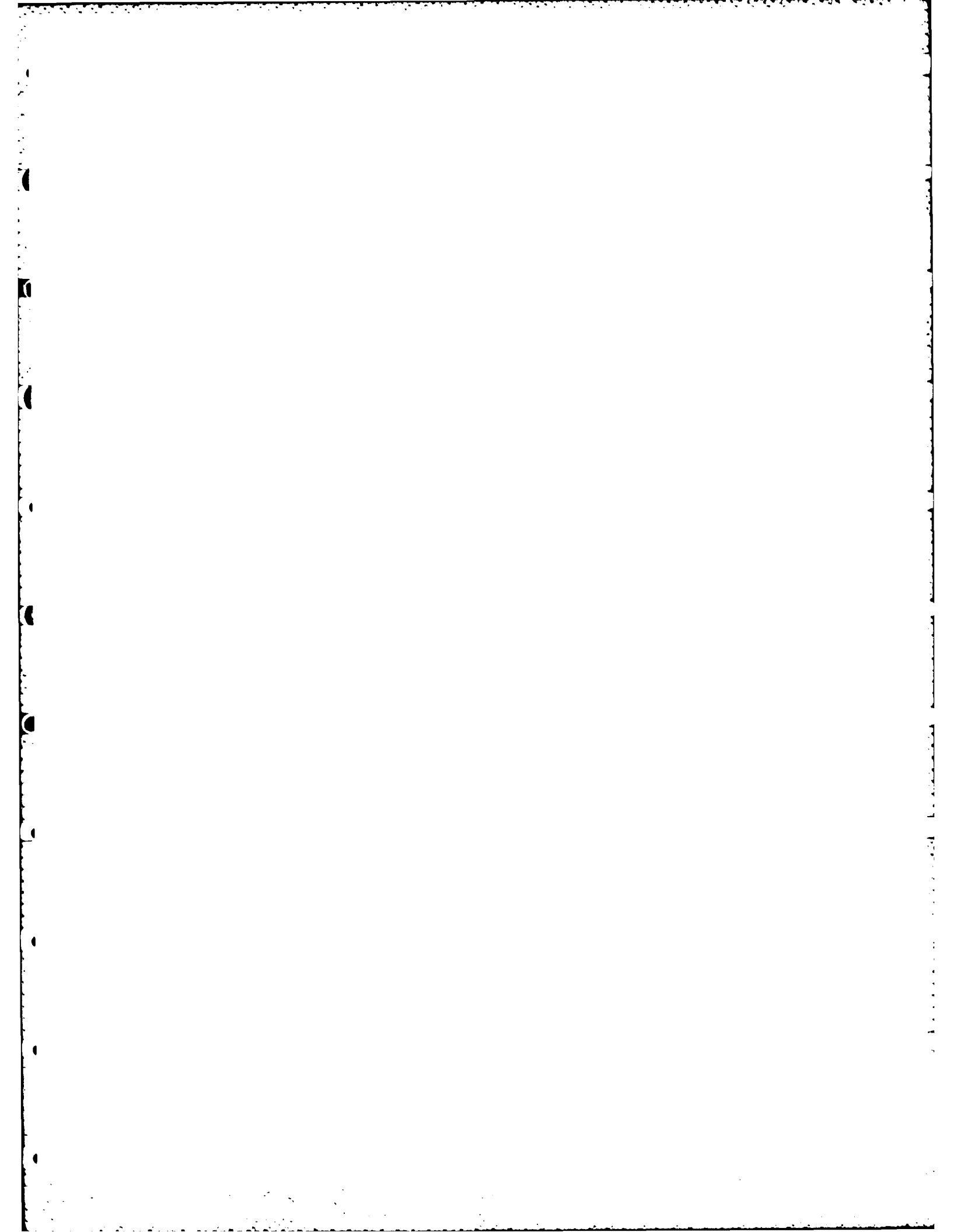
How big is this going to be?

MR. HYATT:

The main unit is packaged in a seven-inch high-rack mount. So it's like seventeen wide, fifteen deep and seven inches high. And of course, there is an antenna unit which is a 3x6x4 assembly that goes on the roof.

DR. REINHARDT:

It's still not the cigarette pack unit, that's a part in 10^{11} but we are getting there.



ON-ORBIT FREQUENCY STABILITY ANALYSIS OF THE GPS NAVSTAR'S 3 AND 4 RUBIDIUM CLOCKS AND NAVSTAR'S 5 AND 6 CESIUM CLOCKS

Thomas B. McCaskill, James A. Buisson, Sarah B. Stebbins,
Naval Research Laboratory, Washington, D. C.

This paper describes the on-orbit frequency stability performance analysis of the GPS NAVSTARs 3 and 4 rubidium clocks, and the NAVSTARs 5 and 6 cesium clocks. Time-domain measurements, taken from the four GPS monitor sites, have been analyzed to estimate the short- and long-term frequency stability performance of the NAVSTAR clocks. The data analyzed includes measurements from 1981, 1982, and the first 100 days of 1983. Short- and long-term results are presented for data collected during 1982. The Allan variance was used as the measure of frequency stability performance in the time domain.

The time-domain noise analysis results indicate a white noise FM process is present, in both rubidium and cesium clocks, for sample times of 900- and 1800-seconds. The projected value of this white noise FM process to a 1-day sample time agrees closely with the 1-day sample time stability results, for both rubidium and cesium clocks, indicating an underlying white noise FM process for sample times ranging from 900 seconds to 1 day.

A random walk FM process was measured for the NAVSTARs 3 and 4 rubidium clocks for sample times of 1 to 10 days. A flicker noise FM process was measured for the NAVSTARs 5 and 6 cesium clocks, for sample times of 1 to 10 days.

The NAVSTARs 3 and 4 rubidium clock long-term frequency stability values are in good agreement with the expected performance. The NAVSTAR-3 short-term stability results indicate an anomaly which has peak effect at a 1.25-hour sample time.

The NAVSTARs 5 and 6 cesium clock long-term frequency stability values are in good agreement with the expected performance. For sample times of 2- to 10-days the cesium clocks have better frequency stability results than the rubidium clocks.

INTRODUCTION

The NAVSTAR Global Positioning System (GPS) is a Department of Defense (DOD) space-based satellite system. When operational in the late 1980's, 18 - 24 satellites in six orbital planes will provide accurate navigation and precise time information to users anywhere in the world. Examples of GPS use are weapons delivery, point-to-point navigation, search/rescue operations and passive rendezvous. It can provide navigational updates to platforms

with other navigation systems.

One role of the Naval Research Laboratory (NRL) in GPS is to provide space-qualified atomic clocks for use in the NAVSTAR spacecraft. The responsibility of NRL includes pre-flight and post-flight frequency stability analyses (1,2) to insure that on-orbit accuracy and stability requirements are met.

This presentation describes the on-orbit frequency stability performance analysis of the GPS NAVSTARs 3 and 4 rubidium clocks, and the NAVSTARs 5 and 6 cesium clocks. Time-domain measurements, taken from the four GPS Monitor Sites (MS), have been analyzed to estimate the short- and long-term frequency stability performance of the NAVSTAR clocks. The results include long-term (1- to 10-day sample times) results for data collected during 1981, 1982, and the first 100 days of 1983. Short- and long-term results are presented for data collected during 1982.

The first part of the presentation briefly describes the NAVSTAR GPS system, with emphasis on the clock measurements. Equations are then presented which permit the separation of the orbital signal, and other smaller effects, from the clock offset between a NAVSTAR clock and a GPS monitor site clock. A time-domain analysis of the NAVSTARs 3, 4, 5, and 6 clocks is then presented. The Allan variance is used as the measure of frequency stability in the time domain. The results presented include a time-domain noise analysis, whose purpose is to identify the random periodic noise processes that are present in the NAVSTAR cesium and rubidium clocks. Readers who are familiar with the mathematical theory of clock analysis may choose to proceed directly to the section on NAVSTAR-3 On-orbit Results.

GPS System Description

The NAVSTAR GPS system is comprised of three major segments:

- (1) Control Segment. The current GPS Control Segment consists of a master control station (MCS), located at Vandenberg, CA and four monitor sites. One monitor site is located adjacent to the master control station at Vandenberg; the remaining three remote monitor sites are located at Hawaii, Alaska, and Guam. These four stations track the GPS space vehicles (SV). Data from these sites are transmitted to the MCS and processed to determine SV orbits and clock offsets. A separate Satellite Control Facility (SCF) is used to transmit commands and navigational information to the GPS spacecraft.
- (2) Space Segment. During the time period covered in this report, the GPS Space Segment constellation consisted of five NAVSTAR SVs; NAVSTAR 8 was launched on July 14, 1983. The launch dates and clock information are detailed by the following table.

TABLE 1

GPS SV Launch Date	Frequency Standard Currently in use
NAV 1 2/22/78	Quartz
NAV 3 10/07/78	Rubidium
NAV 4 12/11/78	Rubidium
NAV 5 2/09/80	Cesium
NAV 6 4/26/80	Cesium
NAV 8 7/14/83	Rubidium

Each GPS space vehicle continuously broadcasts spread spectrum signals in L-band. The center frequency values are at 1227.6- and 1575.42-MHz, which are designated as L_1 and L_2 , respectively. The signal waveform is a composite of two pseudo-random noise (PN) phase-shift-key (PSK) signals transmitted in phase quadrature. These two signals are referred to as the P-signal and the C/A signal.

The P-signal provides the capability for precise navigation, is resistant to ECM and multipath, and could be denied to unauthorized users by means of transmission security (TRANSEC) devices.

The C/A signal provides a ranging signal for users whose navigation requirements are less precise. In addition, this signal serves as an acquisition aid for authorized users to gain access to the P-signal. The C/A designation indicates the "clear" and "acquisition" functions of this waveform.

Orthogonal binary coded sequences, transmitted from each GPS satellite, provide a capability for identifying each individual satellite. This technique is known as Code Division Multiple Access (CDMA). By means of a correlation detector, the apparent time difference between transmission of the signal and arrival of the signal as determined by the user's receiver clock is measured. This apparent time difference is composed of two parts: the signal propagation delay from the satellite transmitter to the user and the unknown offset of the user clock. Each GPS spacecraft transmits a navigation message which is modulated onto the signal, and may be decoded and used in the calculation of the user's position, velocity, and clock offset.

- (3) User Segment. The GPS User Segment is comprised primarily of users from DOD and the NATO community. Selective civilian use of GPS is being considered, with appropriate restrictions to limit the accuracy.

A high accuracy GPS navigational solution is obtained from

four simultaneous measurements of apparent time difference. These apparent time difference measurements are called pseudo-range measurements because the signal must travel from the GPS spacecraft to the user's receiver, a distance on the order of 20,000 to 25,000 km. Hence this delay is present in addition to the actual clock difference. The time differences are taken between the user receiver clock and each of the NAVSTAR spacecraft clocks. Using a computer-controlled receiver, the GPS user tunes and locks the GPS receiver to signals broadcast from the NAVSTAR SVs, and then makes four simultaneous pseudo-range measurements. The four NAVSTAR SV positions are calculated from the GPS navigation message, which is modulated onto each GPS signal. These four pseudo-range measurements are then used to calculate a navigational solution (3,4) for the user's latitude, longitude, height, and clock offset. GPS provides a near-instantaneous navigation capability for users on a world wide basis.

A GPS navigational solution for the user's velocity and clock-rate may be computed through the use of four additional simultaneous measurements of apparent frequency difference. These apparent frequency difference measurements are called pseudo-range rate measurements, because the relative motion between the GPS spacecraft is present in addition to the clock-rate difference. The basic GPS navigation solution for user position and clock offset is independent of the user's velocity and clock rate; however, the user's position is required for the velocity solution. Alternately, the solution for velocity and clock-rate may be estimated from two or more successive GPS position and clock offset solutions.

GPS On-Orbit Clock Analysis

The GPS instantaneous navigation capability is possible because each NAVSTAR clock is synchronized to a common GPS time. The clock offset, orbital elements, and spacecraft health parameters of all spacecraft in the GPS constellation are periodically determined at the GPS master control station. These clock offsets, orbital elements, and spacecraft health parameters are then uploaded to each NAVSTAR SV and inserted into the GPS navigation message. Each NAVSTAR clock must then keep time, to within GPS specifications, until the next clock update. The time stability of a clock is related to its frequency stability; therefore, a fundamental measure of GPS clock performance is the frequency stability of the clocks. The Allan variance is the statistical measure of frequency stability that is used for reporting clock performance.

The procedure that has been devised at NRL (5, 6) for determining GPS clock performance is presented in Figure 1. The goal of this technique is to separate the clock offset, from the orbital and other smaller effects that are present in the GPS signal. This procedure utilizes a highly redundant

set of pseudo-range, and pseudo-range rate measurements, that are collected from all four GPS monitor sites during two-week intervals. This redundant set of measurements allows the determination of smoothed orbit states and bias parameters that are independent of the GPS Master Control Station realtime Kalman estimation procedure. A description of this technique follows, with emphasis on the variables related to clock performance analysis.

Measurements of pseudo-range (PR) and integrated pseudo-range rate are taken between the NAVSTAR SV clock and the MS clock using a spread spectrum receiver. The MS receivers are capable of making measurements from four GPS SVs, simultaneously, whenever four or more SVs are above the MS horizon. The measurements are taken once every six seconds and then aggregated and smoothed once per 15 minutes. Figure 2 presents a plot of a typical pseudo-range signature obtained from a single NAVSTAR satellite pass over a monitor station. Each measurement is corrected for equipment delay, ionospheric delay, tropospheric delay, earth rotation, and relativistic effects. The data are then edited and smoothed after subtracting the predicted SV ephemeris and clock offset, which removes most of the signal. Following the smoothing procedure, the predicted values are added to the smoothed values to produce the smoothed measurements. The apparent clock offset is evaluated near the midpoint of the 15-minute data span, using a cubic polynomial model and both the pseudo-range and the pseudo-range-rate measurements.

The pseudo-range measurements are resolved to $1/64$ of a P-code chip, which corresponds to 1.5 ns of time, or 46 cm in range. Nominal values of pseudo-range noise levels are $\sigma_{PR} = 1.3$ m for the L_1 measurements, and $\sigma_{PR} = 2.0$ m for the L_2 measurements. The L_1 and L_2 measurements are combined to correct for ionospheric refraction, which results in an increase to $\sigma_{PR} = 4.53$ m for the corrected pseudo-range measurements. The accumulated delta pseudo-range measurement noise levels are 0.31 cm for L_1 and 0.56 cm for L_2 . These measurements are also combined to correct for ionospheric refraction. The smoothing procedure uses the pseudo-range rate measurements to aid in the pseudo-range smoothing of each 15-minute segment of data. This process, as outlined in reference 7, results in a smoothed pseudo-range measurement noise level of 18.5 cm.

The equation that relates the pseudo-range measurement to the clock difference between the NAVSTAR SV clock and the MS clock is:

$$PR = R + c (t_{MS} - t_{SV}) + c t_A + \epsilon \quad \text{Eq (1)}$$

where

PR = the measured pseudo-range

R = the slant range (also known as the geometric range)
from the SV (at the time of transmission) to the MS (at
the time of reception)

c = the speed of light

t_{MS} = the MS clock time

t_{SV} = the SV clock time

t_A = ionospheric, tropospheric, and relativistic delay, with
corrections for antenna and equipment delays

ϵ = the measurement error

The clock difference, $(t_{SV} - t_{MS})$, is obtained by dividing by c, the speed of light, and rearranging Eq (1) into

$$(t_{SV} - t_{MS}) = R/c + t_A + \epsilon/c - PR/c \quad \text{Eq (2)}$$

In Eq (1), the pseudo-range is a measure of distance, typically expressed in kilometers (km). In Eq (2) the unit of measure is time, typically expressed in milliseconds (ms).

The clock difference $(t_{SV} - t_{MS})$ may be defined as a new variable $x(t_k)$.

$$x(t_k) = (t_{SV} - t_{MS}) \quad \text{Eq (3)}$$

The subscript k is used to denote the time of measurement as determined by the monitor site clock. This definition of $x(t_k)$ is made so that the clock difference notation will agree with referenced literature; the clock difference is also denoted by the variable Δt_k .

$$\Delta t_k = (t_{SV} - t_{MS}) \quad \text{Eq (4)}$$

The variables $\{ x(t_k), \Delta t_k \}$ are equivalent; the choice of variable will be one of convenience.

All of the smoothed pseudo-range measurements from the four GPS monitor sites are collected at the GPS Master Control Station. These measurements are processed to produce a realtime estimate of each of the NAVSTAR clock and ephemeris states. These smoothed measurements are further processed in post-flight analysis to produce a smoothed estimate of the NAVSTAR ephemerides.

The realtime estimates of the NAVSTAR SV clock and ephemeris states are made using a Kalman (8, 9) estimator which has been adapted for GPS use, as described in reference 10. The success of the estimation technique is critically dependent on the stability of the NAVSTAR SV and MS clocks. For example, Figure 2 presents the time delay that occurs as the NAVSTAR signal travels from the spacecraft to a GPS monitor site. Reference to Figure 2 indicates a change in apparent time differences of 15 milliseconds or 15,000,000 nanoseconds during the first 3 hours of this NAVSTAR pass. Current GPS specifications call for a maximum clock uncertainty of less than 5 nanoseconds during the pass. If the NAVSTAR SV clock does not meet this specification, then the Kalman estimator has difficulty in separating the orbit part of the GPS signal from the clock noise. Reference to Eq (2) shows that the monitor site clock has the same weight in the measurement as the NAVSTAR clock; therefore, it is highly desirable to have a MS clock of equal, or better time stability at each GPS monitor site. Figure (3) presents theoretical frequency models for the GPS cesium and rubidium clocks. In figure (3), the on-orbit clocks are preceded by "SV", the monitor site clocks are all cesium and are designated by "MS cesium".

It will be assumed that the reference GPS MS clocks are significantly more stable than the on-orbit GPS SV clocks. This assumption will be tested, and verified, using a clock ensemble composed of the GPS MS clocks.

Smoothed estimates for the NAVSTAR orbits are routinely made by the Naval Surface Weapons Center (NSWC), using an orbit estimation program (11). The model includes dynamics of the satellite motion, solar radiation pressure, pole wander, earth tides and orbit adjust maneuvers. The smoothed orbits are made once per week, using all available observations for a two-week span from each of the four GPS monitor sites. The pseudo-range measurements are differenced to compute delta-pseudo-range values which are used as the measured quantity in the NSWC program. The model incorporates a segmented bias parameter solution, with analysis of the resulting residual patterns of the smoothed orbit estimation.

The major advantage of the smoothed orbit estimate, over the Kalman realtime estimate, is the production of a smoothed orbit which is almost completely determined by the data, without restrictive assumptions on the uncertainty in clock and orbit states.

Time-Domain Clock Analysis

GPS operation requires that the on-orbit NAVSTAR SV clocks keep the current GPS time. Because the clocks are periodically updated, interest is in evaluating clock performance as a function of the sample time, τ , which is the difference between two successive values of running time.

Given two clock measurements, $x(t_k)$ and $x(t_j)$, which were made at running times t_k and t_j (by the GPS monitor site clock), the sample time τ is given by Eq (5).

$$\tau = (t_k - t_j) \quad \text{Eq (5)}$$

The sample time will be varied from 900 seconds to 10 days (in this presentation) to evaluate clock performance.

One clock model used to describe the NAVSTAR clock as a function of time is a quadratic equation of the form

$$x(t) = x_0(t_0) + y_0(t_0)(t-t_0) + \frac{\dot{y}_0(t_0)}{2}(t-t_0)^2 + \epsilon(t) \quad \text{Eq (6)}$$

In Eq (6) $x_0(t_0)$ is the initial clock offset, $y_0(t_0)$ is the clock rate (also known as the fractional frequency offset), $\dot{y}_0(t_0)$ is the drift in the fractional frequency (also known as the aging rate), and $\epsilon(t)$ is the error term.

By choosing $\tau = (t-t_0)$ and omitting the error term, Eq (6) can be written as

$$x(t) = x_0(t_0) + y_0(t_0)\tau + \frac{\dot{y}_0(t_0)}{2} \tau^2 \quad \text{Eq (7)}$$

By holding the value of τ fixed, and evaluating Eq (7) for many data samples of t and t_0 , the statistical error in the clock coefficients and the error term can be estimated.

The measure of clock performance used in the analysis of this paper is the Allan variance (12), which is defined by

$$\sigma_y^2(\tau) = \frac{1}{2} \langle (\bar{y}_{k+1} - \bar{y}_k)^2 \rangle \quad \text{Eq (8)}$$

where y_k denotes the average fractional frequency, τ denotes the sample time, and the brackets $\langle \rangle$ denote the infinite time average. Two other parameters are involved in the Allan variance analysis. The first is the repetition interval T , which is equal to the sample time in Eq (8). The other parameter is f_b , the system noise bandwidth, which does not explicitly appear in the Allan variance equation. The system noise bandwidth is receiver dependent, and depends upon user dynamics. Information on the GPS monitor site receivers may be found in reference 13.

The fractional frequency, denoted by the variable y , is given by

$$y = \frac{(\nu - \nu_0)}{\nu_0} \quad \text{Eq (9)}$$

where ν denotes the instantaneous frequency, and ν_0 is the reference, or nominal frequency. The average fractional frequency, denoted by \bar{y}_k , is given by

$$\bar{y}_k = \frac{1}{\tau} \int_{t_k}^{t_k + \tau} y(t) dt \quad \text{Eq (10)}$$

Reference to Eq (10) shows that \bar{y}_k depends on t_k and τ , as well as $y(t)$; so \bar{y}_k could be written as $\bar{y}(t_k, \tau)$ to show this dependence on t_k and τ . The values for \bar{y}_k used in this report are obtained from values of clock offset, $x(t_k)$, computed according to Eq (3). The average frequency \bar{y}_k may be evaluated in terms of $x(t)$, as given by

$$\bar{y}_k = \frac{1}{\tau} [x(t_k + \tau) - x(t_k)] \quad \text{Eq (11)}$$

The infinite time average required in Eq (8) for the Allan variance is, of course, unobtainable in the real world. Therefore, a finite approximation of the Allan variance, given by Eq (12), is used.

$$\sigma_y^2(2, \tau, M) = \frac{1}{(M-1)} \sum_{k=1}^{M-1} \frac{(\bar{y}_{k+1} - \bar{y}_k)^2}{2} \quad \text{Eq (12)}$$

The arguments of the finite approximation, $\sigma_y^2(2, \tau, M)$, are 2, τ , M , respectively. The number 2 specifies that pairs of fractional frequencies are used, τ denotes the sample time, and $(M-1)$ denotes the number of frequency pairs.

The difference between $\sigma_y^2(\tau)$ and $\sigma_y^2(2, \tau, M)$ is that $\sigma_y^2(\tau)$ is the desired quantity defined by an infinite series; $\sigma_y^2(2, \tau, M)$ is a partial series obtained from a finite number of data points. The use of a finite number of data points does not introduce any bias in the estimate of $\sigma_y^2(\tau)$, as shown by reference 14. The ratio of the variables $\sigma_y^2(2, \tau, M)$ and $\sigma_y^2(\tau)$ will be used in establishing confidence limits for the finite estimate of $\sigma_y^2(\tau)$.

The convergence of this finite-sample average, $\sigma_y^2(2, \tau, M)$, towards a theoretical limit has been investigated by researchers (13). The confidence of this quantity as a measure of $\sigma_y^2(\tau)$ has also been investigated (14, 15). These theoretical results indicate that a high-confidence estimate of $\sigma_y^2(\tau)$ may be obtained through the use of large data bases, which result in a large number of frequency pairs. In practice it is desirable to have a data base length which is at least a factor of ten larger than the sample time.

The square root of the Allan variance is called the Allan deviation. The Allan deviation is defined by Eq (13).

$$\sigma_y(\tau) = [\sigma_y^2(\tau)]^{1/2} \quad \text{Eq (13)}$$

Frequency Stability Set Selection Criteria

The GPS measurements may be aggregated into sets for the short- and long-term frequency stability analysis. Figure 4 presents a flow diagram of

this procedure. The smoothed pseudo-range measurements are combined with the reference ephemeris to produce smoothed clock offsets. Each smoothed measurement is obtained from up to 150 six-second pseudo-range and 149 delta pseudo-range measurements. This procedure includes corrections for ionospheric, tropospheric, and equipment delays, and a correction for relativity effects. The set selection criteria are then applied to construct subsets of clock offset values, $\{x(t_k)\}$, which are then used to produce the $\sigma_y^2(\tau)$ Allan variance values.

For the short-term frequency stability analysis, the Allan variance is computed from the set of smoothed clock offsets, using one or more satellite passes. Reference to Figure 4 indicates that sets of 5, 10, or more days have been used to compute one value of $\sigma_y^2(\tau)$.

Figure 5 presents an example of a five day set of NAVSTAR-3 observations as recorded at the Vandenberg MS. The plot presents the elevation angle of NAVSTAR-3 as a function of time for five days beginning at day 180. The elevation angle is computed every 15 minutes, and plotted as a "dot" on Figure 5. Inspection of this plot indicates that a partial pass may occur at the beginning, or ending, of the five-day set.

Note the repeating pass signature in Figure 5 which is characteristic of all GPS orbits. This repeating signature is a result of the 12-sidereal-hr GPS orbits which produce repeating ground tracks. Therefore the number of points-per-pass remains constant. For example, in Figure 5 a total of 28 values of smoothed data are available from this NAVSTAR-3 pass over the Vandenberg MS. A five-day set would contain approximately 140 data segments which could be used to obtain smoothed NAVSTAR clock offset values.

The 5-day set has been chosen for use in this paper because of a tradeoff between the confidence in the Allan variance and the length of the set. The primary reason for choosing the shortest set possible is to see changes in the NAVSTAR clocks as a function of time. The reason for choosing longer sets is to increase the total number of samples in each Allan variance calculation.

The number of Allan variance values that are calculated may be maximized, using a procedure based on the one given in reference 15. This procedure involves defining a base sampling time τ_0 , which is defined by Eq (14).

$$\tau_0 = \text{MIN} \{(t_k - t_j) : j \neq k\} \quad \text{Eq (14)}$$

For the short-term frequency stability results, a nominal base sampling time of 15-minutes (or 900 seconds) will be used. For the long-term frequency stability results a base sampling time of 1-day will be used. Multiples of the base sampling time may be calculated according to

$$\tau = n\tau_0$$

where the variable n takes on integer values 1, 2, A maximum value of $n = 8$ will be used for the short-term frequency stability analysis, and $n = 10$ for the long-term frequency stability analysis.

The number of clock offsets in a set will be denoted by the variable N . Assuming that all of the clock offsets are equi-spaced at sample time τ , the total (with maximal use of data) number of Allan variance values is given by the expression $(N - 2n)$. This is not the case with the data used in this report due to the nature of the GPS orbits. For both the short- and the long-term processing algorithms each sample time is calculated according to Eq (5), and each fractional frequency according to Eq (11).

A calculation has been performed to produce typical values for the confidence in the Allan variance. The Allan variance value is then converted to the Allan deviation according to Eq (13). Most of the reference literature expresses frequency stabilities in terms of $\sigma_y(\tau)$ rather than $\sigma_y^2(\tau)$.

The confidence limits are calculated according to the method outlined in reference 15, using a white noise FM process, because this is the dominant noise type that was encountered in the short-term frequency stability values. The confidence limits for a 95% confidence level, calculated for a five-day set (Figure 4), are presented in Table 2. These calculations have been made assuming 25 points-per-pass; however, the total number of samples for the five-day set has been modified to account for the pass-to-pass break in the data. The pass-to-pass break in the data effectively reduces the number of samples that may be computed.

Table 2
95% Confidence Limits
for a
5-Day Set and a
White noise FM process

Sample Time (hrs)	Confidence Limits		Number of $\sigma_y^2(\tau)$ Samples	Degrees of Freedom
	UPPER	LOWER		
0.25	1.189	.816	115	76
.5	1.211	.798	105	63
.75	1.253	.772	95	47
1.00	1.299	.748	85	36
1.25	1.344	.726	75	29
1.5	1.403	.702	65	23
1.75	1.444	.687	55	20
2.00	1.499	.669	45	17

The typical confidence limits may be used to separate random sampling fluctuations from systematic changes in clock behavior, or other changes in clock performance. For example, if a stability of 1×10^{-12} was computed for a 0.25 hour sample time, the upper 95% confidence would be $(1 \times 10^{-12}) \times (1.189) = 1.189 \times 10^{-12}$. A sequence of Allan deviations, computed using successive five-day sets, could then be analyzed using these 95% confidence limits as a guide to separate random sampling from systematic and other

effects. Further inspection of Table 2 indicates that for sample times greater than 2 hours, larger sets would be required to produce acceptable confidence limits in $\sigma_y(\tau)$ values.

The Allan variances obtained from successive 5-day sets can be further averaged to obtain one value for the entire data span. For a 1-year data span, a total of 72 five-day sets would be available for the $\sigma_y^2(\tau)$ calculation. Multiplying the degrees of freedom for a typical 5-day set (Table 2) by 72 five-day sets per year results in 3240 Allan variance samples for a 2-hour sample time, and for a 15-minute sample time. The number of Allan variance samples versus sample time is presented in Figure (7) for a 5-day set, and a 1-year data set from the four GPS monitor sites.

For the long-term (1- to 10-day sample times) frequency stability analysis, one pass of a NAVSTAR SV over a monitor site is used as an operational set selection criteria. Figure 6 depicts one pass of NAVSTAR-6 as observed from the Vandenberg MS. Using the set of clock offsets from one pass, a single value of clock offset is computed for the pass. The epoch for the calculation is chosen to be the Time-of-Closest Approach (TCA) of the spacecraft to the monitor site. This value of clock offset is denoted as $x(t_{TCA})$. A least square objective function is used with data editing to identify and remove statistical outliers, and to limit the set points within ± 1.5 hours of TCA. In addition to this procedure, a pass-to-pass constraint on the sample time τ must be met before an Allan variance can be computed.

For the long-term frequency stability values, two types of noise processes were encountered. These two types of noise processes were: random walk FM for the NAVSTAR rubidium clocks, and flicker noise FM for the NAVSTAR cesium clocks. Tables 3 and 4 present the 95% confidence limits for a 1-year data set assuming no pass-to-pass break in the data.

Table 3
95% Confidence LIMITS
for a
1-year set and a
Random walk FM noise process

Sample Time (days)	Confidence Limits		Number $\sigma_y^2(\tau)$ Samples	Degrees of Freedom
	UPPER	LOWER		
1	1.07	0.93	363	364
2	1.09	.91	361	180
3	1.15	.89	359	119
4	1.17	.87	357	88
5	1.20	.86	355	70
6	1.22	.84	353	58
7	1.25	.83	351	49
7	1.25	.83	351	49
8	1.27	.82	349	42
9	1.32	.81	347	37
10	1.33	.80	345	33

Table 4
95% Confidence LIMITS
for a
1-year set and a
Flicker noise FM process

Sample Time (days)	Confidence Limits		Number of $\sigma_y^2(\tau)$ Samples	Degrees of Freedom
	UPPER	LOWER		
1	1.07	.92	363	315
2	1.08	.91	361	224
3	1.13	.90	359	148
4	1.15	.89	357	110
5	1.17	.87	355	87
6	1.20	.86	353	72
7	1.22	.85	351	61
8	1.24	.84	349	53
9	1.25	.83	347	47
10	1.27	.83	345	42

NAVSTAR-3 On-orbit Results

Two types of plots will be used to present the NAVSTAR time domain clock data. The first type of plot presents the Allan deviation, averaged over 5-day sets, as a function of running time. The second type of plot presents the Allan deviation as a function of sample time.

Figure (8) presents the NAVSTAR-3 $\sigma_y(\tau)$ versus running time t , for 1982. A total of 64 five day sets were used to produce these results. These calculations were made using the 1-year average as a reference. The 95% confidence limits used were those presented in Figure (8). Inspection of Figure (8) indicates only two outliers that obviously exceed the 95% confidence limits.

For brevity only one $\sigma_y(\tau)$ versus running time t plot will be presented in this paper. Those readers interested in a more complete treatment may reference the forthcoming NRL report #8778.

Figure (9) presents the NAVSTAR-3 frequency stability results as a function of sample time. The independent variable in Figure (9) is the sample time, which varies from 900 seconds to 10 days. The NAVSTAR-3 aging rate, which averaged -3.5 PP10(13)/day for 1982, was removed before calculating the Allan variance. The aging rate was calculated using a least-squares curve fit to a quadratic equation, given by Equation (6), and a data length significantly greater than 10-days, which was the longest sample time analyzed. The theoretical curves for the SV rubidium and MS cesium clocks are plotted in Figure (9) as solid curves. The on-orbit measured values, which are referenced to each of the GPS monitor site cesium clocks, are plotted as discrete points connected by dashed line segments. The short-term sample times values range from 900-seconds to 2-hours, with increments of

900-seconds. The long-term sample times vary from 1 to 10 days, with increments of 1-day.

Figure (10) presents the NAVSTAR-3 frequency stability results referenced to an ensemble of clocks, consisting of the four GPS MS clocks. The presentation of the NAVSTAR-3 plots, referenced to individual GPS monitor site clocks, allows statistical comparison of the reference clocks, in addition to the NAVSTAR-3 clock.

The NAVSTAR-3 short-term frequency results indicate a value of 21.3 PP10(13) for a 900-second sample time. From 900- to 1800-seconds, the NAVSTAR-3 clock followed a white noise FM process. Inspection of Figure (9) indicates an anomaly that was first noticed for a 2700-second sample time. This anomaly reaches a peak value of 17.1 PP10(13) for a 1.25-hour sample time. Following presentation of the NAVSTARs 4, 5, and 6 results, it will be concluded that this anomaly is entirely due to the NAVSTAR-3 clock.

The NAVSTAR-3 long-term frequency stability results indicate a stability of 1.11 PP10(13) for a 1-day sample time. For sample times of 1- to 6-days, the NAVSTAR-3 rubidium clocks follow a random walk FM process, which was expected for the rubidium type clocks. For sample times of 6- to 10-days, there was a small departure from the random walk FM process. Reference to Figure (9) indicates that this is due to the behavior of data received from the Guam MS.

NAVSTAR-4 On-orbit Results

The NAVSTAR-4 short- and long-term frequency stability results are presented in Figures (11) and (12). Figure (11) presents the NAVSTAR-4 results referenced to each individual GPS MS clock. Figure (12) presents the results referenced to the ensemble of the four GPS MS clocks.

The NAVSTAR-4 short-term frequency stability results indicate a value of 21.3 PP10(13) for a 900-second sample time. From 900- to 1800-seconds, the NAVSTAR 4 rubidium clock follows a white noise FM process. From 1800- to 3600-seconds a small change in slope occurs, which indicates a change in the noise process. From 3600- to 7200-seconds, a distinct change in the noise process is evident. The slope of this data indicates that a flicker noise FM process is present. This solution is obtained by solving the power law model of the Allan variance, given by Equation (15), for the coefficients a and the exponent μ . This solution yields a value of $\mu = -0.17$, which is close to the value of $\mu = 0$ for a flicker noise FM process.

$$\sigma_y^2(\tau) = a(\tau)^\mu \quad \text{Eq (15)}$$

The NAVSTAR-4 long-term stability results indicate a stability of 1.34 PP10(13) for a 1-day sample time. For sample times of 1- to 6-days, the NAVSTAR-4 rubidium clock follows a random walk FM process. For between 6- and 10-days sample time, a small change in slope occurs, which is due to data received from the Guam GPS MS.

NAVSTAR-5 On-orbit Results

AD-A149 163

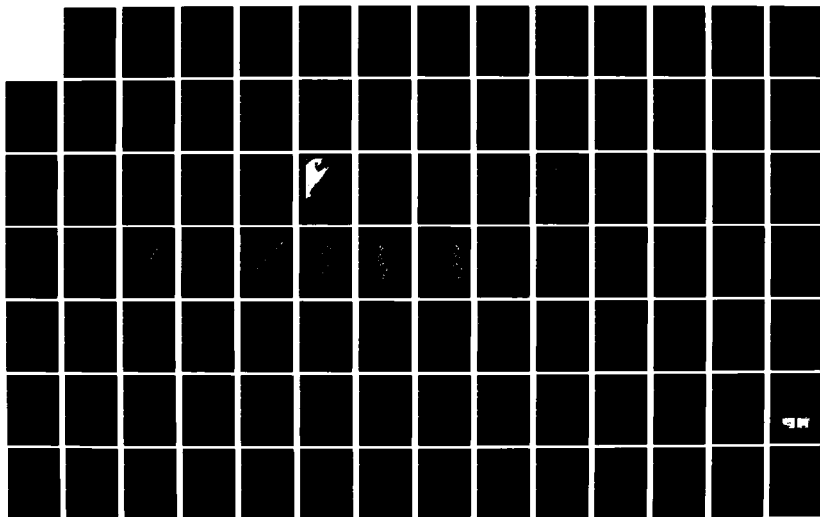
PROCEEDINGS OF THE ANNUAL PRECISE TIME AND TIME
INTERVAL (PTTI) APPLICATI. (U) NAVAL RESEARCH LAB
WASHINGTON DC J A MURRAY 02 APR 84

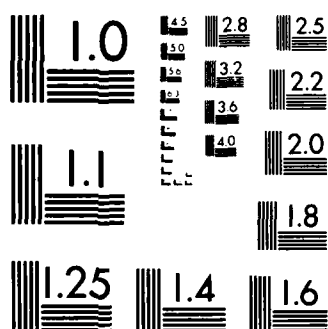
3/8

UNCLASSIFIED

F/G 5/9

NL





MICROCOPY RESOLUTION TEST CHART
NATIONAL BUREAU OF STANDARDS-1963-A

The NAVSTAR-5 short- and long-term frequency stability results are presented in Figures (13) and (14). Figure (13) presents the NAVSTAR-5 results referenced to each individual GPS MS clock. Figure (14) presents the results referenced to the ensemble average of the four GPS MS clocks. No aging rate correction was calculated, or necessary, for the cesium clock.

The NAVSTAR-5 short-term results indicate a value of 23.5 PP10(13) for a 900-second sample time. The NAVSTAR-5 short-term results are slightly higher than the NAVSTAR-4 results, except for the results referenced to the GPS Guam MS. In the ensemble results, presented in Figure (14), the Guam MS data have been deleted from the ensemble average for sample times between 1800- and 7200-seconds. The ensemble average results indicate a flicker noise FM process for sample times of 3600- to 7200-seconds.

The NAVSTAR-5 long-term stability results indicate a stability of 1.58 PP10(13) for a 1-day sample time. From 1- to 5-days sample time, a small slope is noted. From 5- to 10-days, a flicker noise FM process is present, with a value of 1 PP10(13).

NAVSTAR-6 On-orbit Results

The NAVSTAR-6 short- and long-term frequency stability results are presented in Figures (15) and (16). Figure (15) presents the NAVSTAR-6 results referenced to each individual GPS MS clock. Figure (16) presents the results referenced to the ensemble average. No aging rate correction was required.

The NAVSTAR-6 short-term results indicate a value of 21.6 PP10(13) for a 900-second sample time. From 900- to 1800-seconds, the NAVSTAR-6 clock followed a white noise FM process. From 1800- to 3600-seconds, a small change in slope occurs similar to the NAVSTAR 4 and 5 results. Likewise, a flicker noise FM process was present from 3600- to 7200- seconds sample time.

The NAVSTAR-6 long-term results indicate a stability of 1.11 PP10(13) for a 1-day sample time. The stability continues to improve to a stability of 7.7 PP10(14) for a 4-day sample time. Between 4- and 5-days sample time, a small change is noted. For sample times between 5- and 10-days, the NAVSTAR-6 cesium clock follows a flicker noise FM process.

NAVSTARs 3/4/5/6 On-orbit Results

The NAVSTARs 3 and 4 rubidium clock results, referenced to the GPS MS clock ensemble, are presented in Figure (17). The short-term frequency stability results are in close agreement for 900, 1800, and 2700-seconds sample time. The NAVSTAR-3 anomaly, at 1.25 hours sample time, clearly departs from the NAVSTAR-4 results. The long-term results are in close agreement, with both rubidium clocks following a random noise FM process.

The NAVSTARs 5 and 6 cesium clock results are presented in Figure (18). The short-term results are in close agreement at 900-seconds sample time. For sample times of 1800- to 2700-seconds, the NAVSTAR-5 results indicate more

noise than the NAVSTAR-6 results.

The long-term results indicate the NAVSTAR-5 cesium clock has more noise for sample times of 1- to 4-days. The cesium clocks agree closely from 5- to 10-days sample time.

The NAVSTARs 3,4,5, and 6 results are presented in Figure (19). The short-term results indicate close agreement between NAVSTARs 3, 4, and 6 for a 900-second sample time. The NAVSTARs 3 and 6 clocks are in close agreement for sample times of 900- to 2700-seconds. The NAVSTAR-5 cesium indicates slightly more noise than the NAVSTAR 3 and 6 results. The NAVSTAR-3 anomaly is significantly different from the other clock results.

The long-term results indicate a random noise FM process for the rubidium clocks, and a flicker noise FM process for the cesium clocks. For sample times of 2- to 4-days, the NAVSTAR-6 cesium clock is the best performer, with a stability of 7.7 PP10(14) for a 4-day sample time.

The Allan variance power law model, given by Equation (15), was fitted to the 900- and 1800-second sample time data from all four NAVSTAR clocks. The projection of the short-term results to a 1-day sample time indicates good agreement with the measured Allan deviation for a 1-day sample time. Because of the close agreement, a fit was made to the 900- and 1-day Allan variance stability results. This solution is given by Equation (16).

$$\sigma_y^2(\tau) = (2.31 \times 10^{-20})(\tau)^{-1.25} \quad \text{Eq (16)}$$

CONCLUSIONS

- * The NAVSTARs 3 and 4 rubidium clock (with drift removed) long-term stability values agreed closely. A random walk FM noise process was present for sample times of 1- to 10-days. These measurements are in good agreement with the expected rubidium long-term performance.
- * The NAVSTAR-3 rubidium frequency had a significant departure, from expected performance, at a sample time of 1.25 hours. A possible cause is thermal fluctuations with a 2.5-hour period. Performance is nominal for 900- and 1800-seconds sample time.
- * For sample times of 1- to 5-days, the NAVSTAR-6 cesium clock exhibited better performance than the NAVSTAR-5 clock. The NAVSTARs 5 and 6 cesium clock long-term stability values agreed closely for sample times of 6- to 10-days. A flicker noise FM process was present, in both cesium clocks, for sample times of 1 to 10 days.
- * For sample times of 2- to 10-days, the NAVSTARs 5 and 6 cesium clocks have better frequency stability results than the NAVSTARs 3 and 4 rubidium clocks.
- * White noise FM was measured, for both rubidium and cesium clocks, for short-term sample times of 900- and 1800-seconds. For sample times of 2700 seconds to 2-hours, a gradual transition to an apparent, as yet

unexplained, flicker noise FM process was observed.

- * The 1-day sample time frequency stability measurements, for both cesium and rubidium clocks, were in close agreement with an average value of 1.3 PP10(13). This average value agreed closely with the projection of the 900-seconds to 1 day. The Allan variance power law solution for this white noise FM process is

$$\sigma_y^2(\tau) = (2.31 \times 10^{-20})(\tau)^{-1.25}.$$

References

1. C. A. Bartholomew, "Satellite Frequency Standards", Navigation: Journal of the Institute of Navigation, 25(2), Summer 1978, pp 113-120.
2. McCaskill, T. B., Stebbins, S. B., Carson, C., and Buisson, J. A., "Long Term Frequency Stability Analysis of the GPS NAVSTAR 6 Cesium Clock", NRL Report 8599, 20 September 1982.
3. J. A. Buisson and T. B. McCaskill, "TIMATION Navigation Satellite System Constellation Study", NRL Report 7389, June 27, 1972.
4. T. B. McCaskill, J. A. Buisson and D. W. Lynch, "Principles and Techniques of Satellite Navigation Using the TIMATION II Satellite", NRL Report 7252, June 17, 1971.
5. T. B. McCaskill and J. A. Buisson, "NTS-1 (TIMATION III) Quartz - and Rubidium-Oscillator Frequency-Stability Results", NRL Report 7932, December 12, 1975.
6. J. A. Buisson, T. B. McCaskill, O. J. Oaks, M. M. Largay, S. B. Stebbins, "GPS NAVSTAR-4 and NTS-2 Long Term Frequency Stability and Time Transfer Analysis", NRL Report 8419, June 30, 1980.
7. "GPS System Critical Design Review", October 26-27, 1981, Book 2 of 3, Section 4.3, Title 5.1, page 3 of 3.
8. Kalman, R. E., "A New Approach to Linear Filtering and Prediction Problems", Trans ASME J Basic Eng. Series D, Vol 82, pp. 34-35, March 1960.
9. Bernard Friedland, "A Review of Recursive Filtering Algorithms", Proceeding of the Spring Joint Computer Conference", pp 163-180, 1972.
10. Russell, S.S., and Schaibly, J. H., "Control Segment and User Performance", Journal of the Institute of Navigation, Vol. 25, No. 6, pp 166-172, Summer 1978.
11. O'Toole, J. W., "CELEST Computer Program for Computing Satellite Orbits", NSWC/DL TR-3565, October 1976.
12. D. W. Allan, J. H. Shoaf and D. Halford, "Statistics of Time and

Frequency Data Analysis", National Bureau of Standards Monograph 140, 1974, Chap. 8.

13. Haefner, G., and Moses, J., "NAVSTAR GPS X-Set Receiver Performance Flow Down Specifications", Magnavox reference number R-5227, 18 December 1975.
14. Lesage, P., and Audoin, C., "Estimation of the Two-Sample Variance with a Limited Number of Data", Proceedings of the Frequency Control Symposium 1977, pp 311-318.
15. Barnes, J. A., "Notes on Confidence of the Estimate and Overlapping Samples", unpublished.
16. McK.Luck, J. "Construction and Comparison of Atomic Time Scale Algorithms", TR#32, Division of National Mapping, Canberra, Australia.

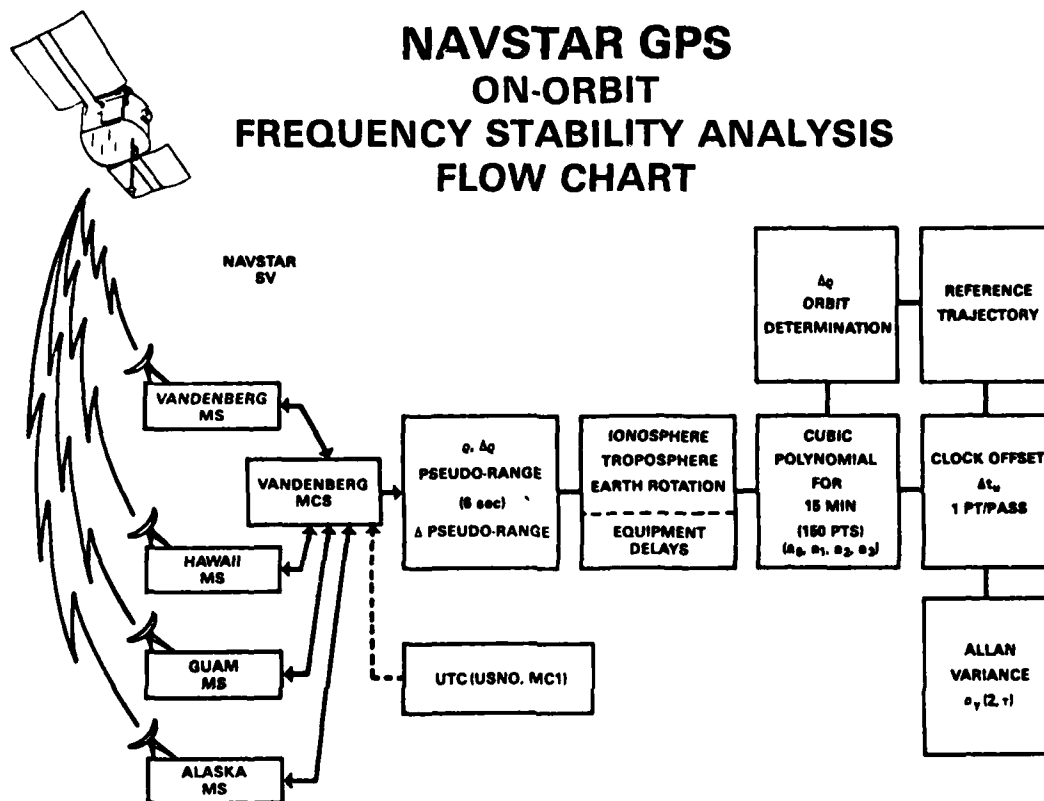


Figure 1

TYPICAL GPS NAVSTAR SV PSEUDO-RANGE SIGNATURE

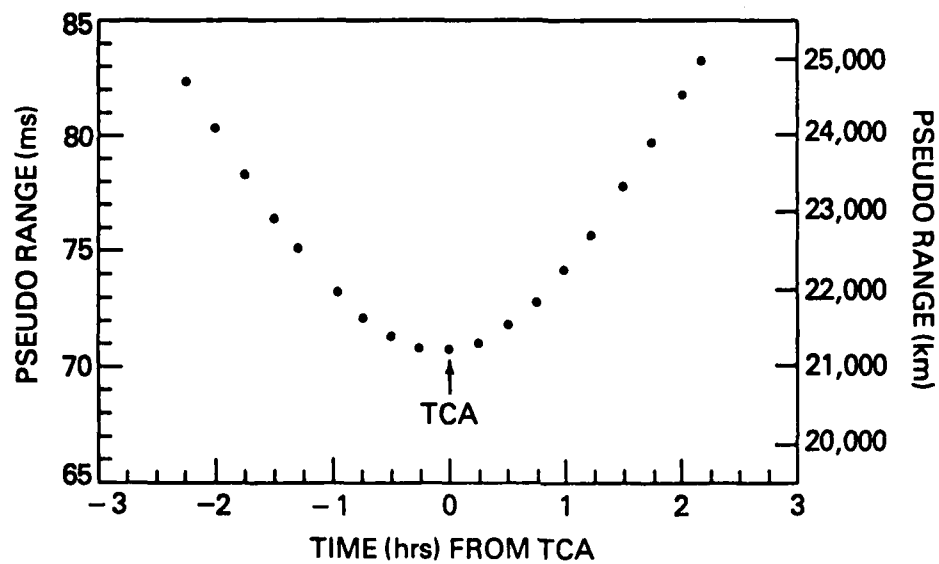


Figure 2

THEORETICAL MODEL OF FREQUENCY STABILITY FOR GPS CESIUM AND RUBIDIUM CLOCKS

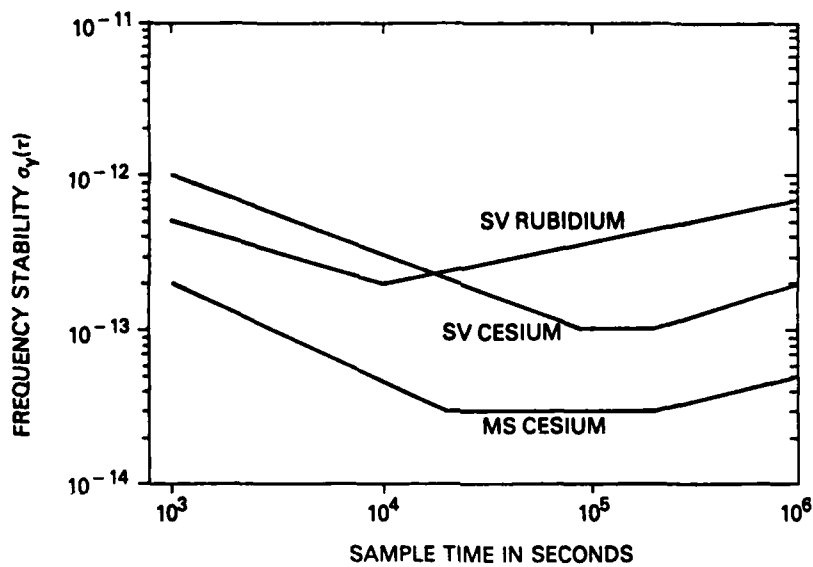


Figure 3

GPS ON-ORBIT DATA SELECTION PROCEDURE FOR ALLAN VARIANCE ANALYSIS

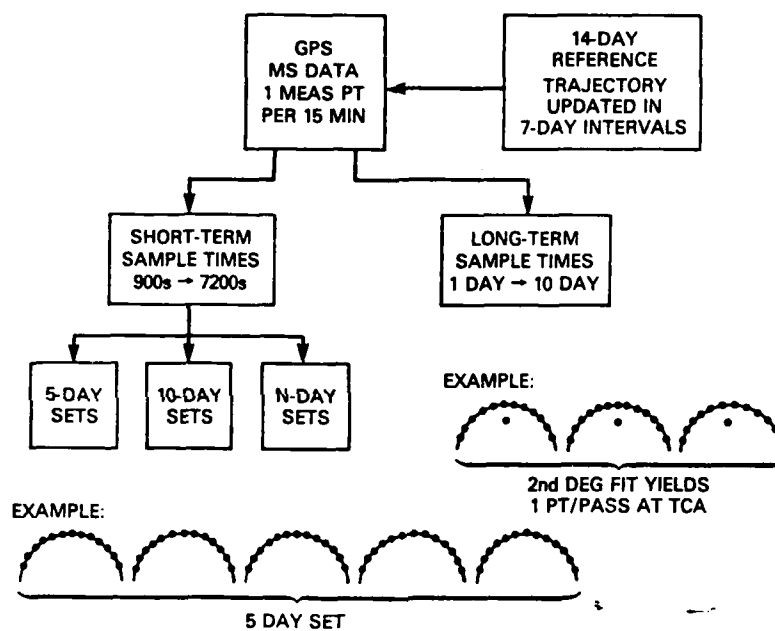


Figure 4

GPS NAVSTAR-3 SV
ELEVATION ANGLE vs TIME
VANDENBERG MS

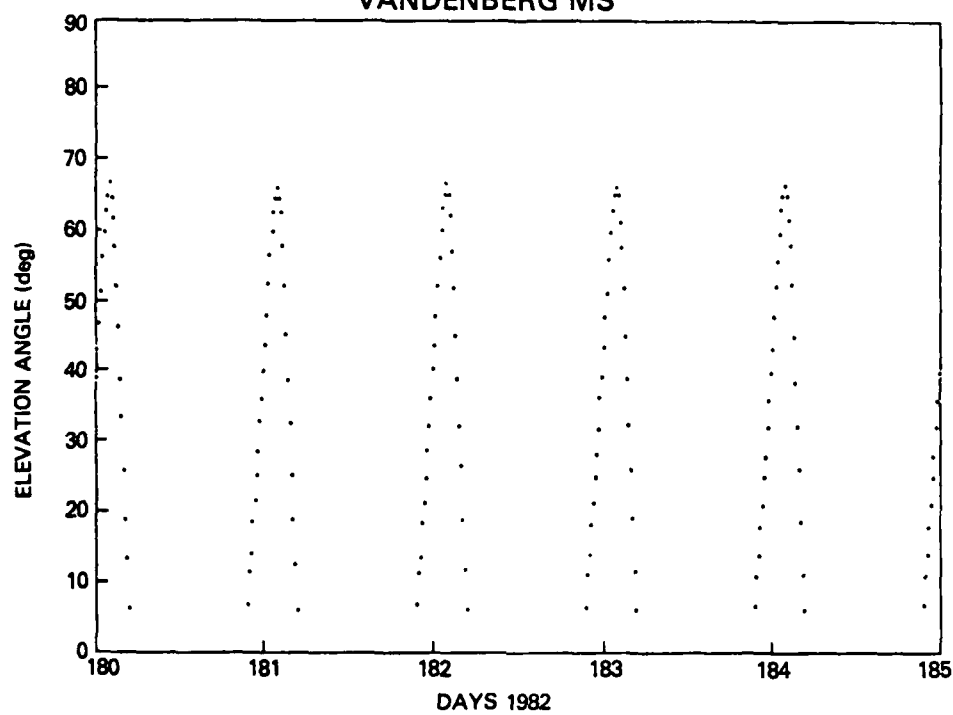


Figure 5

GPS NAVSTAR-3 SV
ELEVATION ANGLE vs TIME
VANDENBERG MS

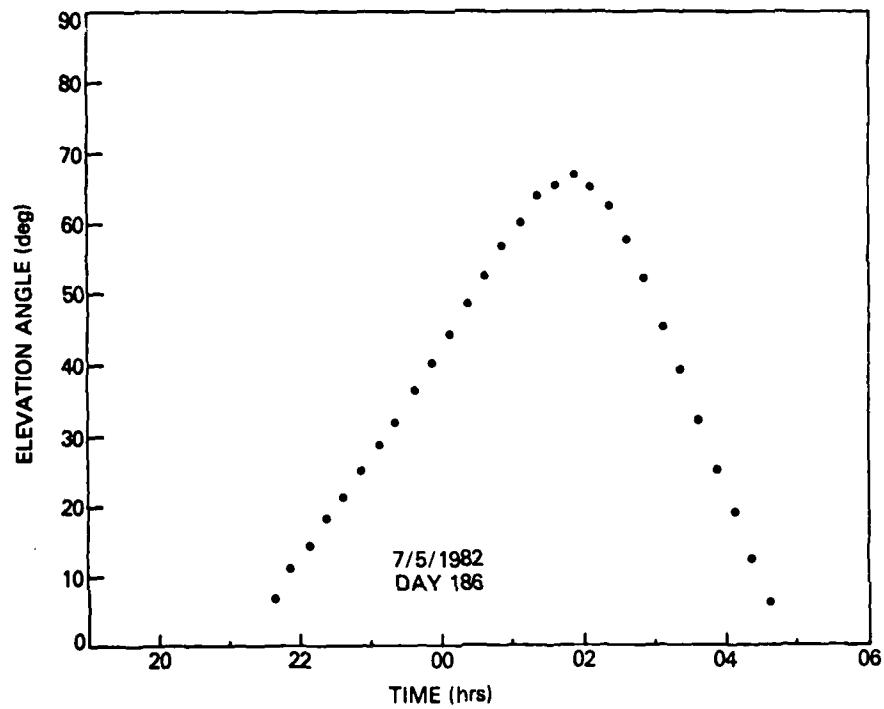


Figure 6

**GPS CLOCK ANALYSIS
NUMBER OF ALLAN VARIANCE SAMPLES
VS
SAMPLE TIME**

SAMPLE TIME T	NUMBER OF SAMPLES		ENSEMBLE	
	5 DAY SET	1 YEAR	4-MS	1-YR
0.25 hrs	115	8280	33120	
0.50	105	7560	30240	
0.75	95	6840	27360	
1.00	85	6120	24480	
1.25	75	5400	21600	
1.50	65	4680	18720	
1.75	55	3960	15840	
2.00 hrs	45	3240	12960	
1 day		503	1452	
2		361	1440	
3		359	1436	
4		357	1428	
5		355	1420	
6		353	1412	
7		351	1404	
8		349	1396	
9		347	1388	
10 days		345	1380	

Figure 7

GPS
CLOCK ANALYSIS
VANDENBERG VS NAVSTAR 3

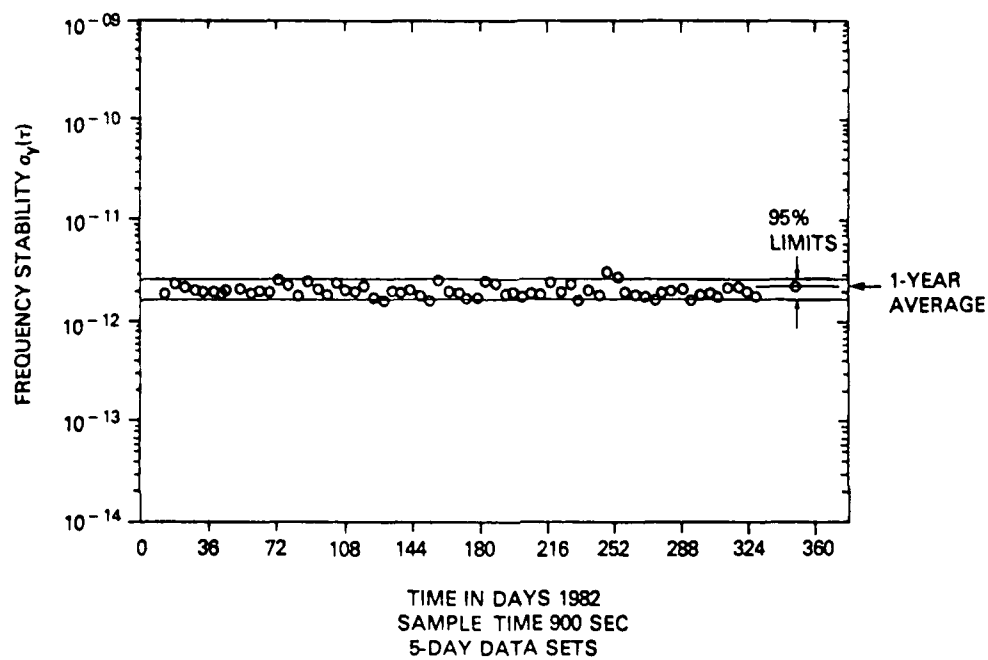


Figure 8

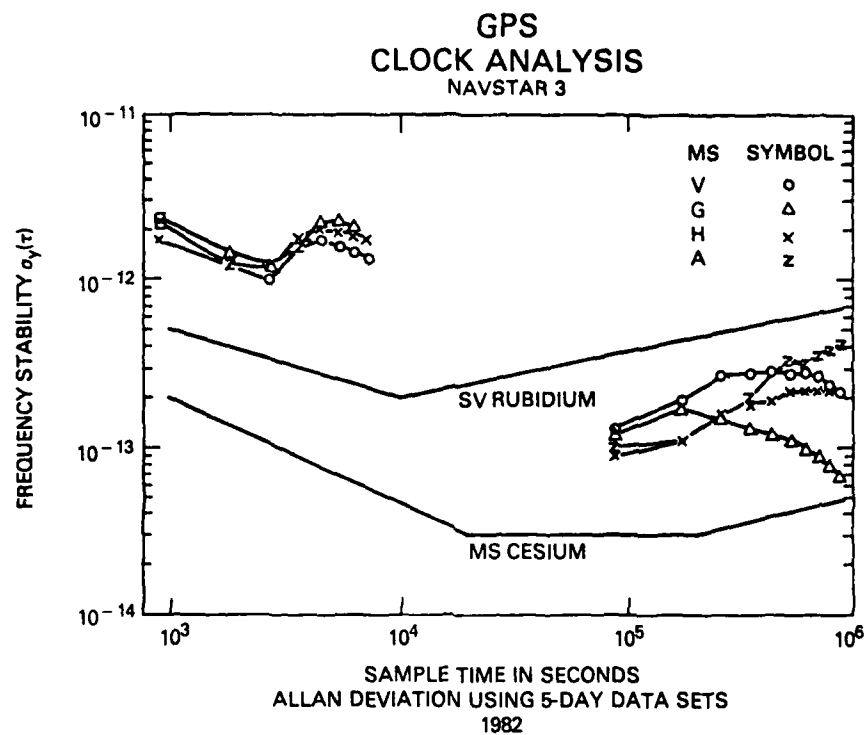


Figure 9

GPS
CLOCK ANALYSIS
STATION ENSEMBLE VS NAVSTAR 3

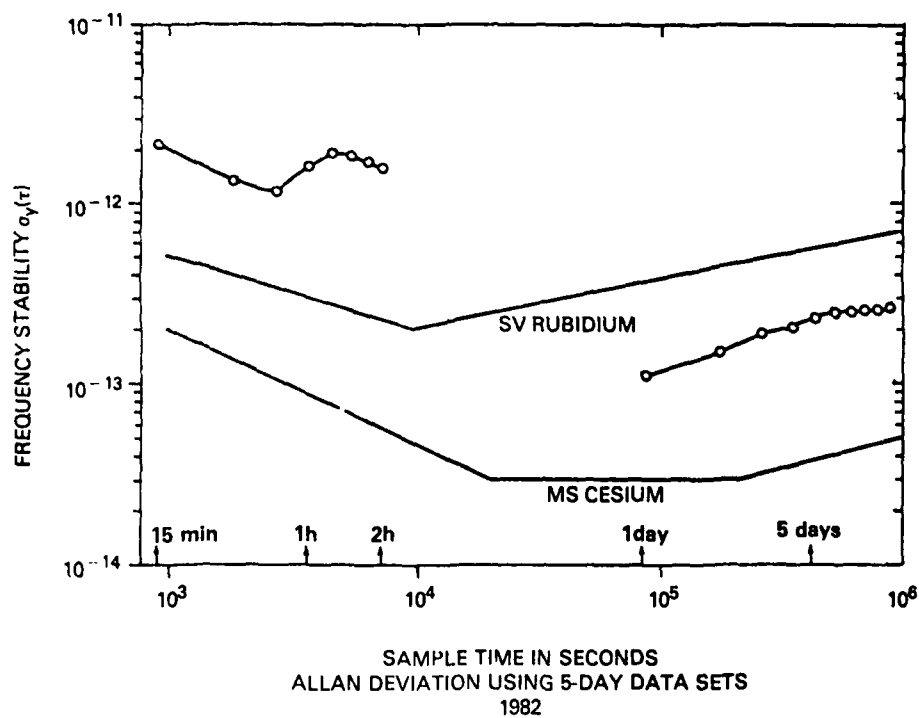


Figure 10

GPS CLOCK ANALYSIS NAVSTAR 4

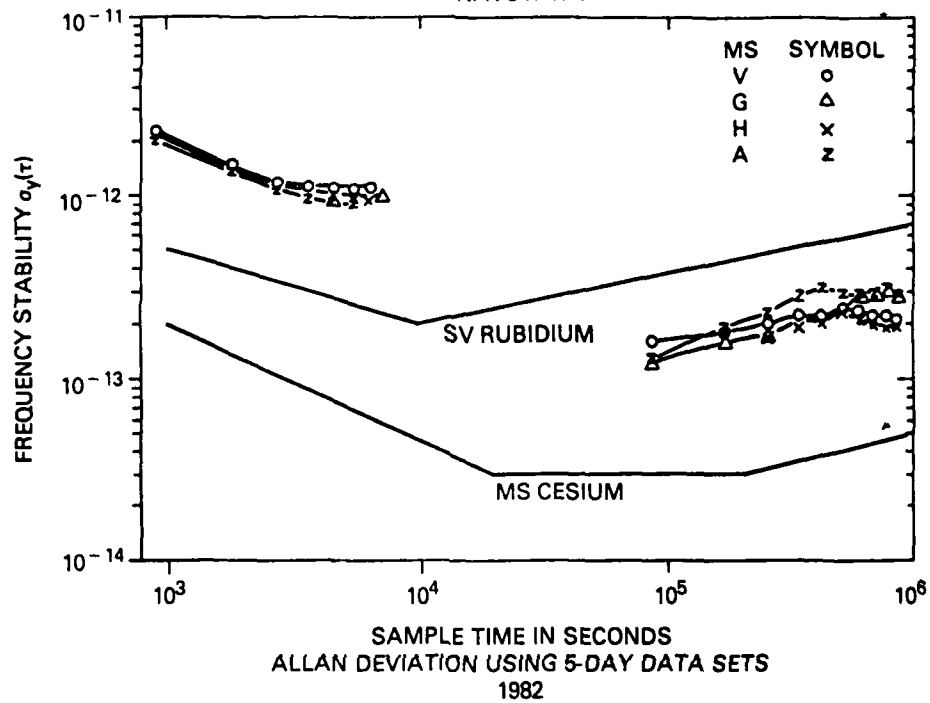


Figure 11

GPS CLOCK ANALYSIS STATION ENSEMBLE VS NAVSTAR 4

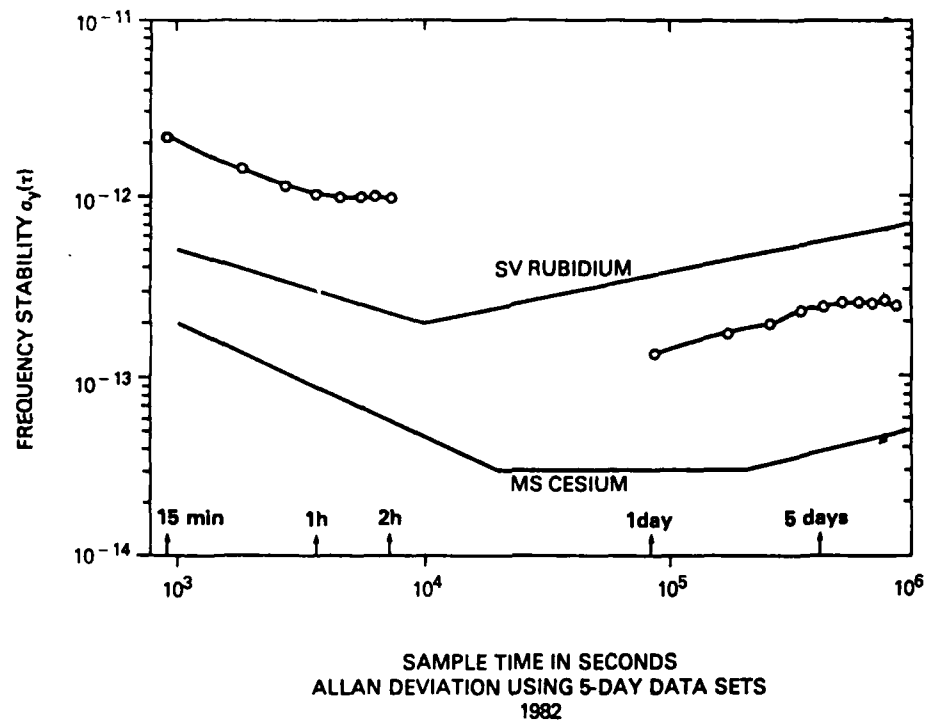


Figure 12

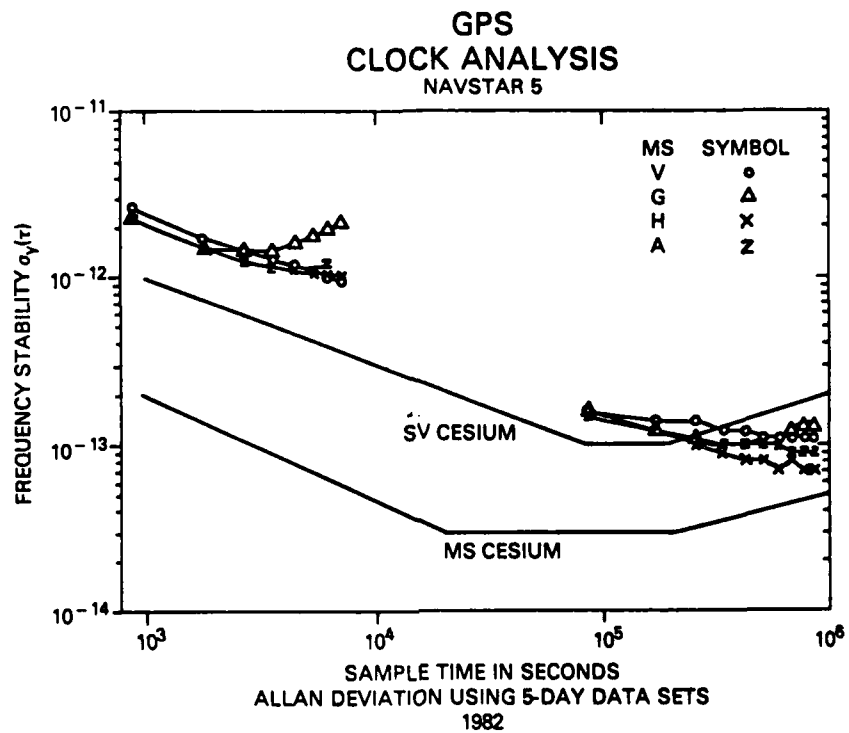


Figure 13

**GPS
CLOCK ANALYSIS
STATION ENSEMBLE VS NAVSTAR 5**

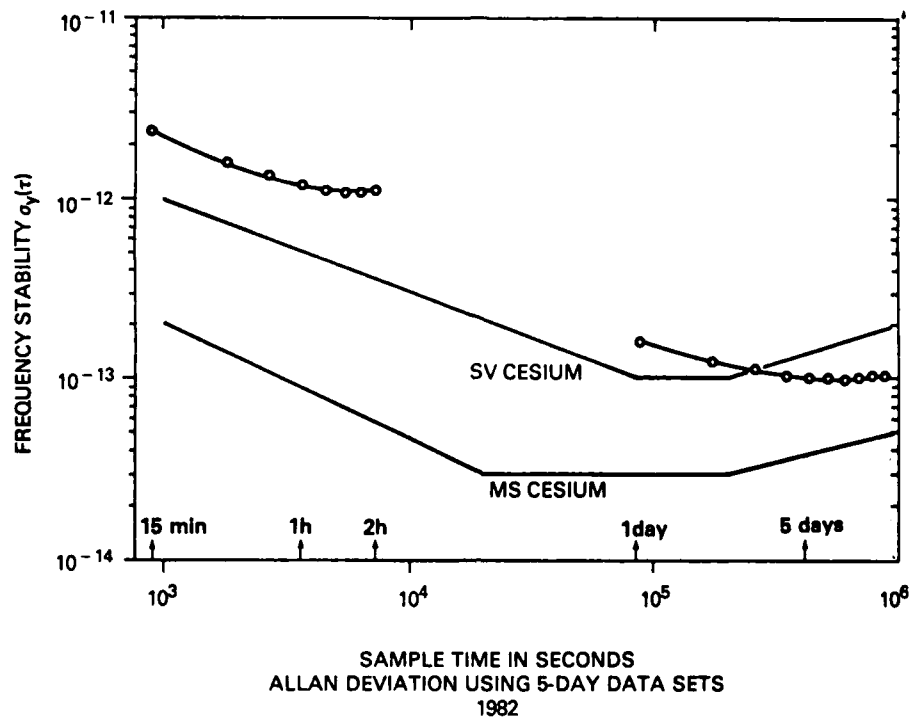


Figure 14

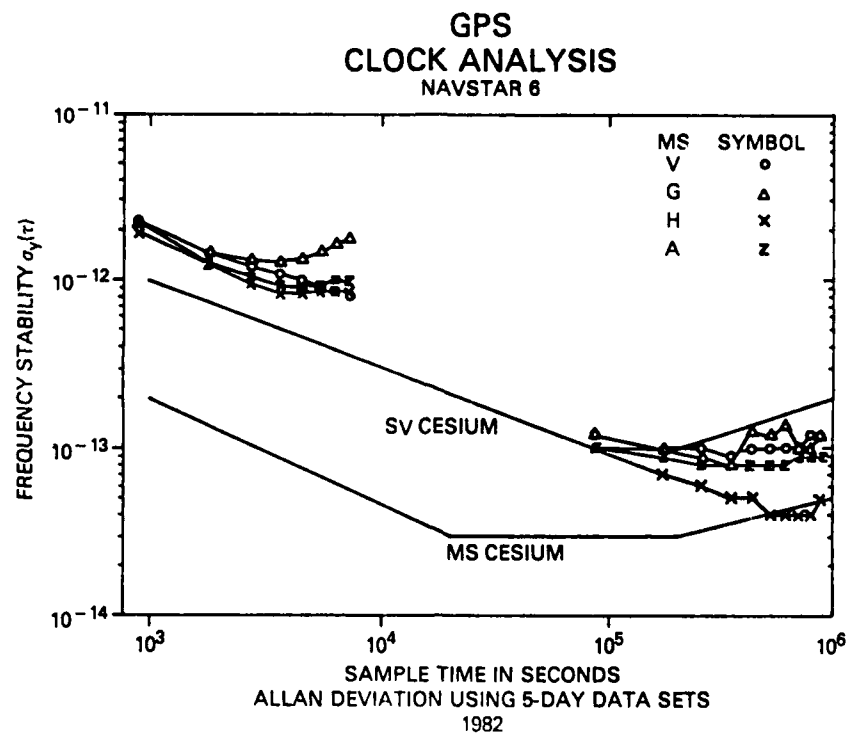


Figure 15

**GPS
CLOCK ANALYSIS
STATION ENSEMBLE VS NAVSTAR 6**

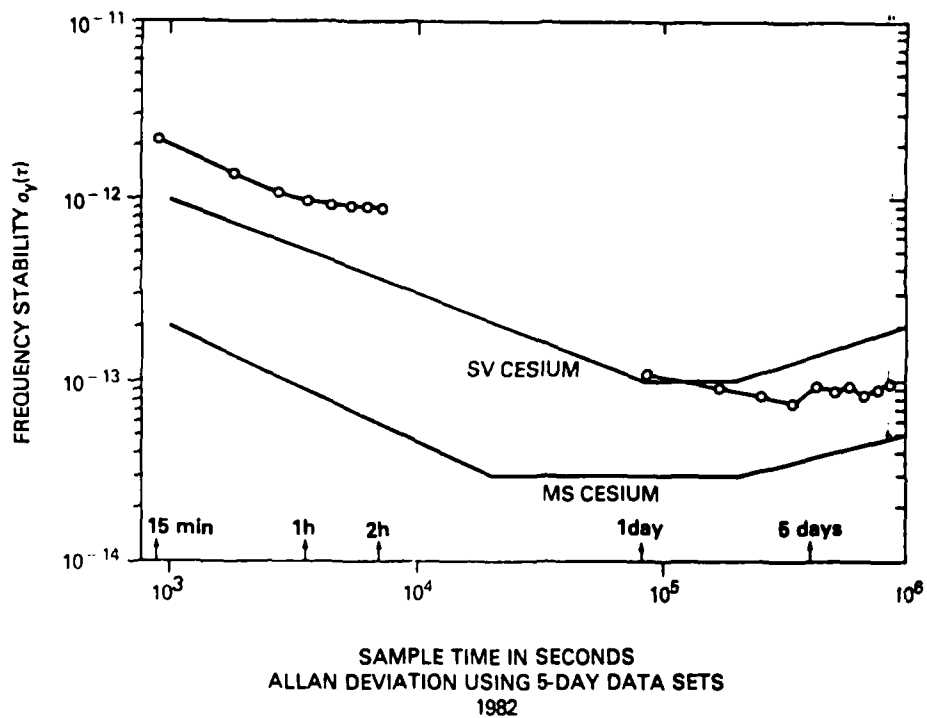


Figure 16

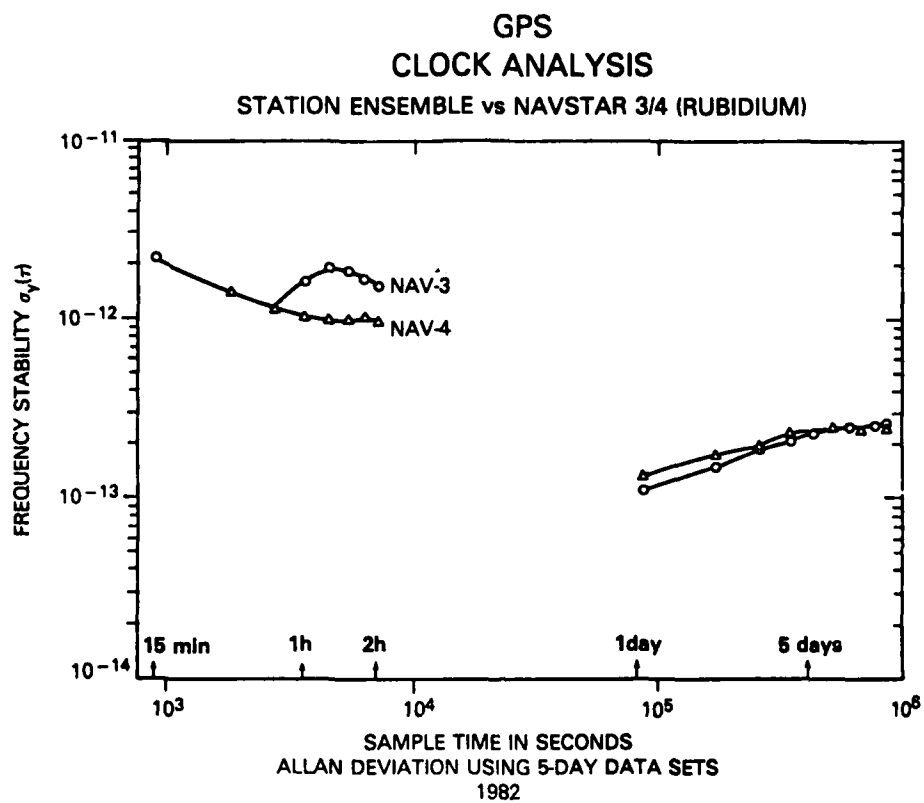


Figure 17

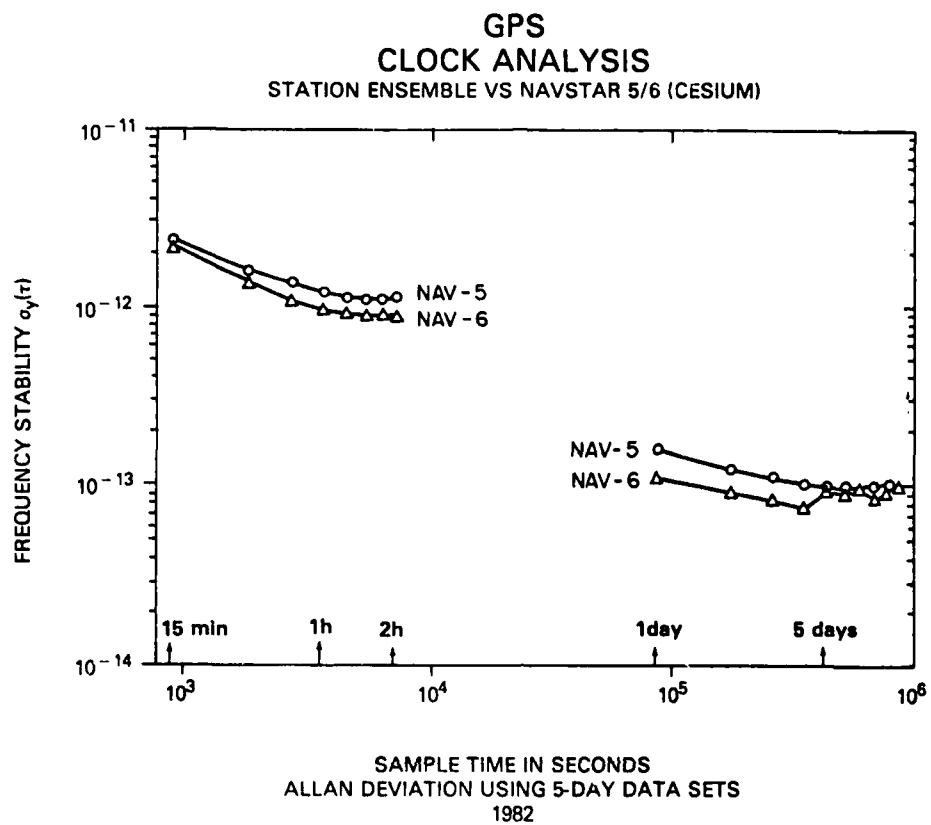


Figure 18

**GPS
CLOCK ANALYSIS
STATION ENSEMBLE VS NAVSTAR 3/4/5/6**

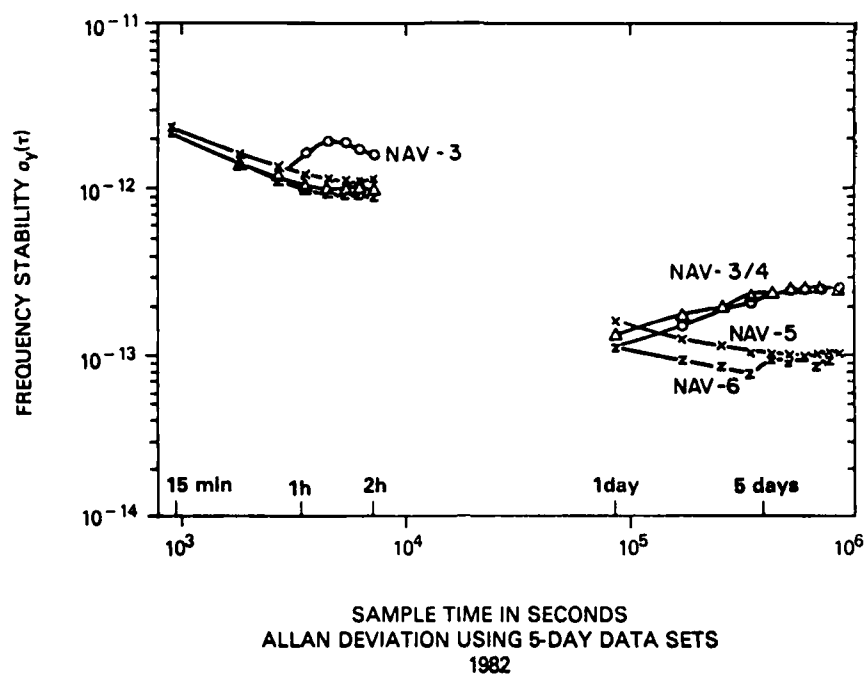


Figure 19

QUESTIONS AND ANSWERS

DR. BARNES:

Jim Barnes, with Austron. A possible suggestion of why you find data that goes as τ to the minus one-half. It might be just the deadtime that you mentioned was in the data. Deadtime can mean that kind of a signature to the allan variance.

MR. McCASKILL:

These data were taken every six seconds continually. So the deadtime corrections for that should be very small. Now, the long term results, we could have possible room for correction there; but I really wouldn't expect much of an effect on short term results.

DR. VESSOT:

Bob Vessot, Smithsonian. On the two hour data, I'm wondering if that anomaly couldn't be the fact that you are using data from a great range of elevation angles; and I think it's rather difficult to estimate the propagation qualities when things are down, say, ten, fifteen degrees. If those enter into the data, then it is likely to cause a wider spread of uncertainties and, hence a larger allan variance.

MR. McCASKILL:

That's a good point, but we do not expect it. We limited the sample time to two hours and if you start at TCA, you would go two hours on one side and two hours on the other, but the typical pass, unless its a short pass, could go up to maybe six hours or more.

So it's possible, if we would have pushed the sample time closer to, let's say, three hours, we could have seen some residual type of results and, of course, it could be there in a two hour sample time, but we just did not expect it at a two hour sample time.

DR. VESSOT:

The prediction of atmospheric is kind of difficult, and these issues, I think, could increase the probability of having noise. That's the point I wanted to raise.

MR. McCASKILL:

It could be, but one thing--there was one slide missing, and I don't know what happened to it, it showed the number of samples. We have collected data for a year, and when you go across the full station ensemble, the number of samples goes into the order of 20 to 30 thousand, so whatever it is, we have high confidence that there's some type of process that flickered out for the short term results; and at the moment we cannot tell you exactly what it is, except that we believe that it's there and is a well defined measurement.

MR. ALLAN:

Dave Allan, N.B.S., two comments. No. 1. There would be no deadtime, because they're measuring time directly; so, there's no deadtime affect on that data. As relates to the two-hour rise in the sigma tau diagram, the recent work we have done, using the separation of various technique has shown serious problems in the ephemeris prediction and, indeed this may be the problem, and is not as good as perhaps they thought it was.

GPS NAVIGATION EXPERIMENT USING HIGH PRECISION GPS
TIMING RECEIVERS

J. Buisson, O. J. Oaks, M. Lister
Naval Research Laboratory
S. C. Wardrip
NASA Goddard Space Flight Center
S. Leschiutta
Politecnico Di Torino
P. G. Galliano, F. Cordara, V. Pettiti
Istituto Elettrotecnico Nazionale
E. Detoma, P. Dachel, H. Warren, T. Stalder
Bendix Field Engineering Corporation
F. Fedele
Italian Navy, MAGNAGHI
R. Azzarone
Italian Navy, MARITELERADAR

ABSTRACT

Global Positioning System (GPS) Time Transfer receivers were developed by the Naval Research Laboratory (NRL) to provide synchronization for the NASA Global Laser Tracking Network (GLTN).

The capabilities of the receiver are being expanded mainly through software modification to:

- * Demonstrate the position location capabilities of a single channel receiver using the GPS C/A code.
- * Demonstrate the time/navigation capability of the receiver onboard a moving platform, by sequential tracking of GPS satellites.

Several advanced navigation algorithms were tested, tracking either a full or reduced constellation of the current Phase I GPS satellites.

The experiment was conducted during October 1983 onboard the Italian Navy hydrographic ship "MAGNAGHI". The ship provided a stable platform, able to move with constant speed, while keeping track of its own position with high accuracy. The ship was equipped with a wide range of radionavigation equipment, including Raydist, Motorola Mini-Ranger, Toran, Loran-C, Omega and Transit receivers. There were also onboard atomic clocks with submicrosecond accuracy. To keep an accurate track of the ship's position at sea during the experiment, the

Mini-Ranger system was used with transponders located on the seashore. The Mini-Ranger system provided position to an accuracy of 5 to 10 meters.

This experiment was a joint effort between the following U.S. and Italian agencies and organizations: The U.S. Naval Research Laboratory, the NASA/Goddard Space Flight Center, with the support of the Bendix Field Engineering Corporation, the Italian Navy, the Istituto Elettrotecnico "G. Ferraris" and the Politecnico of Torino (Italy).

INTRODUCTION

The Naval Research Laboratory developed a GPS time transfer receiver for the NASA/Goddard Spaceflight Center which was first deployed and tested in June 1981¹. Since then, six receivers have been completed and delivered to NASA for deployment in the NASA Global Laser Tracking Network (GLTN). The receiver was designed to provide precise time measurements between the time standard of the U.S. Naval Observatory and clocks at remote locations.² The primary application is synchronization of remote clocks and clock evaluation. NASA is using the receivers to synchronize remote mobile laser stations to the U.S. Naval Observatory time standard. Precise time is required at each station in order to time tag the data and to acquire satellites with the laser ranging systems.

Before time measurements can be made with the receiver, the position of the antenna must be input in WGS-72 coordinates. Currently, this position is determined by an independent survey before deployment of the receiver. This experiment tests the capability of the GPS time transfer receiver to perform a navigation both on a fixed point and on a slow moving platform. An accurate fixed point navigation capability would allow the GPS receiver to perform cold start synchronizations of field deployed clocks in a stand alone capacity. The moving navigation was performed in order to evaluate the feasibility of providing accurate time synchronization on a slow moving platform.

This navigation experiment uses the existing Phase I NAVSTAR GPS satellites which are a partial set of the final constellation of satellites to be deployed in the 1980s. The results presented here are an evaluation of a time transfer receiver operating in a navigation mode. They are not intended to be used as an evaluation of NAVSTAR GPS accuracy or capability.

Moving Navigation Solution

To perform a navigation, the GPS receiver makes independent range measurements to a number of NAVSTAR satellites. The position of each satellite at the time of measurement is computed from ephemeris data transmitted by each satellite. A ground antenna position is assumed, and the distance to each satellite is calculated. The calculated ranges are subtracted from the measured ranges giving residuals which are used to correct the assumed position. The corrected position is then used to

calculate a new residual, and the iterative process continues until the position converges to within some delta value of error. The basic equation in matrix form is

$$P = (A^T W A)^{-1} A^T W (O - C) \quad (1)$$

where P is the improvement in position

A is the measurement matrix

W is a weighting matrix

and $(O - C)$ is the matrix of differences between measured and computed ranges.

The sequential range navigation is explained in detail in reference 3 and reference 4 and therefore, is presented here as the method used without derivation.

In the moving navigation solution, a five dimensional navigation is performed to determine latitude, longitude, clock offset, course direction, and velocity. A minimum of five satellite measurements are made for each position determination. The solution assumes a constant velocity and course for each fix and a constant height on the surface of the earth at all times. These assumptions are reasonable for the case of a slow moving ship in open seas.

In order to determine the goodness of each solution fit to the data, the geometric dilution of precision (GDOP) was calculated. The GDOP is defined here as:

$$GDOP = \sqrt{\sigma_{LAT}^2 + \sigma_{LONG}^2 + \sigma_{CLOCK}^2} \quad (2)$$

where σ_{LAT}^2 , σ_{LONG}^2 , and σ_{CLOCK}^2 are diagonal terms of the covariance matrix $(A^T W A)^{-1}$ in the navigation solution. GDOP in the classical sense may include all five diagonal terms of the covariance matrix, however, the intention is only to provide a relative measure of goodness of solution for the data presented.

Navigation Exercise

The moving navigation was performed onboard the Italian Navy research vessel "Ammiraglio Magnaghi". The ship's home port is in LaSpezia, Italy, and the experiment was performed off the coast of LaSpezia as shown in figure 1. The ship had a Motorola Mini-Ranger system of navigation which was used as a comparison for the GPS receiver results. The Mini-Ranger system consisted of a two channel transceiver onboard the ship and two transponders located at

known positions on the shore. One transponder was located at P^{ta} del Mesco and the other at I.^a Palmaria. The navigation was performed while the ship was steering courses of approximately 090° and 270° with a velocity of 8-9 knots. The Mini-Ranger system provided continuous positions of the ship to an accuracy of 5-10 meters. The data was recorded at the epochs of GPS measurements for later comparison at the conclusion of the experiment.

GPS Measurements

A minimum of five satellite tracks were made for each navigation solution. Each satellite track requires approximately five minutes as shown in figure 2(a). Two minutes are required for signal search and acquisition, and then one minute for locking and synchronizing to the satellite data. Once locked and synchronized, satellite ephemeris and clock information is read from the data. Last, satellite range measurements are made, one measurement every six seconds for a period of a minute. A minimum of five of these such tracks are used in each navigation solution. Ideally five different satellites would be tracked as illustrated in figure 2(b). However, because of the limited satellite visibility using the Phase I satellites in Italy, most of the time less than five satellites were tracked, but they were repeated as shown in the example of figure 2(c).

GPS NAVSTAR Visibility

Figures 3 and 4 are two different ways of describing the satellite visibility for the time and place where the experiment was performed. Figure 3 shows the elevation versus time for each satellite. The navigations were performed during the time period from 6 to 9 hours. The plot shows the maximum of five satellites visible above 10° from 0630 to 0730. During the remainder of the time between 0600 and 0900, only three or four satellites were visible.

Figure 4 shows the satellite azimuth and elevation relative to the ship between 0600 and 0900 hours. The best satellite geometry occurs at approximately 0630 when all five satellites are in view above 10° elevation and separated the greatest distance in azimuth. As time approaches 0900 the satellites move closer together, and NAVSTAR 4 goes out of view giving poor geometry for navigation. The accuracy of the results can be correlated to the goodness of satellite geometry and is apparent in the data presented.

Navigation Data

Figures 5 - 14 are plots of the computed navigation solutions. The position of the ship is plotted in latitude and longitude for different sets of navigation data. Each set represents a run by the ship from one end of the area shown in figure 1 to the other. GPS determined positions are represented by O's and Mini-Ranger positions are X's. A value for accuracy is given as a range from the minimum to the maximum deviation of the GPS position from the Mini-Ranger position. The GDOP value as defined in equation (2), is also given. A NAVSTAR visibility plot shows the positions of the satellites used during each navigation solution. The X's on the satellite position arrows represent the times data were taken by the GPS receiver.

For example, figure 5 is run number 1 on October 5 and shows agreement between GPS and Mini-Ranger solutions of from 4 to 52 meters. The NAVSTAR visibility diagram shows that the solution was obtained from eight satellite tracks, three on NAVSTAR 5, one on NAVSTAR 4, and two each on NAVSTAR 3 and NAVSTAR 6. The GDOP of 1.1 is a factor of the number of total measurements used and satellite geometry. GDOP's of lower values indicate better fits of the data to the navigation solution. GDOP is reduced as the number of measurements increase and as the satellites are separated in position. The plot of Mini-Ranger data shows the deviation of the ship from a straight course. Some of the error is attributed to the assumption in the GPS solution that the course is a straight line and constant speed. The straight line fit is apparent in the GPS data.

The other figures (6 - 14) show absolute accuracy results in the range of 50 meters or better for various geometries and number of tracks. Figures 15 - 17 summarize the results of the GPS navigation accuracy for this experiment using a time transfer receiver. Figure 15 is a plot of the differences in the latitude solutions of GPS from Mini-Ranger for all solutions obtained. The average difference in latitude was 10.8 meters. Figure 16 is the same type of plot showing an average difference in longitude of 23.6 meters. Figure 17 is a plot of $\Delta TNAV$, which is the RSS position difference between the two systems, for all the solutions obtained. The average difference of 45.1 meters is an indication of how good the GPS time transfer receiver can navigate using a partial GPS constellation and, at times, poor geometry.

Stationary Position Determination

The solution of the stationary position determination is the same as the moving navigation with the velocity constrained to zero. Equation (1) becomes three dimensional solving only for latitude, longitude, and clock offset. A position determination was made using GPS measurements obtained over a period of six days at the Istituto Elettrotecnico Nazionale in Turin, Italy. The results are presented in figure 18. A known position was given in WGS-72 coordinates and the GPS solutions for each day are tabulated. The data used to obtain the solutions were taken over a period of hours from all NAVSTAR satellites whenever the satellites were in view and at positions which provided good geometry. Since the receiver was not moving there was no time constraint to take data from all satellites simultaneously. The results show the differences in latitude and longitude to be less than 10 meters.

Conclusions

The results of the moving navigation experiment demonstrate accuracy of 10 to 50 meters. This shows promise of the possibility of an accurate time transfer on a slow moving platform using existing GPS time transfer receivers.

The 10 meter accuracy in determining the position of a stationary platform demonstrates the ability of the GPS time transfer receiver to become a stand alone system for setting field deployed clocks. NASA has plans to implement

this capability on existing receivers in the future and make it operational in the mobile laser systems.

References

1. J. Oaks, A. Frank, et. al., "Global Positioning System Time Transfer Receiver (GPS/TTR) Prototype Design and Initial Test Evaluation," proceedings 13th Annual PTTI Applications and Planning Meeting, December 1 - 3, 1981.
2. C. Wardrip, J. Buisson, et. al., "An International Time Transfer Experiment," Proceedings 37th Annual Symposium on Frequency Control, 1983.
3. T. B. McCaskill, J. A. Buisson, and D. W. Lynch, "Principles and Techniques of Satellite Navigation Using the TIMATION II Satellite," NRL Report 7252, June 17, 1971.
4. A. Bunaguro, T. B. McCaskill, and J. A. Buisson, "Sequential Range Navigation for the NAVSTAR Global Positioning System," NRL Report 7880, July 11, 1975.
5. S. C. Wardrip, et. al., "International Time Transfer and Portable Clock Evaluation Using GPS Timing Receivers," Proceedings 15th Annual PTTI Applications and Planning Meeting, December 6 - 8, 1983.

GPS NAVIGATION EXPERIMENT IN LA SPEZIA, ITALY

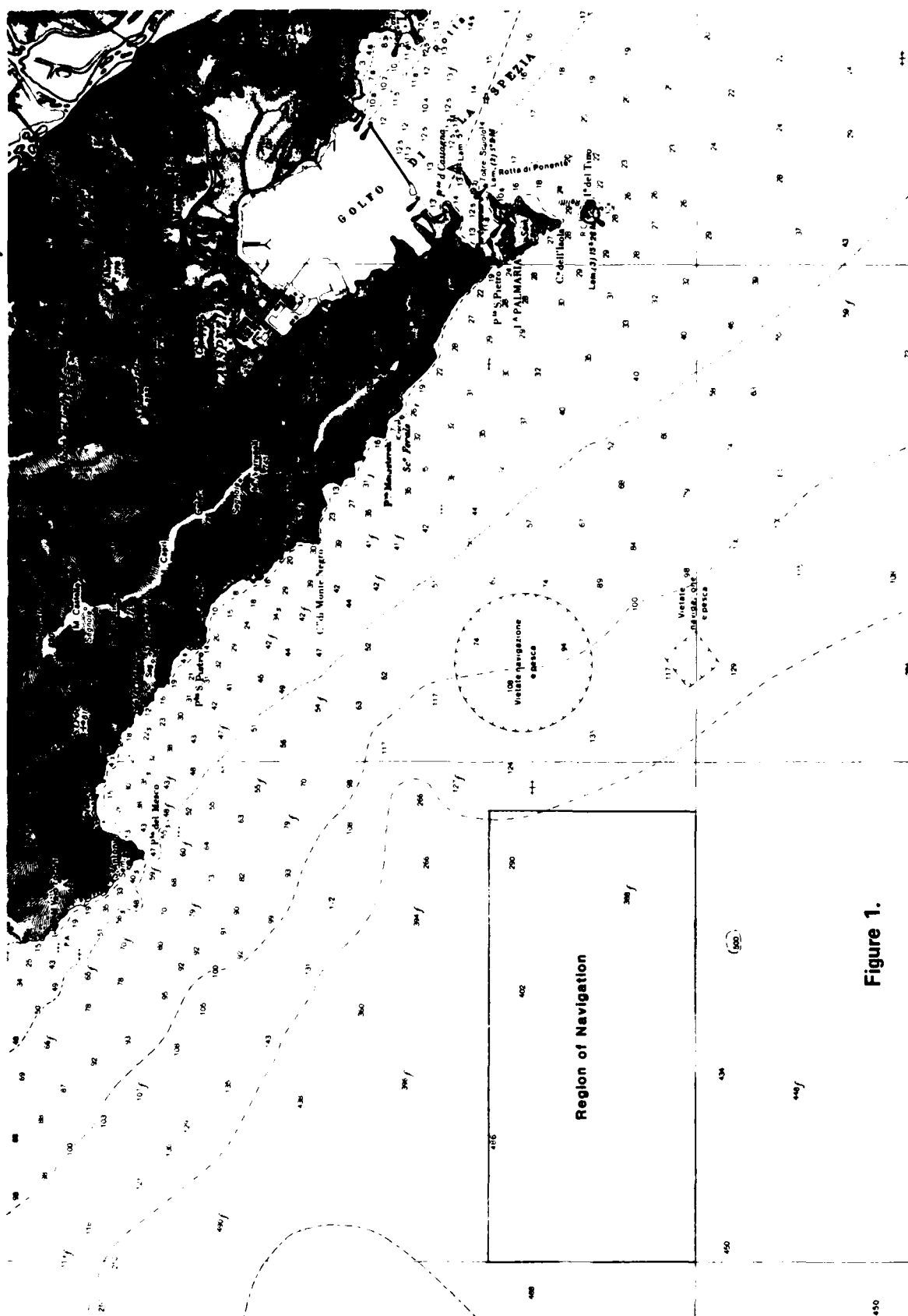
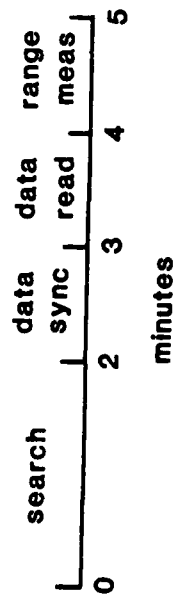


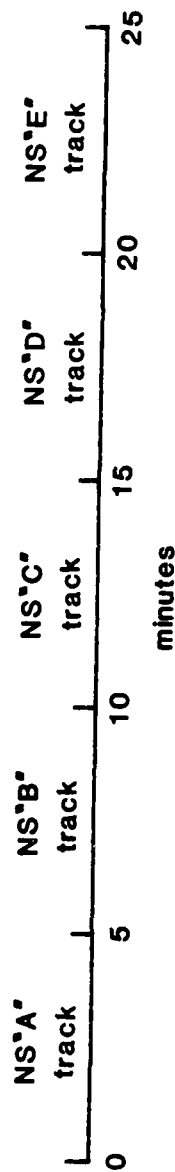
Figure 1.

NAVIGATION MEASUREMENTS

a) Satellite track



b) Navigation fix (2 to 5 satellites, 5 tracks minimum)



c) Example: navigation fix (3 satellites, 5 tracks)

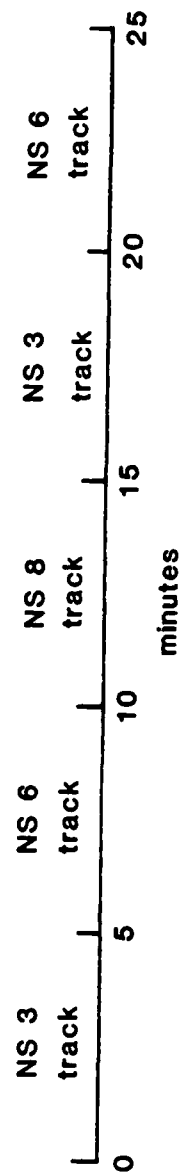


Figure 2.

NAVSTAR GPS TIME & ELEVATION VISIBILITIES ON OCT 5, 1983 FOR 44° 6' N LATITUDE 9° 19' E LONGITUDE

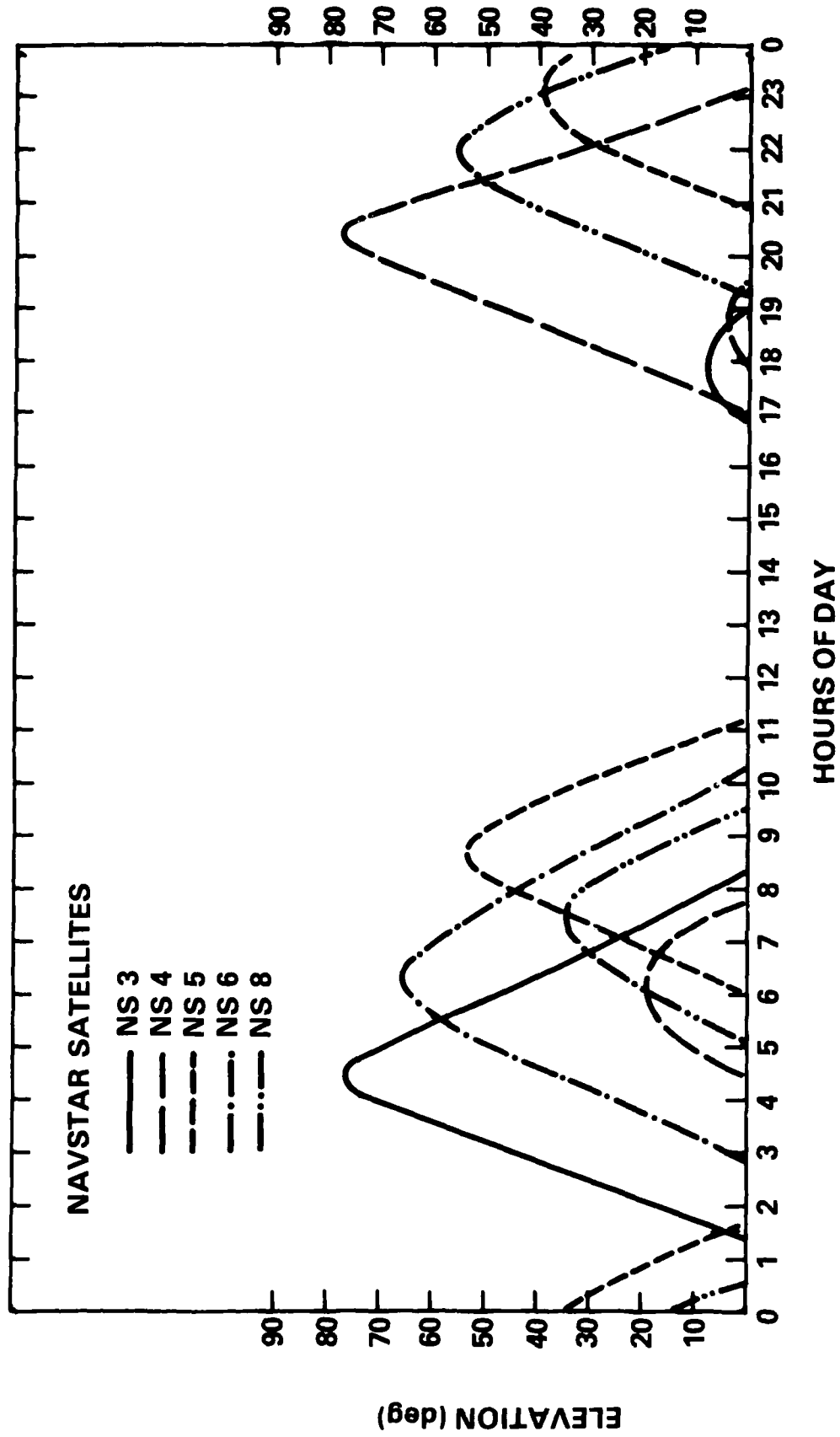


Figure 3.

**GPS NAVSTAR AZIMUTH & ELEVATION VISIBILITIES ON
OCT 5, 1983
FOR 44°6' N LATITUDE
9°49' E LONGITUDE**

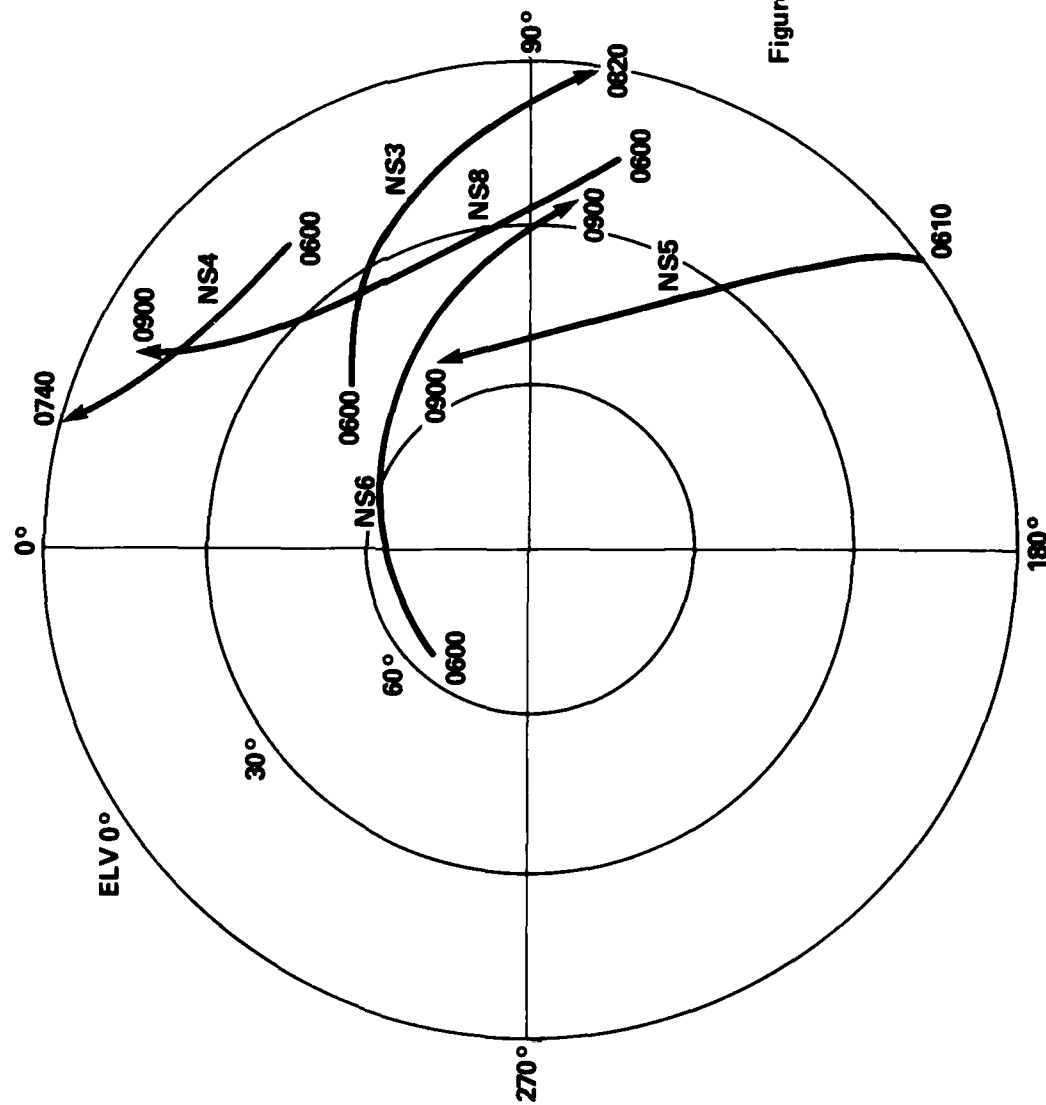


Figure 4.

NAVIGATION COURSE SOLUTION

RUN NO. 1 10/5/83

ACCURACY = 4-52 M
G10P = 1.1

GPS
MINI-RANGE X

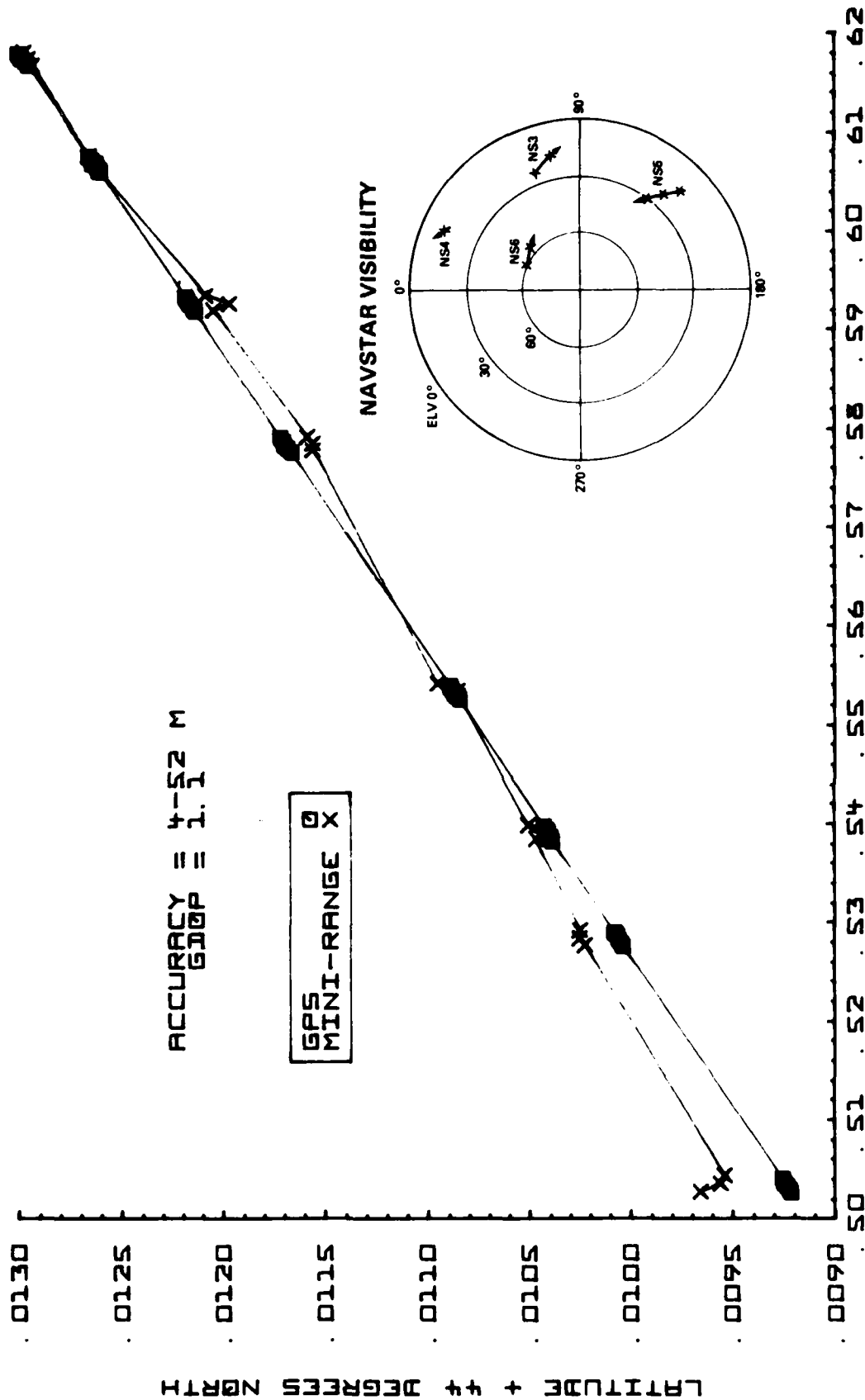


Figure 5.

NAVIGATION COURSE SOLUTION

RUN NO. 2 10/5/83

ACCURACY = 10-80 M
GDOP = 14

GPS
MINI-RANGE X

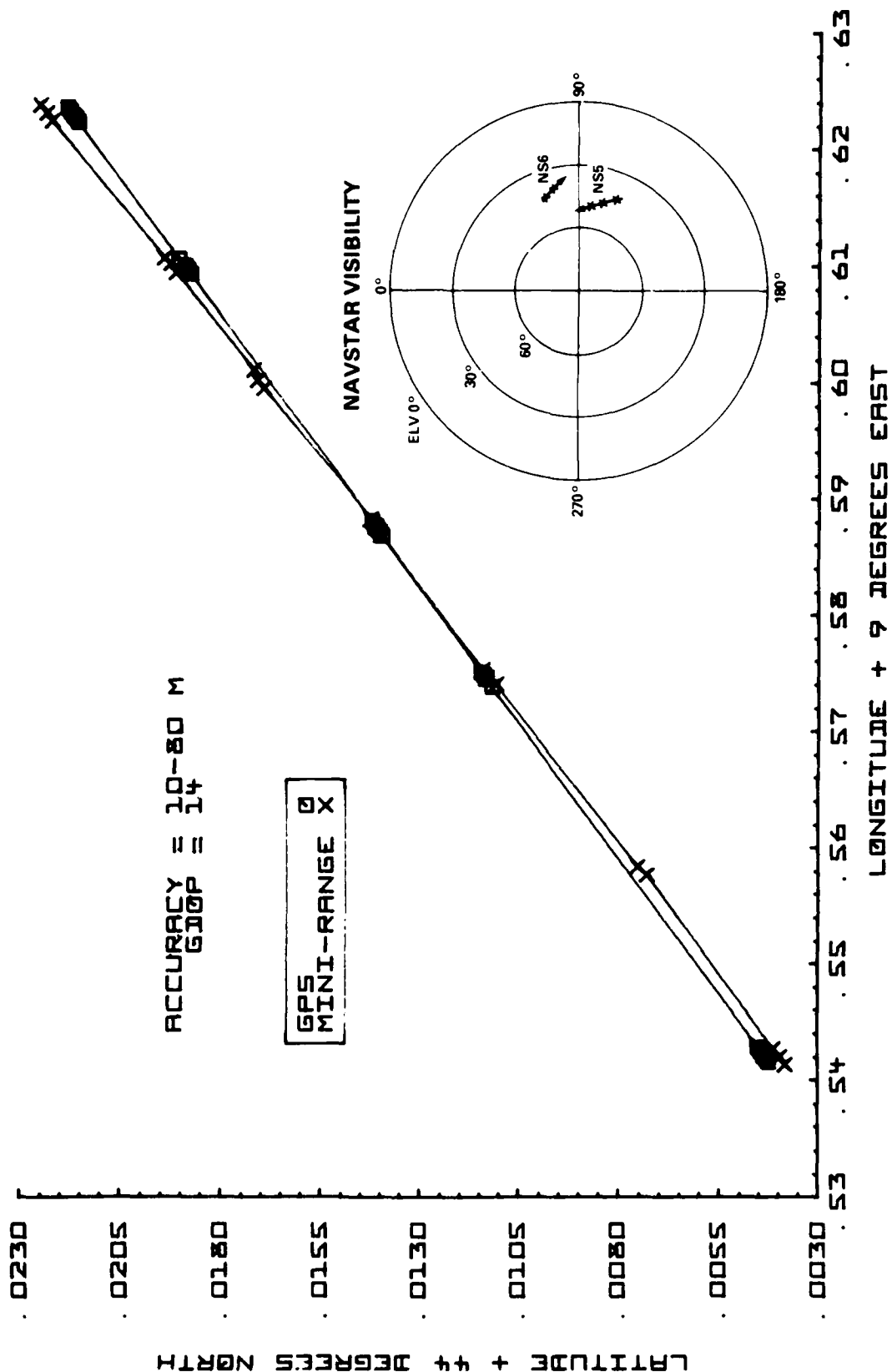


Figure 6.

NAVIGATION COURSE SOLUTION

RUN NO. 1 10/6/83

ACCURACY = 2-40 M
GDOP = 1.6

GPS MINI-RANGE X

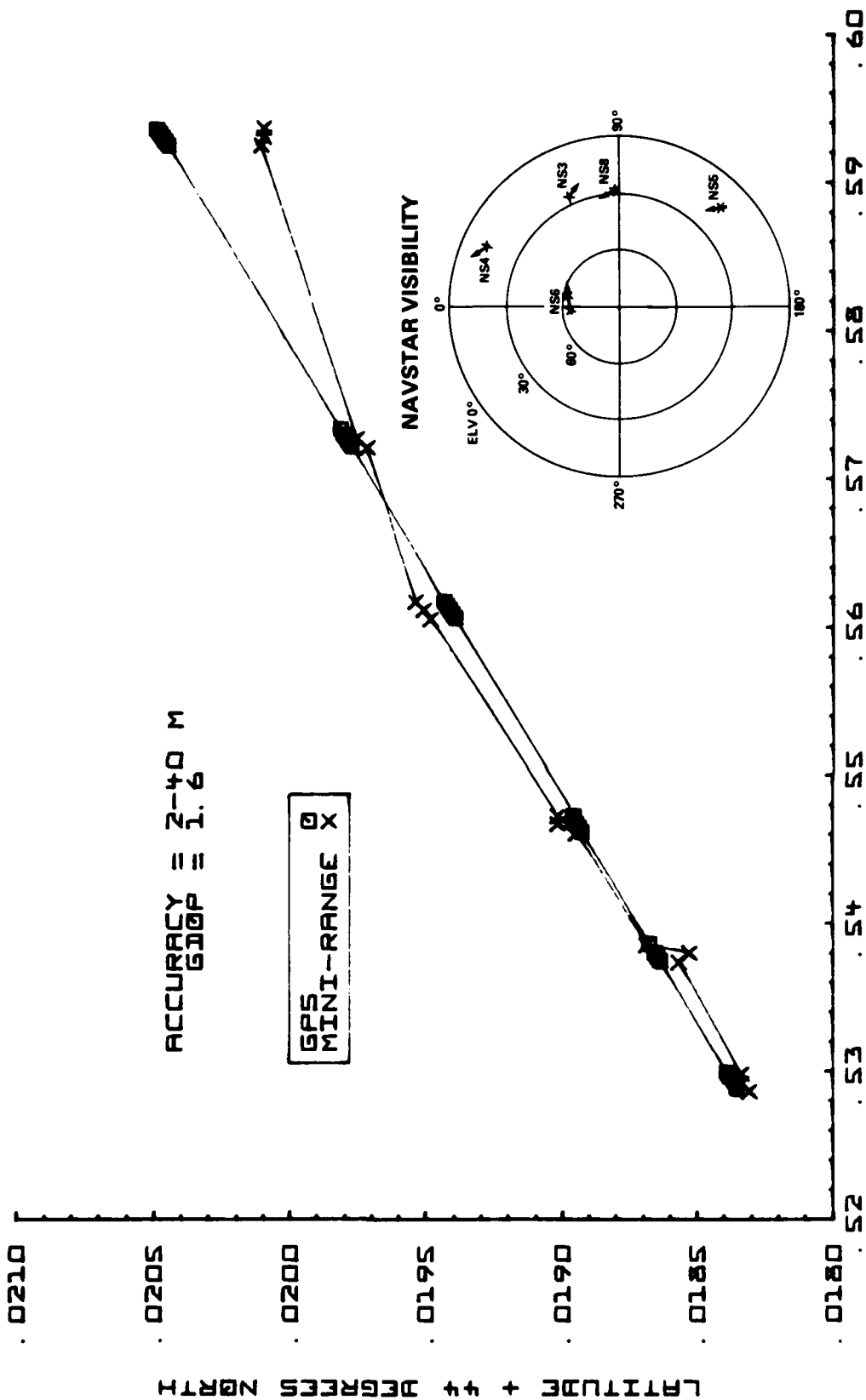


Figure 7.

NAVIGATION COURSE SOLUTION

RUN NO. 2 10/6/83

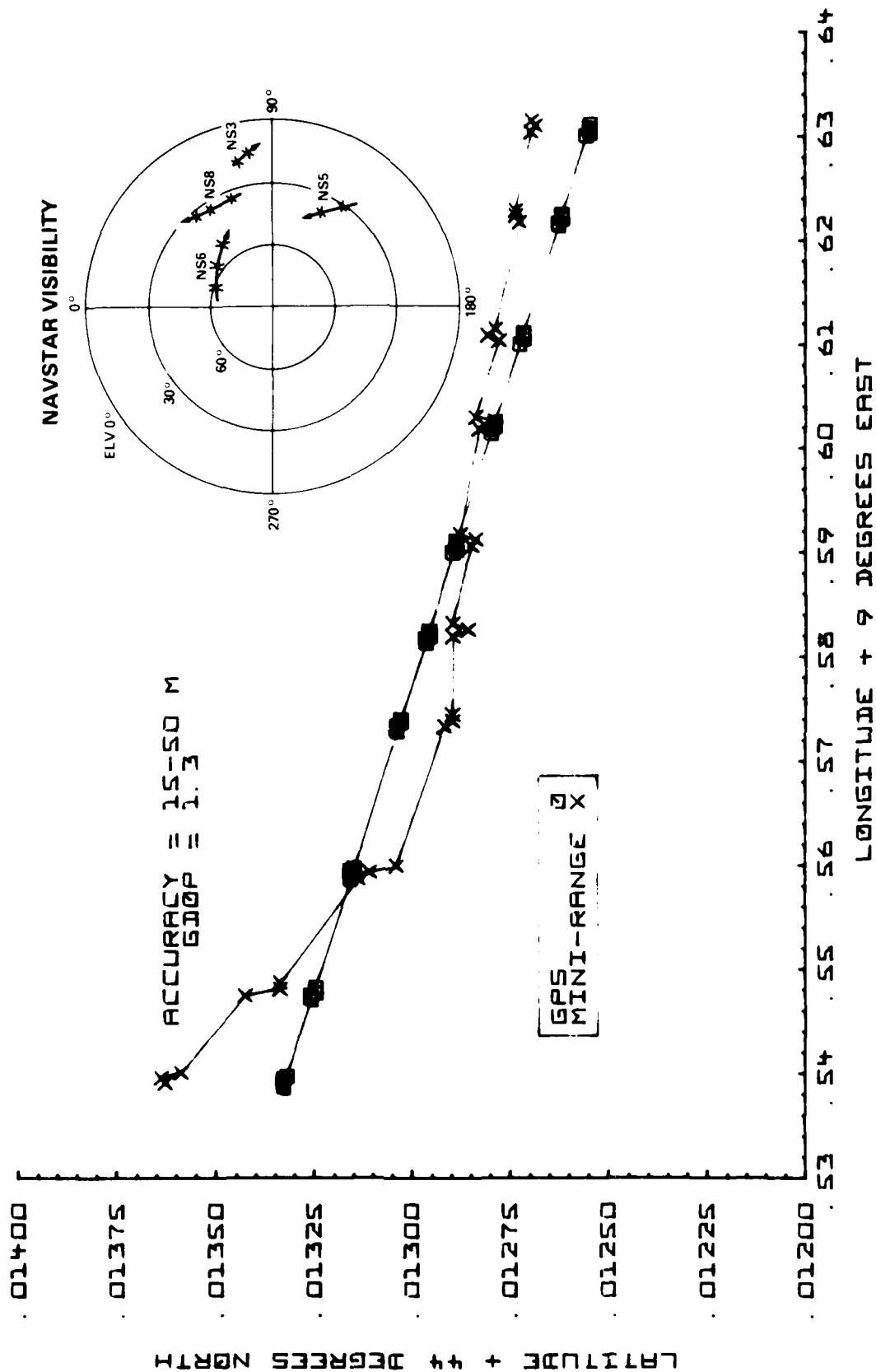


Figure 8.

NAVIGATION COURSE SOLUTION

RUN NO. 1 10/10/83

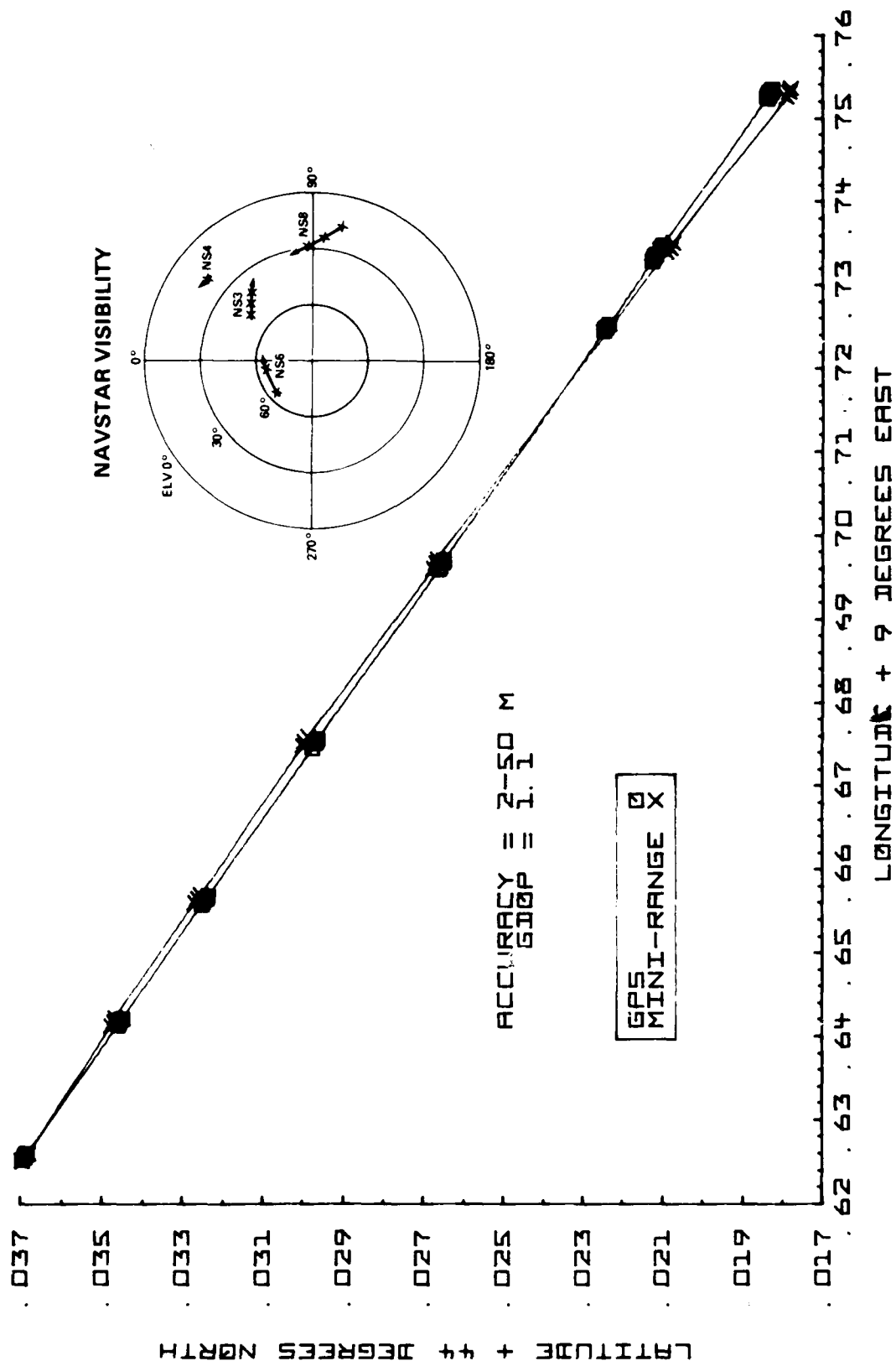


Figure 9.

NAVIGATION COURSE SOLUTION

RUN NO. 2 10/10/83

ACCURACY = 60-110 M
GDOP = 1.9

GPS
MINI-RANGE X

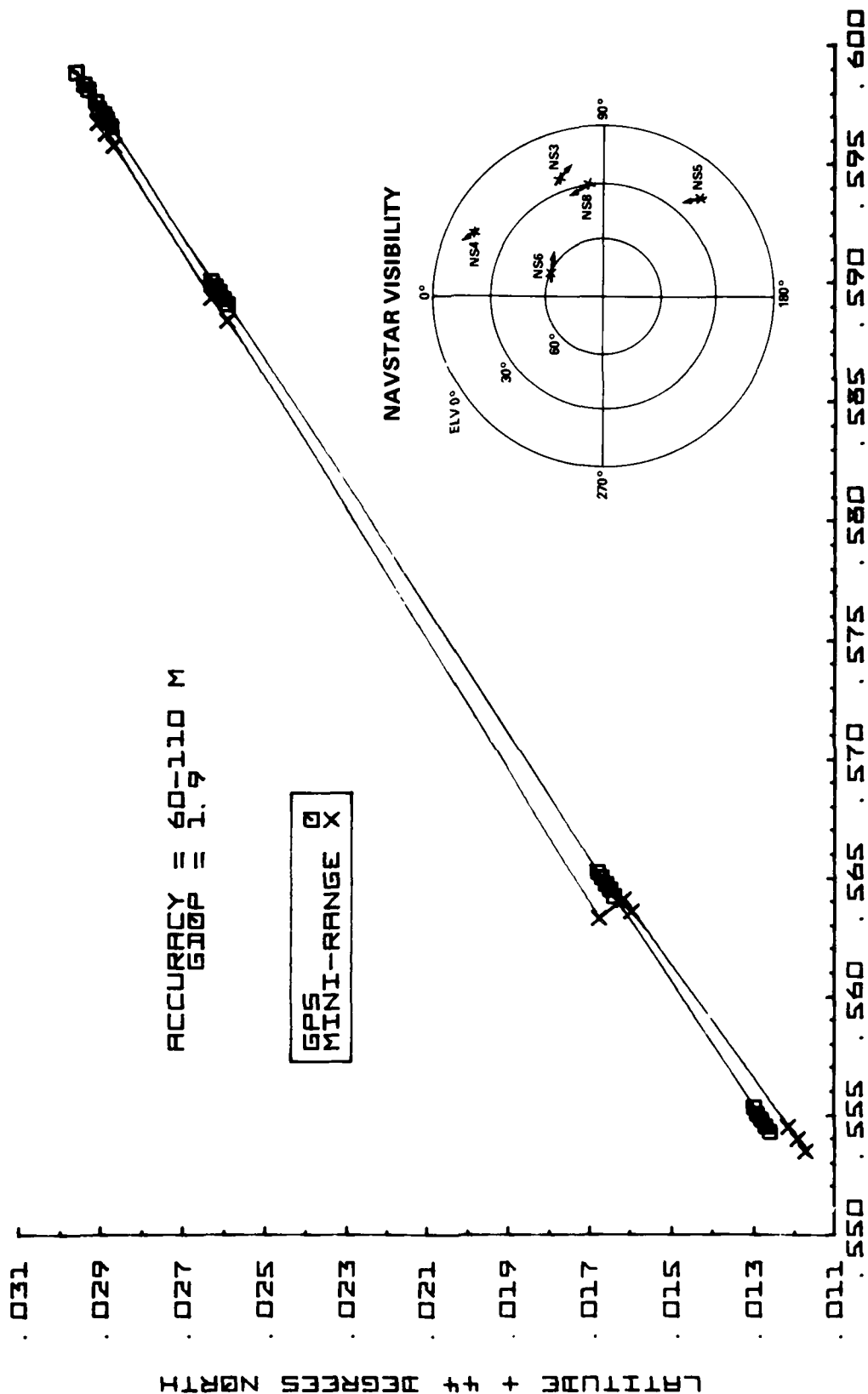


Figure 10.

NAVIGATION COURSE SOLUTION

RUN NO. 3 10/10/83

ACCURACY = 15-100 M
GDOP = 1.4

GPS
MINI-RANGE X

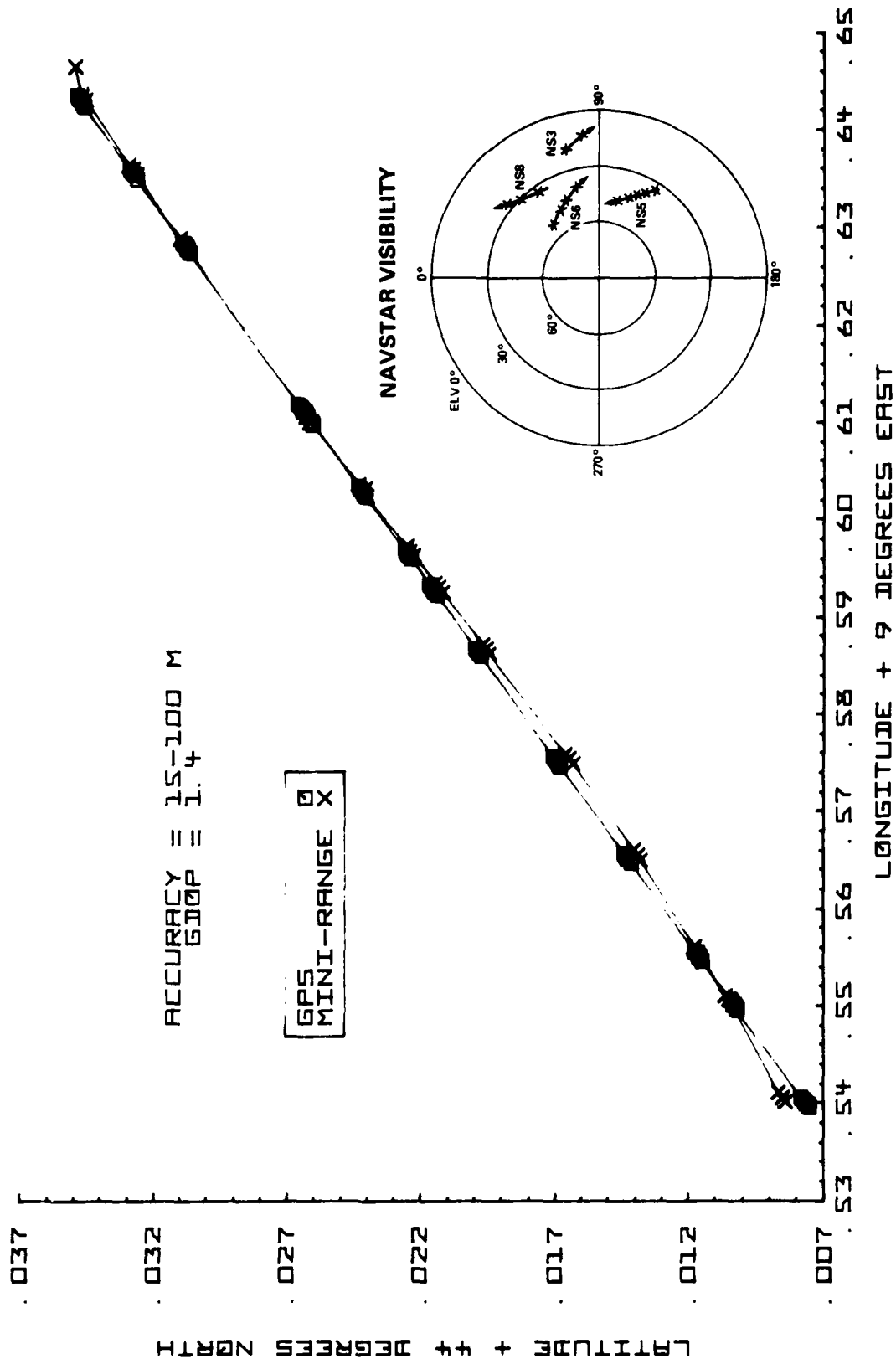


Figure 11.

NAVIGATION COURSE SOLUTION

RUN NO. 1 10/11/83

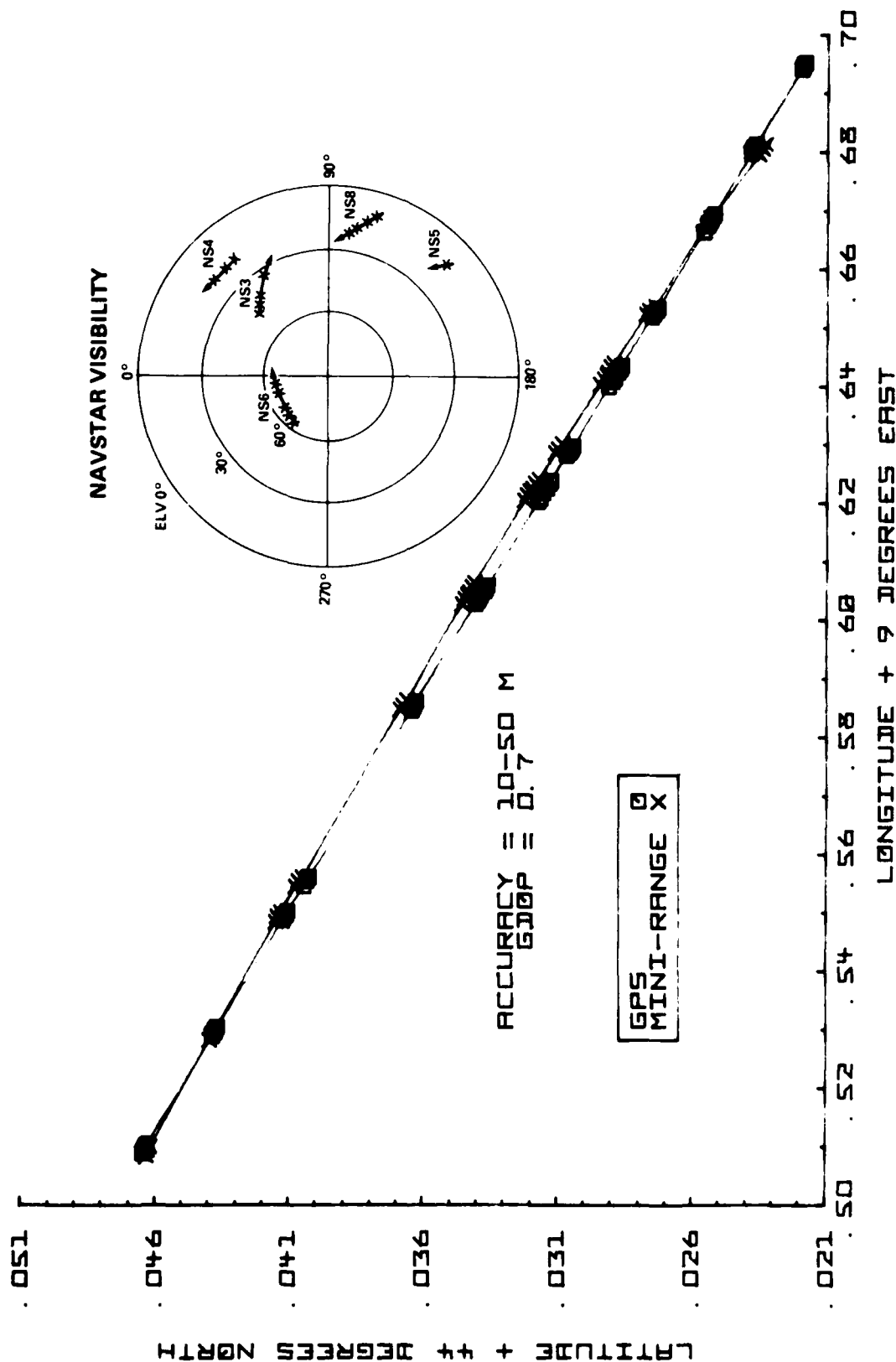


Figure 12.

NAVIGATION COURSE SOLUTION

RUN NO. 2 10/11/83

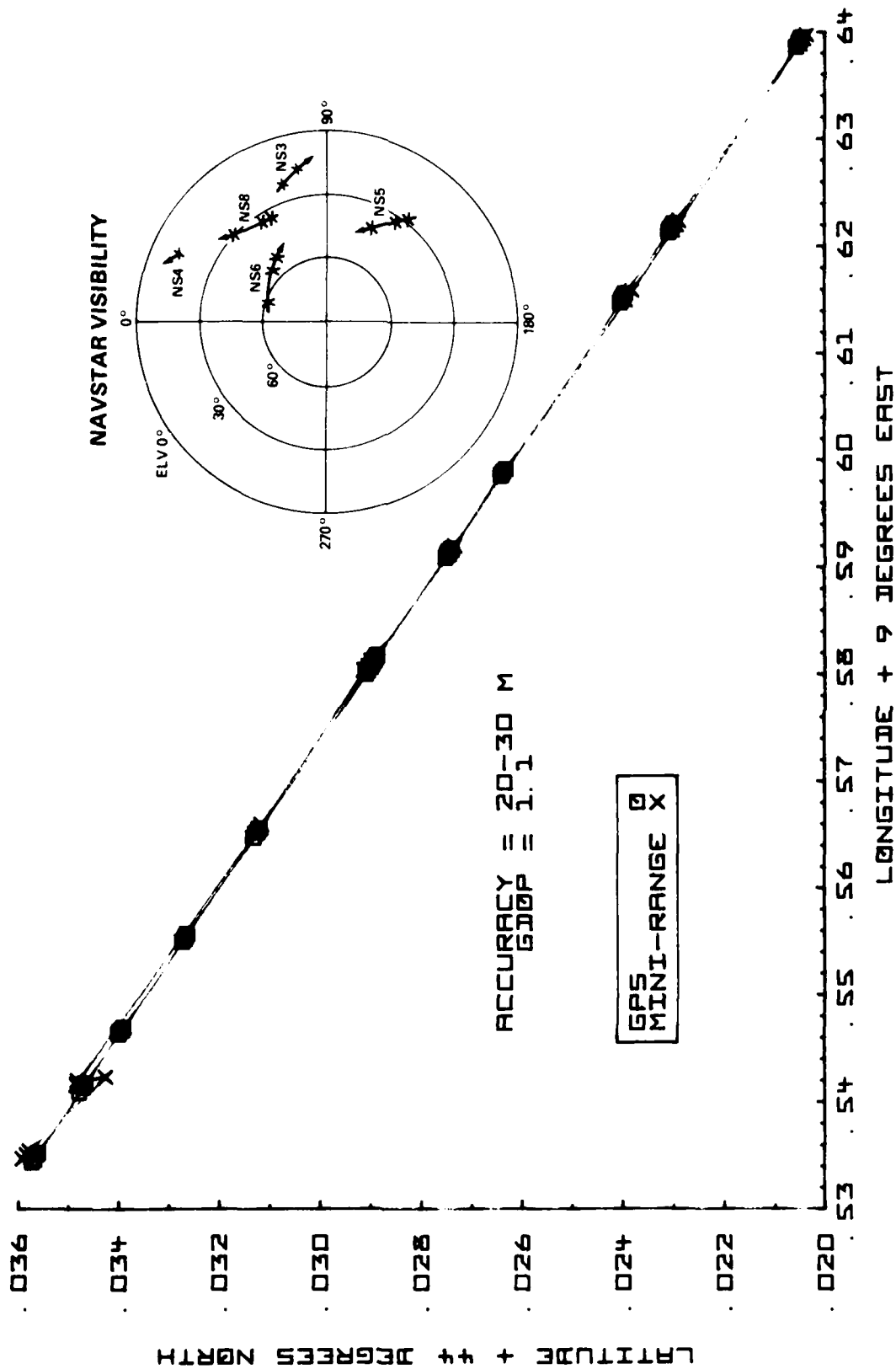


Figure 13.

NAVIGATION COURSE SOLUTION

RUN NO. 3 10/11/83

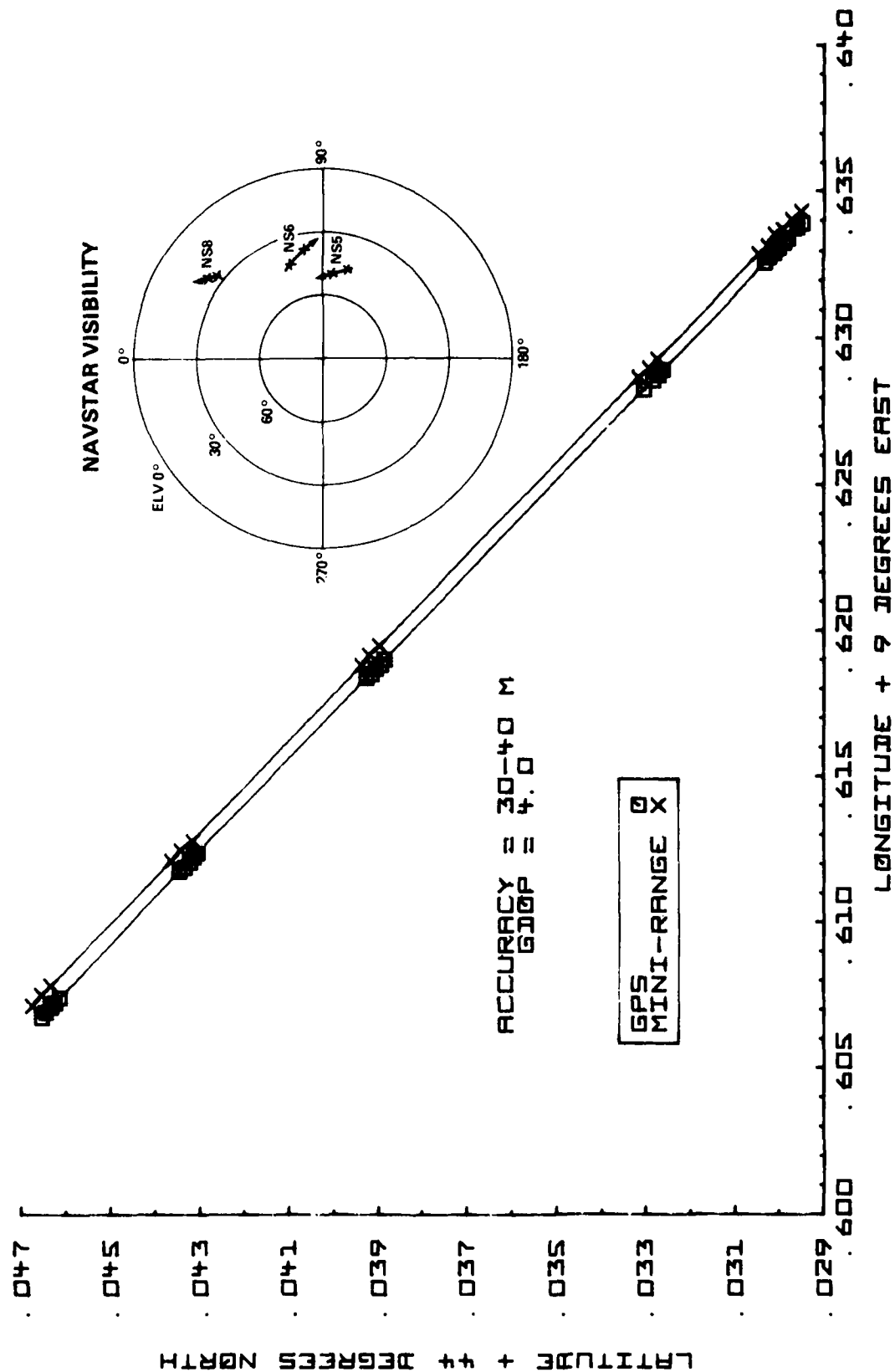


Figure 14.

NAVSTAR GPS NAVIGATION ACCURACY VIA NRL TIME TRANSFER RECEIVER

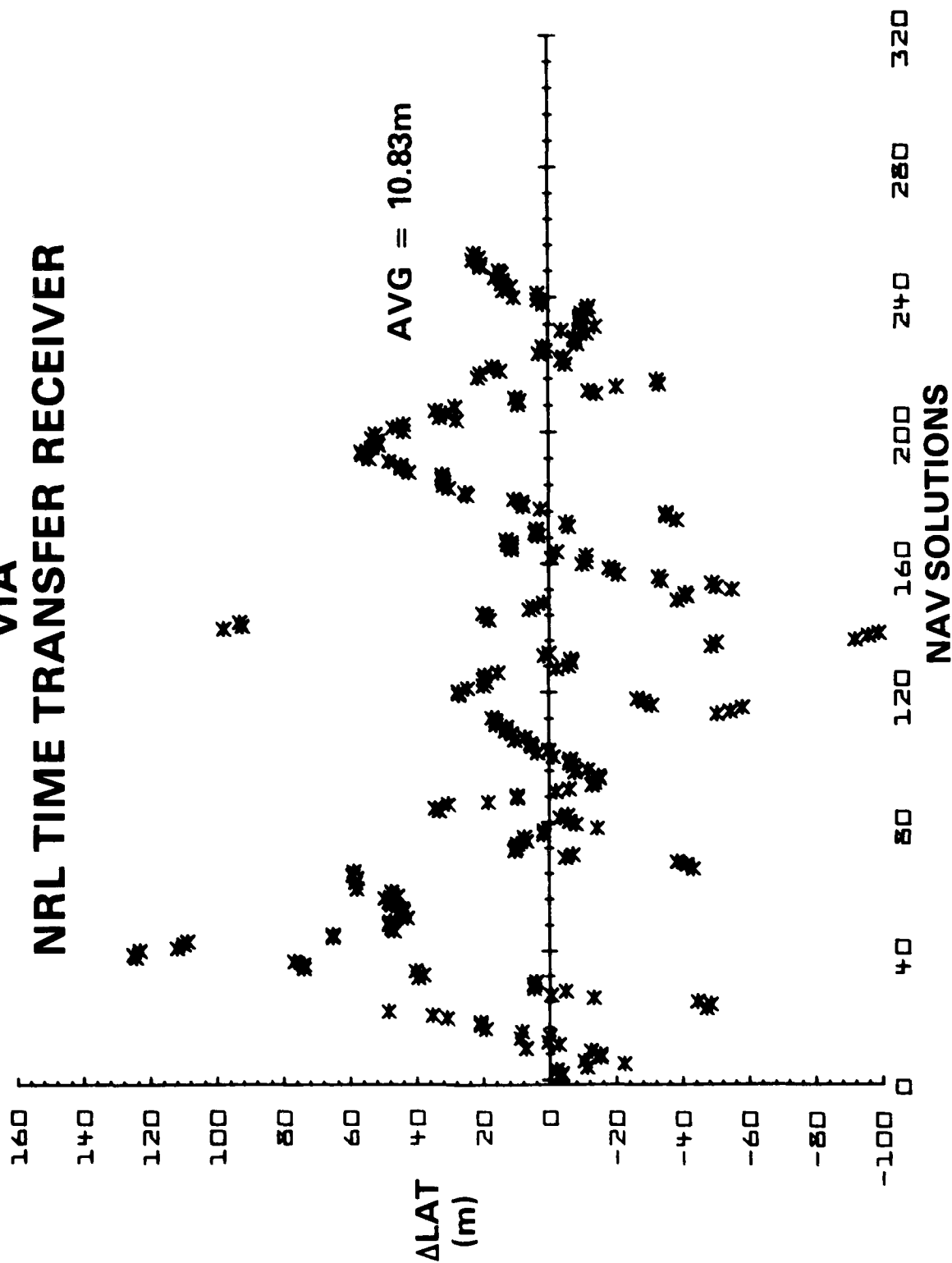


Figure 15.

NAVSTAR GPS NAVIGATION ACCURACY VIA NRL TIME TRANSFER RECEIVER

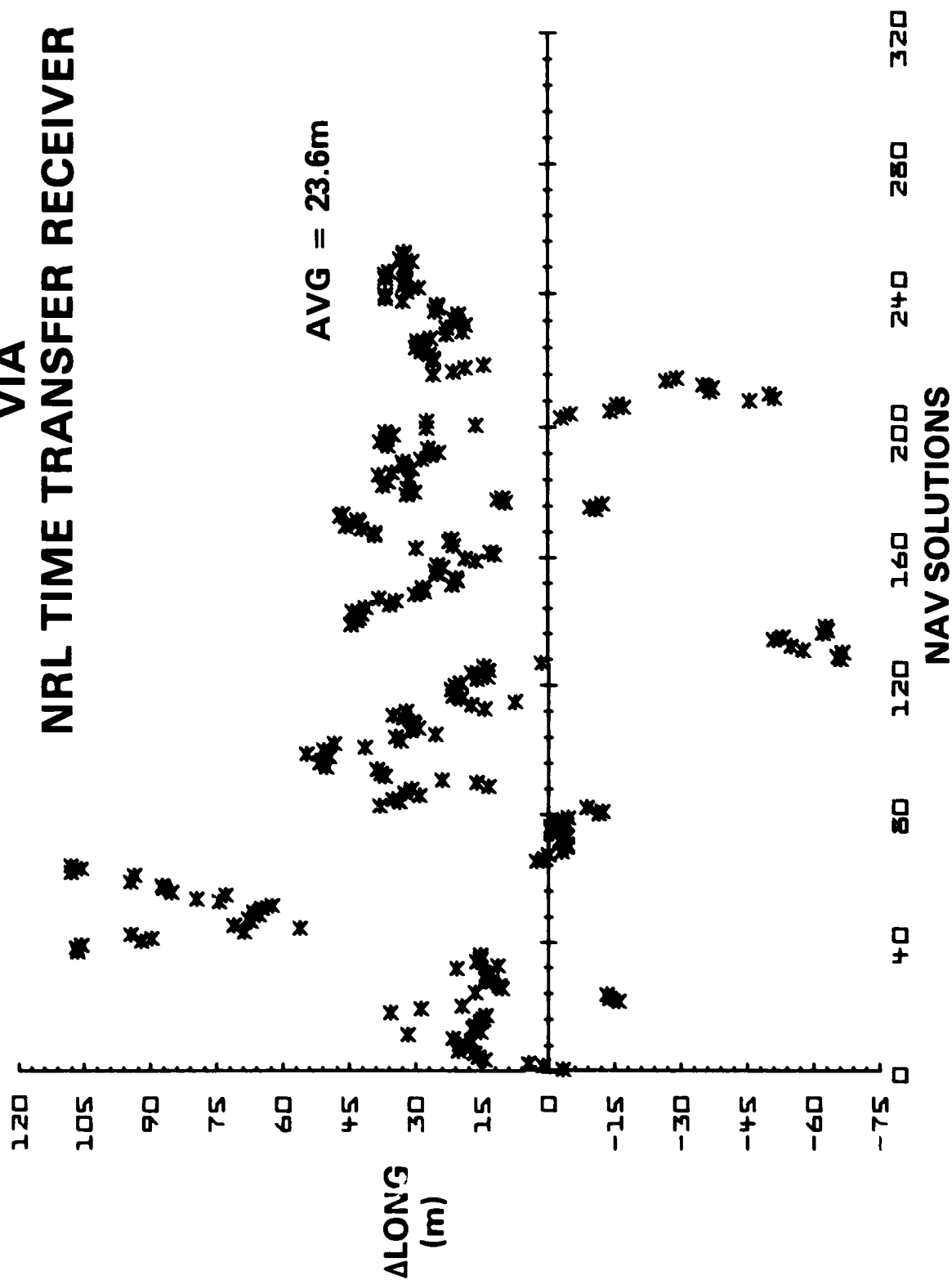


Figure 16.

NAVSTAR GPS NAVIGATION ACCURACY VIA NRL TIME TRANSFER RECEIVER

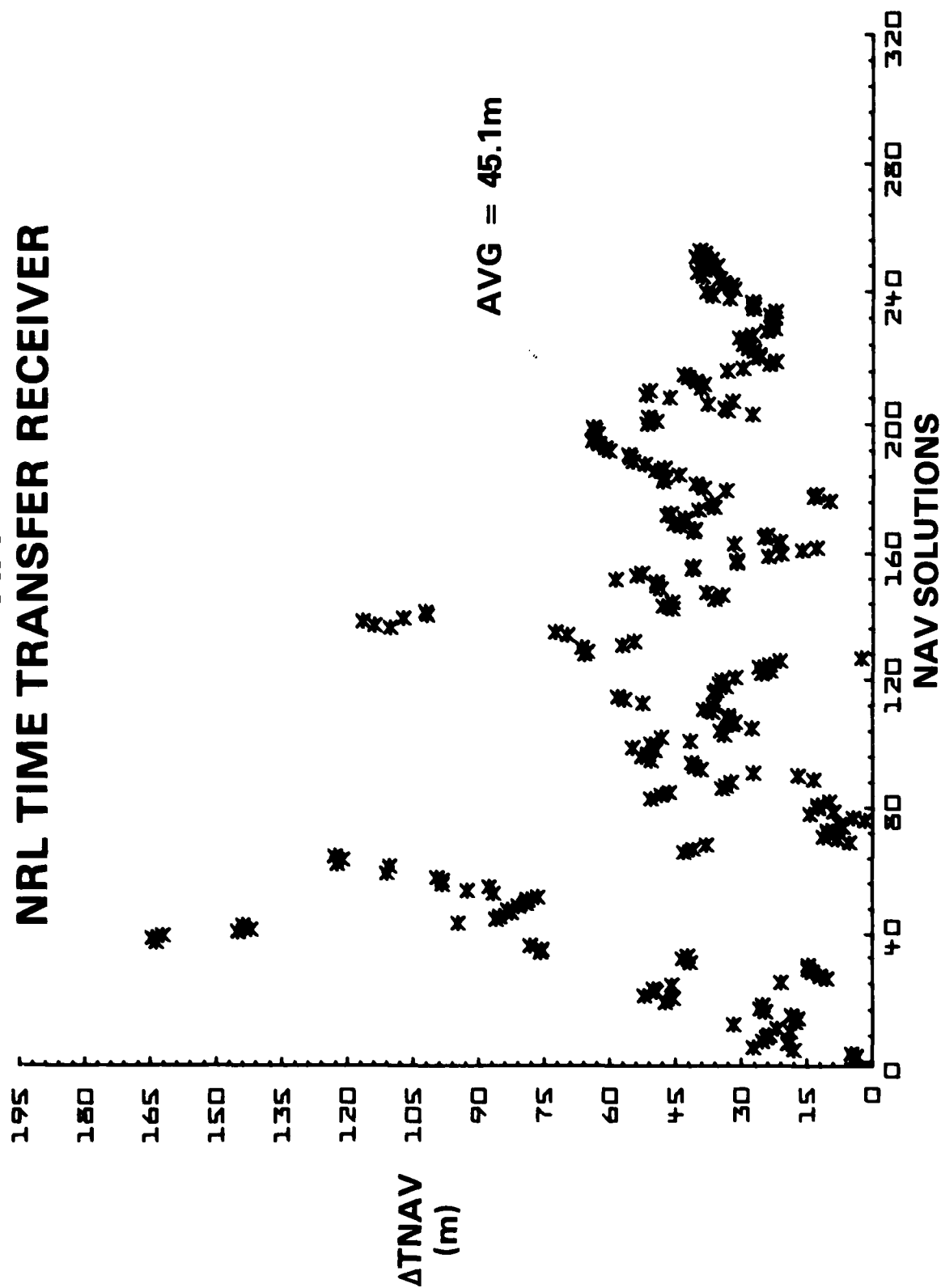


Figure 17.

NAVSTAR GPS NAVIGATION POSITION RESULTS AT IEN VIA NRL TIME TRANSFER RECEIVER

KNOWN POSITION WGS-72	MEASURED POSITION					
	DAY 287	DAY 288	DAY 289	DAY 290	DAY 291	DAY 292
LAT 45° 0' 53.78''	53.35''	53.68''	53.79''	54.11''	53.95''	53.78''
LNG 7° 38' 20.05''	19.63''	19.98''	19.87''	19.57''	19.83''	19.86''
HGT 299.37m						
ΔLAT (ARCSEC)	0.43	0.10	-0.01	-0.33	-0.17	0.00
ΔLNG (ARCSEC)	0.42	0.07	0.18	0.48	0.22	0.19
≈ ΔLAT (m)	13	3	-.3	-10	-5	0
≈ ΔLNG (m)	13	2	5	15	6	6

Figure 18.

QUESTIONS AND ANSWERS

MR. WARD:

Errors caused by tidal bulge, I would expect, to be of that magnitude, when you compared it with the ranging system, the ranging system is not sensitive to that Z-axis.

MR. OAKS:

I'm sorry. Errors caused by what?

MR. WARD:

Tidal bulge. When you're at sea, the tidal bulges on land, but it's much larger on the sea; and the space craft ephemeris is referred to the geoid and the higher the elevation of the space craft, the larger that error becomes; and you could see that the periodic function in your data there is basically, I guess, tied to the solar-lunar tide period.

MR. OAKS:

As I said, we constrained the height to be a constant in the navigation solution, and we hadn't really looked at how--what you're saying is that what we want to do is look at the elevation of the satellites as compared to the periods when we had disagreements in the navigation solution.

MR. WARD:

That's correct.

DR. REINHARDT:

I have one comment. You should RMS errors, not average them. You should average the squares of the errors if you want to talk about the total error of the experiments.

MR. OAKS:

In which data?

DR. REINHARDT:

In the data where you showed the average error for all the individual runs. I'm saying errors add in the square. You should average the square to get a proper answer for the average error, and then take the square root of that, rather than to average the individual errors.

IMPROVED MASTER CLOCK REFERENCE SYSTEM AT USNO

Gernot M. R. Winkler
U. S. Naval Observatory
Washington, D. C.

ABSTRACT

The first phase of the NAVELEX/NRL/USNO Master Clock (MC) upgrade program¹ has been completed with the delivery of two VLG11B Hydrogen Masers to the U. S. Naval Observatory (USNO). After installation in a specially prepared Maser Laboratory with redundant environmental control, and a ten-day "burn-in" operation, the masers were independently tuned. Their subsequent performance caused a review of our plans for their operational use as part of the USNO MC complex. A revised concept is the basis for system integration presently in progress.

INTRODUCTION

For short time intervals, the performance of the USNO Master Clock is limited by the performance of the frequency standard which drives the phase stepper, pulse divider, time code generator and distribution amplifier complex. The data amplifier complex comprises one of the several "Reference Clocks" which implement the master clock time reference. For long time intervals, currently longer than one day, the reference clocks are phaselocked to the computed reference time scale MEAN(USNO). This phase lock is done by a once a day setting by computer of the respective phase microstepper.

In September 1983 USNO received delivery of two VLG11B hydrogen MASERS (produced by Dr. Vessot's group at Smithsonian Astrophysical Observatory, production number S-18 and S-19) which are currently being incorporated into the master clock as superior driving frequency standards. The performance we have measured will permit us to operate the reference clock (which is to be driven by one of the MASERS) in an improved way.

INITIAL MASER PERFORMANCE

Figure 1 shows a conventional sigma-tau plot for the differential stability of the MASERS. These data have been obtained by the offset-beat method. For our application, however, the actual overall performance within our system is of greater relevance. Figure 2 tabulates 5-day solutions of the MASERS in reference to our MEAN(USNO). Two observations are obvious. First, we note the drift of both units (which is entirely within specifications and was expected to be larger by a factor of two to three). Second, we can see that the residuals of the 120 hourly time measurements are indeed less than one nanosecond, i.e. the stability of both the time scale and the MASERS is slightly better than we expected on the basis of older data. Figure 3 is a plot of MASER #18 which shows a change in the drift rate which we correlate with work in the room at that time (#19 was tuned).

The following pictures show the differential stability of the two MASERS expressed as residuals after subtraction of a quadratic fit in phase for progressively longer time intervals. If the drift stays very constant, then we can apply the phasestepper corrections with a time constant longer

than one day and thereby further reduce the phase noise in the reference clock (the noise of the MASER is considerably less than the noise from the time scale for time intervals up to a few days). Table 1 summarizes the essential features of Figures 5-8.

LENGTH OF FIT days	RMS RESIDUALS ps
7	150
15	196
26	1150
40	1870

Table 1

Figure 8 is particularly impressive because it shows that for the full duration of 40 days only three incremental (over and beyond the constant drift) frequency changes occurred. These are 6.7, -4.5 and 3.0 parts in ten to the fifteen. The belief is, therefore, justified that we will be able to utilize the outstanding stability of these two units for times much longer than one day.

MASTER CLOCK MASER SUBSYSTEM CONCEPT

The MASERS are not only superior clocks and cost commensurately more than industrial high performance cesium clocks, they also require much more attention. They must be tuned every month in the interest of continuing high stability. We also expect more interruptions for other reasons. It is for the provision of more required operational flexibility which will be required that we arrived at a subsystem concept as depicted in Figure 9. At the heart of the system is our standard system controller, an HP9915 computer with two interfaces: An IEEE 488 bus for measurement and control and an RS 232C for communication with our IBM Series 1 mini-computer. The concept allows for switching the driving standards at any time because the synthesizer of one unit will be remotely adjusted to keep the output of both units in phase at all times. This way tuning and repair can be performed on a unit without interruptions in the operating system, barring catastrophic failures. Forty channels of test voltages for each unit are under constant surveillance for diagnostic purposes. The system concept follows our general principle of local control so that this subsystem is entirely independent in between the data communications with the IBM operations controller. It also uses to the maximum extent high quality industrial components and subsystems. This subsystem is currently being assembled and interfaced. We expect to be in operation in spring 1984.

REFERENCE

- 1) Ralph Allen (1980), The Navy PTTI Program (Update), Proceedings 12th PTTI Conference, p. 127

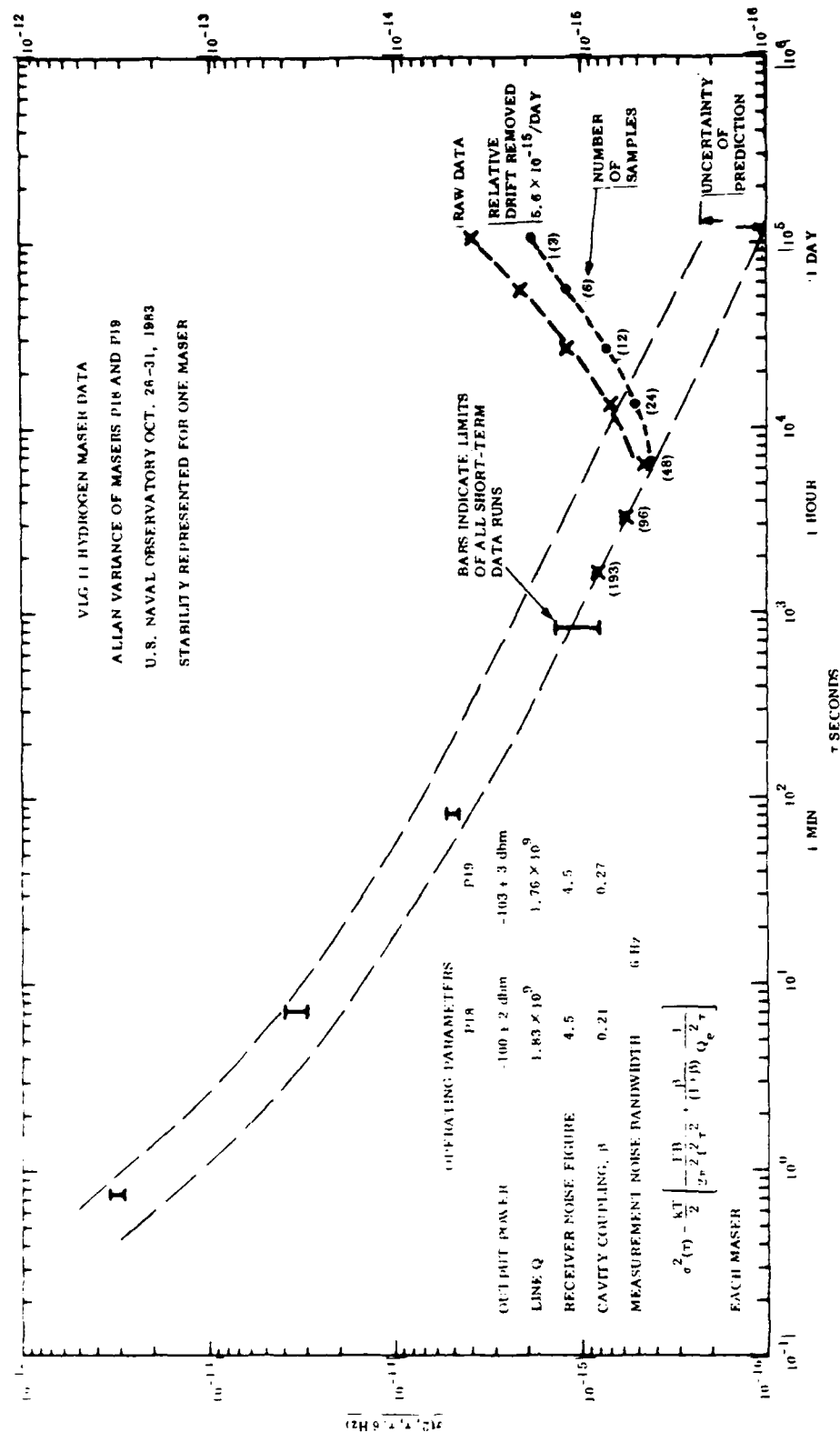


FIGURE 1 STABILITY DATA TAKEN WITH THE OFFSET - METHOD (COURTESY DR. VESSOT)

5-DAY SOLUTIONS FOR USNO VLQIIB MASERS
(MEAN(USNO - MASER))

MJD	Maser A		Maser B	
	S-18		S-19	
	Rate(ns/d)	Sigma	Rate(ns/d)	Sigma
45607	-17.0	0.8		
45612	-12.8	0.9		
45617	-6.4	1.0		
45622	-4.1	0.6		
45627	-1.2	0.5		
45632	+2.9	0.6		
45637	+5.9	0.8		
45642	+7.7	0.5	-3.1	1.1
45647	+10.6	1.1	+3.4	1.6
45652	+12.9	0.8	+9.4	1.6
45657	+15.4	0.6	+15.8	1.3
45662	+17.0	0.5	+20.5	1.0
45667	+19.4	0.5	+25.3	0.4

FIGURE 2 LONG-TERM MASER STABILITY MEASURED IN REFERENCE TO MEAN (USNO)

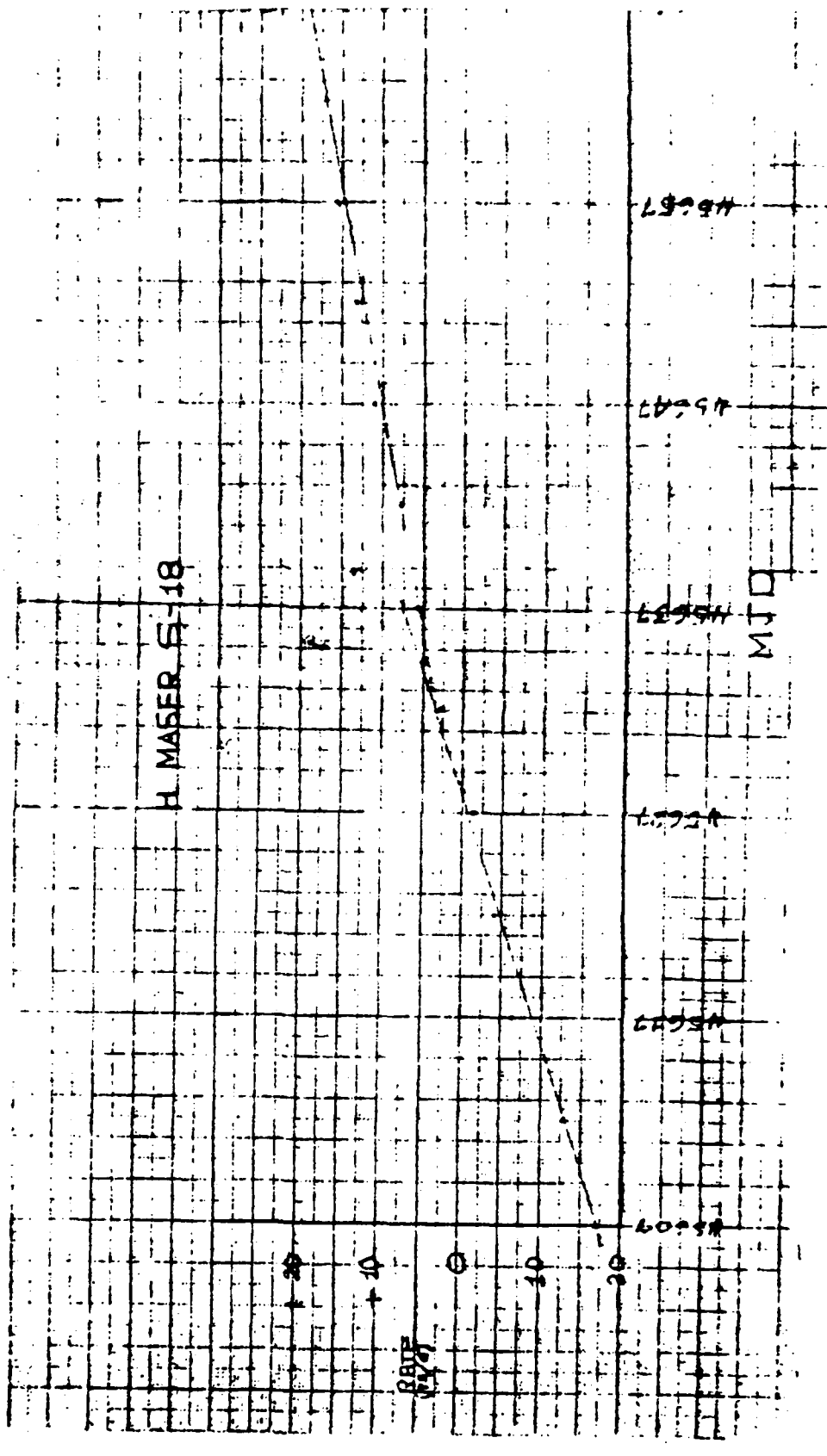


FIGURE 3 FIVE-DAY RATES OF MASER #18

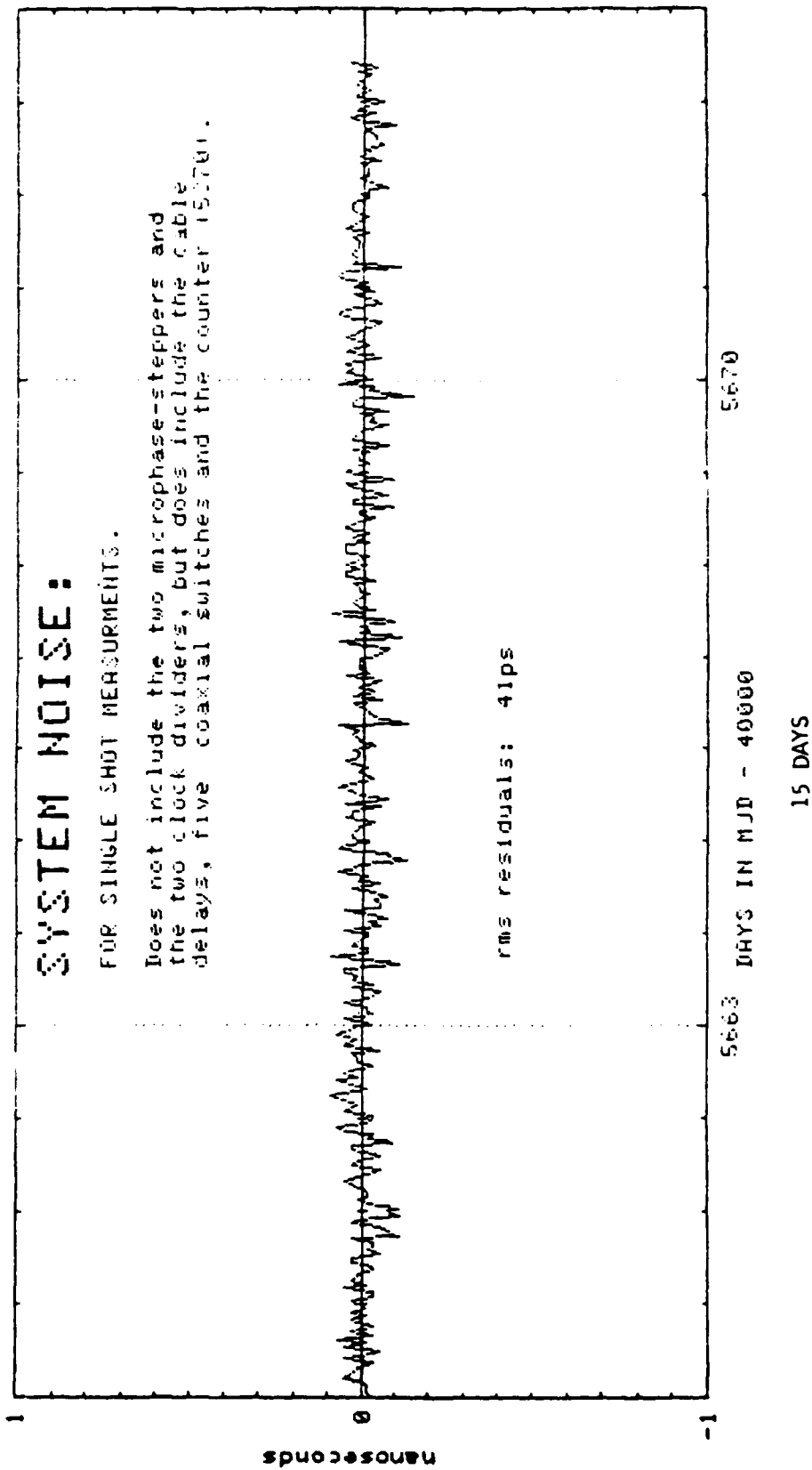


FIGURE 4 SYSTEM NOISE FOR THE HOURLY 1pps TIME DIFFERENCE MEASUREMENTS.

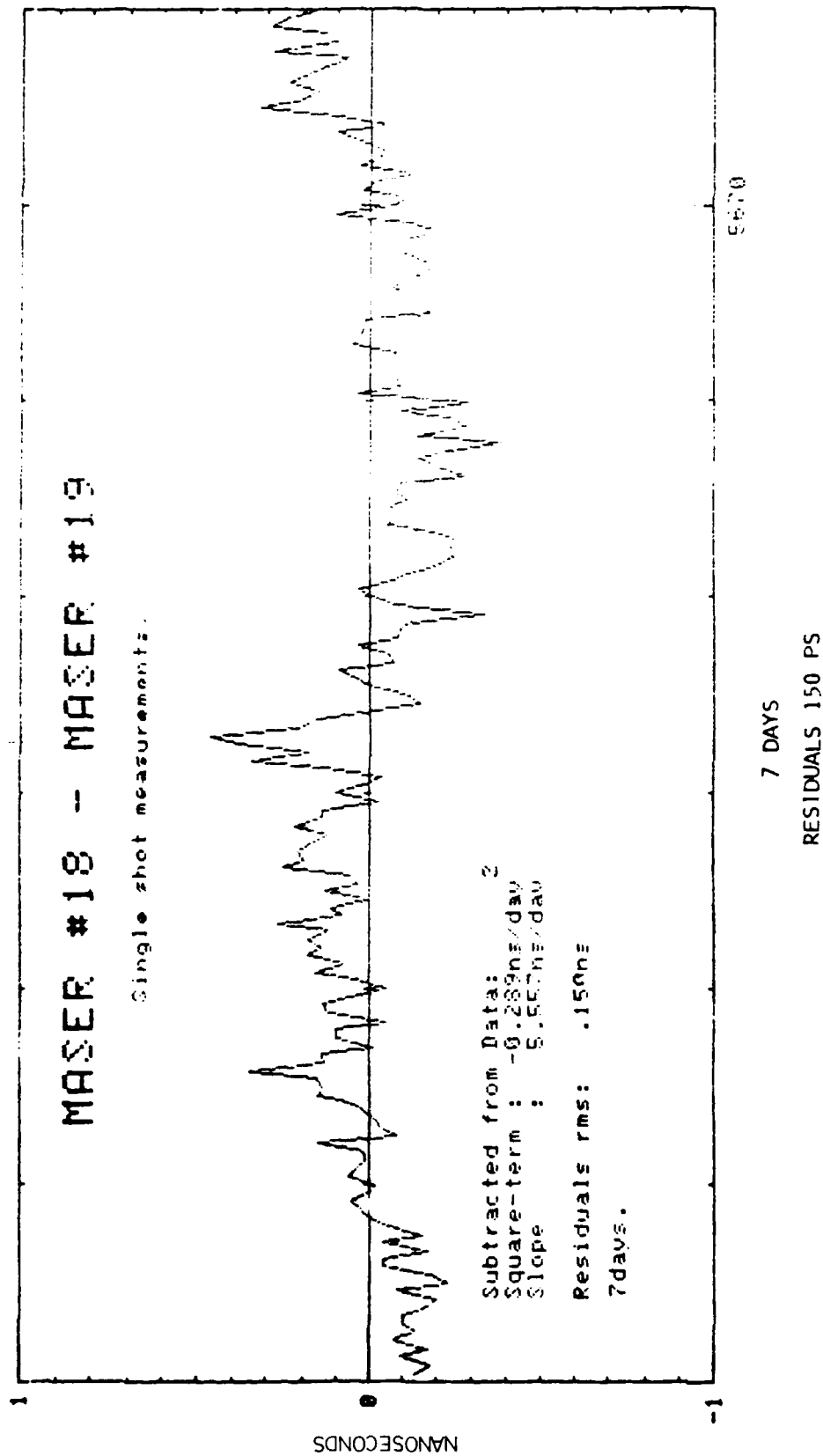


FIGURE 5 MASER DIFFERENTIAL STABILITY

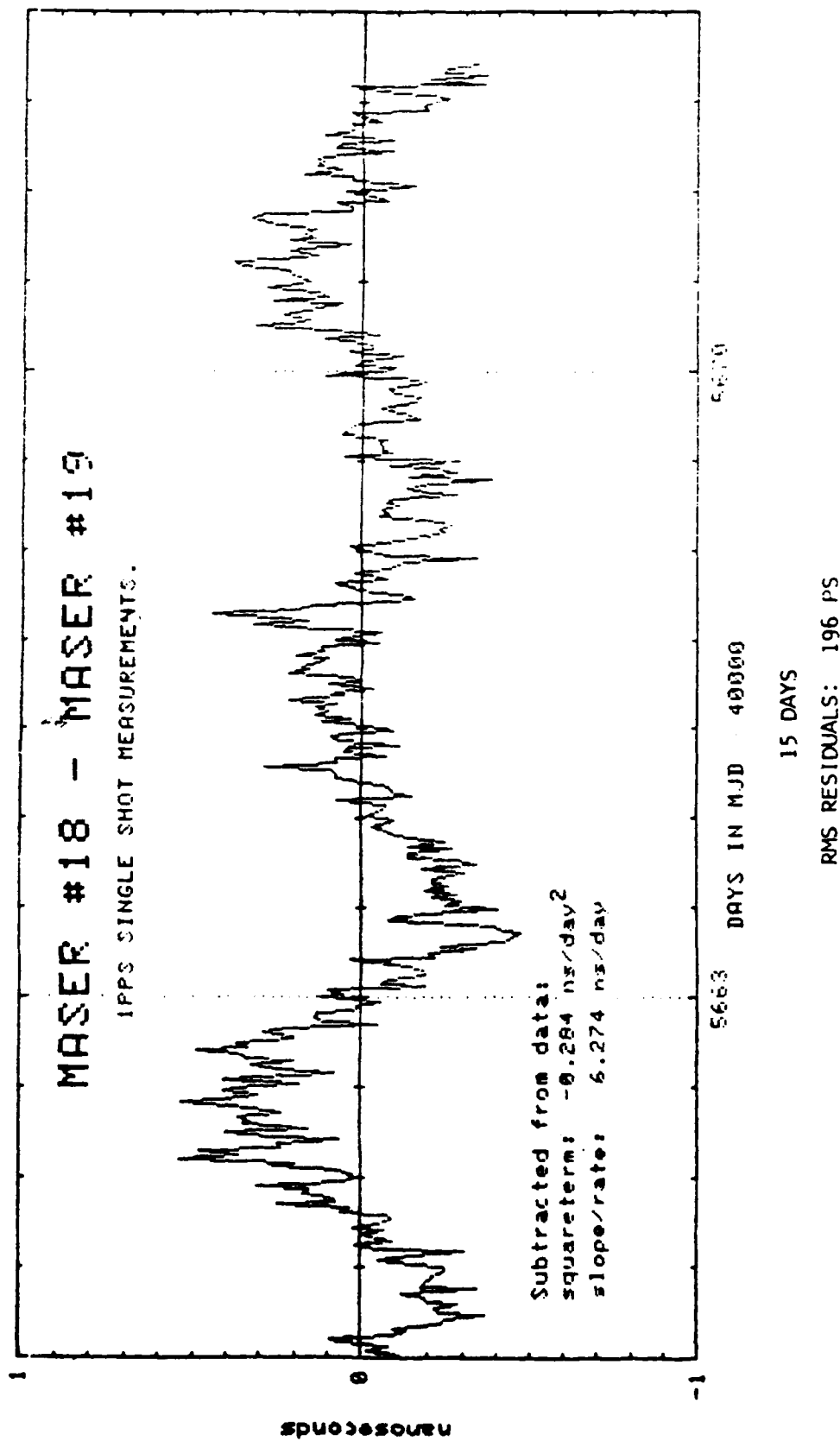


FIGURE 6 MASER DIFFERENTIAL STABILITY

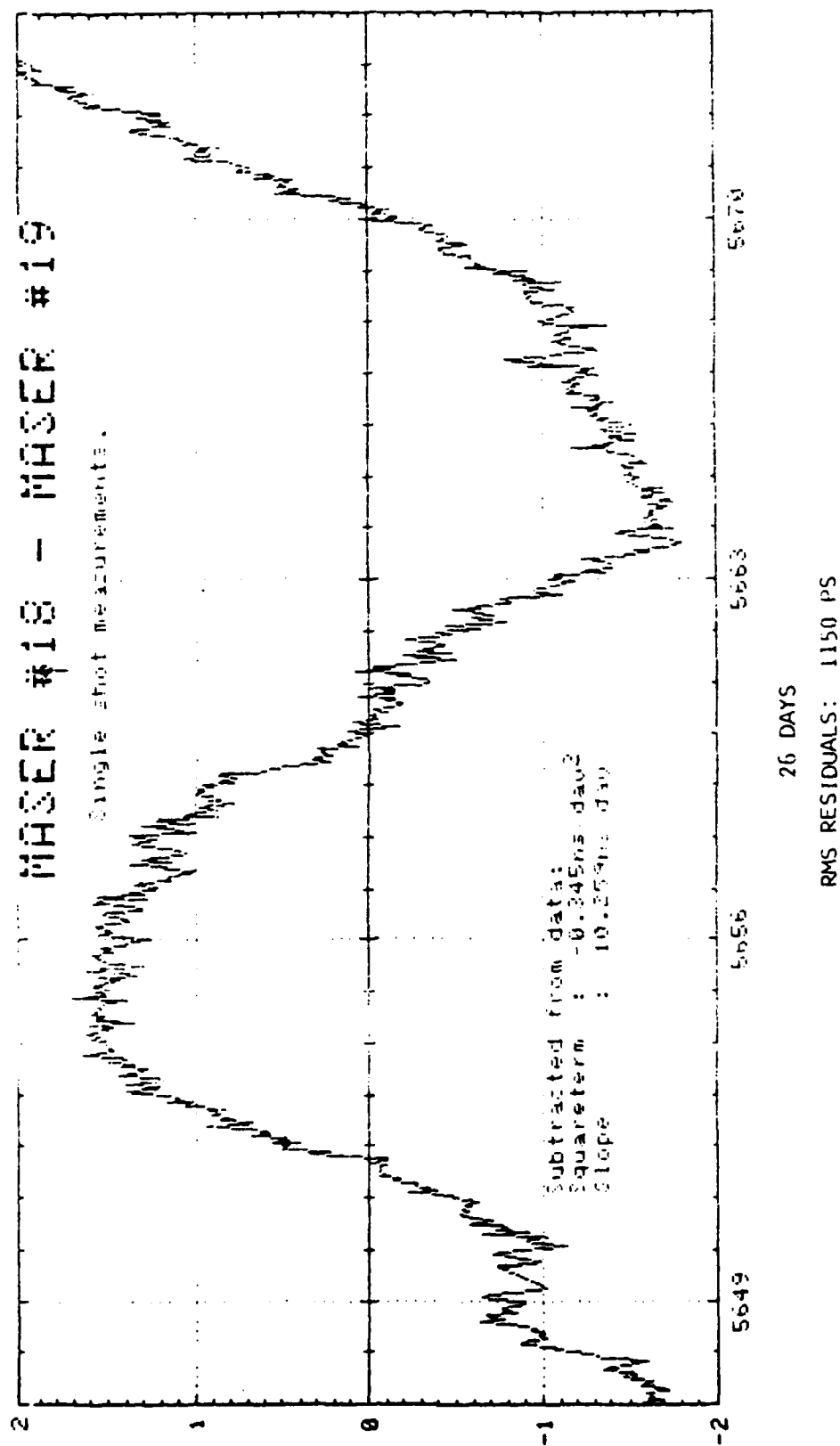


FIGURE 7 MASER DIFFERENTIAL STABILITY

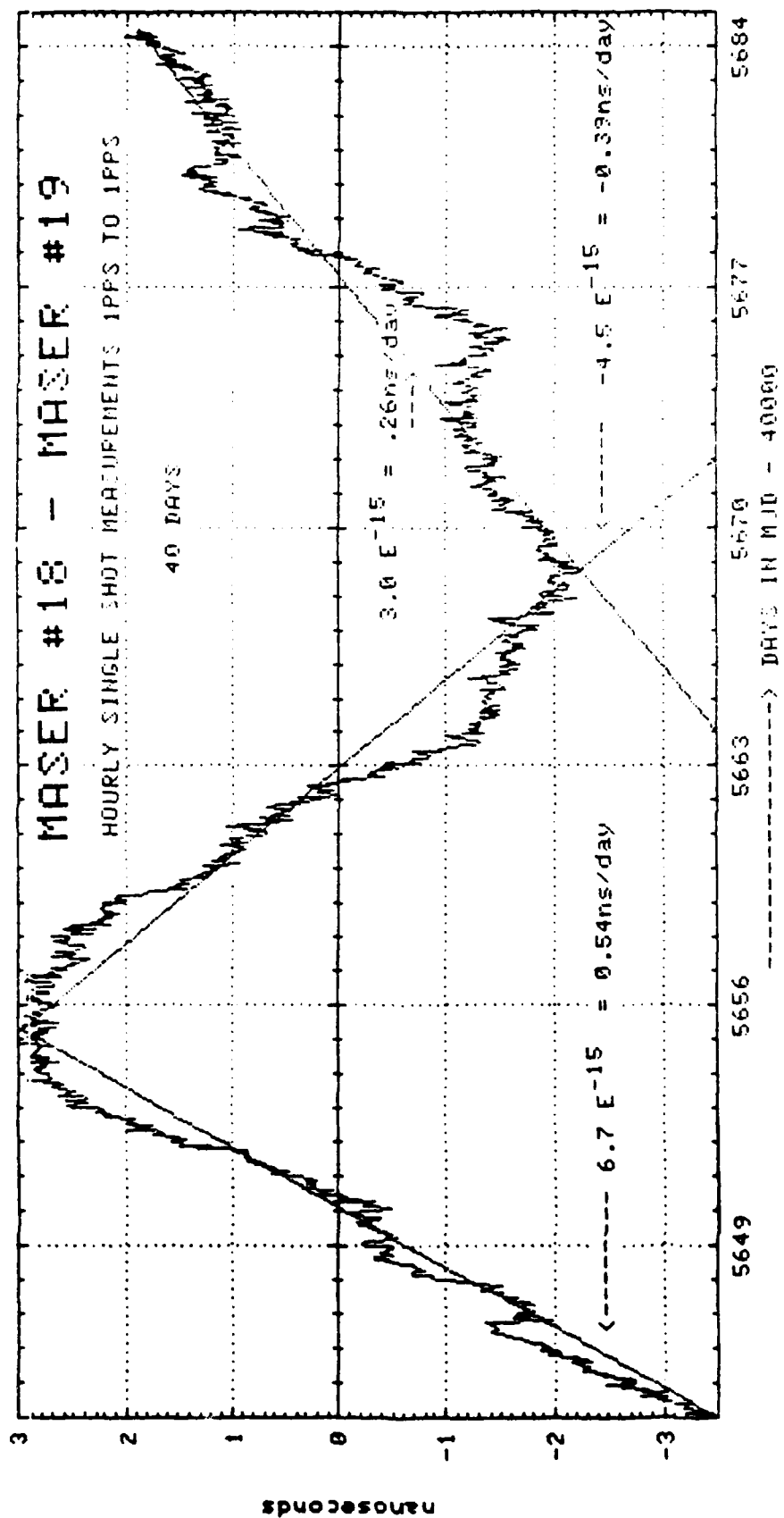


FIGURE 8 QUADRATIC FIT RESIDUALS, SLOPE: 7.7ns/d , SQUARE TERM -0.33ns/d^2 , RMS. RESIDUALS: 1.66ns .

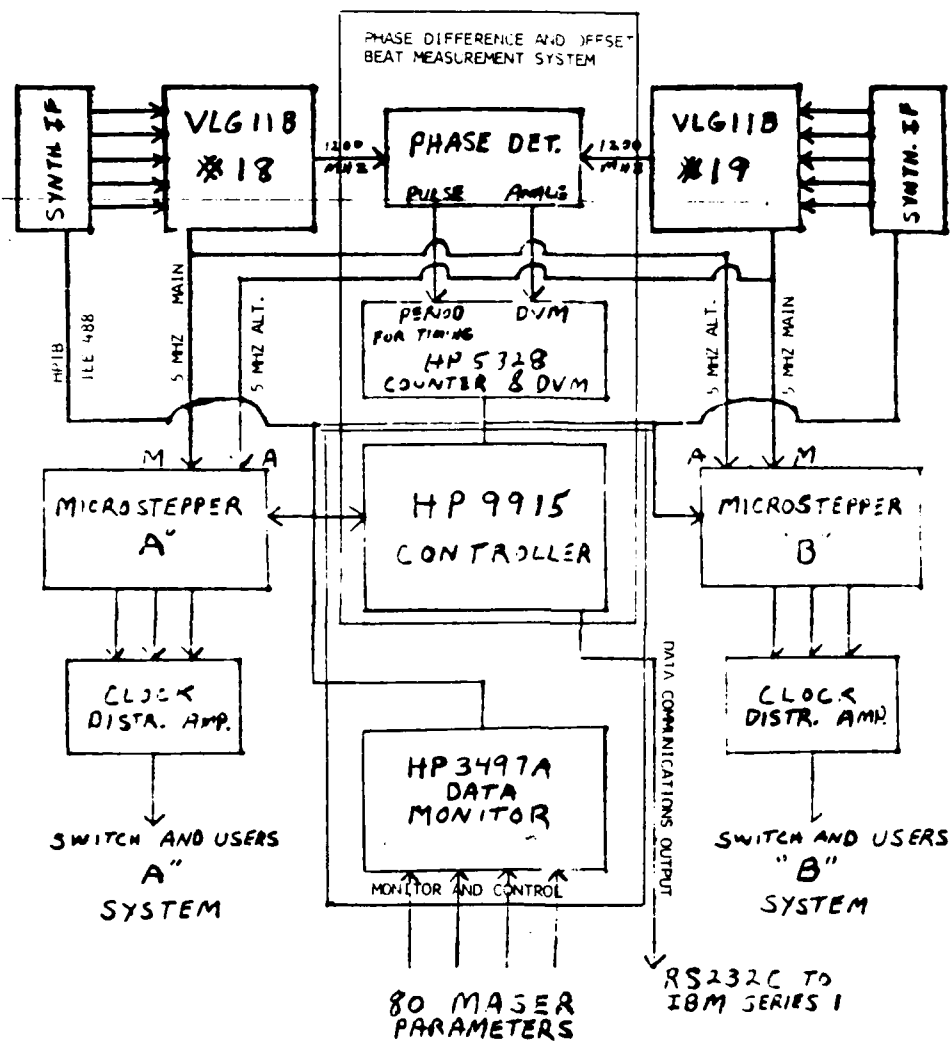


FIGURE 9 NEW MASTER CLOCK MASER SUBSYSTEM

QUESTIONS AND ANSWERS

MR. WARD:

Sam Ward. I have two questions. First, what is causing that periodicity that I saw in the sort of data?

DR. WINKLER:

That is an effect that you can see in every record which has a limited data length. The affect has been discussed at length by Jim Barnes a few years ago. It's simply the low frequency spectral content of the variations which the masers show; and you have the combination of a filter due to the cutoff of the data, and low frequency content appears for a final data piece as some kind of indication of a sine wave.

If, however, you take the next spot, the sine wave looks different. If you continue sampling the sine wave changes period. It is really not the sine wave. It is the low frequency content of the disturbances, and you find it in any such record between highly stable standards. Your second question?

MR. WARD:

The second question deals with the convenient means of measuring the Zeeman so that you can see whether the magnetic environment for both of them has changed.

DR. WINKLER:

We plan to be able at any time, by pushing a button on the controller, to shift--System B, for instance, if that one requires a Zeeman measurement to be operated from the first maser, or in fact from an additionally available Cesium signal that will come from one of our cesium clock vaults and then the maser is available for anything. You can make your Zeeman measurements. You can take it apart if you want to, and you can do anything. You can tune it as often as you please. The idea has been to have a system which will allow maximum use of these two beautiful clocks that we now have and are better by a factor of 10 what our specifications have called for; and I am very happy to acknowledge here the excellent cooperation between the three Navy agencies involved, namely, NAVELEX which provided the program management; N.R.L., with Joe White who wrote the specifications, and our contractor, Smithsonian Astrophysical Observatory, which delivered the masers, and really took every pain to make sure that they operate at this performance level.

My purpose was to report the initial performance of the masers, and to do that I felt some kind of an obligation because in the past there were some quite critical remarks which I made about the performance of masers, and I'm happy to correct myself and say that now we have clocks that are better than anything I have ever seen. Thanks.

THE STEERING OF GPS TIME

H. F. Fliegel

The Aerospace Corporation

El Segundo, California

ABSTRACT

The Navstar Global Positioning System (GPS) will be one of the most widely available means by which to distribute exact time. By agreement between the GPS Control Segment and the US Naval Observatory (USNO), GPS time will be maintained an integral number of seconds, n , from UTC, with an error less than or equal to one microsecond:

$$T = \text{GPS-UTC} - n \leq 1 \mu \text{ sec},$$

where n is the number of leap seconds which will have elapsed between early 1980 and current time. The GPS Navigation Message will give the value of T to 100 nanoseconds or better, real time. After the fact, values of the GPS-UTC offset should be available to qualified users with accuracy of 20 nanoseconds or better. GPS time will be steered by altering its adopted offset bias and drift from a Reference Clock. This paper summarizes the mathematics of the steering algorithm, and the interface between the USNO and the GPS Controller.

INTRODUCTION

The Global Positioning System (GPS) of satellites is designed to disseminate to its users, along with the spacecraft ephemeris information necessary to derive user position, the current value of UTC. The maintenance of GPS time is a responsibility of the Master Control Station (MCS) of the GPS Control Segment, which serves as the

directing center for all data collection and data generation, and also as the primary point of contact with such supporting agencies as the US Naval Observatory (USNO) and the Defense Mapping Agency (DMA). The MCS controls the uploading of navigational messages to the GPS satellites, and these messages include the parameters input to users' receiver sets to convert from GPS time to UTC. Feedback is provided by the USNO, which monitors the GPS navigational messages, and continually estimates the GPS-UTC offset in time and frequency.

The Navigation Data Message represents this GPS-UTC offset as

$$\text{GPS-UTC} = a_0 + a_1 t + n,$$

where a_0 and a_1 are values appropriate to the clock of the satellite broadcasting the message, and n is the number of GPS leap seconds which have accumulated since the GPS epoch of 6 January 1980. Thus, GPS time is offset from International Atomic Time (TAI) by approximately 19 seconds. The exact value of the offset between GPS time and either TAI or UTC depends, of course, on how precisely GPS time/frequency can be estimated and, once estimated, how precisely it can be steered. This paper will be addressed only to the problem of steering.

The tolerance allowed in the steering of GPS time is defined for the final phase of GPS development, the Operational Control Segment (OCS), as follows (Reference 1):

GPS Time is defined in the OCS as the time determined from a particular MS Clock (the Reference Clock), when offset by a bias and drift. The offset bias and drift of the Reference Clock are not estimated in the Kalman Filter but are assumed to be fixed in value. The offset bias and drift can be modified using a controller directive, and hence GPS Time can be "steered" into alignment with UTC. In particular, GPS time will be steered to attempt to maintain

$$|\text{UTC (USNO)} - t_{\text{GPS}} + \Delta \text{LS} [\equiv n, \text{ above}]| \leq 1 \text{ microsecond.}$$

No such requirements are specified for the present Interim Control Segment (ICS), but it is understood that the ICS will satisfy the OCS requirement as nearly as circumstances permit.

This Interim Control Segment, which has been used throughout the Phase I Concept Validation Phase, consists of four Monitor Stations (MS), an Upload Station (ULS), and a Master Control Station (MCS). The Monitor Stations are located at Hawaii; Elmendorf AFB, Alaska; Guam; and Vandenberg AFB, California. The remote Monitor Stations are unmanned data-collection centers under direct control of the MCS. Each MS contains a four-channel user-type receiver, environmental data sensors, an atomic frequency standard, and a computer processor. The receiver measures the pseudorange and delta pseudorange (integrated doppler) of the satellite spread-spectrum signal with respect to the atomic standard. It also detects the navigation data on the spread-spectrum signal. The environmental sensors collect local meteorological data for later tropospheric signal delay corrections at the MCS. The computer processor controls all data collection at the MS, and provides the data interface with the MCS. All data obtained by the MS is buffered at the MS and then relayed upon request to the MCS for processing.

The ULS, located at Vandenberg AFB, provides the interface between the Control Segment and the satellites. Its function is to utilize an S-band uplink to upload data into a satellite navigation processor. This upload data can be user navigation data, requests for processor diagnostics, or commands to change the satellite time provided by the user.

The MCS is also located at Vandenberg AFB, and completely controls the operation of the Control Segment. It performs the computations necessary to determine satellite ephemeris and atomic clock errors, generates satellite upload of user navigation data, and maintains a record of satellite navigation processor contents and status. The MCS also has interfaces with the Satellite Control Facility (SCF) and Naval Surface Weapons Center (NSWC). The SCF provides a backup upload capability in case of ULS failure and also provides satellite telemetry and command information. NSWC generates a predicted reference ephemeris from MCS-smooth pseudorange measurements for use by the MCS in the ephemeris estimation process.

The current configuration at the Master Control Station has been upgraded by an IBM 3033 computer, which will provide increased reliability and capacity for the Phase II Development and System Test Program support. The converted software will provide for operational

enhancements as well as the navigation message changes required to be compatible with the Phase II User Equipment. The upgraded configuration has been installed and is operating at Vandenberg Air Force Base.

The IBM 3033 computer will eventually be installed in the Operational Control System (OCS), which is currently under development and scheduled to initiate satellite operations support in 1985. The OCS will provide worldwide coverage for monitoring and uploading of the full eighteen to twenty-one satellite constellation. The OCS will also consolidate into a single facility the functions currently performed by the AFSCF and NSWC (see Figure 1).

Then the overall MCS operation with regard to maintaining GPS time can be resolved into three tasks:

- a) The weight of each satellite contributing to GPS time must be assigned, based on some objective criterion of satellite performance;
- b) GPS time must be calculated in such a way that it does not change discontinuously when clocks are added or dropped;
- c) the daily estimates of GPS time offset, which are received from the USNO in the form

$$(1) \text{ GPS} - \text{UTC} = a_0 + a_1 t,$$

must be combined into an ongoing, long term sequence of messages, somewhat as the hour-by-hour measurements of pseudorange are combined by the Kalman filter to provide an estimate of the dynamical history of each ephemeris and clock parameter.

Figure 2 illustrates the estimates of the GPS-UTC offsets actually logged at Vandenberg MCS in the beginning of this year. Figure 3 shows GPS - UTC values for the middle of 1983 as determined by the USNO, and the results of several efforts of steering, as recorded in the MCS log.

Any method proposed by which to steer GPS time at the present Interim Control Facility must reckon with the constraints imposed by the present ICS software. To be sure, many of these constraints will be relaxed when the superior OCS software is delivered.

The present system (Phase I) does automatically maintain continuity in GPS time when the master clock is switched. However, it does not maintain continuity in rate. Furthermore, there is no provision in the Phase I system for automatic steering of time, by any algorithm. The operator must change the frequency by hand whenever steering is required (Reference 2). Therefore, the effort of the analysts at Vandenberg has been, not to implement the principles of control theory according to textbook, but to satisfy certain practical requirements:

- 1) The algorithm used must be simple. The more complicated the algorithm, the more likely becomes an operator error.
- 2) The algorithm must not introduce errors in Kalman filter determination of clock and ephemeris parameters. Now, the only algorithm implemented in the Kalman filter for estimation of clock states is a second order polynomial:

$$\Delta T = A_0 + A_1 T + A_2 T^2,$$

where ΔT is any clock offset being solved for,

ΔT is GPS time,

A_0 , A_1 , and A_2 may either be solved for or held fixed by imposing a priori values.

- 3) The steering must not interfere with the determination of the GPS - UTC offset -- e.g., by the Naval Observatory. Practically, this means that any frequency drift rate imposed in the steering operation must be small. In fact, the working rule of thumb is that frequency changes shall not exceed 1 part in 10^{13} per day

$$= 8.64 \text{ nanoseconds/day}^2$$

Several methods of steering have been proposed to satisfy these working conditions.

The simplest and most direct approach was suggested by Gernot Winkler (Reference 3). The operator is to make only small changes, not to exceed 1 part in 10^{13} per day. After each change, he observes the effect by means of the US Naval Observatory determinations of GPS - UTC value and rate. The operator makes these changes only when indicated, according to four simple rules (Figure 4):

- I) If $|GPS - UTC|$ is sensibly increasing, first reduce the rate to zero. Do not attempt to reverse the rate while it is still nonzero.
- II) If $|GPS - UTC|$ is rapidly decreasing, reduce the rate to zero.
- III) If $|GPS - UTC|$ is slowly decreasing, DO NOTHING!
- IV) If GPS - UTC is about to change sign, reduce the rate to zero.

An independent proposal for GPS time steering was made by R. Castro (Reference 4). He observed that the most nearly error-free way to steer at present is to input a frequency drift term manually and to allow it to operate for a preselected time. Mathematically, this is equivalent to letting the quantity GPS - UTC change as a second order polynomial of time -- in other words, to move along a parabola. Castro considered the case when GPS - UTC is slowly decreasing. He observes the rate of change $\dot{\phi}$, which is the frequency offset between GPS time and UTC. Let S be the preassigned span of time over which a frequency drift is to be imposed. He calculates the parameters of the parabola which will bring the GPS - UTC offset to zero in both value and rate:

$$\phi + \dot{\phi} (t - t_0) + \frac{\ddot{\phi}}{2} (t - t_0)^2$$

where $t_1 - t_0 \equiv S$,
 and where ϕ , $\dot{\phi}$, and $\ddot{\phi}$ are GPS - UTC
 and its first and second derivatives,
 t_0 is the time (date) at which steering is to begin,
 and t_1 is where it is to end,
 and S is preassigned in such a way as not to
 violate the constraint that $\ddot{\phi}$ must not
 exceed the aforementioned part in 10^{13} per day.

In practice, the quantities ϕ and $\ddot{\phi}$ are known from USNO reports, and one solves for the quantities t_1 and $\dot{\phi}$ (Figure 5).

At the October meeting of the Data Analysis Working Group at Vandenberg, the author proposed a method similar to Castro's, but replacing the parabola by the function which characterizes the critically damped oscillator (Figure 6).

The function

$$y = (K_1 + K_2 t) e^{-\lambda t}$$

approaches zero asymptotically. As is well known, it displays three forms, depending on the sign of K_2 . In Figure 7, the three cases are displayed, assuming that K_1 and λ are positive. Then, if $K_2 > 0$, the curve of $y(t)$ at first rises, dominated by the first term $(K_1 + K_2 t)$, and then declines nearly exponentially to zero. If $K_2 = 0$, only the second term remains, and of course the curve declines exactly exponentially to zero. If $K_2 < 0$, the curve first crosses the $t = 0$ axis, and then returns toward that axis nearly exponentially. The speed of approach is determined by λ ; and $1/\lambda$ corresponds to the preassigned time span S in the Castro method. It was proposed that one steer by the following steps:

- 1) Smoothed values of GPS - UTC from the US Naval Observatory should be employed, using five day means.
- 2) The value of λ in the damped oscillator function just given be fixed a priori. Simulations have shown that $\lambda = 1/20$ days would be appropriate.

- 3) Using this a priori λ and the USNO value and rate of GPS - UTC for current epoch, one should determine the other two parameters K_1 and K_2 of the damped oscillator function.

The equations are

$$\Delta T(t) = (K_1 + K_2 t) e^{-\lambda t}$$

$$\Delta \dot{T}(t) = K_2 e^{-\lambda t} - \lambda (K_1 + K_2 t) e^{-\lambda t}$$

$$\Delta \ddot{T}(t) = \lambda^2 (K_1 + K_2 t) e^{-\lambda t} - 2\lambda K_2 e^{-\lambda t}$$

so that, at current time $t = 0$,

$$\Delta T_0 = K_1$$

$$\Delta \dot{T}_0 = K_2 - \lambda K_1$$

$$\Delta \ddot{T}_0 = \lambda^2 K_1 - 2\lambda K_2$$

Therefore, since the US Naval Observatory supplies ΔT and $\Delta \dot{T}$ (GPS - UTC offset and rate), we may compute

$$K_1 = \Delta T_0$$

$$K_2 = \lambda K_1 + \Delta \dot{T}_0$$

and apply

$$\Delta \ddot{T} \equiv \ddot{\gamma} = \lambda^2 K_1 - 2\lambda K_2,$$

which is the steering rate, that is, the frequency offset to be applied each day, as in Castro's method.

Figure 8 shows what the effect would have been if the damped oscillator algorithm had been applied during the crucial events of this past year. For the computer simulations illustrated here, the value of λ was chosen to give an exponential decay time of 20 days. The results seem quite satisfactory. The maximum steering rate $\Delta \ddot{T}$

never exceeds one part in 10^{13} per day ($= 8.64 \text{ nanoseconds/day}^2$). The exponential decay is sufficiently gradual that neither the US Naval Observatory nor system users will be affected. Above all, the damped oscillator algorithm prevents oversteering, and so minimizes an important source of user error. Thus, it preserves the best Features of Methods I and II.

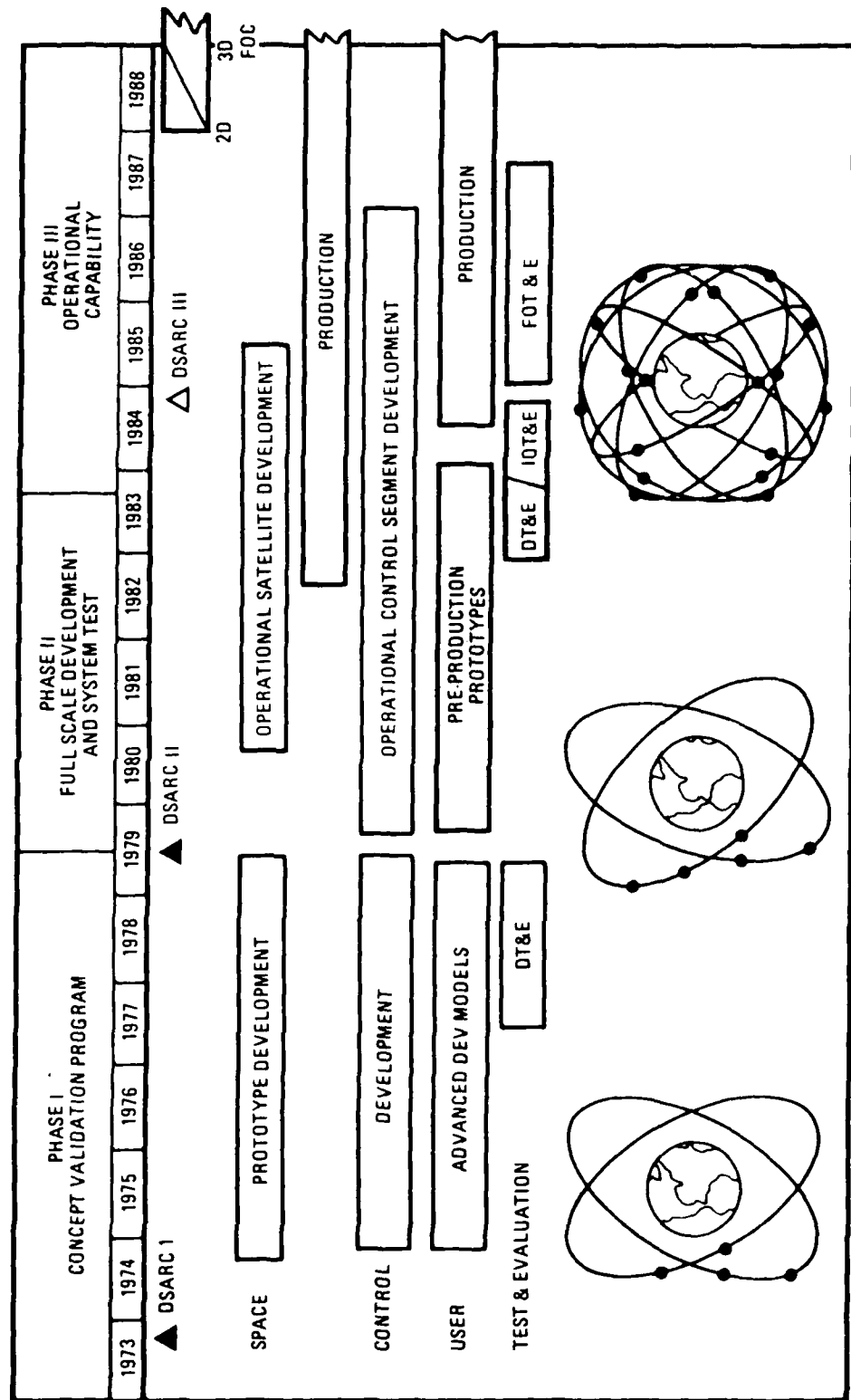
CONCLUSIONS:

The mathematics of GPS time steering are straightforward. To put the mathematics into practice should be equally straightforward, now that the IBM 3033 is available at the Vandenberg Master Control Station. We expect that software embodying the principles presented here will be implemented in the coming year.

References

- 1) Interface Control Document GPS 202, "Navstar GPS Control Segment/
US Naval Observatory Time Transfer Interfaces", Section
3.2.1.2.1.2, preliminary draft 12 April 1982.
- 2) Fran Varnum, Memo for Record to OAO and IBM/V, 3 November 1982.
- 3) Gernot Winkler, private communication, 7 October 1983.
- 4) R. Castro, OAO Corporation Memorandum, 5 October 1983.

FIGURE 1
Navstar Program Evolution



C11019

FIGURE 2
GPS-UTC
AS LOGGED AT THE GPS MASTER CONTROL STATION
(EARLY 1983)

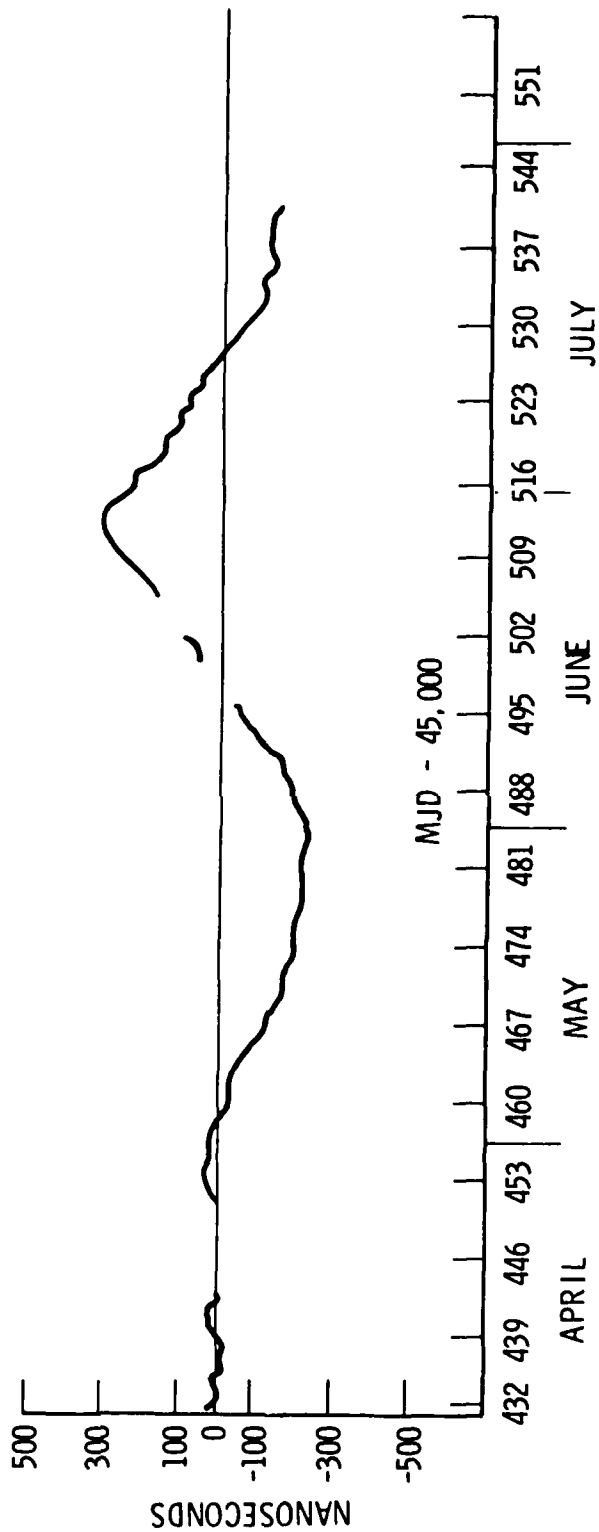


FIGURE 3

GPS — UTC As Reported by the USNO

MID 1983

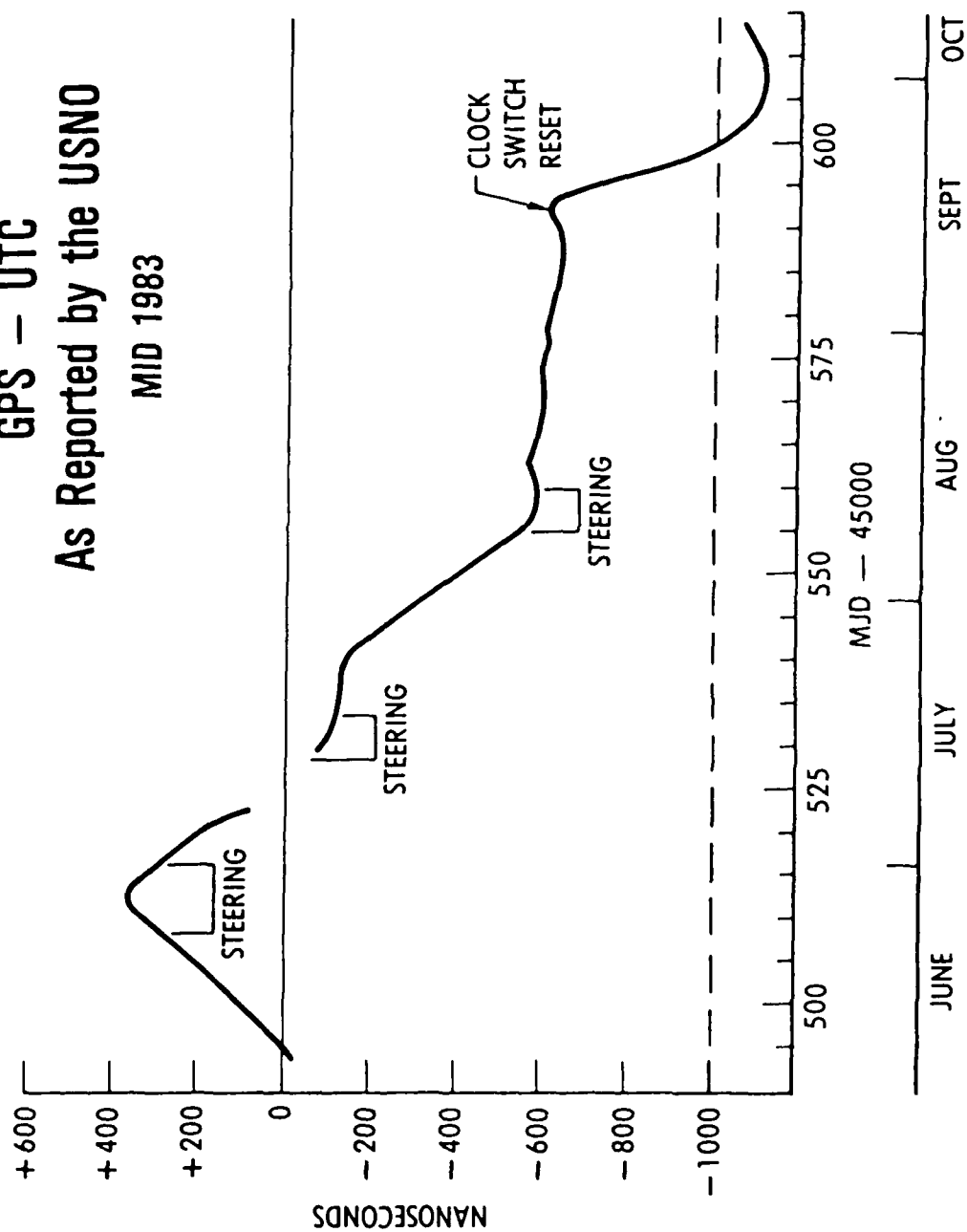


FIGURE 4

GPS Steering Methods (I) THE FOURFOLD WAY

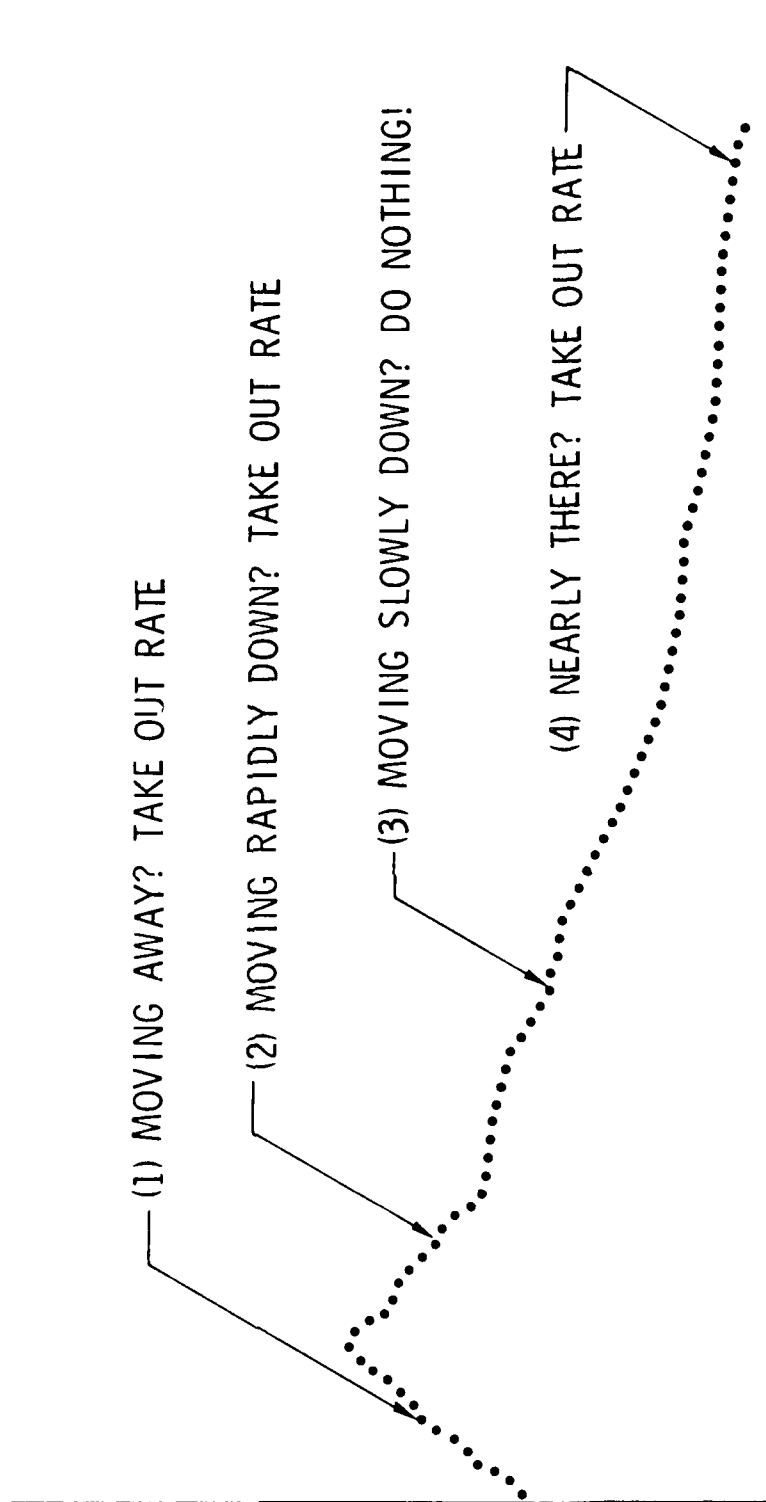


FIGURE 5
GPS Steering Methods (II)
THE PARABOLIC METHOD

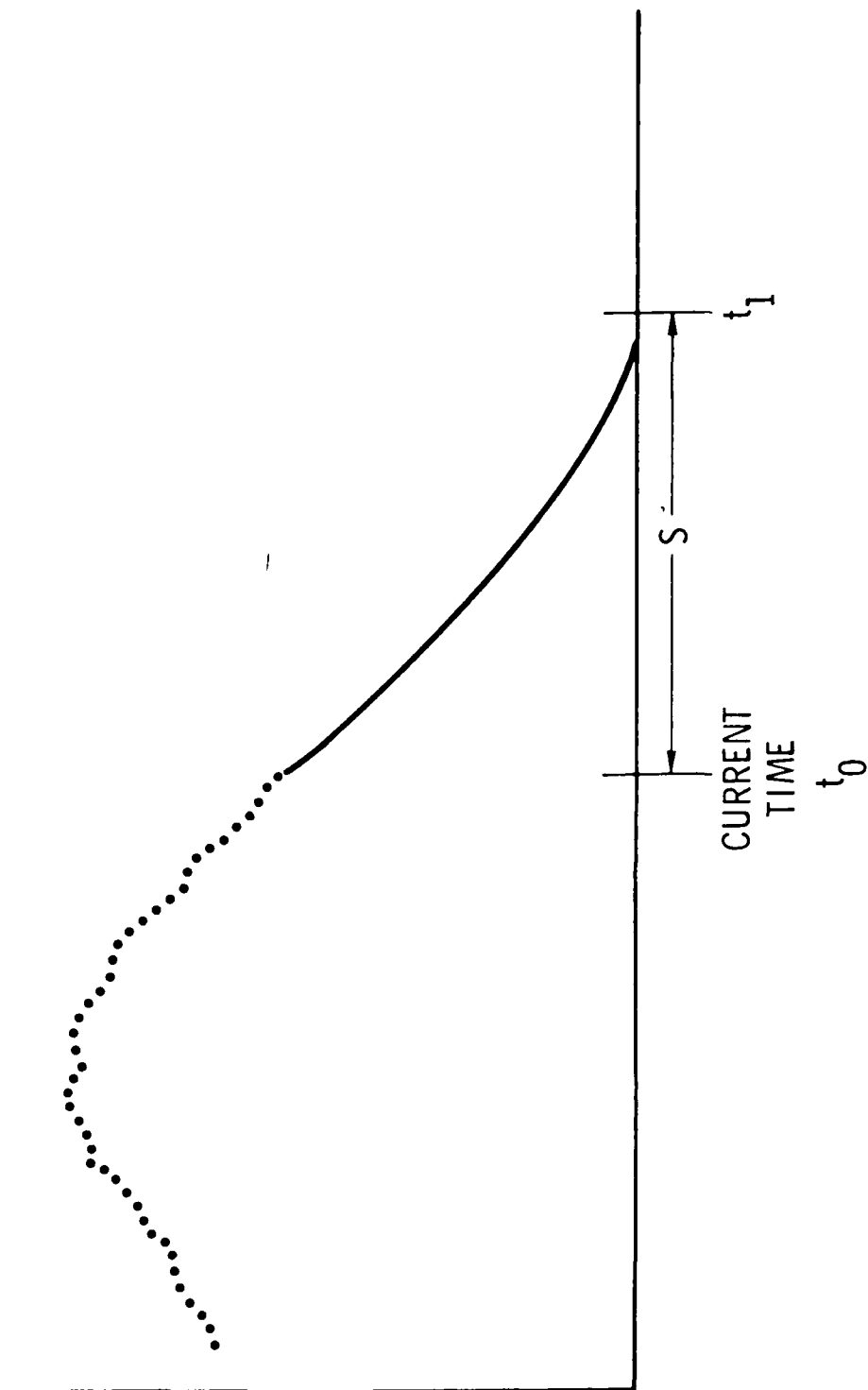
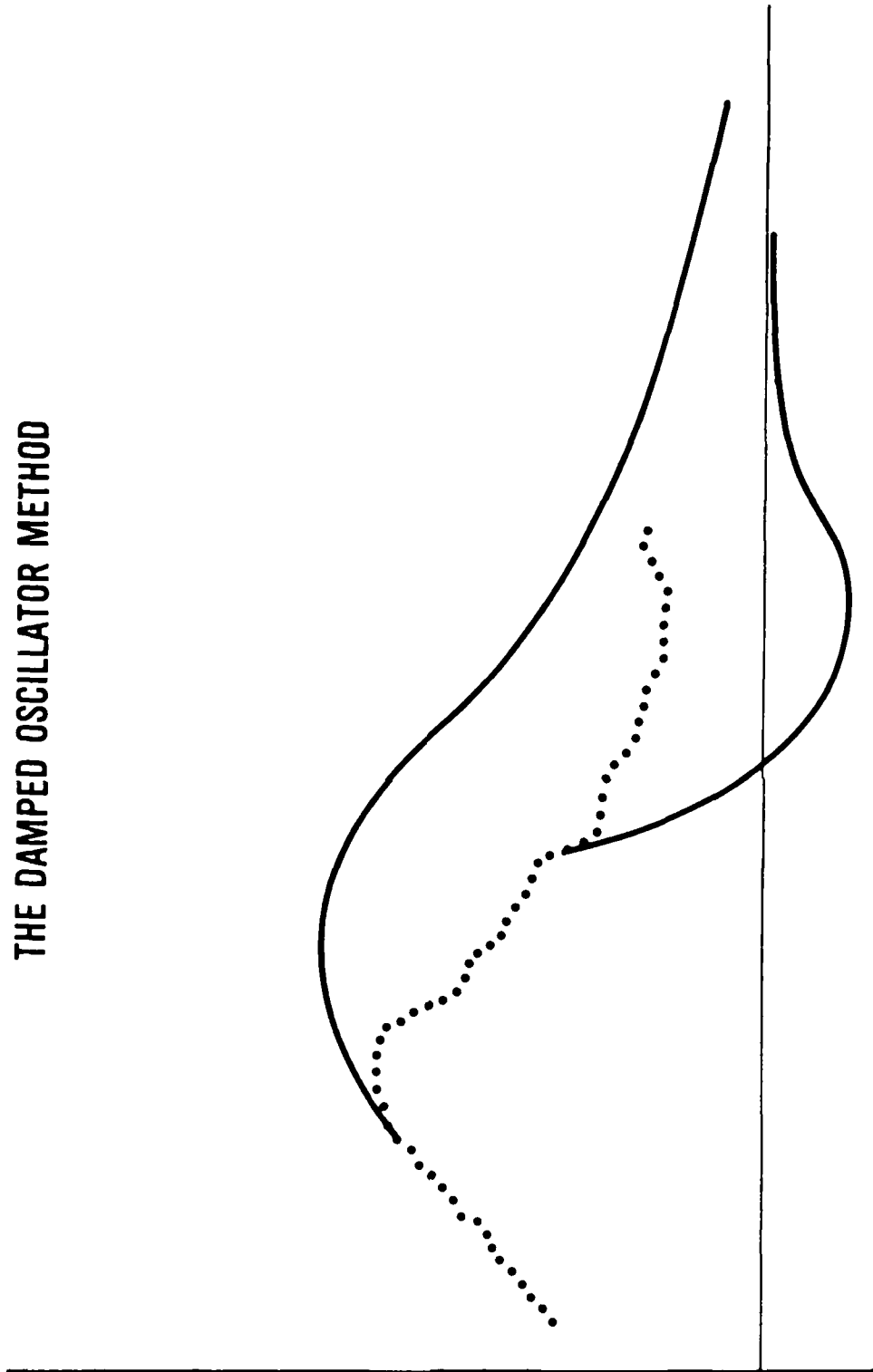


FIGURE 6

GPS Steering Methods (III) THE DAMPED OSCILLATOR METHOD



Critically Damped Oscillator

$$y = (K_1 + K_2 t) e^{-\lambda t}$$

$$K_2 > 0:$$



$$K_2 = 0:$$

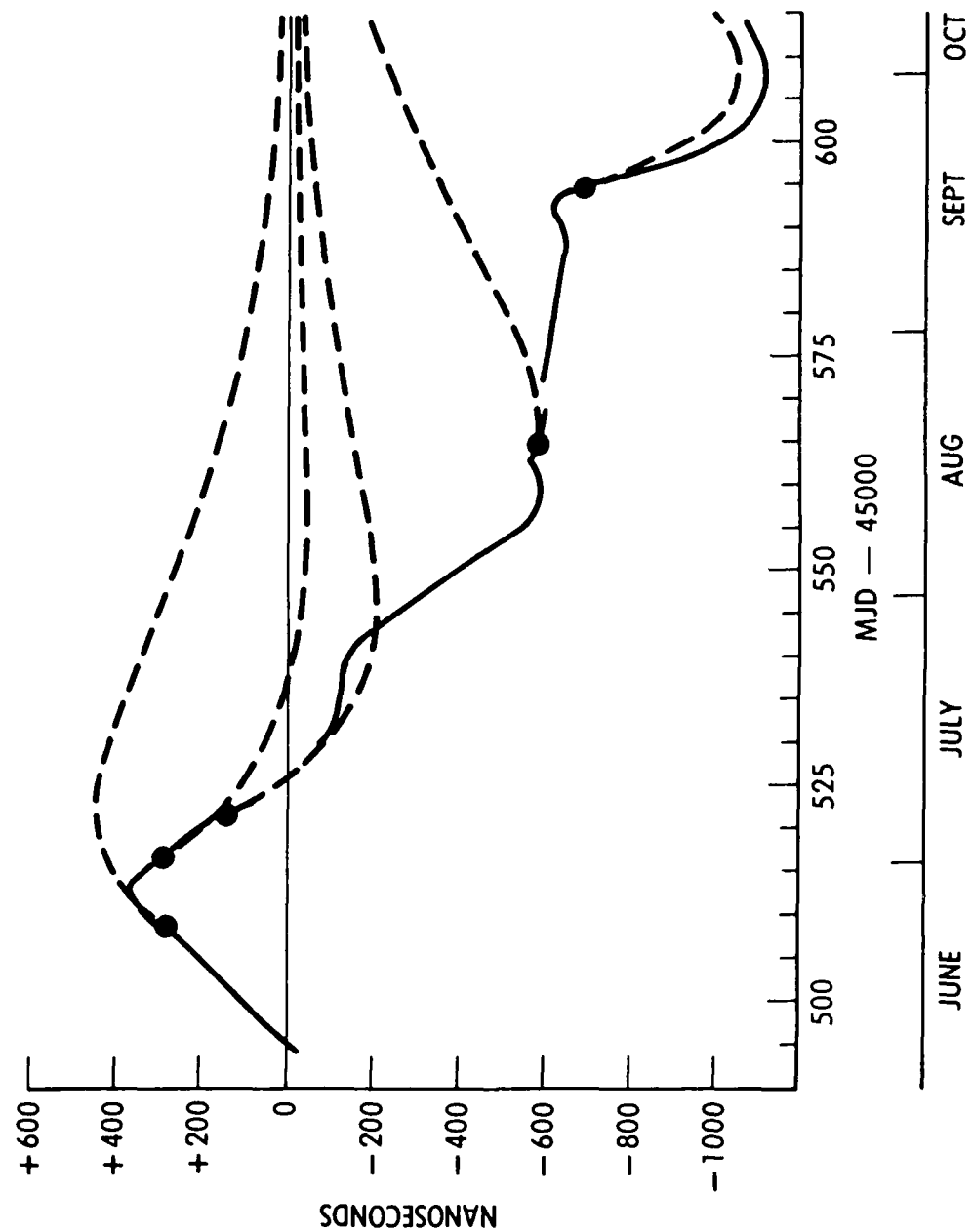


$$K_2 < 0:$$



FIGURE 8

GPS — UTC Damped Oscillator Algorithm



QUESTIONS AND ANSWERS

MR. McCALLUM:

How does one decide between frequency steering and making steps, like leap seconds, or as we do in the navigation system, adding small increments 20 nanoseconds or whatever to the system? How do you decide between these two strategies?

DR. FLIEGEL:

Well, the steps are verboten according to agreement, the software that has been delivered to the enhanced I.C.S. which we are using now does not permit the phase to change discontinually, that would be harmful to many users, but you can put in a step in frequency, and that is the technique that has been used up 'til now.

PROF. ALLEY:

Can you remind us please of physically how you are changing the frequency? Is it a magnetic field adjustment or are you doing it some digital electronic way?

DR. FLIEGEL:

I was afraid somebody would ask me that, because I really do not know. It is done on the GPS master clock. Somebody here may know, but I do not know physically how that adjustment is made?

DR. REINHARDT:

Gernot do you know?

DR. WINKLER:

It is simply done by instructing the computer to assume a different frequency of the driving reference clock so it is a pure paper affair and it is reflected in the different messages which are uploaded into the satellites. There is really no one pulse per second reference tick available at the master station and it is a very complicated thing to make a time comparison directly. But, since I have the microphone, I cannot resist to make another comment. That is, the problem of steering as such would be quite simple, but you have to compare the situation with a bus which is driving over an icy road, and the problem is how do you instruct a committee how to steer that bus without falling off the road. There are two approaches to it, and one is to give it some simple rules the other one is replace the driver with a microprocessor and program it so that you have some reasonable slopes with which you can keep within the confines of the road. But the problem is really more with the committee rather than the roads.

TEST RESULTS FOR PROTOTYPE GPS RUBIDIUM CLOCKS

T.J. Lynch and W.J. Riley
EG&G, Inc.
Salem, Massachusetts

ABSTRACT

This paper presents the results of a series of stability and qualification-level environmental and performance tests on two prototype rubidium frequency standards for the GPS navigation satellite program. One unit was subjected to a 140-day stability test at NBS and demonstrated a drift-corrected stability of $\sigma_y(\tau) = 2.8 \times 10^{-12} \tau^{-1/2} + 3.0 \times 10^{-16} \tau^{+1/2}$ for $1 \leq \tau \leq 10^6$ seconds, thus meeting the goal of 1×10^{-13} at 10^5 seconds. The average drift was -2×10^{-13} /day. The other unit was successfully subjected to a variety of performance and thermal, mechanical, EMI, and magnetic testing. It exhibited a smooth temperature coefficient of $-1 \times 10^{-13}/^\circ\text{C}$. The test program and subsequent additional work have resulted in a better understanding of instability mechanisms and promise a stability below 1×10^{-13} out to 10^6 seconds.

INTRODUCTION

EG&G, Inc., has been engaged since early 1980 in a program to develop a Rubidium Frequency Standard (RFS) for the Global Positioning System (GPS). The design of the EG&G GPS RFS was described at this conference in 1981^[1], and the basic concepts have changed very little since then. Subsequent work has resulted in the building and testing of two prototypes (see Figure 1).

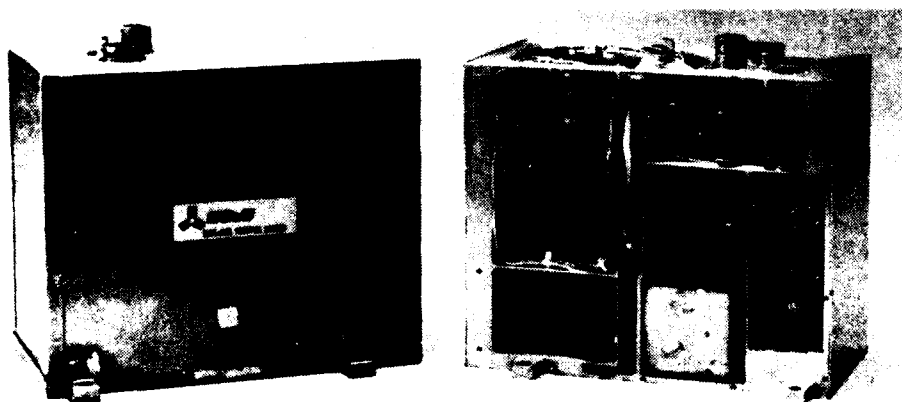


Figure 1. Photograph of EG&G GPS RFS Prototypes.

One unit was subjected to long-term stability testing over a 7½-month period without failure at the National Bureau of Standards (NBS). The other prototype was subjected to qualification levels of electromagnetic, mechanical, and thermal tests. That unit was then put on a stability test which accumulated over 7 months of failure-free operation. This paper summarizes results of those tests.

140-DAY STABILITY TEST

The primary objective of the 140-day stability test was to determine the Allan variance of the frequency scatter at averaging times between 10^5 and 10^6 seconds. Secondary objectives were to observe the phase and frequency records, to determine the stability at shorter averaging times, and to monitor the general behavior of the unit over an extended period of time.

This test was conducted at NBS between September 1982 and January 1983 in a specially built test setup that simulated the $+35^\circ\text{C}$ baseplate temperature and vacuum conditions that the unit would experience in operation on a GPS spacecraft. The test facility included a thermovac chamber, a fail-safe power system, monitoring equipment, and provisions for measuring RFS performance against the NBS clock ensemble. The frequency was adjusted to an absolute value of about -4.5×10^{-10} as required to compensate for the in-orbit gravitational red shift.

The RFS ran normally throughout the test and did not exhibit any performance degradation.

The frequency record is shown in Figure 2 and the residuals after subtraction of the linear least-squares drift of $-2 \times 10^{-13}/\text{day}$ are shown in Figure 3. This drift was twice the specified value of $\pm 1 \times 10^{-13}/\text{day}$ but was smooth and highly modelable, and thus was not a severe problem for the GPS application. (The current GPS rubidium clocks have a drift specification of $\pm 1 \times 10^{-12}/\text{day}$.) Furthermore, subsequent testing on Prototype No. 2 has identified a probable dominant cause of drift that, when eliminated, should result in a significant improvement in this parameter. The most prominent features of the residuals are occasional jumps of about $+5 \times 10^{-13}$. These are the primary limitations on the modeled long-term clock performance and were apparently related to jumps of about -0.25% in the rubidium lamp output.

This unit had a lamp with a heavy rubidium fill (474 μgrams) as compared with a normal fill of 70-100 μgrams which is adequate for a life greater than the specified 7.5 years. It is believed that the heavy lamp fill is responsible for the jumps. No such behavior has been observed in the other unit, which has a lamp with a normal rubidium fill. Both units were tested with the lamp tip upward, so there were opposing thermal and gravitational forces acting on the molten rubidium.

The scatter of the drift-corrected frequency fluctuations is shown on the Allan variance plot of Figure 4. The measured results lie well below the specification limits shown by the dashed line and meet the goal of 1×10^{-13} at 10^5 seconds. The unit displays a $2.8 \times 10^{-12} \tau^{-1/2}$ white frequency noise characteristic in the region below about 10^4 seconds (corrected for the reference noise) that is in good agreement with theoretical predictions[1]. At longer averaging times, the plot shows a random-walk frequency characteristic at a level of about $3.0 \times 10^{-16} \tau^{+1/2}$. There is no significant region of flicker frequency noise. During those intervals when no jumps occurred, the drift-corrected Allan variance was about 5×10^{-14} at 10^5 seconds.

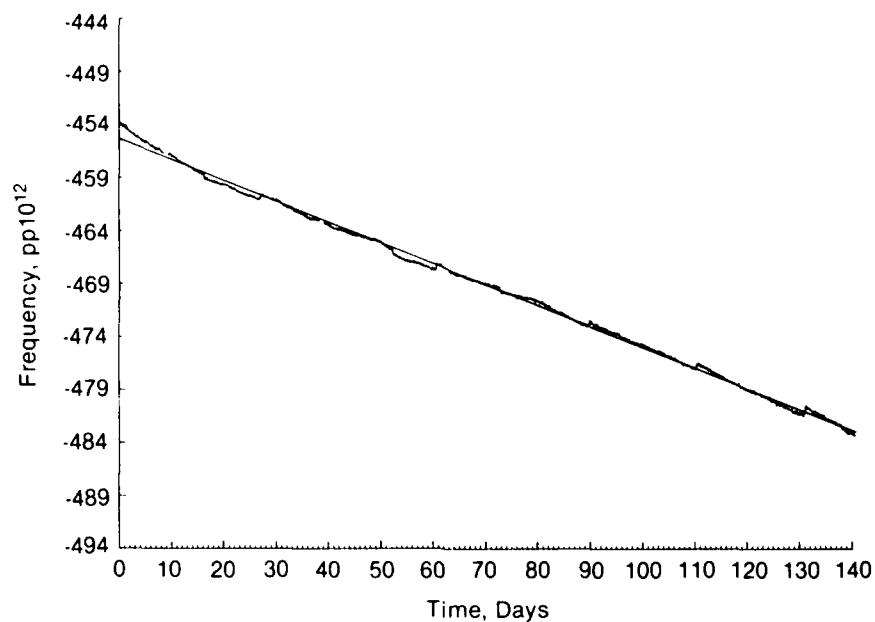


Figure 2. Tau = 2-hour frequency record versus NBS clock ensemble 9/6/82-1/25/83, EG&G GPS RFS Prototype No. 1.

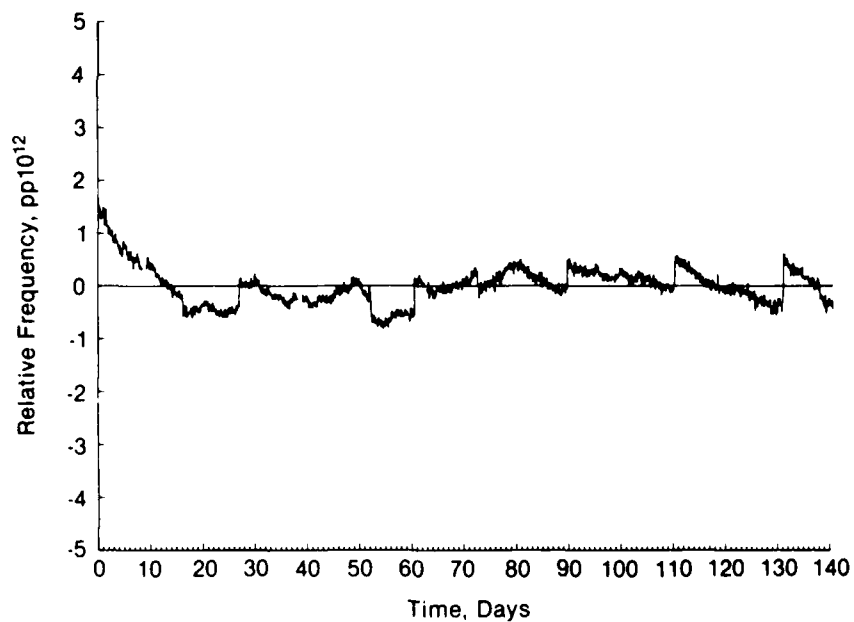


Figure 3. Tau = 2-hour residuals versus NBS clock ensemble after drift correction, EG&G GPS RFS Prototype No. 1.

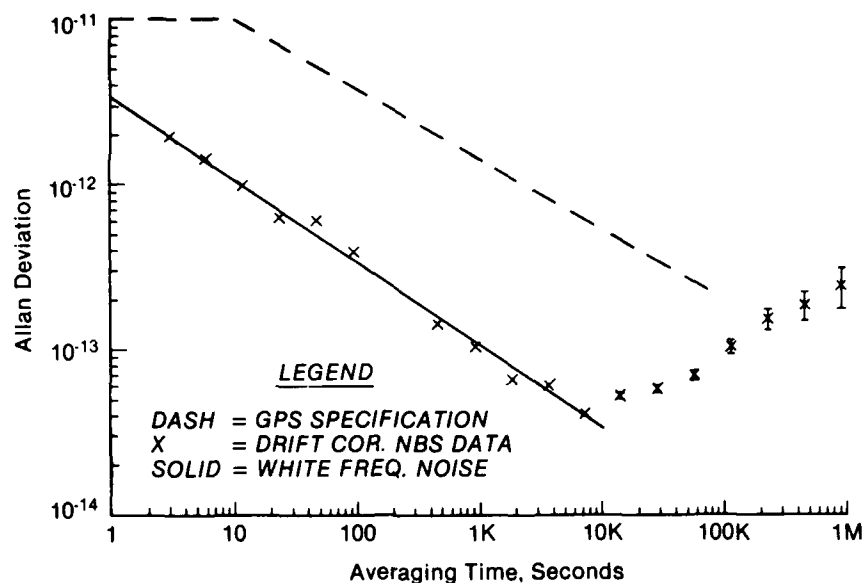


Figure 4. Time-domain frequency stability measured at NBS 9/6/82-1/25/83, EG&G GPS RFS Prototype No. 1.

The subtraction of a least-squares linear frequency drift tends to filter out long-term fluctuations and thus give an overly optimistic result at long averaging times. Nevertheless, the results of an ARIMA maximum likelihood estimate of stability made by NBS are essentially the same as the drift-corrected Allan variance values out to about 3×10^5 seconds.^[2] These data are shown in Figure 5.

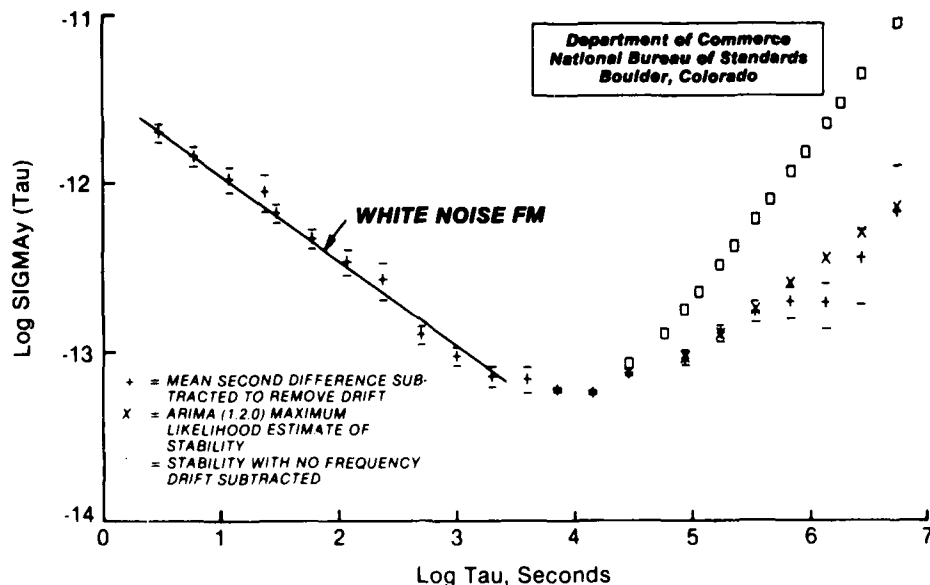


Figure 5. EG&G RB versus NBS ensemble.

ADDITIONAL STABILITY TESTS

In addition to the 140-day stability test, shorter runs were made between January and April 1983 at maximum and minimum C-field and a restart test was done. The C-field value did not have any significant influence on the RFS stability. The unit showed a frequency offset of about $+3 \times 10^{-12}$ when restarted after a 3-day shutdown.

Stability tests were also conducted on Prototype No. 2 at EG&G after qual-level testing. Typical of the excellent results are Figure 6 which shows a drift well below 1×10^{-13} /day and Figure 7 which shows a scatter below 3×10^{-14} at 10^5 seconds. The stability at the shorter averaging times is limited by the cesium reference (HP 5061A Opt. 004). No frequency jumps were observed over a 7-month test period.

QUALIFICATION-LEVEL TESTS

Qualification-level testing was performed on EG&G GPS RFS Prototype No. 2 during the period between October 1982 and March 1983. The primary objectives were to discover and correct design deficiencies. The test conditions were as specified for formal qualification, but the terminology "qual level" was used because the test unit was built as a prototype, rather than with high reliability parts and strict quality control.

Many of the tests were conducted more than once, as retests to verify corrective actions to the test unit or because of deficiencies in the initial test equipment or procedure.

Certification Tests

Testing of Prototype No. 2 began with a series of expanded certification tests intended to establish the general performance of the unit. Besides the standard functional tests conducted after each test sequence (frequency accuracy, dc power, and rf output power and harmonics), tests were performed for phase noise, backup tuning, primary tuning, frequency versus input voltage, frequency stability at fixed temperature, and frequency versus normal operating temperature. Most of these tests, as well as the above stability tests, were performed in vacuum to simulate the GPS environment, to produce effects such as component temperature increase due to loss of convective cooling, and to provide the vacuum insulation for which the physics package design is optimized.

No serious difficulties were experienced. The only discrepancies were associated with the secondary loop OCVCXO. The unit had insufficient varactor tuning range (-0.9 to $+1.8 \times 10^{-7}$ versus the specified $\pm 2 \times 10^{-7}$) and could not maintain lock above about $+40^\circ\text{C}$ (versus the specified $+60^\circ\text{C}$). These problems are expected to be corrected in the next unit.

The RFS easily met its phase noise, primary tuning range, and voltage coefficient requirements. The measured voltage coefficient was $-8 \times 10^{-14}/\text{V}$. The stability test gave a 10^5 seconds Allan variance of 1×10^{-13} , a final drift rate below $1 \times 10^{-13}/\text{day}$, and a TC of $-1 \times 10^{-13}/^\circ\text{C}$. These results show that the RFS prototype is capable of excellent stability.

The average TC of $-1 \times 10^{-13}/^\circ\text{C}$ over the normal operating temperature range of $+20$ to $+45^\circ\text{C}$ was confirmed to be smooth and was $\times 10$ lower than the specification limit. The RFS is free of any region of large incremental temperature sensitivity. This was

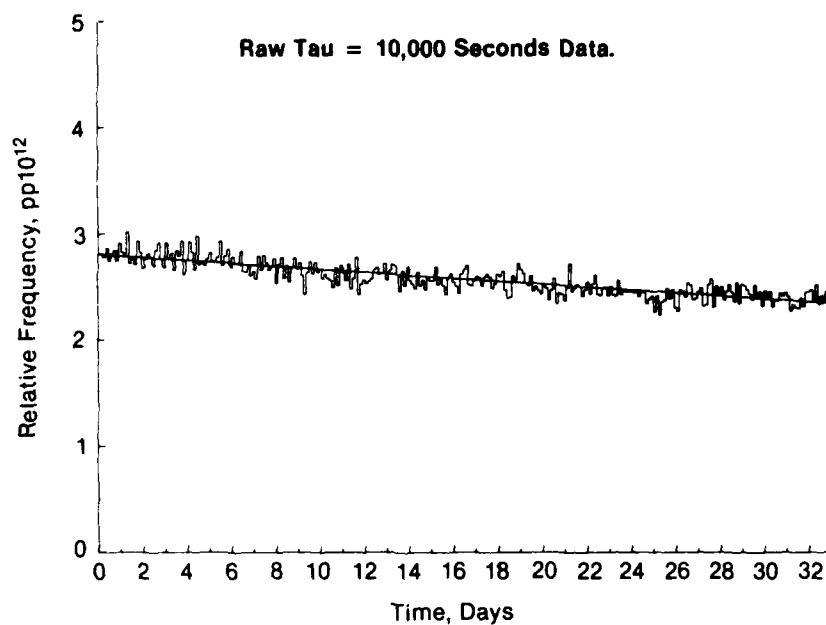


Figure 6. EG&G GPS RFS Prototype No. 2 stability test, 6/16/83-7/19/83.

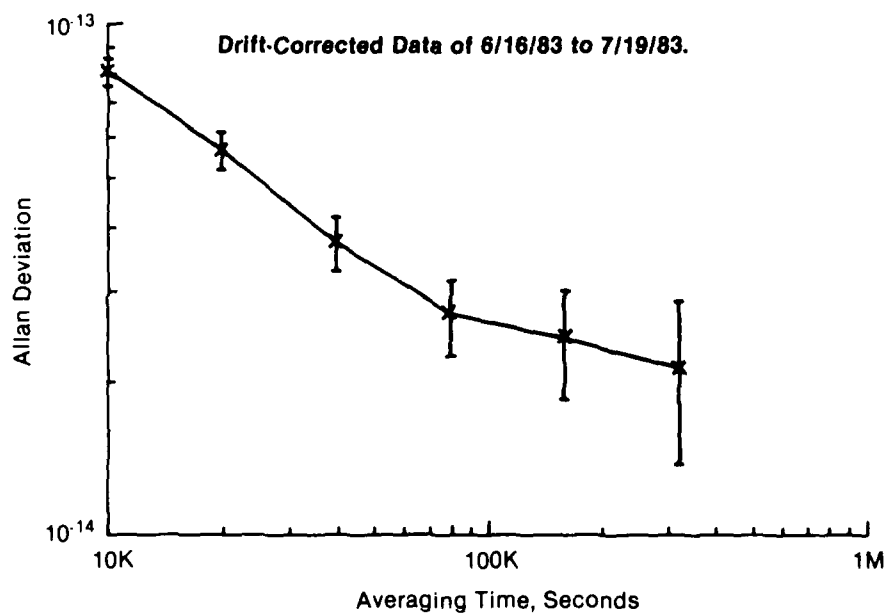


Figure 7. Time-domain stability of EG&G GPS RFS Prototype No. 2.

confirmed by observing the frequency record while varying the baseplate temperature from 20°C to 45°C to 20°C in 1°C steps. One hour was allowed for each step with 8 hours at 45°C. The results are shown in Figure 8. The scatter in the data is determined primarily by the stability of the cesium reference.

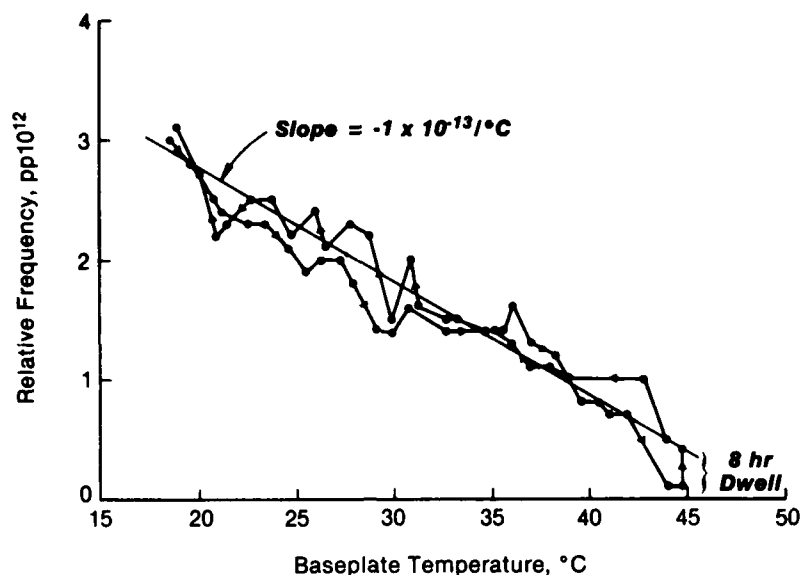


Figure 8. Frequency versus temperature.

EMI Tests

EMI testing proceeded quite well, and, although several deficiencies were found, most are felt to result from the use of improper cabling and cable terminations. During testing, several problems were improved greatly by altering cable terminations. These tests showed the importance of utilizing the exact cables and terminations to be used in flight and also the need to simulate the space vehicle power supply. Input ripple measurements are dependent on the characteristics of the supply.

There was no conducted susceptibility at the critical servo modulation frequencies. This is usually the most difficult aspect of an RFS under exposure to EMI, and therefore the result was most encouraging. An audio frequency power line susceptibility was associated with the +5V portion of the switching power supply and its effect on the synthesizer phase detector was corrected by the addition of a regulator.

The only other susceptibility of real concern occurred as a result of monitor cable pickup at the primary loop frequencies and a few frequencies related to the cable length. It is unclear whether any change is required in the RFS, since a better cable may eliminate the problem.

The few excessive radiated emissions were also associated with the monitor cable and its grounding and termination. An excessive power supply conducted ripple was observed and corrected.

Additional testing will be required with improved cables to determine if other improvements are needed.

Temperature Cycling Tests

Temperature cycling between +50°C and -30°C was performed at 1 atmosphere (dry nitrogen) and in vacuum. At each temperature extreme, the RFS was turned off, then restarted after 30 minutes.

The purpose of these tests was to establish proper RFS startup and operation, although performance requirements did not apply over this temperature range. The results were satisfactory except that secondary oscillator unlock occurred at the high end. This resulted from use of a crystal having too low a turnover temperature and has been corrected.

Because the 30-minute Off time was not sufficient for the RFS (in particular, the ovenized crystal in the secondary oscillator) to stabilize at low temperature, an additional test was performed. The RFS, unpowered, soaked overnight at -19°C in vacuum, was restarted, and warmed up within 1 hour.

Vibration Tests

The qualification random vibration spectrum had a peak level of 0.35 g^2/Hz from 120 to 500 Hz and an overall level of 17 g rms from 20 to 2000 Hz. The duration was 3 minutes per axis. The RFS was powered and monitored during vibration. In service, the RFS would not be operating during (launch) vibration. It was powered and monitored during testing to detect failures such as intermittents, not to verify performance. The shaker magnetic field and its effects on the RFS were evaluated and made acceptable by modifying the setup.

RFS Prototype No. 2 was subjected to vibration testing on four occasions. Failures, with the exception of the secondary oscillator, were corrected by minor changes as described below and the vibration test passed. In the final testing, a laboratory synthesizer functionally replaced the secondary oscillator, which had no output. During vibration, loss of primary and secondary loop lock occurred, but lock was recovered after vibration and thus is not considered a failure.

Most of the failures which occurred during the first tests were associated with mounting of electronic components, such as fracture of leads and solder joints. The corrective action was to bond heavier components to the printed circuit boards with epoxy.

A number of threaded fasteners came loose. The corrective action was to lock the threads by applying Solithane 113/300 urethane coating at assembly (split lock washers and Loctite are prohibited).

A problem was encountered where the center conductor in a connector on flexible coaxial cable withdrew into the connector due to flexing of the cable from vibration or handling. The connector was changed to a design which has mechanical support behind the center contact.

A diode failure (fracturing of the glass body) occurred on a printed circuit board which had been subjected to an uncontrolled mechanical shock due to test equipment malfunction before the start of the qualification-level test program. A new board with five diodes passed qual vibration.

The secondary oscillator had two failures during vibration testing. The first was a change in frequency which was reset by the supplier. The second failure was a loss of output. It was determined by the supplier that the crystal had broken. The crystal was replaced and reportedly the oscillator was subjected by the vendor to the qual vibration level and passed.

Magnetic Susceptibility

The RFS contains three magnetic shields that reduce its susceptibility to frequency changes caused by external magnetic fields. At maximum internal C-field (250 mG), the physics package has a worst-case magnetic sensitivity of $4.2 \times 10^{-8}/\text{G}$ along the optical axis. This requires an overall shielding factor of 126,000 to meet the magnetic susceptibility requirement of $1 \times 10^{-12}/3$ gauss.

Shielding factor measurements were made using Model 124A EG&G lock-in amplifier, a Model DH-200 audio power amplifier, a custom made pick-up coil the size of the absorption cell, and a Helmholtz coil. A frequency of 23 Hz with an amplitude of 8 V rms (6 gauss peak to peak) was used to drive the Helmholtz coil. With all three shields hydrogen annealed and nested and the pick-up coil in the same location as the absorption cell, a shielding factor over 200,000 was measured.

Shielding factors were also measured during assembly of the physics package in order to determine if and when any degradation of its two shields occurred due to rework and assembly operations. No significant changes were measured. The two nested cylindrical shields had a shielding factor of 11,400 initially and 10,400 after assembly.

An overall magnetic susceptibility test was conducted on RFS Prototype No. 2. As expected from the shielding factor measurements, the overall results were excellent. Under worst case conditions of maximum internal C-field and orientation of the external field along the physics package optical axis, the magnetic susceptibility was $1 \times 10^{-12}/6$ gauss (reversal of a 3-gauss field) or $2 \times 10^{-13}/\text{gauss}$. This is at least 2:1 better than specified and the actual susceptibility is probably even less, since the measurement resolution is limited by the stability of the reference and the unit under test.

Acceleration Test

RFS Prototype No. 2, with the secondary oscillator replaced by a dummy load, was subjected to acceleration of 20 g for 5 minutes in each direction of three mutually perpendicular axes (total of 6 runs) using a centrifuge with a 4-foot radius. During exposure, the RFS was powered and the input current was monitored. Between exposures, complete sets of monitor readings were taken.

A slight increase in input current was observed during acceleration. After acceleration in the +Z direction, there was an increase in the light and signal, apparently due to movement of (molten) rubidium from the back of the lamp onto the hotter surfaces. This condition did not result in any malfunction and was partially reversed by subsequent acceleration in the opposite (-Z) direction and was fully corrected by overnight operation.

The RFS showed normal frequency and frequency stability after the test.

Shock Test

RFS Prototype No. 2, with the secondary oscillator replaced by a dummy load, was subjected to three pyro shocks in each of three axes (both directions excited by each shock). The shock spectrum extended from 100 to 10,000 Hz with a peak value of 1250 g from 1250 to 3200 Hz. An electrodynamic shaker and shock synthesizer were used. During exposure, the RFS was not powered. Monitor readings were taken between axes, during which an intermittent short circuit was discovered. The cause was contact between the lamp oscillator enclosure and the main chassis due to a misalignment in the physics package mounting. This was corrected by inserting a strip of insulation between the enclosure and the chassis. After subsequent shock testing, monitor readings were normal.

Conclusions Obtained from Qualification-Level Tests

The qualification level testing of RFS Prototype No. 2 indicates that this design is capable of meeting the GPS requirements. Most of the failures were minor and were easily corrected. They reflected that the test unit was a prototype, not initially constructed as a qualification unit with strict quality control. The only major failure was with the secondary oscillator, which also was an engineering model not initially constructed for qualification testing. Corrective actions to the oscillator have been implemented and have reportedly been verified by the vendor. The packaging design of the RFS, which provided easy access for initial assembly, also facilitated troubleshooting and rework.

DEVELOPMENT TESTS

Besides the stability and qual level testing of the RFS prototypes, a significant amount of other testing was performed on various assemblies. The purpose was to obtain empirical design data, to measure performance, and/or to verify reliability. A brief list of the more important tests follows:

1. Lamp aging with measurements of rubidium consumption by calorimetry.
2. Measurements of thermal contact resistances in vacuum for heat sinks and bolted joints, including PC board mounting.
3. Temperature cycling of potted thermistors with measurements of dissipation constants, coaxial cable assemblies with X-rays, and the large area photodetector assembly (manufactured in house).
4. Measurements of oven temperature stability, thermal gain of oven temperature controllers, and thermal time constants of ovens, heaters, and thermistors.
5. Measurements of magnetic field uniformity in C-field coils of various configurations.
6. Magnetic shielding factor measurements of nested shields with various end gaps.
7. Vibration testing of lamps to investigate the displacement of (molten) rubidium.
8. Thermal profile of the RFS: measurement of temperatures in vacuum to verify that component junction temperatures do not exceed 125°C.

CONCLUSIONS

This paper has presented test results on two prototype rubidium frequency standards that are among the best such devices yet reported. A summary of their characteristics is shown in Table 1. They have demonstrated excellent stability and reliability when operated many months under GPS thermovac conditions. They showed low sensitivity to environmental factors such as temperature, magnetic field, and supply voltage, and they are capable of meeting the GPS environmental requirements of shock, vibration, acceleration, and temperature cycling. This has been accomplished by careful attention to all aspects of classical RFS design. It has been satisfying to see how successfully the size, weight, power, and signal-to-noise advantages of rubidium clock technology could be combined with low physics package parametric sensitivities and other design details to achieve excellent overall performance.

Table 1. Characteristics of EG&G GPS RFS.

Size:	4.46" X 8.36" X 6.89" high
Weight:	10 lb.
Power:	13 watts (at +35°C baseplate in vacuum)
Operating Temperature Range:	+20 to +45°C
Drift:	$\pm 1 \times 10^{-13}$ /day (spec)
Stability:	$2.8 \times 10^{-12} \tau^{-\frac{1}{2}} + 3.0 \times 10^{-16} \tau^{+\frac{1}{2}}$ (typical $\sigma_y(\tau)$ for $1 \leq \tau \leq 10^5$ sec)
Temperature Coefficient:	$-1 \times 10^{-13}/^\circ\text{C}$ (typical)
Magnetic Susceptibility:	2×10^{-13} /gauss (typical)
MTBF:	178,000 hours (calculated)

ACKNOWLEDGMENTS

This work was supported by Rockwell International Space Operations/Integration and Satellite Systems Division and the U.S. Air Force Space Division.

The authors wish to acknowledge the excellent manner in which the National Bureau of Standards Time and Frequency Division staff set up, conducted, and analyzed the results of the long-term stability test.

Many persons contributed to the success of this effort at EG&G. In particular, P. Labrecque and K. Lyon were deeply involved in the qualification-level testing and S. Goldberg provided overall scientific direction of the program.

REFERENCES

1. W.J. Riley, "A Rubidium Clock for GPS," Proceedings of the 13th Precise Time and Time Interval (PTTI) Applications and Planning Meeting, pp. 609-630, December 1981.
2. "Final Report for 140-Day Stability Test of GPS Rubidium Frequency Prototype," NBS Test No. 801590, Time and Frequency Division, National Bureau of Standards, Boulder, Colorado 80303.

QUESTIONS AND ANSWERS

MR. WARD:

Sam Ward, J.P.L. How about the projected life between cesium and the rubidium?

MR. RILEY:

Well, earlier rubidium had lamp problems. That is why we emphasize this lamp problem, but we believe we have it licked. Cesium seems to have a finite life, depending on the design. Myself, being very prejudiced, I would guess that the rubidium could be extended out over a longer period of time than the cesium, but that is a very prejudiced point of view.

A VOICE:

Some of your competitors are indicating 25 years life for rubidium standards, can you comment on that?

MR. RILEY:

The unit I'm describing is twenty years. That's almost entirely an electronic number. Twenty years on the lamp does not frighten us; twenty years on the other cells would frighten us even less.

A VOICE:

What is going into the present, the new birds rubidium, cesium or a combination?

MR. RILEY:

It's a fifty-fifty mix, I understand; two each, and not one of this design. We have gotten to the prototype stage, and that's as far as the new design has been taken.

SESSION III

TIME TRANSFER/SYNCHRONIZATION

Mr. Hugh Fosque, Chairman
NASA Headquarters

CALL TO SESSION III

MR. FOSQUE: Well, good morning, ladies and gentlemen. We are getting off to a little bit of a late start this morning, and so we will have to pay a little stricter accounting to the time as we go through the papers. I would like to ask the authors for their cooperation in that they please try to stick to the allotted time; and, if possible, cut that short by a minute or two so that we can allow for one or two questions after each paper. We have a number of papers this morning.

INTERNATIONAL TIME TRANSFER AND PORTABLE CLOCK EVALUATION
USING GPS TIMING RECEIVERS: PRELIMINARY RESULTS

S. C. Wardrip, NASA Goddard Space Flight Center

J. Buisson, O. J. Oaks, and M. Lister,
Naval Research Laboratory

E. Detoma, P. Dachel, T. Stalder, and H. Warren,
Bendix Field Engineering Corporation

G. Winkler and G. Luther, U.S. Naval Observatory

S. Leschiutta, Politecnico di Torino

P. G. Galliano, F. Cordara, and V. Pettiti,
Istituto Elettrotecnico Nazionale

R. Azzarone and F. Fedeles, Italian Navy

INTRODUCTION

Four portable cesium clocks and two single channel Global Positioning System (GPS) timing receivers were deployed in Italy during October 1983 at the Naval Base in La Spezia, onboard the Italian Navy hydrographic ship "Magnaghi", and at the Istituto Elettrotecnico Nazionale (IEN) in Torino.

The experiment was a joint effort between the following U.S. and Italian agencies and organizations: the NASA Goddard Space Flight Center (GSFC) with the support of the Bendix Field Engineering Corporation (BFEC), the Italian Navy, the U.S. Naval Research Laboratory (NRL), the U.S. Naval Observatory (USNO), the Istituto Elettrotecnico Nazionale (IEN) "G. Ferraris", and the Politecnico of Torino, Italy.

The timing data collected in this effort provided mutual synchronization between the U.S. Naval Observatory and other international time-keeping institutions and laboratories to within an accuracy of ± 50 nanoseconds(ns).

In addition, the experiment provided an excellent opportunity to perform field tests of portable cesium standards during actual trip conditions. Onboard the hydrographic ship was an ensemble of three cesium clocks, which were intercompared via an automated measurement system. Two external time references, Loran-C and GPS, and one additional cesium standard were continuously available on shore, providing a redundant and reliable reference time base. Similar portable clock and GPS data was taken at the IEN, while performing a GPS synchronization for a period of one week.

PURPOSE OF THE EXPERIMENT

The overall experiment was designed to test the positioning and navigation capabilities of the GPS timing receivers developed by the Naval Research Laboratory (NRL) for the NASA Goddard Laser Tracking Network (GLTN).

To perform this experiment, a reliable and redundant time scale was set up onboard the ship, and a back-up system on shore. This situation provided the opportunity to perform simultaneously a timing experiment ideally divided into two parts, the main objectives of the experimentation being:

- 1.) To test GPS timing receiver synchronization capabilities on a moving platform, and to perform an intercontinental synchronization via GPS between participating international timing laboratories in Europe and in the United States.
2. To evaluate the performance of cesium portable clocks in the field.

SYNCHRONIZATION AND PORTABLE CLOCKS

The portable cesium clock synchronization technique represents one of the most accurate means to synchronize remote clocks via a transfer standard.

To perform a portable clock synchronization, the frequency offset of the cesium portable clock with reference to a known time scale should be measured with great accuracy; this will allow an estimate of the time position of the travelling clock during the trip, with reference to the same time scale, after an initial time position measurement has been made.

The behaviour of the portable clock during the trip is essential to obtain good results. When the clock returns, a time closure measurement with the master reference provides an estimate of how well the clock behaved during the trip. If an abnormal behaviour occurs, this can be classified into two categories: (1) a change in the frequency of the travelling standard (fig. 1a), or (2) a change in its time (phase jump) where the frequency before and after the trip appears to be the same (fig. 1b).

Abnormal behaviour of a portable cesium clock can be caused by several factors, but is mainly due to the random behaviour of the standard itself and by systematic effects.

RANDOM BEHAVIOUR OF THE CLOCK

The random behaviour of the clock is primarily due to the standard's own noise processes, leading to uncertainties in the determination of the frequency of the oscillator over a certain time interval, or to small fluctuations in the phase of the oscillator itself in a short time interval.

The error caused by the random behaviour of the clock can be reduced considerably by carefully monitoring the clock parameters before the trip, and by implementing various models of clock performance during the trip. It has been suggested to carry two or more cesium standards on a trip, and monitor one against the other.

However, the statistical analysis of the clock should only be considered at the level at which the systematic errors do not play a dominant role in contributing to the total trip error. In other words, it is not useful to have a good statistical model of the clock when the main error contribution is due to systematic effects.

AD-A149 163 PROCEEDINGS OF THE ANNUAL PRECISE TIME AND TIME
INTERVAL (PTTI) APPLICATI. (U) NAVAL RESEARCH LAB
WASHINGTON DC J A MURRAY 02 APR 84

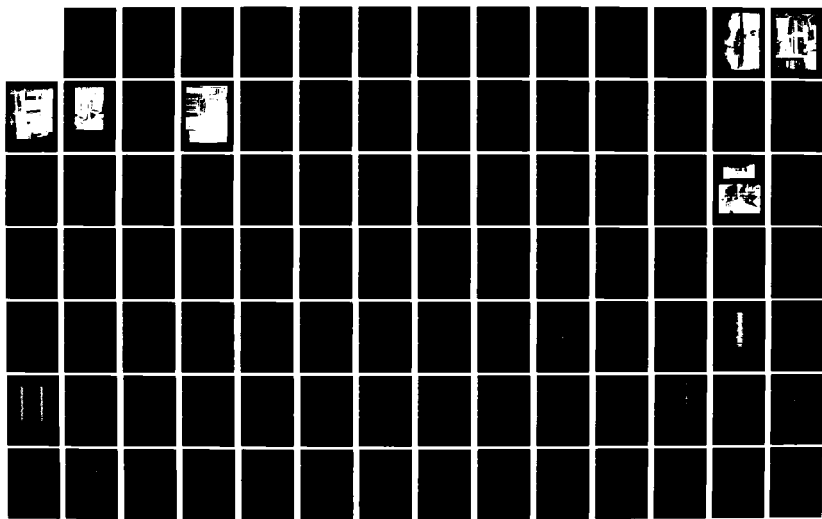
PROCEEDINGS OF THE ANNUAL PRECISE TIME AND TIME
INTERVAL (PTTI) APPLICATI. (U) NAVAL RESEARCH LAB
WASHINGTON DC J A MURRAY 02 APR 84

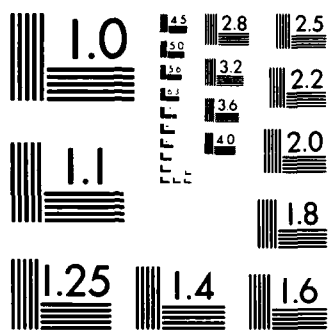
4/8

UNCLASSIFIED

F/G 5/9

NL





MICROCOPY RESOLUTION TEST CHART
NATIONAL BUREAU OF STANDARDS-1963-A

SYSTEMATIC ERRORS

Inaccuracies in a portable clock during a trip can be traced to such systematic errors as temperature effects, acceleration and shock, power supply noise and/or voltage spikes, magnetic field sensitivity, and others.

Until a complete study of systematic errors is made, it is suggested (and in several cases it has already been done) to send a redundant set of 2 or more clocks, of different manufacturer and type, on portable clock trips, along with a portable data acquisition system, to allow a continuous intercomparison of the clocks for the trip duration.

In addition, clock reliability should be addressed by careful evaluation of clock performance, looking for the weak points of each design and suggesting ways to improve the confidence in the operation of the clock and clock subsystems (i.e., power supply modules).

MEASUREMENT SYSTEM CONFIGURATION

During the month of October 1983, personnel from the NASA, the NRL, and the BFEC performed a joint experiment with the Italian Navy and the IEN, with the aim to test the navigation capabilities of the GPS timing receivers onboard a hydrographic ship of the Italian Navy (fig. 2). This provided the opportunity to perform field tests of cesium standards during actual trip conditions.

Three portable cesium standards were available onboard the ship. One was provided by the IEN (HP5061 - CS1230), one by the USNO (HP5061, opt. 004 - CS1809) and the other by the NASA (FTS4010 - CS107). These three clocks provided redundant clock information during the experiment (fig. 3).

An automated measurement system was installed and operated onboard the ship for the duration of the experiment (fig. 6).

External time references were continuously available on shore, such as a LORAN-C timing receiver, TV links, an additional GPS timing receiver and one cesium standard, providing a reliable clock system that was mainly used as a backup to the main timing system onboard the ship.

INSTRUMENTATION ONBOARD THE SHIP

The measurement system is shown in fig. 4 and 5 and a block diagram is shown in fig. 6. An HP-85 computer acts as the system controller. The three cesium standards are intercompared via an HP59307 switch (shown in fig. 5 on top of the HP5370 counter), using an HP5370 counter in the time interval mode (20ps resolution).

The 1 pps signal from the USNO standard (CS1809) provides the master reference start signal to the counter. In this way, the 1 pps pulses and the 5 MHz signals of the cesium standards are intercompared.

A Time Systems Technology (TST model 6459) clock (fig. 4) was used as a precise 1 pps distribution amplifier. The same figure shows a 5 MHz distribution amplifier and the two GPS timing receivers onboard.

An HP Interface Bus (HPIB) compatible digital multimeter was used to monitor (via a standard thermistor) the ambient temperature, while an HPIB compatible clock (HP59309) provided time tags to the data.

The HP5370 and the other instruments were controlled by the HP-85 via the HPIB. The data was collected approximately every 30 minutes and stored on tape for further processing.

In addition, manual readings were taken between the 1 pps signals. Phase monitoring of two 5 MHz signals was provided by a Tracor phase comparator and recorder unit (fig. 3).

The 1 pps and 5 MHz signals generated by each clock were compared against the 1 pps signal of the reference cesium (CS1809). Each data consisted of the average and standard deviation of ten time interval readings between the 1 pps reference signal and the signal being measured (fig. 6). Both the average and the standard deviation of each measurement was stored on tape, along with the time of the measurement and the ambient temperature.

The system failed to operate several times, mainly because of electrical power interruptions (the system had no battery backup). Power interruptions occurred when switching from onboard to shore power and vice versa, and when power was redistributed to balance the load on various distribution lines. Power interruptions were the cause of one of the power failures on CS107, the other was an unplugged power cable.

As a consequence of the power failures, the computer stopped. The auto-start provision was not enabled since the time-tagging digital clock needed to be reset to the proper time, which required operator intervention.

Inproper setting of the digital clock (perhaps caused by noise or spikes on the power line) resulted in uncertain time tagging of the data on October 6 and 7. Even though this data cannot be referenced to pre or post data, it was used to monitor the frequency of the clocks during that period (see tables I, II, and III).

BACK-UP TIMING SYSTEM ON SHORE

The back-up timing system (fig. 7) was installed by the IEN on shore, in a building inside the Naval Base complex. A block diagram of this system is shown in fig. 8.

The local time base was obtained from a HP5061A (CS609) cesium standard. External references included a TV link to UTC (IEN), while LORAN-C and GPS measurements were provided by an Austron 2005 LORAN-C timing receiver and a second NRL GPS time transfer receiver, installed on shore from October 4 to October 8 and later installed onboard the ship for redundant operation.

The measurement system included a HP5345A time interval counter (2ns measurement resolution in the time interval mode), a HP59307 switch, and a HP9815 desk top calculator, which acted as the system controller and data logger. The measured data was stored on tape.

CESIUM CLOCKS PERFORMANCE

The reference cesium standard (CS1809 - HP5061A opt. 004) performed very well, with a 120 ns closure error versus UTC(USNO) after the 17 day trip.

One of the two cesium standards onboard (CS1230 - HP5061A) experienced a phase shift that will be discussed later. The other (CS107 - FTS4010) had two power failures onboard, the first time due to an unplugged connector, and the second time during a switch between shore to onboard power while changing the battery pack.

The frequency of each clock (CS1230 and CS107) versus the reference clock (CS1809) was estimated from the 1 pps comparisons over the measurement intervals listed in table I. The fractional frequency offset was computed as the slope of the fit (line) to the phase data. The standard deviation of the fit and the standard deviation of the slope (frequency) were computed and are given in table II (CS107) and table III (CS1230). The uncertainty in the fractional frequency offset estimate was weighted for the number of data points used in the fitting process by using the Student t-distribution to correct the standard deviation of the slope.

The results of the analysis for CS107 are summarized in fig. 9. The vertical axis is the fractional frequency offset between CS1809 and CS107, the horizontal axis is time (days, October 1983). Each frequency estimate is plotted as a horizontal bar extended over the measurement period. The height of the box around the bar represents the uncertainty of the frequency offset determination over the same period (see legend, fig. 9). The asterisks mark the time of the power failures. Since the vertical scale is 10ns/day per division, this is roughly equivalent to 1×10^{-13} per vertical division.

During the first week the behaviour of CS107 was excellent, then there was the first power failure on the morning of October 8 and the second one on the morning of the 10th. After a warm-up period of approximately two days, the frequency returned to about the original value. The lower frequency on day 11 is unexplained. Notice, however, the large uncertainty.

This change does not appear so dramatic in a phase plot over the same period (fig. 10). Fig. 10 shows the phase behavior of CS107 versus CS1809 on October 10 and 11, 1983, when CS107 was just recovering after the two power failures. The change in slope on October 11 is evident. In the plot to the right (fig. 10) the line fitted over the measurement period is superimposed on the data. The average slope tends to be slightly higher than the slopes estimated on partial intervals covering the same period of time. This is caused by non-linear behaviour of the data.

The average fractional frequency offset between the two clocks after the power failure was then 198 ± 2.6 ns/day (on days 10 and 11); during the first week (on days 5 and 6, fig. 11) the average slope was 208.7 ± 2.3 ns/day. The difference was only 10.7 ns/day (± 5.6 ns/day in the worst case), roughly 1×10^{-13} in frequency difference before and after the power failure.

CS1230 was noisier than CS107 and showed a more random phase behaviour (fig. 12). There is a definite change in the frequency of CS1230 from October 4 to October 5 and 6 (fig. 12). The random walk of CS1230 is evident in fig. 13 (October 10 to 12); however, the long term performance was satisfactory.

On the morning of October 7 there was a phase shift in CS1230 (see fig. 14, top plot). The magnitude of the phase jump was roughly 100ns in less than 4 hours. The bottom plot in fig. 14 shows the simultaneous temperature recording. There was a large temperature inversion, due to the turn-on of the ship's air conditioning equipment, at the time when the phase shift started. The absolute temperature was not very high (about 76° F). The slope on October 6 and 7 was about 121 +/- 2.1 ns/day. After the shift, the average slope was about 129 +/- 3.4ns/day. The shift in phase does not appear to have affected the frequency of the cesium.

Table IV presents a summary of the comparison of the two cesiums (CS107 and CS1230) versus the reference CS1809. The average fractional frequency offset is the arithmetic mean of the frequency offsets shown in tables II and III, with two data points removed on days 8 and 10, where an external power failure interrupted the operation of CS107. One data point was removed on day 7 for the large phase jump in CS1230 which affected the normal behavior of the clock. The standard deviation shown is the standard deviation on the above computed average.

TEMPERATURE ANALYSIS

The purpose of the temperature measurements was to monitor frequency changes due to temperature variations in the field. These can be monitored against a remote reference time scale or against a local standard, but are unaffected by the same temperature changes (absolute frequency dependence on temperature). Alternatively, given an ensemble of clocks exposed to the same temperature variations, frequency changes in one standard versus the others can be monitored (relative frequency dependence on temperature).

The main limitation that was found in carrying on such measurements was that, in both cases, the frequency changes due to short term temperature variations are the same order of magnitude or less than the uncertainty in the short term evaluation of the frequency of the cesium standard. In this experiment, it was not possible to find any substantial correlation between frequency changes and short term temperature variations in the field. Moreover, external references and existing time transfer links do not provide enough accuracy to monitor short term frequency changes.

SYNCHRONIZATION LINKS AVAILABLE DURING THE GPS EXPERIMENT.

Figure 15 shows the various synchronization links that were available during the experiment.

Two time scales were used as a reference: UTC (USNO) and UTC(IEN). Both are reporting to the Bureau International de l'Heure (BIH) and their relative positions can be obtained from the BIH report. As a direct link, two systems were available, in

addition to two GPS timing receivers: (1) Transit Time Transfer receivers (FTS T-200), located at the IEN and at the USNO, provided 10 to 25 microseconds accuracy in time transfer, and (2) LORAN-C, provided indirect synchronization across the Atlantic Ocean of 1 to 10 microseconds.

In contrast, the GPS timing receivers provided time comparison of remote clocks with an accuracy of 50 to 100ns between the USNO, the ship, the La Spezia harbour and the IEN.

To have an independent synchronization link between La Spezia and the IEN in Torino, one LORAN-C timing receiver was installed by the IEN on shore. This provided synchronization to better than 100ns, and an additional, independent reference to UTC (USNO), even if with less certainty.

Moreover, to provide a more precise synchronization between the IEN and La Spezia, the IEN personnel set-up a TV measurement system, taking daily readings at 0900Z at IEN and La Spezia, with an estimated accuracy between 10 and 50ns.

In this way, it was possible to insure accuracy, reliability and redundancy to the clocks in the field, while referencing them continuously to existing time scales.

As shown in table V, there is a wide spread of accuracies available from existing systems, but no one system provides better than 10 to 50ns for comparison of remote clocks. Local (direct) time interval readings between cesium clocks usually have an uncertainty of 1 to 10ns within a 1 day period, equivalent to the typical noise floor of a good cesium standard.

TEMPERATURE BEHAVIOUR

Fig. 16 shows typical plots of temperature versus time during the experiment. The temperature onboard was not controlled, except for a manually operated air conditioning system; the thermistor probe was suspended above the ensemble of the three clocks.

The chart shown in fig. 17 presents the temperature variations onboard the ship. The horizontal bar extended over the measurement period is the average temperature over the same period. The height of the box around the bar represents the standard deviation of the average. Dot and cross symbols indicate the minimum and maximum temperature recorded within each measurement period.

As shown in table VI, (which presents a summary of the temperature measurements), despite large short term temperature variations, the average temperature during the experiment was fairly constant (around 70° Fahrenheit). The largest standard deviation is 5.8° Fahrenheit, however the average standard deviation is only 2.6° Fahrenheit.

Short term temperature variations do not seem to affect the behaviour of portable cesium clocks, at least to increase substantially the phase error at a measurable level.

A redundant set of portable clocks traveling together will certainly improve the reliability, but not necessarily the accuracy of the synchronization.

TIME TRANSFER USING GPS RECEIVERS ONBOARD A MOVING PLATFORM

The primary objective of the synchronization experiment was to evaluate the time transfer capability of a single channel C/A Code GPS timing receiver while onboard a moving platform.

THE NAVSTAR GLOBAL POSITIONING SYSTEM

NAVSTAR GPS is a tri-service Department of Defense (DOD) program. The first GPS satellite flown was The Navigation Technology Satellite (NTS-II) which was designed and built by NRL personnel. GPS will provide the capability of very precise instantaneous navigation and transfer of time from any point on the Earth. GPS comprises three segments: the Space Segment, the Control Segment and the User Segment. The phase III Space Segment will consist of a constellation of 18 to 24 satellites, six to eight in each of three orbital planes. The satellite orbits are nearly circular at an altitude of about 20,000 km and inclined 55° to the equator. The period is one half of a sidereal day, resulting in a constant ground track, but with the satellite appearing 4 minutes earlier each day.

Each satellite transmits its own identification and orbital information continuously. The transmissions are spread spectrum signals, formed by adding the data to a direct sequence code, which is then biphase modulated onto a carrier. At the present time, the control segment consists of a Master Control Station (MCS) and four monitor stations.

The monitor stations collect data from each satellite and transmit to the MCS. The data are processed to determine the orbital characteristics of each satellite, and the trajectory information is then uploaded to each satellite once every 24 hours as the spacecraft passes over the MCS. The user segment consists of a variety of platforms containing GPS receivers, which track the satellite signals and process the data to determine position and/or time by simultaneous or sequential reception of at least four satellites.

GPS TIME TRANSFER RECEIVER (TTR)

As an outgrowth of the NTS timing receiver development in 1977 by the NRL and the GSFC, a joint effort was started in 1979 to develop GPS TTR's using signals radiated by the GPS satellites. In support of the GSFC Crustal Dynamics Program, the GPS TTR's were designed for use in the GSFC Transportable Laser Ranging Network, which requires submicrosecond timing for correlation of highly accurate satellite tracking data with time.

The capabilities of the receiver are being expanded, mainly through software modifications, for the following reasons:

- o Demonstrate the position location capabilities of a single channel receiver using the GPS C/A code.
- o Demonstrate the time/navigation capability of the receiver onboard a moving platform, by sequential tracking of GPS satellites.
- o Develop a timing receiver capable of worldwide synchronization from a moving platform.

The GPS TTR is a microcomputer based system which operates at the single L-band frequency of 1575 MHz. The receiver uses the C/A code only (1.023 MHz), tracking this code to within 3% of a chip (30ns). The receiver has the capability to track satellites throughout their doppler range from horizon to horizon, and can track any GPS satellite by changing the receiver internal code. Operator interface with the receiver is provided by a keyboard and CRT display. The time data is stored on disks and can also be output to an external printer/computer via a serial data interface (fig. 19).

TIME TRANSFER METHOD

The GPS TTR's (fig. 4) installed onboard the ship were driven directly by the reference cesium standard CS1809. The time transfer was obtained as part of a five dimensional navigation solution (see ref. 1), solving for latitude, longitude, heading, speed of the ship, and time. Time here refers to the difference between the GPS system time and the local clock.

The time solution was usually obtained over a 30 minute integration time; the measurements were gathered from 3 to 5 NAVSTAR satellites. The time transfer results were compared with the estimated position of CS1809 (used as the local time reference in the synchronization).

The plot shown in fig. 20 presents the results of the time transfer onboard the moving ship. The square symbols represent the time difference between UTC(USNO) and CS1809 via the GPS solution. The crosses represent the same difference, but estimate the position of the portable clock CS1809 with reference to the USNO. The error bars represent the uncertainty in the estimated clock position in time.

Except for two large discrepancies (around 200ns) on October 5 (day 278) and on October 10 (day 283), the average accuracy was around 100ns.

RESULTS OF THE SYNCHRONIZATION AT THE ISTITUTO ELETTRATECNICO NAZIONALE (IEN).

From October 13 to October 19, identical GPS receivers were installed at the IEN facilities (fig. 22) in Torino, to perform a final synchronization via the GPS.

The two GPS receivers (see the block diagram in fig. 21) were driven by the IEN master clock (An HP5061A, opt. 004, cesium standard), that is part of an ensemble of commercial cesium clocks kept in an underground vault (fig. 22).

The four clocks participating in the navigation experiment (CS1809, CS107, CS1230 and CS609, the last being the one installed on shore at La Spezia) were continuously monitored against each other and against UTC(IEN) for one week.

In addition, measurements via GPS were carried on by temporarily driving the receivers with the portable clocks CS107 and CS1809, to check the time position of the traveling clocks with reference to UTC(USNO).

TIME TRANSFER METHOD VIA GPS FOR A STATIONARY RECEIVER

The major objective of a satellite time transfer receiver is to determine precise time differences between a given satellite and a local ground clock. Precise time

can then be obtained between the space vehicle (SV) and a single remote ground station clock or between the SV and any number of remote stations. The remote sites could then be synchronized among themselves (fig. 18).

To perform a satellite time transfer with GPS, pseudo-range measurements are made that consist of the propagation delay in the signal plus the difference between the satellite clock and the ground station receiver reference clock. Data from the navigation message contain the satellite clock information and the satellite ephemeris, which allows one to compute the satellite position. Since the position of the satellite and of the ground station are known, the computed propagation delay can be subtracted from the pseudo-range and then corrected for the GPS time offset, to determine the final result of ground station time relative to GPS time, which can be referenced to the USNO.

If two ground station clocks are synchronized to GPS time, the results can be subtracted to obtain the time difference between the ground station clocks. This can be done at any time, but best results are obtained when data is taken simultaneously by each ground station from the same satellite (common view), since any error contributed by the satellite clock is cancelled when the data is subtracted.

The GPS time offset, that is the difference between GPS time and UTC(USNO), can be obtained directly in real time as a part of the information broadcast by each satellite.

However, the synchronization results can be improved (as will be shown later), if the difference between UTC(USNO) and GPS time is measured simultaneously or nearly simultaneously (within a few hours) by a GPS time transfer receiver operated at the USNO. This data is made available by the Naval Observatory.

The Phase I GPS time is maintained at the Vandenberg MCS using a cesium oscillator. The Phase III GPS time is planned to be referenced from the MCS to the USNO Master Clock. The final results obtained from a single-frequency receiver, will contain a small error due to the ionospheric delay which may be modeled and corrected.

Fig. 24 shows the time difference between UTC(USNO) and CS107 measured at the IEN. CS107 was directly driving one of the GPS receivers; the asterisks show the estimated position of CS107 with reference to UTC(USNO). NAVSTAR 5 was the satellite used in the time transfer.

The difference between GPS time and UTC(USNO) was obtained in real time from the navigation message transmitted by the satellite.

When the same difference between GPS time and UTC(USNO) was obtained via direct measurements carried on almost simultaneously at the Naval Observatory, the results show a better agreement between the predicted clock position and the GPS time transfer, as shown in fig. 25.

Fig. 26 shows the time difference between UTC(USNO) and CS1809, the latter driving one of the GPS timing receivers at the IEN. Again, the difference between GPS time and UTC (USNO) was obtained from the navigation message. An offset is clearly visible between the estimated clock position (asterisks) and the GPS time transfer

indicated by the number 5, indicating NAVSTAR 5. However, if the measurements carried on at the Naval Observatory are used in place of the prediction broadcasted in real time by the satellite, again the offset disappears (fig. 27).

Fig. 28 presents a summary of the time transfer between the USNO and the IEN. The asterisks show the difference between UTC(USNO) and UTC(IEN) via the portable clock references. The numbers plotted identify the time transfer obtained via a particular NAVSTAR satellite (number 3, 4, 5, 6 and 8). Again, the difference between UTC(USNO) and GPS time was obtained in real time from the navigation message. When the direct measurements at the Naval Observatory are used to evaluate the difference between the USNO and GPS time, the time transfer via GPS shows a better agreement with the portable clock data (fig. 29). The accuracy of estimated time position of the portable clocks was within 50 to 100ns for the days shown.

This experiment proved that the time transfer using NRL GPS timing receivers can achieve a worldwide, reliable accuracy within 50 to 100ns, which is well within the requirements for the synchronization of the NASA Laser Tracking Network.

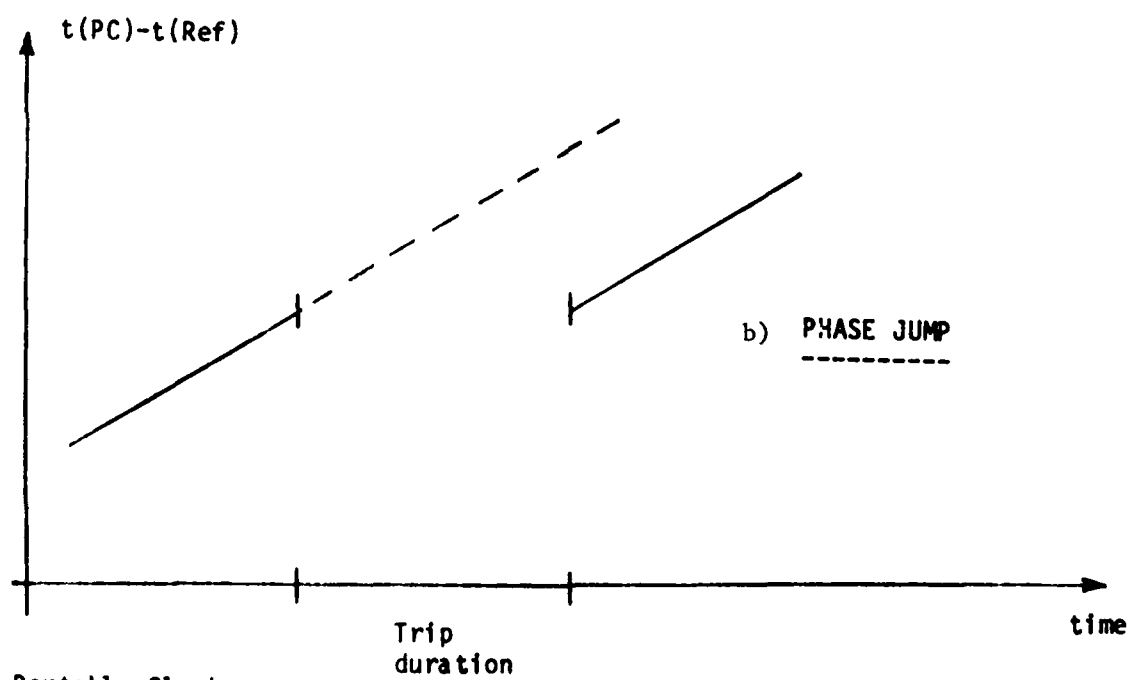
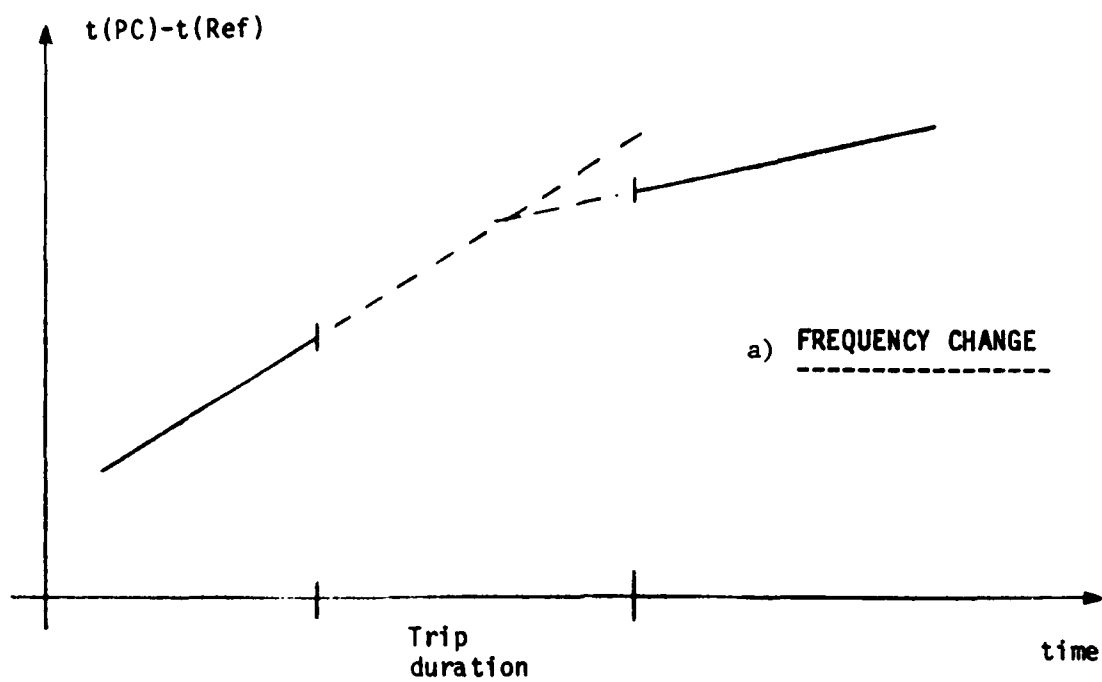
ACKNOWLEDGMENTS

This work would not have been possible without the efforts and the cooperation of many people. In particular we would like to express our sincere thanks to the Captain and the crew of the ship "Magnaghi", to the Mini-Ranger and Raydist ground stations support teams and to the engineers and technicians of the BFEC, the NRL, the Italian Navy and the IEN.

This work was jointly funded by the National Aeronautics and Space Administration, the Italian National Council of Research (National Space Plan) and by the Italian Navy.

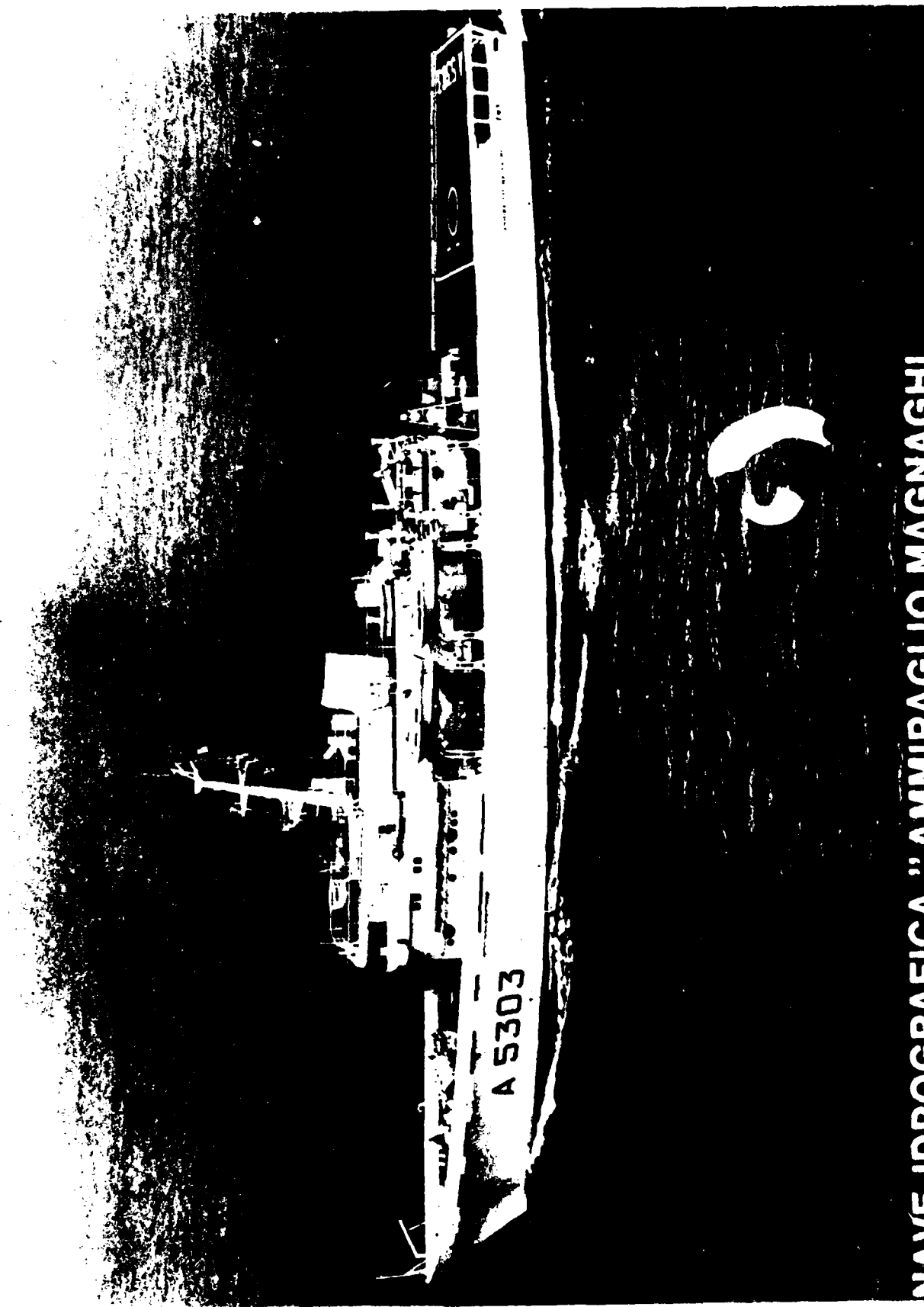
REFERENCES

- 1) - J. Buisson et al., GPS NAVIGATION EXPERIMENT USING HIGH PRECISION GPS TIMING RECEIVERS, Proceedings of the 15th Precise Time and Time Interval Meeting.
- 2) - C. Wardrip et al., AN INTERNATIONAL TIME TRANSFER EXPERIMENT VIA THE GLOBAL POSITIONING SYSTEM (GPS), Proceedings of the 37th Annual Symposium on Frequency Control (Philadelphia, 1-3 June 1983), pp. 61-66.



PC = Portable Clock
 Ref = Reference time scale

Fig. 1 - UNCERTAINTIES AFFECTING
 PORTABLE CLOCKS PERFORMANCE



NAVE IDROGRAFICA " AMMIRAGLIO MAGNAGHI."

Fig. 2

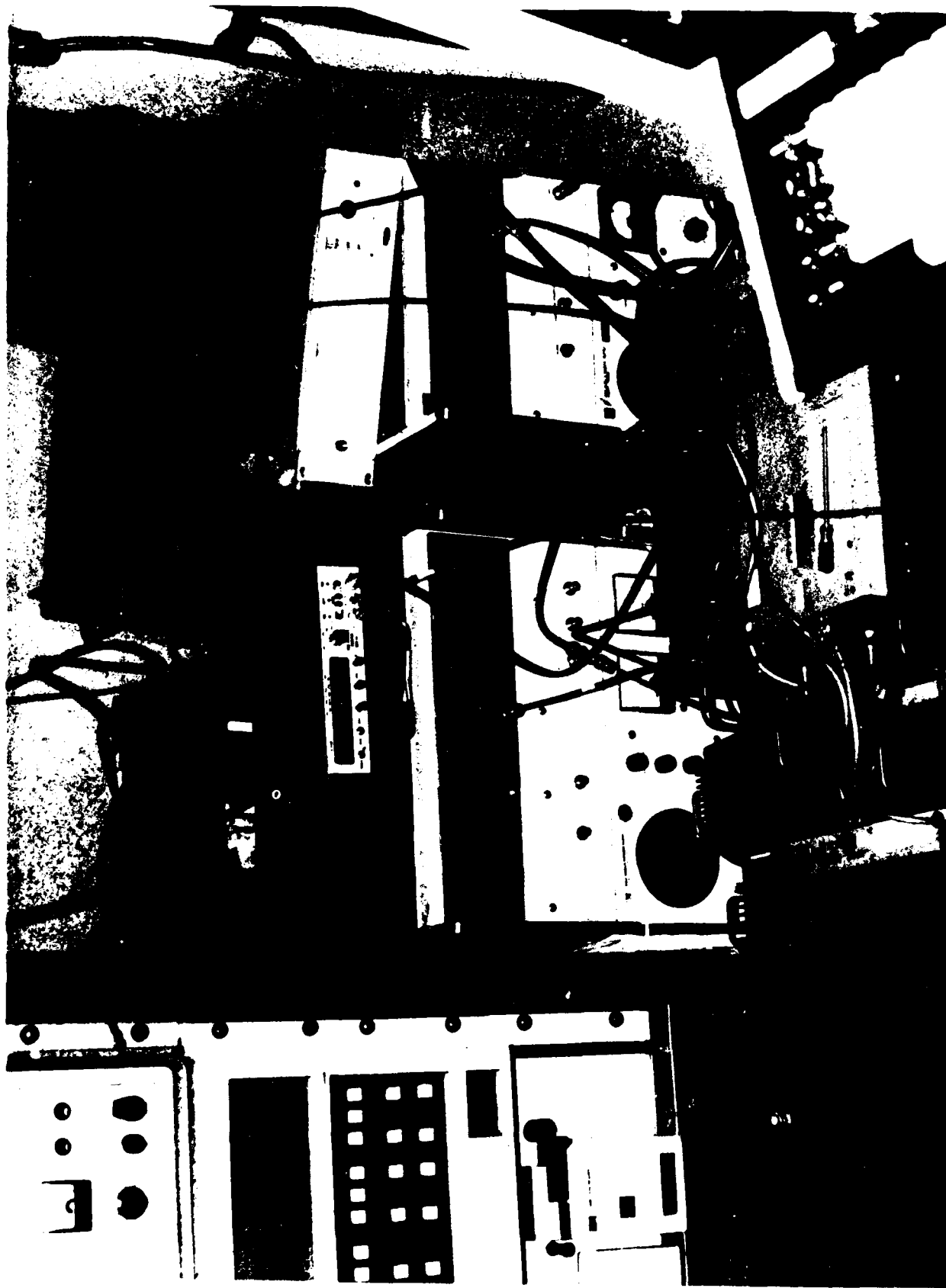


Fig. 3 - Cesium standards onboard the ship

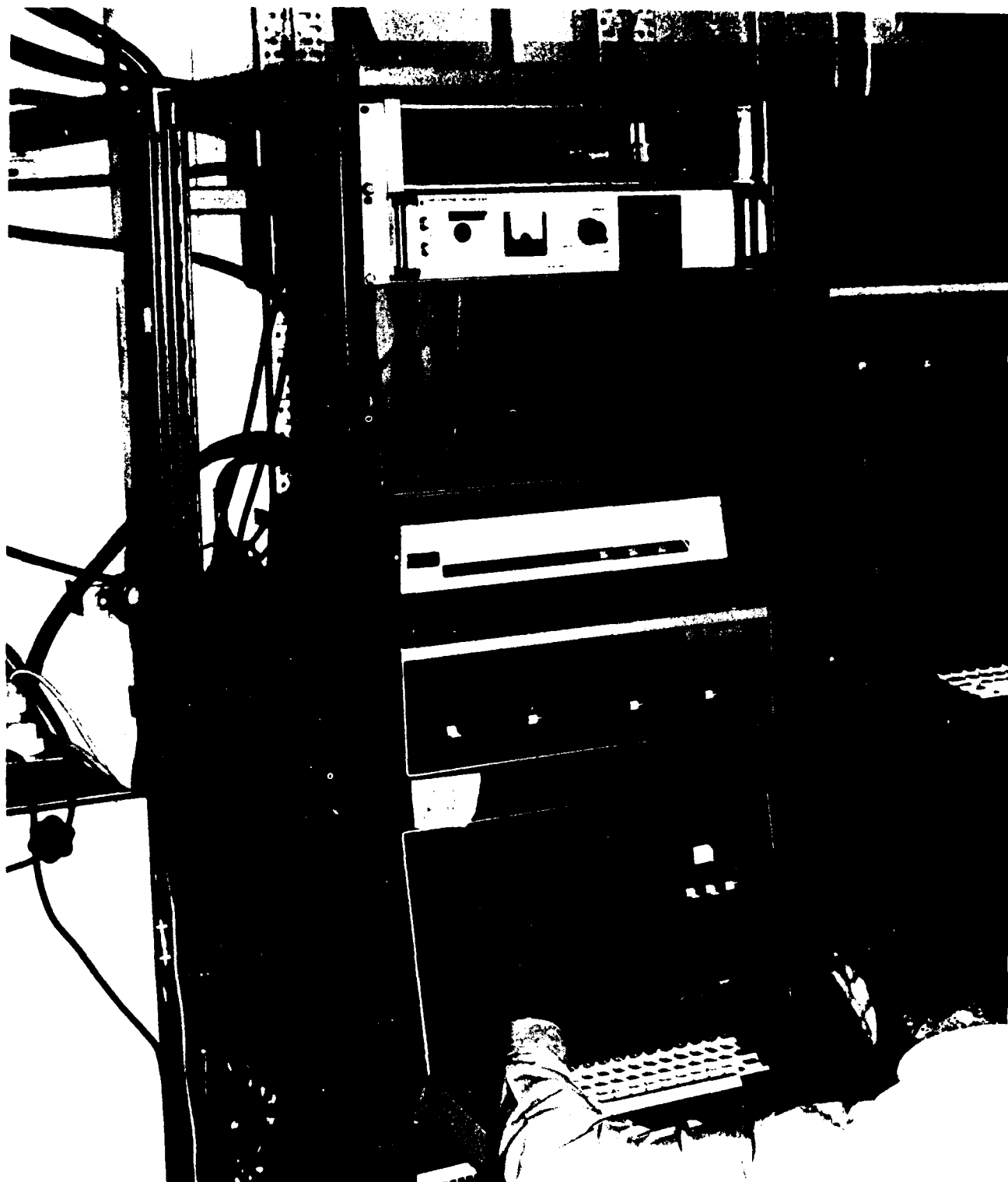


Fig. 4 - GPS time transfer receivers onboard



Fig. 5 - GPS time transfer receivers and data acquisition system (bottom)

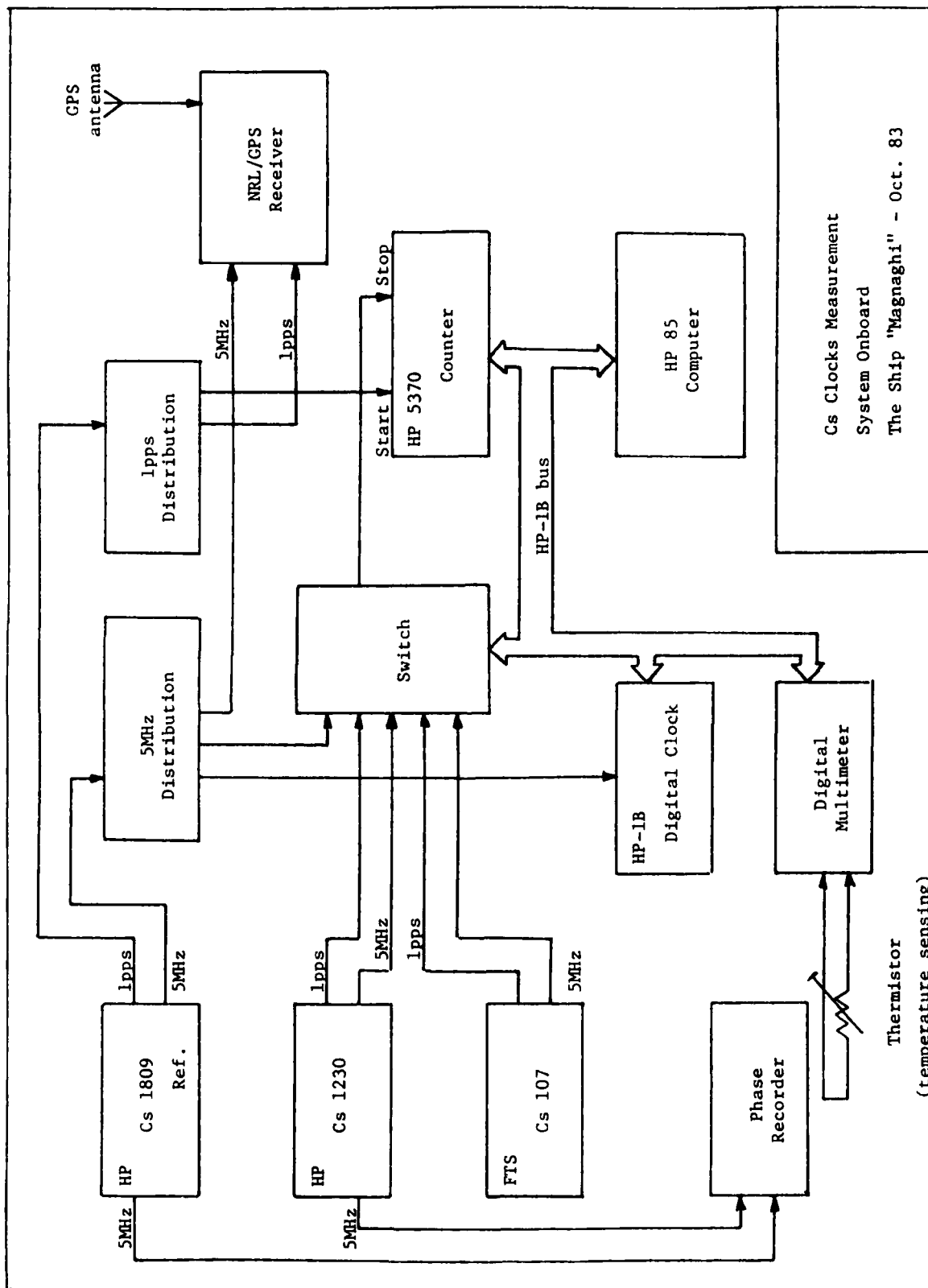


Fig 6

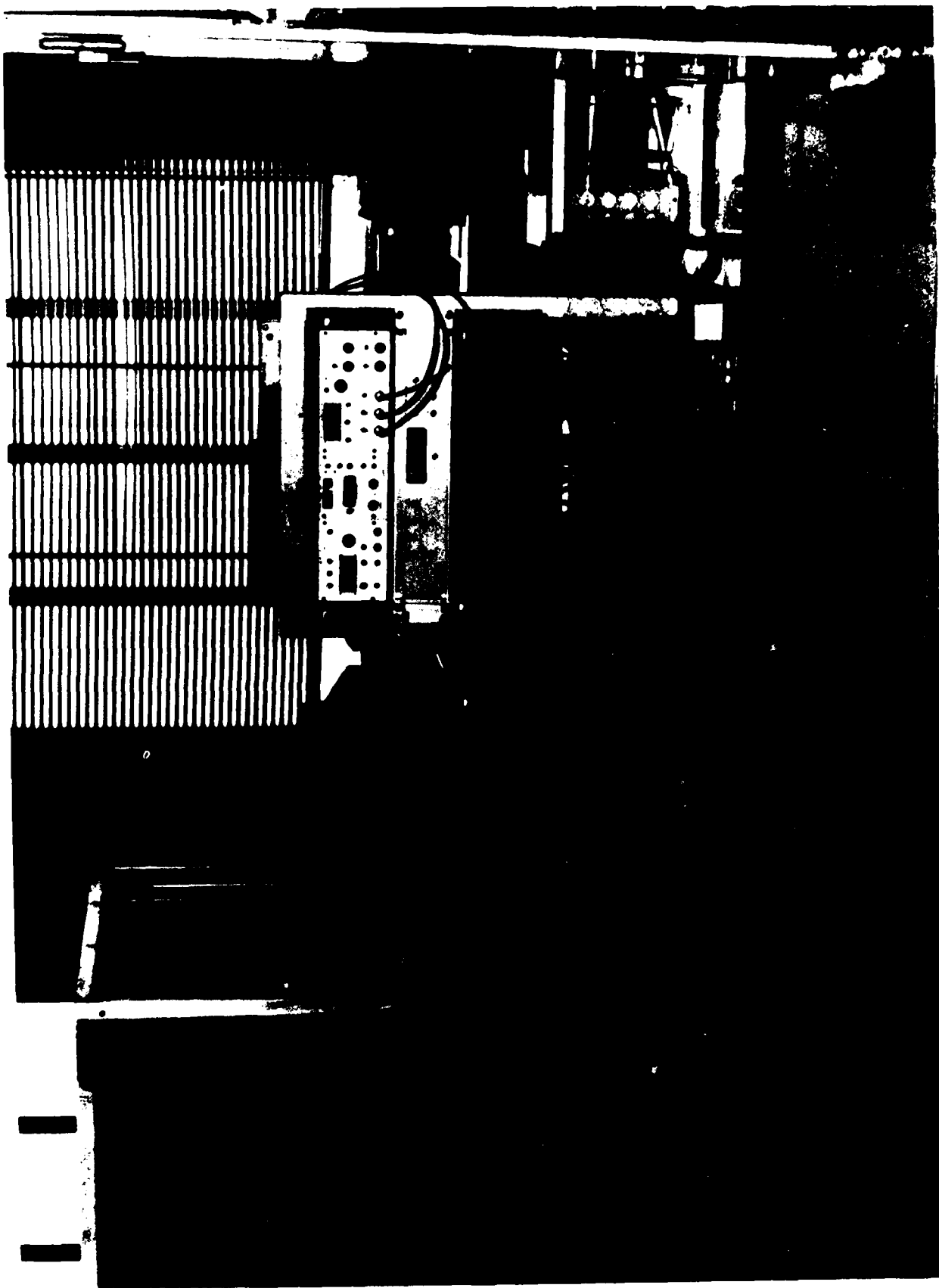
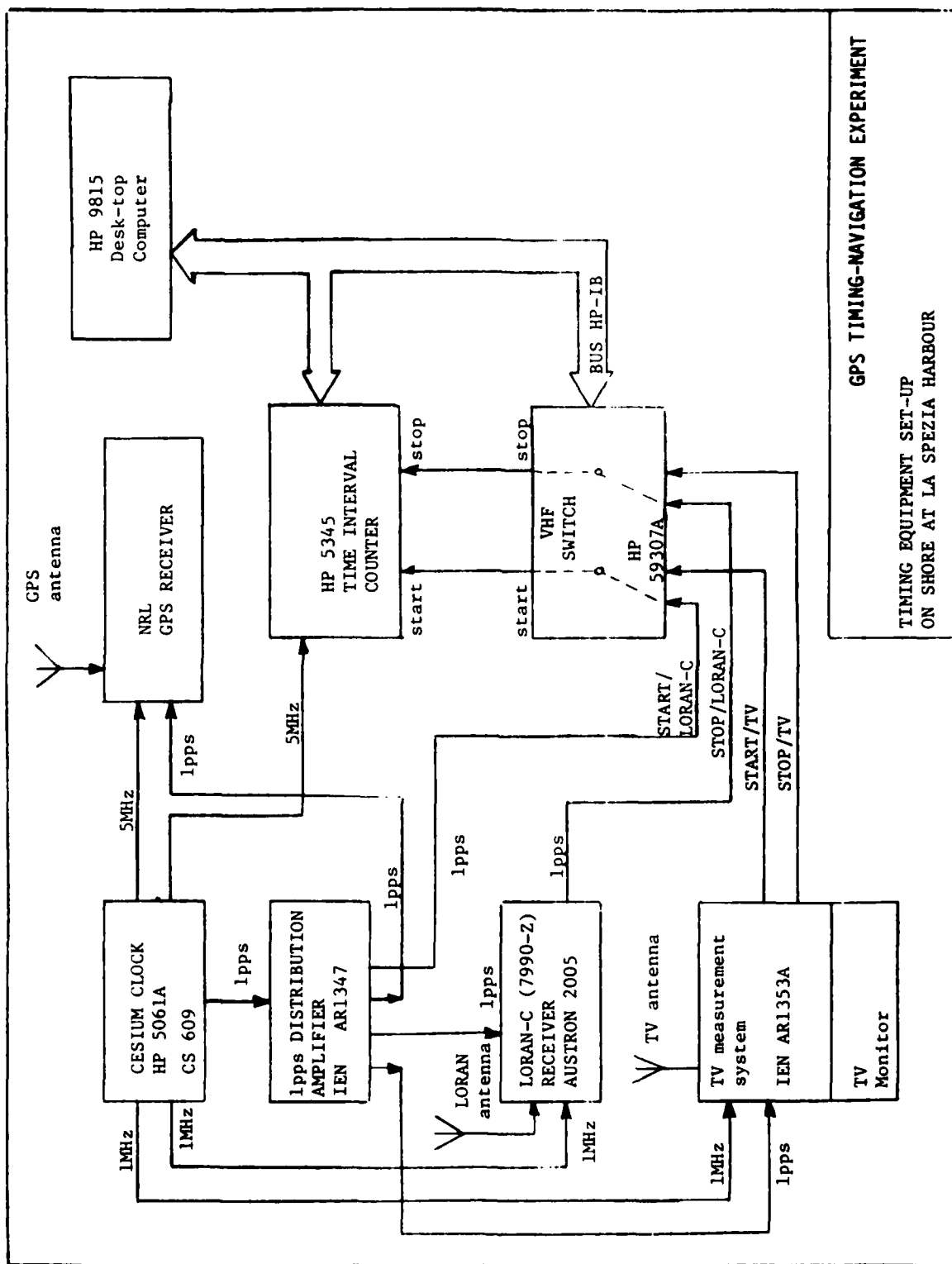


Fig. 7 - Back-up Timing System on shore (La Spezia)



GPS TIMING-NAVIGATION EXPERIMENT
TIMING EQUIPMENT SET-UP
ON SHORE AT LA SPEZIA HARBOUR

FIG. 8

DATA FILE - TIME COVERAGE
=====

DATA FILE	DAY (October)	Start time (Z)	Stop time (Z)	
DATA1	4/5	1804	0325	
DATA2	5	0712	1356	
DATA3	5/6	1441	0012	
DATA4	6/7	1253	0048	(*)
DATA5	7	0247	1707	(*)
DATA6	8	1145	1803	
DATA7	10	0309	1431	
DATA8	10/11	1630	0743	
DATA9	11/12	0746	0133	

NOTE: (*) - Uncertain time tagging

TABLE I

DATA SET	NUMBER OF POINTS	FREQUENCY OFFSET		σ_f ($\mu\text{s}/\text{min}$) (ns/day)	FREQUENCY OFFSET UNCERTAINTY (95%) (ns/day)	σ_{fit} (ns)
		($\mu\text{s}/\text{min}$)	(ns/day)			
1F	19	1.431 10^{-4}		3.297 10^{-6}	± 8.2	2.5
		206.1		4.7		
2F	14	1.441 10^{-4}		3.619 10^{-6}	± 9.3	1.7
		207.5		5.2		
3F	20	1.393 10^{-4}		1.444 10^{-6}	± 3.6	1.2
		200.6		2.1		
4F	23	1.441 10^{-4}		1.030 10^{-6}	± 2.6	1.0
		207.6		1.5		
5F	15	1.423 10^{-4}		2.776 10^{-6}	± 7.1	1.5
		204.9		4.0		
6F	13	9.171 10^{-5}		5.265 10^{-6}	± 13.6	2.2
		132.1		7.6		
7F	11	1.348 10^{-4}		2.199 10^{-6}	± 5.8	1.4
		194.0		3.2		

TABLE IIa PORTABLE CLOCK CS1809 - CS107
EVALUATION

* FREQUENCY PREDICTION TABLE *

DATA SET	NUMBER OF POINTS	FREQUENCY OFFSET		σ_f		FREQUENCY OFFSET UNCERTAINTY (95%) (ns/day)	σ_{fit} (ns)
		($\mu\text{s/min}$) (ns/day)	($\mu\text{s/min}$) (ns/day)				
8F	30	1.369	10^{-4}	1.413	10^{-6}	± 3.5	2.1
		197.1		2.0			
9F	9	1.167	10^{-4}	5.622	10^{-6}	± 15.3	1.3
		168.0		8.1			
9FA	17	1.418	10^{-4}	2.742	10^{-6}	± 6.9	1.7
		204.2		3.9			

PORTABLE CLOCK CS1809 - CS107
EVALUATION

TABLE IIb

* FREQUENCY PREDICTION TABLE *

DATA SET	NUMBER OF POINTS	FREQUENCY OFFSET		σ_f		FREQUENCY OFFSET UNCERTAINTY (95%) (ns/day)	σ_{fit} (ns)
		(μ s/min)	(ns/day)	(μ s/min)	(ns/day)		
1F	19	5.450	10^{-5}	1.974	10^{-6}	+ 4.9	1.5
		78.5		2.8			
2F	14	1.353	10^{-4}	3.165	10^{-6}	+ 8.2	1.5
		194.8		4.6			
3F	20	1.049	10^{-4}	3.219	10^{-6}	+ 8.0	2.6
		151.0		4.6			
4F	24	8.458	10^{-5}	8.396	10^{-7}	+ 2.1	0.9
		121.8		1.2			
5F	15	-2.411	10^{-4}	2.592	10^{-5}	+66.1	14.0
		(#) -347.2		37.3			
6F	13	6.327	10^{-5}	4.116	10^{-6}	+10.6	1.8
		91.1		5.9			
7F	13	8.791	10^{-5}	2.882	10^{-6}	+ 7.5	2.5
		126.6		4.1			

TABLE IIIa

PORTABLE CLOCK CS1809 - CS1230
EVALUATION

Note

(#) - Frequency change

* FREQUENCY PREDICTION TABLE *

DATA SET	NUMBER OF POINTS	FREQUENCY OFFSET		σ_f		FREQUENCY OFFSET UNCERTAINTY (95%) (ns/day)	σ_{fit} (ns)
		(μ s/min)	(ns/day)	(μ s/min)	(ns/day)		
8F	31	7.025 10^{-5}		1.328 10^{-6}		+ 3.2	2.0
		101.2		1.9			
9F	26	1.203 10^{-4}		2.932 10^{-6}		+ 7.2	5.3
		173.2		4.2			

TABLE IIIb PORTABLE CLOCK CS1809 - CS1230 EVALUATION

* FREQUENCY PREDICTION TABLE *

CS1809-CS107 FREQUENCY OFFSET EVALUATION

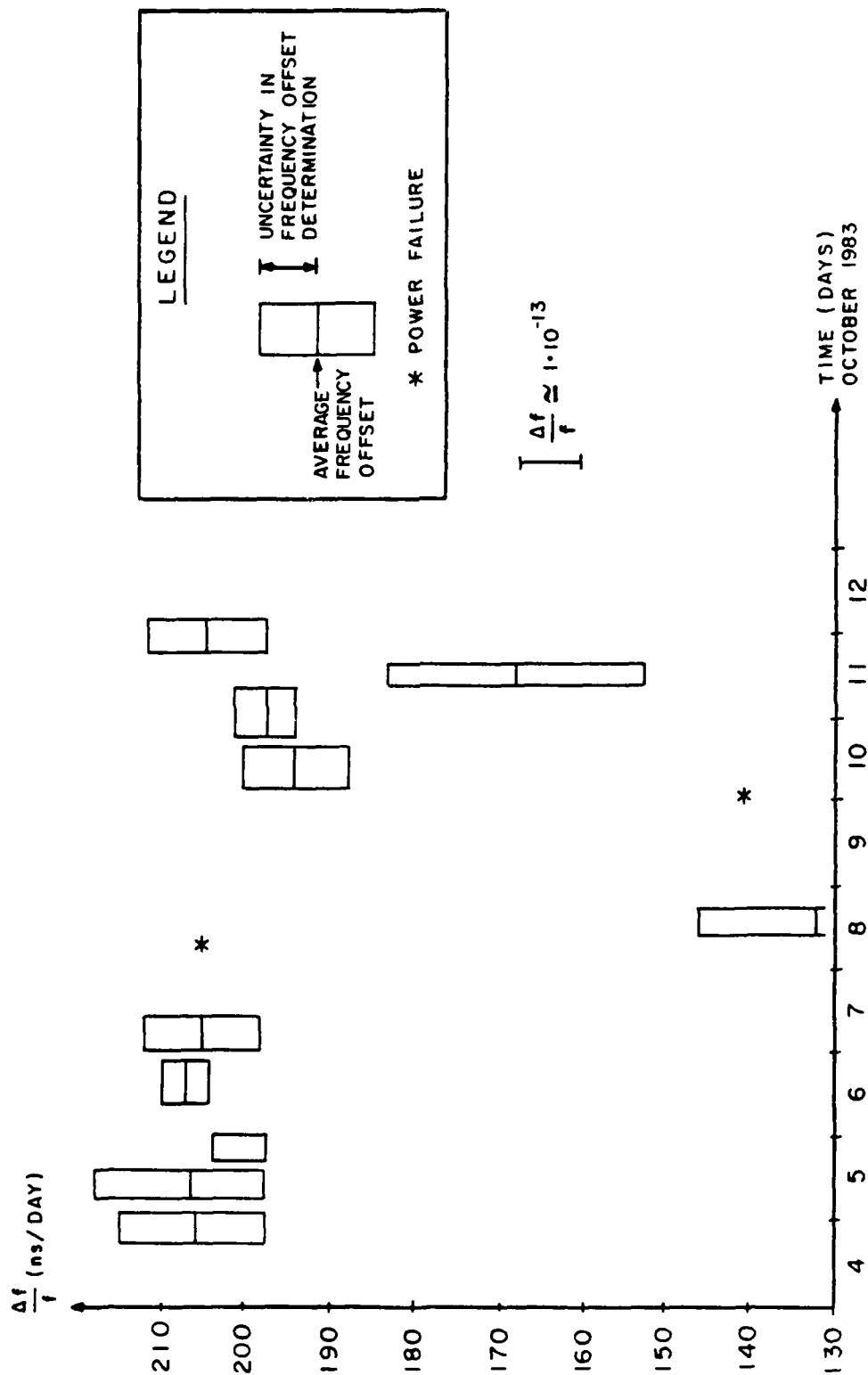
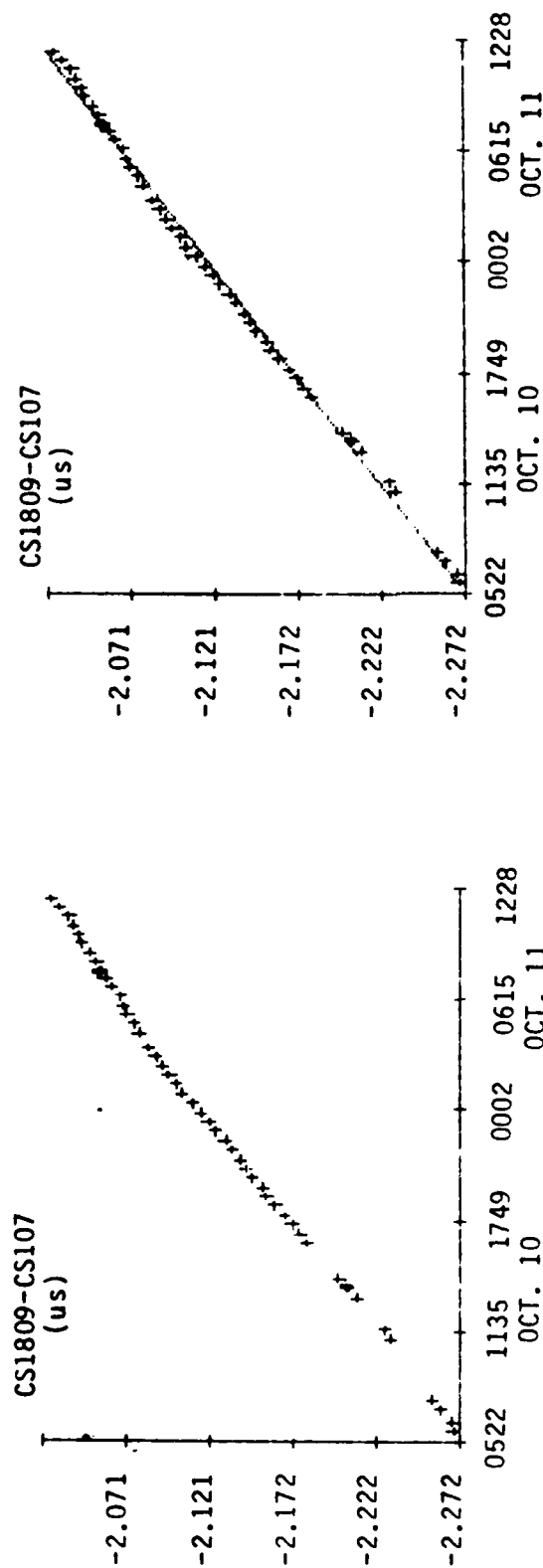


Fig. 9

CS 1809 - CS 107

=====

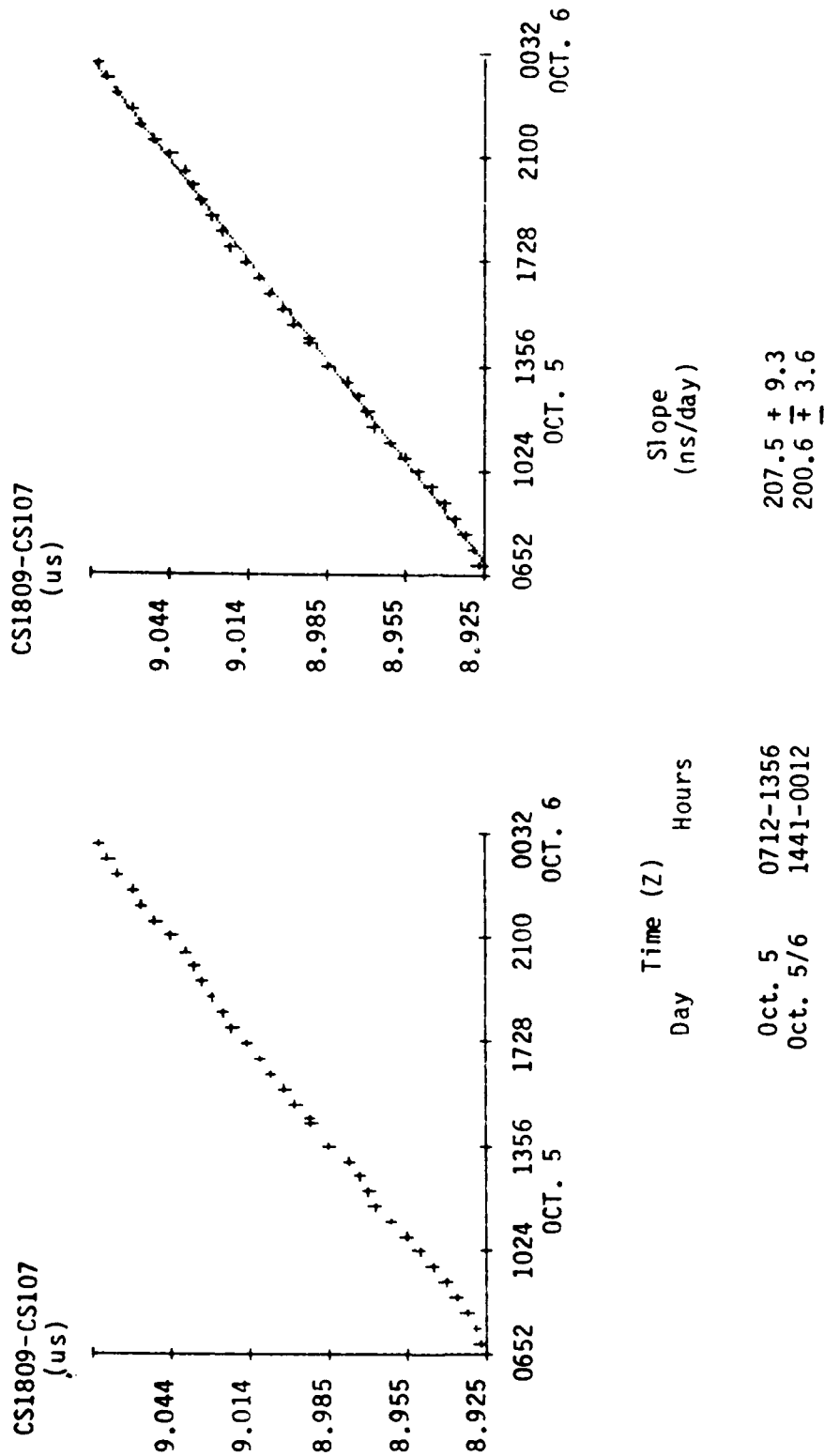


Day	Time (Z)	Hours	Slope (ns/day)
Oct. 10	0558-1431		194.0 ± 5.8
Oct. 10/11	1630-0743		197.1 ± 3.5
Oct. 11	0746-1153		168.0 ± 15.3

Average slope = 198.0 ± 2.6 (ns/day)

Fig. 10 INTERNATIONAL TIME TRANSFER AND PORTABLE CLOCK EVALUATION
USING GPS TIMING RECEIVERS

CS 1809 - CS 107



Average slope = 208.7 ± 2.3 ns/day

Fig. 11 - INTERNATIONAL TIME TRANSFER AND PORTABLE CLOCK EVALUATION
USING GPS TIMING RECEIVERS

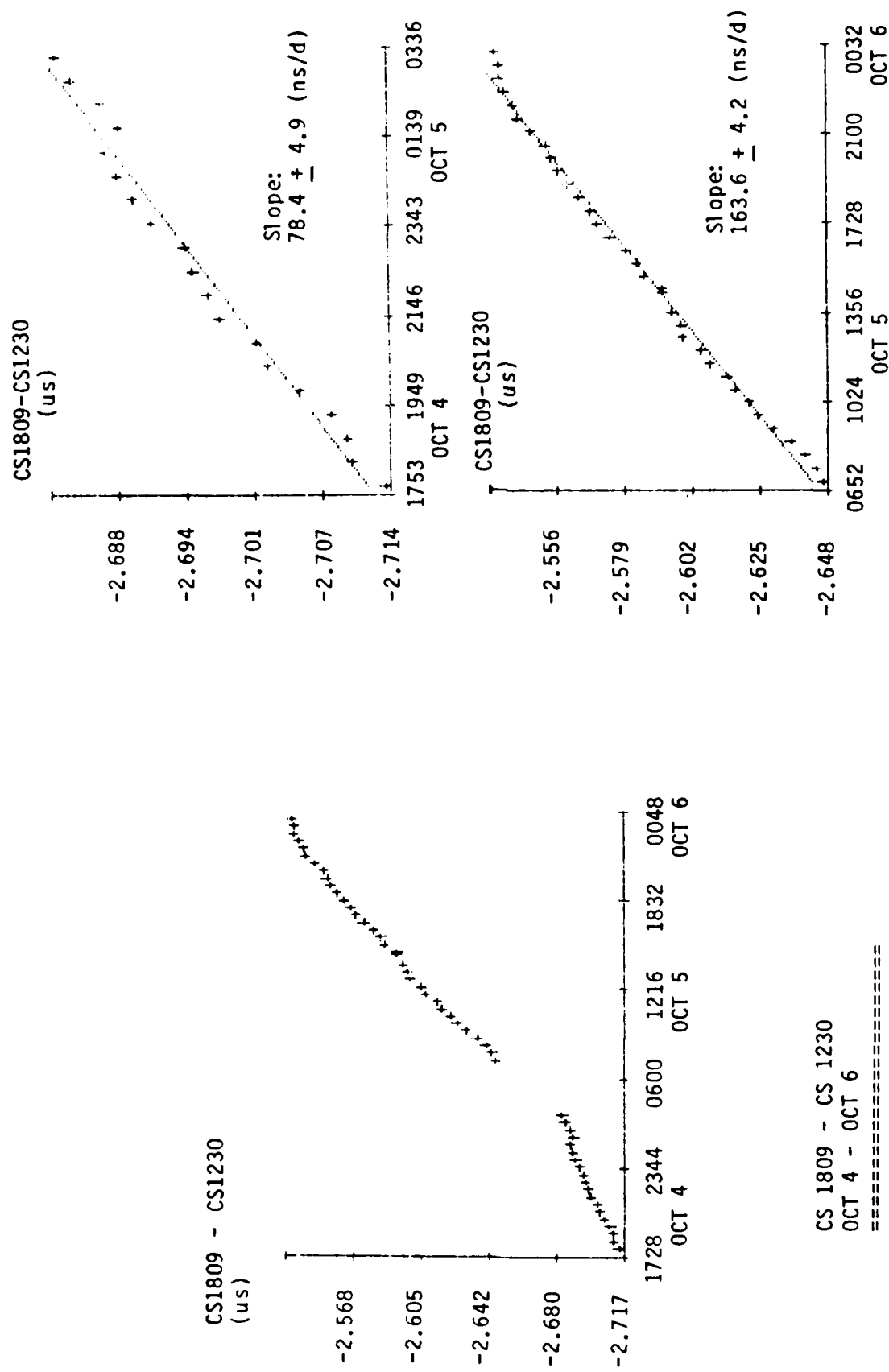


FIG. 12 - INTERNATIONAL TIME TRANSFER AND PORTABLE CLOCK EVALUATION USING GPS TIMING RECEIVERS

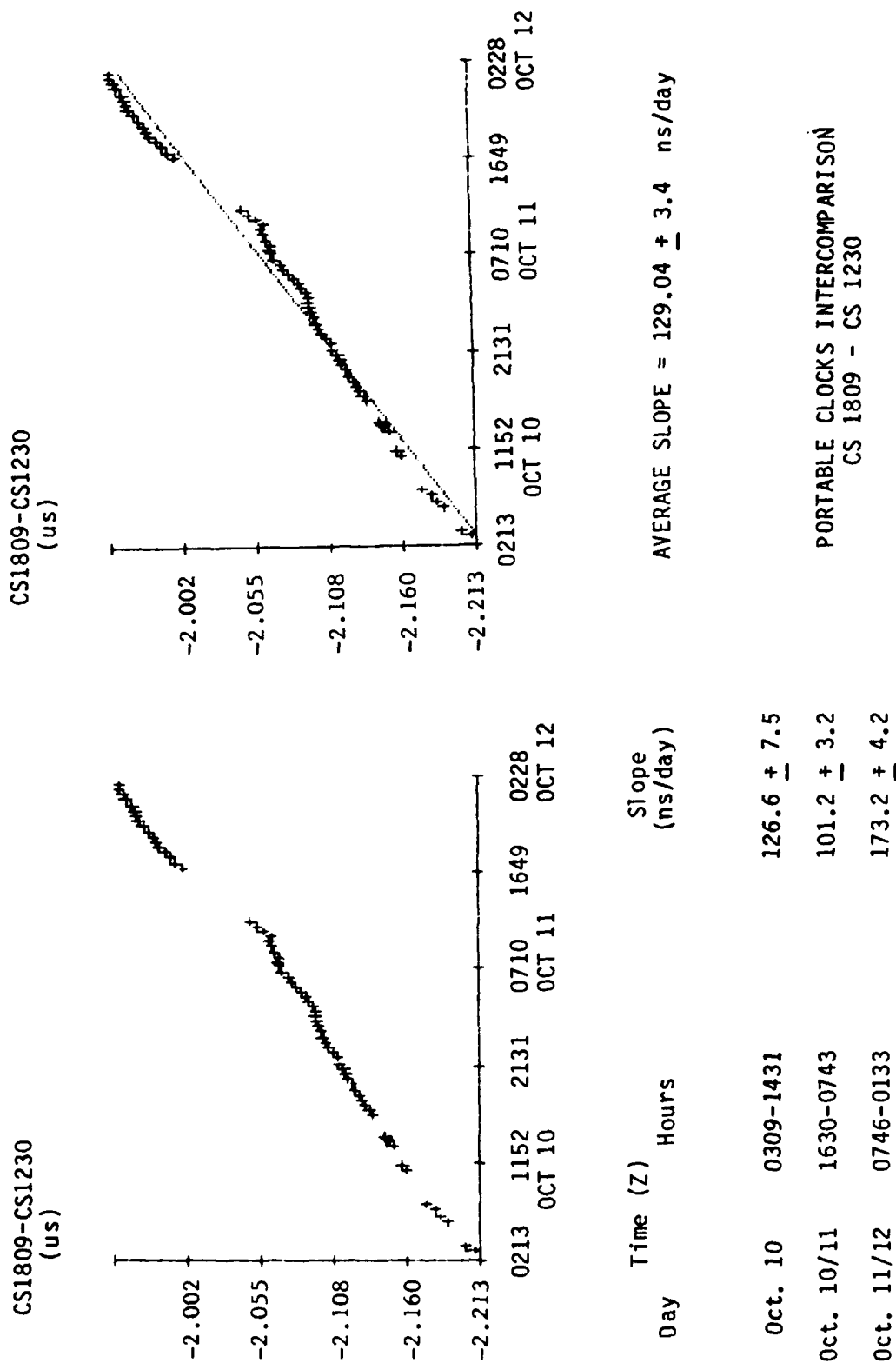
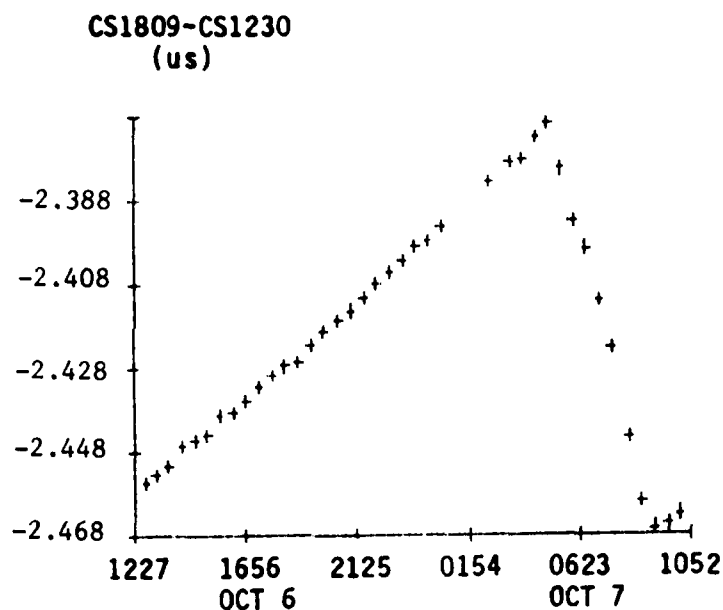
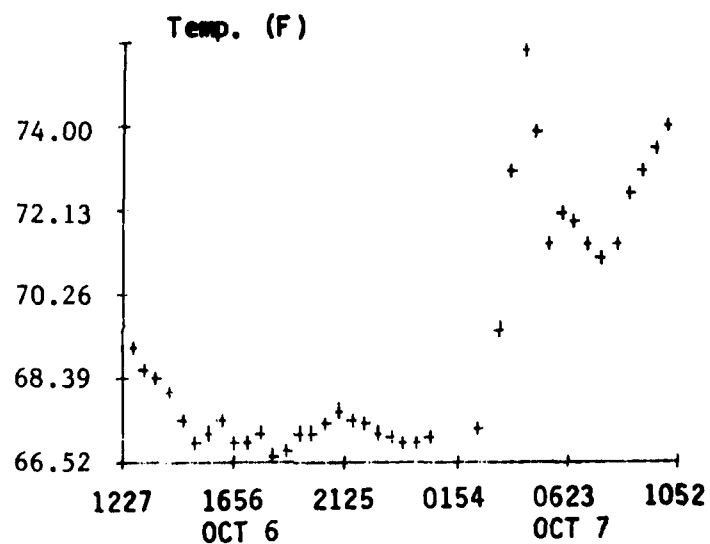


FIG. 13 - INTERNATIONAL TIME TRANSFER AND PORTABLE CLOCK EVALUATION
USING GPS TIMING RECEIVERS

PORTABLE CLOCKS INTERCOMPARISON
CS 1809 - CS 1230



Slope = 121.9 ± 2.1 ns/day



AVERAGE TEMPERATURE = 69.2 degrees (F)

FIG. 14 INTERNATIONAL TIME TRANSFER AND PORTABLE CLOCK EVALUATION
USING GPS TIMING RECEIVERS

CLOCKS STATISTICS TABLE

=====

CS 1809 - CS 107 (\$)

- * AVERAGE FRACTIONAL FREQUENCY OFFSET = 198.9 ns/day
- * STANDARD DEVIATION = 12.50 ns/day = 1.4×10^{-13}
- * MAXIMUM FREQUENCY OFFSET = 207.6 ns/day
- * MINIMUM FREQUENCY OFFSET = 168.0 ns/day
- * RANGE (MAXIMUM - MINIMUM) = 39.6 ns/day

CS 1809 - CS 1230

- * AVERAGE FRACTIONAL FREQUENCY OFFSET = 129.8 ns/day
(1 point filtered)
- * STANDARD DEVIATION = 40.67 ns/day = 4.7×10^{-13}
- * MAXIMUM FREQUENCY OFFSET = 194.8 ns/day
- * MINIMUM FREQUENCY OFFSET = 78.5 ns/day
- * RANGE (MAXIMUM - MINIMUM) = 116.3 ns/day

Note:

(\$) - Days Oct. 8 and 9 were not considered (two power failures)

 *
 * SYNCHRONIZATION LINKS CAPABILITIES *
 *

Link -----	Expected accuracy -----	Comments -----
PORTABLE CLOCKS	10-100 ns	Degrading with elapsed time
GPS RECEIVERS	50-100 ns	Worldwide
LORAN-C	100 ns	Local (between IEN and La Spezia)
LORAN-C	1-10 us	Intercontinental (between IEN and USNO)
TV	10-50 ns	Local (between IEN and La Spezia)
TRANSIT	10-30 us	Worldwide
CS CLOCKS INTERCOMPARISON	1-5 ns	Local (within the same laboratory)

TABLE V
314

GPS TIMING-NAVIGATION EXPERIMENT

REAL-TIME SYNCHRONIZATION LINKS

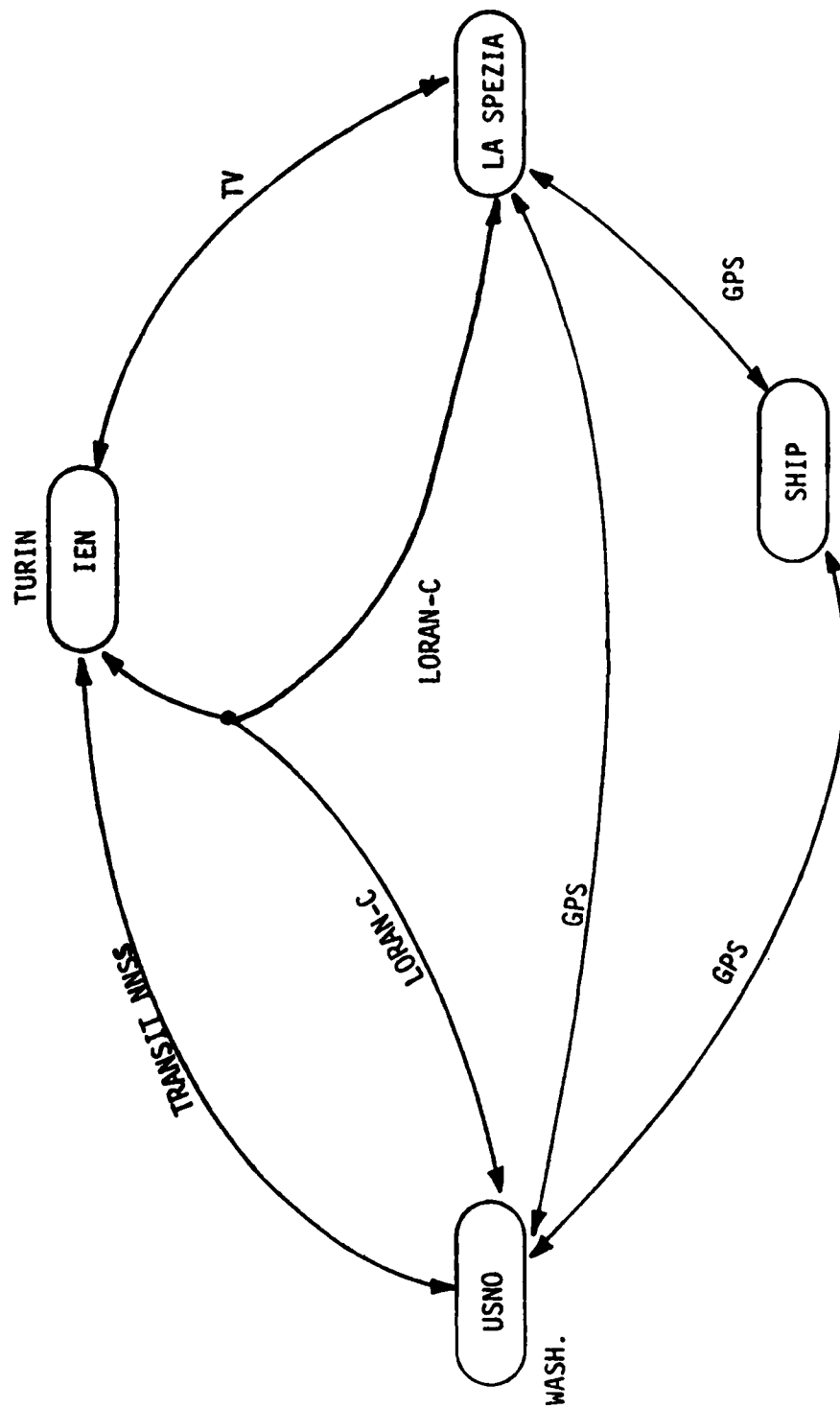
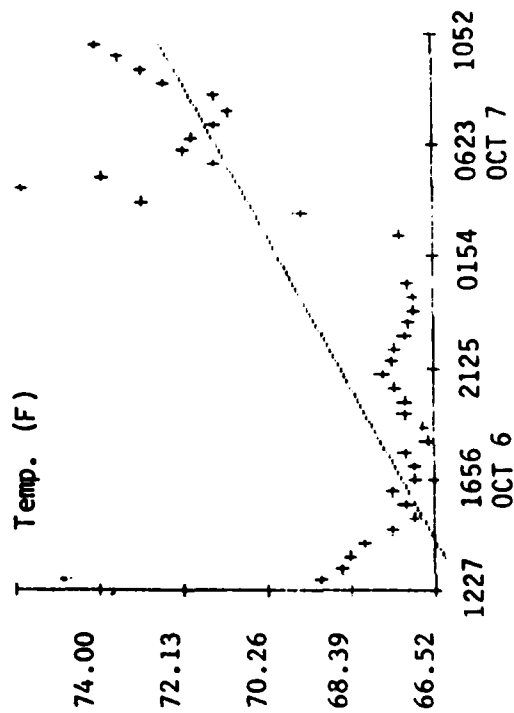


FIG. 15



TEMPERATURE ANALYSIS CHART

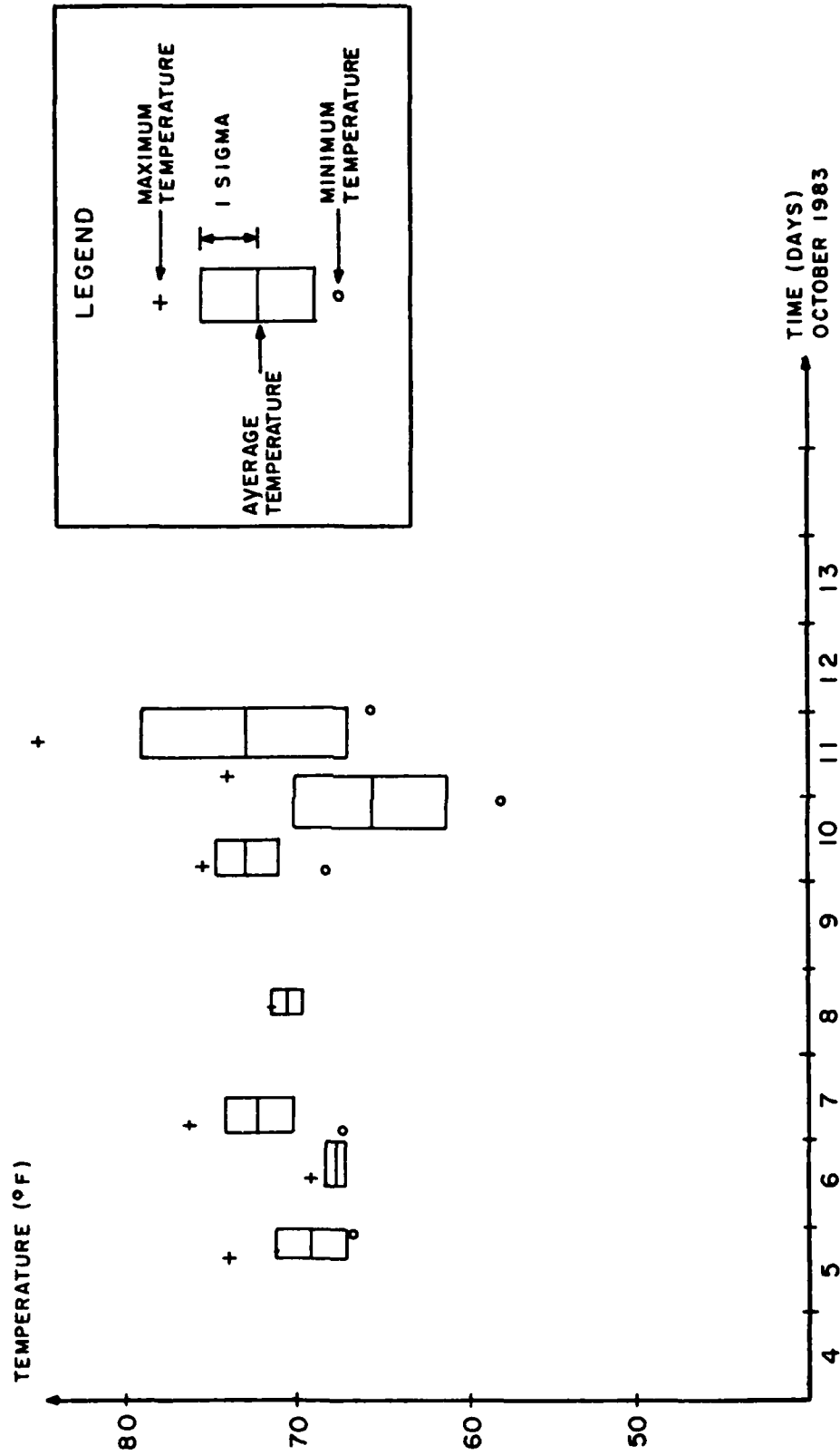


FIG. 17

TEMPERATURE STATISTICS =====

DAY	Start time (Z)	Stop time	Average Temperature	Standard Deviation	Max Temp.	Min Temp.	Max-Min
(October)							
5/6	1441	0012	69.14	2.11	72.8	66.9	5.90
6/7	1253	0048	67.41	0.59	69.1	66.7	2.40
7	0247	1707	72.2	1.9	75.7	67.3	8.4
8	1145	1803	70.5	0.7	71.4	69.4	2.0
10	0309	1431	72.6	1.8	75.2	69.2	6.0
10/11	1630	0743	65.4	5.4	73.6	57.9	15.7
11/12	0746	0133	72.8	5.8	85.1	65.9	19.2

INTERNATIONAL TIME TRANSFER AND PORTABLE CLOCK EVALUATION
USING GPS TIMING RECEIVERS

TABLE VI

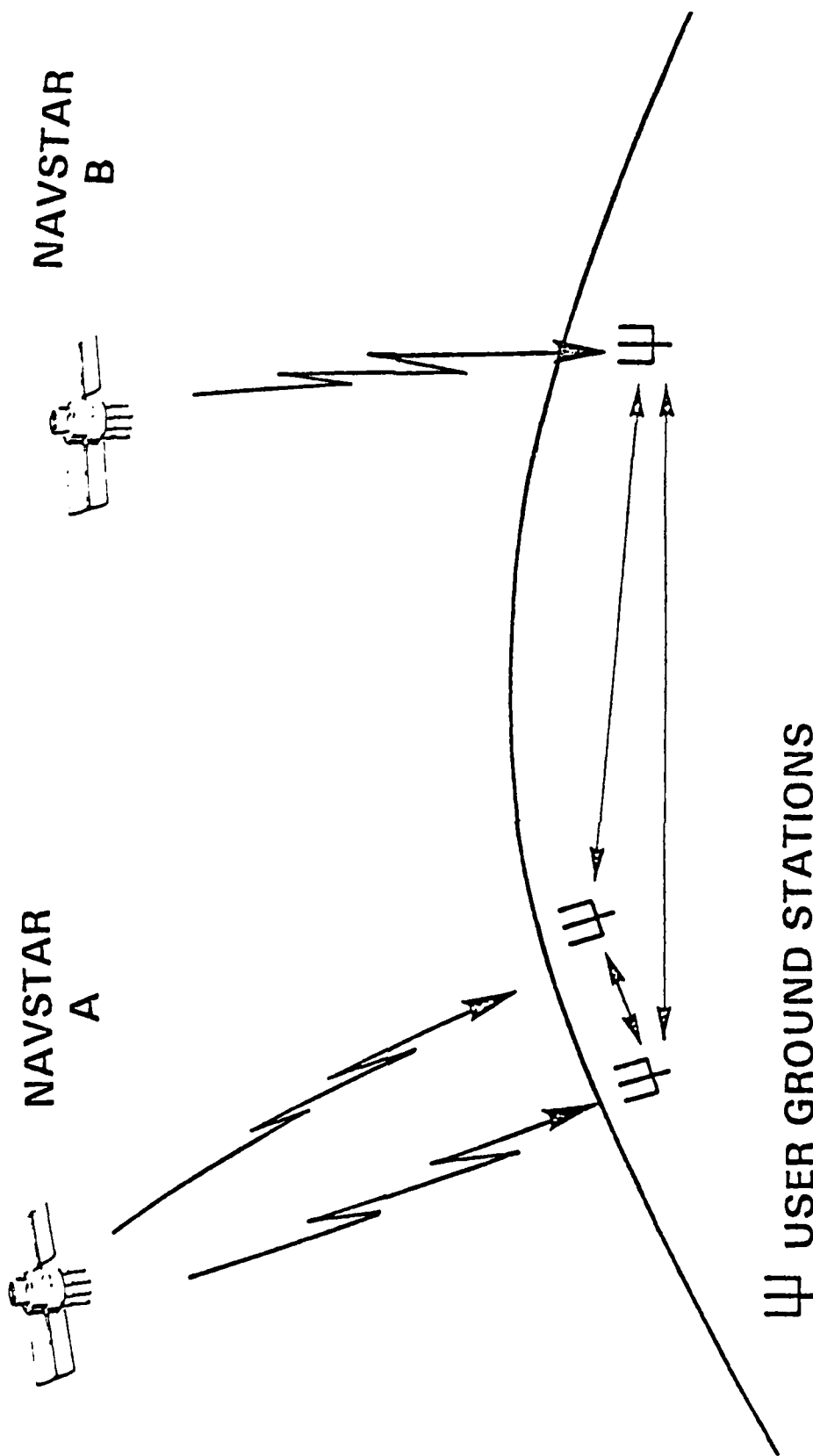


FIG. 18
NAVSTAR GPS Station Synchronization by Time Transfer

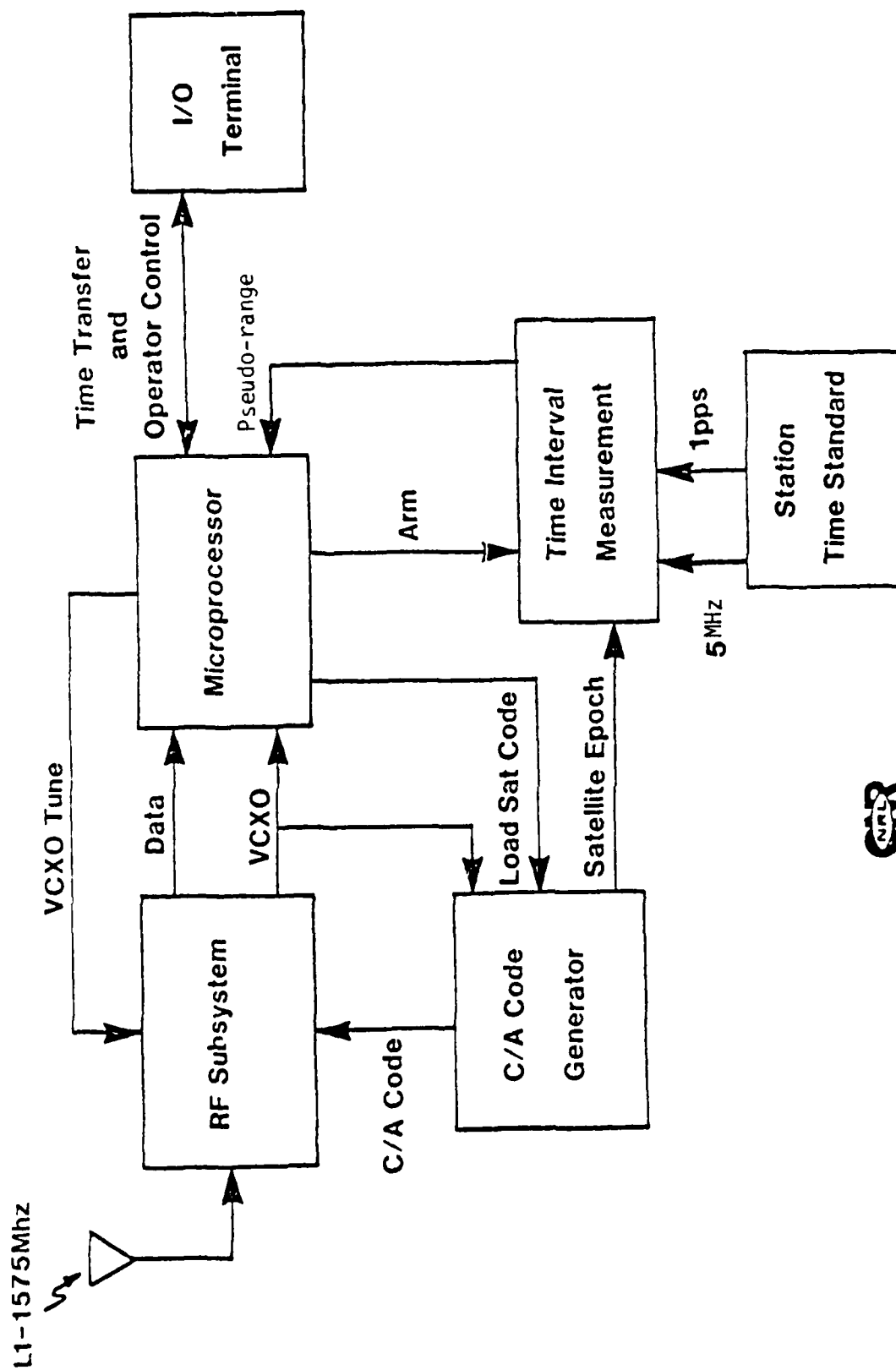
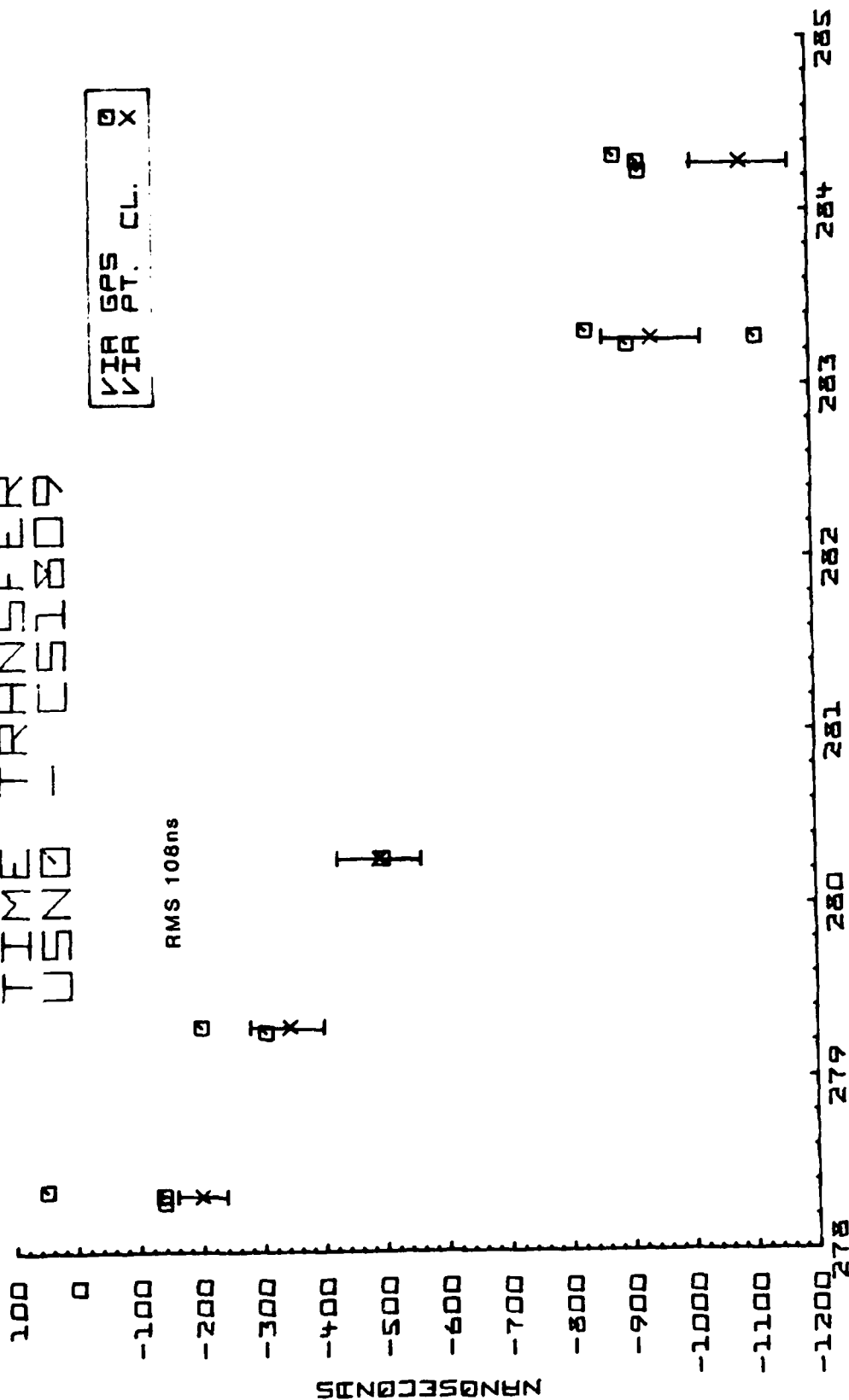


FIG. 19,
GPS Time Transfer Receiver Block Diagram

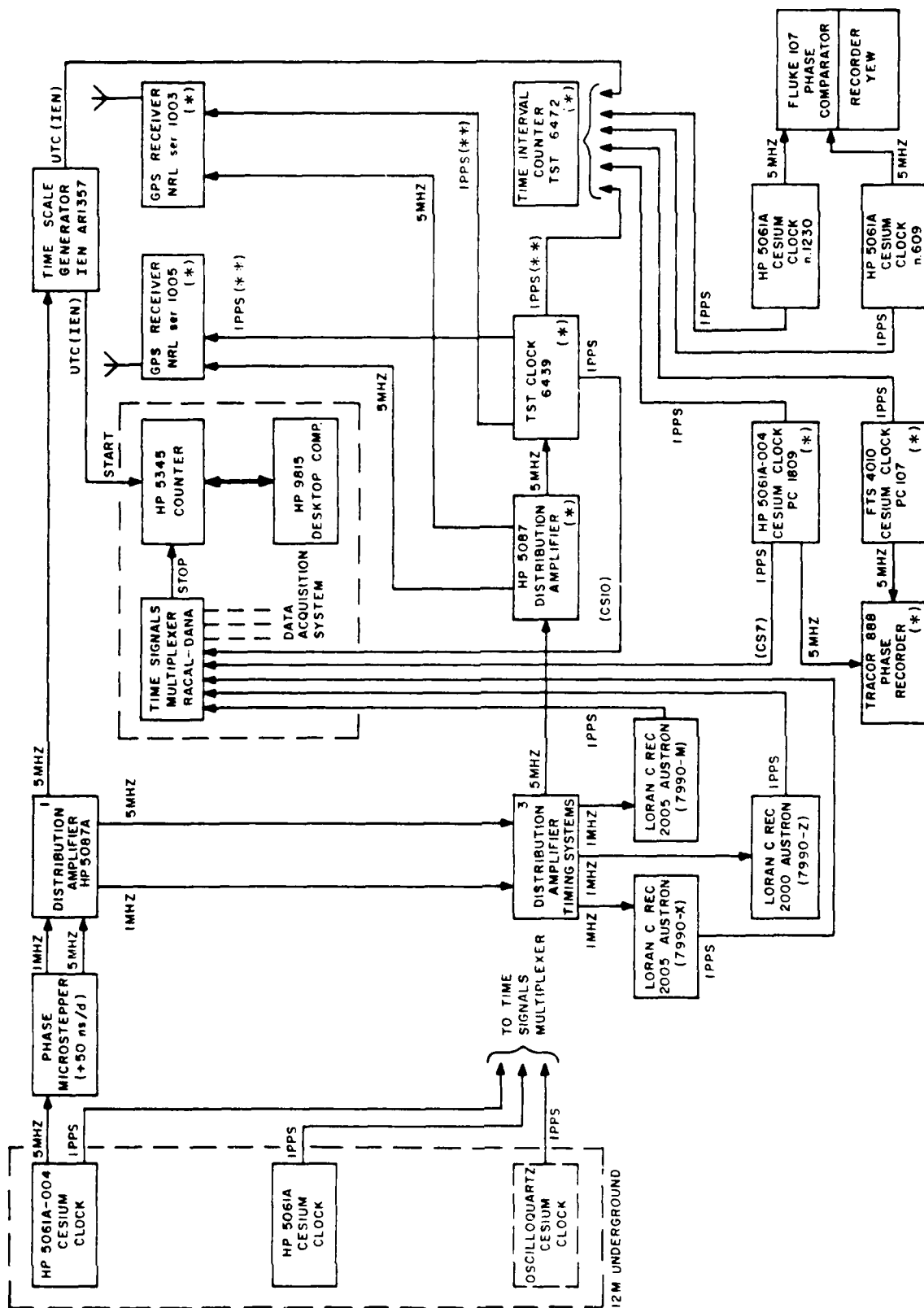
MOVING SHIP TIME TRANSFER USNO - C51809



DAY - 1983

Fig. 20

EQUIPMENT SET-UP AT IEN DURING THE GPS EXPERIMENT 13-20 OCT 1983



(*) U.S. EQUIPMENT
 (**) 1PPS ≡ UTC (IEN)

FIG. 21



Fig. 22 - The Time-keeping facilities at IEN (Torino)



Fig. 23 - Underground clock vault at IEN

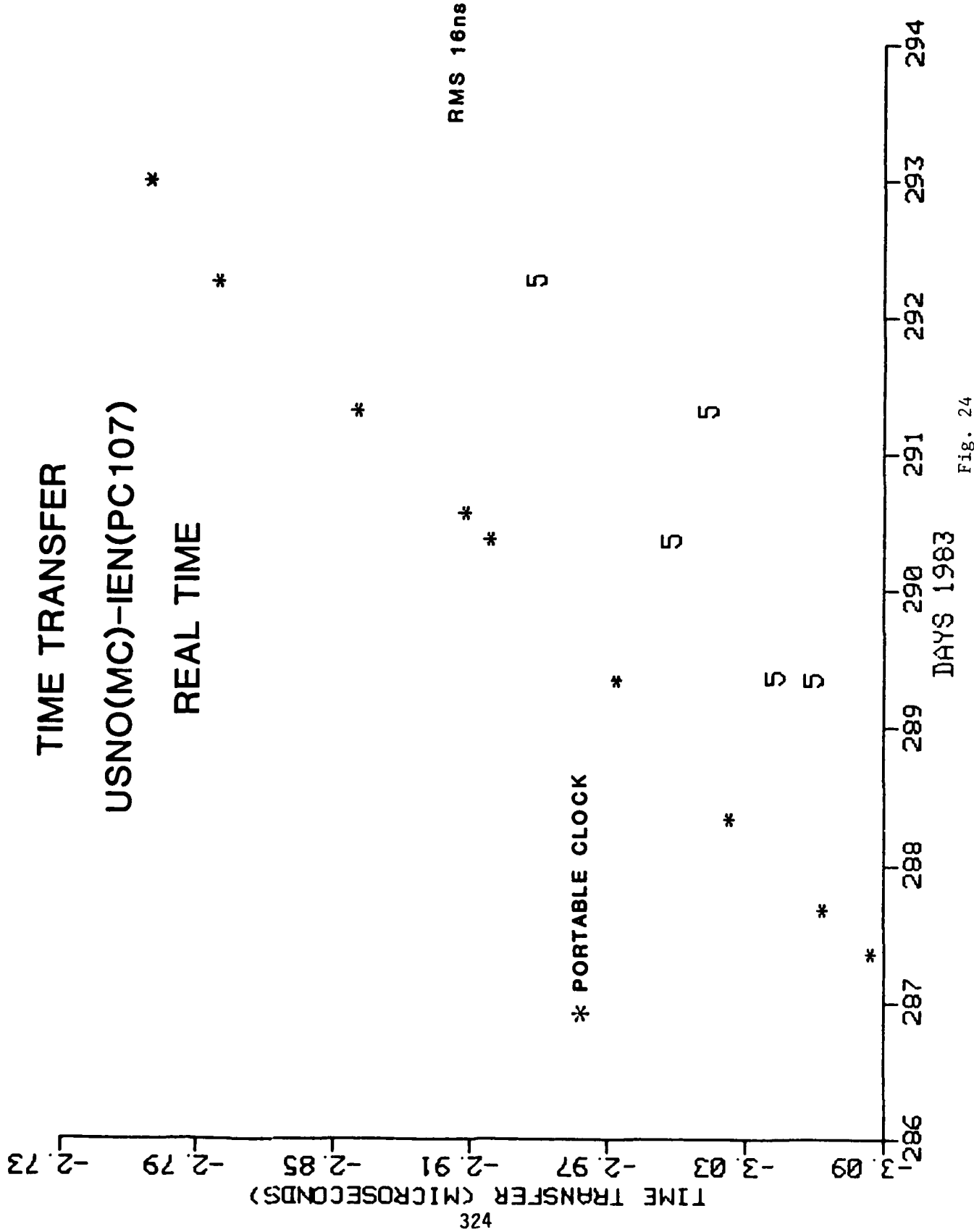


Fig. 24

TIME TRANSFER USNO(MC)-IEN(PC107)

PRECISE

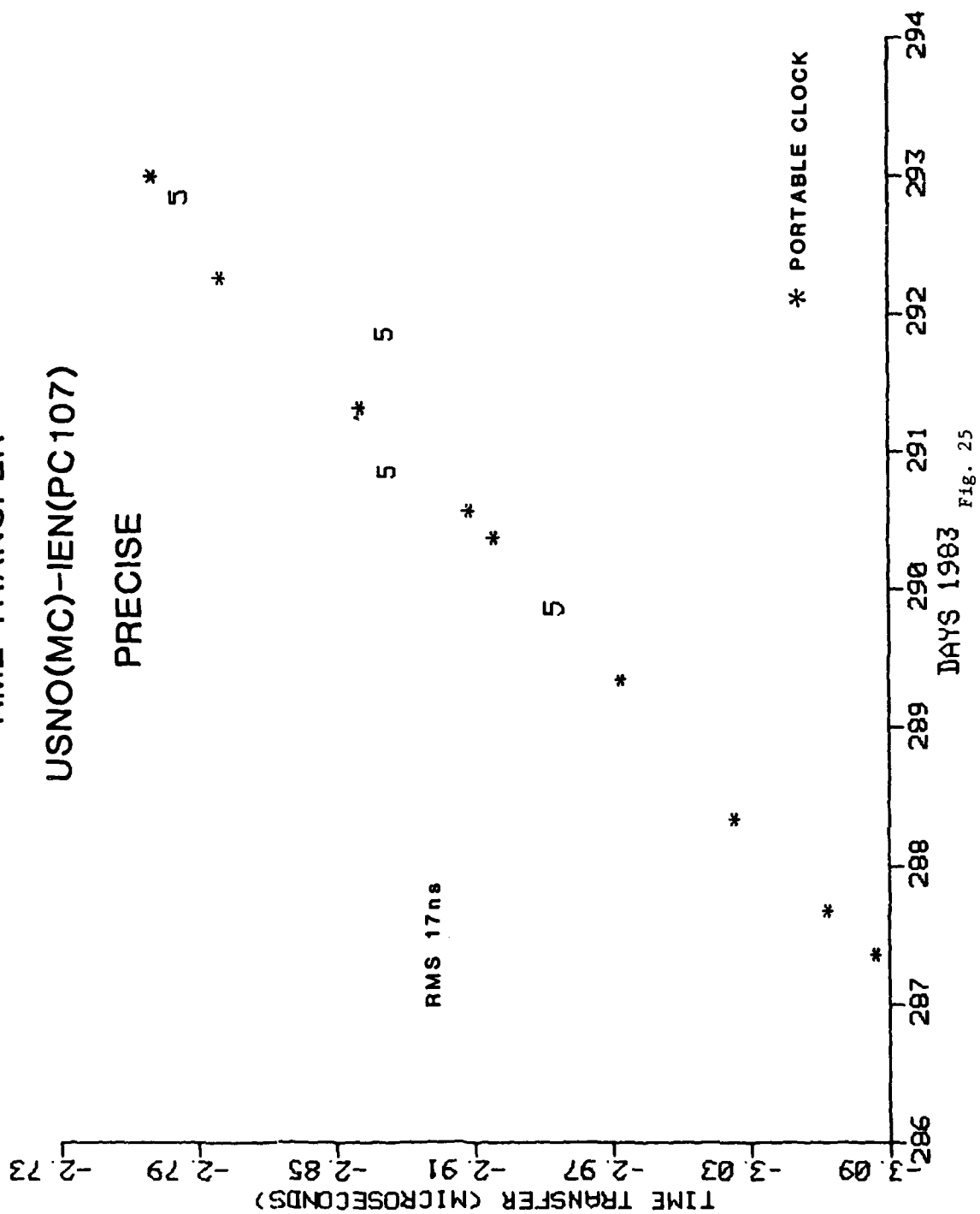


Fig. 25

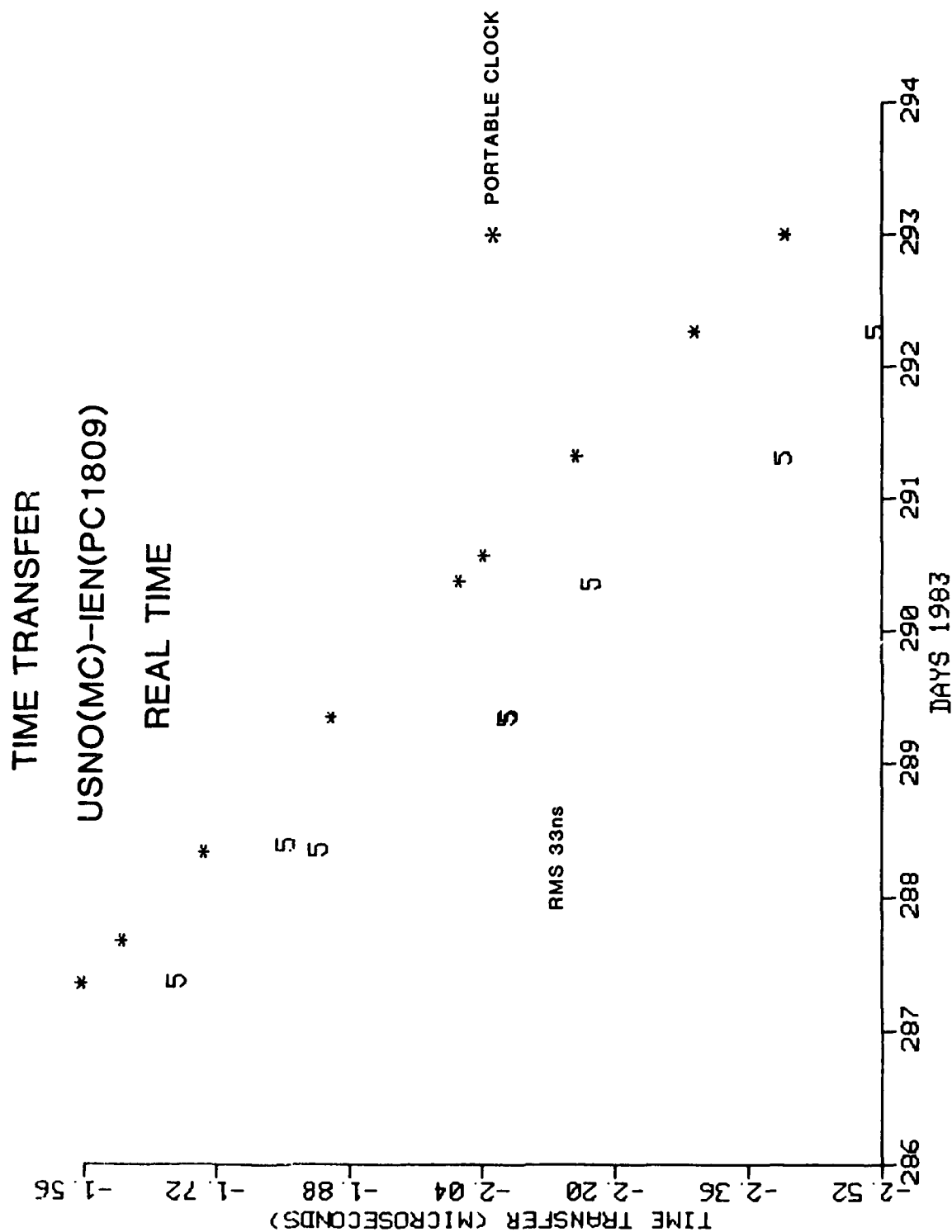


Fig. 26

TIME TRANSFER USNO(MC)-IEN(PC1809) PRECISE

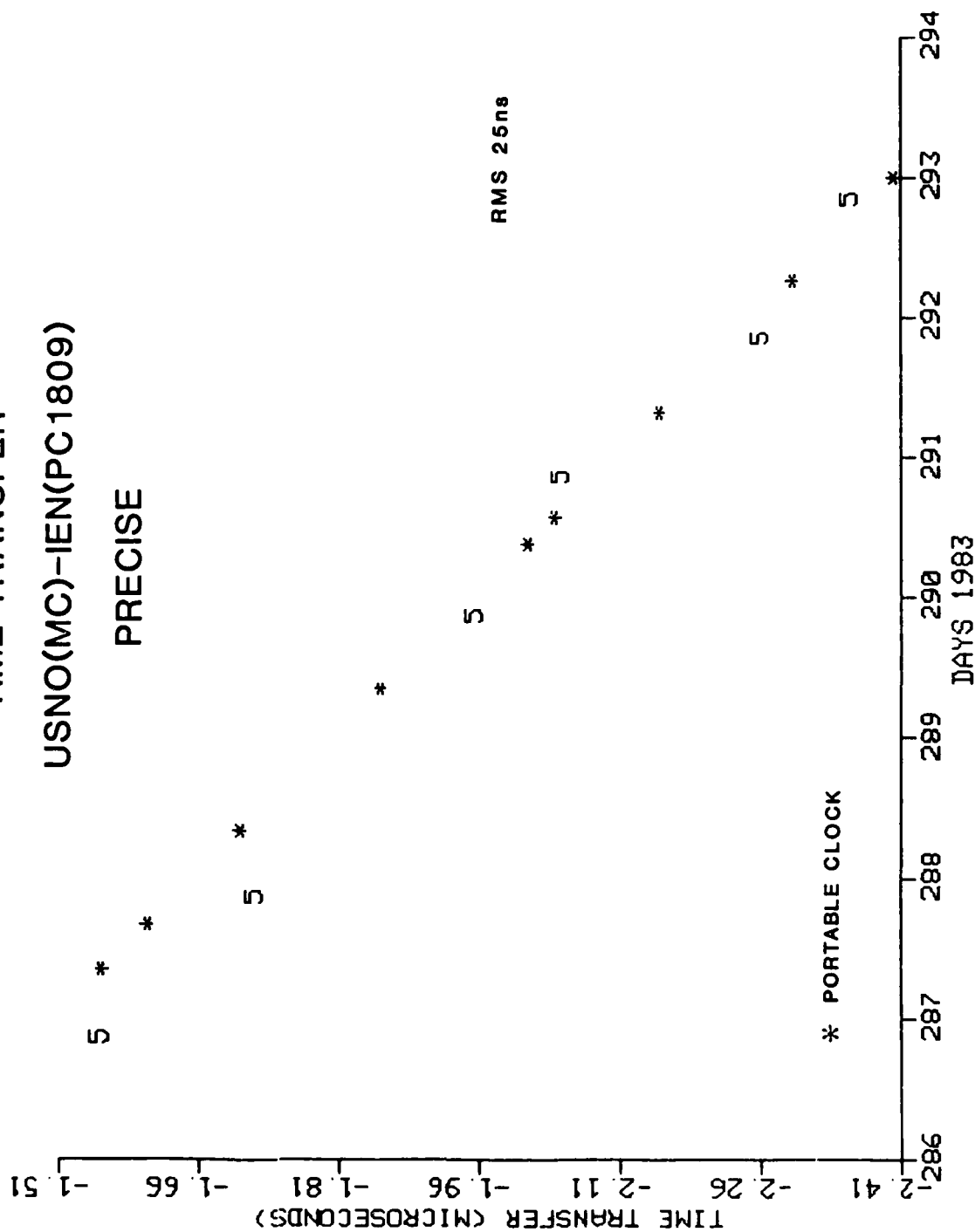


Fig. 27

TIME TRANSFER

USNO(MC)-IEN

REAL TIME

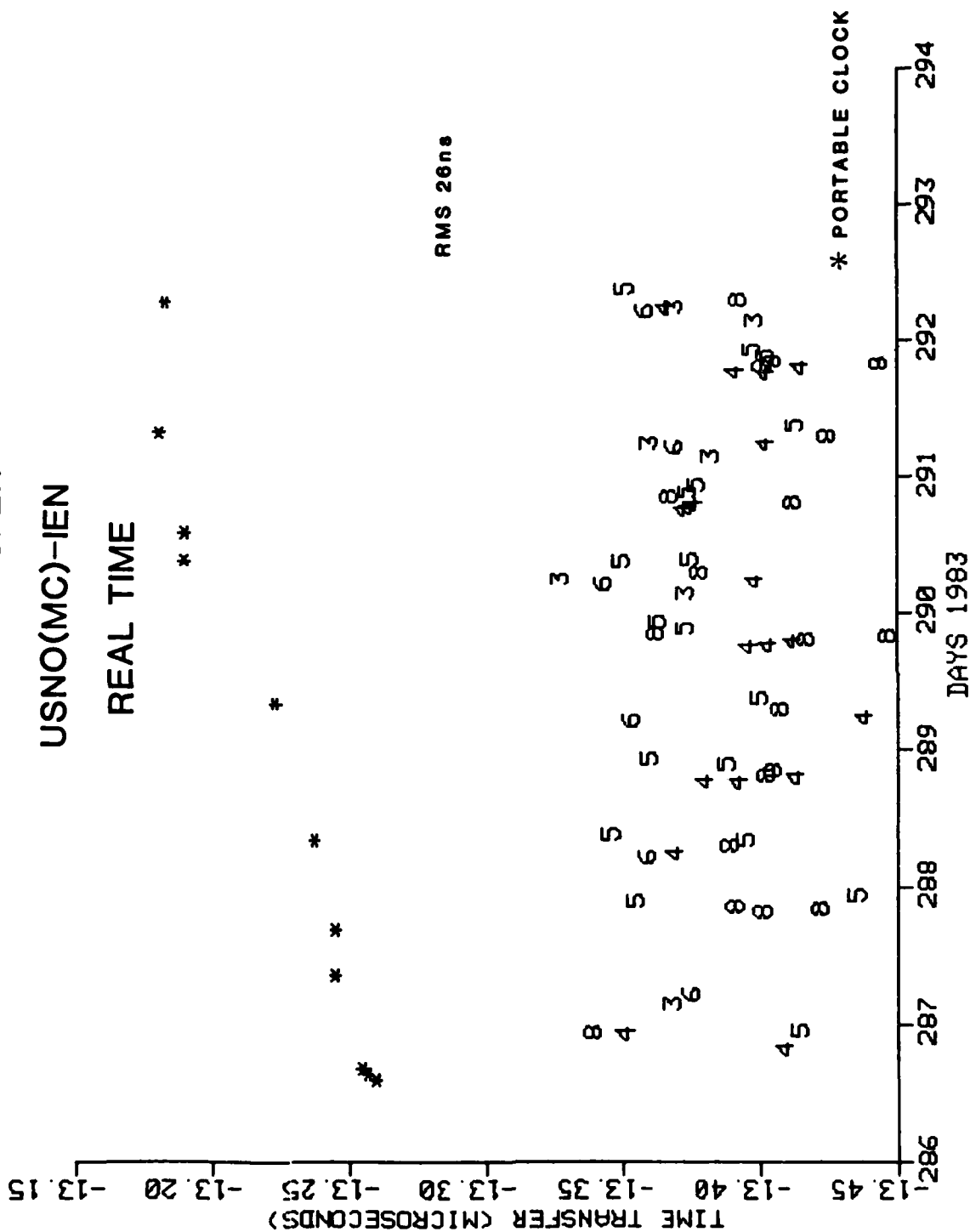


Fig. 28

TIME TRANSFER

USNO(MC)-IEN

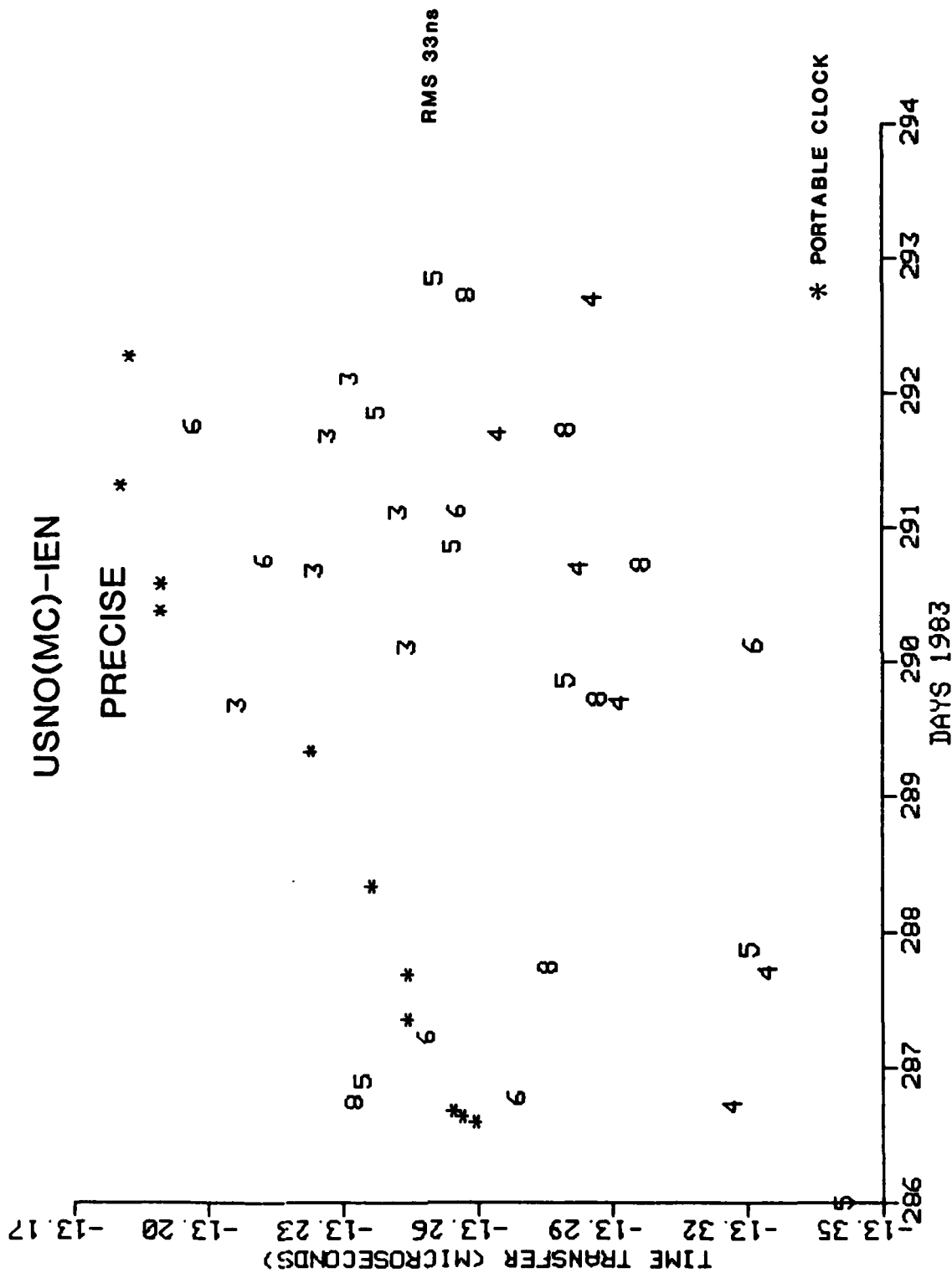


Fig. 29

QUESTIONS AND ANSWERS

MR. JOHNSON:

Andy Johnson, Naval Observatory. Could that thirty meters be reduced by repeated observations over several days from the G.P.S.?

MR. DETOMA:

Yes. As was shown yesterday, the positioning accuracy is much better than the navigation accuracy. This is for a lot of reasons. Also, not only for inaccuracy of the measurement itself, but also for the reason to maintain a straight course of the ship during the period of time between thirty minutes and one hour.

So you can expect an improvement in the order of magnitude, well, probably not in the order of--but at least three times when you perform the synchronization without knowing your position in a fixed site. The results I presented at the I.E.N. were obtained by using the coordinates that were given in the WGS-72 System. But, as was shown yesterday, they were not significantly different from the coordinates obtained from the positioning solution from the receiver.

They were different, if I remember, around ten to fifteen meters maximum in longitude, and less than ten meters in latitude. In average, they were less than ten meters in absolute position. So you can expect almost as good result as was presented here, in a fixed position; but for the time synchronization aboard the ship, we were talking about synchronizing clock while the ship was moving, which is a completely different environment.

SPREAD SPECTRUM TIME TRANSFER EXPERIMENT VIA INTELSAT

Dr. P. Hartl, Institut für Navigation der
Universität Stuttgart, West Germany

L. Veenstra, COMSAT Laboratories,
Clarksburg, Maryland

N. Gieschen, K.-M. Mussener, W. Schafer,
C.-M. Wende, Institut für Luft und
Raumfahrt der Technischen

Universität Berlin, West Germany

Dr. W. Klepczynski, USNO, Washington, DC

H.-H. Nau, R. Stoiber, Deutsche Forschungs
und Versuchsanstalt für Luft
und Raumfahrt, Oberpfaffenhofen,
West Germany

ABSTRACT

A two-way time synchronization experiment was performed in July 1983, between Washington, D.C. and Oberpfaffenhofen, Federal Republic of Germany. The experiment used the 14/11-GHz transponders on the INTELSAT V Atlantic spacecraft. The MITREX (Microwave Time and Ranging Experiment) modem designed, developed, and constructed at the Technical University of Berlin was employed. The experiment was jointly conducted by COMSAT Laboratories and the Institute for Nachrichtentechnik, DFVLR, Oberpfaffenhofen, FRG, in cooperation with the United States Naval Observatory and the Institut für Luft- und Raumfahrt, TU Berlin.

The spread spectrum signal occupied a bandwidth of 4 MHz and used the power normally required by a single-voice carrier. The ground stations involved had parabolic dishes of 2.4 m ($G/T = 20$ dB/K) and 4.5 m ($G/T = 26$ dB/K). In the 4-MHz occupied bandwidth, the carrier-to-noise ratio was -11 dB. At this power level, the time transfer performance had rms-standard deviations of better than 1 ns.

The experimental results confirm that an international time transfer and clock synchronization network using communications satellites is economically viable when using a spread spectrum transmission format.

INTRODUCTION

During 1978 and 1979, COMSAT Laboratories participated in an experiment of time and frequency synchronization via the CTS satellite [1],[2]. This experiment demonstrated the use of a conventional PSK data transmission to transfer time between primary standards. These previous experiments used a technique applicable to situations where it was desired to send time or frequency via an existing high speed digital satellite link. The disadvantage of the system was its high link requirements, 75 dB-Hz or more. This generally precluded use of such a system to directly interconnect standards labs with simple low cost small terminals.

In 1983 a new spread spectrum modem, the MITREX, was made available that did not require as much link power as the old PSK system. This unit required a nominal 55 dB-Hz, the same power as that of an SCPC voice channel [3].

The MITREX (Microwave Time and Ranging Experiment) modems, designed, developed, and constructed at ILR*, were originally intended for use with the SIRIO-2 satellite

- to support the LASSO (Laser Synchronization from Stationary Orbit) project with additional ranging information
- for comparison of different time transfer techniques (laser/microwaves) under the same conditions.

The applied concept makes use of the operating transponders in the same way as do telecommunication systems. First modem tests in the laboratory showed a very promising performance; therefore, after the launch failure of the SIRIO-2 satellite, the U.S. Naval Observatory (USNO) arranged with COMSAT for time transfer tests

*ILR = Institut für Luft- und Raumfahrt, the Aerospace Institute of Technical University of Berlin (TUB)

with this modem. For the ILR this experiment is part of an experimental study for time and ranging concepts which is sponsored by the German Ministry for Science and Technology (BMFT).

This experiment evaluated the performance of the MITREX modem under simulated and actual satellite links. As part of the experiment, a time transfer between UTC (USNO) and UTC (PTB) was made. The experiment was conducted using the 11/14-GHz spot beam transponders on the INTELSAT primary Atlantic Ocean region satellite (INTELSAT V F3). COMSAT provided a transportable 2.4-m earth station at USNO that was connected directly to the master clock. In Germany, a 4.5-m fixed station at DFVLR* (Oberpfaffenhofen) was used. A portable cesium clock was used to close the time transfer link to the PTB master clock.

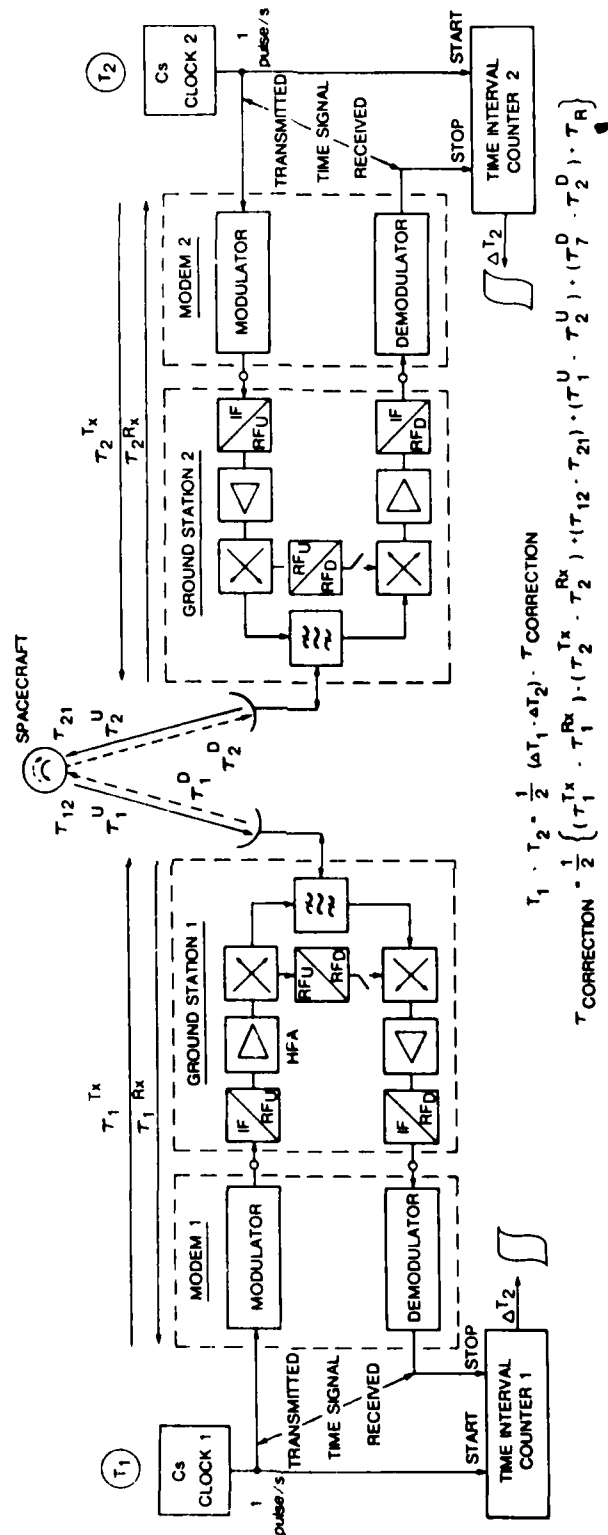
MODEM DESCRIPTION

The time transfer techniques require each station to transmit a "time mark," e.g., a pulse, and to receive the time mark transmitted by the opposite station. The transmitted time mark need not appear periodically; only coordination with the local time scale is necessary. The basic concept for 2-way satellite time transfer is described in Figure 1. Two separated clocks (representing the local time scale) are compared in their time values via the telecommunication channel of a geostationary satellite.

A special unit is needed to interface between the 70-MHz IF of a satellite ground station and the time-keeping hardware necessary to manage and to compare the time scale. This unit is called a modem (modulator/demodulator). It is housed in a 19-in. drawer and operates at the transmit part as a pseudo-random (pn) signal encoder and at the receive part as a corresponding pn signal decoder (Figure 2). The pn sequence which is used to spread the time signal over a large frequency band is of 2-MHz chip rate and has a period of 10^4 chips.

The generation of periodic sequences of the pn-type is accomplished by means of a shift register with prescribed feedback connections. An n-stage shift register is capable of generating a periodic output sequence whose maximum length is $p = 2^n - 1$. These maximal sequences have certain properties which

*DFVLR = Deutsche Forschungs-und Versuchsanstalt für Luft-und Raumfahrt



Time
JS-50E

Figure 1

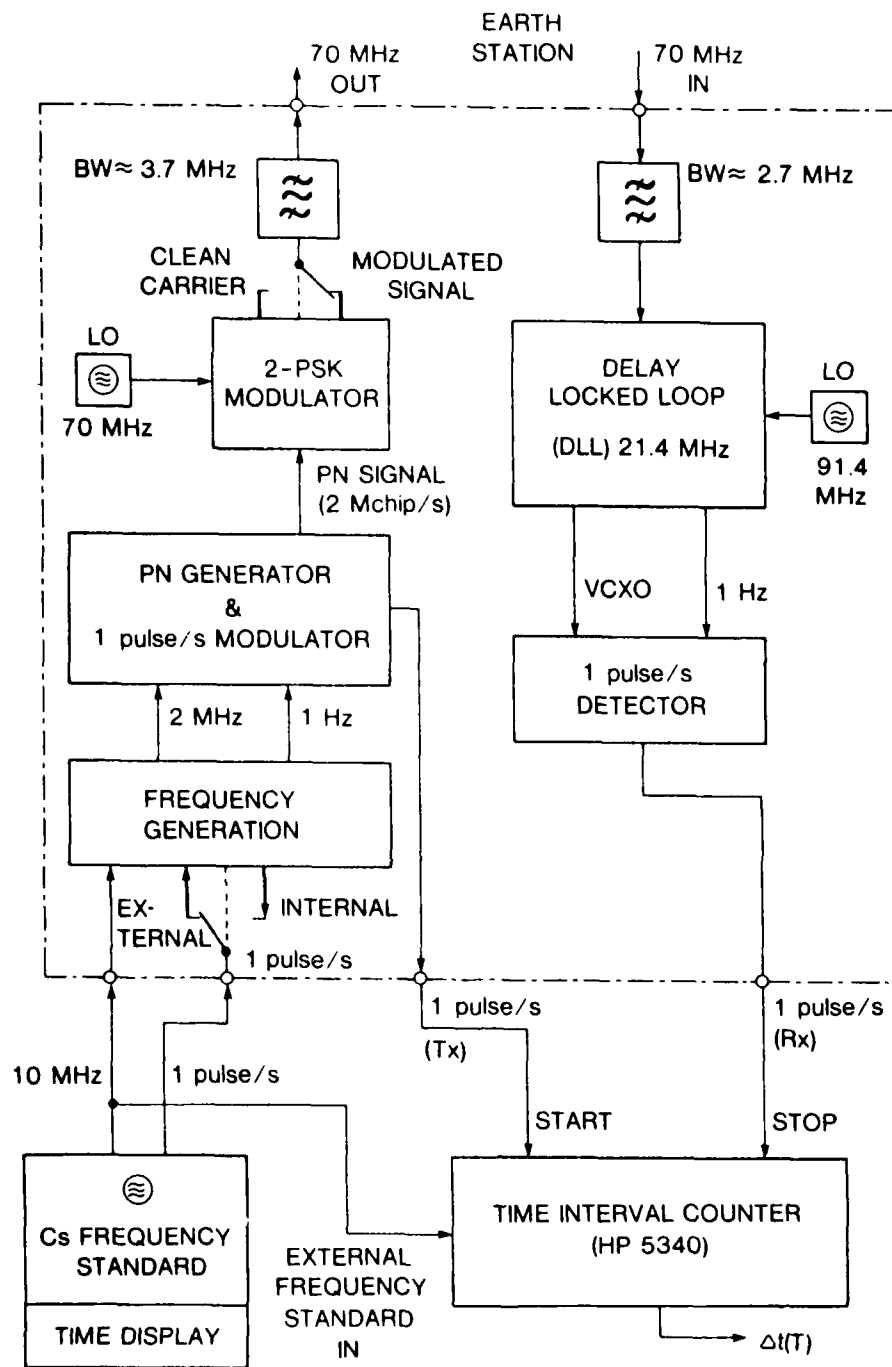


Figure 2

make them very useful, especially in ranging systems (see Figure 3). Our basic sequence of 10^4 chips is a truncated part of a maximal sequence of 16 383 chip length. The choice of this length is a weighing between acquisition time which grows with the length and cross correlation which is the smallest for a maximal length sequence. To ease the overall system design, especially the frequency generation, a sequence with a period which is an even number and some decade is used. To get the unambiguous range of 1 s, this basic sequence will be repeated continuously so that 199 times the same sequence is generated before in the period 200, the 1 pps (1 peak per second) is indicated (Figure 4). This indication happened by a sort of phase modulation. At the beginning of the sequence one chip will be deleted and in the middle one additional chip will be inserted. This modulation, called COBIPAM (Coded Bi-Phase Pulse Amplitude Modulation), will be detected in the receiver.

MULTIPLEXING

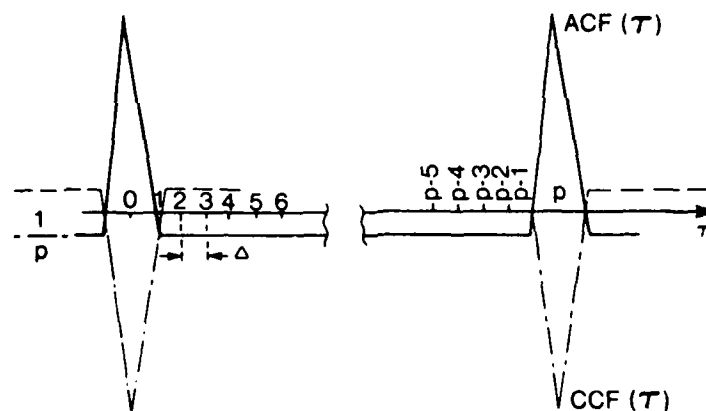
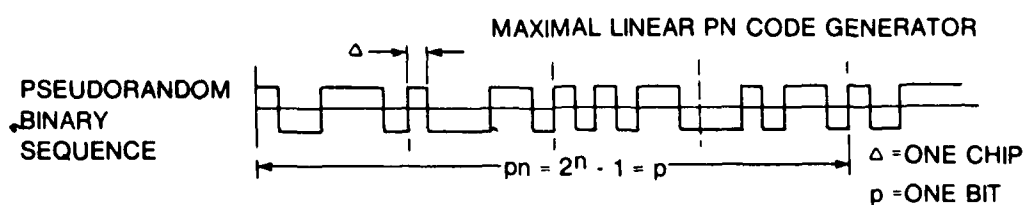
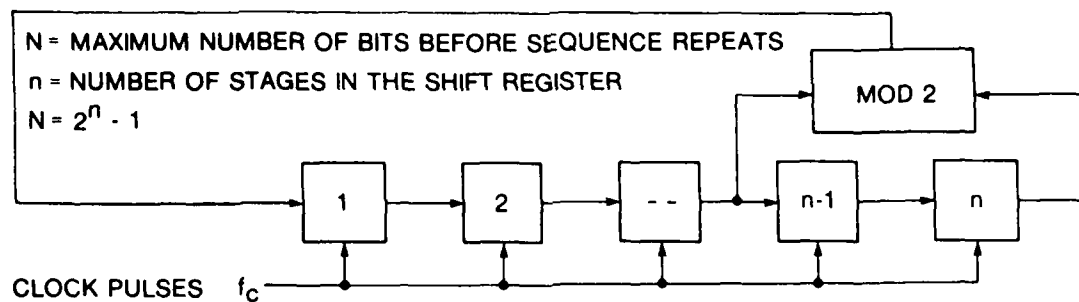
An important feature of pn-sequences is the code, multiplexing property. By using sufficiently orthogonal codes, it is possible to use the same frequency band for different users without disturbing each other. In the current modem, two codes are implemented but a number of 4 or 8 codes (with a sequence length of 10^4 chips) are possible without deterioration of the current modem quality.

TRANSMITTER (Figure 5)

Baseband input signals to the modem are standard frequency and the time tick 1 pps generated by the time standard to be compared, i.e., a cesium clock normally. In the current version, the standard frequency has to be 10 MHz, but with a simple modification, 5 MHz could also be used.

The incoming standard frequency is divided down to 2 MHz and then fed to the clock input of the pn-generator where the 1 pps is used to synchronize the generator with the atomic clock. This synchronizer provides also the pulse for starting the time interval counter.

Output signal of the pn-generator is the continuously repeated code pattern with a chip rate of 2 Mchip/s which is applied on the data input of a double balanced mixer to spread the spectrum of the 70-MHz carrier to the RF-bandwidth (2 PSK modulation). The RF spectrum has a $(\sin x/x)^2$ characteristic



$$ACF(T) = pn(T) \odot pn(t - T)$$

$$CCF(T) = pn(T) \odot \bar{pn}(t - T)$$

$$pn = \text{pn SEQUENCE } p = 2^n - 1$$

$$\bar{pn} = \text{THE SAME AS } pn, \text{ BUT INVERTED}$$

AUTOCORRELATION FUNCTION

CROSS-CORRELATION FUNCTION

Figure 3

pn SEQUENCE, 1 FRAME

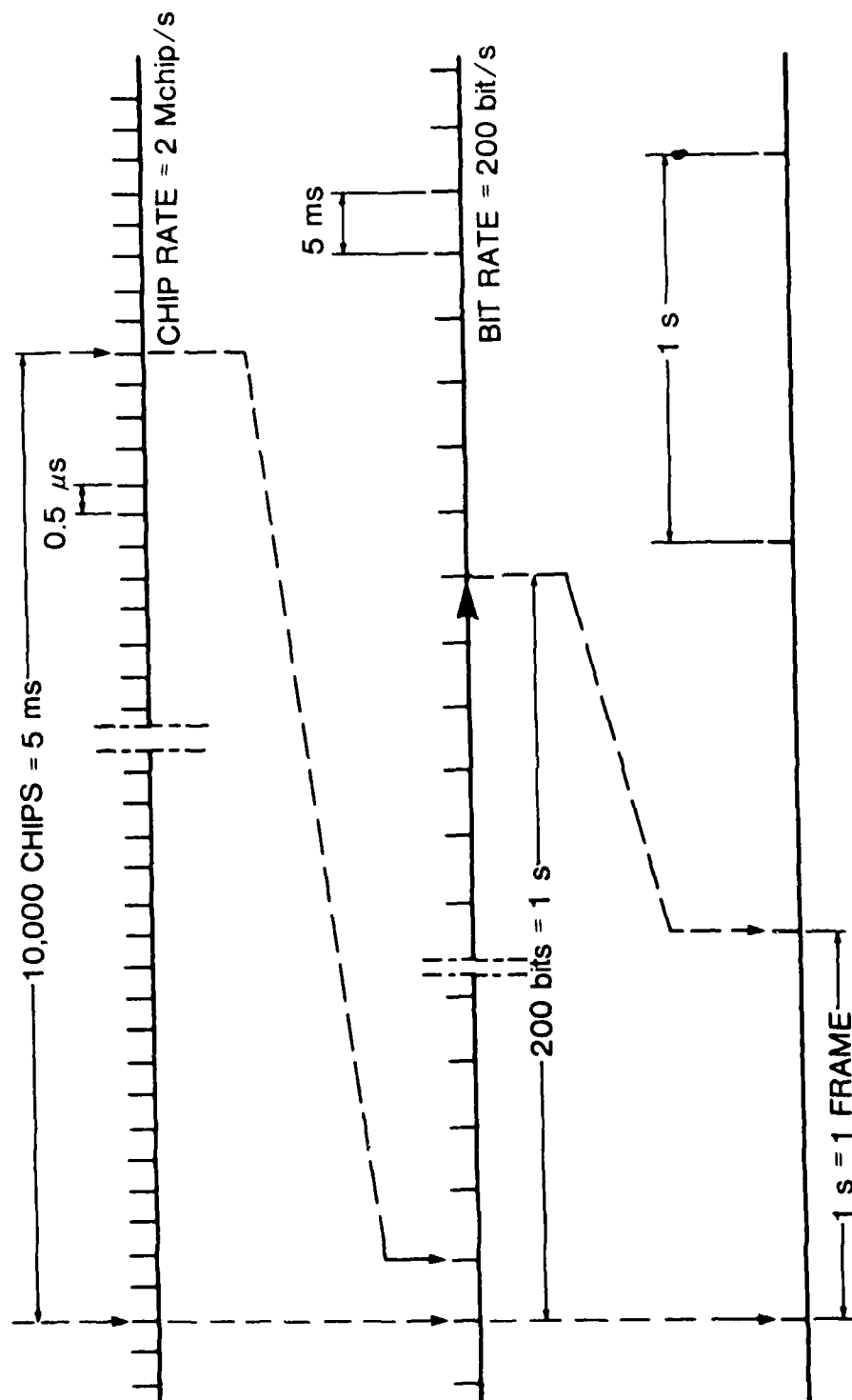


Figure 4

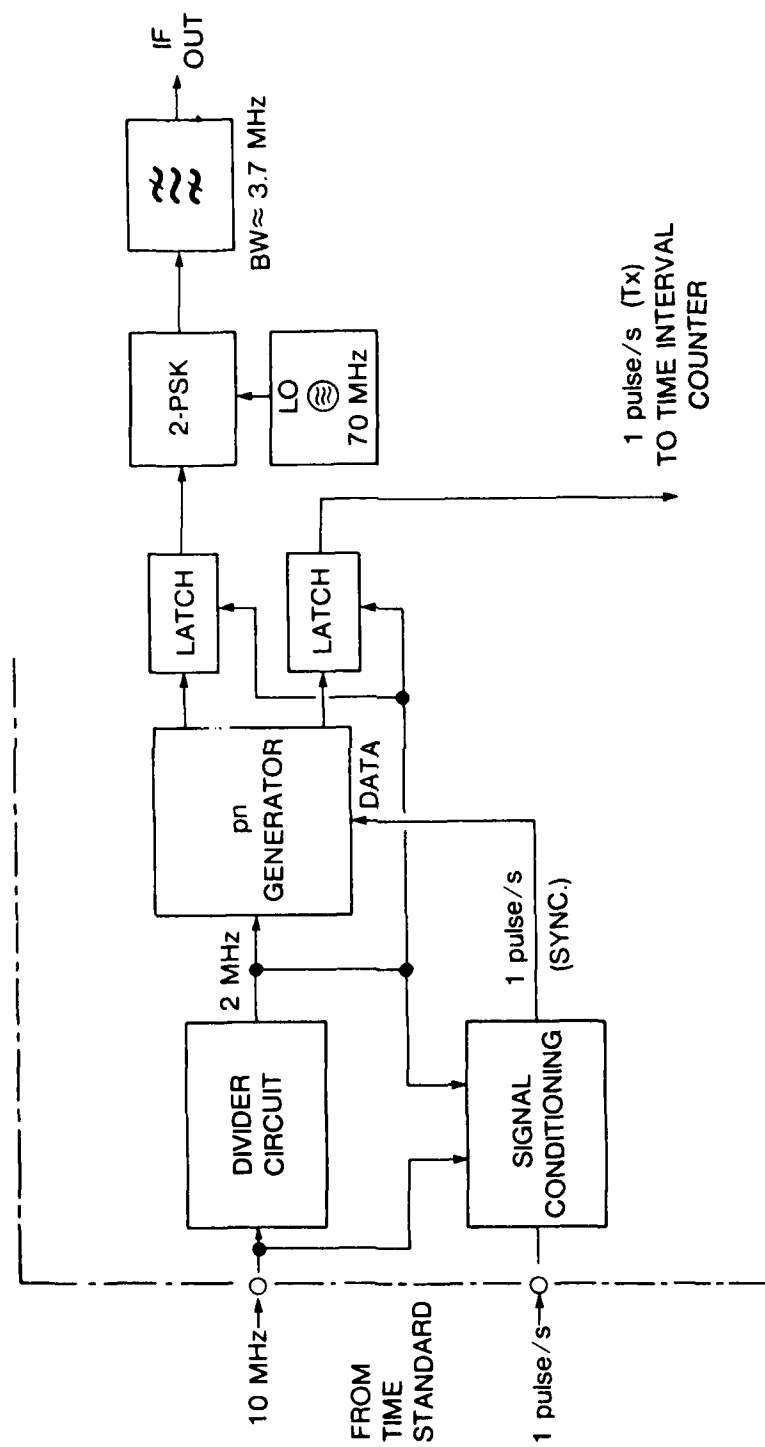


Figure 5

with a bandwidth of about 4-MHz (main lobe) and is suitable for satellite transmission (Figure 6).

Whereas a truly random chip stream has a continuous spectrum, this chip stream generates a spectrum with a fine structure of separate lines whose spreading is determined by the sequence repetition rate (200 Hz).

RECEIVER (Figure 7)

The received signal, after down-conversion to 70 MHz, will be applied on the IF input of the modem and will then pass a predetection filter with a bandwidth of about 2.7 MHz (3 dB). The choice of this bandwidth gives an additional receiver gain of about 1.5 dB (the noise contribution is proportional to the bandwidth while the correlation loss depends on the $(\sin x/x)^2$ shape) but the additional signal delay (and therefore the delay variations by ambient effects) are relatively small. The main part of the receiver is the delay-lock loop (DLL) which is a tracking loop with two separate correlators driven by identical, but delayed in time by one chip, code reference signals. The code itself is identical to the transmitter code. The correlator output signals, the auto correlation function (ACF) between local and transmitter code, are used to control the clock oscillator (VCXO) of the receivers pn-generator in such a way that the ACF is at the maximum level. Now, because the transmitter code reaches the receiver delayed by the transmission time, a reference mark generated at the local pn-generator can be used to stop the time interval measurement. The counter output is therefore proportional to the transmission time with some additional equipment delays which have to calibrate out.

The actual implementation of the tracking loop is shown in Figure 7. It is an IF correlator (IF frequency = 21 MHz) with phase detector for generating the VCXO control voltage. The 1 pps signal is detected by an amplitude discriminator of the auto correlation function. The jittered demodulated one pulse per second signal is used to gate out a single pulse of the VCXO clock; therefore, the resulting measurement jitter is that of the VCXO clock that is in turn used to generate the PN receive sequence.

In order to achieve the minimum of tracking jitter, the tracking loop is a modification of the "delay locked loop" [4]. In the MITREX modem, it is not the classical design of the DLL

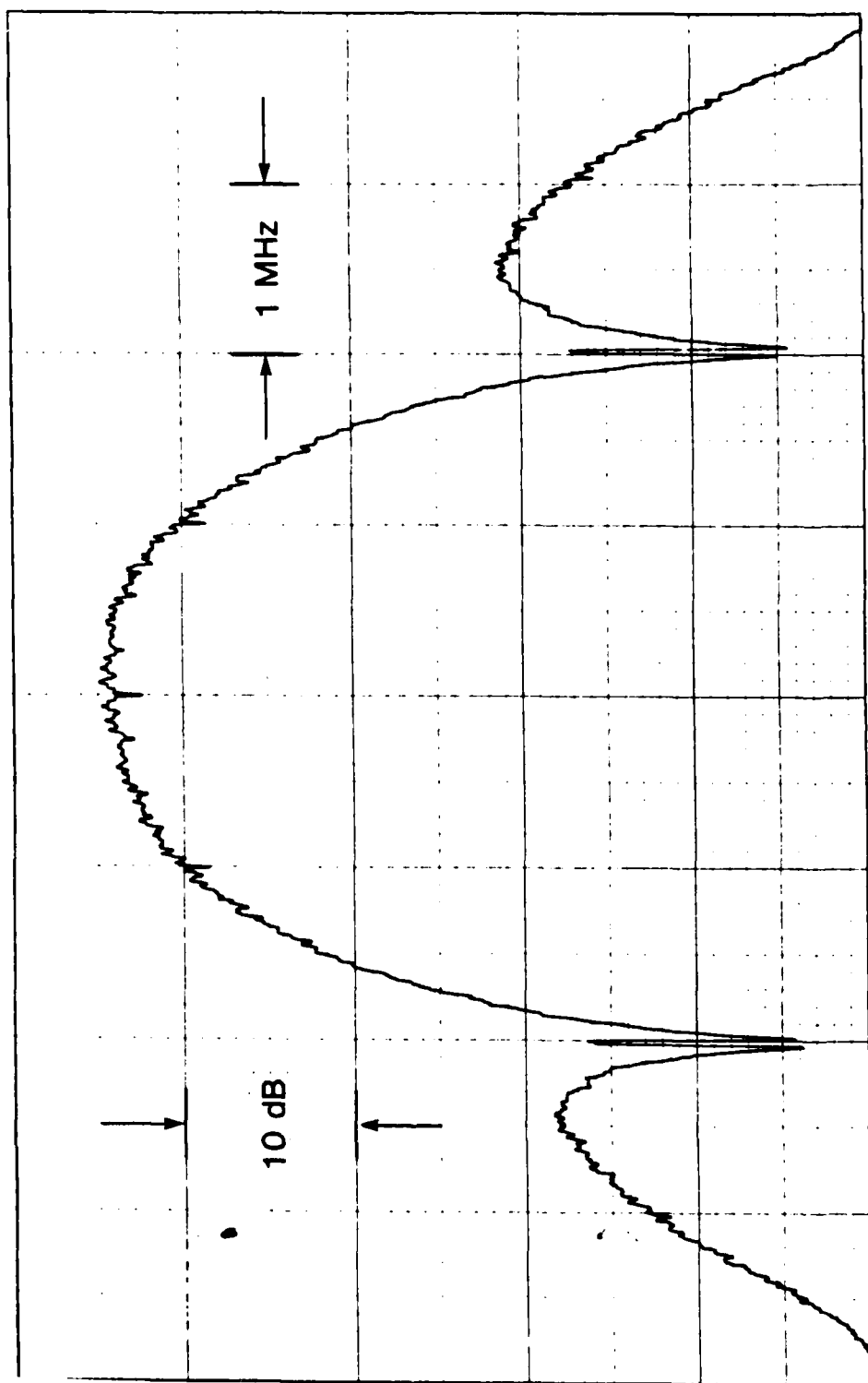


Figure 6

which is used, but rather a modified one, the idea of which goes back to Osborne [4].

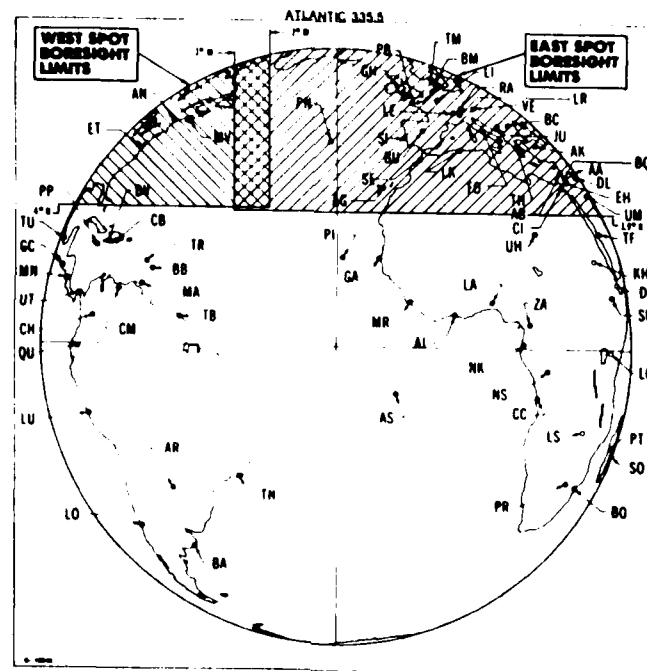
EARTH TERMINALS AND SATELLITE LINK

Two earth terminals that employed different antenna diameters were used in the experiment. The USNO site had an Advanced Communications Terminal (ACT) with a 2.4-m diameter antenna. The DFVLR used a roof-mounted 4.5-m antenna. Table 1 gives the details on the stations. Both stations were equipped with TWT amplifiers of the 200-W class although less than a watt was used. In fact, the exact transmit power was difficult to measure at this low level because of the broadband noise generated by the TWTA.

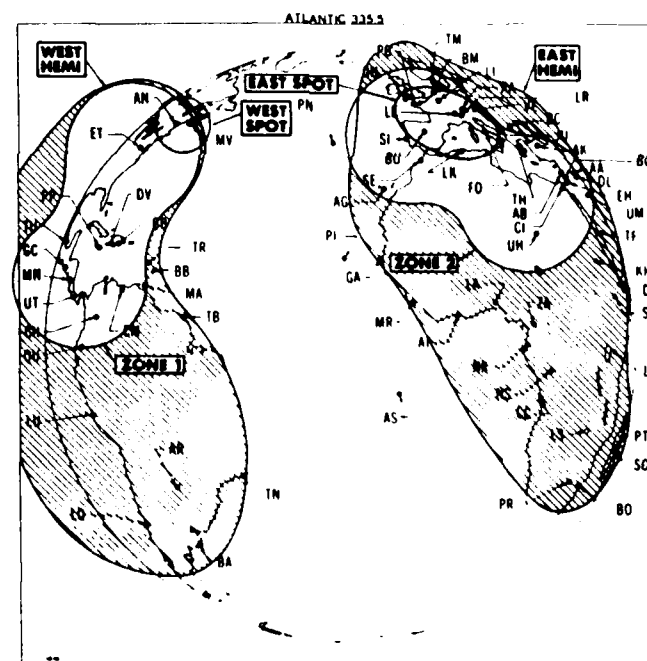
Table 1. Earth Station Parameters

	USNO ACT	DFVLR Oberpfaffenhofen
Antenna Diameter	2.4 m	4.5 m
Type	Prime Focus Parabolic	Prime Focus Parabolic
Polarization	Dual-Orthogonal Linear	Dual-Orthogonal Linear
Receive System Figure of Merit (G/T)	20 dB/K	26 dB/K
Maximum Possible e.i.r.p.	69 dBW	75 dBW

The satellite used was one of the new Atlantic region INTELSAT V spacecraft [6]. These are the first INTELSAT satellites to include 11/14-GHz transponders. The 11/14-GHz service is provided via spot beam antennas. These spots have limited steerability and coverage area, Figure 8. This restricts the service area that they can provide to the time transfer community. However, within the service area, the high gain resulting from the narrow spot beam antennas provides an excellent transponder for small terminal use. The link budget and the operational satellite specifications are shown in Tables 2 and 3. The low powers required in this experiment, 80 mW from the DFVLR transmitter and 170 mW from the USNO transmitter, are a function



*Spot-Beam Steering Capabilities
INTELSAT V Coverages*



*Atlantic Ocean Region
INTELSAT V Coverages*

Figure 8

Table 2. Transponder Characteristics

IS-503

West Spot	
Flux to saturate	-79.1 dBW/m ²
G/T	9.0 dB/K
e.i.r.p.	50.0 dBW
East Spot	
Flux to saturate	-77.6 dBW/m ²
G/T	6.5 dB/K
e.i.r.p.	46.5 dBW
Path Loss	
Up-Link	-207.9 dB
Down-Link	-205.9 dB

Table 3. Link Budget

From To	U.S. DFVLR	DFVLR U.S.	
Transmitter Power	0.17	0.08	W
Transmitter Power	-7.7	-10.8	dBW
Transmitter Gain	46.9	54.0	dB
e.i.r.p.	39.2	43.2	dBW
PL Up	207.9	207.9	dB
S/C G/T	9.0	6.5	dB/K
C/T Up	-159.7	-158.2	dBW/K
e.i.r.p.	39.2	43.2	dBW
PL Up	207.9	207.9	dB
Gain 1m ²	44.5	44.5	dB
Flux at Satellite	-124.2	-120.2	dBW/m ²
Flux to Satellite	-79.1	-77.6	dBW/m ²
Input Backoff	-45.1	-42.6	dB
Output Backoff	-40.1	-37.6	dB
Maximum e.i.r.p.	46.5	50.0	dBW
S/C e.i.r.p.	6.4	12.4	dBW
PL Down	205.9	205.9	dB
G/T	26.0	20.0	dB/K
C/T Down	-173.5	-173.5	dBW/K
C/T Up	-159.7	-158.2	dBW/K
C/T Link	-173.6	-173.6	dBW/K
C/N ₀ Link	55.0	55.0	dB-Hz

of the low requirements of the MITREX modem and the gain of the INTELSAT V transponders. This means that modest solid state amplifiers on 3.5-or 4.5-m antennas could support an operational link. The link does, however, have to be between areas served by the spot beams. This means for the normal antenna pointing, the north east United States, down to the D.C. area, and up to the Canadian maritime provinces, as well as Ontario and Quebec. In Europe, most countries, except northern England and Scandinavia, are served.

Figure 9 shows the signal and noise spectrum at a station receiving a 55-dB-Hz MITREX spread spectrum signal. At this level, the signal is just obvious above the noise by about 1 dB. This means that if this signal were being used in a system where all stations had the same G/T (25 dB/K for Class E1 stations) and other stations were using narrowband signals at the same frequency, those other narrowband stations would receive a degrading interference of 1 dB. It is likely that the time transfer system will share transponders with normal traffic between much higher G/T stations. For example, INTELSAT Class C stations, with a G/T of 39 dB/K, would see the time transfer signal as 10-11 dB higher than the noise. This clearly would not be tolerated in a frequency reuse situation. Thus, it is clear that a network of INTELSAT Class E1 stations (3.5-4.5-diameter antennas G/T greater than 25 dB/K) used for time transfer would not be transparent to other users of the transponder.

In this experiment, the east-to-west and west-to-east transponders were used. This enabled both stations to use the same frequency and the same PN code sequence. Service within a spot beam, say west to west, would require different codes to reuse the frequency. The frequency reuse is desirable in time transfer to minimize any differential time of transmission effects in the link.

MODEM PERFORMANCE

In laboratory tests using noise generators at 70 MHz, the modem performance is close to that expected [3],[5]. Figure 10 indicates the one sigma jitter in the time transfer performance of a single link for each one second data point. This indicates that at the nominal 55-dB-Hz operating point, an uncertainty of 700 ps can be expected. Prior to the link with Germany, the USNO modem was tested in a ranging mode looped back to itself via a transponder on the domestic SBS satellite (12/14 GHz). These tests achieved the same one pulse per second

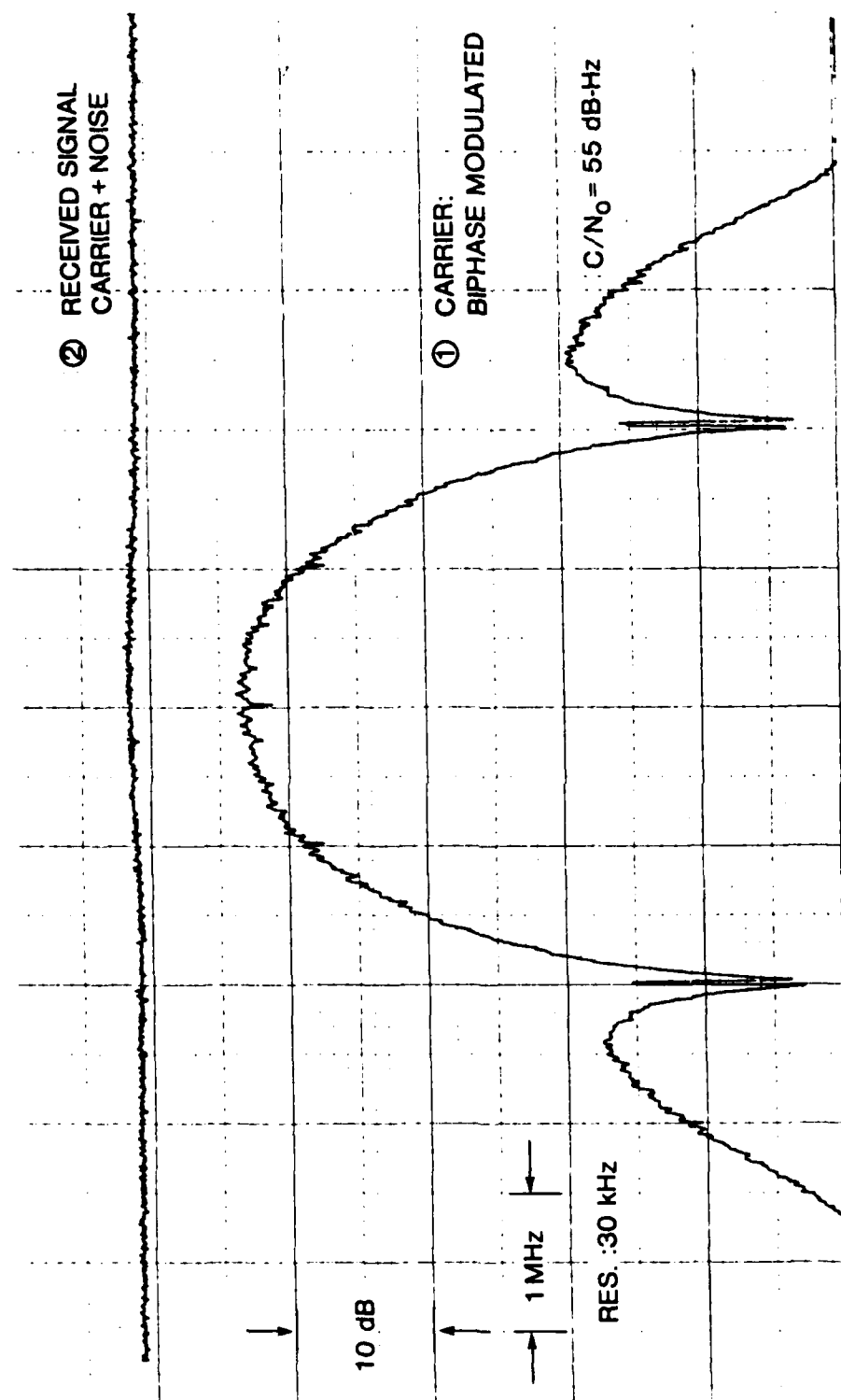


Figure 9. Signal Spectrum at Receiver Input

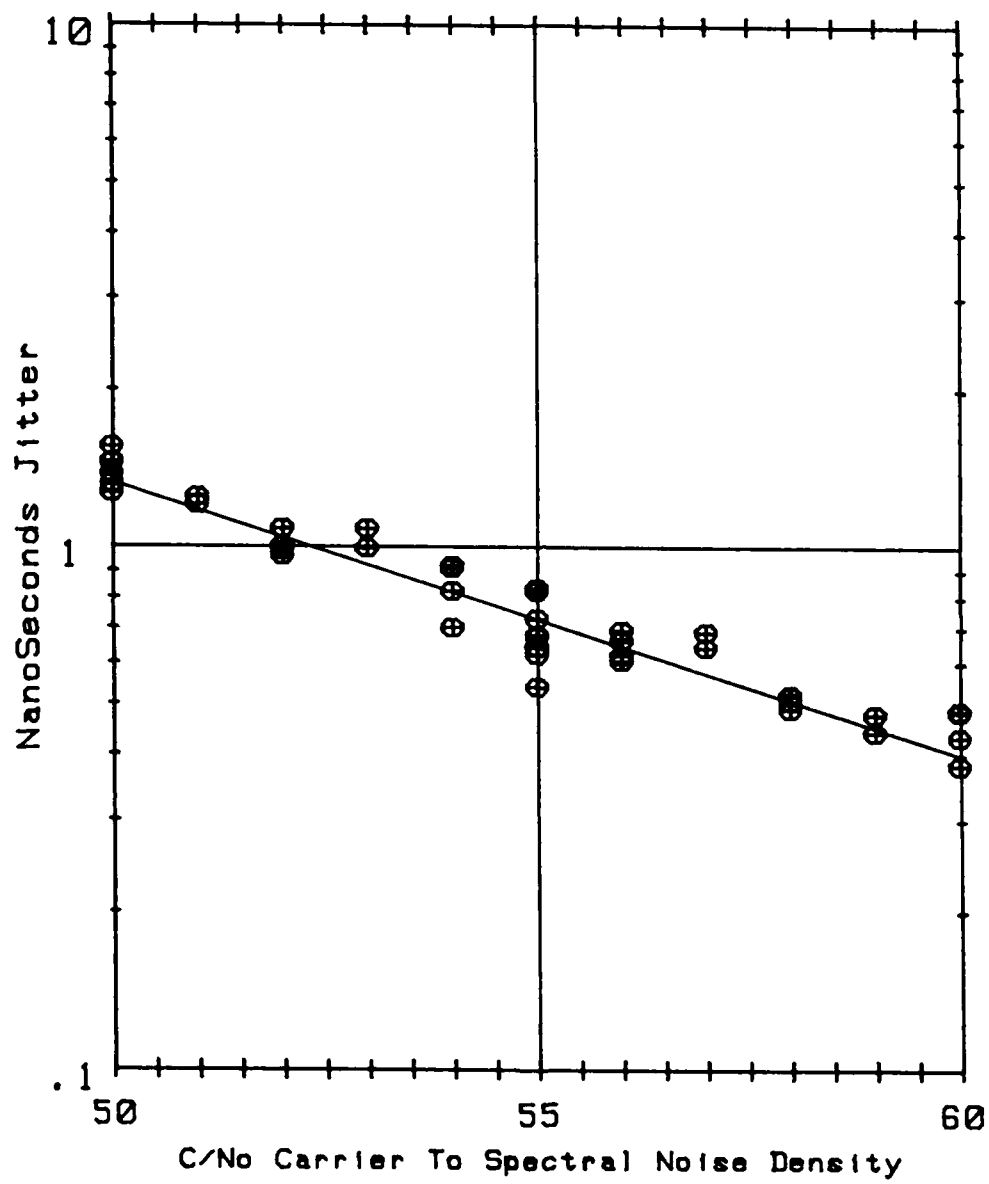


Figure 10

jitter at a given C/N_0 as was observed in the laboratory 70-MHz IF loop tests. This would indicate that for the particular frequency converter chains used and for the satellite transponder, the oscillator noise was not significant at this C/N_0 . The modem's performance is self limited by internal noise after about 90 dB-Hz. The limit is about 10 ps in the absence of noise.

The model used for these tests had two code sets available. This allows two spread spectrum signals to reuse a common frequency without interference due to the orthogonality of the selected codes. At the nominal links tested, 50-60 dB-Hz, the addition of the second signal caused no degradation in the performance.

The internal time delay of the modem between the 1 pulse per second pps input from the local clock and 1 pps (Tx) output that is used to start the time interval counter is not fixed. The synchronization process with 10 MHz also from the standard causes an uncertainty in the internal time delay each time the system is turned on. This uncertainty is in the form of some integer number of 50 ns steps (2-MHz internal clock). Table 4 shows the delays measured on the unit at DFVLR.

Table 4

Day	Internal Delay 1 pps IN/TX(1 pps) (ns)	Internal Delay Modulo 50 (ns)
11 July	980.6	30.6
12 July	781.5	31.5
14 July	978.9	28.9
18 July	734.9	34.9
19 July	634.6	34.6
20 July	733.0	33.0
26 July	1078.3	28.3
27 July	973.6	23.6

For time transfer this internal delay as well as the time delay to the master clock reference must be known.

EXPERIMENTAL TESTS

During the month of July 1983, the MITREX modem was used in a time transfer experiment between USNO, Washington, D.C. and DFVLR, Oberpfaffenhofen, Germany. The two sites were linked via the INTELSAT V primary path satellite at 11/14 GHz for eight days, one hour per day. The satellite transponders used were simultaneously carrying commercial FDM/FDMA traffic of about 1500 two-way voice circuits between INTELSAT class C stations (18-m diameter) located in the United States, France, and Germany. The spread spectrum signal frequency did not overlap with the frequency used by the FDM carriers. There was no detectable cross-talk to the FDM service from the 2 MCPS spreading signal.

The data in the form of the time delay between the local transmit pulse and the received pulse from the opposite station was recorded along with the time of day at the start pulse. These data were recorded in files of 100 points, one point per second. The data were reduced offline with each day's data for the satellite link combined into one file and the third order regression coefficients calculated. To evaluate the quality of the link the residuals were plotted as a scatter diagram as well as used to calculate the standard deviation.

To effect a time transfer the regression coefficients at each site were used to calculate the time interval observed at some point of time common to both data sets. The difference in the time intervals observed at each site is the difference in their clock times after the clock to start pulse time delays are accounted for. Unfortunately, the necessary modem delay times were not recorded each day at the USNO site. Without this correction, the data is unusable due to the random multiple 50-ns jumps in the interval. However, the nature of the scatter diagrams, Figure 11 and 12, show a good agreement with a Gaussian or normal distribution. There are some wild points associated with the start of each one hundred point file but they do not affect the regression coefficients. Figure 13 shows this data set before and after removing all points more than three sigma from the regression curve. The resulting change in the time interval is only 0.013 ns.

CONCLUSION

The MITREX spread spectrum modem is an efficient time transfer system. Its low-link power and lower flux density allow it to be used via communication satellite transponders with a

File US07261326 Sigma = 7.7E-10
Number of points 2111
Delay at 1315Z 262165342.889 NS

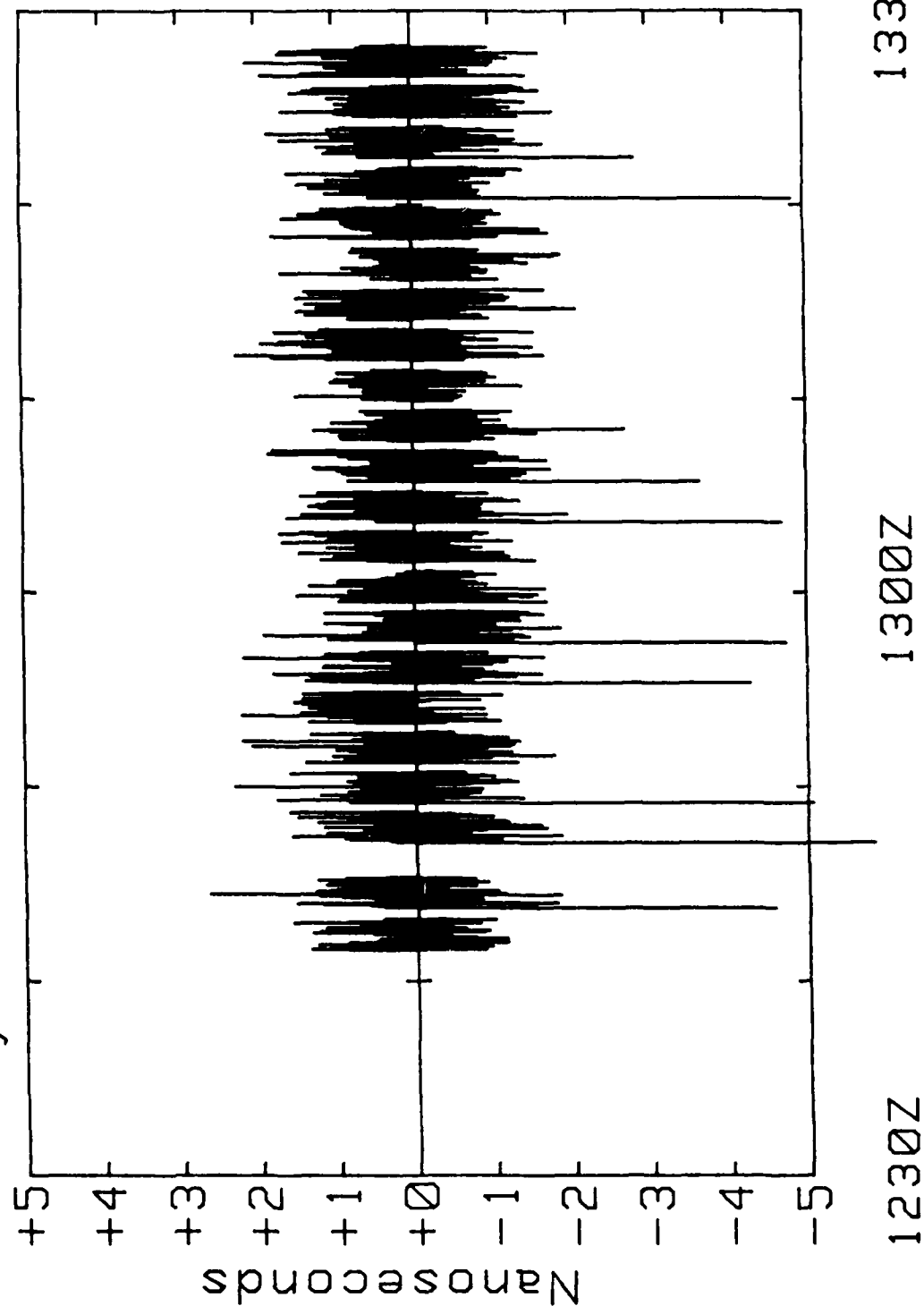


Figure 11

Error Distribution
File US07261326
Number of points 2111

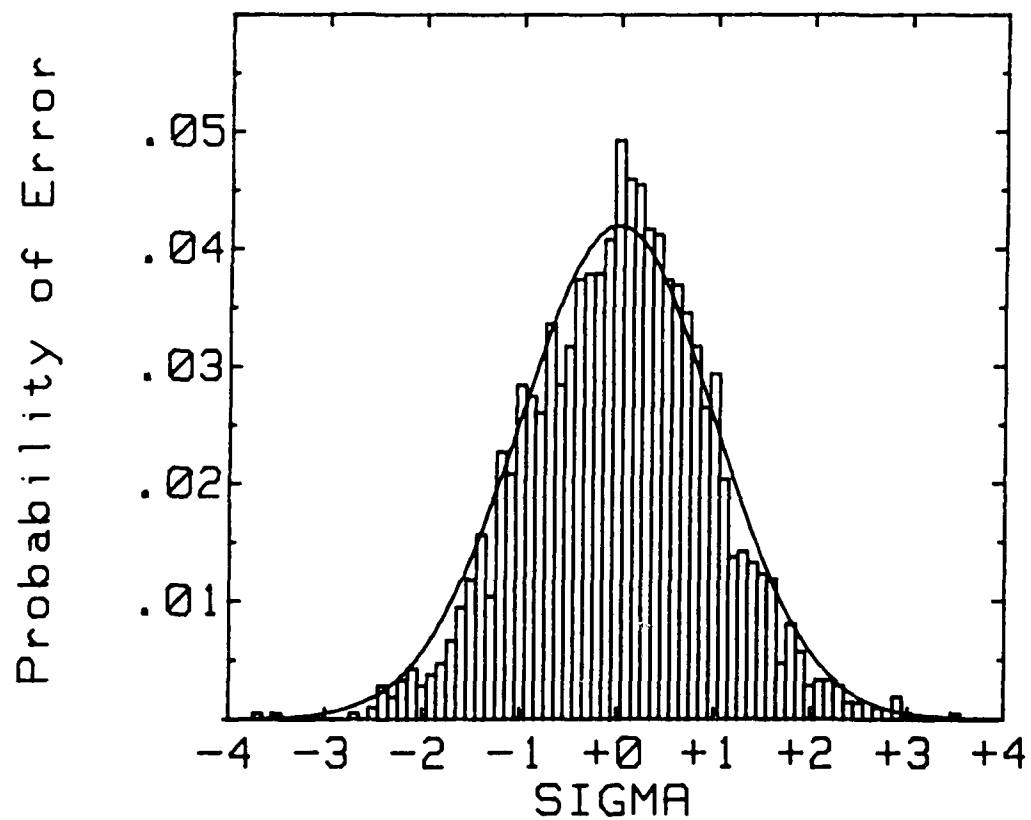


Figure 12

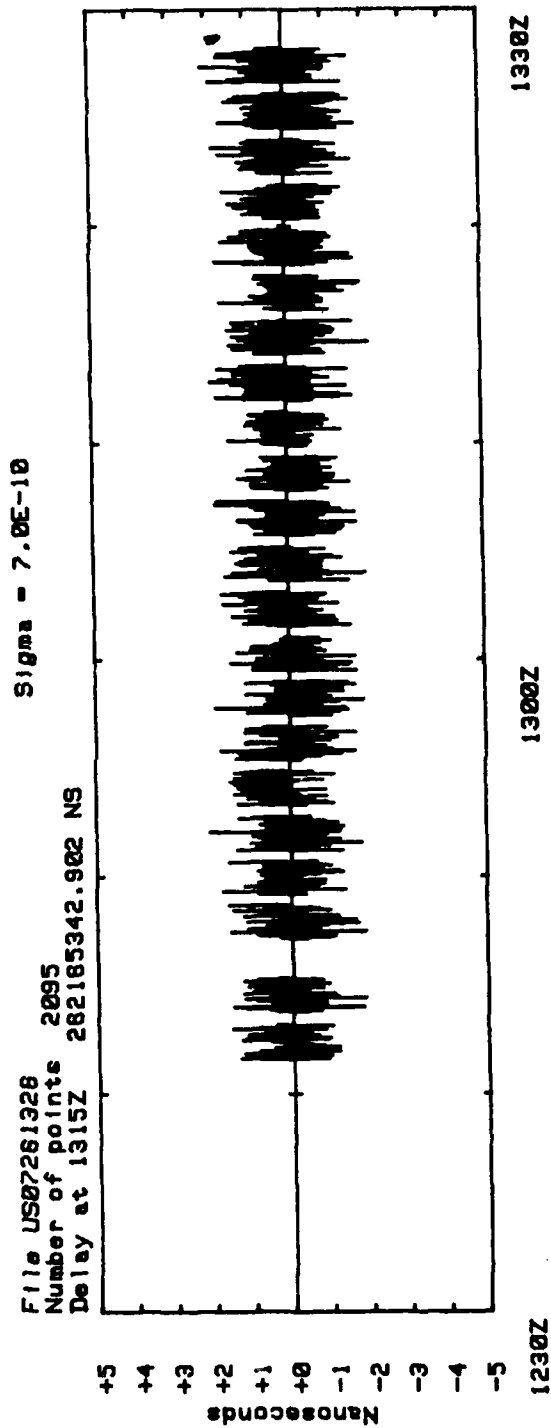
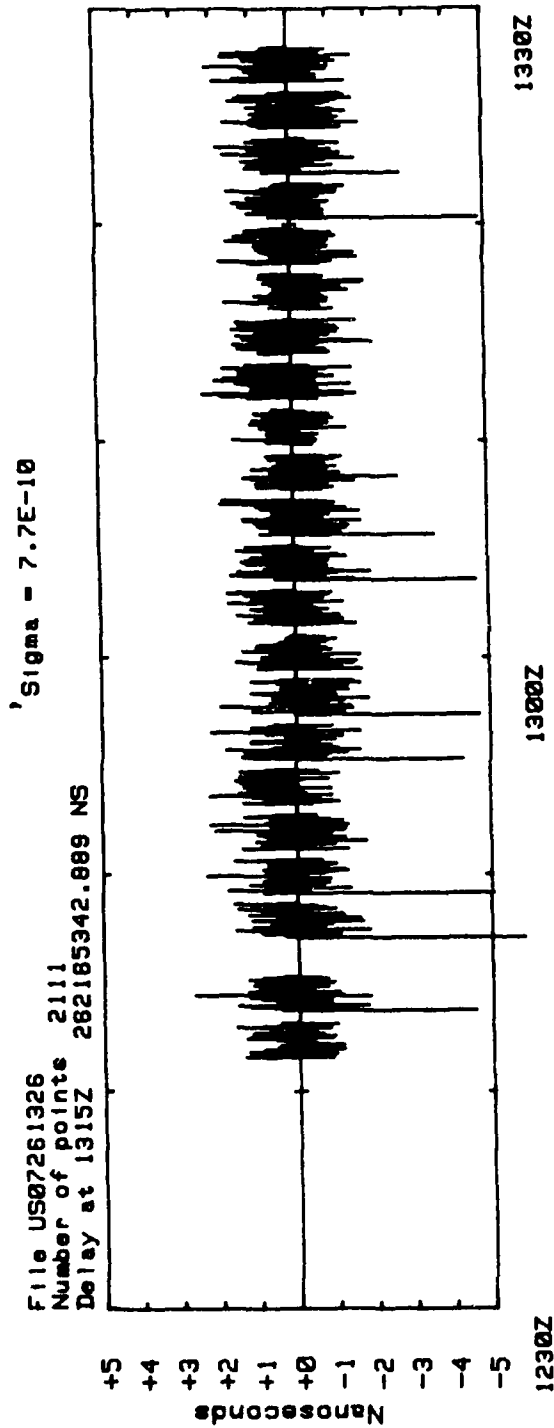


Figure 13

minimum of impact on other users. The sub-nanosecond accuracy of the transfer and the modest earth station requirements make it possible to locate the station directly at the master clock site. The accuracy of the link exceeds that of conventional means, loran, clock carry, GPS. Therefore, work is needed to verify the absolute error caused by earth station path length differences. In addition, the interface with the local clock needs additional work with respect to the use of 5 MHz and the internal time delay stability. It is clear that the experimental results confirm that an international time transfer and clock synchronization network is practical using this spread spectrum implementation.

REFERENCES

- [1] L. Veenstra et al., "Frequency and Time Coordination via Satellite," COMSAT Technical Review, Vol. 11, No. 2, Fall 1981, pp. 369-402.
- [2] C. Costain, J. S. Boulanger, H. Daams, D. W. Hanson, R. E. Beehler, A. J. Clements, D. D. Davis, W. J. Klepczynski, L. Veenstra, J. Kaiser, B. Guinot, J. Azoubib, P. Parcelier, G. Freon, and M. Brunet, "Two-Way Time Transfer via Geostationary Satellites NRC/NBS, NRC/USNO and NBS/USNO via Hermes and MRC/LPTF (France) via Symphonie," Proceedings, Eleventh Annual Precise Time and Time Interval Applications and Planning Meeting, November 1979, NASA Conference Publication 2129.
- [3] P. Hartl et al., "High Accuracy Global Time Transfer via Geosynchronous Telecommunications Satellites With MITREX," Zeitschrift für Flugwissenschaften und Weltraumforschung, Vol. 7, No. 5, 1983, pp. 335-342.
- [4] J. K. Holmes, Coherent Spread Spectrum Systems, New York: John Wiley and Sons, 1982.
- [5] E. F. Osborne and T. A. Schonfott, "Delay Locked Receivers With Phase Sensing of the Correlation Function," National Telemetry Record, 1972/1973, pp. 26B1-26B6.
- [6] J. Fuenzalida, P. Rivalan, and H. Weiss, "Summary of the INTELSAT V Communications Performance Specifications," COMSAT Technical Review, Vol. 7, No. 1, Spring 1977, pp. 311-326.

QUESTIONS AND ANSWERS

MR. ALLAN:

David Allan, National Bureau of Standards. A question, and a comment or two before you answer the question. The question is, do you have a feeling for how well, in fact, you can calibrate the transmit and received delays, and then I would like to clarify, as compared to G.P.S. common view? In this case, all that is important for time transfer is to know the differential delay between two receivers and then you can transfer time in an absolute sense per what we have described earlier. In this case we are talking about time stability, not time accuracy, and there's quite a difference. So one has to calibrate the delay, and I am curious about the kinds of numbers you anticipate, or maybe it's premature to say that.

MR. VEENSTRA:

Time accuracy is very difficult because it's very hard to separate time delays out between seventy megahertz and fourteen gigahertz. That is the transmit only, twelve gigahertz back to seventy megahertz the receive only chain. However, we do have a pretty good idea of what the stability of the earth station is, because at the beginning and end of every day, we did make loop back measurements via local loop back, that is; satellite simulators. These showed at U.S.N.O. stabilities, and this was stabilities on a day-to-day basis, in the order of one to two nanoseconds.

We say stabilities between the end--between the beginning and end of each day's trial in the order of a half nanosecond.

In other words, if you are willing to calibrate your station each day, you could get well below a nanosecond. If you want to forget about calibrating the earth station, and assume it stayed constant, you could assume two or three nanosecond accuracy in the small terminals that we were using.

Incidentally, the small terminal we were using at U.S.N.O. had about a two-hundred foot run of coax going and coming between the modem and earth station; and that sitting out in the grass, taking the ambient temperature variations of July.

DR. DETOMA:

It's true what you said, that if you make a loop measurement you can go down to one to two nanoseconds, but this is not very important in a two-way time transfer, in the sense that you don't need to sum the delays, but you need the difference and that is much harder; and you are usually not able to measure that at the one or two nanosecond levels like you mentioned.

MR. VEENSTRA:

It's very difficult, particularly in the typical international situation, where you can never get the two earth stations together to try to make these measurements. It's very difficult to try to separate receive and transmit time delays; and this really has been traditionally, and I see no solution, short of spending lots of money. If it's worth it, it could be done. To attempt to calibrate half of the earth stations as far as time delay stability, we make the assumption that both earth stations have comparable delays, split it between them, and then they solve out of the equation. But that is really an assumption born by a lack of any better information, not very rigorously justified.

MR. ALLAN:

David Allan, N.B.S. again. Mr. Beehler was mentioning to me a suggestion, I think it was made by Dr. Costain, N.R.C., that perhaps one could use a transportable calibrator and go from one site to another and perhaps accomplish the mission that's needed here to do absolute time transfer.

MR. VEENSTRA:

The question is, you have to build the transportable calibrator, and I feel it can be done. I have had some thoughts of how it could be done, but you need money to build things like this and prove it can be done; and this has not been done at this point. So all we can do is make a guess as to what the stability is, based on what the round-trip delay of the earth station is. Based on that guess, we'll say that if you had a calibrator we might be able to achieve this kind of accuracies.

UNATTENDED TV TIME TRANSFER RESULTS

John A. Waak and John H. Spencer
E. O. Hulburt Center for Space Research,
Naval Research Laboratory, Washington, D. C. 20375

ABSTRACT

We report on the results of more than eight thousand relative television time transfers to Maryland Point Observatory over a 14 month period beginning in December 1981. The data were taken at intervals of 30-60 minutes using a Hewlett-Packard 1000 computer operating in an unattended mode. After correction for linear drifts of our maser with respect to the master clock of the USNO, the results are internally consistent to within roughly ± 65 nsec over timespans up to three months, under the assumption of invariant propagation delay. The major disadvantages to this method of time transfer are the relatively poor precision and the dependency upon constant propagation times.

INTRODUCTION

The Naval Research Laboratory operates the Maryland Point Radio Observatory for a variety of projects that require a very precise station clock including very long baseline interferometry (VLBI). It is therefore necessary to conduct regular clock checks and time transfers from the U.S. Naval Observatory (USNO) master clock. The station clock used in the conduct of these experiments is a Smithsonian Astrophysical Observatory (SAO) VLG10 hydrogen maser. A Hewlett-Packard 5065A rubidium clock is also present at the observatory and is used for testing and backup.

The traditional method of transferring time involves the use of a portable clock which is compared to the master clock before and after being transported to the remote site. This procedure is time consuming and requires the commitment of significant manpower and other resources if it is to be done frequently on a continuing basis. An alternative to the traditional method is to make use of transmitted signals which are simultaneously monitored at the USNO and at the remote site. The Global Positioning Satellite (GPS) system and commercial television broadcasts provide facilities which can be used as such an alternative. The television method requires no moving parts, and when controlled by a multi-user computer, promises more or less continuous operation and a high data return in exchange for the small amount of resources it requires. Various schemes for and uses of television time transfers have previously been discussed in these conferences (cf. Inouye and Takeuchi 1975; Kovacevic 1977; Kaarls and de Jong 1979; Chiu and Shaw 1981), but large numbers of such measurements have not been presented.

Since December 1981 we have been carrying out automatic unattended television time transfers to both the hydrogen maser and the rubidium clock at Maryland Point Observatory. Occasional portable clock time transfers were also conducted, and the data from these can be used to aid in evaluating the suitability of the TV measurements as a time transfer method between the USNO and Maryland Point. In the course

of approximately 14 months we have obtained 9744 measurements.

REVIEW OF THE TV TIME TRANSFER METHOD

The video transmissions from Channel 5 (WTTG) in Washington, D.C. are synchronized such that the line 10 odd TV horizontal pulses are transmitted on particular seconds of a UTC scale referenced to the USNO master clock (Lavanceau and Carroll, 1971). It is termed a "time of coincidence" or "TOC" when the TV line 10 odd pulse occurs at the same instant as a one second pulse of the master clock. The rep-rate of the TV pulse train is 29.97003 pps, which means that TOC's occur at intervals of 1001 seconds (i.e. every 30000 TV pulses).

One consequence is that the local atomic clock should be preset to better than 33.366 milliseconds so that the TV pulse identity is correctly established. The quantity actually measured is the time interval between a 1 pulse per second pulse from one of the local clocks and the next TV line 10 odd pulse. Our station clock is compared to the television signal emitted by Channel 5, whose signal is phase locked to a cesium frequency standard, and is monitored daily by the USNO. This TV signal is easily received at Maryland Point, which is approximately 70 km from the transmitter. The daily monitoring by the USNO enables us to obtain USNO master clock-Maryland Point station clock comparisons by permitting the removal of the effect of cesium drift at the transmitter.

THE MEASUREMENTS

Employing an IEEE-488 interface bus, our Hewlett-Packard 1000 computer is used to read an HP 5345 time interval counter, which has a dual 4-position vhf switch in front of it. A measurement consists of taking a reading from each of the 16 possible stop/start combinations. The start pulses were: rubidium 1 pps, the maser 1 pps, the Mark II VLBI formatter 1 pps (slaved to the maser 5 Mhz), and a delayed pulse from the maser having a period of 1.001 sec. The stop pulses were the TV (the signal out of the McBee Industries line 10 decoder), the maser 1 pps, the Mark II formatter 1 pps, and a switch position where a portable clock or other miscellaneous clock could be read.

A complete measurement is obtained over a short time span (roughly thirty seconds), thus the entire matrix can be considered as virtually simultaneous. For the purpose of this paper, we adopt the convention of referring to a measurement as "identity of stop pulse minus identity of start pulse". In addition to real time and near real time displays at Maryland Point, the data log is dumped to magnetic tape and brought back to NRL for further processing at intervals of approximately two months.

Because of the nature of our measurement technique, the internal clock of the HP 1000 computer is involved in the processing of the over-the-air measurements. The non-rational rep-rate of the TV signal (as described above---29.97003 pps; period = 33.3666 milliseconds), means that an error by the computer clock will produce an offset of 1000 microseconds per second of clock error in the (TOC-start pulse) data. As long as the computer clock reads the correct second, the software correctly identifies the TV pulse, so for example, a 0.5 second error by the computer clock will produce no offset. Offsets arise from both software misidentification of the TV pulse and computer clock error. The HP clock runs on an internal crystal which drifts. In view of the 1000 microsec/sec effect of computer clock error, all of the TV (over-the-air) data is subjected to a modulo 1000 correction before plotting.

While the raw counter readings are a measure of the interval between the 1 pps from a station clock and the next TV line 10 pulse, a correction is made to the readings by applying an offset due to the time elapsed since the most recent TOC. If the time since the last TOC is large or small enough that the clock error caused the misidentification of the correct TOC, the irrational part of the period is added or subtracted causing a few of the reduced readings to be offset by ± 633.3 , ± 266.7 , and ± 900.0 μsec . Due to the large number of good readings we obtain, we did not bother to correct these data.

DISCUSSION OF RESULTS

A. Maser Comparisons

Figure 1 depicts the relationship between the transmitted WTTG television signal and the master clock of the USNO obtained from Series 4 of the USNO Time Service Announcements, interpolated to the time of each of our measurements, and plotted against modified Julian date (MJD is defined as $\text{JD}-2440000.5$). The maximum excursion in this data was less than 4.5 microseconds over the time spanned by this experiment, and the maximum long term rate of drift was less than 40 nsec/day.

A time plot of the relationship between our maser and the WTTG signal received over the air at Maryland Point is presented in Figure 2a, and exhibits a large amount of scatter. Note that these points are all the actual observed values corrected only for the time since last TOC offset and the modulo 1000 corrections already mentioned. We attribute the large scatter to a variety of causes including improperly set trigger levels and the computer aliasing mentioned above. Five days per week, WTTG goes off the air from about 0230-0530 local time. If a TOC measurement is attempted in the absence of a TV carrier, the result is random. Accordingly, we have excluded from the figure all TOC data taken from 0630-1030 UT (the four hour range accomodates the changes between standard and daylight times). There still remain 8200 measurements which include admitted TOC measurements. No measurement has been excluded from the figure for any other reason. A histogram of this data is given in Figure 2b, which shows that more than 70 percent of the observed values lie within a 60 μsec range near 220 μsec .

A number of low-level local maxima are seen in this histogram. Most of them occur at the discrete offsets from the nominal value which were predicted above. Those occurring near 600, 950, and 320 are likely due to the recovered reading being off by 1, 2, and 3 periods, respectively. The maximum near 860 μsec is probably due to the reading being off by one period in the opposite sense. The peaks near 430 and 170 μsec are extremely localized in time (as can be seen in Figure 2a). We know that the 170 μsec readings were obtained when the rubidium clock served as the station clock. The data at the predicted offsets could be recovered, but because of the large number of "good" points that require no recovery, we elected to "clip" all data outside of the 60 microsecond range. This constitutes an error in our procedure of reducing readings to TOC's in the presence of known computer clock errors, and is not intrinsic to the TV time transfer method. Application of recovery techniques would increase the percentage of points within the 60 μsec window by about 15 percent.

The 70 percent of the data within the window is replotted in Figure 3a, where it is clearly seen that the maser drifted slowly relative to the over-the-air TV signal. The breaks in the data were the result of various malfunctions which required us to

(among other things) resync the maser, after which the drift rate was somewhat changed. We found the three most extended groups of continuous data (those beginning near MJD 5030, 5130, and 5220) to have linear drift rates of 157, 52, and 48 nsec/day, respectively. These rates are not significantly larger in magnitude than that of the TV signal relative to the master clock. Note the extended break in data coverage from MJD 5060-5130. Most of that break was the result of computer software failure, and not due to maser problems.

One of our built in observational redundancies is the direct over the air observation of (TV-Maser) via hardware using a time base generator which transforms the 4 mhz pulse from the maser into a pseudo 1/1.001 pps, which triggers the counter. This hardware measurement is independent of the computer clock, for there are exactly thirty line 10 odd pulses in each 1.001 second interval. If all is well, this data should be identical to the (TOC-Maser) results, but with none of the clustering seen in that data which resulted from computer clock error. These "TV-1001" data are shown in Figure 3b. The similarity between this data and the (TOC-Maser) data of Figure 3a is reassuring.

The relationship between our maser and the USNO's master clock as measured over the air and shown in Figure 4 results from combining the data from Figure 1 (WTTG-master clock) with that from Figure 3a (TOC-Maser). The gross characteristics of this data are rather similar to those of Figure 3a. The rates of drift for the (master clock-Maser) results are 147, 23, and 53 nsec/day, respectively, for the three groupings of data mentioned previously. These results do not include any correction for delay due to the time required for the TV signal to travel to Maryland Point. When the above mentioned slopes are removed from the three data groupings, the resulting distributions suggest an uncertainty of ± 65 nsec (HWHM). We saw no evidence of systematic diurnal differences. Kaarls and de Jong (1979) previously reported a TV time transfer experiment where "except for throw-out measurements the average over these 3 months seems to be well within 500 nsec." Our error may be smaller because we have a data density almost two orders of magnitude greater than theirs, a shorter baseline, and a fully automatic recording system.

We attempted to apportion our 65 nsec uncertainty among independent sources of error. Such sources include our maser, counter, the atmosphere, and the transmitter-receiver combination. Adopting a scale height of 7 miles for atmospheric water vapor, taking into account the distance from the transmitter, and noting that the uncertainty due to the maser is ± 1 nsec (based upon VLBI data), and that due to the counter is ± 2 nsec, we find that the transmitter-receiver combination is responsible for almost all of the uncertainty.

B. Propagation Delay

There have been a number of occasions when a high quality cesium portable clock was brought to Maryland Point from the USNO in connection with VLBI experiments. Such trips permit the direct comparison of our clocks to the master clock without the inclusion of TV propagation delay. The differences between the (master clock-Maser) results over-the-air and those via portable clock is the propagation delay. In the latter half of 1978 the result of ten portable clock trips to Maryland Point showed a total range of 120 nsec with an rms deviation of 40 nsec. Since only four portable clock transfers were performed within the time interval spanned by our data, there is little that can be said about systematic propagation delay variations. The four delay values thus obtained yield an average of 224.1 ± 3.3 (rms) microseconds for

the transmitter-Maryland Point delay. Chiu and Shaw (1981) have reported that the delays they measured over the 30 km path between WTTG and the Johns Hopkins University Applied Physics Laboratory during a span of approximately 15 months in 1980-1981 had a total range of <60 nsec and an rms deviation of 11 nsec, based upon 30 portable clock trips. We do not obtain a similar result over our 70 km path. Instead, there is a range of almost 11 microseconds in our delay measurements (see Figure 5). The antenna at Maryland Point is beyond the direct line of sight from the transmitter, and thus the signal is subject to considerably more complex propagation paths.

We experienced a number of hardware problems during the period of the December 1981 delay measurement, so its value (the smallest in our new sample) should be regarded as suspect. If this delay is discarded, the remaining 3 determinations yield an rms of $\pm 0.3 \mu\text{sec}$. At the time of the delay measurement on 19 October 1982 we noticed the following phenomenon: just before 1400 UT, the over-the-air TV signal exhibited an apparent 34 microsecond jump. We saw a similarly abrupt return to the normal value eight hours later (just before 2200 UT). These points can be seen as a "clump" near 198 μsec and MJD=5262 in Figures 3. On this day the portable clock was at Maryland Point 1600-1800 UT, and we used the average of TV data taken before 1400 and after 2200 in computing the propagation delay. We know from the consistency of the propagation delay that the 34 microsecond jump was a problem with the television transmitting system rather than with the Maryland Point system.

C. Rubidium Clock Comparisons

Figure 6 shows the over-the-air relationship between the master clock and our rubidium clock determined in a manner analogous to that used on the maser data. The sharp jumps in this data result from the resetting of the Rb clock. The drift rates are of the order of 1 microsecond/day, significantly larger than those observed for the maser.

Another of the redundancies built into our automatic data acquisition system is the direct on-site intercomparison of the maser and rubidium clocks. A plot of this data along with a histogram of its distribution is provided in Figure 7. Much of the apparent width of this distribution is due to the drift of the Rb clock relative to the maser, and not to inherent measurement scatter. The two clocks can also be compared indirectly by combining the TV measurements of both. Ideally, both the direct and indirect determinations of Maser-Rb should yield the same value (since the effect of TV propagation delay should cancel), and certainly their differences should cluster about zero. When this is done, 56 percent of the differences cluster within 5 μsec of zero.

CONCLUSIONS

With the possibility of undocumented errors as large as 34 microseconds in the transmitted TV signal, and the inability to determine the propagation delay, the unattended television time transfer method appears to be primarily useful as a tool for the detailed monitoring of the station clocks.

For the future, since only slightly more than 55 percent of the direct and indirect intercomparisons of the station clocks give consistent results, we need to monitor more often the performance of the data taking system. The addition of a battery backup system to the Mark II formatter is also desirable. Finally, we must acquire

propagation delay measurements much more frequently, so that we can track any significant changes and remove their effect from our (future) data.

REFERENCES

- Chiu, M.C. and Shaw, B.W. (1981), Proc. 13th Annual PTTI Applications and Planning Meeting, p.299
- Inouye, T. and Takeuchi, C. (1975), Proc. 7th Annual PTTI Applications and Planning Meeting, p.297
- Kaerls, R. and de Jong, J. (1979), Proc. 11th Annual PTTI Applications and Planning Meeting, p.485
- Kovacevic, B.Z. (1977), Proc. 9th Annual PTTI Applications and Planning Meeting, p.277
- Lavanceau, J.D. and Carroll, D. (1971), Proc. 3rd Annual DoD PTTI Strategic Planning Meeting, p.331

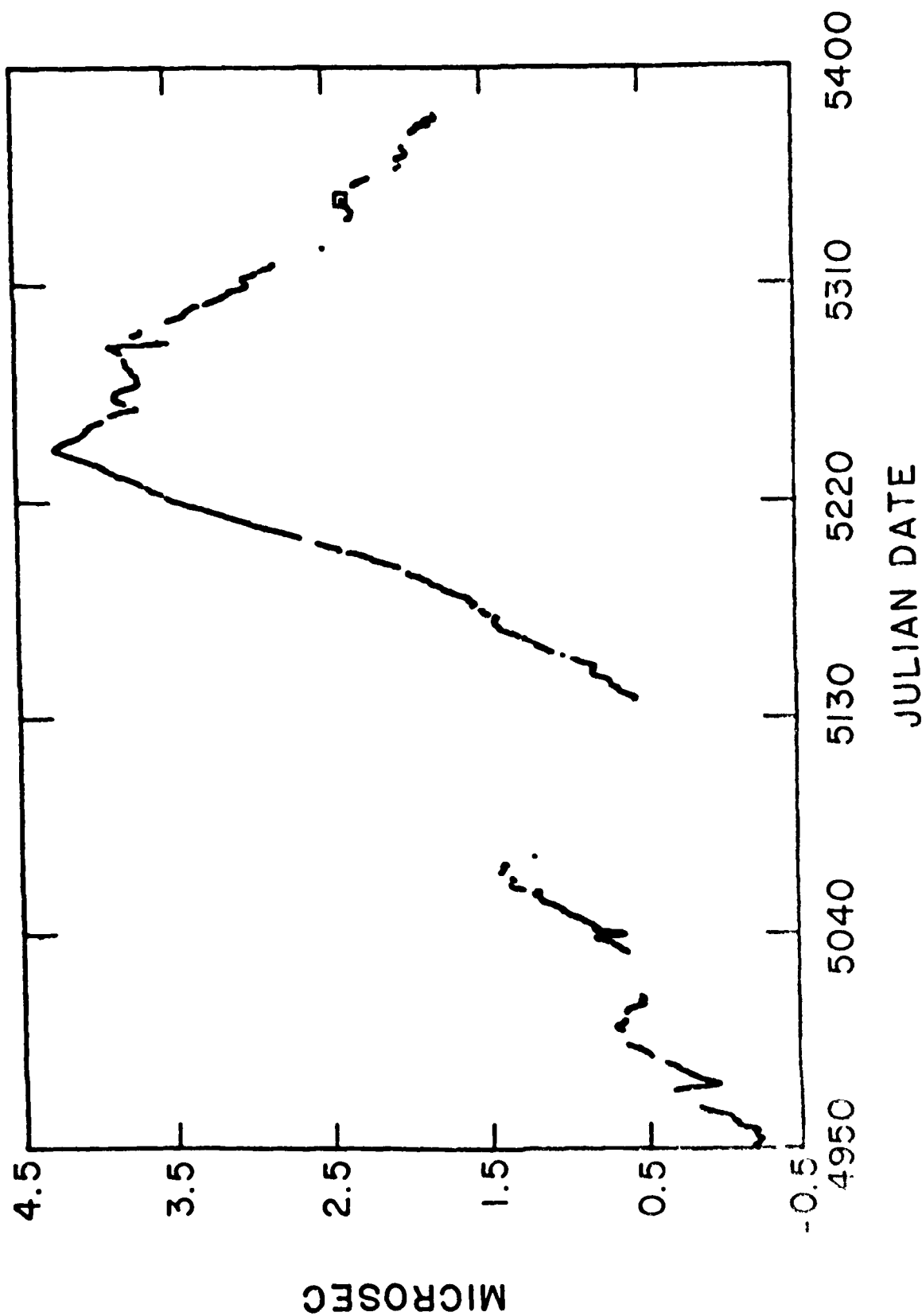


Figure 1 - Drift of WTTG television signal relative to the USNO master clock interpolated to the times of our measurements from the daily values given in Series 4 of the USNO Time Service Publications.

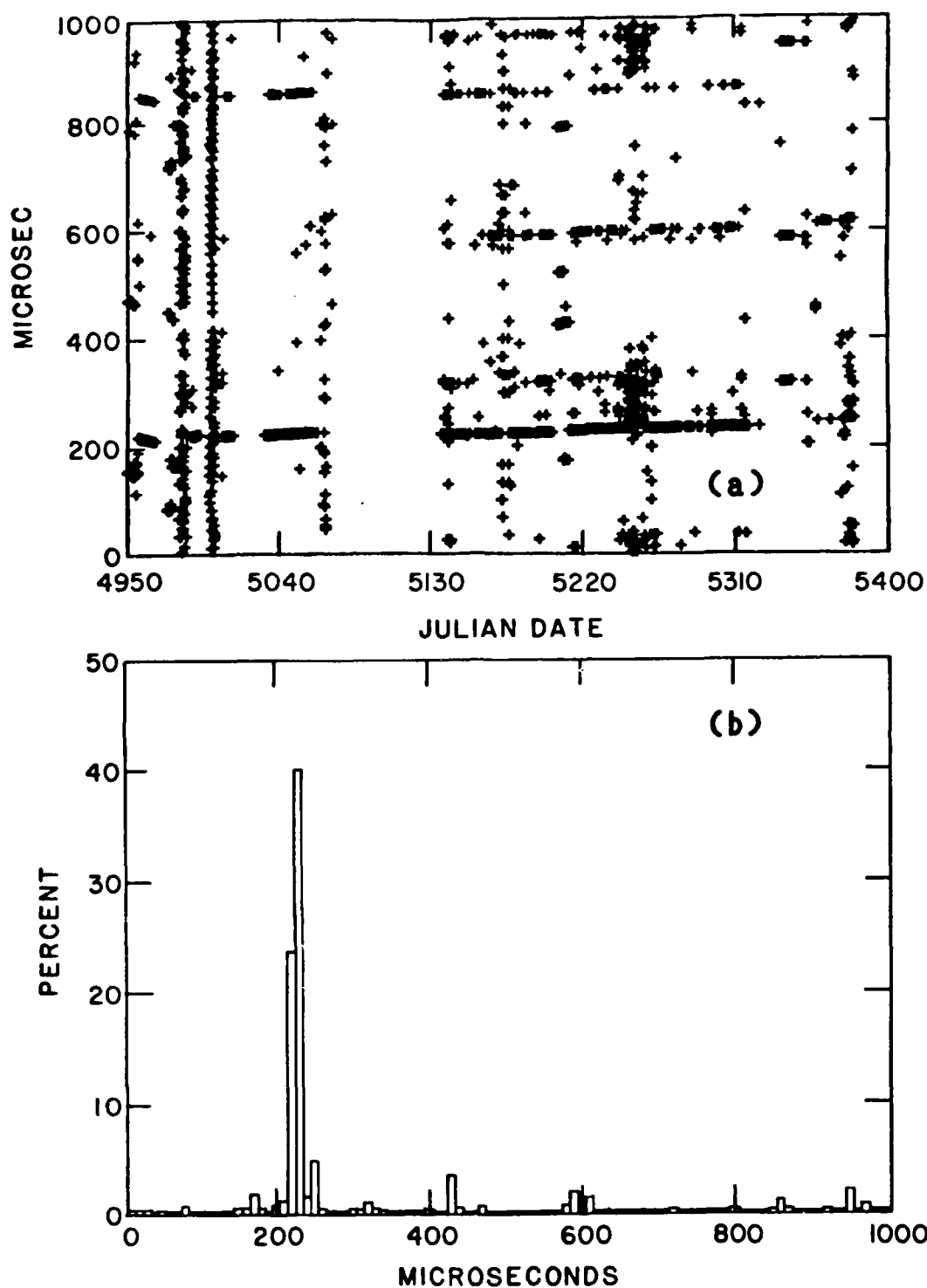


Figure 2(a) - Drift of NRL maser relative to WTTG television signal as received at Maryland Point. No correction for propagation delay has been applied. (b)- Frequency distribution of the data shown in 2(a).

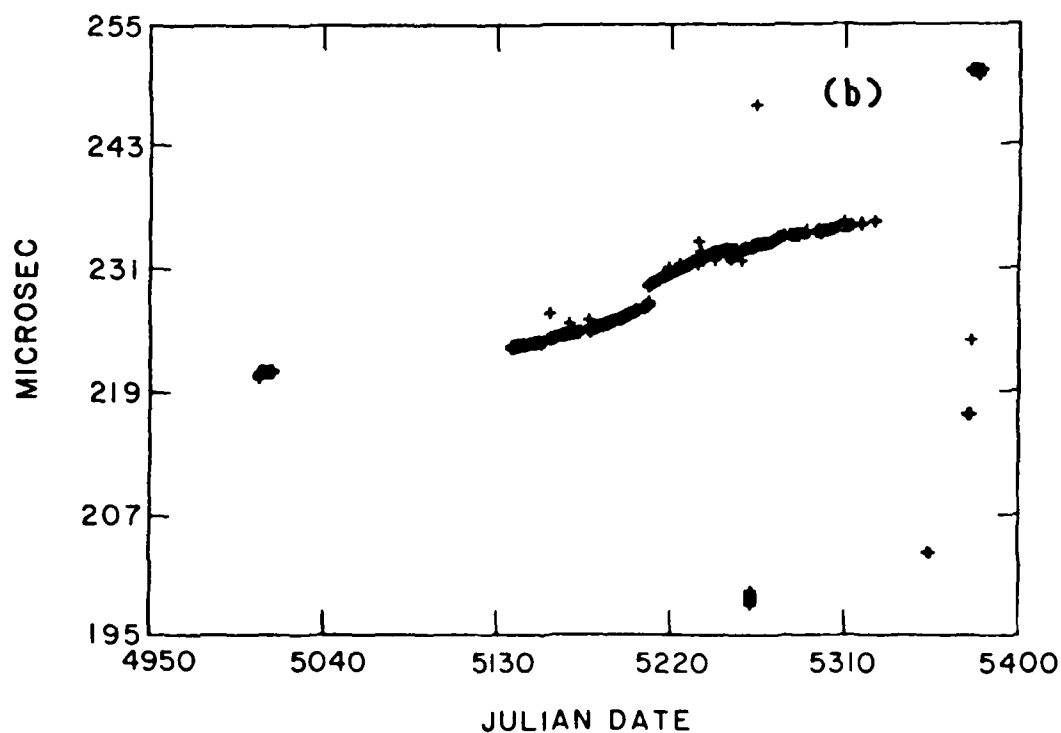
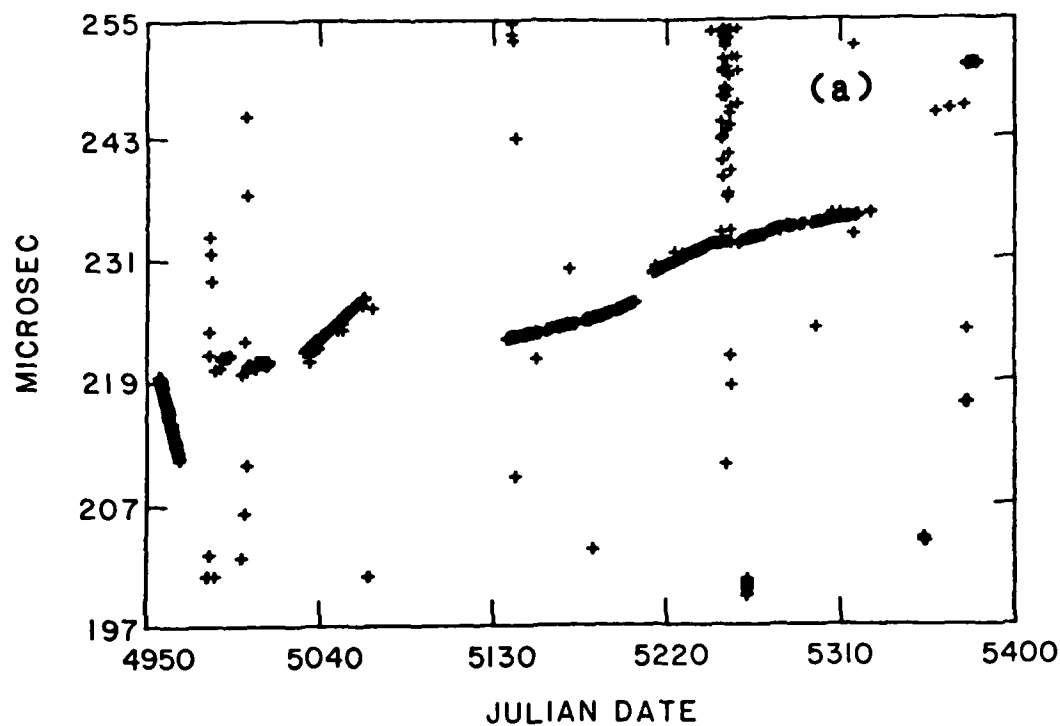


Figure 3(a) - Expanded and clipped view of drift of NRL maser relative to the received WTTG television signal. The clump at 198 μ sec is discussed in the text. (b) - Hardware measurement of maser/WTTG drift using pseudo 1/1.001 pps.

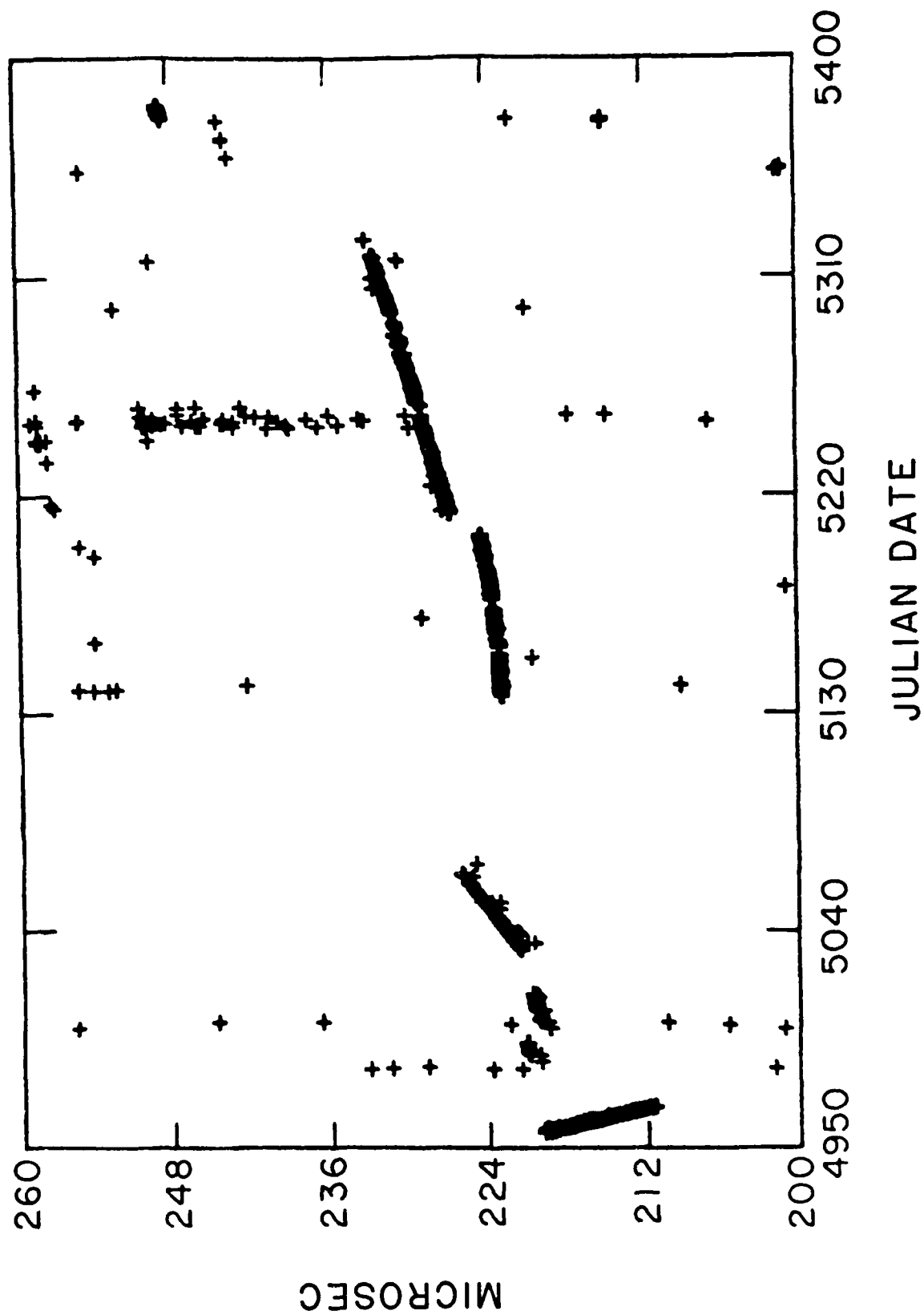


Figure 4 - Clipped view of drift of NRL maser relative to the USNO master clock.

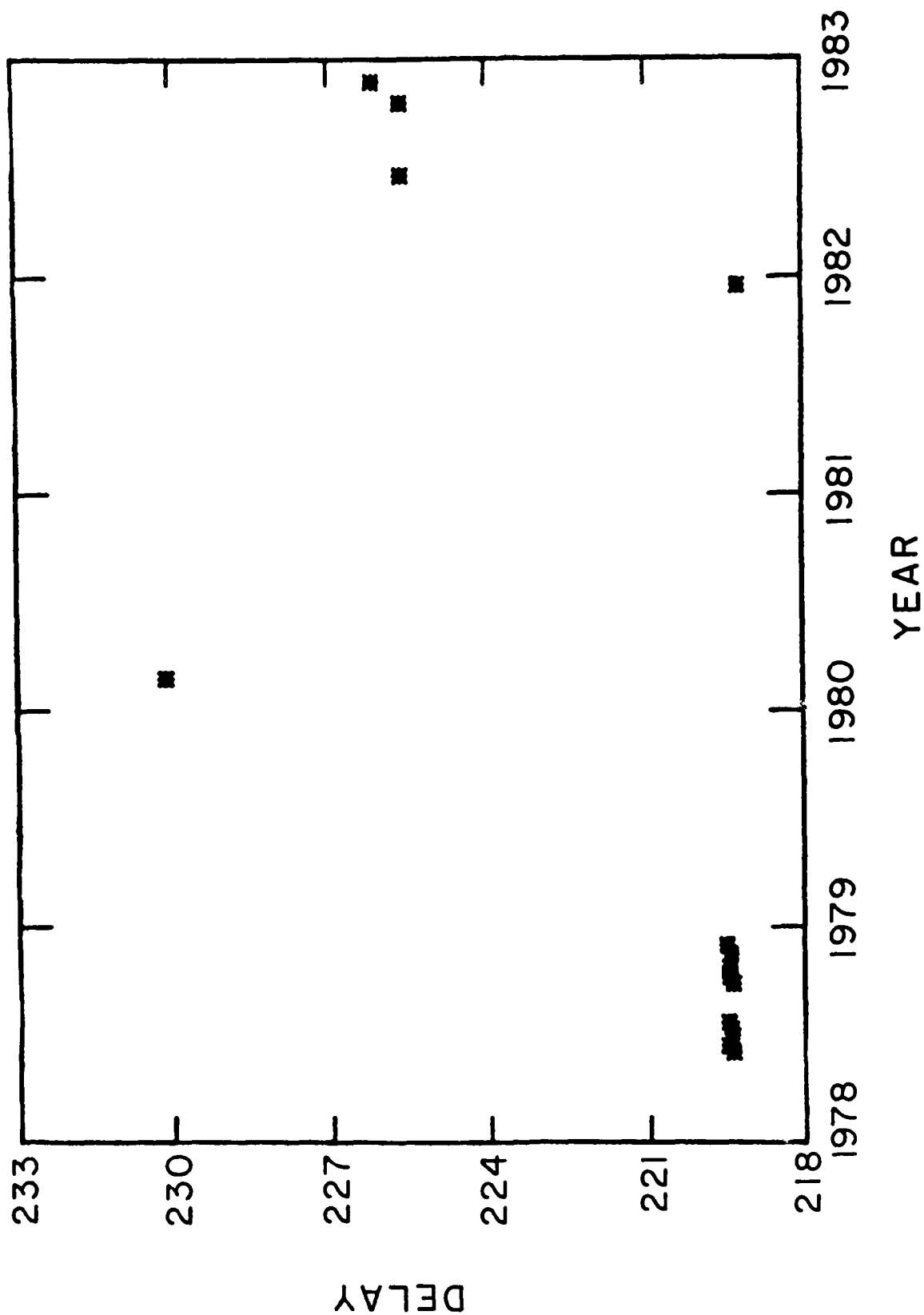


Figure 5 - Propagation delay between WTTG and Maryland Point determined by portable clock trips.

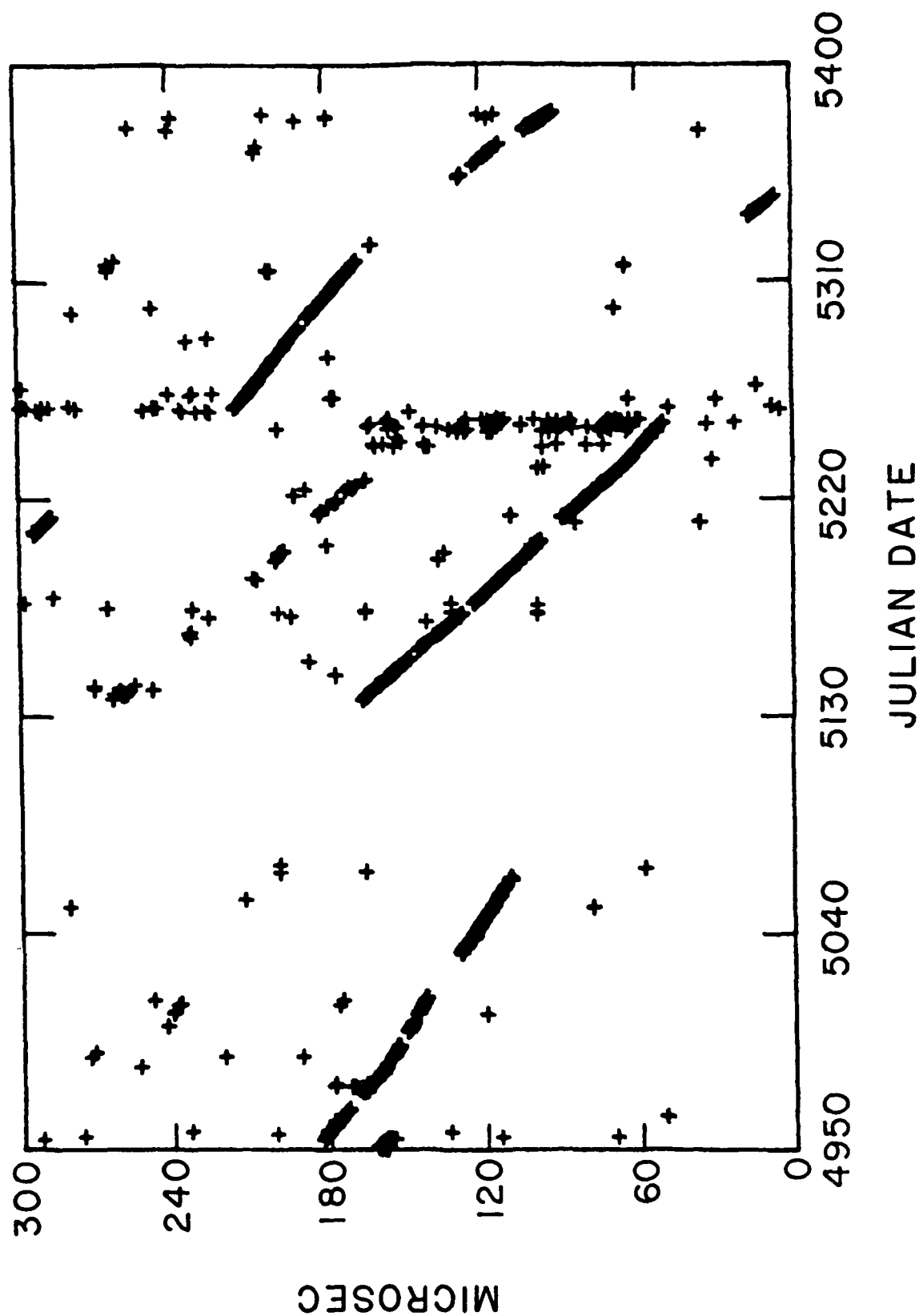


Figure 6 - Clipped view of drift of NRL rubidium clock relative to the USNO master clock.

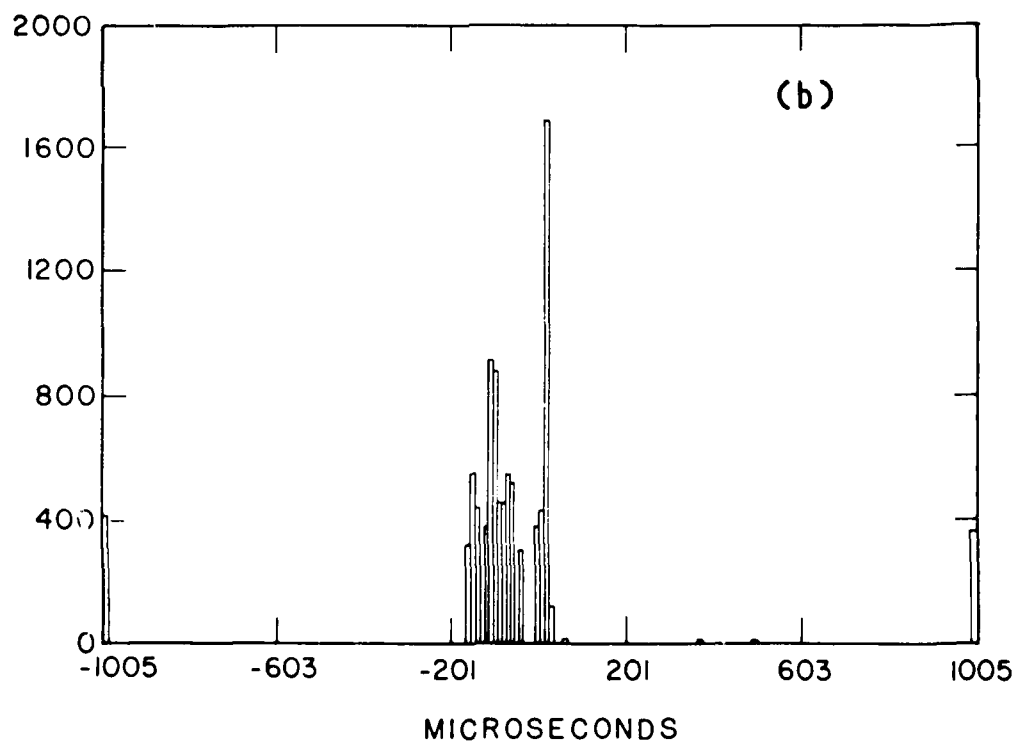
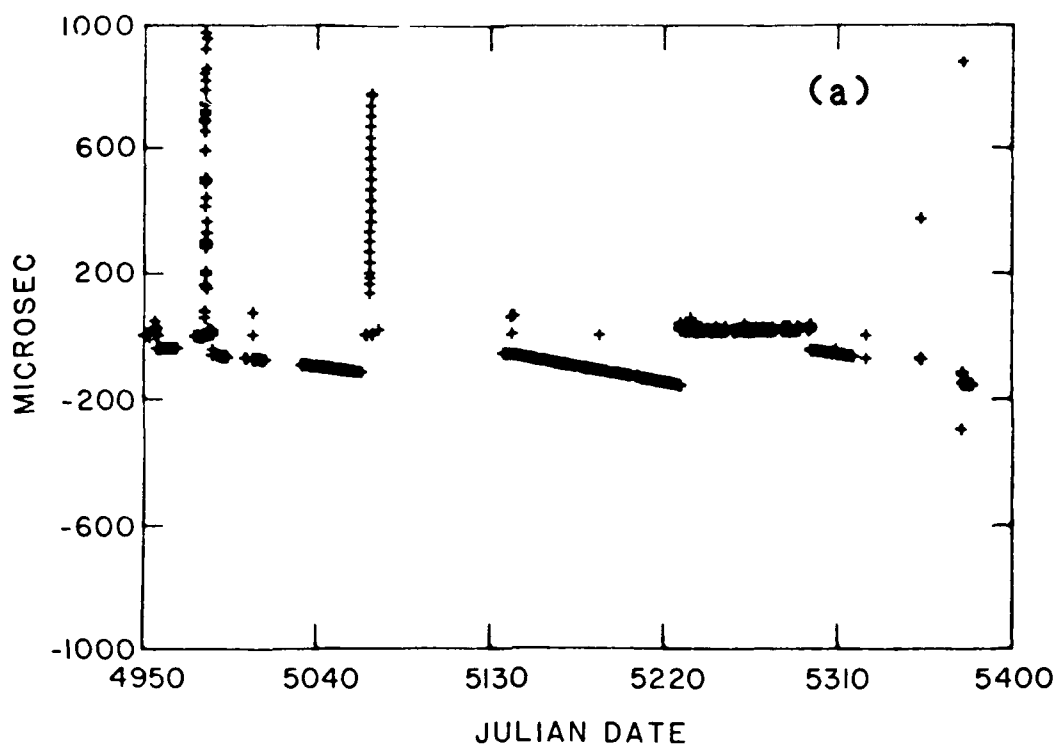


Figure 7(a) - Direct on site comparison of Maryland Point station clocks not involving any television signal. (b) - Frequency distribution of the data shown in 7(a).

QUESTIONS AND ANSWERS

None for Paper #18.

THE ROLE OF A LOW EARTH ORBITER IN INTERCONTINENTAL
TIME SYNCHRONIZATION VIA GPS SATELLITES*

Sien-Chong Wu and V. John Ondrasik
Jet Propulsion Laboratory
4800 Oak Grove Drive
Pasadena, California 91109

ABSTRACT

Time synchronization between two sites using differential GPS has been investigated by a number of researchers. When the two sites are widely separated, the common view period of any GPS satellite becomes shorter; low elevation observations are inevitable. This increases the corrupting effects of the atmospheric delay and, at the same time, narrows the window for such time synchronization. This difficulty can be alleviated by using a transit site located midway between the two main sites. The main sites can now look at different GPS satellites which are also in view at the transit site. However, a ground transit site may not always be conveniently available, especially across the Pacific Ocean; also, the inclusion of a ground transit site introduces additional errors due to its location error and local atmospheric delay. An alternative is to use a low earth orbiter (LEO) as the transit site. A LEO is superior to a ground transit site in three ways: (1) It covers a large part of the earth in a short period of time and, hence, a single LEO provides worldwide transit services; (2) it is above the troposphere and thus its inclusion does not introduce additional tropospheric delay error; and (3) it provides strong dynamics needed to improve GPS satellite positions which are of importance to ultra-precise time synchronization.

*The research described in this paper was carried out at the Jet Propulsion Laboratory, California Institute of Technology, under contract with the National Aeronautics and Space Administration.

This paper investigates the use of a LEO, at 1300-km altitude, as a transit site for intercontinental time synchronization via GPS. Results of analysis indicate the capability of time synchronization over intercontinental baselines (~10,000km) to 1-2 nanoseconds.

INTRODUCTION

By the end of this decade, the operational phase of the Global Positioning System (GPS) will be completed. A constellation of 18 satellites in six orbit planes (Ref. 1) will be dedicated to time keeping, positioning and navigation. The concept of differential GPS for time synchronization between two remote sites was introduced in the early stage of GPS development and has been investigated by several groups of researchers (Refs. 2-4). Time synchronization accurate to about 10 nanoseconds across a 3000-km baseline has been demonstrated using differential GPS (Ref. 4).

The concept of differential GPS is analogous to that of Very Long Baseline Interferometry (VLBI) (Refs. 5,6). That is, the same signal emitted from a distant radio source is simultaneously received at two widely separated sites and later brought together and compared. The difference in arrival times of this signal at the two sites contains information of time offset between the sites as well as the geometrical group delay, propagation delays and instrument delays. Precision time synchronization can be performed provided the positions of the two sites and the distant radio source are accurately known and the propagation and instrument delays properly calibrated. In the case of VLBI the distant radio source is an extragalactic source such as a quasar. To perceive the faint signal of a quasar, large antennas and ultra-low-noise receivers are required. Also, to extract time delay information from the random signal emitted by a quasar, cross-correlation between the signals received at the two sites is essential. This calls for high data rate to maintain a certain usable signal-to-noise ratio. On the other hand, a GPS satellite transmits a much stronger, coded signal. The strong signal allows the use of compact antennas and receivers; the coded signal structure eliminates the need for a cross-correlation process, and a much lower data rate can be used. Hence, differential GPS provides a low-cost vehicle for time synchronization between remote sites and is highly preferred over VLBI approach.

Differential GPS relies on common view of a satellite at the two sites simultaneously. When the two sites are separated by a large distance around the earth, a simultaneous common view of a GPS satellite may not always be available. For instance, with the full constellation of

18 GPS satellites in orbit, a common view between two of the NASA Deep Space sites at Goldstone, California and Canberra, Australia is not available two thirds of the time, as shown in Fig. 1(a). In the remaining one third there is only one satellite in common view and the viewing elevation angles are conceivably low. When the two sites are both at high latitudes (north or south) the situation is not as bad, as shown in Fig. 1(b) for a baseline between Goldstone and another NASA Deep Space site at Madrid, Spain.

The problem of lacking a common view can be alleviated if a transit site located midway between the two main sites is used. Better still, a low earth orbiter (LEO) can be used as a transit. This paper investigates the use of a ground transit and of a LEO transit in intercontinental time synchronization. The results of a covariance analysis are presented comparing the estimated time synchronization accuracies using the two approaches.

TIME SYNCHRONIZATION VIA A GROUND TRANSIT SITE

Fig. 2 describes schematically the use of a ground transit site in intercontinental time synchronization. This transit site is selected to be somewhere midway between the two main sites between which time synchronization is to be performed. Differential GPS pseudo-range measurement is made between this transit site and each of the main sites. A second difference is then taken between these differential GPS measurements. This second difference completely removes whatever clock error at the transit site, thus a precision clock is not needed there. Now there is no need for the two main sites to have a common view of any GPS satellite. These main sites can look at different satellites, as long as these satellites are also in view simultaneously at the transit site. Therefore more satellites can be in view at higher elevation angles. Fig. 3 shows, in chronological order, the number of GPS satellites in common view between a transit site at Johnston Island in central Pacific and either of the two main sites at Goldstone and Canberra. There are 4 to 5 satellites in common view for nearly all the time, as opposed to only one satellite in common view between the two main sites which happens only about one third of the time (cf. Fig. 1(a)). Therefore, a transit site increases the opportunity for intercontinental time synchronization with differential GPS.

However, a ground transit site may not always be conveniently available, especially across the Pacific Ocean. Also, the use of a ground transit site introduces additional station location and tropospheric delay errors. These concerns lead to the concept of using a LEO in place of a ground transit site.

TIME SYNCHRONIZATION VIA A LOW EARTH ORBITER

Fig. 4 provides a conceptual view of using a LEO in intercontinental time synchronization with differential GPS. Here, the differential GPS pseudo-range measurement between a main site and the LEO is differenced with that between another main site and the same LEO. Hence the LEO plays the same role as a ground transit site as before. However, a LEO is superior to a ground transit site in three ways:

- (1) The ground track of a LEO covers a large part of the earth in a short time. Hence, a LEO is capable of providing transit for time synchronization for a world-wide community.
- (2) A LEO is above the earth's troposphere and, hence, its inclusion does not introduce additional tropospheric delay error.
- (3) The rapidly changing geometry of a LEO provides strong dynamics needed to improve the GPS satellite positions which will in turn improve time synchronization accuracy.

GEOMETRY AND ERROR MODELS

To predict the accuracy with which times between intercontinental sites can be synchronized using differential GPS, a covariance analysis was performed. For this purpose, the three NASA Deep Space sites were selected as the main sites between which time synchronization was to be performed. A 1300-km LEO at an inclination of 65 degrees was used as a transit. For comparison, the case using a ground transit site was also studied. The ground transit site between Goldstone and Canberra was selected to be at Johnston Island in central Pacific; and that between Goldstone and Madrid was selected to be at the site of Haystack Observatory in Massachusetts. The ground track of the LEO over a period of two hours is shown in Fig. 5 together with the geographical locations of the ground sites. The full constellation of 18 GPS satellites was assumed. The key orbit parameters of these GPS satellites can be found in Reference 1.

Table I summarizes the error models used in the analysis. A data noise of 10 cm was assumed for the GPS pseudo-range measurement. This implies a 14-cm differential GPS (for time synchronization without a transit) and a 20-cm double differential GPS (for time synchronization via a transit). Two sets of errors, optimistic and conservative, for the transit station location, the LEO position and the GPS satellite positions are shown in Table I. When the optimistic errors were used, they were modeled into time

synchronization error; when the conservative errors were used, these parameters were adjusted simultaneously with the time synchronization solution.

RESULTS OF COVARIANCE ANALYSIS

When optimistic GPS satellite position errors are assumed, time synchronization using only instantaneous measurements is possible. Fig. 6 compares the estimated errors of such instantaneous time synchronization using a LEO as transit with those using a ground transit. The instantaneous measurements were taken at a time when the LEO was nearly midway between the two main sites. For the baseline between Goldstone and Canberra, it was at the beginning of the 2-hour arc; for the baseline between Goldstone and Madrid, it was at 25 minutes later. Both optimistic and conservative errors for the LEO and the ground transit positions were studied. In all cases, the errors are lower when a LEO is used in place of a ground transit site.

In practice, the optimistic sub-meter GPS positions are very hard to maintain. The conservative errors of 10 meters may be more realistic. When such conservative GPS satellite position errors are used, time synchronization to a few nanoseconds can be achieved only when these GPS satellite positions are adjusted simultaneously with time synchronization using measurements over a period of time. The results using differential GPS over a 2-hour arc are shown in Fig. 7. Also included is the case when no transit was used. While a suitably located ground transit improves time synchronization using differential GPS by 30-40%, a LEO provides an improvement by a factor of 5 to 6. Such vast improvement is a result of the strong dynamics of the LEO which can better determine the GPS satellite positions. With such a LEO, time synchronization is accurate to about 1.5 nsec between intercontinental sites.

A breakdown of the 1.5-nsec time synchronization error into its component contributions from individual error sources is shown in Fig. 8. Because the GPS and LEO positions were adjusted, the effects of their a priori errors were buried in the data noise effects. To separate them from one another, the covariance analysis was repeated with perfect GPS and/or LEO a priori positions.

The major error sources are seen to be the 10-cm tropospheric delay error and the 10-m a priori errors of the GPS satellite positions. Sub-nanosecond time synchronization is possible if these errors are reduced by a factor of 2 to 3. It should be pointed out that an increase in the data noise will also increase the effects of satellite position errors because these satellite

positions, being adjusted using the same data set, will be worse determined.

The larger effects of the earth's mass and geopotential errors on time synchronization over one of the two baselines can be explained as follows: The information for time synchronization is strongest when the ground track of the LEO falls between the two ends of the baseline. Referring to Fig. 5, we observe that the information over the baseline between Goldstone and Canberra concentrates mainly at two separate segments near the two ends of the 2-hour data arc. However, it is well known that the effects of unmodeled force parameters on the orbit determination of a LEO are also largest at the two ends of a data arc. This larger LEO orbit error in turn results in larger time synchronization error. For the baseline between Goldstone and Madrid, the information concentrates mainly in a single short segment within the 2-hour data arc and the effects of these unmodeled force parameters are expected to be much smaller. Therefore, the effects of these unmodeled force parameters can be kept small by selecting the proper data arc. The larger errors on the baseline between Goldstone and Canberra is simply an artifact.

REMARKS

A LEO at an altitude of 1000-1500 km is capable of improving intercontinental time synchronization using differential GPS to 1-2 nsec. Time synchronization using an earth orbiter much lower than these altitudes will suffer from larger geopotential and atmospheric drag errors. On the other hand, time synchronization using a much higher earth orbiter will be more sensitive to GPS satellite position errors. Using a LEO as transit, sub-nanosecond time synchronization between intercontinental sites is possible provided that 3-cm zenith tropospheric delay calibration and 5-m GPS satellite positions are available.

Due to a complete cancellation of its effects, the clock on board the LEO need not be of high precision. Also, because no GPS clock information is used in differential GPS, a simple SERIES receiver (Ref. 7) can be used at all sites including the LEO. Such a receiver extracts GPS pseudo-range without having to know the GPS transmitted codes. However, an independent knowledge of time synchronization better than half a microsecond is required to resolve the cycle ambiguity corresponding to the 1-MHz chip rate of the C/A code modulating the GPS transmitted signal.

The proposed Ocean Topography Experiment (TOPEX), if approved and funded which is very likely, will begin its mission in the later part of this decade. A LEO will be put in a circular orbit at an altitude of 1300 km. An experimental GPS receiver will be placed on

board this LEO for testing out a newly developed radio metric tracking technology (Ref. 8). This will provide an opportunity for experimenting the time synchronization system proposed in this paper. The differential GPS data needed for time synchronization can be derived from the tracking data of TOPEX satellite. As a matter of fact, the 1300-km LEO used in the above analysis has been adopted from TOPEX with its possible capability of providing precision global time synchronization in mind.

References:

1. P. W. Parkinson and S. W. Gilbert, "NAVSTAR: Global Positioning System -- Ten Years Later," Proc. IEEE, vol. 71, no. 10, 1983.
2. D. W. Allan and M. A. Weiss, "Accurate Time and Frequency Transfer During Common-View of a GPS Satellite," Proc. 34th Annual Frequency Control Symp., 1980.
3. P. A. Clements, "Intercontinental Time and Frequency Transfer using a Global Positioning System Timing Receiver," Proc. 14th Annual PTTI Application and Planning Meeting, Greenbelt, Maryland, 1982.
4. D. D. Davis, et. al., "Remote Synchronization Within a Few Nanoseconds by Simultaneous Viewing of the 1.575 GHz GPS Satellite Signals," Proc. 37th Annual Frequency Control Symp., 1983.
5. C. C. Councilman, III, et. al., "VLBI Clock Synchronization," Proc. IEEE, vol. 65, no. 11, 1977.
6. T. A. Clark, et. al., "Synchronization of Clocks by Very-Long-Baseline Interferometry," IEEE Trans. Instr. Meas., vol. IM-28, September 1979.
7. P. F. MacDoran, et. al., "SERIES: Satellite Emission Range Inferred Earth Surveying," 3rd Int. Geod. Symp. on Satellite Doppler positioning, Las Cruces, NM, 1982.
8. V. J. Ondrasik and S. C. Wu, "A Simple and Economical Tracking System with Subdecimeter Earth Satellite and Ground Receiver Position Determination Capabilities," 3rd Int. Symp. on the Use of Artificial Satellites for Geodesy and Geodynamics, Ermioni, Greece, 1982.

TABLE L. Error Models

Data Noise:	10 cm GPS pseudo-range
Main Site Locations:	10 cm
Ground Transit Location:	50 cm --- optimistic 5 m --- conservative
GPS Satellite Positions*:	(0.4m, 0.4m, 0.8m) optimistic (3m, 10m, 10m) conservative
LEO Position*:	(10cm, 15cm, 30cm) optimistic (5m, 5m, 5m) conservative
Zenith Tropospheric Delay:	10 cm
Mass of Earth:	1 part in 10^7
Geopotential (on LEO only):	10% of GEM 6 - APL 5.0

* The three components of satellite position errors are in altitude, cross-track and in-track directions, respectively.

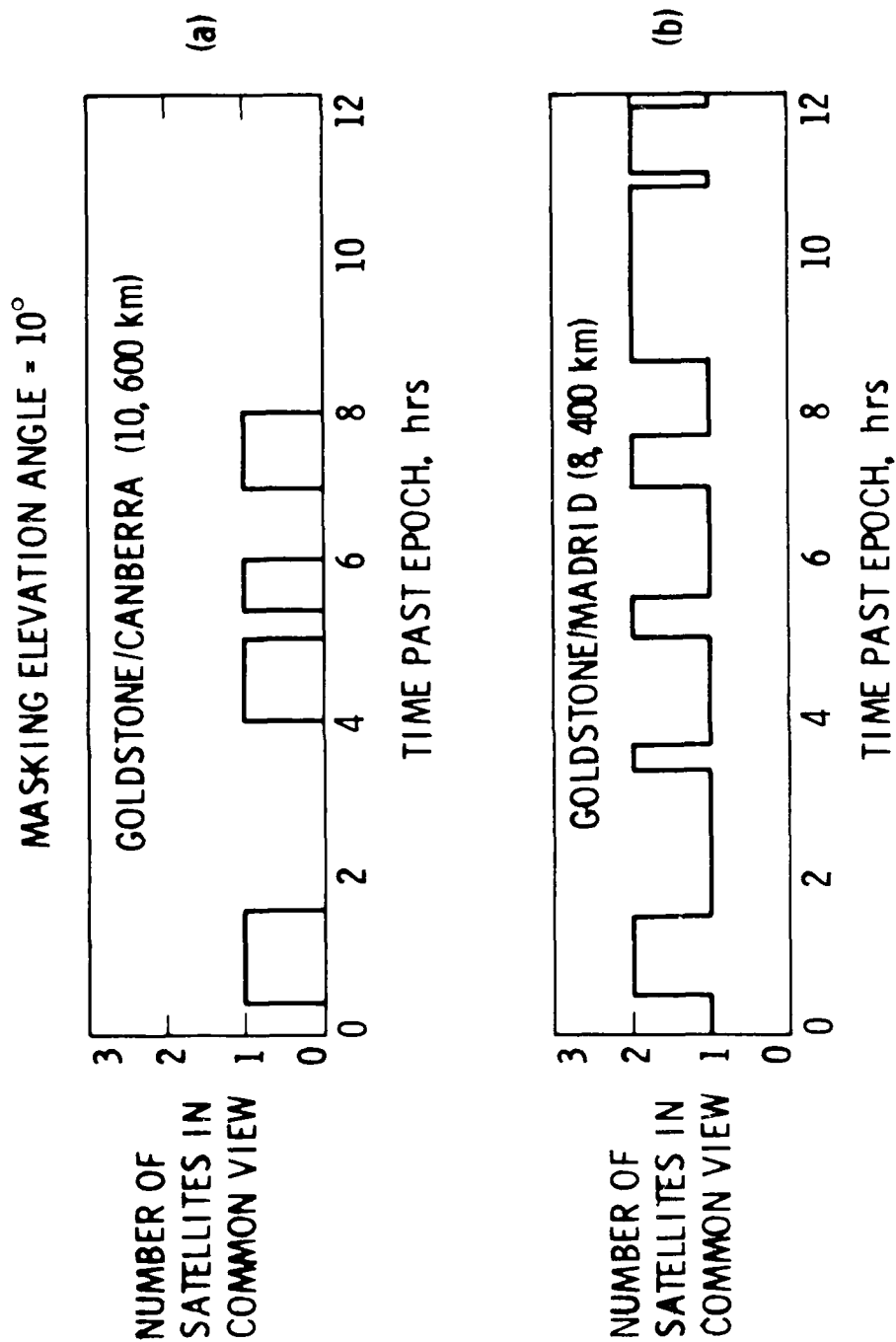


Figure 1. Number of GPS Satellites In Common View Between Remote Sites

AD-A149 163

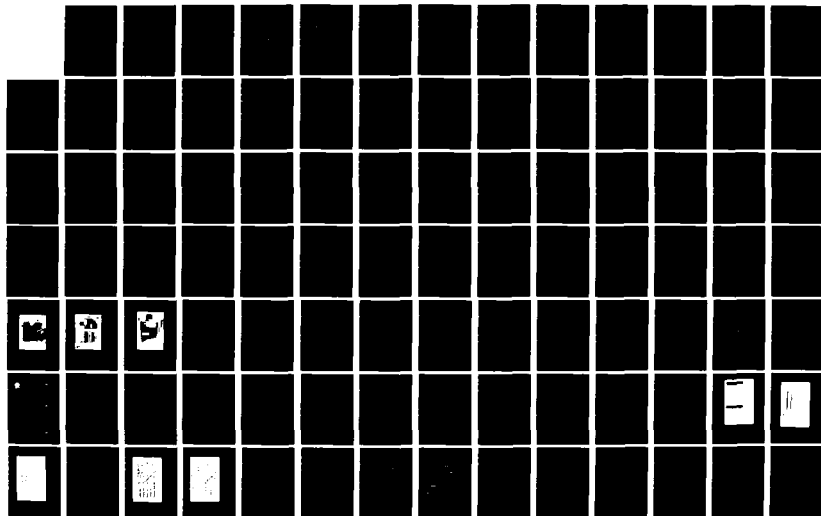
PROCEEDINGS OF THE ANNUAL PRECISE TIME AND TIME
INTERVAL (PTTI) APPLICATI. (U) NAVAL RESEARCH LAB
WASHINGTON DC J A MURRAY 02 APR 84

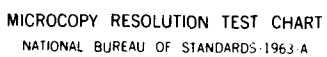
5/8

UNCLASSIFIED

F/G 5/9

NL





MICROCOPY RESOLUTION TEST CHART
NATIONAL BUREAU OF STANDARDS-1963-A

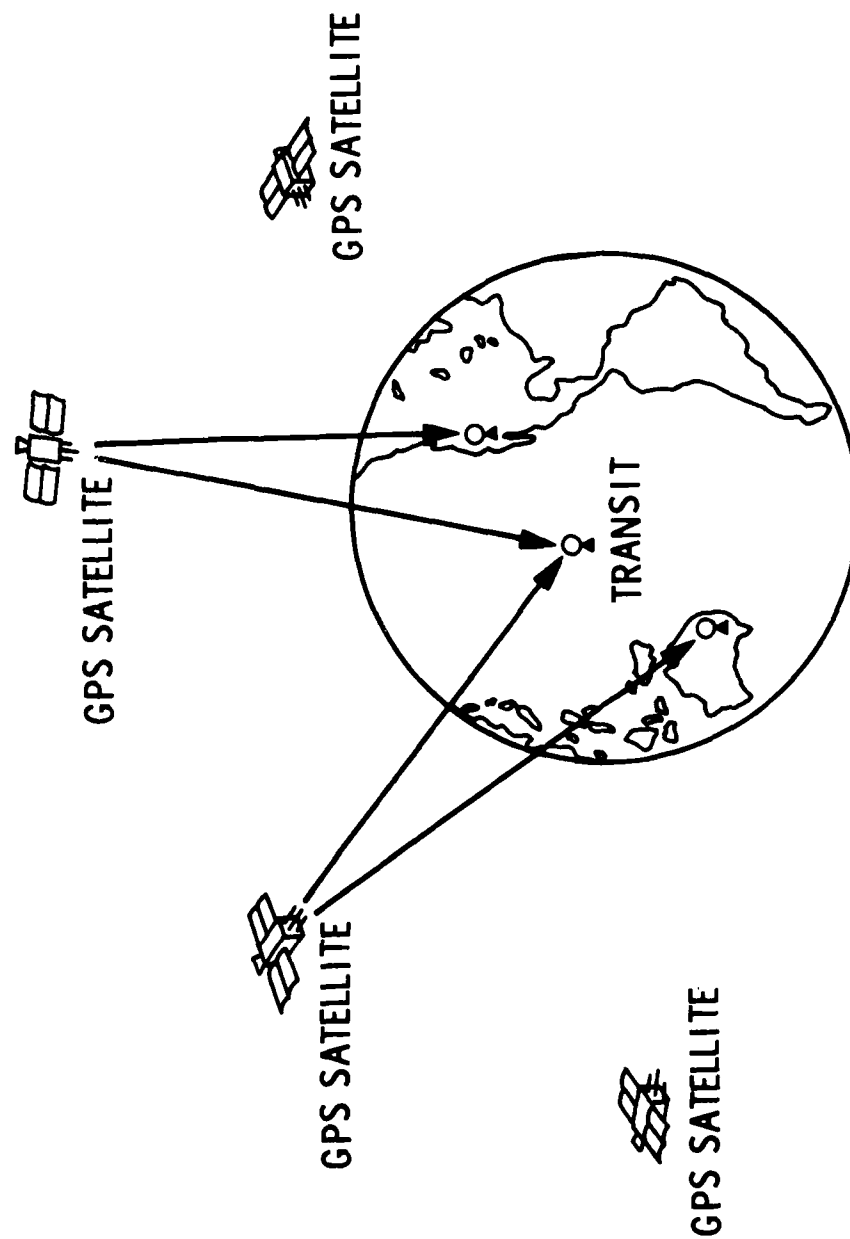


Figure 2. GPS Intercontinental Time Synchronization Via A Transit Station

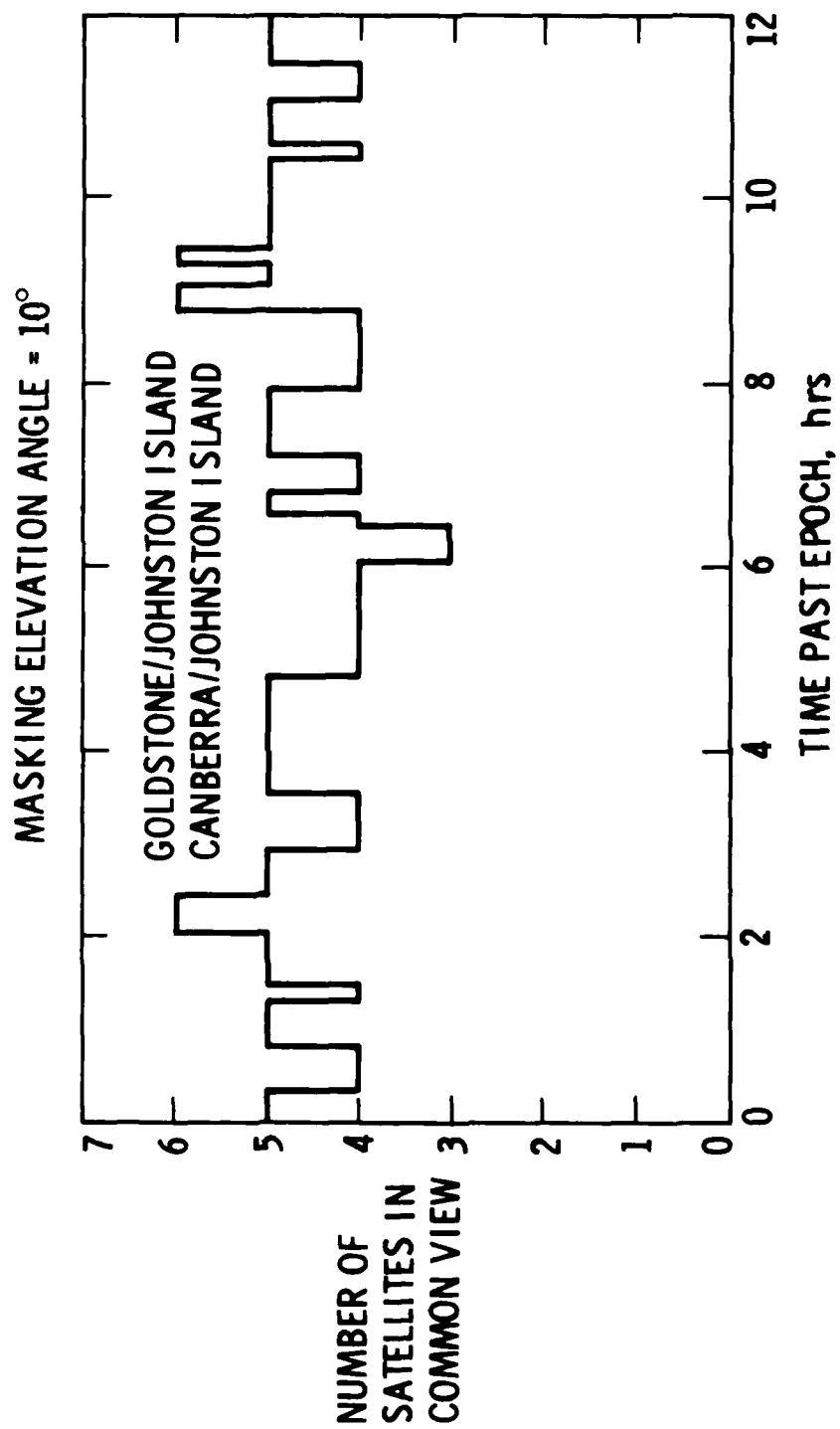


Figure 3. Number of GPS Satellites In Common View Between A Transit Site and One of The Main Sites

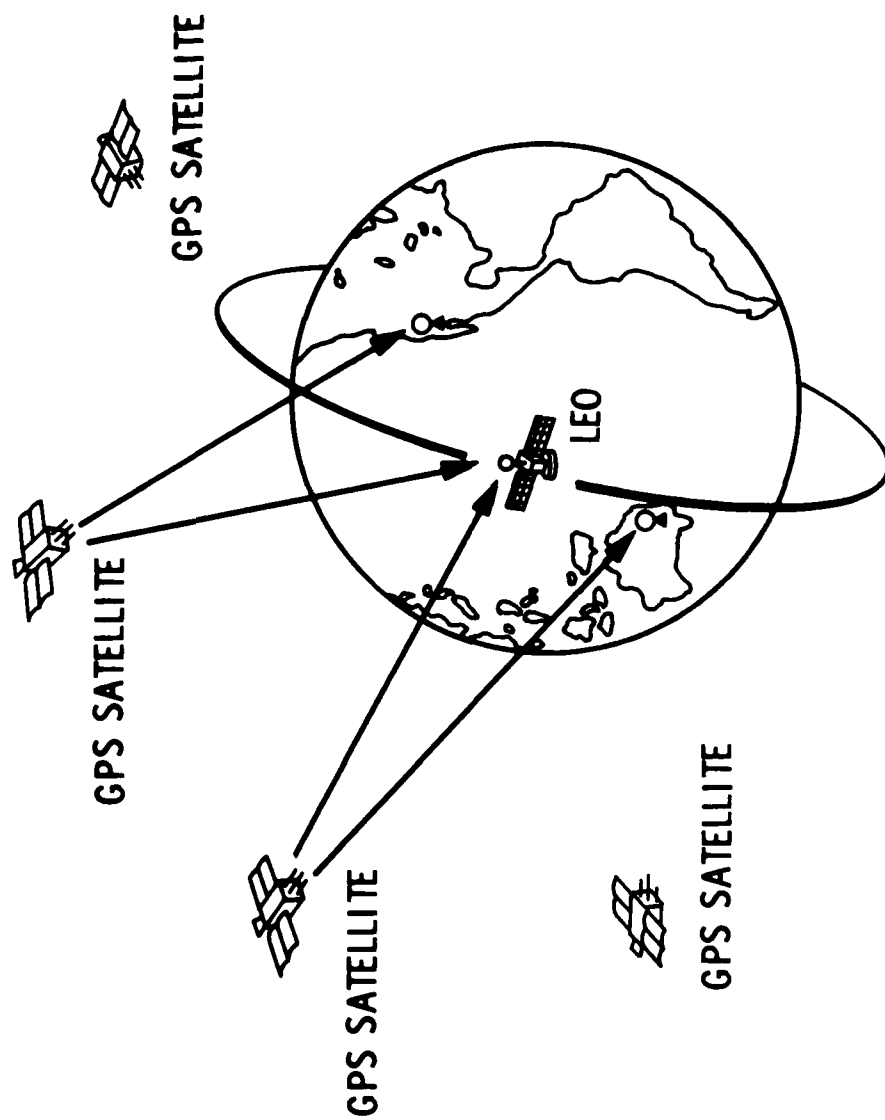


Figure 4. GPS Intercontinental Time Synchronization Via A Low Earth Orbiter

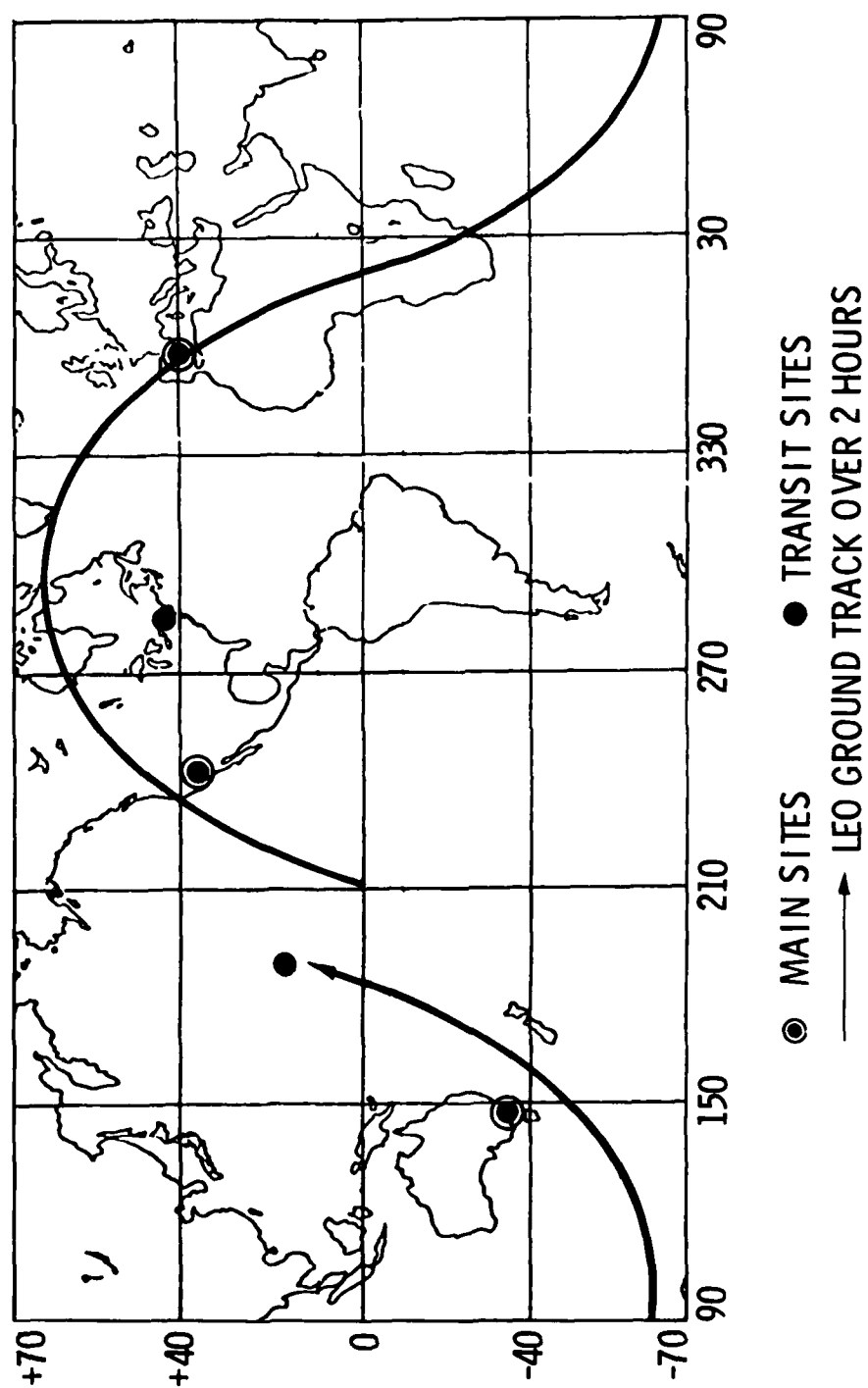


Figure 5. Geometry of The Problem

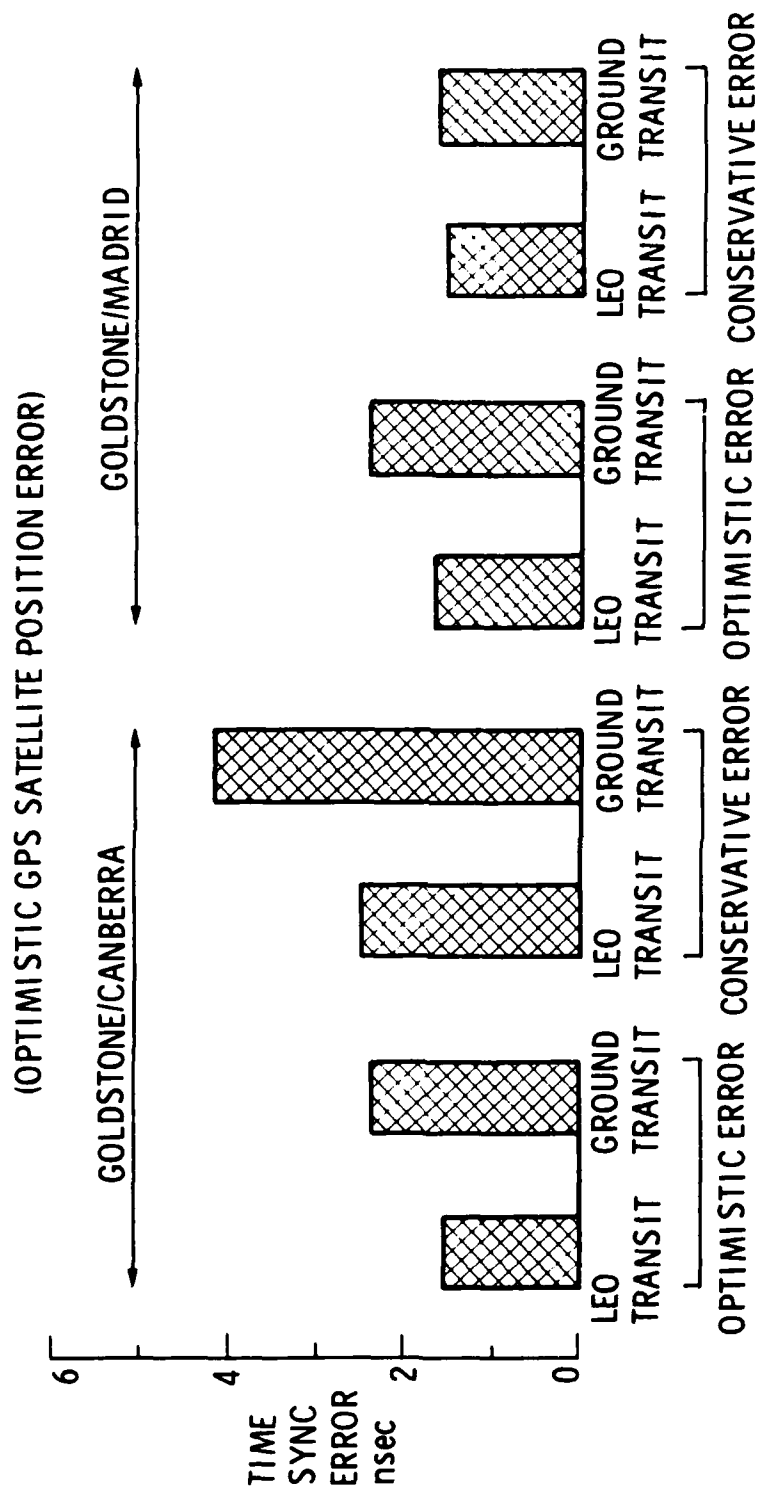


Figure 6. Estimated Time Synchronization Error Using Instantaneous Differential GPS Pseudo-Range

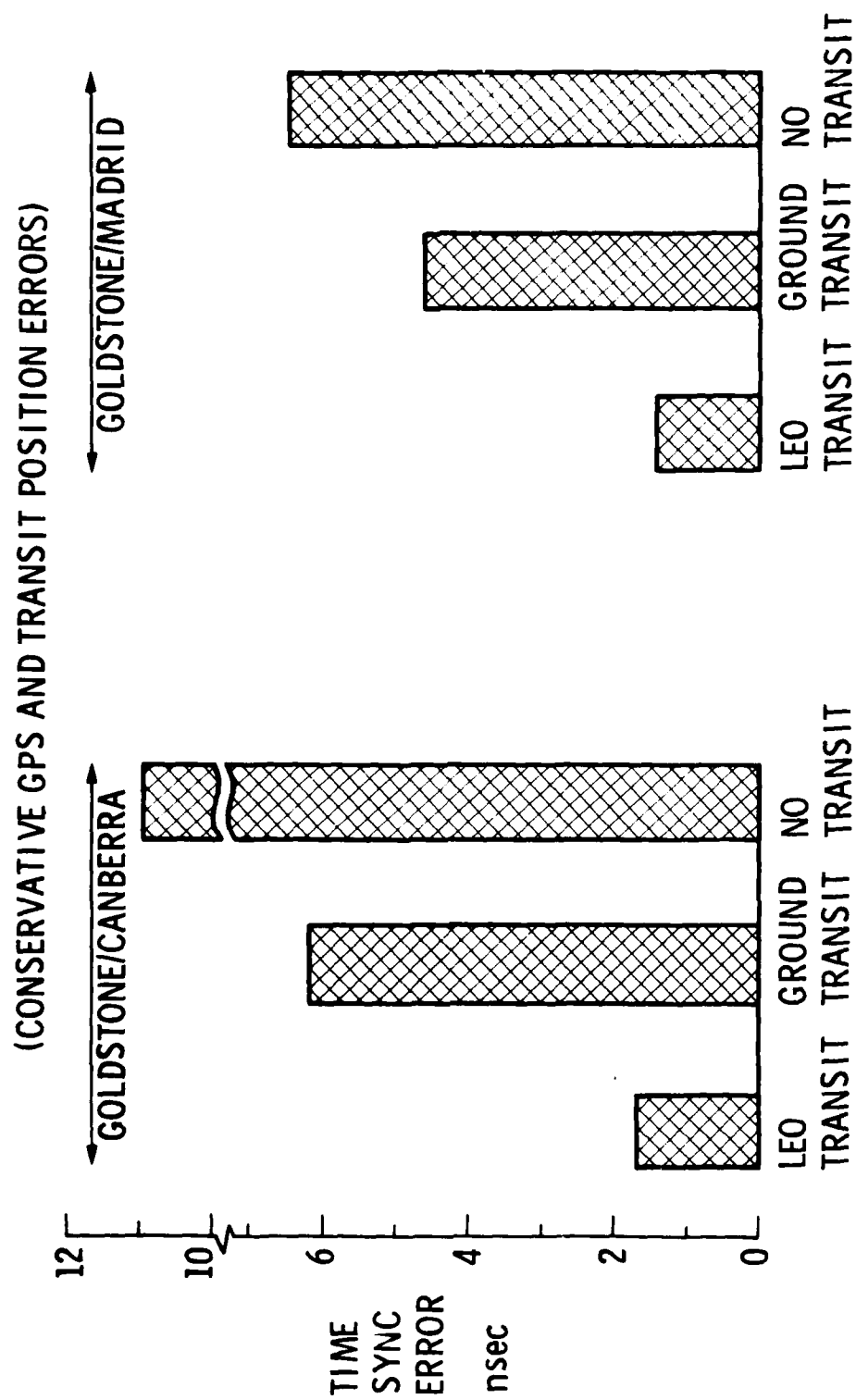


Figure 7. Estimated Time Synchronization Error Using Differential GPS Pseudo-Range Over 2 Hours

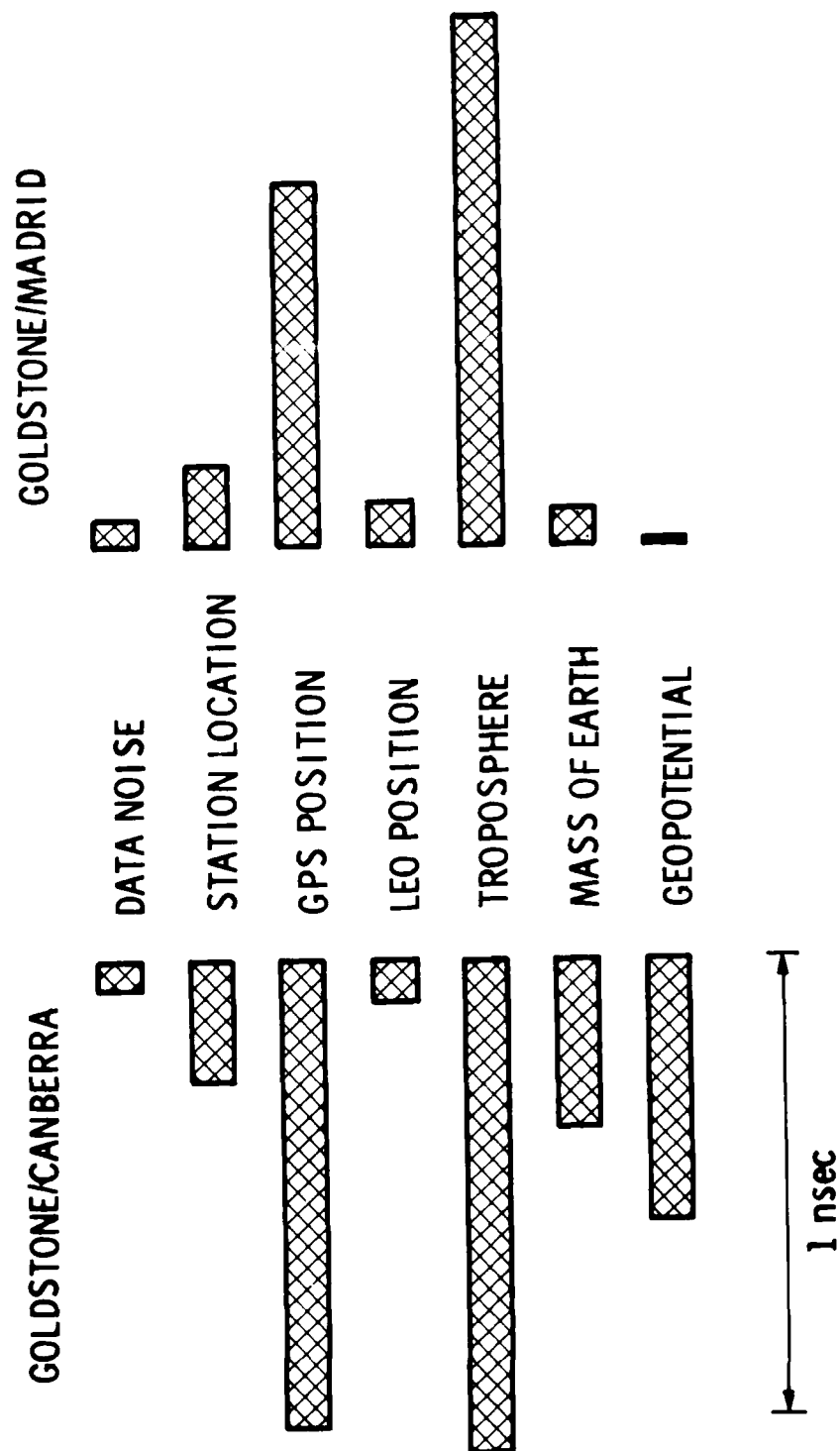


Figure 8. Breakdowns of Time Synchronization Errors

QUESTIONS AND ANSWERS

DR. VESSOT:

Bob Vessot, Smithsonian. At what level do you need tracking data for the low earth orbiter?

MR. WU:

Would you make it more specific?

DR. VESSOT:

Well, at what level of precision was tracking data needed for the low earth orbiter.

MR. WU:

Oh, for tracking the low earth orbiter it can be either a short arc which is about one centimeter, for the pseudo range, or you can do a long arc solution, which can be twenty centimeters, or you can use integrated doppler.

MR. ALLAN:

When is the low earth orbiter planned to be launched?

MR. WU:

The proposed Topex will be launched in February '89.

TIMING OF SPACECRAFT DATA

Time Accuracy Requirements and Timing Facilities
of the European Space Agency (ESA).

H.P. Dworak, European Space Operations Centre,
Darmstadt, West Germany

ABSTRACT

The time accuracy requirements for various ESA satellite missions are analysed; the requirements are grouped by the type of mission. The evolution of satellite timing techniques since 1968 is shown, and the requirements for future ESA missions (until the late 80's) are assessed.

Timing systems and their configuration at various ESA ground stations and the operations control centres are described.

Based on practical experience operational aspects will be presented, covering mainly Time Synchronisation, Time and Frequency corrections and typical problems encountered during routine operations such as routine monitoring, reporting, time/frequency offset calculations and adjustments.

Common time reference techniques operationally used, such as VHF transmission, LORAN-C, TRANSIT and travelling Clocks are compared in terms of availability, reliability and time accuracy.

The equipment performances of standard commercial timing systems, based on Caesium, Rubidium and Crystal oscillators are presented. Based on actual maintenance data acquired in ESA ground stations, the overall reliability of these systems and actual performance parameters in terms of MTBF, MDT, operational availability etc. are shown.

Two studies on future techniques in the field of time dissemination and time synchronisation conclude this paper: The LASSO mission (Laser Synchronisation from Stationary Orbit) and a low-cost time dissemination technique using METEOSAT, the European meteorological satellites, are briefly outlined.

1. INTRODUCTION TO THE ACTIVITIES OF ESA

1.1 General

The European Space Agency (ESA) was set up in 1975, grouping in a single body the complete range of European space activities. These had previously been conducted by ESRO - the European Space Research Organisation - and ELDO - the European Launcher Development Organisation - in their respective fields of scientific satellite development and launcher construction.

Under the terms of its convention, the Agency's task is to provide, for exclusively peaceful purposes, co-operation among European States in space research and technology, with a view of their use for scientific purposes and for operational applications systems.

1.2 Funding

The general budget and the scientific programmes are funded by the 11 European Member States on the basis of their national income. Other programmes - mainly applications programmes, are optional with varying contributions from different States, depending on their interest and involvement in the respective programme. Examples are the ARIANE launcher development, Spacelab, Telecommunications or Earth Observation programmes.

1.3 Establishments

The headquarters of the Agency is in Paris and there are two main technical establishments - a Technology Centre in the Netherlands, called ESTEC and an Operations Centre at Darmstadt, Germany. The technology centre is responsible for the development of Spacecraft, whereas the operations centre (ESOC) is in charge of the satellite orbital operations.

1.4 Ground Stations

In performing this task, ESOC uses a network of 7 ground stations, linked to the control centre by means of suitable data communications links (Fig. 1).

Carnarvon (Australia), Kourou (French Guiana), Malindi (Kenya), Redu (Belgium), and three specialised stations for the geostationary satellites, Odenwald (Germany), Villafranca (Spain), and Ibaraki (Japan).

The technical role of these stations and the ESOC control centre will be displayed in more detail - in the context of Timing techniques - in the following sections.

1.5 Satellite Missions

A total of 13 scientific ESA satellites were launched from 1968 to date, all of which were highly successful (Table 2). Some exceeded expectations as to both lifetime and scientific return.

The ESA applications satellites were all in the field of Communications or Earth Observation (Table 3.).

More details about these science and applications missions will be given in the following section.

2. TIME ACCURACY REQUIREMENTS FOR SPACECRAFT DATA

2.1 Evolution of Time Accuracy of Station Clocks

Table 1 shows the improvement achieved during the last 15 years in the timing of satellite data.

Whereas VLF or HF time dissemination methods were used for synchronisation of station clocks during the early 70's, LORAN-C and TRANSIT are now the standard reference systems in use. If higher precisions are required, time comparison by means of portable clocks are performed.

This will be explained in more detail in the following section.

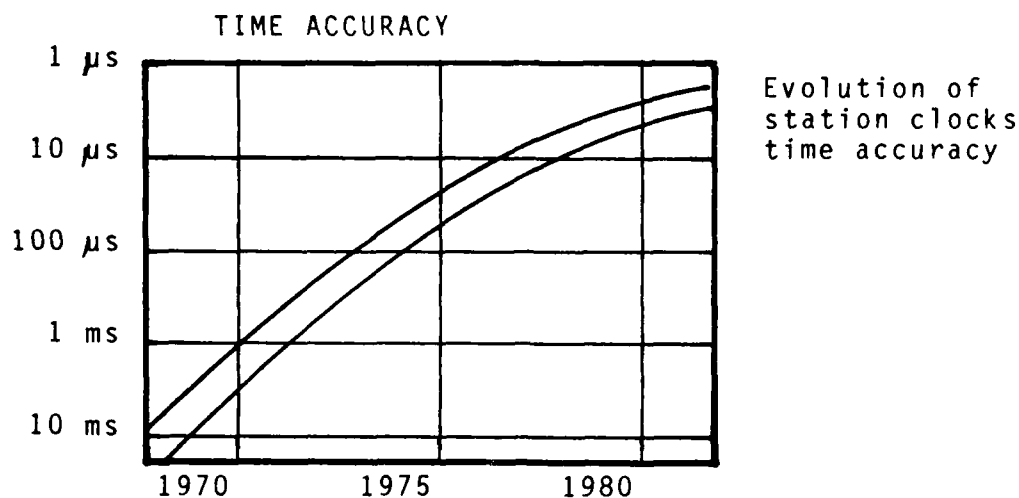


TABLE 1

2.2 In tables 2 and 3 the ESA satellite missions are listed with the associated time accuracy requirement. They are grouped into scientific and applications satellites and include current missions and a selection of future missions. From the tables one can conclude that Science Missions are the main driver for High Accuracy Timing Systems. In addition to the absolute accuracy with respect to UTC a good short term frequency stability (typ. 10^{-13}) is required for all future science missions.

In the field of applications satellites the absolute time accuracy is of lesser importance. The criteria of the high frequency stability however also applies to the meteorological and earth observation missions.

Common to all missions the determination of the orbital position is one of the drivers for precise timing of data. For certain future mission, like the Navigation Satellite, this requirement will be in the order of 3 - 10 ns.

ESA SCIENTIFIC SATELLITES

SATELLITE	LAUNCH DATE	MISSION	TIME ACCURACY
ESRO-II/ IRIS	170568	COSMIC RAYS AND SOLAR X-RAYS	100...
ESRO-IA/ AURORAE	031068	POLAR IONOSPHERE AND AURORAL PHENOMENA	
HEOS-1	051268	SOLAR WIND AND INTERPLANETARY MEDIUM	
ESRO-IB/ BOREAS	011069	POLAR IONOSPHERE AND AURORAL PHENOMENA	10 ms
HEOS-2	310172	POLAR MAGNETOSPHERE AND INTER-PLANETARY MEDIUM	
TD-1	120372	ULTRAVIOLET ASTRONOMY	
ESRO-IV	221172	IONOSPHERE AND SOLAR PARTICLES	1 ms
COS-B	090875	GAMMA RAY ASTRONOMY	
GEOS-1	200477	MAGNETOSPHERE	
ISEE-B	221077	MAGNETOSPHERE AND SUN-EARTH RELATIONS	50 μ s
IUE	260178	ULTRAVIOLET ASTRONOMY	
GEOS-2	140778	MAGNETOSPHERE	
EXOSAT	260583	X-RAY ASTRONOMY	10 μ s
HIPPARCOS	1988	ASTRONOMY	
GIOTTO	1985	HALLEY COMET ENCOUNTER	
ISO	1990	INFRARED ASTRONOMY	5 μ s
			100 μ s

TABLE 2

ESA APPLICATIONS SATELLITES

SATELLITES	LAUNCH DATE	MISSION	TIME ACCURACY
OTS MARECS-A ECS-1	11/05/78 20/12/81 16/06/83	TELECOMMUNICATIONS	100..250 μ s
METEOSAT-1 METEOSAT-2 METEOSAT-OP	23/11/77 19/06/81 198	METEOROLOGY	100..250 μ s
OLYMPUS	1986	COMMUNICATIONS	100 μ s
EURECA	1986	MICROGRAVITY MAT.SCIENCE	100 ms
ERS	1988	EARTH OBSERVATION	100 μ s
NAVSAT	1990 +	NAVIGATION	t.b.d.
POPSAT	1990 +	TERRESTRIAL POSITIONING/ KINEMATICS	t.b.d.

TABLE 3

3. OPERATIONS ASPECTS

3.1 Equipment Configurations

Three examples shall illustrate typical timing equipment configurations at ESA ground stations.

3.1.1 Odenwald Station

Fig. 2 shows a diagram of the timing and frequency subsystem in use at our ODENWALD station, the prime station for the meteorological satellites METEOSAT 1 and 2 and the telemetry receiving station for the scientific satellite GEOS.

Two caesium standards are used to generate 5 MHz outputs with a frequency stability of $\pm 5 \times 10^{-12}$.

The 5 MHz outputs are fed into a switching module consisting of two phase shifters, two divider units, and two switching units. The phase shifters provide manual adjustment of the phase of the off-line standard to enable signal switching without any phase jumps. The dividers provide the 1 MHz and 100 KHz outputs for the station. The outputs from the switching module feed four amplifier modules; each amplifier module has sixteen frequency outputs.

Time Code Generators provide further outputs of serial encoded data and 1 Hz pulses to the majority decision unit and master/slave selection unit, which compares the numerous inputs from the different chains and makes a decision which input to use on a 'best two from three' basis. The majority 1 Hz pulse is made available at the output for comparison with the LORAN-C reference.

The time accuracy which is achieved with this configuration is within $\pm 20 \mu\text{s}$ of UTC.

3.1.2 Redu Station

Slightly simpler variant of the timing subsystems used in other ESA stations is shown in Fig. 3. It is the timing section of the REDU ground station. This station is the prime TT&C station and control centre for the ECS telecommunications satellites. It further provides back-up support in VHF to all other ESA

missions. Since the time accuracy requirements are less stringent, the frequency standards used in this configuration are two Quartz oscillators. They generate 5 MHz, which is compared to a standard frequency derived from a LORAN-C receiver. An error signal is produced, which forms the basis for correction of the station oscillators. The outputs from the two oscillators are taken via a switching module and amplifiers to two time code generators, which in turn supply the time code generator selection module with IRIG-B, PDM, 1, 5 and 10 MHz time signals.

Since the Redu station also includes the control centre for ECS, the timing system includes stop clocks, time displays, and other control centre specific equipment.

With this system configuration the time accuracy achieved is in the order of 50 μ s of UTC.

3.1.3 Transfer Orbit Network

Another variant of timing systems is shown in Fig. 4. This configuration is implemented at the equatorially located stations of the transfer orbit network i.e. Kourou, Malindi, Carnarvon. It can be seen that there is not much redundancy built in, apart the double frequency generator, consisting of a Rubidium standard backed up by a Quartz.

Since LORAN-C reception is not possible in the said stations, time is checked against a TRANSIT Satellite receiver. The resultant time accuracy which is achieved with these systems is in the order of 50 - 100 μ s.

3.2 Synchronisation of Timing Systems

- 3.2.1 Synchronisation of the various timing systems described above, with respect to UTC, is achieved by means of VLF reception, LORAN-C, TRANSIT Satellites or Travelling Clocks. Table 4 shows the normal ways of synchronising station clocks and the references used.

Reference Ground Stations	V L F	L O R A N	T R A N S I T	T R A V E L L I N G C L O C K
OCC	X			(X)
ODENWALD (Germany)		X		(X)
REDU (Belgium)		X		(X)
VILLAFRANCA (Spain)		X		(X)
MALINDI (Kenya)			X	
KOUROU (Fr. Guyana)			X	
CARNARVON (Australia)			X	

Table 4

3.2.2 VLF Reception of timing signals is in use at all stations for coarse time synchronisation and as back-up reference to the respective higher-precision reference systems.

3.2.3 LORAN-C is the standard time comparison technique at sites where LORAN reception is possible. The time offset of station clocks is determined in the normal way by measuring the interval between the reception of the LORAN-C pulse and the station's 1 pps signal and subtracting the fixed propagation delay. The latter is obtained from USNO (US Naval Observatory), calculated on the basis of the station coordinates, and corrected by means of Travelling Clock measurements.

The time offsets are measured by means of LORAN-C on a daily basis. They are corrected retroactively after availability of the "Series-4" LORAN-C offsets. Typical recordings of these time and frequency offset measurements are shown in the following section.

3.2.4 TRANSIT satellites are used for time synchronisation at our equatorial stations MALINDI, KOUROU, and CARNARVON, where LORAN-C reception is difficult or impossible. The operation of TRANSIT satellite timing receivers is not described here; the principle is assumed to be well known. Two important operational aspects, however, are the simplicity of operation and the reliability of the equipment. In particular in the smaller ESA stations mentioned above, with a typical manning of not more than 5 or 6 M+O Technicians, the fully automatic operation of the Satellite Timing receivers without operator attention is a particular advantage.

The time accuracy achieved by means of TRANSIT time comparison is in the order of 5 μ s of UTC.

3.2.5 A Travelling Clock is used for synchronisation of station timing systems, whenever higher precision is required. A home-made portable Rubidium clock is used for this purpose. The autonomy of this clock - limited by the battery capacity - is approximately 4.5 hours. During longer trips the battery has to be recharged - this takes about 1 hour - but for synchronisation of the European ESA sites, the 4.5 hr autonomy is usually sufficient.

The accuracy achieved by time comparison with the portable Rubidium clock is better than 1 μ s which is largely sufficient for our present applications.

3.3 Time and Frequency Corrections

The offsets of the station timing systems are determined from daily measurements, using the reference systems outlined above. Examples of time offset recordings are shown in Fig. 5.

Three figures show the typical behaviour of a clock driven by a Rubidium oscillator. You will note the negative frequency drift, characteristic of Rb oscillators. The offsets are determined against LORAN-C as reference. Please note that the recordings are not "Series-4 corrected", i.e. the retroactive corrections of time offsets in the LORAN-C system have not been performed.

From the time offset curve the frequency offset is determined and compensated for from time to time. Time offset corrections are normally not performed by clock-resetting, but through over-compensation of the frequency offset, except if time jumps occur. The obvious advantage of this method is the fact that no excessive deviation of the frequency from the nominal frequency can build up.

In the portable rubidium clock mentioned in the previous chapter, the "time transport" is normally performed when the time offset parabola reaches its horizontal part, thus minimizing the effects of frequency offsets (and thus time drifts) during the time comparison trip.

3.4 Typical Operational Problems

The following is a short summary from the user's point of view of the most frequent problems in operating timing systems at satellite ground stations:

1) Time Jumps

- a) Reason: Equipment failure, mostly power supply of TCG.
- b) Detection: Regular checks of time consistency.
- c) Corrective action: Time reset, correction of time-coded data.

2) Frequency_Jumps

- a) Reason: Equipment (oscillator) malfunction
- b) Detection: Change of time offset drift
- c) Corrective action: Frequency adjustment or corrective maintenance.

3) Incorrect_Frequency_Setting

- a) Reason: Operator error or incorrect calibration of frequency adjustment.
- b) Detection: Excessive time drift or drift in wrong direction.
- c) Corrective action: Frequency correction, Establishment of frequency "calibration curve".

4) Wrong_Leap_Second_Introduction

- a) Reason: Operator error (mostly)
- b) Detection: Course time check by means of VLF.
- c) Corrective action: Time correction with full synchronisation (VLF, LORAN-C, possibly Travelling clock).

5) LORAN-C_Reference_Incorrect

- a) Reason: Receiver locked on wrong cycle of LORAN pulse.
- b) Detection: Travelling clock time comparison.
- c) Corrective action: Resynch of LORAN receiver.

6) LORAN-C_Propagation_Delay_Error

- a) Reason: Error in calculation of propagation delay, wrong coordinates.
- b) Detection: Travelling Clock.
- c) Corrective action: Correction of fixed delay for LORAN chain.

4. EQUIPMENT PERFORMANCE

The reliability of the timing systems described above is continuously being monitored at the ESA ground stations. From equipment failure records over the past 4 years some performance parameters are summarised below.

Two categories of timing systems were analysed:

- Three systems based on Rubidium clocks, and
- One system based on a Caesium standard.

All systems were in continuous operation.

The results are as follows:

TYPE OF CLOCK	MTBF	MTTR
Rubidium	2100 h	113 h
Caesium	1700 h	503 h

From these figures it is concluded that systems based on Caesium clocks have a slightly higher failure rate than Rubidium clocks. The main difference, however, is in the MTTR which is 4...5 times longer for Caesiums. Mainly due to their higher complexity these systems required frequent corrective maintenance intervention by the manufacturer, which caused long times to repair.

5. TIME DISSEMINATION VIA METEOSAT (STUDY)

5.1 Introduction

A study was carried out on the possibility to use the existing METEOSAT satellites for time dissemination. Similar to the GOES time dissemination system, which uses the DCP (Data Collection Platform) interrogation function, a method was worked out which could provide a similar service with an accuracy and stability in the order of 10 μ s, with a target of 2...3 μ s. The METEOSAT system could thus bridge the gap between the performance of a commercial Rubidium standard and a prime standard, at a cost of less than \$10,000.

5.2 System Concept

The time dissemination system proposed consists of the following elements (Fig. 6):

- A satellite, carrying a transponder of reasonable propagation delay stability, and having an orbit determination system allowing position determination to within about 100 m.
- A ground station which can at any moment be supplied with satellite position information. The station should be equipped with a timing subsystem which allows timekeeping to the microsecond accuracy. The station will transmit timing and position information to the spacecraft.
- User stations. These receive the timing message, apply a correction for the propagation delay to their specific location, and set a local (running) clock accordingly.
- A monitoring and calibration facility consisting essentially of a set of user equipment located at a primary timing reference.

In order to avoid operational conflicts the additional occupation of the satellite communication link should be limited to one percent. Timing transmission will therefore take the form of updates: At regular intervals a message is transmitted containing essentially an "event" occurring at an instant, identified in Universal Time. The user equipment will note the local time at reception of the event and from the difference (corrected for propagation delay) it will calculate and implement a correction to the locally generated time.

A detailed description of the system is contained in Ref. (1).

6. LASSO MISSION: LASER SYNCHRONISATION FROM STATIONARY ORBIT

6.1 Introduction

The concept of the LASSO mission is briefly outlined. This mission was designed to be flown on the SIRIO-2 Spacecraft. Due to a malfunction of the ARIANE launch vehicle the satellite was destroyed during the launch in Sept 1982. In the meantime the LASSO mission has been taken up again and is now planned to be integrated into the METEOSAT-3 payload, due to be launched in 1985.

6.2 Principle of Operations

Fig. 7 illustrates the synchronisation of two atomic clocks, e.g. one in the United States and one in Europe. Each clock triggers a laser pulse from a nearby laser station towards the satellite at a predefined time. The satellite sensor and oscillator assembly will then time-tag the arrival of the two pulses. Assuming equal distances between the laser stations and the spacecraft, any difference in arrival times of the two pulses will be proportional to the synchronisation offset between the atomic clocks. This measured difference can be transmitted along with the satellite's telemetry to the ground for clock synchronisation.

In practice the earth - satellite laser propagation time varies with the distance between the participating station and the satellite. To allow the stations to calculate this distance and perform the necessary corrections for the propagation delay, the satellite is equipped with so-called "Retro-reflectors", i.e. mirrors which reflect the incoming laser pulse back to its originating station.

This principle is shown in Fig. 8, where t_A and t_B are the departure times of the laser pulses, T_A and T_B are the propagation delays, R is the interval measured on-board the satellite. From these values the required clock correction C is calculated, according to the formula

$$C = t_A + T_A + R - T_B - t_B$$

The precision of the clock comparison to be obtained is obviously dependent on the precision to which each term of the above equation can be measured; in principle, it can be as good as 1 ns.

In the time available it is obviously not possible to describe in detail all the elements and the operational set-up of the LASSO system. This information can be found in Ref (2).

REFERENCES

- (1) Transmission of Precision Timing by METEOSAT
ESOC/GEED/Studies Branch
GEED/7030/EEL/SLE
- (2) SIRIO-2 Programme
ESA SP-1039, August 1981

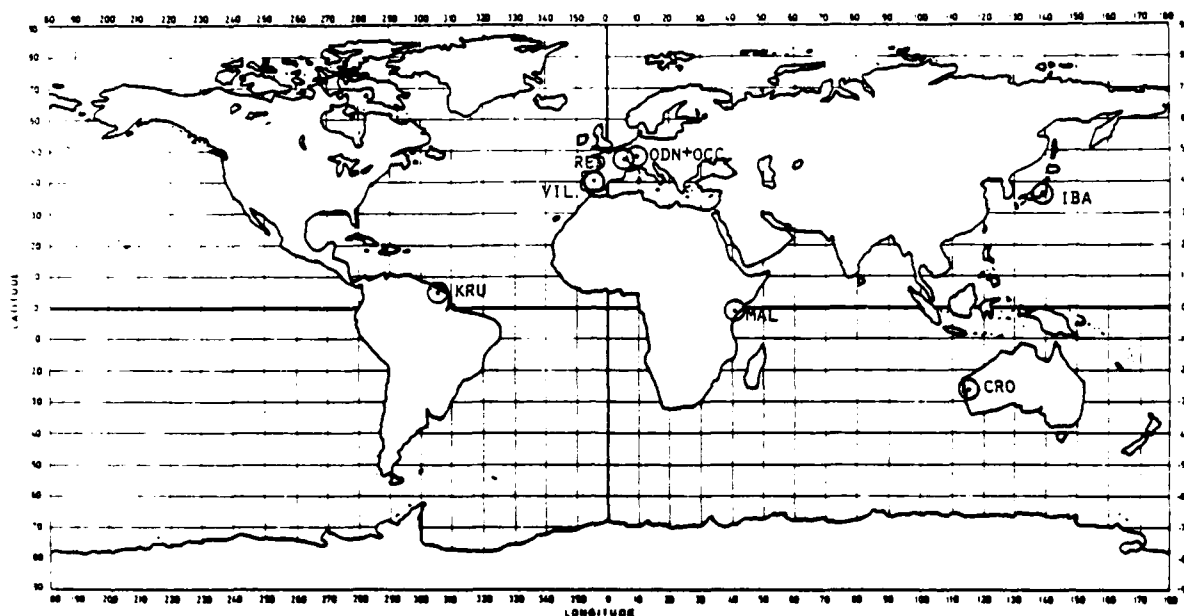


FIG. 1. ESTRACK GROUND STATIONS

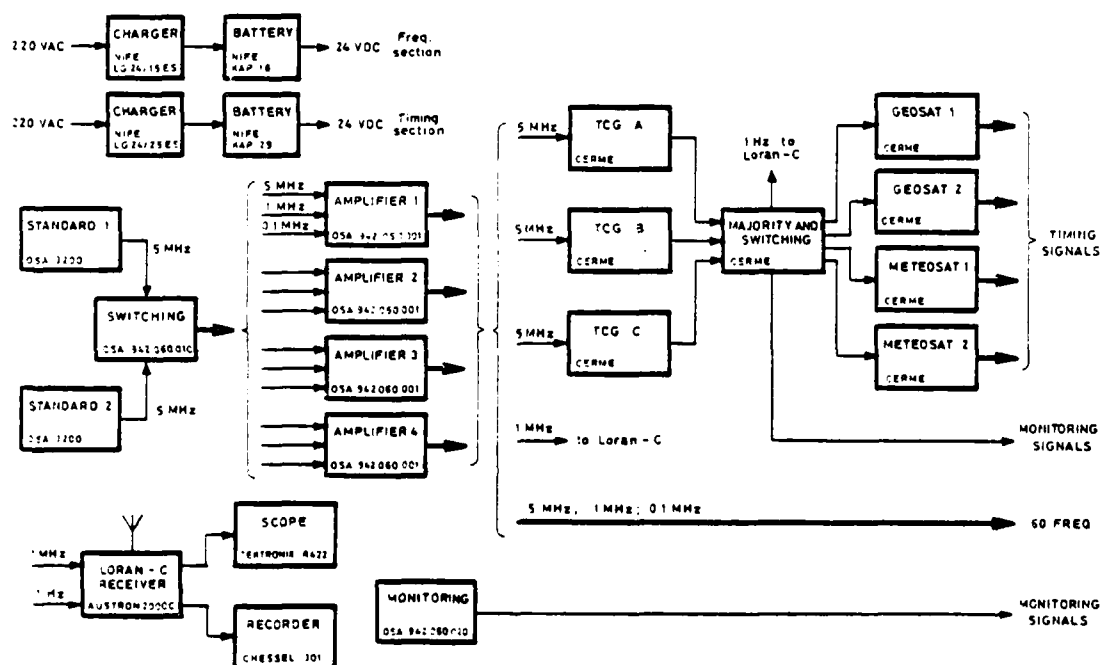


FIG. 2. BLOCK DIAGRAM FOR GEOS-METEOSAT GROUND STATION

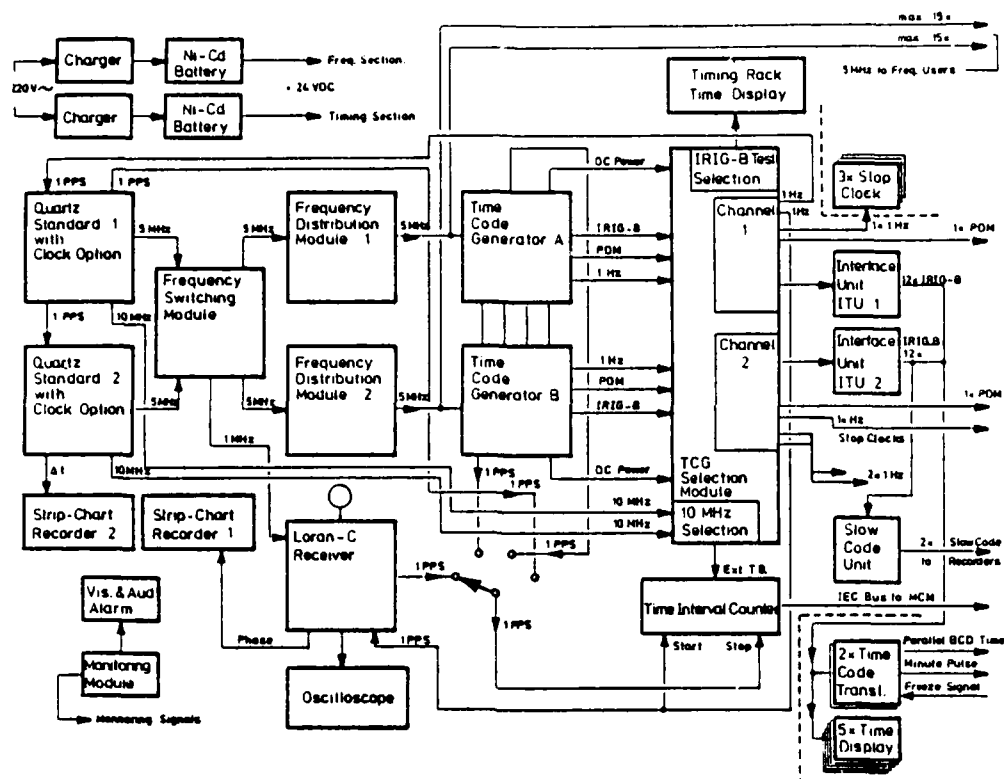


FIG. 3. REDU FREQUENCY AND TIMING SUBSYSTEM BLOCK DIAGRAM

TIMING SUBSYSTEM
BLOCKDIAGRAM

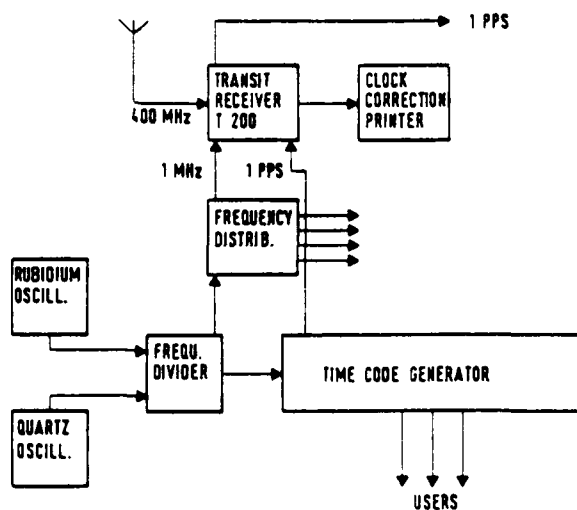


FIG. 4. TRANSFER ORBIT NETWORK STATION

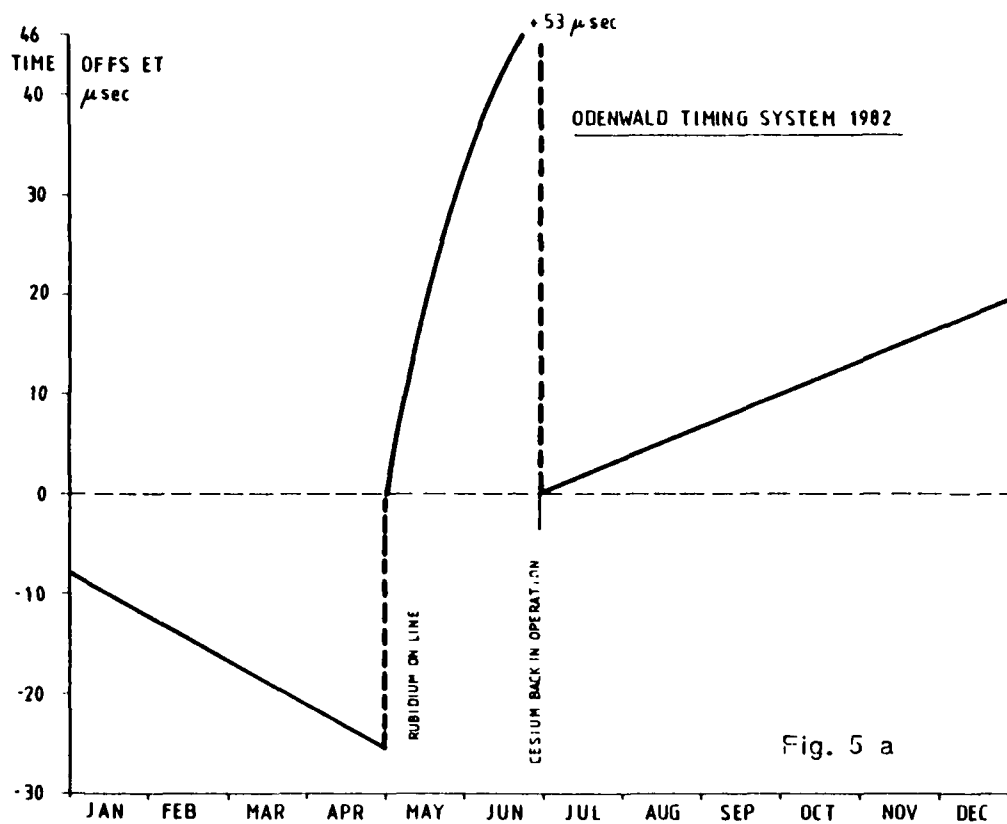


Fig. 5 a

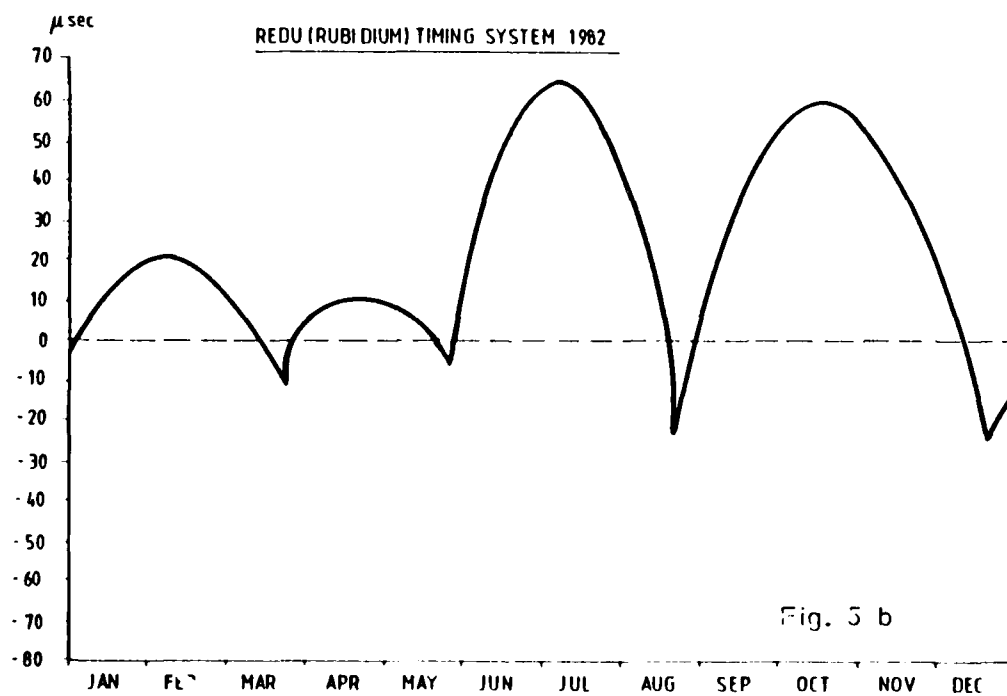
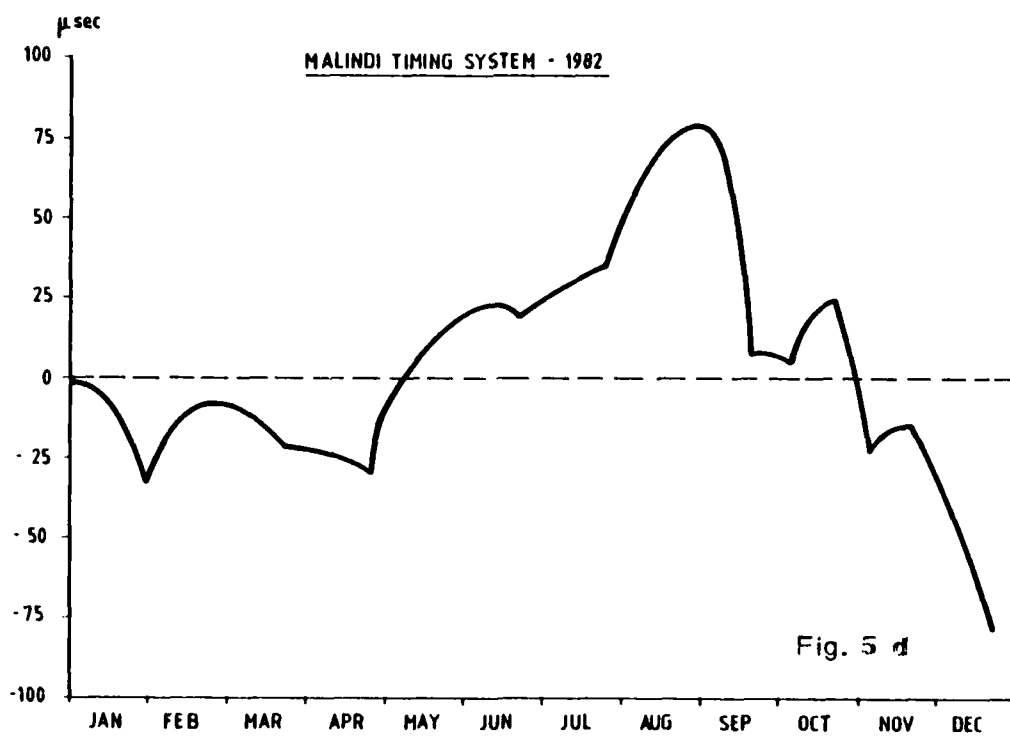
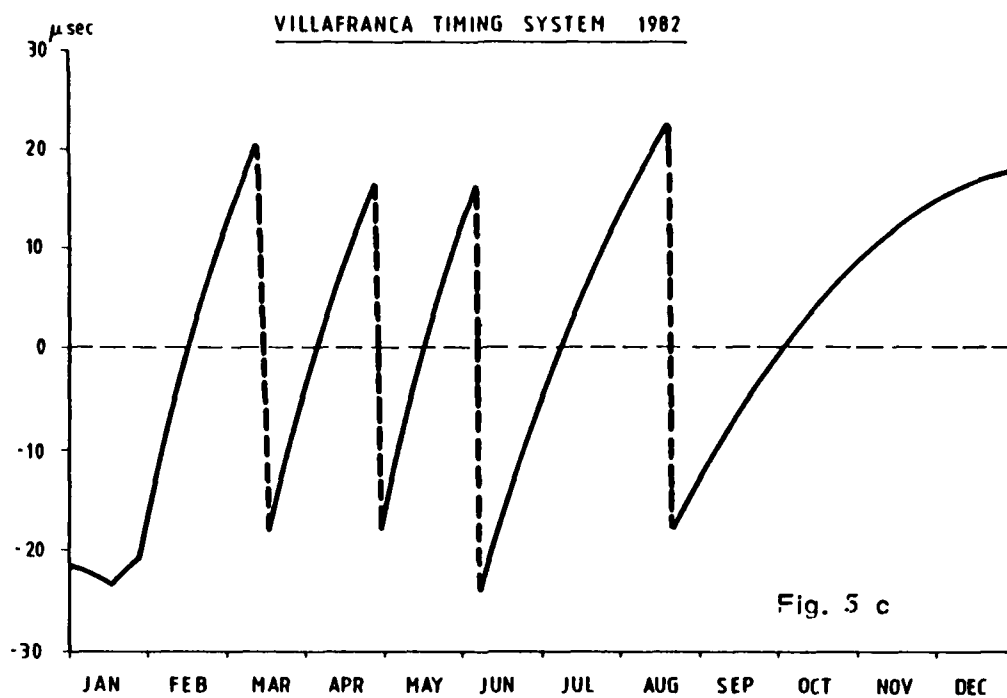


Fig. 5 b



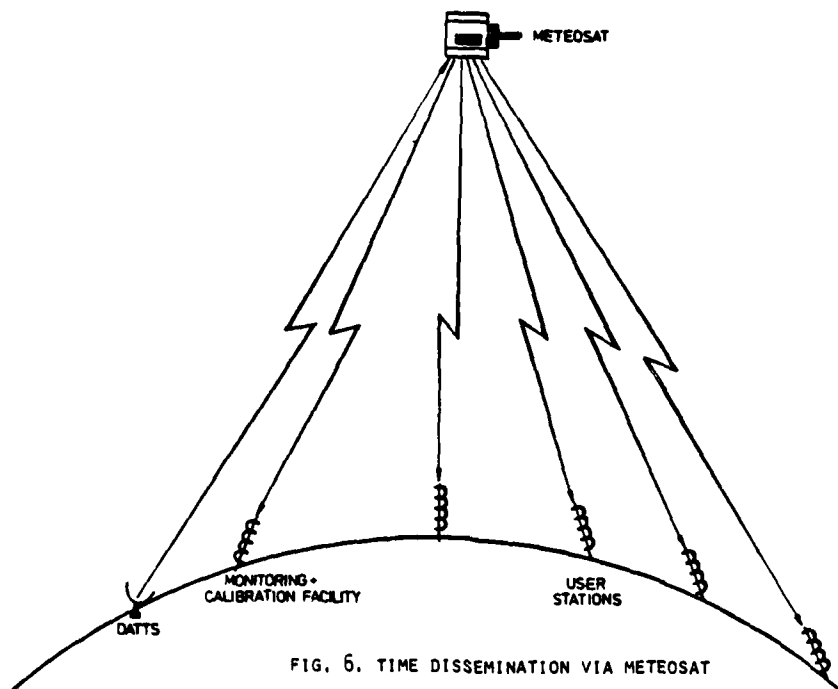


FIG. 6. TIME DISSEMINATION VIA METEOSAT

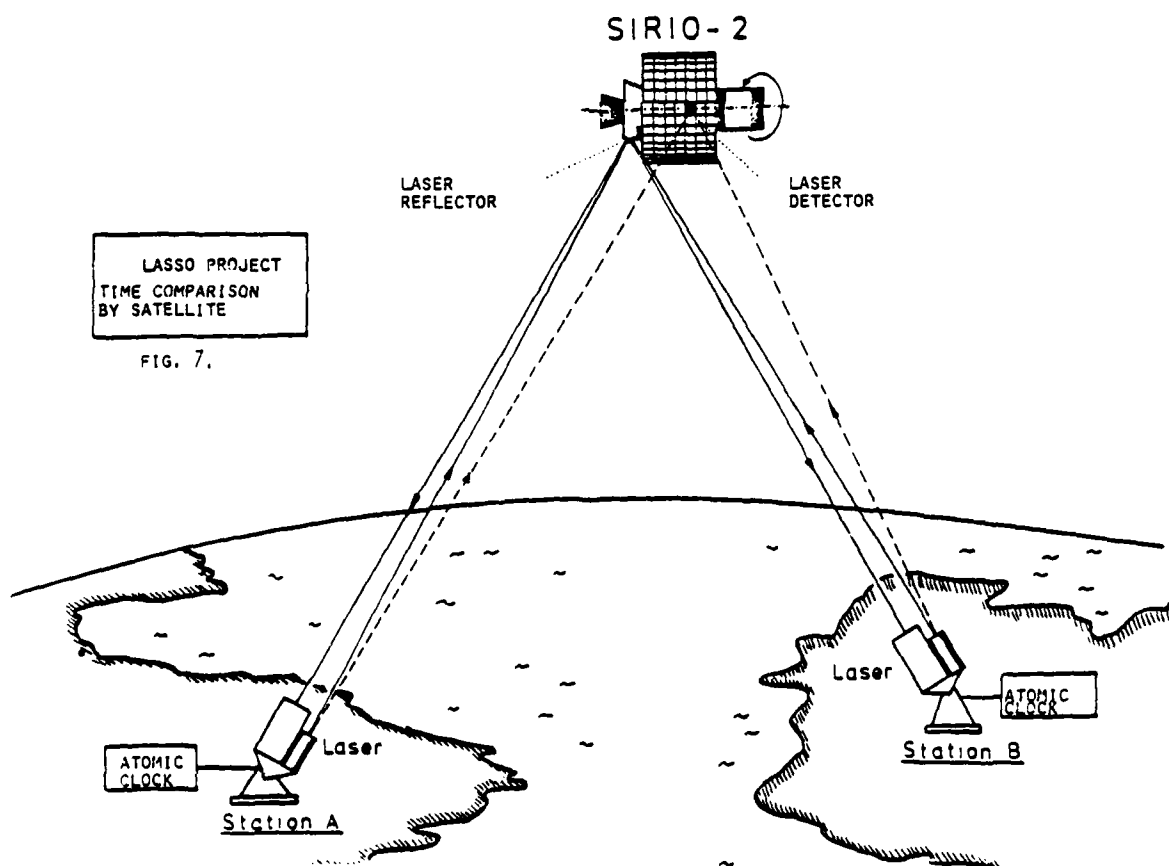
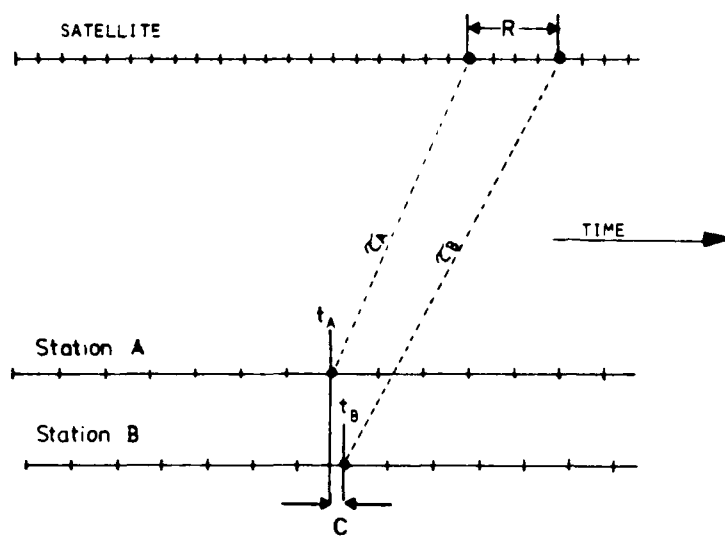


FIG. 7.



$$C = t_A - t_B + \tau_A - \tau_B + R$$

FIG. 8. TIME COMPARISON BETWEEN STATION A AND B

QUESTIONS AND ANSWERS

None for Paper #20.

UHF IRIG G DISTRIBUTION SYSTEM

M. Tope
Kode, Inc.
Tustin, California

This system is designed to transfer precision time from the VAFB Master Timing System to a remote location.

Figure one is a block diagram showing the Master Timing System, the Local IRIG G System, the Transmit/Receive System and the Remote IRIG G System. Notice that the timing is transmitted to the remote site via an RF link. This method was chosen because of the rough terrain at VAFB. In other applications land lines could be used in lieu of the RF link.

The Master System is dual redundant and its time base is a pair of Cesium standards also in a dual redundant configuration. The two timing terminal generators (TTG) in the Kode Local System synchronize to the time code supplied by the Master System. Their outputs are monitored by the Fault Sense and Switching unit. This unit automatically switches to the secondary TTG if a failure is detected in the primary. The outputs of the Fault Sense unit drive the Distribution Amplifiers that buffer the timing signals from the system to the local users and the Transmit System.

The IRIG G transmitter is a fully redundant unit which accepts the IRIG-G002 input, converts it to Bi-phase modulation, and amplifies it to a power level of 40 watts at a frequency of 1740 MHz. The transmitter system contains a separate Fault Sensing and Switch Unit which monitors critical parameters of both transmitters and switches to the standby unit upon primary source failure. The Transmitter output feeds an omnidirectional antenna through a pressurized coaxial cable. This antenna radiates throughout the entire base as does the previously existing 100 watt IRIG A Transmitter.

At the receive sites, two 4 foot parabolic antennas aimed at both the IRIG G and IRIG A sources feed a special receiver assembly through individual pressurized coaxial cables. The receivers contain fully independent dual IRIG G receivers and one IRIG A receiver. The overall Timing Distribution reliability is assured by use of this redundant system.

The Remote Kode System also contains two TTG's. These TTGs each phase lock to the codes supplied by the RF receivers. The outputs of the TTG's are monitored by an identical Fault Sense Unit which again places the outputs of the secondary TTG on line in the event of a failure in the primary TTG. The Distribution Amplifier furnishes buffered outputs to the remote users.

The Local and Remote Systems are identical except that the Local System does not contain the receiver chassis.

The systems are enclosed in an equipment cabinet (see figure 3) that contains a Power Control Panel, the two TTG's, the Fault Sense unit, a Signal Bypass chassis and five Distribution Amplifiers chassis.

The Power Control Panel contains the circuit breakers for the primary power and also contains two heat sensors; one for over heating and one for fire.

The TTG's are the heart of this system. They are capable of operating as stand alone time code generators. In this mode they may be preset, stopped and started and have advance/retard controls that allow them to be manually synchronized to within 50 nanoseconds. The time base is derived from an internal oven controlled quartz oscillator. The outputs of the TTG's include five IRIG time codes, four sine waves and various decade pulse rates.

In the Synchronized Generator mode the TTG's phase lock to the input time code and frequency correct the internal oscillator to match the frequency of the oscillator that is generating the input code, in this case the Cesium standards in the Master System.

The phase error between the TTG and the input code is resolved to less than 100 nanoseconds, typically 70 nanoseconds. The

frequency error is resolved to 1.5 parts in 10^{10} and can handle frequency errors of greater than 1 part in 10^6 . In the event of input code failure the frequency error correction is continued using the last known correction constant.

The front end of the TTG contains sophisticated error detection logic allowing it to ignore faulty code data or incorrect code formats. This logic also compensates for input signal propagation delay. The delay is user programmable in 100 nanosecond steps to a maximum of one millisecond.

(Figure 2 is a simple block of a TTG).

The Fault Sense unit monitors the outputs of each of the TTG's. TTGA is designated as the primary. Should certain of its outputs fail, TTGB will be automatically placed on line assuming that there are no pre-existing failures in TTGB. Also once TTGB has been selected TTGA can not be returned to on line until it is determined to be error free. The criteria for auto switching include code amplitude and ratio, sine wave amplitude and input code failure. Also monitored are bit errors and phase errors between the two TTG's. These errors do not enable auto switching in this system because the lack of a third, or reference input, prevents the Fault Sense unit from determining which TTG is in error.

(Subsequent designs incorporate this feature with the third input being logically synthesized).

The Fault Sense unit also incorporates a very flexible self test program which allows the user to simulate any of the possible TTG failure modes. The Fault Sense unit will in every way respond to the simulated faults as if they were caused by the TTG(s). This feature allows sophisticated diagnostic testing to be run prior to times of anticipated critical timing needs.

The IRIG G System also includes a Signal Bypass chassis. This device allows the time code outputs from a user selected TTG to be applied to the Distribution Amplifier inputs. This feature allows the Fault Sense unit to be removed for maintenance and still supply timing to the users.

The remainder of the system is dedicated to the five Distribution Amplifier chassis. Each chassis will handle up to 30 channels of AC or DC amplifiers. The inputs to each amplifier are user programmable from one of five input sources. The amplifiers are wide band and will buffer any of the available TTG output signals. These signals range from the IRIG H time code modulating a 1KHz carrier up to a 1MHz sine wave. Each amplifier is thoroughly protected from short circuits to either ground, another amplifier, or a voltage. In the unlikely event that an amplifier is damaged, the isolation between amplifiers is such that any of the other channels will not be affected.

In summary these systems provide a method of transferring time derived from Cesium time standards to remote locations. The timing accuracy provided approaches the accuracy of the Cesium standard over a long period of time and also provides a wide variety of very reliable timing signals to the users.

FIGURE 1.

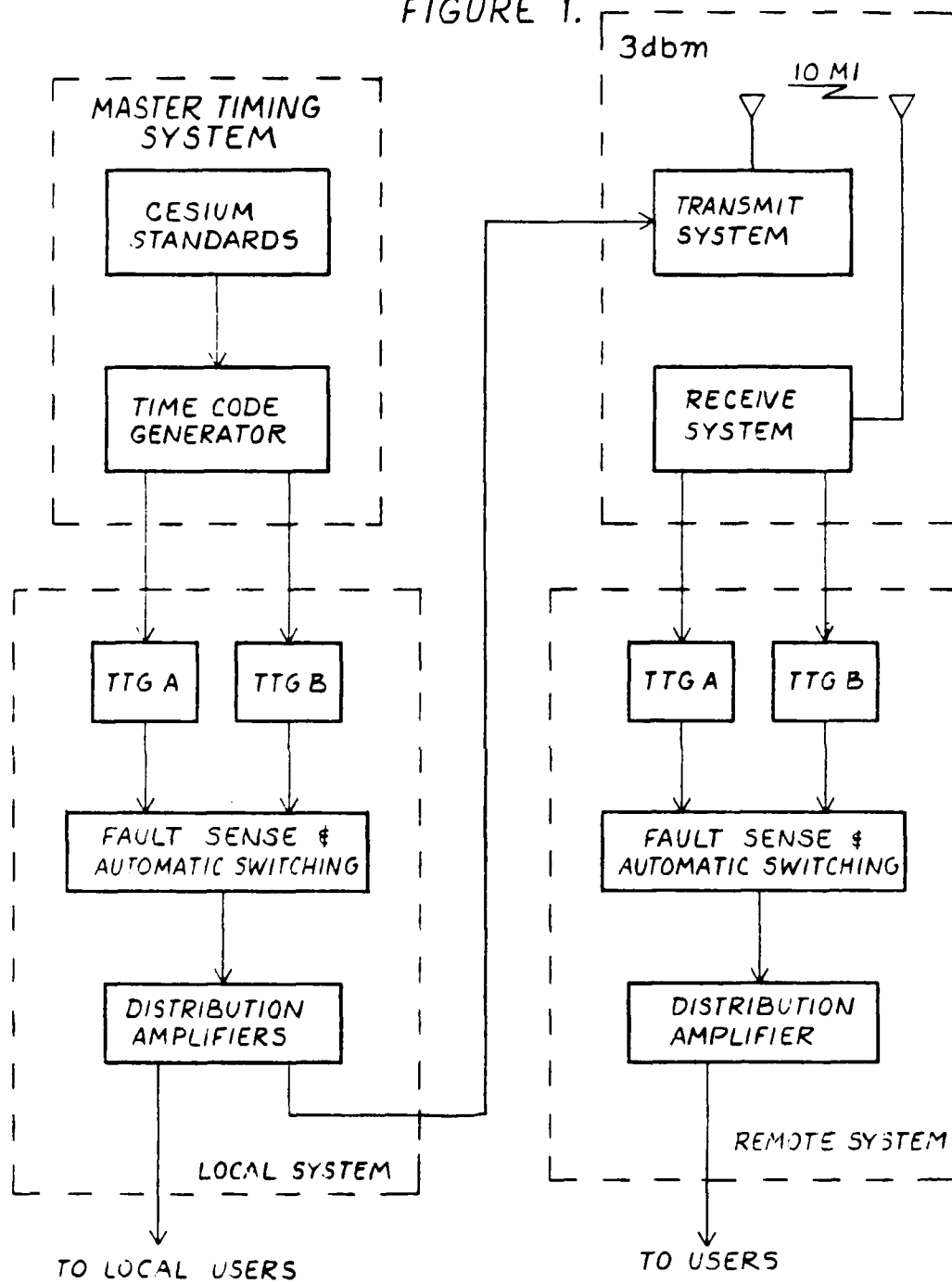
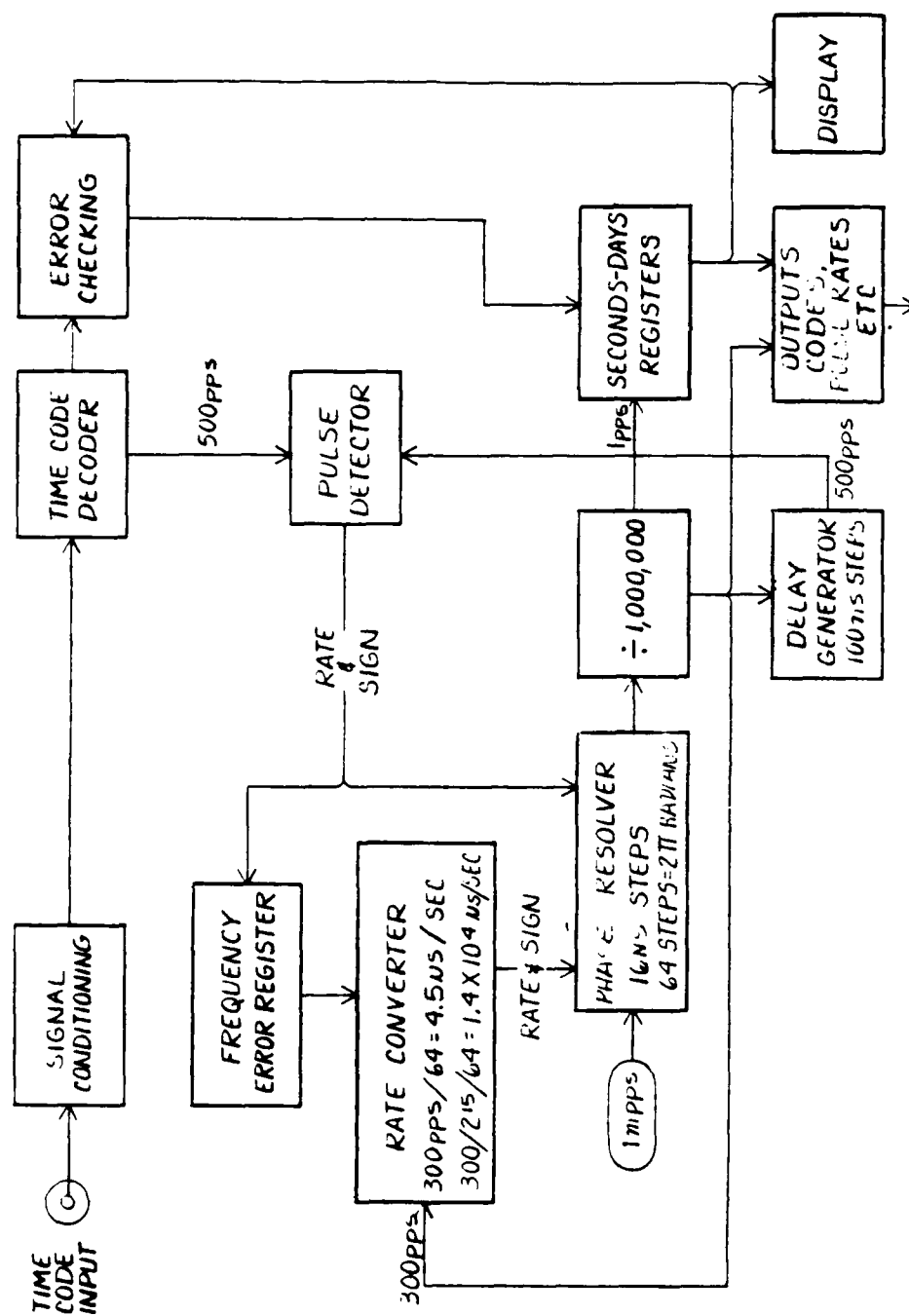


FIGURE 2



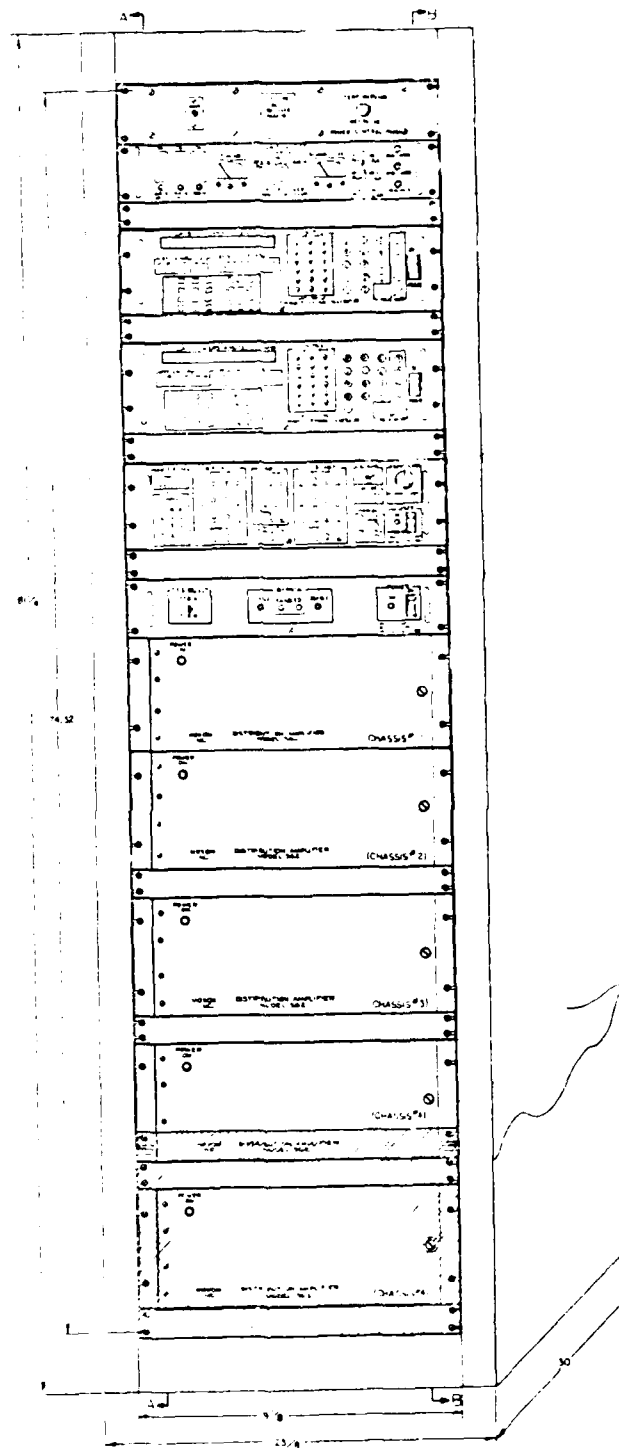


FIGURE 3

QUESTIONS AND ANSWERS

None for Paper #21.

TIMING SYSTEM DESIGN CONSIDERATIONS FOR A MOBILE ASTROLABE

Carl F. Lukac, Paul J. Wheeler, Richard E. Keating, and Randolph T. Clarke
U. S. Naval Observatory
Washington, D. C. 20390

ABSTRACT

The Danjon Astrolabe at the Naval Observatory has been traditionally used to determine Universal Time and improve the systematic accuracy of star positions. During the past year, it has been used to determine latitude and longitude at remotely scattered sites for geodetic purposes. Operating this instrument away from the Observatory necessitated a mobile support and timing system rugged enough to operate dependably in ever changing, and sometimes harsh, environmental conditions.

This paper describes the performance of the astrolabe timing system, gives the basic engineering design considerations, and describes the equipment and instrumentation.

INTRODUCTION

In cooperation with the Defense Mapping Agency an evaluation study was made of astronomical observations acquired using a Danjon Astrolabe at reference points in the western United States extensively used in the past for astro-geodesy.

When the idea was conceived of improving the deflection of the vertical at specific locations with position determination by astronomical measurement and extending this accuracy to large geodetic nets, a high-precision observatory instrument was considered. The Danjon Astrolabe was selected for this work because its accuracy and mobility make it well suited for basic astro-geodetic work. The optical Danjon Astrolabe determines position to within one meter accuracy and requires a timing system that records time-of-day for timing events with 100 microsecond precision. It is an observatory instrument which can be transported and set up overnight.

The astrolabe had been previously used at the Naval Observatory on a regular basis for the determination of Universal Time (UT0) and for reducing the systematic errors in the positions of the stars observed. Like the Photographic Zenith Tube (PZT), the visually operated astrolabe is an efficient instrument for the simultaneous determination of time and latitude. Unlike the PZT, the astrolabe can observe a much larger subset of the so-called "fundamental stars" (i.e., stars for which accurate, precise and consistent positions and proper motions are available), thus yielding better coordinates in a relatively short time. This is important when moving from one place to another because a different subset of the fundamental star catalog is selected for each observing site.

Since the astrolabe would not be operating in an observatory environment, which is essentially a research laboratory environment, it was necessary to provide the astrolabe with rugged field peripheral support equipment which could survive under adverse temperature and weather conditions (e.g., snow, rain, electrical storms, poor and unreliable electrical power, blizzards, desert heat, etc.). The field equipment described herein includes a portable atomic frequency

standard and clock, a "Datachron" chronometer interfaced by means of a Fairchild 4880 coupler unit to a HP9915A modular computer with both a built-in magnetic tape cartridge drive (Option 001) and a video, keyboard, and audio speaker interface (Option 002). An HP-IB Interface (HP Part No. 82937A) card was inserted into one of the three available I/O slots in the rear of the HP9915A. Additionally, an HP85 desktop computer with an HP82939 serial interface communications card and an Anderson-Jacobson Model AJ1234 (Mfr. code 2852) communications modem was used for editing and transmitting the recorded astrolabe data back to the Naval Observatory. A motor vehicle provided housing and transport for the above equipment; and, when the astrolabe was being transported to a new site, the same vehicle provided 12 VDC power to the portable atomic clock. At the observation sites, the motor vehicle also served as a field operations center and as a dressing room for the observers. While on site, external electrical 110 VAC 60 Hz power was provided by extension cables only to the motor vehicle. Electric power to all other instrumentation, including the portable atomic clock and the Danjon Astrolabe, was provided from a common distribution box in the motor vehicle.

OBSERVATIONS AND SYSTEM DESIGN

Basically, time-of-day data to 0.1 millisecond accuracy is acquired by the Danjon Astrolabe (Figure 1) by timing stellar images as the star, in its diurnal sidereal path, crosses the 30° almucantar (a small spherical circle centered on the zenith and having a radius of 30° of arc). Normally, three groups of stars are observed every night. Each group consists of about 30 stars with magnitudes between 3.0 and 6.5, whose almucantar transits are uniformly, or nearly so, distributed in azimuth among the four azimuth quadrants. By forming the time difference between the observed time-of-day of almucantar passage and the calculated time-of-day based upon the positions of the stars as found in a precision astrometric star catalog such as the FK4, it is possible to determine the observed zenith distances for each star at the time of its passage through the almucantar. By combining the observed zenith distances in the same manner that a marine sextant navigator combines intersecting LOP's (Lines of Position) to determine a position "fix", the astrolabe determines an astronomical "fix" and the associated astronomical latitude, longitude, and refraction correction are determined with high precision.

When a stellar almucantar passage is observed, a motor-driven micrometer carriage causes electrical contacts to open and close twelve times, thus causing 24 electrical signals to be generated and whose time-of-day occurrence must be recorded by a chronometer. During the observation interval, i.e., the time interval during which the electrical contact signals are being generated, the star may move as much as 312 seconds of arc in altitude. A speed reducer varies the speed with which the star is tracked in a manner proportional to the sine of the azimuth; and the observer needs only to make slight differential adjustments in the speed with which the star is tracked to maintain the optical null condition of the star images in the eyepiece. In this manner, the observer controls the occurrence of the contact timing signals. The observer has only two variables to reckon with: (1) the instant at which to begin the observing sequence, and (2) having started the observation, to differentially adjust the speed at which the timing contact signals occur so as to first achieve and then maintain the optical null condition of the star images in the telescope eyepiece.

The micrometer of the Danjon Astrolabe is based on standard Repsold transit micrometer techniques. At each micrometer position at which an electrical contact generates a signal, a linear micrometer reading in say tens of micrometers is recorded. The average time of all 24 timing contact signals then equals the time at which the micrometer was located at the average of the 24 linear micrometer readings. By also determining the linear micrometer reading for the position of the focal point of the Danjon Astrolabe objective lens, it is then possible, from a knowledge of the azimuth, to determine a correction to reduce the centroid of the 24 timing contact signals to the time corresponding to the null passage of the star's images through the

focus of the Danjon telescope objective. It is necessary, in order to determine these corrections, to be able to record the time-of-day of each timing contact signal. It is also necessary to form the first differences of the times-of-day in order to set the basic driving motor speed, which is proportional to the latitude of the field site.

Thus, the field timing system for the astrolabe not only had to record timing pulses that arrived at separation intervals that could be as small as 0.3 seconds and no greater than 10.0 seconds, but also had to be able to form and display, on a TV monitor, the time of day and its first difference with the previous time of day. The TV monitor shown in Figures 2 and 3 could be used inside the vehicle or outdoors next to the Danjon Astrolabe.

The transfer and readout capability, including the necessary programming, for field operations of the astrolabe was designed by the Time Service Precise Time and Time Interval (PTTI) Branch of the Naval Observatory. This capability (illustrated in Figures 2, 3 and 4) consists of a HP9915A computer, which served as a control and recording unit, an electronic "Datachron" chronometer, and a portable cesium atomic clock. Use of an atomic clock might be thought of as "overkill", but in field experience, the ability to avoid propagation errors and constant worries over crystal oscillator behavior, proved to be invaluable.

The micrometer contact electrical signals are sent from the astrolabe to a "Datachron", a chronometer built at the Naval Observatory. The Datachron operates off the 5 MHz signal from the portable cesium clock, which also maintains the basic field time of day for the system. The Datachron is manually synchronized with the cesium clock and there are circuits which check for synchronization faults between the cesium and the Datachron. The portable cesium clock operates off an HP K02 portable power supply continuously. The HP K02 is operated mostly from an external power source or, during periods when the vehicle carrying the instrumentation is in motion, off of the vehicle battery. A special heavy duty alternator was installed to insure that the vehicle had enough power to operate both day and night without discharging the vehicle battery. The vehicle cesium clock was always kept within 10 microseconds of the U.S. Naval Observatory Master Clock, UTC(USNO MC) by means of portable clock visits and by visits from nearby laboratory clocks with known traceability to the USNO MC.

The contact signals from the astrolabe are conditioned by a low pass filter, an optical isolator, and a one-shot trigger in order to avoid jagged contact noise and transient oscillations. The conditioned signal causes the Datachron to momentarily lock into a register, the current time of day. The 12 digit (hours, minutes, seconds, and six fraction of a second digits) time of day locked into the Datachron is then transferred to the Fairchild 4880 coupler. The Fairchild coupler next initiates a data transfer of the time of day over a standard IEEE-488 (HPIB) interface to the HP9915A computer. The Fairchild 4880 instrument coupler converts the Datachron high speed parallel data output into the standard IEEE-488 (HPIB) interface format. This conversion of the Datachron electrical wiring and timing interface to the IEEE-488 (HPIB) standard interface simplified the connection between the Datachron and the HP9915A computer. The transfers from the Datachron to the HP9915A are high speed; and any need for stacked data buffering of closely spaced timing signals is eliminated.

The HP9915A has a 16K byte memory. It can be expanded to 32K bytes maximum. Of the 16K bytes, approximately 2.5K bytes are used by manufacturer software, including the interface routines. The language in which the programming was written is BASIC. The application program uses 2.5K bytes and was burned into EPROM memory to avoid problems that may arise when programs have to be field loaded from magnetic cartridges under severe temperature conditions and the harsher electrical power environment encountered in the field. The EPROM program is listed, along with a running commentary in Appendix A. The running commentary includes a description of the IEEE-488 control and data messages used across the HPIB bus. The control message sequences implemented over the HPIB bus were carefully designed to allow high speed transfer of the Datachron TOD data to the HP 9915A.

Whenever the timing signals (or "ticks") from the astrolabe stop for more than 10 seconds, the HP9915A writes the timing data (in the form of an array containing up to 30 times-of-events) onto a magnetic tape cartridge. The 10 second pause in the signals from the astrolabe is interpreted by the HP9915A BASIC program as indicating that observations for a particular star are complete and that the time-of-event data may now be written to the magnetic tape cartridge. While the HP9915A was writing the time-of-event data for a star on the magnetic tape cartridge, a pair of audio beeps, the first at a high tone, the second at a lower tone, were issued to the observer at the Danjon Astrolabe. After the time-of-event data had been recorded and the HP9915A system enabled to again accept astrolabe timing signals, another pair of audio beeps, the first beep at a low tone, the second at a higher tone, was issued to the observer to let him know that the system was now ready to accept timing signals for the next star.

Normally, only 24 time ticks are recorded per star. Because temperature and humidity changes, contact bounce, and contact wear can cause more or less than 24 ticks, a maximum of 30 ticks may be recorded for each star observed. As many as 90 stars were observed each night and recorded on the magnetic cartridge. At the end of the night, the time-of-event data file on the magnetic tape cartridge was "closed" by pressing a programmer defined "END" button and the cartridge removed.

At the hotel or other convenient location the timing data on the cartridge was then combined with hand recorded environmental and instrumental data, observer comments, and other messages. This was accomplished using an HP85 computer. The HP85 computer was furnished with an Anderson-Jacobson 1200 baud telephone modem. By dialing the Naval Observatory HP1000 computer over the switched public telephone net from motel rooms and government phones, the data on the tape cartridge was transferred daily to the Naval Observatory. The data was then transferred from the Observatory HP1000 system to the IBM Series 1 system where preliminary editing of the data was done. Then the data was transferred to the Observatory mainframe IBM 4341 computer either by a RJE link or by magnetic tape. The final reductions and analysis of the data were done on the IBM 4341; and, for each group of stars, the resulting latitudes and longitudes were obtained daily. This near real time transfer and analysis of the data prevented serious problems from going undiscovered; and it may be stated that this procedure is to be greatly recommended because otherwise there is a high probability (higher than otherwise might be expected) that long intervals of measurements might be made which are subsequently found to be useless because of the invalidity or absence of a critical datum or measured quantity.

Occasionally modem data transfers were interrupted (usually by the HP1000 because it was busy and had to attend to other matters) and the data had to be retransmitted. Sometimes the data arrived garbled (this was rare, but it did happen). Problems with data transmission as such were rare. The doubling of the measurement and transmission of both the measurement and its doubled value served as a check on the accuracy of the transmitted data. Most problems encountered with the system were associated with the HP1000 being busy or transmitting strange messages. As there were known reliability problems with the HP1000 during this time, such behavior is not unanticipated. Fortunately the problems with the HP1000 were not so severe that data transfer was disrupted in ways which would have endangered field operations.

SOFTWARE DESIGN

The software for this system, shown in Figure 5, consists of three programs, one for automatic data collection of astrolabe timing signals, the second for manual entry of observer recorded data onto the magnetic tape cartridge, and the third for transfer of the data over the public switched telephone system to the Naval Observatory. The program in the HP9915A for automatic capture of the astrolabe timing signals operates in three modes.

The first mode is the star observation mode. In this mode the HP9915A collects the times-of-event for the astrolabe timing signals, insures that the time-of-event is for a stellar observation (it is possible for the observer to cause isolated timing signals from the astrolabe accidentally; these isolated timing signals from the astrolabe are identified by the HP9915A and ignored; the magnetic tape cartridge is thus not cluttered up with accidental sets of timing signals of no interest), and stores the data on the magnetic tape cartridge when the observation for each star is complete. If the data being collected by the HP9915A does not meet the criterion (12 or more time-of-events must have been received) used to determine if the time-of-event data is from a star observation, then, as already stated, in this mode of operation the time-of-event data is merely discarded.

The second mode is used to calibrate the astrolabe after it is installed at a new observation site. The time-of-event data is collected by the HP9915A, a calculation to form the first difference between the time-of-event for the current event and the previous event performed, and then both the time-of-event and its first difference are displayed on a TV monitor. This information is used by the observer at the Danjon Astrolabe to set the astrolabe motor speed. The main BASIC program is structured so that the observer can put the HP9915A into this "calibration" mode at any time. Mode selection is performed by the observer by pressing a button on the front face of the HP9915A computer.

The third mode, the fast TICK mode, is used to determine certain telescopic instrumental corrections related to the Danjon Astrolabe micrometer carriage (i.e., Vm corrections). In this mode, which is entered by pressing the TICK button on the HP9915A, the astrolabe timing signals are merely beeped back to the observer & he reads the micrometer carriage linear readings at which each timing signal is generated. No times-of-event are recorded on the magnetic cartridge. These micrometer readings allow the centroid of the timing signals to be corrected to the time at which the astrolabe stellar images coincided in the focal plane of the objective of the astrolabe.

The second program, the manual data entry program for the HP85 computer, allows the observer to manually enter all necessary information such as number of stars observed, ambient temperatures, barometric pressures, wire corrections, 2 or 4 ticks per revolution, observing conditions, and comments concerning each observation. The same magnetic tape cartridge used by the HP9915A to record the time of event data for each star is used by the HP85 and this program. A second file, created by the HP9915A when the observer set up for the evening's observing program but left empty, is opened for the manual entry of the observer's information, the necessary data entries made, and then again closed. A later version of this program allowed a certain amount of manual data entry in a "question and answer format."

The third program, the data transfer program, is then executed. This program requests the operator/observer to dial the telephone number of the HP1000 computer at the Observatory, provides the telephone numbers needed by displaying them on a small video screen, and then, when the HP1000 answering tone is heard, to place the telephone into the cradle of the 1200 baud Anderson-Jacobson modem. A special high quality transmission microphone (a Novation "Super Mike") was used in place of the standard carbon telephone microphone. This improved the quality of the data communications bit error rate by increasing the signal to noise ratio. The communication link over the public switched telephone is carried out in 7-bit ASCII, 1 start bit, 1 stop bit, and in even parity. Once the telephone connection has been established, a conversational protocol is executed by the talking computers (i.e. the HP85 and the HP1000). The HP85 first identifies itself to the HP1000 and requests access to the pre-established astrolabe data file on the HP1000 system. The HP1000 opens the astrolabe data files and then informs the HP85 that it may proceed to send data to the HP1000, which will direct all subsequent received data into the HP1000's pre-established astrolabe data file.

The HP85 first opens the manual information file on the magnetic tape cartridge and transfers the entire file to the HP1000; then, without breaking the telephone link, it opens the time-of-event file on the cartridge and transfers this file, in its entirety, to the HP1000. Finally, the HP85 requests the HP1000 to send to the HP85 a file containing messages and other information which the astronomers at the Observatory wish to send to the observer. Typical of such messages are queries concerning problems with pathological time-of-event data, missing data, and administrative messages. All messages sent from the HP1000 to the HP85 are displayed on the CRT of the HP85. The observer may thus evaluate the quality of the telephone connection. The observer may also print out these messages.

To prevent errors and to check the validity of the data transmission, both the time of event and twice the value of the time of event are transmitted to the Observatory by the HP85. This allowed another check to be performed upon the data as received at the Observatory from the field observer. In some cases, retransmission was deemed necessary because the error rate was too high.

When all data transfer operations were complete, the data files on both computers were closed and the computers send each other "GOODBY" and hang up.

SUMMARY

This project lasted about 11 months (August 1982 ---June 1983) and used three observers on a rotating basis. The building, testing, and installation of the data acquisition and timing system required no more than 6 weeks preparation. The timing system used provided considerably more numerical precision than actually needed because of other limitations (errors in star catalog positions); but the reliability was outstanding for field operations and was proven under severe weather conditions (blizzard, desert heat, electrical storms, driving rain and flash flood conditions). Uncertainties in star positions mean that star transits need be timed only with an error not to exceed a millisecond in the time of day. But time errors must not be systematic and they must not be allowed to creep in as ambiguous delays or confused corrections. Systematic errors were to be kept below 0.01 arcseconds. The electronic instrumentation operated successfully over temperature ranges of from 12° to 95° Fahrenheit although an average temperature in the vehicle was about 65°F. On at least one occasion, an electrical storm caused a power failure and damage to the cesium clock. The clock was immediately replaced and a study initiated to determine why the K02 power supply did not protect the cesium clock. It was quickly determined that the K02 had also been damaged by the electrical activity. This pointed to the need for more levels of power filtering and backup battery supply. The damaged clock was quickly replaced and the program continued.

Most survey work, particularly geodetic point-positioning depends upon recording time of day to at least millisecond accuracy. Nanosecond and microsecond timing is not necessary; but older atomic clocks which no longer are capable of functioning adequately for high precision PTTI applications can and should be put to good use in field applications such as this. The only requirement is that the older atomic clocks must be capable of operating to at least 50 microseconds absolute accuracy under severe weather and field conditions. Most older atomic clocks which are still operable have had most problems eliminated and good advantage may be taken of the inherent reliability of the electronics of such clocks even though, for high precision PTTI applications, such older clocks are now unsatisfactory.

In conclusion a complete PTTI timing system, which had been brought from design to implementation in 6 weeks, successfully permitted taking on a new task---the determination of precise astronomical positions in the field. This system, which required high quality, reliable timing, has demonstrated a proven capability for collecting PTTI data at primitive field sites, including examination and, if necessary, editing the data in the field; and finally for easily and rapidly sending that data back to the home office.

ACKNOWLEDGEMENTS

The authors are happy to acknowledge the work of Anthony Kubik, who built the USNO Datatron Chronometer used in this project; the work of Robert Hull, who installed, checked out, and tested the operation of the field timing system with the Danjon Astrolabe; the work of Patrick Lloyd, who drew some of the illustrations; and, finally, the work of F. Neville Withington, who kept the field operations on a successful track by her daily processing of the observations and her timely messages from the home office.

REFERENCES

1. HP 9915 Modular Computer", Hewlett-Packard, Fort Collins, CO., Pub. No. 5953-4550(40), May 1981.
2. HP9915 Installation Manual", Hewlett-Packard, Fort Collins, CO., Pub. No. 09915-90000, Oct. 1980.
3. "HP85 Owner's Manual and Programming Guide", Hewlett-Packard, Corvallis, OR., Pub. No. 00085-90002 Rev. D, Jan. 1981.
4. "I/O Programming Guide, Series 80", Hewlett-Packard, Corvallis, OR., Pub. No. 00085-90142 Rev. D, Oct. 1981.
5. "HP-IB Installation and Theory of Operation Manual", Hewlett-Packard, Corvallis, OR., Pub. No. 82937-90007 Rev. B, Oct. 1980.
6. "HP82939A Serial Interface Installation and Theory of Operation Manual", Hewlett-Packard, Corvallis, OR., Pub. No. 82939-90001 Rev. B, Jun. 1981.
7. "Fairchild Model 4880 Instrument Coupler Instruction Manual", Rev. 5, 1981, Fairchild Instruments, Los Angeles, CA. (Available for \$25 from ICS Electronics, 1620 Banker Rd., Sandose, CA. 95112, Part No. 120002.)
8. "Fundamental Astrometry", V.V. Podobed, (Eng. Ed. by A.N. Vyssotsky), University of Chicago Press, Chicago, IL., 1965, pg. 107ff.

APPENDIX A
HP9915A EPROM BASIC PROGRAM

No.	Statement	Comments
10	ON ERROR GOSUB 390	For any error, go to subroutine 390
20	ERASETAPE	Initialize magnetic tape cartridge and create a directory on it.
30	CREATE "TEXT",15 @ CREATE "DATA",125,512	Create two files on the magnetic tape cartridge. The first file is named "TEXT" and consists of 15 physical records, each 256 bytes in length. The second file is named "DATA" and consists of 125 logical records, each 512 bytes in length.
40	OPTION BASE 1	Specifies that the lowest value of the index for an array is 1 rather than 0.
50	DIM D(60)	Define an array of 60 real numbers

60	OFF TIMEOUT 7 @ RESET 7	Disables any timeout interrupt on the IEEE-488 bus and then resets the IEEE-488 bus, returning it to its power on state. The HP9915A then sends Interface Clear (IFC) and then Remote Enable (REN) to the Fairchild Coupler.
70	ASSIGN#2 TO "TEXT"	Opens the "TEXT" file.
80	PRINT# 2 ; "NO TEXT DATA ENTERED *****"	Writes the above data into the TEXT file to cause the file to be properly initialized (null files cannot be processed).
90	ASSIGN# 2 TO *	Close the TEXT file.
100	ASSIGN# 1 TO "DATA"	Open tick file "DATA"
110	ON KEY# 1 GOTO 360	END processing. If button No. 1 is pushed, go to program segment starting at statement 360.
120	ON KEY# 2 GOTO 440	1'st Difference processing. If button No. 2 is pushed, go to program segment starting at statement 440
130	ON KEY# 3 GOTO 630	TICK processing. If button No. 3 is pushed, go to program segment starting at statement 630.

Star Observation Mode---Default Mode.		
140	ON TIMEOUT 7 GOTO 270	If a timeout occurs on the IEEE-488 bus, go to program segment starting at statement 270. This timeout will normally occur after the astrolabe has transferred 24 ticks and ten seconds have elapsed since the 24'th tick.
150	SET TIMEOUT 7;10000	Set the timeout interval on the IEEE-488 bus to ten seconds.

<pre> 160 ON INTR 7 GOTO 200 165 RESET 7 170 ENABLE INTR 7;8 180 V=SLITE(0,1) @ V=SLITE(0,-1) 190 GOTO 180 200 OFF INTR 7 210 V=SLITE(2,1) 220 FOR R=1 TO 60 STEP 2 230 ENTER 700 USING "K" ; D(R) </pre>	<p>BEGIN MAIN ACQUISITION LOOP. If a service request is received from the Fairchild Coupler, then the Datatron has recorded a tick and wishes to transfer the tick to the HP9915A. The Fairchild Coupler raises the SRQ (Service Request) line to the HP9915A and, if statement 170 below has enabled this SRQ interrupt, then the HP9915A will branch to the program segment beginning at statement 200. Note that after the branch to statement 200 another SRQ interrupt will not be serviced until a subsequent ENABLE INTR 7;8 statement has been executed.</p> <p>Reset IEEE-488 bus, issue IFC and REN.</p> <p>Enable SRQ (Service Request) interrupts from the IEEE-488 bus (bit 3 in control register CR1 is set on)</p> <p>Turn the top (0) HP9915A light on (1), then turn it off (-1).</p> <p>Loop. This is an idle loop which is used to keep the HP9915A busy while waiting for a service request from the Datatron/ Fairchild coupler.</p> <p>A service request SRQ has been received from the Datatron/Fairchild coupler. First disable the ON INTR 7, GOTO 200 instruction at statement 160</p> <p>Turn the third (2) from top HP9915A light on. Inner Read Loop. Read in up to 30 ticks. The step increment is 2 because both the tick and twice the tick will be stored in the array.</p> <p>This command unlistens all devices; then designates the HP9915A as listener; next designates the Fairchild Coupler as talker at address "00" on the IEEE-488 bus ("7"); and then allows the Fairchild Coupler to begin talking by setting the attention ATN line to false. Note that this command allows subsequent bus transfer activity to occur at intervals controlled by the Datatron/ Fairchild Coupler. There is no need to re-interrupt the HP9915A since the HP9915A is now waiting, or "Listening" to the Datatron/ Fairchild Coupler. Each time SRQ is now raised, SRQ is ignored because it has been</p>
--	--

		disabled. Each tick data transfer is indicated complete by the Line Feed that occurs when a tick has been transferred to the HP9915A, and not by using the SRQ interrupt. The USING specification of "K" means that the string or numeric field is entered in the so-called "free field" format. For numeric data, the number is left justified (with leading space or sign) and filled on the right with blanks.
240	D(R+1)=D(R)*2	Double the tick value to form the check number.
250	BEEP 10,100	Beep at 2500 Hz for 0.04 sec.
260	NEXT R	End Inner Read Loop for Datachron/ Fairchild coupler. The inner read loop is normally ended by the ten second timeout set up by statements 140 and 150.
270	IF R<24 THEN RESET 7 @ BEEP 100,100 @ BEEP 100,100 @ V=SLITE(2,-1) @ GOTO 160	If less than 12 ticks were sent to the HP9915A while it listened for ticks, then beep twice (at 492 Hz for 0.2 sec each), ignore values, and go start over at statement 160.
280	RESET 7 @ BEEP 100,200 @ BEEP 200,200	Good data & more than 12 ticks. Beep at 492 Hz for 0.4 sec, then change tone to 261 Hz for 0.8 sec.
290	PRINT# 1 ; D()	Write the array D to the magnetic tape cartridge.
300	FOR R=1 TO 60	Loop to clear D to zero.
310	D(R)=0	
320	NEXT R	
330	BEEP 200,100 @ BEEP 100,200	Beep at 261 Hz for 0.4 sec, then change to 492 Hz for 0.4 sec. to tell observer that he can now observe another star.
340	V=SLITE(2,-1)	Turn third from top HP9915A light off.
350	GOTO 160	END MAIN ACQUISITION LOOP
End Star Observation Mode (Default Mode)		

END Button Routine

```

360      ASSIGN# 1 TO *           Close file "DATA"
370      V=SLITE(4,1)           Turn fifth from top HP9915A light on.
380      END                     Stop HP9915A processor

```

General ERROR Routine

This routine handles all errors.

```

390      IF ERRN=67 THEN CREATE "TEXT",15 @ CREATE "DATA",125,512
      @ RETURN                  If no file error, then create the "TEXT" and
                                "DATA" files and return.
400      DISP "ERROR"; ERRN;"ON LINE";ERRL
                                This line displays on the TV monitor a
                                message which reads "ERROR error-number ON
                                LINE line-statement-number". The error
                                numbers are those in appendix E of the HP85
                                Owners Manual and Programming Guide (00085-
                                90002 Rev. D 1/81).
410      V=SLITE(6,1) @ V=SLITE(7,1) Turn on the bottom two HP9915A lights.
420      BEEP 100,10000         Beep at 492 Hz for 20 sec. to warn observer
                                that catastrophic error has occurred.
430      RETURN                 Go return from error routine and attempt to
                                continue anyway in hope that error was a
                                fluke.

```

Second Mode. (First Difference Program Segment).

```

440      ASSIGN# 1 TO *           Close the "DATA" file
450      OFF INTR 7              Disable the SRQ interrupt processing
                                specified in statement 160 or 520
460      OFF TIMEOUT 7          Disable timeout processing specified in
                                statements 140 and 150.
470      RESET 7                IFC and REN the IEEE-488 Bus.
480      OFF KEY# 3 @ OFF KEY# 1 Disable TICK and END buttons. Only the first
                                difference button (KEY# 2) is to remain
                                active. This key will be used to indicate
                                that first differencing is to be ended.
490      ON KEY# 2 GOTO 60       When 1'ST DIFFERENCE button is pressed (a
                                second time--- the first time is to enter
                                this mode) this program segment is ended and
                                the normal default program segment is
                                restored.
500      SET TIMEOUT 7;5000     Datachron must transfer ticks within 5
                                seconds if a timeout is not to occur.
                                HP9915A does not remain in a "Listen" mode
                                for more than 5 seconds.
510      ON TIMEOUT 7 GOTO 450   If a timeout occurs, then the IEEE-488 bus is
                                reset, IFC and REN issued and then
                                instructions executed which terminate in the
                                idling loop at statements 530 and 540.

```

520 ON INTR 7 GOTO 550 530 ENABLE INTR 7;8 540 V=SLITE(1,1) @ V=SLITE(1,-1) @ GOTO 530 550 ENTER 700 USING "K" ; D1 560 BEEP 10,100 570 DISP D1 580 ENTER 700 USING "K" ; D2 590 BEEP 10,100 600 DISP D2;D2-D1 610 D1=D2 620 GOTO 580	If Datachron/Fairchild Coupler issues a SRQ, then go put HP9915A in listen mode and Coupler in talk mode. Allow SRQ interrupts to occur. Turn second HP9915A light from top on, then off, then loop back. This is an idling loop while waiting for SRQ from Datachron/Fairchild Coupler. Put HP9915A in listen mode; put Datachron/Fairchild Coupler in talk mode; drop ATN line and let Datachron/Fairchild coupler transfer time tick to HP9915A. Data transferred goes into variable D1. Beep at 2500 Hz for 0.04 sec. Display the tick on the video monitor. Put HP9915A in listen mode again; talk mode for Datachron/Fairchild Coupler; and transfer another tick. But this time put tick into another variable D2 Beep at 2500 Hz for 0.04 sec. Display tick and first difference. Make current tick previous tick Go get another tick and loop indefinitely. Loop is ended by pressing 1'st Difference button or by 5 sec. timeout set up by statements 500 & 510.
---	---

End Second Mode (First Difference Segment)

Third Mode. (Fast TICK processing, Button No. 3).

630	ASSIGN# 1 to *	Close file "DATA"
640	OFF INTR 7	Disable interrupt processing set up in statement 150 or 710.
650	OFF TIMEOUT 7	Disable timeout processing set up in statements 140 and 150.
660	RESET 7	Reset IEEE-488 bus, issue IFC and REN.
670	OFF KEY# 2 @ OFF KEY# 1	
680	ON KEY# 3 GOTO 60	Disable END and 1'ST DIFFERENCE buttons.
690	SET TIMEOUT 7;5000	When TICK key is pressed again, go restore normal processing and recording of ticks.
700	ON TIMEOUT 7 GOTO 640	Allow HP9915A to wait in listen mode for no more than 5 seconds when waiting to receive ticks from the Datachron/Fairchild Coupler.
		If HP9915A waits too long (more than 5 sec), then go to statement 640, reset IEEE-488 bus, and execute code which ends in idle loop at statements 720 and 730. This prevents the HP9915A from sitting endlessly in a listen mode waiting for the Datachron/Fairchild coupler to do something.
710	ON INTR 7 GOTO 740	
		When SRQ comes in from Datachron/Fairchild coupler, go place the HP9915A in listen mode and the coupler in talk mode.
720	ENABLE INTR 7;8	Allow Datachron/Fairchild coupler to cause interrupt.
730	V=SLITE(3,1) @ V=SLITE(3,-1) @ GOTO 720	HP9915A turns fourth light from top on, then off, then loops back to previous statement in an indefinite idling loop. Loop is ended when a SRQ from Datachron/Fairchild Coupler comes in.
740	ENTER 700 USING "K" ; D1	Place HP9915A in listen mode, coupler in talk mode, make ATN false to allow coupler to talk. Put tick into variable D1
750	BEEP 10,100	Beep at 2500 Hz for 0.04 sec.
760	GOTO 740	Loop indefinitely. Loop is ended by either timeout of 5 seconds or by pushing the TICK button again.

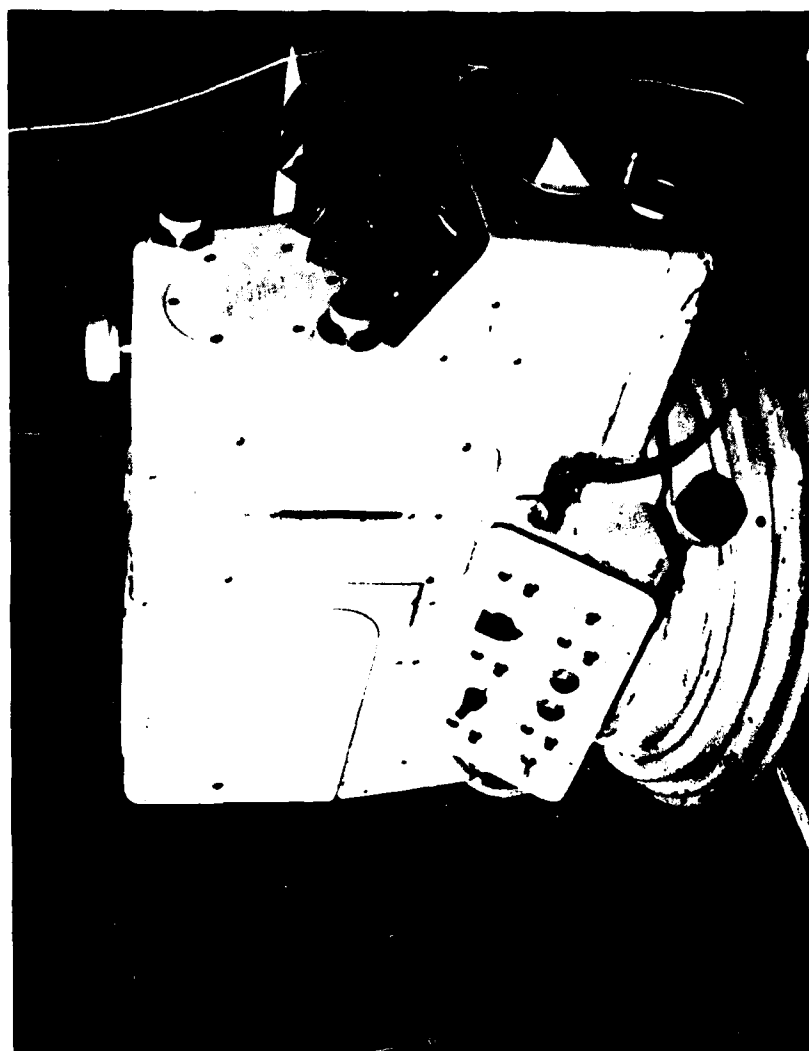


Figure 1. Danjon Astrolabe.

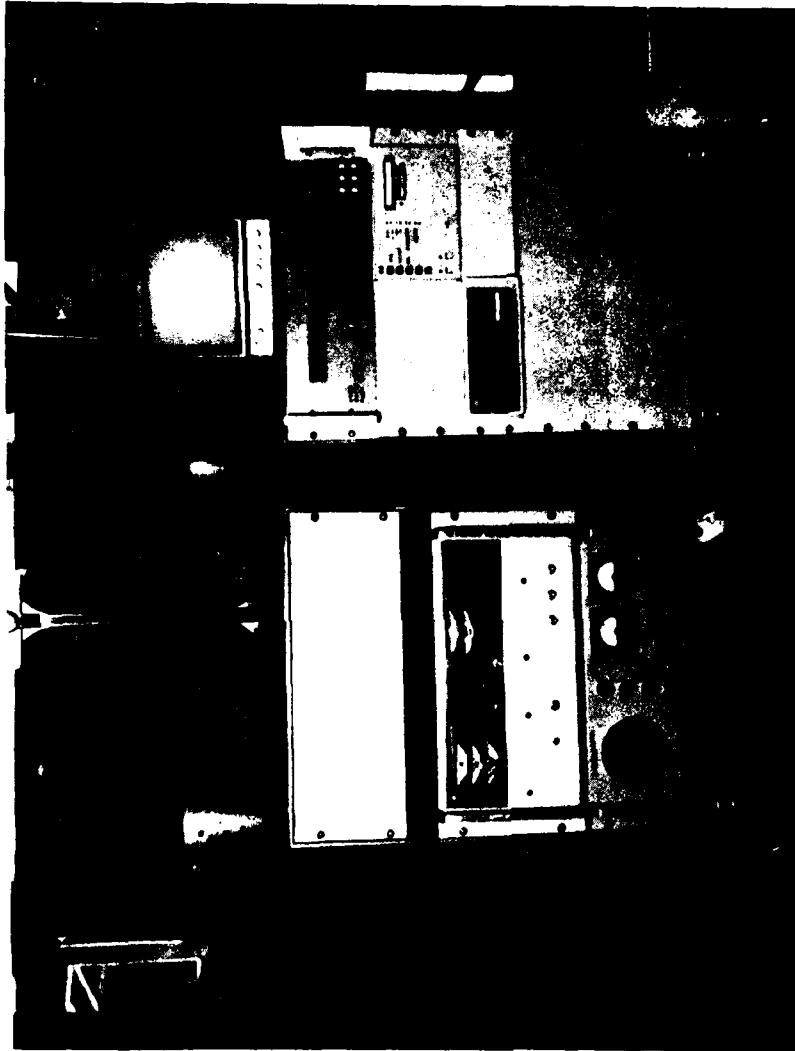


Figure 2. General View of Data Acquisition and Timing System showing cesium standard, TV monitor, Datatron, 9915A computer, and 4880 Interface Coupler.

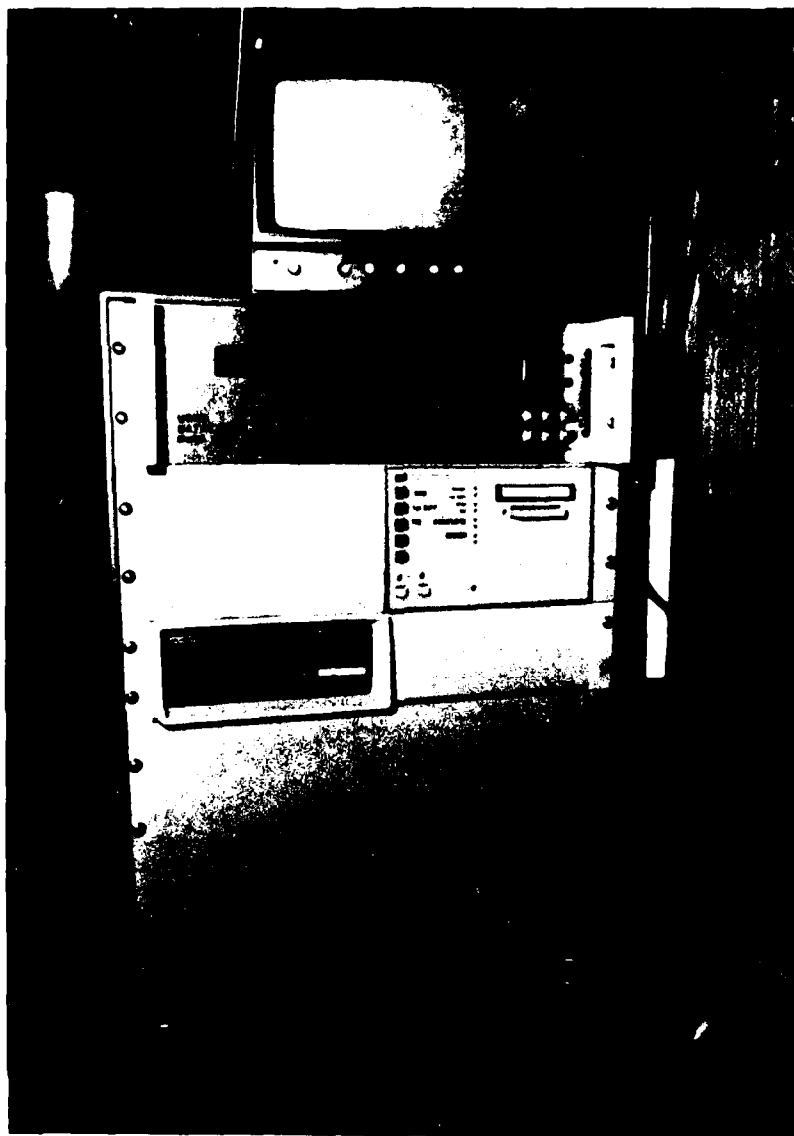


Figure 3. Data Acquisition and Timing System.

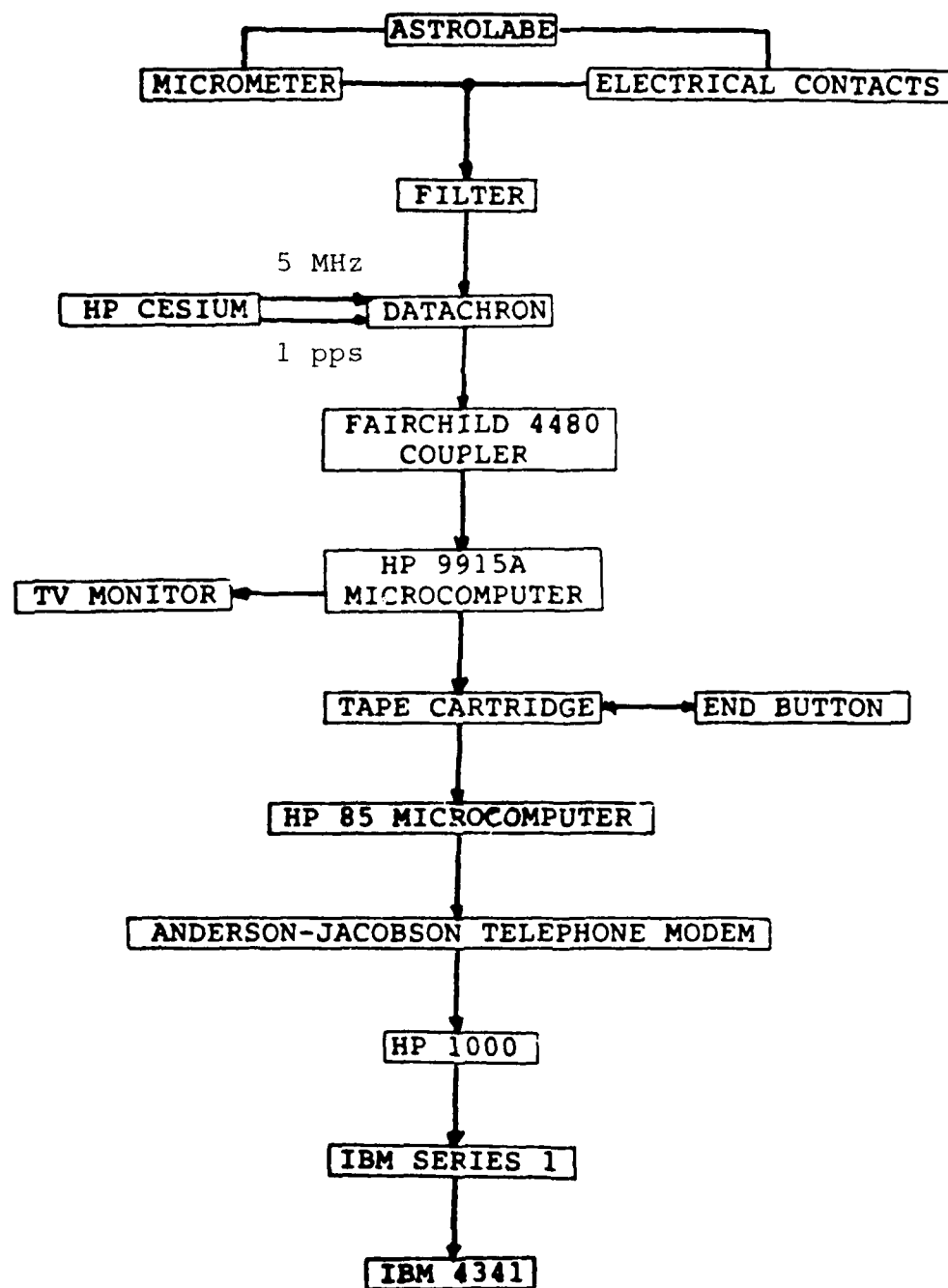


Figure 4. Time Measurement and Transfer System.

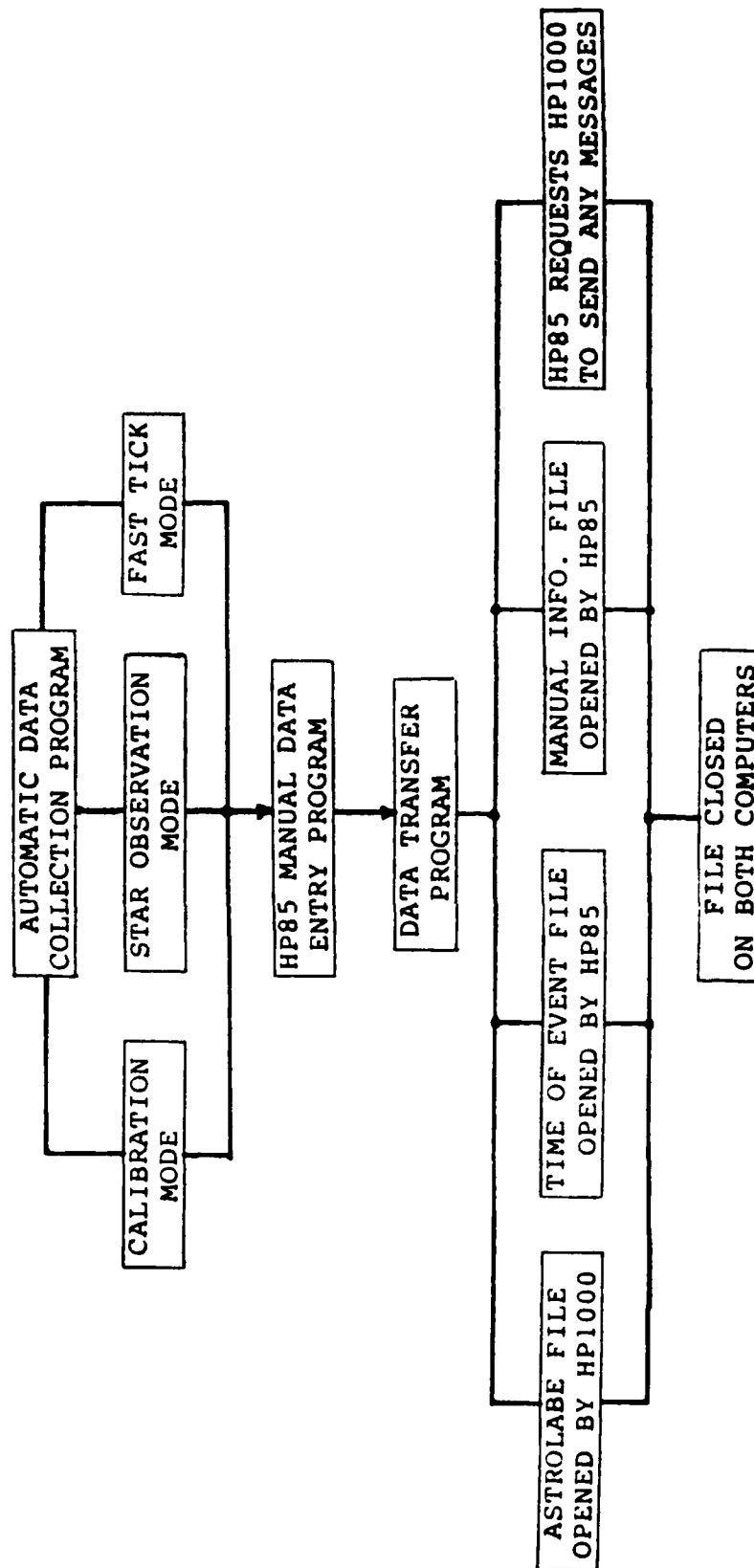


Figure 5. General Software Diagram.

QUESTIONS AND ANSWERS

None for Paper #22.

PRECISE TIME TRANSFER USING MKIII VLBI TECHNOLOGY

K. J. Johnston, J. A. Buisson, M. J. Lister, O. J. Oaks,
J. H. Spencer, W. B. Waltman,
Naval Research Laboratory
G. Elgered, G. Lundqvist,
Onsala Space Observatory
A. E. E. Rogers,
Haystack Observatory
T. A. Clark, C. Ma,
NASA-GSFC
A. C. Johnson, K. Kingham, W. J. Klepczynski, G. Luther,
A. J. Kubic, and D. D. McCarthy,
United States Naval Observatory

ABSTRACT

It is well known that Very Long Baseline Interferometry (VLBI) is capable of precise time synchronization at subnanosecond levels. This paper deals with a demonstration of clock synchronization using the MKIII VLBI system. The results are compared with clock synchronization by traveling cesium clocks and GPS. The comparison agrees within the errors of the portable clocks (± 5 ns) and GPS (± 30 ns) systems. The MKIII technology appears to be capable of clock synchronization at subnanosecond levels and appears to be a very good benchmark system against which future time synchronization systems can be evaluated.

INTRODUCTION

The VLBI technique is quickly maturing. The positions of many antennas are now known to a few centimeters, celestial sources to ~ 2 milliarcseconds, and corrections for the ionosphere and atmosphere are approaching the 1 cm level. This technique has essentially an all weather capability. Therefore if the instrumental delays are understood, as in the case of the MKIII system, there is no reason why one can not synchronize clocks at subnanosecond levels with only a few minutes of data.

The synchronization of clocks via VLBI has been the subject of many papers at PTI meetings in the past. This measurement is simply the difference in time of arrival of a "noise" signature from a celestial radio source which is located at cosmological distances. These sources may be looked upon as fixed radio beacons in the sky. Counselman *et al.* (1977) pointed out that from a few minutes of data using a priori knowledge of the baselines, source positions, etc., the delay differences scattered by an rms of 2 ns for continental U. S. baselines. After estimating two earth rotation parameters, and an average clock rate difference, the "formal" scatter was reduced to subnanosecond levels (Counselman *et al.* 1977). In order to verify the accuracy of VLBI, two experiments were performed on March 28 and September 23, 1977 by Clark *et al.* (1979) in which observations were made in eight 360 kHz bands distributed between 8.4 and 8.5 GHz which resulted in "formal" synchronization below a ns. In this experiment careful corrections were made of the contribution to delay by the antenna feeds, receiver systems, and recorders, yielding absolute determinations of the clock epoch differences. Portable clocks from the U. S. Naval

Observatory were taken to each site and the traveling clock data agreed to within 18 and 14 ns.

NEW TECHNOLOGY DEVELOPMENTS

The development of the Mark III VLBI system (Rogers et al. 1983) offers an improved design for clock synchronization in that the delays in the electronics and cables can be measured quite easily and changes in the delays are monitored.

The delay in the cables connecting the receiver at the focus of the antenna to the recording system are monitored. These cable lengths are sometimes of one hundred meters in length and are far from identical among antennas involved in VLBI experiments. The change in delay for cable length at Maryland Point Observatory for an experiment performed on October 18, 1982 amounted to approximately two nanoseconds. In an earlier experiment using MKII VLBI technology, there was a 59 ns difference between time synchronization when compared with portable clocks. This was well outside the errors attributed to either technique and was ascribed to an epoch difference between the MKII VLBI formatter and the station clocks (Spencer et al. 1981). This problem would not be encountered with the MKIII system.

THE VLBI EXPERIMENTS

A series of experiments were performed between NRL's Maryland Point Observatory, NEROC's Haystack/Westford Observatory and the Onsala Space Observatory in Onsala, Sweden. Experiments were performed on June 19, October 18, and November 23, 1982 and August 29, 1983. These experiments were always performed following a POLARIS measurement which are twenty-four hour measurements made to measure earth rotation parameters. The initial experiments in June and October 1982 established a reliable baseline between the 85' antenna of Maryland Point Observatory and the antennas of Westford/Haystack and Onsala. Figure 1 shows the locations of these antennas. The data were recorded in the standard POLARIS scheme (Robertson and Carter 1982) which has 14 frequency channels of 2 MHz width, 8 at X band between 8210.99 and 8570.99 MHz and 6 at S band between 2215.99 and 2300.99 MHz.

The delays associated with the antenna geometry and feeds were estimated. The delays due to cable lengths, receiver front end and back end, and tape recording system were measured during the experiments. The data was correlated at Haystack Observatory. The data was further analyzed at the Goddard Space Flight Center where the ionospheric delay was removed by differing the S and X band data. The X band data were used to estimate the delay. After adopting source positions, baselines, and correcting for the tropospheric delay using a model atmosphere, the delay epoch and an average clock rate were solved for along with an offset for Universal Time and polar motion. It was found that the formal error in the solutions accumulated around the time of the epoch of the solution. This 95% confidence level of the "formal" delay for the Westford-Maryland Point baseline was below the nanosecond level. The errors accumulate as a function of time around the solved for epoch. This is due to the frequency rate offsets between the oscillators used to generate the local oscillators at each site. An accurate assessment of the errors for an individual observation are given in Table 1. These do not include errors due to oscillator drift. Figure 2 shows the delay residuals for the 29 August 1983 experiment for the Maryland Point-Westford baseline. These residuals allow us to evaluate the "formal" error which is at the 0.4 nanosecond level. However for these measurements we have carefully accounted for the system delays at all the sites.

These are believed to be at the nanosecond level. Therefore these measurements are of the absolute delays between the sites at the nanosecond level. Improvements need to be made to reliably measure waveforms at the subnanosecond level.

Table 1

VLBI Error Sources

Position Location (2 cm)	0.07 ns
Atmosphere/Ionosphere Delays (2 cm)	0.07 ns
Receiver Delay	0.1 ns
Receiver Noise	0.01 ns
Source Position Error (QSO) (0.001 over 7000 km)	0.1 ns

COMPARISON

In order to determine the absolute accuracy of the VLBI technique, portable clocks were dispatched successfully to the Maryland Point and Westford antennas for the last two experiments. For the August 1983 experiments, measurements were made using GPS receivers. Figure 3 shows a schematic representation of the experiment for August 1983.

GPS Receiver

The NRL GPS receiver provides precise time measurements of less than 50 ns between remote station clocks and the U. S. Naval Observatory time standard. The receiver measures directly the difference between a NAVSTAR satellite clock and the remote ground station clock. Data transmitted from the satellite allow computation of the difference between the satellite clocks and the U. S. Naval Observatory time standard.

The basic measurement of the receiver is a phase difference between the satellite clock and a user clock as measured on the ground through the satellite signal. This phase difference, referred to as pseudo-range, contains the phase difference of the two clocks and the phase difference due to propagation delay of the signal. The satellites transmit orbital data which allow software in the receiver to compute the precise position of the satellite. The ground position is precisely known and a theoretical distance to the satellite is computed. The propagation delay of the signal is computed directly from the theoretical distance, with ionospheric and tropospheric effects calculated from a model. These delays are subtracted from the pseudo-range phase measurements and the results are the phase difference between the satellite and the ground clocks.

Common measurements were made on August 29, 1983 when NRL GPS receivers were co-located at Maryland Point and Haystack/Westford observatories. Due to problems with initially implementing an experiment at remote field sites, reliable data were obtained on only one day. This difficulty made it impossible to fit the clock rate to the data. Only nearly simultaneous satellite passes were used. These are listed in Table 2. The average delay between Maryland Point and Haystack/Westford had an rms of 15 ns which is not very significant since there are only four data points. However this gives us some confidence that the data is reliable.

Table 2

Summary of GPS Time Transfer

<u>Day</u> no.	<u>NAVSTAR</u> no.	<u>TIME</u> (hrs:min:sec)	<u>MPT -GPS</u> (μ sec)	<u>TIME</u> (hrs:min:sec)	<u>HAY -GPS</u> (μ sec)	<u>HAY -MPT</u> (μ sec)
241	4	20:08:57	-5.554	20:07:57	-1.653	3.901
241	3	21:17:09	-5.550	21:06:57	-1.676	3.874
241	6	23:02:15	-5.509	23:07:57	-1.648	3.861
242	5	00:57:39	-5.514	00:32:57	-1.645	3.869

In order to evaluate the accuracy of this data, Table 3 presents the sources of error in these measurements. By and far the largest source of error is due to the fact that we have made a very small number of measurements and cannot solve for the clock drift between the two stations.

Table 3

GPS Time Transfer Error Sources

<u>Source</u>	<u>Expected Error</u>
Ionosphere/Troposphere	5-15 ns
Ground Position	10-15 ns
Small Number of Measurements and Frequency	
Offsets between Station Clocks	15-30 ns
Satellite Ephemeris	5-10 ns

Portable Clock Measurements

Portable clocks were transported from USNO to the Haystack/Westford and Maryland Point observatories for the last three experiments and to Onsala Observatory for the final experiment. There was a clock jump of 190 ns for the portable clock transported to the Haystack/Westford Observatory in October 1982. There was also a clock jump during the Onsala measurement. Thus data were deleted. The last two clock trips to Maryland Point and Haystack/Westford were successful. Figure 4 displays the residual "time" versus the USNO master clock after a linear drift rate has been removed for the portable clock used for the August 1983 Maryland Point measurement. The VLBI experiment was performed on modified Julian Date of 45575.6 which is marked by an arrow in figure 4. Thus one can see that if a polynomial is fit to the data and the clock is not away from the master clock for periods longer than a day, one should probably approach an accuracy of better than 5 ns in clock synchronization. This accuracy was shown to be achievable by Spencer *et al.* (1981) who compared four clocks which continuously traveled between VLBI sites for a period of a week.

Comparison

Table 4 shows the comparison between the VLBI portable clock and GPS results. The VLBI measurement has been extrapolated to the time of the portable clock and GPS measurements. This clock synchronization is the difference in the clocks at the VLBI sites. This agrees to within 2 ns of the portable clock measurements and within 28 ns of the GPS measurement. The earlier measurement in November 1982

showed agreement between the VLBI and portable clocks of 2 ns. Thus these measurements are within the errors expected. These measurements are very promising but are only two data points in the case of portable clocks and only one measurement in the case of the GPS comparison.

Table 4
Time Transfer Between VLBI Stations
(Haystack-Maryland Point)

<u>Day</u>	<u>UT</u>	<u>VLBI</u>	<u>GPS</u>	<u>Portable Clock</u>	<u>Δ</u>
241	18 ^h 00 ^m	3.891 μ s	—————	3.889 μ s	2 ns
241	22 ^h 21 ^m	3.814 μ s	3.787 μ s	—————	28 ns

FUTURE IMPROVEMENTS

These measurements have shown that improved "station" clocks could help all three techniques of time synchronization. The difficulty in extrapolating time synchronization from one epoch where it was measured by VLBI, GPS, or portable clocks to another later or earlier epoch depends entirely on the reliability and modelability of the station clocks. The clocks are usually located at field sites as at VLBI stations where maintenance may not be ideal or as in the case of portable clocks, they are exposed to non-ideal conditions as they are moved from one site to another.

The GPS data can be vastly improved by taking a more extended data set, i.e., data obtained over several days in order to remove clock drifts, etc. Improvements can also be made in the electronics. In addition, simultaneous satellite passes should be used for the synchronization as was done here. Improved corrections can be made for the ionospheric and tropospheric delays. In this way the only major cause of error would be the satellite positions.

Finally improvements must be implemented to measure waveforms at subnanosecond levels. This applies to all techniques of time synchronization. With improvements in the GPS method, a series of experiments should be performed to obtain a larger data set to evaluate the accuracies of these techniques for time synchronization.

FUTURE USE OF VLBI

The VLBI system is capable of subnanosecond time synchronization with MKIII technology. It is difficult at this time to see an operational use for this accuracy. The need to use large antennas (in this case about 100-200 tons each) to obtain the signal-to-noise necessary when using natural celestial sources makes this system less than portable. In cases where time synchronization between sites with large antennas is wanted this may be practical. However at this time, the major use of VLBI should be as a benchmark system against which to evaluate other systems.

A CHALLENGE

The successful time synchronization experiments between the Maryland Point, Haystack/Westford and Onsala Space Observatory shows that these stations can perform these experiments with a minimum of instrumental development. These stations

therefore provide an excellent testbed for future precise time synchronization systems. Therefore we challenge any precise system (< 10 ns) to an evaluation against the VLBI technique using these baselines.

REFERENCES

- Clark, T. A., Counselman, C. C., III, Ford, P. G., Hanson, L. B., Hinteregger, H. F., Klepczynski, W. J., Knight, C. A., Robertson, D. A., Rogers, A. E. E., Ryan, J. W., Shapiro, I. I., and Whitney, A. R., 1979, IEEE Trans. on Instrumentation and Measurement, Vol. 28, 184.
- Counselman, C. C., III, Shapiro, I. I., Rogers, A. E. E., Hinteregger, H. F., Knight, C. A., Whitney, A. R., Clark, T. A., 1977, Proc. of IEEE, Vol. 65, 1622.
- Robertson, D. S. and Carter, W. E., 1982, "High Precision Earth Rotation and Earth-Moon Dynamics", ed. O. Calme, D. Reidel, Dordrecht, Holland, pg. 97.
- Rogers, A. E. E., Cappallo, R. J., Hinteregger, H. F., Levine, J. I., Nesman, E. F., Weber, J. C., Whitney, A. R., Clark, T. A., Ma C., Ryan, J., Corey, B. E., Counselman, C. C., Herring, T. A., Shapiro, I. I., Knight, C. A., Shaffer, D. B., Vandenberg, N. R., Lacasse, R., Mauzy, R., Rayhrer, B., Schupler, B. R., and Pigg, J. C., 1983, Science, 219, 51.
- Spencer, J. H., Waltman, E. B., Johnston, K. J., Santini, N. J., Klepczynski, W. J., Matsakis, D. N., Angerhofer, P. E., and Kaplan, G. H., 1981, Proc. of Thirteenth PTTI Applications and Planning Meeting, pg. 231.

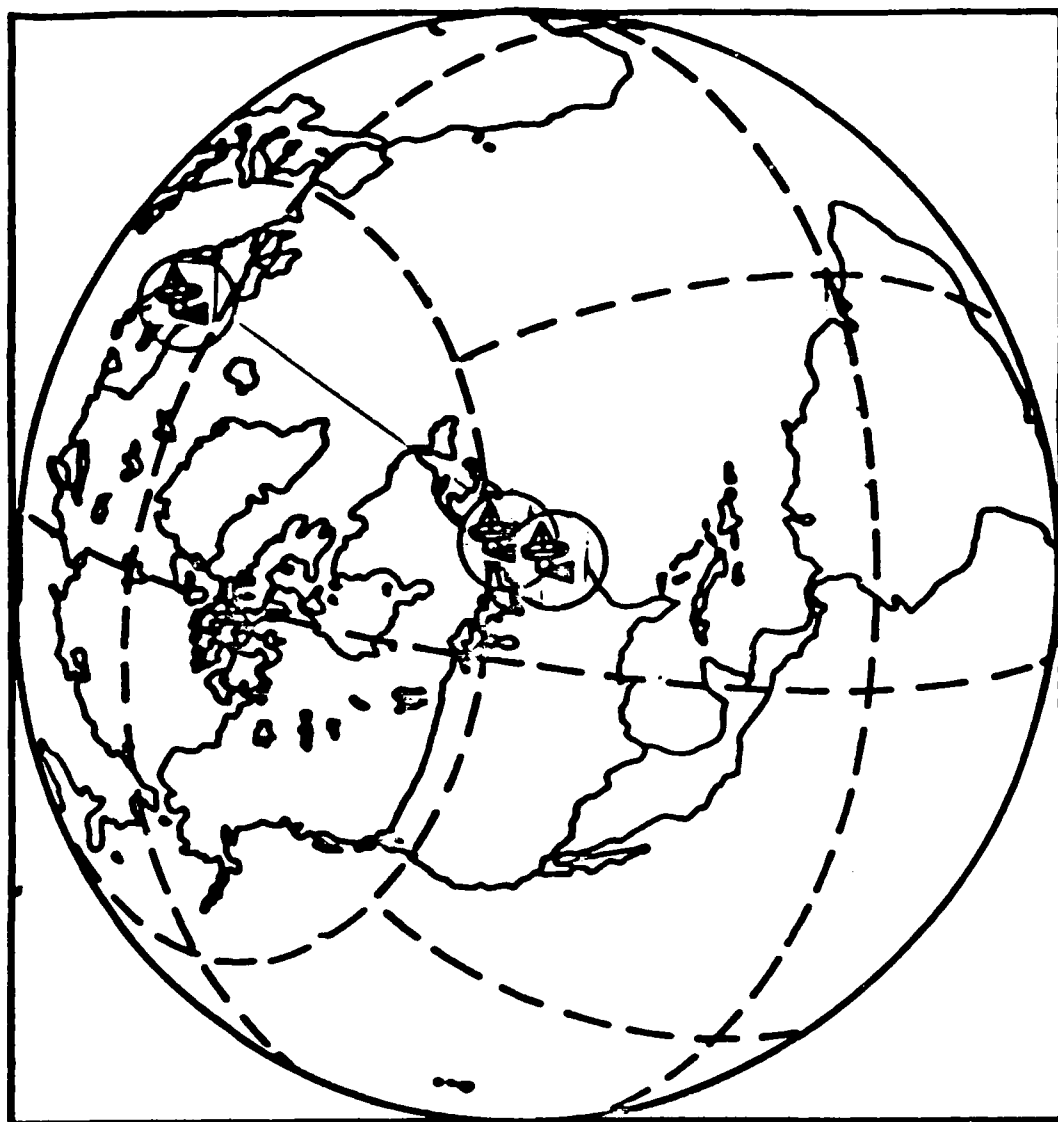
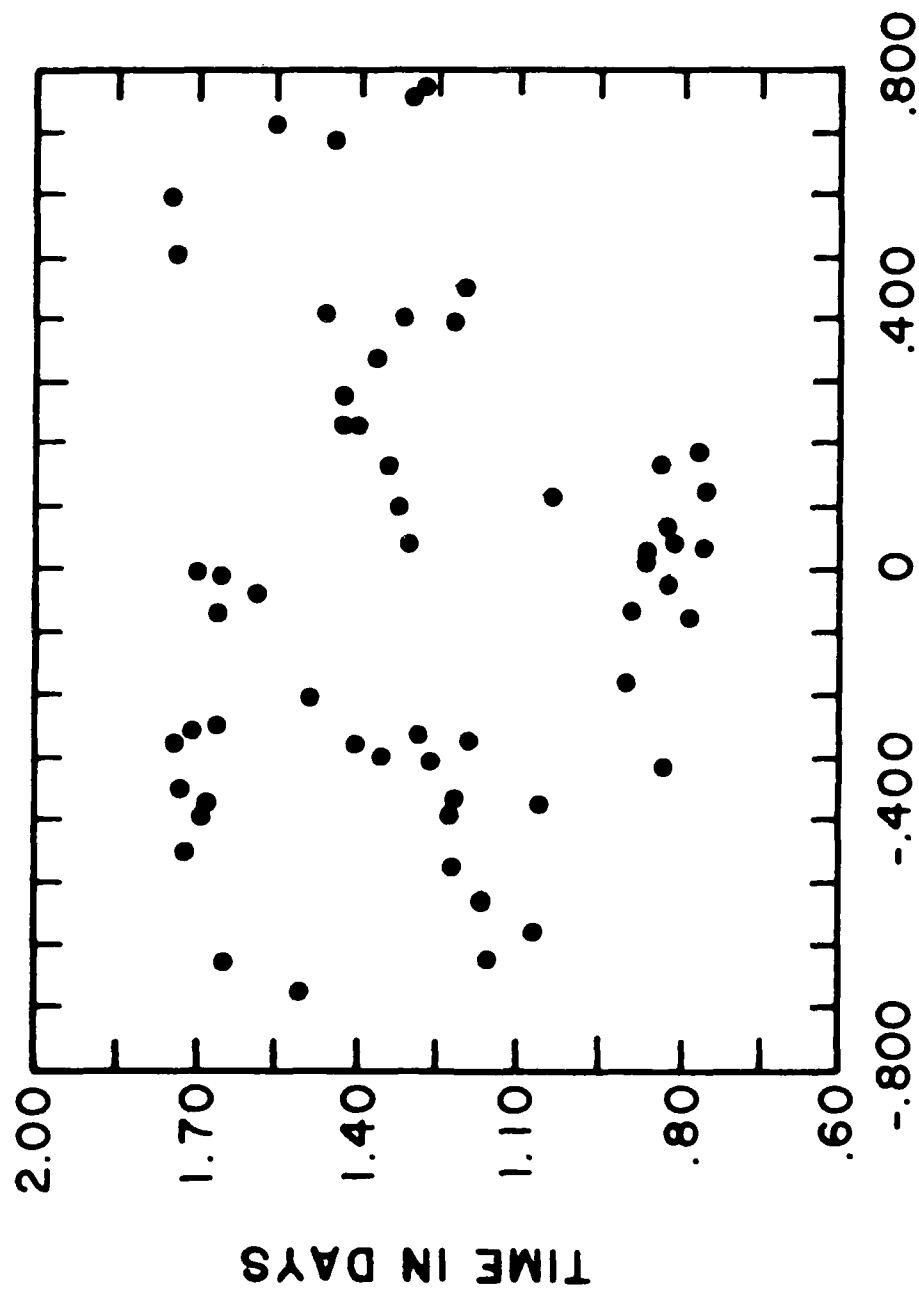


Figure 1 - The location of the Maryland Point, Haystack/Westford, and Onsala Space Observatories.



MEAN = -0.04 ± 0.35 ns

Figure 2 - The delay residuals for the Maryland Point-Westford baseline after the clock epoch and drifts have been removed from the data. The mean is 0.04 ns with an rms scatter of 0.35 ns.

Time Transfer via VLBI, GPS Satellite, and Portable Clock

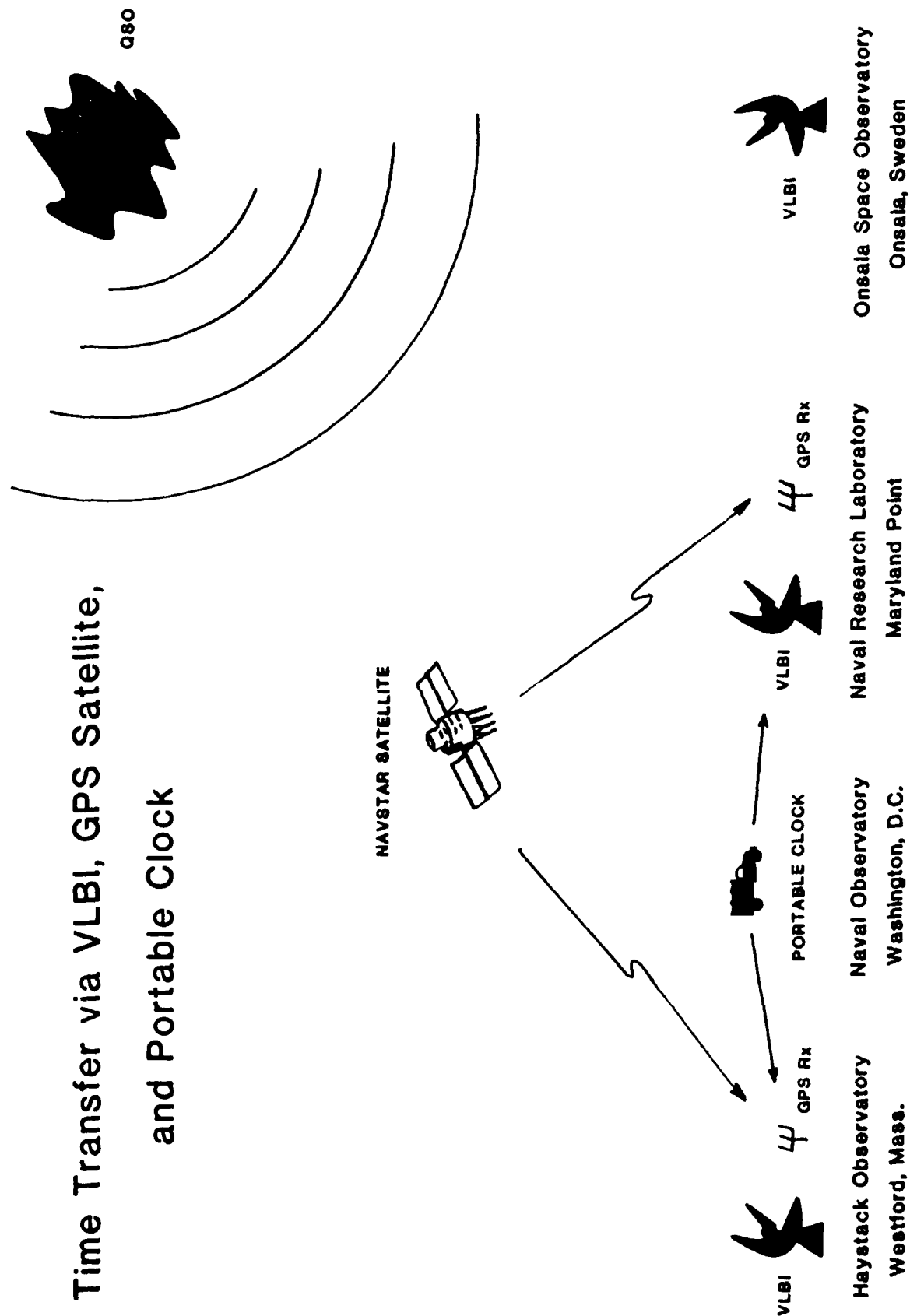


Figure 3 - Schematic representation of the August 29, 1983 experiment which compared VLBI, portable clock, and GPS techniques for precise clock synchronization.

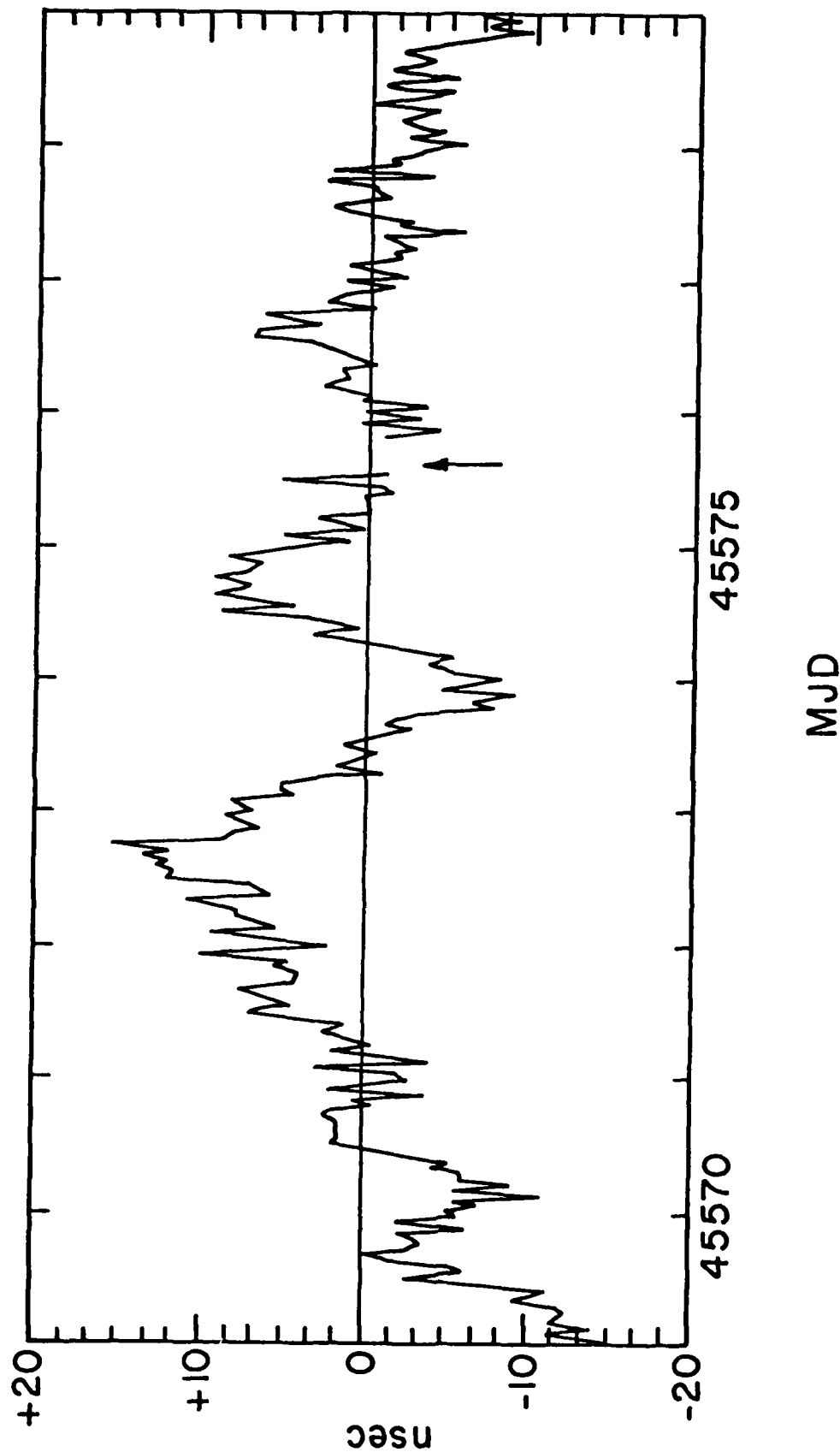


Figure 4 - The residuals in ns for the portable cesium clock used to transfer time between the USNO Master Clock and Maryland Point Observatory for the August 1983 experiment. λ linear drift has been removed from the portable clock residuals. The time is in Modified Julian Days. MJD 45575 is 0^h UT on August 29, 1983. The arrow denotes the time synchronization at Maryland Point.

QUESTIONS AND ANSWERS

DR. WINKLER:

You are complaining about your oscillators, but I must say that none of the sites which I have seen takes proper care of them. It's the conditions of operation which ought first to be improved; and when I say that, I mean to include power supplies, public power. As you probably don't realize, if the input voltage changes by one volt, it will produce a frequency change in your maser later on, and if your temperature changes, it will produce phase shifts. You are talking about fractions of a nanosecond, and these things have to be considered as error. Second comment: A portable clock properly operated, and I think ours are, does not jump around. It develops rate changes, and it develops these changes particularly under the impact of temperature, exposure, and so on, but, of course, the portable clock will never be able to compete, certainly, with the ones now, with the precisions that you have mentioned of a few nanoseconds.

The benefit of the portable clock is that it is very convenient, can be sent almost anywhere and you do not have to calibrate delays, and this is something which has been completely ignored or is not mentioned. This brings me to the 3rd point; today where we had Mr. Veenstra's paper, he gave a very conservative estimate of the difficulty of making these delayed calibrations. When you talk about accuracy, you mean accuracy, that means what is the time difference between two stations and not what is the precision with which you determine these time differences.

I believe most of these numbers, which you have just seen, actually are estimates of precision.

MR. JOHNSTON:

For the VLBI number, I tried to estimate accuracy because we measured delay throughout the whole VLBI system very carefully; that is the one thing that the Mark III can do, because there are calibration signals sent throughout the system and you actually can measure these things now.

DR. WINKLER:

But when you compare the G.P.S. time and a two-way method such as the communication satellite spread spectrum intercomparison, one has to realize that they both deal with the difficulty of calibrating a spread spectrum signal and calibrating the delays starting with the antenna, the preamplifier, the correlator and so on, its exactly the same problem. The only difference is in the G.P.S. In addition, you have the problem of estimating the one-way delay change-through the troposphere and ionosphere, and estimating the errors of the satellite position, which you do not

have in the two-way communication satellite experiments; and this did not come out properly this morning. So if you compare all of these methods, it appears to me that each one of them has unique advantages, but each one, of course, suffers from also unique problems which have not yet been completely solved. I would agree that the VLBI is an extremely useful thing to serve as a benchmark, because it's likely that in view of the Mark III capability to have internal calibrations and the fact that you deal with very large antennas, probably the delay through those large systems can be kept constant to a better degree than so many others; and you at least don't have the ephemeris problem, and so on. But I would not say that one system is better than another, without qualification. They each have individual unique features and problems.

MR. ALLAN:

I completely agree with Dr. Winkler's comments and would add a couple of others. First of all, G.P.S. uses common view. One must take care to make simultaneous measurements because of multipath and other concerns. We have found doing that, for example, for similar baseline, between Boulder and Goldstone that we are seeing three or four nanosecond precision. We have not verified the accuracy; but again the common view technique, all that is important to do, for accurate time transfer, is that you calibrate the differential delay between two receivers because it's a receiver only kind of signal, and you take one receiver from one point to another point and in fact transfer time, the same as you would with a portable clock, with the uncertainties, of course, of the propagation at that new site.

Another thing I would say, we compared GPS common view by Boulder between Paris and the U.S.N.O. and compared it with a portable clock trip that they made, and they agreed to one nanosecond. I don't believe that, either.

MR. JOHNSTON:

On the G.P.S. part of the experiment, I tried to use the common passes for G.P.S., but we didn't have a lot of data, and those were the best ones I could choose. I agree with what Gernot is saying, but I think if you want to find what the accuracy of these systems are--then, that's why I issued this challenge. It will make me clean up my numbers. We really need more data. We don't even have side-by-side comparisons. We need another system satellite. The problem is, I can't move my two-hundred foot antenna; it's too prohibitive in cost.

MR. WARD:

About this request for more data, I will make the commitment today that for the Sixteenth P.T.T.I., we will have five G.P.S. data points and at least a hundred VLBI points; just comparing the two systems with the Australian-U.S. baseline and the U.S.-Europe baseline and for the G.P.S. a direct measurement of Europe-Australia; and by that time we will have a system that will have the full calibrations in for the VLBI.

MR. JOHNSTON:

Presently, that is only partially implemented. Well, I have some data now, but it's only partial; but I guess I have about ten times more data than you have and I have some of it in the report with me. And a point for the useability of the VLBI, it's excellent and it produces UT-1 data. G.P.S. can't produce UT-1 data, but it's superior to the VLBI for deriving the kind of rate which I am interested in. I have some data that is showing accuracy to parts in 10^{16} .

We are doing an experiment over about a year-and-a-half--four experiments, three to get the calibration right. I really have to emphasize that calibration is not straightforward and easy. You have to really sit down and measure delays through the systems and constantly monitor them. If you don't do that part right, you come up with the unexpected, a hundred nanoseconds here and a hundred nanoseconds there. You can get the number right by always subtracting constants in the experiment. Calibration is really important.

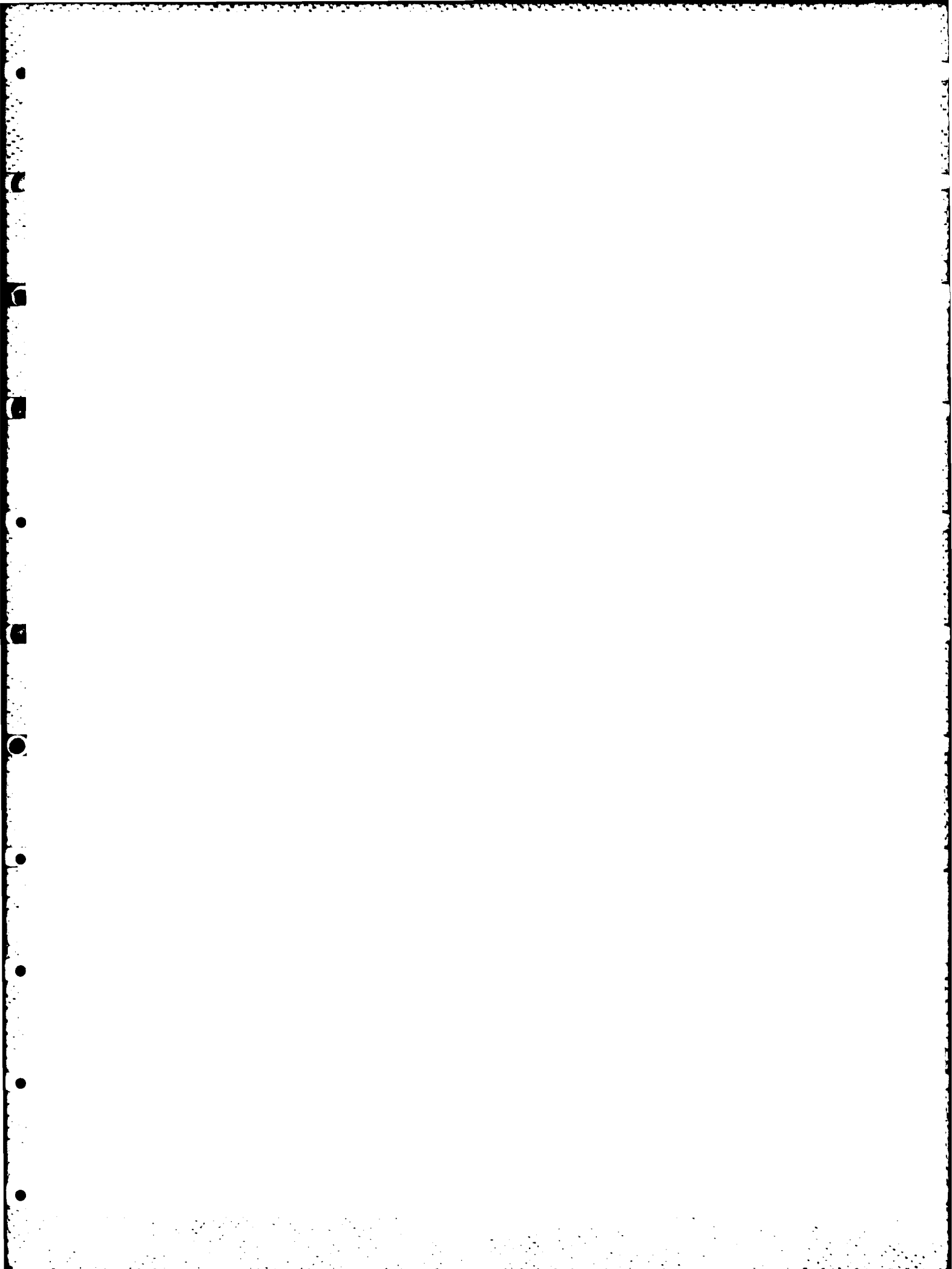
SESSION IV

MATHEMATICAL AND STATISTICAL TECHNIQUES AND THEIR APPLICATION TO PTTI

Dr. James A. Barnes, Chairman
Austron, Inc.

CALL TO SESSION IV

(Nothing transcribed)



CLOCK CHARACTERIZATION TUTORIAL

David W. Allan
Time and Frequency Division
National Bureau of Standards
Boulder, Colorado 80303

ABSTRACT

Managers are often required to make key program decisions based on the performance of some elements of a large system. This paper is intended to assist the manager in this important task in so far as it relates to the proper use of precise and accurate clocks. An intuitive approach will be used to show how a clock's stability is measured, why it is measured the way it is, and why it is described the way it is. An intuitive explanation of the meaning of time domain and frequency domain measures as well as why they are used will also be given.

Explanations of when an "Allan variance" plot should be used and when it should not be used will also be given. A more efficient way to measure clock frequency drift will be explained. The relationship of the rms time error of a clock to a $\sigma_y(\tau)$ diagram will also be given. The environmental sensitivities of a clock are often the most important effects determining its performance. Typical environmental parameters of concern and nominal sensitivity values for commonly used clocks will be reviewed.

Systematic and Random Deviations in Clocks

This paper is tutorial in nature with a minimum of mathematics -- the goal being to characterize clock behavior. First, time deviations or frequency deviations in clocks may be categorized into two types: systematic deviations and random deviations. The systematic deviations come in a variety of forms. Typical examples are frequency sidebands, diurnal or annual variations in a clock's behavior, time offset, frequency offset and frequency drift. Figure 1 illustrates some of these.

If a clock has a frequency offset, the time deviations will appear as a ramp function. On the other hand, if a clock has a frequency drift, then the resulting time deviations will appear as a quadratic time function -- the time deviations will be proportional to the square of the running time. There are many other systematic effects that are very important to consider in understanding a clock's characteristics and Figure 1 is a very simplistic picture or nominal model of most precision oscillators. The random fluctuations or deviations in precision oscillators can often be characterized by power law spectra. In other words, if the time residuals are examined, after removing the systematic effects, one or more of the power law spectra shown in Figure 2 are typically observed. The meaning of power law spectra is that if a Fourier analysis or spectral density analysis is performed on the residuals, the intensity at various Fourier frequencies, f is proportional to f^β ; β designates the particular power law process ($\beta = 0, -1, -2, -3, -4$ and $\omega = 2\pi f$). The first process shown in Figure 2 is called white noise phase modulation (PM). This noise is typically observed in the short term fluctuations.

for example, of an active hydrogen maser for sample times of from one second to about 100 seconds. This noise is also observed in quartz crystal oscillators for sample times in the vicinity of a millisecond and shorter. The flicker noise PM, f^{-1} , is the second line in Figure 2. This kind of noise is often found for sample times of one millisecond to one second in quartz crystal oscillators. The f^{-2} or random walk PM indicated by the third line is what is observed for the time deviations of rubidium, cesium, or hydrogen frequency standards. If the first difference is taken of a series of discrete time readings from the third line, then the result is proportional to the frequency deviations, which will be an f^0 process or a white noise frequency modulation (FM) process. In other words the time and the frequency are related through a derivative or an integral depending upon which way one goes. The derivative of the time deviations yields the frequency deviations, and the integral of the frequency deviations yields the time deviations. So, random walk time deviations result from white noise FM. In general, the spectral density of the frequency fluctuations is ω^2 times the spectral density of the time fluctuations. The fourth line in Figure 2 is an f^{-3} process. If this were representative of the time fluctuations then the frequency would be an f^{-1} or a flicker noise FM process. This process is typical of the output of a quartz crystal oscillator for sample times longer than one second or the output of rubidium or cesium standards in the long term (on the order of a few hours, few days, or few weeks depending upon which standard). We find that in very long term, most atomic clocks have an f^{-2} type behavior for the time fluctuations -- making the frequency fluctuations an f^{-2} process or random walk FM. These five power law processes are very typical and one or more of them are appropriate models for essentially every precision oscillator. Characterizing the kind of power-law process thus becomes an important part of characterizing the performance of a clock (1). Once a clock has been characterized in terms of its systematic and its random characteristics then a time deviation model can be developed. A very simple and useful model that is commonly used is given by the following equation (2):

$$x(t) = x_0 + y_0 \cdot t + \frac{1}{2} D \cdot t^2 + \varepsilon(t) \quad (1)$$

where $x(t)$ is the time deviation of the clock at time t , x_0 is the synchronization error at $t = 0$, and y_0 is the syntonization error at $t = 0$, which produces a linear ramp in the time deviations. D is the frequency drift term, which is almost always an applicable model element in commercial standards. This $\frac{1}{2}Dt^2$ term in the time deviation due to the frequency drift yields a quadratic time deviation. Lastly, the $\varepsilon(t)$ term contains all of the random fluctuations. It is this term which is typically characterized by one or more of the various power law processes. Once a clock has been fully characterized, then it is possible to do optimum time prediction. Shown in Figure 3 are some examples. The even power law spectra have simple algorithms for prediction. In the case of white noise PM, the optimum predictor is the simple mean. In the case of random walk PM, it is the last value. In the case of random walk FM, an f^{-4} process on the time, the optimum predictor is the last slope. In the case of flicker noise, the prediction algorithms are significantly more complicated but not intractable, and ARIMA techniques can be employed in order to develop optimum prediction algorithms (3).

The Concept of an Allan Variance

Figure 4 illustrates a simulated random walk PM process. Suppose this process is the time difference between two clocks or the time of a clock with respect to a perfect clock. Again this process is typical of the time deviations for rubidium, cesium, and passive hydrogen clocks. Choose a sample time τ , as indicated, and note the three time deviation readings (x_1 , x_2 , and x_3) indicated by the circles and spaced by the interval τ . The frequency deviation y_1 is proportional to the slope between x_1 and x_2 ($y_1 = (x_2 - x_1)/\tau$). Similarly y_2 is proportional to the slope between x_2 and x_3 ($y_2 = (x_3 - x_2)/\tau$). The difference in slope, Δy , is a measure of the frequency change from the first τ sample interval to the next adjacent τ sample interval. With a fixed value of τ , imagine averaging through the entire data set for all possible readings of x_1 , x_2 , and x_3 displaced by τ each yielding a Δy . The average squared value of Δy divided by 2 is called the "Allan variance". In theory, it is the average over all time. In practice, finite data sets yield rapidly converging estimates. The square root of the Allan variance is denoted $\sigma_y(\tau)$; $\sigma_y(\tau)$ is an efficient estimator of the power law spectra model for the data. How $\sigma_y(\tau)$ changes with τ indicates the exponent for the power law process. In fact, in the case of random walk FM, $\sigma_y(\tau)$ is statistically the most efficient estimator of this power law process. If power law processes are good models for a clocks random fluctuations, which they typically are, then the Allan variance analysis is faster and more accurate in estimating the process than the Fast Fourier Transform. Some virtues of the Allan variance are: It is theoretically and straightforwardly relatable to the power law spectral type ($\beta = -\mu - 3$, $-2 < \mu < 2$, where μ is the exponent on τ). Once a data set is stored in a computer it is simple to compute $\sigma_y(\tau)$ as a function of τ . The difference in frequency, Δy , is often closely related to the actual physical process of interest, e.g. frequency change after a radar return delayed by τ , effects of oscillator instabilities in a servo with loop time constant τ , the change in frequency after a calibration over an interval τ , etc. Some drawbacks of the Allan variance are: it is transparent to periodic deviations where the period is equal to the sample time τ . It is ambiguous at $\mu = -2$, i.e. $\sigma_y(\tau) \sim \tau^{-1}$ may be either white noise PM or Flicker noise PM. Remembering from above the relationship between the spectral density of the frequency deviations and the spectral density of the time deviations, if $S_x(f) \sim f^\beta$ and $S_y(f) \sim f^\alpha$, then $\alpha = \beta + 2$ and $\alpha = -\mu - 1$ ($-2 < \mu < 2$), where $S_x(f)$ is the spectral density of the time deviations and $S_y(f)$ is the spectral density of the fractional frequency deviations. Figure 5 shows the noise type and the relationship between μ and α . There are some ways around the ambiguity problem at $\mu = -2$. For noise processes where $\alpha > 1$ there is a bandwidth dependence (4). A software trick can be employed to effectively vary the bandwidth rather than doing it with the hardware. Rather than calculating $\sigma_y(\tau)$ from individual phase points the phase can be averaged over an interval τ . Hence the x_1 , x_2 , and x_3 from Figure 4 become phase or time difference averages. As τ increases the effective measurement system bandwidth decreases. This technique removes the ambiguity problem. We have called this the modified Allan variance or modified $\sigma_y(\tau)$ analysis technique. Figure 6 shows the μ , α mapping for the modified Allan variance. For white noise PM, μ is equal to -3, and for flicker noise PM, μ is equal to -2.

Time Prediction Error of a Clock

Another concept which has become useful is the computation of the time error of

prediction. In the case of white noise FM and random walk noise FM, $\tau \sigma_y(\tau)$ is the optimum time error of prediction. For white noise PM the optimum value achievable is $\tau \sigma_y(\tau)/\sqrt{3}$, and for flicker noise FM it is $\tau \sigma_y(\tau)/\ln 2$.

Applying some of the above concepts to state of the art frequency standards yields the frequency stability plot shown in Figure 7 (5), and the corresponding RMS time prediction error plot shown in Figure 8. The RMS time prediction error plot is based on reference (2) and is a function of the levels of noise in the clock and also the uncertainties associated with determining the systematic deviations due to a finite data length.

Environmental Efforts on Clocks

From a management point of view, the characteristics of the various clocks should be related to the needs of a particular program. It is important to keep in mind that, in practice, systematic and environmental effects often are the predominant influence on the time and frequency deviations of a clock. The reliability of a clock is often a basic issue, and the manager should assure himself that adequate reliability has been documented. The manager also needs to ask the following questions in each application that he may have. What are the environmental conditions; e.g., the temperature, the temperature gradients, the temperature fluctuations, the rapidity of the temperature changes, the magnetic field conditions, the shock and vibration conditions, and the humidity conditions? How do these conditions affect the clock's performance? All clocks are affected at some level by changes in the above environmental parameters plus some others as well. Some clocks are affected by barometric pressure. Vibration can be extremely important. In some clocks the servos will unlock, for example, if a 1 kHz vibration is present. (6). Some clocks are acoustically sensitive. What is the gravitational or g sensitivity? What are the cost, size, weight and power requirements? Line voltage power fluctuations can affect clocks. Changes in the dc power can affect some clocks. We have found that a good clock environment can improve clock performance considerably, and we have provided a highly controlled environment for the NBS clock ensemble to improve the performance over that obtained in typical laboratory environments. Another very important question to ask is what is a clock's lifetime? Redundancy and/or multiple clocks are sometimes necessary to overcome lifetime and reliability problems. It is important to take a system's approach in establishing the best clock(s) and clock(s) configuration. In some cases the program needs are for synchronization to UTC, in other cases the needs are for syntonization, i.e. the frequencies within a system need to agree. Often the need is for time or frequency self consistency within a program, e.g. GPS requires time consistency. It seems many people are buying cesium standards as a panacea, when in fact they may not be solving the problem at hand. Buying a cesium standard does not guarantee synchronization. However, it does guarantee syntonization within some accuracy. All clocks will diverge and eventually depart from synchronization tolerance. It's just a matter of time! Knowing a clock's characteristics, the system requirements, and the environmental conditions will allow the manager to know the best clock or clocks to buy and the best way to implement them. For example, a rubidium clock coupled to a GPS receiver (used in the common-view mode with UTC(USNO MC) or with UTC(NBS)) would have better short term and better long term stability than any commercial cesium clock available. The stability would be somewhat worse in the vicinity of τ equal to one day. In practice, there are some

problems with this idea, but it illustrates the point.

Lastly, Figures 9 through 13 show nominal values for some important clock coefficients that managers and design engineers need to properly assess when evaluating which clock or clocks will best serve their needs. These are only nominal values and there will be exceptions. A band of values is listed for these coefficients ranging from nominal best performance available from laboratory-type standards through the range of typical values observed and specified for commercially available standards.

Acknowledgments

The author wishes to express appreciation to Mr. Roger Beehler and Dr. Richard Jones for their assistance in proofing the text and to Dr. Lindon Lewis and Dr. Fred Walls for assistance with the data in Figures 9-13.

References

1. Barnes, J. A., Chi, A., Cutler, L. S., Healey, D. J., Lesson, D. B., McGunigal, T., Mullen, J. Jr., Smith, W., Sydnor, R., Vessot, R., and Winkler, G. M., "Characterization of Frequency Stability", Proc. IEEE Trans. on Instrumental and Measurement IM-20, 105 (1971) NBS Tech. Note 394 (1971).
2. Allan, D. W. and Hellwig, H., "Time Deviation and Time Prediction Error for Clock Specification, Characterization and Application," IEEE Position Location and Navigation Symposium Proceedings, 29-36 (1978).
3. Box, G. E. P. and Jenkins, G. M., Time Series Analysis Forecasting and Control, Holden-Day, 1970, Catalog No. 77-79534.
4. Vessot, R., Mueller, L., and Vanier, J., "The Specification of Oscillator Characteristics from Measurements Made in the Frequency Domain," Proc. of the IEEE, Vol 54, No.2 pp. 199-207 (1966).
5. Winkler, G. M. R., "Improved Master Clock Reference System at USNO," PTTI (1983) to be published.
6. Walls, F. L., "Vibration and Acceleration Induced Timing Errors of Clocks and Clock Systems," 36th Annual Symposium on Frequency Control, p. 371 (1982).

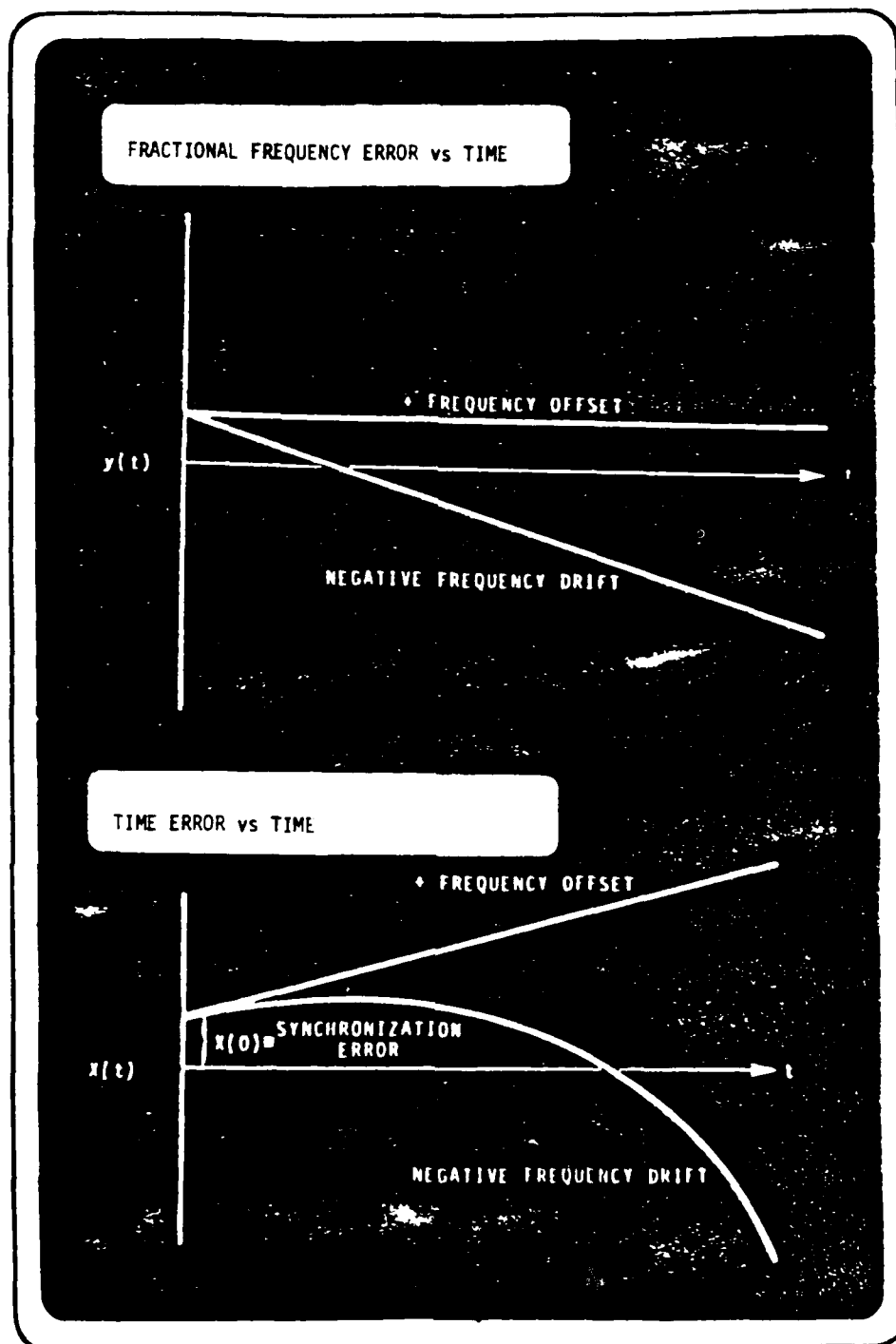


Figure 1. Frequency, $y(t)$, and time, $x(t)$, deviations due to frequency offset and to frequency drift in a clock.

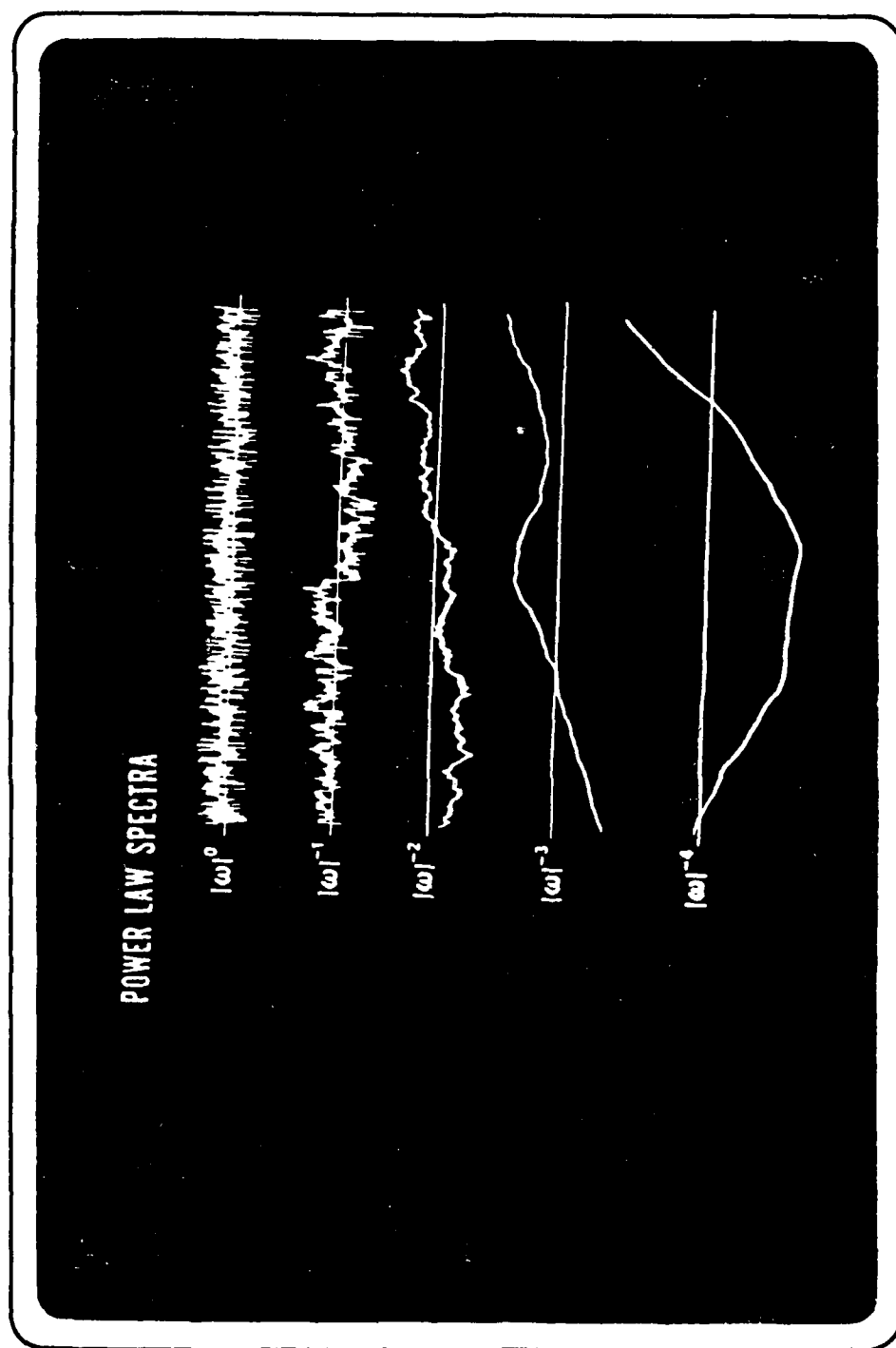


Figure 2. Simulated random processes commonly occurring in the output signal of atomic clocks. Power law spectra $S(\omega)$, are proportional to ω to some exponent, where ω is the Fourier frequency.

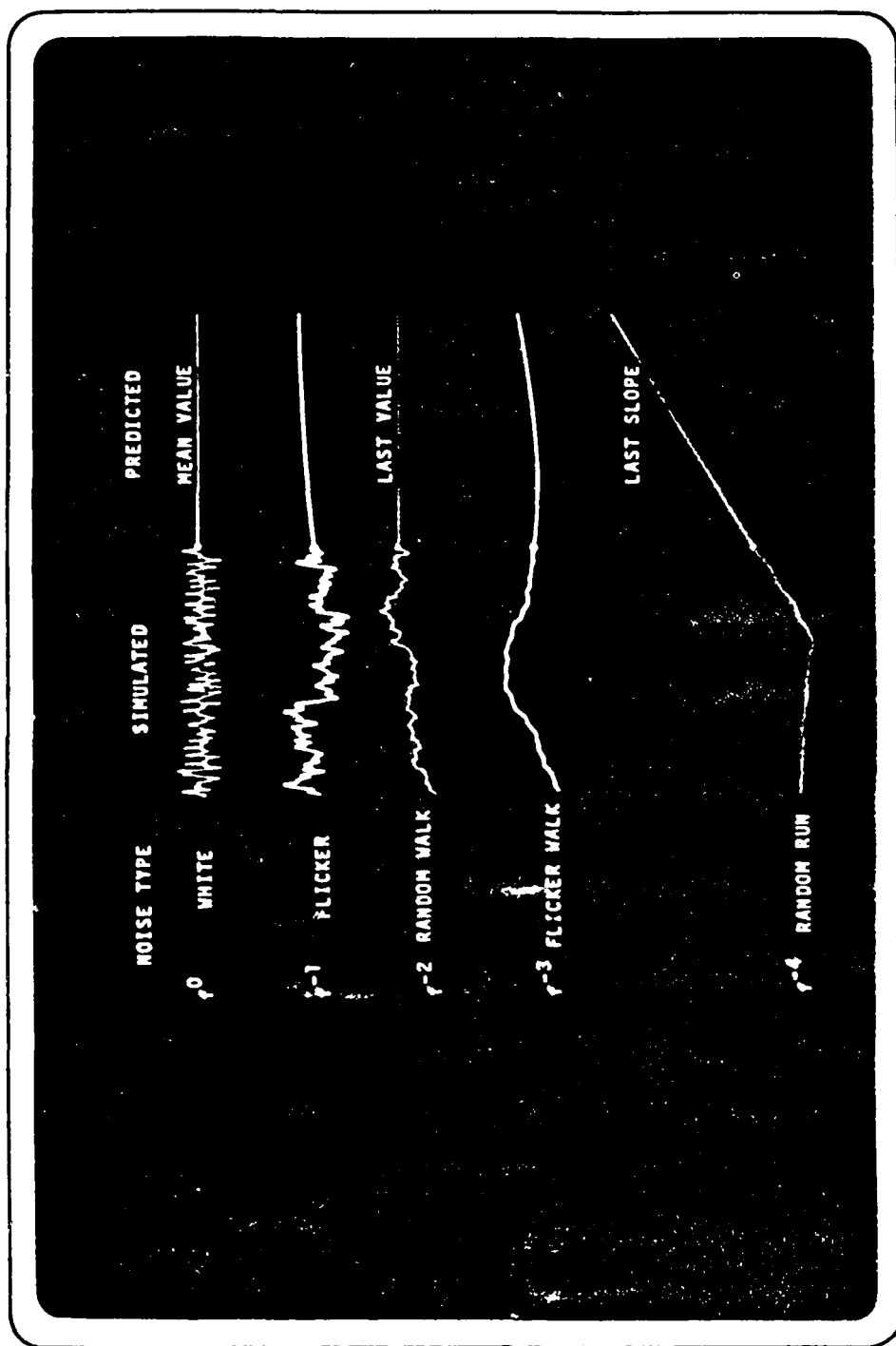


Figure 3. Simulated power law noise processes with their optimum predicted estimates.

'Allan variance' concept

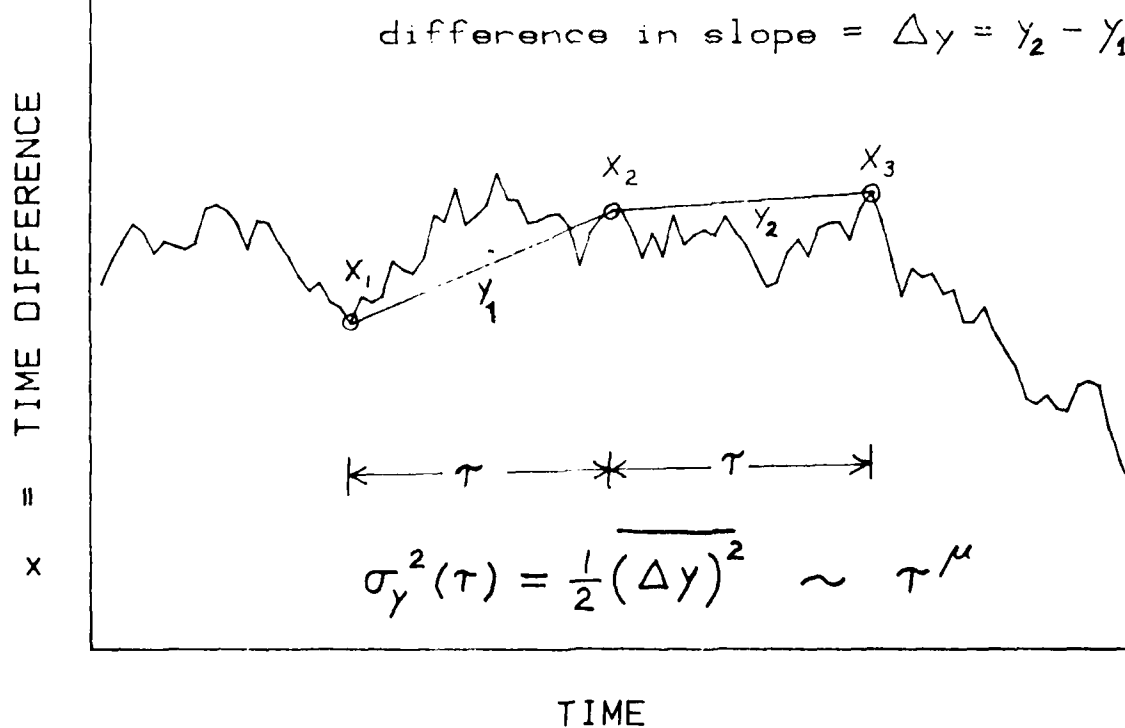


Figure 4. Pictorial of computation of "Allan variance".

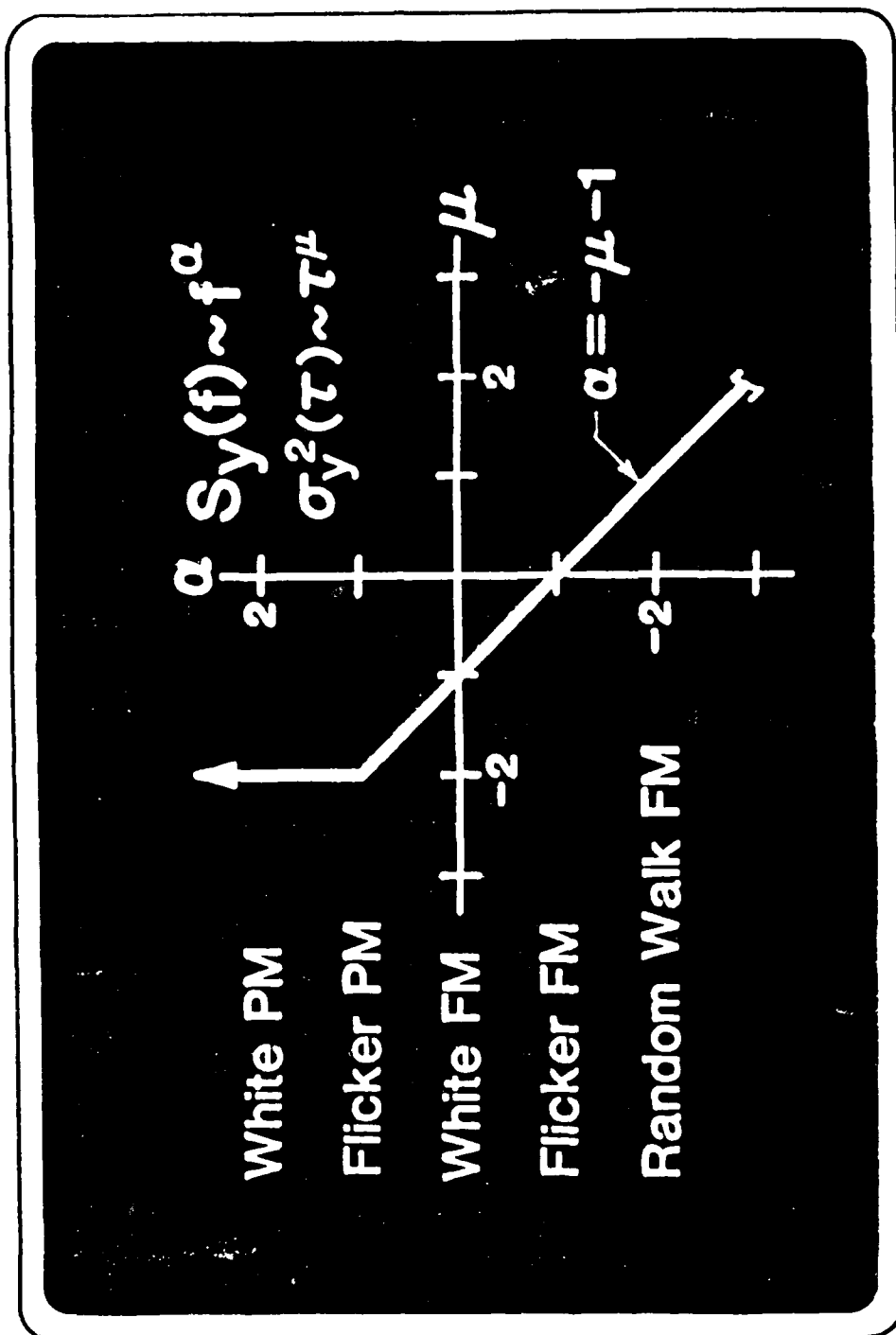


Figure 5. Various power law noise types commonly occurring in the precision clocks and the mapping between the exponent α of the frequency domain measure and the exponent μ of the time domain measure.

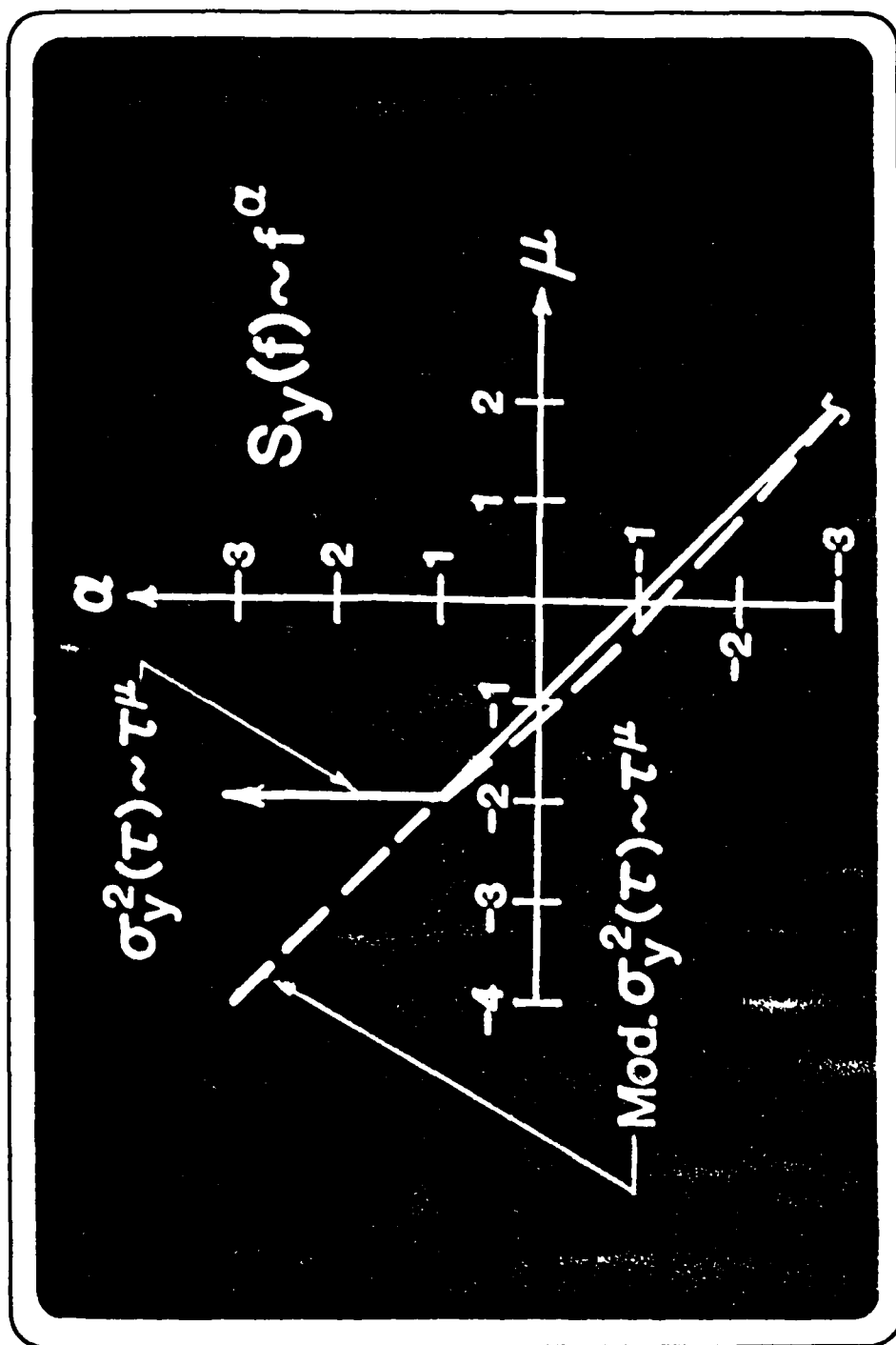


Figure 6. The mapping of the τ exponent μ of the Allan variance and of the modified Allan variance to the power law spectrum exponent α .

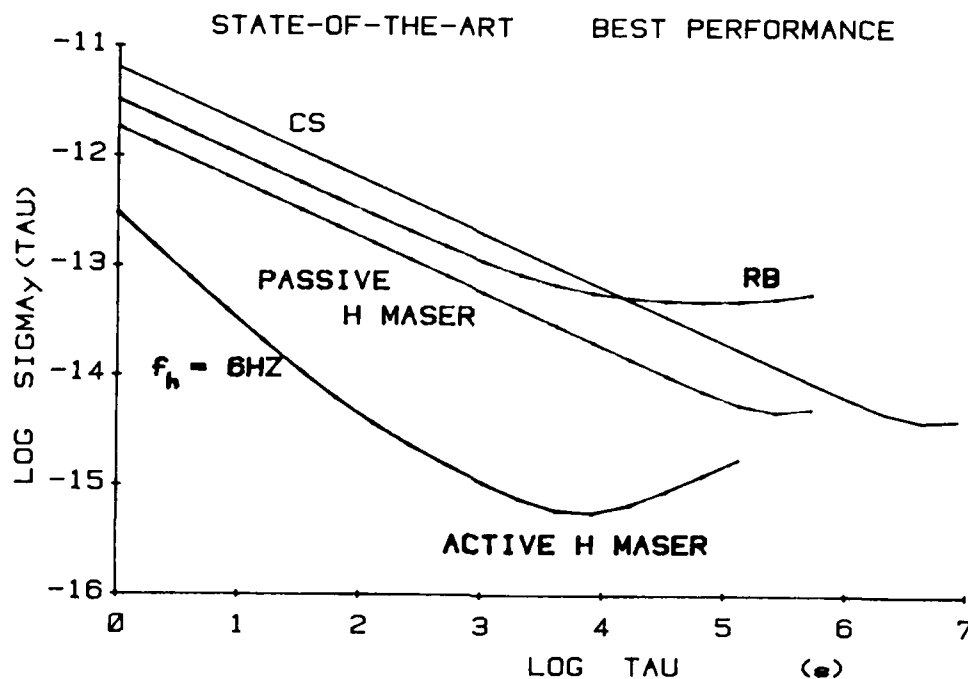


Figure 7. Frequency stability of some of the best performing frequency standards from each of four main types: CS = cesium beam, RB = rubidium gas cell, H = hydrogen (active and passive). Note: $\log 10^1 = 1$; e.g. $\log 10^{-14} = -14$.

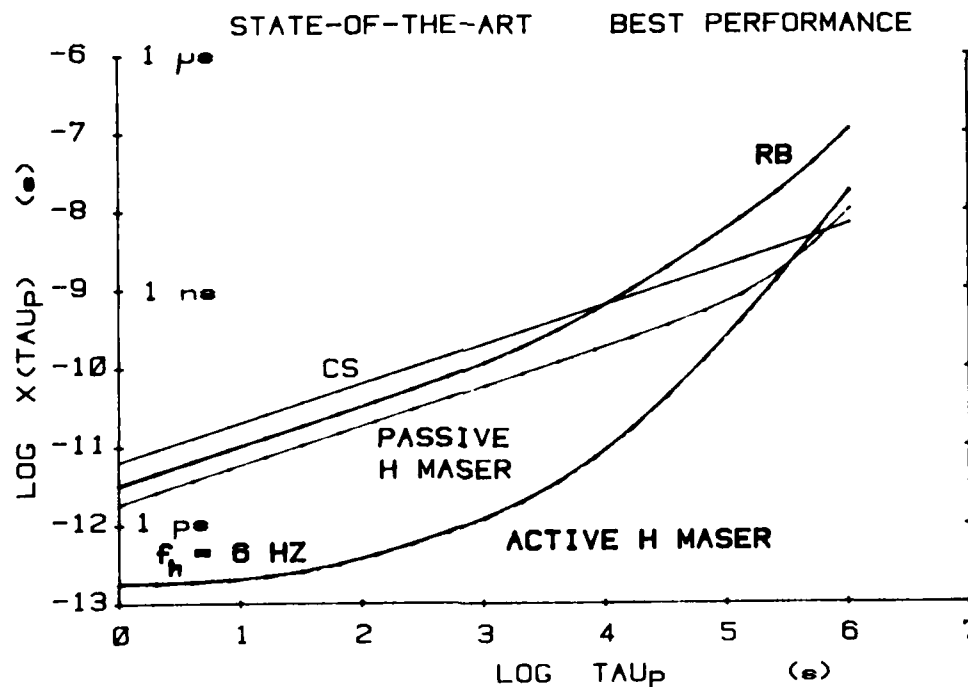


Figure 8. RMS time prediction error plot for the same frequency standards as shown in Figure 7. Note: $\log 10^1 = 1$; e.g. $\log 10^{-14} = -14$.

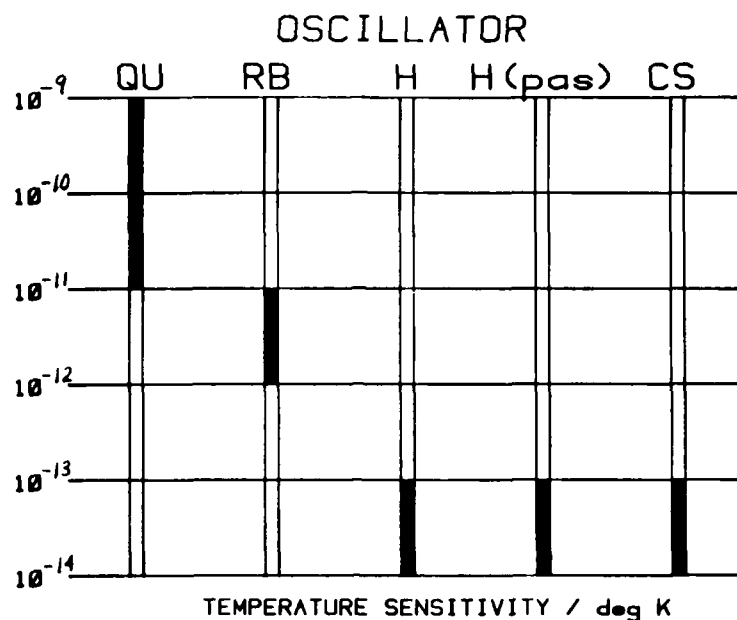


Figure 9. Nominal values for the temperature coefficient for the frequency standards: QU = quartz crystal, RB = rubidium gas cell, H = active hydrogen maser, H(pas) = passive hydrogen maser, and CS = cesium beam.

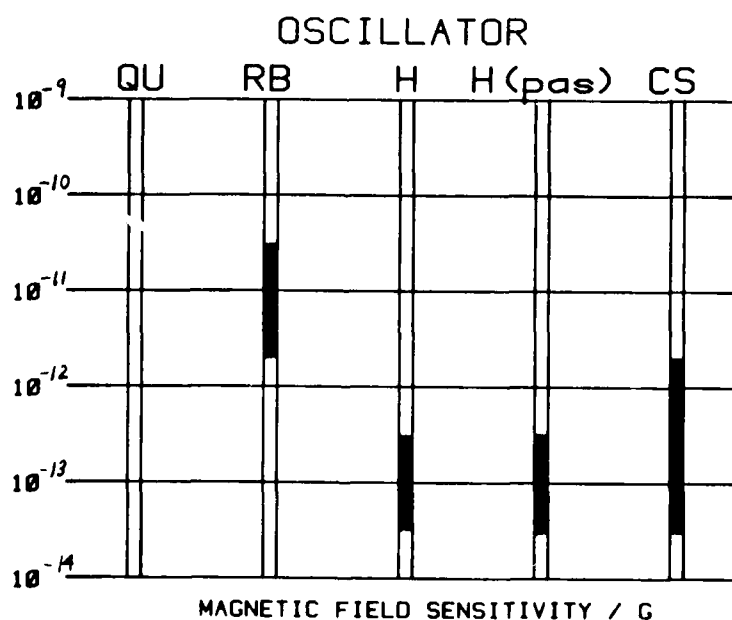


Figure 10. Nominal values for the magnetic field sensitivity for the frequency standards: QU = quartz crystal, RB = rubidium gas cell, H = active hydrogen maser, H(pas) = passive hydrogen maser, and CS = cesium beam.

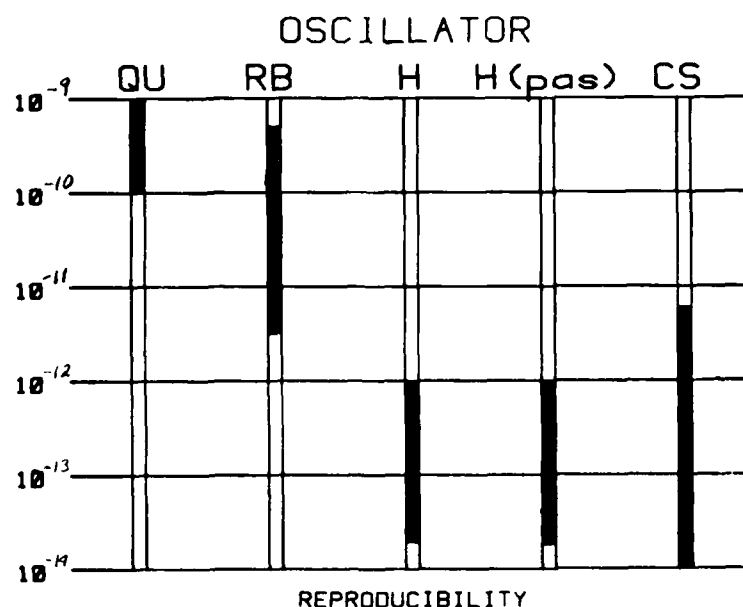


Figure 11. Nominal capability of a frequency standard to reproduce the same frequency after a period of time for the standards: QU = quartz crystal, RB = rubidium gas cell, H = active hydrogen maser, H(pas) = passive hydrogen maser, and CS = cesium beam.

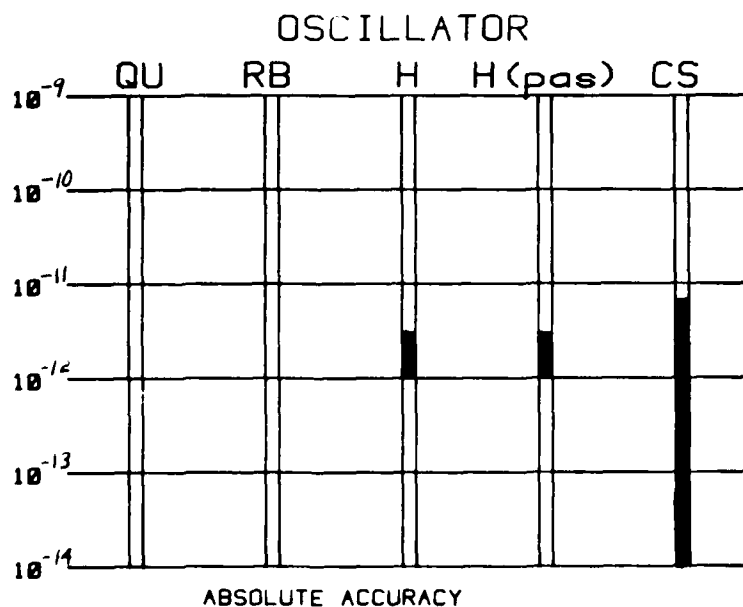


Figure 12. Nominal capability for a frequency standard to produce a frequency determined by the fundamental constants of nature for the standards: QU = quartz crystal, RB = rubidium gas cell, H = active hydrogen maser, H(pas) = passive hydrogen maser, and CS = cesium beam.

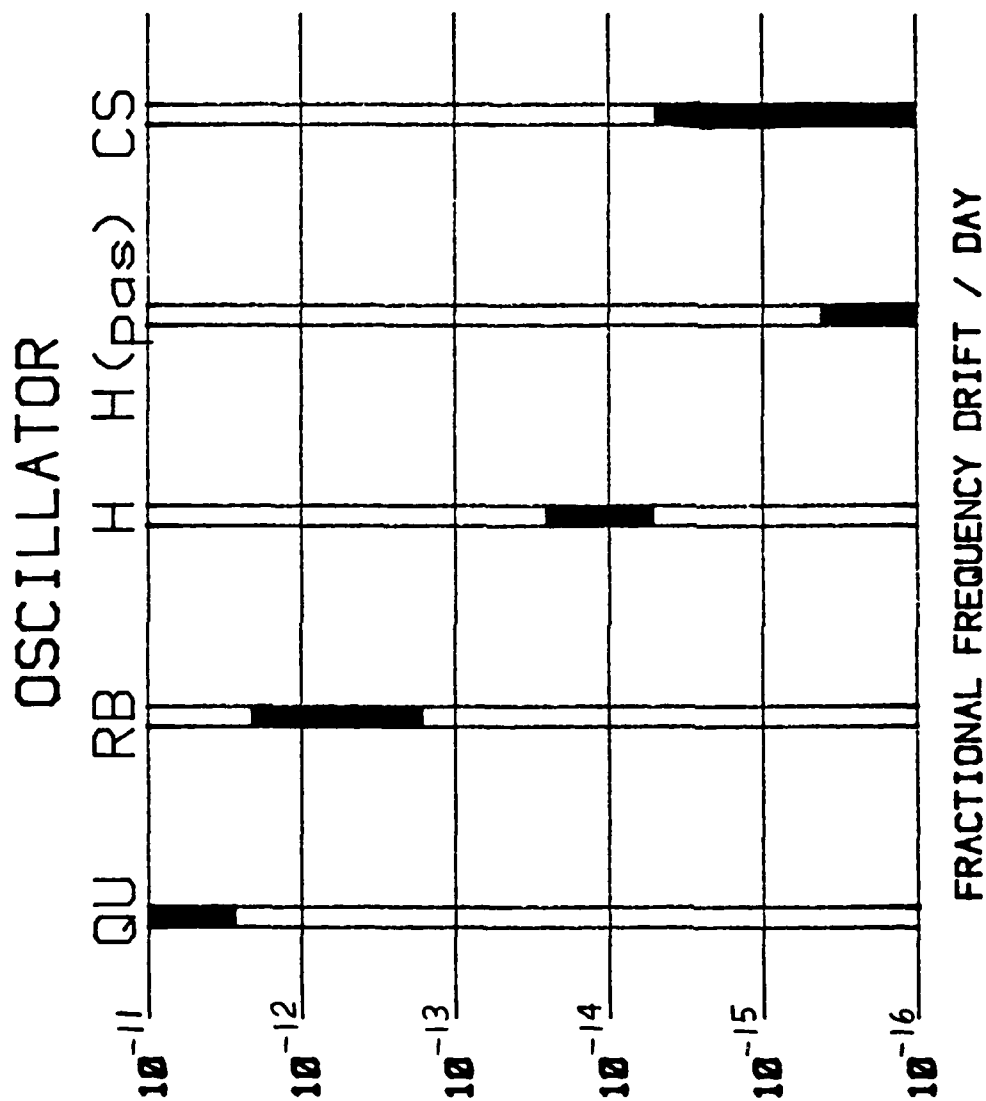


Figure 13. Nominal values (ignoring the sign) for the frequency drift for the frequency standards: QU = quartz crystal, RB = rubidium gas cell, H = active hydrogen maser, H(pas) = passive hydrogen maser, and CS = cesium beam.

QUESTIONS AND ANSWERS

DR. WINKLER:

I would like to qualify your statement that one should operate a rubidium standard with a GPS receiver and have a better performance for very short and very long times. That statement is true, but incomplete, because if you would buy a set of cesium clocks, a clock ensemble, you gain one more point and for strategic systems that is of strategic importance, that is independence. That's a very important point and I want to emphasize that.

MR. ALLAN:

I said there are practical reasons that you don't choose to do that. That's a very good example.

MR. WARD:

Sam Ward, Jet Propulsion Lab. Is that modified Allan variance useful on an active hydrogen below TAU values of a hundred seconds?

MR. ALLAN:

It would be useful because active hydrogen does have a white pm and so for the short term analysis you get tau to the $3/2$ power, yes, it would be useful.

DR. VESSOT:

In relation to that last point of TAU $-3/2$ behavior, in fact, arose from such measurements of Phase Noise 1956. That's not the comment I want to make. There are two things I implore you to do. The first one is, please lower the floor on the colored graph of the hydrogen maser; the ten to the minus fourteen; I think we are safely below one in the fifteenth. So I respectfully suggest that you back it down by a factor of ten and still be as honest as you could possibly want to be. You are safe by a factor of about three, if you do that.

The second comment is the fact that as we have long discussed, ever since 1956, that besides making the variances a function of time, I respectfully suggest also that we include the bandwidth. It's increasingly important, I think, to recognize that short term stability is limited by additive noise and that additive noise is necessarily bandwidth dependent. And those people who are to specify oscillators' stability, particularly if they're involved in rather shorter terms, must, in the giving of the Allan variance, specify the averaging in time and the stability.

The definition of the Allan variance implies that the sample number is two. So by saying that, we have cornered that issue as two. The dead time is another question, and I don't think one should complicate it further at this point, but I would urge you to at least admit that we should have the averaging time and the bandwidth; and we have been around the barn with that, Jim, on that committee. I would just like to take one more lap.

MR. ALLAN:

Thank you, Bob, and I would fully concur on any sigma-tau graph that you're looking at a tau to the minus one behavior. You need to have bandwidth specified as well.

DR. BARNES:

I will take just a moment to mention that some years ago. Dr. Vessot did a bandwidth variable measure of frequency stability and the tau of the three halves came out of his work. So the tau of the three halves is not a stranger.

METHODS FOR OPTIMAL RECURSIVE ESTIMATION OF NON-STATIONARY TIME
SERIES, APPLICATIONS TO ATOMIC TIME AND FREQUENCY METROLOGY

Z.Y. Weng and J. Rutman
Laboratoire Primaire du Temps et des Fréquences
61, avenue de l'Observatoire, 75014 Paris, France
and

J. Uebbersfeld
Département d'Electronique
Université Pierre et Marie Curie
Place Jussieu, 75005 Paris, France

ABSTRACT

In time and frequency metrology, the problems of characterization, prediction, approximation and modelization are of fundamental importance for theoretical and experimental studies. In this paper, an improved unified approach is proposed and developed, which is based on the optimal estimation theory and the digital recursive processing methods. For two different models of non-stationary time series, the digital recursive methods of optimal estimation are presented. By these unified methods one can synthesize some digital predictors, digital filters and digital differentiators. These digital estimators are used to characterize the frequency instabilities of atomic clocks, to predict the random variations of atomic time scales, and to smooth the time series data. For the modelization of the statistics of frequency and phase fluctuations some analytical procedures are proposed. Then the Markov models of atomic clock instabilities can be deduced. In order to emphasize the utility of the theory, application examples are given for some time comparison data between commercial cesium atomic clocks.

I. INTRODUCTION

In time and frequency metrology, there are some problems of fundamental importance for the theoretical and experimental studies of oscillators and atomic clocks: (1) modelization of the statistics of frequency and phase fluctuations; (2) characterization of frequency and phase instabilities; (3) prediction of random variations of atomic time scales; (4) approximation or smoothing of the frequency and time measurement data.

The commonly used methods of modelization and characterization are based on stationary models as the basic assumption. In general, one must assume the non-stationary models of variations of frequency and time. In this case, the method of structure functions is used for the characterization problem, the least-squares method is used for the approximation problem, and the fixed filter method or the ARIMA method are used for the prediction problem. But the solutions of problems provided by the above mentioned methods are not always completely satisfactory.

In this paper, improved unified methods are proposed and developed, which are based on the optimal estimation theory and the digital recursive processing methods. For the study of non-stationary fluctuations of frequency and phase

in atomic clocks, two different approaches are used. The first approach relies on deterministic polynomial models with exponential weighting of data. The second approach utilizes non-stationary stochastic models with stationary increments. The optimal digital recursive methods for the estimation of non-stationary time series are developed for each of these two approaches. By the unified methods one can synthesize digital predictors, digital filters and digital differentiators. These digital recursive estimators are used for solving the problems of characterization, prediction and approximation.

From time comparison data between atomic clocks, one can use the digital differentiators for the characterization of frequency instability. The transfer functions of the differentiators are composed by two operations: pure differentiation and low-pass filtering. This method allows us to estimate the variance function and the power spectral density function. Therefore one can characterize frequency instabilities both in the time and in the Fourier frequency domains only from clock time comparison data.

From time comparison data between atomic clocks, one can use the digital recursive predictors for the prediction of random variations of atomic time scales. In the design of optimal predictors the additive measurement noise is taken into account, which is not negligible for the time comparisons between distant atomic clocks.

Time comparisons between atomic clocks via a satellite provide time series data. The conventional method for the smoothing of time series data is the classical least-squares method. But this method is not suited for the real-time data processing. One can use the digital recursive filters for the smoothing of time series by real-time data processing.

For the modelization of the statistics of frequency and phase fluctuations, some analysis of internal noises in atomic clocks will be given, and some theoretical Markov models of atomic clocks will be deduced. Then some analytical procedures of spectral approximation and model identification will be proposed. One can obtain the corresponding ARIMA models by the method of Z-transformation.

II. METHOD FOR OPTIMAL RECURSIVE ESTIMATION OF NON-STATIONARY TIME SERIES REPRESENTED BY DETERMINISTIC POLYNOMIAL MODELS

2.1 Problem Statement

In time and frequency metrology one often encounters problems where optimal estimators must be determined, which reproduce or transform random signals carrying useful information constituting non-stationary random processes. In this paragraph one will discuss the methods for determining optimal estimators in the case where besides a stationary random process the input data contain a mathematical expectation which can be represented in the form of a polynomial of finite order with respect to time.

When an optimal estimator is determined where the non-stationary part of the signal is present, a more complicated problem must be solved for the conditional minimum of the estimation error. Additional conditions arise from the fact that the mathematical expectation of the signal must be estimated with a given accuracy. At the same time, it is necessary to satisfy the condition of "exponentially fading memory" of the estimator, which re-

duces to the condition that the signal at the output of the estimator must be formed from the observed values of the input signal with an exponential weighting.

In the solution of the above mentioned problem, the classical Wiener filtering theory is not applicable for two reasons: (1) it assumes that the input signals are stationary random processes with zero mathematical expectations, (2) it assumes that the output signal is formed from an input signal observed over the semi-infinite time interval without weighting. Some authors have solved the filtering problem for non-stationary polynomial inputs with finite observation time. But the optimal filters resulting from their methods are difficult to realize in applications. [15]

In this paragraph the main attention is focussed on the solution of the problem of synthesis of optimal digital estimators for polynomial models with exponential weighting of data. This approach has not been considered until very recently. But it can yield some important results for practical applications.

2.2 Optimization with exponential weighting

One assumes that the time series data of measurements is represented by $y(iT) = g(iT) + n(iT)$ and $g(iT) = \sum_{j=0}^r g_j(iT)^j$ (2.1) where $g(iT)$ is the deterministic polynomial component, $n(iT)$ is the stationary random component with autocorrelation function $R_n(lT)$ and power spectral density $G_n(z)$. The output of the estimator is designated by $x(iT)$, and the desired output by $x_d(iT)$. The impulse response of the real estimator is $k(iT)$, and the impulse response of the ideal estimator is $h(iT)$.

Therefore one can obtain $x_d(lT) = T \sum_{i=-\infty}^{\infty} h(iT)g(lT-iT)$ (2.2)

$$x(lT) = T \sum_{i=0}^{\infty} k(iT)[g(lT-iT) + n(lT-iT)] \quad (2.3)$$

The error of estimation is $\epsilon(lT) = x_d(lT) - x(lT) = \epsilon_g(lT) + \epsilon_n(lT)$ (2.4)

where $\epsilon_g(lT) = T \sum_{i=-\infty}^{\infty} g(lT-iT)h(iT) - T \sum_{i=0}^{\infty} g(lT-iT)k(iT)$ (2.4a)

$$\epsilon_n(lT) = -T \sum_{i=0}^{\infty} n(lT-iT)k(iT) \quad (2.4b)$$

The variance of random error of the estimation is

$$\bar{\epsilon}_n^2 = T \sum_{i_1=0}^{\infty} k(i_1T) T \sum_{i_2=0}^{\infty} R_n(i_1T-i_2T)k(i_2T) \quad (2.5)$$

One can determine the optimal impulse response function $k(iT)$ by the variational calculus with Lagrange multipliers. The minimum of the following expression will be determined.

$$J\{k\} = T \sum_{i_1=0}^{\infty} k(i_1T) T \sum_{i_2=0}^{\infty} R_n(i_1T-i_2T)k(i_2T) + pT \sum_{i=0}^{\infty} g(lT-iT)[h(i,T)-k(i,T)] \exp(-aiT) \quad (2.6)$$

The decomposition of $g(lT-i,T)$ to the Taylor series gives

$$g(lT-i,T) = g(lT) - iT g'(lT) + \frac{(iT)^2}{2!} g''(lT) + \dots + (-1)^r \frac{(iT)^r}{r!} g^{(r)}(lT) \quad (2.7)$$

Thus one can obtain $J\{k\} = T \sum_{i_1=0}^{\infty} k(i_1T) \left\{ T \sum_{i_2=0}^{\infty} R_n(i_1T-i_2T)k(i_2T) - [2p_0 + 2p_1(i_1T) + 2p_2(i_1T)^2 + \dots + 2p_r(i_1T)^r] \exp(-ai,T) \right\} + pT \sum_{i=0}^{\infty} g(lT-i,T)k(i,T) \exp(-ai,T)$ (2.8)

where $2p_i = \frac{(-1)^i}{i!} g^{(i)}(lT)$ for $i=0,1,2,\dots,r$

By the rules of the calculus of variations, the optimal impulse response $k(iT)$, transforming the expression $J\{k\}$ into a minimum, is determined from

$$\frac{\partial}{\partial \Delta} J\{k + \Delta k\} \Big|_{\Delta=0} = 0 \quad (2.9)$$

where Δ is an arbitrary number. This formula is a necessary and sufficient condition for obtaining the minimum of $J\{k\}$. In this way, substituting $k(iT) + \Delta k(iT)$ for $k(iT)$ in (2.8), one obtains $J\{k + \Delta k\} = J\{k\} + 2\Delta E_1 + \Delta^2 E_2$ (2.10)

$$\text{where } E_2 = T \sum_{i_1=0}^{\infty} k(i_1, T) T \sum_{i_2=0}^{\infty} k(i_2, T) R_n(i_1, T - i_2, T) \quad (2.10a)$$

$$E_1 = T \sum_{i_1=0}^{\infty} k(i_1, T) \left\{ T \sum_{i_2=0}^{\infty} k(i_2, T) R_n(i_1, T - i_2, T) - [p_0 + p_1 i_1 T + p_2 (i_1, T)^2 + \dots + p_r (i_1, T)^r] \exp(-a_1 T) \right\} \quad (2.10b)$$

Thus one finds that the condition for the minimum of $J\{k\}$ is determined by $E_1 = 0$, or equivalently, by the following equation:

$$T \sum_{i_1=0}^{\infty} R_n(i_1, T - i_2, T) k(i_2, T) = [p_0 + p_1 i_1 T + p_2 (i_1, T)^2 + \dots + p_r (i_1, T)^r] \exp(-a_1 T) \quad (2.11)$$

2.3 Solution of the Equation for the Optimal Impulse Response of the Digital Estimator

One will now solve the equation (2.11), which determines the impulse response of an optimal estimator. If the noise $n(iT)$ is a statistically independent time series, then the correlation function of $n(iT)$ can be expressed by $R_n(iT) = R_{n0} \delta(iT)$ (2.12)

where $\delta(iT)$ is the Kronecker function defined by the following conditions: $\delta(iT) = 1$ for $i=0$, and $\delta(iT) = 0$ for $i \neq 0$ (2.12a)

In this case one can obtain

$$k(iT) = [A_0 + A_1 iT + A_2 (iT)^2 + \dots + A_r (iT)^r] \exp(-a_1 T) \quad (2.13)$$

$$\text{where } A_0 = R_{n0}^{-1} p_0, \quad A_1 = R_{n0}^{-1} p_1, \quad A_2 = R_{n0}^{-1} p_2, \dots, \quad A_r = R_{n0}^{-1} p_r \quad (2.13a)$$

By performing the Z-transformation one can find the transfer function

$$W(z) = T \sum_{i=0}^{\infty} k(iT) z^{-i} = T \sum_{i=0}^{\infty} [A_0 + A_1 iT + A_2 (iT)^2 + \dots + A_r (iT)^r] \exp(-a_1 T) z^{-i} \quad (2.14)$$

In this formula $A_0, A_1, A_2, \dots, A_r$ are the constants to be determined.

If the noise $n(iT)$ is a statistically correlated time series, the solution of equation (2.11) is more complicated. One supposes that the spectral density function of the noise $n(iT)$ can be represented by

$$S_n(z) = N(z)N(z^{-1}) = \frac{A(z)}{B(z)} = \frac{a_K z^K + a_{K-1} z^{K-1} + \dots + a_1 z + a_0 + a_1 z^{-1} + \dots + a_{K-1} z^{-K+1} + a_K z^{-K}}{b_m z^m + b_{m-1} z^{m-1} + \dots + b_1 z + b_0 + b_1 z^{-1} + \dots + b_{m-1} z^{-m+1} + b_m z^{-m}} \quad (2.15)$$

$$\text{where } N(z) = \frac{E(z)}{C(z)} = \frac{e_0 + e_1 z + e_2 z^2 + \dots + e_K z^K}{c_0 + c_1 z + c_2 z^2 + \dots + c_m z^m}$$

One supposes that the function $N(z)$ has neither zero nor pole outside the unit circle in the Z plane. In this case, it can be demonstrated that the solution of equation (2.11) is the following:

$$k(iT) = [A_0 + A_1 iT + A_2 (iT)^2 + \dots + A_r (iT)^r] \exp(-a_1 T) + E_1 d_1^i + E_2 d_2^i + \dots + E_{2K} d_{2K}^i \quad (2.16)$$

In this formula $A_0, A_1, \dots, A_r, E_1, E_2, \dots, E_{2K}$ are the constants to be determined, and d_1, d_2, \dots, d_{2K} are the roots of the equation

$$A(z) = a_K z^K + a_{K-1} z^{K-1} + \dots + a_1 z + a_0 + a_1 z^{-1} + \dots + a_{K-1} z^{-K+1} + a_K z^{-K} = 0 \quad (2.17)$$

By performing the Z-transformation one can find the transfer function

$$W(z) = T \sum_{i=0}^{\infty} k(iT) z^{-i} = T \sum_{i=0}^{\infty} [A_0 + A_1 iT + A_2 (iT)^2 + \dots + A_r (iT)^r] \exp(-a_1 T) z^{-i} + T z \sum_{i=1}^{2K} \frac{E_i}{z - d_i} \quad (2.18)$$

The optimal estimator must satisfy the following additional

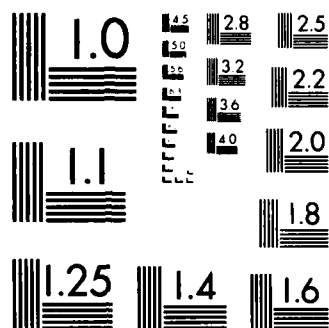
PROCEEDINGS OF THE ANNUAL PRECISE TIME AND TIME
INTERVAL (PTTI) APPLICATI. (U) NAVAL RESEARCH LAB
WASHINGTON DC J A MURRAY 02 APR 84

6/8

F/G 5/9

NL

A 10x10 grid of squares. The grid is mostly black, with a few white squares forming a small pattern in the upper right quadrant. The white squares are located at the following coordinates (row, column): (1, 8), (2, 8), (2, 9), (3, 9), (4, 9), (5, 9), (6, 9), (7, 9), (8, 9), (9, 9), (10, 9), (10, 10). All other squares are black.



MICROCOPY RESOLUTION TEST CHART
NATIONAL BUREAU OF STANDARDS 1963 A

condition: $\epsilon_r(lT) = T \sum_{i=-\infty}^{\infty} g(lT-iT)h(iT) - T \sum_{i=-\infty}^{\infty} g(lT-iT)k(iT) = 0$ (2.19)
 Substituting the formula (2.7) into this condition one can obtain

$$\epsilon_r(iT) = \sum_{l=0}^r (d_l - m_l) \frac{(-1)^l}{l!} g^{(l)}(iT) = 0 \quad (2.20)$$

where $d_l = T \sum_{i=-\infty}^{\infty} (iT)^l h(iT)$, $m_l = T \sum_{i=-\infty}^{\infty} (iT)^l k(iT)$ (2.20a)
 Therefore one must satisfy the following $(r+1)$ conditions:

$$m_l = d_l \text{ or } T \sum_{i=-\infty}^{\infty} (iT)^l k(iT) = T \sum_{i=-\infty}^{\infty} (iT)^l h(iT) \text{ for } l=0, 1, 2, \dots, r \quad (2.21)$$

In the case of prediction for a time interval $t_0 = l_0 T$, one can obtain $h(iT) = \delta(iT + l_0 T)$. Thus $d_l = T \sum_{i=-\infty}^{\infty} (iT)^l \delta(iT + l_0 T) = (-l_0 T)^l$ for $l=0, 1, 2, \dots, r$
 Therefore the $(r+1)$ conditions are the following:

$$m_l = T \sum_{i=-\infty}^{\infty} (iT)^l k(iT) = (-l_0 T)^l \text{ for } l=0, 1, 2, \dots, r \quad (2.22)$$

In the case of filtering one can obtain $h(iT) = \delta(iT)$, $d_l = T \sum_{i=-\infty}^{\infty} (iT)^l \delta(iT)$
 Therefore the $(r+1)$ conditions are the following:

$$m_0 = 1, \quad m_l = 0 \text{ for } l=1, 2, \dots, r \quad (2.23)$$

In the case of estimation of the first derivative one can obtain the following $(r+1)$ conditions: $m_0 = 0$, $m_1 = -1$, and $m_l = 0$ for $l=2, 3, \dots, r$ (2.24)

In the case of estimation of the second derivative one can obtain the following $(r+1)$ conditions: $m_0 = 0$, $m_1 = 0$, $m_2 = 2$, and $m_l = 0$ for $l=3, 4, \dots, r$ (2.25)

2.4 Synthesis of Some Digital Recursive Estimators

Using the general method, presented in the sections 2.2 and 2.3, one can synthesize some digital recursive estimators (predictors, filters and differentiators). The results of synthesis are presented in the following table, where the simplified notation $\theta = \exp(-aT)$ is used throughout.

Estimator type	Signal $g(iT)$	Noise $R_{n0}(iT)$	Transfer function $W(z)$
filter	g_0	$R_{n0} \delta(iT)$	$\frac{z(1-\theta)}{z-\theta}$
filter	$g_0 + g_1 iT$	$R_{n0} \delta(iT)$	$z \frac{(1-\theta^2)z + 2\theta^2 - 2\theta}{(z-\theta)^2}$
differentiator(1)	$g_0 + g_1 iT$	$R_{n0} \delta(iT)$	$z \frac{(z-1)(1-\theta)^2}{T(z-\theta)^2}$
filter	$g_0 + g_1 iT + g_2 (iT)^2$	$R_{n0} \delta(iT)$	$z \frac{(1-\theta^3)z^2 - 3\theta(1-\theta^2)z + 3\theta^2(1-\theta)}{(z-\theta)^3}$
differentiator(2)	$g_0 + g_1 iT + g_2 (iT)^2$	$R_{n0} \delta(iT)$	$z \frac{(z-1)^2(1-\theta)^3}{T^2(z-\theta)^3}$
differentiator(1)	$g_0 + g_1 iT + g_2 (iT)^2$	$R_{n0} \delta(iT)$	$z(1-\theta)^2 \frac{(z-1)[1.5(1+\theta)z - 0.5(5\theta+1)]}{T(z-\theta)^3}$
predictor for $t_0 = l_0 T$	$g_0 + g_1 iT$	$R_{n0} \delta(iT)$	$z \frac{(1-\theta^2)(1+l_0 \frac{1-\theta}{1+\theta})z - 2\theta(1-\theta)[1+\frac{l_0}{2\theta}(1-\theta)]}{(z-\theta)^2}$

III. METHODS FOR OPTIMAL RECURSIVE ESTIMATION OF NON-STATIONARY TIME SERIES REPRESENTED BY STOCHASTIC MODELS WITH STATIONARY INCREMENTS

3.1 Problem Statement

The random variations of frequency and phase of oscillators and atomic clocks are non-stationary processes. In this paragraph one will develop the methods for optimal recursive estimation of non-stationary time series with stationary increments, represented by the ARIMA models or the Markov models. If the frequency fluctuations of atomic clocks are stationary and the frequency drift is negligible, one must consider the phase (time) fluctuations of atomic clocks as non-stationary processes with the stationary increments of first order. If the frequency fluctuations of atomic clocks are stationary, and the frequency drift has a constant value and is not negligible, one must consider the phase (time) fluctuations of atomic clocks as non-stationary processes with the stationary increments of second order. This stochastic approach is more complicated than the deterministic approach presented in the previous paragraph, because the statistics of random processes must be taken into account. In order to synthesize the optimal estimators one must have the knowledge of the signal and noise statistics. But from the viewpoint of the physical phenomena in the oscillators and atomic clocks, the stochastic approach is more reasonable.

In the solution of the above mentioned problem, the classical Wiener filtering theory is not directly applicable, because it assumes that the signal and the noise are stationary random processes. One will resolve the problem of synthesis of digital estimators by the method of variational calculus. This is a modification and extension of the Wiener's method to the optimization problem for the non-stationary sampled random signals with stationary increments. By this method one can determine the transfer functions of optimal recursive digital estimators. One can also deduce the algorithms for the realization of these digital estimators. In section 3.2 will be presented the direct method of optimal synthesis of digital estimators. In some cases, one can alternatively use the indirect method of synthesis. That is to say that one will synthesize the optimal continuous estimators at first. And then one can obtain the corresponding digital estimators by the transformation methods. The indirect method for synthesis of digital estimators will be presented in section 3.3. In section 3.4 will be presented the method for optimal synthesis of digital estimators for Markov models. For the non-stationary time series with stationary increments and for the case of steady-state optimization, using the general theory of Kalman filtering, one can obtain the time-invariant digital filters. And the transfer functions of these digital recursive filters can be deduced.

3.2 Direct Method for Optimal Synthesis of Digital Estimators

3.2.1 General Method for Optimal Synthesis of Digital Estimators

One assumes that the time series is represented by $y(iT) = u(iT) + n(iT)$ where T is the sampling period, $u(iT)$ is a non-stationary signal with stationary increment of m -th order, $n(iT)$ is a stationary noise. One can represent the problem of optimal estimation by the following diagram.

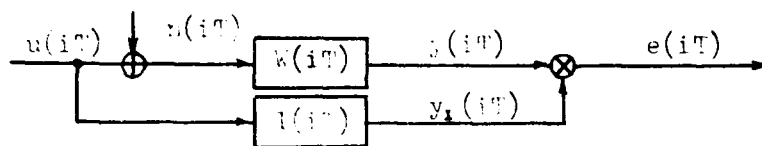


Fig. 3.1

where $W(iT)$ is the impulse response of a real estimator, which is a linear constant system, $I(iT)$ is the impulse response of the ideal estimator. One wishes to minimize the mean-square error

$$\sigma_e^2 = \mathcal{E}[e^2(iT)] = \mathcal{E}[y_1^2(iT) - 2y_1(iT)y(iT) + y^2(iT)] \quad (3.2.1)$$

By performing the Z-transformation one can obtain

$$Y_1(z) = U(z)I(z), \quad Y(z) = [U(z) + N(z)]W(z) \\ E(z) = U(z)I(z) - [U(z) + N(z)]W(z) = U(z)[I(z) - W(z)] - W(z)N(z) \quad (3.2.2)$$

Because $u(iT)$ is a non-stationary signal with stationary increment of m -th order, one obtains $U(z) = \frac{D(z)}{(1-z^{-1})^m}$ (3.2.3)

where $D(z)$ is a stationary time series. Thus one can obtain

$$E(z) = \frac{D(z)}{(1-z^{-1})^m} [I(z) - W(z)] - W(z)N(z) \quad (3.2.4)$$

If one assumes no correlation between signal and noise, then $S_{dn}(z) = 0$, $S_{nd}(z) = 0$. The expected value of $E(z)E(z^{-1})$ becomes

$$\mathcal{E}[E(z)E(z^{-1})] = S_{ee}(z) = \frac{S_{dd}(z)}{(1-z^{-1})^m (1-z)^m} [I(z) - W(z)][I(z^{-1}) - W(z^{-1})] + W(z)W(z^{-1})S_{nn}(z) \quad (3.2.5)$$

This expression gives the spectral density of the error in terms of the spectral density of the derivative of the signal and the spectral density of the noise. One uses the formula of inversion to obtain the mean-square error as

$$\sigma_e^2 = \frac{1}{2\pi j} \oint_{|z|=1} S_{ee}(z) z^{-1} dz \quad (3.2.6)$$

One will derive the equation for the best $W(z)$, which minimizes the mean-square error σ_e^2 . By using the following short notations

$$W(z) = W_+, \quad W(z^{-1}) = W_-, \quad I(z) = I_+, \quad I(z^{-1}) = I_- \quad (3.2.7)$$

one obtains

$$\sigma_e^2 = \frac{1}{2\pi j} \oint_{|z|=1} \left\{ \frac{S_{dd}(z)}{(1-z^{-1})^m (1-z)^m} (I_+ - W_+)(I_- - W_-) + S_{nn}(z) W_+ W_- \right\} z^{-1} dz \quad (3.2.8)$$

By the rules of variational calculus, to determine the minimum of σ_e^2 one must give a variation $\Delta\eta(z)$ to the transfer function $W(z)$ and find the quantity $\sigma_e^2\{W + \Delta\eta\}$. In this case the optimal transfer function is determined from

$$\frac{\partial \sigma_e^2\{W + \Delta\eta\}}{\partial \Delta\eta} \Big|_{\Delta\eta=0} = 0. \text{ In this way one can obtain } \sigma_e^2\{W + \Delta\eta\} = \\ \frac{1}{2\pi j} \oint_{|z|=1} \left\{ \frac{S_{dd}(z)}{(1-z^{-1})^m (1-z)^m} (I_+ - W_+ - \Delta\eta_+)(I_- - W_- - \Delta\eta_-) + S_{nn}(z) (W_+ + \Delta\eta_+)(W_- + \Delta\eta_-) \right\} z^{-1} dz \quad (3.2.9)$$

$$\frac{\partial \sigma_e^2\{W + \Delta\eta\}}{\partial \Delta\eta} \Big|_{\Delta\eta=0} = \frac{1}{2\pi j} \oint_{|z|=1} \left\{ \frac{S_{dd}(z)}{(1-z^{-1})^m (1-z)^m} [(I_+ - W_+)(-\Delta\eta_-) + \Delta\eta_+(I_- - W_-)] + \right. \\ \left. + S_{nn}(z)(W_+ \Delta\eta_- + W_- \Delta\eta_+) \right\} z^{-1} dz = 0 \quad (3.2.10)$$

This may be written as the sum of two integrals :

$$\frac{1}{2\pi j} \oint_{|z|=1} \eta_- \{ S_{dd}(z) (1-z^{-1})^{-m} (1-z)^{-m} (W_+ - I_+) + S_{nn}(z) W_+ \} z^{-1} dz + \\ \frac{1}{2\pi j} \oint_{|z|=1} \eta_+ \{ S_{dd}(z) (1-z^{-1})^{-m} (1-z)^{-m} (W_- - I_-) + S_{nn}(z) W_- \} z^{-1} dz = 0 \quad (3.2.11)$$

If, in the second integral, one makes the change of variable $z = -\bar{z}$

and uses the evenness property of $S_{dd}(z)$ and $S_{nn}(z)$, one can show that the two integrals are identical. Thus one obtains

$$\frac{1}{2\pi j} \oint_{|z|=1} \eta(z^{-1}) \{S_{dd}(z)(1-z^{-1})^{-m}(1-z)^{-m}[W(z)-I(z)] + S_{nn}(z)W(z)\} z^{-1} dz = 0 \quad (3.2.12)$$

Now one defines the spectral factorization as following

$$S_{dd}(z)(1-z^{-1})^{-m}(1-z)^{-m} + S_{nn}(z) = \Delta(z)\Delta(z^{-1}) \quad (3.2.13)$$

and requires that $\Delta(z)$ has poles and zeros inside the unit circle only, and that $\Delta(z^{-1})$ has poles and zeros outside the unit circle only.

$$\text{Using the notation } \Gamma(z) = S_{dd}(z)(1-z^{-1})^{-m}(1-z)^{-m} I(z) \quad (3.2.14)$$

$$\text{one obtains } \frac{1}{2\pi j} \oint_{|z|=1} \eta(z^{-1}) \Delta(z^{-1}) [W(z)\Delta(z) - \frac{\Gamma(z)}{\Delta(z^{-1})}] z^{-1} dz = 0 \quad (3.2.15)$$

Expanding the term $\Gamma(z)/\Delta(z^{-1})$ in partial fractions, one obtains

$$\frac{\Gamma(z)}{\Delta(z^{-1})} = \left[\frac{\Gamma(z)}{\Delta(z^{-1})} \right]_+ + \left[\frac{\Gamma(z)}{\Delta(z^{-1})} \right]_- \quad (3.2.16)$$

where $\left[\frac{\Gamma(z)}{\Delta(z^{-1})} \right]_+$ has the poles inside the unit circle, and $\left[\frac{\Gamma(z)}{\Delta(z^{-1})} \right]_-$ has the poles outside the unit circle.

$$\text{Thus } \frac{1}{2\pi j} \oint_{|z|=1} \eta(z^{-1}) \Delta(z^{-1}) \left\{ W(z)\Delta(z) - \left[\frac{\Gamma(z)}{\Delta(z^{-1})} \right]_+ - \left[\frac{\Gamma(z)}{\Delta(z^{-1})} \right]_- \right\} z^{-1} dz = 0 \quad (3.2.17)$$

Note that $\eta(z^{-1}) \Delta(z^{-1}) \left[\frac{\Gamma(z)}{\Delta(z^{-1})} \right]_-$ has the poles outside the unit circle only, then one obtains

$$\frac{1}{2\pi j} \oint_{|z|=1} \eta(z^{-1}) \Delta(z^{-1}) \left[\frac{\Gamma(z)}{\Delta(z^{-1})} \right]_- z^{-1} dz = 0 \quad (3.2.18)$$

Thus the requirement of realizability of the optimal estimator becomes

$$\frac{1}{2\pi j} \oint_{|z|=1} \eta(z^{-1}) \Delta(z^{-1}) \left\{ W(z)\Delta(z) - \left[\frac{\Gamma(z)}{\Delta(z^{-1})} \right]_+ \right\} z^{-1} dz = 0 \quad (3.2.19)$$

from which one obtains $W(z) = \frac{1}{\Delta(z)} \left[\frac{\Gamma(z)}{\Delta(z^{-1})} \right]_+$

3.2.2. Synthesis of some digital recursive estimators

Using the general method, presented in the section 3.2.1, one can synthesize some digital recursive estimators for the non-stationary time series with stationary increments of m -th order. The results of synthesis of the digital recursive estimators can be represented in the following table.

$\frac{S_{dd}(z)}{(1-z^{-1})^m(1-z)^m}$	$S_{nn}(z)$	$I(z)$	Transfer function $W(z)$	Parameters values	ARIMA (pnq)
$\frac{d^2}{(1-z^{-1})^2(1-z)^2}$	c^2	1	$\frac{1-r_1}{z-r_1}$	$r_1 = 1 + \frac{d^2}{2c^2} \sqrt{(1 + \frac{d^2}{2c^2})^2 - 1}$	(010)
$\frac{d^2}{(1-z^{-1})^2(1-z)^2}$	c^2	1	$\frac{(2-r_1-r_2)z+r_1r_2-1}{(z-r_1)(z-r_2)}$	$y_1 = 2+jd/c,$ $y_2 = 2-jd/c,$ $r_1 = 0.5y_1 - \sqrt{0.25y_1^2 - 1}$	(020)
$\frac{d^2}{(1-z^{-1})^2(1-z)^2}$	c^2	$\frac{1-z^{-1}}{T}$	$z \frac{(z-1)(1-r_1)(1-r_2)}{T(z-r_1)(z-r_2)}$	$r_2 = 0.5y_2 - \sqrt{0.25y_2^2 - 1}$	(020)
$\frac{d^2}{(1-z^{-1})^2(1-z)^2}$	c^2	$\frac{(1-z^{-1})^2}{T^2}$	$z \frac{(z-1)^2(1-r_1)(1-r_2)(1-r_3)}{T^2(z-r_1)(z-r_2)(z-r_3)}$	r_1, r_2 and r_3 are the roots of equation	(030)
$\frac{d^2}{(1-z^{-1})^2(1-z)^2}$	c^2	$\frac{1-z^{-1}}{T}$	$\frac{(z-1)(z+\theta')(1-r_1)(1-r_2)(1-r_3)}{T(1+\theta')(z-r_1)(z-r_2)(z-r_3)}$	$(z-1)^4 - \frac{d^2}{c^2} z^3 = 0$ inside the unit cycle. θ', θ_0 and θ_1 are constants	(030)
$\frac{d^2}{(1-z^{-1})^2(1-z)^2}$	c^2	1	$\frac{(z^3+\theta z+\theta_0)(1-r_1)(1-r_2)(1-r_3)}{(1+\theta+\theta_0)(z-r_1)(z-r_2)(z-r_3)}$		(030)

3.3 Indirect Method for Optimal Synthesis of Digital Estimators

In some cases, the synthesis of optimal digital estimators is more difficult than the synthesis of corresponding optimal continuous estimators, because the algebraic procedure of spectral factorization is more cumbersome. One can alternatively use the indirect method of optimal synthesis. At first one will synthesize optimal continuous estimators. Then one can obtain the corresponding digital estimators by transformation methods.

3.3.1 General Method for Optimal Synthesis of Continuous Estimators

One defines $u(t)$ as the signal and $n(t)$ as the additive noise. One can represent the problem of optimal estimation by the following diagram. $W(t)$ is the impulse response of a real estimator, $I(t)$ is the impulse response of an ideal estimator. The criterion of optimization is the mean-square error $\sigma_e^2 = \mathcal{E}[e^2(t)]$

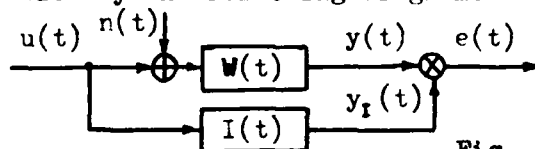


Fig. 3.2

By performing the Laplace transformation one can obtain

$$E(s) = U(s) [I(s) - W(s)] - W(s)N(s) \quad (3.3.1)$$

Because $u(t)$ is a non-stationary signal with a stationary increment of m -th order, one obtains $U(s) = D(s)/s^m$, where $D(s)$ is a stationary signal. One assumes that the spectral densities $S_{dn}(s) = S_{nd}(s) = 0$, then the expected value of $E(s)E(-s)$ is

$$\mathcal{E}[E(s)E(-s)] = S_{ee}(s) = \frac{S_{dd}(s)}{s^m(-s)^m} [I(s) - W(s)] [I(-s) - W(-s)] + W(s)W(-s)S_{nn}(s) \quad (3.3.2)$$

$$\text{The mean-square error is } \sigma_e^2 = \frac{1}{2\pi j} \int_{-j\infty}^{j\infty} S_{ee}(s) ds \quad (3.3.3)$$

By the rules of variational calculus one can obtain

$$\frac{1}{2\pi j} \int_{-j\infty}^{j\infty} \eta(-s) \{ S_{dd}(s) s^{-m} (-s)^m [W(s) - I(s)] + S_{nn}(s) W(s) \} ds = 0 \quad (3.3.4)$$

Now one defines spectral factorization as the following

$$\frac{S_{dd}(s)}{s^m(-s)^m} + S_{nn}(s) = \Delta(s)\Delta(-s) \quad (3.3.5)$$

and requires that $\Delta(s)$ has poles and zeros inside the left half-plane (LHP) only, and $\Delta(-s)$ has poles and zeros inside the right half-plane (RHP) only.

$$\text{Then one obtains } \frac{1}{2\pi j} \int_{-j\infty}^{j\infty} \eta(-s) \Delta(-s) \left[W(s) \Delta(s) - \frac{\Gamma(s)}{\Delta(-s)} \right] ds = 0 \quad (3.3.6)$$

where $\Gamma(s) = S_{dd}(s) s^{-m} (-s)^m I(s)$. Expanding the term $\Gamma(s)/\Delta(-s)$ in partial fractions, one obtains

$$\frac{\Gamma(s)}{\Delta(-s)} = \left[\frac{\Gamma(s)}{\Delta(-s)} \right]_+ + \left[\frac{\Gamma(s)}{\Delta(-s)} \right]_- \quad (3.3.7)$$

where $[\Gamma(s)/\Delta(-s)]_+$ has the poles inside the LHP only, and $[\Gamma(s)/\Delta(-s)]_-$ has the poles inside the RHP only. Noting that

$$\frac{1}{2\pi j} \int_{-j\infty}^{j\infty} \eta(-s) \Delta(-s) [\Gamma(s)/\Delta(-s)]_- ds = 0 \quad (3.3.8)$$

one can obtain the transfer function of optimal continuous estimator

$$W(s) = \frac{1}{\Delta(s)} \left[\frac{\Gamma(s)}{\Delta(-s)} \right]_+ \quad (3.3.9)$$

3.3.2 Synthesis of Some Optimal Continuous Estimators

Using the general method, presented in the section 3.3.1, one can synthesize some optimal continuous estimators (predictors, filters and differentiators). The results of synthesis are presented in the following table.

ARIMA (pnq)	$\frac{S_{dd}(s)}{s^m(-s)^m}$	$S_{nn}(s)$	$I(s)$	$w(s)$	Parameter values
(110)	$\frac{d^2}{s(-s)(-s^2+c^2)}$	c^2	e^{cs}	$\frac{q, s+1}{(ab)^{-1}s^2+(a+b)(ab)^{-1}s+1}$	$a = \left[\frac{\theta^2}{2} + \left(\frac{\theta^2}{4} - \frac{d^2}{c^2} \right)^{1/2} \right]^{1/2} (*1)$
(110)	$\frac{d^2}{s(-s)(-s^2+c^2)}$	c^2	se^{cs}	$\frac{ks}{(ab)^{-1}s^2+(a+b)(ab)^{-1}s+1}$	$b = \left[\frac{\theta^2}{2} - \left(\frac{\theta^2}{4} - \frac{d^2}{c^2} \right)^{1/2} \right]^{1/2} (*2)$
(020)	$\frac{d^2}{(-s)^2 s^2}$	c^2	e^{cs}	$\frac{(\sqrt{2}T_c + \tau)s+1}{T_c^2 s^2 + \sqrt{2}T_c s + 1}$	$T_c = \sqrt{c/d}$
(020)	$\frac{d^2}{(-s)^2 s^2}$	c^2	s	$\frac{s}{T_c^2 s^2 + \sqrt{2}T_c s + 1}$	$T_c = \sqrt{c/d}$
(030)	$\frac{d^2}{(-s)^3 s^3}$	c^2	e^{cs}	$\frac{(2T_c^2 + 2T_c\tau + \frac{\tau^2}{2})s^2 + (2T_c + \tau)s + 1}{T_c^3 s^3 + 2T_c^2 s^2 + 2T_c s + 1}$	$T_c = \sqrt[3]{c/d}$
(030)	$\frac{d^2}{(-s)^3 s^3}$	c^2	se^{cs}	$\frac{s[(2T_c + \tau)s + 1]}{T_c^3 s^3 + 2T_c^2 s^2 + 2T_c s + 1}$	$T_c = \sqrt[3]{c/d}$
(030)	$\frac{d^2}{(-s)^3 s^3}$	c^2	s^2	$\frac{s^2}{T_c^3 s^3 + 2T_c^2 s^2 + 2T_c s + 1}$	$T_c = \sqrt[3]{c/d}$
(111)	$\frac{d^2(-s^2+\xi^2)}{s(-s)(-s^2+c^2)}$	c^2	e^{cs}	$\frac{q, s+1}{a_1^2 s^2 + a, a_1^2 s + 1}$	$a_1 = \sqrt{2d\xi/c + \theta^2 + d^2/c^2}$ $a_2 = d\xi/c, (*3)$
(021)	$\frac{d^2(-s^2+\xi^2)}{(-s)^2 s^2}$	c^2	e^{cs}	$\frac{(a_1 a_1^2 + \tau)s + 1}{a_1^2 s^2 + a, a_1^2 s + 1}$	$a_2 = d\xi/c$ $a_1 = \sqrt{2d\xi/c + d^2/c^2}$
(011)	$\frac{d^2(-s^2+\xi^2)}{(-s)s}$	c^2	1	$\frac{1}{T_c s + 1}$	$T_c = \sqrt{1 + \frac{d^2}{c^2}} \left(\frac{d}{c} \xi \right)^{-1}$
(*1) $q_1 = \frac{1}{\theta} \left[1 - \frac{a\tau \exp(-\tau\tau)}{(\theta+a)(\tau+b)} \right],$ (*2) $k = \frac{\exp(-\theta\tau)}{(ab)^{-1}\theta^2 + (a+b)(ab)^{-1}\theta + 1}$ (*3) $q_1 = \frac{1}{\theta} + \frac{a_2(\tau^2 - \xi^2)\exp(-\theta\tau)}{\xi^2\theta(\theta^2 + a, \theta + a_2)}$					

3.3.3 Calculation of digital estimators by methods of transformation

One has obtained transfer functions of continuous estimators. By the method of Z-transformation or the state variables method one can determine the transfer functions of corresponding digital estimators, which are necessary for the realizations or for computer solutions. One will explain the state variables method only.

Given the transfer function of a continuous estimator $w(s) = \frac{Y(s)}{U(s)} = \frac{b_p s^p + b_{p-1} s^{p-1} + \dots + b_1 s + b_0}{a_p s^p + a_{p-1} s^{p-1} + \dots + a_1 s + a_0}$ where $q \leq p-1$ (3.3.10)

one can find a differential equation of order p . Then one can represent the continuous estimator by a set of first order differential equations, called state variables equations.

$$\begin{aligned} \dot{X}(t) &= FX(t) + GU(t) \\ Y(t) &= CX(t) + DU(t) \end{aligned} \quad (3.3.11)$$

where F, G, C and D are matrices, $X(t), U(t), Y(t)$ and $Y(t)$ are vectors. Then for the corresponding discrete estimator, one can determine the state transition matrix Φ and the input matrix Γ by the following formulas:

$$\Phi = \exp(FT), \quad \Gamma = \int_0^T \Phi(p)Gdp \quad (3.3.12)$$

Thus for the discrete estimator one can obtain the following state variables equations:

$$\begin{aligned} X_{k+1} &= \Phi X_k + \Gamma U_k \\ Y_k &= C X_k + D U_k \end{aligned} \quad (3.3.13)$$

These equations give the algorithm of a digital estimator. They are natural and convenient for computer solution of problems. In order to analyse the

digital estimator, one can perform the Z-transformation of these equations. one obtains $X(z) = (zI - \phi)^{-1} \Gamma z U(z)$

$$Y(z) = C X(z) + D U(z) = [C(zI - \phi)^{-1} \Gamma z + D] U(z)$$

Therefore the transfer function of the digital estimator is

$$W(z) = Y(z) [U(z)]^{-1} = C(zI - \phi)^{-1} \Gamma z + D \quad (3.3.14)$$

One will illustrate this method by two simple examples.

(1) The continuous estimator is $W(s) = \frac{Y(s)}{U(s)} = \frac{1}{T_c s + 1} \quad (3.3.15)$

Thus $\dot{x}(t) = -\frac{1}{T_c} x(t) + \frac{1}{T_c} u(t)$, $y(t) = x(t)$.

One obtains $F = -1/T_c$, $G = 1/T_c$, $\phi = \exp(FT) = \exp(-T/T_c)$, $\Gamma = 1 - \exp(-T/T_c)$, $C = 1$, $D = 0$. The transfer function of the digital estimator is $W(z) = C(zI - \phi)^{-1} \Gamma z + D = z \frac{1 - \exp(-T/T_c)}{z - \exp(-T/T_c)} \quad (3.3.16)$

(2) The continuous estimator is $W(s) = \frac{Y(s)}{U(s)} = \frac{\sqrt{2} T_c s + 1}{T_c^2 s^2 + \sqrt{2} T_c s + 1} \quad (3.3.17)$

One obtains the state equations $\dot{X}(t) = F X(t) + G U(t)$ $Y(t) = C X(t) + D U(t) \quad (3.3.18)$

where $X(t) = \begin{bmatrix} x_1(t) \\ x_2(t) \end{bmatrix}$, $F = \begin{bmatrix} 0 & 1 \\ -T_c^{-2} & -\sqrt{2} T_c^{-1} \end{bmatrix}$, $G = \begin{bmatrix} 0 \\ T_c^{-2} \end{bmatrix}$, $C = (1 \quad \sqrt{2} T_c)$, $D = 0$

The state equations for digital estimator are

$$\begin{aligned} X_{k+1} &= \phi X_k + \Gamma U_{k+1} \\ Y_k &= C X_k + D U_k \end{aligned} \quad (3.3.19)$$

where $X_k = \begin{bmatrix} x_k \\ \dot{x}_k \end{bmatrix}$, $X_{k+1} = \begin{bmatrix} x_{k+1} \\ \dot{x}_{k+1} \end{bmatrix}$, $\phi = \begin{pmatrix} e^{-\alpha} (\cos \alpha + \sin \alpha) & \sqrt{2} T_c e^{-\alpha} \sin \alpha \\ -\sqrt{2} T_c^{-1} e^{-\alpha} \sin \alpha & e^{-\alpha} (\cos \alpha - \sin \alpha) \end{pmatrix}$ $\Gamma = \begin{bmatrix} 1 - e^{-\alpha} (\sin \alpha + \cos \alpha) \\ \sqrt{2} T_c^{-1} e^{-\alpha} \sin \alpha \end{bmatrix}$, $C = (1 \quad \sqrt{2} T_c)$, $D = 0$, $U_k = u_k$, $Y_k = y_k$, $\alpha = T/(\sqrt{2} T_c)$

The transfer function of the digital estimator is

$$W(z) = C(zI - \phi)^{-1} \Gamma z + D = z \frac{[1 + e^{-\alpha} (\sin \alpha - \cos \alpha)] z + e^{-2\alpha} - e^{-\alpha} (\sin \alpha + \cos \alpha)}{z^2 - 2ze^{-\alpha} \cos \alpha + e^{-2\alpha}} \quad (3.3.20)$$

Using this method, one can resolve more complicated problems.

3.4 Optimal Synthesis of Digital Estimators for Markov Models

For the optimal estimation of non-stationary time series, represented by Markov models, one can use the Kalman filtering theory. In general, one obtains digital estimators with time-varying parameters, which are difficult to realize in applications. For the cases of non-stationary time series with stationary increments, and for the cases of steady-state optimization, one can obtain digital estimators with time-invariant parameters, which are easy to realize in applications. One will at first summarize the basic results of Kalman filtering theory, and then develop some aspects of application to the estimation problems of non-stationary time series with stationary increments.

3.4.1 Basic Formulas of Optimal Filtering for the Case of White Noise [17]

One supposes that the state equations of the model are the following

$$\begin{aligned} X_k &= \phi_{k,k-1} X_{k-1} + \Gamma_k W_k \\ Y_k &= H_k X_k + V_k \end{aligned} \quad (3.4.1)$$

where W_k and V_k are zero mean white noises, so that $EW_k = 0$, $EV_k = 0$, $\text{Cov}(W_k, W_j) = Q_k \delta_{kj}$, $\text{Cov}(V_k, V_j) = R_k \delta_{kj}$, $\text{Cov}(W_k, V_j) = 0$.

Then the linear optimal estimation \hat{X}_k for the time series X_k can be determined by the following recursive formula :

$$\hat{X}_k = \phi_{k,k-1} \hat{X}_{k-1} + K_k (Y_k - H_k \phi_{k,k-1} \hat{X}_{k-1}) \quad (3.4.2)$$

$$\text{The gain matrix is } K_k = P_{k/k-1} H_k^T (H_k P_{k/k-1} H_k^T + R_k)^{-1} \quad (3.4.3)$$

$$\text{The a priori variance is } P_{k/k-1} = \phi_{k,k-1} P_{k-1} \phi_{k,k-1}^T + \Gamma_{k-1} Q_{k-1} \Gamma_{k-1}^T \quad (3.4.4)$$

$$\text{The posterior variance is } P_k = (I - K_k H_k) P_{k/k-1} (I - K_k H_k)^T + K_k R_k K_k^T \quad (3.4.5)$$

$$\text{The estimation error is } \tilde{Y}_{k/k-1} = Y_k - H_k \phi_{k,k-1} \hat{X}_{k-1} \quad (3.4.6)$$

In general, the matrices $\phi_{k,k-1}$, Γ_k , H_k , Q_k , R_k , K_k , $P_{k/k-1}$ and P_k depend on k , so that one obtains time-varying estimators. But for non-stationary time series with stationary increments, one can have the matrices ϕ , Γ , H , Q and R , which are independent of k . For ease of implementation, one will focus the main attention on the optimization for the steady state, but not for the transient state. In this case, one can obtain the matrices K , P^* and P , which are independent of k . Therefore, one can obtain suboptimal estimators with time-invariant parameters, expressed by the following equations :

$$X_k = \phi X_{k-1} + \Gamma W_k, \quad Y_k = H X_k + V_k \quad (3.4.1a)$$

$$E W_k = 0, \quad E V_k = 0, \quad \text{Cov}(W_k, W_j) = Q \delta_{j-k}, \quad \text{Cov}(V_k, V_j) = R \delta_{j-k}, \quad \text{Cov}(W_k, V_j) = 0$$

$$\text{The estimator equation is } \hat{X}_k = \phi \hat{X}_{k-1} + K (Y_k - H \phi \hat{X}_{k-1}) \quad (3.4.2a)$$

$$\text{The gain matrix is } K = P^* H^T (H P^* H^T + R)^{-1} \quad (3.4.3a)$$

$$\text{The a priori variance is } P^* = \phi P \phi^T + \Gamma Q \Gamma^T \quad (3.4.4a)$$

$$\text{The posterior variance is } P = (I - K H) P^* (I - K H)^T + K R K^T \quad (3.4.5a)$$

$$\text{The estimation error is } \tilde{Y}_{k/k-1} = Y_k - H \phi \hat{X}_{k-1} \quad (3.4.6a)$$

By performing the Z-transformation, one can determine transfer functions of the time-invariant estimators. One obtains

$$X(z) = (zI - \phi)^{-1} \Gamma z W(z), \quad Y(z) = H(zI - \phi)^{-1} \Gamma z W(z) + V(z) \quad (3.4.7)$$

$$\hat{X}(z) = (zI - \phi)^{-1} K z \tilde{Y}(z), \quad \hat{Y}(z) = H \phi z^{-1} \hat{X}(z) = H \phi (zI - \phi)^{-1} K [Y(z) - \hat{Y}(z)] \quad (3.4.8)$$

Thus the transfer function of the digital estimator is

$$A(z) = \hat{Y}(z) [Y(z)]^{-1} = [I + H \phi (zI - \phi)^{-1} K]^{-1} H \phi (zI - \phi)^{-1} K \quad (3.4.9)$$

The open loop transfer function of the digital filter is

$$B(z) = H \phi (zI - \phi)^{-1} K = \hat{Y}(z) / \tilde{Y}(z) \quad (3.4.10)$$

3.4.2 Method for Solution of Optimal Filtering Problems for the Case of Coloured Perturbation

According to the definition, the ARIMA(p,n,q) time series corresponds to a continuous process, expressed by the following state variables equations :

$$\begin{aligned} \dot{X}(t) &= F X(t) + G L(t) \\ Y(t) &= H X(t) + V(t) \end{aligned} \quad (3.4.11)$$

where

$$F = \begin{bmatrix} 0 & 1 & 0 & \dots & 0 \\ 0 & 0 & 1 & \dots & 0 \\ \vdots & \vdots & \vdots & \ddots & \vdots \\ 0 & 0 & 0 & \dots & 1 \\ 0 & 0 & 0 & \dots & 0 \end{bmatrix}, \quad G = \begin{bmatrix} 0 \\ 0 \\ 0 \\ \vdots \\ 1 \end{bmatrix}, \quad X(t) = \begin{bmatrix} x_1(t) \\ x_2(t) \\ \vdots \\ x_n(t) \end{bmatrix}, \quad \dot{X}(t) = \begin{bmatrix} \dot{x}_1(t) \\ \dot{x}_2(t) \\ \vdots \\ \dot{x}_n(t) \end{bmatrix}, \quad H = (1 \ 0 \ 0 \ \dots \ 0)$$

$L(t)$ is a coloured perturbation, $V(t)$ is a white noise. One supposes that

$L(s)=M(s)W(s)$, where $M(s)=N(s)/D(s)$, $W(t)$ is a white perturbation. If all roots of the equation $D(s)=0$ are real and different, the state equations for the coloured perturbation $L(t)$ become

$$\begin{aligned} \dot{P}(t) &= A P(t) + B W(t) \\ L(t) &= C P(t) \end{aligned} \quad (3.4.12)$$

where

$$A = \begin{bmatrix} \theta_1 & & 0 \\ & \theta_2 & \\ & & \ddots \\ 0 & & & \theta_p \end{bmatrix}, \quad B = \begin{bmatrix} 1 \\ 1 \\ \vdots \\ 1 \end{bmatrix}, \quad C = (c_1 \ c_2 \ \dots \ c_p)$$

One can associate the state equations for $L(t)$ to the state equations of the model. One obtains

$$\begin{bmatrix} \dot{X}(t) \\ \dot{P}(t) \end{bmatrix} = \begin{bmatrix} F & GC \\ 0 & A \end{bmatrix} \begin{bmatrix} X(t) \\ P(t) \end{bmatrix} + \begin{bmatrix} 0 \\ B \end{bmatrix} W(t) \quad (3.4.13)$$

One supposes that $p_1(t)=x_{n+1}(t), \dots, p_p(t)=x_{n+p}(t)$, $X^*(t) = \begin{bmatrix} X(t) \\ P(t) \end{bmatrix}$, $F^*(t) = \begin{bmatrix} F & GC \\ 0 & A \end{bmatrix}$, $G^* = \begin{bmatrix} 0 \\ B \end{bmatrix}$

Then the extended state equations are the following :

$$\begin{aligned} \dot{X}^*(t) &= F^* X^*(t) + G^* W(t) \\ Y^*(t) &= H X^*(t) + V(t), \quad \text{where } F^* = \begin{bmatrix} F & GC \\ 0 & A \end{bmatrix}, \quad G^* = \begin{bmatrix} 0 \\ B \end{bmatrix} \end{aligned} \quad (3.4.14)$$

By the methods of matrix calculus one can determine $\Phi^* = \exp(F^* T)$ and

$\Gamma^* = \int_0^T \Phi^*(\psi) G^* d\psi$. Therefore the extended discrete state equations are the following :

$$\begin{aligned} X_k^* &= \Phi^* X_{k-1}^* + \Gamma^* W_{k-1} \\ Y_k^* &= H X_k^* + V_k \end{aligned} \quad (3.4.15)$$

Then one can use the basic formulas of section 3.4.1 for resolve the optimal filtering problems for the process model, expressed by the extended discrete state equations.

3.4.3 Calculation of Some Digital Recursive Filters

Using the general methods presented in sections 3.4.1 and 3.4.2, One can design some digital recursive filters. The results are presented in the following table.

ARIMA (pnq)	$\dot{X}(t)=FX(t)+GW(t)$ $Y(t)=HX(t)+V(t)$	$X_k = \Phi X_{k-1} + \Gamma W_k$ $Y_k = H X_k + V_k$	K	Transfer function $A(z)$	Coeff. of ϵ_p
(010)	$F=0, G=1, H=1$	$\Phi=1, \Gamma=T, H=1$	a	$\frac{a}{z-1+a}$	$c_0=0$ $c_1=T/a$
(020)	$F = \begin{bmatrix} 0 & 1 \\ 0 & 0 \end{bmatrix}, G = \begin{bmatrix} 0 \\ 1 \end{bmatrix}, H = (1 \ 0).$	$\Phi = \begin{bmatrix} 1 & T \\ 0 & 1 \end{bmatrix}, \Gamma = \begin{bmatrix} T^2/2 \\ T \end{bmatrix}, H = (1 \ 0).$	a b/T	$\frac{(a+b)z-a}{z^2+(a+b-2)z+1-a}$ where $a=-b/2+\sqrt{2b}$	$c_0=0$ $c_1=0$ $c_2=2T^2/b$
(110)	$F = \begin{bmatrix} 0 & 1 \\ 0 & \theta \end{bmatrix}, G = \begin{bmatrix} 0 \\ 1 \end{bmatrix}, H = (1 \ 0).$	$\Phi = \begin{bmatrix} 1 & \theta^{-1}(e^{\theta T}-1) \\ 0 & e^{\theta T} \end{bmatrix}, \Gamma = \begin{bmatrix} \theta^{-1}[\theta(e^{\theta T}-1)-T] \\ \theta^{-1}(e^{\theta T}-1) \end{bmatrix}, H = (1 \ 0).$	a b/T	$\frac{(a+\Gamma_1 b)z-a\Gamma_2}{z^2+(a+\Gamma_1 b-1-\Gamma_2)z+(1-\Gamma_2)\Gamma_2}$ where $\Gamma_1=(\theta T)^{-1}(e^{\theta T}-1)$, $\Gamma_2=\exp(\theta T)$.	$c_0=0$ $c_1=\frac{T(1-\Gamma_2)}{a(1-\Gamma_2)+\Gamma_1 b}$
(030)	$F = \begin{bmatrix} 0 & 1 & 0 \\ 0 & 0 & 1 \\ 0 & 0 & 0 \end{bmatrix}, G = \begin{bmatrix} 0 \\ 0 \\ 1 \end{bmatrix}, H = (1 \ 0 \ 0).$	$\Phi = \begin{bmatrix} 1 & T & T^2/2 \\ 0 & 1 & T \\ 0 & 0 & 1 \end{bmatrix}, \Gamma = \begin{bmatrix} T^3/6 \\ T^2/2 \\ T \end{bmatrix}, H = (1 \ 0 \ 0).$	a b/T 2c/T^2	$\frac{q_3 z^2 + q_1 z + q_0}{z^3 + p_2 z^2 + p_1 z + p_0}$ where $q_2=a+b+c$, $q_0=a$, $p_2=a+b+c-3$, $p_1=-2a-b+c+3$, $q_1=-2a-b+c$, $p_0=-1+a$.	$c_0=0$ $c_1=0$ $c_2=0$ $c_3=3T^3/c$

IV. APPLICATIONS OF DIGITAL RECURSIVE ESTIMATORS TO ATOMIC TIME AND FREQUENCY METROLOGY

In this paragraph, one will demonstrate the applications of digital recursive estimators to characterize the frequency instabilities of atomic clocks, to predict the random variations of atomic time scales, and to smooth time series data, obtained by the comparisons of atomic clocks.

4.1 Characterization of Frequency Instabilities of Atomic Clocks by Recursive Digital Differentiators

4.1.1 Estimation of Variance σ_y^2 by Using Recursive Digital Differentiators

For the characterization of frequency instabilities, phase comparison data of atomic clocks will be used. For the determination of the first derivative of phase fluctuations, one can use the digital differentiator

$$w_1(z) = z \frac{(z-1)(1-r_1)(1-r_2)}{T_c(z-r_1)(z-r_2)} = \frac{z-1}{T_c} W_L(z), \text{ where } W_L(z) = \frac{z(1-r_1)(1-r_2)}{(z-r_1)(z-r_2)} \quad (4.1.1)$$

The corresponding continuous differentiator is

$$w_1(s) = \frac{s}{T_c^2 s^2 + \sqrt{2} T_c s + 1} = s W_L(s), \text{ where } W_L(s) = \frac{1}{T_c^2 s^2 + \sqrt{2} T_c s + 1} \quad (4.1.2)$$

For the determination of the second derivative of phase fluctuations, one can use the digital differentiator

$$w_2(z) = z \frac{(z-1)^2 (1-r_1)(1-r_2)(1-r_3)}{T_c^2 (z-r_1)(z-r_2)(z-r_3)} = \frac{(z-1)^2}{T_c^2} W_L(z) \quad (4.1.3)$$

where $W_L(z) = \frac{z(1-r_1)(1-r_2)(1-r_3)}{(z-r_1)(z-r_2)(z-r_3)}$ is the transfer function of a digital low-pass filter. The corresponding continuous differentiator is

$$w_2(s) = \frac{s^2}{T_c^3 s^3 + 2T_c^2 s^2 + 2T_c s + 1} = s^2 W_L(s), \text{ where } W_L(s) = \frac{1}{T_c^3 s^3 + 2T_c^2 s^2 + 2T_c s + 1} \quad (4.1.4)$$

Therefore the transfer functions of optimal differentiators are composed by two operations: pure differentiation and low-pass filtering. The corresponding low-pass filters are the Putterworth filters, which are the approximations to the ideal low-pass filter within the pass-band $\omega_c = 1/T_c$. From the time series y_i obtained at the output of the digital differentiator $w_1(z)$, one can determine the mean value and the variance by the following formulas: $m_y = \frac{1}{N} \sum_{i=1}^N y_i$, $\sigma_y^2 = \frac{1}{N-1} \sum_{i=1}^N (y_i - m_y)^2$ (4.1.5)

For each value of the parameter T_c one can obtain a value of the variance σ_y^2 . By changing the parameter T_c , one can determine the curve of variance function $\sigma_y^2(T_c)$. When the parameter T_c increases, the variance σ_y^2 decreases. From the curve $\sigma_y^2(T_c)$ one can obtain the curve $\sigma_y^2(\omega_c)$ by a simple computation. The curves $\sigma_y^2(T_c)$ give the frequency instability characterization in the time domain. (see Appendices, Fig. A1).

From the time series d_i obtained at the output of the digital differentiator $w_2(z)$, one can determine the mean value and the variance by the following formulas: $m_d = \frac{1}{N} \sum_{i=1}^N d_i$, $\sigma_d^2 = \frac{1}{N-1} \sum_{i=1}^N (d_i - m_d)^2$ (4.1.6)

The values of m_d and σ_d^2 give the frequency drift characterization of oscillators.

4.1.2 Filtering Method for the Power Spectral Density Determination

One supposes that there is a curve of the power spectral density $S_Y(\omega)$. The spectral function $F_Y(\omega)$ can be determined by $F_Y(\omega) = \int_0^\omega S_Y(\omega) d\omega$

And the variance is $\sigma_Y^2 = \frac{1}{\pi} \int_0^\infty S_Y(\omega) d\omega = \frac{1}{\pi} F_Y(\omega) \Big|_{\omega=\infty}$ (4.1.7)

One can obtain also $S_Y(\omega) = \frac{dF_Y(\omega)}{d\omega}$ (4.1.8)

Therefore $F_Y(\omega)$ is the primitive function of $S_Y(\omega)$, and $S_Y(\omega)$ is the first derivative of $F_Y(\omega)$. The value of $F_Y(\omega)$ for $\omega=\infty$ is the total variance σ_Y^2 . The value of $F_Y(\omega)$ for $\omega=\omega_i$ is a partial variance.

$F_Y(\omega_i) = \int_0^{\omega_i} S_Y(\omega) d\omega = \pi \sigma_Y^2(\omega_i)$. From the curve $\sigma_Y^2(\omega_i)$ one can determine the curve $\sigma_Y^2(\omega_c)$. Then one can compute the spectral function $F_Y(\omega_c) = \pi \sigma_Y^2(\omega_c)$ for different values of ω_c . The power spectral density $S_Y(\omega)$ can be obtained by the differentiation of the curve $F_Y(\omega_c)$:

$$S_Y(\omega_i) = \frac{\Delta F_Y(\omega_i)}{\Delta \omega_i} = \frac{F_Y(\omega_i) - F_Y(\omega_{i-1})}{\omega_i - \omega_{i-1}} \quad (4.1.9)$$

4.1.3 Relations to the Conventional Characterization Methods

It is of interest to compare the proposed characterization method with the conventional methods, especially with the Allan-variance method and the three samples variance method. In this section, some comparisons between these methods are given.

(1) Comparison with the Allan-variance method

According to the definition of the Allan variance one obtains (see [8])

$$\sigma_Y^2(2, \tau, \tau) = \frac{1}{2} \langle (\bar{y}_2 - \bar{y}_1)^2 \rangle. \text{ Thus } \sigma_Y(\tau) = \frac{1}{\sqrt{2}} (\bar{y}_2 - \bar{y}_1) \quad (4.1.10)$$

where $\bar{y}_1 = \frac{1}{\tau} \int_{t_1}^{t_1+\tau} y(\theta) d\theta$, $\bar{y}_2 = \frac{1}{\tau} \int_{t_1+\tau}^{t_1+2\tau} y(\theta) d\theta$, and $t_2 = t_1 + \tau$

Hence one obtains the following transfer function

$$H(s) = \frac{1}{\sqrt{2}\tau s} (1 - e^{-\tau s})^2, \quad |H(j\omega)|^2 = \frac{2 \sin^4 \pi f \tau}{(\pi f \tau)^2}, \text{ where } s = j\omega = j2\pi f \quad (4.1.11)$$

According to the Padé approximation one can obtain (see [16])

$$e^{-\tau s} = \frac{1 - s\tau/2}{1 + s\tau/2}, \text{ so that } 1 - e^{-\tau s} = \frac{\tau s}{\tau s/2 + 1} \quad (4.1.12)$$

Thus the approximate transfer function of the Allan variance method is

$$H(s) = \frac{1}{\sqrt{2}\tau s} (1 - e^{-\tau s})^2 \approx \frac{1}{2} \tau s H_L(s), \text{ where } H_L(s) = \frac{1}{\tau s^2/4 + \tau s + 1} \quad (4.1.13)$$

The equivalent pass-band of the low-pass filter $H_L(s)$ is $f_e^* = 1/(4\tau)$

For the optimal continuous differentiator

$$W_L(s) = \frac{s}{\tau_c^2 s^2 + \sqrt{2} \tau_c s + 1} = s W_L(s), \text{ where } W_L(s) = \frac{1}{\tau_c^2 s^2 + \sqrt{2} \tau_c s + 1} \quad (4.1.14)$$

the equivalent pass-band of the low-pass filter $W_L(s)$ is $f_e = (4\sqrt{2} \tau_c)^{-1}$

Therefore the condition of equivalence is $\tau = \sqrt{2} \tau_c$ or $\tau_c = \tau/\sqrt{2}$ (4.1.15)

(2) Comparison with the three samples variance method

According to the definition of the three samples variance method [8] one

$$\text{obtains } \sigma_Y^2(3, \tau, \tau) = \frac{1}{9} (2\bar{y}_2 - \bar{y}_1 - \bar{y}_3)^2. \text{ Thus } \sigma_Y(\tau) = \frac{1}{3} (2\bar{y}_2 - \bar{y}_1 - \bar{y}_3) \quad (4.1.16)$$

The transfer function of this method is

$$H(s) = \frac{1}{3\tau s} (1 - e^{-\tau s})^3, \quad |H(j2\pi f)|^2 = \frac{1}{9} \frac{\sin^6 \pi f \tau}{(\pi f \tau)^2} \quad (4.1.17)$$

$$\text{Using the Padé approximation } e^{-\tau s} = \frac{1 - s\tau/2}{1 + s\tau/2} \text{ and } 1 - e^{-\tau s} = \frac{s}{\tau s/2 + 1} \quad (4.1.18)$$

one can obtain the approximate transfer function of this method

$$H(s) = \frac{1}{3\tau s} (1 - e^{-\tau s})^3 \approx \frac{1}{3} \tau^2 s^2 H_L(s), \text{ where } H_L(s) = \frac{1}{(\tau s/2 + 1)^3} \quad (4.1.19)$$

The equivalent pass-band of the low-pass filter $H_L(s)$ is $f_e^* = 3/(16\tau)$
For the optimal continuous differentiator

$$W(s) = \frac{s^2}{T_c^3 s^3 + 2T_c^2 s^2 + 2T_c s + 1} = s^2 W_L(s), \text{ where } W_L(s) = \frac{1}{T_c^3 s^3 + 2T_c^2 s^2 + 2T_c s + 1} \quad (4.1.20)$$

the equivalent pass-band of the low-pass filter $W_L(s)$ is $f_e = (6T_c)^{-1}$

$$\text{Therefore the condition of equivalence is } \tau = \frac{9}{8} T_c \text{ or } T_c = \frac{8}{9} \tau \quad (4.1.21)$$

4.2 Prediction of Random Variations of Atomic Time Scales by Digital Recursive predictors

4.2.1 Statement of the Atomic Time Scale Prediction Problem

The time scale prediction problem is one of practical importance in such areas as utilization of portable clock data, control of time and frequency at remote autonomous stations, and atomic time scale formation with extrapolation. Several prediction methods have been proposed. They fall into two general classes: fixed polynomial filter methods and autoregressive integrated moving average (ARIMA) methods. By these methods, some results of prediction of atomic time scales have been obtained. [9] [11].

But there are three main problems in prediction, which have not been resolved. (1) The fixed polynomial filter method by the least-squares is not a recursive method. Thus it is not applicable for real-time data processing. (2) According to the ARIMA prediction method of Box and Jenkins, the additive measurement noise is not taken into account. (3) By these two methods one cannot make the prediction of derivatives of time series data. Therefore they are not applicable to the frequency prediction problem.

To resolve the above mentioned problems, one will use digital recursive predictors for atomic time and frequency prediction. Hence the additive measurement noise can be taken into account, and one can predict time and frequency variations simultaneously.

4.2.2 Realization of Digital Recursive Polynomial Predictors with Exponential Weighting of Data

The transfer function of polynomial predictor of second degree is

$$W(z) = \frac{z^2 X(z)}{Y(z)} = \frac{(1-\theta^2)[1+l_0(1-\theta)(1+\theta)^{-1}] - 2\theta(1-\theta)[1+l_0(1-\theta)(2\theta)^{-1}]z^{-1}}{1 - 2\theta z^{-1} + \theta^2 z^{-2}} \quad (4.2.1)$$

Thus the algorithm of this predictor is the following :

$$x_{n+l_0} = 2\theta x_{n+l_0-1} - \theta^2 x_{n+l_0-2} + (1-\theta^2)(1+l_0 \frac{1-\theta}{1+\theta})y_n - 2\theta(1-\theta)(1+l_0 \frac{1-\theta}{2\theta})y_{n-1} \quad (4.2.2)$$

where the prediction time is $t_0 = l_0 T$, T is the sampling period.

The transfer function of polynomial predictor of third degree is

$$W(z) = \frac{z^3 X(z)}{Y(z)} = \frac{A_0 T + \theta(-2A_0 T + A_1 T^2 + A_2 T^3)z^{-1} + \theta^2(A_0 T - A_1 T^2 + A_2 T^3)z^{-2}}{1 - 3\theta z^{-1} + 3\theta^2 z^{-2} - \theta^3 z^{-3}} \quad (4.2.3)$$

where $A_0 T = (1-\theta^3) \left[1 + \frac{3l_0(1-\theta^2)}{2(1+\theta+\theta^2)} + \frac{l_0^2(1-\theta)^2}{2(1+\theta+\theta^2)} \right]$, $A_1 T^2 = -\frac{3}{2}(1-\theta)^2(1+\theta) \left[1 + l_0 \frac{(1-\theta)(9\theta+1)}{6\theta^2} + l_0^2 \frac{(1-\theta)^2(3\theta+1)}{6\theta^2(1+\theta)} \right]$, $A_2 T^3 = \frac{(1-\theta)^3}{2} \left[1 + l_0 \frac{(3\theta+1)(1-\theta)}{2\theta^2} + l_0^2 \frac{(1-\theta)^2}{2\theta^2} \right]$

The algorithm of this predictor is the following :

$$x_{n+l_0} = 3\theta x_{n+l_0-1} - 3\theta^2 x_{n+l_0-2} + \theta^3 x_{n+l_0-3} + (A_0 T)y_n + \theta(-2A_0 T + A_1 T^2 + A_2 T^3)y_{n-1} + \theta^2(A_0 T - A_1 T^2 + A_2 T^3)y_{n-2}$$

$$+A_2 T^3)y_{n-2} \quad (4.2.4)$$

4.2.3 Realization of Digital Recursive Predictors Based on Stochastic Models with Stationary Increments

In the paragraph III the synthesis of optimal predictors for several models has been done by the indirect method. At first, the transfer functions for continuous predictors have been obtained. Then one must use the Z-transformation method or the state variables method in order to obtain the corresponding digital recursive predictors.

For the model ARIMA(0,2,0), the optimal continuous predictor is

$$W(s) = \frac{(\sqrt{2} T_c + \tau)s + 1}{T_c^2 s^2 + \sqrt{2} T_c s + 1} \quad \text{where } T_c = \sqrt{c/d} \quad (4.2.5)$$

For the model ARIMA(0,3,0), the optimal continuous predictor is

$$W(s) = \frac{(2T_c^2 + 2T_c\tau + \tau^2/2)s + (2T_c + \tau)s + 1}{T_c^3 s^3 + 2T_c^2 s^2 + 2T_c s + 1} \quad \text{where } T_c = \sqrt[3]{c/d} \quad (4.2.6)$$

For the model ARIMA(0,3,0), the optimal continuous predictor of first derivative is

$$W(s) = \frac{s[(2T_c + \tau)s + 1]}{T_c^3 s^3 + 2T_c^2 s^2 + 2T_c s + 1} \quad \text{where } T_c = \sqrt[3]{c/d} \quad (4.2.7)$$

In order to demonstrate the digital realization method of continuous predictors, one will transform a continuous predictor of second degree by using the state variables method. For a given transfer function (4.2.5) one can determine the following state equations:

$$\begin{aligned} \dot{X}(t) &= FX(t) + GU(t) \\ Y(t) &= CX(t) + DU(t) \end{aligned} \quad (4.2.8)$$

where $X(t) = \begin{bmatrix} x_1(t) \\ x_2(t) \end{bmatrix}$, $\dot{X}(t) = \begin{bmatrix} \dot{x}_1(t) \\ \dot{x}_2(t) \end{bmatrix}$, $F = \begin{bmatrix} 0 & 1 \\ -T_c^{-2} & -\sqrt{2}T_c^{-1} \end{bmatrix}$, $G = \begin{bmatrix} 0 \\ T_c^{-2} \end{bmatrix}$, $C = \begin{bmatrix} 1 & (\sqrt{2}T_c + \tau) \end{bmatrix}$, $D=0$. One designates $V_k = \dot{X}_k T$, $V_{k+1} = \dot{X}_{k+1} T$ and $\alpha = T/(\sqrt{2}T_c)$.

The state variables equations for the digital predictor are the following:

$$\begin{aligned} X_{k+1} &= \Phi X_k + \Gamma U_{k+1} \\ Y_k &= C X_k + D U_k \end{aligned} \quad (4.2.9)$$

where $X_k = \begin{bmatrix} x_k \\ v_k \end{bmatrix}$, $X_{k+1} = \begin{bmatrix} x_{k+1} \\ v_{k+1} \end{bmatrix}$, $\Phi = \begin{bmatrix} e^{-\alpha}(\cos\alpha + \sin\alpha) & \alpha^{-1}e^{-\alpha}\sin\alpha \\ -2\alpha e^{-\alpha}\sin\alpha & e^{-\alpha}(\cos\alpha - \sin\alpha) \end{bmatrix}$, $\Gamma = \begin{bmatrix} 1 - e^{-\alpha}(\sin\alpha + \cos\alpha) \\ 2\alpha e^{-\alpha}\sin\alpha \end{bmatrix}$, $C = \begin{bmatrix} 1 & (\alpha^{-1} + \tau/T) \end{bmatrix}$, $D=0$.

4.3 Approximation of Non-stationary Time Series Data by Digital Recursive Filters

4.3.1 Statement of the Approximation Problem of Non-stationary Time Series Data

In atomic time and frequency metrology, especially for the time comparison between distant atomic clocks by satellite, one often has necessity to solve the approximation or smoothing problem of time series data. Conventionally, one can use the least-squares method of approximation by algebraic polynomials. In order to simplify the algorithm of computation, one can use the least-squares method of approximation by orthogonal polynomials (Legendre polynomials). In this case, one can save the operation of matrix inversion in the determination of coefficients of polynomials. But these least-squares methods are essentially batch-wise processing methods. They are not well suited for real-time digital processing of time series data.

For the processing of non-stationary time series of long duration and

for real-time processing, one must use digital recursive filtering methods. When one compares two distant atomic clocks by a satellite, there are no knowledges of the statistics of the process. In this case, one can use digital recursive polynomial filtering with exponential weighting for the data approximation or smoothing.

4.3.2 Time Series Approximation by Digital Recursive Polynomial Filtering with Exponential Weighting of Data

Using the results, obtained in paragraph II, one can solve the problem of non-stationary time series approximation by digital recursive polynomial filtering. One will demonstrate this application by two simple examples. (1) For the smoothing of stationary time series data, one can use the digital recursive polynomial filter of first degree. The transfer function of this filter is

$$W(z) = \frac{X(z)}{Y(z)} = z \frac{1-\theta}{z-\theta} = \frac{1-\theta}{1-\theta z^{-1}} \quad (4.3.1)$$

Thus the algorithm of realization of this filter is the following :

$$x_n = \theta x_{n-1} + (1-\theta)y_n \quad \text{or} \quad x_n = x_{n-1} + (1-\theta)e_n, \quad \text{where} \quad e_n = y_n - x_{n-1} \quad (4.3.2)$$

(2) If the time series data contain linear deterministic component, one must use the digital recursive polynomial filter of second degree. The transfer function of this filter is

$$W(z) = \frac{X(z)}{Y(z)} = z \frac{(1-\theta^2)z + 2\theta(\theta-1)}{(z-\theta)^2} = \frac{(1-\theta^2) + 2\theta(\theta-1)z^{-1}}{1-2\theta z^{-1} + \theta^2 z^{-2}} \quad (4.3.3)$$

The algorithm of realization of this digital filter is

$$x_n = 2\theta x_{n-1} - \theta^2 x_{n-2} + (1-\theta^2)y_n + 2\theta(\theta-1)y_{n-1} \quad (4.3.4)$$

One can also use another algorithm for realization of this digital filter, expressed by the following matrix equation :

$$\begin{pmatrix} x_{n+1} \\ v_{n+1} \end{pmatrix} = \begin{pmatrix} 1 & 1 \\ 0 & 1 \end{pmatrix} \begin{pmatrix} x_n \\ v_n \end{pmatrix} + \begin{pmatrix} 1-\theta^2 \\ (1-\theta)^2 \end{pmatrix} e_{n+1}, \quad \text{where} \quad e_{n+1} = y_{n+1} - x_n - v_n \quad (4.3.5)$$

Using this method, one can solve more complicated problems by the same procedure.

V. NON-STATIONARY TIME SERIES MODELIZATION BY DIGITAL RECURSIVE METHODS

5.1 Problem Statement

The problem of atomic time and frequency modelization has a fundamental importance for theoretical and experimental studies. The conventional method for modelization of the statistics of frequency fluctuations is based on stationary models. The commonly used model of frequency instabilities is the power-law spectral density model, expressed by the following formulas:

$$S_y(f) = \sum_{\alpha=-2}^2 h_\alpha f^\alpha \quad \text{for} \quad 0 \leq f \leq f_A \quad \text{and} \quad S_y(f) = 0 \quad \text{for} \quad f > f_A \quad (5.1.1)$$

Based on this model, the phase fluctuations can be expressed by the following model:

$$S_x(f) = (4\pi^2 f^2)^{-1} S_y(f) \quad (5.1.2)$$

The second widely used model is the deterministic polynomial model. When there is a linear frequency drift, expressed by a first-order polynomial model, the phase drift can be modeled by a second order polynomial.

The third proposed method for modelization of frequency and phase fluctuations is the ARIMA stochastic models. These models can be used for the modelization of non-stationary time series with stationary increments.

But there are some problems in modelization of atomic clocks, which have

not been resolved completely. (1) The power-law spectral density models are not completely suited for modelization of non-stationary frequency and phase fluctuations. And the procedures of modelization are not natural and convenient for computer simulations. (2) The deterministic polynomial models can not reflect the statistics of frequency and phase random fluctuations. (3) The ARIMA models have been constructed by empirical methods. The physical origins of different ARIMA models have not been explained and derived. The ARIMA representations of models can be further modified in order to get the Markov representations, which are more natural and convenient for computer solutions and simulations.

In the section 5.2 one will analyze the internal noises of atomic clocks in order to interpret the physical origins of different ARIMA models. Then some theoretical Markov models can be deduced. In the section 5.3, analytical procedures of spectral approximation and model identification will be proposed.

5.2 Analysis of Internal Noises and Deduction of Theoretical Models for Atomic Clocks

5.2.1 Analysis of Internal Noises of Atomic Clocks

Consider the system block diagram of a cesium atomic clock, shown in the following figure.

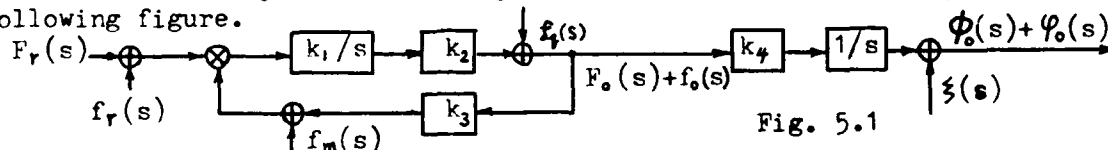


Fig. 5.1

One supposes that the noise of the oscillator $f_q(t)$, the noise of the frequency multiplier $f_m(t)$, and the noise of the atomic reference $f_r(t)$ are uncorrelated. Then the random variations of the frequency of the atomic clock is determined by the following formula :

$$f_o(s) = f_r(s) \frac{k_1 k_2}{s + k_1 k_2 k_3} + f_q(s) \frac{s}{s + k_1 k_2 k_3} - f_m(s) \frac{k_1 k_2}{s + k_1 k_2 k_3} \quad (5.2.1)$$

The random variations of the phase of the atomic clock is determined by the following formula :

$$\phi_o(s) = f_o(s) \frac{k_4}{s} + \xi(s) \quad (5.2.2)$$

Using these general formulas, one can analyze frequency and phase fluctuations for different cases of noises $f_r(s)$, $f_q(s)$ and $f_m(s)$. And then one can obtain different theoretical models for atomic clocks. The results of some theoretical analysis can be represented in the following table.

Noise type	$f_r(s)$	$f_q(s)$	$\xi(s)$	$f_o(s)$	$\phi_o(s)$	ARIMA (p,n,q)
White noises	r	b	0	$\frac{b(s+rb^{-1}k_1k_2)}{s+k_1k_2k_3}$	$\frac{bk_4(s+rb^{-1}k_1k_2)}{s(s+k_1k_2k_3)}$	(1,1,1)
Random walks	r/s	b/s	0	$\frac{b(s+rb^{-1}k_1k_2)}{s(s+k_1k_2k_3)}$	$\frac{bk_4(s+rb^{-1}k_1k_2)}{s^2(s+k_1k_2k_3)}$	(1,2,1)
Freq. drift	0	d/s ²	0	$\frac{d}{s(s+k_1k_2k_3)}$	$\frac{dk_4}{s^2(s+k_1k_2k_3)}$	(1,2,0)
W.N.+ F.D.	r	b + d/s ²	0	$\frac{bs^2+rk_1k_2s+d}{s(s+k_1k_2k_3)}$	$\frac{ks^2+rk_1k_2s+d}{k_4s^2(s+k_1k_2k_3)}$	(1,2,2)

5.2.2 Deduction of Markov Models for Atomic Clocks

All formulas, which express the theoretical models of atomic clocks, can be represented by Markov models. Using state variables method, one can transform the formulas of $f_0(s)$ and $\varphi_0(s)$ to matrix equations, which have the Gauss-Markov properties. This method of representation is more convenient for computer simulation and computer solution of problems.

From the formulas $\varphi_0(s)$, expressed by the Laplace transformation, one can obtain the continuous state equations

$$\begin{aligned}\dot{X}(t) &= F X(t) + G B(t) \\ \varphi_0(t) &= C X(t) + D V(t)\end{aligned}\quad (5.2.3)$$

where $B(t)$ is a unity white noise, which generates the stochastic model, $V(t)$ is the noise of observation or additive measurement noise. Performing the transformation, one can obtain the discrete state equations

$$\begin{aligned}X_{k+1} &= \Phi X_k + \Gamma B_{k+1} \quad \text{where } \Phi = \exp(FT), \quad \Gamma = \int_0^T \Phi(p) G dp \\ \varphi_{0k} &= C X_k + D V_k\end{aligned}\quad (5.2.4)$$

Performing the Z-transformation, one obtains

$$X(z) = (zI - \Phi)^{-1} \Gamma z B(z), \quad \varphi_0(z) = C X(z) + D V(z) = C(zI - \Phi)^{-1} \Gamma z B(z) + D V(z) \quad (5.2.5)$$

Therefore the transfer function of the discrete model is

$$H(z) = \varphi_0(z)/B(z) = C(zI - \Phi)^{-1} \Gamma z \quad (5.2.6)$$

As an example, one will transform a simple atomic clock model to the corresponding Markov model. One supposes that

$$\varphi_0(s) = \frac{bk_4 s + rk_1 k_2 k_4}{s(s + k_1 k_2 k_3)} \quad (5.2.7)$$

One can obtain the continuous state equations

$$\begin{aligned}\dot{X}(t) &= F X(t) + G B(t) \\ \varphi_0(t) &= C X(t) + D V(t)\end{aligned} \quad \text{where } F = \begin{bmatrix} 0 & 1 \\ 0 & -\alpha \end{bmatrix}, \quad G = \begin{bmatrix} 0 \\ 1 \end{bmatrix}, \quad C = (rk_1 k_2 k_4 \quad bk_4), \quad D = 0 \quad (5.2.8)$$

The discrete state equations are

$$\begin{aligned}X_{k+1} &= \Phi X_k + \Gamma B_{k+1} \\ \varphi_{0k} &= C X_k + D V_k\end{aligned}\quad (5.2.9)$$

where $\Phi = \begin{bmatrix} 1 & \Omega \\ 0 & \theta \end{bmatrix}$, $\Gamma = \begin{bmatrix} \alpha^{-1}(T - \Omega) \\ \Omega \end{bmatrix}$, $C = (rk_1 k_2 k_4 \quad bk_4)$, $D = 0$

In the formulas (5.2.8) and (5.2.9) the coefficients are the following:

$$\alpha = k_1 k_2 k_3, \quad \theta = \exp(-\alpha T), \quad \Omega = \alpha^{-1} [1 - \exp(-\alpha T)] \quad (5.2.10)$$

5.3 Analytical Methods of Spectral Approximation and Model Identification

There are two methods for the identification of models of time series data. The time domain method is based on the curves of autocorrelation functions. The frequency domain method is based on the curves of power spectral densities. The commonly used time domain method of identification of general ARIMA models is quite complicated, except for simple autoregressive models. Therefore, it is of interest to study the frequency domain method for identification of models. For a non-stationary time series with stationary increments of n -th order, one must at first take the n -th order differences in order to obtain stationary time series. Then one determines the curves of autocorrelation function and the curves of power spectral density. One will identify the models from the power spectral density curves $S(\omega)$.

5.3.1 Interpolation Method of Spectral Approximation

For a given curve $S(\omega)$ one will make the approximation by the following rational function

$$S^*(\omega) = \frac{B_0 + B_1 \omega^2 + B_2 \omega^4 + \dots + B_m \omega^{2m}}{1 + A_1 \omega^2 + A_2 \omega^4 + \dots + A_n \omega^{2n}} \quad (5.3.1)$$

In order to determine the $(n+m)$ coefficients, one supposes that $\omega = \omega_i$ and requires that $S^*(\omega_i) = S(\omega_i)$ for $i=1,2,3,\dots,(n+m)$. (5.3.2)

Then one obtains

$$(1+A_1\omega_i^2+A_2\omega_i^4+\dots+A_n\omega_i^{2n})S(\omega_i)-(B_0+B_1\omega_i^2+B_2\omega_i^4+\dots+B_m\omega_i^{2m})=0 \quad (5.3.3)$$

for $i=1,2,3,\dots,(n+m)$, where $B_0=S(\omega)|_{\omega=0}=S_0$.

From these $(n+m)$ linear equations one can determine the coefficients

$A_1, A_2, A_3, \dots, A_n$ and $B_1, B_2, B_3, \dots, B_m$.

For example, one supposes that $S^*(\omega) = \frac{B_0+B_1\omega^2}{1+A_1\omega^2+A_2\omega^4}$, where $B_0=S_0$. (5.3.4)

One can determine the coefficients A_1, A_2 and B_1 from the following equations

$$(1+A_1\omega_i^2+A_2\omega_i^4)S_i-(S_0+B_1\omega_i^2)=0 \quad \text{for } i=1,2,3. \quad (5.3.5)$$

5.3.2 Least-squares Method of Spectral Approximation

For a given curve $S(\omega)$, one will make the approximation by two steps. The first step is the least-squares approximation by a polynomial as

$$S(\omega) \approx \sum_{i=0}^n a_i \omega^{2i} = a_0 + a_1 \omega^2 + a_2 \omega^4 + \dots + a_n \omega^{2n} \quad (5.3.6)$$

The second step is the utilization of the Padé approximation method, which yields

$$a_0 + a_1 \omega^2 + a_2 \omega^4 + \dots + a_n \omega^{2n} \approx \frac{p_0 + p_1 \omega^2 + p_2 \omega^4 + \dots + p_L \omega^{2L}}{1 + q_1 \omega^2 + q_2 \omega^4 + \dots + q_M \omega^{2M}} \quad (5.3.7)$$

At the first step one obtains the error of approximation

$$d(\omega) = S(\omega) - \sum_{i=0}^n a_i \omega^{2i}. \quad \text{For the minimization of the integral}$$

$$D = \int_0^\infty [S(\omega) - \sum_{i=0}^n a_i \omega^{2i}]^2 d\omega, \quad \text{one obtains the necessary condition } \frac{\partial D}{\partial a_j} = 0$$

for $j=0,1,2,\dots,n$. Thus one obtains $(n+1)$ equations in order to determine the coefficients $a_0, a_1, a_2, \dots, a_n$. These equations are the following:

$$\sum_{i=0}^n a_i \left[\int_0^\infty \omega^{2(i+j)} d\omega \right] = \int_0^\infty \omega^{2j} S(\omega) d\omega \quad \text{for } j=0,1,2,\dots,n \quad (5.3.8)$$

For example, one can obtain the following approximation:

$$S(\omega) \approx a_0 + a_1 \omega^2 + a_2 \omega^4 + a_3 \omega^6 \approx \frac{B_0 + B_1 \omega^2}{1 + A_1 \omega^2 + A_2 \omega^4} \quad (5.3.9)$$

$$\text{where } B_0 = a_0, \quad B_1 = a_1 + \frac{a_0 a_1 a_2 - a_0^2 a_3}{a_0 a_2 - a_1^2}, \quad A_1 = \frac{a_0 a_3 - a_1 a_2}{a_0 a_2 - a_1^2}, \quad A_2 = \frac{a_1 a_3 - a_2^2}{a_0 a_2 - a_1^2}$$

5.3.3 Determination of Parameters of the Model by Spectral Factorization

In order to determine the parameters of the model, one must perform the spectral factorization according to the following formula:

$$S^*(\omega) = \frac{B_0 + B_1 \omega^2 + B_2 \omega^4 + \dots + B_m \omega^{2m}}{1 + A_1 \omega^2 + A_2 \omega^4 + \dots + A_n \omega^{2n}} = B_0 H(j\omega) H(-j\omega) \quad \text{where } j\omega = s \quad (5.3.10)$$

For example, if $S^*(\omega) = \frac{B_0 + B_1 \omega^2}{1 + A_1 \omega^2 + A_2 \omega^4}$, one can obtain

$$H(s) = \frac{\sqrt{B_0 B_1} s + 1}{\sqrt{A_2} s^2 + (A_1 + 2\sqrt{A_2}) s + 1} \quad (5.3.11)$$

Then, by the Z-transformation method or by the state variables method, one can determine the corresponding discrete model ARMA (2,1), expressed by the following formula:

$$H(z) = \frac{b_1 z + b_0}{a_2 z^2 + a_1 z + a_0} \quad (5.3.12)$$

VI. CONCLUSIONS

In time and frequency metrology, the conventional used methods are essentially non-recursive methods. They have been developed separately according to the envisaged problems, either for the characterization, or for the prediction, or for the approximation, or for the modelization. The interrelations between these problems and corresponding methods have not been clarified. One finds very little common points of these problems and these used methods.

In this paper, an attempt to unify these problems and the corresponding methods is made. The principal ideas are based on the optimal estimation theory and the digital recursive processing methods. Also the mathematical methods of statistics and linear systems theory have been extensively used. Several methods for optimal recursive estimation of non-stationary time series have been used and developed. Two different models of non-stationarities have been supposed: the deterministic polynomial models and the stochastic models with stationary increments. For these two types of models, one has synthesized optimal digital recursive estimators (predictors, filters and differentiators). One has applied these estimators to the atomic time and frequency metrology. It is clarified that the problems of characterization, prediction, approximation and modelization are particular cases of the general problem of optimal estimation of the states and the parameters. Thus, one can resolve these problems by the unified theory and methods. This new approach allows us to establish the fundamental problems of time and frequency metrology on a sound and rigorous mathematical basis regardless of the user's applications. It can also provide much insight into more complicated problems. Then the interrelations between the proposed methods and the conventional methods can be easily derived.

From the viewpoint of the study of mathematical and statistical methods, the main contributions of this work are the following :

- (1) Utilization of the exponential weighting method to resolve the problem of optimal estimation for the deterministic polynomial models. This method allows us to avoid the difficulties and drawbacks in the realization of the finite memory polynomial filters.
- (2) Optimal synthesis of digital recursive estimators for the stochastic models of non-stationary time series with stationary increments. This is an extension of the classical Wiener filtering theory to the non-stationary and discrete cases.
- (3) Proposition of the design method of suboptimal digital filters according to the general theory of Kalman filtering. For the non-stationary time series with stationary increments and for the case of steady-state optimization, one has obtained some time-invariant digital filters. The transfer functions of these digital filters have been deduced.
- (4) Synthesis of different optimal digital recursive estimators (predictors, filters and differentiators) by the unified methods. Though digital filters are widely used in many other domains, the digital predictors and digital differentiators are more particular and are especially important for time and frequency metrology.

From the viewpoint of the applications of statistical methods to atomic time and frequency metrology, the main contributions of this work are the

following :

(1) Application of digital recursive differentiators to characterize the frequency and phase instabilities of atomic clocks. This method allows us to estimate the variance and power spectral density function of frequency instability. Therefore one can characterize frequency instabilities both in the time and in the Fourier frequency domains.

(2) Application of digital recursive predictors to predict the random variations of atomic time scales. Two types of digital predictors can be used : the optimal predictors for deterministic polynomial models with exponential weighting of data, and the optimal predictors for stochastic non-stationary models with stationary increments.

(3) Application of digital recursive filters to smooth the time series data, obtained from time comparisons of distant atomic clocks via a satellite. This method is better than the least-squares method for real-time data processing.

(4) For the modelization of the statistics of frequency and phase fluctuations, one has deduced some theoretical models from the structure of atomic clocks. Then, two analytical procedures of spectral approximation and the spectral factorization method are proposed, which allows us to identify the parameters of stochastic models of atomic clocks.

We have developed several methods for optimal estimation of non-stationary time series. We have also applied these methods to atomic time and frequency metrology. Several new concepts and definitions have been proposed. For the latter, we have pointed out their specific advantages in applications. At present, the existing models and methods for time and frequency metrology are well documented. They provide a good background for actual applications. However, future researches will certainly include the development of more sophisticated approaches, that may possibly improve the methods of time and frequency metrology. In this regard, it seems that the optimal estimation theory can play a key role. This is a very promising approach, because this theory has a rigorous mathematical basis, and its concepts are quite general to cover the domain of time and frequency metrology. Many practical problems can be deduced from this theory as the particular cases. Using the optimal estimation theory, we have tried to solve some fundamental problems of time and frequency metrology. However, the problems of time and frequency metrology are quite diversified and very profound. This rich domain is still widely open for further researches.

REFERENCES

- [1] Special Issue on Frequency Stability, Proc.IEEE, vol.54, pp. 101-338, Feb. 1966.
- [2] L.S. Cutler and C.L. Searle, "Some aspects of the theory and measurement of frequency fluctuations in frequency standards," in [1], pp. 136-154.
- [3] D.W. Allan, "Statistics of atomic frequency standards," in [1], pp. 221-230.
- [4] J.A. Barnes, et al. "Characterization of frequency stability", IEEE Trans. Instrum. Meas., vol. IM-20, pp. 105-120, May 1971.
- [5] G.M.R. Winkler, "A brief review of frequency stability measures," in Proc. 8th Annu. PTTI Applications and Planning Meeting, Nov.30-Dec.2, 1976, pp. 489-527.
- [6] P. Kartaschoff, "Frequency and Time", Academic Press, London, New York, San Francisco, 1978.
- [7] W.C. Lindsey, C.M. Chie and W.E. Leavitt, "Interpretation and application of oscillator instability measures using structure functions," in Proc. 8th Annu. PTTI Applications and Planning Meeting, Nov.30-Dec.2, 1976, pp.535-560.
- [8] J. Rutman, "Characterization of phase and frequency instabilities in precision frequency sources : fifteen years of progress," Proc.IEEE, vol.66, pp. 1048-1075, Sept. 1978.
- [9] D.B. Percival, "Prediction error analysis of atomic frequency standards," in Proc. 31st Annu. Frequency Control Symp.,(Atlantic City,NJ), USA, June 1-3, 1977, pp. 319-326.
- [10] J. Uebersfeld, "Bruit de scintillation, stabilité ultime," Seminaire sur les étalons de fréquence, leur caractérisation et leur utilisation. LPMO Besançon France, Du 23 au 25 Mars 1981, pp. U1-U10.
- [11] G.E.P. Box and G.M. Jenkins, "Time Series Analysis, Forecasting and Control," San Francisco, CA, Holden-Day, 1976.
- [12] Special Issue on System Identification and Time Series Analysis, IEEE Trans. on Automatic Control, vol. AC-19, No 6, Dec. 1974.
- [13] R.J. Bennett, "Spatial Time Series : Analysis-Forecasting-Control," Pion Limited, London, 1979.
- [14] H.J. Blinichoff and A.L. Zverev, "Filtering in the Time and Frequency Domains." Wiley- Interscience, 1976.
- [15] P.D. Krut'ko, "Statistical Dynamics of Sampled- Data Systems" ILIFFE Books LTD, London, 1969.
- [16] G.A. Baker, "Essentials of Padé Approximation", Academic Press, New York, 1975.
- [17] A.H. Jazwinski, "Stochastic Processes and Filtering Theory" Academic Press, New York and London, 1970.
- [18] J.A. Cadzow, "Discrete- Time Systems " Prentice- Hall, Inc., New Jersey , 1973.
- [19] R.A. Gabel and R.A. Roberts, "Signals and Linear Systems " John Wiley and Sons, Inc. New York, Toronto, 1980.
- [20] J.S. Bendat and A.G. Piersol, "Random Data : Analysis and Measurement Procedures" Wiley-Interscience, New York, 1971.
- [21] M. Kunt, "Traitement Numérique des Signaux." Editions Georgi, Lausanne, 1980.

Appendices

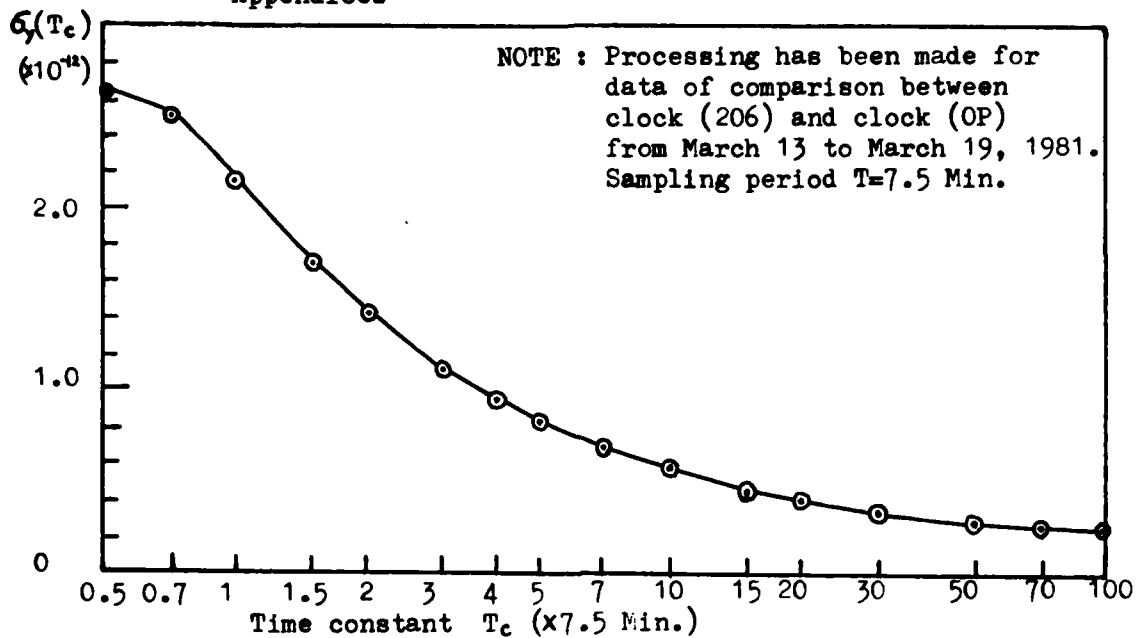


Fig. A1 - Variance function $\sigma_y(T_c)$

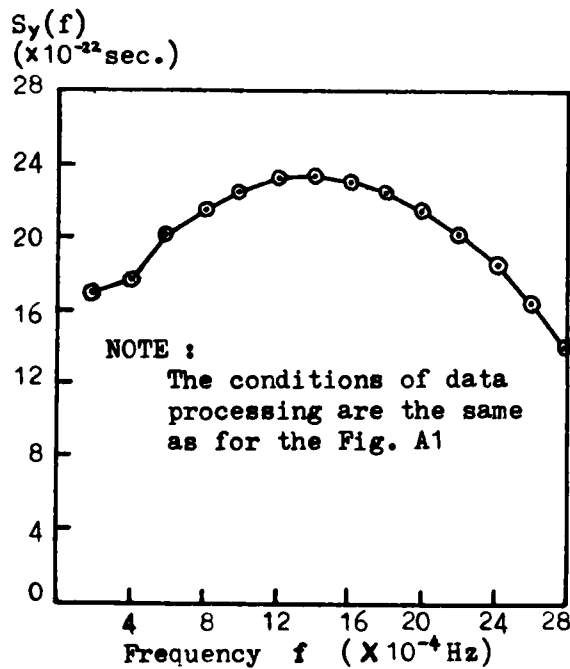
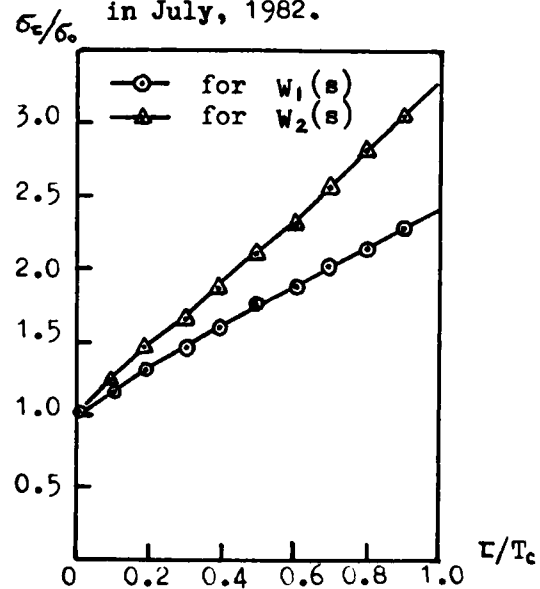


Fig.A2- Power spectral density $S_y(f)$

NOTE: Processing has been made for data of comparison between clock (195) and clock (OP) in July, 1982.



$T=30$ Min. $T/T_c=0.1$, $\sigma_0=3.2$ ns

Fig.A3 - Variance of time prediction
 $W_1(s)$ is determined by (4.2.5)
 $W_2(s)$ is determined by (4.2.6)

QUESTIONS AND ANSWERS

None for Paper #25.

APPLIED KALMAN FILTERING: AN OVERVIEW

R. Grover Brown
Electrical Engineering Department
Iowa State University

ABSTRACT

A brief resume of the evolution of Kalman filtering from classical filter theory is presented. The required format of the discrete filter model is discussed. The recursive equations for the discrete Kalman filter are then presented, but not derived. Two scalar examples are given to illustrate the use of the recursive equations. The first deals with estimation of a random constant; the second illustrates the Wiener process.

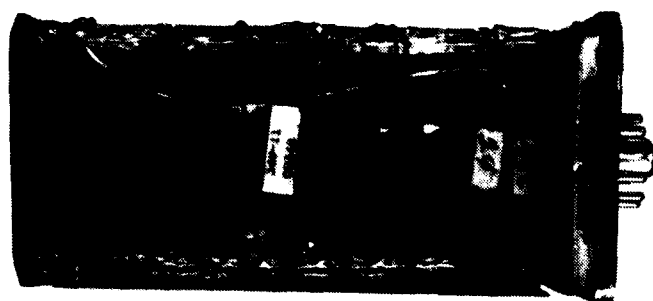
1. INTRODUCTION

It has been about 20 years since R. E. Kalman published his classic paper on recursive least-squares filtering [1]. In addition to its theoretical elegance, Kalman filtering has proved to be eminently practical. This, no doubt, accounts for its continued durability. The first applications in the early 1960's were in position and velocity determination [2,3,4], both in space and terrestrial settings. Since then, applications outside the navigation field have become more common. For example, a recent issue of the Bell System Technical Journal was devoted entirely to applications of Kalman filtering to load forecasting [5]. Also, a recent issue of the IEEE Transactions on Automatic Control was dedicated to new applications of Kalman filtering, many of which were outside the traditional application area of navigation [6]. Thus, Kalman filtering is alive and well, and the list of applications continues to grow!

Of necessity, this paper must be brief. Thus, it will be largely an overview or, if you like, a guided tour of the bare essentials of Kalman filtering. With this thought in mind, it is appropriate that we begin with a brief historical perspective.

2. HISTORICAL PERSPECTIVE

Figure 1 shows a conventional telephone bandpass filter side-by-side with a Kalman filter. At first glance, it looks ridiculous even to try to compare the two. On one hand, we have a circuit consisting of resistors, capacitors, etc.; on the other, we have just a set of mathematical equations. One might logically ask, "How in the world did that set of equations ever become known as a 'filter'?" The answer lies in the historical evolution of modern statistical filter theory from classical theory.



BAND-PASS
TELEPHONE FILTER

$$K_k = P_k^{-1} H_k^T [H_k P_k^{-1} H_k^T + R_k]^{-1}$$

$$\hat{x}_k = \hat{x}_k^- + K_k (z_k - H_k \hat{x}_k^-)$$

$$P_k = [I - K_k H_k] P_k^-$$

$$\hat{x}_{k+1}^- = \Phi_k \hat{x}_k$$

$$P_{k+1}^- = \Phi_k P_k \Phi_k^T + Q_k$$

KALMAN FILTER
RECURSIVE EQUATIONS

Fig. 1 (a) Conventional analog filter and (b) Kalman filter

Figure 2 shows a simplified chronology of the three major branches of filter theory as we know it today. Classical filter theory began in the early days of telegraphy, and it continues today as an active discipline within electrical

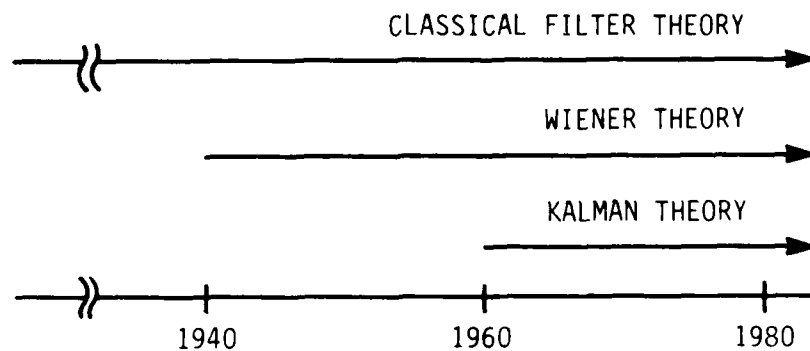


Fig. 2 Chronology of filter theory

engineering. The basic problem of classical theory is shown in Figure 3. It is basically one of synthesizing a given frequency response with R, L, C and (nowadays) active elements. The word given is underscored to emphasize the fact that the designer is assumed to know a priori what response is desirable in the application at hand. The only problem remaining then is that of practical implementation of the desired response (to some degree of approximation). Obviously, this problem is just as fresh and important today as it was in the 1800's.

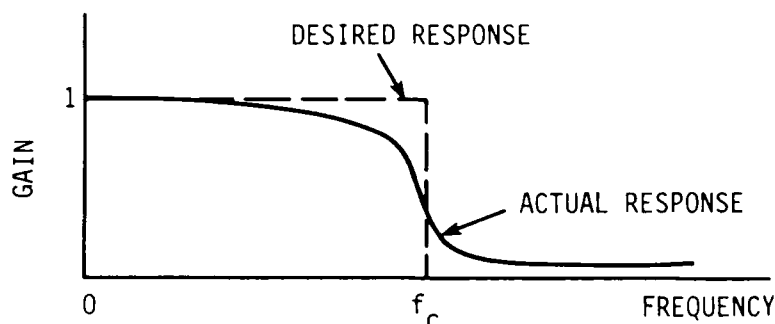


Fig. 3 The classical filter problem (low-pass example)

In the early 1940's, Norbert Wiener considered a different type of filtering problem [7]. Suppose, as shown in Fig. 4, that one has an additive combination of signal and noise with overlapping frequency spectra. We wish to remove the noise from the signal. However, it should be apparent that no filter in the usual sense will do a perfect job of removing noise without destroying the signal. Furthermore, it is not at all obvious what sort of compromise filter response will get rid of most of the noise with minimal damage to the signal. This is the problem that Wiener addressed during the World War II period.

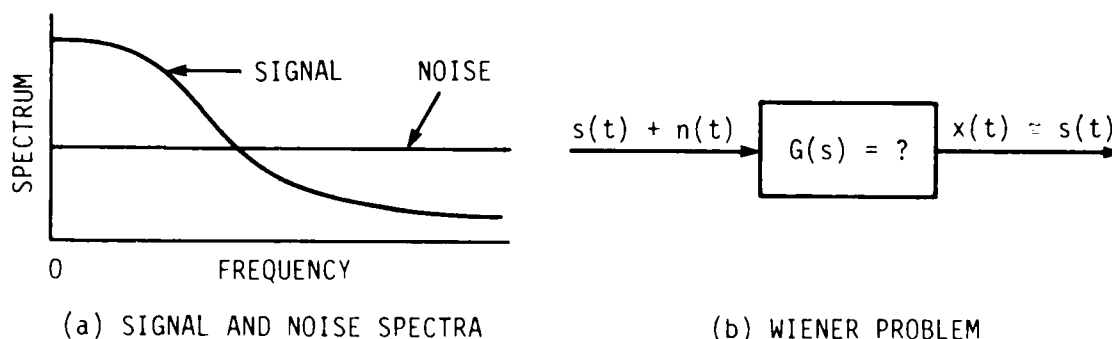


Fig. 4 Wiener filter problem

Wiener began by assuming both the signal and noise to be noiselike in character with known spectral characteristics. He then chose minimum-mean-square-error as the performance criterion, and he proceeded to develop a solution for the weighting function (inverse transform of the frequency response) of the filter. The "solution" which is in the form of an integral equation can be solved (with some difficulty) in the stationary (time invariant) case, and Wiener theory is still used in some applications. However, its extension to discrete, multiple-input multiple-output situations is awkward, to say the least. Thus, in a large class of problems the older Wiener methods have been replaced by those of Kalman. Note that the final solution of the Wiener problem is just a transfer function. The classical problem of synthesizing the transfer function still remains after the Wiener problem is solved.

In 1960, R. E. Kalman published a new solution of the least-squares filtering problem [1]. Even though Kalman's methods were much different than those of Wiener, the underlying assumptions were the same. In Kalman's formulation of the problem, the noisy measurements were assumed to be discrete rather than continuous in time, and the signal and noise were modeled in vector rather than scalar form. Kalman then proceeded to develop a solution for the conditional mean of the vector process (i.e., the "signal"), conditioned on all available measurements. In the Gaussian case, this conditional mean also minimizes the mean square error, so the end result is the same as that obtained with the Wiener theory. Kalman's solution is recursive in form, though, which makes it readily amenable to programming on a digital computer, either in real time or off line.

In summary, we might characterize the Wiener approach as a scalar weighting function method, whereby the desired estimate of the signal is computed as a weighted sum of past measurements. This procedure has been modified somewhat in recent years to ease the computational burden, but it still is basically a weighting function approach. On the other hand, Kalman's solution was discrete from the outset, and it is characterized by vector modeling of the noise and signal processes and recursive processing of the measurement data. Over the past 20 years, this approach has proved to be remarkably versatile in its ability to accommodate a wide variety of practical filtering problems. There is every reason to expect this activity will continue in the future.

The evolution of linear filter theory from frequency-selective RLC circuits to a set of mathematical equations should now be clear. Once one makes the transition from continuous to discrete measurement, the filter becomes just a prescribed set of arithmetic operations on the sequence of samples. The prescribed operation in the Kalman filter case is developed using the methods of probability and statistics because of the minimum-mean-square-error performance criterion. Thus, at times, the theory looks more like statistics than electrical engineering. Yet, its roots go back to the early days of telegraphy.

3. A SIMPLE AVERAGING EXAMPLE

The recursive philosophy which is essential in Kalman filter theory can be illustrated with a simple example. Suppose we have a sequence of noisy measurements of some unknown constant. We wish to simply average the available measurements and use this as a measure of the unknown constant. Assume that the measurements come to us sequentially in time, and denote them as $z_0, z_1, \dots, z_k, \dots$

The last measurement, z_k , is the measurement at current time t_k . We can now compute the average at each point in time in either of two ways:

<u>Batch Processing</u>		<u>Recursive Processing</u>	
<u>Time</u>	<u>Averaging Formula</u>	<u>Time</u>	<u>Averaging Formula</u>
t_0	$(Ave)_0 = z_0$	t_0	$(Ave)_0 = z_0$
t_1	$(Ave)_1 = \frac{z_0 + z_1}{2}$	t_1	$(Ave)_1 = \frac{1}{2} (Ave)_0 + \frac{1}{2} z_1$
t_2	$(Ave)_2 = \frac{z_0 + z_1 + z_2}{3}$	t_2	$(Ave)_2 = \frac{2}{3} (Ave)_1 + \frac{1}{3} z_2$
	\vdots		\vdots
	\vdots		\vdots
	\vdots		\vdots
	etc.		etc.

Clearly, both methods lead to the same sequence of sample averages. However, as the process progresses, the recursive computation has two distinct advantages over the batch method: (1) The measurements z_0, z_1, \dots, z_k do not have to be stored individually, and (2) the number of arithmetic operations remains the same with each step. Thus, the recursive approach avoids an escalation of the computational problem as the amount of measurement data increases. This is certainly important in problems involving a large number of measurements. In effect, with recursive processing the new measurement is simply used to update or refine the old estimate. The updated estimate is then projected ahead to the next step, and the process is repeated. This is the basic computational philosophy of the Kalman filter; it is to be contrasted with the batch philosophy, whereby all available measurements are stored and then summed with appropriate weight factors to yield the desired estimate.

4. THE DISCRETE KALMAN FILTER

The theory and details of Kalman filtering can be found in a number of textbooks [8,9,10], so we will only touch on the high points here. In discrete Kalman filter theory, the process to be estimated must be modeled in the following vector form:

$$x_{k+1} = \phi_k x_k + w_k \quad (1)$$

where

x_k = State vector at time t_k

ϕ_k = State transition matrix

w_k = Input white noise sequence characterized by a covariance matrix Q_k

which is defined as

$$E[w_k w_i^T] = \begin{cases} Q_k, & i=k \\ 0, & i \neq k \end{cases} \quad (2)$$

Equation (1) may result from sampling a continuous system driven by white noise. This does not have to be the case, though. Some physical problems are inherently discrete at the outset and there need be no continuous counterpart. The discrete process equation, Eq. (1), stands in its own right.

The measurement relationship connecting the noisy measurement z_k to the state vector x_k must be of the form

$$z_k = H_k x_k + v_k \quad (3)$$

where

z_k = Measurement at time t_k

H_k = Linear connection matrix

v_k = White measurement noise sequence characterized by a covariance matrix R_k

which is defined by

$$E[v_k v_i^T] = \begin{cases} R_k, & i=k \\ 0, & i \neq k \end{cases} \quad (4)$$

and

$$E[w_k v_i^T] = 0, \text{ for all } i \text{ and } k. \quad (5)$$

Equations (3), (4) and (5) simply state that there must be a linear connection between the measurement and the process to be estimated, and that the process (which is driven by w_k) and measurement noise must be uncorrelated.

Equations (1) and (3) are sometimes loosely referred to as the Kalman filter "model", and they may seem unduly restrictive at first glance. However, experience of the past 20 years has shown that the model is remarkably versatile in its ability to accommodate a wide variety of physical applications. Formulating the model is, without a doubt, the most difficult part of any applied Kalman filter problem, and there is no one simple rule for doing this. In the case of continuous processes, one must ask the question, "What set of linear differential equations relates the various random processes under consideration to white noise inputs?" Or, saying the same thing another way, "What linear dynamical operations will shape a set of white noise inputs into the processes being considered?" If the appropriate linear dynamical connection can be found, then the problem can be put into state space form, and the discrete form specified by Eq. (1) can be found. Of course, the linear connection between the measurement sequence and the process must also be formulated. This, though, is usually the easier half of the modeling problem.

5. THE RECURSIVE EQUATIONS

We begin by assuming that the estimation problem at hand fits the form given by Eqs. (1) and (3). We then pose the question: What sequence of estimates of the state vector will minimize the mean square error? The recursive solution of this problem is summarized in Fig. 5. Its derivation is given in the tutorial references previously cited, so it will not be included here. However, each major step in the recursive loop deserves further comment.

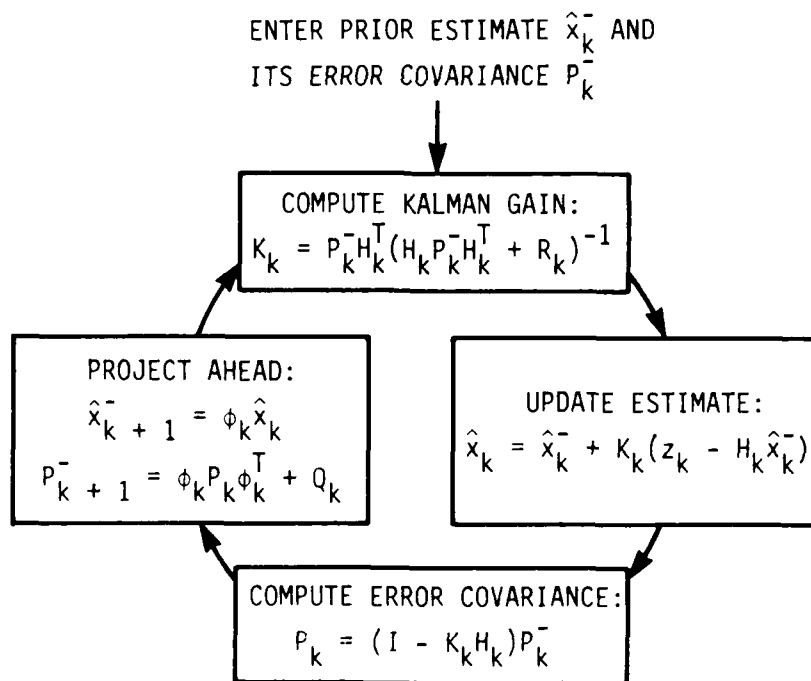


Fig. 5 Kalman filter recursive loop (super minus denotes a priori)

We enter the loop with an initial estimate and its error covariance. The starting point in time occurs with the first measurement, and we usually let this be $t=0$ ($k=0$). The initial estimate \hat{x}_0^- is based on our prior knowledge of the process, and this is zero for processes where we have no prior measurements and we know this process mean to be zero. In this case, the initial error covariance P_0^- is just the covariance of the process itself, which is assumed to be known a priori.

The first step in the loop is to compute a matrix known as the Kalman gain. Note from the first block of the loop in Fig. 5 that the Kalman gain depends on the known model parameters H_0 , R_0 and the initial P_0^- , but it does not depend on the actual measurement z_0 .

The next step in the recursive process is to use the measurement z_0 to update the prior estimate \hat{x}_0^- . The equation for doing this is shown in the second block of the loop, and note that it is similar in form with that of the simple averaging example considered in Section 3. That is, the updated estimate \hat{x}_0 is formed as the sum of the prior estimate \hat{x}_0^- plus a correction term which is the measurement residual weighted by the Kalman gain.

The third step is to update the prior error covariance P_0^- and obtain the error covariance associated with updated estimate. One can think of P_0 as a measure of the "fuzziness" associated with the updated estimate \hat{x}_0 . The terms along the major diagonal of P are the variances of the estimation errors for the respective components of the state vector. The off-diagonal terms are the corresponding covariances.

The final step in the recursive loop is to project \hat{x}_0 and P_0 ahead to time t_1 . This is done via the equations given in the fourth block of the loop shown in Fig. 5. In effect, the state estimate is projected ahead through the natural dynamics of the system as determined by the state transition matrix. Additional uncertainty is added to the projected estimate because of the process noise w_k , and this is accounted for with the Q_k matrix in the error covariance projection.

After the projection step, the estimator is ready to repeat the recursive loop and assimilate the next measurement z_1 at time t_1 . If the time between measurements is sufficient to permit all the required computations, the recursive estimation can be done on line. If not, it must be done off line. Two simple scalar examples will now illustrate the use of the recursive equations.

6. KALMAN FILTER EXAMPLES

(a) Estimating an Unknown Random Constant

Suppose we wish to estimate an unknown constant based on a sequence of noisy samples of the constant. For example, this might be the bias on a particular instrument that had just come off the assembly line and is now ready for calibration. Let us say that our past experience with similar instruments tells us that the bias is as likely to be positive as negative, and most of the previous instruments tested were found to have biases in the range of ± 2 units. Based on this crude prior information, it would be reasonable to model the unknown constant (i.e., the bias of the untested instrument) to be a zero-mean Gaussian random variable with a variance of 2^2 units.

A typical sequence of measurements for this examples is shown in Fig. 6.

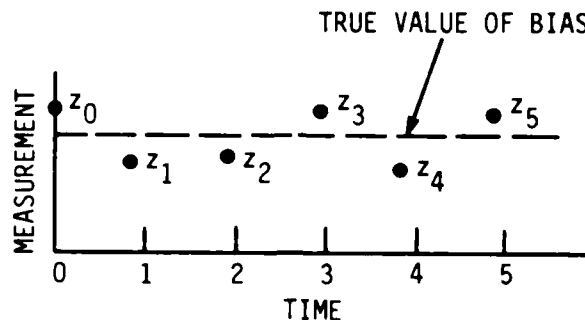


Fig. 6 Constant bias example

Suppose the master instrument used for measurement has a random error of 0.5 units rms, and that this error uncorrelated from step to step in the measurement process. The model parameters can now be specified as follows:

- (1) The process satisfies the discrete state equation $x_{k+1} = 1 \cdot x_k + 0$, because x is assumed to be constant. Thus

$$\phi_k = 1$$

$$Q_k = 0$$

- (2) We assumed a direct one-to-one noisy measurement of x . Thus

$$H_k = 1$$

- (3) We assumed the measurement error to be 0.5 units rms, or a variance of 0.25. Therefore, R_k is

$$R_k = .25$$

Note that ϕ_k , Q_k , H_k , and R_k do not depend on time, so the subscript k could be omitted in this simple example.

As stated previously, prior knowledge of the process led us to assume x to be a zero-mean Gaussian random variable with a variance of 4 units. Thus, the initial conditions are

$$\hat{x}_0^- = 0$$

$$P_0^- = 4$$

We now enter the loop at $t=0$ and compute the Kalman gain (see Fig. 5).

$$K_0 = 4 \cdot 1 (1 \cdot 4 \cdot 1 + .25)^{-1} = \frac{16}{17}$$

We update the estimate next.

$$\begin{aligned}\hat{x}_0 &= 0 + \frac{16}{17} (z_0 - 1 \cdot 0) \\ &= \frac{1}{17} \cdot 0 + \frac{16}{17} \cdot z_0\end{aligned}$$

The P matrix associated with \hat{x}_0 is then computed as

$$P_0 = (1 - \frac{16}{17} \cdot 1)4 = \frac{4}{17}$$

Finally, we project \hat{x}_0 and P_0 ahead to the next measurement.

$$\begin{aligned}P_1^- &= 1 \cdot \frac{4}{17} \cdot 1 + 0 = \frac{4}{17} \\ \hat{x}_1^- &= 1 \cdot \hat{x}_0\end{aligned}$$

We are now ready to repeat the process at t_1 and assimilate z_1 in a similar manner, and so forth.

Before leaving this example, it should be noted that the Kalman filter result is not the same as that obtained by simply averaging the measurements (Section 3). The difference arises because the Kalman filter gives the initial a priori estimate nonzero weight when blending it with the first measurement z_0 . This will, of course, cause the a priori estimate to propagate indirectly into the subsequent estimates as the recursive process proceeds. This distinguishes the Kalman filter from maximum likelihood estimation, where we usually assume that no a priori information is available. To make a Kalman filter artificially look like maximum likelihood estimation, all one has to do is make the initial P matrix very large. Then the initial estimate is given zero weight on the first step, and all subsequent estimates will depend only on the measurement sequence.

(b) Brownian Motion (Wiener) Process

Figure 7 shows a noise process which is being generated as the output of an integrator driven by Gaussian white noise. This experiment can be readily demonstrated in the laboratory just by connecting the output of a wideband noise source to an analog integrator with the initial condition being set at zero. Such a process is known as a Brownian-motion or Wiener process. Clearly, $x(t)$ satisfies the first order differential equation

$$\dot{x} = f(t) \tag{6}$$

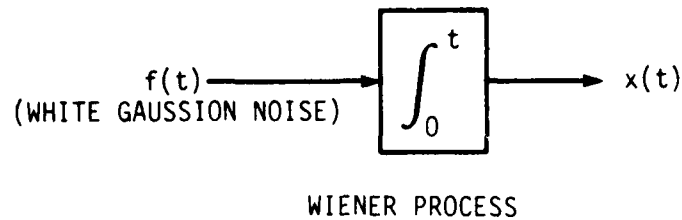


Fig. 7 Generation of a Wiener process

Thus, discrete samples of $x(t)$ are related by the recursive equation

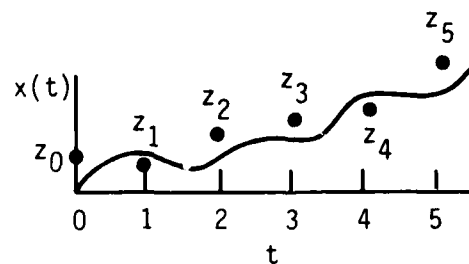
$$x_{k+1} = x_k + w_k \quad (7)$$

where

$$w_k = \int_{t_k}^{t_{k+1}} f(t) dt \quad (8)$$

Clearly, if $f(t)$ is white noise, the w_k sequence will be white and the process model fits the required format.

Suppose we have a sequence of noisy measurements of this process as shown by the dots in Fig. 8. Further, suppose that the rms measurement error is 0.5, and that



MEASUREMENT SITUATION

Fig. 8 Typical measurement situation for random walk example

w_k for a sampling interval of 1 sec is normal with zero mean and unit variance. The model parameters are then

$$\phi_k = 1$$

$$Q_k = 1$$

$$H_k = 1$$

$$R_k = (.5)^2 = .25$$

The initial conditions in this case are

$$\hat{x}_0^- = 0$$

$$P_0^- = 0$$

Note that the P_0^- condition is unusual. It says that we know the initial process state at $t=0$ perfectly! This is due to initial zero condition on the integrator; we know its output cannot change instantaneously. To see how this unusual P_0^- affects the estimator, we cycle through the recursive loop at $t=0$ (see Fig. 5):

$$\text{Calculate gain: } K_0 = 0 \cdot 1 (1 \cdot 0 \cdot 1 + .25)^{-1} = 0$$

$$\text{Update estimate: } \hat{x}_0 = 0 + 0 \cdot (z_0 - 1 \cdot 0) = 0$$

$$\text{Update P: } P_0 = (1 - 0 \cdot 1) \cdot 0 = 0$$

$$\text{Project ahead: } \hat{x}_1^- = 1 \cdot 0 = 0$$

$$P_1^- = 1 \cdot 0 \cdot 1 + 1 = 1$$

Note that the Kalman filter gives the noisy measurement z_0 zero weight. This is just as it should be; it is worthless relative to our perfect knowledge of the state at $t=0$.

It is instructive now to cycle through one more step of the recursive process. At $t=1$:

$$\text{Calculate gain: } K_1 = 1 \cdot 1 (1 \cdot 1 \cdot 1 + .25)^{-1} = \frac{4}{5}$$

$$\text{Update estimate: } \hat{x}_1 = 0 + \frac{4}{5} (z_1 - 1 \cdot 0) = \frac{4}{5} z_1$$

Update P: $P_1 = (1 - \frac{4}{5} \cdot 1) = \frac{1}{5}$

Project ahead: $\hat{x}_2^- = 1 \cdot \hat{x}_1$

$$P_2^- = 1 \cdot \frac{1}{5} \cdot 1 + 1 = \frac{6}{5}$$

Notice now that the a priori estimate at $t=1$ is only given a weight of $1/5$, and the measurement receives a weight of $4/5$. This is due to the process "random walk" that takes place in the interval from $t=0$ to $t=1$. The a priori estimate is thus quite uncertain at $t=1$, and the measurement, even though noisy, contains valuable new information about the process.

The recursive data processing can now be continued on ad infinitum. It might be mentioned that this least-squares estimation problem works out to be elementary when viewed from the Kalman viewpoint. It is somewhat elusive, though, when viewed from the Wiener viewpoint because of the nonstationary character of the Wiener process.

7. CLOSING COMMENT

We will close with these two simple examples, knowing that there are a number of application papers to follow in this session of the PTTI meeting. Hopefully, this tutorial overview will be of help in understanding the subsequent papers.

References

- [1] R. E. Kalman, "A New Approach to Linear Filtering and Prediction Problems", Trans. of the ASME--Jour. of Basic Engr., pp. 35-45, March 1960.
- [2] S. F. Schmidt, "Application of State-Space Methods to Navigation Problems, in Advances in Control Systems, Vol. 3, C. T. Leondes (Ed.), New York, Academic Press, 1966.
- [3] R. G. Brown and D. T. Friest, "Optimization of a Hybrid Inertial Solar-Tracker System", IEEE International Convention Record, Part 7, pp. 121-135, 1964.
- [4] B. E. Bona and R. J. Smay, "Optimum Reset of Ship's Inertial Navigation System", IEEE Trans. on Aerospace and Electronic Systems, AES-2, No. 4, pp. 409-414, July 1966.
- [5] Bell System Technical Journal, January 1982.
- [6] IEEE Trans. on Automatic Control, Vol. AC-28, No. 3, March 1983.
- [7] N. Wiener, Extrapolation, Interpolation and Smoothing of Stationary Time Series, New York, John Wiley, Inc., 1949.
- [8] R. G. Brown, Introduction to Random Signal Analysis and Kalman Filtering, New York, John Wiley, Inc. 1983.
- [9] A. Gelb (Ed.), Applied Optimal Estimation, Cambridge, MA, The M.I.T. Press, 1974.
- [10] P. S. Maybeck, Stochastic Models, Estimation and Control, Vol. 1, New York, Academic Press, 1979.

QUESTIONS AND ANSWERS

MR. BROWN:

What you always wanted to know about Kalman Filtering but were afraid to ask, or something like that.

MR. McCONAHY:

Mac McConahy, JHU/Applied Physics Lab. Grover would you like to say a few words about one of the things that I think rather puzzles many people about Kalman Filters, and that is, 'choosing' the process noise co-variance matrix in a practical application?

MR. BROWN:

Okay. The process noise co-variance matrix, that is the Q-matrix you're talking about. Well, I got to go clear back here, I'm afraid. Can I get the projector turned on again, please?

Going back to this particular model here, you have to have the characterization of W_K and, of course, the Q-matrix is W_K times W_K transposed and then the expectation of that; so it is a covariance matrix, and what you have to do is describe this in terms of the dynamics of the system. Usually, you end up getting this equation by starting out with some kind of continuous dynamics that relate the state vector to white noise inputs. Now, if you have that, if that's the starting point, then you can write a set of dynamical--you know, you can write it out explicitly what this W_K is; usually write it out as a convolution integral. Now, you take W_K transpose times W_K , take the expectation of that, and you end up having to evaluate a whole bunch of double integrals, is what it amounts to; and I guess I can't say more than that, except that is one of the most difficult parts of the problem. It's a very doggy job.

One of the sneaky approaches is the risk of adding something to that. There is a sneaky approach sometimes. If the step size is relatively large, sometimes the effective way of getting the Q-matrix is to subdivide the large integral into infinitesimal integrals, approximate the Q_K for the infinitesimal integral as being a diagonal matrix. No, not a diagonal matrix, but a matrix consisting of only first order terms of delta t.

Then you cycle through a whole bunch of steps to find the Q for the whole integral, just using the projection on the P-matrix form.

Use $Q\Phi Q^+$, that extra term, and you keep cycling through that. That is sort of a vague description, but the Q-matrix is kind of hard to find.

MR. WEISS:

Mark Weiss, N.B.S. To what extent does using a Kalman Filter assume a certain form of a noise, such as excluding flicker noise?

MR. BROWN:

I'll simply say this, if this is a bit of a cop-out that will apply to any situation if you can make it fit the model that is up there now. Now, there are certain cases where you can always fit it into this particular form. If you start out with the processes of--if you start out with stationary processes that are describable in terms of--well, where the spectral characteristics are rational. Then you can always choose the state vector to describe that which is such that it's the result of putting input white noise into some kind of linear dynamics to give that spectral characteristic. So any time the spectral characteristics are describable by rational spectral functions, then you're in business as far as the Kalman Filter is concerned--. But that is not the only case. You can also handle non-stationary cases.

You can model any case where the process that you are talking about can be thought of as the result of--let's see what I want to say--putting white noise inputs into a system of linear dynamics.

MR. WEISS:

Would you handle flicker noise?

MR. BROWN:

No, I don't think so. You see, that's something you people know a lot more about than I do, but it appears to be that that's a case where you have a spectral function, which is not rational. It's fractional powered, and I don't know how to do that.

DR. BARNES:

You can approximate it with an empirical approach.

MR. BROWN:

If it's truly a spectral function where it involves fractional powers of Ω , then I don't know any way to model it exactly, using the Kalman Filtering methods.

KALMAN FILTERING WITH A TWO-STATE CLOCK MODEL

Fran B. Varnum, Defense Mapping Agency

ABSTRACT

In this paper, a formulation of the operative equations that might be employed to filter measurements taken of an atomic clock are developed in an intuitive way. Emphasis is upon making clear, in a practical example, concepts and matrix components that might otherwise appear somewhat abstract to the uninitiated in a formal derivation.

Particular attention is given to the concept and calculation of the process noise required to process timing data in a Kalman filter. The author has tried to present the material in such a manner that a person with little or no experience could begin experimenting with the use of a Kalman filter to process real or simulated timing data.

INTRODUCTION

This paper assumes a rudimentary understanding of the Kalman filter concept and algorithm. Its purpose is to extend that understanding through the intuitive development of a practical example. The example chosen is a 2-state (phase and frequency) filter to process time difference data between a subject clock and a reference clock. The reference is assumed perfect and the subject clock is assumed to be perturbed by white noise on its frequency. How to include a white noise source on the frequency drift (random walk FM) is an extension that will be developed but not included in the full example.

The behavior of a cesium clock system is, for the most part, deterministic. However, random fluctuations in the on-going physical processes give rise to some measure of unpredictable behavior. It will be the function of the Kalman filter to make optimum estimates of the deterministic parameters (phase and frequency states) given measurements that are a function not only of these parameters but also of the perturbing noise source(s). This task is ideally suited for a Kalman filter.

One practical reason for estimating deterministic parameters is to use those parameters to predict a clock's behavior. For example, this is the purpose of estimating satellite clock states at the Master Control Station of the Global Positioning System (GPS).

Prediction of a clock's behavior will generally always be in error for two reasons. First, even though given the best possible values for the deterministic parameters describing past behavior, one could not predict subsequent random motion. Second, the original estimates of the deterministic parameters must necessarily have been made in the presence of

random behavior and are, themselves, subject to error. The function of the Kalman filter is to make an "optimum" estimate of the deterministic parameters based on whatever data is available in the belief that these will provide the best possible prediction under the circumstances.

Included, additionally, as part of these circumstances is the user-specified "model" which describes the dynamical relationships between the selected filter states together with a specification of the noise sources that are assumed to exist within the clock. It is very important that the model adequately represent the system under consideration in order to obtain the best possible result. The model is usually expressed very compactly in the form of a vector matrix differential equation. In the following section, the standard clock model in state-space, vector-matrix notation will be examined.

CLOCK MODEL

$$\dot{X} = A X + B N \quad (1)$$

Equation 1 is the matrix differential equation form of the clock model. X is the matrix vector of the states chosen to describe the deterministic behavior of the clock. In our case, as previously stated, we have chosen phase and frequency. Call these states $X1$ and $X2$ respectively. N is a matrix vector of the noise sources we are identifying as the cause of random behavior. Call these $N1$ and $N2$.

Equation (1) can be expanded as:

$$\begin{bmatrix} \dot{X1} \\ \dot{X2} \end{bmatrix} = \begin{bmatrix} 0 & 1 \\ 0 & 0 \end{bmatrix} \begin{bmatrix} X1 \\ X2 \end{bmatrix} + \begin{bmatrix} 1 & 0 \\ 0 & 0 \end{bmatrix} \begin{bmatrix} N1 \\ N2 \end{bmatrix} \quad (2)$$

N is a matrix vector consisting of zero mean, white, normally distributed noise sources. In our example, white FM is being modeled, so the elements in the B matrix are set appropriately to reflect this model.

If random walk frequency were to be modeled, then $N2$ should be incorporated into the model (random walk frequency is generated from white noise on frequency drift) by setting the zero in the lower right-hand corner of the B matrix to a one.

Performing the indicated matrix multiplication in equation (2), a pair of differential equations are obtained:

$$\dot{X1} = X2 + N1 \quad (3)$$

$$\dot{X2} = 0 \quad (4)$$

These equations are an identical but a more explicit statement of the clock model of equation (1). Equation (3) states that the time derivative of state 1 equals state 2 plus a white noise term. Remembering that states 1 and 2 are phase and frequency respectively and that only white noise FM is being considered, the reader should have no difficulty accepting this equation. Equation (4) states that the time derivative of the second state is zero, or, in other words, the frequency is being modeled as a constant. The fact that a real cesium exhibits a random walk in frequency is being ignored. If it were to be considered, then equation (4) would be:

$$\dot{X}_2 = N_2$$

Because phase, frequency, and frequency drift are integrally related and perfectly analogous to position, velocity, and acceleration, the basic clock model is identical in form to that used to model many dynamic systems in state space.

The next step, in preparation for implementing our Kalman filter, is to note the solution to the clock model. What is required is the solution to a stochastic differential equation and in our case one with constant coefficients (the A matrix).

SOLUTION TO THE CLOCK MODEL

The solution to the deterministic part of matrix equation (1) is:

$$e^{At} = \phi(t) = \sum_{n=0}^{\infty} \frac{1}{n!} t^n A^n \quad n = 0, 1, \dots$$

Since $A = \begin{bmatrix} 0 & 1 \\ 0 & 0 \end{bmatrix}$

$$\phi(t) = \begin{bmatrix} 1 & t \\ 0 & 1 \end{bmatrix} \quad (n = 0, 1 \text{ are the only nonzero terms})$$

$\phi(t)$ is the "transition matrix" which plays an important role in the Kalman filter algorithm. As the solution to equation (1), it describes the evolution of the modeled states with time and is a very aptly named quantity. The value of the states at any time, t , is:

$$X(t) = \phi(\delta t) X(t-\delta t) \quad (5)$$

where δt is some interval of time prior to t . For the sake of notational simplicity let this earlier time be (T_0) . In expanded form (5) is:

$$\begin{bmatrix} X_1(t) \\ X_2(t) \end{bmatrix} = \begin{bmatrix} 1 & \delta t \\ 0 & 1 \end{bmatrix} \begin{bmatrix} X_1(0) \\ X_2(0) \end{bmatrix}$$

Notice that $X(T_0)$ has been simplified to $X(0)$.

Performing the indicated multiplication gives:

$$X_1(t) = X_1(0) + X_2 \delta t$$

$$X_2(t) = X_2(0)$$

Expressing our state variables X_1 and X_2 (phase and frequency) as T and \dot{T}

$$T(t) = T(0) + \dot{T}(0)\delta t \quad (6)$$

$$\dot{T}(t) = \dot{T}(0) \quad (7)$$

Intuitively we see that these equations are correct. Equation (6) states that the phase at any time (t) is equal to the phase at an earlier time plus an accumulation due to the constant frequency offset. Equation (7) states that the frequency is constant.

The next concern, in finding the solution to equation (1), is to consider it's nondeterministic term. The solution to this part is a difficult integral. However the covariance of that integral is the quantity of interest (1). It is, itself, another integral, but one easily evaluated. Before examining it, a short discussion of it's physical significance is in order.

The covariance matrix of the solution to the random part of the clock model specifies the uncertainty in the clock's output due to the white noise sources incorporated in the model. In other words, it is a statistical measure of the inability of the deterministic states to completely model the clock's behavior. This is precisely the quantity needed to "Q" the Kalman filter; or more properly stated, it specifies the amount of "process noise" to be incorporated for each filter state.

The solution to the random part of the clock model is:

with covariance:

$$\int_{t-\delta t}^t \phi(u) BN du$$

$$\int_{t-\delta t}^t \phi(u) \text{cov} (BN) \phi(u)' du \quad (9)$$

Evaluation of this integral (Eq. 9) will specify the "Q's" required for each state in the filter. Because of its importance, the evaluation will be outlined for a more general model incorporating three states (frequency drift is added) and a random forcing function (white noise) associated with each state. The appropriate choice of zeros in the A and B matrices will tailor these results for a particular application.

EVALUATION OF CLOCK STATE NOISE COVARIANCE MATRIX

$$\text{Write } \mathbf{B} \mathbf{N} \text{ (Eq 1)} = \begin{bmatrix} S1 & 0 & 0 \\ 0 & S2 & 0 \\ 0 & 0 & S3 \end{bmatrix} \begin{bmatrix} N1 \\ N2 \\ N3 \end{bmatrix}$$

where $S1$, etc. are the standard deviations of the respective white noises in the model. In the previous development, the \mathbf{B} matrix contained 1's which implied unit standard deviations.

By definition: $\text{COV } \mathbf{B} \mathbf{N} = \mathbf{E} (\mathbf{B} \mathbf{N} (\mathbf{B} \mathbf{N})') = \mathbf{B} \mathbf{E} (\mathbf{N} \mathbf{N}') \mathbf{B}'$

where \mathbf{E} is the expectation and the prime indicates the matrix transpose.

Assuming the noise sources to be uncorrelated:

$$\mathbf{E} (\mathbf{N} \mathbf{N}') = \delta \begin{bmatrix} 1 & 0 & 0 \\ 0 & 1 & 0 \\ 0 & 0 & 1 \end{bmatrix}$$

where δ indicates the Dirac delta function.

So:

$$\text{COV } \mathbf{B} \mathbf{N} = \begin{bmatrix} V1 & 0 & 0 \\ 0 & V2 & 0 \\ 0 & 0 & V3 \end{bmatrix}$$

where $V1$, etc., are the variances of the noise sources.

Now $\phi \text{ COV } (\mathbf{B} \mathbf{N}) \phi'$ is determined by performing the indicated multiplication. For the three state model, the transition matrix $\phi(\delta t)$ is:

$$\begin{bmatrix} 1 & t & \frac{\delta t^2}{2} \\ 0 & 1 & \delta t \\ 0 & 0 & 1 \end{bmatrix}$$

The result is:

$$\phi(\delta t) \text{ COV } \mathbf{B} \mathbf{N} \phi(\delta t)' = M1 + M2\delta t + M3\delta t^2 + M4\delta t^3 + M5\delta t^4 \quad (10)$$

The matrices $M1$ through $M5$ are:

$$M1 = \begin{bmatrix} V1 & 0 & 0 \\ 0 & V2 & 0 \\ 0 & 0 & V3 \end{bmatrix}$$

$$M2 = \begin{vmatrix} 0 & \frac{V1}{2} & 0 \\ \frac{V1}{2} & 0 & \frac{V2}{2} \\ 0 & \frac{V2}{2} & 0 \end{vmatrix}$$

$$M3 = \begin{vmatrix} 0 & 0 & \frac{V1}{6} \\ 0 & \frac{V1}{3} & 0 \\ \frac{V1}{6} & 0 & \frac{V2}{3} \end{vmatrix}$$

$$M4 = \begin{vmatrix} 0 & 0 & 0 \\ 0 & 0 & \frac{V1}{8} \\ 0 & \frac{V1}{8} & 0 \end{vmatrix}$$

$$M5 = \begin{vmatrix} 0 & 0 & 0 \\ 0 & 0 & 0 \\ 0 & 0 & \frac{V1}{20} \end{vmatrix}$$

Finally, equation (10) is integrated over the interval δt , from $(t-\delta t)$ to t to obtain the $Q(\delta t)$ matrix required to optimally tune the Kalman filter. The result is:

$$Q(\delta t) = M1\delta t + M2(\delta t)^2 + M3(\delta t)^3 + M4(\delta t)^4 + M5(\delta t)^5$$

This same process, applied to the simpler model chosen for our example, gives:

$$Q(\delta t) = \begin{vmatrix} V1\delta t & 0 \\ 0 & 0 \end{vmatrix}$$

By inspection one sees that non-zero process noise (Q) is applied to the phase state only and that its magnitude is proportional to time: specifically, the time between measurement updates to the filter. In other words, while the last measurement will have presumably decreased the uncertainty in the phase state over what it had been previously, the uncertainty should start growing again until the next measurement. Some sense of the dynamics of a Kalman filter can be had at this point by imagining that due to a loss in some measurements, a longer than normal time elapses between the latest and the previous measurement. Because of the relatively larger value for " Q " (δt increased) and hence growth in uncertainty in the state, the Kalman gain will be correspondingly larger than otherwise for the state. This, in turn, causes the delayed measurement to have a larger impact on the estimate of this state than under the postulated "normal conditions".

It is this process that gives rise to the idea of a kalman filter "memory", and the fact that it is effected by the filter process noise. Generally larger values of process noise tend to weight the latest measurements more heavily.

The converse is that without the incorporation of adequate process noise, too little weight is given to the latest measurements. Suffice it to say, the choice of "Q's" is critical and can mean the difference between optimum and worthless results in a given situation. It is for this reason that some attention has been given to the concept of filter "Q'ing" in this discussion.

THE KALMAN FILTER ALGORITHM

The state variables (X) to be estimated have already been established as the phase and frequency (X1 and X2). Let it further be specified at this point that these are "epoch states". That is to say, a phase and frequency will be estimated for a specified time in the past such that when propagated to current time by the transition matrix, one obtains the corresponding "current-time" states. It can be shown that epoch and current-time state formulations result in identical estimates of the current-time states (3). If there is an advantage to estimating epoch states it is the relative ease with which predictions can be made relative to a fixed vs a variable epoch.

Use of epoch states introduces a conceptual subtlety that initially caused this author some difficulty in formulating the filter algorithm under discussion. It has to do with the state-transition matrix which has already been introduced and described validly as the model for the time-evolution of states. But note that epoch states, themselves, are generally constant by definition. Continuous reestimation is required due to the stochastic behavior of the clock, but in the absence of data the transition matrix for the epoch states is unity. There are, in other words, two transition matrices: the first describes the time evolution of states and was used to calculate the process noise. The second propagates epoch states between measurements. More importantly, it propagates the epoch state covariance matrix between measurements—a process called the "time update" and the first step in the Kalman cycle.

TIME UPDATE

This process propagates the epoch state covariance from its computed value immediately following the last measurement update to the time of the next measurement. Call these covariances $P(k+)$ and $P(k+1-)$ respectively. In this notation $k+$ means immediately after the last measurement update, $k+1-$ means at the time of but before processing the next measurement. The time update consists of computing $P(k+1-)$ given $P(k+)$ from the last Kalman cycle.

$$P(k+1-) = P(k+) + \phi^{-1} Q \phi'^{-1} \quad (11)$$

The inverse of the transition matrix means that the process noise added to account for the growth in uncertainty during the interval between measurements is propagated back to epoch. In our example pre and post multiplication by the inverse and the inverse of the transpose of the transition matrix leaves the Q matrix unchanged. If there had been a noise term associated with the frequency rate term (random walk frequency) this would not be the case. Note that the transition matrix normally encountered with the propagation of the P matrix itself is missing. This is, of course, because it is unity as discussed above.

The three remaining steps in the Kalman cycle are to:

- compute the gain
- make the new estimate (measurement update)
- compute the new state covariance

Once this is complete, the cycle starts again with the time update as described in the previous paragraph.

Before writing the three equations that describe these steps only two new matrices need to be introduced. They are the measurement noise covariance matrix (R) and the measurement matrix (H).

The measurement noise matrix for our example is simply a 1 x 1 with its single element equal to the variance of the measurement error.

The measurement matrix (H) is the matrix that defines the relationship between the measurement and the states being estimated. In our example, the phase difference between a subject clock and a reference clock is being measured. The measurement is the state X1 propagated to current time (the time of the measurement). The transition matrix provides the relationship, namely, equation (6) which in matrix form is written:

$$T(t) = \begin{bmatrix} 1 & \Delta t \end{bmatrix} \begin{bmatrix} T(0) \\ \cdot \\ T(0) \end{bmatrix}$$

Where Δt is the elapsed time since epoch.

Letting $T(t) = Z - v$, where Z is the measurement incorporating a measurement error (v) and defining $\begin{bmatrix} 1 & \Delta t \end{bmatrix} = H$

$$Z = H X - v \quad (12)$$

which is the standard form for the measurement equation in the Kalman algorithm.

Notice that in order for equation (12) to be correct X must be the true clock states and not the estimated states. We expect some error in the estimate or else there would be no need to update it. The quantity $Z - H\hat{X}$ (where the hat indicates the estimate) plays a major role in the measurement update process. This residual carries the information relating to the difference between the actual measurement and measurement predicted from existing estimates.

To complete the Kalman cycle the operative equations are:

$$K = P(k+1-) H' [H P(k+1-) H' + R]^{-1} \quad (\text{compute gain})$$

$$\hat{X}(k+1) = \hat{X}(k) + K [Z - H\hat{X}(k)] \quad (\text{update estimate})$$

$$P(k+1+) = [I - K H] P(k+1-) \quad (\text{update covariance})$$

These equations are easily implemented on a small computer. The largest matrix is a 2×2 and the entire algorithm is reducible to a few algebraic manipulations. Performance of the filter under a variety of conditions can be empirically evaluated. Simulated data can be created by integrating the output of a Gaussian random number generator where the numbers are interpreted as white noise on frequency. The standard deviation of the number generator should be chosen to appropriately represent the noise characteristics of the clock being simulated. This follows from the sample time chosen and the Allen variance that characterizes the clock. While the model chosen for this tutorial is over-simplified for a real situation, it should serve quite well as a first step in developing insight and experience with the use of Kalman filters to process timing data.

The two-state Kalman filter described in this paper was implemented and a simulated set of 500 data points processed with three different values of process noise. The magnitudes of the process noise were chosen to represent under, over, and optimum "Q'ing" respectively. In all other respects, including the input data, the runs were identical. The input data samples, (representing simulated phase difference measurements) were generated by integrating (summing) over a set of normally distributed random numbers. The resulting filter source data is shown plotted in Figure 3. The "true" states, in this instance, are zero for both phase and frequency since the only source of variation in the data is the random component. The filter states were initialized with values of 20ns and + 1 part in 10×10^{13} respectively. The covariance matrix was initialized with the square of these values.

The resulting phase estimates for the three cases cited are shown plotted in Figure 1. Clearly, increasing the "Q" increases the variation in the phase estimate. In accordance with the development of the "Q" matrix for our simplified noise model, process noise is added to the phase state only, and it follows that this should happen. Perhaps it is not quite as obvious that just the reverse should happen to the frequency estimate even though it is not being "Q'ed". It is because the filter insures that the time history of the estimated "state pair" is such that it will always closely predict the measurement data (via the measurement matrix). Increasing the range over which the phase estimate is allowed (or forced) to vary, will result in a decrease in the variation required of the companion state. The plots of the frequency state estimates in Figure 2 confirm this. In fact, too much process noise for the phase state prevented the frequency estimate from changing at all. The important general observation is that the choice of "Q" for even a single state can effect the estimates of other states.

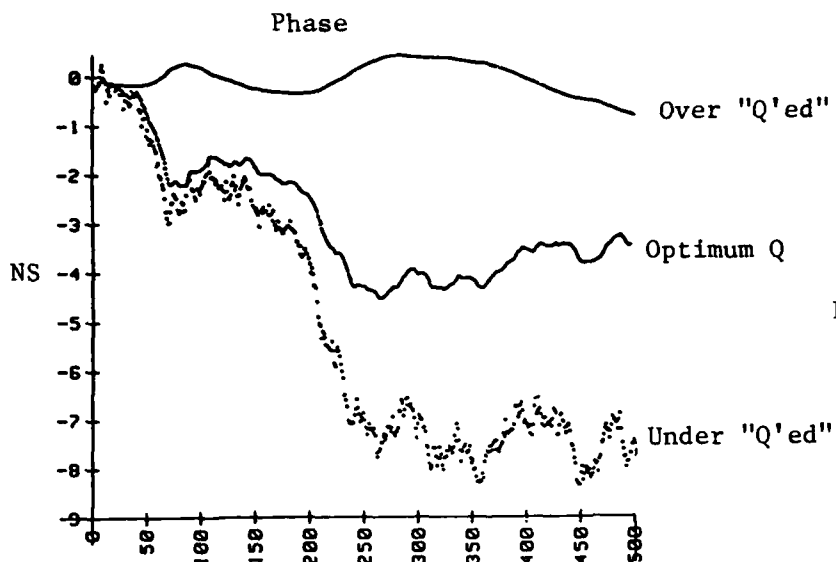


Figure 1

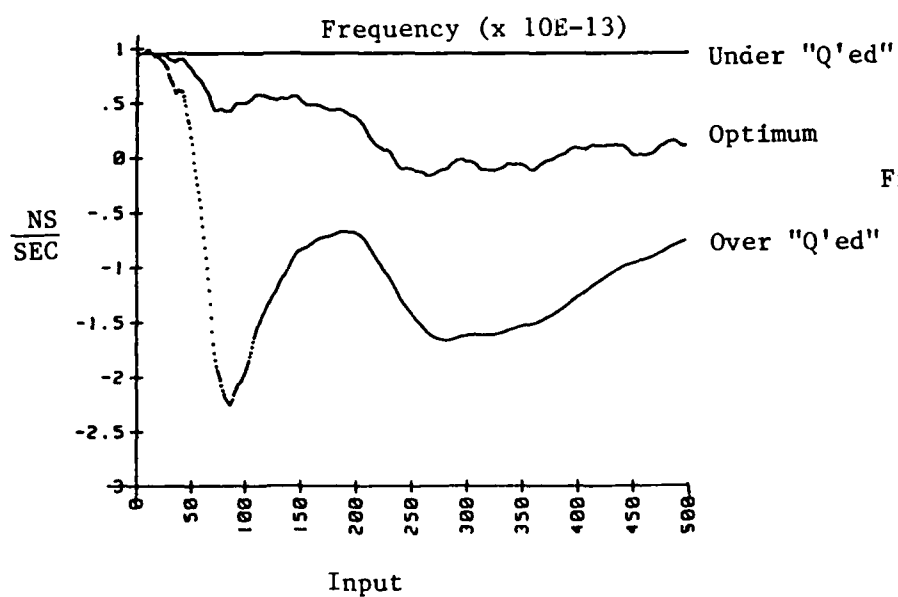


Figure 2

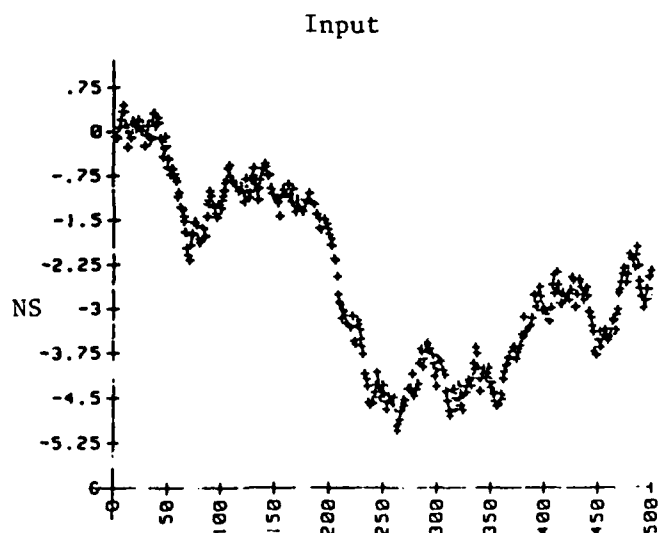


Figure 3

REFERENCES

1. Maybeck, P.S. "Stochastic Models, Estimation, and Control", Vol.1 Academic Press, 1979
2. Chaffee, J. "Derivation of the Process Noise Matrix for Satellite Clocks", unpublished memorandum (QAO Corp), March 1982.
3. Chaffee, J. "Exact Relationship between Epoch and Current Time Filters", unpublished memorandum (QAO Corp), October 1982.
4. Sorenson, H.W., Stubberud, A.R. "Linear Estimation Theory", Ch 1 "Theory and Applications of Kalman Filtering", distributed by The National Technical Information Service (NTIS), U.S. Department of Commerce, AGARDograph No. 139 1970.
5. Barham P.M., Humphries, D.E. "Further Comments on the Derivation of Kalman Filters", same publication as above.
6. Barnes, J.A., Jones, R.H., Tryon, P.V., Allen, D.W. "Stochastic Models for Atomic Clocks", NASA Conference Publication 2265 (PTTI) 1982.

QUESTIONS AND ANSWERS

DR. WEISS:

UnderQ'ing is assuming a sigma too large or too small?

MR. VARNUM:

UnderQ'ing means that Q'ing is too small. I have under Q'd the phase state.

DR. WEISS:

So you are assuming that the sigma is smaller than it actually is for the variance of the process.

MR. VARNUM:

That's right. With the result that if you look in the filter, the uncertainty in that estimate is collapsing, and the gain is going down and less and less can be done to vary that state and it will tend to converge on a constant value, which you really don't want to happen for the phase if you have modeled the frequency as a constant. But underQ'd generally means you have put too little process noise in and overQ'd too much.

KALMAN FILTER ESTIMATES OF THE NAVSTAR SATELLITE CLOCK PARAMETERS

Paul S. Jorgensen
The Aerospace Corporation
El Segundo, California

ABSTRACT

As is now well known, the Navstar/Global Positioning System is being used for precise time transfer between widely separated locations on earth. A part of this service is to provide users with information regarding the clocks in the GPS satellites. This data comes from the Kalman filter estimates in the Master Control Station at Vandenberg. This paper presents the results of an analysis of the Kalman filter data and illustrates the day-to-day characteristics of the satellite clock parameters that are provided to the time transfer user community. The monitor station tracking data also has been investigated and this paper illustrates the characteristics of the data acquired at the four monitor stations located at Vandenberg, Guam, Hawaii and Alaska. The paper shows that there are systematic and random variations in the Kalman filter estimates of the clock parameters, as well as in the tracking data. The relationship between the tracking data and the Kalman filter estimated parameters is discussed in this paper.

INTRODUCTION

Before going into the body of this paper, a brief overview of how GPS works is appropriate. There are now five fully operating satellites: Navstar 3, 4, 5, 6, and 8 - plus Navstar 1, which is operating with a quartz oscillator. Navstar 3, 4, and 8 are operating with rubidium clocks and Navstar 5 and 6 employ cesium beam frequency standards. These satellites are tracked by the four monitor stations located at Vandenberg in California, and at Guam, Hawaii, and Alaska. These stations track the satellites whenever they are visible and transmit the tracking data to the Master Control Station at Vandenberg. Here the data are processed and the ephemeris and clock parameters for each satellite are continuously updated. Actually, the update occurs every 15 minutes, 96 times per day. The upload station is also located at Vandenberg. At least once per day a revised estimate of the satellite's ephemeris and clock parameters is uploaded to the satellite which, in turn, transmits this data down on its navigating signal. In this way, GPS navigation users know the satellite's precise location in space, as

well as the offset of the satellite clock from "GPS time." In general, GPS time is defined as the time of a selected monitor station clock, and usually the Vandenberg monitor station is selected for this purpose.

The ephemeris and clock parameters are updated in a complex Kalman filter. As of last August, Navstar 3, 4, 5, and 6 have their parameters estimated in a common partition, with a total of 57 parameters being solved for simultaneously. For each satellite there are 11 parameters (six ephemeris, two solar radiation pressure, and three clock states). There are two clock states for the three non-master monitor stations, a troposphere parameter for all four monitor stations, and three pole wander states.

A detailed study has been made of the day-to-day variations in the Kalman filter estimates of the satellite clock states, as well as in the satellite-to-monitor-station measurements. This results in a large mass of data. To limit the data to a manageable amount, this paper will discuss only one satellite, Navstar 3. The data covers the last two weeks of August 1983. Navstar 3 data was selected because it best illustrates the systematic behavior of the Kalman filter.

SATELLITE CLOCK PARAMETERS

The Kalman filter estimates three satellite clock parameters: phase, frequency, and frequency rate. All are estimated with reference to GPS time and, for the data presented here, the reference was the Vandenberg monitor station clock. Frequency rate is also called the "aging" parameter and is a parameter more peculiar to rubidium clocks than to cesium clocks.

A word about units may be of value. At the Master Control Station, the clock parameters are estimated in units of nanoseconds, nanoseconds per second, and nanoseconds per second squared for phase, frequency, and frequency rate, respectively. For the purpose of this paper, it was more meaningful to use units that relate closely to the navigation problem; instead of nanoseconds, meters are used and instead of seconds, days are used. Thus, the units are meters, meters per day, and meters per day squared.

A difficulty presented by the data is that the phase and frequency estimates can be very large values. In order to be able to "see" the data, the phase estimates are least-squares fitted to a straight line and only the residuals to this straight line fit are analyzed and plotted. Thus, the average phase and frequency are removed from the phase estimates. Likewise, the average frequency is removed from the Kalman filter frequency estimates. No adjustment is made to the Kalman filter estimates of frequency rate.

USER RANGE ERROR

A yardstick often used by the Navstar/GPS Program Office is "user range error" (URE). This consists of two components, ephemeris and clock. Let us concern ourselves only with the clock component. After the satellite is uploaded with the latest Kalman filter estimates of the three clock parameters, the filter continues to update its estimate of the satellite clock parameters. However, users must rely on the three parameters that were uploaded earlier in time. The new, revised estimate of the satellite clock phase is not available to the users until a new upload is sent up to the satellite. The difference between the current estimate of clock phase and the clock phase that users obtain from the satellite's navigation data message is the clock component of the user range error. It should be noted that the users depend heavily on the Kalman filter estimate of satellite clock frequency at the time of upload to determine the phase offset of the clock for the time they are navigating. On the other hand, the Kalman filter estimate of satellite clock phase does not have this dependability. This difference between the real-time Master Control Station determination of satellite clock phase and how the user obtains clock phase suggests the following as a reasonable measure of the difference in the data available at the two situations.

The basic question is the consistency between the Kalman filter estimates of phase and frequency. These parameters are the integral and differential of each other. A way to evaluate the performance of the Kalman filter at the Vandenberg Master Control Station is to numerically integrate the estimate of frequency, thereby creating a phase estimate based on the frequency estimate (this is akin to what the user must contend with). By subtracting this frequency-derived phase estimate from the actual real-time Kalman filter estimate of phase, a measure of the internal consistency of the Kalman filter is obtained. Several plots of this measure are given in this paper and will be related to the Navstar/GPS measurements obtained at the monitor stations.

MEASUREMENT RESIDUALS

The inputs to the Kalman filter are the smoothed measurements of pseudo-range and delta pseudo-range, which are obtained once every 15 minutes from every monitor station that can observe the satellite. These times are referred to as K-points. It should be noted that, with the current configuration of satellites and monitor stations, as many as 24 sets of measurements can, in principle, be made at each K-point. In practice, geometrical limitation limits the maximum to some lesser number; but, in any event, a great deal of data are fed into the filter. The delta pseudo-range data are the measured changes in the pseudo-range measurement within a 15-minute interval. It has been shown that the delta measurements play a very small role in the Kalman

filtering process. For all intents and purposes, the filter operates almost entirely on the pseudo-range measurements.

The Kalman filter actually uses, as inputs, the so-called measurement residuals. The Master Control Station computes the expected value of pseudo-range, based on its latest estimate of the values of all the states being estimated. The residual is the difference between the actual pseudo-range measurement and the predicted value. Note that, if the system states were known perfectly, these two pseudo-ranges would be the same. Thus, the pseudo-range measurement residual is a measure of one or more of the states not being correctly estimated. At the present time, the tuning of the Kalman filter is such as to place most of the "blame" on the satellite clock parameters. The filter tends to adjust the satellite clock parameters more often than it does other system parameters, such as ephemeris and monitor station clocks.

In attempting to observe a correlation between the measurements and the satellite clock parameters, a simple device has been adopted to condense the measurement residual data. At each K-point all the measurement residuals from a particular satellite to whichever monitor stations can observe the satellite are added to form a composite total measurement residual. (The same convenience might be obtained by plotting all the measurement data on the same page.)

RESULTS

Analysis data have been collected for the period from 15 August 1983 through 28 August 1983. The Kalman filter estimates of the phase, frequency, and frequency rate of the rubidium clock on Navstar 3, relative to the Vandenberg monitor station clock, are shown on Figures 1, 2, and 3, respectively. In the case of phase, the plot is the residual from a least-squares fit to a straight line. The average has been removed from the frequency plot.

An examination of these figures reveals two distinct characteristics. For all three parameters there is a clearly repetitive day-to-day structure in their estimates. The second characteristic is the obvious correlation in the estimates of phase, frequency, and frequency rate. This flies in the face of mathematical reality in that one would not expect direct correlation between a quantity and its time differential (or time integral). The inexorable conclusion is that this repetitive structure and correlation between parameters is a reflection of the operation of the Kalman filter and is not a true day-to-day picture of satellite clock performance.

The data in Figure 4 show the integral of the Kalman filter frequency estimate and are, therefore, a phase measurement based on frequency. The initial value was set to the initial actual phase estimate shown in Figure 1. This integral is obviously smoother than the direct Kalman

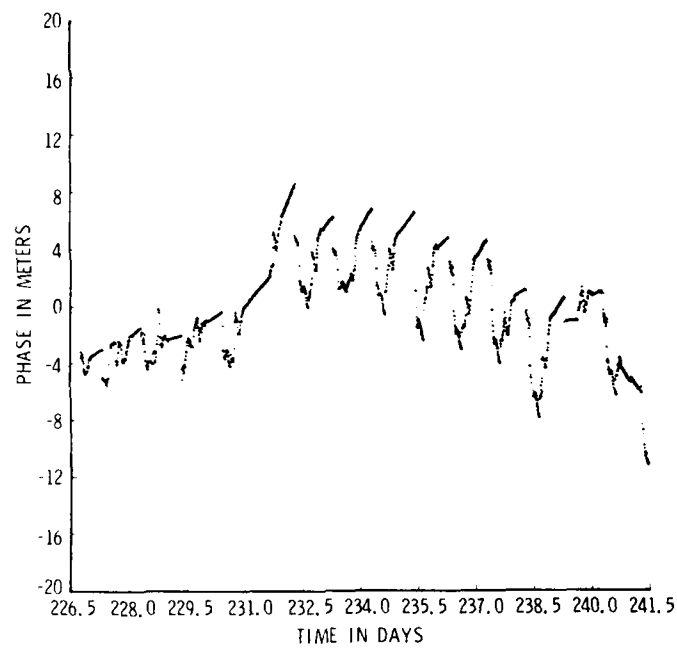


Figure 1. Kalman Clock Data, Navstar 3, Phase

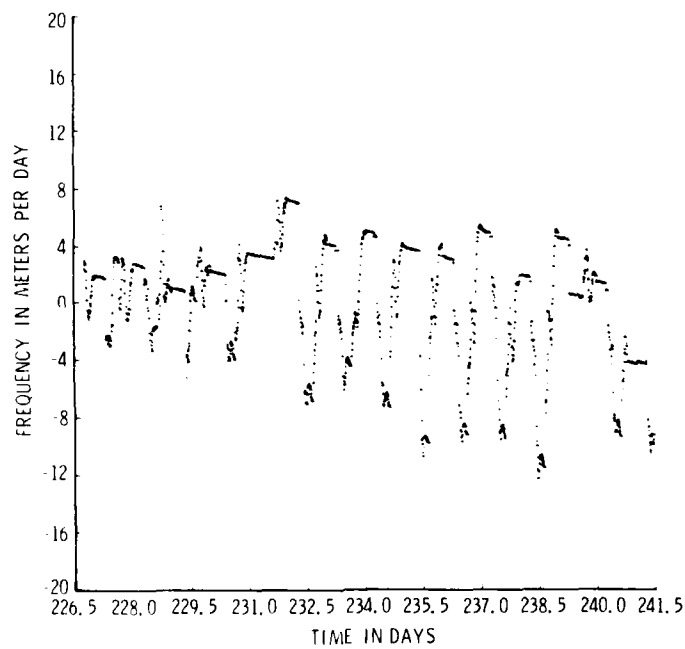


Figure 2. Kalman Clock Data, Frequency

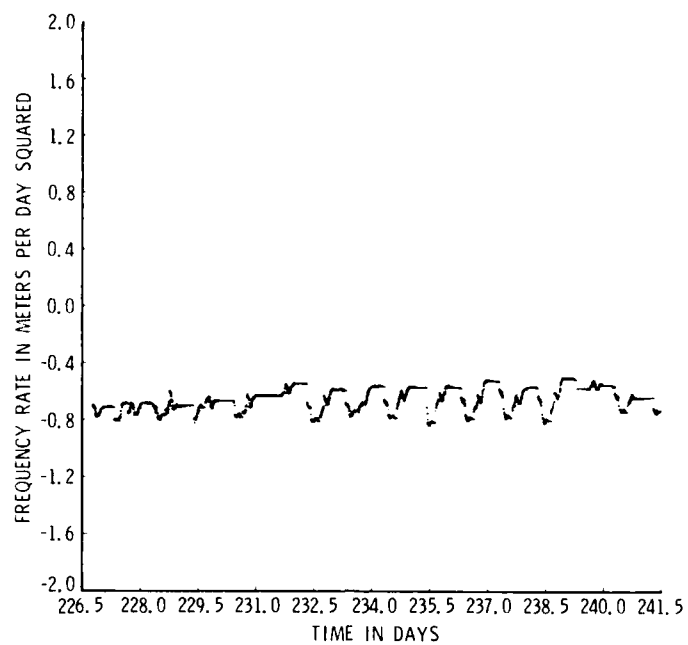


Figure 3. Kalman Clock Data, Frequency Rate

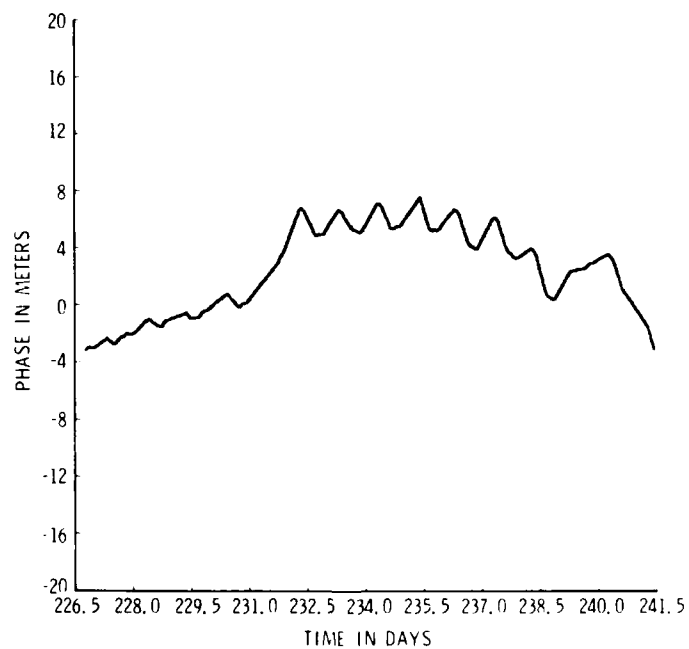


Figure 4. Kalman Clock Data, Frequency Integral

filter estimates shown in Figures 1 through 3. Yet, note the distinctive saw-tooth pattern over most of the two weeks. The difference between the actual real-time estimate of phase (Figure 1) and the phase obtained by integrating the frequency estimate (Figure 4) is shown in Figure 5. This quantity has been discussed previously and is akin to "user range error." It will be shown that this measure of satellite clock performance is related to the pseudo-range measurement residuals. Let us refer to the plot on Figure 5 as phase difference. The value of this representation is that it shows the day-to-day activity of the Kalman filter, whereas the long term (two weeks) variation in clock behavior is removed.

A part of the data on Figure 5 has been expanded to better observe the day-to-day response of the Kalman filter estimate of clock phase to the pseudo-range residuals. The data for five days, 22 August through 26 August 1983, are shown in Figures 6 through 10. A comparison of these five plots clearly shows the repetitive nature of the Kalman filter from one day to the next.

The pseudo-range measurement residuals at the four monitor stations are shown in Figures 11 through 14 for Vandenberg, Guam, Hawaii, and Alaska, respectively, for 22 August 1983. This corresponds in time to the phase difference Kalman filter estimates in Figure 6. A comparison of Figure 6 with Figures 11 through 14 reveals how the Kalman filter reacts to the inputs to the filter.

To better illustrate the relationship between the Kalman filter estimates of satellite clock phase and the measurement residuals, the residual data in Figures 11 through 14 have been combined. This is done simply by adding up the measurement residuals at the four monitor stations for each 15-minute K-point. The resulting total measurement residuals are shown in Figure 15. An examination of Figures 6 and 15 clearly shows how the Kalman filter estimate of satellite clock phase responded to the measurements on 22 August 1983. The total measurement residuals have also been obtained for the next four days, August 23 through 26. These total residuals are shown in Figures 16 through 19. Comparing Figures 7 and 16, 8 and 17, 9 and 18, and 10 and 19, gives a clear illustration of the response of the Kalman filter to the measurements for these four days. In addition, an examination of Figures 15 through 19 reveals the highly repetitive characteristics of the pseudo-range measurements from one day to the next. This, of course, accounts for the day-to-day repetition of the Kalman filter estimate of the satellite clock parameters.

DISCUSSION

With satellites 10,900 nmi above the earth and monitor stations located at intervals of several thousand miles across the Pacific, it should come as no surprise that some unknown bias lurks in the system. Some

systematic effect is causing a day-to-day repeated pattern in the pseudo-range measurements taken at the monitor stations, an effect on the order of a few meters. Overall, the effect on the GPS user's navigation accuracy is quite acceptable. Nevertheless, being repetitive, it should be possible to root out this effect and eliminate it. Hopefully, this will be accomplished for the operational configuration of 18 satellites, five monitor stations distributed worldwide, and three or four ground antennas that allow for the uploading of each satellite three times per day.

The Kalman filter overreacts to the pseudo-range measurements taken at the monitor stations. It simply does not filter enough. The Kalman filter is "tuned" to a mythical world where all errors in the system emanate from a Gaussian, random noise process. That is not the real world, in which systematic, unknown effects are present. The strong correlation between the Kalman filter estimates of phase, frequency, and frequency rate (parameters that are differentials and integrals of each other) is a clear-cut indication of mis-tuning of the filter. The day-to-day repetition in these estimates, together with their overreaction to the measurement residuals, further supports this contention.

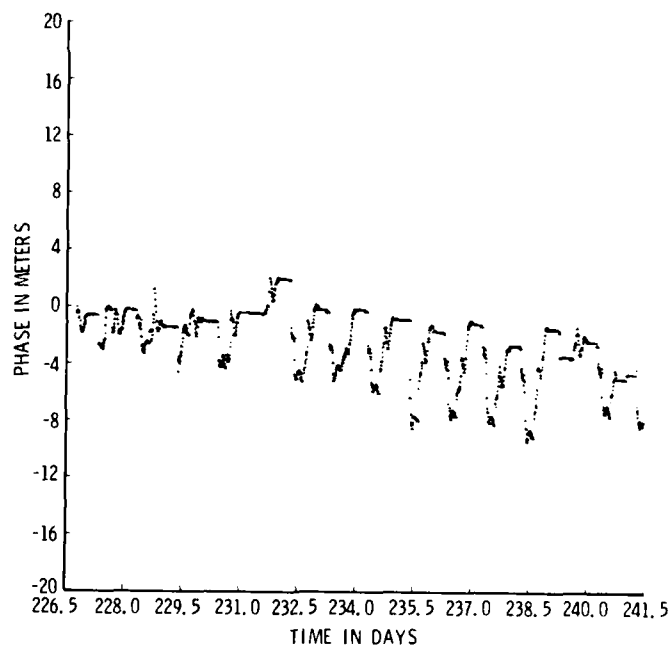


Figure 5. Kalman Clock Data, Phase Difference

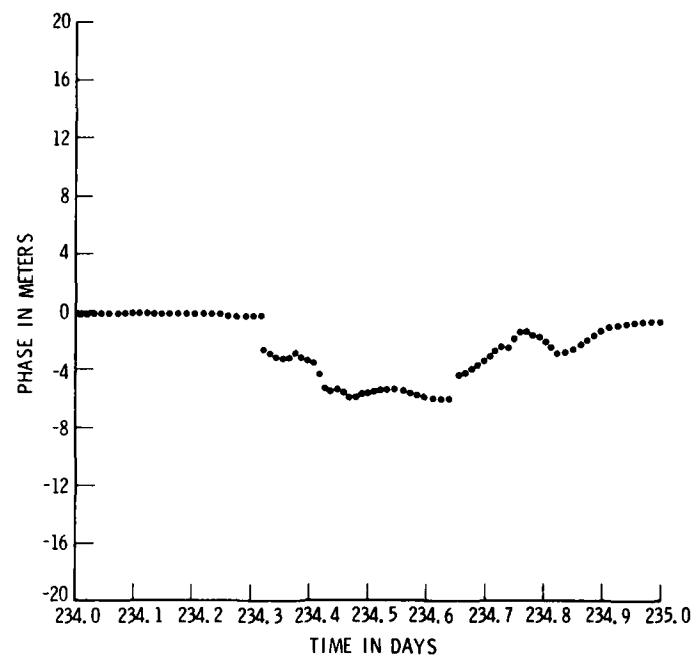


Figure 6. Kalman Clock Data, 22 August 1983

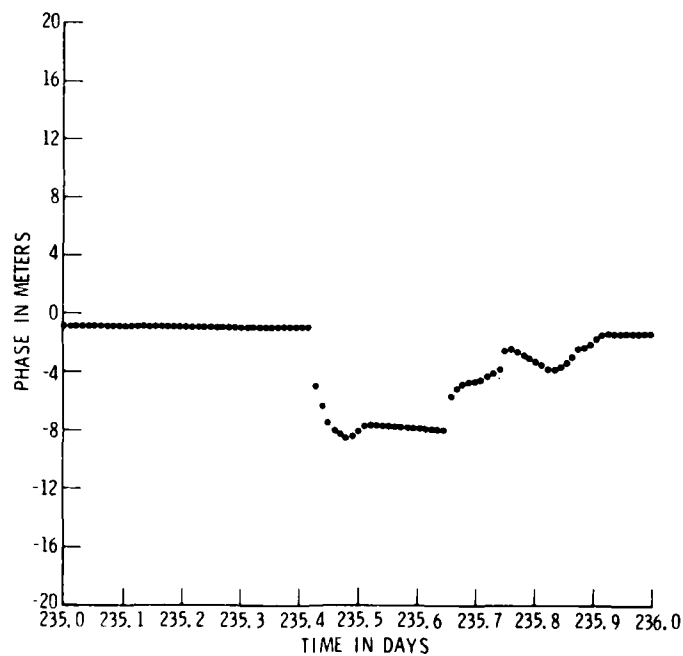


Figure 7. Kalman Clock Data, 23 August 1983

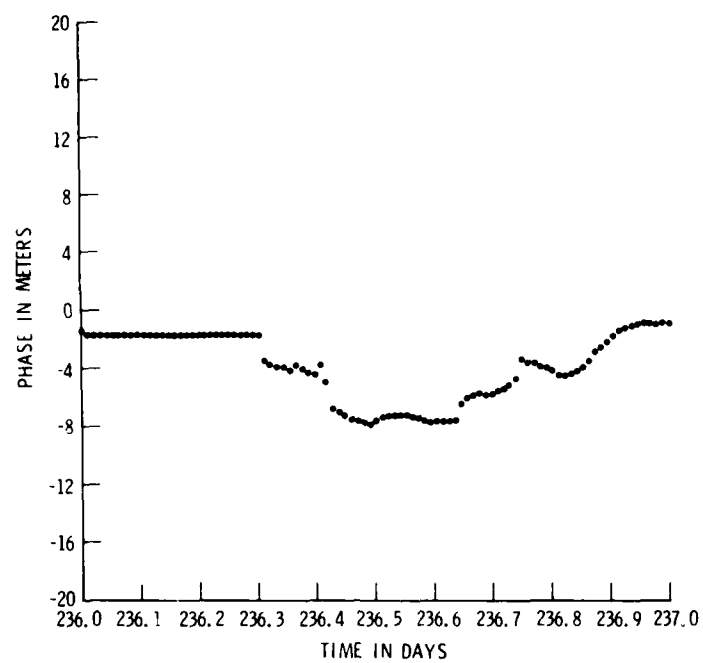


Figure 8. Kalman Clock Data, 24 August 1983

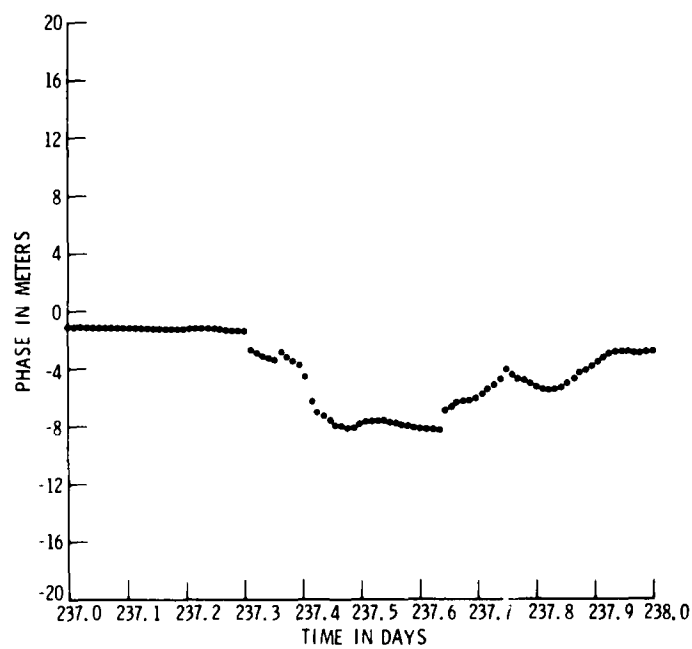


Figure 9. Kalman Clock Data, 25 August 1983

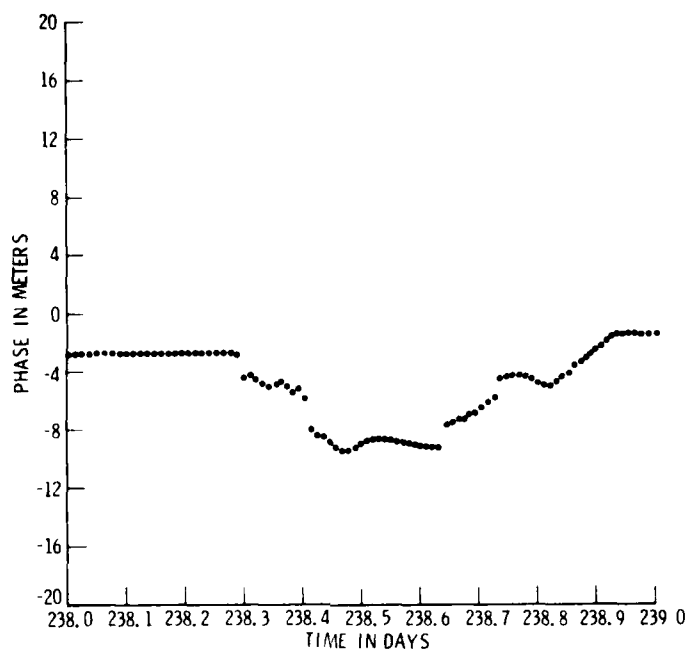


Figure 10. Kalman Clock Data, 26 August 1983

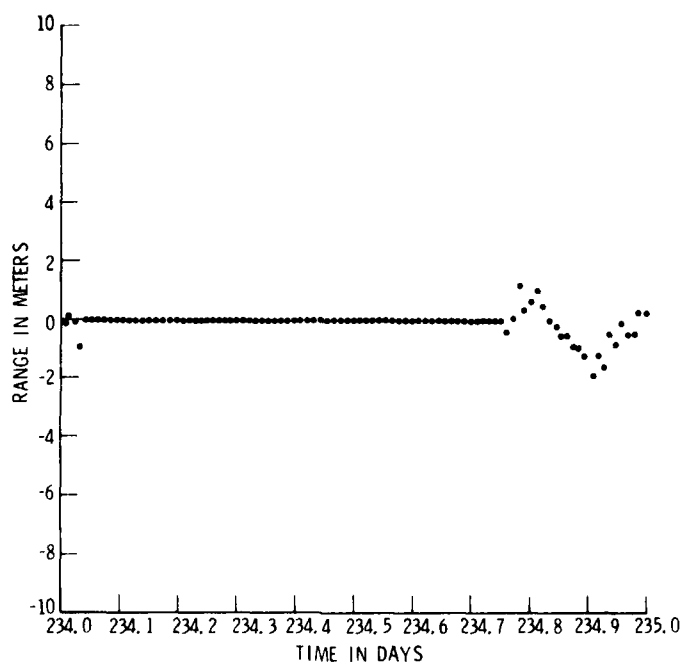


Figure 11. Kalman Residual Data, Vandenberg

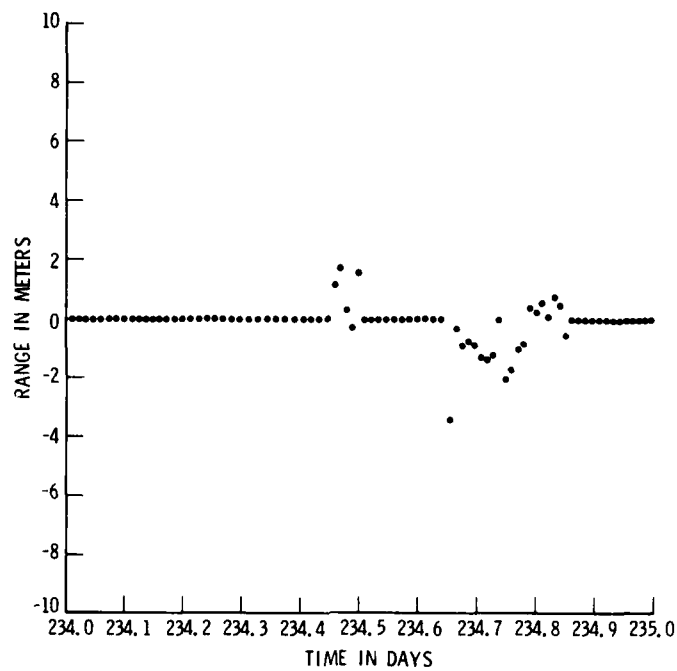


Figure 12. Kalman Residual Data, Guam

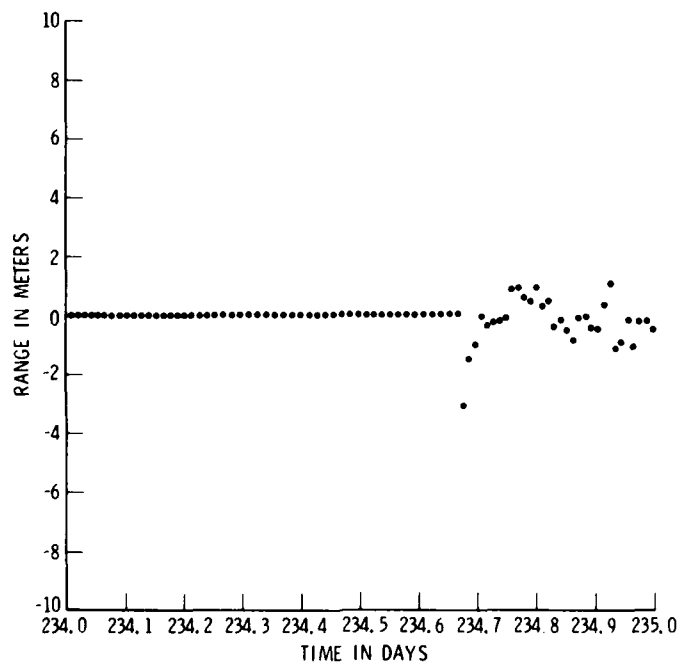


Figure 13. Kalman Residual Data, Hawaii

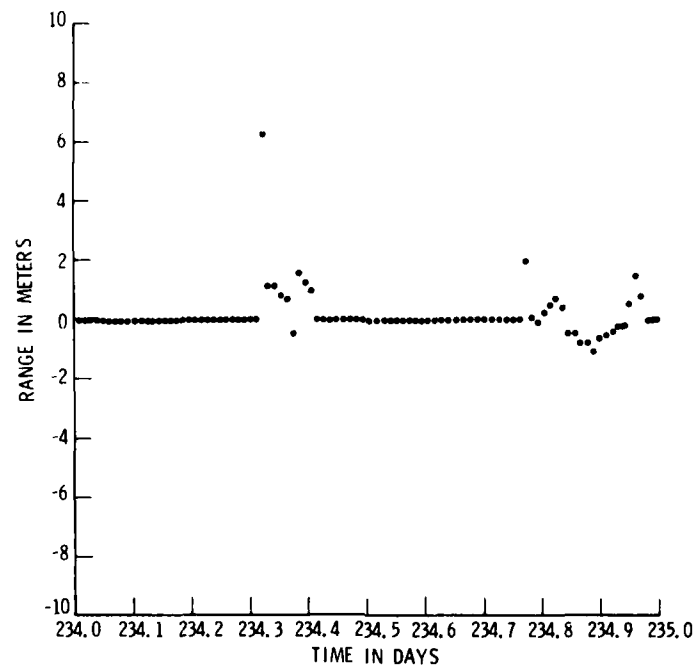


Figure 14. Kalman Residual Data, Alaska

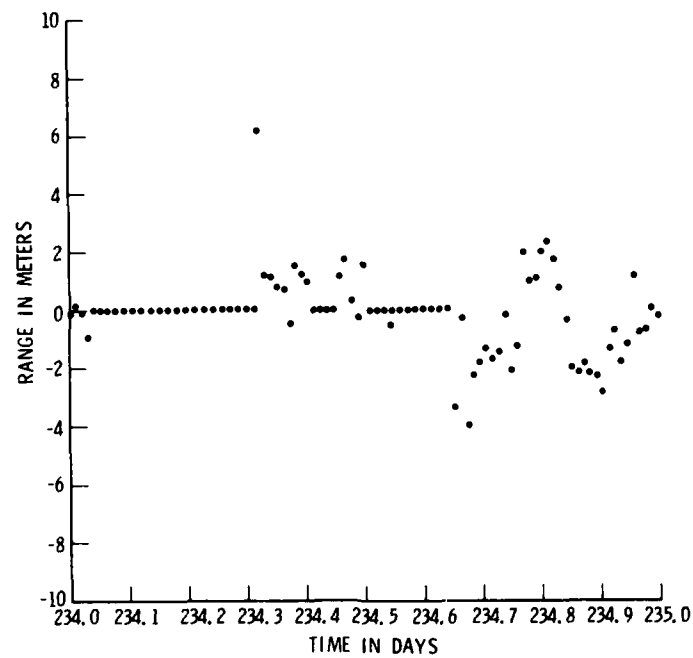


Figure 15. Kalman Residual Data, Total, 22 August 1983

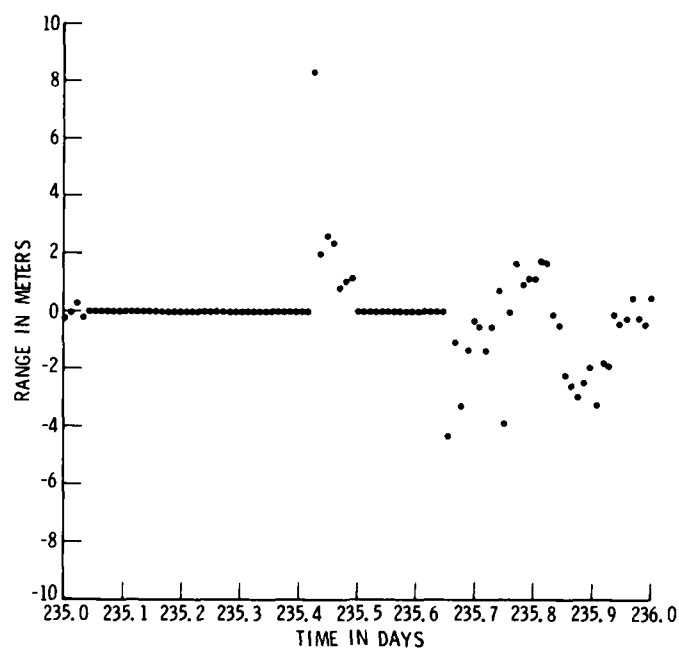


Figure 16. Kalman Residual Data, Total, 23 August 1983

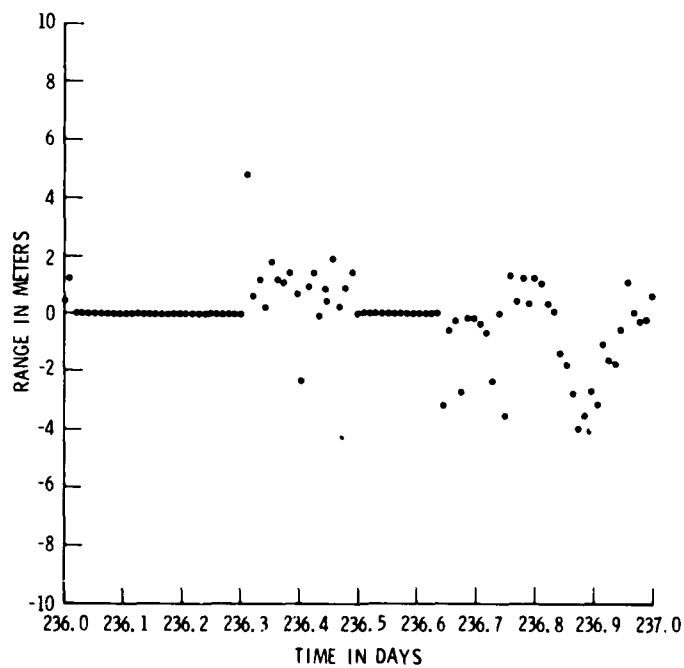


Figure 17. Kalman Residual Data, Total, 24 August 1983

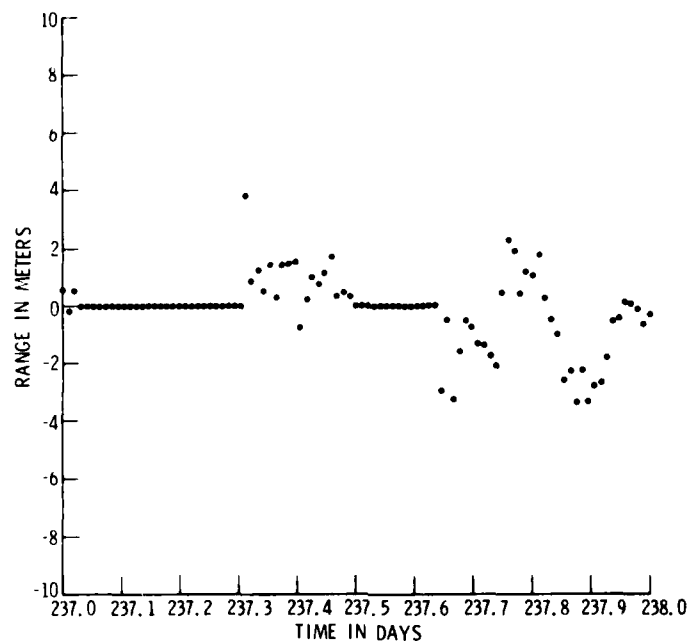


Figure 18. Kalman Residual Data, Total, 25 August 1983

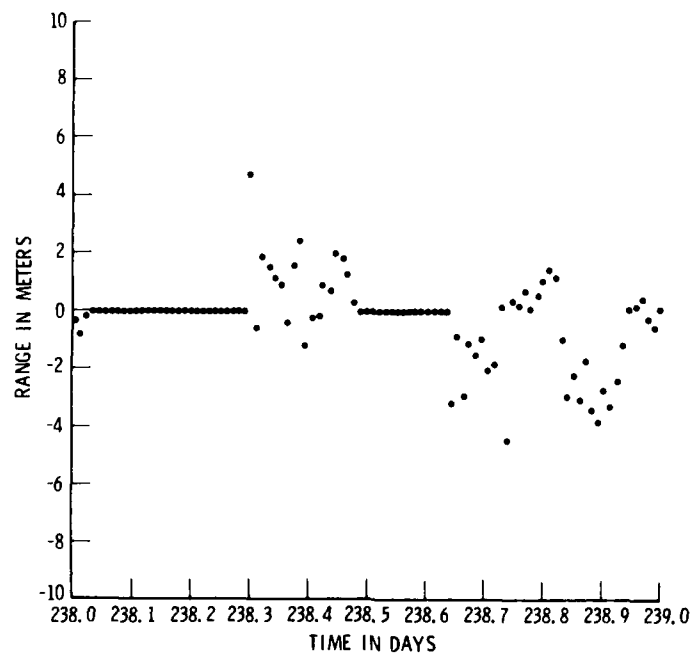


Figure 19. Kalman Residual Data, Total, 26 August 1983

QUESTIONS AND ANSWERS

MR. CARMAN:

I would like to ask one quick question. Are those epoch or current state plots?

MR. JORGENSEN:

These are current time.

MR. CARMAN:

I would like to point out for some that don't maybe know too much about G.P.S., that we are processing data for short periods each day, so that you would expect that you would get periodic phenomena with one-day periods. So the fact that you saw structure in the long term plots that had one-day periods, you could expect that.

In fact, between the time you process data during one day and the next day, you are propagating whatever states that have estimated for fifteen, maybe twenty, hours.

MR. JORGENSEN:

Right.

MR. CARMAN:

So that any miss-estimation you had in the ephemeris, even if you had perfect clock estimates, the random behavior in the clock is going to do something different than you are systematically trying to predict. So you would expect at the time of processing data the following day, you are going to have residuals with which to contend. I don't think those residuals that were shown were that bad.

MR. JORGENSEN:

That's right. The satellites are limited to fourteen-thousand miles away; and in the case of Alaska we should keep in mind that during one pass, the satellite is over there and in a second pass of satellite over there, so we are talking about enormous geometry; geometry that in totality is of the order of forty-thousand kilometers. We're talking about the worst case residual being eight meters. That point should be put into perspective.

MR. CARMAN:

The other point--because the ephemeris or satellite model behavior can be expected to be rather constant from one day to the next, when a residual appears in the order of five or six or eight meters, the first place the filter is going to try to put it is into the clock, specifically into the phase because it's the most observable state, directly correlating to range; one to one. So the immediate response of the filter is to adjust the phase to satisfy the measurement. So you might get a little over-reaction in the phase, but I think you have to let the filter settle a bit and that first residually doesn't mean very much. The fact that integrated frequency measurements, or frequency estimates, should be the same as your phase measurements, I don't understand that, because if that were really to be true, you wouldn't be estimating phase and frequency. You would only have to estimate the frequency state, integrate it and you would have the phase state.

So the filter is free, I think, within the mathematics to readjust its allocation between phase and frequency from one measurement to the next and there's no constraint that says that the integrated frequency estimate has to be the same as the phase estimate. I don't think it's an absurdity that it happens and I don't think it's a mathematical impossibility.

MR. ALLAN:

The analysis that we have done on separation of ephemeris that Dr. Weiss reported yesterday would very much support your conclusion that there are other systematics besides the clocks and those, in fact, are probably in the ephemeris. I think that strongly supports your conclusion.

DR. WINKLER:

One fact I think one has to accept is the measurement, and it's the time of arrival measurement, and you put the error into the clock because you don't want to do anything else. But my question is: does the Kalman filter--use, as a model, the oscillating elliptical elements?

MR. JORGENSEN:

Yes.

DR. WINKLER:

And it's quite clear that 12-hour orbit will have systematic perturbations with a period of only one day, half-day and multiples of that, and if his perturbations are not included in the filter, you would exactly expect the kind of performance that you get because we see the same thing. If we observe time measurements in distant places, we have again this up, down, up, down with a period of one day, and the amplitude is precisely the same as you have shown here.

MR. JORGENSEN:

All right. As Fran Varnum pointed out earlier, we use epoch states; that is to say, we use essentially the initial conditions, at say, the beginning of the two week period; however, in the operation of the whole process, we also use a two-week reference orbit developed by the Naval Surface Weapons Laboratory, which covers ahead from that two-week period which has the whole nine yards. It has all the physical things you can think about; all the gravity terms, solar radiation pressure, and what have you.

So it's really not quite oscillating elements. It's really the elements at zero time at the beginning of the two-week period.

DR. WEISS:

It's hard to believe that the time and frequency of the clocks themselves are correlated.

MR. JORGENSEN:

That's right. So the conclusion must be that what you saw regarding what the Kalman Filter is estimating has to do with the total estimation process, the combination of the ephemeris and clock estimation, and I think you must agree what must be is some really small systematic affect that, on a day-to-day basis, exists in the system.

DR. WEISS:

Well, my question is, how are the frequency and time of the clocks themselves measured, because it seems to me that what that implies is that there is a correlation in the measurement of those two quantities.

DR. JORGENSEN:

Well, the Kalman Filter estimates of the satellite clock parameters is it. That is what the world of users take the satellite clock to be doing; and, indeed, on a short term basis, there does appear to be some uncertainty in those estimates. But, on the other hand, as I pointed out, over the entire two-week period, the thing works.

You do have the proper relationship between frequency and phase, and if you notice also, the frequency rate plot appears to be consistent with the other two parameters over the two-week period. For all intents and purposes, the only thing we measure is the one-way ranging measurements from the satellite to the monitor stations.

DR. WEISS:

So you don't measure the frequency of the transmitted frequency at all?
You just measure the time of arrival?

MR. JORGENSEN:

That's correct.

DR. WEISS:

Well, then you are not actually directly measuring the frequency of the clock.

DR. JORGENSEN:

That's correct. Well, I would like to clarify that. In the particular Kalman Filter we now use there is also a so-called Delta range measurement, which is within the fifteen minute period, the change in range. It turns out that if you look into the details of the thing, the way the filter works depends much more heavily on pseudo range measurements as opposed to the Delta pseudo range measurements.

MR. VANMELA:

Mr. Vannela from Rockwell. To bring a little reality to the problem, we have a space craft up there right now, spacecraft II that was launched in July, and it just so happens that we have some Kalman Filter plots, nanoseconds per second and they have a very periodic change. Every day, it goes up and down, up and down, every day. So therefore, if everybody believed that, then the clock is really in trouble; but there seem to be other parameters involved, like the ephemeris data may be wrong or the Kalman Filter may be wrong, or slightly Q'd different. So that in the real world Rockwell has to look and Air Force has to look. We talked to each other, and the Air Force says the clock is jumping around too much, but it may be due to the application of the Kalman Filter. So that's what's actually happening. This was in the latter part of November.

DR. KLEPCZYNSKI:

Everybody seems to be accusing the ephemeris of the orbit. One thought that came to my mind here is that you are combining observations made at four different sites, which in my thoughts give you very poor geometry for orbit determination, in the first place. It seems that the inverse problem of--if there are any errors in the station coordinates at your four stations and they're systematically different, not of the same system, errors in this will find their way into the orbits or the satellites because you are making your observations, or combining your observations in the four different stations at different times and if each one is off in position and you find an error in your satellite ephemeris.

MR. JORGENSEN:

You are expressing the obvious suspicion about something wrong with the coordinates of the Alaskan monitor station. On the other hand, I have been told that the station has been surveyed very accurately. So that's all I can say, as to the location of the monitor stations, don't forget the four locations were selected many years ago for the purpose of the Phase I program primarily to test out the system at Yuma, Arizona.

In the operational system we will have stations at totally different locations on earth, spread out around the entire globe, which of course will be better.

THE MEASUREMENT OF LINEAR FREQUENCY DRIFT IN OSCILLATORS

James A. Barnes
Austron, Inc., Austin, Texas

ABSTRACT

A linear drift in frequency is an important element in most stochastic models of oscillator performance. Quartz crystal oscillators often have drifts in excess of a part in ten to the tenth power per day. Even commercial cesium beam devices often show drifts of a few parts in ten to the thirteenth per year. There are many ways to estimate the drift rates from data samples (e.g., regress the phase on a quadratic; regress the frequency on a linear; compute the simple mean of the first difference of frequency; use Kalman filters with a drift term as one element in the state vector; and others). Although most of these estimators are unbiased, they vary in efficiency (i.e., confidence intervals). Further, the estimation of confidence intervals using the standard analysis of variance (typically associated with the specific estimation technique) can give amazingly optimistic results. The source of these problems is not an error in, say, the regressions techniques, but rather the problems arise from correlations within the residuals. That is, the oscillator model is often not consistent with constraints on the analysis technique or, in other words, some specific analysis techniques are often inappropriate for the task at hand.

The appropriateness of a specific analysis technique is critically dependent on the oscillator model and can often be checked with a simple "whiteness" test on the residuals. Following a brief review of linear regression techniques, the paper provides guidelines for appropriate drift estimation for various oscillator models, including estimation of realistic confidence intervals for the drift.

I. INTRODUCTION

Almost all oscillators display a superposition of random and deterministic variations in frequency and phase. The most typical model used is^[1]:

$$X(t) = a + b \cdot t + Dr \cdot t^2/2 + \phi(t) \quad (1)$$

where $X(t)$ is the time (phase) error of the oscillator (or clock) relative to some standard; a , b , and Dr are constants for the particular clock; and $\phi(t)$ is the random part. $X(t)$ is a random variable by virtue of its dependence on $\phi(t)$.

Even though one cannot predict future values of $X(t)$ exactly, there are often significant autocorrelations within the random parts of the model. These correlations allow forecasts which can significantly reduce clock errors. Errors in each element of the model (Eq. 1) contribute their own uncertainties to the prediction. These time uncertainties depend on the duration of the forecast interval, τ , as shown below in Table 1:

TABLE 1. GROWTH OF TIME ERRORS

<u>MODEL ELEMENT NAME</u>	<u>CLOCK PARAMETER</u>	<u>RMS TIME ERROR</u>
Initial Time Error	a	Constant
Initial Freq Error	b	$\sim \tau$
Frequency Drift	D_r	$\sim \tau^2$
Random Variations	$\phi(t)$	$\sim \tau^{3/2*}$

*The growth of time uncertainties due to the random component, $\phi(t)$, can have various time dependencies. The three-halves power-law shown here is a "worst case" model.[2]

One of the most significant points provided by Table 1 is that eventually, the linear drift term in the model over-powers all other uncertainties for sufficiently long forecast intervals! While one can certainly measure (i.e., estimate) the drift coefficient, D_r , and make corrections, there must always remain some uncertainty in the value used. That is, the effect of a drift correction based on a measurement of D_r , is to reduce (hopefully!) the magnitude of the drift error, but not remove it. Thus, even with drift corrections, the drift term eventually dominates all time uncertainties in the model.

As with any random process, one wants not only the point estimate of a parameter, but one also wants the confidence interval. For example, one might be happy to know that a particular value (e.g., clock time error) can be estimated without bias, he may still want to know how large an error range he should expect. Clearly, an error in the drift estimate (see Eq. 1) leads directly to a time error and hence the drift confidence interval leads directly to a confidence interval for the forecast time.

II. LEAST SQUARES REGRESSION OF PHASE ON A QUADRATIC

A conventional least squares regression of oscillator phase data on a quadratic function reveals a great deal about the general problems. A slight modification of Eq. 1 provides a conventional model used in regression analysis[3]:

$$X(t) = a + b \cdot t + c \cdot t^2 + \phi(t) \quad (2)$$

where $c = Dr/2$. In regression analysis, it is customary to use the symbol "Y" as the dependent variable and "X" as the independent variable. This is in conflict with usage in time and frequency where "X" and "Y" (time error and frequency error, respectively) are dependent on a coarse measure of time, t , the independent variable. This paper will follow the time and frequency custom even though this may cause some confusion in the use of regression analysis text books.

The model given by Eq. 2 is complete if the random component, $\phi(t)$, is a white noise (i.e., random, uncorrelated, normally distributed, zero mean, and finite variance).

II. EXAMPLE

One must emphasize here that ALL results regarding parameter error magnitudes and their distributions are totally dependent on the adequacy of the model. A primary source of errors is often autocorrelation of the residuals (contrary to the explicit model assumptions). While simple visual inspection of the residuals is often sufficient to recognize the autocorrelation problem, "whiteness tests" can be more objective and precise.

This section analyzes a set of 94 hourly values of the time difference between two oscillators. Figure 1 is a plot of the time difference (measured in microseconds) between the two oscillators. The general curve of the data along with the general expectation of frequency drift in crystal oscillators leads one to try the quadratic behavior (Model #1; models #2 and #3 discussed below). While it is not common to find white phase noise on oscillators at levels indicated on the plot, that assumption will be made temporarily. The results of the regression are summarized in a conventional Analysis of Variance, Table 2.

TABLE 2. ANALYSIS OF VARIANCE QUADRATIC FIT TO PHASE
(Units: seconds squared)

<u>SOURCE</u>	<u>SUM OF SQUARES</u>	<u>d.f.</u>	<u>MEAN SQUARE</u>
Regression	2.32E-9	3	
Residuals	4.26E-12	91	4.68E-14
Total	2.329E-9	94	2.48E-11

Coefficient of simple determination 0.99713

Parameters:

$$\begin{aligned}\hat{a} &= 1.10795E-5 \text{ (seconds)} & t\text{-ratio} &= 161.98 \\ \hat{b} &= 1.4034E-10 \text{ (sec/sec)} & t\text{-ratio} &= 152.02 \\ \hat{c} &= -3.7534E-16 \text{ (sec/sec}^2\text{)} & t\text{-ratio} &= -143.51\end{aligned}$$

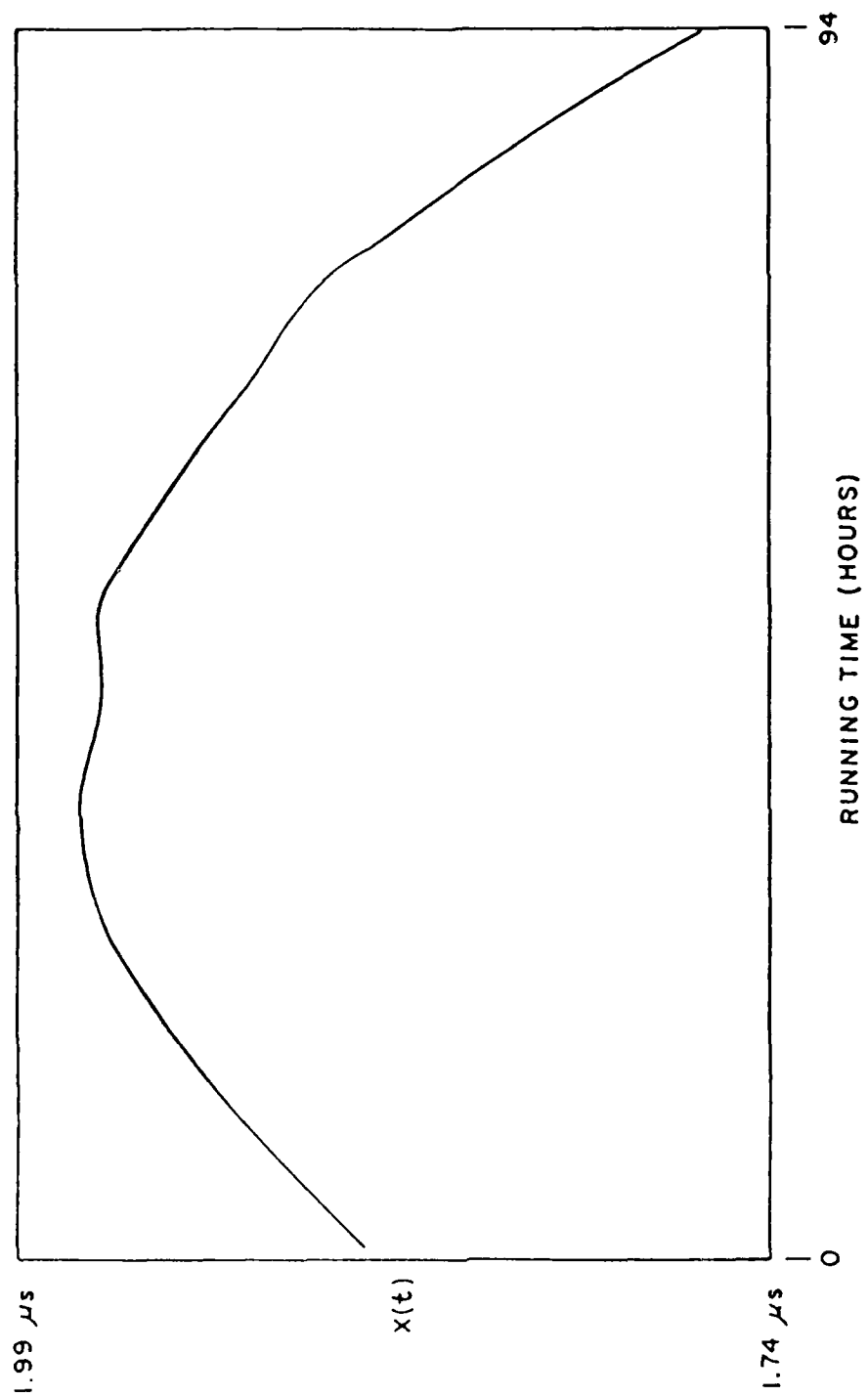


Fig. 1 - Phase difference

$$\hat{D}_r = 2\hat{c} = -7.507E-16 \text{ (about } -6.5E-11 \text{ per day)}$$

$$\text{Std. Error} = 0.05231E-16$$

(Note: \hat{a} is the value estimated for the a-parameter, etc.)

The Analysis of Variance, Table 2, above suggests an impressive fit of the data to a quadratic function, with 99.71% of the variations in the data "explained" by the regression. The estimated drift coefficient, D_r , is $-7.507E-16$ (sec/sec²) or about $-6.5E-11$ per day --- 143 times the indicated standard error of the estimate. However, Figure 2, a plot of the residuals, reveals significant autocorrelations even visually and without sensitive tests. (The autocorrelations can be recognized by the essentially smooth variations in the plot. See Fig. 5 as an example of a more nearly white data set.) It is true that the regression reduced the peak-to-peak deviations from about 18 microseconds to less than one microsecond. It is also true that the drift rate is an unbiased estimate of the actual drift rate, but the model assumptions are NOT consistent with the autocorrelation visible in Fig. 2. This means that the confidence intervals for the parameters are not reliable. In fact, the analysis to follow will show just how extremely optimistic these intervals really are.

At this point we can consider at least two other simple analysis schemes which might provide more realistic estimates of the drift rate and its variance. Each of the two analysis schemes has its own implicit model; they are:

- (2) Regress the beat frequency on a straight line.
(Model: Linear frequency drift and white FM.)
- (3) Remove a simple average from the second difference of the phase.
(Model: Linear frequency drift and random walk FM.)

Continuing with scheme 2, above, the (average) frequency, $\bar{Y}(t)$, is the first difference of the phase data divided by the time interval between successive data points. The regression model is:

$$\bar{Y}(t) = b + D_r \cdot t + \epsilon(t) \quad (3)$$

where $\epsilon(t) = [\phi(t + \tau_0) - \phi(t)]/\tau_0$. Following standard regression procedures as before, the results are summarized in another Analysis of Variance Table, Table 3.

TABLE 3. ANALYSIS OF VARIANCE LINEAR FIT TO FREQUENCY
(Units: sec²/sec²)

<u>SOURCE</u>	<u>SUM OF SQUARES</u>	<u>d.f.</u>	<u>MEAN SQUARE</u>
Regression	1.879E-18	2	
Residuals	2.084E-20	91	2.29E-22
Total	1.899E-18	93	2.042E-20

(Note: Taking the first differences of the original data set reduces the number of data points from 94 to 93.)

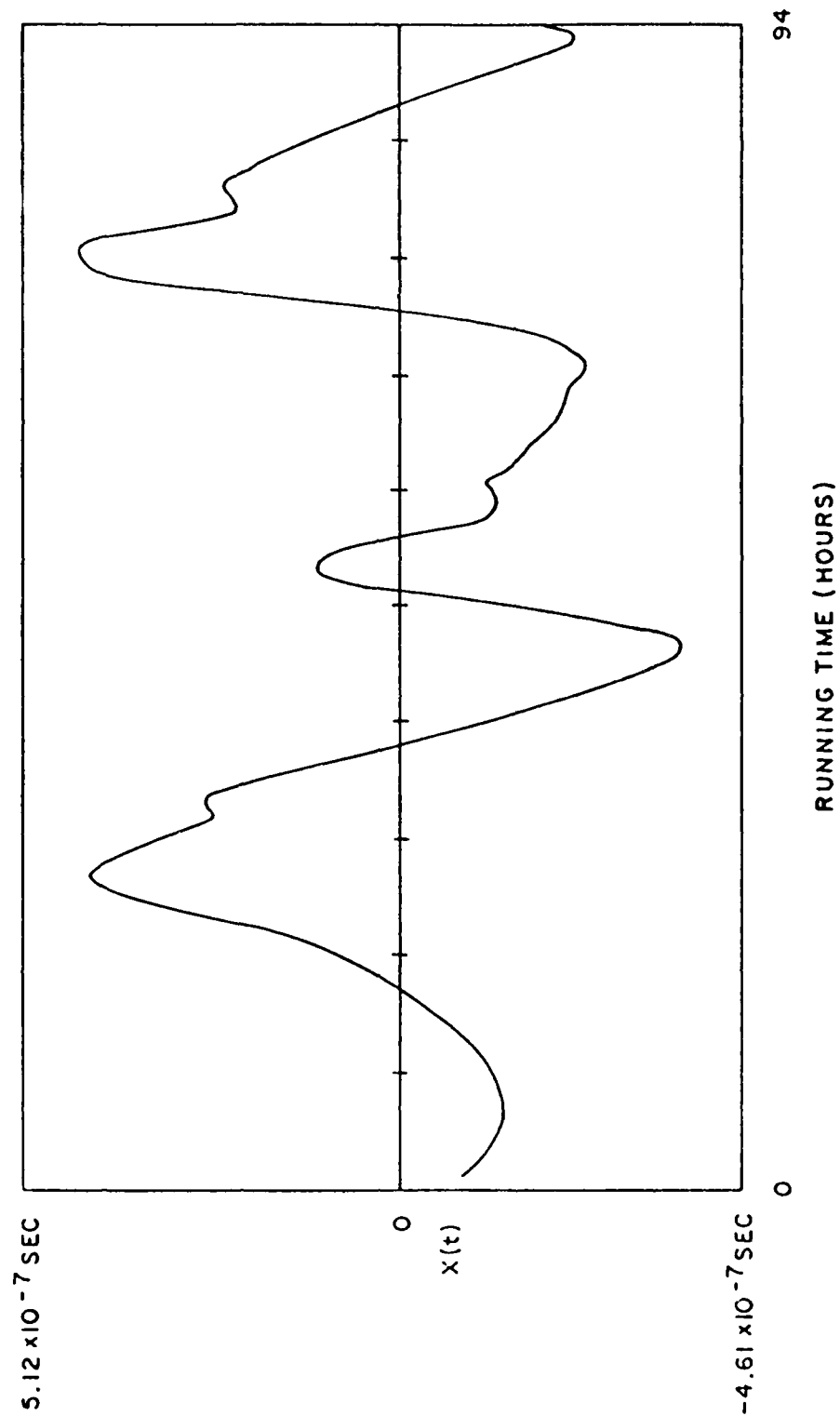


Fig. 2 - Residuals from quadratic fit to phase

Coefficient of simple determination 0.9605

Parameters:

$$\hat{b} = 1.049E-10 \text{ (sec/sec)} \quad t\text{-ratio} = 3.32$$

$$\hat{D}_r = -7.635E-16 \text{ (sec/sec}^2\text{)} \quad t\text{-ratio} = -4.70$$
$$\text{Std. Error} = 0.1624E-16 \text{ (sec/sec}^2\text{)}$$

While the drift rate estimates for the two regressions are comparable in value ($-7.507E-16$ and $-7.635E-16$), the standard errors of the drift estimates have gone from $0.052E-16$ to $0.162E-16$ (a factor of 3). The linear regression's coefficient of simple determination is 96.05% compared to 99.17% for the quadratic fit. Figure 3 shows the residuals from the linear fit and they appear more nearly white. A cumulative periodogram^[4] is a more objective test of whiteness, however. The periodogram, Fig. 4, does not find the residuals acceptable at all.

IV. DRIFT AND RANDOM WALK FM

In the absence of noise, the second difference of the phase would be a constant, $D_r \cdot \tau_0^2$. If one assumes that the second difference of the noise part is white, then one has the classic problem of estimating a constant (the drift term), in the presence of white noise (the second difference of the phase noise). Of course, the optimum estimate of the drift term is just the simple mean of the second difference divided by τ_0^2 . The results are summarized below, Table 4:

TABLE 4. SIMPLE MEAN OF SECOND DIFFERENCE PHASE

$$\text{Simple mean} \quad \hat{D}_r = -6.709E-16 \quad t\text{-ratio} = -2.45$$

$$\text{Degrees of Freedom} = 91$$

$$\text{Standard Deviation} \quad \hat{s} = 26.2405E-16$$

$$\text{Standard Deviation of the Mean} = 2.7358E-16$$

Figure 5 shows the second difference of the phase after the mean was subtracted. Visually, the data appear reasonably white, and the periodogram, Fig. 6, cannot reject the null hypothesis of whiteness. Now the standard error of the drift term is $2.735E-16$, 52 times larger than that computed for the quadratic fit! Indeed, the estimated drift term is only 2.45 times its standard error.

V. SUMMARY OF TESTS

The analyses reported above were all performed on a single data set. In order to verify any conclusions, all three analyses used above were performed a total of four times on four different data sets from the same pair of oscillators. Table 5 summarizes the results:

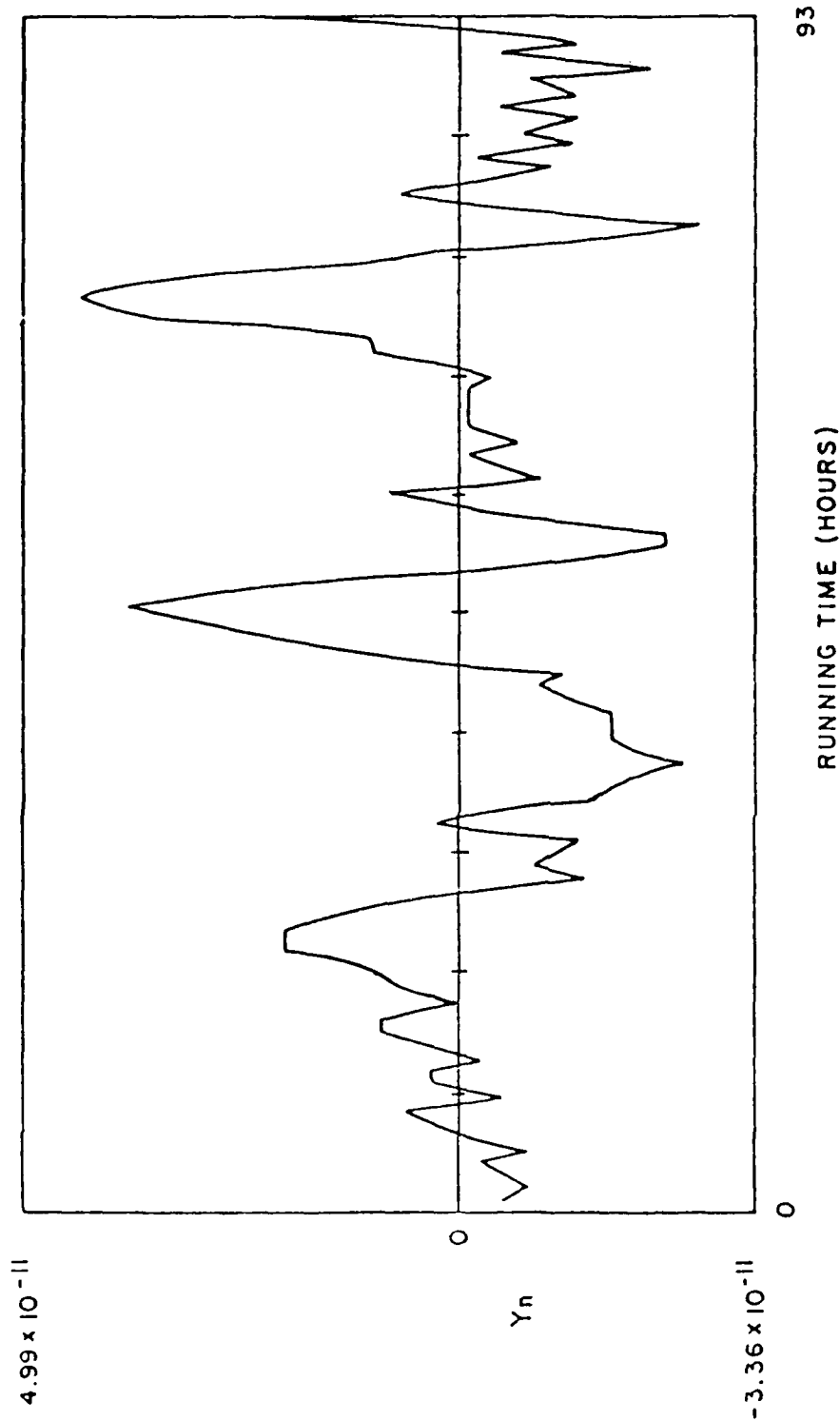


Fig. 3 - Frequency residual
(1st diff-lin)

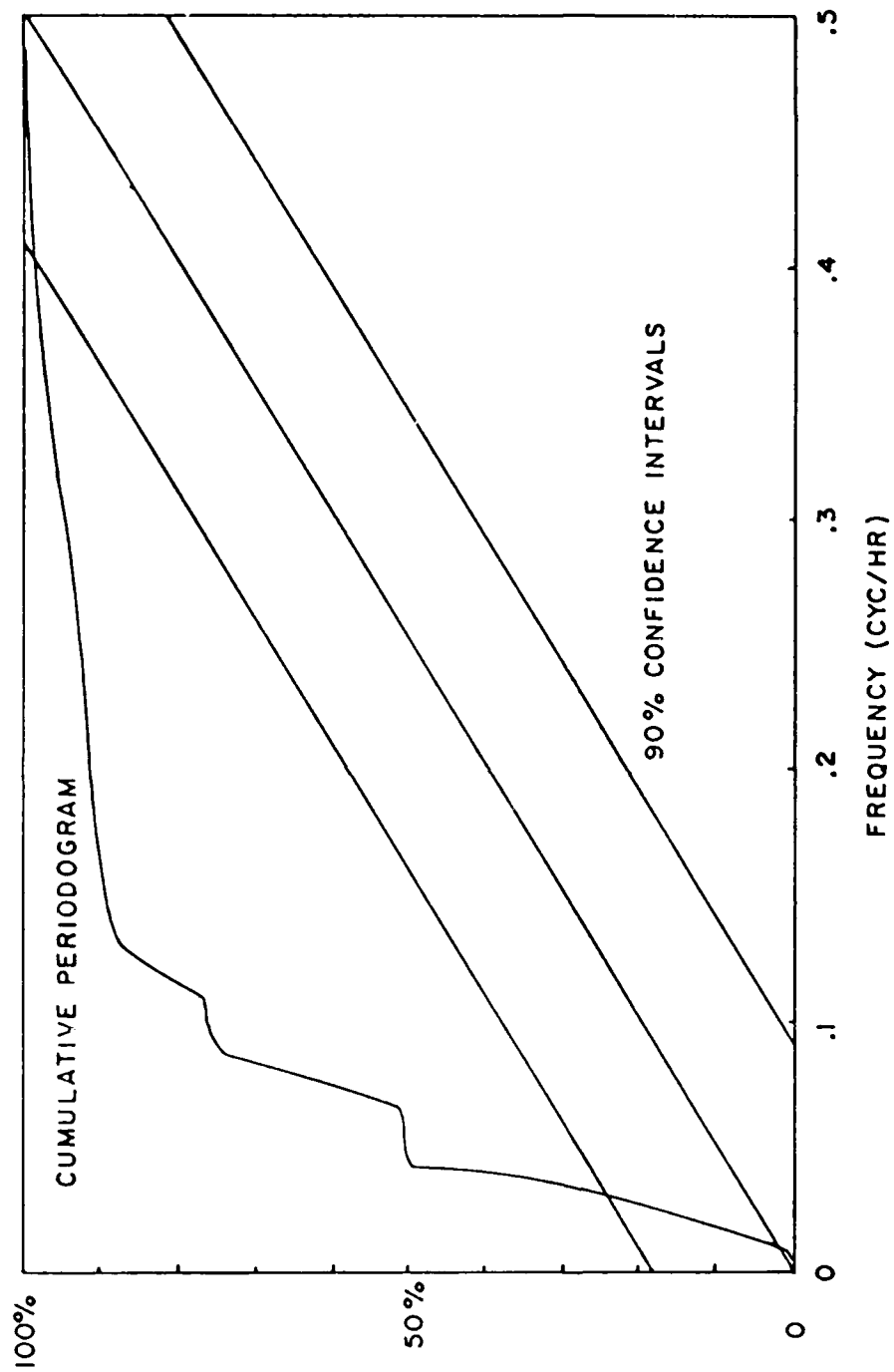


Fig. 4 - First diff - linear

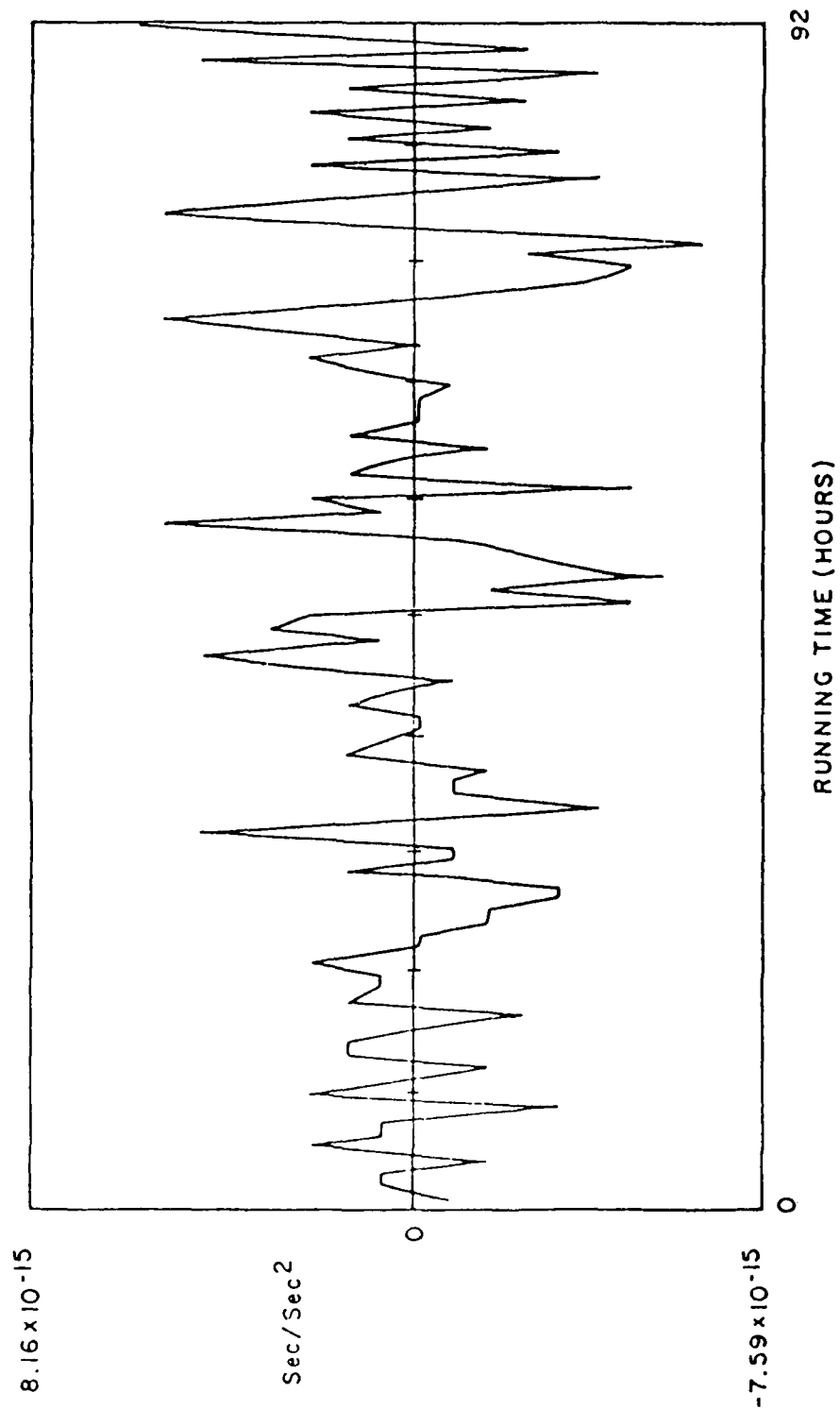


Fig. 5 - Second diff of phase

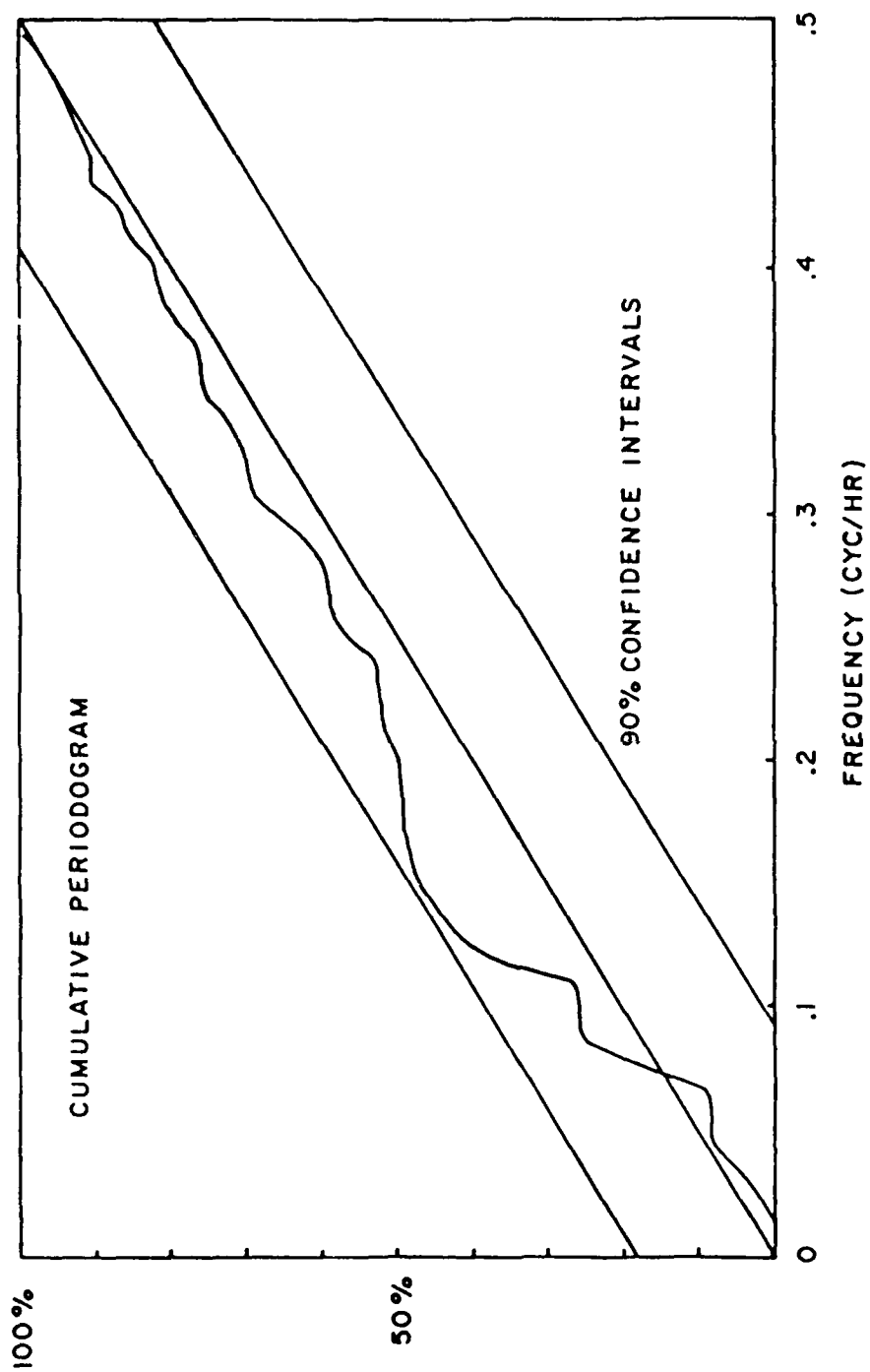


Fig. 6 - Second diff - avg.

TABLE 5. SUMMARY OF DRIFT ESTIMATES
(Units of $1.E-16$ sec/sec²)

ESTIMATION PROCEDURE & MODEL	DRIFT ESTIMATE	COMPUTED STANDARD ERROR	PASS WHITENESS TESTS?
Quad Fit (White FM and Drift)	-7.507	.0523	No
	-8.746	.0493	No
	-6.479	.0645	No
	-6.468	.0880	No
1st Difference Linear Fit (White FM and Drift)	-7.635	.162	No
	-8.558	.206	No
	-6.443	.192	No
	-6.253	.295	No
Second Difference Less Mean (Random Walk FM and Drift)	-6.710	2.736	Yes
	-7.462	9.335	No
	-6.870	3.424	Yes
	-6.412	3.543	Yes

One can calculate the sample means and variances of the drift estimates for each of the three procedures listed in Table 5, and compare these "external" estimates with those values listed in the table under "Computed Standard Error," the "internal" estimates. Of course the sample size is small and we do not expect high precision in the results, but some conclusions can be drawn. The comparisons are shown in Table 6.

It is clear that the quadratic fit to the data displays a very optimistic internal estimate for the standard deviation of the drift rate. Other conclusions are not so clear cut, but still some things can be said. Considering Table 5, the "2nd Diff - Mean" residuals passed the whiteness test three times out of four. The external estimate of the drift standard deviation lies between the internal estimates based on the first and second differences. Since the oscillators under test were crystal oscillators, one expects flicker FM to be present at some level. One also expects the flicker FM behavior to lie between white FM and random walk FM. This may be the explanation of the observed standard deviations, noted in Table 6.

TABLE 6. STANDARD DEVIATIONS

PROCEDURE (Model)	EXTERNAL ESTIMATE (Std. Dev. of Drift Estimates from Col. #2, Table 5)	INTERNAL ESTIMATE (RMS Computed Std. Dev. Col. #3, Table 5)
Quad Fit (White PM)	1.08	0.065
1st Diff - Lin (White FM)	1.08	0.203
2nd Diff - Mean (Rand Wlk FM)	0.44	5.45

VI. DISCUSSION

In all three of the analysis procedures used above, more parameters than just the frequency drift rate were estimated. Indeed, this is generally the case. The estimated parameters included the drift rate, the variance of the random (white) noise component, and other parameters appropriate to the specific model (e.g., the initial frequency offset for the first two models). If these other parameters could be known precisely by some other means, then methods exist to exploit this knowledge and get even better estimates of the drift rate. The real problems, however, seem to require the estimate of several parameters in addition to the drift rate, and it is not appropriate to just ignore unknown model parameters.

To this point, we have considered only three, rather ideal oscillator models, and seldom does one encounter such simplicity. Typical models for commercial cesium beam frequency standards include white FM, random walks FM, and frequency drift. Unfortunately, none of the three estimation routines discussed above are appropriate to such a model. This problem has been solved in some of the recent work of Jones and Tryon^{[5],[6]}. Their estimation routines are based on Kalman Filters and maximum likelihood estimators and these methods are appropriate for the more complex models. For details, the reader is referred to the works of Jones and Tryon.

Still left untreated are the models which, in addition to drift and other noises, incorporate flicker noises, either in PM or FM or both. In principle, the methods of Jones and Tryon could be applied to Kalman Filters which incorporate empirical flicker models^[7]. To the author's knowledge, however, no such analyses have been reported.

VII. CONCLUSIONS

There are two primary conclusions to be drawn:

- (1) The estimation of the linear frequency drift rates of oscillators and the inclusion of realistic confidence intervals for these

estimates are critically dependent on the adequacy of the model used and, hence the adequacy of the analysis procedures.

- (2) The estimation of the drift rate must be carried along with the estimation of any and all other model parameters which are not known precisely from other considerations (e.g., initial frequency and time offsets, phase noise types, etc.)

More and more, scientists and engineers require clocks which can be relied on to maintain accuracy relative to some master clock. Not only is it important to know that on the average the clock runs well, but it is essential to have some measure of time imprecision as the clock ages. For example, the uncertainties might be expressed as, say,, 90% certain that the clock will be within 5 microseconds of the master two weeks after synchronization. Such measures are what statisticians call "interval estimates" (in contrast to point estimates) and their estimations require interval estimates of the clock's model parameters. Clearly, the parameter estimation routines must be reliable and based on sound measurement practices. Some inappropriate estimation routines can be applied to clocks and oscillators and give dangerously optimistic forecasts of performance.

APPENDIX A

REGRESSION ANALYSIS (Equally Spaced Data)

We begin with the continuous model equation:

$$X(t) = a + b \cdot t + c \cdot t^2 + \phi(t) \quad (A1)$$

We assume that the data is in the form of discrete readings of the dependent variable $X(t)$ at the regular intervals given by:

$$t = n\tau_0 \quad (A2)$$

Equation (A1) can then be written in the obvious form:

$$X_n = a + \tau_0 b \cdot n + \tau_0^2 c \cdot n^2 + \phi(n\tau_0) \quad (A3)$$

for $n = 1, 2, 3 \dots, N$.

Next, we define the matrices:

$$\underline{N} = \begin{bmatrix} 1 & 1 & 1 \\ 1 & 2 & 4 \\ 1 & 3 & 9 \\ \dots & \dots & \dots \\ 1 & N & N^2 \end{bmatrix}$$

$$\underline{X} = \begin{bmatrix} X_1 \\ X_2 \\ X_3 \\ \dots \\ X_N \end{bmatrix}$$

$$\underline{T} = \begin{bmatrix} 1 & 0 & 0 \\ 0 & \tau_0 & 0 \\ 0 & 0 & \tau_0^2 \end{bmatrix}$$

$$(\underline{NT})' \underline{X} = \begin{bmatrix} \sum_{n=1}^N X_n \\ \tau_0 \sum_{n=1}^N X_n n \\ \tau_0^2 \sum_{n=1}^N X_n n^2 \end{bmatrix} = \underline{T} \cdot \begin{bmatrix} \sum_{n=1}^N X_n \\ \sum_{n=1}^N X_n n \\ \sum_{n=1}^N X_n n^2 \end{bmatrix} = \underline{T} \cdot \begin{bmatrix} S_x \\ S_{nx} \\ S_{nnx} \end{bmatrix}$$

where four quantities must be calculated from the data:

$$S_x = \sum_{n=1}^N X_n \quad S_{nnx} = \sum_{n=1}^N X_n n^2$$

$$S_{nx} = \sum_{n=1}^N X_n n \quad S_{xx} = \sum_{n=1}^N X_n^2$$

Define

$$\underline{B} = \begin{bmatrix} a \\ b \\ c \end{bmatrix}$$

With these definitions, Eq. A3 can be rewritten in the matrix form:

$$\underline{X} = \underline{N} \underline{T} \underline{B} + \underline{\epsilon} \quad (\text{A4})$$

and the coefficients, B, which minimize the squared errors are given by:

$$\underline{\hat{B}} = \begin{bmatrix} \hat{a} \\ \hat{b} \\ \hat{c} \end{bmatrix} = \underline{T} \cdot (\underline{N}'\underline{N})^{-1} \cdot (\underline{N}'\underline{X}) \quad (\text{A5})$$

The advantage of evenly spaced data for these regressions is that, with a bit of algebra, the matrix, $(\underline{N}'\underline{N})^{-1}$, can be written down in closed form:

$$(\underline{N}'\underline{N})^{-1} = \begin{bmatrix} A & B & C \\ B & D & E \\ C & E & F \end{bmatrix} \cdot 1 / G \quad (\text{A6})$$

where

$$A = 3 [3 (N + 1) + 2]$$

$$B = -18 (2N + 1)$$

$$C = 30$$

$$D = 12 (2N + 1) (8N + 11) / [(N + 1) (N + 2)]$$

$$E = -180 / (N + 2)$$

$$F = 180 / [(N + 1) (N + 2)]$$

and

$$G = N (N - 1) (N - 2)$$

Also, the inverse of T is just:

$$\underline{T}^{-1} = \begin{bmatrix} 1 & 0 & 0 \\ 0 & 1/\tau_0 & 0 \\ 0 & 0 & 1/\tau_0^2 \end{bmatrix}$$

The complete solution for the regression parameters can be summarized as follows:

There are four quantities which must calculate from the data:

$$S_X = \sum_{n=1}^N X_n \quad S_{nnx} = \sum_{n=1}^N X_n n^2$$

$$S_{nx} = \sum_{n=1}^N X_n n \quad S_{xx} = \sum_{n=1}^N X_n^2$$

for $n = 1, 2, 3, \dots, N$. Based on these four quantities, the regression parameters are calculated from the seven following equations:

$$\hat{a} = (A S_X + \tau_0 B S_{nx} + \tau_0^2 C S_{nnx}) / G$$

$$\hat{b} = (B S_X + \tau_0 D S_{nx} + \tau_0^2 E S_{nnx}) / (G \tau_0)$$

$$\hat{c} = (C S_X + \tau_0 E S_{nx} + \tau_0^2 F S_{nnx}) / (G \tau_0^2)$$

$$\hat{\sigma}^2 = (S_{xx} - \hat{a} S_X - \tau_0 \hat{b} S_{nx} - \tau_0^2 \hat{c} S_{nnx}) / (N - 3)$$

$$\hat{\sigma}_a^2 = \hat{\sigma}^2 A / G$$

$$\hat{\sigma}_b^2 = \hat{\sigma}^2 D / (G \tau_0^2)$$

$$\hat{\sigma}_c^2 = \hat{\sigma}^2 F / (G \tau_0^4)$$

where the coefficients A, B, C, etc., are given by:

$$A = 3 [3N (N + 1) + 2]$$

$$B = -18 (2N + 1)$$

$$C = 30$$

$$D = 12 (2N + 1) (8N + 11) / [(N + 1) (N + 2)]$$

$$E = -180 / (N + 2)$$

$$F = 180 / [(N + 1) (N + 2)]$$

and

$$G = N (N - 1) (N - 2).$$

In matrix form, the error variance for forecast values is:

$$\text{Var} (\hat{X}_k) = \hat{\sigma}^2 [1 + \underline{N}_k' (\underline{N}'\underline{N})^{-1} \underline{N}_k]$$

where $\underline{N}_k' = [1 \ n_0 \ n_0]$ and $\tau_0 \ n_0$ is the date for the forecast point, \hat{X}_k . That is, $n_0 = N + K$ and K is the number of lags past the last data point at lag N .

APPENDIX B

REGRESSIONS ON LINEAR AND CUBIC FUNCTIONS

The matrixes $(N'N)^{-1}$ for the linear fit and cubic fit, which correspond to Eq. A6 in Appendix A are as follows:

For the linear fit:

$$(N'N)^{-1} = \begin{bmatrix} A & B \\ B & C \end{bmatrix} 1 / D$$

where

$$A = 2 (2N + 1)$$

$$B = -6$$

$$C = 12 / (N + 1)$$

and

$$D = N (N - 1)$$

For the cubic fit:

$$(N'N)^{-1} = \begin{bmatrix} A & B & C & D \\ B & E & F & G \\ C & F & H & I \\ D & G & I & J \end{bmatrix} 1 / K$$

where

$$A = 8 (2N + 1) (N + N + 3)$$

$$B = -20 (6N^2 + 6N + 5)$$

$$C = 120 (2N + 1)$$

$$D = -140$$

$$E = 200 (6N^4 + 27 N^3 + 42 N^2 + 30 N + 11) / L$$

$$F = -300 (N + 1) (3N + 5) (3N + 2) / L$$

$$G = 280 (6N^2 + 15N + 11) / L$$

$$H = 360 (2N + 1) (9N + 13) / L$$

$$I = -4200 (N + 1) / L$$

$$J = 2800 / L$$

and

$$K = N (N - 1) (N - 2) (N - 3)$$

$$L = (N + 1) (N + 2) (N + 3).$$

The restrictions on these equations are that the data is evenly spaced beginning with $n = 1$ to $n = N$, and no missing values. For error estimates (and their distributions) to be valid, the residuals must be random, uncorrelated, (i.e., white).

REFERENCES

1. D.W. Allan, "The Measurement of Frequency and Frequency Stability of Precision Oscillators," Proc. 6th PTTI Planning Meeting, pl09 (1975).
2. J.A. Barnes, et al., "Characterization of Frequency Stability," Proc IEEE Trans. on Inst. and Meas., IM-20, pl05 (1971).
3. N.R. Draper and H. Smith, "Applied Regression Analysis," John Wiley and Sons, N.Y., (1966).
4. G.E.P. Box and G.M. Jenkins, "Time Series Analysis," Holden-Day, San Francisco, p294, (1970).
5. P.V. Tryon and R.H. Jones, "Estimation of Parameters in Models for Cesium Beam Atomic Clocks," NBS Journal of Research, Vol. 88, No. 1, Jan-Feb. 1983.
6. R.H. Jones and P.V. Tryon, "Estimating Time from Atomic Clocks," NBS Journal of Research, Vol. 88, No. 1, Jan-Feb. 1983.
7. J.A. Barnes and S. Jarvis, Jr., "Efficient Numerical and Analog Modeling of Flicker Noise Processes," NBS Tech. Note 604, (1971).

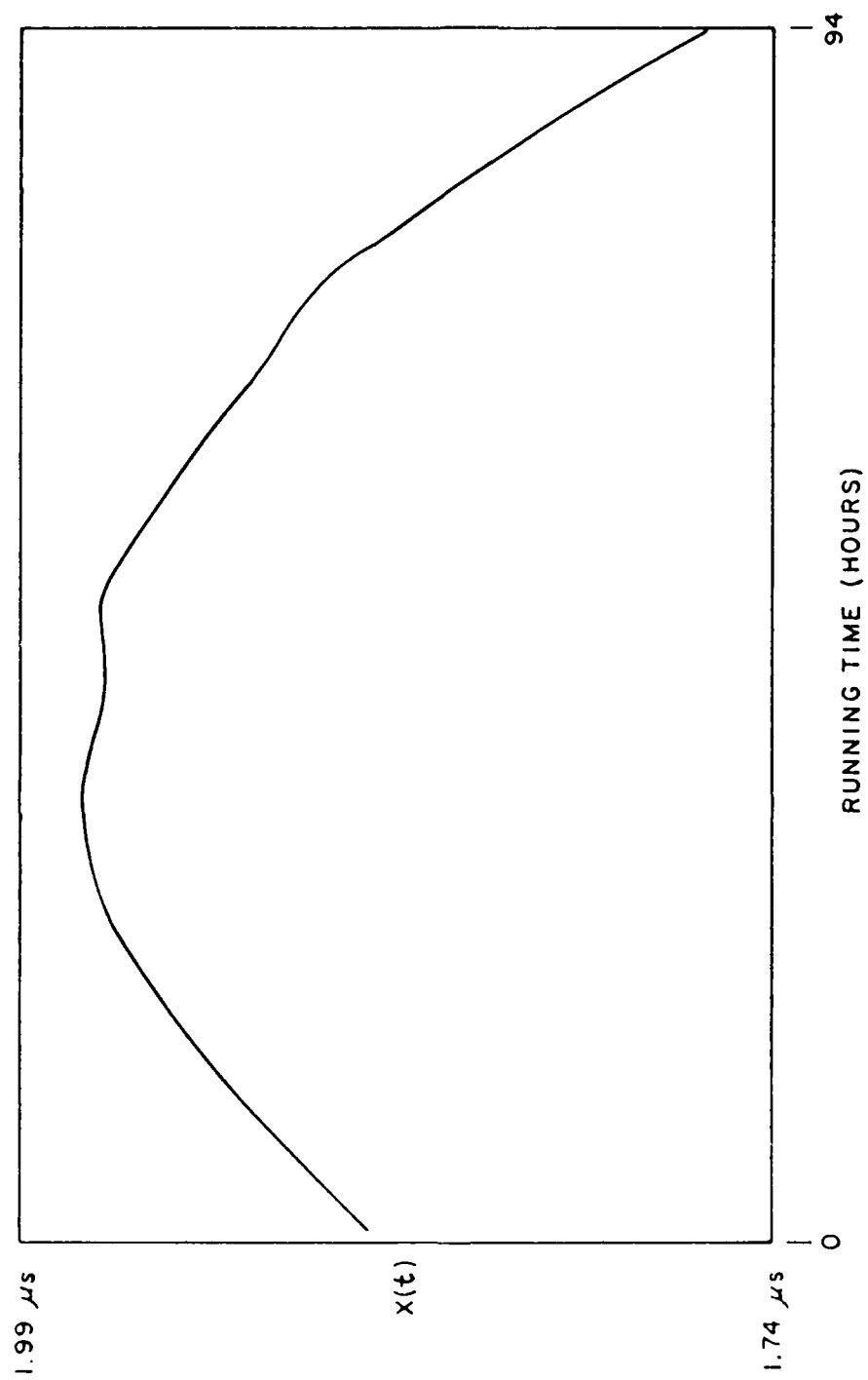


Fig. 1 - Phase difference

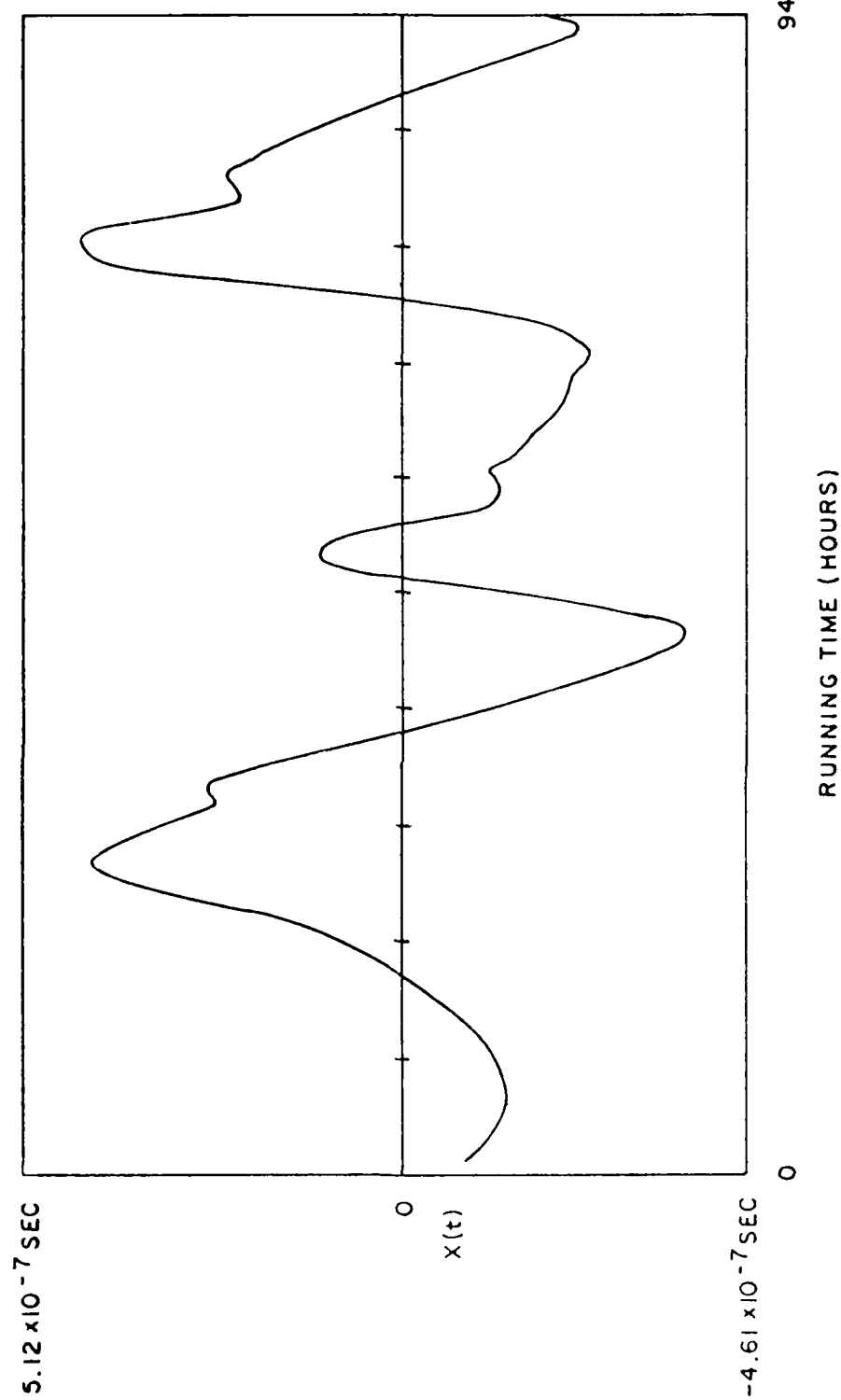


Fig. 2 - Residuals from quadratic fit to phase

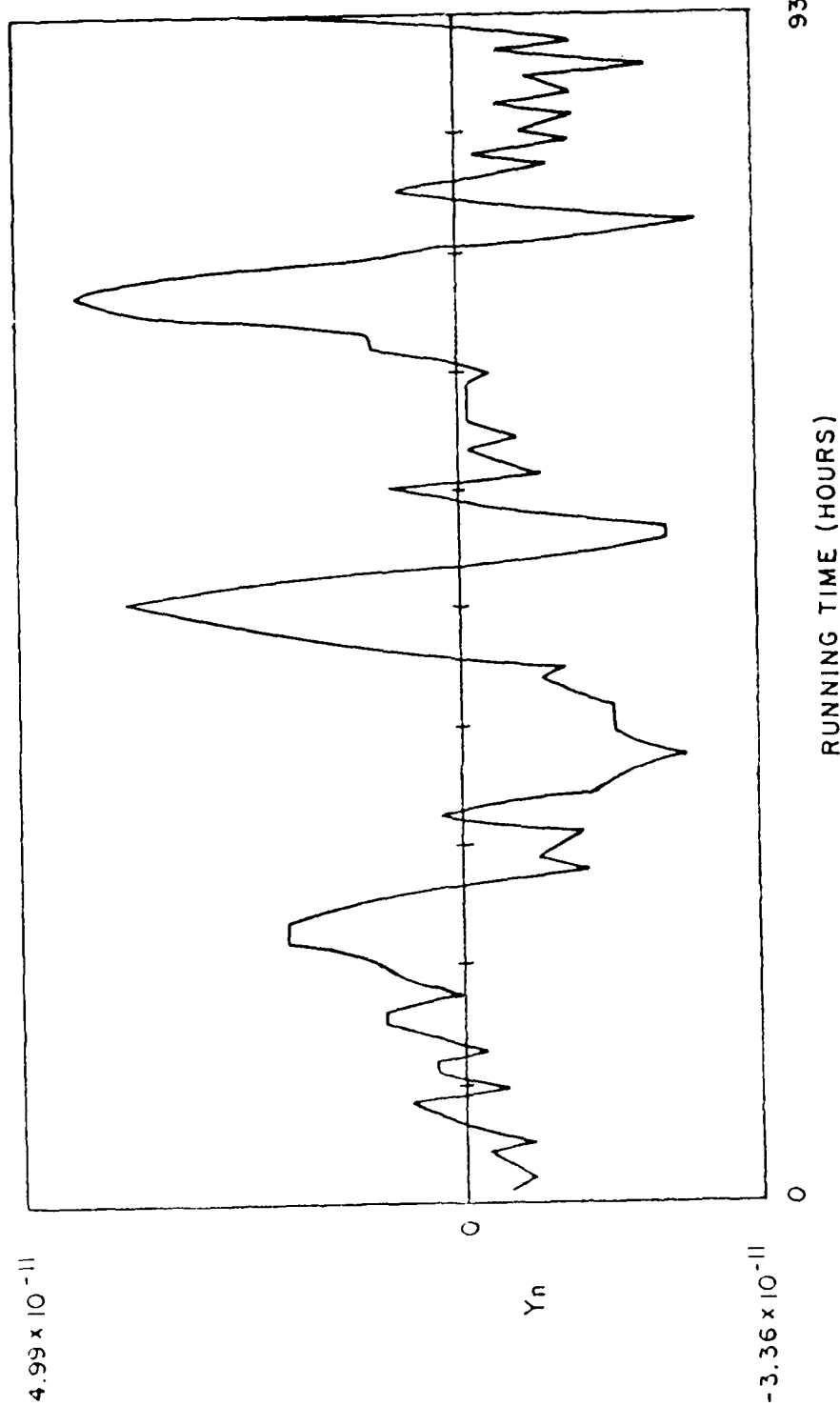


Fig. 3 - Frequency residual
(1st diff-lin)

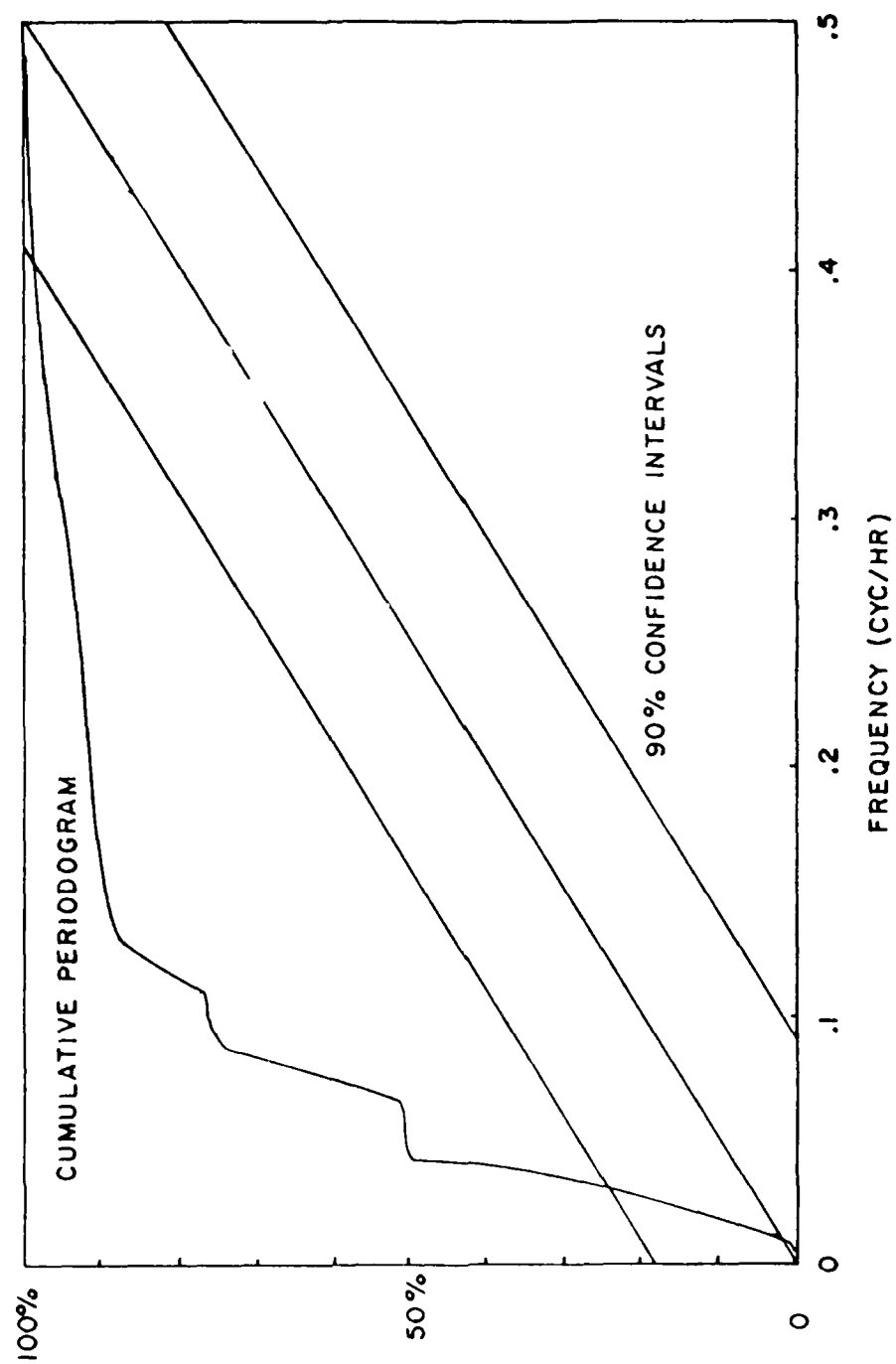


Fig. 4 - First diff - linear

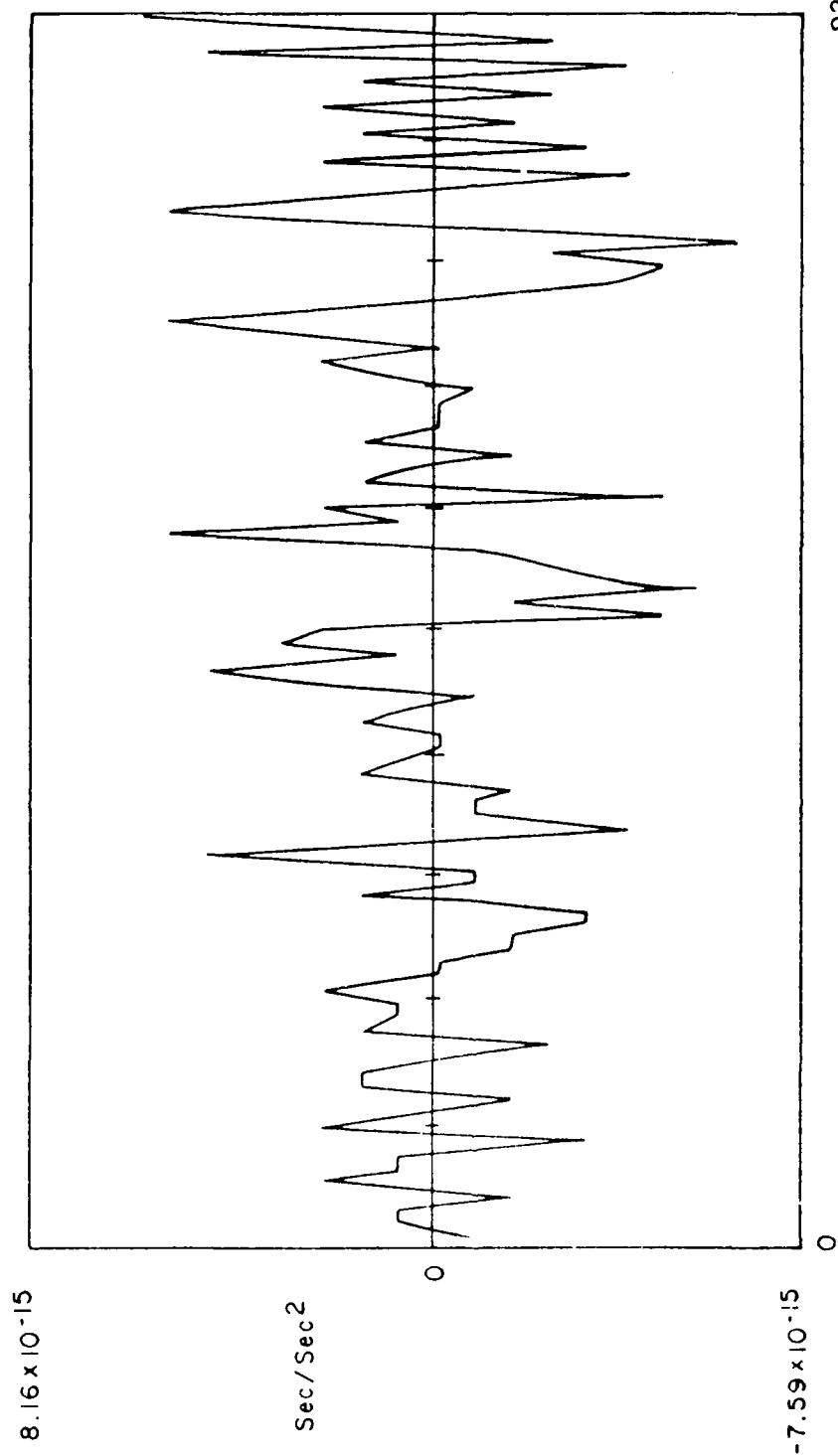


Fig. 5 - Second diff of phase

AD-A149 163

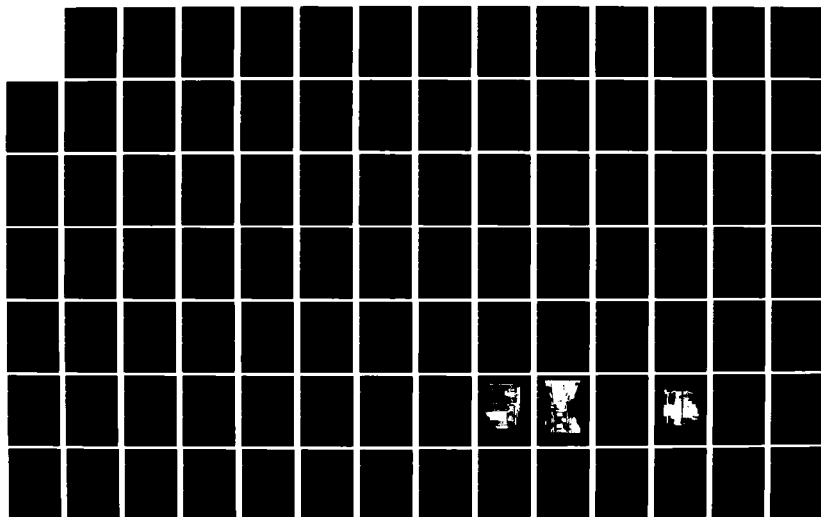
PROCEEDINGS OF THE ANNUAL PRECISE TIME AND TIME
INTERVAL (PTTI) APPLICATI. (U) NAVAL RESEARCH LAB
WASHINGTON DC J A MURRAY 02 APR 84

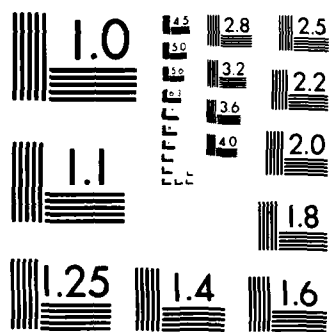
7/8

UNCLASSIFIED

F/G 5/9

NL





MICROCOPY RESOLUTION TEST CHART
NATIONAL BUREAU OF STANDARDS-1963-A

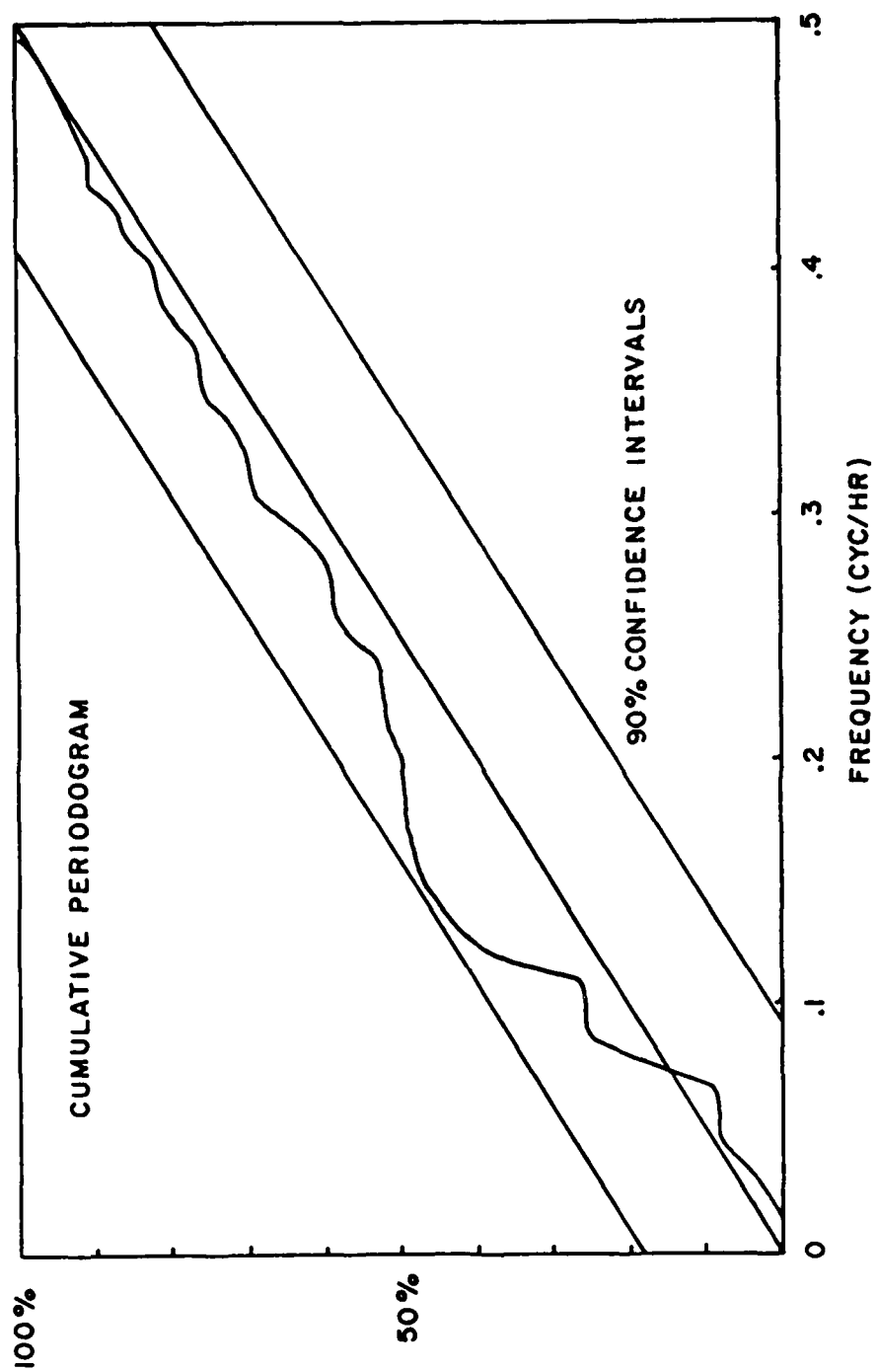
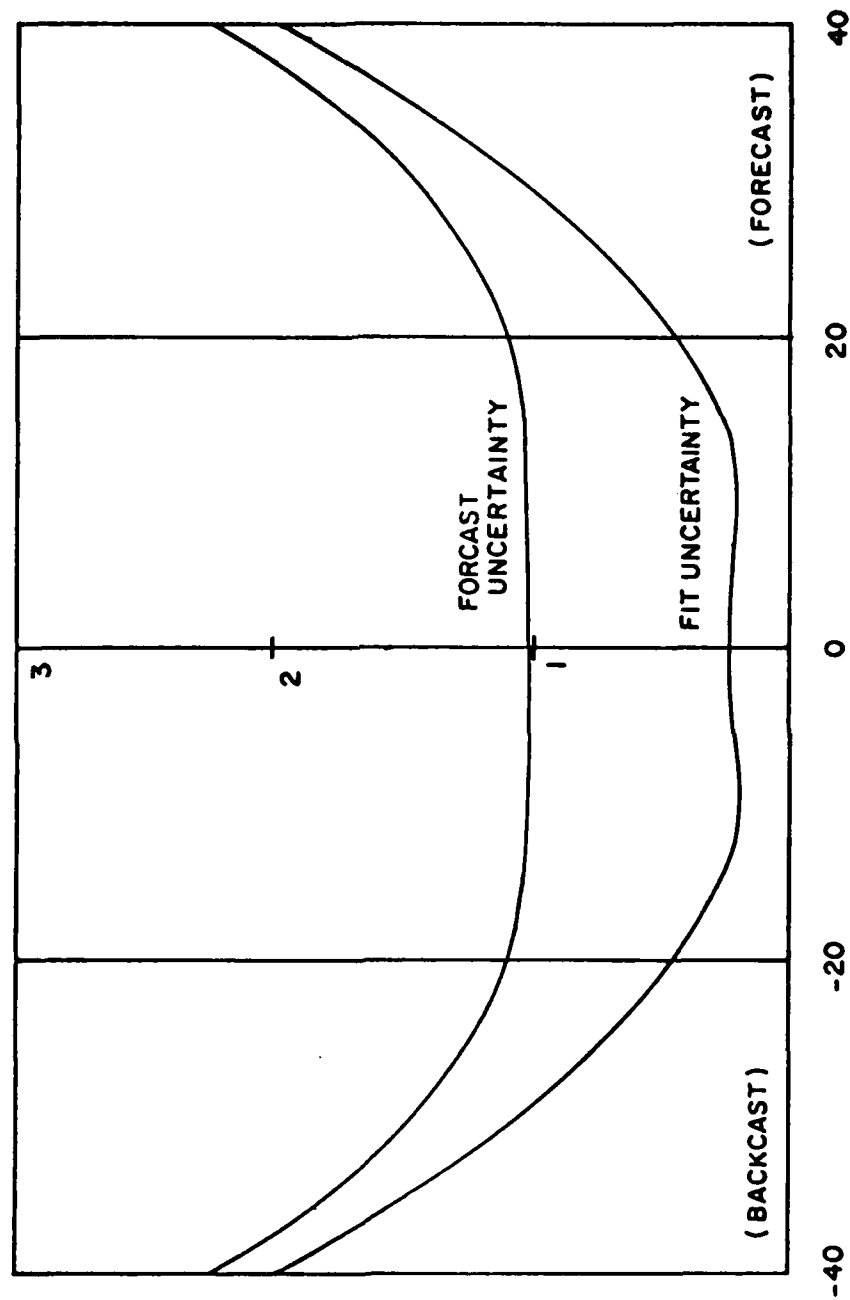
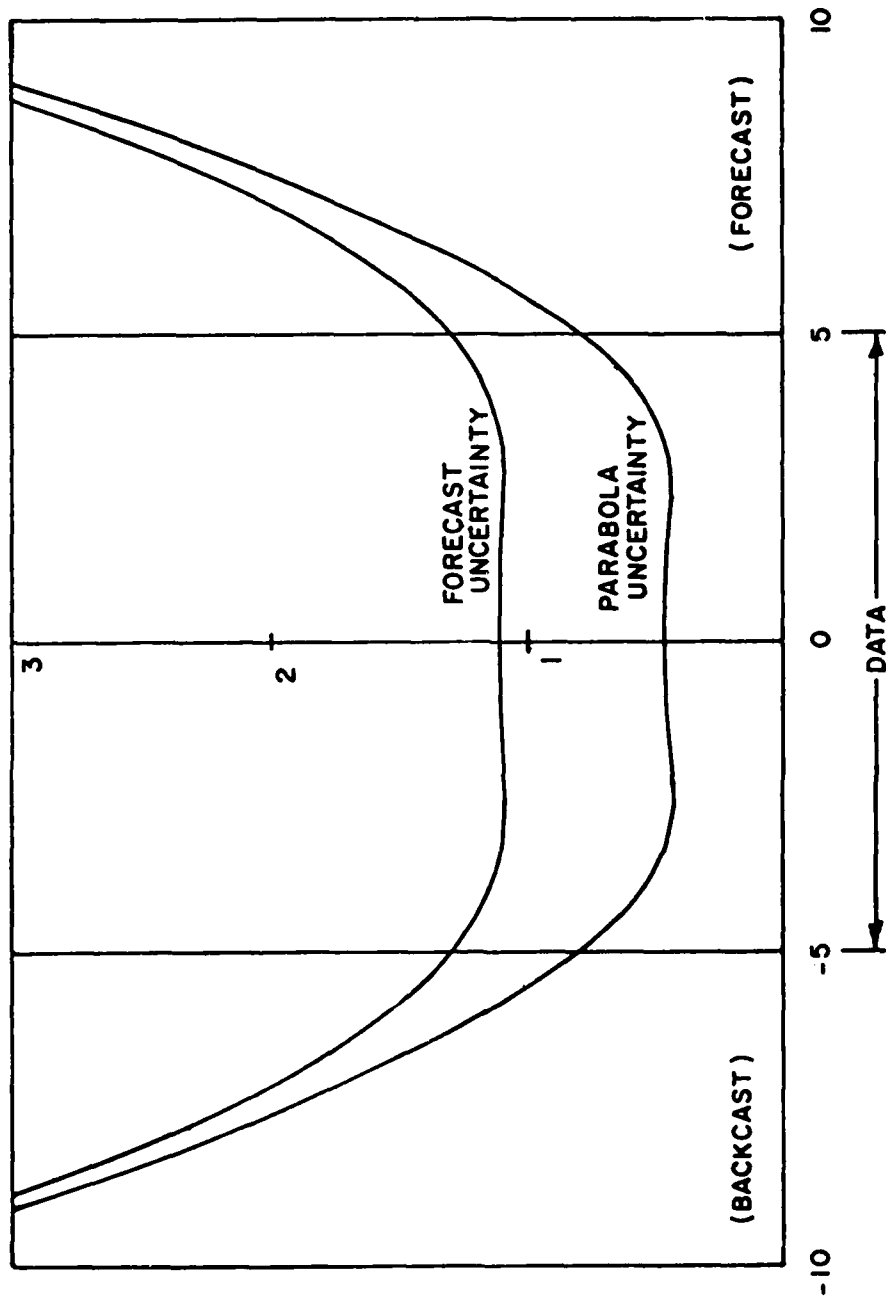


Fig. 6 - Second diff - avg.

FREQUENCY DRIFT AND WHITE PM STANDARD DEVIATIONS



FREQUENCY DRIFT AND WHITE PM STANDARD DEVIATIONS



QUESTIONS AND ANSWERS

MR. ALLAN:

We have found the second difference drift estimator to be useful for the random walk FM process. One has to be careful when you apply it, because if you use overlapping second differences, for example, if you have a cesium beam, and you have white noise FM out to several days and then random walk FM beyond that point, and you are making hourly or 2 hour measurements, if you use the mean of the second differences, you can show that all the middle terms cancel, and in fact you are looking at the frequency at the beginning of the run and the frequency at the end of the run to compute the frequency drift and that's very poor.

DR. BARNES:

My comment would be: There again the problem is in the model, and not in the arithmetic. The models applied here were 3 very simple models, very simple, simpler than you will run into in life. It was pure random walk plus a drift or pure frequency noise plus a drift, or pure random walk of frequency noise plus a drift and it did not approach at all any of the noise complex models where you would have both white frequency and random walk frequency and a drift. That's got to be handled separately, I'm not even totally sure how to perform it in all cases at this point.

MR. McCASKILL:

I would like to know if you would comment on the value of the sample time and the reason why, of course, is that the mean second difference does depend on the sample time? For instance, if you wanted to estimate the aging rate or change in linear change of frequency, what value of sample time would you use in order to make that correction. So, really, the question is, how does the sample time enter into your calculations?

DR. BARNES:

At least I will try to answer in part. I don't know in all cases, I'm sure, but if you have a complex noise process where you have at short term different noise behavior than in long term, it may benefit you to take a longer sampling time and effectively not look at the short term, and then one of the simple models might apply. I honestly haven't looked in great detail at how to choose the sample time. It is an interesting question.

MR. McCASKILL:

Well, let me go further, because we had the benefit of being out at NBS and talking with Dr. Allan earlier and he suggested that we use the mean second difference, and the only problem is if we want to calculate or correct for our aging rate at a tau of five days or ten days, and you calculate the mean second difference, you come up with exactly the Allan Variance. What appears is that in order to come up with the number for the aging rate, you have to calculate the mean second difference using a sample time whenever you take your differences of longer than, let's say, ten days sample time. So we use, of course, the regression model, but we use on the order of two or three weeks in order to calculate an aging rate correction for, say, something like the rubidium in the NAVSTAR 3 clock. It looks like in order to come up with a valid value for the Allan Variance of five or ten day sample time you have to calculate the aging rate at a longer, maybe two or three times longer sample time.

DR. BARNES:

Dave Allan, do you think you can answer that?

MR. ALLAN:

Not to go into details, but if you assume that in the longer term you have random walk frequency modulation as the predominant noise process in a clock, which seems to be true for rubidium, cesium and hydrogen, you can do a very simple thing. You can take the full data length and take the time at the beginning, the time in the middle and the time in the end and construct a second difference, and that's your drift.

There is still the issue of the confidence interval on that. If you really want to verify your confidence interval, you have to have enough data to do a regression. You need enough data to test to be sure the model is good.

DR. WINKLER:

That argument is fourteen years old, because we have been criticized here. I still believe that for a practical case where you depend on measurements which are contaminated and maybe even contaminated by arbitrarily large errors if they are digital. These, theoretical advantages that you have outlined may not be as important as the benefits which you get when you make a least square regression. In this case you can immediately identify the wrong data. Otherwise, if you put the data into an algorithm you may not know how much your data is contaminated. So for practical applications, the first model even though theoretically it is poor, it still gives reasonable estimates of the drift and you have residuals which let you identify wrong phase values immediately.

DR. BARNES:

I think that's true and you may have different reasons to do regression analysis, if your purpose is to measure a drift and understand the confidence intervals, then I think what has been presented is reasonable, if you have as your purpose to look--to see if there are indications of funny behavior in a curve that has such strong curvature or drift that you can't get it on graph paper without doing that, I think it is a very reasonable thing to do. I think looking at the data is one of the healthiest things any analyst can do.

A PLAN FOR THE DEVELOPMENT OF
INERTIAL RECONSTRUCTION OF INITIAL STATE CLOCK (IRIS)

Ernest G. Kimme, Ph.D.
Cobit, Inc.

ABSTRACT

Increasing utilization of wideband low energy/Hertz signalling techniques in the electronic communications and allied arts is creating an urgent need for significant improvements in the stability characteristics of small, rugged, low-cost time standards. One approach to obtaining such improvements is to apply currently available sophisticated signal processing techniques to the homely crystal oscillator. The uncompensated crystal oscillator exhibits performance limitations due explicitly and directly to the physical and electrical characteristics of the crystal resonant element. Compensation improves the performance of the oscillator by in effect isolation of the resonator from the external environment. An alternative approach would be to attempt to create a system "image" of the resonator at a fixed point in time and synthesize the oscillator output from this fixed image. This concept suggests application of plant estimation theory to the design of a crystal-based high-performance time standard. The basic crystal can be used to provide state evolution information to a processing subsystem which simply utilizes this information to provide a statistically stable estimate of the state of the resonator at some fixed point in its history, say at "turn-on time." This paper develops the theoretical basis for such a system. Kalman filtering techniques are utilized to provide initial-state estimation, and a suitable signal synthesis technique produces the time standard output signal. The crystal oscillator runs uncompensated and is merely utilized to obtain data to present to the filter on the current state of the crystal resonator. The paper includes complete generic flow charts of the proposed state estimation process and supporting signal processing. The program of development of a prototype IRIS system is described.

1. Introduction and Motivations

Provision of stable low-noise timing signals is an essential requirement in modern instrumentation, communications, and navigation systems, which utilize highly complex signal structures. High-performance distributed and spatially flexible communications systems require some sort of functional subsystem which provides the effect of universal synchronization. System approaches to date have generally involved (locally or globally) star configurations insofar as communication of timing information is concerned, relying upon remote acquisition of timing from central high-precision sources. Environmental and cost considerations have dictated this type of approach; stable sources have been both expensive and vulnerable to extremes of external system stresses.

A common system implementation of a timing source is the electronic oscillator. The design technology for this generic device is well understood, and for the purposes of this exposition can be represented by a high-gain amplifier with a resonant feedback path, as in Figure 1-1.

The quality of this device, in the limit as gain of the amplifier is increased, is determined by the qualities of the resonator: spectral purity of the output timing signal is directly related to the resonator bandwidth, for example, and the stability of the frequency of the output is a direct function of the stability of the resonator.

The crystal oscillator, in which the resonant element is a piezoelectric crystal, is the common intermediate-technology implementation of the generic device. The rationale for this choice is a matter of history and needs no expository emphasis here. It suffices to observe that achievement of high performance qualities in such designs depends upon the characteristics of available crystal resonant elements, and that inherent physical limitations on the quality of crystal resonators translate directly to inherent performance limitations of crystal oscillators.

These physical limitations are understood in piezoelectric crystal technology in terms of the dependence of the resonance characteristics of crystals upon a set of definable physical parameters. These parameters fall into two categories, which will be oversimplified by describing them as external and internal. Internal parameters will be here considered to be those associated with the physical and chemical structure of the crystal, while external parame-

ters will be identified with properties of the current operating environment of the crystal. Thus, e.g., crystal geometry and chemical composition are deemed internal parameters, and temperature, acceleration, and aging are deemed external.

Internal parameters of crystals are traditionally considered to be determined by the fabrication process. External parameters are managed by a variety of oscillator design techniques which are intended to attenuate the effect of these parameters upon oscillator performance. In extremis, certain external parameters are subjected to processes designed to create an artificial microenvironment for the crystal resonator in which the variation of these parameters are constrained to regions in which their effects are constant on the crystal. Temperature compensation and factory aging are examples of such techniques.

These methods increase costs of finished goods while impairing reliability and longevity; in this regard, a significant attribute of these procedures is that they are basically ad hoc processes. Conventional crystal fabrication technologies have not supported systematic application of sophisticated technologies to this problem.

Current improvements in crystal fabrication technologies have broken through this particular barrier and crystals are now being manufactured with well controlled internal parameters, resulting in increased yields and greater predictability of effects of variations in external parameters. It is, therefore, now feasible to consider borrowing methods from the established technology of system theory to provide more effective ways of dealing with these external effects. In fact, contemplation of this possibility leads to the more general idea of treating the whole crystal oscillator, not just the resonator, as a part of a total estimation and control system.

2. Applicable System-Theoretic Technologies

The ultimate system performance objective for an oscillator as a time standard is the production of an output signal which is a pure sinewave of specified frequency without any variations in that frequency. Physical difficulties in measurement of frequency immediately force compromises with this ideal and actual performance criteria seek to achieve small maximum frequency fluctuations measured over specified time intervals (long-term and short-term).

In the case of the crystal oscillator, variations of output frequency are largely produced by the resonator or crystal itself and are due to aforementioned evolution of physical characteristics of the crystal and environmentally induced variations of the external parameters. Pursuant to holistic system design philosophies, the designer may contemplate methods of controlling the effects of parameter variations rather than controlling the variations directly. A synthesized oscillator design concept emerges from this kind of reasoning, in which the designer effectively takes a snapshot of the crystal at some point in time and uses this fixed image to control a signal generation process for all subsequent time. The obvious difficulty with this idea, apart from the problems associated with measuring all relevant parameters of a crystal at a fixed point in time, is that any signal generation process ultimately requires a time base; physical intuition then strongly suggests that the quality of the synthesized timing signal will not be better than that of the processing time base.

Digital signal processing technology, however, has developed synthesizing algorithms which are largely independent of their time base signals. "Time-tagged" processing algorithms do, in fact, require only sequential clocking and can, in principle, even run independently of real time. Time base dependence reappears, however, when the results of such processing are to be converted to real output signals. If, however, the output timing signal is synthesized as a band-limited signal from a sequence of impulse amplitudes, random sequential timing variations which remain bounded by the reciprocal of the repeat bandwidth will not appear, but non-random (i.e., slow) or very large timing deviations will produce distortions of the output which will be seen as frequency deviations. These phenomena are well-known and discussed at length in published sampled-data literature of considerable vintage.

Review of prior art in this field suggests that the problem addressed here is analogous to the problem of stabilizing and correcting inertial navigation system outputs. Gyroscopes at best vaguely resemble crystals, but the problems of correcting for their internal and external parameter variations are strongly similar, in kind if not quantitatively. The inertial system technologies suggest, in fact, that slow frequency variations of a synthesized oscillator could also be controlled by appropriate design of the synthesis algorithm if their behavior is susceptible to some form of prediction and if it is possible to introduce some form of correction utilizing inputs from a sensor of the

oscillator's behavior. The oscillator itself, in this case, can provide a reference for relative or differential sensing, and careful review of the established technologies is therefore indicated.

The body of applicable mathematics which supports the design of stabilized inertial systems is known as recursive system theory and has seen much development in recent times. The general conceptual approach of this discipline involves three basic ideas:

- i) Identification of internal versus observable variables.
- ii) Definition of a recursive functional relation governing evolution of the internal variables
- iii) Definition of the functional dependence of the observable variables upon the internal variables.

The internal variables of this paradigm are referred to as the "states" of the system, and the recursion describing their evolution is the state transition functional of the system.

In application of these concepts to crystal oscillator design, it is to be noted that the output (observable) is a band-limited signal; the Nyquist sampling theorem is then invoked to create a sequential representation of the observable variables. A standard technical device of system theory translates this sequential representation to the internal state representation as well, and accordingly, the above three steps are followed by a fourth step:

- iv) Selection of a sampling period T less than the reciprocal of the half-bandwidth of the observable function and restructuring the previously defined functional dependencies in sequential form, time-tagged at integral multiples of T .

Two final steps permit introduction of powerful mathematical methods into subsequent analyses: linearization and modeling of uncertainties. The steps are:

- v) Representation of functional relations as linear functionals plus higher-order terms.

- vi) Incorporation of additive stochastic terms in all functional relations modeling approximation and measurement errors.

The impact of these last two steps is, first, to make the vast machinery of matrix algebra available to the analyst, and, secondly, to bring the statistical estimation techniques to the tasks of finding design parameters and predicting system performance. Appendix A elaborates these concepts.

3. Mathematical Formulation of the Plan

The state structure of an oscillator system is modeled, following the steps of Section 2 above, in vector/matrix form as

$$x(n+1) = \Phi(n) \cdot x(n) + u(n), \quad n \geq 0 \quad (3.1)$$

where

$$x(n) = \begin{pmatrix} x(n;1) \\ \vdots \\ x(n;N_s) \end{pmatrix}$$

$$u(n) = \begin{pmatrix} u(n;1) \\ \vdots \\ u(n;N_s) \end{pmatrix},$$

and

$$\Phi(n) = \begin{pmatrix} \Phi(n;1,1) & \dots & \Phi(n;1,N_s) \\ \vdots & & \\ \Phi(n;N_s,1) & \dots & \Phi(n;N_s,N_s) \end{pmatrix}$$

The components of $x(n)$ are values of the N_s internal states of the oscillator at time nT (identified with the parameters of the resonator), the components of $u(n)$ are random variables evaluated at times nT of zero mean and known covariance $Q(n;i,j) = E\{u(n;i)u(n;j)\}$, and the components of $\Phi(n)$ are elements of the state transition matrix at time nT .

The measurement or observation process produces the output of the oscillator in sampled-data form; let,

$$y(n;k) = s((nN_0 + k)T) \quad (3.2)$$

for $k = 0, 1, \dots, N_0 - 1$, and $n \geq 0$. N_0 is arbitrary, within limits discussed later.

Then

$$y(n) = K(n) \cdot x(n) + e(n), n \geq 0$$

where

$$y(n) = \begin{pmatrix} y(n;1) \\ \vdots \\ y(n;N_0) \end{pmatrix}, \quad (3.3)$$

are the N_0 measured values of the system output produced by each state vector $x(n)$,

$$e(n) = \begin{pmatrix} e(n;1) \\ \vdots \\ e(n;N_0) \end{pmatrix} \quad (3.4)$$

are errors in measurement of this output, and

$$K(n) = \begin{pmatrix} K(n;1) & \dots & K(n;1,N_s) \\ \vdots & & \\ K(n;N_0,1) & \dots & K(n;N_0,N_s) \end{pmatrix} \quad (3.5)$$

is the measurement matrix effecting the $x(n) \rightarrow y(n)$ transformation.

This model assumes that the system states transition every N_0 sample times of the output.

Measurement errors are assumed to be independent random variables with known covariance $R(\)$:

$$E\{e(n)e(r)^T\} = \delta(n,r)R(n) \quad (3.6)$$

Denote this covariance matrix by R .

Specification of K and Φ are essential elements in construction of this system model. K is definable nearly ad hoc upon the assignment of the $x(n)$, but Φ requires prior application of the methods of mathematical physics to prediction of the way in which the parameters of the crystal resonator behave in time. The combination of availability of powerful high-speed digital processing devices and development of predictable crystal fabrication processes makes such a definition of Φ feasible, and provides renewed motivation for development of the methods here proposed.

4. General Description of the Oscillator Stabilization Plan

The approach first proposed to produce a highly stable timing signal was to observe the system states at a fixed point in time and forever after synthesize a sinusoidal signal of frequency defined by that one state. A point brushed aside at that time was the form this state observation would take. In point of fact, the best measurement data available to make this determination is the crystal oscillator output itself; that is to say, the state of the system at any point in time is best estimated from the oscillator output defined for that state. Unfortunately, the presence of measurement and approximation errors prevents exact determination of the states corresponding to a given output sequence even if the K transformations are invertible, which they are not in general (since, at the very least, it may be impossible to select $N_s = N_0$).

The fact that to a degree the successive values of the states of the system are related (via Φ), suggests that the fixed-state description can be achieved via statistical techniques. The applicable theory in this case is that of linear recursive estimation (LRE), also known as Kalman filtering. From Appendix A, the following is a realization of LRE techniques applied to the model of Section 3.

Let $\hat{x}(n)$ be an estimate of the state at time $(n-1)T$, and let $P(n)$ be $N_s \times N_s$ correction matrix, assumed symmetric.

Form the auxiliary matrix

$$S(n) = (K(n)P(n)K(n)^T + R(n))^{-1} \quad (4.1)$$

Then update $\hat{x}(n)$ by

(4.2)

$$\hat{x}(n+1) = \phi(n) \cdot P(n) K(n)^T S(n) (y(n) - K(n) \hat{x}(n)) + \phi(n) \hat{x}(n)$$

Then update $P(n)$ by

(4.3)

$$P(n+1) = \phi(n) (P(n) - P(n) K(n)^T S(n) K(n) P(n)) \phi(n) + Q(n)$$

$\hat{x}(n+1)$ is the minimum-variance estimate of $x(n+1)$ based upon $\hat{x}(n)$ and the observation of $y(n)$; the $y - K\hat{x}$ term is the prediction error.

The random process $u(n)$ is represented by the correction term of (4.2):

$$\hat{u} = \phi(n) \cdot P(n) \cdot K(n)^T \cdot S(n) \cdot (y(n) - K(n) \hat{x}(n)) \quad (4.4)$$

If the system is known to be time-varying, the covariance of $u(n)$ can be estimated from these residuals; if $\hat{Q}(n)$ is the estimate of $Q(n)$ used in obtaining $\hat{x}(n+1)$, then

$$\hat{Q}(n+1) = \frac{n\hat{Q}(n) + \hat{u}(n) \hat{u}(n)^T}{n+1} \quad (4.5)$$

provides an estimate of \hat{Q} for the next recursion.

Similarly, if $\hat{R}(n)$ is a current estimate of $R(n)$, $e(n)$ is estimated by

$$\hat{e}(n) = y(n) - K(n) \cdot \hat{x}(n) \quad (4.6)$$

and an estimate of $R(n)$ for the next recursion is

$$\hat{R}(n+1) = \frac{n\hat{R}(n) + \hat{e}(n) \hat{e}(n)^T}{n+1} \quad (4.7)$$

These two error covariance estimation techniques are the mechanism through which the proposed system will have the capability of compensating the synthesis process for large

changes of the environmental forces affecting the system. Thus, the system will be able, to an extent depending upon the artfulness of implementation, to responding to (at least) and correct for (as a performance objective of the design) such factors as short-term high-G forces, and G-tipover, to name just two of the more troublesome aspects of the crystal oscillator environment. Equations (4.5) and (4.7) assume uniform weighting of variance components in time; performance of the proposed system is expected to be modified by selection of more exotic weightings, as exponential.

The entire process begins with an initial estimate of x ; there is no reason not to select $t=0$ or $n=0$ as the initial time of this process, so an initial minimum-variance estimate of $x(0)$, based on observation of $y(0)$ only, is computed according to

$$\hat{x}(0|0) = (K^T(0)K(0))^{-1} \cdot K^T(0) \cdot y(0) \quad (4.8)$$

(See again Appendix A.)

It is a consequence of the theory of the LRE process that $\hat{x}(0|n)$, the minimum variance estimate of $x(0)$ based upon the first n system transition and subsequent LRE of corresponding states, is given by

$$\hat{x}(0|n) = (\Phi(n-1) \cdot \Phi(n-2) \dots \Phi(0))^{-1} \hat{x}(n) \quad (4.9)$$

This is the "fixed state" which was to be used to control the synthesis process.

Finally, the design constructs a synthesis process, described here as K (i.e., independent of n), which operates on $\hat{x}(0|n)$ to produce the stabilized output at the n^{th} epoch:

$$\hat{y}(0|n) = K \cdot \hat{x}(0|n) \quad (4.10)$$

K is a constant-frequency version of the family of measurement transformations $\{K(n)\}$. K may be constructed to provide a signal whose frequency is offset from that of the internal oscillator.

Equation (4.10) describes the production of the vector of observables, which were modeled as samples of the oscillator output signal. The actual output signal of this signal generation process is constructible as a band-limited

signal using the Nyquist sampling theorem. In idealized implementation,

$$S(t|n) = \sum_k y(o|n;k) \delta(t-kT) \quad (4.11)$$

This signal is applied to a band limiting filter; the impulse response of which is

$$h(t) = \cos 2\pi f_0 t \cdot \frac{\sin \frac{\pi t}{T}}{\frac{\pi t}{T}} \quad (4.12)$$

where f_0 is the center frequency of the filter.

In practice, this ideal construction is unachievable since the function $h(t)$ is not realizable, and one of the vast collection of available approximate realizations of an ideal bandpass device will be used.

This point in the output signal synthesis process is, as was noted earlier, a critical point in this development plan. In (4.11), the signal is constructed from modulated impulses occurring at the times $t=nT$ exactly.

The LRE process adjusts the system states once an epoch, and observable timing deviations from the $\{nT\}$ sequence that persist over an epoch will contribute to the prediction error and, thus, be susceptible to correction. Short-term deviations that average out over an epoch will not be incorporated in the LRE process. A development of the Nyquist sampling theorem, however, states that when $s(t)$ has bandwidth $< 1/T$,

$$S(t) = \sum_n S((n+\tau_n)T) \frac{\sin \frac{\pi}{T}(t-(n+\tau_n)T)}{\frac{\pi}{T}(t-(n+\tau_n)T)} \quad (4.13)$$

in the sense of convergence in mean-square (L2), when $\{\tau_n:n\}$ is a sequence of independent random variables such that $|\tau_n| \leq 1/2$ with probability one. The designer's problem is to ensure that the sampling clock satisfies these conditions; equation (4.13) then guarantees that short-term timing deviations are removed by band limiting of the synthesized signal.

5. Implementation of the System

5.1 First Design Considerations

The foregoing discussion describes the mathematical basis for a time-signal generation system utilizing an uncompensated crystal oscillator as a control element for a digital sampled-data synthesis process. The technology is based upon that developed for and applied to the stabilization of inertial navigation systems; the proposed system has for this reason been called an "Inertial Reconstruction of Initial State" (IRIS) clock. Better names may be found, but this one must do for present documentation.

The general structure of the IRIS system has been described, and details of implementation need to be examined. The general problem of implementation of high-speed large-scale digital processed is being swept away by currently developed VHSIC technology; in fact, large-scale array processing microcircuits are a target of several of these development programs. There are, however, two problems yet to consider.

Realizations of large-scale sequential signal-processing techniques encounter significant difficulties due to the presence of systematic, or nearly so, effects of discretization:

- 1) A/D conversions on a large scale are generally required to be sequential and timing errors interact with the various truncation and rounding operations that must be performed.
- 2) Internal arithmetic operations of multiplication and division also require truncations and rounding and even with an ideal time base, systematic errors can be introduced. Intermodulation effects are common.

Signal processing technology has dealt with this problem by introducing various species of randomization. A technique exists that has several attractive features, including the potential for the ultimate utilization of fast single-bit (e.g., band limiting) digitization of signal amplitudes.

This technique is referred to here as the CNM-transform and amounts to representation of signals as linear combinations of basis elements of an orthonormal family of arithmetic binary sequences. These basis sequences are all translates of each other so that the representation can be implemented

by convolutions. This technique is discussed in further detail in Cobit 00002; in that reference the application of the CNM-representation to the direct A/D conversion is described. Very high speed correlators are in current development (Ref. 3) and can ultimately be expected to find application here.

This transform process has the effect of modifying, by a fixed unitary transformation, the measurement matrices $\{K(n)\}$.

The internal clock (hereinafter referred to as the "strobe" clock) can, from the previous discussions, be implemented in a technology consistent with that used for the digital processing; a simple delay-line digital multivibrator is suggested. The strobe frequency must be significantly higher than the reciprocal of the update epoch $N_0 T$, and possibly also higher than the reciprocal of the sample time T .

The previous discussion also indicates that management of inter-stage delay will also be a significant implementation problem; this is, however, dealt with adequately in current digital design technologies.

As said earlier, an important factor in developing the algorithms implementing an IRIS system is the physical description of the oscillator, and particularly, of the oscillator's frequency-determining element. It is obvious that this step requires understanding and control of the significant performance-related parameters of this element. The introductory remarks cited current improvements in fabrication technologies for crystals, and application of these technologies and of the physical understanding behind them to the development of specifications of state-transition descriptions for the IRIS application will be a significant area of activity in the proposed plan.

The term "precision" will be used here to emphasize these attributes of the oscillator and its crystal resonator: "PXTL" will designate the "precision crystal" and "PXC0" will designate the "precision crystal oscillator".

5.2 The IRIS System

Figure 5-1 depicts the general plan of the IRIS clock. Figure 5-2 depicts a proposed first implementation of the strobe clock. In Figure 5-1, this clock drives the spec-

trum-spreading A/D conversion subsystem, and is counted down to derive sample and update epoch timing. Initial State Estimation and Signal Synthesis operations are implemented as N_s -dimensional array processors. The CNM-transform step converts the synthesized band spread representatives of the signal to signal amplitudes, which are (in pulse-amplitude modulated form) applied to the smoothing filter.

5.3 CNM Transforms (A/D)

Figure 5-3 exhibits a proposed implementation of the CNM-transform operation. The signal is ideally processed in analog form; discretization is accomplished prior to handing off the signal to the estimation process. [Ref. 1] provides theoretical background for this transform process. Due to its spectrum-spreading attributes, the subsequent estimation process needs no frequency tracking or similar bandwidth adjustments. The process is referred to as "direct sequence modulation" in the world of spread spectrum communications.

The analog multipliers of Figure 5-3 need not be true multipliers, as seen in Figure 5-4. They are there implemented as switched attenuators, with consequent linearity of response.

The strobe frequency is counted down by a fixed integer Nf_0 , an "update" frequency; that is to say, the system model assumes that internal system dynamics effect a change in the values assigned to the internal states of the system once every N sample times of the oscillator output.

Appendix A describes the mathematical details of the development of initial state estimation algorithms based upon the system model assuming deterministic state transitions $u(n) \equiv 0$, $\phi(n) \equiv \phi$. It is shown in Appendix A that this model amounts to a mathematical assignment of state transition uncertainties to the role of unknown components of the observational error $\{e(n):n\}$. This deterministic case represents a first approximation to the truth, and performance of the resulting IRIS-type system will be predictably sub-optimal, particularly in the presence of large transient external effects rendering the state transition inaccurate for a few data frames. Proof of concept can be achieved, however, with these simplifying assumptions, and the estimation process described in Figure 5-6 will be used for the first exploratory efforts. Figure A3-2 of Appendix A is a detailed flowchart of this estimation process derived from the detailed estimation equation 3.7 of Appendix A.

5.4 Signal Synthesis

Referring to the system definition (5.1) above, signal synthesis is simply the matrix multiplication operation $(K^*())$ modeling the measurement or observation process, that is, if $\hat{x}(o|n)$ is the estimate of the initial state obtained at the n^{th} observation of the PXO output, then

$$\hat{y}(o|n) = K^* \hat{x}(o|n) \quad (5.2)$$

represents the (CNM transform of the) output if the states had remained constant with this estimated value and the measurements were produced by the operation $K^*()$.

5.5 CNM Transform (D/A)

In principle, the two CNM transforms are identical: they have identical sampled-data representations. However, the synthesized signal is in digital form, and applicable transform processes must be implemented digitally. Figure 5-7 exhibits a version of the form this process could assume. The subsystem design plan of Figure 5-8 is presently structured around a hypothetical microcomputer implementation. The actual hardware configuration of this subsystem may have to be considerably more complex due to speed limitations of currently available low-cost microcomputer chips. Certain economies suggest themselves as well, notably, the possibilities of time-sharing the z-multiply (D) functions and of implementing the accumulator recursively. The straightforward plan of Figure 5-7 will, however, be followed initially.

The z-multiply (D) function is exhibited in Figure 5-8. Note that this is a true digital multiplication.

Incorporation of this second transform operation into the synthesis algorithm is a considered option.

5.6 Smoothing

The smoothing process is required to achieve removal of the strobe clock transitions and minimize the effects of quantizing noise. At frequencies of interest, it seems likely that RC realizations will be entirely adequate; this filter should therefore have little impact upon size and cost parameters for IRIS-type timing sources.

6. Summary and Development Plan

The proposed IRIS development will eventually produce a working hardware prototype system. Steps toward achievement of this objective are as follows:

Phase I: Oscillator Subsystem Modeling:

Technical Objective: Develop modeling techniques for representation of oscillators (resonant elements) as linear dynamic systems of display (5.1) above.

Approach: Computer implementation of relations (5.1) and verification of accuracy thereof by comparisons of laboratory measurements and computer outputs using standard statistical criteria.

Phase II: IRIS Simulation

Technical Objective: Develop verified source codes implementing the predictor-corrector process of Figure 5-7.

Approach: Write computer code implementations of the overall predictor-corrector process following the flow-chart of Figure 5-7, and combine this with the oscillator subsystem model from Phase I to produce an IRIS simulator; prepare a test and evaluation plan for concept verification and execute this plan using the IRIS simulation system.

Phase III: IRIS Prototype

Technical Objective: Construct an IRIS frequency source and obtain laboratory data on its operation; this is to be proof-of-concept IRIS realization using a precision crystal as the oscillator resonant element.

Approach: Design and fabricate interface and control equipments to permit replacement of the oscillator subsystem simulator of Phase I in the overall IRIS simulation with a real oscillator, and develop a (test and) demonstration plan for the resulting prototype system. Incorporate available high-speed digital correlators in the implementation (ICOR).

Phase IV: IRIS Improvement

Technical Objective: Extend IRIS capabilities to accommodate non-random transient external parameter variations and verify the projected performance enhancement.
(Implement the relation (4.1) and (4.2) in full generality.)

Approach: Modify the oscillator model of Phase I above to include state transition uncertainty, modify the predictor-corrector software accordingly (theoretical development and attendant modifications of the predictor-corrector algorithms), modify the test and evaluation plan as needed, and repeat the process of Phase III.

Phase V: Full-Scale IRIS Implementation

Technical Objective: Develop an advanced development model of a manufacturable IRIS device.

Approach: Replace general purpose digital computer host by microcomputer(s), using available microcomputer development aids to translate the predictor-corrector code into machine code for the microcomputer(s) selected. Develop test and evaluation plan and observe and evaluate IRIS operation.

This program, as outlined, is estimated to require between 18 months and three years depending upon applied levels of effort. The result, be it noted, is not merely an enhanced type of crystal oscillator, but an altogether novel device best described as a crystal-controlled synthesized timing standard. Furthermore, the basic techniques employed here utilize crystals as stable elements, but are clearly applicable to other types of devices, e.g., rubidium standards. In such applications, the strobing elements might be crystal oscillators and the internal signal processing bandwidths would be correspondingly higher, requiring higher-speed digital devices.

Appendix A
Initial State Estimation for Sampled Data Linear Systems:
Deterministic Case

Section 1. General Model:

Let $\{x(t;i): 1 \leq i \leq N_s\}$ denote the states of an (ideal) linear system. For fixed i , $x(t;i)$ is a real function of time t . Let T be a fixed sampling interval, and let for each i and n

$$x(n;i) = x(nT;i) \quad (A1.1)$$

The linearity property is an attribute of the system states; for each n there are numbers $\{\phi(n;i,j)\}$ for which

$$x(n+1;i) = \sum_{j=1}^{N_s} \phi(n;i,j) x(n;j) \quad (A1.2)$$

It will be convenient to adopt matrix notation: let

$$x(n) = \begin{pmatrix} x(n;1) \\ \vdots \\ x(n;N_s) \end{pmatrix} \quad (A1.3)$$

and

$$\phi(n) = \begin{pmatrix} \phi(n;1,1) & \phi(n;1,2) & \dots & \phi(n;1,N_s) \\ \phi(n;2,1) & & & \vdots \\ \vdots & & & \\ \phi(n;N_s,1) & & \dots & \phi(n;N_s,N_s) \end{pmatrix} \quad (A1.4)$$

Then the state evolution relation (A1.2) can be stated as

$$x(n+1) = \phi(n) \cdot x(n) \quad (A1.5)$$

The observable or output variables are $\{y(t;i): 1 \leq i \leq N_o\}$, and they are sampled as above to produce

$$y(n;i) = y(nT;i) \quad (A1.6)$$

The $\{y(n;i)\}$ are derived from the states $\{x(n;i)\}$ by a linear measurement process: there are numbers $\{K(n;i,j): 1 \leq j \leq N_S; 1 \leq i \leq N_O\}$ for which

$$y(n;i) = \sum_{j=1}^{N_S} K(n;i,j) x(n;j) \quad (A1.7)$$

Again, in matrix notation, let

$$y(n) \equiv \begin{pmatrix} y(n;1) \\ \vdots \\ y(n;N_O) \end{pmatrix} \quad (A1.8)$$

and let

$$K(n) \equiv \begin{pmatrix} K(n;1,1) & \dots & K(n;1,N_S) \\ K(n;2,1) & \dots & K(n;2,N_S) \\ \vdots & & \vdots \\ K(n;N_O,1) & \dots & K(n;N_O,N_S) \end{pmatrix} \quad (A1.9)$$

Then the measurement relations are

$$y(n) = K(n) \cdot x(n) \quad (A1.10)$$

It will be assumed $\dim y(n) = N_O \neq N_S = \dim x(n)$.

If $x(0)$ is an initial vector of state, the linear system under consideration has the specification

$$\begin{aligned} x(0) &= \text{initial states} \\ x(n+1) &= \Phi(n) \cdot x(n) \quad \text{evolution} \\ y(n) &= K(n) \cdot x(n) \quad (\text{measurement}) \end{aligned} \quad (A1.11)$$

Figure A1-1 depicts this situation.

Section 2. Time-Stationary Case

Of particular interest are those systems which are time-stationary, that is, those systems whose descriptions (A1.11) can be formulated so that $\Phi(n)$ and $K(n)$ are constant functions of n :

$$\begin{aligned}x(0) &= \text{initial states} \\x(n+1) &= \Phi \cdot x(n) \quad (\text{evolution}) \\y(n) &= K \cdot x(n) \quad (\text{measurement})\end{aligned} \tag{A2.1}$$

The essential feature of (A2.1) is, as seen in Figure A2-1, the absence of the explicit "clock" variable n in the evolution and measurement algorithms.

Time-stationary systems have a unique position in this regard: internal timing of the system can be decoupled from external clocks, since absolute or external time is not required for the evaluation of the internal parameters Φ and K .

In the time-stationary case, Φ is referred to as the state-transition matrix, and K is referred to as the measurement matrix.

Section 3. Estimation Under Uncertainty

The previous sections deal with deterministic linear system models. The linear case is regarded as an important object of study because it serves as an approximation to the general case. In the general case, the system of (A1.11) has the form

$$\begin{aligned}x(0) &= \text{initial state} \\x(n+1) &= \Phi[x;n] \quad (\text{state transition}) \quad n \geq 0 \\y(u) &= K(x;n) \quad (\text{measurement})\end{aligned} \tag{A3.1}$$

where $\Phi[x;n]$ denotes a vector-valued functional depending upon $x(0), \dots, x(n)$, and $K(x;n)$ is a general vector function of the vector $x(n)$.

The linear approximation is made by noting that under (A3.1), $x(n)$ is defined by recursion upon its history $x(0), \dots, x(n-1)$, and hence without loss of generality $\phi[x:n]$ can be assumed to depend on $xz(n)$ only. Hence, it makes sense to ask for that linear functional of $x(n)$, which will be temporarily denoted $\phi_L[x:n]$, that makes

$$\phi[x:n] - \phi_L[x:n]$$

small for all $x(n)$ of interest. Depending on the sense taken for the phrase "small for all $x(n)$ of interest," $\phi_L[x:n]$ is one or another of the species of differentials defined for functionals of a vector space into itself. If the Euclidean norm is used to define "small" and $\phi[\]$ is given suitable continuity properties, $\phi_L[x:n]$ is representable as a matrix operation on $x(n)$, as in (A1.2).

By suitable renormalizations of the $x(n)$, the state transition relation of (A3.1) can be written

$$x(n+1) = \phi[x:n] = \phi(n) \cdot x(n) + (\phi[x:n] - \phi(n) \cdot x(n)) \quad (A3.2)$$

The residual term can be made small for $x(n)$ of interest.

A similar process yields

$$y(n) = K(x;n) = K(n) \cdot x(n) + (K(x;n) - K(n) \cdot x(n)) \quad (A3.3)$$

with the same residual argument.

The residuals are next treated as statistical rather than descriptive errors. Conceptual justifications for this step abound, but a simplistic view is that (A3.1) reflects at best the extent to which the dynamic behavior of the general system is quantitatively described, and that description is almost certainly incomplete. (A3.1), therefore, can be regarded as statements made under uncertainty and the Bayesian philosophy invoked to introduce stochastic terms.

In the sense of these remarks, the system of (A3.1) is describable as a linear system with additive random components, thus:

$$x(0) = \text{initial state}$$

$$x(n+1) = \phi(n) \cdot x(n) + u(n) \quad n \geq 0 \quad (A3.4)$$

$$y(n) = K(n) \cdot x(n) + e(n)$$

where $\{u(n)\}$ and $\{e(n)\}$ are taken to be random variables of specifiable distribution. The deterministic cases of the previous sections correspond to $u(n) \equiv e(n) \equiv 0$, $n \geq 0$.

Figure A3-1 depicts the general recursive linear system model under uncertainty.

Under very general conditions on the random variables $u(n)$ and $e(n)$, the system of Figure A3-1 is equivalent, in the sense of convergence in the mean, to a time-stationary system, under uncertainty. As noted in the previous section, this implies that the limiting behavior of the general linear system can be studied in terms of an equivalent system for which $\phi(n) \equiv \phi$ and $K(n) \equiv K$ for all n . (In the deterministic case,

$$\phi = \lim_{N \rightarrow \infty} \left(\prod_{k=0}^N \phi(k) \right)^{1/N+1}$$

as would be expected. The corresponding relation for K is more complicated.)

The problem of estimating the state of the system is generally solved: Given an initial state $x(0)$, the minimum-variance estimate of $x(n)$, denoted by $\hat{x}(n)$, based upon the measurements $y(0), \dots, y(n)$, is updated to a minimum-variance estimate of $x(n+1)$ by the generalized Kalman-Bucy relations, otherwise known as the minimum-variance linear recursive estimator (LRE). If $\{u(n)\}$ are independent with covariance $Q(u)$ and $\{e(n)\}$ are independent with covariance $R(n)$, then:

Given $\hat{x}(n)$, $y(n)$, $\phi(n)$, $K(n)$, and $P(n)$:

$$S(n) \triangleq (K(n)P(n)K(n)^T + R(n))^{-1} \quad (A3.5)$$

$$P(n+1) = \phi(n) (P(n) - P(n)^T K(n)^T S(n) K(n) P(n)) \phi(n)^T + Q(n)$$

$$\hat{x}(n+1) = \phi(n) (\hat{x}(n) + P(n) K(n)^T S(n) (y(n) - K(n) \hat{x}(n)))$$

The matrix $P(n)$ is symmetric; its initial value is

$P(0) = E\{x(0) \cdot x(0)^T\}$, which can be replaced by $x(0)$.

$x(0)^T$ for computational purposes. Note that (A3.5) supposes that $\hat{x}(n)$ is used to find a predicted $y(n)$, and that the error of this prediction (the term $y - K\hat{x}$ in the

equation for $\hat{x}(n+1)$) is used to correct the estimate of the new state $\hat{x}(n+1)$, which otherwise would be simply $\phi(n)\hat{x}(n)$. It is for this reason that the LRE is sometimes referred to as a predictor-corrector filter,

The equations (A3.5) are susceptible of considerable algebraic manipulation and can be found in many different forms. The form used here is that given in reference [2].

Section 4. Time-Stationary Systems with Deterministic State Transition

Time-stationarity, as noted previously, implies $\phi(n) \equiv \phi$ and $K(n) \equiv K$. It is also possible to incorporate the state uncertainty $u(n)$ into the measurement error $e(n)$ in (A3.4) and set $u(n) \equiv 0$. The LRE then corrects the estimated states suboptimally, so that, although the system model is conceptually equivalent, the state estimation process will not have the minimum-variance property.

The equations (A3.5) simplify, however, and this fact makes study of this special case attractive as an intermediate step to achieving the full benefit of (A3.5). Let $\phi(n) \equiv \phi$, $K(n) \equiv K$; if $u(n) \equiv 0$, then $Q(n) \equiv 0$. If the measurement process is modified to effect randomization of the measurement error, and these errors are already time-stationary, then

$$R(n) = E\{e(n)e(n)^T\} = \sigma^2 I \quad (A3.6)$$

where I is the identity matrix of appropriate dimension, and σ^2 is independent of n . With these relations, (A3.5) becomes:

Given $\hat{x}(n)$, $y(n)$, ϕ , K , and $P(n)$:

$$S(n) \triangleq (KP(n)K^T)^{-1} \quad (A3.7)$$

$$P(u+1) = \phi(P(n) - P(n)K^T S(KP(n))\phi^T + \sigma^2 I$$

$$\hat{x}(n+1) = \phi(\hat{x}(n) + P(n)K^T S(n)(t(n) - K\hat{x}(n)))$$

Let $P(n) = P(n)/\sigma^2$; then,

$$S(n) = (K P(n) K^T)^{-1} = (K \sigma^2 P(n) K^T)^{-1} = \frac{1}{\sigma^2} (K P(n) K^T)^{-1}$$

$$\bar{D} = \frac{1}{\sigma^2} S(n) \quad (A3.8)$$

The recursion on P becomes

$$\begin{aligned} P(n+1) &= \sigma^2 P(n+1) = \Phi(P(n) \sigma^2 - \sigma^2 P(n) \cdot K^T \cdot \frac{1}{\sigma^2} S(n) \cdot K \cdot \sigma^2 P(n)) \cdot \Phi^T + \sigma^2 I \\ &= \sigma^2 (\Phi(P(n) - P(n) \cdot K^T S(n) \cdot K \cdot P(n)) \Phi^T + I) \end{aligned}$$

or

$$P(n+1) = \Phi(P(n) - P(n) K^T S(n) \cdot K \cdot P(n)) \Phi^T + I \quad (A3.9)$$

The corrected \hat{x} becomes

$$\begin{aligned} \hat{x}(n+1) &= \Phi(\hat{x}(n) + \sigma^2 P(n) \cdot K^T \cdot \frac{S(n)}{\sigma^2} (y(n) - K \hat{x}(n))) \\ &= \Phi(\hat{x}(n) + P(n) \cdot K^T \cdot S(n) (y(n) - K \hat{x}(n))) \end{aligned} \quad (A3.10)$$

The error variance σ^2 enters the recursive estimation process only at the initial step, where now

$$P(0) = \frac{x(0) x(0)^T}{\sigma^2} \quad (A3.11)$$

The relations (A3.7) will next be trivially restated in a form preparatory to computer program implementation:

Initialization: Assign σ^2 , Φ , and K.

Enter x

$$\text{Compute } P = (xx^T) / \sigma^2 \quad (A3.12)$$

Set $\hat{x} = x$

Algorithm:

Given \hat{x} , y, and P.

$$S = (KPK^T)^{-1}$$

$$\text{New} \quad \hat{x} = \phi(\hat{x} + PK^T S(y - K\hat{x}))$$

$$\text{New} \quad P = \phi(P - PK^T SKP) \phi^T + I$$

Figure A3-2 is a flowchart of the relations (A3.12).

The initial state is always estimated (minimum variance) from the transition matrix: if $\hat{x}(0|n)$ denotes the initial state estimate based on the observations $y(0), \dots, y(n)$, then

$$\hat{x}(0|n) = (\phi(0) \cdot \phi(1) \cdot \dots \cdot \phi(n-1))^{-1} \cdot \hat{x}(n) \quad (\text{A3.13})$$

In the present case,

$$\hat{x}(0|n) = (\phi^n)^{-1} \hat{x}(n) \quad (\text{A3.14})$$

The initial state estimation process can be concluded in the algorithm:

$$\text{Initialize:} \quad \psi = I$$

$$\text{Given:} \quad \psi \quad (\text{A3.15})$$

$$\text{New} \quad \psi = \phi^{-1} \cdot \psi$$

which provides a current-time estimate $\hat{x}(0|n)$ of the initial system state.

References:

- [1] Representation and Analysis Techniques of Wideband Signalling Systems, Cobit 00002, Rev. 2; CUES Workshop, 19-20 July 1983; ANSER Corp. Arlington, VA.

- [2] Optimization by Vector Space Methods, David G. Luenberger; John Wiley and Sons, New York, NY 1969 (Chapter 4, pp. 78-102).

- [3] U.S. Patent #4,205,302; ICOR Co., Bellevue, WA, May 27, 1980.

- [4] Optimization Over Time: Dynamic Programming and Stochastic Control, Vol. I, Peter Whittle F.R.S., Wiley & Sone, New York

- [5] Probability, Random Variables, and Stochastic Processes, Athanasios Papoulis, McGraw-Hill, 1965

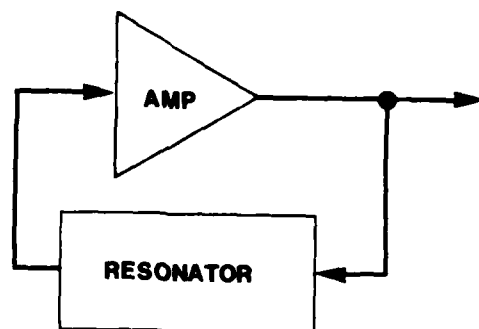


FIGURE 1-1
GENERIC OSCILLATOR

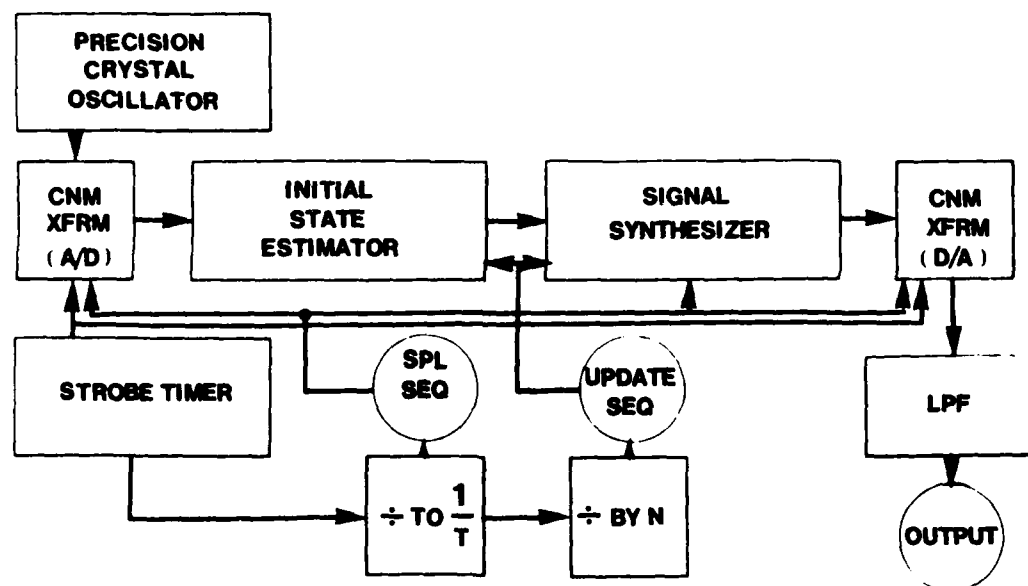


FIGURE 5-1
IRIS SYSTEM ORGANIZATION

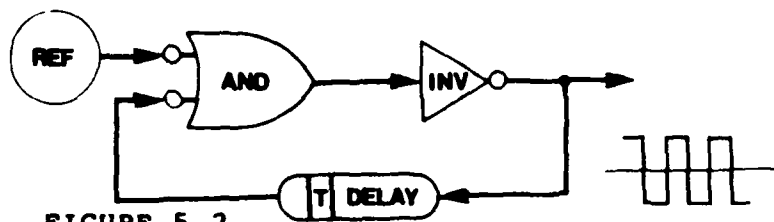


FIGURE 5-2
STROBE TIMER

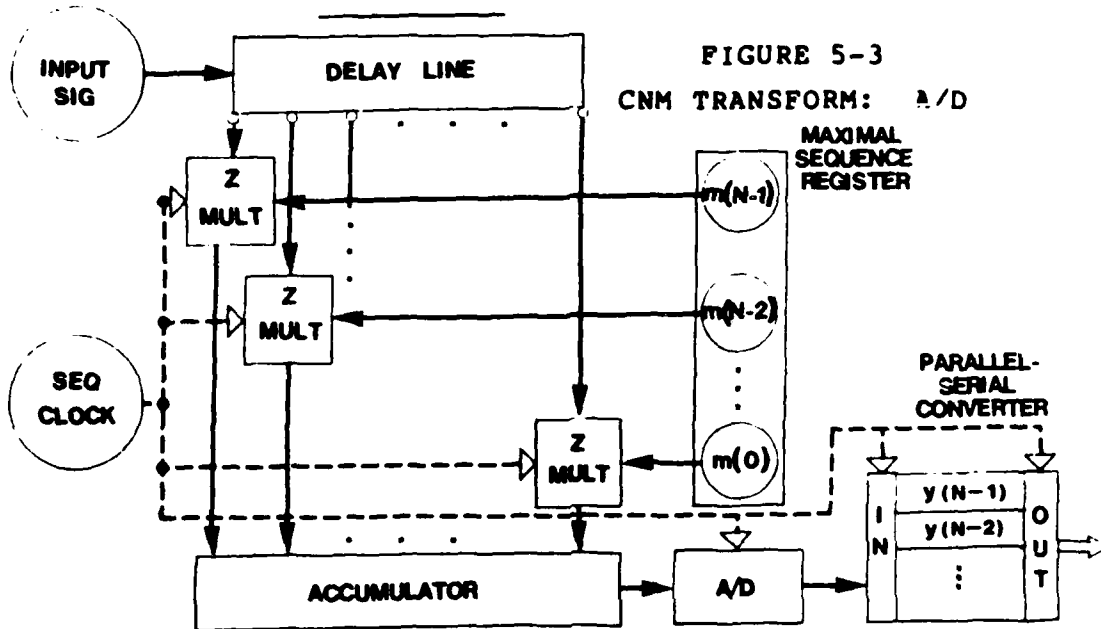


FIGURE 5-3
CNM TRANSFORM: A/D

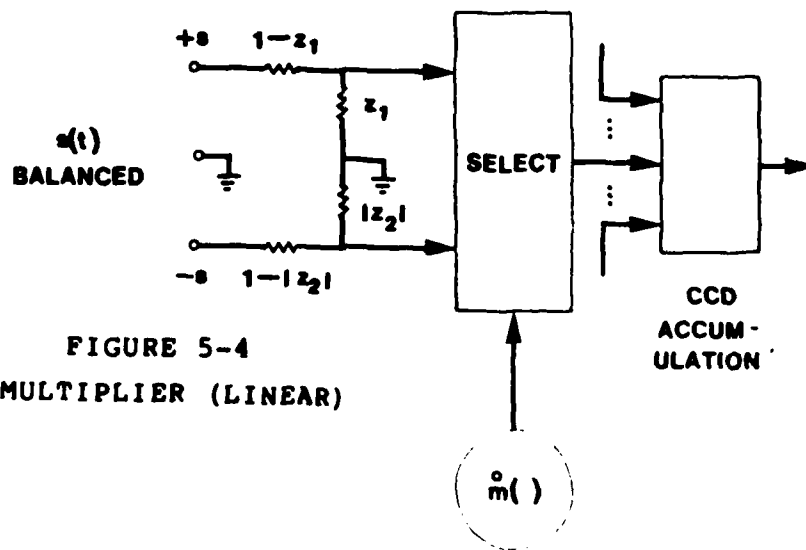


FIGURE 5-4
Z-MULTIPLIER (LINEAR)

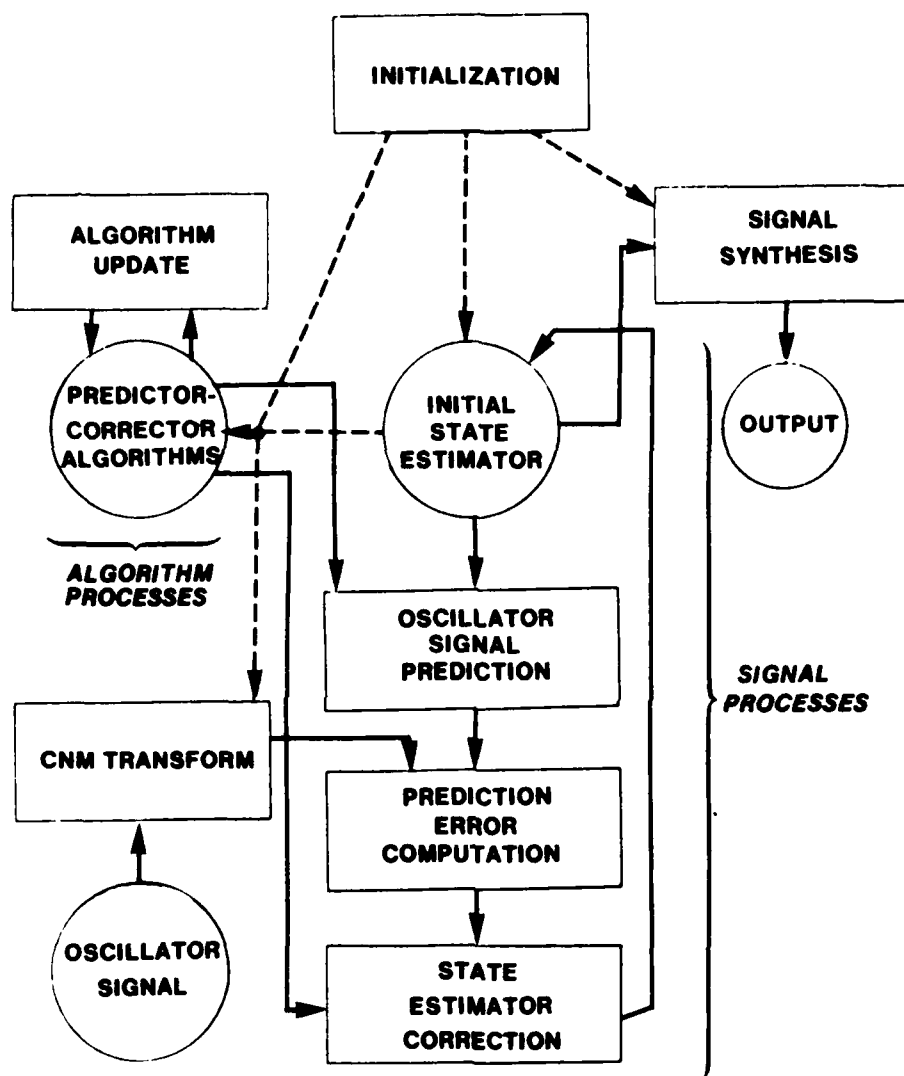


FIGURE 5-5
INITIAL STATE ESTIMATION PROCESSES

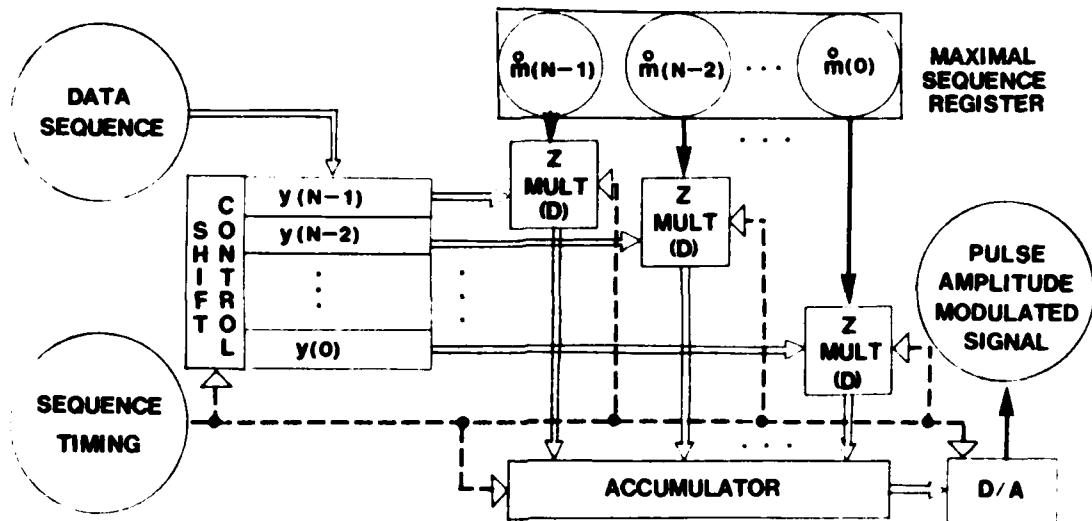


FIGURE 5-6
CNM TRANSFORM: D/A

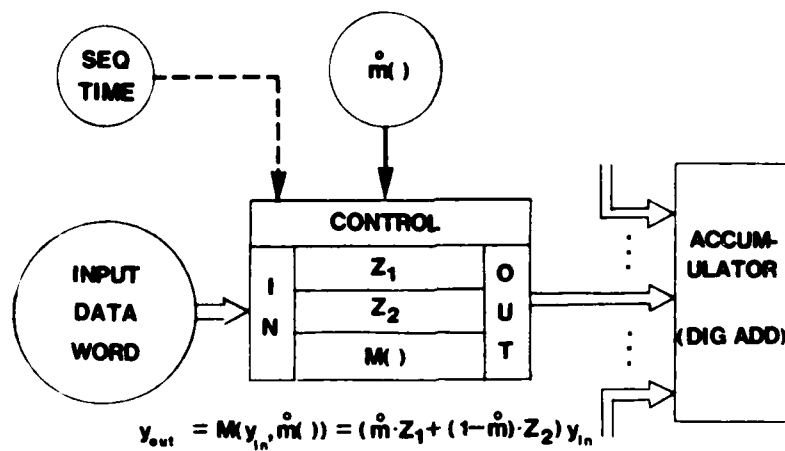


FIGURE 5-7
Z-MULTIPLIER (DIGITAL)

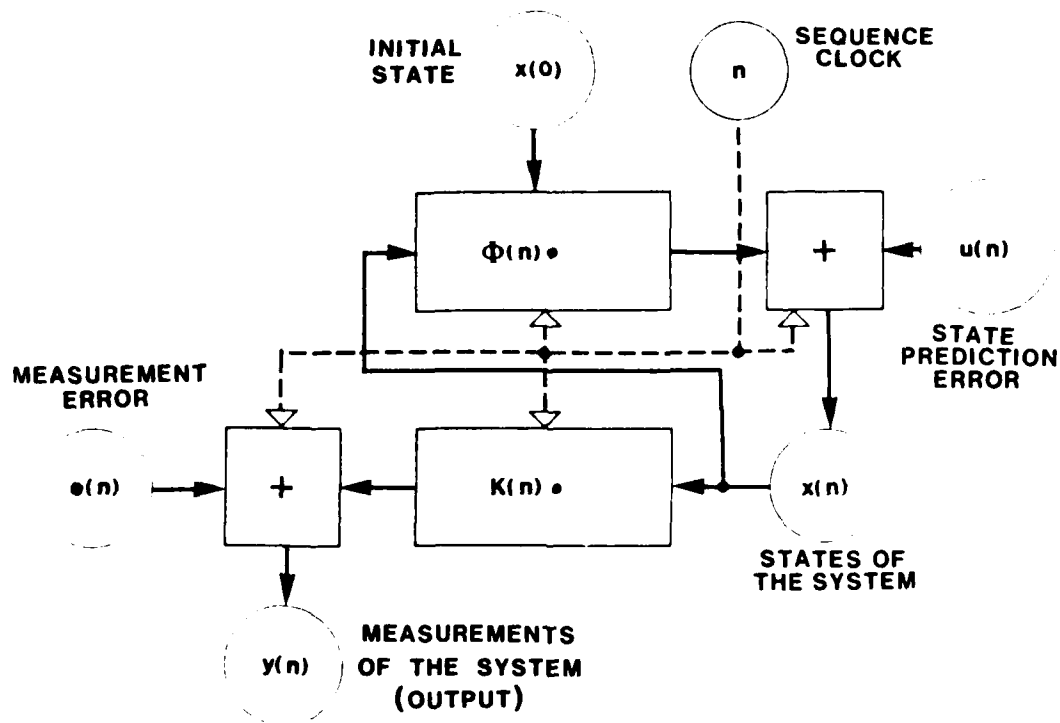


FIGURE A3-1
GENERAL RECURSIVE LINEAR SYSTEM WITH UNCERTAINTY

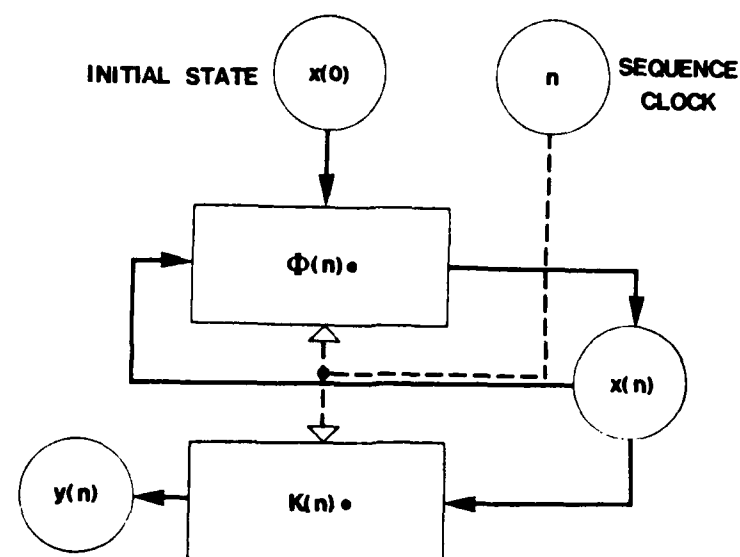


FIGURE A1-1
IDEAL LINEAR SYSTEM

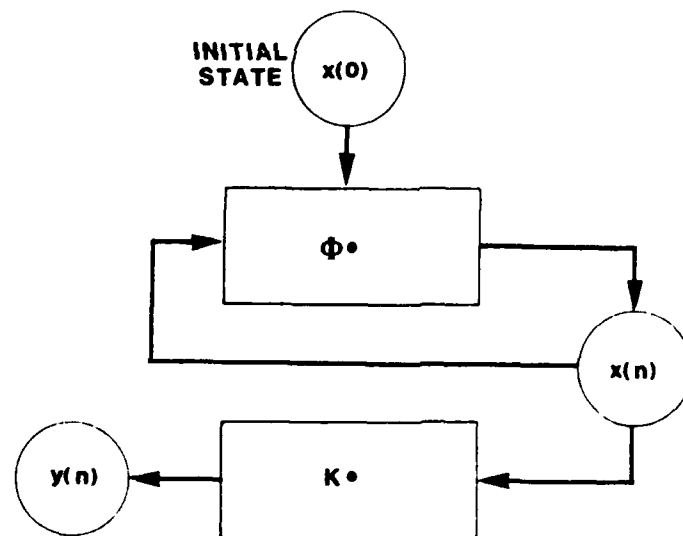


FIGURE A2-2
IDEAL TIME-STATIONARY LINEAR SYSTEM

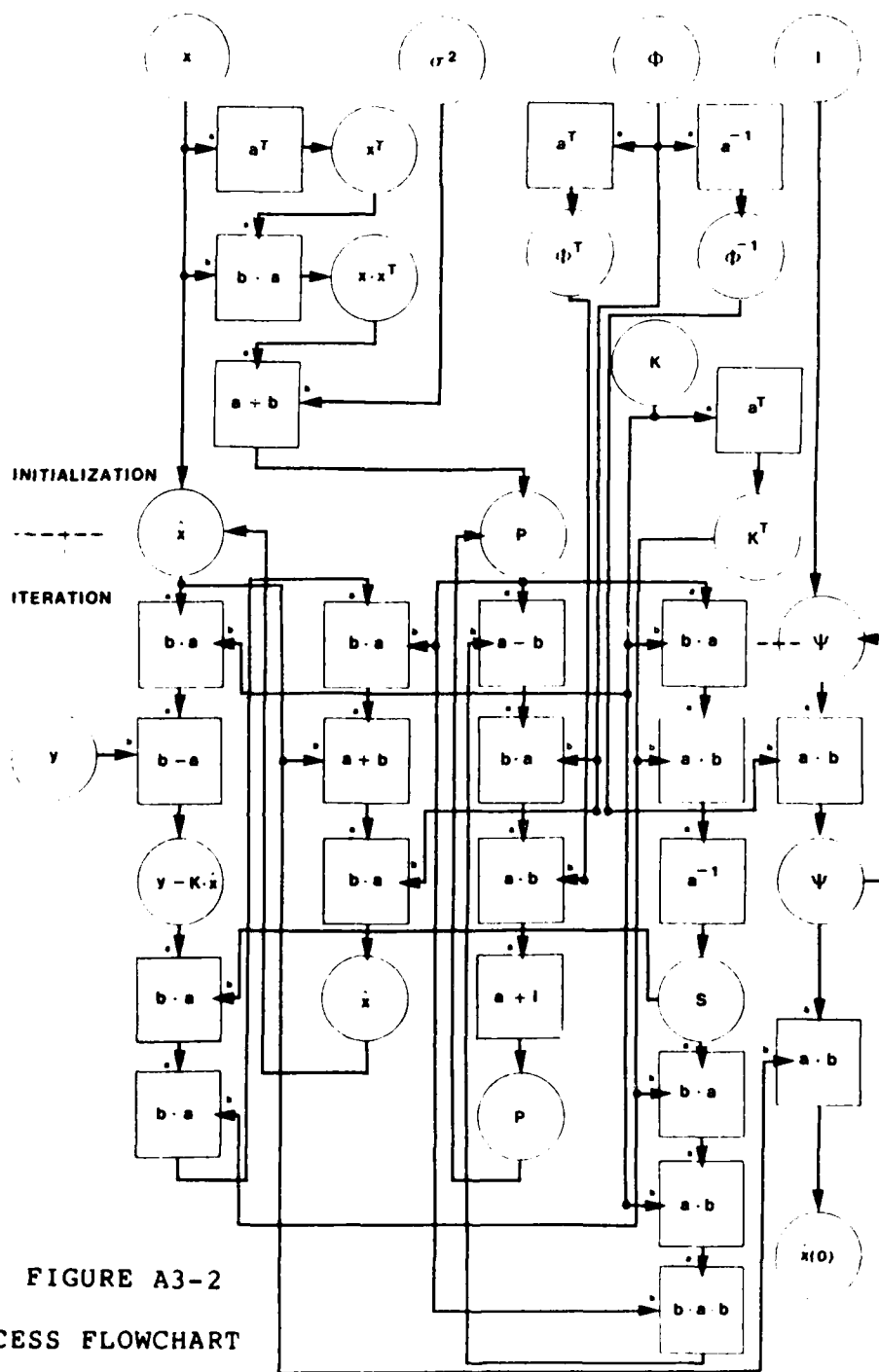


FIGURE A3-2
PROCESS FLOWCHART

QUESTIONS AND ANSWERS

DR. WINKLER:

I'm sorry, but I still do not understand why you deliberately almost, seem to avoid having your sequence timer coherent with your precision frequency source. Is there any advantage with not having it coherent? Unless for cheapness.

MR. KIMME:

I wish it to be cheap.

SESSION V

PTTI COMPONENTS

Dr. Authur O. McCoubrey, Chairman
National Bureau of Standards

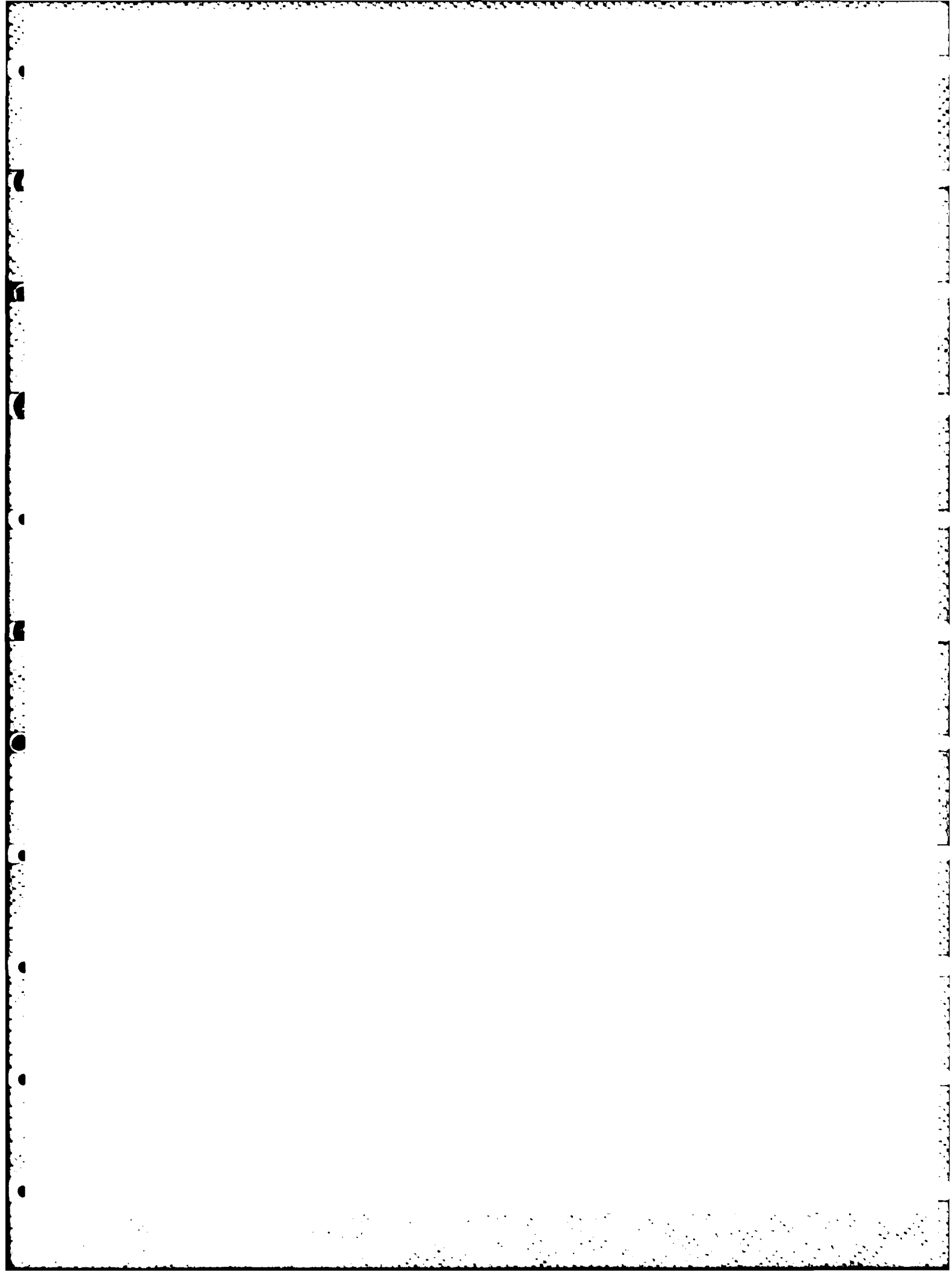
CALL TO SESSION V

DR. MCCOUBREY: I welcome you all this morning to the final session of the Fifteenth P.T.T.I. Meeting. The program this morning is somewhat different than listed in your booklet; it's been revised a little bit. In the first place, Paper No. 31, listed in your program, will not be given. The authors of that paper did not arrive. Paper No. 36, as listed in your agenda, is also withdrawn, and in its place there will be a paper for which the abstract is on Page 45 of your program.

The title of this paper will be, The Superconducting Cavity Stabilized Ruby Maser Oscillator, by G. J. Dick, Low Temperature Physics of California Technology and D. M. Strayer, J.P.L.

Finally, Paper No. 38, will also not be given, since the authors were not able to attend.

Paper #31 was neither given nor submitted for publication.



HIGH PERFORMANCES FROM A NEW DESIGN
OF CRYSTAL OSCILLATOR

C. BEAUVY , G. MAROTEL , P. RENOULT .

Compagnie d'Electronique et de Piézo-Electricité .

ARGENTEUIL FRANCE

ABSTRACT

This paper describes new designs developed and applied in order to increase the performance of crystal oscillators for military and space applications, requiring high performances.

The following performances have been reached :

- at frequencies of 10 MHz or 10,230 MHz : long term stability 10^{-10} per month ; drift in temperature range (from -40 to $+70^{\circ}\text{C}$) some parts of 10^{-10} ; short term $5 \cdot 10^{-13}$; spectral density $< 160 \text{ dBc/Hz}$, g-sensitivity $< 2.5 \cdot 10^{-10}$ per g, which allows high immunity against induced side bands under vibrations.

These results have been obtained from :

- the developments of a new technology applied to crystal resonators
- the use of a low noise design of the electronics associated with the resonator
- highly miniaturized oven with PID control
- assembly of these elements have met these specifications during mechanical environment tests.

INTRODUCTION

Since several decades, oven controlled crystal oscillators in a large range of frequencies from 1 MHz to 200 MHz, offering high performances in stability and spectral density, have been improved by CEPE. From this large experience for research, development and manufacturing OCXO and other kinds as XO, TCXO, VCXO ; with the contribution of new techniques on resonators and with the support of precise systems of measurements, a new generation of ultra stable oscillator, (USO), is now under development to satisfy the requirements during the next decade.

These USO are designed for a nominal frequency of 10 MHz ; frequencies about 10 MHz, for example 10.230 MHz can be also achieved. The domain of stability involved is 10^{-10} per month and under environmental conditions. According to the environment, it has been defined three types corresponding to the fields of application (fig 1).

1. USO for fixed equipments : continuous operation; easy environmental conditions, volume and power consumption are not critical.
2. USO for transportable or airborne equipments : intermittent operation, severe operating conditions, volume and possibly power consumption to be minimized.
3. USO for satellite applications : performances to be maintained after launch, volume and power consumption to be minimized.

Considering these different domains which could lead to contradictions, it has been nevertheless possible to define a basic design, with extensions suitable for specific requirements.

The study and development have been done on the following elements which are described in the first part :

- High Q resonators

- Circuits of the oscillator and the oven
- Mechanical assembly.

In the second part, tests results of following parameters are presented :

- Long term stability
- Mean term stability
- Short term stability
- Spectral density
- Influence of environmental conditions
- Turn on time and retrace.

DESCRIPTION OF INCORPORATED ELEMENTS

An ultra stable oscillator has to be considered as a sub-assembly in an equipment ; each function is depending of the others. Nevertheless, three main subjects can be considered as shown in block diagram (fig 2).

Crystal resonators

In this field, CEPE has now the capability of manufacturing high Q resonators at 10 MHz or 10.230 MHz standard frequencies ; it is also possible to provide other frequencies in the range of 5 MHz to 20 MHz, having a product $Q \times F$ of 12×10^{12} with the support of the following facilities :

- choice of the overtone : 3rd or 5th
- choice of the doubled rotated cut : SC ...
- choice of the assembly technologies : classic means with plated electrodes and mounted on springs: QAS plated electrodes, isolated from the active part of the plate by quartz bridges ; BVA electrodes separate from the quartz active

- plate, using quartz bridges as QAS and assembled by clips.
- improved experience on technics of machining and polishing the plates, of metallisation, outgasing and closing procedures.

In other respects, the facilities of measurement of the achieved resonators have been completed by precision test sets allowing short term 0,1 to 1000 s and g-sensitivity measurements at the operational temperature of the oven adjustable between 50 and 90°C.

These facilities and capabilities allow the choice of the resonator adapted for each domain of utilization and improved before mounting in the oscillator in the oven.

Electronic circuitry

Two main parts can be distinguished :

- the oscillator (fig 3)
- and the oven (fig N° 4)

The oscillator includes the following elements :

- the transistorized oscillator which is a Clapp giving a low drive level of about 30 μ W on the resonator. The components must have a low noise level especially the transistor.
- the varactor, in series with the resonator, permits the adjustment of the frequency by a control voltage.
- the voltage regulator has to be designed for a low noise and effective protection against the ripple of the power supply.
- the additional buffer amplifiers give an insulation between the oscillator and the external mismatch of the frequency output.

The circuits of the oven are constituted by thermistors, DC proportional amplifier and heating elements. The thermistors located

near the crystal case, are glass welded small size type because they have a good long term stability. The proportional amplifier associated with integrator and derivator circuits ensures with a high sensibility, a good stability without ondulation. The heating elements are made with power transistors on which it is possible to adjust the required power.

Mechanical assembly

The purpose was to reduce as much as possible the volume to be maintained within several hundredths of degree centigrade. For this reason the elements to be in the oven: crystal and the oscillator and some other parts of the electronics have been designed in mini electronic or hybrid assembly (fig N° 5).

Also specific hybrid circuits including the thermistor and a chip of power transistor were developed on BeO substrate to ensure a tight thermal coupling between these elements and the crystal housing.

Mechanical design of the assembly takes in account the thermal losses corresponding to the optimization between a fine regulation and a power consumption as low as possible fig N° 6).

Thermal insulation can be eccofoam, or still air between non radiative walls, or vaccum. If necessary , in particular requirements, a second oven can be added.

RESULTS OF THE PERFORMANCES

In this section, the key parameters of the performances are presented.

Long term stability

This parameter is measured in stable conditions : continuous operating, supply voltage, load and external temperature are constant at the moment of the measurement. For this type of USO, in the perfor-

mance of $\pm 10^{-11}$ per day is obtained after 10 days of continuous operation. The level of some 10^{-10} per month is obtained after 2 months of continuous operation and we expect $\pm 1.10^{-9}$ per year.

These measurements are done on a fully automatic testing equipment referenced by a Cesium standard (figure 7) on which the result of stability per day is given on the last ten days.

Mean term stability

This domain concerns the stability between 100 s and one day, in continuous operation, taking into account the drifts due to slight changes in power supply, load and temperature. This requirement is specifically expressed by the drift of the external temperature at about 5 or 10°C / per hour related to the kind of the mission.

The measurments are made with a programmable test chamber and the the frequencies are recorded each 10 s during 15 minutes, the slope p and the dispersion σ are calculated with goal of $p = 1.10^{-12}$ / min. and $\sigma = 3.10^{-12}$.

Short term stability

This parameter, also designed by stability in time domain, can be achieved by comparaisn of two or three USO of the same type running in continuous operation. The measurments are made on a specific test system including a low noise mixer, a low noise amplifier, a low band pass filter giving a resolution better than 10^{-11} over 10 ms and 5.10^{-14} over 100 s. The results are expressed by $\sigma_y(\tau)$ as function of τ by the formula of Allan or Pincibono variance. The results are given on fig N°8.

Spectral density

The spectral density $\mathcal{L}(f)$ is defined as a ratio between the power of the phase noise in a bandwidth of 1 Hz at the frequency f from the

carrier and the total power of the signal. Because of the high Q factor of this oscillator, the spectral density will be at -130 dBc/Hz at 10 Hz and -160 dBc / Hz at 1 KHz (fig N° 9). The measurement set has the basic configuration of the previous one, coupled with a low frequency analyzer and a graphic plotter; the resolution reaches - 170 dBc / Hz.

Influence of the environment

The characteristics of stability and spectral density have to be maintained in the proper environmental conditions specified for each application. The following parameters have been taken into consideration :

a) - external temperature

by using SC crystals and a precision electronic compact design for the oven, the stability of $2 \cdot 10^{-11}$ peak-peak from + 10 to + 40°C or $2 \cdot 10^{-10}$ peak-peak from - 40 to + 70°C in the total temperature range (fig N° 10).

b) - g-sensitivity

Due to the new developments on crystal, a stability as low as $3 \cdot 10^{-10}$ per g in all directions is achieved. This value drops to $5 \cdot 10^{-11}$ per g in all directions, if required.

c) - vibrations and shocks

by a ruggedized conception of PCB and assembly, the USO is able to support high levels of mechanical stresses :

- under sine vibration 20 g up to 2000 Hz
- under random vibrations 25 g rms up to 2000 Hz
- under shocks 100 g - 11 ms

c) - pressure

the performances under vacuum are also guaranteed by a specific design due to thermal losses.

Turn-on time and retrace

The performances in this domain are mostly important in intermittent operational conditions. In order to make comparative measurements, the following procedure is applied : after the measure of the slope $p_1 \Delta F / F$ per day before turn off, the oscillator is stored at ambient temperature during 24 hours and the frequency is recorded after turn-on at t_0 . The retrace is defined as the gap of frequency between the frequency before turn-on and the frequency obtained when the slope p_2 is equal to p_1 (fig N° 11).

This gap depends on the power available, on the capability of resonators and the miniaturization of the oven. The influence of the number of retraces and of the temperature of storage will be also measured.

The results obtained with a power consumption of 5 W during less than 1 min., with a QAS resonator is shown in fig N° 12 which gives retrace of $\pm 2 \cdot 10^{-10}$ after 100 min. and even the stability of $\pm 1 \cdot 10^{-9}$ have been reached after 10 min. operation.

CONCLUSIONS

Since the USO are tuneable by external adjustment of voltage applied on the varactor, the long term drift can be permanently or periodically compensated by the external circuitry shown on fig N° 13 .

By combination of QAS and BVA resonators and new design of the electrical and mechanical parts of the ovenized oscillator, it is now possible to define a new generation of USO (fig N° 1bis) giving at great improvement to the different fields of application.

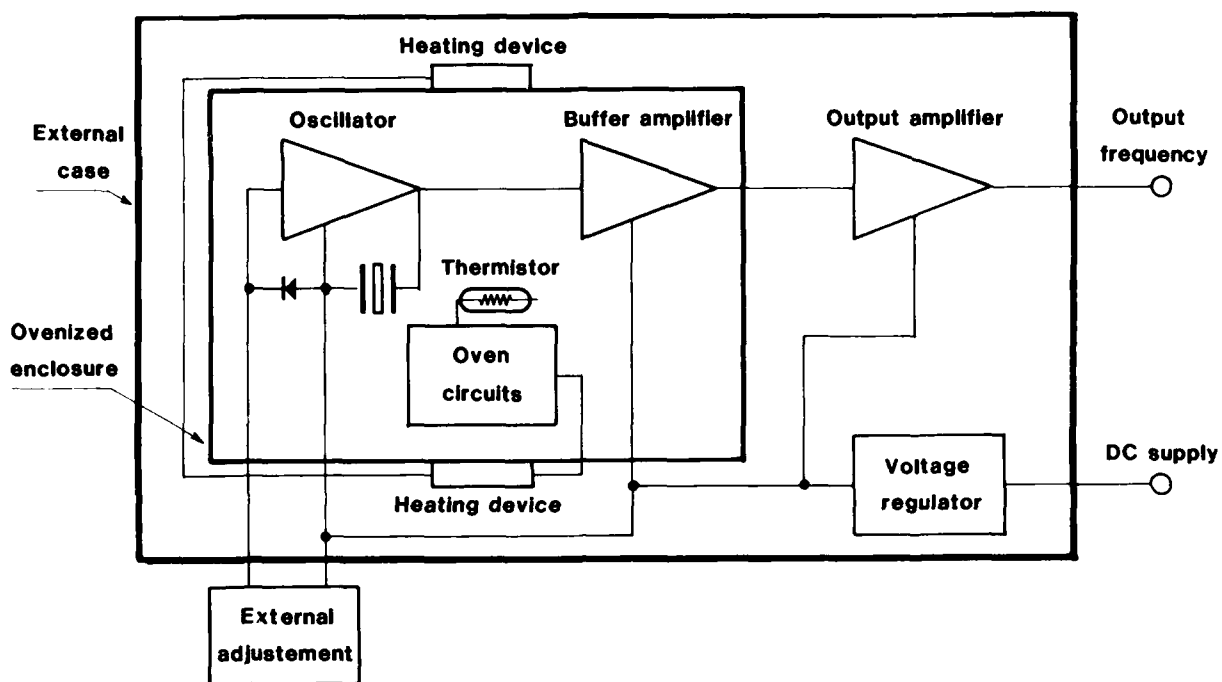
Thus, these USO offer with an expected duration of life of ten years, performances comparable and even better, than those offered by other secondary references of frequency.

	① USO-Metrology	② USO-Transportable	③ USO-Satellite
Operation	continuous	alternative storage/continuous	storage + continuous
Environmental conditions			
-operating temperature	0 to 50°C	-40 to +70°C	10 to 40°C
- vibrations - shocks - accelerations	no	yes	yes in storage no in operation
Power consumption	no	no	yes
Small size	no	yes	yes

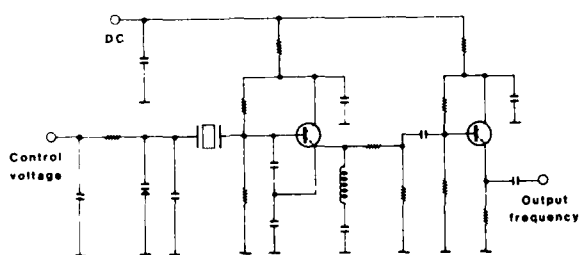
1 - Classification of Ultra Stable Oscillators

		OCXO PMT.P	USO
Long term stability	$\left[\begin{array}{l} 1\text{day} \\ 1\text{month} \\ 1\text{year} \end{array} \right.$	$\pm 5.10^{-10}$ to $\pm 5.10^{-11}$ $\pm 1.10^{-8}$ to $\pm 1.10^{-9}$ $\pm 5.10^{-8}$ to $\pm 1.10^{-8}$	$\pm 5.10^{-11}$ to $\pm 1.10^{-11}$ $\pm 1.10^{-9}$ to $\pm 2.10^{-10}$ $\pm 1.10^{-8}$ to $\pm 2.10^{-9}$
Mean term stability	$\left[\begin{array}{l} +10 \text{ to } 40\text{C} \\ -40 \text{ to } 70\text{C} \end{array} \right.$	3.10^{-9} pp 1.10^{-8} pp	5.10^{-11} pp 2.10^{-10} pp
Short term stability	$\left[\begin{array}{l} 1\text{ms} \\ 1\text{s} \\ 10\text{s} \end{array} \right.$	4.10^{-10} 5.10^{-12} 5.10^{-12}	4.10^{-11} 6.10^{-13} 5.10^{-13}
Spectral density dB/Hz	$\left[\begin{array}{l} 10 \text{ Hz} \\ 100 \text{ Hz} \\ 1 \text{ KHz} \end{array} \right.$	120 135 150	130 147 158
Retrace after turn on	$\left[\begin{array}{l} 10 \text{ mn} \\ 100 \text{ mn} \end{array} \right.$	1.10^{-8} 2.10^{-9}	1.10^{-9} 2.10^{-10}
g-sensitivity	per g	5 to 2.10^{-9}	5.10^{-10} to 5.10^{-11}

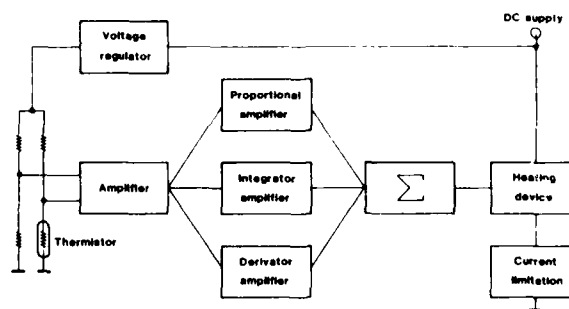
1bis - Comparaison between OCXO and USO



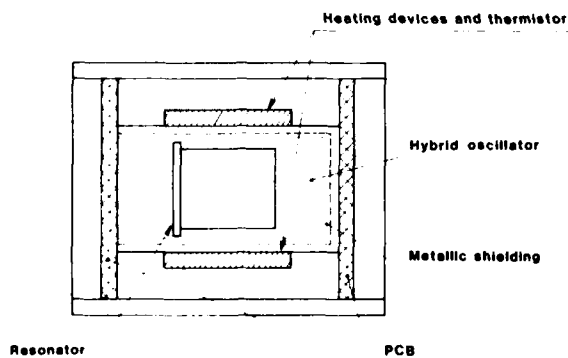
2 - Block diagram



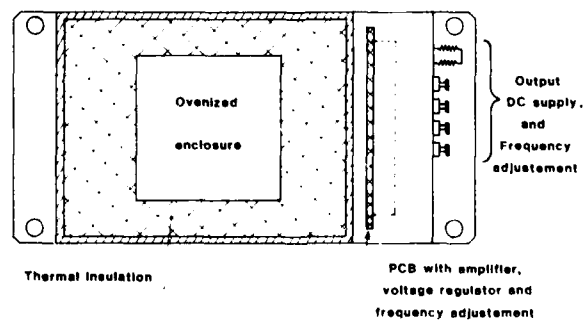
3 - Clapp oscillator



4 - Oven circuits



5 - Ovenized enclosure



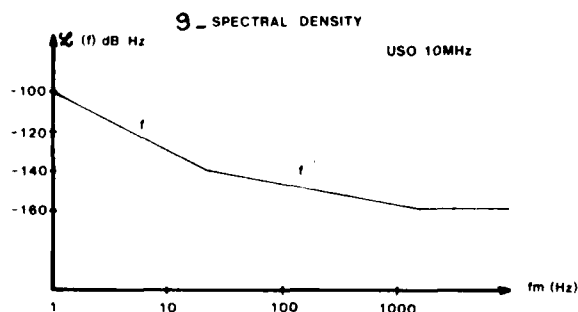
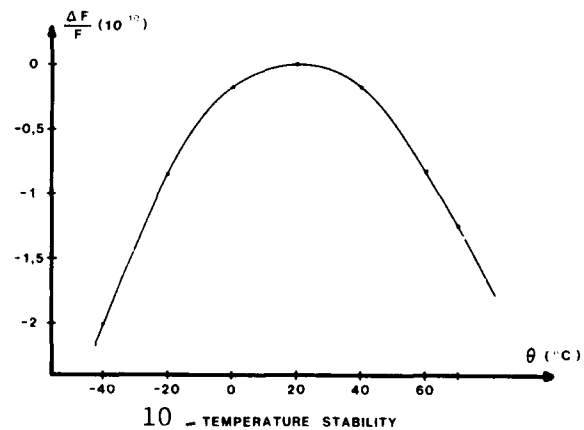
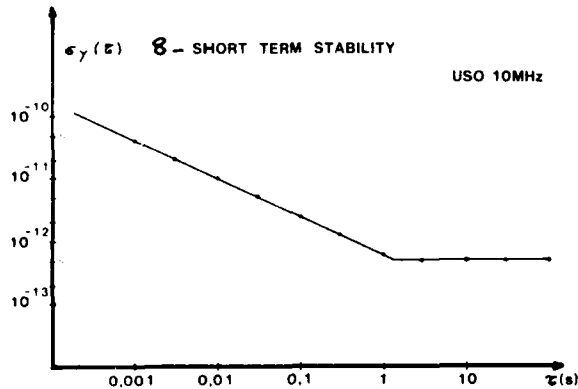
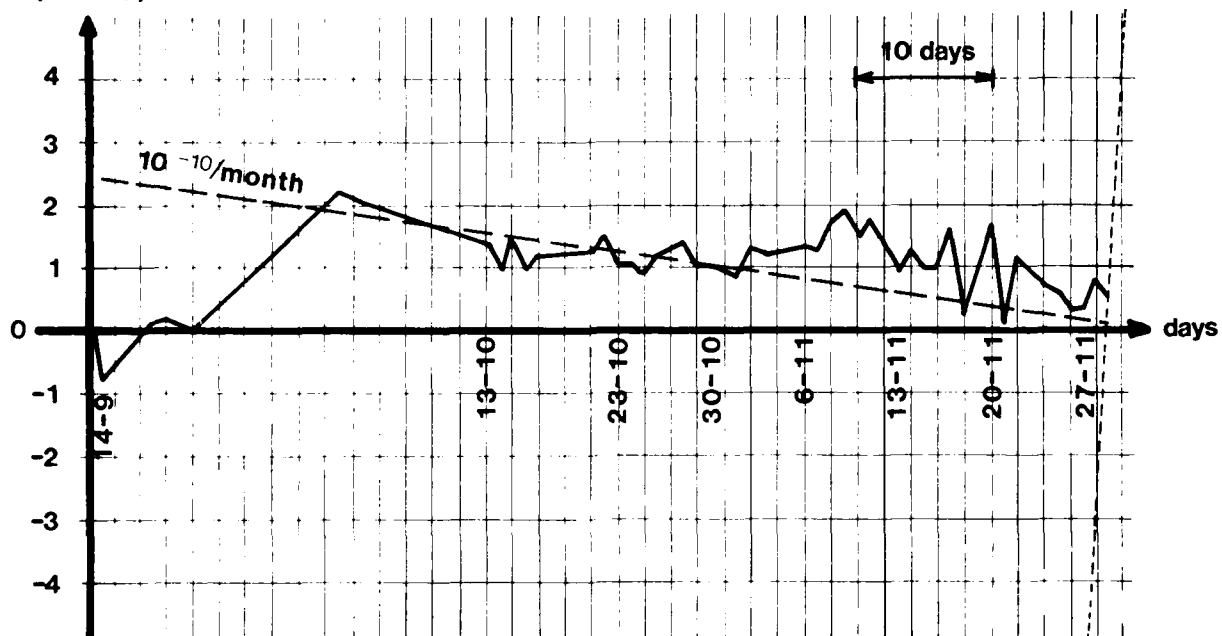
6 - USO mechanical design

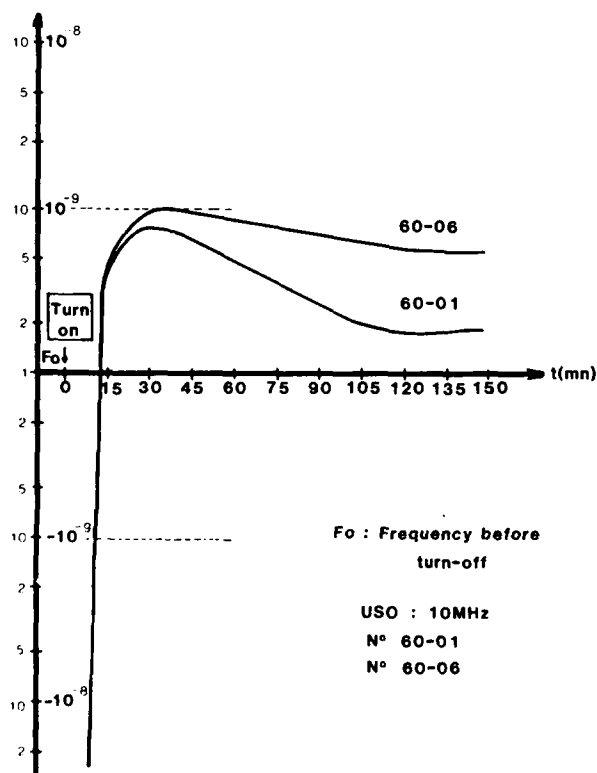
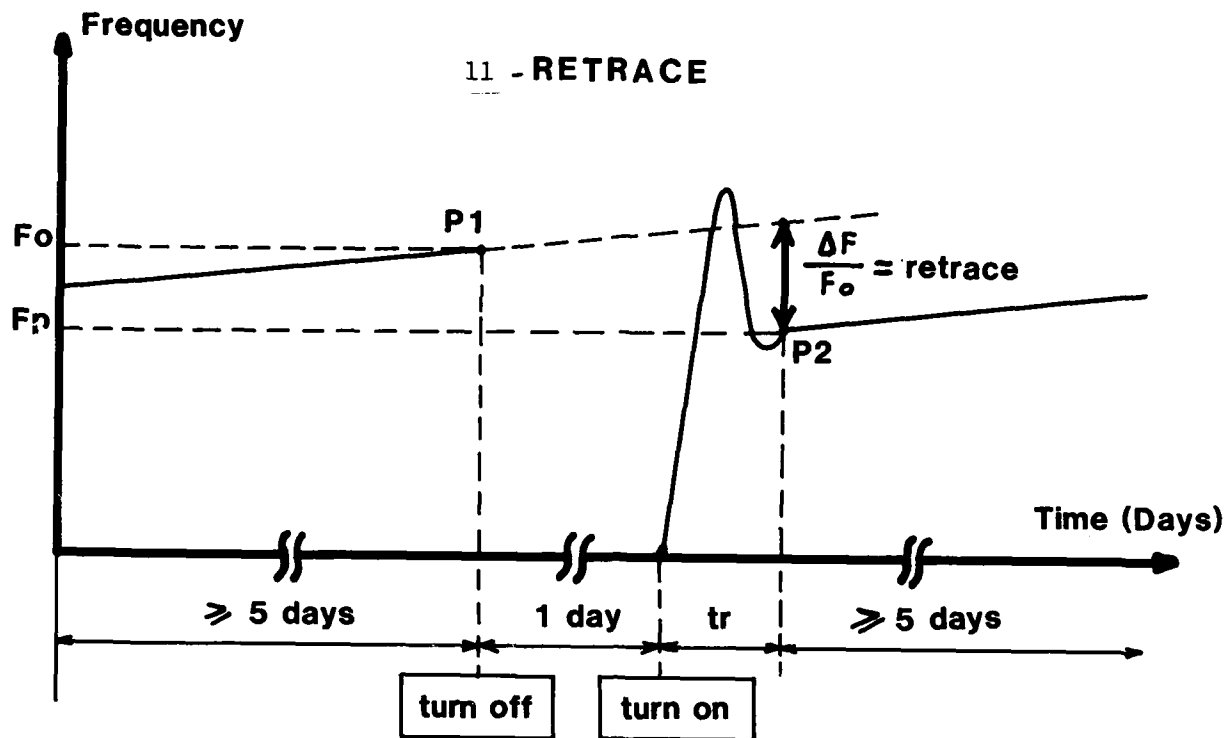
7 - AGEING

$\frac{\Delta F}{F}$
(1E-10)

Slope per day : $-6.92E-12$

USO 375
Number : 4 L16157
Fo : 10 MHz



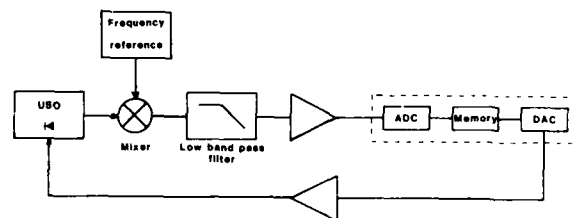


F_0 : Frequency before
turn-off

USO : 10MHz

N° 60-01

N° 60-06



13 - EXTERNAL ADJUSTMENT

12 - MEASUREMENT OF RETRACE

QUESTIONS AND ANSWERS

MR. CAMP:

The warmup time that you showed for SC seems to be relatively long. You mentioned one of the limits was the amount of power available. How long did it take for the oven to cut back on the power?

MR. BEAUVY:

This time was some three minutes, or something like that if you start at 20°C.

MR. GOLDBERG:

EGG. What is the size oscillator you showed?

MR. BEAUVY:

External, about ten centimeter cubic. Ten centimeters on each side.

MR. McCOUBREY:

To what extent is the spectral density of the noise performance and the short term stability achieved considering the theoretical limits?

MR. BEAUVY:

Do you mean the theoretical limits which are located about -130 db for spectral density?

MR. McCOUBREY:

Yes.

MR. BEAUVY:

There is some progress to be done, but there are also limitations due to the electronic circuits and also the loaded Q value of the resonator, and some things like that. So I think this improvement is one of the best that can be done today.

MR. McCOUBREY:

What is the most important source of noise now, is it the crystal or the electronics?

MR. BEAUVY:

I would say both of them, it depends if you are at a place near the carrier or far from the carrier. So for some radar applications, we build oscillators for 100 or 200 megahertz, and what is important, is not noise near the carrier, but noise far from the carrier.

We can achieve much better results, starting with a hundred megacycle direct, instead of starting with ten megacycles with multiplication, but of course you are not so good right near the carrier in this case.

DESIGN OF SC CUT 10 MHZ H.Q. CRYSTALS
WITH G. SENSITIVITY BETTER THAN 2.10^{-10} /G.

A. Debaisieux, J.P. Aubry, Compagnie d'Electronique et de Piézo Electricité - Argenteuil
J. Groslambert, Laboratoire de Physique et
Métrologie des Oscillateurs du C N R S à
Besançon - France

ABSTRACT

Several theoretical and experimental studies on the force-frequency effect have shown that the g sensitivity of a crystal resonator is directly related to the location and structure of the mounting support.

Our work has lead to the definition of a new design of crystal resonator having low sensitivity. The effects of both surface and body forces applied to the vibrating part of the crystal must be considered.

In this paper, the details of this new design are presented.

Statistical results show that g sensitivity between 3.10^{-11} /g and 2.10^{-10} /g on the worst axis are currently obtained on an industrial basis.

These values are measured by a 2 g tip over test in all directions either with Phase Modulated Reflectometer (which are also described at 5 and 10 MHz) or in classical oscillators.

INTRODUCTION

In numerous fields of the aerospace industry for communications, localization ... the needs of highly stable crystal oscillators has continually increased in quality as well as in performances.

In an hostile and vibration environment, the full potential of many

systems is severely limited by the acceleration sensitivity of the resonator.

The search of g sensitivity lower than $3 \cdot 10^{-10}/g$ and a high spectral purity of oscillator required by some modern applications leads to the development of new manufacturing processes which involve high technologies such as SC cut, ultrasonic machining, ultra high vacuum...

The first theoretical approach of the acceleration sensitivity was presented by Lee and Kuang Ming Wu in 1976. / 2 /

At the same time, this problem was investigated by Valdois, Janiaud, Gagnepain. / 1, 5, 7 /

The force frequency effect is also of interest when dealing with g sensitivity of crystals resonators.

The first theoretical explanation of the force frequency effect was presented by PCY Lee Wang and Markenscof . They use an isotropic assumption for the determination of the plane stress distribution induced by the mounting support of a plate submitted to in-plane acceleration. Their results, given for AT cut, were in good agreement with the experimental values.

A more precise solution making allowance for the anisotropy of crystal was given by Ballato EerNisse and Lukasek. This study was applied to doubly rotated quartz resonator. / 4 /

Nevertheless, even if some of the phenomenon implicated in g sensitivity have been extensively described, there are not yet many crystal resonators which have been demonstrated with a low g sensitivity in all directions of space. / 3, 11 /

However, some interesting results have been obtained with the B V A design quartz crystal resonators. It is assumed that the quartz bridges support of the resonator in the B V A design allow reduction of most of the stresses, applied on the vibrating area involved in g sensitivity.

The goal of this study was to achieve a g sensitivity better than

3.10^{-10} /g with a HQ SC cut resonator encapsulated in HC 40 can (to be easily used in classical oscillators) in order to reach a good compromise between performances (ageing, g sensitivity, retrace), volume, warm up time and price.

This paper describes the design of such a resonator and the reproducibility of g sensitivity results from batch to batch.

The g sensitivity measurements are performed with a phase modulated reflectometer locked on the crystal mounted in a separated oven allowing a " 2 g tip over " test. Two different phase modulation systems are described at 5 MHz and 10 MHz. (Fig. 7 - Fig. 8)

The 2 g test results are confirmed by 2 g test on oscillators and also by induced FM side bands under vibrations.

. I) THE PASSIVE REFERENCE SYSTEM

The principle of this system was presented by S.R. Stein in 1978 (ref.9) (Fig. 1). It consists in locking an oscillator of medium stability on a Xtal resonator driven in reflection. The output signal of the oscillator is phase modulated at an fm frequency. The output of this phase modulator is applied on the Xtal resonator with the help of a structural coupler. The reflected signal is amplified then detected. The oscillator is locked by using a synchronous detector working at the fm frequency.

In this system the most important part is the phase modulator which must be realized with care : this phase modulator must not exhibit amplitude modulation at its output. As a matter of fact the phase modulated signal after reflection on the Xtal resonator gives an amplitude modulated signal which presents a modulation index proportional to the frequency shift between the frequency of the oscillator and the resonance frequency of the Xtal. In this case all amplitude modulations at the phase modulator output have the same effects as frequency shift of the Xtal.

PHASE MODULATORS

Two types of phase modulators have been used in the present work.

The first one is a digital modulator which exhibits a phase modulation index proportional to the frequency to be modulated : consequently this system is limited when the modulation index becomes too large, but since this modulator is a digital one, an exactly signal $\pi/2$ out of phase with respect to the modulating signal can be obtained. This signal is used as reference signal in the synchronous detector.

The second one is an hybrid modulator (analog and digital), its upper working frequency depends only on the elements which are used to construct it. It needs a traditional phase shifter to obtain a quadrature signal for the reference channel of the synchronous detector.

- 1) Digital phase modulator

The phase modulation is obtained by using the time delay existing between the input/output signals of logic gates. A time delay ΔT produces a phase shift $\Delta\phi$ corresponding to

$$\Delta\phi = 2\pi \frac{\Delta T}{T} \quad \text{where } T \text{ is the HF signal period}$$

By associating N gates in series, a phase shift can be obtained in the range 0 to $N\Delta\phi$ with $\Delta\phi$ steps.

A four bits multiplexer (Fig. 2) gives the possibility by using eight gates and one 4193 divider to obtain a triangular phase modulation by connecting together the 1-15, 2-14, 3-13, 4-12 multiplexer input pins. The resulting phase modulation is given on Fig.3. This modulator works correctly below 7 MHz with an amplitude modulation rejection of about 80 dB.

- 2) Analog and digital phase modulator

This system (Fig. 4) provides the addition of the modulating signal and the high frequency signal and the application of the resulting signal to a Schmitt trigger. The output pulse of the Schmitt trigger is phase

modulated with pulse width modulation. A monostable circuit sets this pulse to a constant value determined by the time constant of the monostable. A sinusoidal modulated phase signal is obtained with this system.

. II) MOUNTING CONFIGURATIONS

Numerous studies have been devoted to force frequency effect and acceleration sensitivity of quartz resonators

To prevent frequency variations due to initial static stresses applied on a resonator by the mounting supports, it has been shown that it does exist angles ψ for which the force-frequency coefficient / 6 /

$$k f (\psi) = \frac{\Delta f}{f_0} = \frac{2hD}{F} \frac{1}{N}$$

becomes equal to zero.

These points are given as $\psi = 60^\circ$ and 120° for an AT cut and $\psi = 86^\circ$ and 179° for an SC cut. Anisotropy was shown to have little effect on the force frequency effect.

In-plane acceleration sensitivity has also been studied.

These phenomenon allow to expect, for a four points mounting (XX' , ZZ') configuration, a small variation of frequency for the AT cut. It must be pointed out that the locations of the mounting supports of an AT cut resonator, which minimizes the acceleration effects on the frequency, are not the same as those giving a null diametral force frequency effect.

Up to now, a study of acceleration sensitivity for the SC cut has not yet been published.

To solve the g sensitivity problem of a crystal resonator, we must consider all the forces (static and dynamic) applied on the vibrating area for all possible directions of acceleration in the full space.

Then we have considered all forces (surface and body forces, dynamic forces, initial stresses ...) which can be due to the mounting support or induced by an acceleration vector applied in a given direction.

Force frequency effect and in plane acceleration sensitivity must be both taken into account for the location of mounting supports, even if they do not give a full explanation of g sensitivity.

A more adequate model has been proposed to explain g sensitivity / 10 / (Fig. 5), involving the blank resonator and the mounting support taken in all directions. In this model, various forces are taken into account :

- . surface and body forces
- . torques coming from geometrical variation of the mounting ribbon
- . induced compressive forces

With the geometry described in this reference (which assumes no initial diametral stresses), one can see that the distribution of volume forces is not equal to zero in the center of the plate, which is the area of interest.

On the other hand, all the static stresses T_j are equal to zero in the center of the crystal .

From the classical equilibrium relation :

$$\rho \frac{\partial^2 u_i}{\partial t^2} = \text{div } T_j + F_i$$

where u_i : are the displacement vector

T_j : strains

F_i : body forces ,

we can see that any change in the distribution of body forces in the vibrating part of the crystal may induce a variation of resonant frequency.

A quartz resonator submitted to in plane acceleration (\ddot{x}) reaches the equilibrium from the balance between body forces ($m\ddot{x}$) and reaction forces due to mounting support, inducing a given stress distribution in the plate.

Submitted to out-of-plane acceleration (\ddot{w}) the resonator can be affected by diametral compression and torques. Furthermore, in this case, there is a lack of symmetry in the plane of the resonator, which changes the diametral compression in static thickness shear stress in the vibrating part of the crystal, inducing a variation of frequency.

The mechanical equilibrium of quartz resonator submitted to any acceleration is modified in terms of the direction of this acceleration, inducing a change of the stress distribution in the plane which leads to a variation of frequency.

In summary, it comes from these studies that the in-plane sensitivity is now more or less completely explained and expected to be solved by an accurate positioning of mounting supports.

Geometrical symmetry of the whole device (including mounting ribbons) around x_1 x_2 plane of the resonator, seems to play an important role in the out-of-plane g sensitivity.

Roughly speaking, we have to solve nearly independently in and out of plane g sensitivities.

Among the studies dedicated to this problem, BVA design has offered an interesting solution to minimize g sensitivity.

The two main concepts of BVA design are non plated electrodes and quartz bridges as mounting supports. These bridges are supported by a quartz ring.

Ultrasonic machining is used to obtain these quartz bridges by removing quartz material.

The quartz bridge technique must reduce greatly the initial stresses due to supports. The mounting configuration can show a good symmetry in the main directions of the quartz plate. Shape, location and orientation of these quartz bridges can be easily chosen to minimize most of the effects involved in g sensitivity. Mounting supports

can be located on the quartz ring, at any place regarding the location of quartz bridges or other parameters, such as Young modulus....

Furthermore this ring is a good mechanical filter, dissipating a part of the mechanical energy by its own deformation.

The whole structure (vibrating area, bridges, quartz ring, ribbons support) is expected to solve or to minimize the q sensitivity by reducing some initial and dynamic stresses.

. III) EXPERIMENTAL RESULTS

Following the conclusion described above, we have manufactured and tested various designs of QAS crystal resonators.

The parameters involved in this study were :

- . number)
- . location) of quartz bridges
- . configuration)

To obtain the QAS design we have used the ultrasonic manufacturing. With this process, the positions of the quartz bridges can be accurately adjusted regarding to the orientation axis of the crystal. The positioning is given by a goniometric table.

In order to achieve a low q sensitivity, it has been shown that the effects of σ_T and σ_N must be solved independently.

To prevent q sensitivity coming from diametral compression (initial stresses, σ_N), the location of bridges were chosen around the zero of the $K_q(\psi)$ curve applying to SC cut. (Fig. 6)

" In-plane " q sensitivity (σ_T) is mostly due to stresses at the boundary between vibrating area and quartz bridges.

The flexibility of the mounting and of the bridges has an effect on σ_N .

Location, various ratios of widths, lengths and thicknesses number of bridges between the vibrating area and the surrounding allow solutions to

both sensitivities.

Among the various designs we have tried, the most significant are :

- . 2 bridges (along ZZ' or XX')
- . 4 bridges (XX' and ZZ' with dimensions eventually different on each axis)
- . 4 bridges located at minimum of young modulus
- . 4 bridges located at ψ angles given by $k_y(\psi) = 0$ (Fig. 6)
- . 4 bridges symmetrical versus given direction

In this later configuration, it is expected that the superposition observed by Lukaszek and Ballato will apply, meaning that two diametral forces giving opposite effects will balance each other.

In each configuration of quartz bridges, we have tried various mounting support (2 or 3 points).

Two bridges and three points have allowed very low g sensitivity results but with a wide dispersion inside each batch of resonators, from $3 \cdot 10^{-11}/g$ to $8 \cdot 10^{-10}/g$

Insofar as our goal was to achieve $3 \cdot 10^{-10}/g$, we have selected a configuration for which we obtain a good percentage of resonators below this limit.

In the first batch manufactured by using this design, the results in g sensitivity can be summarized by the following table :

$\leq 2 \cdot 10^{-10}/g$	$\leq 3 \cdot 10^{-10}/g$	$\leq 4 \cdot 10^{-10}/g$	$\leq 5 \cdot 10^{-10}/g$	$\leq 7 \cdot 10^{-10}/g$
16 %	36 %	50 %	60 %	80 %

To test the reproducibility of the design and of the working procedure, we have manufactured three batches (50 pieces each) using the same structure.

The statistical results are given by figure 9 on which we can

see, more or less, the same g sensitivity distribution.

We verify that 35% of resonators, in each batch, have a g sensitivity smaller than $3 \cdot 10^{-10}/q$. These resonators being devoted to highly stable oscillators, g sensitivity with good electrical parameters, short term stability, retraceability ... are of great interest.

The Table II gives standard parameters and short term stability measured with the phase modulated reflectometer (Fig 10) or oscillator. Additional results reached by oscillators using such resonators can be founded in the paper given by C. BEAUVY

F (MHz)	L (H)	R (Ω)	Q (10^6)	$\sigma_y (f)$ (PMR)		Retrace 25°C 24 H
				10 s	100 s	
10 MHz or 10.130 MHz	1,2	63	1,2	$1 \cdot 10^{-12}$ $6 \cdot 10^{-13}$	$1 \cdot 10^{-12}$ $5 \cdot 10^{-13}$	$2 \cdot 10^{-10}$

TABLE II

From table II, we see that these resonators could be successfully used in high quality oscillators.

These results show that the QAS design has allowed great improvement to some interesting features such as short term stability or retraceability.

These improvements are assumed to be mostly due to homogeneity of the mounting of the quartz on its base through the quartz bridges.

CONCLUSION

Our work leads to the definition of a new design of HQ 10 MHz SC cut resonators (QAS).

With this design, we obtain for all directions of space a low g sensitivity with a good reproducibility from batch to batch.

35 % resonators manufactured have g sensitivity better then $3.10^{-10}/g$.
The best resonator was measured down to $3.10^{-11}/g$ on the worst axis.

We are still working on the design of quartz bridge in order to increase the ratio of low g sensitivity resonators by batch.

These resonators are shown to have very interesting factors to be used in high quality oscillators for military or space applications (low ageing rate, good retraceability, fast warm up) in addition to all advantages of classical SC cut (static and dynamic thermal behaviour, anisochronism ...).

It must be pointed out that the equipment we have described (PMR) allow sorting of the crystals during final production tests before the implantation in oscillators (g sensitivity, short term stability).

CEPE is using B.V.A. techniques due to R. J. Besson and his group (P. Maitre, J. P. Valentin and others...). Manufacturing is being developed with proper cooperation of the group.

(Patents No. 7601035 and No. 8315652-8315653-8315654)

REFERENCES

- 1) M. VALDOIS, R. BESSON and J.J. GAGNEPAIN, " Influence of support. Configuration on the acceleration sensitivity of quartz resonator plates " Proc. of the 31st Annual Symposium on Frequency Control 1977
- 2) P.C.Y. Lee and Kuang MING WU, " The influence of support configuration on the acceleration sensitivity of quartz resonator plates " Proc. of the 31st Annual Symposium on Frequency Control 1977
- 3) R.L. FILLER and J.R. VIG, " The acceleration and warm up characteristics of Four Point Mounted SC and AT cut resonators " Proc. 35th AFCS, 1981
- 4) A. BALLATO, E.P. EERNISSE and T. LUKASZEK, " The Force Frequency effect on doubly rotated quartz resonators " Proc. 31th AFCS June 1977
- 5) D. JANIAUD, L. NISSIM and J.J. GAGNEPAIN, " Analytical calculation of initial stress effects on anisotropic crystals : application to quartz resonators " Proc. 32th AFCS 1978
- 6) J.M. RATAJSKI, " The force sensitivity of AT cut quartz crystal " Proc. 20th AFCS 1966
- 7) M. VALDOIS " Influence des conditions d'environnement sur un résonateur à quartz " Thèse Université de Besançon 1974
- 8) Dr Donald A. EMMONS " Acceleration sensitivity compensation in high performance crystal oscillators. 10 th PTTI 1978
- 9) S.R. STEIN, C.M. MANNEY, Jr., F.L. WALLS, James E. GRAY " A system

approach to high performance oscillators ", Proceedings of the
32nd Annual Symposium on Frequency Control (1978), pp. 527-530

- 10) D. JANIAUD " Influence du support sur la sensibilité aux accélérations d'un résonateur à quartz " C.R. Acad. Sc Paris t 28> B
(1977)
- 11) Raymond L. FILLER, J.A. KOSINSKI and J.R. VIG, " Further Studies
on the acceleration sensitivity of quartz resonators "
- 12) R.J. BESSON French patent N° 7601035
CEPE French patents N° 8315652 - 8315653 - 8315654

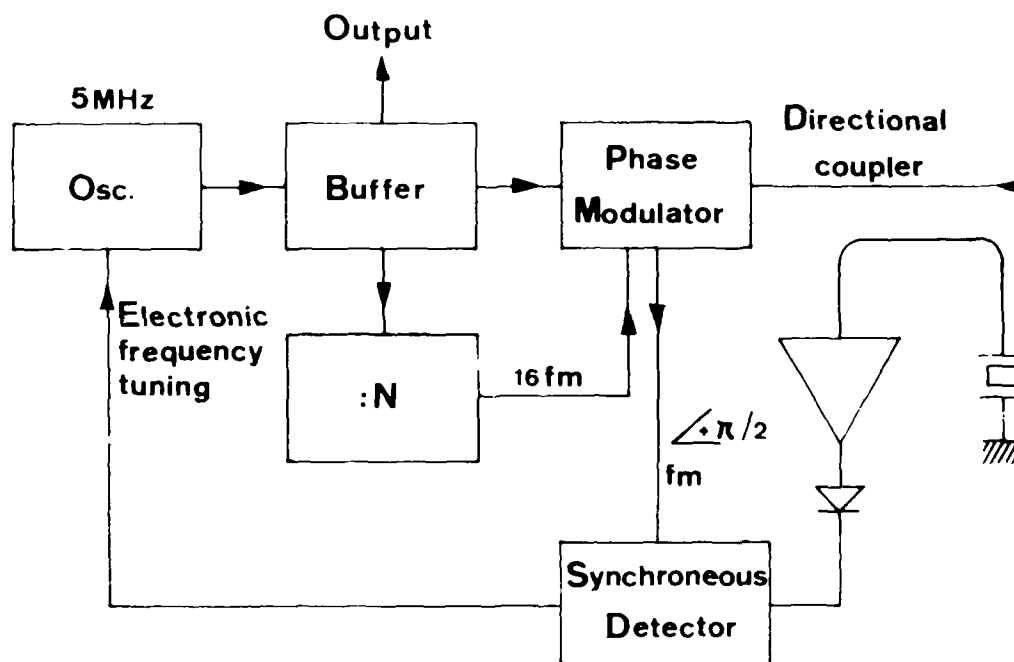
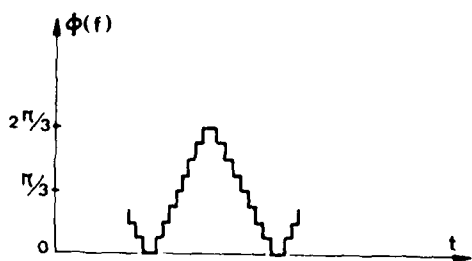
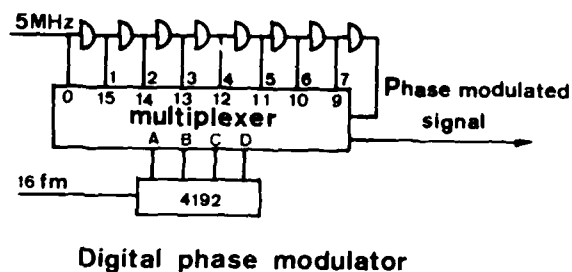
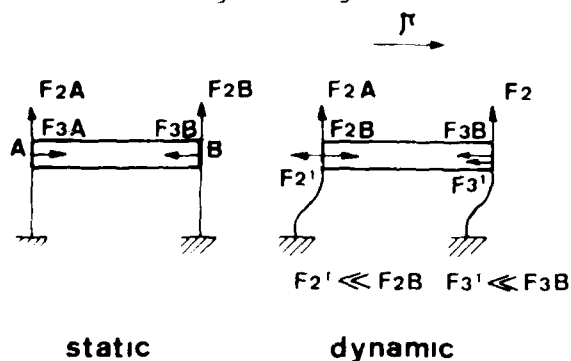


**Fig 1 SCHEMATIC DIAGRAM
OF THE PASSIVE REFERENCE SYSTEM**



Resulting phase modulation obtained with the digital phase modulator

Fig. 2 Fig. 3



STRESS MODEL

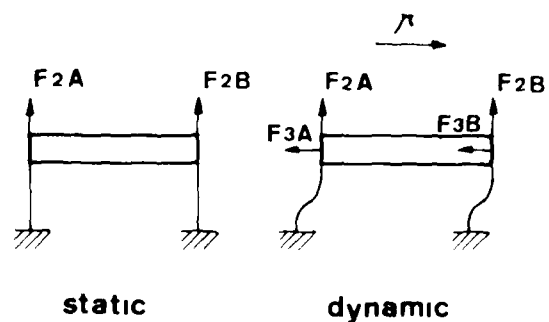
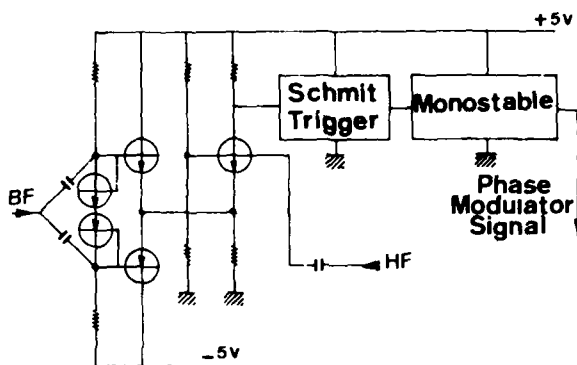


Fig5 ACCELERATION MODEL



ANALOG AND DIGITAL PHASE MODULATOR

Fig. 4

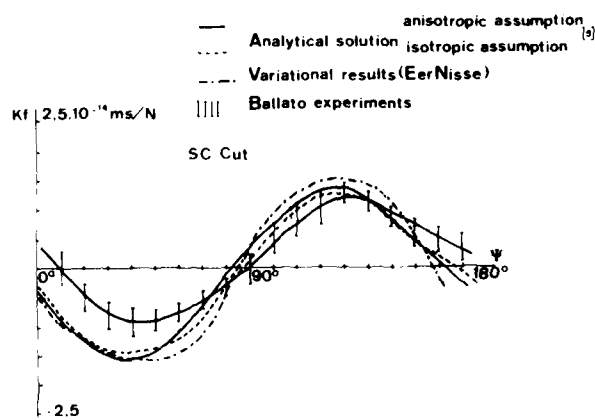
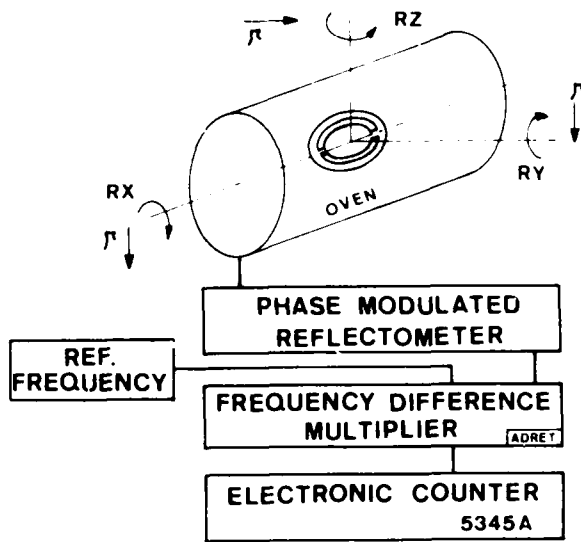
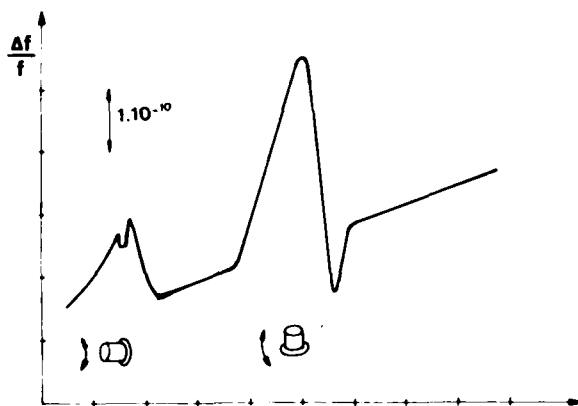


Fig. 6

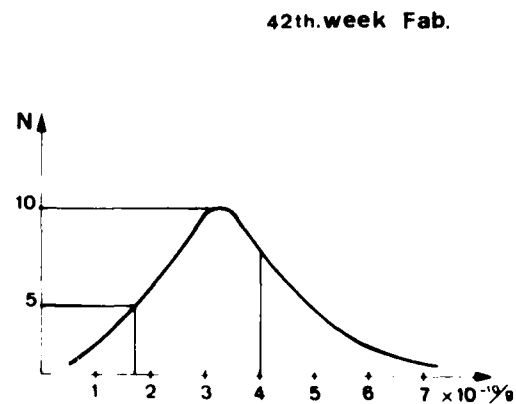
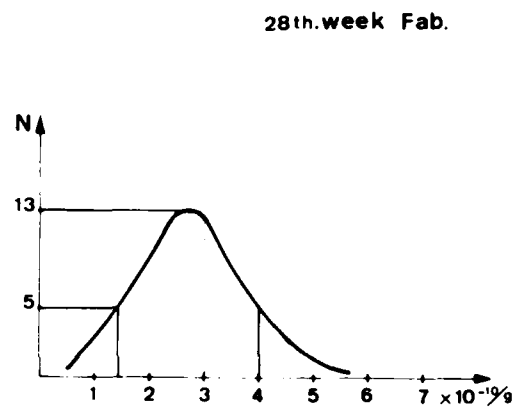
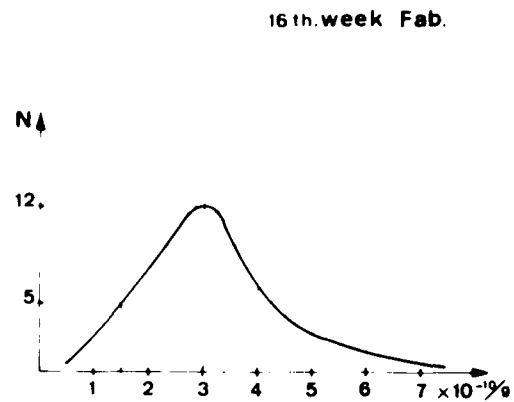


**Fig7 G. SENSITIVITY TEST BENCH
AND
SHORT TERM TEST BENCH**



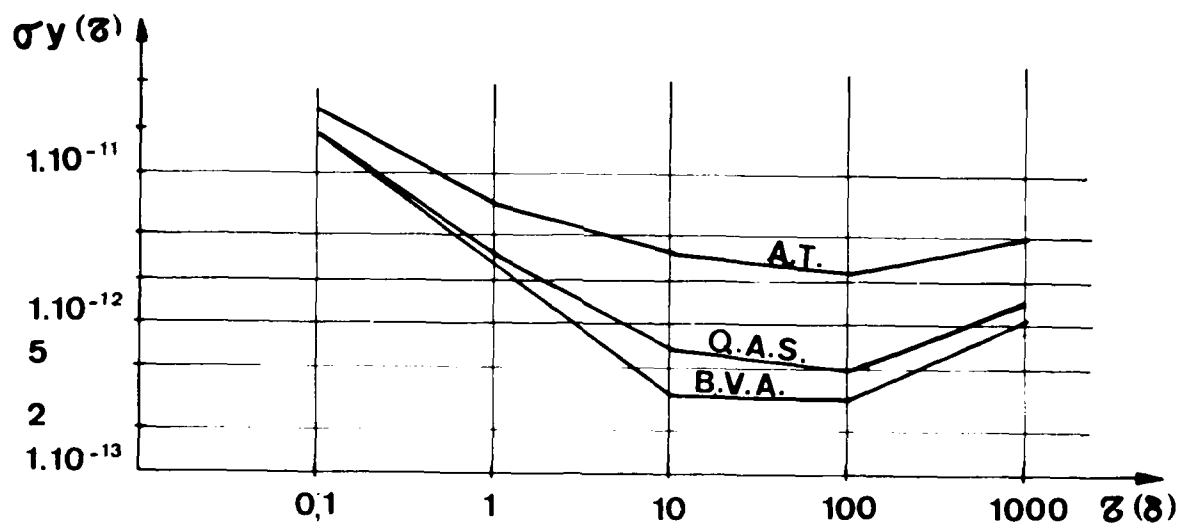
2 G TIP OVER TEST

Fig. 8



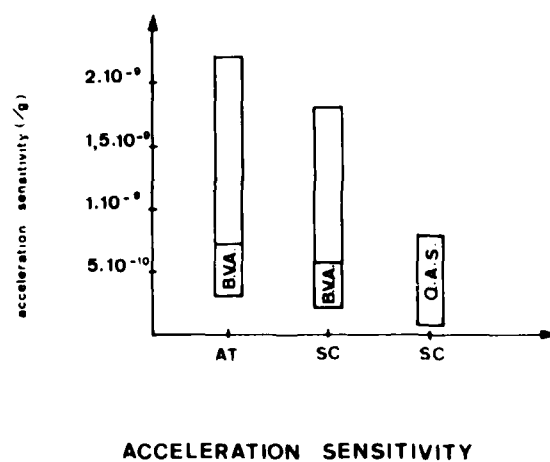
**g SENSITIVITY VALUES OF
SEVERAL BATCHS**

Fig. 9



SHORT TERM STABILITY

Fig. 10



ACCELERATION SENSITIVITY

Fig. 11

QUESTIONS AND ANSWERS

MR. VIG:

Mr. Vig, U.S. Army. The blank size of your resonators is significantly larger than the conventional resonator. Have you ever made any resonators without the bridges to see what a large diameter resonator without the bridges would do, compared to the one with the bridges? What I'm really asking, is the improved performance definitely due to the bridges or could it be due to the fact that you are using a much larger diameter blank?

MR. DEBAISIEUX:

The ten mehgertz resonators, the dimension of the blanks is 15mm and the dimension of the ring is variable. For example, we have two designs where the dimension of the ring is different. The dimension of the ring is very important for the sensitivity to acceleration. And the dimensions of the quartz bridge is also very important.

MR. CLARK:

I have one question. Do you think it's the dimensions of the quartz bridge that accounts for the range of a factor of ten in g sensitivity, of three parts in ten to the eleventh? It's mainly the dimension of the quartz bridge that accounts for that?

MR. DEBAISIEUX:

Yes. At the present time we have resonators with g sensitivity as low as 5 parts in 10^{-11} per g. Mr. Vig, I see an oscillator in your laboratory where the g sensitivity of resonator is five times 10^{-11} /g.

MR. WALLS:

Fred Walls, N.B.S. Have you had a chance to look at the differences with different quartz for the blank; swept quartz, natural quartz, etc. on the sensitivity? Does the g sensitivity or your resonators depend upon the quartz from which it is made? Have you looked at the differences in performance for natural quartz, synthetic quartz, swept quartz?

MR. DEBAISIEUX:

No. At the present time we use two quartz: Sawyer and (Essisan's) quartz and we cannot see the difference of the g sensitivity of quartz, caused by quartz.

MR. WALLS:

Do you have some speculation as to why the wide variance of the three-ten-eleven range, and yet many of them are still above 2×10^{-10} ? Why the wide dispersion in g sensitivity?

DR. McCOUBREY:

He is asking, I think, why differences in g sensitivity from the one batch of crystals to the other? I think you already mentioned that the dimensions of the quartz bridge connecting the oscillator plate to the framework makes a difference, but perhaps you can comment on reasons for the difference.

MR. WALLS:

The dimensions of the quartz bridge are very carefully controlled in thickness and so forth, so I don't understand why that would explain the wide dispersion. Do you have some idea as to why there is such a difference in one batch between one resonator and another on g sensitivity?

MR. DEBAISIEUX:

The dimension and location of the bridges are important. The dimensions are more important than the location but it's not necessary to look at the quartz bridge with high precision.

RECENT RESULTS ON THE PERFORMANCE OF EFOS, NP, AND NX HYDROGEN MASERS

V. Reinhardt, J. Ingold, T. Stalder, M. Saifi, P. Dachel
Bendix Field Engineering Corporation, Columbia, Maryland 21045
and
S. C. Wardrip
NASA/Goddard Space Flight Center, Greenbelt, Maryland 20771

INTRODUCTION

In response to a NASA Goddard Space Flight Center (GSFC) Work Assignment, Bendix Field Engineering Corporation (BFEC) evaluated the performance of the Oscilloquartz EFOS-2 hydrogen maser along with that of NASA NX-3 and NP-2 hydrogen masers in early 1983. This paper presents the results of that evaluation.

The hydrogen maser was brought to BFEC's Hydrogen Maser Facility at Columbia, Maryland by Oscilloquartz personnel at the request of the National Radio Astronomy Observatory (NRAO) who purchased the maser from Oscilloquartz. Figure 1 shows the EFOS-2 maser soon after arriving at the BFEC Hydrogen Maser Facility. During the evaluation period, the maser was maintained by Oscilloquartz personnel. BFEC would like to thank the NRAO and Oscilloquartz personnel who made this evaluation possible and who helped BFEC perform the various tests involved.

During most of the tests, the EFOS-2 maser was intercompared with the NASA NX-3 and NASA NP-2 hydrogen masers which were both operating in hydrogen maser thermal chambers built by BFEC. For the long-term stability and temperature coefficient tests, EFOS-2 was also placed in a BFEC thermal chamber. The measurement area with the thermal chambers is shown in Figure 2. At NASA's request, the evaluation was performed on a best effort basis within the confines of existing funding. Some tests, therefore, such as a pressure sensitivity test, were not performed because of funding and time limitations even though they would have been highly desirable.

The remainder of the report describes the specific tests that were performed and the results obtained. For the reported results, all reported errors are standard errors. These are indicated in parentheses and are to be interpreted as error values on the last places of the number stated.

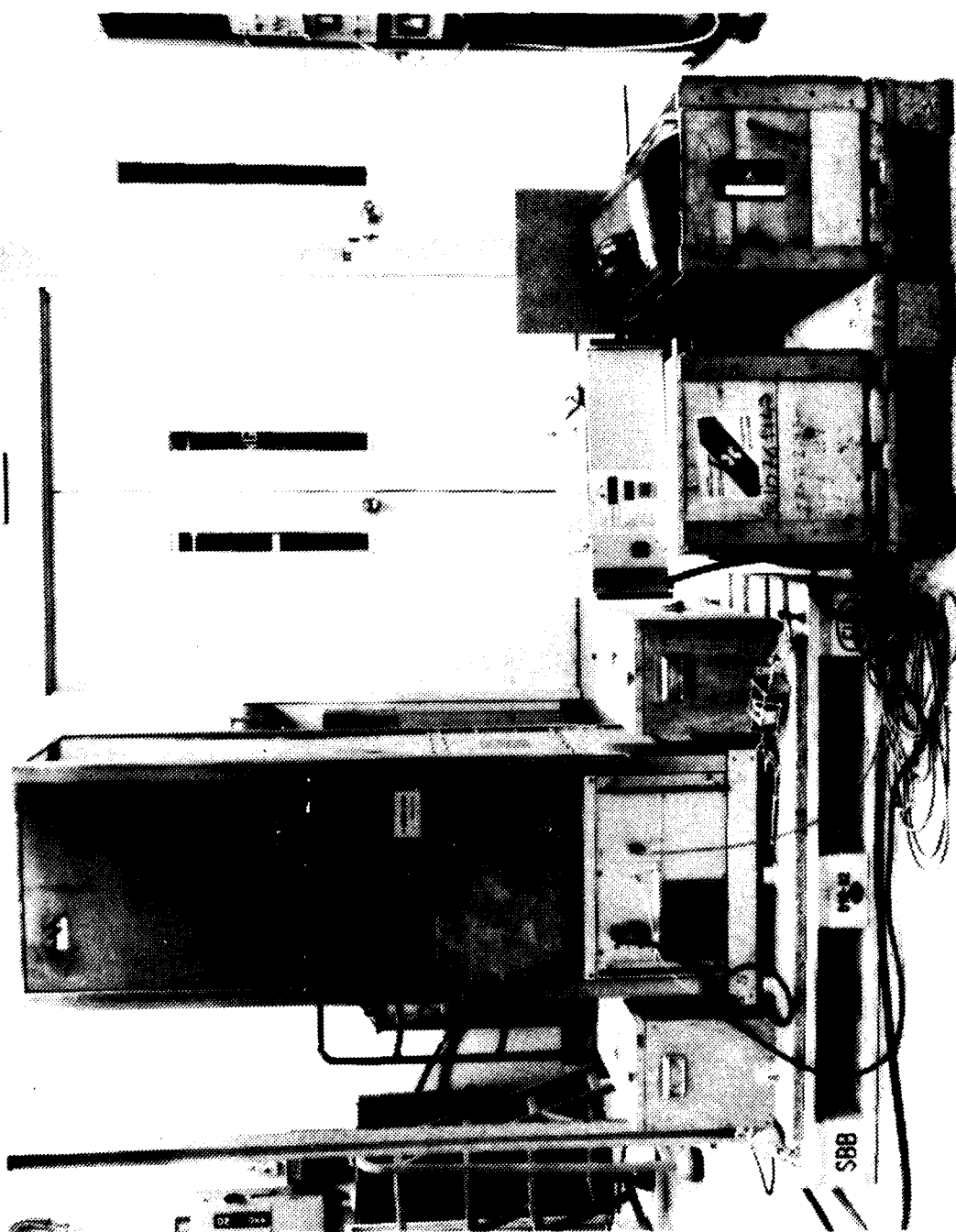


Figure 1. EF0S-2 Soon After Arriving at Bendix, Columbia

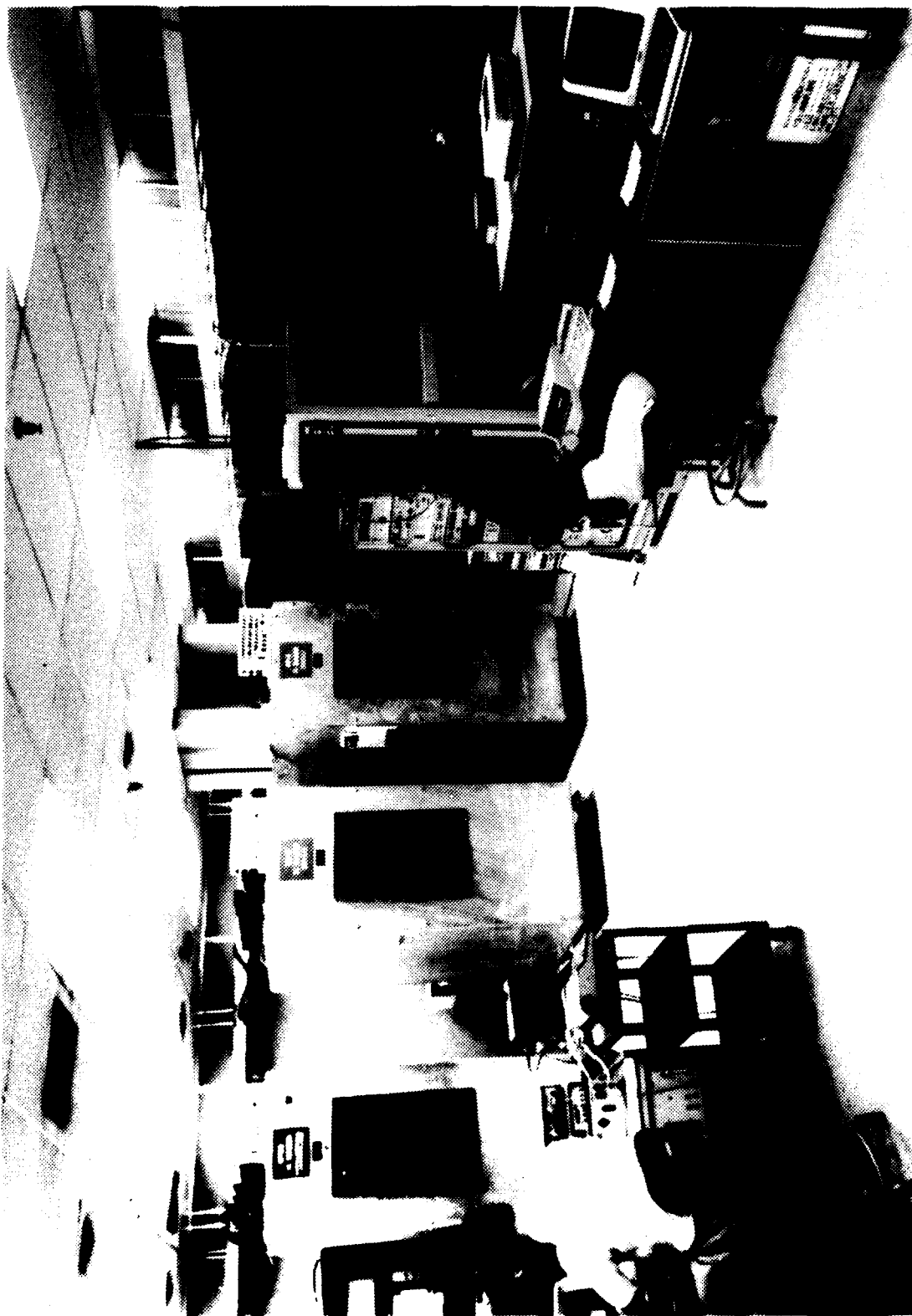


Figure 2. Measurement Area with Thermal Chambers

MAGNETIC TESTS

For the magnetic tests, the EFOS-2 hydrogen maser was placed in a large solenoid as shown in Figure 3. The solenoid was switched back and forth between +0.2 gauss and -0.2 gauss while a 100 second average frequency measurement was performed for each solenoid polarity after waiting about 20 seconds for the maser frequency to settle down. The measurements were made after Oscilloquartz personnel degaussed the EFOS-2 maser and set the maser to its recommended Zeeman and cavity settings. The results of the average of 10 measurements at each solenoid polarity are shown in Table 1.

Table 1. Magnetic Sensitivity:

$$\Delta f/f/\Delta H = 5.2(36) \times 10^{-14} / \text{gauss}$$

for $\Delta H = 0.4$ gauss

TEMPERATURE COEFFICIENT

For the temperature coefficient test, the EFOS-2 maser was placed in a BFEC thermal chamber. After the EFOS-2 maser was in the thermal chamber more than 41 hours and after the maser was operating 22 hours without any environmental disturbances, the thermal chamber was stepped from 28C to 23C. Figure 4 shows the frequency response of the EFOS-2 maser to this temperature step. The results obtained from this data are shown in Table 2.

Table 2. Temperature Sensitivity in Thermal Chamber:

$$\Delta f/f//\Delta T = -7.00(47) \times 10^{-14} / \text{C}$$

for $\Delta T = -5.4\text{C}$ and after 22 hours

$$\text{Time Constant in Thermal Chamber} = 4.02(33) \text{ hours}$$

Caution must be used, however, in using this data because the time constant of the hydrogen maser was severely shortened in the thermal chamber because of the high-speed air flow around the maser. (In a room with relatively still air, the maser was observed to have a time constant of more than 12 hours.) The measurement results given represent a good measurement of a static temperature sensitivity (theoretically one with infinite settling time), but do not give a true picture of the maser behavior after 22 hours in a normal laboratory environment. In a normal laboratory environment, from the difference in the time constants, one would expect the temperature sensitivity after 22 hours to be 16 percent lower or about $-6 \times 10^{-14} / \text{C}$.

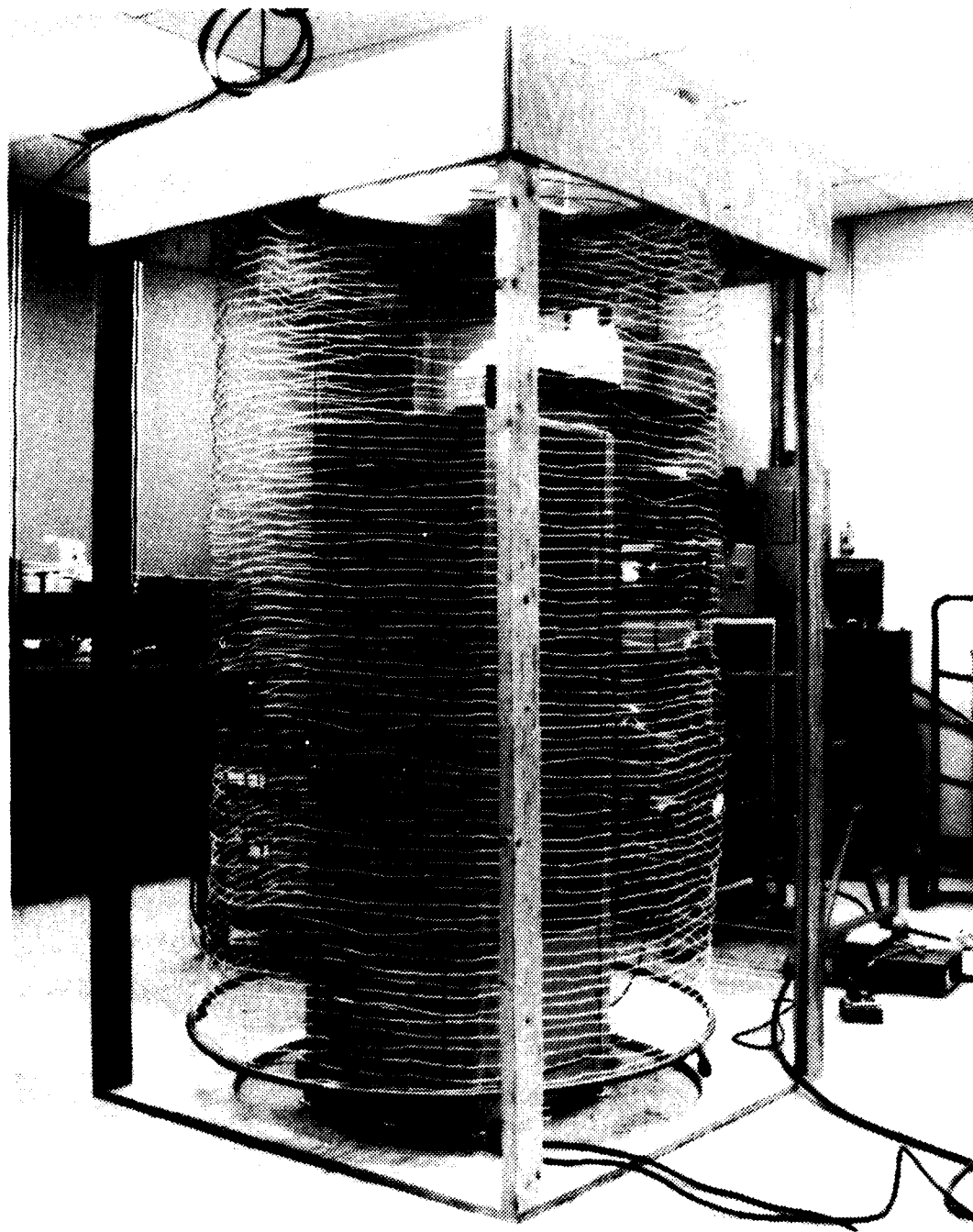
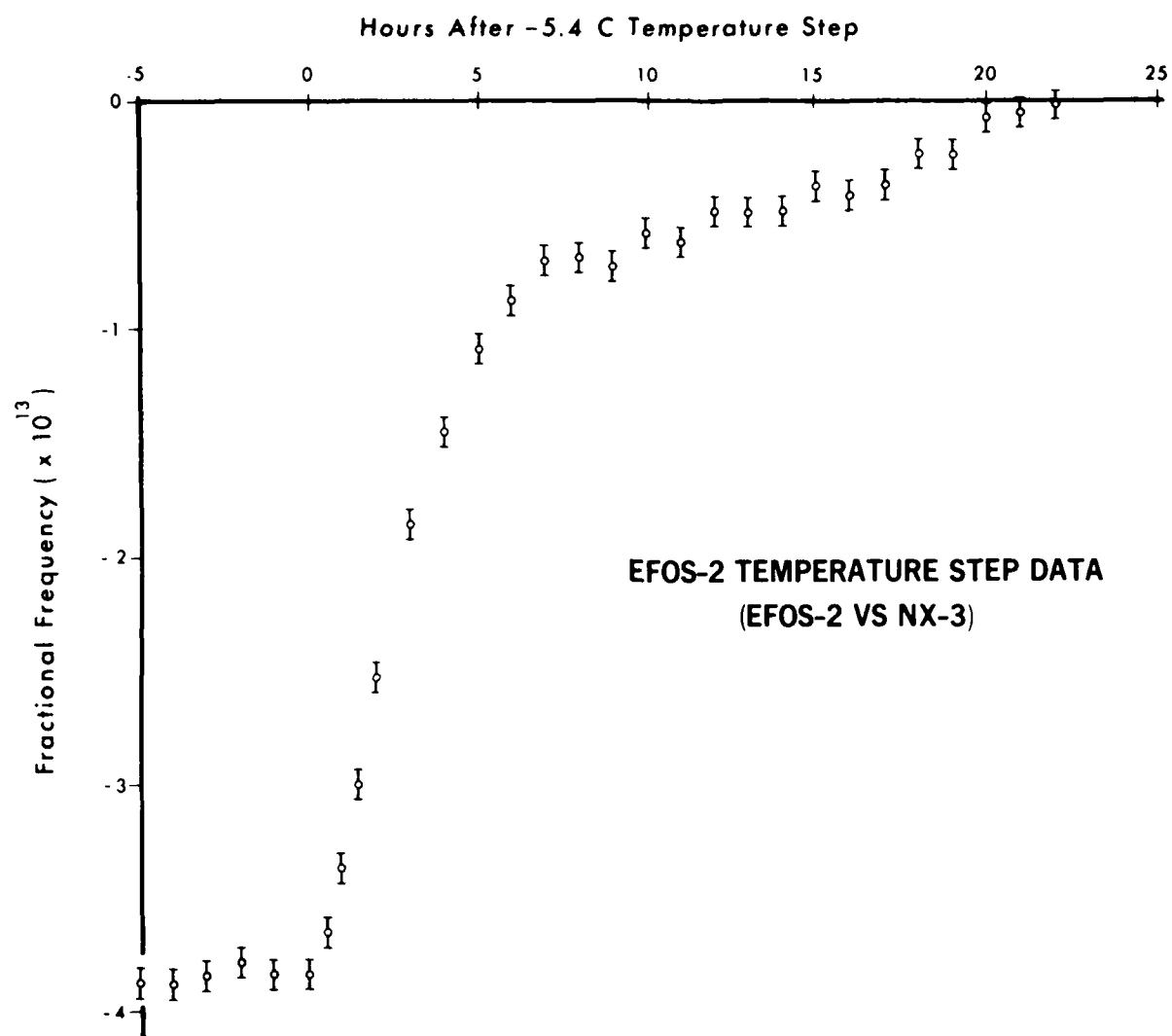


Figure 3. EFOS-2 in the Test Solenoid



5.83-VR

Figure 4. EFOS-2 Frequency Response to Temperature Step

The errors in Table 2 are based totally on the short-term noise of the data. The data in Figure 4 though, seems to indicate that the data is not completely described by a single time constant. With hindsight, it would have been better to have taken data for another day but time constraints forced us to move on to other tests.

SHORT TERM STABILITY

Short-term stability tests were run comparing EFOS-2 to NP-2 and NX-3, but an anomalous noise level of about 0.6ps, probably caused by ground loops between the masers in the thermal chambers, clouded the data. We therefore reran the tests with both ports of our measurement system measuring EFOS-2 versus NX-3 in order to subtract out the noise of the measurement system. The theory behind this technique is as follows.

The time average of the fractional frequency offsets out of the two beat frequency ports is given by:

$$y_A = y + y_a \quad (1a)$$

$$y_B = y + y_b \quad (1b)$$

where y_A and y_B represent the total offsets, where y_a and y_b represent the contributions of the 2 measurement systems, and where y represents the contribution of EFOS versus NX-3. Differencing (1a) and (1b), we obtain approximately:

$$y_d = y_a - y_b \quad (2)$$

Taking the Allan variance of this quantity yields an estimate of the total system noise:

$$\sigma_d^2 = \sigma_a^2 + \sigma_b^2 \quad (3)$$

assuming the noise processes are independent. Summing (1a) and (1b) yields:

$$y_s = 2y + y_a + y_b \quad (4)$$

The Allan variance of this becomes:

$$\sigma_s^2 = 4\sigma_y^2 + \sigma_a^2 + \sigma_b^2 \quad (5)$$

again assuming that all noise processes are independent. Combining (3) and (5) yields our desired estimate of the Allan variance of the masers alone:

$$\sigma_a^2 = (\sigma_s^2 - \sigma_d^2)/4 \quad (6)$$

If all the noise sources are not independent, there would be deviations from (6) due to correlations between y, a, and b. These correlations could only occur through some environmental parameter affecting the measurement system and the masers or 60 Hz interference. Temperature and other similar environmental parameters usually affect the performance of masers and measurement systems only for averaging times of 1000 seconds or longer. Since we are only considering stabilities up to 100 seconds, these effects would not cause any problems.

The 60 Hz interference, however, is another matter. It would cause short term correlations which could generate positive or negative correlation terms. (Positive terms would cause our estimate of the masers' stability to be high and negative terms would cause our estimate of the masers' stability to be low.) The sign of 60 Hz correlations is a periodic function of the averaging time with a period equal to the 60 Hz period, so 60 Hz interference usually causes Allan deviate data, as a function of averaging time, to have scatter from a smooth power law behavior larger than the statistical error bars associated with the data (unless the averaging times under consideration just happen to be exact multiples of the 60 Hz period). Therefore, smoothness of the data is a good test for the presence of 60 Hz effects. In the data presented later in the paper using this analysis, there is no such evidence of 60 Hz correlation problems.

Equation (2) is only approximately true because, if the zero crossings of the beats of the 2 ports are not exactly synchronized, there will be an extra term equal to:

$$y_e = y(t, \tau) - y(t + \epsilon, \tau) \quad (7)$$

where:

$$y(t, \tau) = \frac{1}{\tau} \int_t^{t+\tau} y(t') dt'$$

If the synchronization error between the beats, ϵ , is much less than, t_c , the correlation time of the low-pass filters in the phase comparators used to generate the beats, (7) makes a negligible contribution to Allan deviate. Numerically for $\epsilon \ll t_c$, (7) yields an Allan deviate of:

$$\sigma_e = (\epsilon/\tau) 2^{1/2} \sigma_y(t_c, \tau)$$

or, because the dominant noise for short averaging times is white noise:

$$\sigma_e = (\epsilon/t_c) 2^{1/2} \sigma_y(\tau, \tau + 1s) \quad (8)$$

For the data taken, $\epsilon < 0.4$ ms and $t_c = 12$ ms, σ_e is only 0.047 times σ_y . Thus, for our case, σ_e makes a negligible contribution in estimating σ_y .

The results obtained after the system noise is subtracted out are shown in Table 3.

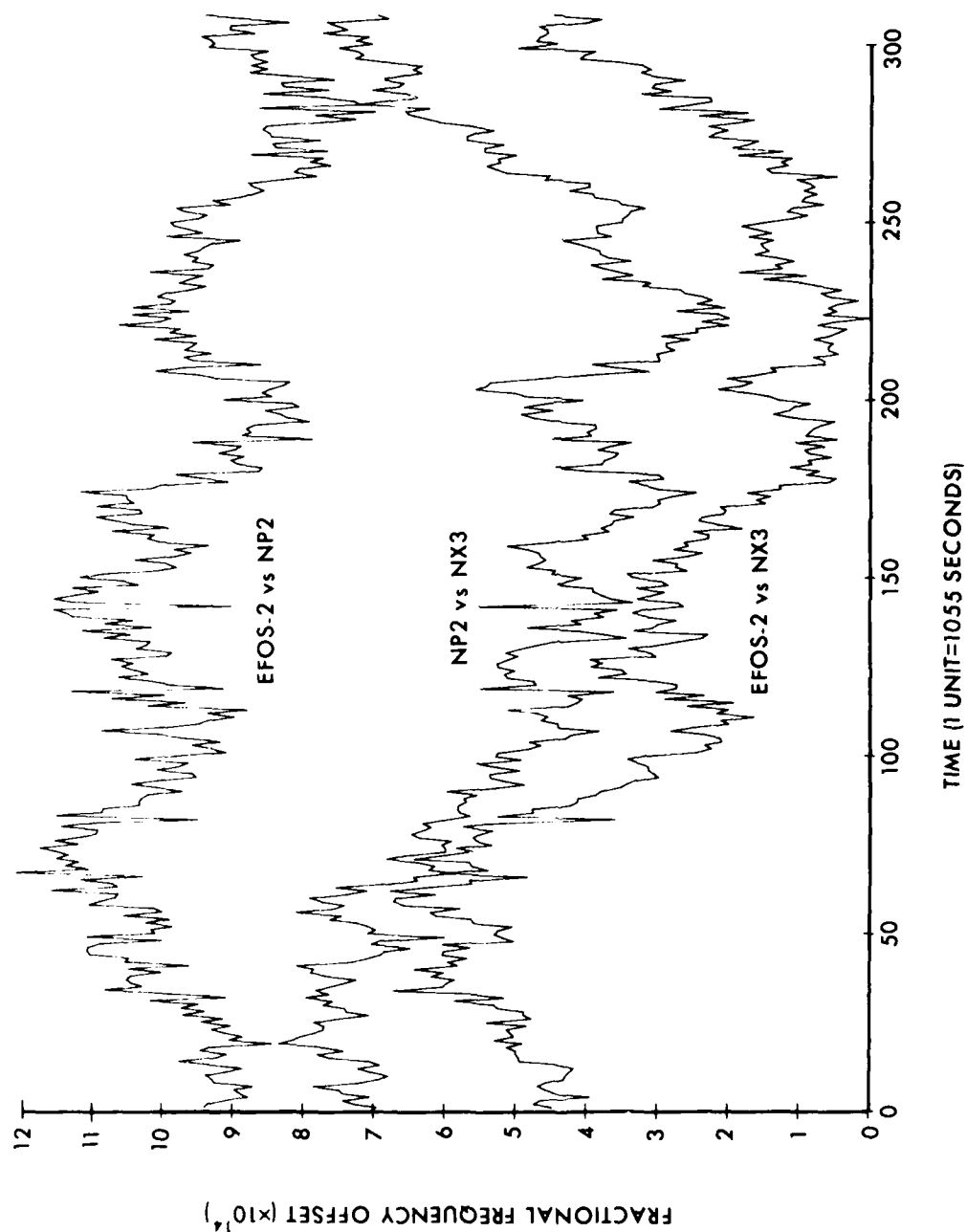
Table 3. Short-Term Stability of EFOS-2 Versus NX-3:

NOTE: All Allan deviates are divided by an extra square root of 2 to normalize to one maser deviate. The noise bandwidth is approximately 12 Hz. The statistic used is $\sigma_y(2, \tau, \tau + 1s)$.

TAU	SIGMA	NUMBER OF POINTS USED
1s	$2.05(46) \times 10^{-13}$	410
10s	$3.29(47) \times 10^{-14}$	380
100s	$4.66(47) \times 10^{-15}$	480

LONG-TERM STABILITY

Long-term stability data was taken for 3.75 days comparing NX-3 with EFOS-2 and NP-2. The data was taken as nearly contiguous 1054 second averages of the two intercomparison beat periods of the 5 MHz signals from the masers. For measurement purposes, NX-3 was offset approximately 0.95Hz lower than the other masers. The period counters used to take the data were reset between readings so the dead time between the data and the lack of synchronization between the data channels is on the order of 1 second. In order to obtain a direct comparison of EFOS-2 and NP-2, the EFOS-2 versus NX-3 and NP-2 versus NX-3 data was differenced to produce a derived EFOS-2 versus NP-2 channel of data. The data is plotted in Figure 5 with frequency drifts removed and with arbitrary frequency offsets so the data can be compared on the same plot.



5.83.VR

Figure 5. Frequency Data with Frequency Drifts Removed and with Arbitrary Frequency Offsets

To analyze the data, a sliding Allan variance technique was used (D. Allan and J. Barnes, "A Modified 'Allan Variance' with Increased Oscillator Characterization Ability," 35th Annual Frequency Control Symposium, Philadelphia, 27-29 May, 1981). In our version of this technique, 2 consecutive frequency averages over N samples were generated by arithmetically averaging the first N consecutive samples and the next N consecutive samples. In general, arithmetic averages are not equivalent to the time averages normally used to generate the Allan variance. However, when the Allan fractional frequency deviate behaves as $\tau^{\epsilon-1/2}$ where $\epsilon > 0$, a time average is equivalent to an arithmetic average of smaller time averages for computing variances. This is true for the hydrogen masers under consideration for averaging times of 100 seconds or greater (which can be verified a posteriori).

The first estimate for the sliding Allan variance is then created by squaring the difference between these two consecutive arithmetic averages and dividing by 2. Successive Allan variance estimates are generated by sliding each of the 2 consecutive averages by one 1054-second data point and by similarly differencing, squaring, and dividing the data by 2. This process is carried out until there are no longer 1054-second data points to create successive averages. Then, all the estimates are averaged to produce a single estimate. In summary, the formula used is:

$$s_y^2(M) = \frac{1}{2N'M^2} \sum_{j=1}^{N'} \left(\sum_{i=j}^{M+j-1} y_i - \sum_{i=M+j}^{2M+j-1} y_i \right)^2 \quad (9)$$

where $N' = N - 2M + 1$ and M is the averaging time in multiples of the averaging time of the original data y_i .

The advantage of using the sliding Allan variance technique is that it produces a better estimate of the theoretical Allan variance, especially for small data samples. When the Allan fractional frequency deviate behaves as τ^{ϵ} where $\epsilon \leq -1/2$, the sliding technique produces a statistically better estimate for the same number of samples. When the Allan fractional frequency deviate behaves as τ^{ϵ} where $\epsilon > -1/2$, the formal statistical advantage of the sliding variance tends to disappear, but the sliding variance still produces an estimate which is much more representative of an ensemble average for relatively small samples. For example, for quasi-periodic noise processes, the sliding variance averages over all phases of the process with a data sample only 3 times the quasi-period. Of course, one of the reasons this is true is that the sliding estimate technique is closer to the infinite time averaging used in theoretical definition of the Allan variance.

The conventional method for estimating the Allan variance yields a fractional error for the Allan deviate estimate given by:

$$\sigma(\sigma_y) / \sigma_y = 1 / (2^{1/4} \times F^{1/2}) \quad (10)$$

when the differences of the average frequencies used to compute the Allan variance are normally distributed. F is the number of degrees of freedom and is given by:

$$F = N_T - 1 \quad (11)$$

where N_T is the number of average frequency samples used to compute the Allan variance. For the sliding average technique, (10) is used to define the number of degrees of freedom. For this technique, F is usually greater than it is for the conventional method. As a worst case it is:

$$F = T/\tau - 1 \quad (12)$$

where τ is the averaging time and T is the total elapsed time for the set of data. This worst-case value of F is used to estimate the errors of the sliding Allan variances computed in this report.

The results of a sliding Allan variance computation on the EFOS-2 versus NX-2 data, the NP-2 versus NX-3 data, and the derived EFOS-2 versus NP-2 data are shown in Table 4. Notice the anomalously high value in the derived EFOS-2 versus NP-2 data for 1054 seconds. This is an artifact of using a derived channel as opposed to a directly measured channel. Because the frequency averages of the differenced channels are not completely synchronized, the contribution of NX-3 to the data does not completely cancel. A residual term is left of the difference of the average fractional frequency offset of NX-3 of the same form as Equation 7. When the data points are averaged over N values, this NX-3 term acts like a white noise term because only fluctuations over 1054 seconds will contribute to the NX-3 difference. This means that the NX-3 contribution to Allan variance of the derived channel is reduced by $1/N$ for the longer averaging times. Because the EFOS and NP-2 contributions to the Allan variance stay the same or get worse as the averaging time is increased, the NX-3 contribution to the Allan variance very quickly becomes negligible.

A three-corner hat estimate of the Allan variance of each of the masers was run on the data. For averaging times greater than 52×1054 seconds, the estimated variance of NP-2 became negative.

Table 4. Long Term Allan Deviate Data (Page 1)

SLIDING ALLAN DEVIATE / SQUARE ROOT OF 2										SIS DAT MAY 17, 1983										EFOS-NP2=- 545467E-15												
DRIFT REMOVED DRIFT PER POINT EFOS-NX3=- 534234E-15										NP2-NX3= 112323E-16																						
THE FRACT ERROR (FOR ALLAN DEVIATES) ASSUMES A NORMAL DISTRIBUTION FOR THE SIGMA'S																																
TAU IS IN UNITS OF 1054 SECONDS																																
FRACTIONAL FREQUENCY IN UNITS OF 1E-15																																
TAU	EF-NX					NP-NX					EF-NP					# OF PTS					DEG OF FREEDOM											
1	2	10793	+/	-	143069	2	09486	+/	-	142182	3	00632	+/	-	204044	305										307						
2	1	75399	+/	-	168631	1	9443	+/	-	186928	2	1796	+/	-	20955	303											153					
3	1	82084	+/	-	214753	2	09442	+/	-	24702	2	02016	+/	-	238261	301											101					
4	2	0336	+/	-	277407	2	29682	+/	-	313312	2	02169	+/	-	275781	299											76					
5	2	28238	+/	-	348665	2	51577	+/	-	38432	2	1203	+/	-	323906	297											60					
6	2	52612	+/	-	423767	2	72954	+/	-	47553	2	24133	+/	-	375695	295											50					
7	2	75549	+/	-	499714	2	94528	+/	-	534134	2	38977	+/	-	43339	293											43					
8	2	96507	+/	-	575807	3	14597	+/	-	610937	2	54852	+/	-	494915	291											37					
9	3	15799	+/	-	651559	3	32625	+/	-	686688	2	69836	+/	-	556727	289											33					
10	3	34015	+/	-	727637	3	49733	+/	-	761879	2	84156	+/	-	619022	287											29					
11	3	51369	+/	-	804153	3	65052	+/	-	835468	2	97533	+/	-	680943	285											27					
12	3	68018	+/	-	881195	3	79223	+/	-	908023	3	09852	+/	-	74192	283											24					
13	3	83686	+/	-	957841	3	92331	+/	-	979423	3	20803	+/	-	80086	281											22					
14	3	98876	+/	-	103511	4	05063	+/	-	105116	3	31042	+/	-	859074	279											21					
15	4	13822	+/	-	111348	4	17005	+/	-	11205	3	40194	+/	-	915369	277											19					
16	4	2844	+/	-	119266	4	28521	+/	-	119288	3	49014	+/	-	971559	275											18					
17	4	42273	+/	-	127124	4	39459	+/	-	126318	3	57928	+/	-	10288	273											17					
18	4	55728	+/	-	135021	4	5001	+/	-	133327	3	66526	+/	-	108592	271											16					
19	4	68427	+/	-	142833	4	59885	+/	-	140228	3	75035	+/	-	114355	269											15					
20	4	80369	+/	-	15054	4	69418	+/	-	147108	3	82917	+/	-	12	267											14					
21	4	90816	+/	-	157886	4	78368	+/	-	153882	3	90171	+/	-	125511	265											13					
22	5	01872	+/	-	165531	4	87057	+/	-	160644	3	96858	+/	-	130894	263											13					
23	5	11455	+/	-	172785	4	96459	+/	-	167719	4	02778	+/	-	136071	261											12					
24	5	19819	+/	-	179703	5	05479	+/	-	174746	4	08065	+/	-	14107	259											11					
25	5	28595	+/	-	186835	5	13743	+/	-	181585	4	12859	+/	-	145927	257											11					
26	5	37226	+/	-	193989	5	22301	+/	-	188599	4	17392	+/	-	150718	255											10					
27	5	43927	+/	-	200506	5	30646	+/	-	19561	4	21555	+/	-	155396	253											10					
28	5	52094	+/	-	207621	5	37652	+/	-	203178	4	23535	+/	-	160027	251											10					
29	5	59414	+/	-	21448	5	4594	+/	-	209314	4	23095	+/	-	164516	249											9					
30	5	66879	+/	-	21455	5	52777	+/	-	215946	4	3206	+/	-	168787	247											9					
31	5	74315	+/	-	22848	5	57885	+/	-	2227	4	343	+/	-	172778	245											8					
32	5	80566	+/	-	235088	5	66863	+/	-	23539	4	35794	+/	-	176465	243											8					
33	5	86429	+/	-	241582	5	74023	+/	-	236471	4	36504	+/	-	179819	241											8					
34	5	95293	+/	-	249375	5	81504	+/	-	243598	4	36542	+/	-	182872	239											8					
35	6	03312	+/	-	256893	5	88971	+/	-	250787	4	35845	+/	-	185585	237											7					
36	6	10807	+/	-	264258	5	95331	+/	-	257562	4	34329	+/	-	187907	235											7					
37	6	17938	+/	-	271531	6	03346	+/	-	265118	4	31938	+/	-	1898	233											7					
38	6	25898	+/	-	279236	6	10064	+/	-	272171	4	28675	+/	-	191247	231											7					
39	6	33664	+/	-	286728	6	16882	+/	-	279329	4	24593	+/	-	192259	229											6					
40	6	40457	+/	-	294245	6	23208	+/	-	286321	4	19737	+/	-	19284	227											6					
41	6	48038	+/	-	301991	6	2822	+/	-	292756	4	14031	+/	-	192942	225											6					
42	6	54544	+/	-	3093	6	32846	+/	-	299047	4	0759	+/	-	192604	223											6					
43	6	61816	+/	-	317034	6	3649	+/	-	304902	4	00305	+/	-	191761	221											6					
44	6	68526	+/	-	324564	6	39212	+/	-	310332	3	92389	+/	-	190502	219											6					
45	6	75824	+/	-	332445	6	41746	+/	-	315682	3	84089	+/	-	189938	217											5					
46	6	83023	+/	-	340347	6	4446	+/	-	321131	3	73561	+/	-	187184	215											5					
47	6	88502	+/	-	347449	6	46241	+/	-	326122	3	66794	+/	-	185101	213											5					
48	6	98791	+/	-	357058	6	48261	+/	-	331239	3	58141	+/	-	182998	211											5					

Table 4. Long Term Allan Deviate Data (Page 2)

49	7	05484	+/-	3	64916	6	50358	+/-	3	36402	3	49414	+/-	1	80737	209	5	28571
50	7	13807	+/-	3	73691	6	52584	+/-	3	4164	3	40526	+/-	1	78481	207	5	16
51	7	22447	+/-	3	82721	6	53951	+/-	3	46435	3	32592	+/-	1	76034	205	5	03922
52	7	30848	+/-	3	91711	6	56203	+/-	3	51704	3	24031	+/-	1	7367	201	4	92308
53	7	37322	+/-	3	99744	6	60697	+/-	3	58202	3	1646	+/-	1	71571	199	4	81132
54	7	43446	+/-	4	08746	6	63679	+/-	3	63912	3	09389	+/-	1	69646	197	4	7037
55	7	56465	+/-	4	19438	6	68071	+/-	3	70426	3	02892	+/-	1	67945	195	4	5
56	7	63961	+/-	4	28275	6	73419	+/-	3	72517	2	97431	+/-	1	66739	193	4	40351
57	7	73541	+/-	4	38371	6	78108	+/-	3	84288	2	9298	+/-	1	66034	191	4	31034
58	7	82789	+/-	4	4838	6	82544	+/-	3	9096	2	89477	+/-	1	65812	189	4	22034
59	7	91684	+/-	4	58285	6	86818	+/-	3	97581	2	86824	+/-	1	66035	187	4	13333
60	7	98871	+/-	4	67287	6	9292	+/-	4	05313	2	85004	+/-	1	66709	185	4	04918
61	8	06663	+/-	4	76223	6	97077	+/-	4	1196	2	8402	+/-	1	67851	183	3	96774
62	8	15055	+/-	4	866	7	01618	+/-	4	18877	2	83712	+/-	1	69381	181	3	88889
63	8	21818	+/-	4	95888	7	04808	+/-	4	25026	2	84162	+/-	1	7136	179	3	8125
64	8	30867	+/-	5	06039	7	10503	+/-	4	32731	2	85164	+/-	1	73679	177	3	73846
65	8	40561	+/-	5	16988	7	13167	+/-	4	38634	2	86772	+/-	1	76379	175	3	6667
66	8	48788	+/-	5	27134	7	18721	+/-	4	46357	2	8888	+/-	1	79407	173	3	59701
67	8	54575	+/-	5	35842	7	23483	+/-	4	53643	2	91346	+/-	1	82682	171	3	46377
68	8	6321	+/-	5	46415	7	27138	+/-	4	60281	2	9408	+/-	1	86154	169	3	3
69	8	71496	+/-	5	56863	7	30636	+/-	4	6687	2	97009	+/-	1	89781	167	3	33803
70	8	81218	+/-	5	68331	7	32661	+/-	4	72521	3	00101	+/-	1	93547	165	3	27778
71	8	88111	+/-	5	78069	7	36958	+/-	4	79684	3	03285	+/-	1	97407	163	3	21918
72	8	97707	+/-	5	89661	7	40876	+/-	4	86646	3	06517	+/-	2	01402	161	3	16216
73	9	07213	+/-	6	11304	7	41982	+/-	4	91788	3	10131	+/-	2	05556	159	3	10667
74	9	14095	+/-	6	11304	7	43911	+/-	4	97492	3	13759	+/-	2	09827	157	3	05263
75	9	21439	+/-	6	21694	7	47925	+/-	5	04624	3	17587	+/-	2	14276	155	3	94872
76	9	32994	+/-	6	35037	7	49511	+/-	5	1015	3	21558	+/-	2	18935	153	2	89873
77	9	40487	+/-	6	45728	7	54822	+/-	5	18353	3	25896	+/-	2	23756	149	2	85
78	9	49614	+/-	6	5764	7	57685	+/-	5	24723	3	30264	+/-	2	28719	147	2	7561
79	9	60301	+/-	6	7075	7	60485	+/-	5	31169	3	3477	+/-	2	3383	145	2	71084
80	9	68228	+/-	6	82045	7	65131	+/-	5	38978	3	39275	+/-	2	38994	143	2	6667
81	9	80774	+/-	6	96716	7	71666	+/-	5	48171	3	43782	+/-	2	44214	139	2	62353
82	9	87368	+/-	7	07277	7	7467	+/-	5	54916	3	48199	+/-	2	49424	137	2	5814
83	9	975	+/-	7	20474	7	79056	+/-	5	62696	3	52495	+/-	2	546	135	2	54023
84	10	0503	+/-	7	31903	7	82627	+/-	5	69939	3	56819	+/-	2	59849	133	2	5
85	10	1614	+/-	7	46052	7	87791	+/-	5	78396	3	60988	+/-	2	65037	129	2	46067
86	10	2655	+/-	7	59819	7	90623	+/-	5	85194	3	65118	+/-	2	70248	127	2	42222
87	10	363	+/-	7	73228	7	95291	+/-	5	934	3	69207	+/-	2	7548	125	2	38462
88	10	455	+/-	7	86339	7	98266	+/-	6	00392	3	73272	+/-	2	80746	123	2	34783
89	10	5524	+/-	7	99587	8	03221	+/-	6	08928	3	77296	+/-	2	86031	121	2	31183
90	10	6275	+/-	8	12051	8	0525	+/-	6	15292	3	81343	+/-	2	91385	119	2	2766
91	10	7415	+/-	8	27202	8	0785	+/-	6	22127	3	85398	+/-	2	96796	117	2	24211
92	10	8628	+/-	8	43073	8	11789	+/-	6	30039	3	89495	+/-	3	02292	115	2	20833
93	10	9364	+/-	8	55374	8	15367	+/-	6	37724	3	9354	+/-	3	078	113	2	17526
94	11	036	+/-	8	69814	8	1931	+/-	6	45748	3	97589	+/-	3	13364	111	2	14286
95	11	1176	+/-	8	82958	8	2363	+/-	6	54126	4	1898	+/-	3	43922	109	2	11111
96	11	2011	+/-	8	96363	8	27091	+/-	6	61879	4	237	+/-	3	49369	107	2	08
97	11	2934	+/-	9	106	8	31072	+/-	6	61879	4	28593	+/-	3	56023	105	2	0495
98	11	3656	+/-	9	23322	8	34605	+/-	6	70102	4	33567	+/-	3	62811	103	2	01961
99	11	4552	+/-	9	37571	8	36405	+/-	6	78019	4	38746	+/-	3	69839	101	1	99029
100	11	5417	+/-	9	51692	8	39848	+/-	6	87389	4	4485	+/-	3	36721	99	1	94154
101	11	6259	+/-	9	65742	8	42375	+/-	6	94594	4	49524	+/-	3	77057	97	1	93333
102	11	7058	+/-	9	79547	8	49742	+/-	7	03863	4	49524	+/-	3	84465	95	1	90566
103	11	8096	+/-	9	95484	8	52227	+/-	7	13148	4	55044	+/-	3	92002	93	1	8785
104	11	8901	+/-	10	0959	8	53914	+/-	7	3355	4	60669	+/-	3	99706	91	1	85185
105	11	9842	+/-	10	2497	8	63918	+/-	7	43503	4	66391	+/-	4	07572			
106	12	1019	+/-	10	4253	8	7492	+/-	7	53708	4	66391	+/-	4	07572			
107	12	219	+/-	10	602	8	80988	+/-	7	64401	4	66391	+/-	4	07572			
108	12	3017	+/-	10	7503	8	86616	+/-	7	748	4	66391	+/-	4	07572			

Table 4. Long Term Allan Deviate Data (Page 3)

109	12 3846 +/- 10 9	8 93235 +/- 7 8615	4 72199 +/- 4 15594	1 82569
110	12 4894 +/- 11 0704	8 90519 +/- 7 94127	4 7808 +/- 4 23762	1 8
111	12 6044 +/- 11 2514	9 00835 +/- 8 04139	4 8962 +/- 4 32014	1 77477
112	12 6885 +/- 11 4064	9 04995 +/- 8 13551	4 8948 +/- 4 40352	1 75
113	12 8043 +/- 11 5914	9 0841 +/- 8 23359	4 9595 +/- 4 48648	1 72566
114	12 8834 +/- 11 7447	9 12727 +/- 8 32051	5 0133 +/- 4 57017	1 70175
115	12 9744 +/- 11 9101	9 14547 +/- 8 39525	5 06754 +/- 4 65184	1 67826
116	13 044 +/- 12 0572	9 17077 +/- 8 47699	5 12011 +/- 4 73276	1 65517
117	13 1491 +/- 12 2386	9 19203 +/- 8 5555	5 1568 +/- 4 81169	1 63248
118	13 2481 +/- 12 4158	9 20984 +/- 8 63125	5 21568 +/- 4 88802	1 61017
119	13 3342 +/- 12 5825	9 23348 +/- 8 71296	5 25817 +/- 4 96175	1 58824
120	13 4189 +/- 12 7493	9 24547 +/- 8 78431	5 29589 +/- 5 03163	1 56667
121	13 4779 +/- 12 8929	9 26806 +/- 8 8658	5 33127 +/- 5 09988	1 54545
122	13 5928 +/- 13 0915	9 27917 +/- 8 93697	5 36398 +/- 5 16617	1 52459
123	13 6653 +/- 13 2508	9 30997 +/- 9 0276	5 39422 +/- 5 23062	1 50407
124	13 742 +/- 13 4156	9 31451 +/- 9 09336	5 42163 +/- 5 29284	1 48387
125	13 8064 +/- 13 5697	9 31059 +/- 9 15091	5 44668 +/- 5 35326	1 464
126	13 8906 +/- 13 7445	9 31682 +/- 9 21881	5 46923 +/- 5 41169	1 44444
127	13 9356 +/- 13 8818	9 31479 +/- 9 27883	5 4915 +/- 5 4703	1 4252
128	13 9914 +/- 14 0309	9 32116 +/- 9 34752	5 51221 +/- 5 52779	1 40625
129	14 0502 +/- 14 1843	9 29337 +/- 9 38208	5 53197 +/- 5 58477	1 3876
130	14 1114 +/- 14 3413	9 26815 +/- 9 41916	5 5513 +/- 5 64175	1 36923
131	14 1437 +/- 14 4701	9 24788 +/- 9 46125	5 56845 +/- 5 69693	1 35115
132	14 1747 +/- 14 5983	9 2042 +/- 9 47925	5 5957 +/- 5 7463	1 33333
133	14 2126 +/- 14 7346	9 17409 +/- 9 51102	5 58633 +/- 5 7915	1 31579
134	14 2182 +/- 14 8381	9 14532 +/- 9 54409	5 59055 +/- 5 83431	1 29851
135	14 2661 +/- 14 9867	9 10666 +/- 9 56666	5 59587 +/- 5 87854	1 28148
136	14 2666 +/- 15 0863	9 056 +/- 9 57433	5 59886 +/- 5 92055	1 26471
137	14 3008 +/- 15 2223	9 01283 +/- 9 59359	5 5999 +/- 5 96073	1 24818
138	14 3063 +/- 15 3285	8 96581 +/- 9 60643	5 59753 +/- 5 99748	1 23188
139	14 2808 +/- 15 4019	8 92941 +/- 9 6304	5 5992 +/- 6 03875	1 21583
140	14 2835 +/- 15 5061	8 88724 +/- 9 64792	5 599 +/- 6 07823	1 1844
141	14 255 +/- 15 5767	8 8398 +/- 9 65943	5 59543 +/- 6 11424	1 16901
142	14 2416 +/- 15 6641	8 8264 +/- 9 70803	5 59234 +/- 6 15094	1 15385
143	14 2144 +/- 15 7366	8 78392 +/- 9 7246	5 59319 +/- 6 19217	1 13889
144	14 215 +/- 15 8403	8 73804 +/- 9 73713	5 59618 +/- 6 23604	1 12414
145	14 2064 +/- 15 9343	8 69331 +/- 9 75063	5 60079 +/- 6 28199	1 10959
146	14 1795 +/- 16 008	8 66588 +/- 9 78339	5 60768 +/- 6 33082	1 09524
147	14 1986 +/- 16 1342	8 64892 +/- 9 828	5 61985 +/- 6 38598	1 08108
148	14 1927 +/- 16 2327	8 62932 +/- 9 86972	5 63501 +/- 6 445	1 06711
149	14 243 +/- 16 3966	8 63165 +/- 9 93678	5 6674 +/- 6 52433	1 05333
150	14 3506 +/- 16 6281	8 68053 +/- 10 0582	5 71935 +/- 6 62706	1 03974
151	14 607 +/- 17 0356	8 82805 +/- 10 2958	5 82804 +/- 6 79702	1 02632
152	15 2832 +/- 17 9404	9 23091 +/- 10 8358	6 10738 +/- 7 16922	1 01307
153	18 61 +/- 21 9879	11 2397 +/- 13 2799	7 44906 +/- 8 80114	
154	0 +/- 0 0 +/- 0	0 +/- 0 -1	1	

In this regime, the EFOS-2 versus NP-2 data is about half that of the other data channels. It is obvious that both EFOS-2 and NP-2 are more stable than NX-3 unless EFOS-2 and NP-2 are moving up and down in frequency together. Under these conditions, it is apparent that the three-corner hat method amplifies the small differences between the EFOS-2 versus NX-3 data and the NP-2 versus NX-3 data beyond that which is statistically significant. We have therefore decided that using the three-corner hat data would be misleading. Instead we recommend that, as a best estimate of EFOS-2's stability:

1. the EFOS-2 versus NX-3 data be used from 1x10⁵4 to 3x10⁵4 seconds.
2. the EFOS-2 versus NP-2 data be used beyond 3x10⁵4 seconds.

BEST ESTIMATE OF EFOS-2 STABILITY

Figure 6 shows our best estimate of EFOS-2's fractional frequency stability from 1.054 seconds to 153x10⁵4 seconds. For 1 to 100 seconds the short-term stability estimates of EFOS-2 versus NX-3 are used. For 1054 to 3x10⁵4 seconds the long-term data of EFOS-2 versus NX-3 are used. Beyond 3x10⁵4 seconds, the long-term data of EFOS-2 versus NP-2 are used.

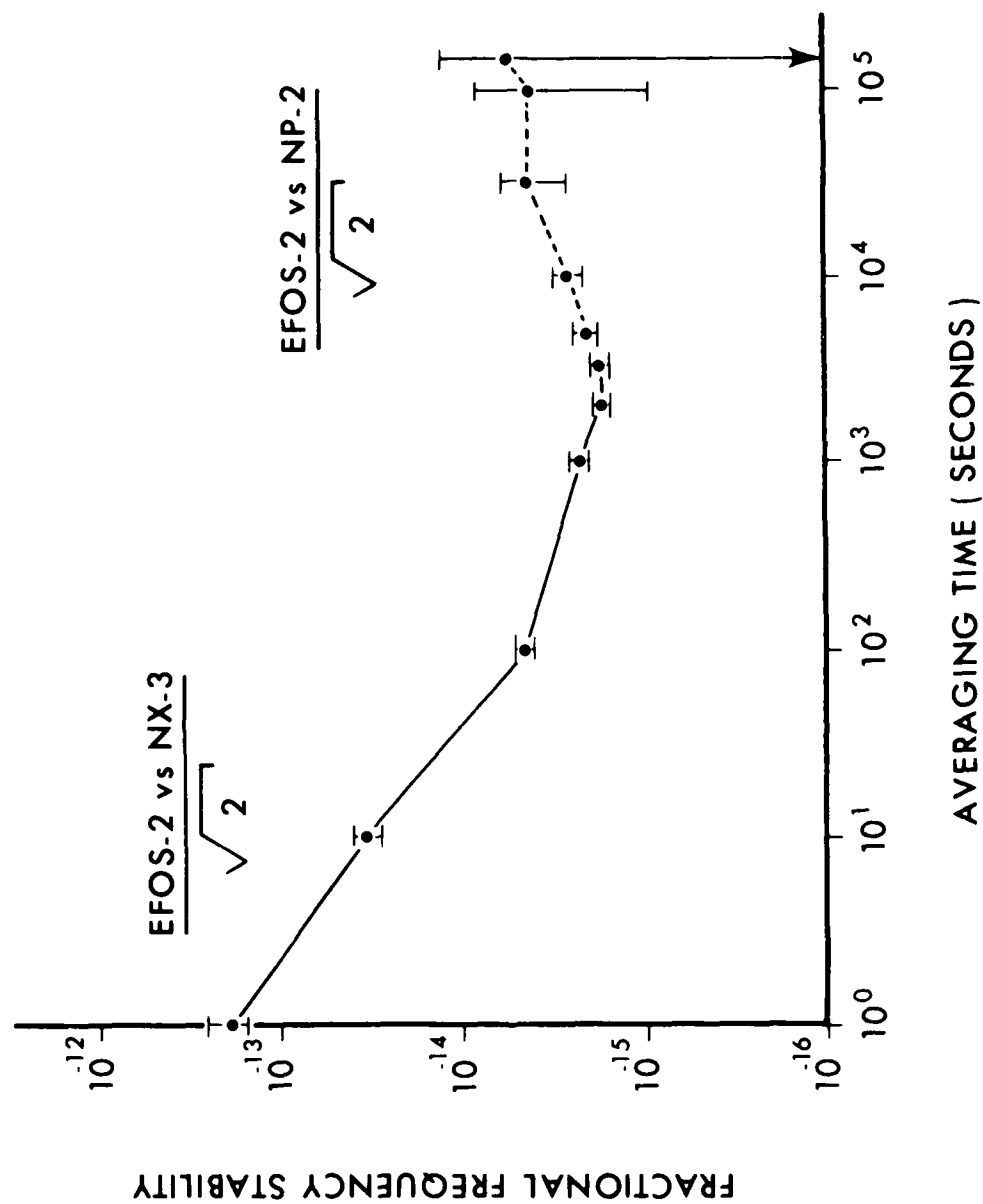
FREQUENCY DRIFT OF THE MASERS

The relative drifts of the masers derived from the long-term data are shown in Table 5.

Table 5. Relative Frequency Drift of the Masers over 3.75 Days:

EFOS-2 vs NX-3	= -4.4(20)x10 ⁻¹⁴ /day
NP-2 vs NX-3	= 0.1(20)x10 ⁻¹⁴ /day
EFOS-2 vs NP-2	= -4.5(28)x10 ⁻¹⁴ /day

During the period from January 14, 1983 to March 18, 1983 NP-2 was monitored relative to UTC(USNO) via LORAN-C, portable clock, television line 10, and GPS receiver. A quadratic fit of the data yields a frequency drift rate relative to UTC(USNO) of -6.55(8)x10⁻¹⁵/day. Using this value and the previous data, the frequency drifts of the 3 masers relative to UTC(USNO) over the 3.75 day measurement period were calculated. The results of this calculation are shown in Table 6.



5-83-VR

Figure 6. Best Estimate of EFOS-2 Frequency Stability

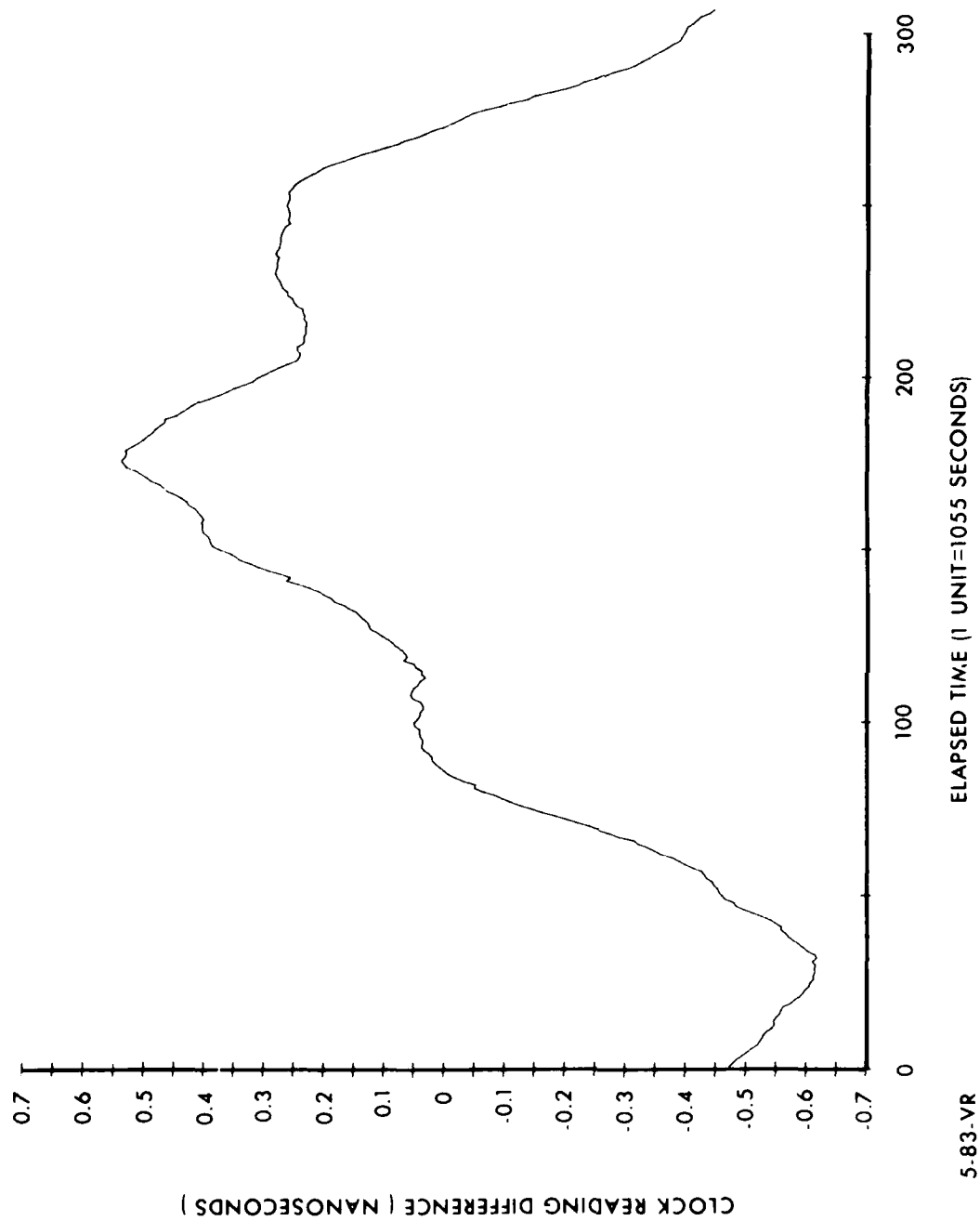


Figure 7. Clock Reading Difference Between EFOS-2 and NP-2 Over 3.75 Days with Average Clock Reading, Frequency Offset and Frequency Drift Removed

Table 6. Frequency Drifts of the Masers Relative to UTC(USNO):

$$\text{EFOS-2 vs UTC(USNO)} = -5.1(29) \times 10^{-14} / \text{day}$$

$$\text{NP-2 vs UTC(USNO)} = -6.55(8) \times 10^{-15} / \text{day}$$

$$\text{NX-3 vs UTC(USNO)} = -0.7(22) \times 10^{-14} / \text{day}$$

PREDICTED LONG-TERM GROUP DELAY RESIDUALS

Clock reading difference (ϕ/ω_0) data between EFOS-2 and NP-2 can be generated by numerically integration the derived EFOS-2 versus NP-2 fractional frequency offset data. The results of this integration are shown plotted in Figure 7 with a quadratic function of time removed (average clock reading, frequency offset, and frequency drift removed). This figure also represents a prediction of the expected group delay residuals from a 3.75-day VLBI run using EFOS-2 and NP-2 when both are in thermal chambers.

One day residuals were determined from the clock reading data by fitting out a quadratic function of time from one day sections of data randomly chosen out of the 3.75 days of data. The results of 11 such random samples are:

Table 7. Predicted One Day Group Delay Residuals with Quadratic Polynomials Removed

$$\text{RMS RESIDUAL} = 83(50) \text{ ps}$$

QUESTIONS AND ANSWERS

MR. WALLS:

Fred Walls, N.B.S. Victor, I don't understand how you get eleven data points from three-and-a-half days worth of data. They are certainly not independent and to do RMS on that gives a very misleading answer if you are trying to say you have 83 picoseconds. I don't believe it.

MR. REINHARDT:

No, they are not independent and the purpose of picking 11 points is to make them not independent.

MR. WALLS:

What do you mean, you only have three and one-half days worth of data, how can you get 11 - you can take different sets.

MR. REINHARDT:

What we attempted to do there in picking more than three samples, from three-and-a-half days of data is to randomize the starting point of the data relative to the data, its equivalent to doing the modified Allan variance. When you have data with very strong correlations, if you pick a certain starting point, your data is very susceptible to the phase of any fluctuation relative to your starting point; and to get a better measurement of the average data over that period, what we did, we took random samples of uncorrected data, perform the one day fit.

MR. WALLS:

Yes, but I think that's only reasonable if you say its stationary and its white, and you can't prove that either is true on such a short data set. I don't think it is a reasonable analysis.

MR. REINHARDT:

No. The error bars are just recorded there. We didn't take the fluctuations for 11 points and divide them by the square root of n.

MR. WARD:

Have you any idea about what the coupling mode was?

MR. REINHARDT:

Coupling mode for what?

MR. WARD:

Why was it correlated?

MR. REINHARDT:

What we are talking about is, if you take one day samples out of three-and-a-half days' data, and take more than three-and-a-half samples, it will overlap in the samples. The data is correlated, but the method I am using here, is equivalent to using the modified Allan variance, you are getting better use of your data by basically sliding your one day sample across your measurement interval rather than taking successive samples. And what I found in these long term data with very low frequency terms you have to be extremely careful because, by chance, you may just pick a phase of the data such that your errors cancel. I haven't been able to quantify this yet; but I think Dave Allan has done some work on this. I have better confidence in the sliding Allan variance for data that is non-stationary than I do with the conventional way of taking the Allan variance because of the sliding method. It averages over all phases of these random patterns much better. I haven't found a way to quantify that, but it produces a better result and it's more typical of an average result.

MR. ALAN:

Dr. Barnes has gone through and looked at that quite carefully, and in fact, you do gain quite a bit by the overlapping estimate as it is sometimes called. I think I understand what you are doing, Victor. And the only problem I have with it is that what we are addressing is a non-white process for the VLBI people. It's their need, they want coherence over the tracking time. I think you just have to do what you have to do to satisfy their need. It's a very reasonable approach.

MR. REINHARDT:

Basically they are using a statistic that is meant for stationary processes to describe a non-stationary process. They want the result of the RMS residual of a one-day run. That's what they want to know. So what we are doing by picking random samples we just didn't have an algorithm at that point to slide things over. It's equivalent to the sliding Allan variance. It's equivalent to taking a least squares fit at the start of the data, getting an estimate for the residual after doing only a one-day fit on the data, and then sliding the data, and just averaging this fit. It certainly gives you no worse result than taking sequences, and I have confidence that this gives a better result. Mathematically for flicker of frequency noise or worse it gives you no better result. But I have better confidence that it is more typical of an average error than if I had just taken three samples out of the data.

AD-A149 163 PROCEEDINGS OF THE ANNUAL PRECISE TIME AND TIME
INTERVAL (PTTI) APPLICATIONS (U) NAVAL RESEARCH LAB
WASHINGTON DC J A MURRAY 02 APR 84

AD-A149 163 PROCEEDINGS OF THE ANNUAL PRECISE TIME AND TIME
INTERVAL (PTTI) APPLICATIONS (U) NAVAL RESEARCH LAB
WASHINGTON DC J A MURRAY 02 APR 84

AD-A149 163 PROCEEDINGS OF THE ANNUAL PRECISE TIME AND TIME
INTERVAL (PTTI) APPLICATIONS (U) NAVAL RESEARCH LAB
WASHINGTON DC J A MURRAY 02 APR 84

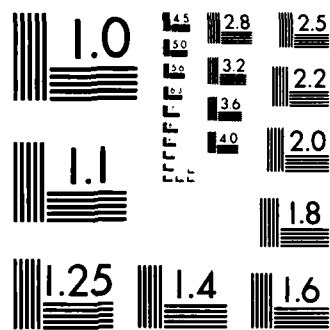
UNCLASSIFIED

UNCLASSIFIED

UNCLASSIFIED WASHINGTON DC 6 11 1984 F/G 5/9 NL

FILMED

DTAC



MICROCOPY RESOLUTION TEST CHART
NATIONAL BUREAU OF STANDARDS-1963-A

MR. KUHNLE:

JPL. Victor, what do you think the temperature coefficient might have been on the maser if the air flow had been considerably lower, like in a room?

MR. REINHARDT:

All I can do is quote what I've been told. Oscilloquartz people told me they got on the order of 5 in 10^{-14} in Switzerland. They remeasured that at NRAO and got on the order of 6 in 10^{-14} per $^{\circ}\text{C}$. Maybe the Oscilloquartz people want to speak for themselves at this point.

MR. BUSCA:

Oscilloquartz. The temperature coefficient is something which should be defined in a more accurate way, in the sense that the data you get depends on how you measure the temperature coefficient itself. We make the test simply by raising the room temperature by 1°C , in a similar way is doing Bob VEssot, and we measured before shipping the maser a value of $10^{-14}/^{\circ}\text{C}$. That was the last measured value. When we talk about a maser with an aluminum cavity as we are, people immediately said "This is not for a maser, because there is a problem of frequency sensitivity with temperature." We feel that if you put the maser in a big room and change the total room temperature by 1° , the time constant is on the order of 12 hours of the maser, and the final temperature coefficient under this condition is on the order of $2 \times 10^{-14}/^{\circ}\text{C}$.

DR. WINKLER:

I think this is very true, and in other words. Temperature coefficients of such systems are senseless and should not be specified in this way. What you should give is the step response of the system. The step response is a transient which may end without any displacement of the frequency after 24 hours or 36 hours. The question of the step response, one should measure it differently. By making a single step, you depend on air temperature, air flow, heat conduction and all of these things. What we should do. Expose the maser to a psuedo-random sequence of temperature changes + and - one degree and after 3 to 5 weeks you cross-correlate. Then the random variations will be suppressed and systematic. The effect of the temperature will be available and you get a very clean step response to temperature. The simple temperature coefficient as it is usually given is too simplistic a concept and leads into trouble.

MR. REINHARDT:

What muddies the water even further, is that we are dealing with non-stationary noise processes and these wall coefficients assume these things are reproducible. The problem in the lab is that when you make the measurements, they are not reproducible. When the device does not return to the same frequency, what do you do? There are other cases like the barometric pressure coefficient. You get two coefficients, an adiabatic and an isothermal, because depending on how fast the pressure is changed, you get different results. We have definitely seen these effects in masers. JPL saw this as a secondary temperature effect. This problem of coefficients is much more suited to devices which are stationary. It's a problem we have to live with.

DR. VESSOT:

I want to clear the record. We put our equipment in a box which we made out of rather poor insulating material and we have a rather substantial fan blowing the air within the box for the tests to make sure we do not have temperature gradients from above and below. This is a blower of considerable size, not a casual motion to the air.

The question of coefficient: it is clear that there are many things that will move. We have found that if we make a sudden step temperature change which we use in an attempt to diagnose what is going on, that in the early phases of the change, we see a change in frequency which moves rather rapidly and has a plus sign. We associate that with a phase change within the receiver system itself. And then there is a very long change carried on for 6 to 8 hours, which we think is effecting the maser itself. The comments by Dr. Winkler as a manner of getting through the noise, a matter of coherency detection, is clearly the only way to get through it. But, I must recommend that these step sizes be long enough to represent the long-term stationary end point behavior of the maser. This is one manner of describing it. If, on the other hand, we are in a room where the temperature fluctuates rather rapidly, then this other term will depend on it. So I think you have to set up sort of a Green's function approach, to say what is the response, and then you go and ask what is the stimulus of the room and then follow through that. It is not easy to do. The best thing to do is make them as immune as possible and stop worrying.

MR. PETERS:

A comment, that has not been properly brought out yet. The thermal control system, the thermal gain is highly dependent upon the insulation quality-conductivity. This is highly dependent on air flow when you are talking about atmospheric conduction and convection. Your time constant is actually a measure of the change in thermal conductivity which you have created and which changes your nominal thermal gain. So that it points out that one probably wants to use a minimal of air flow or at least something typical of the situation where you are going to use the maser.

If you put a rapid flow in, you are throwing in rapid and untypical changes. You are also changing the actual value because the thermal gain depends on this very strongly. In this case it could be a factor of 2 or something like that.

MR. REINHARDT:

A comment on what Bob Vessot said. You can see in this data, unfortunately we had to truncate it because we were under a time limit. I would love to let the maser sit here for 3 days. There were clearly 2 time constants here and that further complicates the issues, especially in hydrogen masers. You get short time constants, long time constants, the coefficients in some masers cancel, they add in others and you clearly, if you do this right, you have to do what Dr. Winkler does, but even more so than a step change, probably a square wave function and sweep the changes. You have to fully characterize the response.

DR. WINKLER:

Excuse me. I did not make myself clear. You expose the maser to a psuedo-random sequence of steps and they contain, or should contain all frequencies, even very low ones, so you are picking up the transient response of the system, which includes the response to all frequencies. That is the only way to describe a system response, properly.

MR. REINHARDT:

I see, you make random steps in time.

PHYSICS ELEMENT DESIGN ASPECTS FOR A TACTICAL
RUBIDIUM FREQUENCY STANDARD

Bruce Grover and Tae M. Kwon

Litton Industries
Guidance and Control Systems
5500 Canoga Avenue, Woodland Hills, California 91365

ABSTRACT

The rubidium frequency standard to be used in tactical applications must be capable of satisfying frequency stability specifications under severe environmental conditions which include a high ambient temperature. This has resulted in a physics element design of lamp, separated filter and resonance cell which operates above the highest ambient temperature, with a simple oven structure. This design differs from previous rubidium standards primarily in its smaller size and higher operating temperatures. The Litton tactical rubidium frequency standard physics element parameters and their effects on frequency stability are presented in this paper.

INTRODUCTION

Guidance and Control Systems Division of Litton Industries has developed a modular rubidium frequency standard for tactical military applications. Frequency standards for tactical applications demand small size, rapid warmup, low power consumption, and extreme ruggedness along with medium frequency stability. The frequency standard to be used in tactical applications must be capable of operating under severe environmental conditions which include extreme temperatures. Specifications call for a broad operating temperature range and for baseplate temperature as high as 80°C. Temperature stability of the physics package elements: lamp, filter cell and resonance cell can be maintained over the environmental range by operating these elements at temperatures above 80°C. This approach leads to a simpler oven design and compliance with the power budget. To date, rubidium standards have operated with resonance cells at temperatures below 70°C and an optical path length between 0.5 and 1.0 inches. As this temperature increases, the ideal balance between absorbed and transmitted light necessary for adequate signal to noise, and hence short term frequency stability, can best be maintained by decreasing the optical path length dimension of the

cell. Since rubidium density increases by two for each 9°C increase in temperature, operation above 80°C might require a resonance cell with path length dimension below 0.25 inches. This is a region where signal loss mechanisms due to rubidium interaction with the cell walls becomes increasingly important. Regardless of the operating temperature, a practical rubidium standard must operate with low frequency sensitivity to temperature (temperature turning point) and rubidium light intensity (light turning point). For these reasons, a portion of our program has been devoted to a study of these physical processes, including a parameterization of the light and temperature turning points as a function of system variables. Much of this work may be found in a final technical report.¹ We wish here to examine the Litton tactical rubidium standard physics element parameters and their effect on frequency stability. Where possible a physical explanation for these dependencies will be given.

EXPERIMENTAL SET-UP

The experimental set-up is shown in Figure 1. The physics package is placed inside a large cylindrical mu-metal shield. A pair of helmholtz coils located inside of the shield provides the static dc magnetic field. 10 MHz signal from a Cs frequency standard provides the reference to the frequency synthesizer and the input to the frequency multiplier. Outputs of the multiplier, 120 MHz, and of the synthesizer, f_1 approximately 5.3 MHz, are mixed at a mixer to generate $f_2 = 120 \text{ MHz} \pm f_1$.

In order to interrogate the atomic resonance at 6.8 GHz, the frequency f_2 is further multiplied by a step recovery diode in the microwave cavity. The cavity is tuned to select the lower sideband, f_3 , of the 57th harmonics of f_2 , i.e., $f_3 = 57 \times 120 \text{ MHz} - f_1$. For f_1 being 5,312,500 Hz, f_3 becomes 6,834,678,500 Hz. In this set-up, the interrogation frequency can be varied by varying the synthesized frequency f_1 . Phase modulation of the interrogation frequency is accomplished by modulating f_1 at the frequency synthesizer. Both frequency f_m and depth of modulation are readily adjustable at the lock-in amplifier. The resonance signal detected in the photodiode contains both in-phase and quadrature-phase components with respect to the modulation. The quadrature signal is detected at the lock-in amplifier. The ^{87}Rb resonance dispersion curve is obtained in an x-y recorder by plotting the signal amplitude as a function of the interrogation frequency f_3 .

The physics package consists of three physics elements: lamp, filter cell and resonance cell, and is shown in Figure 2. Later studies were made using a modification of this unit with both

filter and resonance cell inside the microwave cavity. The entire physics package is assembled within two layers of magnetic shield, the outer dimension of which measures $1\frac{1}{4} \times 1\frac{1}{4} \times 3$ inches.

The lamp consists of a 1720 glass blank, $\frac{1}{2}$ mm wall, of cylindrical shape 9 mm diameter and 10 mm overall length with a slight convex exit window and pinchoff at the opposite end. About 100 micrograms of isotopically pure ^{87}Rb is filled with 2.5 torr of buffer gas. The lamp is excited in a helical resonator driven by a modified Colpitts oscillator at ~ 90 MHz. Lamp luminance for D_1 and D_2 rubidium radiation increases with lamp temperature over the range of interest, here 100°C to 120°C . Lamp temperature is monitored and controlled closely to maintain a constant spectral output. Filter cells used in this study are made from 12 mm diameter 1 mm wall glass tubing cut to length with 1 mm glass disks attached as end windows. The fill stem is attached on the side wall of the filter. Filter cells used in this work range from 7 mm to 9 mm overall length and are filled with isotopically pure ^{85}Rb and either Ar, N_2 , or both gases. The filter cell temperature is controlled and monitored in the range 85°C to 92°C . The filter cell serves two primary functions. One is to establish enough preferential optical pumping of the $F=1$ hyperfine level over the $F=2$ level for sufficient signal to noise ratio. The second function is to establish a spectral condition for minimum dependence of rubidium resonance frequency on light intensity. Resonance cells used in this work are made of glass in a fashion identical to our filter cells. These cells range from 8 mm to 10.5 mm in length and are filled with isotopically pure ^{87}Rb and varying amounts of N_2 and Ar, approximately 10 torr N_2 and 14 torr Ar.

The resonance cell is placed in a small rectangular microwave cavity operating in the TE_{101} mode.² The cavity is partially loaded with a low loss dielectric slab. A 0.3" diameter in each end of the cavity allows light to pass through the resonance cell and be collected at a photo cell mounted on the outside of the cavity. Two 10 mm diameter plano-convex lenses are placed in the cavity to optimize the optical process. Table 1 lists some of the physics package parameters used in this work.

LIGHT SHIFT

To minimize dependence of clock frequency on rubidium light intensity, the physics package parameters are adjusted to allow unit operation at the so called light turning point where light shift, i.e., the change in clock frequency with light intensity, is zero. All physics package parameters that we have studied appear to influence the light turning point (LTP) to some extent,

however the filter cell parameters: length, temperature and buffer pressure have the greatest effect. Figure 3 shows light shift as a function of filter length for several cavity temperatures and constant pressure. Light shift here is defined as the change in resonant frequency with a 15% change in light intensity. Figure 4 gives cavity temperature at the LTP as a function of filter cell length. Figure 5 shows light shift versus buffer pressure based on N_2 buffered filter cells and shows the trend in light shift over a wide pressure range. In general, we observe that light shift changes sign on passing thru a LTP indicating that the integrated light shift spectrum also changes sign. This is to be contrasted with light shift which asymptotically approaches zero from one side only. This behavior as a function of the filter pressure parameter is shown in Figure 6.

Since data for Figures 3 and 4 was taken from an integrated cavity configuration, the temperature dependence indicated could in general arise from both filter and resonance cells. However, separated measurements as in Figure 7 indicate that light shift is a weak function of resonance cell temperature in this range.

Light shift is also influenced by lamp temperature. Figures 8 and 9 show clock frequency and light shift versus lamp temperature, respectively, and indicate that both frequency and light shift increase positively with lamp temperature in the region of a light turning point. Figure 10 relates light shift to the RB87 lamp spectrum filtered by a RB85 filter cell and provides a qualitative understanding of the light shift vs. filter pressure, length and temperature behavior shown here.

TEMPERATURE COEFFICIENT

We find that the temperature coefficient of the resonance cell, i.e., the change in clock frequency with resonance cell temperature is determined by several processes. The dominant process is the well known pressure shift arising from an increase or decrease in hyperfine level spacing due to $Rb-N_2$ and $Rb-Ar$ atom collisions respectively. In practice, the Ar/N_2 ratio is adjusted to minimize the temperature coefficient at the LTP. Figure 11 shows frequency vs. cavity temperature for several resonance cells of differing buffer ratio (N_2/Ar) as measured in the integrated cavity. It should be mentioned that the filter cell contributes a negative temperature coefficient to this data. The negative filter cell coefficient appears to be an unavoidable consequence in this range of increased filtering of the positive light shift, $F=2$, component with increasing filter temperature. This contribution to the temperature coefficient of the integrated cavity scales with the total light intensity. The cavity temperature coefficient should then be a strong function of light level as Figure 12 indicates.

MAGNETIC FIELD GRADIENT

When a magnetic field gradient is present across the resonance cell, inhomogeneous effects cause light shift, resonance cell temperature coefficient and microwave sensitivity values to be altered. Figures 13 and 14 illustrate microwave sensitivity and light shift as a function of c-field when the c-field produces approximately a 30% gradient across the resonance cell.

SUMMARY

Due to the influence of the many parameters involved it is not suggested that data presented here should be exactly reproducible in rubidium frequency standards of others. However, the more general qualitative behavior of the physics package elements discussed here should apply to the tactical rubidium standards of others in this higher temperature and smaller cell size regime.

ACKNOWLEDGEMENTS

The authors wish to acknowledge the support by the USAF RADC/ESD. Contributions to this work have been made by all members of our group. Particular thanks go to W. Debley for cell fabrication.

REFERENCES

1. Rubidium Frequency Standard Study, Feb. 1982 to March 1983, USAF, Electronic Systems Division. F19628-83-C-0046.
2. H.E. Williams, T.M. Kwon, T. McClelland, 1983 Frequency Contr. Symp. p.12.

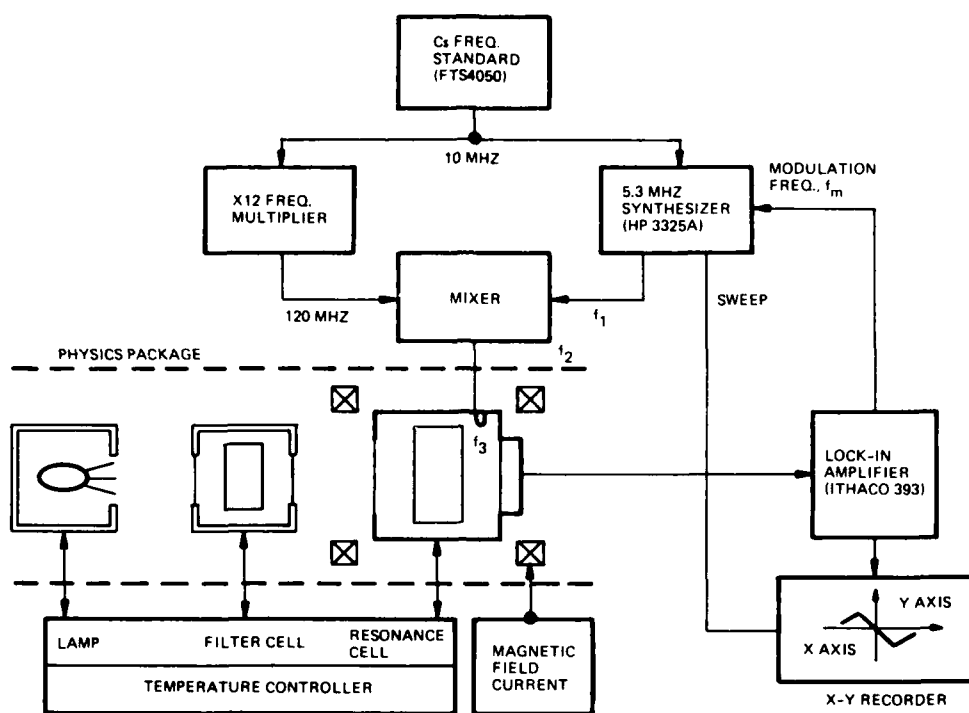


Fig. 1-Experimental Apparatus

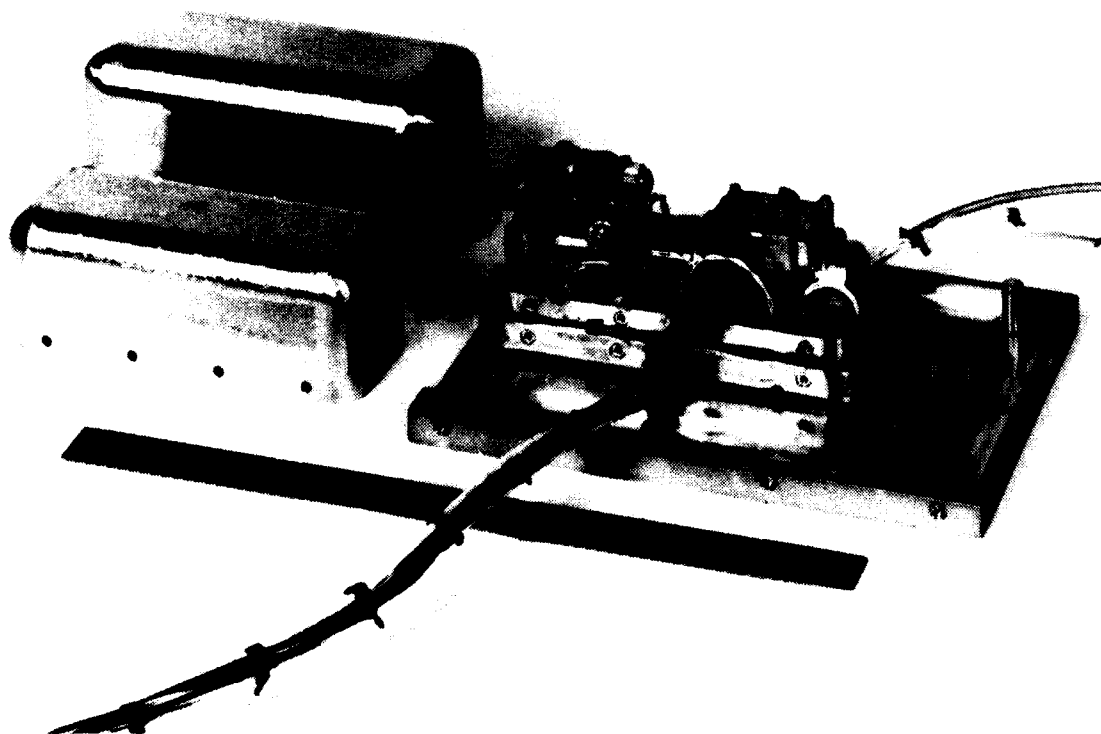


Fig. 2-Litton Engineering Model FSU Physics Package

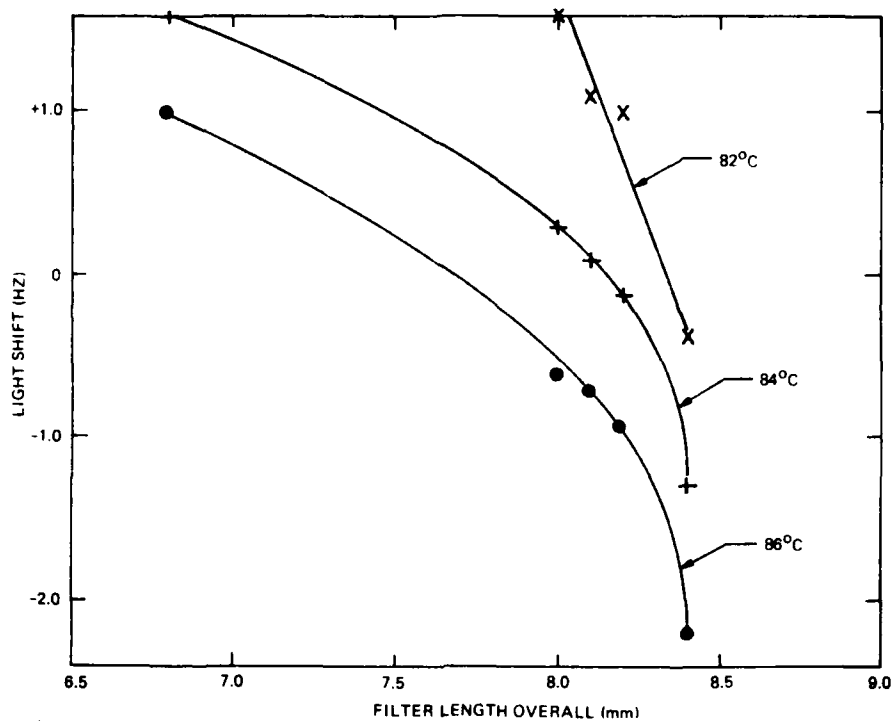


Fig. 3-Light Shift Vs. Filter Length for Several Cavity Temperatures
Filter Pressure = 120 TORR Ar, Lamp Temperature = 118°C

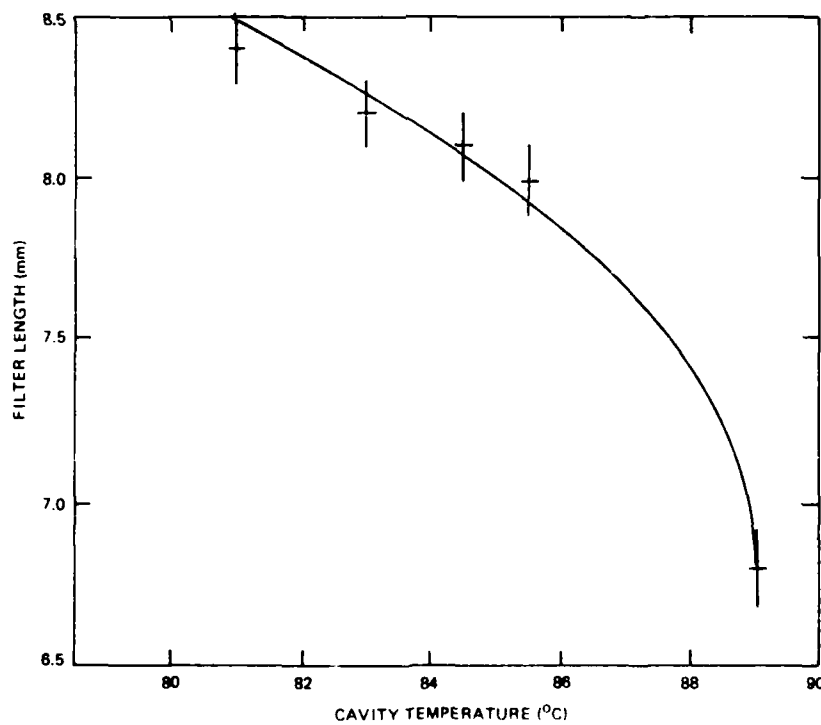


Fig. 4-Cavity Temperature at LTP Vs. Filter Length-Parameters as in Figure 3

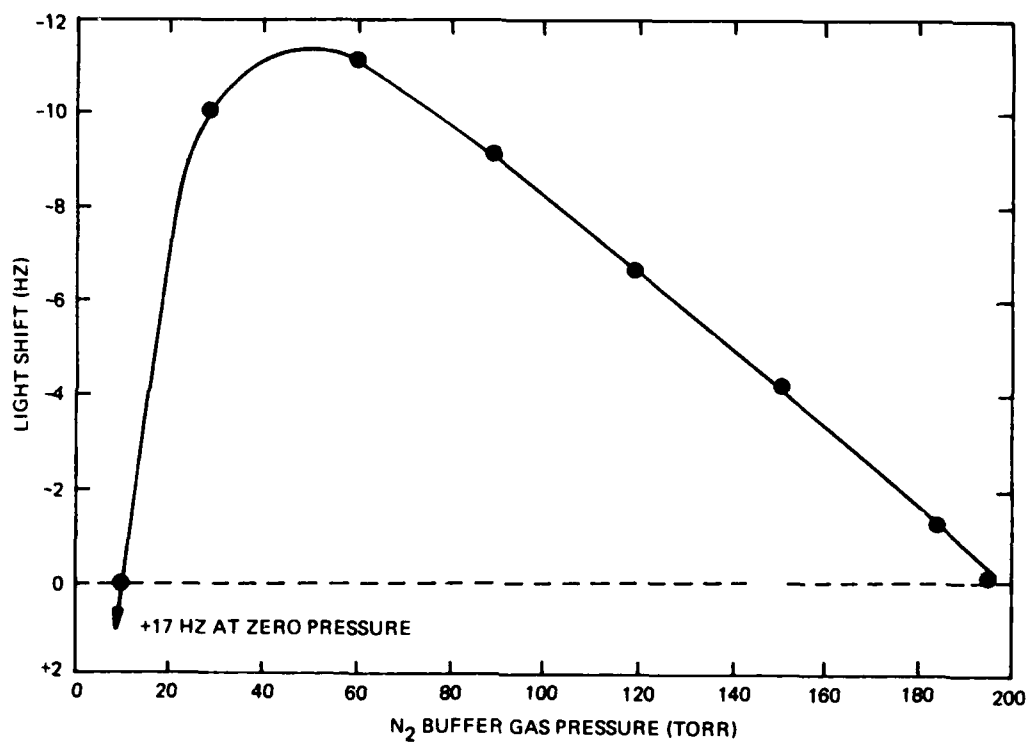


Fig. 5-Light Shift Vs. Filter Buffer Gas Pressure (N_2)
 Lamp - 116.5C, Filter - 88C, Resonance Cell - 9.2 mm, 83C
 Filter Length Nominal 8.4 mm

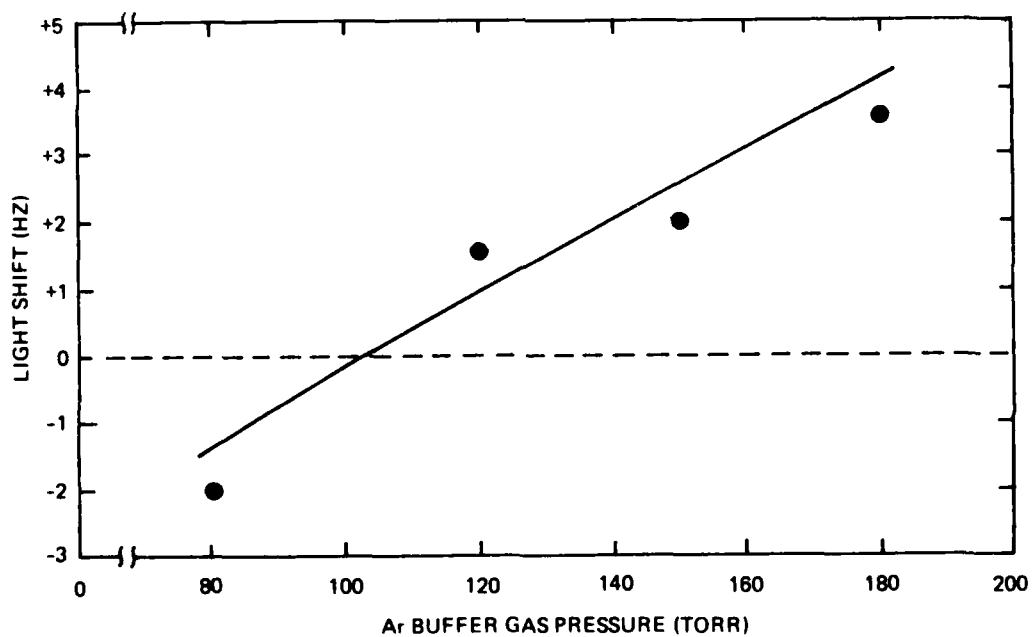


Fig. 6-Light Shift Vs. Ar Buffer Gas Pressure of Filter Cell

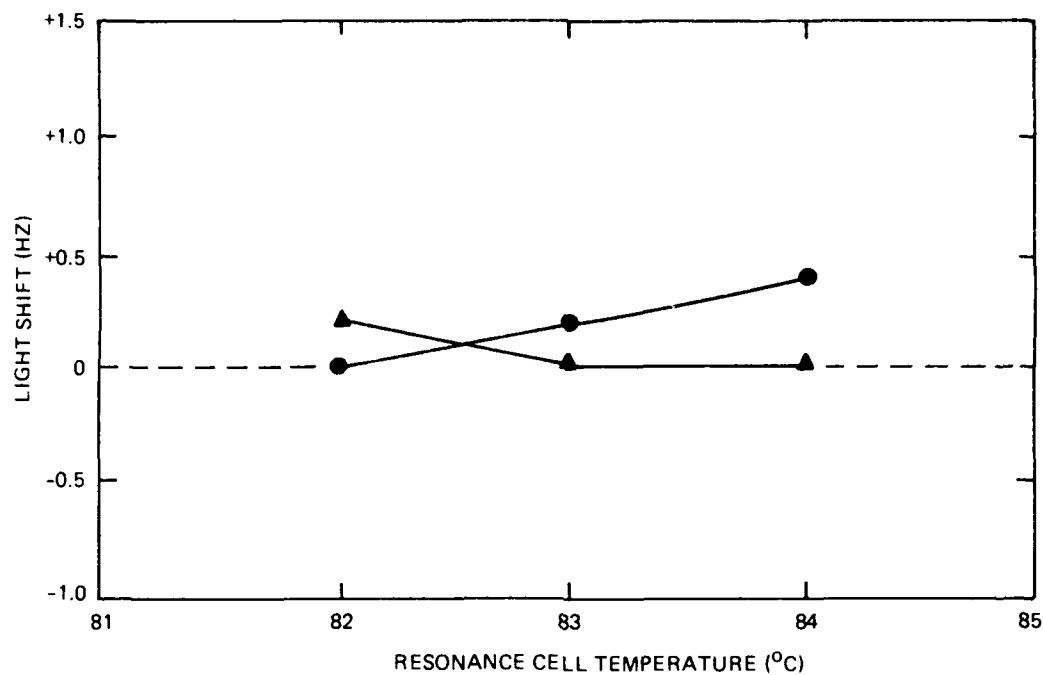


Fig. 7-Light Shift Vs. Resonance Cell Temperature
Lamp - 116.8C, ●90C Filter, ▲91C Filter

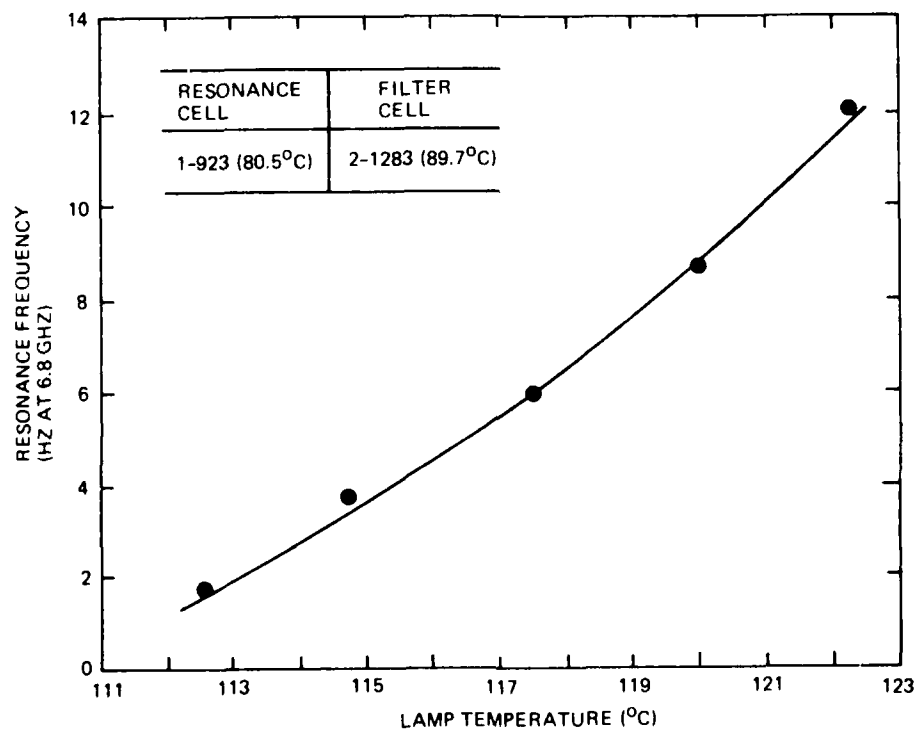


Fig. 8-Rb87 Resonance Frequency Vs Lamp Temperature

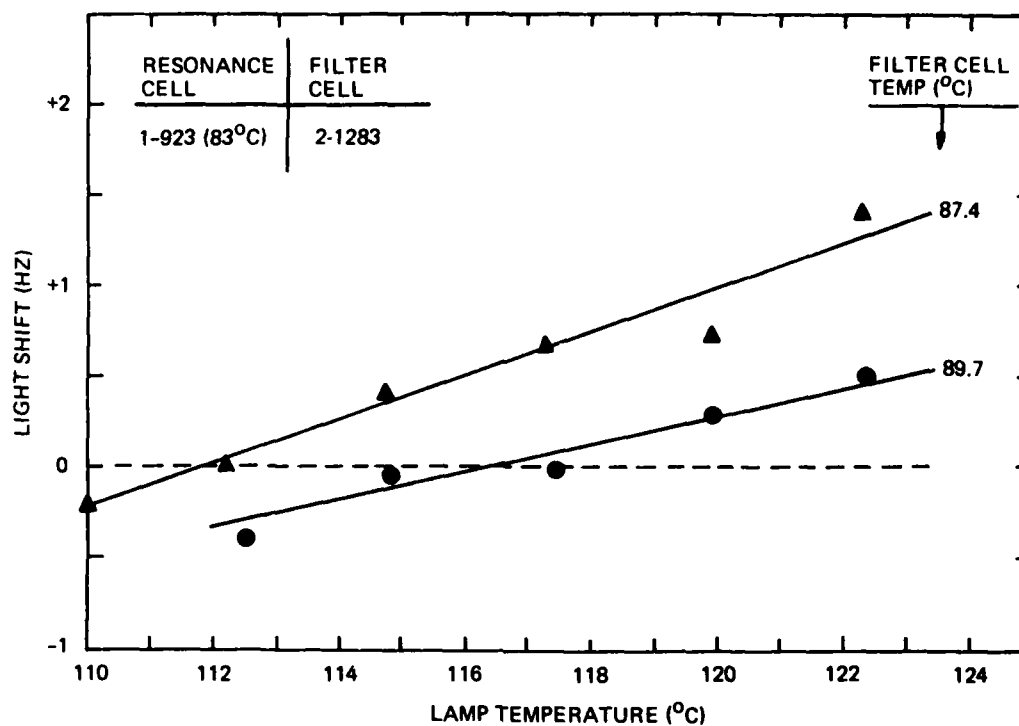


Fig. 9-Light Shift Vs. Lamp Temperature

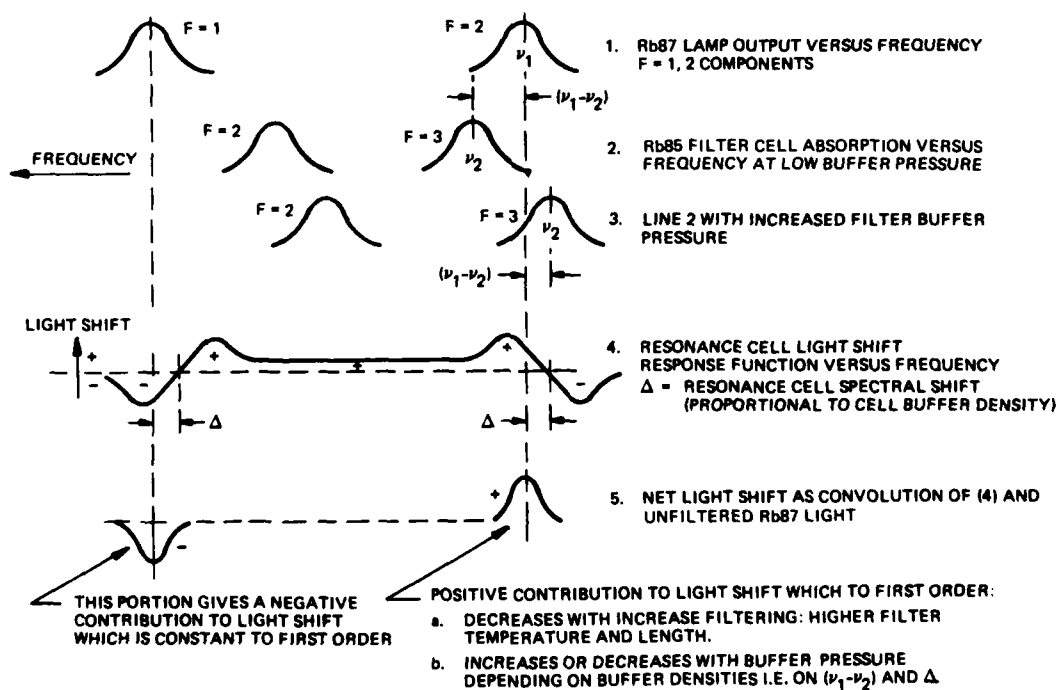


Fig. 10-Light Shift Model

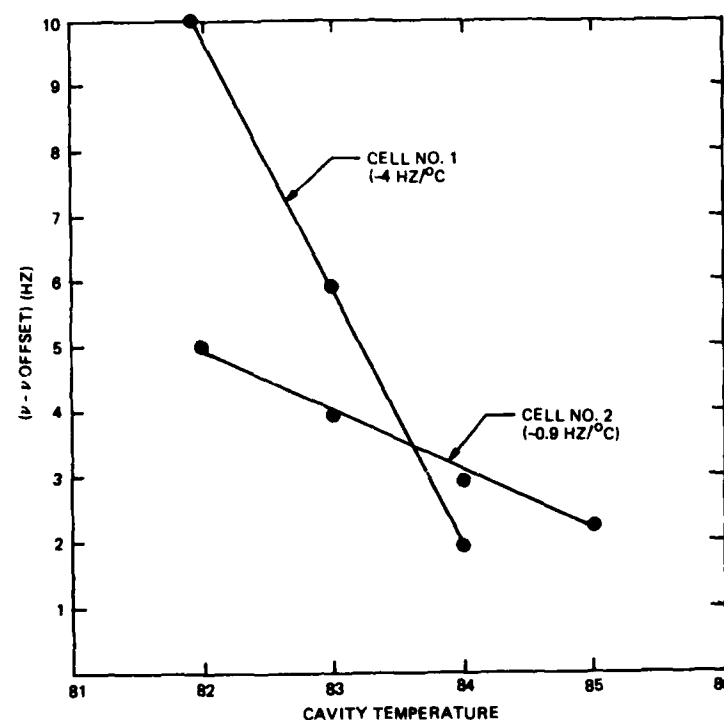


Fig. 11-Frequency Vs. Cavity Temperature for Resonance Cells of Differing Buffer Ratio (N_2/Ar)

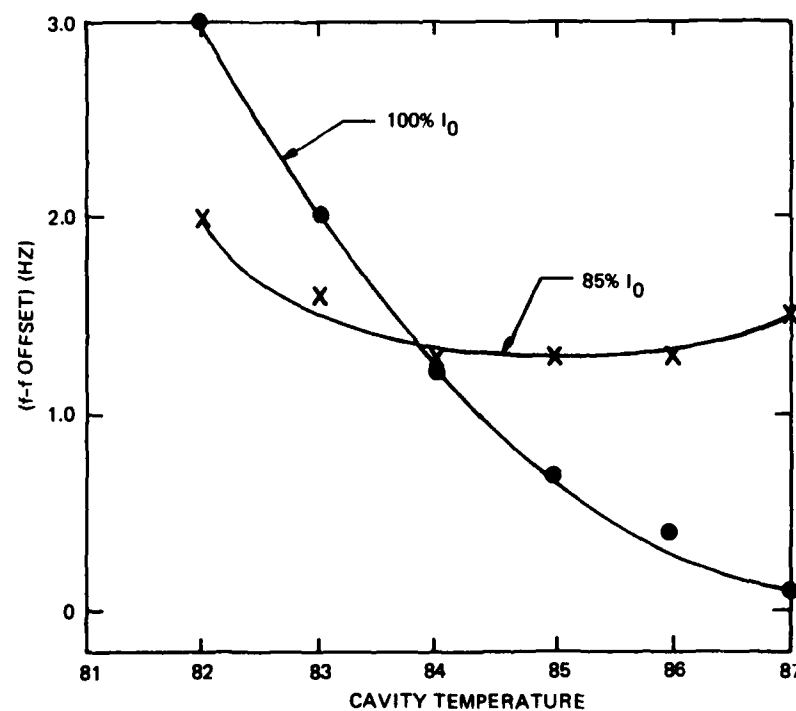


Fig. 12-Frequency Vs. Cavity Temperature as a Function of Light Intensity (I_0)

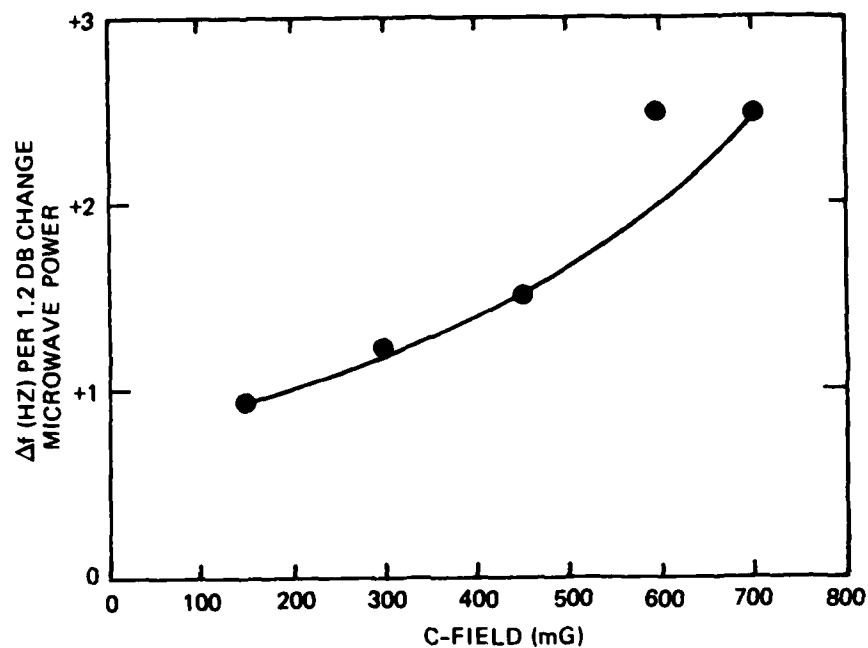


Fig. 13-Microwave Sensitivity Vs. C-Field With Gradient

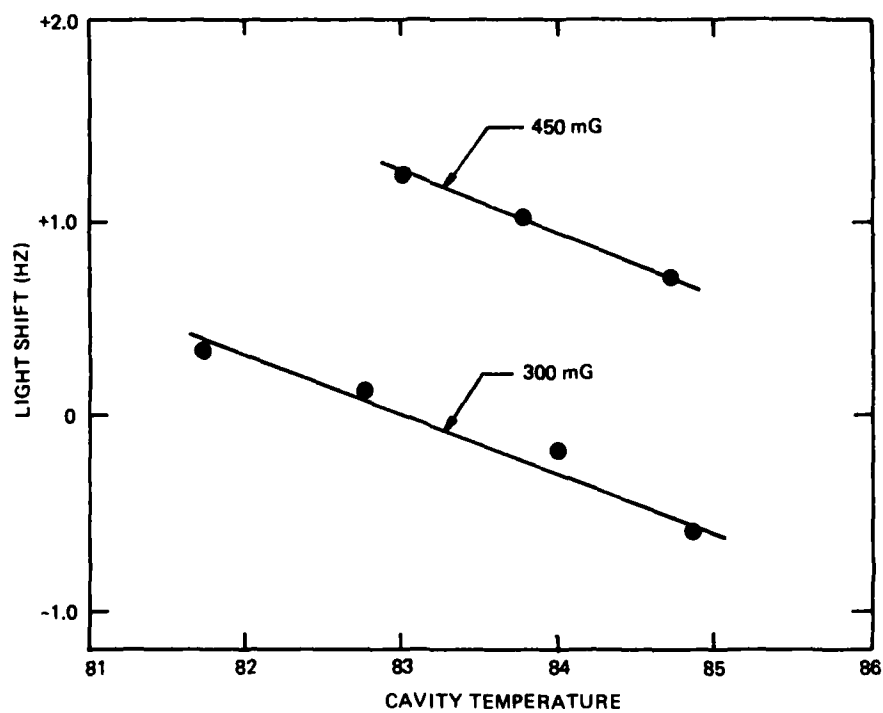


Fig. 14-Light Shift Vs. Cavity Temperature as a Function of C-Field with Gradient

TABLE I. PHYSICS PACKAGE PARAMETERS USED IN THIS STUDY

LAMP SIZE	9mm DIAMETER X 10mm LONG
LAMP FILL	Rb87 + 3 TORR Xe
LAMP TEMPERATURE	115 – 120°C
FILTER CELL SIZE*	12mm DIA X 7-9mm LONG
FILTER CELL FILL	Rb85 + N ₂ OR Ar
FILTER CELL TEMPERATURE	85C – 92C
RESONANCE CELL SIZE*	12mm DIA X 8-11mm LONG
RESONANCE CELL FILL	Rb87 + 10 TORR N ₂ + 14 TORR Ar
RESONANCE CELL TEMPERATURE	80C – 85C
DC PHOTODETECTOR CURRENT	≈ 75 μA
LINEWIDTH BETWEEN INFLECTION POINTS	800 – 1200 Hz
DISCRIMINATOR SLOPE AT PHOTODETECTOR	210 – 36 PA RMS PER 1 X 10 ⁻¹⁰
FREQUENCY STABILITY IN SHOT NOISE LIMIT	5 X 10 ⁻¹² τ ^{-1/2} – 3 X 10 ⁻¹¹ τ ^{-1/2}

*INCLUDES 1mm END WINDOWS

QUESTIONS AND ANSWERS

None for Paper #35.

Paper #36 was neither given nor submitted for publication.

CRYSTAL RESONATOR/OSCILLATOR TEST FACILITY and TEST RESULTS

V.J. Rosati and R. L. Filler

US Army Electronics Technology & Devices Laboratory (ERADCOM)
Fort Monmouth, New Jersey 07703

Introduction

The primary mission of the Frequency Control and Timing Branch of the U.S. Army Electronics Technology and Devices Laboratory (ETDL) is to advance the state of the art in quartz crystal resonators and oscillators in order to meet the requirements of military users. Secondary missions include consultative support to project managers and systems designers and the maintenance of the military specifications for quartz crystal resonators and crystal oscillators (i.e., MIL-C-3098⁽¹⁾ and MIL-O-55310.⁽²⁾)

These activities require an intimate and practical knowledge of the state-of-the-art.

In the course of fulfilling the above missions and activities, comprehensive test facilities have been established at ETDL for quartz crystal resonators and oscillators. The purpose of this paper is to outline the capabilities of the laboratory, present the results of some investigations, and offer to DOD-sponsored users our assistance with the testing, selection, specification and development, when necessary, of crystal oscillators.

Crystal Resonator Test Facility

Computer controlled instruments such as impedance instruments and Pi network/vector voltmeter combinations are used to measure resonators' frequency and equivalent circuit parameters, i.e., the motional resistance, motional capacitance, motional inductance, and shunt capacitance.^(3,4)

For room temperature measurement of equivalent circuit parameters, the impedance instruments have been found to be convenient and accurate. All parameters can be measured as a function of drive current and various environmental stimuli such as radiation, shock, etc.

Frequency versus temperature (f-T) and resistance versus temperature (R-T) measurements are done with a multiposition pi network system. The pi networks are inexpensive thick film resistors deposited on ceramic substrates. The input and output are isolated by more than 100 dB by incorporating appropriate shielding between the network halves, then enclosing the whole assembly in an aluminum "minibox". Short circuit amplitude and phase data for each network are stored in the computer. A block diagram of the "temperature run" system is shown in Figure 1.

Each resonator to be measured is inserted into a pi network and the chamber is set to the lowest test temperature for a low temperature "soak". Temperature is then increased, stepwise, until the highest test temperature is reached. Frequency and pi-network input and output voltages are measured, after an appropriate stabilization time, prior to the next temperature step. This is called a "quasi static" temperature profile.

Figure 2 is a representation of the time-temperature profile used for these tests. For a single temperature run, only the first half of the cycle is used. For thermal repeatability and hysteresis measurements, reverse cycles are also used. The cycles are repeated when thorough hysteresis data is desired.

The data are stored and at the conclusion of a run the f-T and R-T data are plotted. Third- and fourth-order polynomials are fitted to the f-T data using a least squares technique. The third order polynomial is used to calculate upper and lower turning points, inflection temperature, and the frequency temperature slope at inflection. The fourth order curve is included for more accurate representation of the data, if needed. A typical temperature run plot is shown in Fig. 3.

If thermal hysteresis or thermal repeatability measurements are desired, the above process is modified. To measure thermal hysteresis, a technique has been evolved which allows self measurement of the resonator temperature via the excitation of two modes in the resonator.⁽⁵⁾ This avoids the apparent hysteresis caused by thermal lag or thermal gradients between the temperature sensing probe and the resonator.

Thermal hysteresis as good as 5×10^{-9} has been measured. Figure 4 shows the results obtainable using the hysteresis test set. In the figure, the abscissa represents temperature and the ordinate represents the values of the residuals after a 6th order polynomial (fitted to the first f-T run) is subtracted from the data of the first run and from three subsequent runs. The hysteresis manifests itself as the spread of the residuals to a fitted polynomial curve. Deviation from the horizontal axis is indicative of the quality of the polynomial fit.

A parameter of increasing interest is the sensitivity of resonators to acceleration or vibration. The sensitivity is represented by Γ and is determined by measuring the "2g tipover" or vibration-induced sidebands.⁽⁶⁾

The "2g tipover" test is accomplished by incorporating the resonator in a stable OCXO and placing the oscillator into a fixture which has a horizontal axis of rotation. The operator rotates the oscillator, stepwise, through 360 degrees. At each step the frequency is measured and recorded. The frequency versus angle data is fitted to a sine curve. Next, the oscillator is rotated 90 degrees such that the axis which was initially horizontal is made vertical. Frequency is recorded and the oscillator is tipped 180 degrees. The frequency is again recorded. The

three components of the acceleration sensitivity vector can then be determined and the sensitivity vector, $\vec{\Gamma}$, calculated.

A representative curve and calculated acceleration sensitivity are shown in Figure 5.

To determine whether there are vibration resonances in the resonator structure, the vibration-induced sidebands are measured as a function of vibration frequency, as follows. A test oscillator, containing the resonator under test, is completely filled with wax (potted), rigidly fastened to the shake table surface, and subjected to sine wave excitation over a range of 50 Hz to 2000 Hz. Oscillator output is mixed down to audio frequency and displayed on a spectrum analyzer. Vibration sideband amplitudes are measured and the components of $\vec{\Gamma}$ are calculated from the relation:

$$\gamma_i = \frac{2 F_{vi}}{a f_o} 10^{L/20}$$

where F_{vi} is vibration frequency in the i direction, a is acceleration, f_o is the oscillator frequency, and L is the sideband amplitude in dBc. A representative L versus F_v curve is shown in Figure 6.

Aging, Allan Variance, and phase noise tests are generally performed with a specially designed test oscillator.⁽⁷⁾ The test oscillator oven temperature is externally adjustable to facilitate setting to the turnover temperature. Resonator drive current is also externally adjustable. Some models of the test oscillator have ovens settable to below -60°C for low temperature aging and stability studies. The aging measurements are straightforward, data being automatically taken every workday. Periodically, the aging data are plotted and fitted to logarithmic, exponential, or combined log-exponential functions.

Allan Variance and phase noise measurements generally follow the procedures of NBS Monograph 140.⁽⁸⁾ The oscillator under test is quadrature phase locked to a reference oscillator to suppress the carrier. Mixer output is displayed on a baseband spectrum analyzer which can be under computer control.

Oscillator Test Facility

Frequency versus temperature tests for complete oscillators are performed in a manner similar to the corresponding resonator test, according to the block diagram in Figure 7.

The apparatus can accommodate 150 oscillators. The power supply leads are isolated and filtered at each oscillator position to avoid crosstalk via the power supply leads. Each oscillator is terminated according to its specification, then matched to 50 ohms for a coaxial cable feed to the RF selector switch.

A temperature run starts with a two hour stabilization at 30°C. At this point, any required frequency adjustments are made. For example, TCXO may be adjusted to their marked calibration offset frequency, or offset by a predetermined amount to observe the trim effect. (The trim effect is the rotation of the resonator f-T characteristic caused by varying the load capacitor). After this initial interval, a temperature profile similar to Fig. 2 is followed, except that longer stabilization times are used to accommodate the thermal time constants of oscillators. Frequency is recorded every degree during the up- and down-cycles.

Upon completion of the temperature run, the chamber is again set to 30°C and a final frequency measurement is made after two hours. Figure 8 is a representative plot a TCXO f-T curve.

The two plotted curves depict the frequency versus temperature behavior in the temperature-increasing and temperature-decreasing directions. The left hand column of figures gives the maximum frequency and the minimum frequency measured during the temperature increasing half of the run. Also in the first column is the frequency at 30°C, taken "on the fly", and the slope of the f-T curve at 30°C. The center column gives similar figures for the temperature-decreasing half of the cycle. The right hand column gives the maximum and minimum frequencies recorded for the full cycle. These are used to compute stability according to the formula:

$$\frac{F_{\max} - F_{\min}}{2}$$

The "del F offset" figure is the frequency offset to which the oscillator must be adjusted (at 30°C) to center the maximum and minimum frequencies about the horizontal (nominal frequency) axis.

Thermal hysteresis can also be determined from the plotted data. This determination is made by measuring the separation of the two curves at each temperature. The maximum deviation is assigned as the hysteresis for the oscillator.

The trim effect is observed by offsetting the oscillator by means of the frequency adjust control as would be required to compensate for aging or other environmental effects. After each frequency adjustment the f-T run is repeated. Figure 9 is a plot of the trim effect for a TCXO.

Frequency aging measurements for oven controlled crystal oscillators (OCXO) are accomplished at laboratory room temperature, (oscillator oven energized, set to resonator upper turning point) and present no particular problem.

For TCXO's, the definition of aging is somewhat clouded: The effect of temperature on aging has not yet been determined; A "standard" TCXO aging temperature has not been defined, there is also the question of

whether aging data taken at a constant temperature can be used to predict how an oscillator will age when it is subjected to variations in temperature.

Notwithstanding these issues, aging measurements are now made at 60°C for at least 30 days. The temperature chamber used for this test has been observed to be stable to $\pm 0.05^\circ\text{C}$ over a 30 day period.

Several additional tests which are soon to be implemented are: observation of hysteresis during repeating temperature cycling (twenty $^\circ\text{C}$ and one hundred $^\circ\text{C}$ swings); trim effect after repeated thermal cycling, hot soak, and cold soak; and aging at various temperatures and after repeated thermal cycling.

Allan Variance and phase noise testing are done as explained above for resonators.

Vibration testing, likewise, is similarly performed except that no potting is used. Peaks in the acceleration sensitivity curve, caused by resonating loose components, wires, or flexing circuit boards can, therefore, be seen. An example of an oscillator suffering this type of defect is seen in Figure 10.

Test Program Results

The results of a continuing oscillator testing program have been reported in detail elsewhere. (9,10)

Table I is a summary of the results to date of that TCXO testing program. From the table, it can be seen that the likelihood of finding TCXO that meet specifications diminishes as the specified stability improves.

Not included in the table are the latest measurements of the trim effect. The data are disappointing, showing that there are no TCXO in the 0.5 ppm stability class that can safely be designed into systems that have as little as five years expected life.

Conclusion

The Frequency Control and Timing Branch of the U.S. Army Electronics Technology and Devices Laboratory (Fort Monmouth, NJ) has established a comprehensive facility for the testing and characterization of quartz crystal resonators and oscillators.

The Branch is happy to offer to military users its assistance with the testing, selection, specification and development of crystal oscillators.

References

1. Military Specification; Crystal Units, Quartz, General Specification for, 1979
2. Military Specification: Oscillators, Crystal, General Specifications for, 1976
3. "Crystal Parameter Measurement Methods", Final report, contract Nr. DAAK-20-82-C-0390, 1983
4. Basic method for the measurement of resonance frequency and equivalent series resistance of quartz crystal units by zero phase technique in a pi network, Publication No. 444, Bureau Central de la Commission Electrotechnique Internationale, Geneva, Switzerland
5. "Resonator Self Temperature Sensing Using a Dual Mode Crystal", S. Schodowski, V. Rosati, and D. Bowman, Classified Session, 37th Annual Frequency Control Symposium, Philadelphia, PA, June, 1983
6. "The Effect of Vibration on Frequency Standards and Clocks", R. Filler, Proc 35th Annual Frequency Control Symposium, USAERADCOM, Fort Monmouth, NJ, May 1981
7. "Update on the Tactical Miniature Crystal Oscillator Program", H. Jackson, Proc. 36th Annual Frequency Control Symposium, USAERADCOM, Fort Monmouth, NJ, June 1982.
8. Time and Frequency: Theory and Fundamentals, NBS Monograph 140, May 1974, Superintendent of Documents, Washington, DC.
9. "Temperature Compensated Crystal Oscillator Survey and Test Results", V. Rosati, S. Schodowski, and R. Filler, Proc 37th Annual Frequency Control Symposium, IEEE Catalog No. 83CH1957-0, June 1983.
10. "State of the Art in Crystal Oscillators", V. Rosati, R. Filler, J. Vig, and S. Schodowski, Proc MILCOM '83, IEEE Catalog No. 83CH1909-1, October 1983.

RESONATOR F-T SETUP

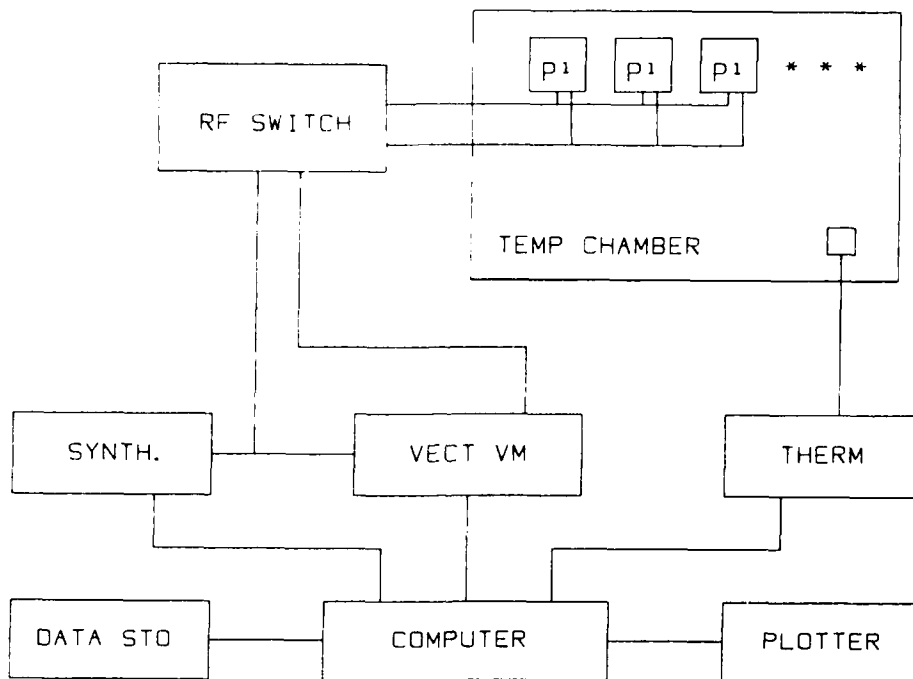


Fig. 1. Block diagram of resonator f-T apparatus.

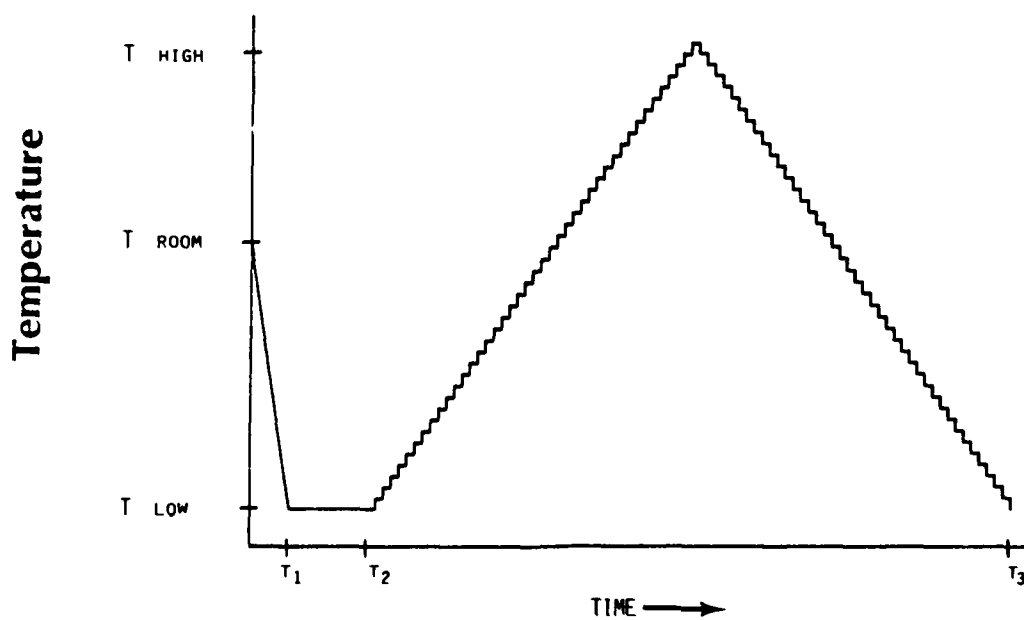
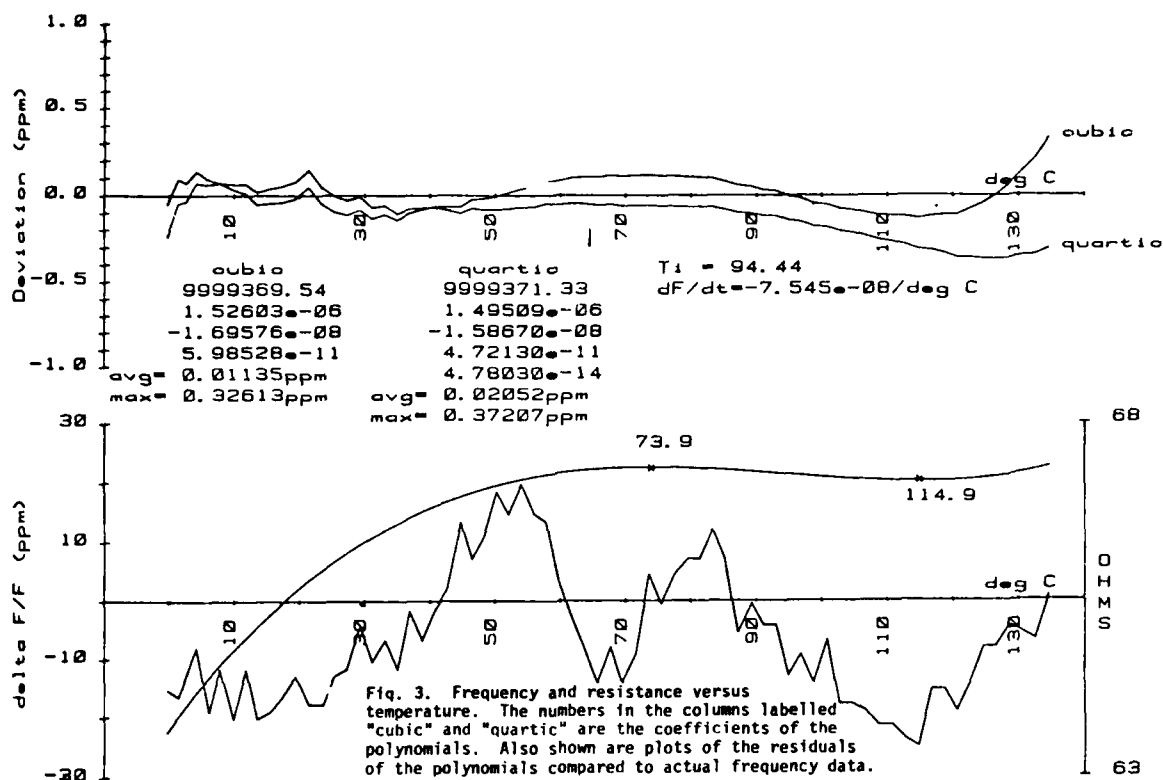
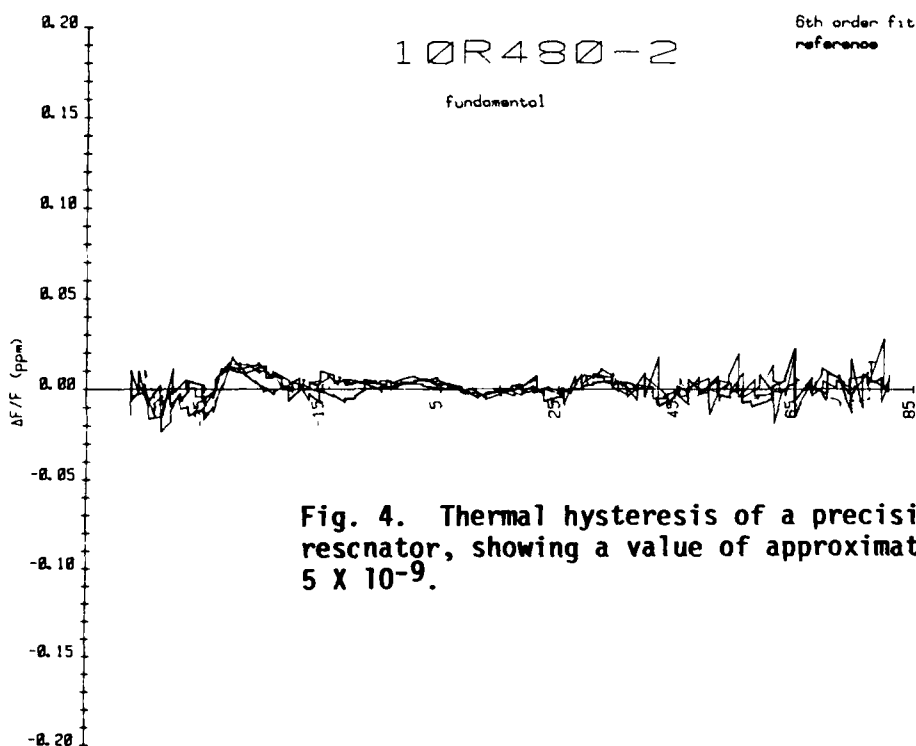


Fig. 2. Stepwise time/temperature profile.



RESONATOR THERMAL HYSTERESIS



CR-696
5.115MHz

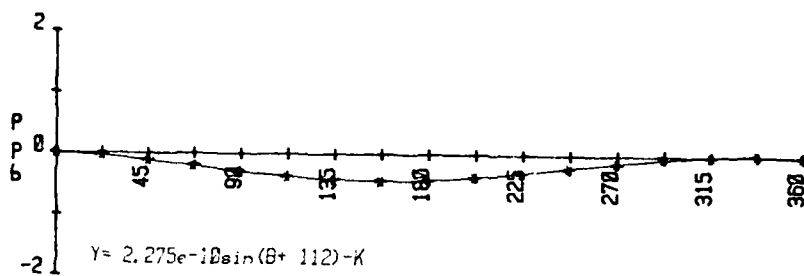
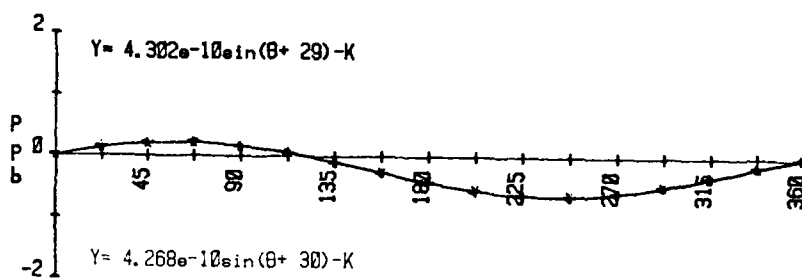


Fig. 5. "Two g tipover" results. The x, y, and z values are the components of the sensitivity vector, \vec{r} .

$$\begin{aligned} X &= 8.523e-11/g \\ Y &= -2.110e-10/g \\ Z &= 3.749e-10/g \end{aligned}$$



$$Y = 4.268e-10 \sin(\theta + 30) - K$$

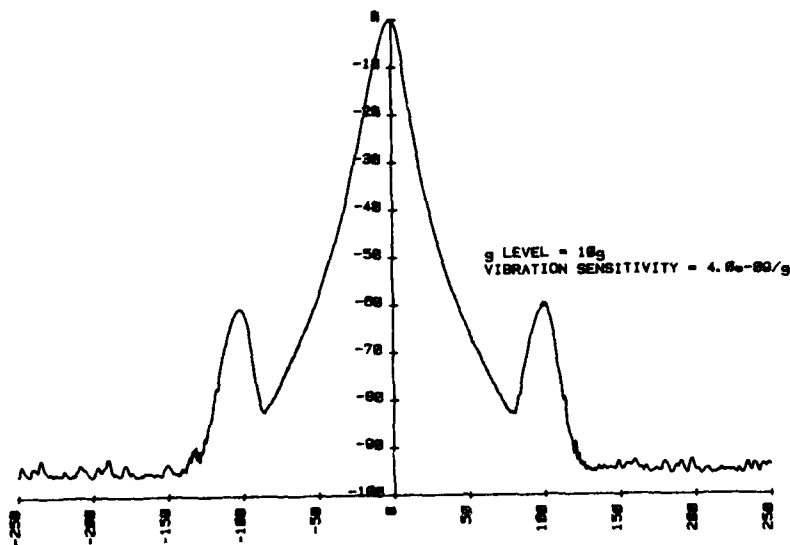


Fig. 6. Vibration-induced sidebands resulting from g acceleration at 100 Hz. The measured sensitivity of this resonator is $4 \times 10^{-9}/g$ in the direction of vibration.

OSCILLATOR F-T SETUP

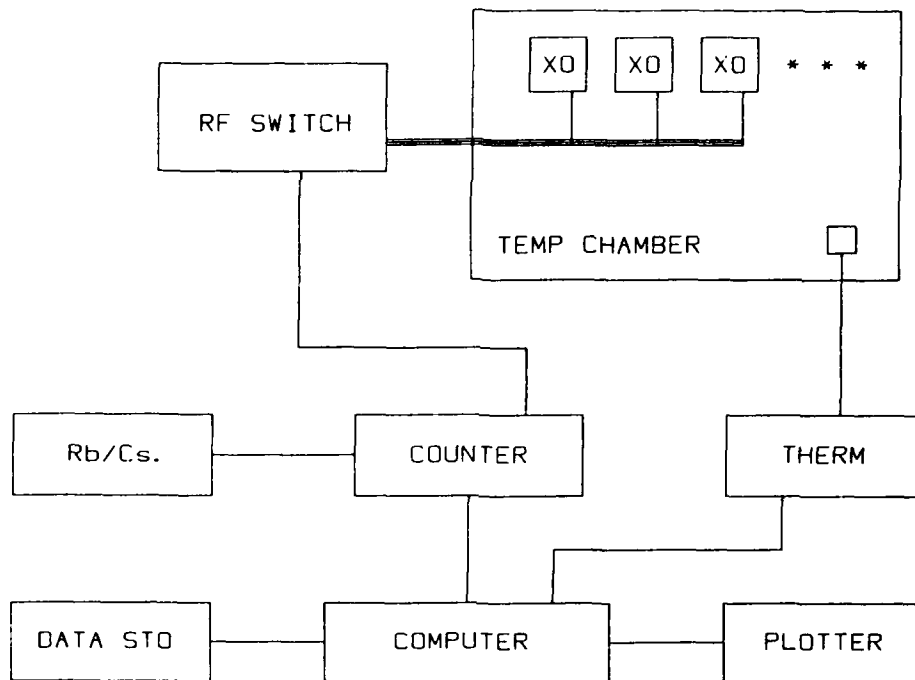


Fig. 7. Block diagram of oscillator f-T apparatus.

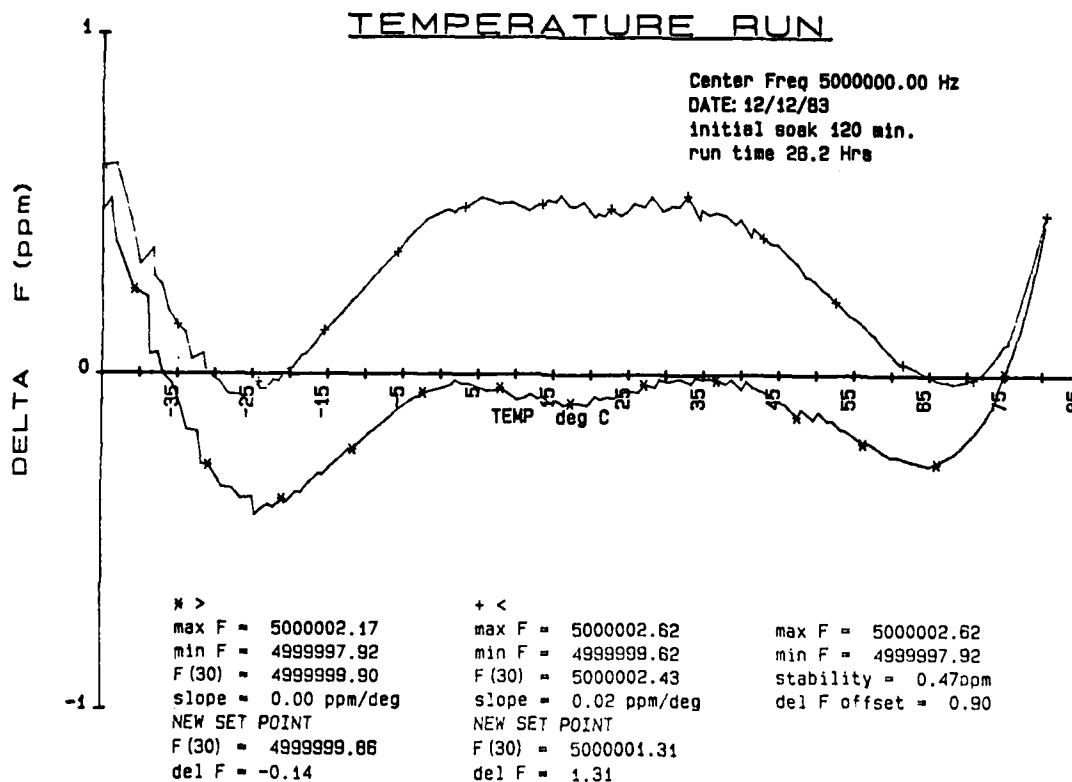


Fig. 8. Representative TCXO f-T curve. The thermal hysteresis of this oscillator is about 0.6 ppm.

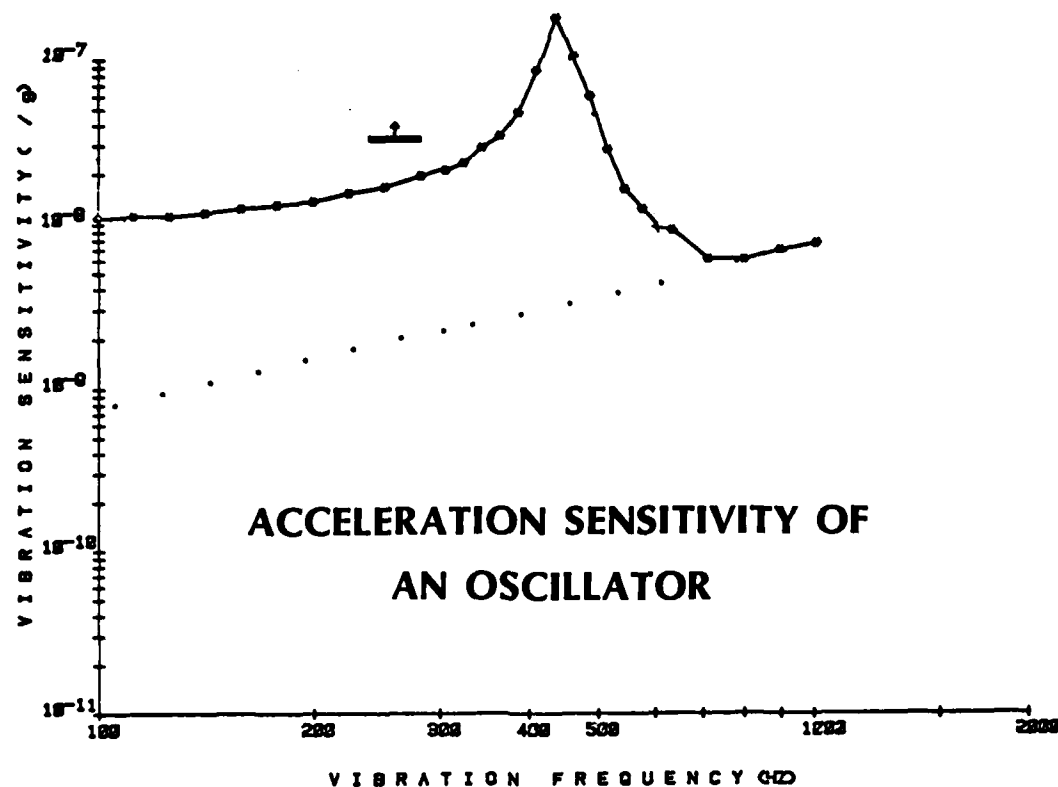
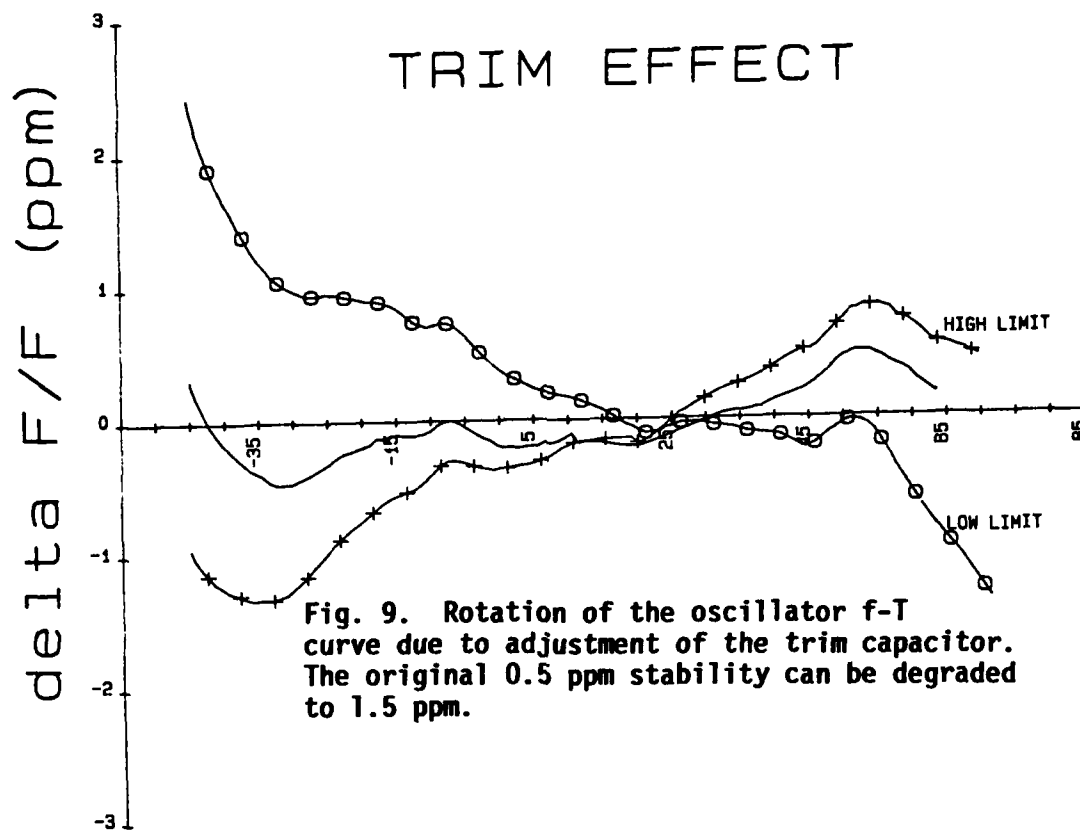


Fig. 10. Degradation of effective vibration sensitivity due to mechanical resonance in the oscillator.

SUMMARY OF ALL OSCILLATORS

STABILITY CLAIMED (PPM)	F-T STABILITY		AGING/MO (PPM)
	#TESTED	#FAILED	
5	30	1	0.2
3	5	0	.25 (E)
2	5	0	.57
1	5	1	.18
0.6	5	5	.34
0.6	5	1	.5 (E)
0.5	5	3	.30
0.5	25	16	.36
0.5	5	2	---

E = ERRATIC

Table I. Summary of the results of testing a group of 90 TCX0. Details of the study can be found in references 8 and 9.

QUESTIONS AND ANSWERS

A VOICE:

That blue slide on the summary, I can't understand that slide as saying that if you need stability or ageing of a half a part per million what you should do is order the cheapest and don't specify.

MR. ROSATI:

If you don't specify anything, I don't know what you would get.

DR. WINKLER:

Well, the conclusion is to spend the least amount of money on procurement and most of it on testing.

MR. ROSATI:

Absolutely. That is what we are trying to get across, that money spent up front in testing and guaranteeing that the oscillator will be good, delivers a good payoff in the logistic costs later on.

TIME SYNCHRONIZATION EXPERIMENTS WITH APPLE

C. L. Jain, K. Kumar, M. R. Sivaraman
Space Applications Centre, Ahmedabad, India

and

B. S. Mathur, P. Banerjee, A. Sengupta, Mithlesh
Saxana, A. K. Hanjura and A. K. Suri
National Physical Laboratory, New Delhi, India

ABSTRACT

Several Time Transfer/Synchronization techniques viz transmissions of 1PPS, TV Passive, TV Active, transmission of INSAT Time Code etc. were tried out on the Indian Experimental Satellite APPLE. The availability of the APPLE Satellite for a long time gave us the opportunity to try out various new techniques which could not be tried out earlier on Symphonie and to firm up the specifications of the hardware required to be developed for various category of users when INSAT becomes available on an operational basis for the dissemination of Standard Time and Frequency.

The drift of APPLE Satellite in its orbit was found to be about 150 meters/sec. Because of such large change in the range of the satellite it was not possible to achieve expected accuracies in the time transfer. Due to the availability of only one transponder on board, most of the experiments were conducted in quasi-simultaneous mode. The use of 2nd order range extrapolation technique to correct for the satellite range helped us to get better time transfer accuracies than was possible with linear extrapolation. Using the techniques of 1PPS, ranging to the APPLE was carried out and orbit computation was attempted and used in a TV passive technique. In this paper results of various experiments conducted on APPLE are presented.

INTRODUCTION

The technique of Standard Time and Frequency (STF) dissemination via satellite is well established. Dissemination of STF via satellite provides many unique advantages over HF propagation technique viz larger coverage, better accuracy, better S/N ratio. A satellite in its orbit is used in two modes, first in which the satellite is the source of Standard Time and Frequency and the second in which satellite is used to transfer time from a Master Station to the User Station. In the first technique the user should know the precise orbital elements of the satellite along with various bias parameters like Onboard Clock accuracy and its drift, propagation path delay, Receiver ground co-ordinates, tropospheric and ionospheric delay, Receiver delay etc. (Satellites like NNSS, GOES, GPS etc. fall in this category). In the second case the various biases that should be known accurately are the propagation path delay from Master Station to the User Station, earth station delay, ionospheric and tropospheric path delay, clock offset of the Master Station with respect to UTC, satellite transponder delay, etc. The advantage of Geostationary satellite for the dissemination of STF is that most of the bias parameters can be determined fairly accurately and they remain unchanged for a long period. In this paper results of various experiments conducted on APPLE Geostationary satellite are presented.

APPLE UTILIZATION PROGRAM

Under APPLE Utilization Program, Space Applications Centre, Ahmedabad and National Physical Laboratory, New Delhi conducted mainly two types of experiments viz:

- (a) Time Dissemination experiments relevant to INSAT
- (b) Ranging of the Satellite

- (a) In India several time dissemination techniques have been tried out on experimental basis using Symphonie (1, 2, 3, 4, 5) and APPLE Geostationary satellites. In Table -1 we have given a list of various techniques tried out on Symphonie and APPLE and accuracies achieved. Out of the various techniques used, three techniques viz TV Passive technique, TV Active technique and Transmission of INSAT Code on RN Channel are found to be more useful on INSAT for the dissemination of STF. These three techniques could be used without affecting the basic usage and with no additional requirement on the Space-craft and with only incremental investments on the ground segment.

The necessary hardware required for the generation of and decoding of the INSAT Format was developed at National Physical Laboratory, New Delhi and tested on APPLE. A narrow band RN Channel in S band has been allotted for this purpose on INSAT-1B. Initially it is planned to use this channel on an experimental basis but it is likely to be made operational as the number of users increase with time.

The Format of Standard Time planned for INSAT-1B is shown in Figure 1. It is a slow code and carries information about the number of days of the year, time of the day in Indian Standard Time, satellite position co-ordinates and DUT1. Distribution of bit information is elaborated in Figure 2, one complete Format of information consists of 59 bits between two consecutive minute marks, the first 29 bits carry information about days, hours and minutes, the remaining 30 bits carry information about satellite co-ordinates.

- (b) In the satellite ranging experiment a station transmits 1PPS (one pulse per second) and receives back the same via satellite and measures the time interval between the transmitted and received pulse. If T is the time interval between the transmitted and received pulse, the range to the satellite is given by $\frac{cT}{2}$ where c is the velocity of electromagnetic waves in free space. The overall accuracy of the range measurements depends on several bias parameters. We have compared in Table-2 the ranging data obtained from Clock synchronization technique with the C-Band tone ranging technique carried out simultaneously. The C-Band tone ranging technique is a conventional technique used for satellite tracking by transmitting a burst of low frequency tone and comparing its phase differences with the received tone burst, transmitted back by the satellite. Range values from clock synchronization data were found to be consistently lower by about 6.5 to 7.0 km from tone ranging values. The difference could be attributed to the unknown bias parameters of either earth stations. This comparison indicated the potentiality of using time synchronization technique for tracking geostationary satellite. A Computer Program for orbit determination using these ranging data was developed. In this program by a least square method the square of the difference between the observed range and theoretically calculated range is

minimized by iteration and updating of the orbital parameters. This was done mainly for the determination of orbital elements required for the INSAT Format. The main aim of ranging and orbit determination was to study the feasibility of generating orbital elements of the satellite to be transmitted with INSAT format keeping in view the accuracy requirements of various users. With such Orbit improvement it was possible to cater the requirement of Users who needs time to an accuracy of better than 50 microsecond.

CONCLUSION

Though the accuracy achieved via APPLE is not as good as was obtained using Symphonie, it gave us an opportunity to try out some of the new techniques which could not be tried out on Symphonie and also to develop and test necessary hardware to be used on INSAT for the dissemination of STF. The main reason for the poor time transfer accuracy was due to the large drift of the APPLE owing to the instability of its Orbit.

ACKNOWLEDGEMENT

The authors would like to thank Director, Space Applications Centre and Project Director, APPLE Utilization for Allotting time on APPLE Satellite for conducting the experiments. Authors would also like to thank the Staff Members of Ahmedabad Earth Station and Delhi Earth Station for providing the necessary help during the Course of Experiment.

REFERENCES

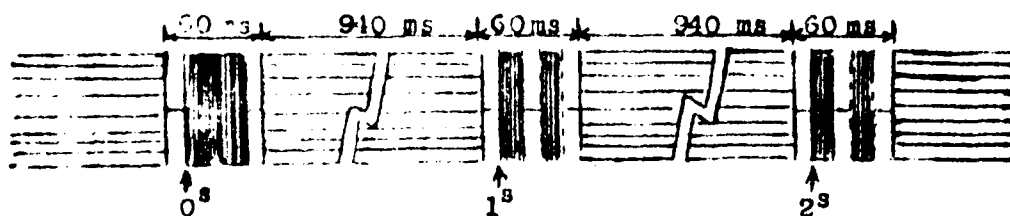
- (1) Clock Synchronization experiment in India using Symphonie Satellite. Somayajulu (YV) et. al. Proceedings of Tenth PTTI Applications and Planning meeting, Nov. 1978, NASA, GSFC, PP (643-658).
- (2) A Study of Time Dissemination via satellite in India. Proceedings of Eleventh Annual PTTI Meeting, Nov. 1979, GSFC, PP (387-402), B. S. Mathur et. al.
- (3) Simultaneous Two way time transfers between NPL, SAC and MES via Symphonie Satellite, B. S. Mathur et. al. Journal of Institute of Electronics and Telecommunication Engineers (JIETE) Vol. 27, No. 6, 1981 PP (207-213).
- (4) Precise Time transfer using Direct TC Broadcast by Satellite Symphonie, P. Banerjee et. al. JIETE, Vol. 28, No. 8, 1982 PP (425-428).

- (5) Broadcast of ATA Time signals via satellite Symphonie.
P. Banerjee et. al., JIETE, Vol. 28, No. 9, 1982
PP (457-462).
- (6) INSAT- 1A, A Multipurpose Domestic Satellite System for
India, IEEE Transactions on Broadcasting. B.C. 25, 4, 1979,
Dhawan(S), Singh(JP) and Kale(PP).

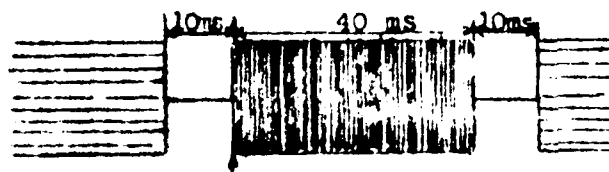
TABLE -1.

S.No.	TIME DISSEMINATION TECHNIQUE	ACCURACY		REMARKS
		SYMPHONIE	APPLE	
1.	Two way quasi simultaneous ⁽¹⁾	Better than 1 Microsecond	Better than 10 Microsecond	Second order range extrapolation technique tried on
2.	Two way simultaneous ^(2, 3)	"	-	
3.	ATA transmission via satellite ^(2, 5)	"	-	
4.	TV Passive technique ^(2, 4)	"	Better than 30 microsecond	
5.	TV Active technique	-	-	Hardware tested & Methodology Established
6.	Transmission of INSAT Time Code	-	-	"

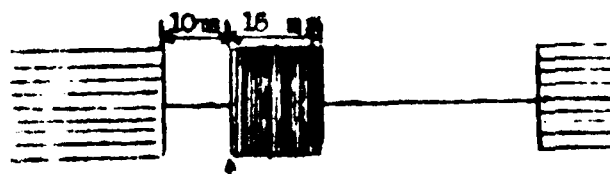
DATE 25-8-82			TABLE -2.		ABSOLUTE DIFFERENCE
HR	MIN	SEC	RANGE IN KMS TONE RANGING TECH- NIQUE	RANGE IN KMS CLOCK SYNCHRO- NISATION	
09	56	32	38070.365	38063.822	6.543
09	59	31	38074.600	38068.020	6.579
10	02	31	38078.83	38072.123	6.709
10	04	31	38081.72	38074.810	6.910



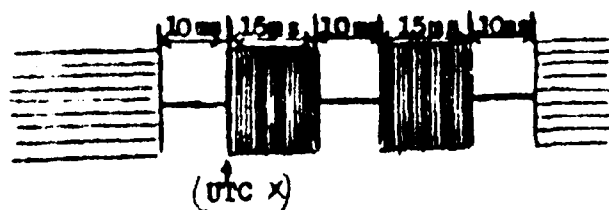
Details Of The Time Signals



⇒ Minute mark



⇒ Zero bit state



⇒ One bit state

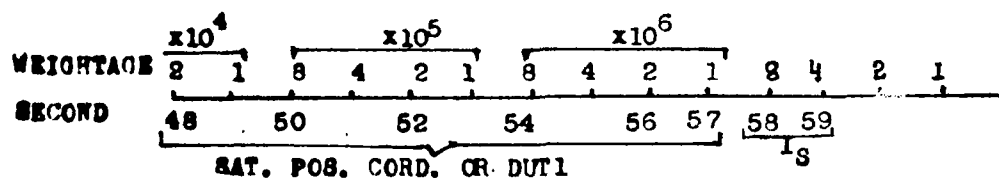
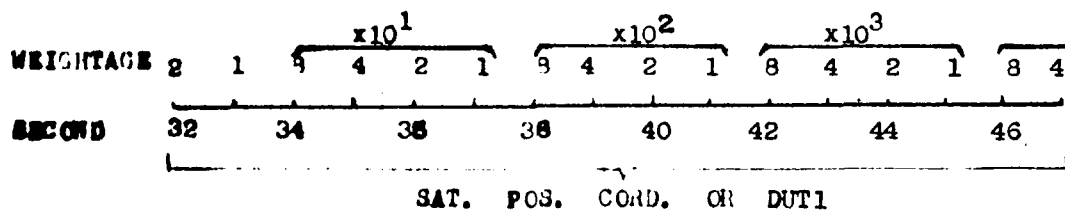
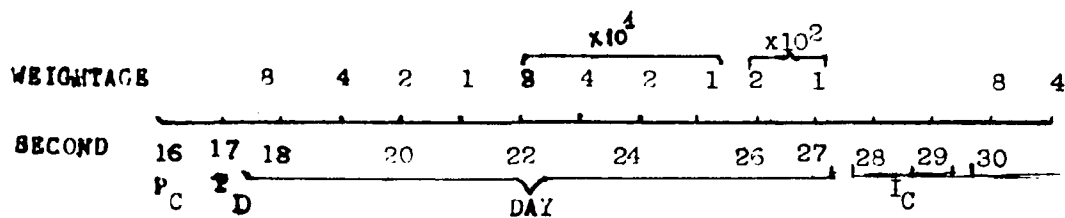
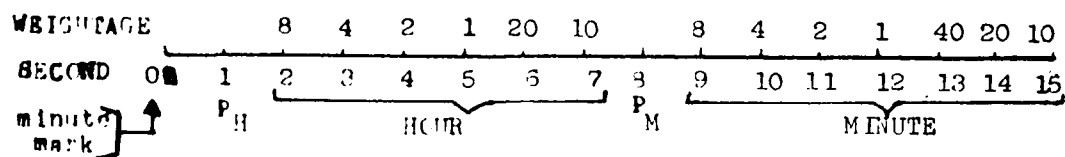


5 KHz



1 KHz

FIG. 1: STF SIGNAL FORMAT VIA INSAT
(RN TYPE CHANNEL)



P _H = Hour Parity	I _D = Status Indicator	1 = Normal
		0 = Poor
P _M = Minute Parity	I _C = Identification for position coordinates.	00 = X 10 = Z
		01 = Y 11 = DUT1
P _C = Combined (Hour and minute) Parity	I _S = Identification for Satellite	11 = INSAT 1A
		00 = INSAT 1B

FIG. 2: DISTRIBUTION OF BIT INFORMATION FOR INSAT TIME SIGNAL FORMAT

Paper #38 was not given.

Papers # 39 - 43 were assigned to the classified section
and were not planned for publication.

DR. MCCOUBREY: As I mentioned earlier, in place of Paper No. 36, we will have Paper No. 44 for which the abstract is on Page 45 of your programs, and the topic is, The Superconducting Cavity Stabilized Ruby Maser Oscillator, and the authors are G. J. Dick, California Institute of Technology, and D. M. Strayer of J.P.L.

The Superconducting Cavity Stabilized Ruby Maser Oscillator

G. J. Dick

Low Temperature Physics
California Institute of Technology
Pasadena, California

D. M. Strayer

Jet Propulsion Laboratory
California Institute of Technology
Pasadena, California

ABSTRACT

We present an analysis of the stability, performance, and design of a new all-cryogenic frequency source, the superconducting cavity stabilized maser oscillator (SCSMO).¹ We also present the results of an experimental study of the various components of such an oscillator which demonstrate the feasibility of achieving a stability better than $\Delta f / f = 10^{-17}$ with this technique.

Previous superconducting cavity stabilized oscillator designs have combined solid niobium cavities at cryogenic temperatures with room temperature microwave electronic components to achieve the highest stability reported to date,² $\Delta f / f = 3 \times 10^{-16}$. The long term performance of these designs suffers due to instabilities in the connecting link between electronics and cavity. A successful all-cryogenic design would eliminate this problem due to the "freezing-out" of thermal expansion coefficients and a complete avoidance of temperature gradients.

The ruby maser currently allows the lowest noise temperature (1.5K) of any microwave amplifier and seems an ideal component for an all-cryogenic oscillator. The power available ($\sim 10^{-7} \text{ W/cm}^2$ at 4.2K) is adequate for measuring times longer than one second, and the gain ($Q_m = -100$) is large enough to allow oscillation with very weak coupling to the stabilizing cavity. Furthermore, power dissipation is very low, allowing operation in the same cryogenic environment as the cavity even at temperatures below 1K. The magnetic field required for maser operation and tuning gives rise to important technical problems, namely, the need to shield the superconducting cavity from the field, and frequency-pulling effects as the field varies. We present an analysis of a multiple-

cavity design which allows the active ruby element to be physically removed from the superconducting cavity. We shall also show maser oscillator stability using a relatively low-Q normal stabilizing cavity where pulling effects are greatly enhanced.

Finally, we will present the results of our work to obtain a superconducting cavity with the highest possible mechanical integrity. Sapphire has a thermal coefficient of expansion 100 times less than niobium and sags 10 times less in the earth's gravity. We have obtained the lowest microwave loss values to date in sapphire (7×10^{-10} at 1.5K) and have demonstrated a superconductor-on-sapphire resonator with $Q = 10^8$, the value required by our design.

1. Design of the SCSMO

1.1. General Features of an All-Cryogenic Oscillator

The two techniques for highest frequency stability are combined in the SCSMO to allow an all-cryogenic oscillator. Superconducting cavity stabilized oscillators (SCSO's) to date show great cavity stability due to very low cavity losses and the freezing out of thermal expansion coefficients at cryogenic temperature, but phase shifts in the cryogenic transition and room temperature electronics limit attainable performance. Hydrogen masers have great stability in the atomic transition itself, but frequency pulling effects due to the high-Q cavity required to induce oscillation introduces drift, and the low power available limits short time performance. Long time instability, in both cases, is due to frequency pulling effects within the bandwidth of the high-Q (10^8 to 10^{10}) stable element, and appear to be principally due to thermal expansion effects in supporting electronic elements. Since overall stability of 10^{-15} to 10^{-17} is desired, the performance required of support components is very high, since these values are 10^{-5} to 10^{-9} of the natural bandwidth of the stabilizing element.

In both cases, the situation is worse than it might seem. In order to obtain oscillation with the low hydrogen densities allowed by the technique, a high-Q (normal) cavity is necessary for the operation of the hydrogen maser. Sensitivity to the cavity frequency is increased proportional to its Q, which is typically 10^4 . Very stable materials and techniques of "auto-tuning" are used to reduce this sensitivity, but it continues to be a principle roadblock to improved performance.

Thermal effects in the SCSO are similarly exacerbated by two effects. The wavelength at the typical operating frequency (10 GHz) is much shorter than the path length required between room temperature electronics and the cryogenic cavity. This increases the sensitivity of the frequency to the fractional length change by 2π times the one-way length divided by the wavelength, a value typically about 10^2 . Secondly, the waveguide must span a temperature differential

of 300K, and thus small fractional changes in the temperature profile imply large temperature changes. To achieve a stability of 10^{-7} times the superconducting bandwidth, an average stability of 3×10^{-8} in the temperature profile is required. Electronic feedback techniques have been used to sense the instantaneous length in order to provide substantial compensation of this effect, with reported results of 3×10^{-16} overall stability, the best to date for any technique.² However, the overall system is cumbersome and expensive, and dramatic improvements seem unlikely.

The reduction in expansion coefficient of a superconducting cavity at low temperature together with its high Q make possible its use as a frequency stabilizing element. Niobium and copper have an expansion coefficient of $\sim 5 \times 10^{-11}/K$ at 1.0K, a value reduced 10^5 from their room temperature values. Together with the short thermal relaxation times (10^{-3} seconds) and accurate temperature control ($10^{-6}K$) possible only at low temperatures, unparalleled structural stability can be achieved. The advantage of an all-cryogenic oscillator is that coefficients of expansion for the entire system are reduced, not just that of the cavity itself. This reduction eliminates frequency pulling effects which are due to thermal instability, the major source of drift in both H-maser and SCSO systems.

1.2. Application of the Ruby Maser

Ruby maser amplifiers are the quietest amplifiers presently available in the microwave frequency range, with device noise temperatures as low as 1.5K reported.³ They operate naturally at temperatures below 4K, and can provide output power of a fraction of a microwatt, a value sufficient for excellent short term measurements and far above the 10^{-11} watts available from the H-maser. Furthermore, the pump power required is related only to the signal power, allowing very low power dissipation and consequently lower temperature operation, if desired. This is in contrast to the available transistor amplifiers which must dissipate several milliwatts of power in order to maintain their operating point.⁴ Operation well below 1K seems feasible, with important consequent reductions in thermally generated frequency shifts in the superconducting cavity itself.

In contrast to the H-maser with its fractional linewidth of 10^{-9} , ruby has a fractional bandwidth of about 10^{-2} , making it unsuitable for determining the frequency itself. However, this wide bandwidth (low Q) is a distinct advantage when used in conjunction with a superconducting cavity, since it results in a reduction of frequency pulling effects. Frequency pulling of the actual operating frequency Δf_0 due to frequency change Δf_c in a lower- Q circuit element is proportional to the ratio of its Q to that of the frequency stabilizing element.

A comparison between frequency pulling effects in the two devices is instructive. While the H-maser's output closely follows the frequency of the masing transition, the sensitivity to its cavity frequency is given by

$$\frac{\Delta f_0}{\Delta f_c} = \frac{Q_c}{Q_m} = \frac{10^4}{10^9} = 10^{-5} \quad (1)$$

for a cavity $Q_c = 10^4$ and maser linewidth characterized by $Q_m = 10^9$. In a similar manner, the frequency of the output of the SCSMO closely follows that of the high-Q superconducting cavity, while its sensitivity to the ruby resonant frequency f_m is

$$\frac{\Delta f_0}{\Delta f_m} = \frac{Q_m}{Q_c} = \frac{10^2}{10^9} = 10^{-7} \quad (2)$$

for maser linewidth characterized by $Q_m = 10^2$ and a cavity $Q_c = 10^9$. It is apparent that the roles of the maser and cavity Q's are reversed.

We expect that the role of this source of frequency pulling will be much less significant in the design of the SCSMO than in the H-maser because of the reduction implied by equations (1) and (2), but more importantly because superconducting magnets allow great stability to be achieved in the applied magnetic field which determines the ruby resonant frequency. Long term stability of better than 10^{-12} has been reported at the relatively low magnetic fields required for maser action, which would imply, from equation (2), frequency drifts less than 10^{-19} from this source.

The magnetic field applied to the ruby must be effectively shielded from the superconductor of the stabilizing cavity, as Q degradation would otherwise result. The ruby material is very strongly amplifying, in comparison to what is needed to induce oscillation at a Q of 10^9 , being able to excite a fully filled cavity with a Q of only 100. Thus it is possible to physically separate regions of high Q and high magnetic field - - conceptually, the ruby need only probe the fringe fields of the stabilizing cavity.

1.3. Superconducting Cavity Design

With the promise of much greater electronic stability allowed by an all-cryogenic design, the relationship of cavity Q to the overall design changes somewhat compared to the SCSO. In particular, a lower Q might be advantageous if it allowed substantially higher frequency stability to be attained in the cavity itself. This appears to be possible by the use of a superconductor-on-sapphire resonator when operated at temperatures somewhat lower than has been previously employed. While the thermal coefficient of expansion of solids follows a T^3 dependence, the penetration depth of the superconductor, which also determines the effective size of the resonator, shows a much more rapid exponential temperature dependence. Thus, for a solid niobium cavity, the frequency variation with temperature decreases rapidly as the temperature is reduced down to a temperature of approximately 1.25K, below which the relatively slowly varying T^3 dependence is dominant.² If the physical size were determined by the characteristics of sapphire, the value of the T^3 contribution could be reduced by more than 10^2 . If the superconducting character of niobium were unchanged, a

reduction in operating temperature to 0.9K would still show the rapid exponential reduction in sensitivity to thermal variations, resulting in an overall improvement of thermal sensitivity from $\sim 10^{-11}/K$ to $10^{-13}/K$.

We have measured the highest Q reported to date in a sapphire-filled superconducting cavity ($Q > 10^9$) and present details in a following section. Such a resonator would additionally be lighter and stronger than a solid niobium cavity, giving a reduction in the shift due to gravity by 10 times. An additional advantage of the sapphire based resonator is that its large dielectric constant ($\epsilon \sim 10$) allows operation at a lower, more convenient frequency ($\sim 3\text{GHz}$) with modest overall size (overall diameter $< 7.5\text{ cm}$).

1.4. Multiple Cavity Oscillator Design

We have chosen to study oscillator designs which, rather than separating the amplifier and resonator functions in separate elements, combine them by the use of multiple electromagnetic resonators. If the ruby could be included in the superconducting cavity itself, a single resonator would suffice, with the negative resistance due to the pumped ruby overcoming the positive resistance in the cavity, and inducing oscillation. However, the magnetic field required for ruby maser operation at microwave frequencies greatly reduces the cavity Q if allowed to penetrate the superconducting surface. The thin films we propose to use are even more sensitive than the bulk superconductor to such fields, and we propose a three-cavity design to isolate the superconducting cavity from the ruby cavity by a third coupling cavity. Most of the features of such a design are common to a two-cavity design, which was used in the present experiments, and we shall confine our present discussion to that case.

The essential electromagnetic features of a coupled two-cavity resonant system designed for this purpose are a high- Q stabilizing cavity, a low- Q cavity containing pumped ruby, and a coupling between the cavities. Such a two-cavity system will always have at least two modes, with the frequency difference between the modes depending on the isolated cavity frequencies f_1 and f_2 , and on the coupling strength k in a particularly simple manner if the frequencies are defined and measured in the presence of the coupling holes, and not their absence.⁵ Eigenfrequencies of the coupled cavities f_a and f_b can then be shown to be related by:

$$f_b - f_a = \sqrt{(f_2 - f_1)^2 + \left(\frac{k}{4}(f_2 + f_1)\right)^2} \quad (3)$$

and

$$f_b + f_a = f_1 + f_2 \quad (4)$$

in the limit that $k \ll 1$ and $f_2 - f_1 \ll f_2 + f_1$. That is to say, if the coupling strength and the difference between the frequencies of the two isolated modes are both small enough, the splitting of the coupled modes is given by adding

these two effects in quadrature.

The energy division between the two parts of the coupled system also has a particularly simple form in this case. If E_1 and E_2 are the energies in physical resonators one and two, energy ratios for modes α and β are given by:

$$\left[\frac{E_1}{E_2} \right]_{\alpha} = \frac{f_{\alpha} - f_2}{f_{\alpha} - f_1} = \left[\frac{E_2}{E_1} \right]_{\beta} = \frac{f_{\beta} - f_1}{f_{\beta} - f_2} \quad (5)$$

The energy involved in the coupling is given by

$$E_c = k\sqrt{E_1 E_2} \quad (6)$$

and is assumed to be small.

In this simplified framework, the Q 's of modes α and β can be written:

$$Q_{\alpha}^{-1} = \frac{E_{1\alpha} Q_1^{-1} + E_{2\alpha} Q_2^{-1}}{E_{1\alpha} + E_{2\alpha}} \quad (7)$$

and

$$Q_{\beta}^{-1} = \frac{E_{1\beta} Q_1^{-1} + E_{2\beta} Q_2^{-1}}{E_{1\beta} + E_{2\beta}} \quad (8)$$

where $E_{1\alpha}$ is the energy in resonator 1 for mode α , etc.

Oscillator design is relatively easy within this framework. The negative resistance associated with the pumped ruby is strongly frequency dependent, and is effective over a range of only a percent or so. Frequencies f_{α} and f_{β} must be chosen to be farther apart than this width to allow selection of the desired mode. If cavity 1 contains the ruby with mode α the coupled mode nearest in frequency to that of the isolated cavity 1, stabilized operation would result by tuning the frequency of the ruby resonance instead to that of mode β where nearly all of the energy is in cavity 2. Thus, the magnetic field is adjusted to give a strongly negative Q_1 at frequency f_{β} while showing a net positive Q_1 at f_{α} , as well as at f_1 the natural frequency of cavity 1. The oscillation condition can then be imposed by setting $Q_{\beta}^{-1} = 0$ in equation (8), from which can be calculated the maximum energy ratio which allows oscillation to occur in mode β . Frequencies and couplings can then be calculated from equations (3), (4), and (5).

This approach can be generalized to cover the case of three coupled resonators. The advantage over other methods is that actual mode and coupling configurations do not enter the calculations, rather, frequencies, energies and Q 's, all easily accessible by experimental measurement, are used.

2. A Low-Q Experiment

Contributions to the frequency error in a high-Q oscillator fall into two categories; those due to variations in the natural frequency of the stabilizing cavity, and those due to deviations in frequency within the bandwidth of the cavity caused by factors other than the cavity itself. These latter frequency pulling effects scale inversely as the Q of the resonator, and thus can be studied effectively by deliberately building an oscillator with a poor Q. Effects that can be studied in this way include those due to output VSWR and a whole host of effects due to the ruby itself. These include thermal (white) noise, possible 1/f noise, possible amplitude and frequency pulling effects related to the pump signal, and the previously discussed pulling with magnetic field. All of these aspects can be fully characterized by reference to a source with very modest stability, if the Q can be reduced by, for example, a value as large as 10^7 . That is, measurement of a stability of 10^{-10} with a Q of 100 would allow direct extrapolation of all these effects to a stability of 10^{-17} at a Q of 10^9 .

Of particular interest and concern in this regard was the possibility of 1/f type modulation noise in the ruby, since no experiments have been previously conducted that place significant limits on such noise. The existence of such noise would place a Q-dependent limit to the stability allowed by the oscillator, and might indicate that a very high Q (10^{10} or above) was necessary, ruling out the use of a sapphire resonator.

To this end we modified an experimental setup designed primarily to measure the more conventional aspects of the ruby response to allow the first measurements of frequency stability in a ruby maser oscillator, and further, added a coupled (low Q) superconducting cavity to study the performance of the coupled cavity system, as well as the Q dependence of frequency pulling effects.

The various aspects of the oscillator were treated with differing degrees of care. The superconducting magnet was carefully constructed as a first attempt at what might be used in the final system. The ruby itself has been previously used in amplifier service, and can be expected to be a good example of what is available. The signal coupling line, however, was not constructed with an eye for stable VSWR, being instead designed to allow a wide range of coupling strengths. Similarly, the pump source had poor amplitude and frequency stability. Due to these reasons we do not feel that these preliminary results represent the best that can be obtained with this technique.

3. Measurements

The SCSMO components have been studied separately to establish the feasibility of the design. To achieve the part in 10^{17} stability level, our performance analysis has shown that the resonator cavity must have a quality factor Q of at least 10^9 . Electromagnetic losses in the cavity can come from the dielectric material, from the superconducting material or from the interface region

between the two. Results of measurements on all three effects will be presented and their implications for the Q of the cavity will be discussed.

The other principal component of the oscillator is the active element, the ruby maser. To determine the maser's suitability for the oscillator, a ruby maser oscillator stabilized with a copper cavity of modest Q was fabricated. The relatively low Q of the stabilizing cavity allows easy measurement of effects such as frequency pulling by the magnetic field and frequency pulling by the amplitude and frequency of the RF pump signal. Results of some of these measurements and some preliminary stability data for this system will be presented below.

3.1. Description of the Two-Cavity Maser Oscillator

Figure 1 shows the configuration that is being used to study the ruby maser oscillator. A size scale can be obtained by noting that the cylindrical ruby crystal (3) is 1.00 cm in diameter and is 1.15 cm tall. Both the cavity (5) containing the ruby and the cavity (8) stabilizing the oscillator are of the coaxial type; the center posts (4) and (7) and the coupling apertures (6) have been adjusted in size to give the operating frequencies and the disposition of energy between the two cavities deemed best for oscillator performance.

The outer wall (2) of the oscillator probe serves both as a waveguide for the ~ 13 GHz pump signal applied to the ruby, and as the outer conductor of a coax for the ~ 2.7 GHz oscillator signal. The inner conductor (1) of this coax is adjustable at the top of the probe to allow the coupling to the oscillation signal to be varied.

The magnet (9) is a superconducting solenoid with a persistent current switch.

Compensating coils at the ends of the solenoid make it an "outside notch" magnet⁶, producing a field constant to sixth order that is uniform to one part in 10^9 over a sphere of 2.54 cm diameter at the solenoid's center.

The pump signal is supplied by a Hewlett-Packard 8690A sweep oscillator. After amplification the oscillator signal is mixed in an HP 934A harmonic mixer with a signal from an Ailtech 360D11 frequency synthesizer. The low frequency output is further amplified and then is continuously sampled both by a HP 5245M counter and by a PDP 11/34 computer. A chart recording of the counter output provides a quick check of the oscillator's stability and drift, while statistical stability analysis is carried out on the computer system.

By measuring the lowest resonant frequencies of each cavity alone and of the two coupled modes, the energy splitting between the cavities in each coupled mode and the coupling strength can be determined. For the data reported below, the coupling strength was 2.5%. The stabilized mode had 85% of the energy in the stabilizing cavity and 15% in the ruby-filled cavity, while the other mode had the opposite ratio.

For magnetic fields applied at right angles to the ruby crystal's optic axis (the crystalline c -axis), there are two values of the magnetic field magnitude that will

give ~ 2.7 GHz splitting between chromium ion energy levels: $\sim .05T$ and $\sim .27T$. For both of these cases the lowest frequency pump signal is ~ 13 GHz. The data reported below were all measured with the ruby in the low-field mode near $.05T$.

3.2. Results of Frequency Stability Measurements

The cavity stabilized ruby maser oscillator described above has operated once successfully, and then only in a somewhat modified form, so the data reported here must be considered of a rather preliminary nature. Even with these reservations, some valuable conclusions and insights can be obtained from the data, so the results are being reported here.

When the oscillator was first cooled to 4.2K in the configuration described in the preceding section, the mode with most of the energy in the stabilizing cavity could not be driven into oscillation. To enable this mode to be studied, the portions drawn with heavy lines in Fig. 1 were plated with superconductor. With this lower loss condition, the stabilized mode was observed to oscillate at ~ 2.71 GHz when cooled to 4.2K and lower temperatures. The upper (ruby-filled) cavity had its outer wall not plated with superconductor, so the mode at ~ 2.87 GHz with most of the energy in the upper cavity displayed lower Q than the stabilized mode. By measuring frequency pulling effects and frequency stabilities for both modes at various temperatures, data for modes having a range of Q values could be obtained.

Fig. 2 shows examples of Allan variances of $\Delta f / f$ calculated from data obtained from several rather quiet periods of the oscillator's operation. The upper portion shows some of the best data obtained for the high- Q ($Q = 70,000$) stabilized mode at low temperature, and shows what our drift-removing algorithm does to the data curves. The lower portion of Fig. 2 shows curves for data obtained under various conditions. Note that cooling the ruby to 2.2K and improving the cavity Q from 25,000 to 70,000 do not yield improvement in the lowest observed σ values. We conclude that the limiting stabilities observed are not characteristic of the ruby maser, but rather are caused by some other device in the measuring system; a good candidate is the quartz crystal stabilized Ailtech frequency synthesizer being used as a local oscillator to beat down the oscillation frequency to audio frequencies.

The HP 8690A sweep oscillator used as a pump source was found to have great effect on the measured values of frequency and on frequency stability. The best data were obtained by carefully tuning this pump source to minimize the frequency pulling effects. A quieter klystron pump signal source has been obtained for comparison purposes for future measurements.

The output power of the oscillator is shown in Fig. 3 for a range of applied pump power, with the magnetic field tuned to optimum. Zero attenuation of the pump signal corresponds to ~ 100 milliwatts of pump power. The maximum output power in the region of saturation is 0.5×10^{-7} watt, a level well within our

expectation and readily usable in our final design. Hence, the ruby volume will not need to be changed substantially in the final configuration of the oscillator.

The change of oscillator frequency with change in magnetic field was measured rather carefully, with results in agreement with our analysis. For the unstabilized mode with $Q = 5,000$, the fractional frequency pulling was found to be $\Delta f / f = 2.5 \times 10^{-3} \Delta H / H$, and this value varied as Q^{-1} for the other oscillation conditions measured. This value implies that, in order to achieve 10^{-17} stability with a cavity Q of 10^9 , the magnetic field must not have a fractional variation larger than 10^{-9} over the measuring time τ . This field stability is tractable for a superconducting magnet operating in persistent mode, and having superconducting shields to attenuate ambient field variations.

Two frequency pulling effects are observed relating to signal amplitudes in the cavity: response to pump power changes, and response to oscillation amplitude changes. In the unstabilized mode with $Q = 5,000$, the two effects are nearly equal in magnitude at $\Delta f / f = \sim 3 \times 10^{-6}$ for a 3 dB power change. The response to changes in pump power is independent of the tuning of the magnetic field and varies as Q^{-1} . The response to changes in oscillation amplitude varies with magnetic field tuning, being positive if the field is tuned high and negative if the field is tuned low; the magnitude of this pulling does not decrease as fast as Q^{-1} when the Q increases. This output amplitude effect may result from magnetic field inhomogeneity at the ruby caused by the superconductors near the crystal. A test is planned with no superconductor on the oscillator probe to examine this possibility.

3.3. Measurements of the Cavity Losses

To obtain the cavity Q of 10^8 required by the design, various sapphire materials have been examined for their electromagnetic losses at frequencies near 2.7GHz and at temperatures below 4.2K. Samples with losses below 10^{-8} have previously been described^{7,8}. Recently a new sample has been obtained⁹ with significantly lower losses, the loss tangent reaching $\delta = 7.0 \times 10^{-10}$ at the temperature of 1.5K. A description of the manufacturing process for this sample and of the loss measurements will be published elsewhere¹⁰.

In measuring the sapphire losses, the samples are placed inside a lead-coated copper cavity and the decay time of the cavity-sapphire system is measured. Since initially lead will also be used to coat the sapphire substrate in forming the stabilizing cavity, the very low loss values reported above are sufficient evidence that losses in the superconducting film will not prevent the cavity from achieving a Q of 10^8 . However, because the electromagnetic field is to be contained inside the cavity, the interface region between the lead film and the sapphire will also be exposed to the signal and could degrade the cavity Q . A measurement was made on a spherical sapphire substrate coated with a lead film to test this loss mechanism. The uncoated sapphire sphere displayed a loss value of $\delta = 1.17 \times 10^{-8}$, while the lead-coated sphere's loss was $\delta = 1.15 \times 10^{-8}$, both

values measured at 1.5K. These results show that the losses in the interface region do not contribute appreciably to the total loss measured at this region near $Q = 10^8$.

Actually, these measurements have indicated the possibility of achieving even higher Q -values in the stabilizing cavity. Both the sapphire loss tangent measurements and the measurements in the spherical cavity have demonstrated that a Q of 10^9 is feasible for this cavity. A ruby maser oscillator stabilized with a cavity having a Q of 10^9 would be expected to have stability approaching $\Delta f / f = 10^{-17}$ for some range of sampling times.

4. Conclusions

Analysis of an application of the ruby maser to a Superconducting Cavity Stabilized Oscillator (SCSO) shows many attractive features. These derive from the mechanical stability inherent in an all-cryogenic design and from the properties of the ruby maser itself. A multiple-cavity design has been developed to allow physical separation of the high- Q superconducting cavity and the ruby element with its required applied magnetic field. Mode selection is accomplished in this design by tuning the ruby by means of the applied field. We conclude that such an oscillator would perform well, even with cavity Q 's as low as 10^8 , allowing the use of a superconductor-on-sapphire resonator with its greater rigidity and lower thermal expansion.

A first test of the Superconducting Cavity Stabilized Maser Oscillator (SCSMO) confirms the efficacy of the multiple-cavity design and the applicability of the ruby maser. Frequency variation less than 4×10^{-11} was measured in the stabilized mode and is attributed to the reference oscillator and to instabilities in the pump source. Variation of 10^{-10} was observed in the low- Q unstabilized mode, again attributable to pump fluctuations. Even so, direct scaling to a Q of 10^9 predicts a stability better than 10^{-15} . Together with results showing the lowest losses to date in sapphire at microwave frequencies, and preliminary experiments on superconductor-on-sapphire resonators, frequency stability levels as low as 10^{-17} are indicated.

5. Acknowledgements

The authors gratefully acknowledge the helpful discussions, contributions and encouragement of J. E. Mercereau and R. C. Clauss. The technical assistance of E. P. Boud has facilitated this work. Initial collaboration with E. Tward is also gratefully acknowledged.

The work described in this paper was carried out at California Institute of Technology with the support of the Jet Propulsion Laboratory under contract with the National Aeronautics and Space Administration.

- 1 W. H. Higa "The Superconducting Cavity Stabilized Maser Oscillator", Tech. Mem. 33-805, NASA, 1976.
- 2 S. R. Stein and J. P. Turneaure, "Superconducting resonators: high stability oscillators and applications to fundamental physics and metrology", Proc. Conf. on Future Trends in Superconductive Electronics, AIP Conf. Proc. No. 44, 192-213, 1978.
- 3 See, for example, J. V. Jelley, "The Potentialities and Present Status of Masers and Parametric Amplifiers in Radio Astronomy" reprinted in MASERS, J. Weber, Gordon and Breach, New York, 1967. Also, R. C. Clauss, private communication.
- 4 S. Weinreb, "Low-noise cooled GASFET amplifiers", IEEE Trans. Microwave Theory Tech., MTT-28, 1041(1980).
- 5 Details to be published, G. J. Dick. See also, for example, H. A. Bethe, "Theory of Diffraction by Small Holes" Physical Review 66,163(1944)
- 6 D. B. Montgomery, Solenoid Magnet Design, Wiley, New York (1969).
- 7 D. M. Strayer, G. J. Dick and E. Tward, "Superconductor-sapphire cavity for an all-cryogenic SCSO", IEEE Trans. Magnetics MAG-19, 512 (May 1983).
- 8 V. B. Braginski, V. I. Panov and S. I. Vasiliev, "The properties of superconducting resonators on sapphire", IEEE Trans. Magnetics, MAG-17, pp. 955-957, 1981. See also "Systems With Small Dissipation" by V. B. Braginski, V. P. Mitrofanov and V. I. Panov, soon to be published by University of Chicago Press.
- 9 Crystal Systems, Inc., 35 Congress Street, Salem, Mass. 01970.
- 10 D. M. Strayer and C. Khatak, to be published.

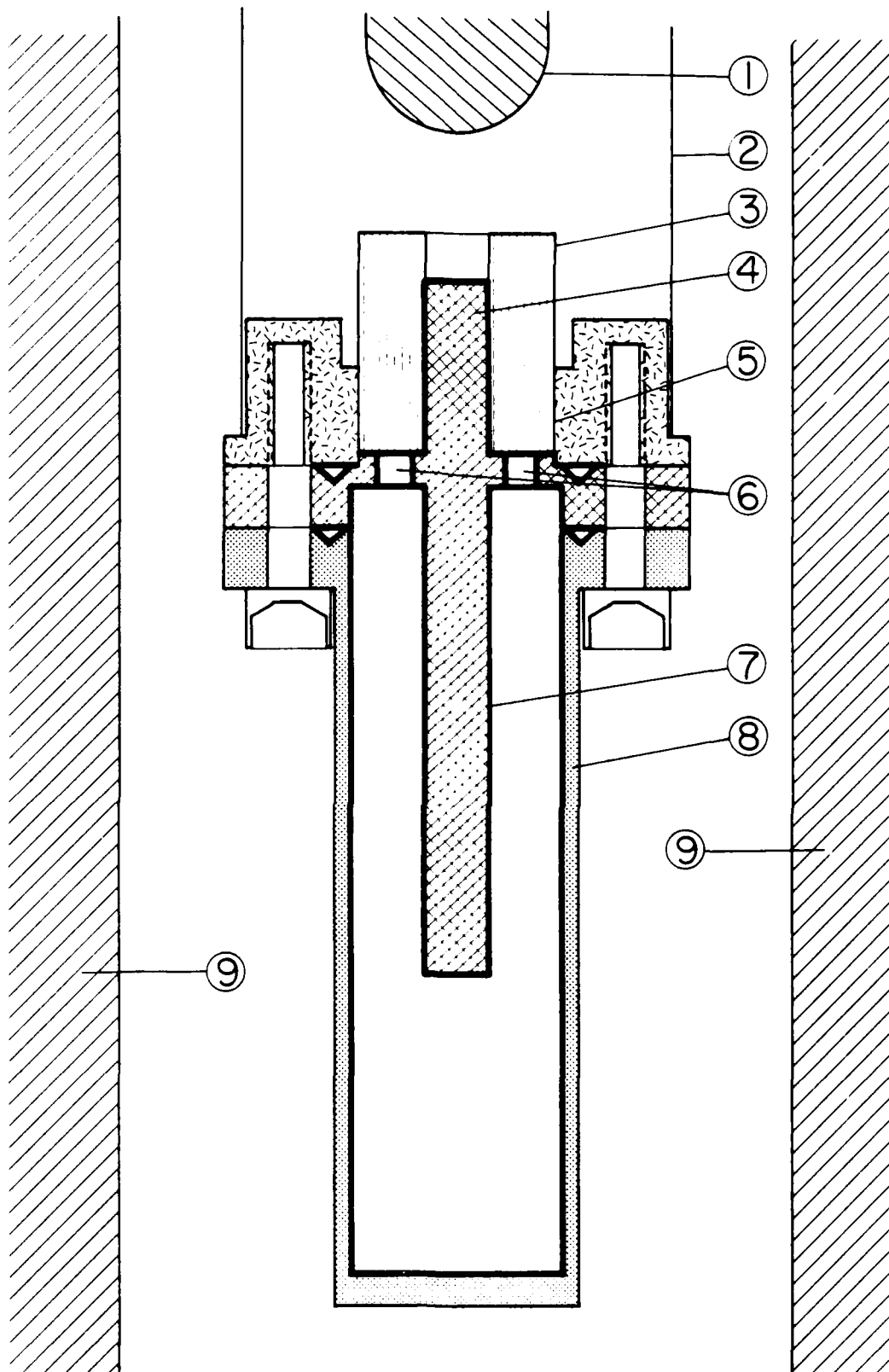


Fig.1 RUBY MASER OSCILLATOR CONFIGURATION

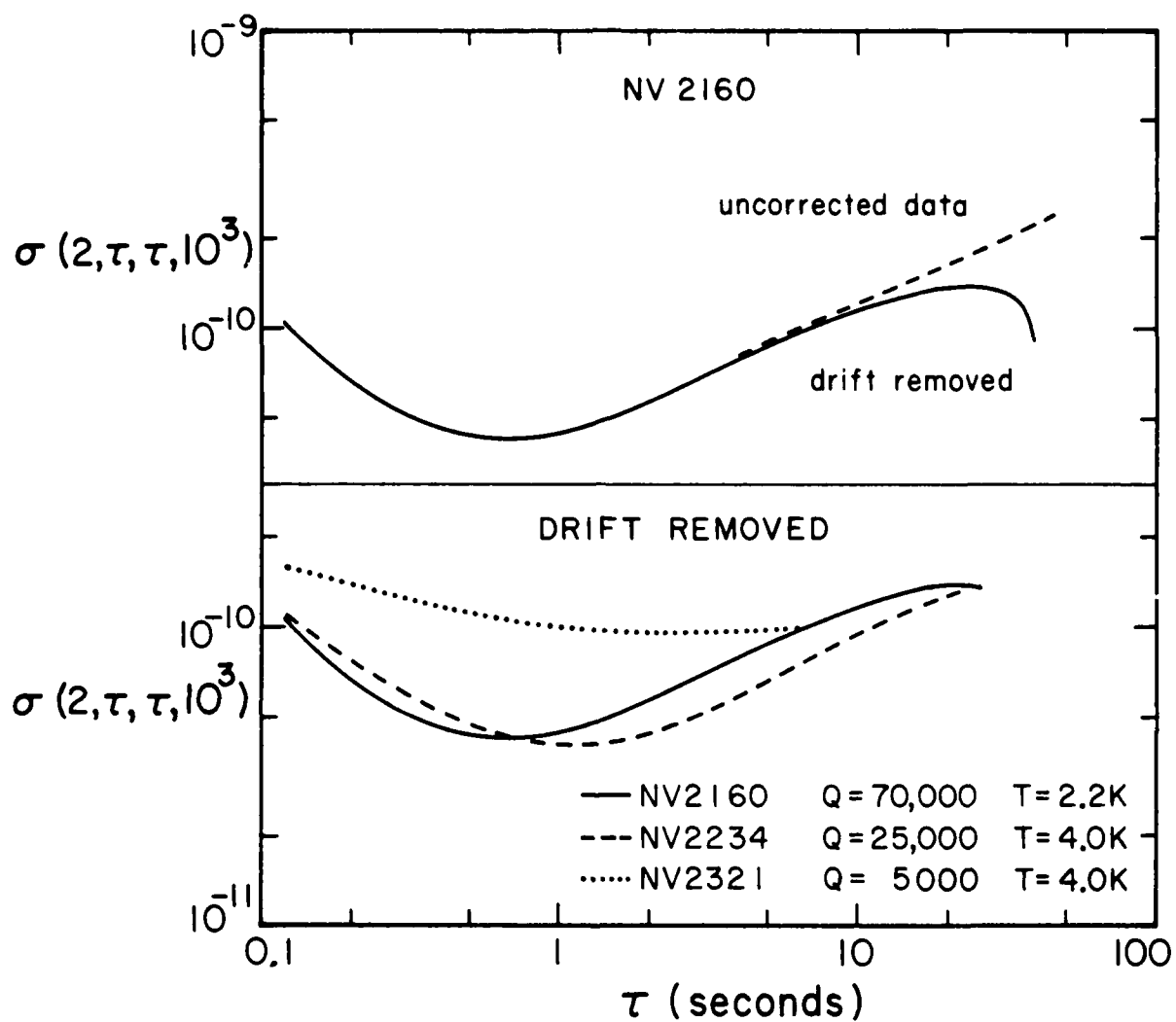


Fig.2 STABILITY DATA FOR THE RUBY MASER OSCILLATOR

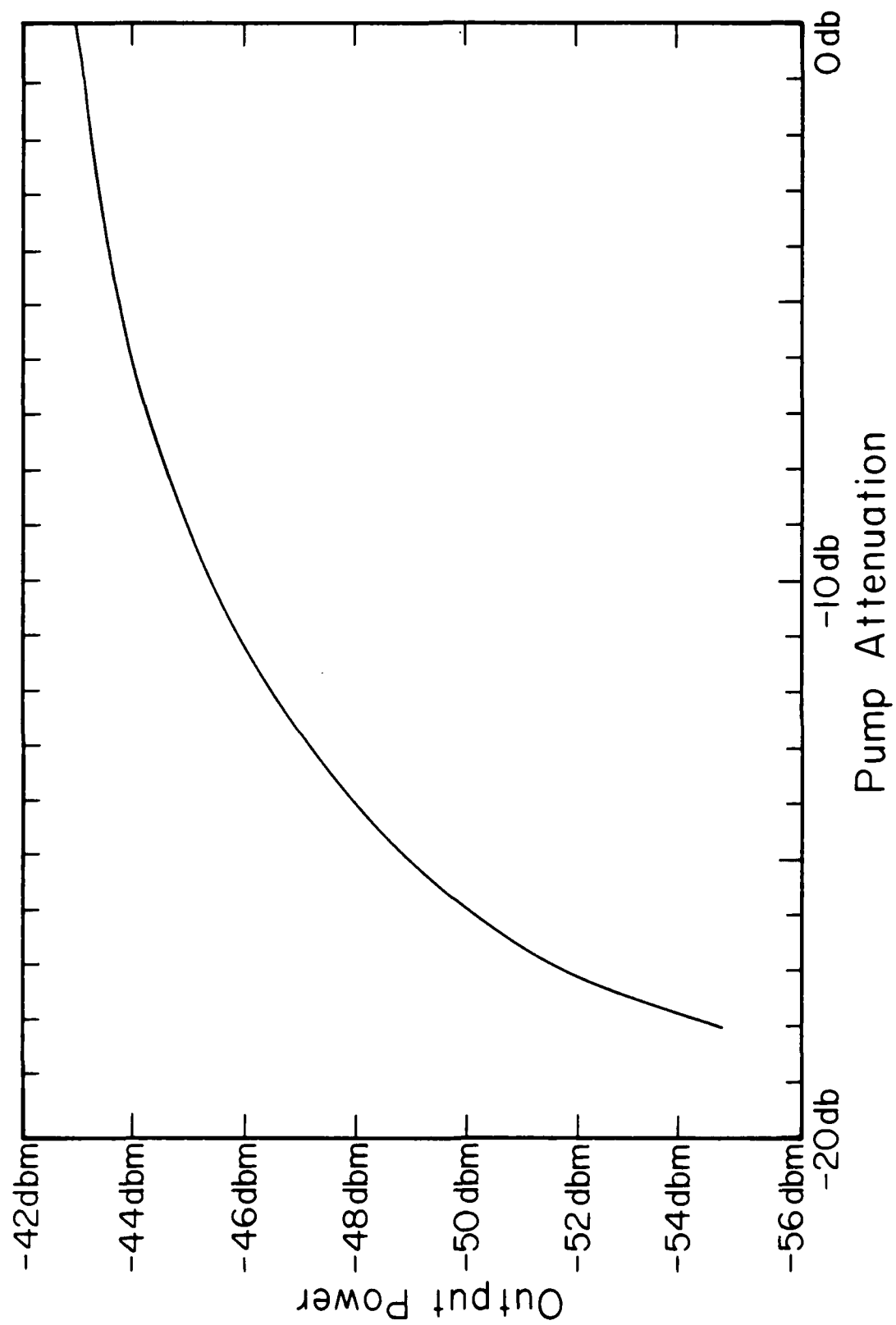


Fig. 3 RUBY MASER OSCILLATOR OUTPUT POWER vs. PUMP ATTENUATOR SETTING

QUESTIONS AND ANSWERS

MR. VESSOT:

The sapphire losses have become an interesting theoretical problem, as in the paper by Brojinski and Panoff on the loss in ionic crystals. I was talking to Bob Clause and he told me to bring this up. His mode of oscillation is that of a whispering gallery, that only internal reflections are used and does not depend on superconducting surfaces at all.

DR. STRAYER:

That's intriguing.

MR. VESSOT:

It really is and I just wanted to bring this up. Perhaps you should tell about it.

DR. STRAYER:

He's wanted to set up a racetrack type resonator of uncoated sapphire that will have very high Q, because the electromagnetic waves do not radiate out. The impedance mismatch at the boundary being enough to keep them in, and use that as a stabilizing element. That should work at room temperature. There is improvement in the Q as you cool it, but one possibility is using at room temperature as a stabilizing element. That should work at room temperature. There is improvement in the Q as you cool it, but one possibility is using at room temperature as a stabilizing element.

PROF. ALLEY:

Is it possible to use other than a Ruby maser amplifier, at some sacrifice, its the low noise of the ruby I gather that prompted you to do this. Could you couple in some more conventional high frequency frequency amplifiers?

DR. STRAYER:

We started to think about a gallium-arsenide FET amplifier operated at low temperatures, they have a high noise. One $1/f$ noise does not improve on cooling from the information I can gather. There are other solid state devices to be considered. The one on the horizon is HEMT which supposedly has low $1/f$ noise.

MR. REINHARDT:

On that doughnut type, what do you expect on something like that at room temperature?

DR. STRAYER:

I can't remember the exact values. I'm sorry.

CLOSING REMARKS

DR. MCCOUBREY: I would like to thank all of the speakers for a most interesting session this morning, and it has been a most interesting Fifteenth P.T.T.I. Meeting. I thank all for attending, and I declare the meeting adjourned.

15TH ANNUAL PRECISE TIME AND TIME INTERVAL REGISTRATION

William J. Affeldt, Jr.
Naval Electronic Systems Engineering Center
P.O. Box 55
Portsmouth, VA 23705

David W. Allan
NBS
Boulder, CO 80303

Burton A. Allen
Interstate Electronics Corp.
707 East Vermont Ave.
Anaheim, CA 92803

Carroll O. Alley
University of Maryland
Department of Physics and Astronomy
College Park, MD 20742

John C. Arnold
Bendix Field Engineering Corporation/TF0
One Bendix Road
Columbia, MD 21045

Rex Backus
Kinematrics - True Time Division
3243 Santa Rosa Ave.
Santa Rose, CA 95407

O. J. Baltzer
Brightline Corp.
P.O. Box 1016
Cedar Park, TX 78613

James F. Barnaba
Air Force Metrology Center
Newark Air Force Station
Newark, OH 43057

James A. Barnes
Austron, Inc.
737 29th St.
Boulder, CO 80303

Edward H. Beals
NADC
Code 4031
Warminster, PA 18974

Loren S. Bearce
Code 7743, Naval Research Lab
Washington, DC 20375

Ronald L. Beard
NRL
Washington, DC 20375

Christian Beauvy
CEPE
46 Avenue de la Glaciere
Argenteuil, France 95100

Renold R. Beck
MITRE (Washington)
1806 Dolley Madison Blvd
McLean, VA 22101

Roger E. Beehler
National Bureau of Standards
325 Broadway
Boulder, CO 80303

Henry M. Beisner
IBM
21 Firstfield Rd.
Gaithersburg, MD 20760

Jose S. Benavente
Spanish Naval Observatory
S/N Cecilio Pujazon
San Fernando (Cadif) Spain

Kim A. Benton
Bendix Field Engineering Corp
One Bendix Road
Columbia, MD 21045

Raymond J. Besson
Ecole Nationale Supérieure
Mecanique Microtechnique
La Bouloie Route de Gray
Besancon, France 25030

Harry B. Bethke
Rockwell International
29582 Vista Plaza Dr.
Laguna Niguel, CA 92677

15TH ANNUAL PRECISE TIME AND TIME INTERVAL REGISTRATION

Ken F. Beutler
JPL
4800 Oak Grove Dr.
Pasadena, CA 91109

Michael T. Bingham
SAI
9512A Lee Hwy
Fairfax, VA 22031

Louis Bidart
CEPE TH/CSF
Phi we de la Mame Hublay, 95
France

Frederick M. Blanchette
Bendix Field Engineering Corp.
One Bendix Road
Columbia, MD 21045

Martin B. Bloch
F.E.I.
55 C.L.B.
Uniondale Michel Field, NY 11553

Richard J. Blume
Naval Research Lab
Code 5352-RJB
Washington, DC 20375

Emery F. Boose
Mitre Corp.
Box 208
Bedford, MA 01730

Susan E. Borutzki
Jet Propulsion Laboratory
4800 Oak Grove Dr.
Pasadena, CA 91109

Robert M. Bowles
U.S. Geological Survey
P.O. Box 465
Falmouth, MA 02541

Daniel E. Brannen
HRB-Singer, Inc.
P.O. Box 60, Science Park Road
State College, PA 16804

Ed Bregstone
USCG
2607 Central Ave.
Alexandria, VA 22302

R. Grover Brown
Iowa State University
Ames, IA 50010

Ellis H. Bryant, Jr.
Weatherchron Co.
5144 Peachtree Rd.
Atlanta, GA 30341

Carl H. Buehrer
CTS Knights
400 Reimann Ave.
Sandwich, IL 60548

Giovanni Luigi Busca
Oscilloquartz SA
16 Brevards
Neuchatel, Switzerland
2002

Jose E. Calavia
Bendix Field Engineering Corp.
One Bendix Road
Columbia, MD 21045

Bob Camp
CINOX
3914 Gray Rd.
Cincinnati, OH 45232

George T. Cannon
USAF, Eastern Test
Range/RSL
Patrick Air Force Base,
FL 32925

Richard J. Carlson
Communications Security
Establishment
Dept. National Defence
101 Col. By Drive
Ottawa, Ontario, Canada KIA
OK2

15TH ANNUAL PRECISE TIME AND TIME INTERVAL REGISTRATION

Clifford F. Casey
Computer Sciences Corporation
6565 Arlington Blvd.
Arlington, VA 22046

Clarence Cassidy
Kode, Inc
2752 Walnut Ave.
Tustin, CA 92680

David N. Chalmers
U.S. Naval Observatory
34th & Massachusetts Ave. N.W.
Washington, DC 20390

Laura G. Charron
U.S. Naval Observatory
34th & Massachusetts Ave. N.W.
Washington, DC 20390

Mary C. Chiu
Johns Hopkins University/Applied Physics Lab
Johns Hopkins Rd.
Laurel, Maryland 20707

Timing Chst
Hughes Aircraft Company
P.O. Box 31979
Aurora, CO 80041

Randolph T. Clarke
USNO - Time Service
Washington, DC 20390

Peter B. Coates
National Physical Laboratory, U.K.
Building 5, N.P.L.
Teddington, Middlesex, U.K.

Jimmie B. Collie
NAVELEX
NC #1 5N20
Washington, DC 20390

William V. Collings, Jr.
Pan American World Airways
Bldg. 989, Mail Unit 840
Patrick AFB, FL 32925

Walter E. Cote
USAF/RADC/DCLW
Griffiss AFB
Rome, NY 13441

Charles L. Daves, Jr.
Hughes Aircraft Company
P.O. Box 31979
Aurora, CO 80010

Duane G. Davis
Hughes Aircraft Company
6251 S. Ulster OP8, Suite 300
Englewood, CO 80111

Andre AD Debaisieux
C.E.P.E.
66 Avenue de la Glaciere
Argenteuil, France 95100

B. F. Dennison
Hughes Aircraft Co.
6926 S. Spruce Dr. West
Englewood, CO 80112

Edoardo Detoma
Bendix Field Engineering Corp.
One Bendix Rd.
Columbia, MD 21045

William F. Dicke
Astron, Inc.
P.O. Box 14766
Austin, TX 78761

Christina E. Dise
U.S. Naval Observatory
34th & Massachusetts Ave. NW
Washington, DC 20390

Lawrence Doepke
DMAAC
9418 Oakwood Manor
St. Louis, MO 63126

Robert W. Donaldson
Westinghouse Electric Corp.
P.O. Box 1897, MS944
Baltimore, MD 21203

15TH ANNUAL PRECISE TIME AND TIME INTERVAL REGISTRATION

Robert J. Douglas
National Research Council
of Canada
Building M-36,
Montreal Road Laboratories
Ottawa, Canada KIA OR6

Joseph E. Dressel
Naval Electronic Systems Command
Elex 08T21, Rm 4W25
Washington, DC 20363

Hugues Duchaussoy
Direction des Recherches Etudes et Techniques
26 Boulevard Victor
Paris, France 75996

Hans P. Dworak
European Space Agency
J. Robert Bosch St.
D 6100 Darmstadt, W. Germany

James D. Echols
Austron, Inc.
P.O. Box 14766
Austin, TX 78758

Warren E. Edwall
RCA/GSD
1901 North Moore Street
Arlington, VA 22209

Richard A. Eichinger
Bendix TFO/CCS
One Bendix Rd.
Columbia, MD 21045

Robert F. Ellis
Austron, Inc.
P.O. Box 14766
Austin, TX 78761

Barry Elson
U.S. Naval Organization
P.O. Box 32418
Washington, DC 20007

Ferdinand Euler
USAF Rome Air Development Center (RADC)
46 Florence Road
Waltham, MA 02154

Bennie W. Falin
Jet Propulsion Laboratory
4800 Oak Grove Drive
Pasadena, CA 91109

Henry F. Fliegel
Aerospace Corp.
2350 East El Seguido
Boulevard
El Seguido, CA 90245

Vincent J. Folen
NRL
Code 6615
Washington, DC 22375

Paul Forman
Smithsonian Institution
MAH-5025 Smithsonian
Washington, DC 20560

D. Earl Fossler
Trak Microwave
4726 Eisenhower
Tampa, FL 33614

Daniel J. Freedman
Bendix Field Engineering Corp.
One Bendix Rd. M/S EOG/TFO
Columbia, MD 21045

Jerome P. Friedrichs
Motorola, Inc.
2553 N. Edgington
Franklin Park, IL 60131

Harold C. Friend
Defense Communications
Engineering Center
1860 Wiehle Ave.
Reston, VA 22090

Hugo Fizuehalif
Efratom, Ball
25881 Ernestine
Laguna Hills, CA 92653

Daniel D. Fryberger
Interstate Electronics
Corporation
1745 Jefferson Davis
Highway, Suite 601
Arlington, VA 22202

15TH ANNUAL PRECISE TIME AND TIME INTERVAL REGISTRATION

Carl R. Gast
TRAK Microwave
4722 Eisenhower Blvd.
Tampa, FL 33614

Nikolaus Gieschen
Technical University Berlin
12-13 Salzufer
Berlin Fed. Rep., Germany 1000

Asbjorn M. Gjelsvik
MITRE
Burlington Road
Bedford, MA 01730

Robert M. Glasmeier
U.S. Air Force
AGMC - MLE
Newark, OH 43057

Steven P. Glicklich
Navy Metrology Eng. Ctr.
P.O. Box 2436
Pomona, CA 91769

Sy Goldberg
EG&G Inc. - Electronic Components Division
35 Congress Street
Salem, MA 01970

Kenneth R. Goldman
CTS Knights
400 Reimann Ave.
Sandwich, IL 60548

Darence H. Grabill
HRB - Singer, Inc.
P.O. Box 60, Science Park Road
State College, PA 16804

Erhard Graf
Oscilloquartz S.A.
CH 2002 Neuchatel, Switzerland

Richard L. Greenspan
CS Draper Lab Inc.
555 Technology Sq.
Cambridge, MA 02139

Bruce Grover
Litton Guidance & Control Systems Division
5500 Canoga Ave.
Woodland Hills, CA 91320

Glenn R. Hall
3612 Spring St
Chevy Chase, MD 20815

William P. Hanson
Piezo Crystal Co.
100 K
Carlisle, PA 17013

Fred R. Harrison
Austron, Inc.
P.O. Box 14766
Austin, TX 78761

Helmut W. Hellwig
Frequency and Time
Systems, Inc.
34 Tozer Road
Beverly, MA 01915

Alex Hertzberg
Litton Guidance & Control
Systems Division
5500 Canoga Avenue
Woodland Hills, CA 91365

Robert J. Hesselberth
Spectracom Corp.
320 N. Washington St.
Rochester, NY 14526

Car E. Hoefener
Interstate Electronics
707 E. Vermont
Anaheim, CA 92803

David C. Holmes
Kernco
237 Providence Rd.
Annapolis, MD 21401

Peter S.P. Hui
Goddard Space Flight
Center, Code 725
Greenbelt, MD 20771

Ron C. Hyatt
Trimble Navigation
1077 Independence Ave.
Mountain View, CA 94043

15TH ANNUAL PRECISE TIME AND TIME INTERVAL REGISTRATION

Jeffrey S. Ingold
Bendix Field Engineering Corp.
One Bendix Road
Columbia, MD 21045

Harold W. Jackson
Bendix Communications Div
1300 E. Joppa Rd.
Baltimore, MD 21204

Chas J. Jensik
Piezo CR4 Stal Co.
P.O. Box 619
Carlisle, PA 17013

Andrew C. Johnson
U.S. Naval Observatory
Washington, DC 20309

Charles B. Johnson
Austron, Inc.
140 Mayhew Way #100
Pleasant Hill, CA 94523

Kenneth J. Johnston
NRL
Code 4130 NRL
Washington, DC 20375

Paul S. Jorgensen
The Aerospace Corp.
El Segundo, CA

Alfred Kahan
USAF/RADC/ES
Hanscom AFB
Bedford, MA 02146

Peter Kartaschoff
PTT, RR Division
Ostetzmundigen BE, Switzerland

Donald C. Kaufmann
GSFC/NASA Code 854.2
Greenbelt Rd.
Greenbelt, MD 20771

William W. Kellogg
Lockheed Missiles and Space -
Research Lab
3251 Hanover
Palo Alto, CA 94304

Robert H. Kern
Kernco
28 Harbor St.
Danvers, MA 01923

Ernest G. Kimme
Cobit, Inc.
227 N. Sunset
Industry, CA 91744

Dittmar Kittler
USAF/ESD
ESD/SCS-4M
Hanscom AFB, MA 01731

Chester J. Kleczek
NRL Code 7969
4555 Overlook Ave. S.W
Washington, DC 20375

David A. Klein
Litton Guidance & Control
Sys. Div.
5500 Canoga Ave.
Woodland Hills, CA 91304

William J. Klepczynski
U.S. Naval Observatory
Washington, DC 20390

Stephen H. Knowles
NRL Code 4183
Washington, DC 20375

M. L. Koonsman
Kode, Inc.
2752 Walnut Ave.
Tustin, CA 92680

Mark E. Kotancheck
HRB - Singer, Inc.
P.O. Box 60
State College, PA 16804

Anthony J. Kubik
U.S. Naval Observatory
34th Massachusetts Ave.
Washington, DC 20390

Paul F. Kuhnle
Jet Propulsion Laboratory
4800 Oak Grove Drive
Pasadena, CA 91109

15TH ANNUAL PRECISE TIME AND TIME INTERVAL REGISTRATION

Ryszard Kanski
Bendix Field Engineering Corporation
One Bendix Road
Columbia, MD 21045

Tae M. Kwon
Litton Guidance & Control Sys. Div.
5500 Canoga Ave. MS-25
Woodland Hills, CA 91364

J. M. Landers
Data Time, Inc.
12600 Viewside Drive
Gaithersburg, MD 20878

Paul G. Landis
NRL
4555 Overlook S.W.
Washington, DC 20375

Jean-Daniel Lavanceau
Lt. International, Inc.
5106 Benton Avenue
Bethesda, MD 20814

Julius C. Law
JPL
4800 Oak Grove Dr.
Pasadena, CA 91107

Felix Lazarus
Hewlett-Packard AG
150 Route Du Nant D'Avril
CH-1217 Meyrin 2, Switzerland

Christoph Lehner
DFVLR/GSOC-ZDBS
Postfach 756
Weilheim, West Germany 8120

David Lerner
Technical Services
P.O. Box MM
Lytle Creek, CA 92358

Vestal R. Lester
Hughes Aircraft Company
19631 Strathern Street
Reseda, CA 91335

Carl F. Lukac
Naval Observatory
34th & Mass. Ave. N.W.
Washington, DC 20390

Donald W. Lynch
Naval Research Lab
4555 Overlook Ave. S.W.
Washington, DC 20375

Thomas Lynch
EG&G Inc. - Electronic
Components Division
35 Congress Street
Salem, MA 01970

Alan D. MacIntyre
Ball Corp. Efratom Div.
18851 Bardeen Ave.
Irvine, CA 92715

Donald E. Mastin
Ballistic Missile Defense
Systems Command (U.S. Army)
P.O. Box 1500
Attn: BMDSC-RDP
Huntsville, AL 35807

Edward M. Mattison
Smithsonian Astrophysical
Observatory
60 Garden St.
Cambridge, MA 02138

Michael D. Mayhue
Austron, Inc.
4114 Sawmill Valley Dr.
Mississauga Ontario, Canada L5L-347

Robert M. McCannon
Weatherchrow
5144 Peachtree Rd.
Atlanta, GA 30341

Thomas B. McCaskill
NRL
Code 7966 4555 Overlook
Ave. S.W.
Washington, DC 20375

15TH ANNUAL PRECISE TIME AND TIME INTERVAL REGISTRATION

Raullo J. McConahy
Applied Physics Lab/Johns Hopkins Univ
Johns Hopkins Rd.
Laurel, MD 20707

Arthur O. McCoubrey
National Bureau of Standards
Washington, DC 20234

James R. McCullough
Woods Hole Oceanographic Inst
Woods Hole, MA 02543

Keith D. McDonald
Federal Aviation Adm
800 Independence Ave.
Washington, DC 20591

Robert L. McGill
Bendix Communications Division
1300 East Joppa Road
Towson, MD 21204

John E. McKeever
U.S. Coast Guard
8413 Ravenswood Rd.
New Carrollton, MD 20784

Richard E. Miller
Kode Inc.
2752 Walnut Ave.
Tustin, CA 29680

Donald H. Mitchell
Datum Inc.
1363 S. State College Blvd.
Anaheim, CA 92806

Joseph A. Molnar
NAVELEX
MC 1
Washington, DC 20363

Billy B. Moon
U.S.A.F.
AGMC/MLEA
Newark AFS, OH 43055

Harry K. Moore
Creative Marketing
Associates, LTD.
6716 Old McLean Village
Drive
McLean, VA 22101

Derek Morris
National Research Council
Montreal Road
Ottawa Ontario, Canada KIA
OR6

Ivan I. Mueller
Ohio State University
Geodetic Science &
Surveying,
1958 Neil Avenue
Columbus, OH 43210

Frank Mullen
FTS Inc.
34 Tozer Rd.
Beverly, MA 01915

James A. Murray
Naval Research Lab
Code 7960
Washington, DC 20375

Arvid E. Myers
U.S. Naval Observatory
34th and Massachusetts
Ave NW
Washington, DC 20390

Stephen Nichols
Naval Electronic Systems
Command
PME 106-6
Washington, DC 20363

Jerry R. Norton
The Johns Hopkins University
Applied Physics Laboratory
Johns Hopkins Road
Laurel, MD 20707

Philip J. Norton
Navastrogru, Systems Dept.
SPM 233
Pt Mugu, CA 93042

15TH ANNUAL PRECISE TIME AND TIME INTERVAL REGISTRATION

Klemens Nottarp
Institut Fuer Angewandte Geodaesie
11, Richard Strauss Allee
Frankfurt/M, FR-Germany, D-6000

Michael J. Nugent
DOD (W36)
9800 Savage Rd.
Ft. George G. Meade, MD 20755

Ernest J. Nyiri
3 dbm System
766 Lakefield Rd.
Westlake Village, CA 91361

Jay O. Oaks
Naval Research Lab
Washington, DC 20375

John T. O'Hara
Marktron FNC/Suite 203
54 Scott Adam Rd.
Hunt Valley, MD 21030

Richard G. Olson
Sonic Sciences Inc.
362 Threenotch Road
Lexington Park, MD 20653

Roger K. Olson
Trak Microwave
4726 Eisenhower Blvd.
Tampa, FL 33614

Harry E. Peters
Sigma Tau Standards Corporation
1675 Northwood
Northport, AL 35476

Edward A Pettit
USAF Eastern Space & Missile
Center/RSM
Patrick Air Force Base, FL 32925

John D. H. Pilkington
Royal Greenwich Observatory
Herstmonceux Castle, Hailsham
East Sussex, England BN27 IRP

David H. Phillips
2901 Accokeek Rd. W.
Accokeek, MD 20607

Ruth E. Phillips
Naval Research Lab
Code 7522, NRL
Washington, DC 20375

Myron A. Pleasure
Chronotechnology Associates
37-13 74th Street
Jackson Heights, NY 11372

Paul J. Pointek
DOD Mail Stop T242
9800 Savage Rd.
Ft. Meade, MD 20755

Timothy C. Pruitt
Naval Avionics Center
6000 E. 21st Street
Indianapolis, IN 46218

Rawlison C. Puig
Dept. of Navy
Box 4265
Point Mugu, CA 93042

Marilyn P. Raines
USNO
34th Street and Massachusetts
Ave., N.W.
Washington, DC 20016

Wilson G. Reid
Naval Research Lab
4555 Overlook Ave. S.W.
Washington, DC 20375

Victor S. Reinhardt
Bendix Field Engineering
One Bendix Road
Columbia, MD 21045

CDR. Leslie W. Renfrey
Royal Australian Navy
1601 Massachussetts Ave. N.W.
Washington, DC 20036

15TH ANNUAL PRECISE TIME AND TIME INTERVAL REGISTRATION

William J. Riley
EG&G Inc. Electronic Components
Division
35 Congress Street
Salem, MA 01970

Ronald G. Robinson
HBB Singer
P.O. Box 60, Science Park Rd.
State College, PA 16803

Richard P. Robson
Raytheon Service Co.
2 Wayside Rd.
Burlington, MA 01803

Ronald C. Roloff
Bendix
8005 McKenstry Dr.
Laurel, MD 20707

Vincent J. Rosati
US Army Electronics Technology
& Devices Lab.
Attn: Delet-EQ
Fort Monmouth, NJ 07703

Lauren J. Rueger
Johns Hopkins University Applied Physics
Laboratory
Johns Hopkins Road
Laurel, MD 20707

Prof. Dr. Reiner Rummel
Geodetic Institut, Tu-Delft
77 Thijsseweg
Delft, Netherlands

Tian Run-ging
P.O. Box, Lintoney, Shaanxi
Peoples Republic of China

Mehjabin Saifi
Bendix Field Engineering
One Bendix Road
Columbia, MD 21045

Jules Schlesinger
HazelTine Co.
Greenlawn, NY 11740

Bernard Rene Schlueter
Oscilloquartz SA
16 Brevards
Neuchatel, Switzerland 2002

Wolfgang Schlueter
Institut fuer Angewandte
Geodasie
SAT - BEOB. - Station
Wetzell
8493 Koetzting, F.R.
Germany D-8493

Prof. Dr. Manfred Schneider
Institut fuer Astron.
U. Physik Geodasie
21 Arcisstrasse
Munich, F.R. Germany D-
8000

Prof. Dr. Guenter Seeber
Institut fuer Theor. Geodasie
6, Nienburger Strasse
Hannover, F.R. Germany D-
3000

Prof. Dr. Hermann Seeger
Geodaetisches Institut,
Univ. Bonn 7F Nuss Allee
Bonn, F.R. Germany D5300

Richard L. Semer
AGMC/MLEA Newark AFS
Newark AFS
Newark, OH 43057

Phillip J. Sentner
Villanova Univ
218 E. Conestoga Road
Devon, PA 1933

David B. Shaffer
Interferometrics
Code 974 NASA/GSFC
Greenbelt, MD 20771

Irving Silverman
US NRL
4555 Overlook Ave
Washington, DC 20375

15TH ANNUAL PRECISE TIME AND TIME INTERVAL REGISTRATION

Alexander Skopetz
NASA/GSFC
11911 Galaxy Lane
Bowie, MD 20715

James A. Slater
Defense Mapping Agency/GST
6500 Brookes Lane
Washington, DC 20315

Arthur E. Smith
Trajectory Inst Div
Range Inst. Syms Dept.
Code 3421.3
Ft. Mugu, CA 93042

Ralph R. Smith
Navy Astronautics Group
SPM 214
Pt Mugu, CA 93042

Thomas M. Stalder
Bendix Field Engineering Corporation
5707 Thunderhill Rd.
Columbia, MD 21045

Samuel R. Stein
National Bureau of Standards-
Time and Frequency Division, 524
325 Broadway
Boulder, CO 80303

C. S. Stone
Brightline Corporation
P.O. Box 1016
Cedar Park, TX 78613

Harris A. Stover
DCA/DCEC
1860 Wiehle Ave
Reston, VA 22090

David Y. Stowell
MITRE
1820 Dolley Madison Blvd.
McLean, VA. 22102

John T. Strain
Frequency Electronics
1688 East Gude Drive
Rockville, MD 20850

Donald M. Strayer
Jet Propulsion Laboratory,
M/S 183-401
4800 Oak Grove Drive
Pasadena, CA 91109

Ed Sullivan
EG&G Inc. Dept. 325
35 Congress St.
Salem, MA 01970

Joe J. Suter
JHU/APL
Laurel, MD 20707

Everett R. Swift
NSWC K12
Dahlgren, VA 22448

David A Symonds
PIEZO Technology Inc.
2525 Shader Rd. Box 7859
Orlando, FL 32854

Richard D. Timblin
HRB-Singer Inc.
P.O. Box 60
State College, PA 16804

Michael Tope
Kode Inc.
2752 Walnut Ave.
Tustin, CA 92680

Kenneth M. Uglow
P.O. Box 2260
Sarasota, FL 33578

Paul J. Underwood
Johns Hopkins University APL
Johns Hopkins Rd.
Laurel, MD 20707

A. J. Van Dierendonck
Stanford Telecommunication
2421 Mission College Blvd.
Santa Clara, CA 95050

15TH ANNUAL PRECISE TIME AND TIME INTERVAL REGISTRATION

John L. van Groos
Kinematics - True Time Division
3243 Santa Rosa Avenue
Santa Rosa, CA 95407

Marinus J. Van Melle
Rockwell Int
8042 Madia
LaPalma, CA 90623

Fran B. Varnum
Defense Mapping Agency
USNO Bldg. 56
Washington, DC 20305

Lester B. Veenstra
Comsat Laboratory
22300 Comsat Dr.
Clarksburg, MD 20871

Robert F.C. Vessot
Smithsonian Astrophysical Observatory
60 Garden Street
Cambridge, MA 02138

Jerome R. Vetter
Applied Physics Laboratory/JHU
Johns Hopkins Road
Laurel, MD 20707

John R. Vig
U.S. Army Electronics Technology & Devices Lab.
Atten: Delet-EQ
Ft. Monmouth, NJ 07703

Camil G. Vigneault
Geodetic Survey of Canada (E.M.R.)
615 Booth St.
Ottawa, Canada K1A 0E9

John A. Waak
NRL
Code 4134 W
Washington, DC 20375

H. Beat Wackernagel
USAF Space Command
Peterson AFB, CO 80914

Elbert S. Walker
Hughes Aircraft Co.
2911 S. Newark Place
Aurora, CO 80014

William C. Walker
Pan Am World Airways
Bldg 989 Mu 840
Patrick AFB, FL 32925

Fred L. Walls
National Bureau of
Standards
325 Broadway
Boulder, CO 80303

Donald J. Walt
USAF 89th FMS OLA
5473 C. Langley Way
Bolling AFB DC 20336

Harry T. M. Wang
Hughes Research
Laboratories
3011 Malibu Canyon Road
Malibu, CA 90265

John C. Warburton
HRB-Singer Inc.
Box 60 Science Park
State College, PA 16804

Samuel C. Ward
Jet Propulsion Laboratory
4800 Oak Grove Drive
Pasadena, CA 91103

S. Clark Wardrip
NASA-GSFC
Code 854
Greenbelt, MD 20771

Hugh E. Warren
Bendix Field Engineering
Code 7966 NRL
4555 Overlook Ave.
Washington, DC 20375

Wemer A. Weidemann
Efraetom
18851 Bardeen Ave.
Irvine CA 92715

Marc A. Weiss
National Bureau of Standards
325 Broadway
Boulder, CO 80303

15TH ANNUAL PRECISE TIME AND TIME INTERVAL REGISTRATION

James E. Wells
J.P. L. Deep Space Network
S. Elwick Place, Lyons
Canberra A.C.T. Australia 2606

Zuyin Weng
Laboratoire Primaire du Temps et des
Frequences Observatoire de Paris
61, avenue de l'observatoire
Paris, France 75014

Gart Westerhout
U.S. Naval Observatory
Washington, DC 20390

Paul J. Wheeler
U.S. Naval Observatory
34th and Massachussetts Ave.
Washington, DC 20390

Joseph D. White
U.S. NRL
Code 7962
Washington, DC 20375

Warren L. Wilson
Fairchild Test Systems
707 Spindrift Dr.
San Jose, CA 95134

Gernot Winkler
USNO
Washington, DC 20396

Jeffrey A. Wisnia
Kernco
28 Harbor St.
Danvers, MA 02188

Frances Neville Withington
U.S. Naval Observatory Time Service
34th St. and Mass Ave. N.W.
Washington, DC 20390

Herman R. Wood
Kentron International
2003 Byrd Spring Road
Huntsville, AL 35802

Raymond F. Woolley
U.S. Army - CECOM
Ft. Monmouth, NJ 07703

Woody K. Wordsworth
Austron, Inc.
1800 Old Meadow Rd.
McLean, VA 22102

C. Robert Wright
DOT/FAA
FAA Technical Center,
APM-164
Atlantic Air Airport, NJ
08405

James L. Wright
Pan American World
Airways
Bldg. 989 MU 840
Patrick AFB, FL 32925

Sien-Chong Wu
Jet Propulsion Laboratory
4800 Oak Grove Dr.
Pasadena, CA 91109

Pam Xiao-pei
P.O. Box 18, Lintong,
Shaanxi
Peoples Republic of China

Miao Yong-Yui
P.O. Box 18 Lintong
Shaanxi
Peoples Republic of China

Larry Young
Jet Propulsion Lab
4800 Oak Grove Drive
Mail Stop 264-737
Pasadena, CA 91109

Thomas P. Yuncck
Jet Propulsion Laboratory
4800 Oak Grove Drive
Pasadena, CA 91109

Robert R. Zeigler
PIEZO Crystal Co.
100 K. St
Carlisle, PA 17013

Philip A. Zirkle
Applied Physics Laboratory
Johns Hopkins Road
Laurel, MD 20707

END

FILMED

2-85

DTIC